NIST NCSTAR 1-2

Federal Building and Fire Safety Investigation of the World Trade Center Disaster

Baseline Structural Performance and Aircraft Impact Damage Analysis of the World Trade Center Towers

Fahim Sadek

NIST National Institute of Standards and Technology • Technology Administration • U.S. Department of Commerce

NIST NCSTAR 1-2

Federal Building and Fire Safety Investigation of the World Trade Center Disaster

Baseline Structural Performance and Aircraft Impact Damage Analysis of the World Trade Center Towers

Fahim Sadek
Building and Fire Research Laboratory
National Institute of Standards and Technology

September 2005

U.S. Department of Commerce
Carlos M. Gutierrez, Secretary

Technology Administration
Michelle O'Neill, Acting Under Secretary for Technology

National Institute of Standards and Technology
William Jeffrey, Director

Disclaimer No. 1

Certain commercial entities, equipment, products, or materials are identified in this document in order to describe a procedure or concept adequately or to trace the history of the procedures and practices used. Such identification is not intended to imply recommendation, endorsement, or implication that the entities, products, materials, or equipment are necessarily the best available for the purpose. Nor does such identification imply a finding of fault or negligence by the National Institute of Standards and Technology.

Disclaimer No. 2

The policy of NIST is to use the International System of Units (metric units) in all publications. In this document, however, units are presented in metric units or the inch-pound system, whichever is prevalent in the discipline.

Disclaimer No. 3

Pursuant to section 7 of the National Construction Safety Team Act, the NIST Director has determined that certain evidence received by NIST in the course of this Investigation is "voluntarily provided safety-related information" that is "not directly related to the building failure being investigated" and that "disclosure of that information would inhibit the voluntary provision of that type of information" (15 USC 7306c).

In addition, a substantial portion of the evidence collected by NIST in the course of the Investigation has been provided to NIST under nondisclosure agreements.

Disclaimer No. 4

NIST takes no position as to whether the design or construction of a WTC building was compliant with any code since, due to the destruction of the WTC buildings, NIST could not verify the actual (or as-built) construction, the properties and condition of the materials used, or changes to the original construction made over the life of the buildings. In addition, NIST could not verify the interpretations of codes used by applicable authorities in determining compliance when implementing building codes. Where an Investigation report states whether a system was designed or installed as required by a code *provision*, NIST has documentary or anecdotal evidence indicating whether the requirement was met, or NIST has independently conducted tests or analyses indicating whether the requirement was met.

Use in Legal Proceedings

No part of any report resulting from a NIST investigation into a structural failure or from an investigation under the National Construction Safety Team Act may be used in any suit or action for damages arising out of any matter mentioned in such report (15 USC 281a; as amended by P.L. 107-231).

National Institute of Standards and Technology National Construction Safety Team Act Report 1-2
Natl. Inst. Stand. Technol. Natl. Constr. Sfty. Tm. Act Rpt. 1-2, 458 pages (September 2005)
CODEN: NSPUE2

U.S. GOVERNMENT PRINTING OFFICE
WASHINGTON: 2005

For sale by the Superintendent of Documents, U.S. Government Printing Office
Internet: bookstore.gpo.gov — Phone: (202) 512-1800 — Fax: (202) 512-2250
Mail: Stop SSOP, Washington, DC 20402-0001

ABSTRACT

The baseline structural performance and aircraft impact damage analysis of the National Institute of Standards and Technology (NIST) Investigation of the World Trade Center (WTC) disaster had two primary tasks: (1) to develop reference structural models of the WTC towers and use these models to establish the baseline performance of each of the towers under gravity and wind loads, and (2) to estimate the damage to the towers due to aircraft impacts and establish the initial conditions for the fire dynamics modeling and the thermal-structural response and collapse initiation analysis. This report provides the technical approach, methodology, and results related to both tasks.

For the first task, the baseline performance of the WTC towers under gravity and wind loads was established in order to assess the towers' ability to withstand those loads safely and to evaluate the reserve capacity of the towers to withstand unanticipated events. The baseline performance study provides a measure of the behavior of the towers under design loading conditions, specifically: (1) total and inter-story drift (the sway of the building under design wind loads), (2) floor deflections under gravity loads, (3) the stress demand-to-capacity ratio for primary structural components of the towers such as exterior walls, core columns, and floor framing, (4) performance of exterior walls under wind loading, including distribution of axial stresses and presence of tensile forces, (5) performance of connections between exterior columns, and (6) resistance of the towers to shear sliding and overturning at the foundation level.

Wind loads were a governing factor in the design of the structural components that made up the frame-tube steel framing system. Wind load capacity was also a key factor in determining the overall strength of the towers and was important in determining not only the ability of the towers to withstand winds but also the reserve capacity of the towers to withstand unanticipated events such as major fire or impact damage. Accurate estimation of the wind load on tall buildings is a challenging task, given that wind engineering is still an evolving technology. For example, estimates of the wind-induced response presented in two recent independent studies of the WTC towers differed from each other by about 40 percent. In this study, NIST developed refined estimates of wind effects by critically assessing information obtained from the Cermak Peterka Peterson, Inc. (CPP) and Rowan Williams Davis and Irwin, Inc. (RWDI) reports and by bringing to bear state-of-the-art considerations. Furthermore, the available prescriptive codes specify wind loads on tall buildings that are significantly lower than wind tunnel-based loads. This case study provided an opportunity to assess effectively current design practices and various code provisions on wind loads.

For the purpose of establishing the baseline performance of the towers, various wind loads were considered in this study, including wind loads used in the original WTC design, wind loads based on two recent wind tunnel studies conducted in 2002 by CPP and RWDI for insurance litigation concerning the towers, and refined wind load estimates developed by NIST.

In order to develop the reference models and conduct the baseline performance analyses, the following steps were undertaken:

- Develop structural databases for the primary structural components of the WTC 1 and WTC 2 towers from the original computer printouts of the structural design documents.

- Develop reference structural analysis models that captured the intended behavior of each of the two towers using the generated databases. These reference models were used to establish the baseline performance of the towers and also served as a reference for more detailed models for aircraft impact damage analysis and thermal-structural response and collapse initiation analysis. The models included: (1) two global models (one for each tower) of the major structural components and systems of the towers, and (2) floor models of a typical truss-framed floor and a typical beam-framed floor.

- Develop estimates of design gravity (dead and live loads) and wind loads on each of the two towers for implementation into the reference structural models. The following three loading cases were considered:

  – *Original WTC design loads case.* Loads included dead and live loads as in original WTC design, in conjunction with original WTC design wind loads.

  – *State-of-the-practice case.* Loads included dead loads; current New York City Building Code (NYCBC 2001) live loads; and wind loads from the RWDI wind tunnel study, scaled in accordance with NYCBC 2001 wind speed.

  – *Refined NIST estimate case.* Loads included dead loads; live loads from the American Society of Civil Engineers (ASCE) 7-02 Standard (a national standard); and refined wind loads developed by NIST.

- Perform structural analyses to establish the baseline performance of each of the two towers under design gravity and wind loads.

For the second task related to aircraft impact, the aircraft impact damage to the exterior of the WTC towers could be visibly identified from the video and photographic records. However, no visible information could be obtained for the extent of damage to the interior of the towers, including the structural system (floors and core columns), partition walls, and interior building contents. Such information was needed for the subsequent fire dynamics simulations and post-impact structural analyses. In addition, for the fire dynamics modeling, the dispersion of the jet fuel and the location of combustible aircraft debris were required. The estimate of the extent of damage to the fireproofing on the structural steel in the towers due to impact was essential for the thermal and structural analyses. The aircraft impact damage analyses were the primary tool by which most of the information on the tower damage could be estimated.

The focus of the analysis was to analyze the aircraft impacts into each of the WTC towers to provide the following: (1) estimates of probable damage to structural systems, including exterior walls, floor systems, and interior core columns; (2) estimates of the aircraft fuel dispersion during the impact; and (3) estimates of debris damage to the building nonstructural contents, including partitions and workstations. The results were to be used to estimate the damage to fireproofing based on the predicted path of the debris field inside the towers. This analysis thus estimated the condition of the two WTC towers immediately following the aircraft impacts and established the initial conditions for the fire dynamics modeling and the thermal-structural response and collapse initiation analysis. The impact analyses were conducted at various levels of complexity including: (1) the component level, (2) the subassembly level, and (3) the global level to estimate the probable damage to the towers due to aircraft impact.

In order to estimate the aircraft impact damage to the WTC towers, the following steps were undertaken:

- Constitutive relationships were developed to describe the behavior and failure of the materials under the dynamic impact conditions of the aircraft. These materials included the various grades of steels used in the exterior walls, core columns, and floor trusses of the towers, weldment metal, bolts, reinforced concrete, aircraft materials, and nonstructural contents.

- Global impact models were developed for the towers and aircraft. The tower models included the primary structural components of the towers in the impact zone, including exterior walls, floor systems, core columns, and connections, along with nonstructural building contents. A refined finite element mesh was used for the areas in the path of the aircraft, and a coarser mesh was used elsewhere. The aircraft model included the aircraft engines, wings, fuselage, the empennage, and landing gear, as well as nonstructural components of the aircraft. The aircraft model also included a representation of the fuel, using the smooth particle hydrodynamics approach.

- Component and subassembly impact analyses were conducted to support the development of the global impact models. The primary objectives of these analyses were to (1) develop an understanding of the interactive failure phenomenon of the aircraft and tower components, and (2) develop the simulation techniques required for the global analysis of the aircraft impacts into the WTC towers, including variations in mesh density and numerical tools for modeling fluid-structure interaction for fuel impact and dispersion. The component and subassembly analyses were used to determine model simplifications for reducing the overall model size while maintaining fidelity in the global analyses.

- Initial conditions were estimated for the impact of the aircraft into the WTC towers. These included the aircraft speed at impact, aircraft orientation and trajectory, and impact location of the aircraft nose. The estimates also included the uncertainties associated with these parameters. This step utilized the videos and photographs that captured the impact event and subsequent damage to the exterior of the towers.

- Sensitivity analyses were conducted at the component and subassembly levels to assess the effect of uncertainties on the level of damage to the towers due to impact and to determine the most influential parameters that affect the damage estimates. The analyses were used to reduce the number of parameters that would be varied in the global impact simulations.

- Analyses of aircraft impact into WTC 1 and WTC 2 were conducted using the global tower and aircraft models. The analysis results included the estimation of the structural damage that degraded their strength and the condition and position of nonstructural contents such as partitions, workstations, aircraft fuel, and other debris that influenced the behavior of the subsequent fires in the towers. The global analyses included, for each tower, a “base case” based on reasonable initial estimates of all input parameters. They also provided a range of damage estimates based on variations of the most influential parameters. This range included more severe and less severe damage cases.

- Approximate analyses were conducted to provide guidance to the global finite element impact analyses. These included: (1) analysis of the overall aircraft impact forces and assessment of the relative importance of the airframe strength and weight distribution, (2) evaluation of the potential effects of the energy in the rotating engine components on the calculated engine impact response, (3) influence of the static preloads in the towers on the calculated impact damage and residual strength predictions, and (4) analysis of the load characteristics required to damage core columns compared to the potential loading from impact of aircraft components.

Keywords: Aircraft impact, finite element analysis, floor system, load, model, structural, truss, wind loads, World Trade Center.

TABLE OF CONTENTS

This page intentionally left blank.

LIST OF FIGURES

This page intentionally left blank.

LIST OF TABLES

LIST OF ACRONYMS AND ABBREVIATIONS

Acronyms

AA	American Airlines
AISC	American Institute of Steel Construction
ALE	Arbitrary-Lagrangian-Eulerian
ARA	Applied Research Associates, Incorporated
ASCE	American Society of Civil Engineers
ASD	Allowable Stress Design
ASTM	American Society for Testing and Materials
CDL	Construction dead load
C.O.V.	coefficient of variation
CPP	Cermak Peterka Peterson, Inc.
CPU	central processing unit
CSU	Colorado State University
DCR	demand/capacity ratio
DL	dead load
E–W	East–West direction
FBI	Federal Bureau of Investigation
FEMA	Federal Emergency Management Agency
HAZ	heat affected zone
HFFB	heat-frequency force-balance
LERA	Leslie E. Robertson Associates, RLLP
LL	live load
LRFD	Load and Resistance Factor Design
MIT	Massachusetts Institute of Technology
NIST	National Institute of Standards and Technology
N–S	North–South direction
NOAA	National Oceanic Atmospheric Administration
NTSC	National Television System Committee
NYCBC	New York City Building Code

PAL	Phase Alternating Line
PANYNJ	Port Authority of New York and New Jersey
RWDI	Rowan Williams Davies and Irwin, Inc.
SDL	superimposed dead load
SOM	Skidmore, Owings, and Merrill
SPH	Smoothed Particle Hydrodynamics
UAL	United Airlines
ULD	unit load device
WAI	Weidlinger Associates, Inc.
WSHJ	Worthington, Skilling, Helle & Jackson
WTC	World Trade Center
WTC 1	World Trade Center 1 (North Tower)
WTC 2	World Trade Center 2 (South Tower)
WTC 7	World Trade Center 7

Abbreviations

±	plus or minus
2D	two dimensional
3D	three dimensional
fps	foot per second
ft	foot
ft^2	square foot
GHz	gigahertz
h	hour
in.	inch
kip	a stress equal to 1,000 pounds
ksi	1,000 pounds per square inch
lb	pound
m	meter
min	minute
mph	miles per hour
pcf	pounds per cubic foot

psf	pounds per square foot
psi	pounds per square inch
s	second
ms	millisecond

This page intentionally left blank.

PREFACE

Immediately following the terrorist attack on the World Trade Center (WTC) on September 11, 2001, the Federal Emergency Management Agency (FEMA) and the American Society of Civil Engineers began planning a building performance study of the disaster. The week of October 7, as soon as the rescue and search efforts ceased, the Building Performance Study Team went to the site and began its assessment. This was to be a brief effort, as the study team consisted of experts who largely volunteered their time away from their other professional commitments. The Building Performance Study Team issued its report in May 2002, fulfilling its goal "to determine probable failure mechanisms and to identify areas of future investigation that could lead to practical measures for improving the damage resistance of buildings against such unforeseen events."

On August 21, 2002, with funding from the U.S. Congress through FEMA, the National Institute of Standards and Technology (NIST) announced its building and fire safety investigation of the WTC disaster. On October 1, 2002, the National Construction Safety Team Act (Public Law 107-231), was signed into law. The NIST WTC Investigation was conducted under the authority of the National Construction Safety Team Act.

The goals of the investigation of the WTC disaster were:

- To investigate the building construction, the materials used, and the technical conditions that contributed to the outcome of the WTC disaster.
- To serve as the basis for:
  - Improvements in the way buildings are designed, constructed, maintained, and used;
  - Improved tools and guidance for industry and safety officials;
  - Recommended revisions to current codes, standards, and practices; and
  - Improved public safety.

The specific objectives were:

1. Determine why and how WTC 1 and WTC 2 collapsed following the initial impacts of the aircraft and why and how WTC 7 collapsed;
2. Determine why the injuries and fatalities were so high or low depending on location, including all technical aspects of fire protection, occupant behavior, evacuation, and emergency response;
3. Determine what procedures and practices were used in the design, construction, operation, and maintenance of WTC 1, 2, and 7; and
4. Identify, as specifically as possible, areas in current building and fire codes, standards, and practices that warrant revision.

NIST is a nonregulatory agency of the U.S. Department of Commerce's Technology Administration. The purpose of NIST investigations is to improve the safety and structural integrity of buildings in the United States, and the focus is on fact finding. NIST investigative teams are authorized to assess building performance and emergency response and evacuation procedures in the wake of any building failure that has resulted in substantial loss of life or that posed significant potential of substantial loss of life. NIST does not have the statutory authority to make findings of fault nor negligence by individuals or organizations. Further, no part of any report resulting from a NIST investigation into a building failure or from an investigation under the National Construction Safety Team Act may be used in any suit or action for damages arising out of any matter mentioned in such report (15 USC 281a, as amended by Public Law 107-231).

Organization of the Investigation

The National Construction Safety Team for this Investigation, appointed by the then NIST Director, Dr. Arden L. Bement, Jr., was led by Dr. S. Shyam Sunder. Dr. William L. Grosshandler served as Associate Lead Investigator, Mr. Stephen A. Cauffman served as Program Manager for Administration, and Mr. Harold E. Nelson served on the team as a private sector expert. The Investigation included eight interdependent projects whose leaders comprised the remainder of the team. A detailed description of each of these eight projects is available at http://wtc.nist.gov. The purpose of each project is summarized in Table P–1, and the key interdependencies among the projects are illustrated in Fig. P–1.

Table P–1. Federal building and fire safety investigation of the WTC disaster.

Technical Area and Project Leader	Project Purpose
Analysis of Building and Fire Codes and Practices; Project Leaders: Dr. H. S. Lew and Mr. Richard W. Bukowski	Document and analyze the code provisions, procedures, and practices used in the design, construction, operation, and maintenance of the structural, passive fire protection, and emergency access and evacuation systems of WTC 1, 2, and 7.
Baseline Structural Performance and Aircraft Impact Damage Analysis; Project Leader: Dr. Fahim H. Sadek	Analyze the baseline performance of WTC 1 and WTC 2 under design, service, and abnormal loads, and aircraft impact damage on the structural, fire protection, and egress systems.
Mechanical and Metallurgical Analysis of Structural Steel; Project Leader: Dr. Frank W. Gayle	Determine and analyze the mechanical and metallurgical properties and quality of steel, weldments, and connections from steel recovered from WTC 1, 2, and 7.
Investigation of Active Fire Protection Systems; Project Leader: Dr. David D. Evans; Dr. William Grosshandler	Investigate the performance of the active fire protection systems in WTC 1, 2, and 7 and their role in fire control, emergency response, and fate of occupants and responders.
Reconstruction of Thermal and Tenability Environment; Project Leader: Dr. Richard G. Gann	Reconstruct the time-evolving temperature, thermal environment, and smoke movement in WTC 1, 2, and 7 for use in evaluating the structural performance of the buildings and behavior and fate of occupants and responders.
Structural Fire Response and Collapse Analysis; Project Leaders: Dr. John L. Gross and Dr. Therese P. McAllister	Analyze the response of the WTC towers to fires with and without aircraft damage, the response of WTC 7 in fires, the performance of composite steel-trussed floor systems, and determine the most probable structural collapse sequence for WTC 1, 2, and 7.
Occupant Behavior, Egress, and Emergency Communications; Project Leader: Mr. Jason D. Averill	Analyze the behavior and fate of occupants and responders, both those who survived and those who did not, and the performance of the evacuation system.
Emergency Response Technologies and Guidelines; Project Leader: Mr. J. Randall Lawson	Document the activities of the emergency responders from the time of the terrorist attacks on WTC 1 and WTC 2 until the collapse of WTC 7, including practices followed and technologies used.

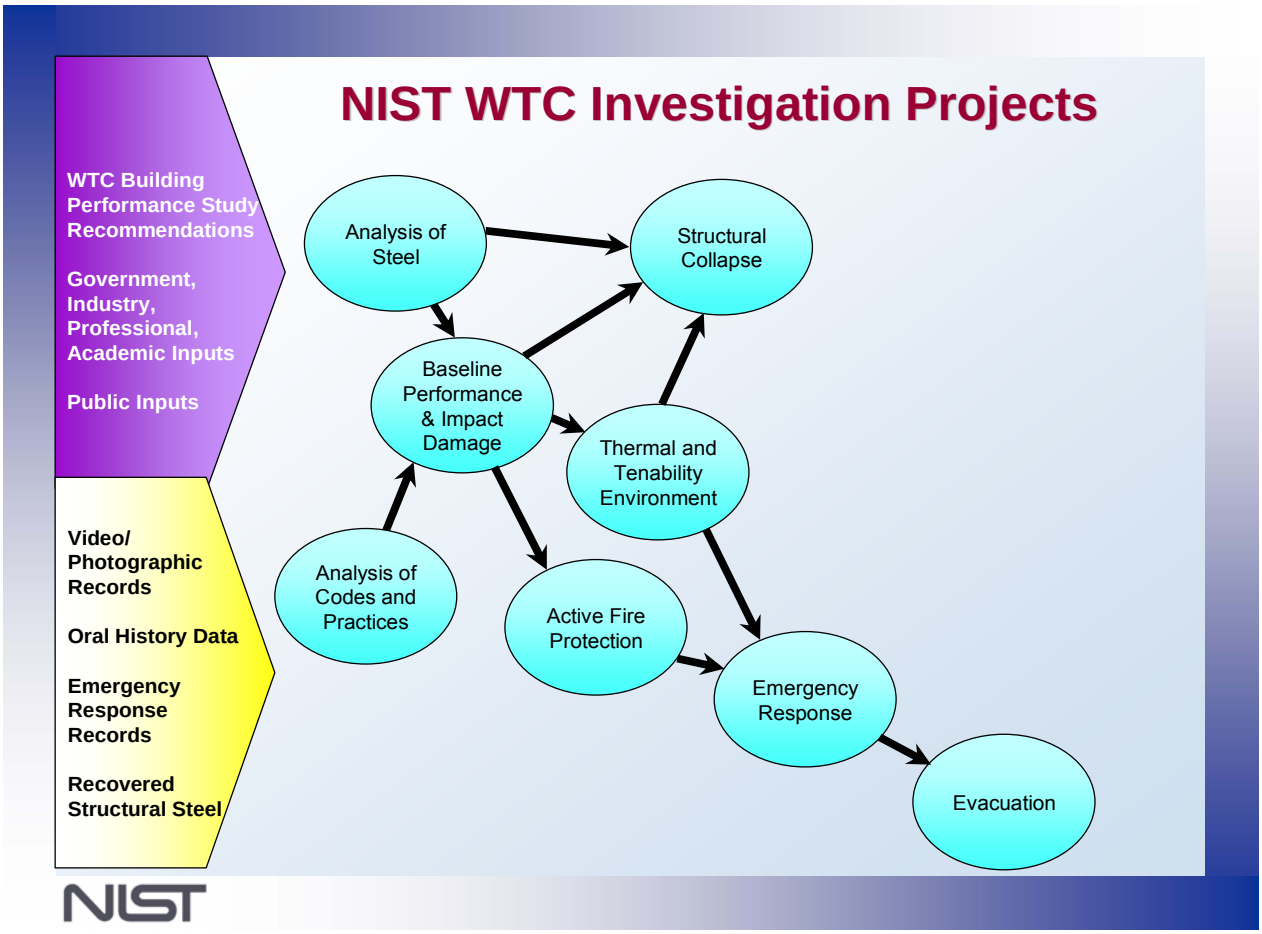

Figure P–1. The eight projects in the federal building and fire safety investigation of the WTC disaster.

National Construction Safety Team Advisory Committee

The NIST Director also established an advisory committee as mandated under the National Construction Safety Team Act. The initial members of the committee were appointed following a public solicitation. These were:

- Paul Fitzgerald, Executive Vice President (retired) FM Global, National Construction Safety Team Advisory Committee Chair
- John Barsom, President, Barsom Consulting, Ltd.
- John Bryan, Professor Emeritus, University of Maryland
- David Collins, President, The Preview Group, Inc.
- Glenn Corbett, Professor, John Jay College of Criminal Justice
- Philip DiNenno, President, Hughes Associates, Inc.

- Robert Hanson, Professor Emeritus, University of Michigan
- Charles Thornton, Co-Chairman and Managing Principal, The Thornton-Tomasetti Group, Inc.
- Kathleen Tierney, Director, Natural Hazards Research and Applications Information Center, University of Colorado at Boulder
- Forman Williams, Director, Center for Energy Research, University of California at San Diego

This National Construction Safety Team Advisory Committee provided technical advice during the Investigation and commentary on drafts of the Investigation reports prior to their public release. NIST has benefited from the work of many people in the preparation of these reports, including the National Construction Safety Team Advisory Committee. The content of the reports and recommendations, however, are solely the responsibility of NIST.

Public Outreach

During the course of this Investigation, NIST held public briefings and meetings (listed in Table P–2) to solicit input from the public, present preliminary findings, and obtain comments on the direction and progress of the Investigation from the public and the Advisory Committee.

NIST maintained a publicly accessible Web site during this Investigation at http://wtc.nist.gov. The site contained extensive information on the background and progress of the Investigation.

NIST's WTC Public-Private Response Plan

The collapse of the WTC buildings has led to broad reexamination of how tall buildings are designed, constructed, maintained, and used, especially with regard to major events such as fires, natural disasters, and terrorist attacks. Reflecting the enhanced interest in effecting necessary change, NIST, with support from Congress and the Administration, has put in place a program, the goal of which is to develop and implement the standards, technology, and practices needed for cost-effective improvements to the safety and security of buildings and building occupants, including evacuation, emergency response procedures, and threat mitigation.

The strategy to meet this goal is a three-part NIST-led public-private response program that includes:

- A federal building and fire safety investigation to study the most probable factors that contributed to post-aircraft impact collapse of the WTC towers and the 47-story WTC 7 building, and the associated evacuation and emergency response experience.
- A research and development (R&D) program to (a) facilitate the implementation of recommendations resulting from the WTC Investigation, and (b) provide the technical basis for cost-effective improvements to national building and fire codes, standards, and practices that enhance the safety of buildings, their occupants, and emergency responders.

Table P–2. Public meetings and briefings of the WTC Investigation.

Date	Location	Principal Agenda
June 24, 2002	New York City, NY	Public meeting: Public comments on the *Draft Plan* for the pending WTC Investigation.
August 21, 2002	Gaithersburg, MD	Media briefing announcing the formal start of the Investigation.
December 9, 2002	Washington, DC	Media briefing on release of the *Public Update* and NIST request for photographs and videos.
April 8, 2003	New York City, NY	Joint public forum with Columbia University on first-person interviews.
April 29–30, 2003	Gaithersburg, MD	NCST Advisory Committee meeting on plan for and progress on WTC Investigation with a public comment session.
May 7, 2003	New York City, NY	Media briefing on release of *May 2003 Progress Report.*
August 26–27, 2003	Gaithersburg, MD	NCST Advisory Committee meeting on status of the WTC investigation with a public comment session.
September 17, 2003	New York City, NY	Media and public briefing on initiation of first-person data collection projects.
December 2–3, 2003	Gaithersburg, MD	NCST Advisory Committee meeting on status and initial results and release of the *Public Update* with a public comment session.
February 12, 2004	New York City, NY	Public meeting on progress and preliminary findings with public comments on issues to be considered in formulating final recommendations.
June 18, 2004	New York City, NY	Media/public briefing on release of *June 2004 Progress Report.*
June 22–23, 2004	Gaithersburg, MD	NCST Advisory Committee meeting on the status of and preliminary findings from the WTC Investigation with a public comment session.
August 24, 2004	Northbrook, IL	Public viewing of standard fire resistance test of WTC floor system at Underwriters Laboratories, Inc.
October 19–20, 2004	Gaithersburg, MD	NCST Advisory Committee meeting on status and near complete set of preliminary findings with a public comment session.
November 22, 2004	Gaithersburg, MD	NCST Advisory Committee discussion on draft annual report to Congress, a public comment session, and a closed session to discuss pre-draft recommendations for WTC Investigation.
April 5, 2005	New York City, NY	Media and public briefing on release of the probable collapse sequence for the WTC towers and draft reports for the projects on codes and practices, evacuation, and emergency response.
June 23, 2005	New York City, NY	Media and public briefing on release of all draft reports for the WTC towers and draft recommendations for public comment.
September 12–13, 2005	Gaithersburg, MD	NCST Advisory Committee meeting on disposition of public comments and update to draft reports for the WTC towers.
September 13–15, 2005	Gaithersburg, MD	WTC Technical Conference for stakeholders and technical community for dissemination of findings and recommendations and opportunity for public to make technical comments.

- A dissemination and technical assistance program (DTAP) to (a) engage leaders of the construction and building community in ensuring timely adoption and widespread use of proposed changes to practices, standards, and codes resulting from the WTC Investigation and the R&D program, and (b) provide practical guidance and tools to better prepare facility owners, contractors, architects, engineers, emergency responders, and regulatory authorities to respond to future disasters.

The desired outcomes are to make buildings, occupants, and first responders safer in future disaster events.

National Construction Safety Team Reports on the WTC Investigation

A final report on the collapse of the WTC towers is being issued as NIST NCSTAR 1. A companion report on the collapse of WTC 7 is being issued as NIST NCSTAR 1A. The present report is one of a set that provides more detailed documentation of the Investigation findings and the means by which these technical results were achieved. As such, it is part of the archival record of this Investigation. The titles of the full set of Investigation publications are:

NIST (National Institute of Standards and Technology). 2005. *Federal Building and Fire Safety Investigation of the World Trade Center Disaster: Final Report on the Collapse of the World Trade Center Towers.* NIST NCSTAR 1. Gaithersburg, MD, September.

NIST (National Institute of Standards and Technology). 2006. *Federal Building and Fire Safety Investigation of the World Trade Center Disaster: Final Report on the Collapse of World Trade Center 7.* NIST NCSTAR 1A. Gaithersburg, MD.

Lew, H. S., R. W. Bukowski, and N. J. Carino. 2005. *Federal Building and Fire Safety Investigation of the World Trade Center Disaster: Design, Construction, and Maintenance of Structural and Life Safety Systems.* NIST NCSTAR 1-1. National Institute of Standards and Technology. Gaithersburg, MD, September.

Fanella, D. A., A. T. Derecho, and S. K. Ghosh. 2005. *Federal Building and Fire Safety Investigation of the World Trade Center Disaster: Design and Construction of Structural Systems.* NIST NCSTAR 1-1A. National Institute of Standards and Technology. Gaithersburg, MD, September.

Ghosh, S. K., and X. Liang. 2005. *Federal Building and Fire Safety Investigation of the World Trade Center Disaster: Comparison of Building Code Structural Requirements.* NIST NCSTAR 1-1B. National Institute of Standards and Technology. Gaithersburg, MD, September.

Fanella, D. A., A. T. Derecho, and S. K. Ghosh. 2005. *Federal Building and Fire Safety Investigation of the World Trade Center Disaster: Maintenance and Modifications to Structural Systems.* NIST NCSTAR 1-1C. National Institute of Standards and Technology. Gaithersburg, MD, September.

Grill, R. A., and D. A. Johnson. 2005. *Federal Building and Fire Safety Investigation of the World Trade Center Disaster: Fire Protection and Life Safety Provisions Applied to the Design and Construction of World Trade Center 1, 2, and 7 and Post-Construction Provisions Applied after Occupancy.* NIST NCSTAR 1-1D. National Institute of Standards and Technology. Gaithersburg, MD, September.

Razza, J. C., and R. A. Grill. 2005. *Federal Building and Fire Safety Investigation of the World Trade Center Disaster: Comparison of Codes, Standards, and Practices in Use at the Time of the Design and Construction of World Trade Center 1, 2, and 7.* NIST NCSTAR 1-1E. National Institute of Standards and Technology. Gaithersburg, MD, September.

Grill, R. A., D. A. Johnson, and D. A. Fanella. 2005. *Federal Building and Fire Safety Investigation of the World Trade Center Disaster: Comparison of the 1968 and Current (2003) New*

York City Building Code Provisions. NIST NCSTAR 1-1F. National Institute of Standards and Technology. Gaithersburg, MD, September.

Grill, R. A., and D. A. Johnson. 2005. *Federal Building and Fire Safety Investigation of the World Trade Center Disaster: Amendments to the Fire Protection and Life Safety Provisions of the New York City Building Code by Local Laws Adopted While World Trade Center 1, 2, and 7 Were in Use*. NIST NCSTAR 1-1G. National Institute of Standards and Technology. Gaithersburg, MD, September.

Grill, R. A., and D. A. Johnson. 2005. *Federal Building and Fire Safety Investigation of the World Trade Center Disaster: Post-Construction Modifications to Fire Protection and Life Safety Systems of World Trade Center 1 and 2*. NIST NCSTAR 1-1H. National Institute of Standards and Technology. Gaithersburg, MD, September.

Grill, R. A., D. A. Johnson, and D. A. Fanella. 2005. *Federal Building and Fire Safety Investigation of the World Trade Center Disaster: Post-Construction Modifications to Fire Protection, Life Safety, and Structural Systems of World Trade Center 7*. NIST NCSTAR 1-1I. National Institute of Standards and Technology. Gaithersburg, MD, September.

Grill, R. A., and D. A. Johnson. 2005. *Federal Building and Fire Safety Investigation of the World Trade Center Disaster: Design, Installation, and Operation of Fuel System for Emergency Power in World Trade Center 7*. NIST NCSTAR 1-1J. National Institute of Standards and Technology. Gaithersburg, MD, September.

Sadek, F. 2005. *Federal Building and Fire Safety Investigation of the World Trade Center Disaster: Baseline Structural Performance and Aircraft Impact Damage Analysis of the World Trade Center Towers.* NIST NCSTAR 1-2. National Institute of Standards and Technology. Gaithersburg, MD, September.

Faschan, W. J., and R. B. Garlock. 2005. *Federal Building and Fire Safety Investigation of the World Trade Center Disaster: Reference Structural Models and Baseline Performance Analysis of the World Trade Center Towers.* NIST NCSTAR 1-2A. National Institute of Standards and Technology. Gaithersburg, MD, September.

Kirkpatrick, S. W., R. T. Bocchieri, F. Sadek, R. A. MacNeill, S. Holmes, B. D. Peterson, R. W. Cilke, C. Navarro. 2005. *Federal Building and Fire Safety Investigation of the World Trade Center Disaster: Analysis of Aircraft Impacts into the World Trade Center Towers*, NIST NCSTAR 1-2B. National Institute of Standards and Technology. Gaithersburg, MD, September.

Gayle, F. W., R. J. Fields, W. E. Luecke, S. W. Banovic, T. Foecke, C. N. McCowan, T. A. Siewert, and J. D. McColskey. 2005. *Federal Building and Fire Safety Investigation of the World Trade Center Disaster: Mechanical and Metallurgical Analysis of Structural Steel.* NIST NCSTAR 1-3. National Institute of Standards and Technology. Gaithersburg, MD, September.

Luecke, W. E., T. A. Siewert, and F. W. Gayle. 2005. *Federal Building and Fire Safety Investigation of the World Trade Center Disaster: Contemporaneous Structural Steel Specifications.* NIST Special Publication 1-3A. National Institute of Standards and Technology. Gaithersburg, MD, September.

Banovic, S. W. 2005. *Federal Building and Fire Safety Investigation of the World Trade Center Disaster: Steel Inventory and Identification.* NIST NCSTAR 1-3B. National Institute of Standards and Technology. Gaithersburg, MD, September.

Banovic, S. W., and T. Foecke. 2005. *Federal Building and Fire Safety Investigation of the World Trade Center Disaster: Damage and Failure Modes of Structural Steel Components.* NIST NCSTAR 1-3C. National Institute of Standards and Technology. Gaithersburg, MD, September.

Luecke, W. E., J. D. McColskey, C. N. McCowan, S. W. Banovic, R. J. Fields, T. Foecke, T. A. Siewert, and F. W. Gayle. 2005. *Federal Building and Fire Safety Investigation of the World Trade Center Disaster: Mechanical Properties of Structural Steels.* NIST NCSTAR 1-3D. National Institute of Standards and Technology. Gaithersburg, MD, September.

Banovic, S. W., C. N. McCowan, and W. E. Luecke. 2005. *Federal Building and Fire Safety Investigation of the World Trade Center Disaster: Physical Properties of Structural Steels.* NIST NCSTAR 1-3E. National Institute of Standards and Technology. Gaithersburg, MD, September.

Evans, D. D., R. D. Peacock, E. D. Kuligowski, W. S. Dols, and W. L. Grosshandler. 2005. *Federal Building and Fire Safety Investigation of the World Trade Center Disaster: Active Fire Protection Systems.* NIST NCSTAR 1-4. National Institute of Standards and Technology. Gaithersburg, MD, September.

Kuligowski, E. D., D. D. Evans, and R. D. Peacock. 2005. *Federal Building and Fire Safety Investigation of the World Trade Center Disaster: Post-Construction Fires Prior to September 11, 2001.* NIST NCSTAR 1-4A. National Institute of Standards and Technology. Gaithersburg, MD, September.

Hopkins, M., J. Schoenrock, and E. Budnick. 2005. *Federal Building and Fire Safety Investigation of the World Trade Center Disaster: Fire Suppression Systems.* NIST NCSTAR 1-4B. National Institute of Standards and Technology. Gaithersburg, MD, September.

Keough, R. J., and R. A. Grill. 2005. *Federal Building and Fire Safety Investigation of the World Trade Center Disaster: Fire Alarm Systems.* NIST NCSTAR 1-4C. National Institute of Standards and Technology. Gaithersburg, MD, September.

Ferreira, M. J., and S. M. Strege. 2005. *Federal Building and Fire Safety Investigation of the World Trade Center Disaster: Smoke Management Systems.* NIST NCSTAR 1-4D. National Institute of Standards and Technology. Gaithersburg, MD, September.

Gann, R. G., A. Hamins, K. B. McGrattan, G. W. Mulholland, H. E. Nelson, T. J. Ohlemiller, W. M. Pitts, and K. R. Prasad. 2005. *Federal Building and Fire Safety Investigation of the World Trade Center Disaster: Reconstruction of the Fires in the World Trade Center Towers.* NIST NCSTAR 1-5. National Institute of Standards and Technology. Gaithersburg, MD, September.

Pitts, W. M., K. M. Butler, and V. Junker. 2005. *Federal Building and Fire Safety Investigation of the World Trade Center Disaster: Visual Evidence, Damage Estimates, and Timeline Analysis.* NIST NCSTAR 1-5A. National Institute of Standards and Technology. Gaithersburg, MD, September.

Hamins, A., A. Maranghides, K. B. McGrattan, E. Johnsson, T. J. Ohlemiller, M. Donnelly, J. Yang, G. Mulholland, K. R. Prasad, S. Kukuck, R. Anleitner and T. McAllister. 2005. *Federal Building and Fire Safety Investigation of the World Trade Center Disaster: Experiments and Modeling of Structural Steel Elements Exposed to Fire.* NIST NCSTAR 1-5B. National Institute of Standards and Technology. Gaithersburg, MD, September.

Ohlemiller, T. J., G. W. Mulholland, A. Maranghides, J. J. Filliben, and R. G. Gann. 2005. *Federal Building and Fire Safety Investigation of the World Trade Center Disaster: Fire Tests of Single Office Workstations.* NIST NCSTAR 1-5C. National Institute of Standards and Technology. Gaithersburg, MD, September.

Gann, R. G., M. A. Riley, J. M. Repp, A. S. Whittaker, A. M. Reinhorn, and P. A. Hough. 2005. *Federal Building and Fire Safety Investigation of the World Trade Center Disaster: Reaction of Ceiling Tile Systems to Shocks.* NIST NCSTAR 1-5D. National Institute of Standards and Technology. Gaithersburg, MD, September.

Hamins, A., A. Maranghides, K. B. McGrattan, T. J. Ohlemiller, and R. Anleitner. 2005. *Federal Building and Fire Safety Investigation of the World Trade Center Disaster: Experiments and Modeling of Multiple Workstations Burning in a Compartment.* NIST NCSTAR 1-5E. National Institute of Standards and Technology. Gaithersburg, MD, September.

McGrattan, K. B., C. Bouldin, and G. Forney. 2005. *Federal Building and Fire Safety Investigation of the World Trade Center Disaster: Computer Simulation of the Fires in the World Trade Center Towers.* NIST NCSTAR 1-5F. National Institute of Standards and Technology. Gaithersburg, MD, September.

Prasad, K. R., and H. R. Baum. 2005. *Federal Building and Fire Safety Investigation of the World Trade Center Disaster: Fire Structure Interface and Thermal Response of the World Trade Center Towers.* NIST NCSTAR 1-5G. National Institute of Standards and Technology. Gaithersburg, MD, September.

Gross, J. L., and T. McAllister. 2005. *Federal Building and Fire Safety Investigation of the World Trade Center Disaster: Structural Fire Response and Probable Collapse Sequence of the World Trade Center Towers.* NIST NCSTAR 1-6. National Institute of Standards and Technology. Gaithersburg, MD, September.

Carino, N. J., M. A. Starnes, J. L. Gross, J. C. Yang, S. Kukuck, K. R. Prasad, and R. W. Bukowski. 2005. *Federal Building and Fire Safety Investigation of the World Trade Center Disaster: Passive Fire Protection.* NIST NCSTAR 1-6A. National Institute of Standards and Technology. Gaithersburg, MD, September.

Gross, J., F. Hervey, M. Izydorek, J. Mammoser, and J. Treadway. 2005. *Federal Building and Fire Safety Investigation of the World Trade Center Disaster: Fire Resistance Tests of Floor Truss Systems.* NIST NCSTAR 1-6B. National Institute of Standards and Technology. Gaithersburg, MD, September.

Zarghamee, M. S., S. Bolourchi, D. W. Eggers, Ö. O. Erbay, F. W. Kan, Y. Kitane, A. A. Liepins, M. Mudlock, W. I. Naguib, R. P. Ojdrovic, A. T. Sarawit, P. R Barrett, J. L. Gross, and

T. P. McAllister. 2005. *Federal Building and Fire Safety Investigation of the World Trade Center Disaster: Component, Connection, and Subsystem Structural Analysis.* NIST NCSTAR 1-6C. National Institute of Standards and Technology. Gaithersburg, MD, September.

Zarghamee, M. S., Y. Kitane, Ö. O. Erbay, T. P. McAllister, and J. L. Gross. 2005. *Federal Building and Fire Safety Investigation of the World Trade Center Disaster: Global Structural Analysis of the Response of the World Trade Center Towers to Impact Damage and Fire.* NIST NCSTAR 1-6D. National Institute of Standards and Technology. Gaithersburg, MD, September.

McAllister, T., R. W. Bukowski, R. G. Gann, J. L. Gross, K. B. McGrattan, H. E. Nelson, L. Phan, W. M. Pitts, K. R. Prasad, F. Sadek. 2006. *Federal Building and Fire Safety Investigation of the World Trade Center Disaster: Structural Fire Response and Probable Collapse Sequence of World Trade Center 7.* (Provisional). NIST NCSTAR 1-6E. National Institute of Standards and Technology. Gaithersburg, MD.

Gilsanz, R., V. Arbitrio, C. Anders, D. Chlebus, K. Ezzeldin, W. Guo, P. Moloney, A. Montalva, J. Oh, K. Rubenacker. 2006. *Federal Building and Fire Safety Investigation of the World Trade Center Disaster: Structural Analysis of the Response of World Trade Center 7 to Debris Damage and Fire*. (Provisional). NIST NCSTAR 1-6F. National Institute of Standards and Technology. Gaithersburg, MD.

Kim, W. 2006. *Federal Building and Fire Safety Investigation of the World Trade Center Disaster: Analysis of September 11, 2001, Seismogram Data*. (Provisional). NIST NCSTAR 1-6G. National Institute of Standards and Technology. Gaithersburg, MD.

Nelson, K. 2006. *Federal Building and Fire Safety Investigation of the World Trade Center Disaster: The Con Ed Substation in World Trade Center 7*. (Provisional). NIST NCSTAR 1-6H. National Institute of Standards and Technology. Gaithersburg, MD.

Averill, J. D., D. S. Mileti, R. D. Peacock, E. D. Kuligowski, N. Groner, G. Proulx, P. A. Reneke, and H. E. Nelson. 2005. *Federal Building and Fire Safety Investigation of the World Trade Center Disaster: Occupant Behavior, Egress, and Emergency Communication.* NIST NCSTAR 1-7. National Institute of Standards and Technology. Gaithersburg, MD, September.

Fahy, R., and G. Proulx. 2005. *Federal Building and Fire Safety Investigation of the World Trade Center Disaster: Analysis of Published Accounts of the World Trade Center Evacuation.* NIST NCSTAR 1-7A. National Institute of Standards and Technology. Gaithersburg, MD, September.

Zmud, J. 2005. *Federal Building and Fire Safety Investigation of the World Trade Center Disaster: Technical Documentation for Survey Administration.* NIST NCSTAR 1-7B. National Institute of Standards and Technology. Gaithersburg, MD, September.

Lawson, J. R., and R. L. Vettori. 2005. *Federal Building and Fire Safety Investigation of the World Trade Center Disaster: The Emergency Response Operations.* NIST NCSTAR 1-8. National Institute of Standards and Technology. Gaithersburg, MD, September.

ACKNOWLEDGMENTS

The analyses presented in this report were conducted in collaboration with four contractors:

- A team of experts from Leslie E. Robertson Associates, whose work included the development of the structural databases, the reference structural models, and the baseline performance analysis of the World Trade Center (WTC) towers. The team was led by Mr. William J. Faschan and Mr. Richard B. Garlock.

- A team of experts from Skidmore, Owings, and Merrill, who provided the third-party review of the structural databases, the reference structural models, the baseline performance analysis, and the refined NIST estimate of the wind loads on the towers. The team included Mr. William F. Baker, Mr. John J. Zils, and Mr. Robert C. Sinn.

- A team of experts from Applied Research Associates, whose work included the analysis of aircraft impacts into the WTC towers. The team was led by Dr. Steven W. Kirkpatrick with major contributions from Dr. Robert T. Bocchieri.

- Dr. David M. Parks, who provided expertise in the area of computational mechanics for the aircraft impact analysis.

In addition, Dr. Shankar Nair of Teng & Associates provided help with the baseline analysis study, Professor Daniele Veneziano of MIT provided help with the uncertainty analyses, and Professor Kaspar Willam of the University of Colorado provided help with the constitutive modeling for aircraft impact.

The following individuals from the National Institute of Standards and Technology (NIST) made contributions to this report:

- Dr. Emil Simiu provided the wind engineering expertise required for the development of Chapter 3 "Wind Loads on the WTC Towers" of this report, of which he was the primary author. He was also co-author of Appendix B "Estimation of Sectorial Extreme Wind Speeds."

- Dr. Michael A. Riley and Dr. William P. Fritz assisted with preliminary stability analyses of the towers that were reported in the Interim Report of June 2004. In addition, Dr. Fritz participated in the wind study and was the primary author of Appendix B.

- The mechanical and metallurgical analysis of structural steel team (Dr. Frank W. Gayle, Dr. Richard J. Fields, Dr. William E. Luecke, Mr. J. David McColskey, Dr. Tim J. Foecke, Dr. Stephen W. Banovic, and Dr. Thomas A. Siewert) provided the mechanical characteristics of the tower steels that were used in the constitutive models for the aircraft impact simulations. In addition, Dr. Foecke conducted the comparison of the calculated and observed damage to the exterior walls of the towers and provided the images presented in Figures 7–65 and 7–73.

- Dr. Therese P. McAllister and Dr. John L. Gross contributed to the interpretation of the impact simulation results and provided the link between the impact analysis and the subsequent fire-structural analyses. They also helped with the review of certain parts of this report.

- Dr. William M. Pitts provided assistance in the identification of videos and photographs relevant to this project, and in the interpretation of the video and photographic data collected by NIST.

- Dr. James Filliben provided guidance in the performance of the uncertainty analyses. He contributed to the methodologies that allowed a large reduction in the total number of analyses required.

NIST acknowledges the parties to an insurance litigation concerning the WTC towers for voluntarily making available to NIST the Cermak Peterka Peterson, Inc. report and the Rowan Williams Davis and Irwin, Inc. (RWDI) reports containing their estimates of wind loads on the towers. NIST also acknowledges Dr. Najib Abboud of Weidlinger and Associates, Inc. and Dr. Peter Irwin of RWDI for their cooperation in providing answers to NIST questions concerning the RWDI reports.

The author also acknowledges Dr. Raymond Daddazio and Mr. David K. Vaughan of Weidlinger and Associates, Inc., and Professor Tomasz Wierzbicki of Massachusetts Institute of Technology for early discussions on aircraft impact analysis.

EXECUTIVE SUMMARY

E.1 INTRODUCTION

The National Institute of Standards and Technology (NIST) investigation into the collapse of the World Trade Center (WTC) towers included eight interdependent projects. The *Baseline Structural Performance and Aircraft Impact Damage Analysis* project had two primary tasks. These were:

1. To develop reference structural models of the towers and use these models to establish the baseline performance of the two towers under gravity and wind loads.

2 To estimate the damage to the towers due to aircraft impacts and establish the initial conditions for the fire dynamics modeling and thermal-structural response and collapse initiation analysis.

For the first task, the baseline performance of the WTC towers under gravity and wind loads was established in order to assess the towers' ability to withstand those loads safely and to evaluate the reserve capacity of the towers to withstand unanticipated events. The baseline performance study provided a measure of the behavior of the towers under design loading conditions, specifically: (1) total and inter-story drift (the sway of the building under design wind loads), (2) floor deflections under gravity loads, (3) the stress demand-to-capacity ratio for primary structural components of the towers such as exterior walls, core columns, and floor framing, (4) performance of exterior walls under wind loading, including distribution of axial stresses and presence of tensile forces, (5) performance of connections between exterior columns, and (6) resistance of the towers to shear sliding and overturning at the foundation level.

This task included the development of reference structural models that captured the intended behavior of the towers under design loading conditions. These reference models were used to establish the baseline performance of the towers and also served as a reference for more detailed models for aircraft impact damage analysis and the thermal-structural response and collapse initiation analysis. The models included: (1) two global models (one for each tower) of the major structural components and systems of the towers, and (2) floor models of a typical truss-framed floor and a typical beam-framed floor. In the towers, tenant floors were typical truss-framed floors, while the mechanical floors (floors 7, 41, 75, and 108) and near mechanical floors (floors 9, 43, 77, 107, 110, and roof) of both towers were typical beam-framed floors.

For the second task, the aircraft impact damage to the exterior of the WTC towers could be visibly identified from the video and photographic records collected. However, no visible information could be obtained for the extent of damage to the interior of the towers, including the structural system (floors and core columns), partition walls, and interior building contents. Such information was needed for the subsequent fire dynamics simulations and post-impact structural analyses. In addition, for the fire dynamics modeling, the dispersion of the jet fuel and the location of combustible aircraft debris were required. The estimate of the extent of damage to the fireproofing on the structural steel in the towers due to impact was essential for the thermal and structural analyses. The aircraft impact damage analyses were the primary tool by which most of the information about the tower damage could be estimated.

The focus of this task was to analyze the aircraft impacts into each of the WTC towers to provide the following: (1) estimates of probable damage to structural systems, including exterior walls, floor systems, and interior core columns; (2) estimates of the aircraft fuel dispersion during the impact; and (3) estimates of debris damage to the building nonstructural contents, including partitions and workstations. The analysis results were used to estimate the damage to fireproofing based on the estimated path of the debris field inside the towers. This analysis thus estimated the condition of the two WTC towers immediately following the aircraft impacts and established the initial conditions for the fire dynamics modeling and the thermal-structural response and collapse initiation analysis.

E.2 DEVELOPMENT OF REFERENCE STRUCTURAL MODELS

The reference structural models were developed to capture the intended behavior of the WTC towers under design loading conditions. The models were used: (1) to establish the baseline performance of the towers under design gravity and wind loads and (2) as a reference for more detailed models used in other phases of the NIST investigation, including aircraft impact analysis and thermal-structural response and collapse initiation analysis. The reference models included the following:

- Two global models of the primary structural components and systems for each of the two towers.
- Two models, one of a typical truss-framed floor (tenant floor) and one of a typical beam-framed floor (mechanical level), within the impact and fire regions.

All reference models were linearly elastic and three-dimensional, and were developed using the Computers and Structures, Inc. SAP2000 software. SAP2000 is a commercial finite element software package that is customarily used for the analysis and design of structures. A summary of the size of the global and floor models of the towers is presented in Table E–1.

Table E–1. Approximate size of the reference structural models (rounded).

Model	Number of Joints	Degrees of Freedom	Number of Frame Elements	Number of Shell Elements	Total Number of Elements
WTC 1 global model[a]	53,700	218,700	73,900	10,000	83,900
WTC 2 global model[a]	51,200	200,000	73,700	4,800	78,500
Typical truss-framed model	28,100	166,000	27,700	14,800	42,500
Typical beam-framed model	6,500	35,700	7,500	4,600	12,100

a. Model does not include floors except for flexible diaphragms at 17 floors as explained later.

The models were developed by Leslie E. Robertson Associates (LERA), the firm responsible for the original structural engineering of the WTC towers, under contract to NIST. The models were reviewed by independent parties to ensure objectivity. The review process included a third-party review by the firm of Skidmore, Owings, and Merrill (SOM), under contract to NIST, and an in-house review by NIST.

For the global models of the towers, the large amount of data required to construct the models dictated that a database of the primary structural components of the towers be developed from the original

computer printouts of the structural design documents. The various databases, developed in Microsoft Excel format, were linked together using the relational database technique. The relational databases, developed using Microsoft Access, were generated in a format suitable for the development of the global finite element models of the towers.

E.2.1 Global Models of the Towers

Three-dimensional models of the 110-story above-grade structure and 6-story below-grade structure within the footprint of each of the two towers were developed. The global models for the towers consisted of all primary structural elements in the towers, including exterior walls (exterior columns, spandrel beams, and bracings in the basement floors), core columns, hat trusses, and rigid and flexible diaphragms representing the floor systems.

For the development of the global models, each tower was divided into several sub-models that included:

- Exterior walls, which in turn was divided into
  - Exterior wall, foundation to floor 4
  - Exterior wall trees (floors 4 to 9)
  - Exterior wall, floors 9 to 106
  - Exterior wall, floors 107 to 110
- Core columns
- Hat truss

After these sub-models were assembled into a unified model, rigid and flexible diaphragms representing the floor systems, boundary conditions, gravity and wind loads, and masses were added to the unified model. Isometric views of the complete WTC 1 model showing exterior walls, core columns, bracings, hat trusses, and flexible floor diaphragms are shown in Figure E–1.

The global models were developed primarily using prismatic and non-prismatic frame (beam) elements. Shell elements were used only to represent the flexible floor diaphragms. For the development of beam element representations of the exterior wall panels, detailed shell element models of the panels were developed and used to calibrate the behavior of the beam element model under gravity and lateral loads (Figure E–2). Similarly, the detailed floor models were used to calibrate the response of a simplified shell element representation of the floor systems for use as flexible diaphragms in the global models.

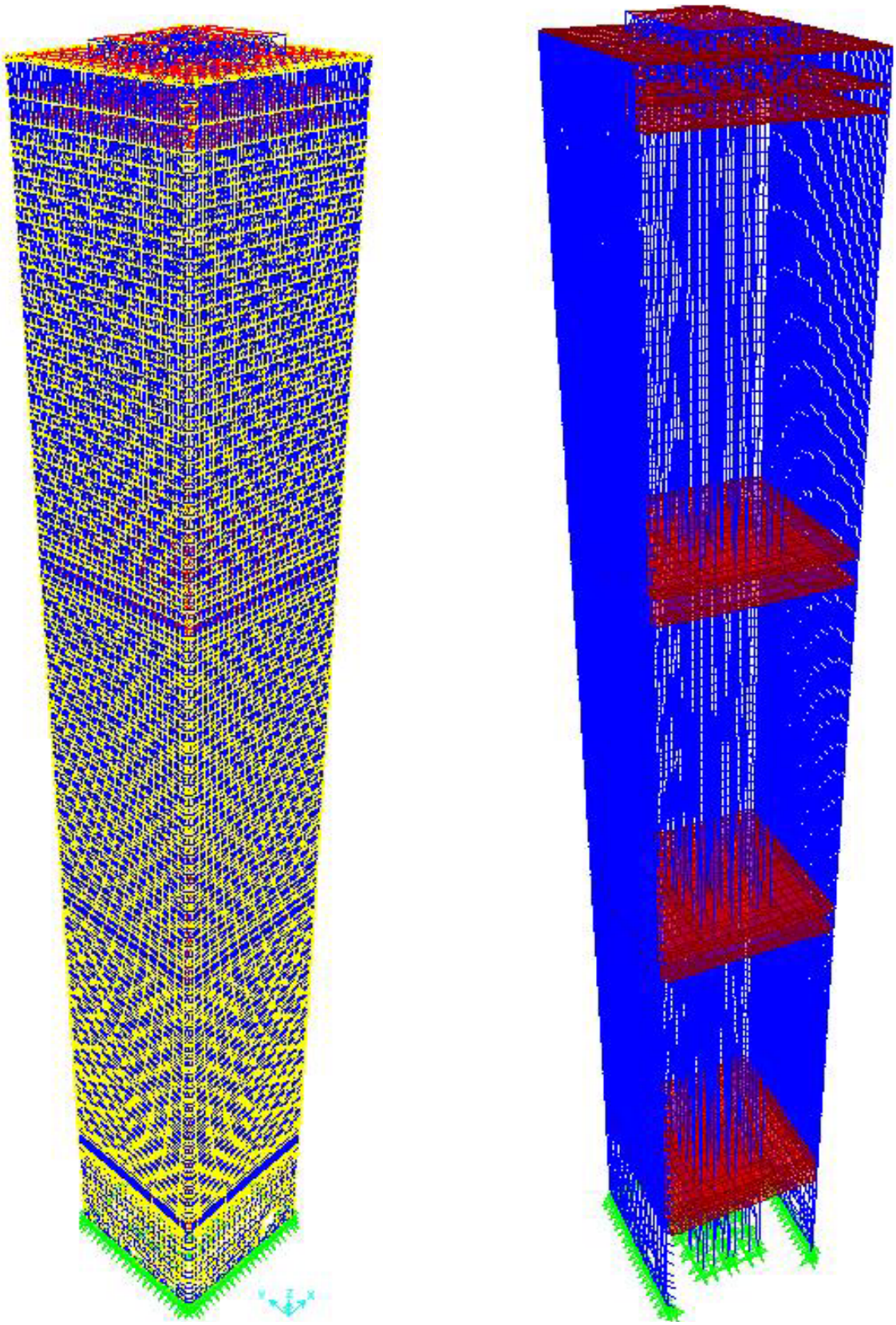

Figure E–1. Rendered isometric views of the WTC 1 global model.

To validate the global models, the natural periods of WTC 1 calculated from the model were compared with those measured on the tower based on analyzing acceleration records obtained from accelerometers installed atop WTC 1. Table E–2 presents a comparison of the calculated first three natural frequencies and periods against measured frequencies and periods for WTC 1. The measurements were taken during the period from 1978 through 1994 for wind speeds ranging from 11.5 mph to 41 mph. The table indicates longer periods measured at larger wind speeds. The natural periods and frequencies predicted in the original design are also presented in the table. The table shows a good agreement between the calculated and measured periods. Thus, Table E–2 indicates that the reference global model provided a reasonable representation of the actual structure.

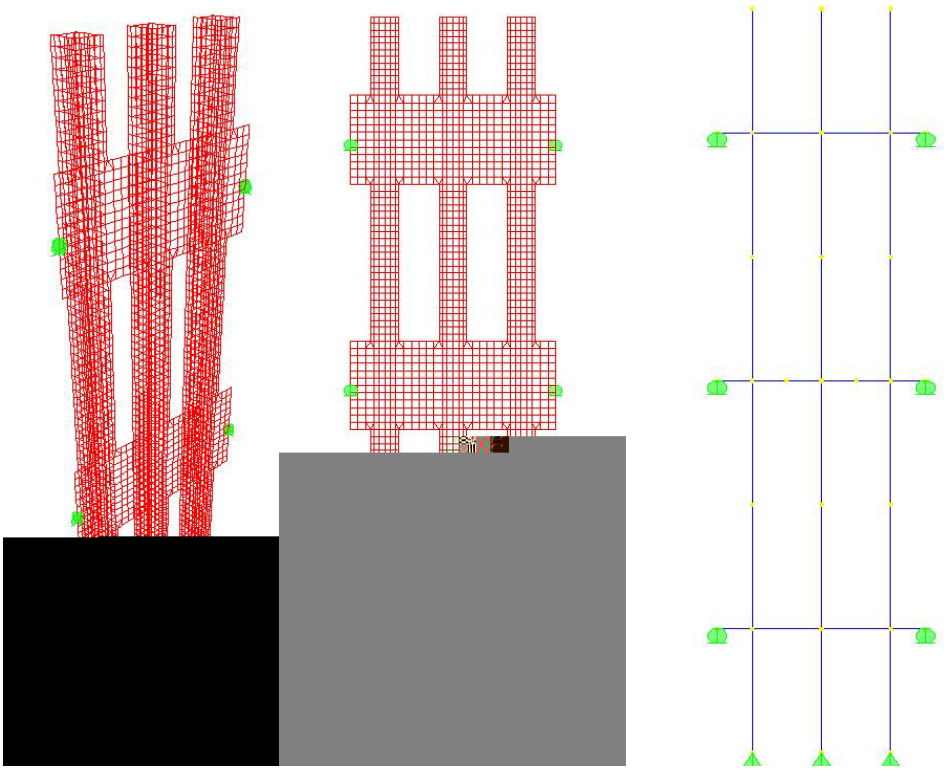

Figure E–2. Shell element and frame element models of an exterior wall panel.

Table E–2. Comparison of measured and calculated natural periods for WTC 1.

Data Source/ Event Date	Wind Speed & Direction	Frequency (HZ)			Period (s)		
		Direction of Motion			Direction of Motion		
		N-S	E-W	Torsion	N-S	E-W	Torsion
Historical Data							
October 11, 1978	11.5 mph, E/SE	0.098	0.105	0.211	10.2	9.5	4.7
January 24, 1979	33 mph, E/SE	0.089	0.093	0.203	11.2	10.8	4.9
March 21, 1980	41 mph, E/SE	0.085	0.092	0.201	11.8	10.9	5.0
December 11, 1992	-	0.087	0.092	-	11.5	10.9	-
February 2, 1993[1]	20 mph, NW	0.085	0.093	0.204	11.8	10.8	4.9
March 13, 1993[1]	32 mph, NW	0.085	0.094	0.199	11.8	10.6	5.0
March 10, 1994[1]	14 mph, W	0.094	0.094	0.196	10.6	10.6	5.1
December 25, 1994[2]	N	0.081	0.091	-	12.3	11.0	-
Average of Measured Data							
Average	-	0.088	0.094	0.202	11.4	10.6	4.9
Orginal Design - Predicted Values							
Theoretical Value	-	0.084	0.096	-	11.9	10.4	-
Reference Global Model							
LERA/NIST - WTC 1 without P-Delta		0.088	0.093	0.192	11.4	10.7	5.2
LERA/NIST - WTC 1 with P-Delta		0.083	0.088	0.189	12.1	11.3	5.3

Notes:

[1]Reported frequency value is the average of the SW corner, NE corner, and center core frequency measurements.

[2]Reported frequency is based on center core data only.

E.2.2 Typical Truss-Framed Floor Model – Floor 96 of WTC 1

The model of the typical truss-framed floor contained all primary structural members of the floor system, including the primary trusses, bridging trusses, spandrel beams, columns above and below the floor level, concrete slabs, dampers, strap anchors, and beams in the core. The model was developed primarily using frame elements with the exception of the floor slabs, which were modeled using shell elements with typical element sizes of 20 in. An isometric view of the model is shown in Figure E–3.

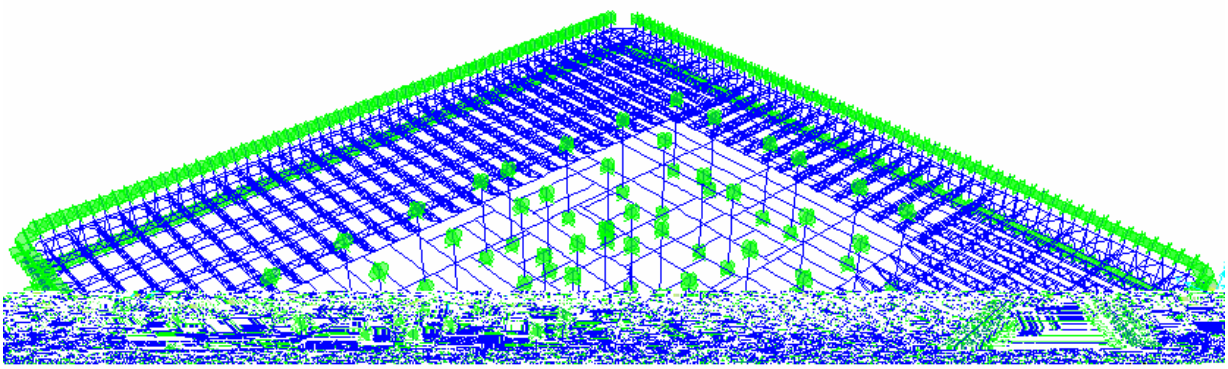

Figure E–3. Typical truss-framed floor model (floor 96 of WTC 1), slab not shown.

E.2.3 Typical Beam-Framed Floor Model – Floor 75 of WTC 2

The model of the typical beam-framed floor contained all primary structural members of the floor system, including the primary composite beams, horizontal trusses, spandrel beams, columns above and below the floor level, concrete slab, dampers, and beams in the core. Similar to the typical trussed-frame model, this model was developed primarily using frame elements with the exception of the floor slabs, which were modeled using shell elements with typical element sizes of 40 in. An isometric view of the model is shown in Figure E–4.

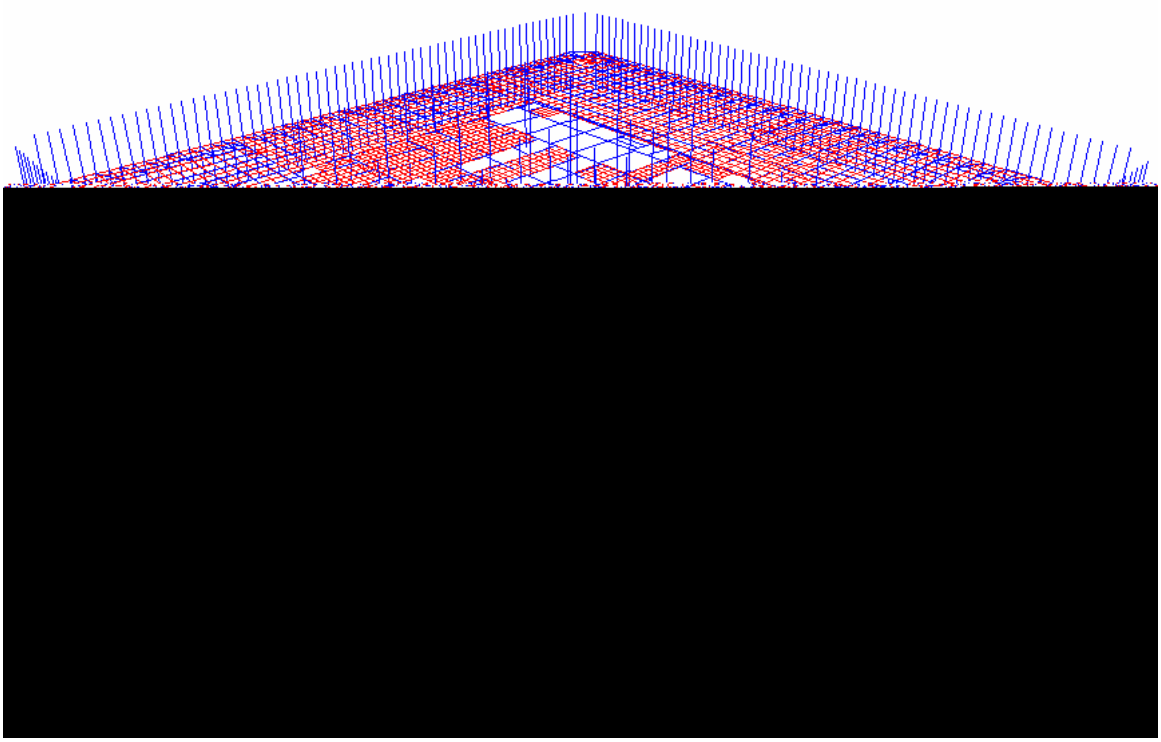

Figure E–4. Typical beam-framed floor model (floor 75 of WTC 2).

E.3 WIND LOADS ON THE WTC TOWERS

Wind loads were a governing factor in the design of the components of the WTC towers' perimeter frame-tube system. Their study was required for evaluating: (1) the baseline performance of the towers under design loading conditions, (2) the towers' reserve capacity to withstand unanticipated events such as a major fire or impact damage, and (3) design practices, procedures, and codes. Accurate estimation of the wind loads on tall buildings is challenging, since wind engineering is still an evolving technology.

Wind estimates for the WTC towers considered in this study included: (1) wind loads used in the original WTC design, (2) wind loads based on two recent wind tunnel studies conducted in 2002 by Cermak Peterka Peterson, Inc. (CPP) and Rowan Williams Davis and Irwin, Inc. (RWDI), and (3) refined wind loads estimated by NIST by critically assessing information obtained from the CPP and RWDI reports and using state-of-the-art knowledge. These estimates are summarized below.

E.3.1 Original WTC Wind Design Loads

Wind loads were determined for the original design of the WTC towers through the development and implementation of a boundary-layer wind-tunnel study, which simulated the mean and fluctuating (turbulence) properties of the wind from ground to gradient height by using the knowledge and techniques available in the 1960s. The wind tunnel tests were conducted at Colorado State University (CSU) and the National Physical Laboratory (NPL), United Kingdom. Aeroelastic tests at CSU were conducted at a scale of 1:500, while the aeroelastic models at NPL were conducted with a scale of 1:400. Results from the tests conducted at NPL were in good qualitative and quantitative agreement with those obtained from the CSU tests. Wind tunnel data were collected for each tower for wind approaching from 24 wind

directions in 15 degree increments. The wind effects were estimated as the summation of static and dynamic components based on results obtained from wind tunnel tests. The most severe wind effects were determined from diagrams of wind-induced shear forces and overturning moments.

E.3.2 State-of-the-Practice Wind Loads

For the WTC towers, two wind tunnel tests and wind engineering studies based thereon were conducted in 2002 by independent laboratories as part of insurance litigation unrelated to the NIST investigation. The tests and studies were conducted by CPP and RWDI. The results of both studies were made available to NIST.

The CPP wind tunnel tests modeled the terrain surrounding the WTC towers over an area with a radius of about 2,300 ft. The tests used a high-frequency force balance (HFFB) model and an aeroelastic model of the south tower only. The test scale was 1:400, and testing was conducted for 36 wind directions at 10 degree intervals. The wind-induced loads and responses were determined by combining the wind tunnel test data with recorded directional wind speeds and unspecified hurricane wind speed data. The recorded wind speeds were obtained at the three airports in the New York area over about 25 years. The directional wind tunnel and wind speed data were combined by using the sector-by-sector approach. Wind effects corresponding to a damping ratio of 2 percent were provided for WTC 2 only for nominal 50 year and 720 year mean recurrence intervals. The wind-induced effects were provided as peak shear forces and bending moments for two orthogonal directions and peak torsional moments. The peak components were not applied to the structural model of the tower simultaneously, but were combined by using the full peak load in one direction and "companion point-in-time" loads in the other direction and in torsion.

The RWDI wind tunnel tests modeled the terrain surrounding the WTC towers over an area with a radius of about 4,000 ft. The tests used an HFFB model of both towers and an aeroelastic model for the north tower only. The test scale was 1:500, and testing was conducted for 36 wind directions at 10 degree intervals. Corrections were made to account for the effects on the flow of the presence of the building model (i.e., of wind tunnel blockage). Predictions of the full-scale wind effects and responses were obtained by combining the wind tunnel test data with a statistical model of winds for New York City, based on surface wind measurements taken at airports between 1948 and 1995 and proprietary simulated hurricane winds. The directional wind tunnel and wind speed data were combined by using an out-crossing approach developed by RWDI. Two sets of wind effects on the towers were developed by scaling the wind loads to the design wind speeds

adequacy of the original design wind loads, but rather to better understand and assess the effects of successive changes in standards, codes, and practices. The analysis yielded refined estimates of wind effects for the north and south WTC towers. These estimates made use of independent extreme wind climatological estimates developed by NIST, based on airport wind speed data obtained from the National Climatic Data Center and on the NIST hurricane wind speed database. The estimates of wind effects relied primarily on RWDI results, since no results for WTC 1 were available from CPP. However, the estimates took into account a comparative assessment of the RWDI and CPP results for WTC 2.

A summary comparison between CPP and RWDI estimates of maximum base moments and shear forces on WTC 2 indicated that the CPP estimates were larger by about 40 percent. The critical base moments from both studies occurred for a wind direction of about 210 degrees. This agreement suggested that a comparison between those results was warranted in some detail for that wind direction. An independent estimate by NIST of the 720 yr, 3 s peak gust speed for that direction was 99.8 mph, while the CPP estimate was about 117.5 mph. The CPP results were therefore multiplied by a factor of approximately $(99.8/117.5)^2=1/1.386$.

In addition, the CPP results were modified to account for the use by CPP of the sector-by-sector approach to integrating aerodynamic data and extreme-wind climatological data. The sector-by-sector approach is not valid from a physical point of view. A study by NIST concluded that the sector-by-sector approach underestimated the wind effects corresponding to a specified mean recurrence interval. According to preliminary estimates, it was assumed that the underestimation was approximately 15 percent. Therefore, the CPP results, modified via multiplication by the factor 1/1.386, were further modified via multiplication by the factor 1.15. The reduction factor applied to the estimated CPP effects was therefore about 1/1.205. To within the limitations inherent in the information available for this investigation, and to within the approximations noted, these reduced values are reasonable estimates of the actual responses of interest.

According to the conclusion concerning the modified CPP results, the RWDI results underestimated the towers' response. This conclusion was consistent with the fact that RWDI assumed wind profiles in hurricanes to be flatter than wind profiles in non-hurricane winds. According to state-of-the-art information on wind profiles at high elevations, hurricane profiles do not differ substantially from non-hurricane wind profiles, and an unconventional model such as the relatively flat hurricane profile model used by RWDI is not supported by measurements

equal to the ratio of the modified CPP estimates to the corresponding RWDI estimates. This factor was found to be about 1.15. The factor 1.15 was reco

Table E–3. Comparison of wind load estimates for WTC 2 based on various sources.

Source	Year	Base Shear 10^3 kip			Base Moment 10^6 kip·ft		
		N-S	E-W	Most unfavorable combined peak	About N-S	About E-W	Most unfavorable combined peak
NYC Building Code	1938	5.3	5.3		4.2	4.2	
NYC Building Code	1968 to date	9.3	9.3		7.6	7.6	
RWDI / NYC Building Code	2002	9.7	11.1	12.3	10.1	9.2	11.3
RWDI / ASCE 7-98	2002	10.6	12.2	13.5	11.1	10.1	12.4
CPP / NYC Building Code	2002	None	None	None	None	None	None
CPP / ASCE 7-98[a]	2002	15.1	15.3	17.1	15.5	14.0	17.0
NIST / third-party SOM review	2004	12.2	14.0	15.5	12.8	11.6	14.3
Original WTC Design	1960s	13.1	10.1	16.5	8.8	12.6	15.4

a. Using ASCE 7-98 sections 6.5.4.1 and 6.6.

Table E–4. Base shears and base moments due to wind loads based on various building codes.

Building Code	1938 NYC Code	1968 to date NYC Code	1964 NY State Code	1965 BOCA/BBC	1967 Chicago Municipal Code
Base Shear (10^3 kip)	5.3	9.3	9.5	9.8	8.7
Base Moment (10^6 kip·ft)	4.2	7.7	7.6	8.5	7.5

E.4 BASELINE PERFORMANCE OF THE WTC TOWERS

E.4.1 Baseline Performance of the Global Models

The reference global models were analyzed under gravity and wind loads to establish the baseline performance of the towers. Three loading cases were considered for this analysis. They included:

- *Original WTC design loads case.* Loads were as follows: dead and live loads as in original WTC design, used in conjunction with original WTC design wind loads (Section E.3.1).

- *State-of-the-practice case.* Loads were as follows: dead loads as in original design; NYCBC 2001 live loads; and wind loads from RWDI wind tunnel study (Section E.3.2), scaled in accordance with NYCBC 2001 wind speed. This wind load was considered to be a lower estimate state-of-the-practice case, as the CPP wind tunnel study produced larger wind loads.

- *Refined NIST estimate case.* Loads were as follows: dead loads as in original design; live loads from ASCE 7-02; and refined wind loads developed by NIST (Section E.3.3).

The following is a summary of the results.

Total and Inter-Story Drift

The calculated total drift of both WTC 1 and WTC 2 induced by the three loading cases is presented in Table E–5. The table lists calculated total drift values at the top of the tower, in absolute terms and as a fraction of the building height, H, from the foundation level to the roof (referred to in the table as the drift ratio). According to LERA, limiting total building drift under wind loads was not part of the original WTC design criteria. Instead, inter-story drifts were determined and compared to the capability of the architectural building systems, such as the partitions and the exterior cladding, to accommodate these inter-story drifts. Accordingly, there are no historical project-specific data available to which the total drifts may be compared.

Table E–5. Total drift for WTC 1 and WTC 2 under the three loading cases.

Loading Case	WTC 1				WTC 2			
	E–W		N–S		E–W		N–S	
	Total Drift (in.)	Drift Ratio	Total Drift (in.)	Drift Ratio	Total Drift (in.)	Drift Ratio	Total Drift (in.)	Drift Ratio
Original design case	56.6	H/304	55.7	H/309	51.2	H/335	65.3	H/263
SOP case	56.8	H/303	68.1	H/253	59.7	H/287	56.1	H/306
Refined NIST case	70.6	H/244	83.9	H/205	75.6	H/227	71.0	H/242

Under the original WTC design loads, the cumulative drifts at the top of the WTC towers ranged from H/263 to H/335. For the lower estimate state-of-the-practice case, those drifts ranged from H/253 to H/306. The drifts obtained from the refined NIST estimate case were about 25 percent larger than those from the state-of-the practice case. Under design loading conditions, the maximum inter-story drift was as high as h/230 and h/200 for WTC 1 and WTC 2, respectively, where h is the story height. Maximum inter-story drifts under the state-of-the practice case were about h/184 and h/200 for WTC 1 and WTC 2, respectively. For the refined NIST estimate case, these inter-story drifts were about 25 percent larger than those from the state-of-the practice case.

Currently no building codes specify a drift limit for wind design. The commentary to Section B.1.2 of the ASCE 7-02 Standard indicates that drift limits in common usage for building design are on the order of 1/400 to 1/600 of the building (for total drift) or story (for inter-story drift) height to minimize damage to cladding and nonstructural walls and partitions. Structural engineers often use in their practice the criterion that total drift ratios should not exceed H/400 to H/500 for serviceability considerations and to enhance overall safety and stability (including second order, nonlinear P-Δ effects). Reducing the drift of the WTC towers to the range of H/400 to H/500 would entail enhancing the stiffness and/or damping characteristics of the towers. For inter-story drifts, structural engineers often use in their practice an inter-story drift limit in the range of h/300 to h/400. This is primarily done for serviceability considerations. Similar to total drift, inter-story drifts of the towers were larger than what is generally used in practice.

Demand/Capacity Ratios (DCRs)

DCRs were based on the allowable stress design procedure and were estimated using the American Institute of Steel Construction (AISC) Specifications (1989). Figure E–5 shows the distribution of DCRs for the four exterior walls of WTC 1 under the original design load case, while Figure E–6 shows DCRs for the WTC 1 core columns on lines 600 and 900. The results of the baseline analyses indicated that, for both towers, the DCRs estimated from the original WTC design load case were in general close to those obtained from the lower estimate state-of-the practice case. For both cases, a fraction of structural components had DCRs larger than 1.0. These were mainly observed in both towers at (1) the exterior walls at the columns around the corners, where the hat truss connected to the exterior walls, and below floor 9; and (2) the core columns on the 600 line between floors 80 and 106 and at core perimeter columns 901 and 908 for much of their height.

While it is a normal design practice to achieve a DCR less than unity, the safety of the WTC towers on September 11, 2001, was most likely not affected by the fraction of members for which the demand exceeded capacity due to the following: (1) the inherent factor of safety in the allowable stress design method, (2) the load redistribution capability of ductile steel structures, and (3) on the day of the attack, the towers were subjected to in-service live loads (a fraction of the design live loads) and minimal wind loads.

The DCRs obtained for the refined NIST estimate case were higher than those from the original WTC design and the lower-estimate state-of-the-practice load cases, owing to the following reasons: (1) the NIST estimated wind loads were higher than those used in the state-of-the-practice case by about 25 percent, and (2) the original WTC design and the state-of-the-practice cases used NYCBC load combinations, which result in lower DCRs than the ASCE 7-02 load combinations used for the refined NIST case.

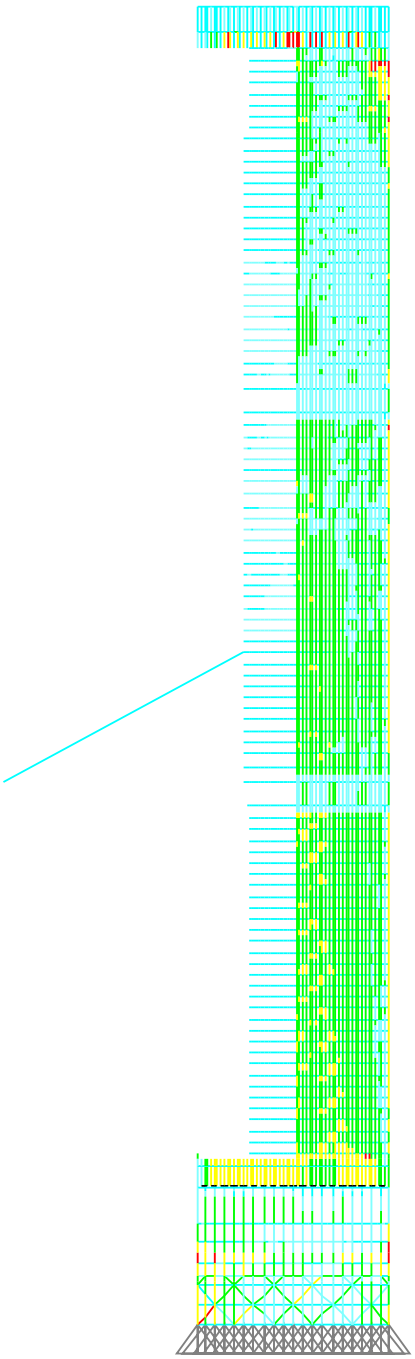

LEVEL	TOWER A, DCR of CORE COLUMN 600's COLUMN NUMBER							
	601	602	603	604	605	606	607	608
106 FL	0.94	1.03	1.29	1.01	1.01	1.05	1.15	0.80
105 FL	1.03	1.10	1.36	1.11	1.08	1.13	1.23	0.92
104 FL	1.12	0.98	1.13	0.94	0.96	0.95	1.12	0.84
103 FL	1.04	1.03	1.18	1.01	1.03	1.01	1.18	0.93
102 FL	1.11	1.08	1.24	1.08	1.09	1.07	1.25	1.02
101 FL	1.19	1.06	1.05	0.88	0.99	1.07	1.05	1.09
100 FL	1.10	1.11	1.10	0.93	1.05	1.13	1.10	1.18
99 FL	1.16	1.16	1.15	0.99	1.10	1.20	1.15	1.27
98 FL	1.23	1.01	0.96	0.96	1.02	1.06	1.00	1.18
97 FL	1.18	1.06	1.00	1.01	1.07	1.12	1.04	1.25
96 FL	1.24	1.10	1.04	1.06	1.12	1.17	1.09	1.33
95 FL	1.31	0.97	0.93	0.98	1.05	1.05	0.96	1.12
94 FL	1.13	1.01	0.96	1.02	1.10	1.09	1.00	1.18
93 FL	1.18	1.04	0.99	1.07	1.14	1.14	1.04	1.24
92 FL	1.23	0.98	0.93	0.83	0.98	1.03	0.88	1.07
91 FL	1.09	1.02	0.95	0.86	1.02	1.07	1.01	1.12
90 FL	1.12	1.05	0.98	0.89	1.05	1.12	1.05	1.17
89 FL	1.17	0.95	0.89	0.93	0.92	1.02	0.94	1.03
88 FL	1.04	0.98	0.92	0.96	0.96	1.06	0.97	1.08
87 FL	1.08	1.01	0.94	1.00	0.99	1.10	1.00	1.12
86 FL	1.12	0.96	0.93	0.87	0.88	1.09	0.99	1.00
85 FL	1.15	0.98	0.95	0.90	0.90	1.13	1.02	1.04
84 FL	1.20	1.01	0.98	0.93	0.93	1.16	1.05	1.08
83 FL	1.25	0.93	0.90	0.96	0.96	0.99	0.96	1.11
82 FL	1.01	0.97	0.93	0.89	0.93	1.02	1.00	1.16
81 FL	1.04	1.02	0.99	1.04	1.03	1.07	1.05	1.21
80 FL	1.08	0.88	0.93	0.72	0.82	1.07	0.86	0.97
79 FL	1.04	0.90	0.96	0.74	0.84	1.09	0.88	1.01
78 FL	1.08	0.92	0.98	0.76	0.87	1.12	0.90	1.05
77 FL	0.76	0.63	0.66	0.62	0.68	0.65	0.66	0.85
76 FL	0.78	0.67	0.70	0.65	0.70	0.68	0.70	0.86
75 FL	0.97	0.84	0.89	0.82	0.91	0.86	0.86	1.00
74 FL	0.97	0.85	0.89	0.82	0.92	0.86	0.86	1.01
73 FL	1.00	0.86	0.91	0.84	0.93	0.88	0.88	1.04
72 FL	1.00	0.83	0.87	0.82	0.85	0.83	0.85	0.95
71 FL	1.03	0.84	0.88	0.83	0.86	0.84	0.86	1.02
70 FL	1.05	0.86	0.90	0.85	0.88	0.86	0.88	1.04
69 FL	0.80	0.78	0.82	0.80	0.84	0.83	0.83	0.96
68 FL	0.84	0.81	0.85	0.84	0.88	0.87	0.87	0.91
67 FL	0.83	0.80	0.85	0.84	0.87	0.86	0.86	0.90
66 FL	0.89	0.82	0.89	0.87	0.89	0.89	0.89	1.07
65 FL	0.90	0.82	0.89	0.87	0.89	0.88	0.89	1.09
64 FL	0.92	0.84	0.92	0.90	0.92	0.90	0.91	1.12
63 FL	0.90	0.81	0.89	0.86	0.88	0.87	0.88	0.99
62 FL	0.91	0.83	0.90	0.88	0.89	0.88	0.89	1.01
61 FL	0.93	0.84	0.92	0.89	0.91	0.89	0.91	1.03
60 FL	0.90	0.81	0.86	0.90	0.87	0.87	0.87	1.05
59 FL	0.91	0.82	0.87	0.91	0.89	0.88	0.88	1.07
58 FL	0.93	0.83	0.88	0.93	0.90	0.89	0.89	1.09
57 FL	0.90	0.81	0.86	0.90	0.87	0.86	0.86	1.05
56 FL	0.92	0.82	0.87	0.92	0.88	0.87	0.87	1.07
55 FL	0.93	0.83	0.88	0.93	0.89	0.88	0.88	1.08
54 FL	0.87	0.81	0.86	0.90	0.91	0.86	0.83	1.04
53 FL	0.88	0.82	0.87	0.91	0.92	0.87	0.84	1.06
52 FL	0.89	0.83	0.88	0.93	0.93	0.88	0.85	1.08
51 FL	0.87	0.81	0.86	0.90	0.90	0.86	0.83	1.04
50 FL	0.89	0.82	0.87	0.91	0.91	0.87	0.83	1.05
49 FL	0.90	0.83	0.88	0.92	0.93	0.88	0.84	1.07
48 FL	0.88	0.81	0.86	0.93	0.90	0.84	0.82	1.03
47 FL	0.89	0.82	0.87	0.94	0.91	0.85	0.83	1.05
46 FL	0.91	0.83	0.88	0.96	0.92	0.86	0.84	1.07
45 FL	0.83	0.77	0.81	0.86	0.84	0.80	0.75	0.92
44 FL	0.85	0.78	0.83	0.89	0.86	0.81	0.77	0.95
43 FL	0.64	0.56	0.60	0.65	0.65	0.61	0.58	0.70
42 FL	0.66	0.56	0.63	0.68	0.68	0.64	0.61	0.72
41 FL	0.85	0.77	0.83	0.88	0.90	0.84	0.81	0.92
40 FL	0.85	0.76	0.82	0.88	0.90	0.84	0.81	0.92
39 FL	0.84	0.77	0.82	0.88	0.88	0.84	0.80	0.90
38 FL	0.85	0.78	0.83	0.90	0.89	0.85	0.81	0.91
37 FL	0.87	0.79	0.84	0.91	0.90	0.86	0.82	0.93
36 FL	0.85	0.78	0.81	0.88	0.87	0.84	0.81	0.91
35 FL	0.86	0.79	0.82	0.89	0.88	0.85	0.82	0.92
34 FL	0.88	0.80	0.82	0.91	0.90	0.86	0.82	0.93
33 FL	0.84	0.77	0.81	0.89	0.87	0.83	0.80	0.92
32 FL	0.85	0.77	0.82	0.90	0.88	0.84	0.81	0.93
31 FL	0.86	0.78	0.83	0.91	0.89	0.85	0.82	0.94
30 FL	0.82	0.77	0.82	0.89	0.87	0.84	0.81	0.92
29 FL	0.83	0.78	0.82	0.90	0.88	0.85	0.82	0.94
28 FL	0.84	0.78	0.83	0.91	0.89	0.86	0.83	0.95
27 FL	0.83	0.77	0.82	0.89	0.88	0.83	0.80	0.93
26 FL	0.84	0.78	0.82	0.90	0.88	0.84	0.81	0.94
25 FL	0.85	0.79	0.83	0.91	0.89	0.85	0.82	0.95
24 FL	0.82	0.78	0.81	0.89	0.88	0.82	0.80	0.94
23 FL	0.83	0.78	0.81	0.90	0.89	0.82	0.81	0.95
22 FL	0.84	0.79	0.82	0.91	0.89	0.83	0.82	0.96
21 FL	0.82	0.78	0.81	0.92	0.88	0.82	0.81	0.94
20 FL	0.83	0.79	0.82	0.93	0.89	0.83	0.82	0.96
19 FL	0.84	0.79	0.83	0.94	0.90	0.83	0.83	0.97
18 FL	0.82	0.78	0.81	0.92	0.88	0.82	0.80	0.93
17 FL	0.83	0.79	0.82	0.93	0.89	0.82	0.80	0.94
16 FL	0.84	0.79	0.83	0.94	0.90	0.83	0.81	0.95
15 FL	0.81	0.77	0.80	0.93	0.90	0.81	0.80	0.93
14 FL	0.82	0.78	0.81	0.93	0.91	0.82	0.81	0.94
13 FL	0.83	0.79	0.82	0.94	0.92	0.82	0.81	0.95
12 FL	0.82	0.78	0.81	0.93	0.90	0.82	0.79	0.94
11 FL	0.83	0.78	0.82	0.94	0.91	0.82	0.79	0.95
10 FL	0.84	0.80	0.83	0.95	0.92	0.84	0.80	0.96
09 FL	0.92	0.76	0.90	1.04	1.01	0.97	0.87	1.03
08 FL	0.92	0.81	0.90	1.04	1.02	0.98	0.87	1.04
07 FL	0.57	0.53	0.56	0.62	0.60	0.60	0.55	0.61
06 FL	0.59	0.55	0.57	0.63	0.62	0.62	0.56	0.62
05 FL	0.59	0.55	0.58	0.64	0.63	0.63	0.57	0.62
04 FL	0.57	0.54	0.56	0.62	0.61	0.61	0.55	0.60
03 FL	0.66	0.61	0.64	0.71	0.70	0.69	0.63	0.69
02 FL	0.69	0.62	0.66	0.74	0.72	0.71	0.64	0.72
01 FL	0.80	0.79	0.82	0.92	0.90	0.88	0.79	0.88
B1 FL	0.79	0.78	0.81	0.91	0.89	0.87	0.79	0.88
B2 FL	0.81	0.79	0.82	0.93	0.90	0.88	0.80	0.89
B3 FL	0.77	0.75	0.81	0.89	0.87	0.87	0.78	0.84
B4 FL	0.79	0.83	0.89	0.99	0.97	0.95	0.86	0.95
B5 FL	0.80	0.83	0.90	1.00	0.98	0.96	0.87	0.96

(a)

LEVEL	TOWER A, DCR of CORE COLUMN 900's COLUMN NUMBER							
	901	902	903	904	905	906	907	908
106 FL	0.76	0.98	0.97	0.80	0.85	1.10	1.02	0.76
105 FL	0.82	1.05	1.02	0.71	0.91	1.16	1.08	0.80
104 FL	0.83	0.95	0.94	1.13	0.75	0.96	0.97	0.80
103 FL	0.92	1.01	0.98	1.21	0.80	1.01	1.02	0.89
102 FL	1.01	1.07	1.03	0.89	0.88	1.05	1.07	0.97
101 FL	0.87	0.96	0.86	0.98	0.78	0.89	0.98	0.84
100 FL	0.94	1.01	0.88	1.04	0.84	0.93	1.03	0.91
99 FL	1.01	1.05	0.91	1.10	0.90	0.97	1.08	0.98
98 FL	1.02	0.92	0.81	0.99	0.88	0.90	0.94	1.00
97 FL	1.09	0.96	0.83	1.05	0.93	0.93	0.98	1.06
96 FL	1.16	1.00	0.86	1.10	0.99	0.97	1.02	1.13
95 FL	0.91	0.84	0.81	0.88	0.86	0.86	0.90	1.08
94 FL	0.96	0.88	0.83	0.92	0.91	0.89	0.94	1.14
93 FL	1.00	0.91	0.85	0.96	0.95	0.92	0.97	1.20
92 FL	0.89	0.86	0.78	0.90	0.90	0.86	0.87	1.04
91 FL	0.98	0.89	0.80	0.94	0.94	0.89	0.90	1.09
90 FL	1.07	0.92	0.82	0.98	0.98	0.92	0.93	1.14
89 FL	1.01	0.84	0.76	0.84	0.84	0.83	0.85	1.00
88 FL	1.05	0.86	0.78	0.87	0.88	0.85	0.88	1.05
87 FL	1.09	0.89	0.80	0.90	0.91	0.88	0.90	1.09
86 FL	0.97	0.85	0.75	0.93	0.78	0.87	0.86	0.97
85 FL	1.01	0.87	0.77	0.96	0.81	0.89	0.88	1.00
84 FL	1.04	0.90	0.79	0.99	0.83	0.92	0.91	1.04
83 FL	1.07	0.79	0.73	0.86	0.79	0.87	0.80	1.07
82 FL	1.11	0.81	0.75	0.89	0.82	0.89	0.82	1.11
81 FL	1.15	0.83	0.77	0.92	0.84	0.91	0.84	1.14
80 FL	1.19	0.86	0.85	0.95	0.87	0.94	0.86	1.19
79 FL	1.25	0.89	0.88	0.99	0.91	0.97	0.89	1.24
78 FL	1.30	0.92	0.90	1.03	0.94	1.00	0.92	1.30
77 FL	0.84	0.67	0.62	0.71	0.60	0.56	0.55	0.88
76 FL	0.85	0.71	0.65	0.73	0.63	0.60	0.60	0.90
75 FL	0.98	0.85	0.84	0.94	0.76	0.85	0.88	1.05
74 FL	0.98	0.85	0.84	0.95	0.77	0.85	0.88	1.06
73 FL	1.01	0.87	0.86	0.97	0.79	0.87	0.90	1.09
72 FL	0.95	0.89	0.79	0.92	0.77	0.82	0.85	1.03
71 FL	0.98	0.91	0.81	0.94	0.79	0.85	0.87	1.06
70 FL	1.00	0.93	0.82	0.96	0.81	0.87	0.88	1.08
69 FL	0.81	0.81	0.79	0.91	0.77	0.82	0.84	0.88
68 FL	0.88	0.87	0.82	0.96	0.82	0.88	0.89	0.95
67 FL	0.86	0.85	0.82	0.96	0.81	0.86	0.87	0.92
66 FL	1.01	0.93	0.85	0.98	0.83	0.88	0.89	1.09
65 FL	1.03	0.93	0.85	0.98	0.83	0.89	0.89	1.11
64 FL	1.06	0.97	0.88	1.02	0.87	0.92	0.92	1.14
63 FL	1.00	0.91	0.83	0.97	0.82	0.94	0.85	1.07
62 FL	1.03	0.93	0.84	0.99	0.84	0.96	0.89	1.10
61 FL	1.05	0.95	0.85	1.01	0.85	0.99	0.91	1.12
60 FL	0.99	0.90	0.83	0.97	0.83	0.93	0.87	1.06
59 FL	1.01	0.92	0.84	0.99	0.85	0.95	0.88	1.08
58 FL	1.03	0.93	0.86	1.01	0.87	0.97	0.90	1.10
57 FL	1.06	0.88	0.84	1.01	0.85	0.93	0.84	1.04
56 FL	1.08	0.90	0.85	1.02	0.86	0.94	0.85	1.06
55 FL	1.10	0.91	0.86	1.04	0.88	0.96	0.87	1.09
54 FL	1.04	0.93	0.84	1.01	0.86	0.91	0.88	1.11
53 FL	1.06	0.94	0.85	1.02	0.87	0.93	0.89	1.13
52 FL	1.08	0.96	0.87	1.04	0.89	0.95	0.91	1.15
51 FL	1.03	0.89	0.85	0.99	0.86	0.97	0.83	1.09
50 FL	1.05	0.90	0.86	1.01	0.87	0.98	0.85	1.11
49 FL	1.07	0.91	0.87	1.03	0.89	1.00	0.86	1.13
48 FL	1.09	0.83	0.83	0.97	0.86	0.89	0.83	1.08
47 FL	1.12	0.85	0.85	0.98	0.87	0.92	0.85	1.11
46 FL	1.14	0.87	0.86	1.00	0.89	0.93	0.87	1.13
45 FL	0.85	0.78	0.77	0.76	0.83	0.84	0.79	0.88
44 FL	0.87	0.80	0.79	0.78	0.85	0.86	0.81	0.90
43 FL	0.75	0.61	0.60	0.69	0.63	0.66	0.62	0.77
42 FL	0.77	0.63	0.63	0.72	0.66	0.68	0.64	0.79
41 FL	1.00	0.85	0.83	0.94	0.86	0.90	0.86	1.00
40 FL	1.00	0.85	0.83	0.94	0.85	0.90	0.86	1.00
39 FL	0.98	0.83	0.84	0.94	0.84	0.89	0.84	1.01
38 FL	1.00	0.84	0.85	0.96	0.85	0.90	0.85	1.02
37 FL	1.01	0.85	0.86	0.97	0.86	0.92	0.86	1.04
36 FL	1.02	0.84	0.85	0.95	0.84	0.90	0.85	1.01
35 FL	1.03	0.85	0.86	0.96	0.85	0.91	0.86	1.03
34 FL	1.05	0.86	0.87	0.97	0.87	0.92	0.87	1.04
33 FL	1.02	0.84	0.85	0.94	0.84	0.90	0.85	1.02
32 FL	1.04	0.85	0.87	0.96	0.85	0.91	0.86	1.03
31 FL	1.05	0.86	0.88	0.97	0.86	0.92	0.87	1.04
30 FL	1.04	0.85	0.86	0.94	0.83	0.91	0.86	1.02
29 FL	1.05	0.86	0.87	0.95	0.84	0.92	0.87	1.03
28 FL	1.06	0.87	0.89	0.96	0.85	0.93	0.88	1.04
27 FL	1.17	0.86	0.87	0.97	0.84	0.91	0.86	1.02
26 FL	1.18	0.87	0.88	0.98	0.85	0.92	0.87	1.03
25 FL	1.07	0.88	0.89	0.99	0.86	0.93	0.88	1.05
24 FL	1.05	0.86	0.88	0.97	0.85	0.91	0.85	1.03
23 FL	1.06	0.87	0.89	0.98	0.86	0.92	0.86	1.04
22 FL	1.07	0.88	0.90	0.99	0.87	0.93	0.87	1.05
21 FL	1.05	0.87	0.89	0.97	0.86	0.92	0.86	1.06
20 FL	1.07	0.88	0.90	0.98	0.87	0.93	0.87	1.07
19 FL	1.08	0.89	0.91	0.99	0.87	0.94	0.88	1.09
18 FL	1.08	0.87	0.88	0.96	0.87	0.92	0.87	1.06
17 FL	1.10	0.88	0.89	0.97	0.88	0.93	0.88	1.08
16 FL	1.11	0.89	0.90	0.98	0.89	0.94	0.89	1.09
15 FL	1.09	0.86	0.89	0.99	0.86	0.93	0.87	1.08
14 FL	1.10	0.87	0.90	1.00	0.87	0.94	0.88	1.09
13 FL	1.11	0.88	0.91	1.01	0.88	0.95	0.89	1.10
12 FL	1.09	0.87	0.90	0.98	0.86	0.94	0.87	1.08
11 FL	1.11	0.88	0.91	0.99	0.87	0.95	0.88	1.09
10 FL	1.13	0.89	0.93	1.01	0.89	0.96	0.89	1.11
09 FL	0.91	0.86	0.89	0.97	0.99	1.03	0.97	1.06
08 FL	0.98	0.91	0.95	1.03	1.00	1.04	0.97	1.06
07 FL	0.63	0.60	0.61	0.62	0.67	0.59	0.59	0.62
06 FL	0.65	0.62	0.63	0.64	0.69	0.61	0.60	0.64
05 FL	0.65	0.63	0.64	0.65	0.70	0.62	0.61	0.64
04 FL	0.63	0.61	0.62	0.63	0.67	0.60	0.59	0.62
03 FL	0.72	0.69	0.71	0.72	0.80	0.68	0.67	0.71
02 FL	0.75	0.71	0.73	0.74	0.83	0.70	0.69	0.74
01 FL	1.07	0.89	0.92	1.01	1.00	0.96	0.90	1.07
B1 FL	1.06	0.88	0.91	1.00	0.98	0.94	0.88	1.06
B2 FL	1.08	0.89	0.92	1.01	0.99	0.96	0.90	1.08
B3 FL	1.02	0.85	0.89	0.97	0.93	0.92	0.86	1.01
B4 FL	1.05	0.87	0.98	1.07	1.05	1.00	0.94	1.13
B5 FL	1.06	0.88	0.99	1.08	1.06	1.01	0.95	1.14

(b)

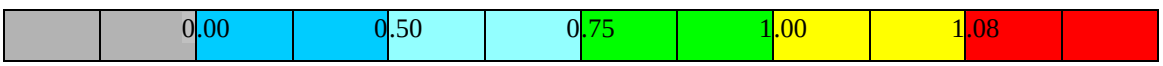

Figure E–6. DCRs for WTC 1 core columns under original design loads, (a) 600 line, and (b) 900 line.

Exterior Columns Behavior

Analysis of the axial stress distribution in the columns under lateral wind loads indicated that the behavior of the lower portion of the towers at the basement floors was that of a braced frame, while the behavior of the super-structure was that of a framed tube system. Under a combination of the original WTC design dead and wind loads, tension forces were developed in the exterior walls of both towers. The forces were largest at the base of the building and at the corners. These tensile column loads were transferred from one panel to another through the column splices. The DCRs for the exterior wall splice connections under these tensile forces for both towers were shown to be less than 1.0.

Resistance of the Towers to Shear Sliding and Overturning Moment

The resistance of the towers to shear sliding and overturning due to wind was provided by the dead loads that acted on the exterior walls of the towers. Considering the resistance to shear sliding under wind load, the factor of safety was calculated to be between 10 and 11.5, while the factor of safety against overturning ranged from 1.9 to 2.7 for both towers.

E.4.2 Baseline Performance of the Typical Floor Models

The reference floor models were analyzed under gravity loads to establish their baseline performance. The following presents a summary of the results:

- For the typical truss-framed floor (floor 96 of WTC 1), the DCRs for all floor trusses were less than 1.14 for the original WTC design loads and less than 0.86 for the ASCE 7-02 loading. Under the original WTC design loads, the DCR was less than 1.00 for 99.4 percent of the floor truss components. Inside the core, the DCRs for all floor beams were less than 1.08, and more than 99 percent of the floor beams had a DCR of less than 1.0. The maximum mid-span deflections of the long span and short span zones under the original design loads were approximately 1.79 in. (≈ L/400) and 0.57 in. (≈ L/750), respectively, where L is the floor span.

- For the typical beam-framed floor under the original WTC design loads, the DCRs for all floor beams were less than 1.0, except for two core beams where the DCRs in shear were 1.125 and 1.09. The maximum mid-span deflections of the long span and short span zones under the original design loads were approximately 1.55 in. (≈ L/450) and 0.70 in. (≈ L/600), respectively.

E.5 DEVELOPMENT OF TOWER AND AIRCRAFT IMPACT MODELS

The WTC tower models for the impact analysis required considerably greater sophistication and detail than was required for the reference models. The reference models provided the basis for the more detailed models required for the impact simulations. The impact models of the towers, which utilized the structural databases described earlier, included the following refinements:

- The material properties used in the impact models accounted for the highly nonlinear behavior of the tower and aircraft materials, including softening and failure of components, and strain rate sensitivity.

- The impact simulations required a much higher level of detail than that in the reference global models. For instance, the impact analyses necessitated that the floors inside and outside the core in the impact region, as well as connections, be modeled in detail. In addition, structural components in the exterior walls and core of the towers were modeled using shell elements (instead of beam elements in the reference models) to properly capture the impact-induced damage to these components.
- The size of the impact models required a very large mesh (more than ten million degrees of freedom). The SAP2000 program cannot accommodate this model size.
- Contact and erosion algorithms were required for the impact analyses. That necessitated the use of appropriate software, specifically LS-DYNA, for the development of the impact models.

As a result, three separate models were developed for the impact analyses. The first two were detailed models of the impact regions of the WTC 1 and WTC 2 towers. The third was a comprehensive model of the Boeing 767 aircraft. All models were developed using the LS-DYNA finite element code, which is a commercially available nonlinear explicit finite element code for the dynamic analysis of structures. The code has been used for a wide variety of crash, blast, and impact applications.

One of the significant challenges in developing the tower and aircraft models for the global impact analyses was to minimize the model size while keeping sufficient fidelity in the impact zone to capture the deformations and damage distributions. The limitation was that for each analysis the combined aircraft and tower models should not exceed approximately 2.3 million nodes. These were distributed between the global WTC tower model and the aircraft so that the tower model would be about 1.5 million nodes and the aircraft about 0.8 million nodes.

E.5.1 Development of Tower Impact Models

The approach used to meet this model size limitation was to develop models for the various tower components at different levels of refinement. Components in the path of the impact and debris field were meshed with a higher resolution to capture the local impact damage and failure, while components outside the impact zone were meshed more coarsely to primarily capture their structural stiffness and inertial properties. A summary of the size of the global impact models of both towers is presented in Table E–6. As the table indicates, the towers were modeled primarily with shell elements, with the exception of the exterior wall bolted connections (beam and brick elements) and the floor truss diagonals (beam elements). The WTC 1 model extended between floors 92 and 100, while the WTC 2 model extended between floors 77 and 85.

Table E–6. Summary of the global impact models for the WTC towers.

	WTC 1 Tower Model	WTC 2 Tower Model
Number of Nodes	1,300,537	1,312,092
Hughes-Liu Beam Elements	47,952	53,488
Belytschko-Tsay Shell Elements	1,156,947	1,155,815
Constant Stress Solid Elements	2,805	2,498

The global impact models of the WTC towers included the following components:

- Exterior walls: The exterior columns and spandrels were modeled using shell elements with two mesh densities, a refined density in the immediate impact zone (typical element sizes were 4 in.) and a coarser far field density elsewhere (typical element sizes were 14 in.). For the bolted connections between exterior panels in the refined mesh areas, brick elements were used to model the butt plates, and beam elements were used for the bolts. The model of the impact face of WTC 1 is shown in Figure E–7.
- Core columns and floors: Core columns were modeled using shell elements with two mesh densities, a refined density in the direct impact area and a coarser far field density elsewhere. Typical element sizes were 2 in. and 8 in. for the impact zone and far field, respectively. The spliced column connections were included in the model with proper failure criteria. The floors within the core were modeled using shell elements representing the floor slabs and beams. A generated model for the core of WTC 1 between floors 94 and 98 is shown in Figure E–8.
- Truss floors: In the direct impact area, the floor model included shell elements for the combined floor slab and metal decking and for the upper and lower chords of the trusses. Beam elements were used for the truss diagonals. In the far field floor segments, simplified shell element representations were used for the floor slab and trusses, with typical element sizes of 30 in. A model assembled for the entire 96th floor of WTC 1 is shown in Figure E–9.
- Interior building contents: The interior nonstructural contents of the towers were modeled explicitly. These included the partitions and workstations, which were modeled with shell elements in the path of the aircraft debris. The live load mass was distributed between the partitions and cubicle workstations. The resulting model of a floor with interior contents is shown in Figure E–10.

Figure E–11 shows the assembled global impact model of WTC 1.

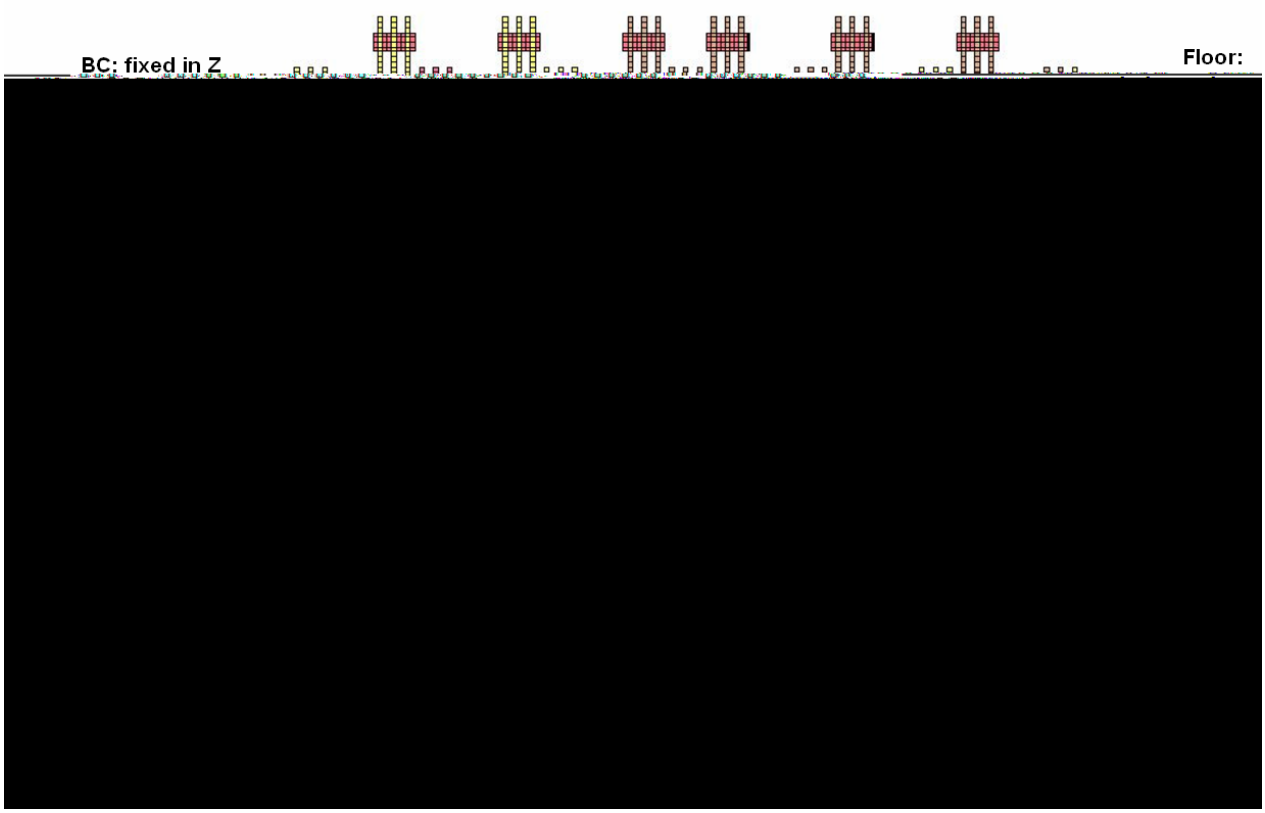

Figure E–7. Impact face of the WTC 1 model, floors 91–101.

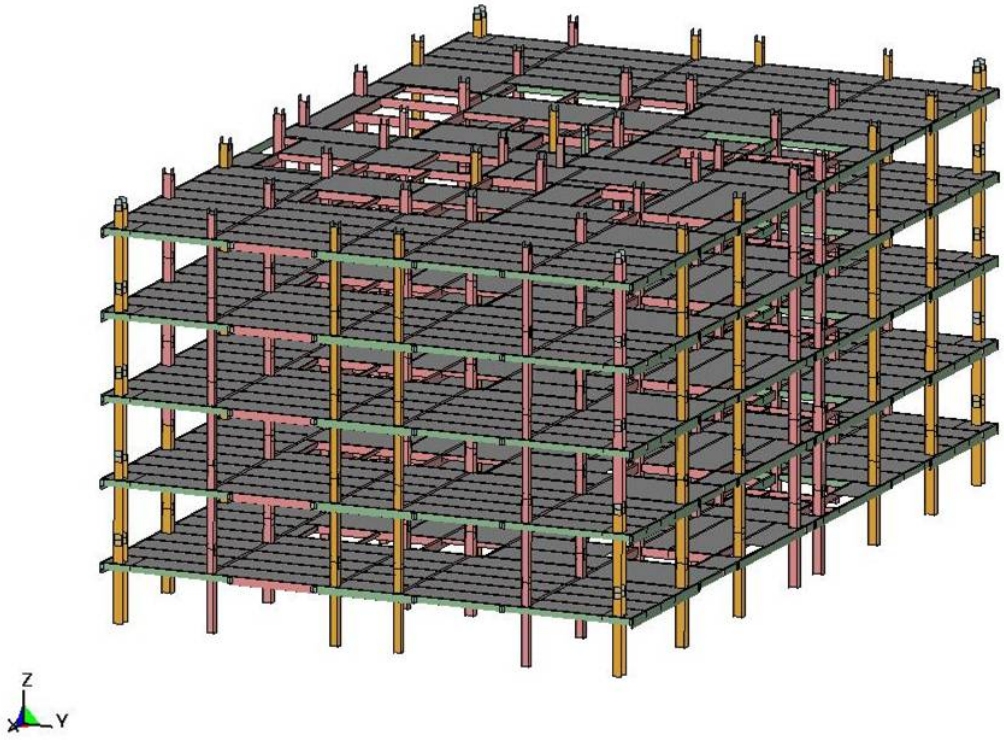

Figure E–8. Model of the WTC 1 core, floors 94–98.

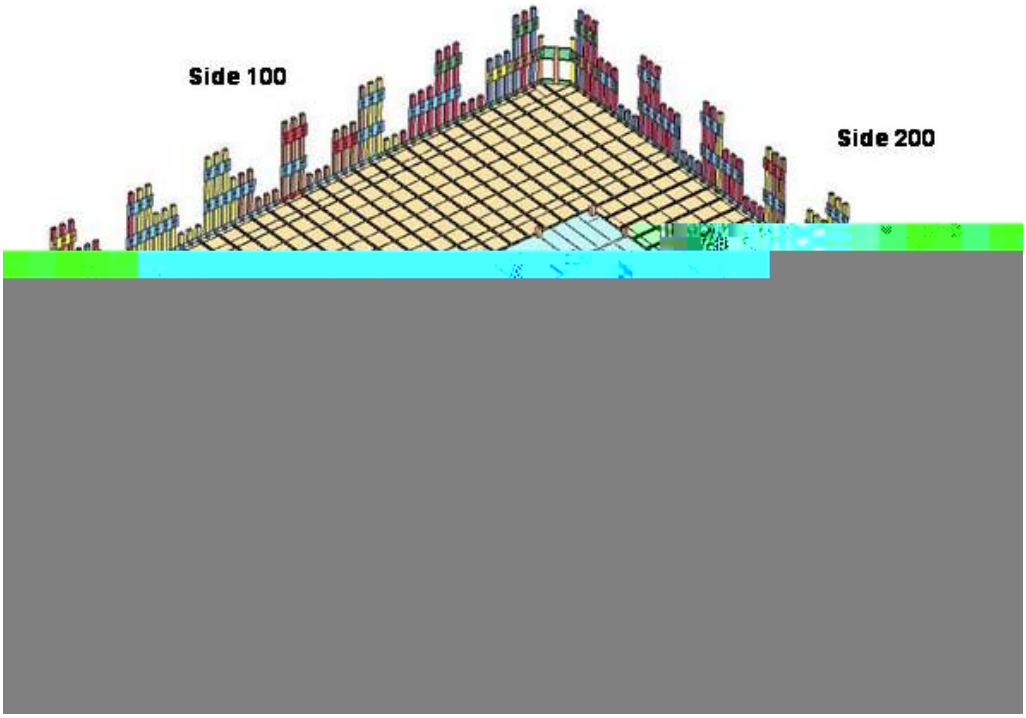

Figure E–9. Model of the 96th floor of WTC 1.

Figure E–10. Model of the 96th floor of WTC 1 including interior contents.

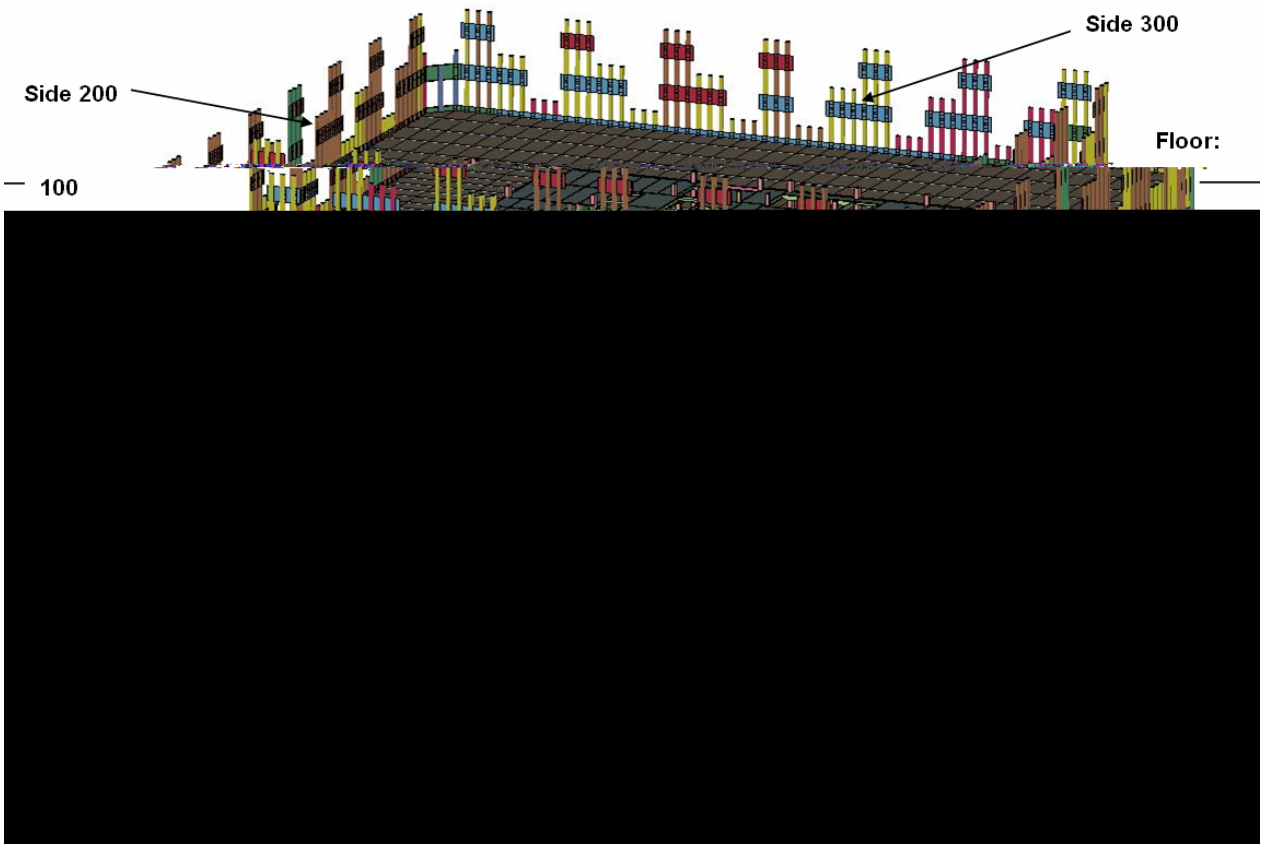

Figure E–11. Multi-floor global impact model of the WTC 1 tower.

Tower Material Constitutive Models

The materials that were considered for the tower modeling included: (1) the several grades of steel used in the columns, spandrels, and floor trusses and beams of the WTC towers, (2) the concrete floor slabs, and (3) the nonstructural contents of the towers. These materials exhibit significant nonlinear rate-dependent deformation and failure behavior that need to be represented in the constitutive relationship. The following is a brief summary of the constitutive models used for these materials.

WTC Tower Steel Constitutive Models—The primary constitutive model that was used for the tower steels was the Piecewise Linear Plasticity model in LS-DYNA. This model is sufficient to model the nonlinear rate-dependent deformation and failure of the steel structures. A tabular effective stress versus effective strain curve was used in this model with various definitions of strain rate dependency. The constitutive model parameters for each grade of steel were based on engineering stress-strain data developed by the mechanical and metallurgical analysis of structural steels part of the NIST Investigation. Finite element analyses of the test specimens were conducted with a fine and a medium mesh (similar to that used in the component level analysis) to capture the nonlinear material behavior up to failure (Figure E–12). The finite element analysis provided a validation that the constitutive model parameters were defined accurately and that the model could reproduce the measured response for the test conditions.

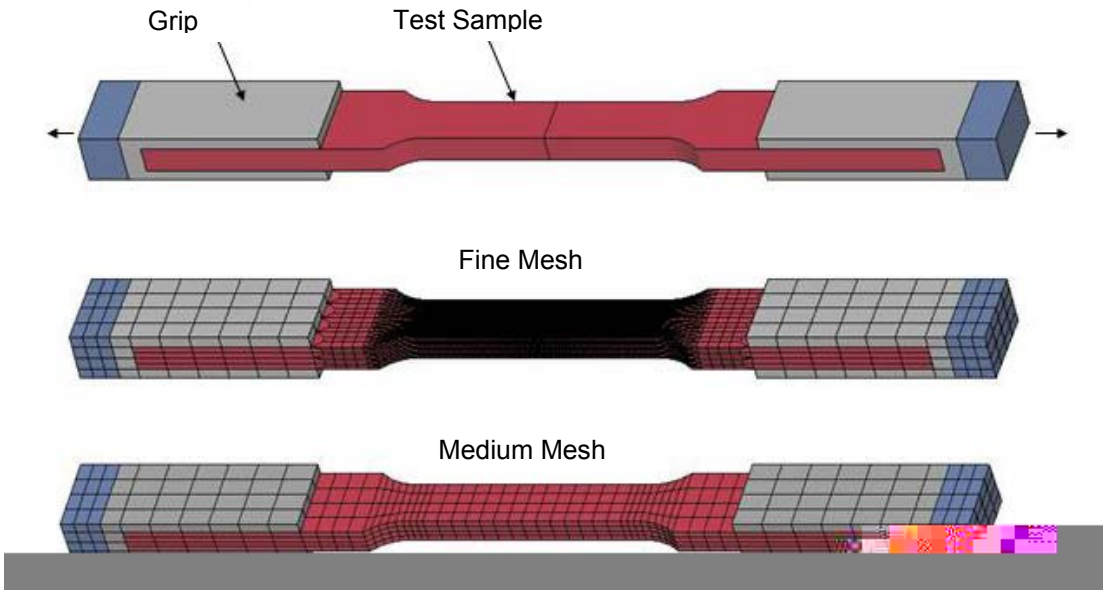

Figure E–12. Finite element models of the ASTM 370 rectangular tensile specimen.

The first step in the constitutive model development process was to obtain a true stress-true strain curve. The typical approach was to select a representative test for each grade of steel and convert the engineering stress-strain curve to true stress-strain. The true stress-strain curve was extrapolated beyond the point of necking onset. This curve was the input used to specify the mechanical behavior in the simulation of the tensile test (Figure E–12). If necessary, the extrapolation of the true stress-strain behavior was adjusted until the simulation matched the measured engineering stress-strain response, including necking and failure. A summary of the true stress-strain curves used in the constitutive models for the various WTC tower steels are summarized in Figure E–13.

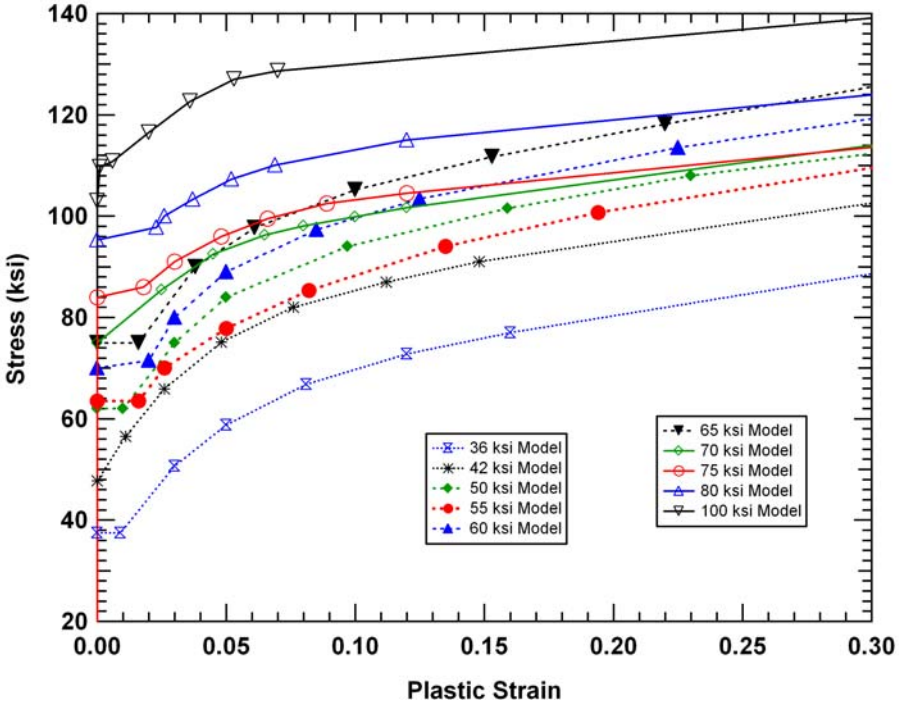

Figure E–13. Tabular true stress-strain constitutive model curves for the tower steels.

Strain-rate effects on the steel yield strength were included in the constitutive model for tower steels with the Cowper and Symonds rate effect model. The resulting rate effects used in the constitutive modeling of tower steels based on this model were compared to the measured high rate test data for the 50 ksi, 75 ksi, and 100 ksi tower steels in Figure E–14. The comparison showed that the Cowper and Symonds model was capable of reproducing the rate effects for the range of data available.

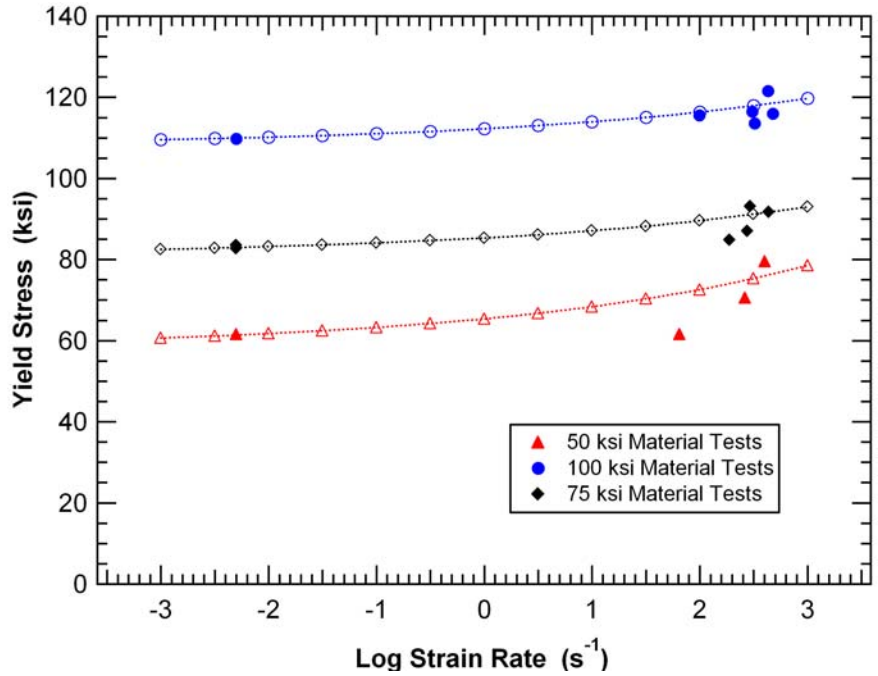

Figure E–14. Comparison of rate effects model and test data.

Concrete Constitutive Models—The LS-DYNA material Type 16 (pseudo-tensor concrete model) was selected for modeling the concrete floor slabs due to its ability to accurately model the damage and softening of concrete, associated with low confinement. The model uses two pressure-dependent yield functions and a damage-dependent function to migrate between curves. This allows for implementation of tensile failure and damage scaling, which are more dominant material behaviors at low confinement. The pseudo-tensor model also accounts for the sensitivity of concrete to high strain rates. Material constitutive parameters for the pseudo-tensor model were developed. A simulation was performed of a standard unconfined concrete compression test to check the constitutive model behavior. The calculated compressive stress-strain response for the 3 ksi concrete was compared to measured compression data for 2.3 ksi and 3.8 ksi strength concretes in Figure E–15.

Figure E–15. Comparison of the calculated unconfined compression behavior with concrete compression test data.

Nonstructural Materials Constitutive Models—The primary influence of the nonstructural components on the impact behavior was their inertial contribution. The effects of their strength were small. As a result, relatively simple approximations of their constitutive behavior were used. Typically, a bilinear elastic-plastic constitutive model was applied for these materials to allow for efficient modeling of deformation and subsequent erosion from the calculations as their distortions became large. The ability to include material failure and erosion of these soft materials was important for the stability of the impact analyses.

E.5.2 Development of Aircraft Impact Model

The finite element model for the Boeing 767-200ER aircraft was constructed through a three-step process: (1) data collection, (2) data interpretation and engineering analysis, and (3) meshing of the structure. The

focus of this effort was on gathering sufficient structural data and including adequate detail in the aircraft model so that the mass and strength distribution of the aircraft and contents were properly captured for implementation in the impact analyses. Structural data were collected for the Boeing 767-200ER aircraft from (1) documentary aircraft structural information, and (2) data from measurements on Boeing 767 aircraft.

A summary of the aircraft model size and parameters is presented in Table E–7. The complete model of the Boeing 767-200ER is shown in Figure E–16. The airframe model contained most of the significant structural components in the aircraft. The models of the fuselage, empennage, and wing structures were developed completely using shell elements. Models for the landing gear and engines were developed primarily using shell elements, but contained some brick elements as well. The typical element dimensions were between one and two in. for small components, such as spar or rib flanges, and three to four in. for large parts, such as the wing or fuselage skin.

Table E–7. Boeing 767-200ER aircraft model parameters.

	American Airlines 11	**United Airlines 175**
No. Brick Elements	70,000	70,000
No. Shell Elements	562,000	562,000
No. SPH Fuel Particles	60,672	60,672
Total Nodes	740,000	740,000
Total Weight (Empty)	183,500 lb	183,500 lb
ULD/Cargo Weight	12,420 lb	21,660 lb
Cabin Contents Weight	21,580 lb	10,420 lb
Fuel Weight	66,100 lb	62,000 lb
Total Weight (Loaded)	**283,600 lb**	**277,580 lb**

Special emphasis was placed on modeling the aircraft engines due to their potential to produce significant damage to the tower components. The engine model was developed primarily with shell elements. The objective was to develop a mesh with typical element dimensions between one and 2 in. However, smaller element dimensions were required at many locations to capture details of the engine geometry. Brick elements were used for some of the thicker hubs and the roots of the compressor blades. The various components of the resulting engine model are shown in Figure E–17. Fuel was distributed in the wing, as shown in Figure E–18, based on a detailed analysis of the likely fuel distribution at the time of impact.

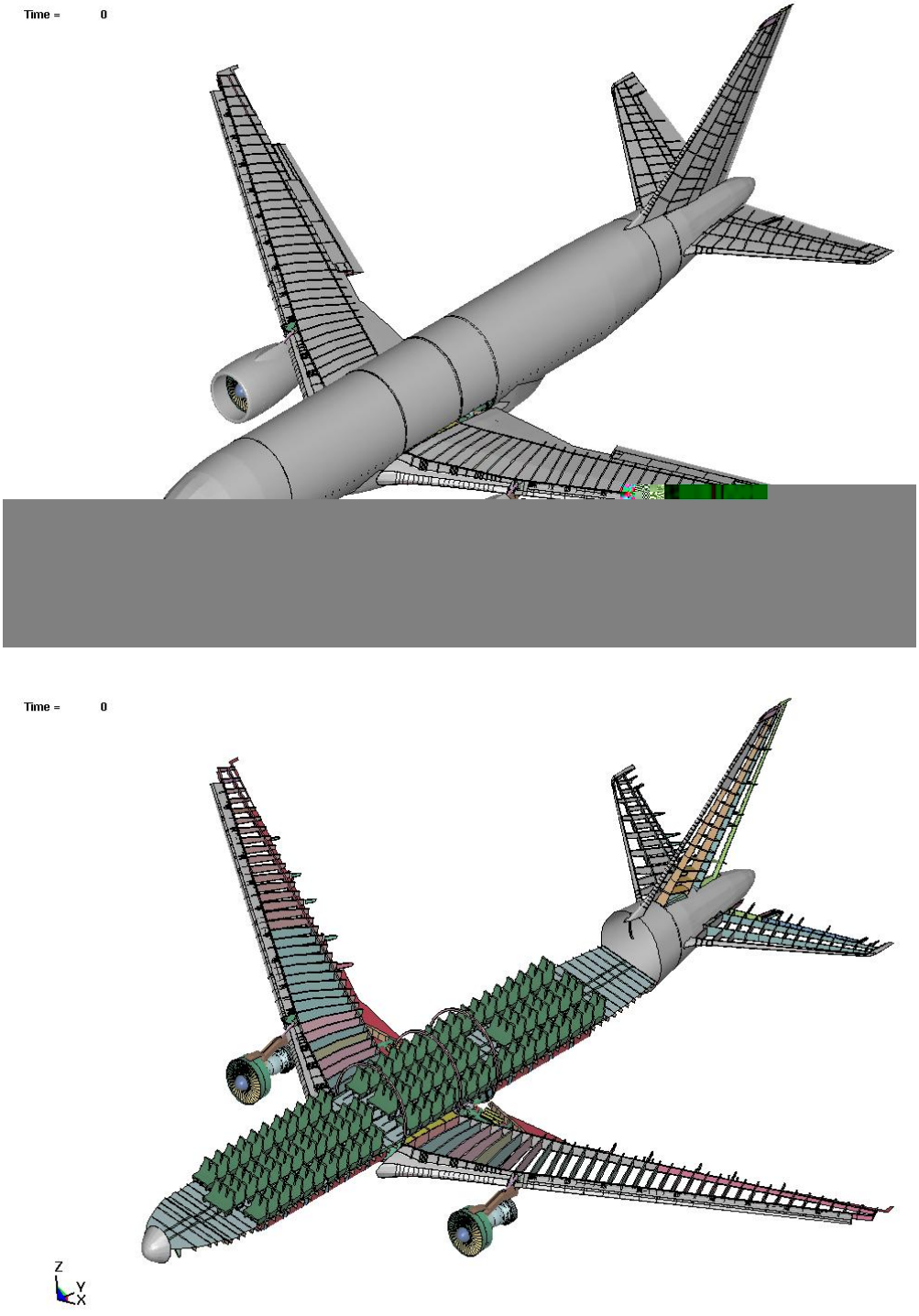

Figure E–16. Finite element model of the Boeing 767-200ER.

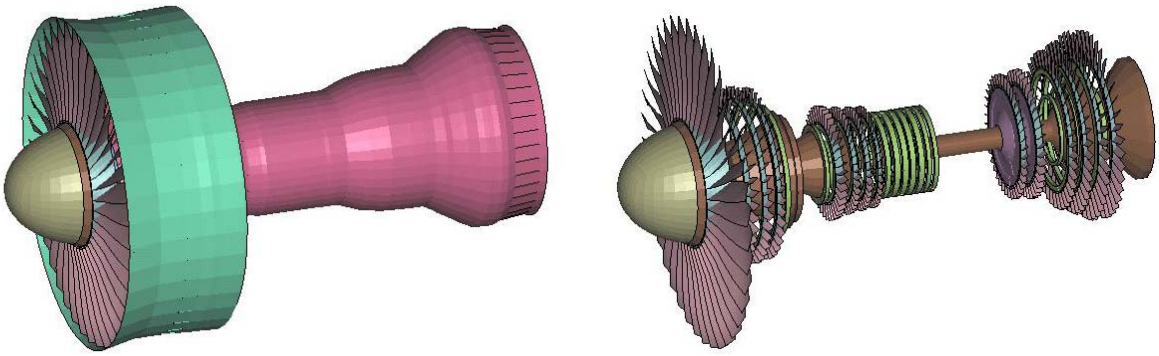

Figure E–17. Pratt & Whitney PW4000 turbofan engine model.

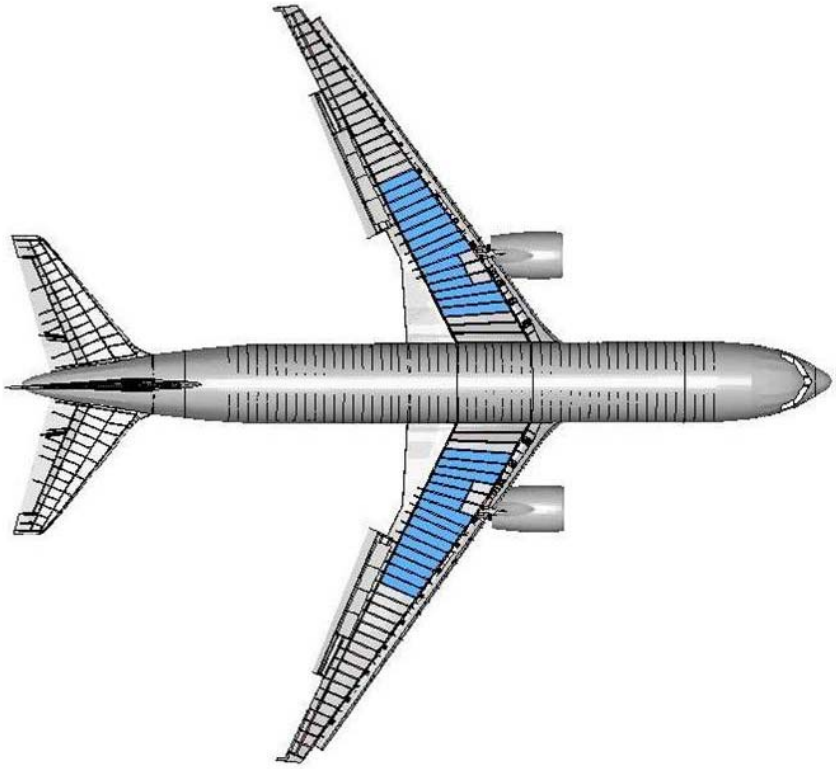

Figure E–18. Boeing 767-200ER with fuel load at time of impact.

Aircraft Materials Constitutive Models

The constitutive and failure properties for the aircraft materials were developed from data available in the open literature. Complete engineering stress-strain curves were obtained for various 2024 and 7075 aluminum alloys that are commonly used in the construction of the Boeing 767 airframe structures. These curves were digitized for the various aluminum alloys. Representative stress-strain curves were then converted into true stress and true strain and used to develop tabular curves for constitutive models. The tabular constitutive model fits are shown in Figure E–19. No rate sensitivity of the aircraft materials was considered.

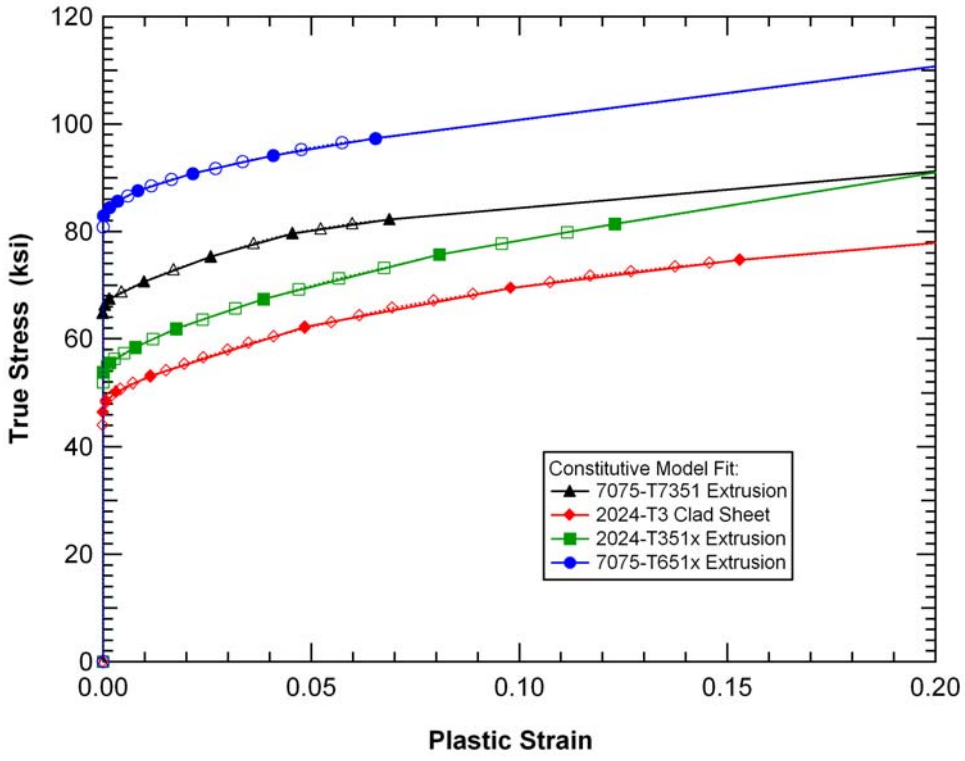

Figure E–19. True stress-strain curves developed for various aircraft aluminum alloys.

E.5.3 Component and Subassembly level analyses

A large array of component and subassembly models were developed and used in the impact simulations. The primary objectives of the component modeling were to (1) develop understanding of the interactive failure phenomenon of the aircraft and tower components, and (2) develop the simulation techniques required for the global analysis of the aircraft impacts into the WTC towers. The approach taken for component modeling was to start with finely meshed, brick and shell element models of key components of the tower structure and progress to relatively coarsely meshed beam and shell element representations that were used for the global models. Other key technical areas were addressed in the component modeling, including material constitutive modeling, treatment of connections, and modeling of aircraft fuel.

Examples of the component impact analyses conducted include:

- Impact of a segment of an aircraft wing with an exterior column.
- Detailed and simplified modeling of exterior panel bolted connection under impact loading.
- Impact of a simplified plow type impactor with truss floor assembly.
- Impact of fuel-filled wing segment with exterior wall panels (Figure E–20).

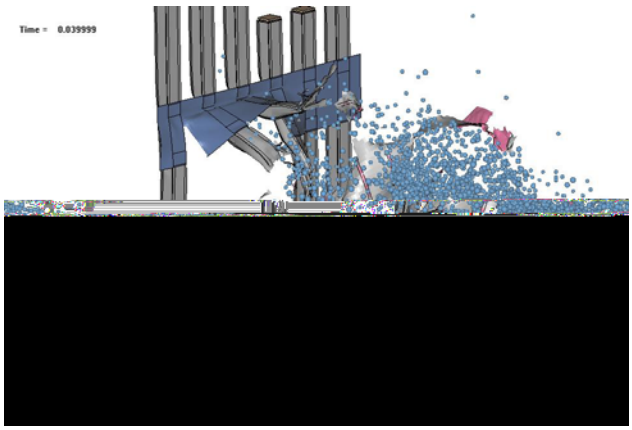

t = 0.0 s **t = 0.04 s**

Figure E–20. Calculated impact of a coarse mesh wing section laden with fuel modeled using SPH particles.

The following results were obtained from the component impact analyses:

- A 500 mph engine impact against an exterior wall panel resulted in a penetration of the exterior wall and failure of impacted exterior columns. If the engine did not impact a floor slab, the majority of the engine core would remain intact through the exterior wall penetration, with a reduction in speed between 10 percent and 20 percent. The residual velocity and mass of the engine after penetration of the exterior wall was sufficient to fail a core column in a direct impact condition. Interaction with additional interior building contents prior to impact or a misaligned impact against the core column could change this result.

- A normal impact of the exterior wall by an empty wing segment from approximately mid-span of the wing produced significant damage to the exterior columns but not complete failure. Impact of the same wing section, but filled with fuel, resulted in extensive damage to the external panels of the tower, including complete failure of the exterior columns. The resulting debris propagating into the building maintained the majority of its initial momentum prior to impact.

- Three different numerical techniques were investigated for modeling impact effects and dispersion of fuel: (1) standard Lagrangian finite element analysis with erosion, (2) Smoothed Particle Hydrodynamics (SPH) analysis, and (3) Arbitrary-Lagrangian-Eulerian analysis. Of these approaches, use of the SPH offered the best viable option due to its computational efficiency.

The subassembly analyses were used as a transition between the component level analyses and the global impact analyses. With the subassembly analyses, more complex structural behavior not captured in the component analyses could be investigated with significantly shorter run times than required for the global analyses. The subassembly analyses were primarily used to investigate different modeling techniques and associated model size, run times, numerical stability, and impact response. The subassembly model used structural components from the impact zone on the north face of WTC 1. The structural components in

the subassembly model included the exterior panels, core framing, truss floor structures, and interior contents (workstations), Figure E–21.

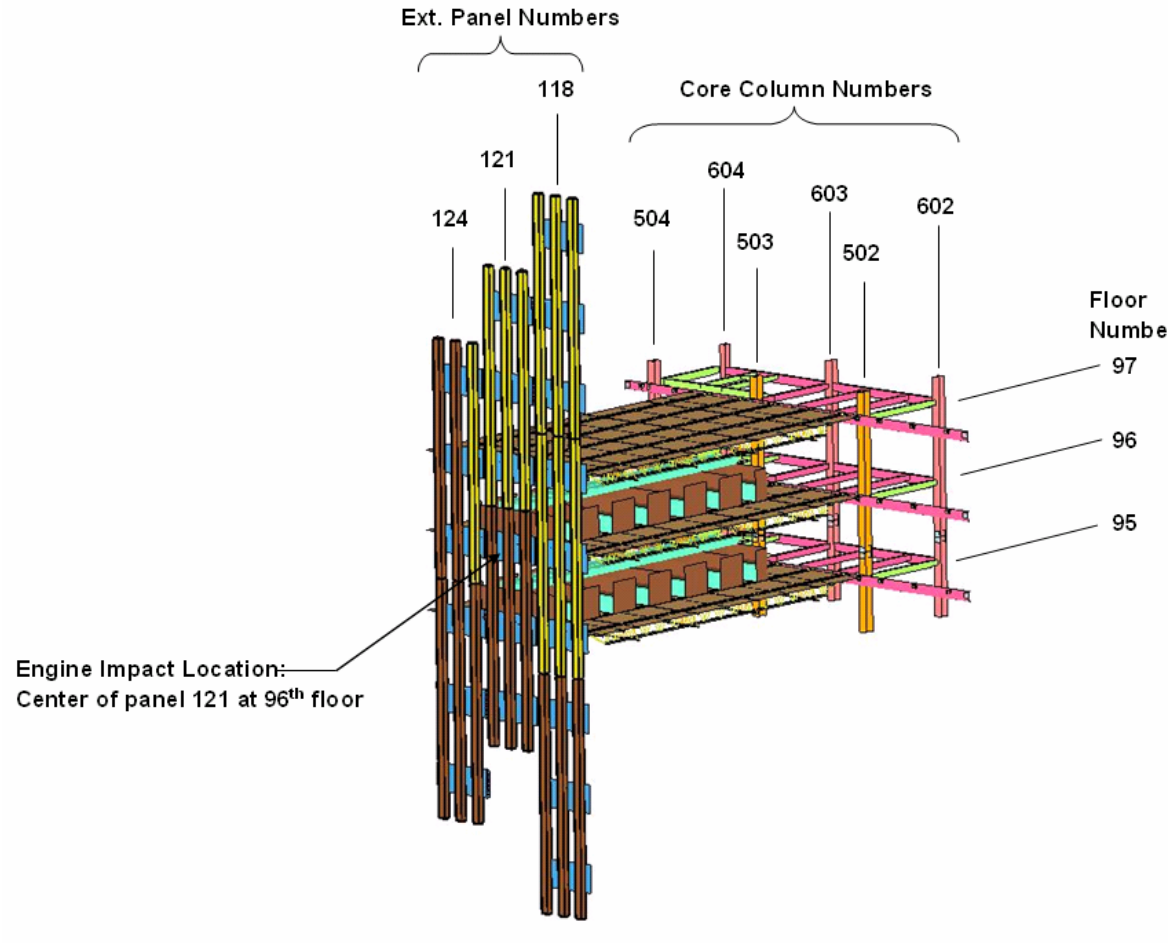

Figure E–21. Final WTC tower subassembly model.

The subassembly model was impacted by an aircraft engine and by a segment of a fuel-filled wing. The response of the structure to the engine impact is shown in Figure E–22. The following results were obtained from the subassembly impact analyses:

- The deceleration profile of the impacting engine indicated that the response of the nonstructural building contents was dominated by the mass of the workstations, rather than by their strength.

- Varying the strength of the floor concrete slab from 3 ksi to 4 ksi did not result in significant change in the impact response. It appears that the mass of the concrete slab had a greater effect on the engine deceleration and damage to the floor than did the concrete strength.

- Varying the ductility of the weld zone in the exterior columns from 8 percent to 1 percent did not result in any noticeable difference in the damage pattern or the energy absorbed by the exterior panels, indicating that the weld ductility had a negligible effect on the impact response.

(a) Time = 0.00 s

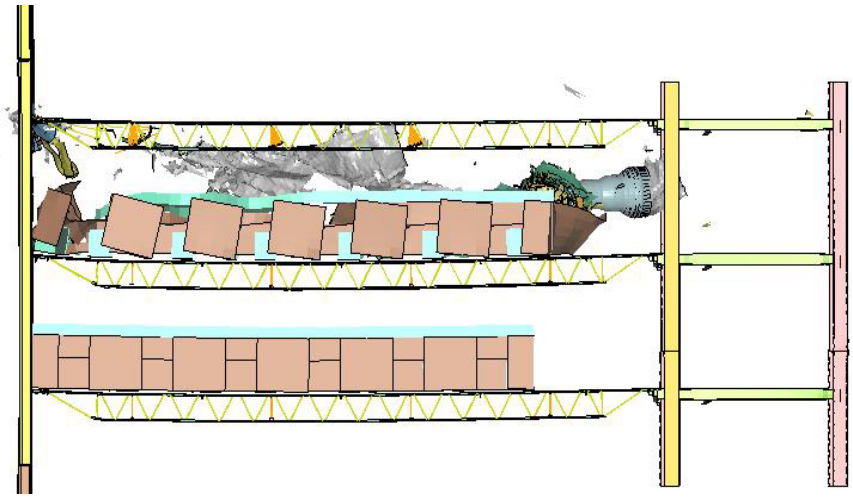

(b) Time = 0.25 s

Figure E–22. Engine impact and breakup behavior (side view).

E.6 AIRCRAFT IMPACT INITIAL CONDITIONS

Three methods were used to determine the initial conditions for the two aircraft that impacted the towers. The first method used a comparison of videos from different positions to calculate the three-dimensional trajectory of the aircraft. The second method used the relative frame-by-frame motion in a single video scaled to the length of the aircraft in the video to calculate the impact speed. Finally, analysis of the impact damage on the face of each tower was used to refine the relative impact orientation and trajectory.

The aircraft impact conditions matching the observed exterior wall damage are shown in Figure E–23 and Figure E–24 for WTC 1 and WTC 2, respectively. The aircraft and exterior wall models were used to visualize the impact scenario in the figures and the view shown was aligned with the aircraft trajectory. Matching the projected impact points of the wings, fuselage, engines, and vertical stabilizer onto the exterior wall of each tower to the observed damage pattern was an important constraint in the determination of impact conditions. The final set of impact conditions from the analyses are summarized in Table E–8.

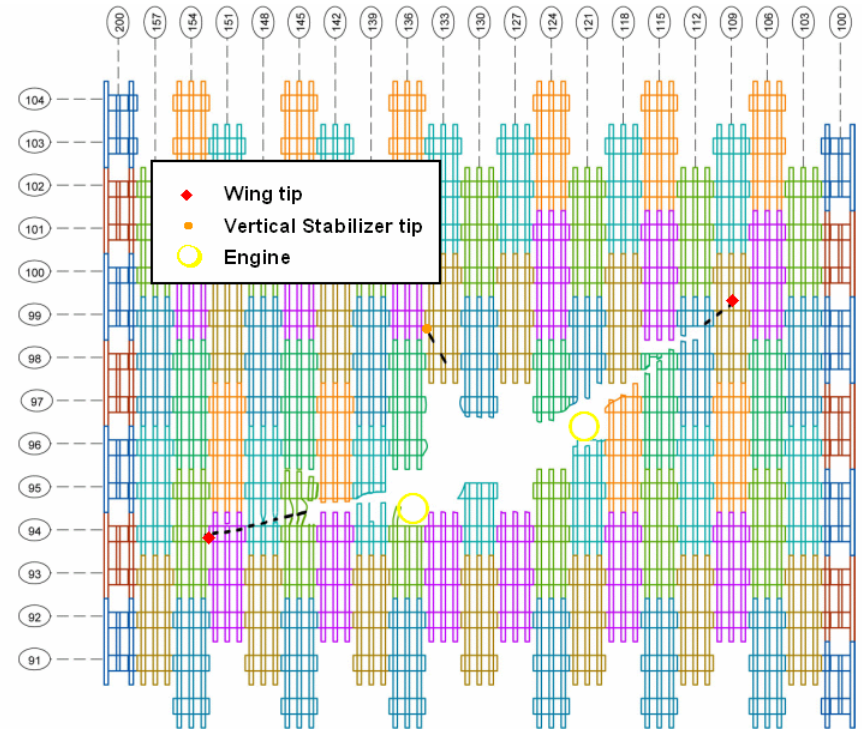

(a) Impact damage

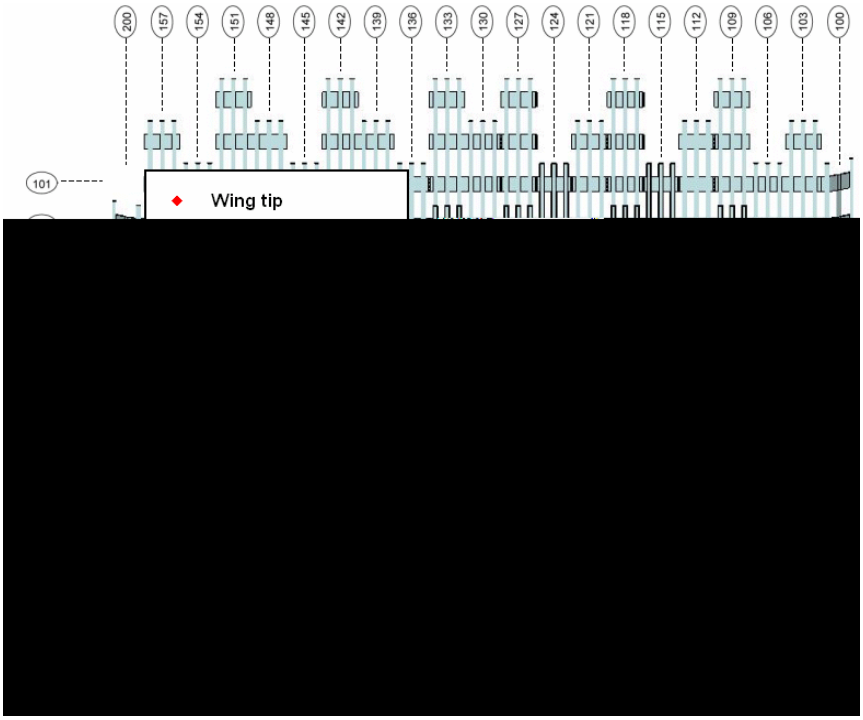

(b) Impact conditions (vertical angle = 10.6°, lateral angle = 0°)

Figure E–23. WTC1 impact conditions and the impact pattern.

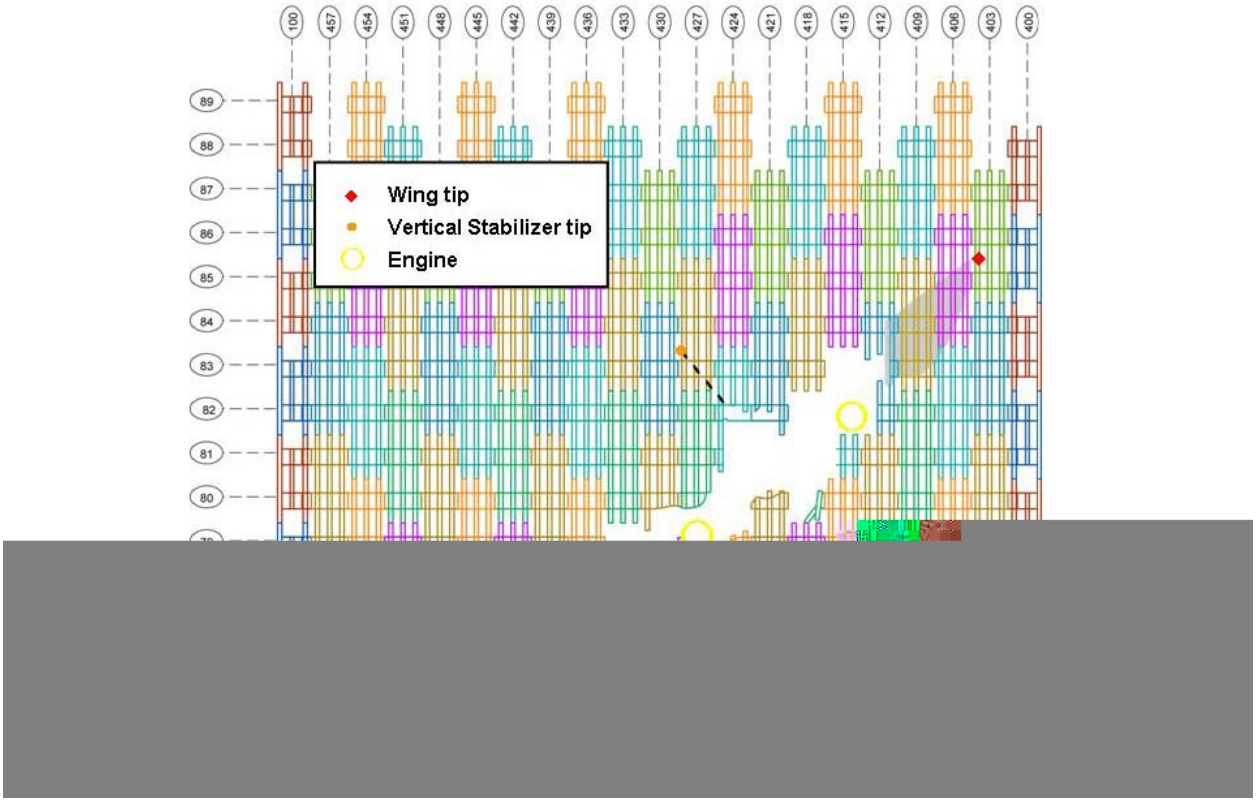

(a) Impact damage

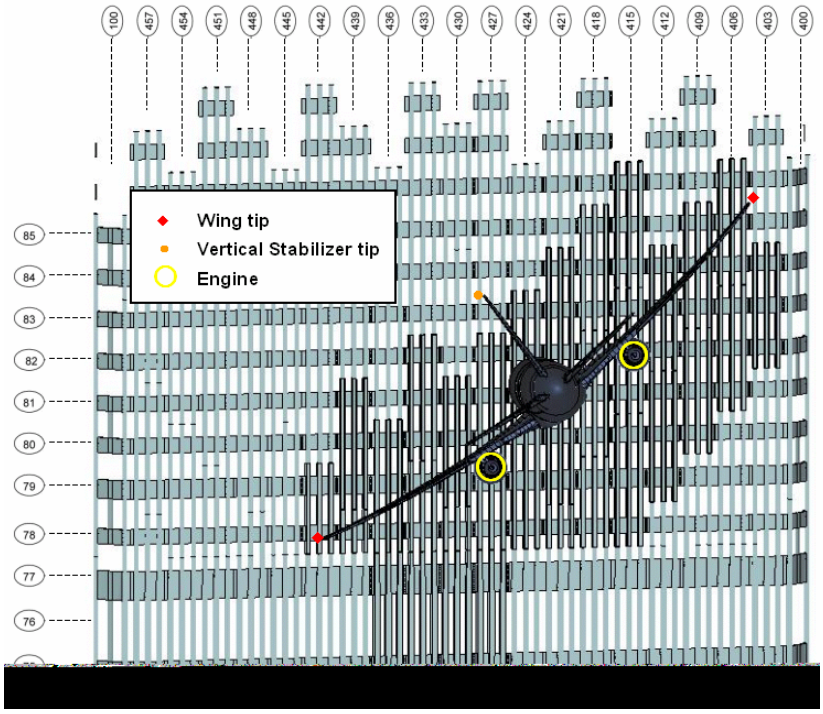

(b) Impact conditions (vertical angle = 6°, lateral angle = 13°)

Figure E–24. WTC 2 impact conditions and the impact pattern.

Table E–8. Summary of refined aircraft impact conditions.

	AA 11 (WTC 1)	UAL 175 (WTC 2)
Impact Speed (mph)	443 ± 30	542 ± 24
Vertical Approach Angle (Velocity vector)	10.6° ± 3° below horizontal (heading downward)	6° ± 2° below horizontal (heading downward)
Lateral Approach Angle (Velocity vector)	180.3° ± 4° clockwise from Structure North	15° ± 2° clockwise from Structure North
Vertical Fuselage Orientation Relative to Trajectory	2° nose-up from the vertical approach angle	1° nose-up from the vertical approach angle
Lateral Fuselage Orientation Relative to Trajectory	0° clockwise from lateral approach angle	-3° clockwise from lateral approach angle
Roll Angle (left wing downward)	25° ± 2°	38° ± 2°

E.7 GLOBAL IMPACT ANALYSES

The objective of these analyses was to estimate the condition of the two WTC towers immediately following the aircraft impacts. This assessment included the estimation of the structural damage that degraded their strength and the condition and position of nonstructural contents such as partitions, workstations, aircraft fuel, and other debris that influenced the behavior of the subsequent fires in the towers. The global impact analyses were the primary method by which the damage to the towers was estimated. The global impact simulations provided, for each tower, a range of damage estimates. These included a base case based on reasonable initial estimates of all input parameters, along with a less severe and a more severe damage scenario. The less severe damage case did not meet two key observables: (1) no aircraft debris was calculated to exit the side opposite to impact and most of the debris was stopped prior to reaching that side, in contradiction to what was observed in photographs and videos of the impact event and (2) The subsequent structural response analyses of the damaged towers indicated that the towers would not have collapsed had the less severe damage results been used. As a result, this report provides detailed description of the results of the analyses pertaining to the base and the more severe cases, which were used as the initial conditions for the subsequent fire dynamics simulations, thermal analyses, and fire-structural response and collapse initiation analyses. Only a brief description is provided for the less severe damage results for comparison purposes.

E.7.1 WTC 1 Base Case Impact Analysis

The combined aircraft and tower model for the base case WTC 1 global impact analysis is shown in Figure E–25. The base case impact analysis was performed for a 0.715 s duration following initial impact of the aircraft nose with the north exterior wall. The analysis was performed on a computer cluster using twelve 2.8 GHz Intel Xeon processors, each on a separate node of the cluster. The run time for this analysis was approximately two weeks. The calculations were terminated when the damage to the towers reached a steady state and the motion of the debris was reduced to a level that was not expected to produce any significant increase in the impact damage. The residual kinetic energy of the airframe components at the termination of a global impact simulation was typically less than one percent of the initial kinetic energy at impact.

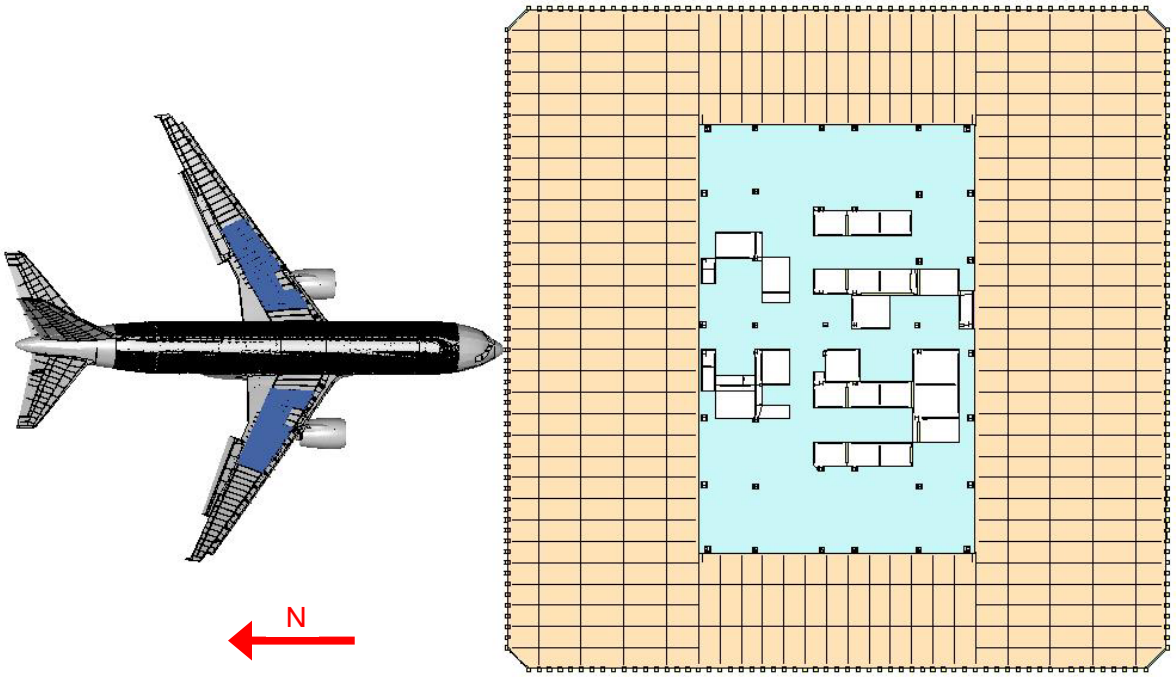

(a) Top view

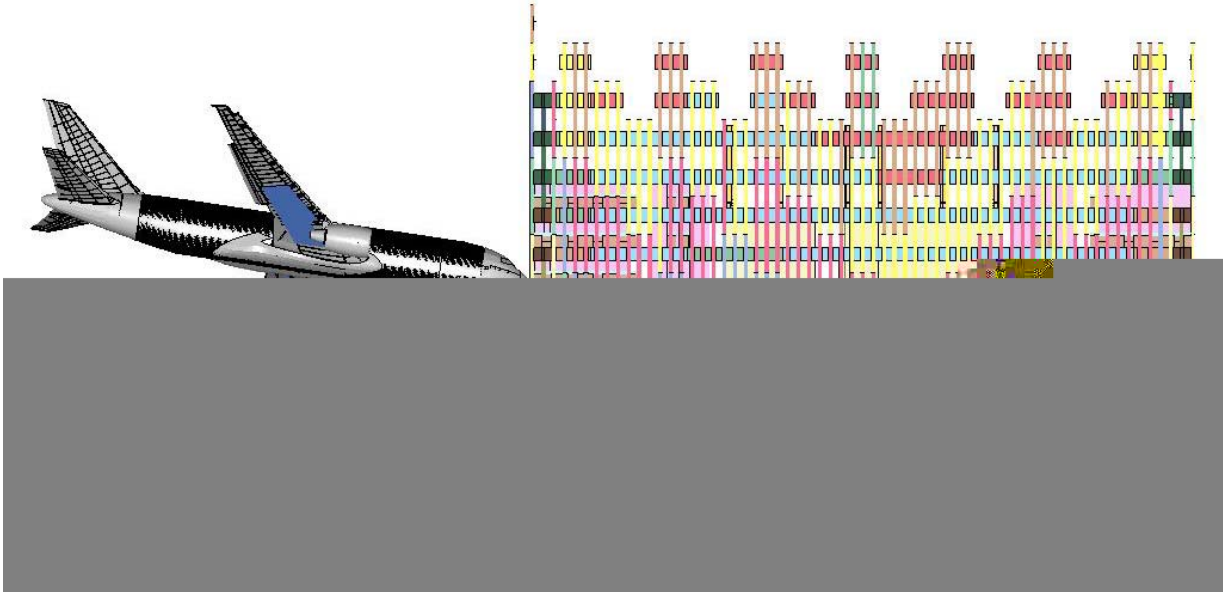

(b) Side view

Figure E–25. WTC 1 global impact model.

A side view of the base case WTC 1 global impact response is shown in Figure E–26. A corresponding top view of the impact response is shown in Figure E–27. The aircraft impact response was dominated by the impact, penetration, and fragmentation of the airframe structures. The entire aircraft fully penetrated the tower at approximately 0.25 s. The fuselage structures were severely damaged both from the penetration through the exterior columns and the penetration of the 96th floor slab that sliced the fuselage

structures in half. The downward trajectory of the aircraft structures caused the airframe to collapse against the floor, and the subsequent debris motion was redirected inward along a more horizontal trajectory parallel to the floor. The downward trajectory of the aircraft structures transferred sufficient vertical load such that the truss floor structures on the 95th and 96th floors collapsed in the impact zone.

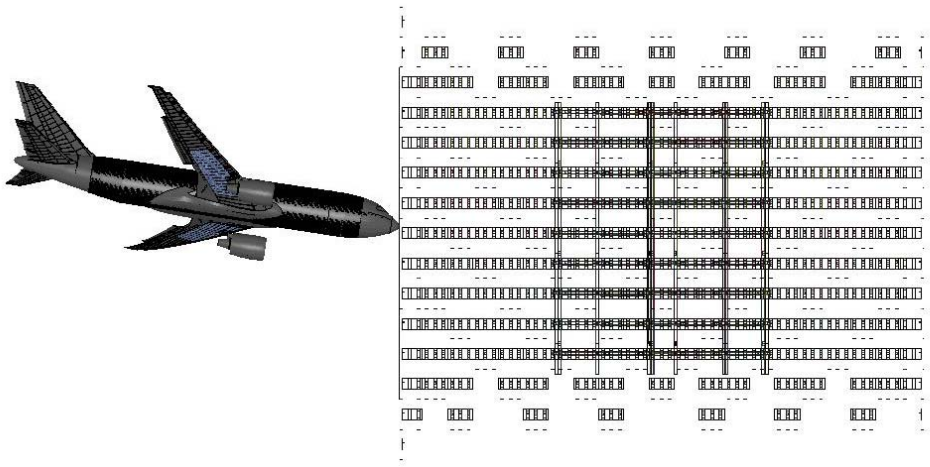

(a) Time=0.00 s

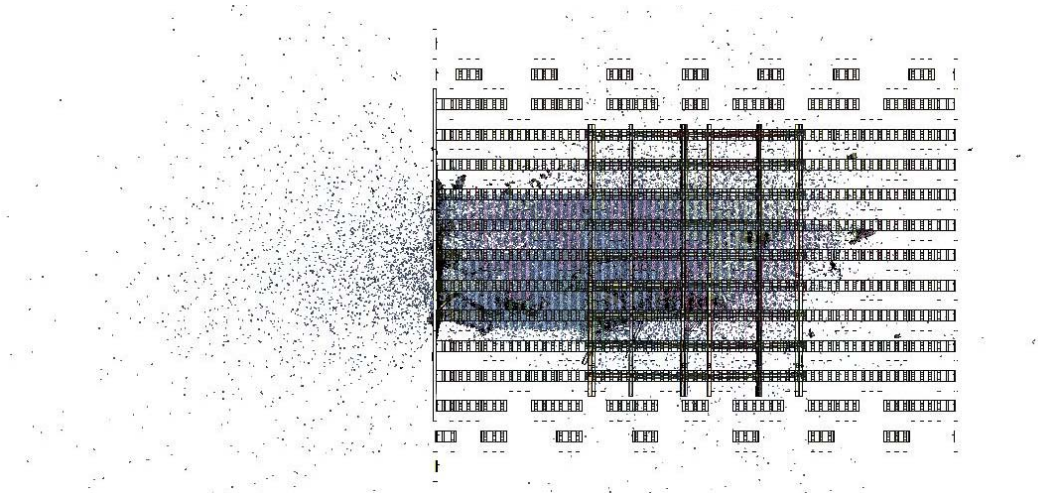

(b) Time=0.50 s

Figure E–26. WTC 1 base case global impact analysis – side view.

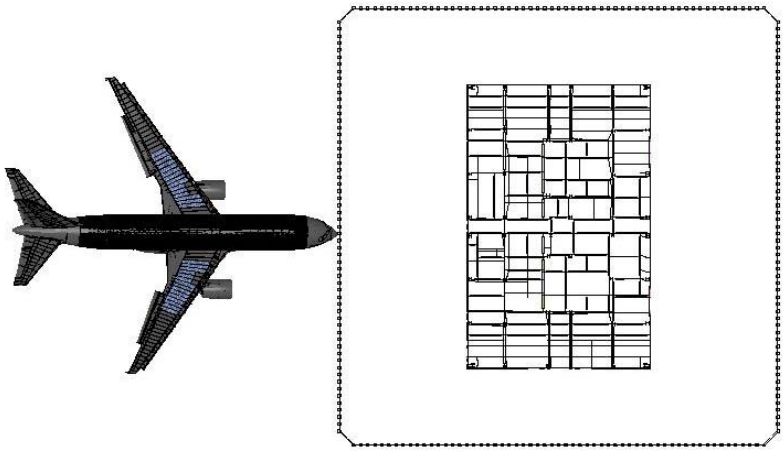

(a) Time=0.00 s

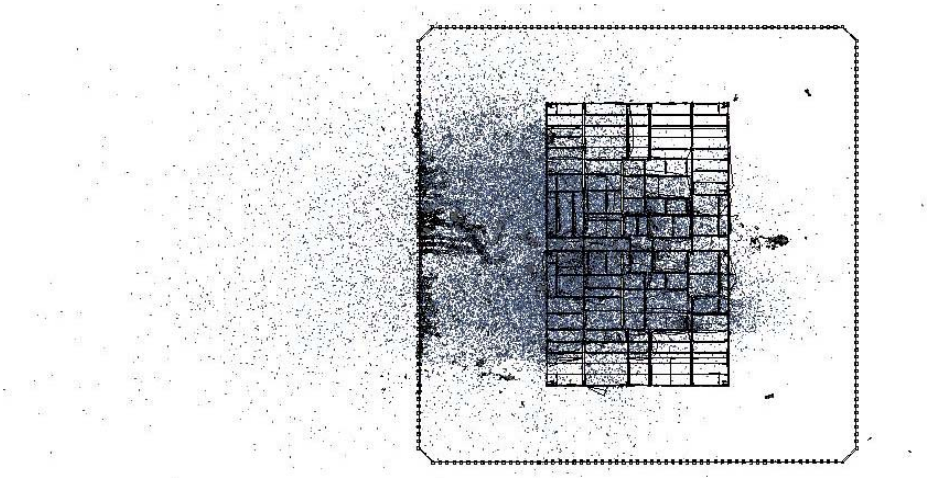

(b) Time=0.50 s

Figure E–27. WTC 1 base case global impact analysis – top view.

The wing structures were completely fragmented by the exterior wall. The aircraft fuel cloud began to spread out after impact but remained relatively dense until the leading edge of the fuel reached the tower core. The aircraft fuel and debris cloud eventually penetrated most of the distance through the core before their motion was halted.

The aircraft was severely broken into debris as a result of the impact with the tower. At the end of the impact analysis, the aircraft was broken into thousands of debris fragments of various sizes and masses. Larger fragments still existed for specific components, such as the engines. At the end of the simulation, the port engine was still inside the core, and the starboard engine was roughly one third of the distance from the core to the south exterior wall. Each had a speed of less than 50 mph.

Exterior Wall Damage

The exterior wall was the one structural system for which direct visual evidence of the impact damage was available. Therefore, the comparison of the calculated and observed exterior wall damage provided a

partial validation of the analysis methodologies used in the global impact analyses. A comparison of the north exterior wall observed and calculated damage from the base case WTC 1 global impact analysis is shown in Figure E–28. The comparison of the calculated and observed damage indicated that the geometry and location of the impact damage zone were in good agreement. This agreement in the position and shape of the impact damage served to validate the geometry of the aircraft model, including the aircraft orientation, trajectory, and flight distortions of the wings.

The comparison also indicated a good agreement in the magnitude and mode of impact damage on the exterior wall. The exterior wall completely failed in the regions of the fuselage, engine, and fuel-filled wing section impacts. Damage to the exterior wall was observed all the way out to the wing tips, but the exterior columns were not completely failed in the outer wing and vertical stabilizer impact regions. Failure of the exterior columns occurred both at the bolted connections between column ends and at various locations in the column depending on the local severity of the impact load and the proximity of the bolted connection to the impact. The agreement of both the mode and magnitude of the impact damage served to partially validate the constitutive and damage modeling of the aircraft and exterior wall of the tower.

Core Structural Damage

The estimation of the damage to the core columns and core beams was important in determining the residual strength for the subsequent analyses of structural stability and collapse. The core had significant damage in the region close to the impact point. The columns in line with the aircraft fuselage failed on the impact side, and several of the core beams were also severely damaged or failed in the impact zone.

The calculated damage to the core columns by row is shown in Figure E–29. A total of three columns were severed, and four columns were heavily damaged. The damage to the core floor framing for floors 95 and 96 is shown in Figure E–30.

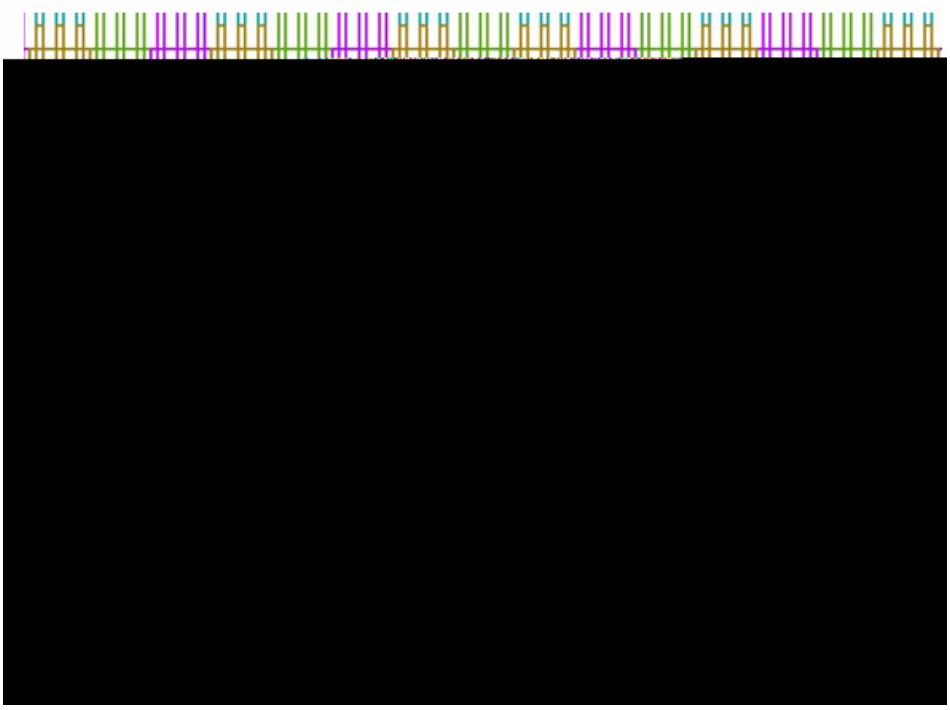

(a) Schematic of observed damage

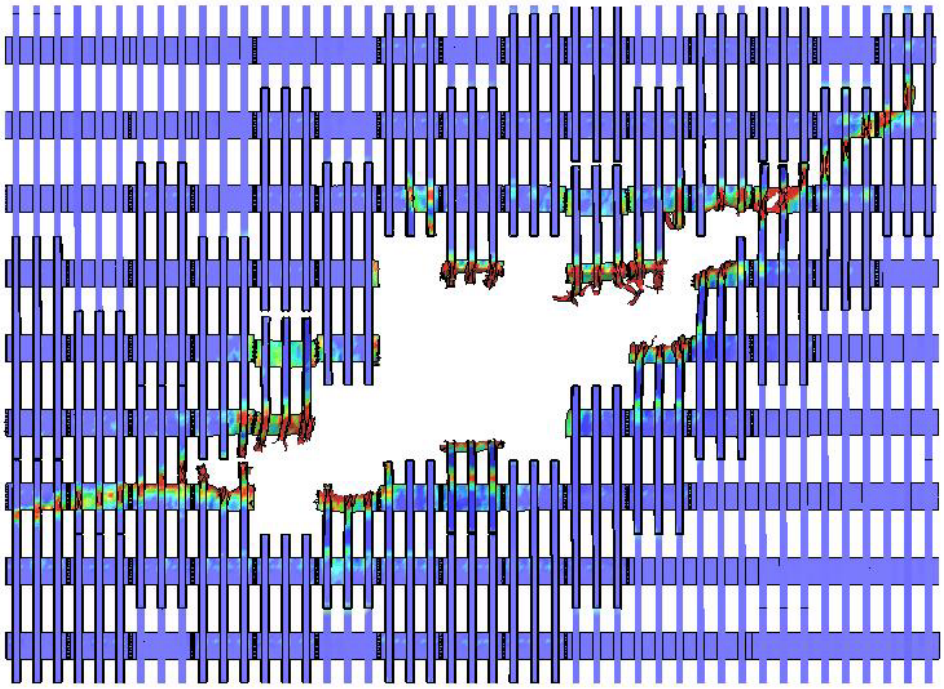

(b) Calculated damage

Figure E–28. Base case impact damage to the WTC 1 exterior wall.

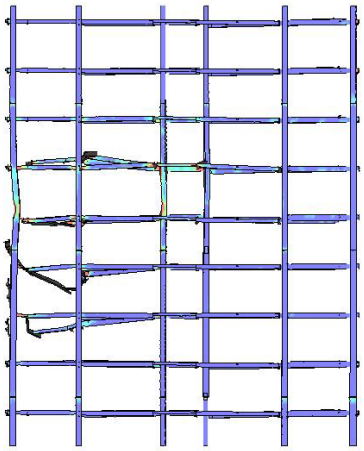

(a) Columns 503-1003

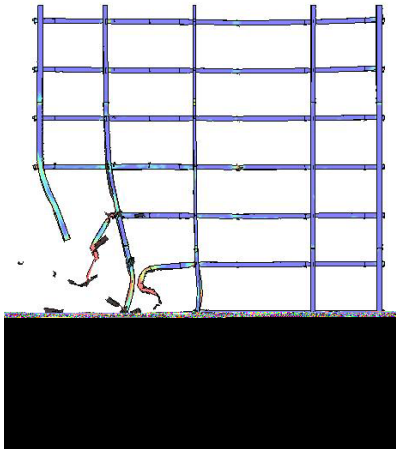

(b) Columns 504-1004

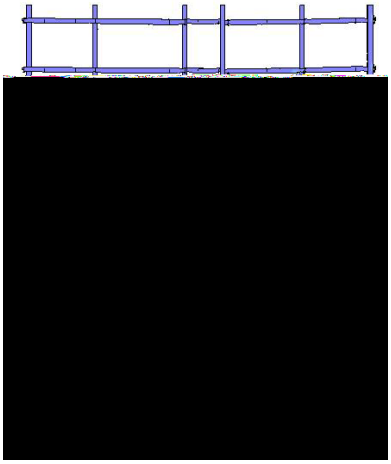

(c) Columns 505-1005

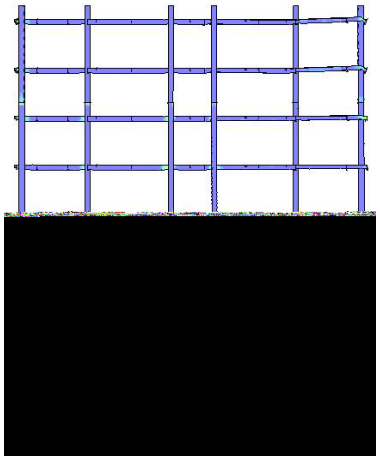

(d) Columns 506-1006

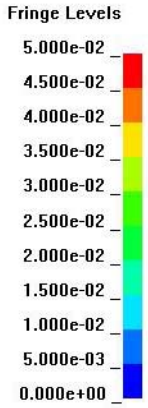

(e) Reference scale

Figure E–29. Base case impact damage to the WTC 1 core columns.

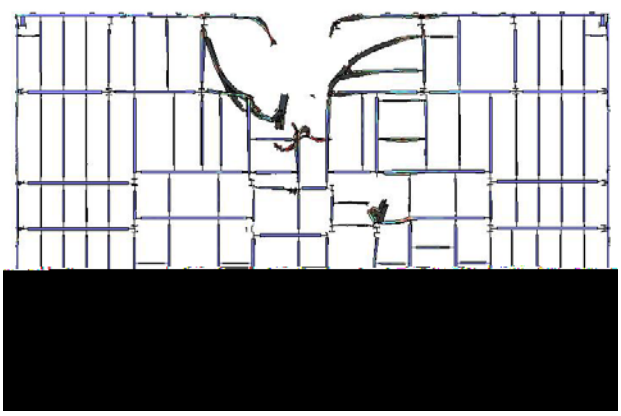

(a) Floor 95 core framing damage

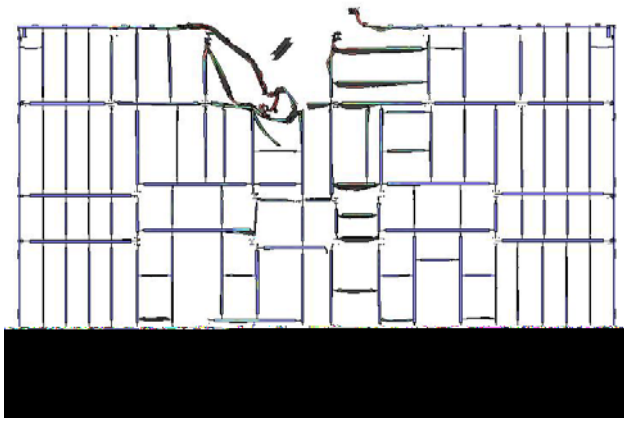

(b) Floor 96 core framing damage

Figure E–30. Base case impact damage to the core beams of floors 95 and 96 of WTC 1.

Floor Truss and Slab Damage

An overall frontal view of the floor trusses in the impact zone, along with the calculated impact damage to the floor trusses, is shown in Figure E–31. The figure shows that the trusses experienced significant damage and sagging in the impact zone. A plan view of the calculated damage to the trusses on floors 95 and 96 is shown in Figure E–32. The calculated impact response produced severe damage to the truss structures in the primary impact path of the fuselage from the exterior wall to the core. The truss floor system on floors 94 through 96 were damaged and sagged downward as a result of the impact loading. The calculated damage to the WTC 1 floor slab for floors 95 and 96 are shown in Figure E–33, where a similar pattern of response to that observed in the trusses can be seen for the floor slabs.

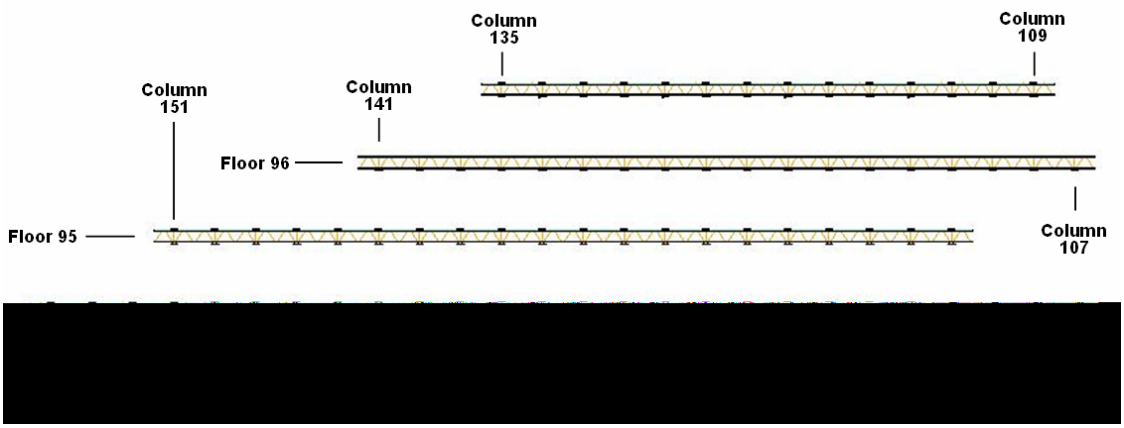

(a) Initial detailed truss structures

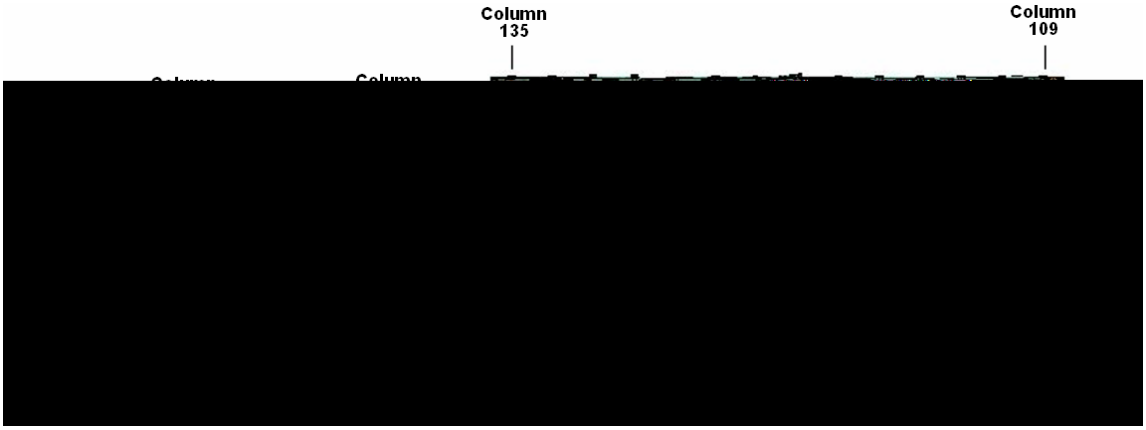

(b) Calculated damage

Figure E–31. Base case impact damage to the WTC 1 floor trusses (front view).

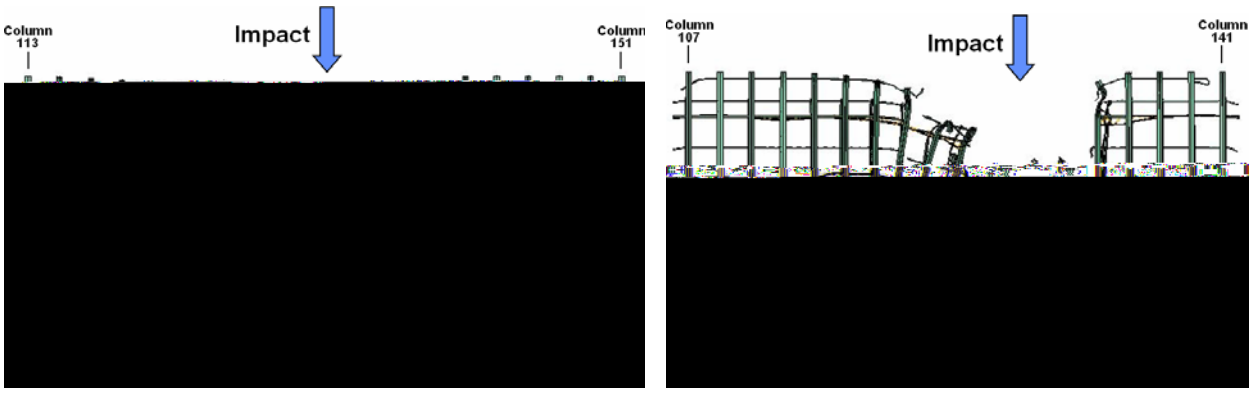

(a) Floor 95 truss damage **(b) Floor 96 truss damage**

Figure E–32. Base case impact damage to the trusses on floors 95 and 96 of WTC 1 (plan view).

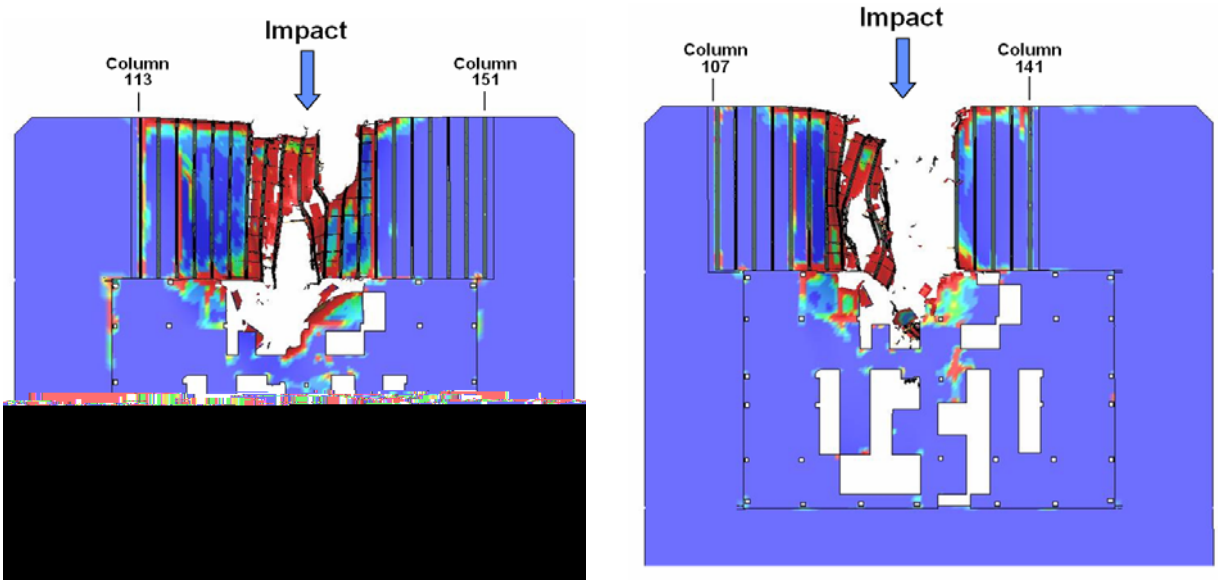

(a) Floor 95 slab damage **(b) Floor 96 slab damage**

Figure E–33. Base Case impact damage to the slabs on floors 95 and 96 of WTC 1 (plan view).

Summary of Structural Damage

The impact-induced structural damage described above was used as the initial conditions for the post-impact fire-structural analyses. Figure E–34 presents the cumulative damage on all affected floors and columns. The damage to the columns at the various levels is identified by the color of the circles, where red, blue, green, and yellow signify severed, heavily damaged, moderately damaged, and lightly damaged columns, respectively. The dotted boxes on the figures indicate areas where the impact created an opening in the floor. These were used to identify slab openings in the fire dynamics simulations. The solid boxes indicate areas in the floor system that had severe structural damage. These areas were removed from the subsequent structural analyses. Figure E–34 shows the damage to the exterior walls due to impact, based on the photographs of the north wall. Note the panel that was severed in the south

wall of the tower. While the analysis did not capture the failure of the connections at the ends of this panel due to the coarse mesh of the south wall, photographic evidence showed that this panel was knocked down by the impact. As a result, this panel was removed from the subsequent structural analyses.

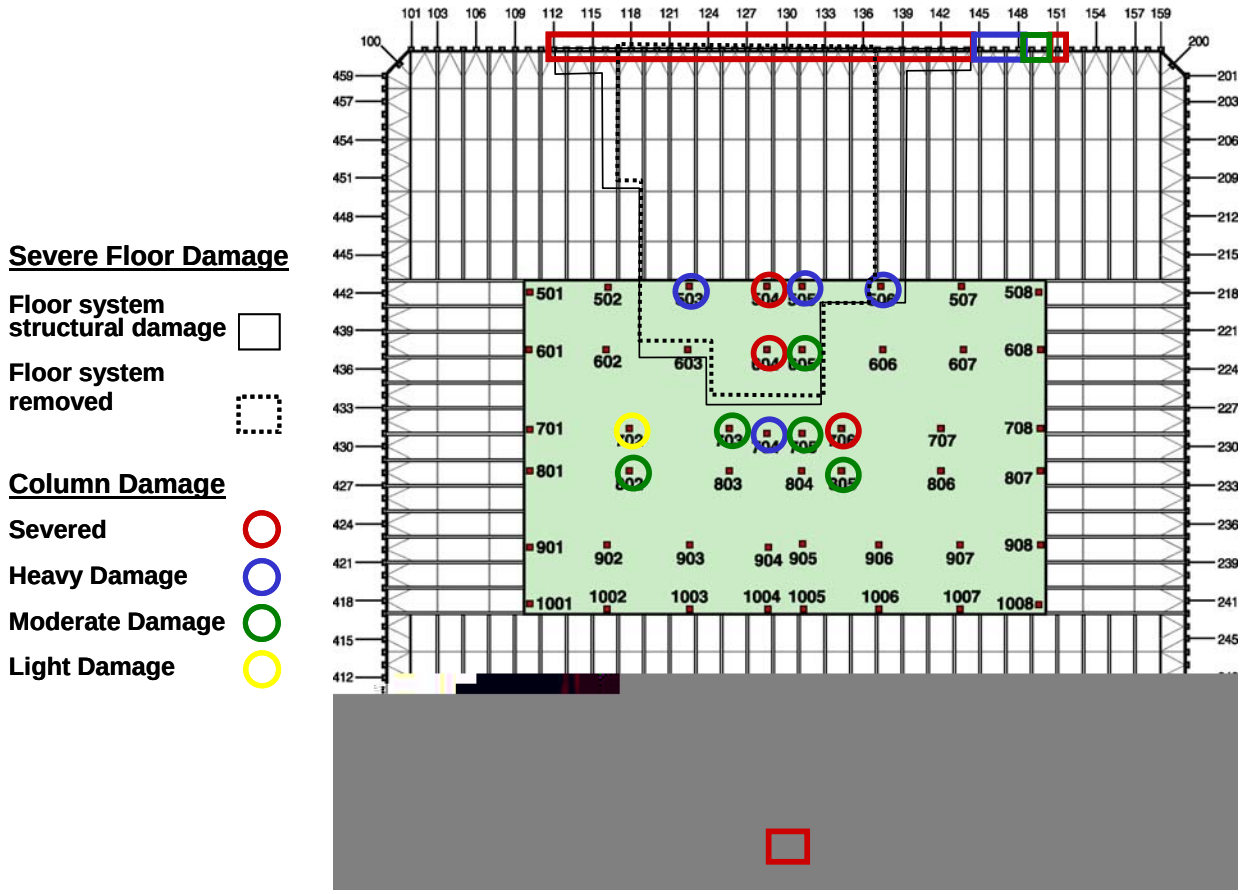

Figure E–34. Cumulative structural damage to the floors and columns of WTC 1 (base case).

Fuel and Debris Distribution

Another primary objective of the global impact analyses was to determine the initial conditions that influenced the initiation and propagation of the fires in the towers. These initial conditions included the distribution of the jet fuel in the towers, the distribution of tower contents and aircraft debris that provided flammable materials for the fires, and the condition of the partitions and walls that provided barriers to air flow and spreading of the fires. For the base case WTC 1 global impact analysis, the calculated distribution of the fuel in the tower and shape of the fuel cloud in a plan view and side view were shown previously in Figure E–26 and Figure E–27, respectively. Figure E–35 shows the distribution of the fuel and damage to the building contents due to impact.

The bulk of the fuel and aircraft debris was deposited on floors 93 through 97, with the greatest concentration on floor 94. The calculated debris cloud included 17,400 lbs of debris and 6,700 lbs of aircraft fuel outside of the tower at the end of the impact analysis, either rebounding from the impact face

(north wall) or passing through the tower (south wall). This amount might have been larger in the calculation since the exterior walls were not modeled with windows that would contain the fuel cloud and other small debris inside the towers. In addition, the impact behavior of the aircraft fuel cloud did not include the ability to stick to, or wet, interior components. Rather, the aircraft fuel SPH particles tended to bounce off of internal structures.

Figure E–35. Calculated fuel distribution and debris damage in the base case WTC 1 analysis.

d E.2(m)-2300(WTC 1)]MogurSeve no(0C Iriol)-5.2(5)1054s. l)

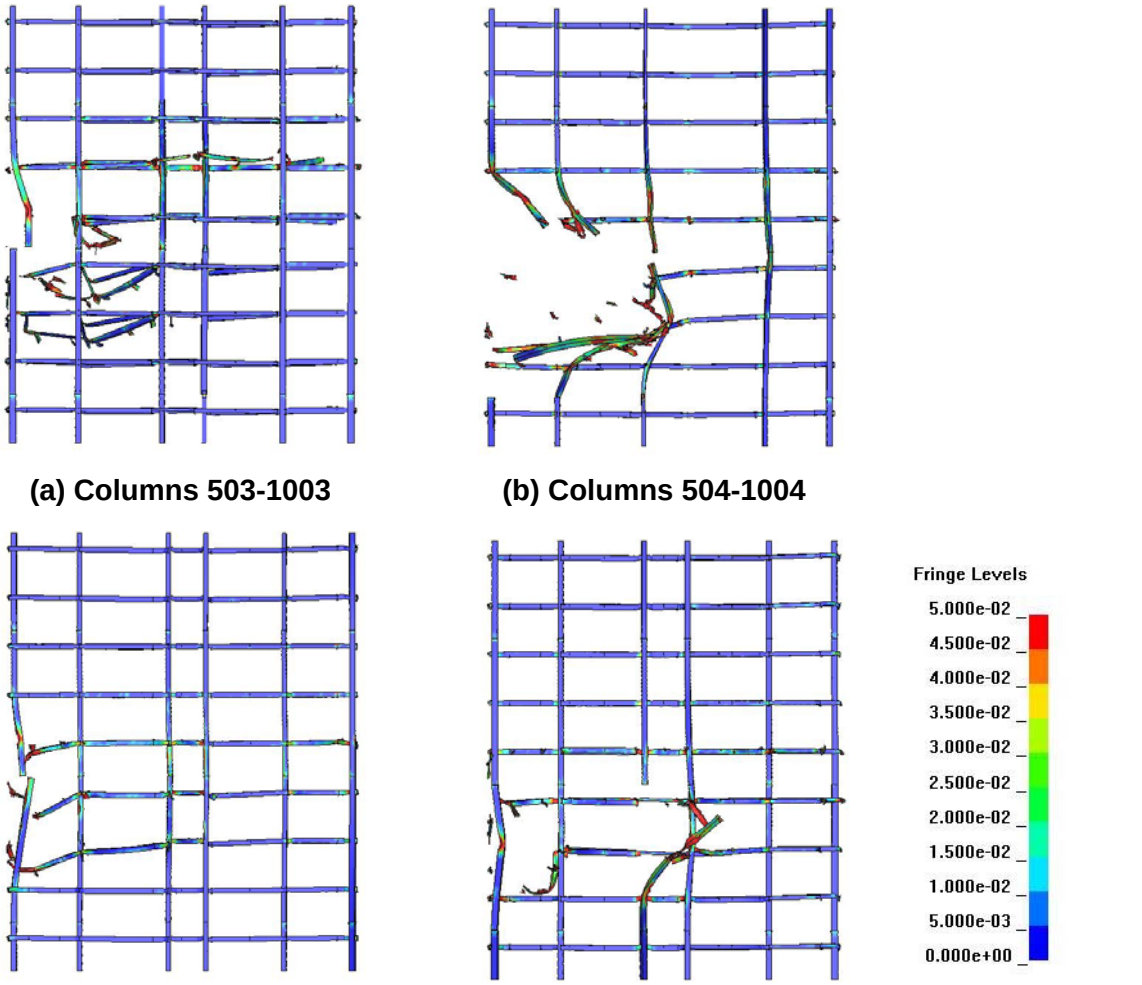

(a) Columns 503-1003 (b) Columns 504-1004

(c) Columns 505-1005 (d) Columns 506-1006 (i) Reference scale

Figure E–37. More severe impact response of the WTC 1 core columns.

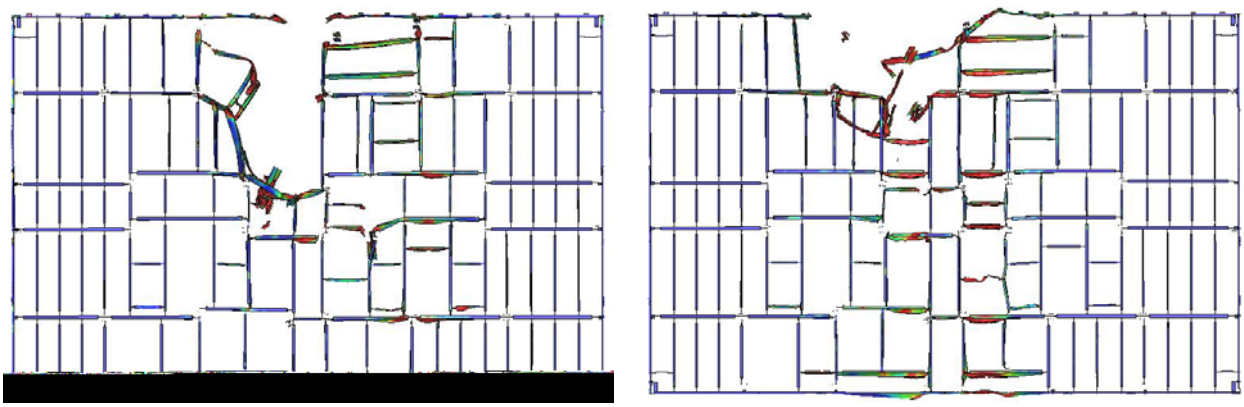

(a) Floor 95 core framing damage (b) Floor 96 core framing damage

Figure E–38. More severe impact damage to the core beams of floors 95 and 96 of WTC 1.

Floor Truss and Slab Damage

An overall frontal view of the calculated more severe impact damage to the floor trusses is shown in Figure E–39. The figure shows that the trusses experienced significant damage in the impact zone. A plan view of the calculated damage to the truss on floors 95 and 96 is shown in Figure E–40. The calculated impact response produced severe damage to the truss structures in the primary impact path of the fuselage from the exterior wall to the core. The truss floor system on floors 94 through 96 were damaged and sagged downward as a result of the impact loading.

When the floor-by-floor damage was compared for the base case and more severe impact analyses, the damage appeared to be slightly less for the more severe impact analysis. The parameters used in the more severe global impact analysis would primarily contribute to an increased damage magnitude for the tower structures. However, the downward impact trajectory angle was reduced from the 10.6 degree angle in the base case analysis to a 7.6 degree angle in the more severe impact analysis. This would have the effect of directing more of the impact energy inward toward the tower core but reducing the normal downward force on the floor structures in the impact zone. As a result, the combined effects of the analysis parameter variations produced slightly less damage to the truss structure in the more severe impact analysis scenario.

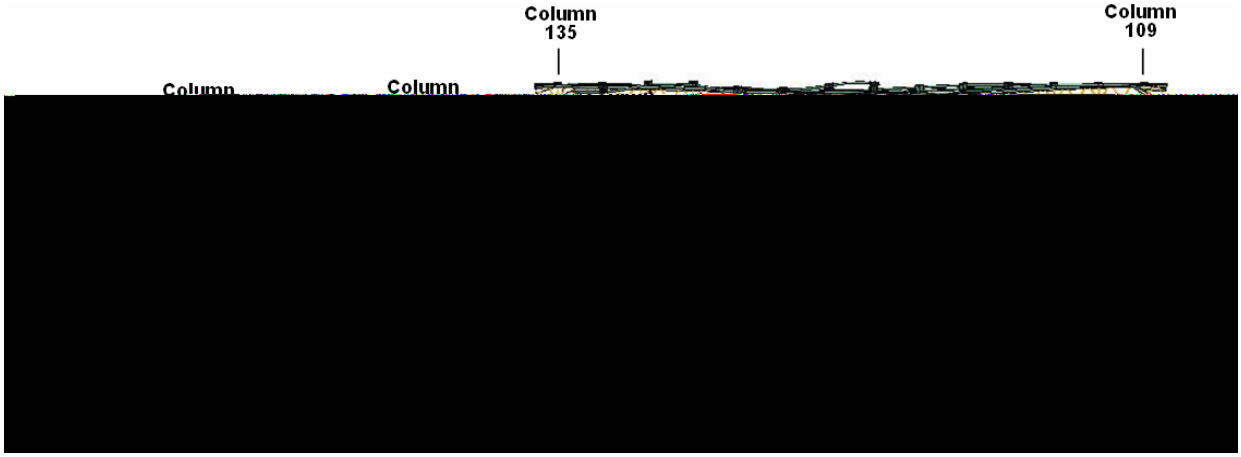

Figure E–39. Calculated more severe impact damage to the WTC 1 floor trusses (front view).

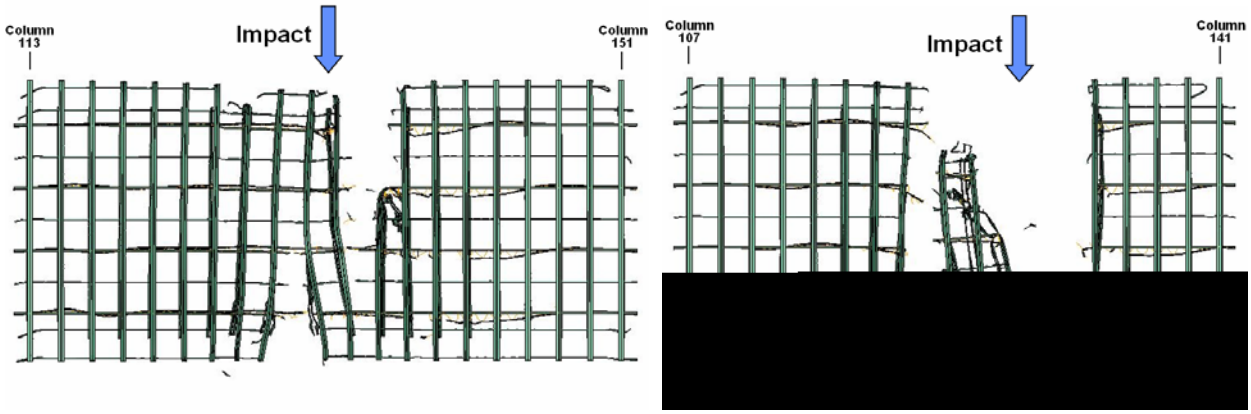

(a) Floor 95 truss damage **(b) Floor 96 truss damage**

Figure E–40. More severe impact damage to the trusses on floors 95 and 96 of WTC 1 (plan view).

The calculated more severe impact damage to the floor slabs for floors 95 and 96 of WTC 1 is shown in Figure E–41. The magnitude of floor slab damage was, in general, very similar for the base case and more severe global impact analyses. When the floor-by-floor damage was compared for the two analyses, the damage appeared to be slightly less for the more severe impact analysis. Similar to the truss damage, the reduced damage in the floor slabs is believed to be the result of the reduction in the downward impact trajectory angle from 10.6 to 7.6 degrees in the more severe impact analysis, reducing the normal downward force on the floor structures.

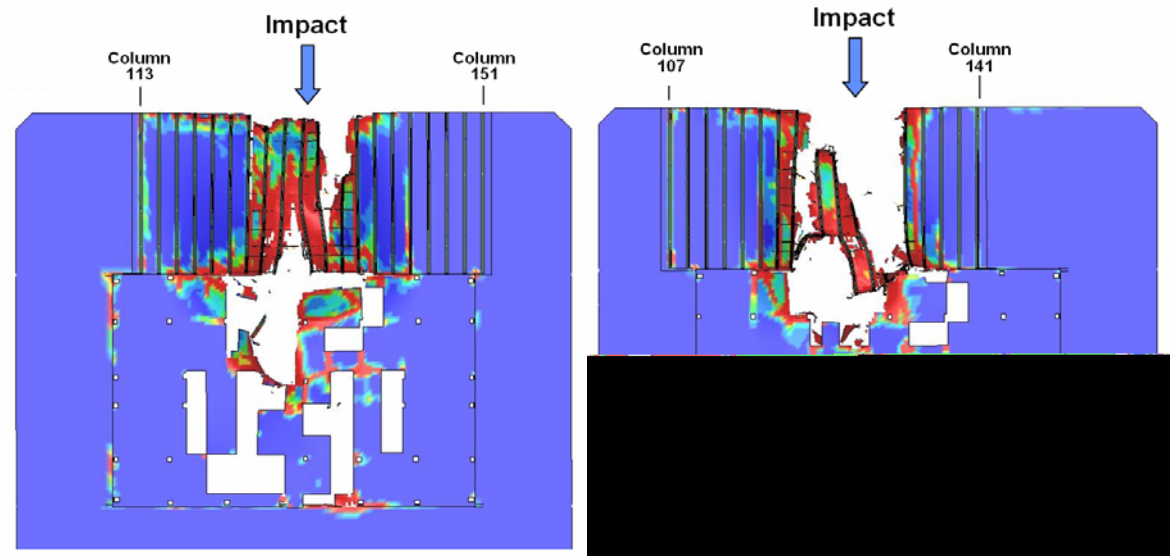

(a) Floor 95 slab damage **(b) Floor 96 slab damage**

Figure E–41. More severe impact damage to the slabs on 1 floors 95 and 96 of WTC 1 (plan view).

Summary of Structural Damage

Figure E–42 presents the cumulative damage to WTC 1 on all affected floors and columns for the more severe case.

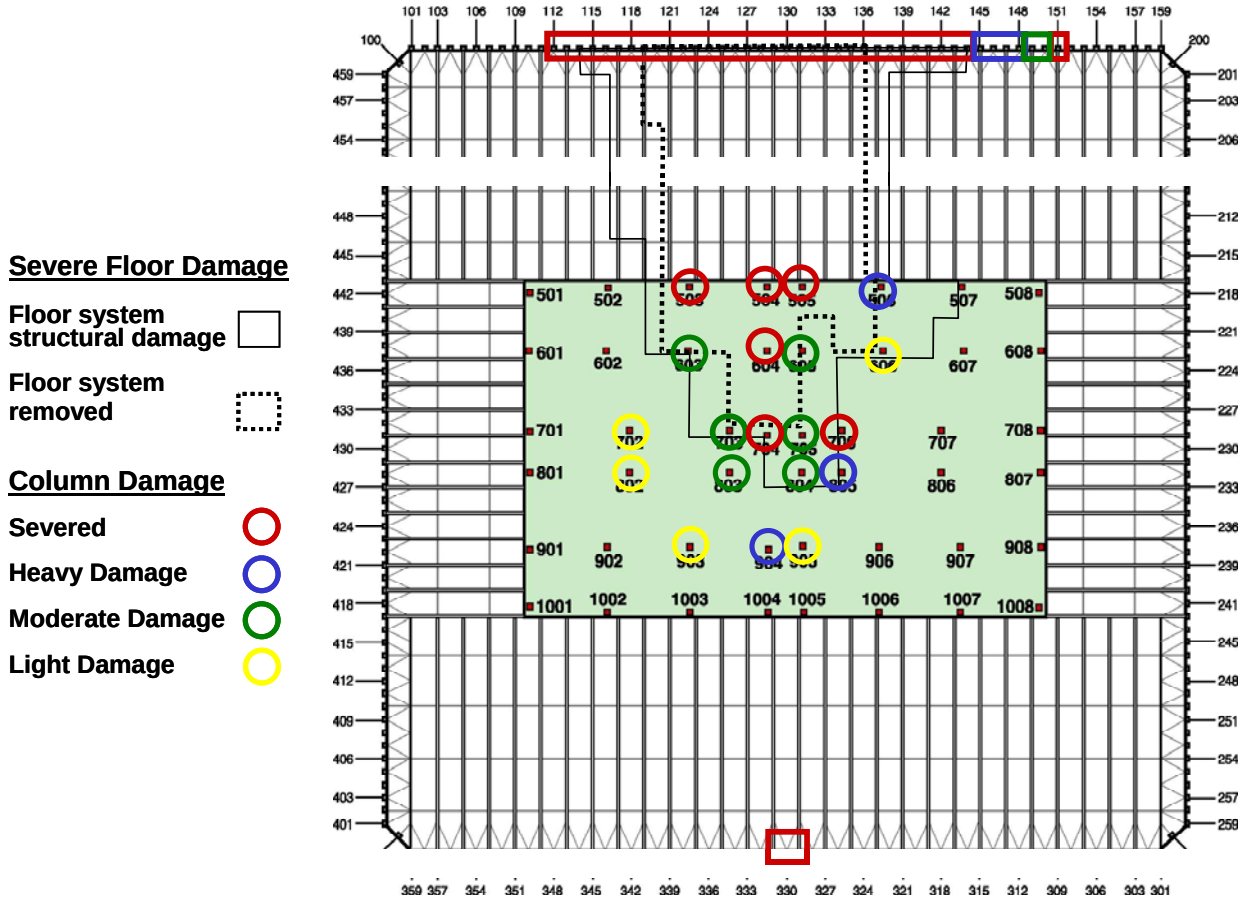

Figure E–42. Cumulative structural damage to the floors and columns of WTC 1 (more severe case).

Fuel and Debris Distribution

The distribution of the fuel in the tower calculated from the more severe case is shown in Figure E–43. A comparison to the calculated damage for the base case WTC 1 impact analysis indicated that the content damage zone is very similar in width but extended further south through the tower in the more severe impact. The more severe impact produced significantly greater content damage on the far side of the core and extended more fully through the tower.

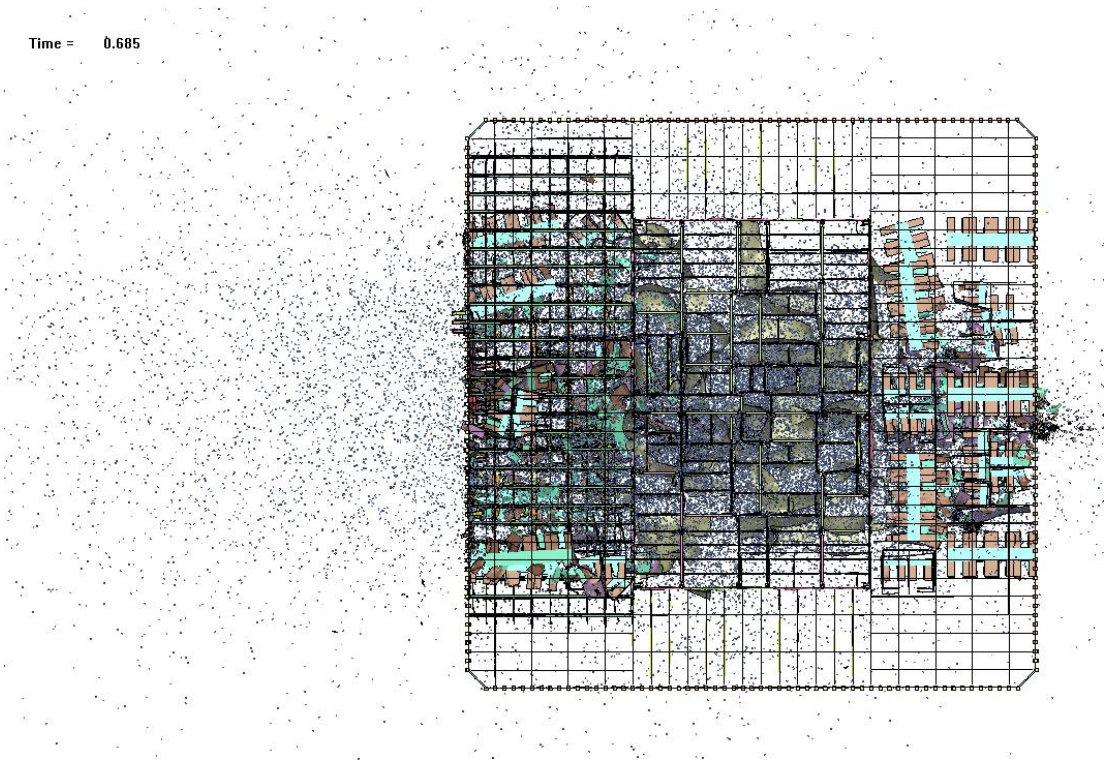

Figure E–43. Calculated fuel distribution and debris damage in the more severe WTC 1 analysis.

E.7.3 WTC 1 Less Severe Impact Analysis

For the north exterior wall of WTC 1, the magnitude and mode of impact damage were in good agreement with the observed damage for the less severe impact scenario. The core had a limited damage confined to the region nearest to the impact point. Only one column was severed, and two columns were heavily damaged for the less severe case, compared to three severed columns and four heavily damaged columns in the base case WTC 1 impact analysis.

The floor trusses experienced significant damage in the impact zone. The calculated impact response produced severe damage to the truss structures in the primary impact path of the fuselage. The truss structures were severely damaged from the exterior wall to the core. The truss floor system on floors 94 through 96 were damaged and sagged downward as a result of the impact loading. When compared with the base case, the magnitude of damage to the floor trusses and floor slabs was slightly increased for the less severe impact analysis. The parameters used in the less severe global impact analysis would primarily contribute to a reduced damage magnitude for the tower structures. However, the downward impact trajectory angle was increased from the 10.6 degree angle in the base case analysis to a 13.6 degree angle in the more severe impact analysis. This would have the effect of directing more of the impact energy downward, increasing the normal force on the floor structures in the impact zone. As a result, the combined effects of the analysis parameter variations produced a small increase in the damage to the truss structure in the less severe impact analysis scenario.

A comparison to the base case and less severe case indicated that the building contents damage zone was very similar in width but did not extend as far through the tower in the less severe impact. The less severe

impact produced little content damage on the far side of the core and did not extend fully through the tower. No debris penetration of the south wall of the tower was observed for the less severe impact condition.

E.7.4 WTC 2 Base Case Impact Analysis

The WTC 2 base case impact analysis was performed for a 0.62 s duration following initial impact of the aircraft nose with the south exterior wall. The side view and top view of the base case WTC 2 global impact response is shown in Figure E–44 and Figure E–45, respectively. Full penetration of the aircraft into the tower was completed at 0.2 s after impact. The aircraft impact response was very similar to that of the WTC 1 impact and was dominated by the penetration and fragmentation of the airframe structures. The fuselage structures were severely damaged both from the penetration through the exterior columns and the penetration of the 81st floor slab that sliced the fuselage structures in half. The downward trajectory of the aircraft structures caused the airframe to collapse against the floor, and the subsequent debris motion was redirected inward along a more horizontal trajectory parallel to the floor. The downward trajectory of the aircraft structures transferred sufficient vertical load that the truss floor structures on the 80th and 81st floors began to collapse in the impact zone by the end of the simulation.

The aircraft wing structures and fuel tank were fragmented by the impact with the tower exterior. The aircraft fuel cloud started to spread out immediately after impact, but the leading edge of the fuel remained relatively dense until passing approximately one-third of the lateral distance through the tower core (approximately 0.2 s after impact). At 0.3 s after impact, the aircraft fuel cloud had penetrated approximately two-thirds the distance through the core and was spreading out. Beyond this time, the subsequent motion of the aircraft fragments and fuel debris cloud was noticeably slowed. The spread of the fuel and debris cloud was more rapid and extensive in the open truss floor regions than through the core as a result of the open volume above the workstations in the truss floor zone.

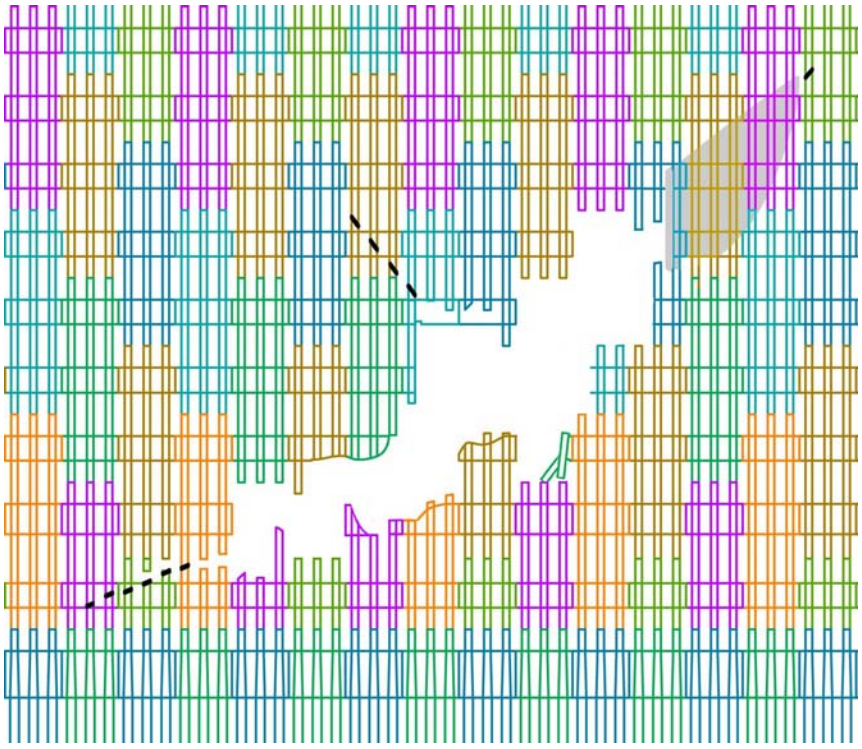

(a) Schematic of observed damage

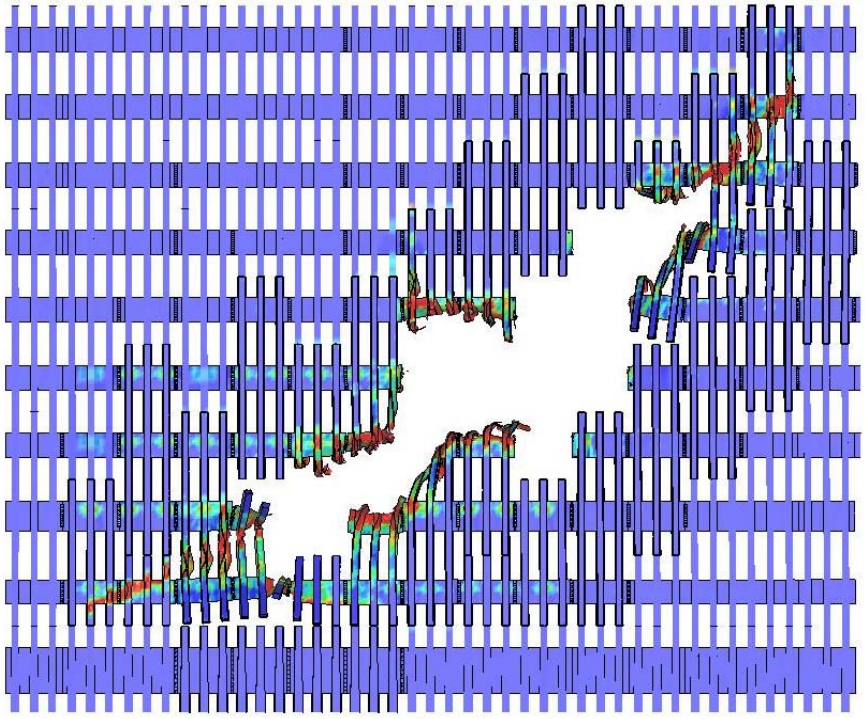

(b) Calculated damage

Figure E–46. Base case impact damage to the WTC 2 exterior wall.

Core Structural Damage

The core had significant damage in the region close to the impact point, in particular the southeast corner of the core. The columns in line with the aircraft fuselage failed on the impact side, and several of the core beams were also severely damaged or failed in the impact zone. In some cases, failure of the column splices located on floors 77, 80, and 83 contributed significantly to the failure of the core columns. This was particularly true for the heavy column number 1001 at the southeast corner of the core that failed at the three splice locations.

The calculated damage to the core columns by row is shown in Figure E–47. A total of five columns were severed, and four columns were heavily damaged. The damage to the core beams for floors 80 and 81 is shown in Figure E–48.

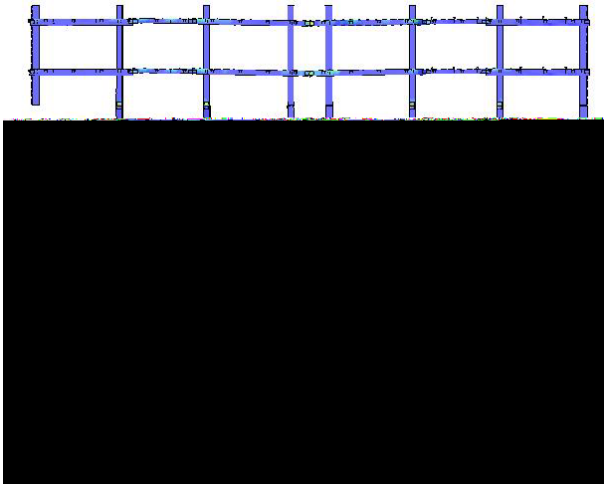

(a) Columns 1001-1008

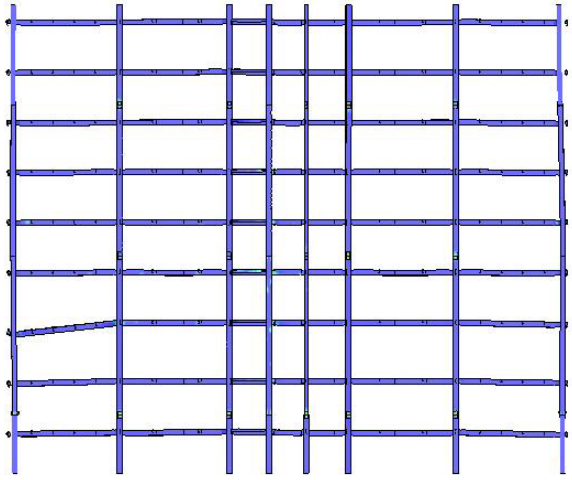

(b) Columns 901-908

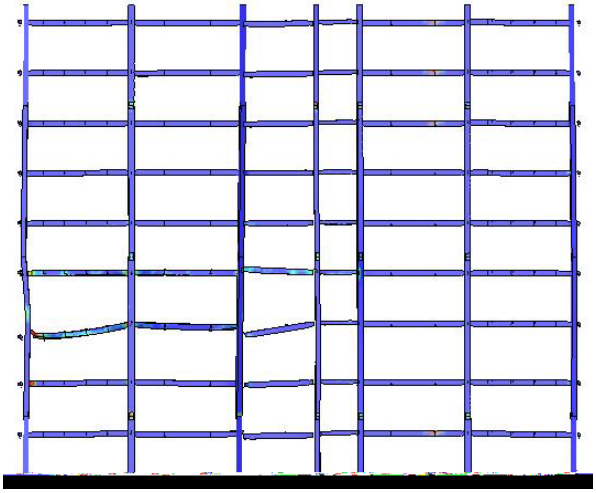

(c) Columns 801-807

(d) Columns 701-708

Figure E–47. Base case impact damage to the WTC 2 core columns.

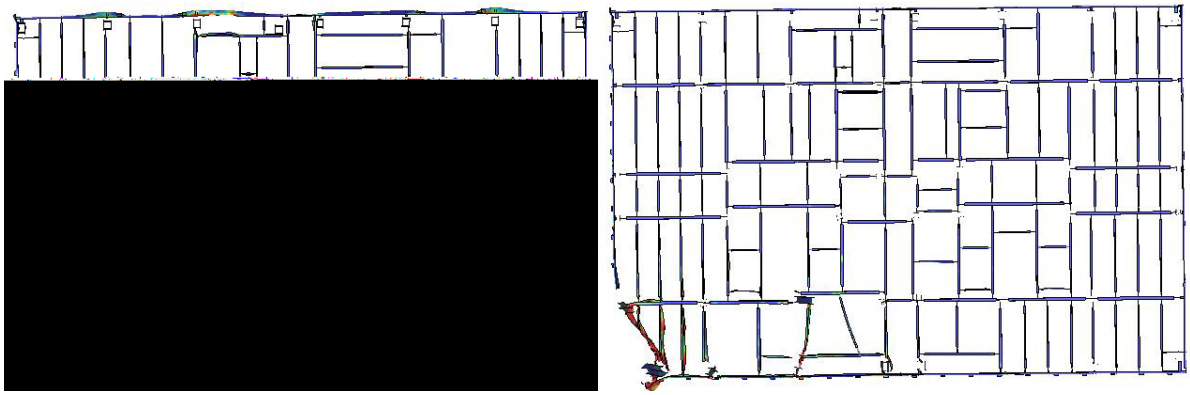

(a) Floor 80 core framing damage **(b) Floor 81 core framing damage**

Figure E–48. Base case impact damage to the core beams of floors 80 and 81 of WTC 2.

Floor Truss and Slab Damage

An overall frontal view for the floor truss structure in the WTC 2 impact zone, along with the calculated base case impact damage to the trusses, is shown in Figure E–49. The figure shows that the trusses experienced significant damage in the impact zone, with the largest damage on floor 81. A plan view of the calculated damage to the trusses on floors 80 and 81 is shown in Figure E–50. The calculated impact response produced severe damage to the truss structures in the primary impact path of the fuselage. The truss structures were severely damaged from the exterior wall to the core. The truss floor system on floors 79 and 81 had sufficient damage from the impact that truss floor sections sagged downward. The calculated damage to the WTC 2 floor slabs for floors 80 and 81 is shown in Figure E–51, where a similar pattern of response to that observed in the trusses can be seen for the floor slabs.

(a) Initial detailed truss structures

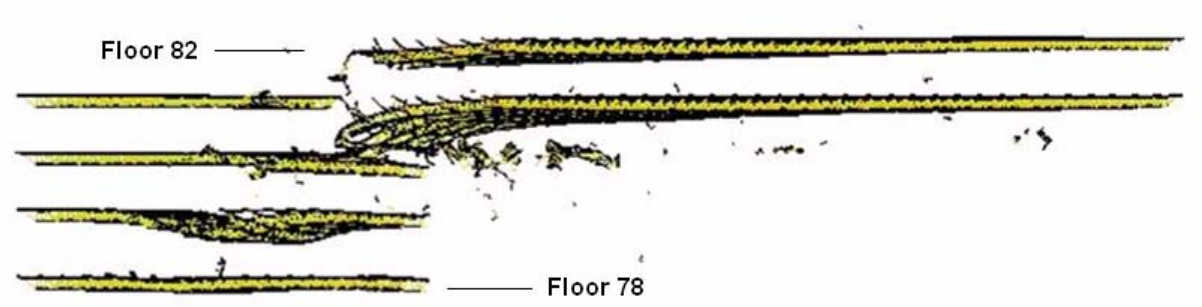

(b) Calculated damage

Figure E–49. Base case impact damage to the WTC 2 floor trusses (front view).

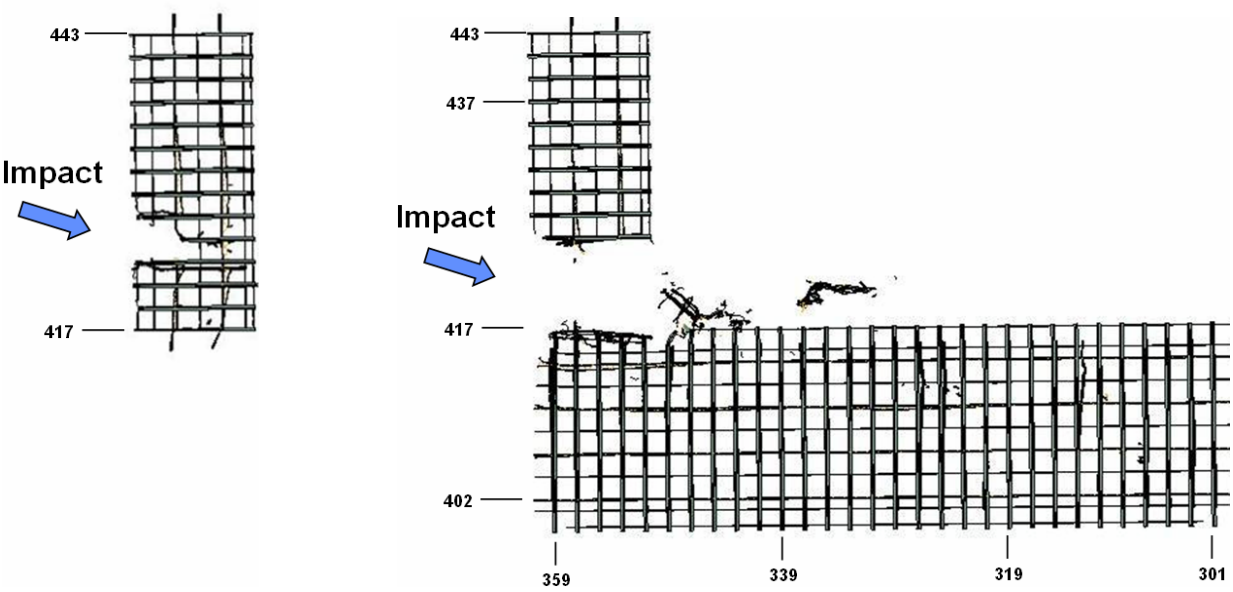

(a) Floor 80 truss damage **(b) Floor 81 truss damage**

Figure E–50. Base case impact damage to the trusses on floors 80 and 81 of WTC 2 (plan view).

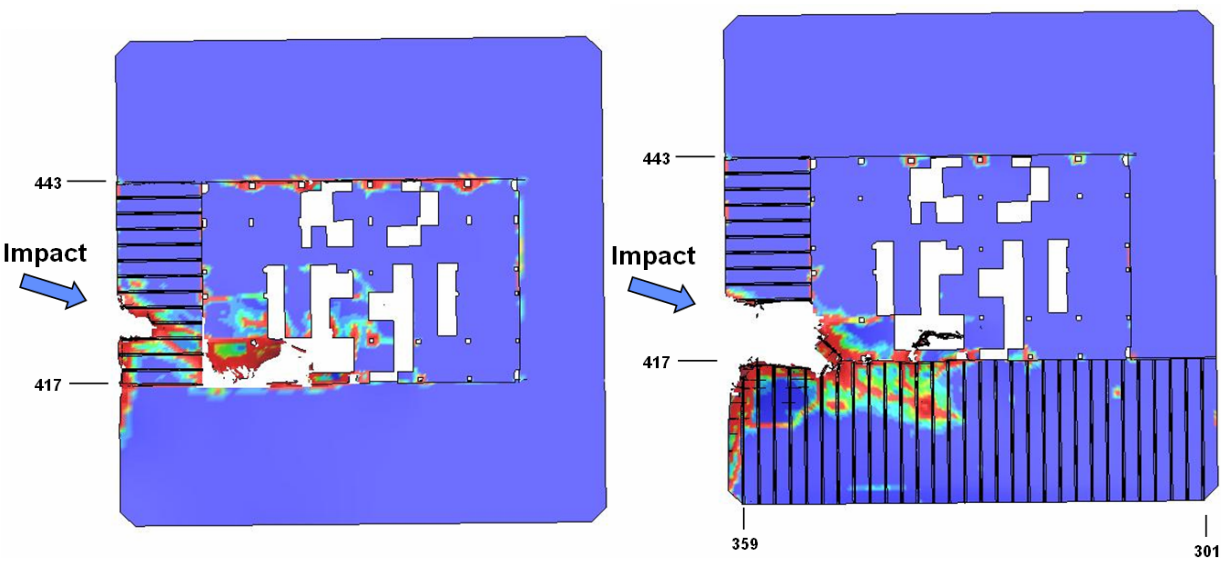

(a) Floor 80 slab damage (b) Floor 81 slab damage

Figure E–51. Base case impact damage to the slabs on floors 80 and 81 of WTC 2 (plan view).

Summary of Structural Damage

The impact-induced structural damage described above provided the initial conditions for the post-impact fire-structural analyses. Figure E–52 presents the cumulative damage on all affected floors and columns. The damage to the columns at the various levels is identified by the color of the circles, where red, blue, green, and yellow signify severed, heavily damaged, moderately damaged, and lightly damaged columns, respectively. The dotted boxes on the figures indicate areas where the impact created an opening in the floor. These were used to identify slab openings in the fire dynamics simulations. The solid boxes indicate areas in the floor system that had severe structural damage. These areas were removed from the subsequent structural analyses. Figure E–52 also shows the damage to columns on the north perimeter wall, which the analysis did not capture due to the coarse mesh on the north wall. This damage was observed in photographs. As a result, this damage was accounted for in the subsequent structural analyses.

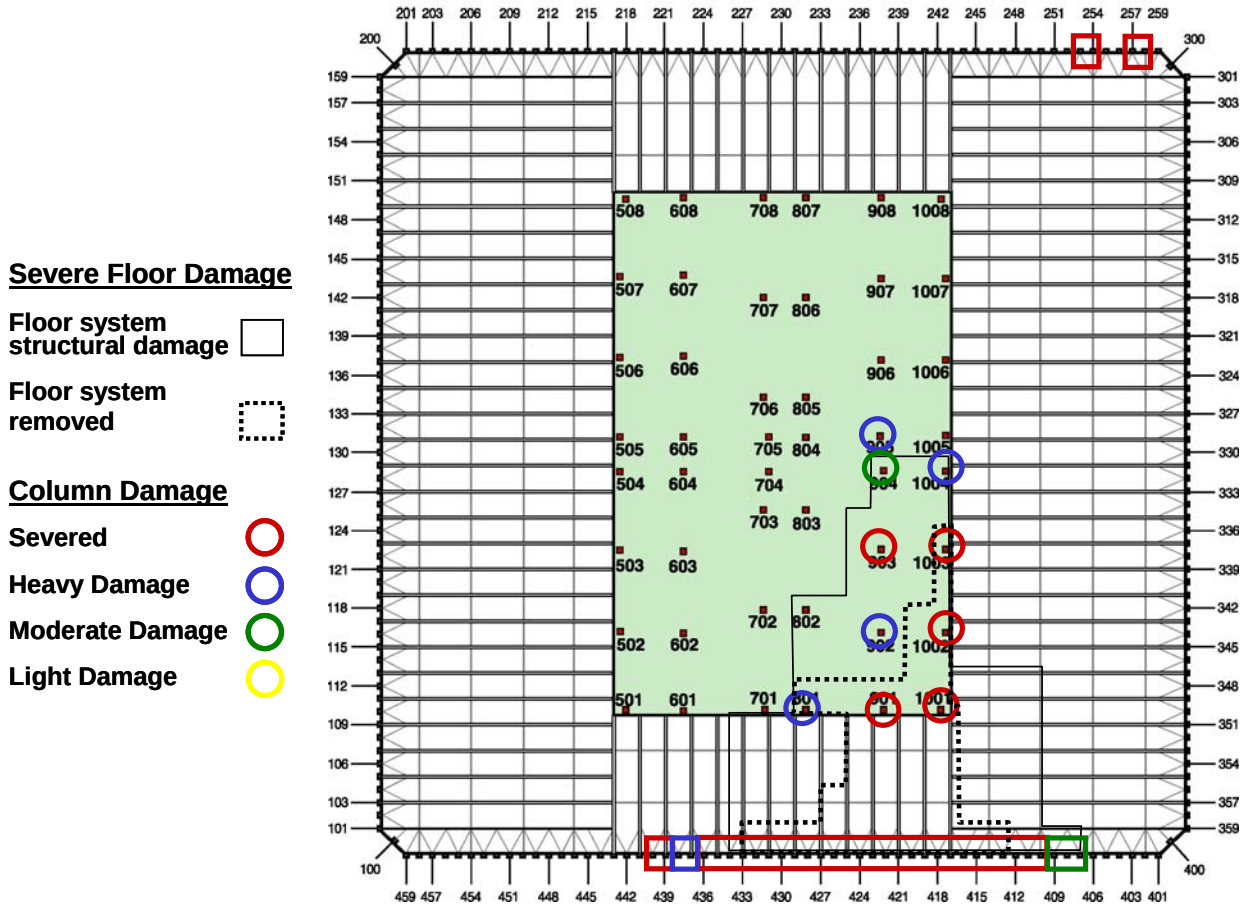

Figure E–52. Cumulative structural damage to the floors and columns of WTC 2 (base case).

Fuel and Debris Distributions

The calculated distribution of the aircraft debris and fuel cloud from the base case WTC 2 global impact analysis was shown previously in Figure E–44 and Figure E–45. Figure E–53 shows the distribution of fuel and damage to the building contents due to impact. The bulk of the aircraft debris and fuel was arrested prior to exiting the tower structures. However, a significant amount of aircraft debris was calculated to exit the north and east sides of the tower (Sides 300 and 200 of WTC 2).

The bulk of the fuel and aircraft debris was deposited in floors 78 through 80, with the greatest concentration of aircraft debris on floor 80, and the largest concentration of aircraft fuel on floors 79, 81, and 82. The calculated debris distribution included 55,800 lbs of debris and 10,600 lbs of aircraft fuel outside of the tower at the end of the impact analysis, either rebounding from the impact face or passing through the tower. The calculated mass outside the tower is believed to be larger than is realistic, since the exterior walls were not modeled with windows that could contain the fuel cloud and small debris inside the tower. In addition, treatment of the aircraft fuel cloud did not include the ability to stick to, or wet, interior components. Rather, the aircraft fuel SPH particles tended to bounce off of internal structures.

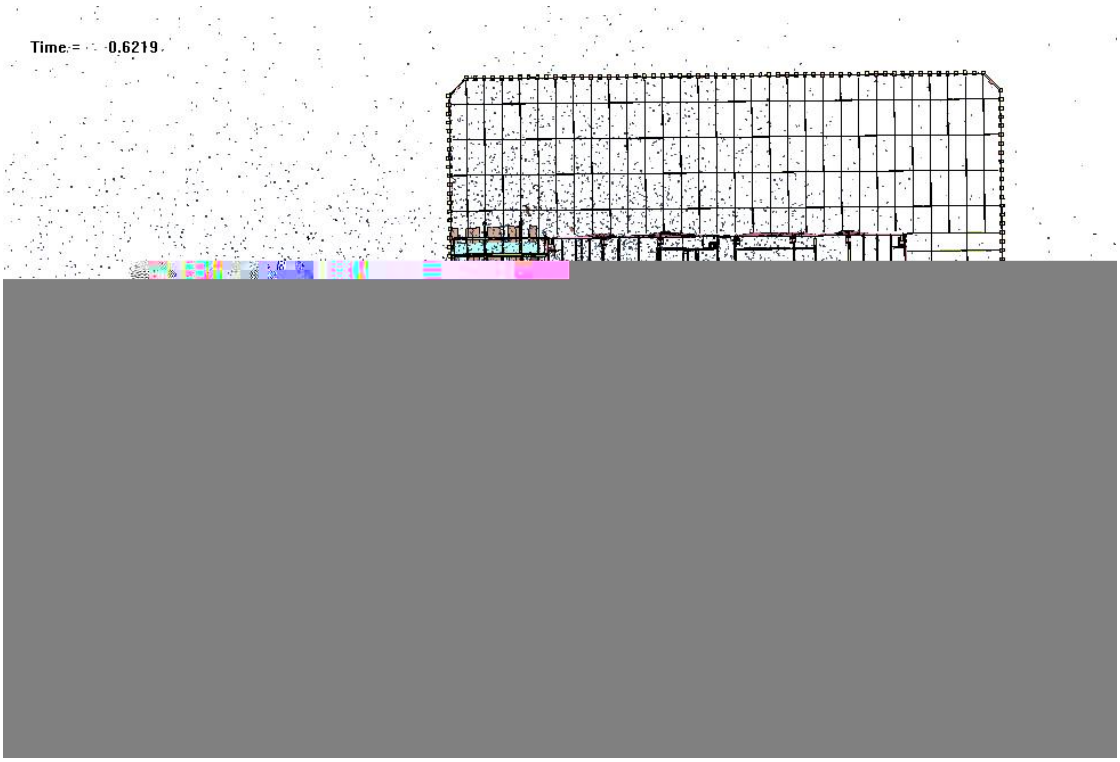

Figure E–53. Calculated fuel distribution and debris damage in the base case WTC 2 analysis.

E.7.5 WTC 2 More Severe Impact Analysis

This section summarizes the results of the more severe impact analysis for WTC 2. The parameters for the more severe and less severe damage cases for WTC 2 were similar to those for WTC 1. Section E.7.6 provides a brief description of the WTC 2 less severe case.

Exterior Wall Damage

The calculated damage to the south wall from the more severe WTC 2 global impact analysis is shown in Figure E–54. A comparison of the south exterior wall observed (Figure E–46a) and calculated (Figure E–54) damage from the more severe WTC 2 global impact analysis indicated that the calculated and observed magnitude and mode of impact damage were still in good agreement.

As was the case for WTC 1, there were small differences in the damage estimates for the south wall of WTC 2 from the base case and the more severe case scenarios (compare Figure E–46b and Figure E–54). Overall, the agreement with the observed damage from photographs was very good for both cases. The most obvious differences were largely due to portions of panels that may have severed columns in one case or have been removed at the connections in another.

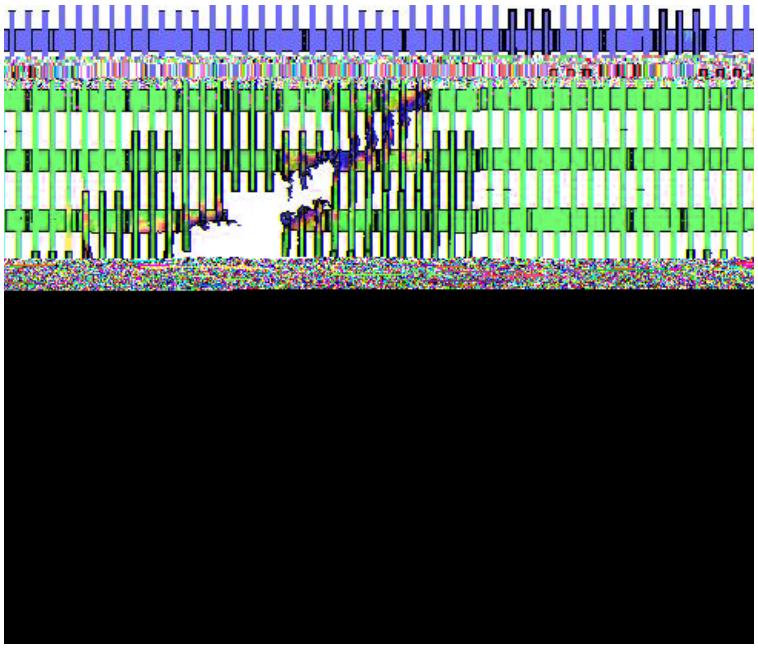

Figure E–54. Calculated more severe impact damage to the WTC 2 exterior wall.

Core Structural Damage

The core had extensive damage in the region close to the impact point. The columns in line with the aircraft fuselage failed on the impact side, and several of the core beams were also severely damaged or failed in the impact zone. In some cases, failure of the column splices located on floors 77, 80, and 83 contributed significantly to the failure of the core columns.

The calculated damage to the core columns by row is shown in Figure E–55, and the damage to the core framing at floors 80 and 81 is shown in Figure E–56. A total of ten columns were severed, and one column was heavily damaged in the WTC 2 more severe case, compared to five columns severed and four columns heavily damaged in the base case WTC 2 impact analysis. This shows a clear correlation between damage magnitude and impact severity.

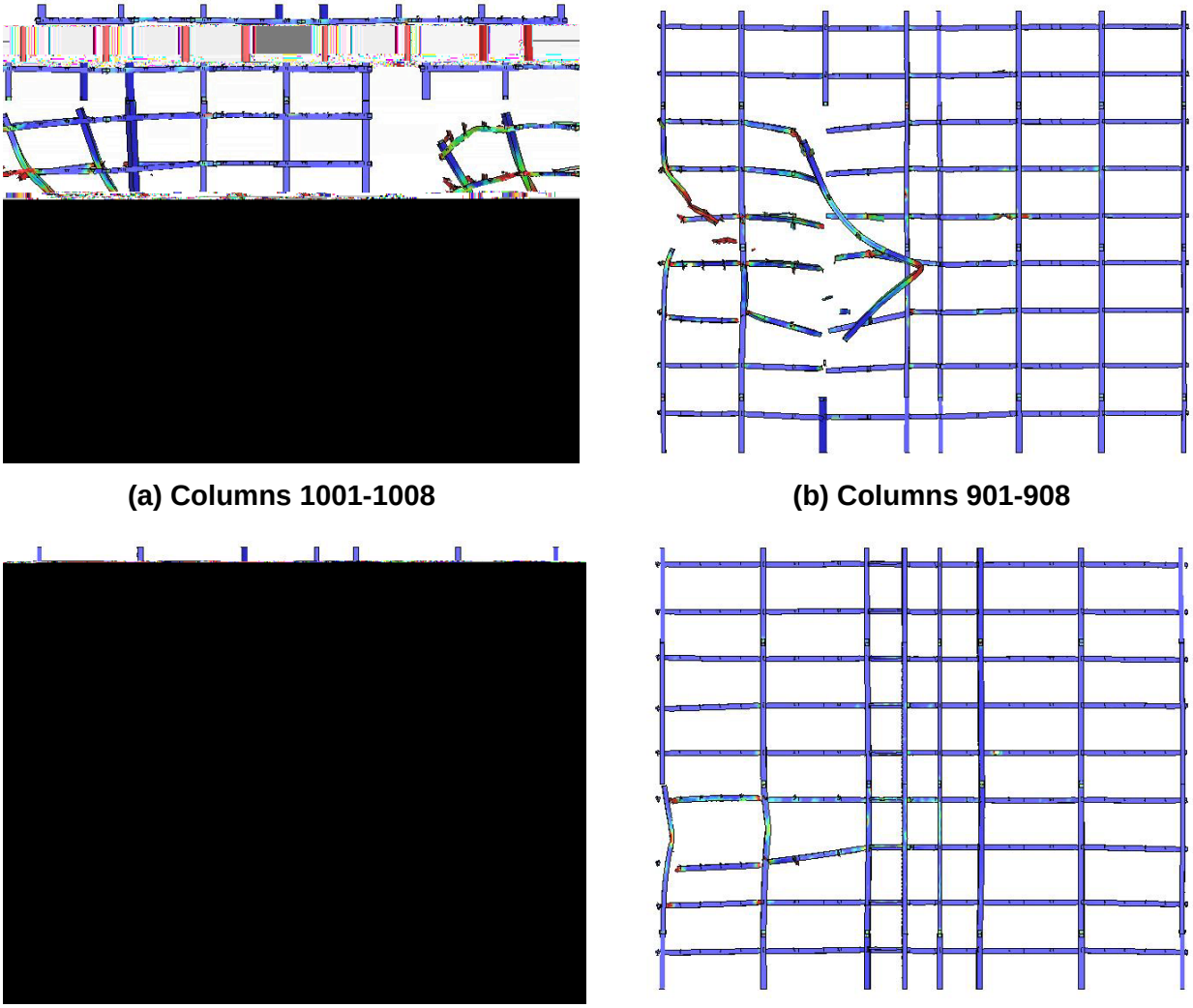

(a) Columns 1001-1008

(b) Columns 901-908

(c) Columns 801-807

(d) Columns 701-708

Figure E–55. More severe impact damage to the WTC 2 core columns.

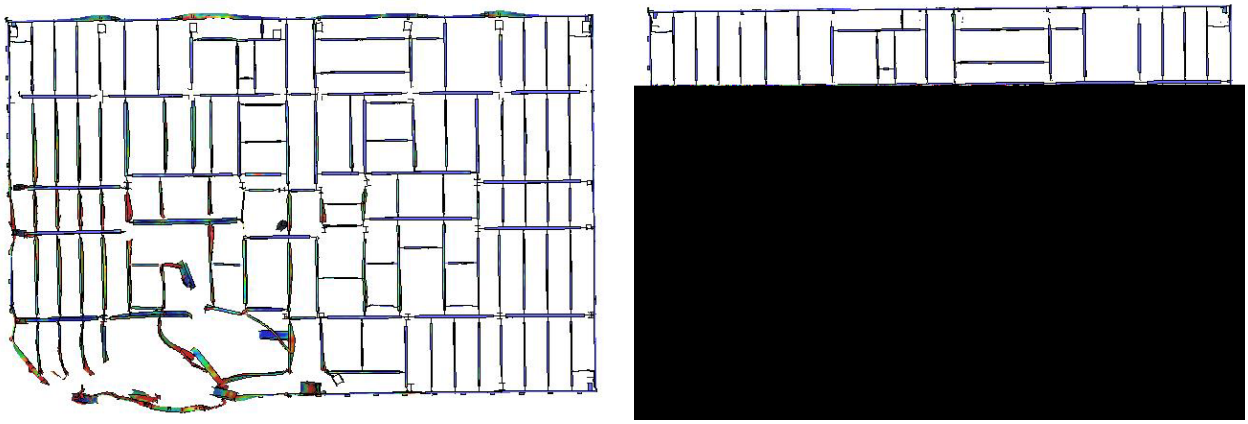

(a) Floor 80 core framing damage **(b) Floor 81 core framing damage**

Figure E–56. More severe impact damage to the core beams of floors 80 and 81 of WTC 2.

Floor Truss and Slab Damage

An overall frontal view for the calculated more severe impact damage to the trusses is shown in Figure E–57. The figure shows that the trusses experienced significant damage in the impact zone, with the heaviest damage on floor 81. A plan view of the calculated damage to the trusses on floors 80 and 81 is shown in Figure E–58. The calculated impact response produced severe damage to the truss structures in the primary impact path of the fuselage. The truss structures were severely damaged from the exterior wall to the core. The truss floor system on floors 79 through 82 had sufficient damage from the impact that portions of the truss floor sections sagged downward as a result of the impact.

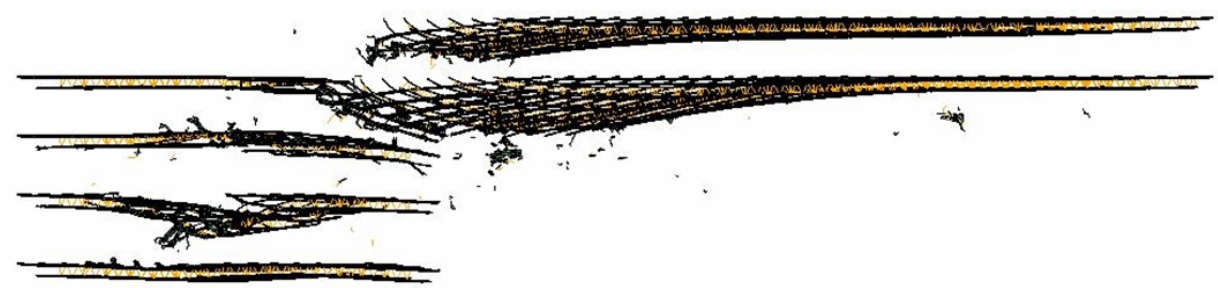

Figure E–57. Calculated more severe impact damage to the WTC 2 floor trusses (front view).

The magnitude of truss floor damage was very similar for the base case and more severe global impact analyses. The parameters used in the more severe global impact analysis would primarily contribute to an increased amount of damage for the tower structures. However, the downward impact trajectory angle was reduced from the 6 degree angle in the base case analysis to a 5 degree angle in the more severe impact analysis. This resulted in directing more of the impact energy inward toward the tower core, but reducing the normal downward force on the floor structures in the impact zone. As a result, the combined effects of the analysis parameter variations produced very similar damage to the truss structure.

The calculated damage to the WTC 2 floor slab for floors 80 and 81 for the more severe impact is shown in Figure E–59. The magnitude of floor slab damage was very similar for the base case and more severe global impact analyses due to the reasons explained above for the floor trusses.

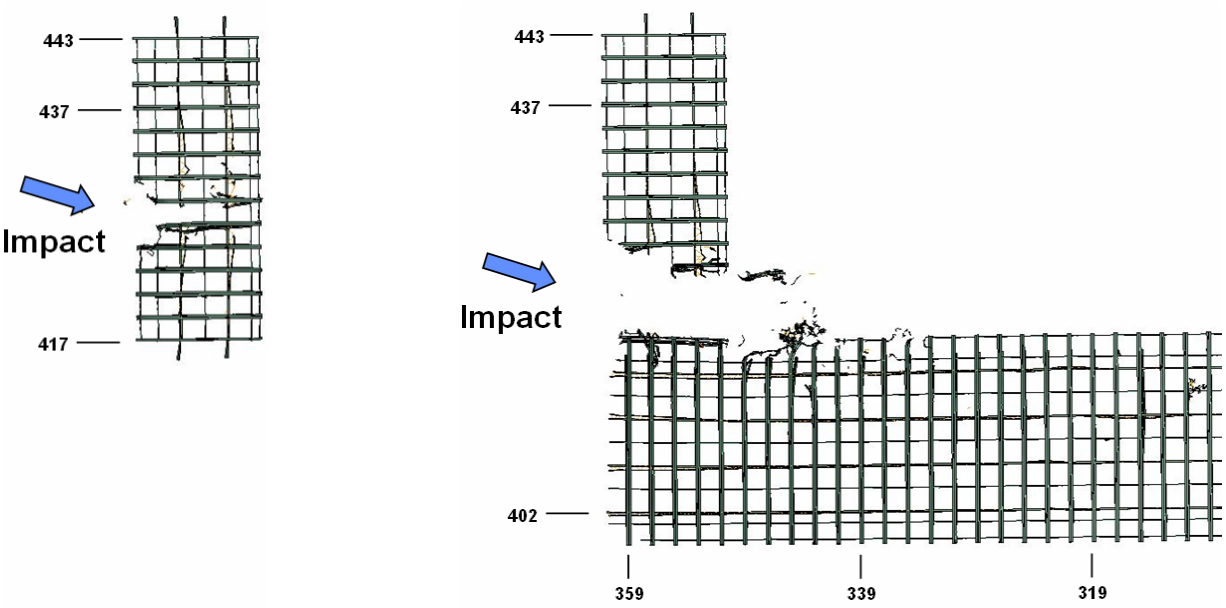

(a) Floor 80 truss damage **(b) Floor 81 truss damage**

Figure E–58. More severe impact damage to the trusses on floors 80 and 81 of WTC 2 (plan view).

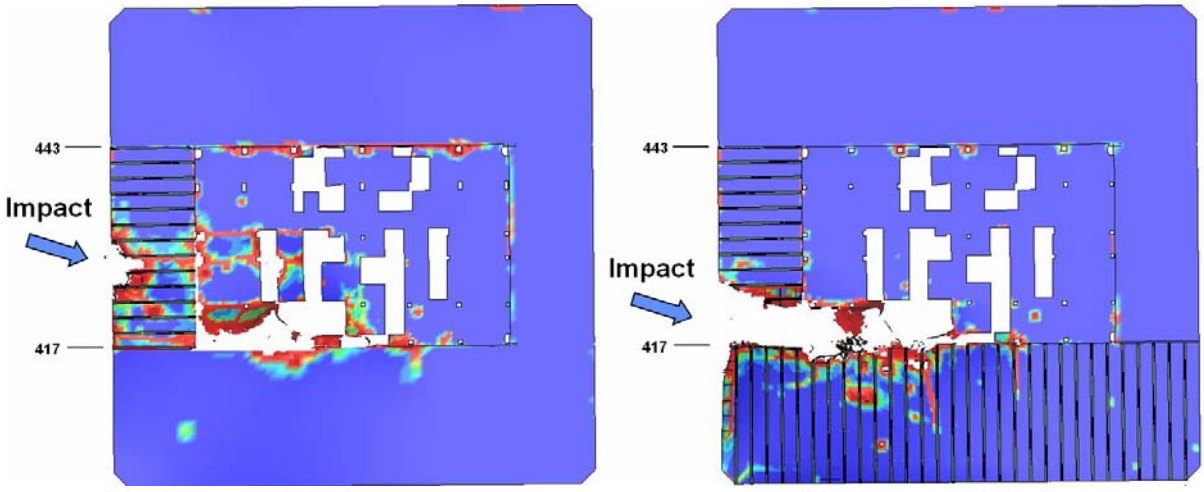

(a) Floor 80 slab damage **(b) Floor 81 slab damage**

Figure E–59. More severe impact damage to the WTC 2 floor slab (plan view).

Summary of Structural Damage

Figure E–60 presents the cumulative damage to WTC 2 on all affected floors and columns for the more severe case.

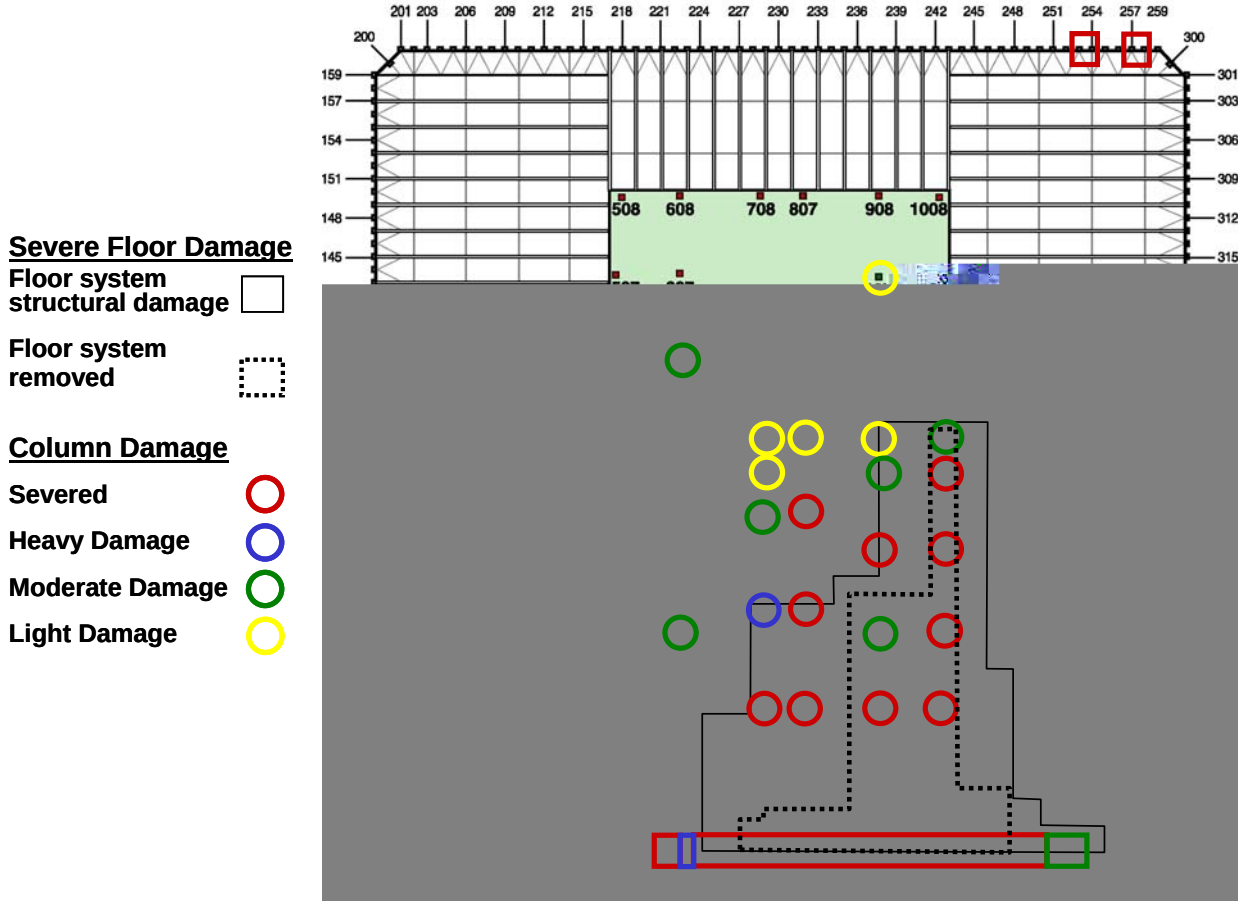

Figure E–60. Cumulative structural damage to the floors and columns of WTC 2 (more severe case).

Fuel and Debris Distributions

The distribution of the fuel in the tower calculated from the more severe case in a plan view and side view is shown in Figure E–61. A comparison to the calculated damage for the base case WTC 2 impact analysis indicated that the tower contents damage zone was similar, with a slight increase in damage for the more severe impact.

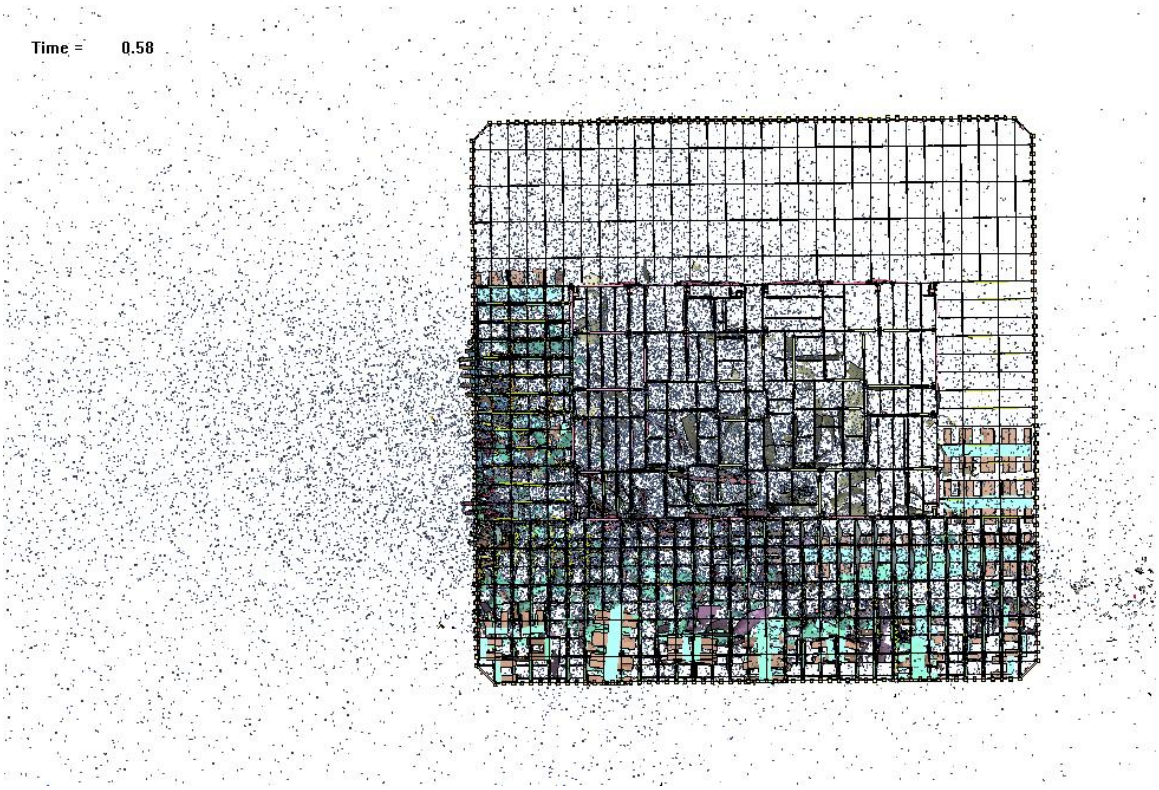

Figure E–61. Calculated fuel distribution and debris damage in the more severe WTC 2 analysis.

E.7.6 WTC 2 Less Severe Impact Analysis

For the south exterior wall of WTC 2, the magnitude and mode of impact damage were in good agreement with the observed damage for the less severe impact scenario. The core had significant damage in the region close to the impact point. The columns in line with the aircraft fuselage failed on the impact side, and several of the core beams were also severely damaged or failed in the impact zone. In some cases, failure of the column splices located on floors 77, 80, and 83 contributed significantly to the failure of the core columns. A total of three columns were severed, and two columns heavily damaged, compared to five severed columns and four heavily damaged columns in the base case WTC 2 impact analysis.

The truss floor system on floors 79 through 82 had sufficient damage from the impact that portions of the truss floor sections sagged downward as a result of the impact. The trusses experienced significant damage in the impact zone, with the heaviest damage on floor 81. The calculated impact response produced severe damage to the truss structures in the primary path of the fuselage. The truss structures were completely destroyed along the impact path on floor 81 from the exterior wall to the core.

When compared with the base case, the magnitude of damage to the floor trusses and floor slabs was slightly increased for the less severe impact analysis. The parameters used in the less severe global impact analysis would primarily contribute to a reduced damage magnitude for the tower structures. However, the downward impact trajectory angle was increased from the 6 degree angle in the base case analysis to an 8 degree angle in the less severe impact analysis. This would have the effect of directing

more of the impact energy downward, increasing the normal force on the floor structures in the impact zone. As a result, the combined effects of the analysis parameter variations produced very similar damage to the truss structure.

A comparison to the base case and less severe case indicated that the building contents damage zone was similar, with a slight reduction in damage for the less severe impact.

E.7.7 Comparison with Observables

The observables available to help validate the global impact analyses included the following:

- Damage to the building exterior (exterior walls and floors in the immediate vicinity of the impact) documented by photographic evidence.
- Aircraft debris external to the towers (landing gear for WTC 1 and a landing gear and an engine for WTC 2) as documented by photographic evidence.
- Eyewitness accounts from survivors who were inside the towers (blocked or passable stairwells).

An example of such comparisons was a detailed comparison between the observed and calculated damage (from the base case analysis) to the north wall of WTC 1 and the south wall of WTC 2. The comparison included the mode, magnitude, and location of failure around the hole created by the aircraft impact. The color code included the following: (1) green circles indicating a proper match of the failure mode and magnitude between the observed and calculated damage, (2) yellow circles indicating a proper match in the failure mode, but not the magnitude, (3) red circles indicating that the failure mode and magnitude predicted by the calculation did not match that was observed, and (4) black circles indicating that the observed damage was obscured by smoke, fire, or other factors. The comparisons shown in Figure E–62 and Figure E–63 for WTC 1 and WTC 2, respectively, indicate that the overall agreement with the observed damage was very good.

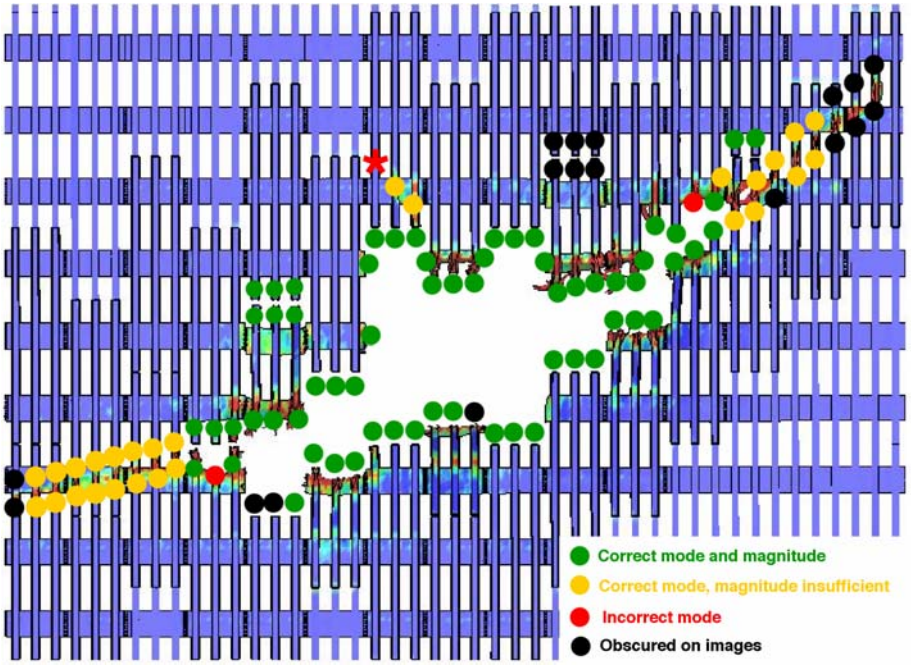

Figure E–62. Comparison of observable and calculated base case impact damage to the north wall of WTC 1.

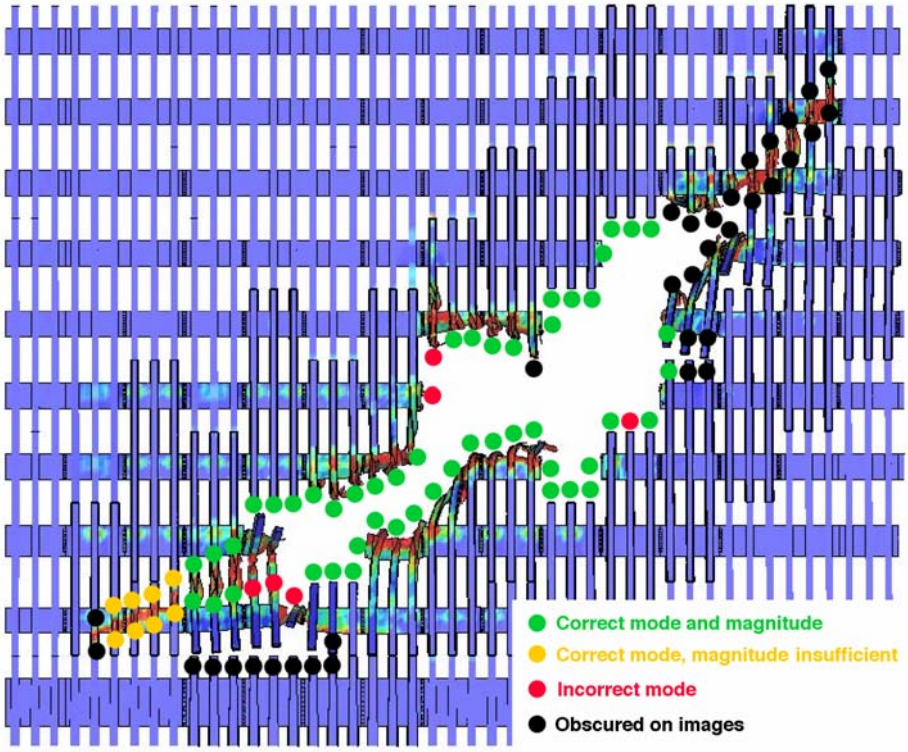

Figure E–63. Comparison of observable and calculated base case impact damage to the south wall of WTC 2.

Not all of the observables were perfectly matched by the simulations due to the uncertainties in exact impact conditions, the imperfect knowledge of the interior tower contents, the chaotic behavior of the aircraft breakup and subsequent debris motion, and the limitations of the models. In general, however, the results of the simulations matched these observables reasonably well.

E.8 FINDINGS

Finding 1: The original design wind loads on the towers exceeded those established by NYCBC prior to 1968, when the WTC towers were designed, and up to and including 2001. The original design load estimates were also higher than those required by other selected building codes of the time, including the relevant national model building code (BOCA). The prescriptive approach in these codes is oversimplified, and as a result, these codes are not appropriate for super-tall building design.

Finding 2: In the majority of the cases, each of the two orthogonal shear components and of the two orthogonal overturning moment components at the base of the towers used in the original wind design were smaller than the CPP, RWDI, and refined NIST estimates. However, the most unfavorable combined peaks (resultant) from the original design were larger, or smaller, by at most 15 percent than estimates based on the CPP, RWDI, and NIST estimates. This is due to the conservative approach used to combine the loads in the original design.

Finding 3: The estimated wind-induced loads on the towers varied by as much as 40 percent between the wind tunnel/climatological studies conducted in 2002 by CPP and RWDI. The primary reasons for these differences were due to the different approaches used in those studies to (1) estimate extreme wind speeds; (2) estimate wind profiles; (3) integrate aerodynamic, dynamic, and extreme wind climatological information; and (4) combine wind effects in two orthogonal directions and in torsion. Such disparity is indicative of the limitations and inconsistencies associated with the current state of practice in wind engineering for tall buildings.

Finding 4: A comparison of wind speeds indicated significant differences among various specified design wind speeds. The basic wind speed specified in ASCE 7-02 for New York City is equivalent to an 88 mph fastest-mile wind speed at 33 ft above ground for open terrain exposure. The wind speed specified in the NYCBC (2001) is 80 mph and is interpreted to be a fastest-mile wind speed at 33 ft above ground. For the original WTC design, the design wind speed was 98 mph averaged over 20 minutes at a height of 1,500 ft above ground, which is equivalent to a fastest-mile wind speed at 33 ft above ground of between 67 mph and 75 mph. The wind speed estimated by NIST for the three airports (La Guardia, Newark International Airport, and John F. Kennedy International Airport), regardless of direction, was equivalent to 96 mph fastest-mile wind speed. An evaluation of the wind speed specifications and the development of improved design wind speeds, as well as protocols for selection of site-specific wind speeds and directionality, are, therefore, in order.

Finding 5: Under the original WTC design loads, the cumulative drifts at the top of the WTC towers ranged from H/263 to H/335. For the lower estimate state-of-the-practice case, those drifts ranged from H/253 to H/306. Under design loading conditions, the maximum inter-story drift was as high as h/230 and h/200 for WTC 1 and WTC 2, respectively. Maximum inter-story drifts under the state-of-the practice case were about h/184 and h/200 for WTC 1 and WTC 2, respectively. For the refined NIST estimate case, the cumulative and inter-story drifts were about 25 percent larger than those from the state-

of-the-practice case. Total and inter-story drifts of the towers were larger than what is generally used in current practice.

Finding 6: DCRs estimated from the original WTC design load case were in general close to those obtained for the lower-estimate state-of-the practice case. For both cases, a fraction of the structural components had DCRs larger than 1.0. These were mainly observed in both towers at (1) the exterior walls: (a) at the columns around the corners, (b) where the hat truss connected to the exterior walls, and (c) below floor 9; and (2) the core columns on the 600 line between floors 80 and 106 and at core perimeter columns 901 and 908 for much of their height. The DCRs obtained for the refined NIST estimate case were higher than those for the original WTC design and the lower-estimate state-of-the-practice load cases.

Finding 7: The safety of the exterior walls, core columns, and hat truss members of the WTC towers on September 11, 2001, was most likely not affected by the fraction of members for which the demand exceeded allowable capacity.

Finding 8: The behavior of the lower portion of the towers at the basement floors was that of a braced frame, while the behavior of the super-structure was that of a framed tube system. Under a combination of the original WTC design dead and wind loads, tension forces developed in the exterior walls of both towers. The forces were largest at the base of the building and at the corners. The DCRs for the exterior wall splice connections under these tensile forces for both towers were shown to be less than 1.0.

Finding 9: For the towers' resistance to shear sliding under wind loads, the factor of safety was between 10 and 11.5, while the factor of safety against overturning ranged from 1.9 to 2.7 for both towers.

Finding 10: For the typical truss-framed floor under the original WTC design gravity loads, the DCRs for all floor trusses were less than unity for 99.4 percent of the floor truss components, with a maximum of 1.14. Inside the core, the DCRs for all floor beams were less than 1.08, and more than 99 percent of floor beams had a DCR of less than 1.0. The maximum mid-span deflections of the long span and short span zones under the original WTC design loads were about L/400 and L/750, respectively, where L is the floor span. For the typical beam-framed floor under the original WTC design gravity loads, the DCRs for all floor beams were less than 1.0, except for two core beams where the DCRs in shear were 1.125 and 1.09. The maximum mid-span deflections of the long span and short span zones under the original design loads were about L/450 and L/600, respectively.

Finding 11: Documents from The Port Authority of New York and New Jersey indicated that the safety of the WTC towers and their occupants in an aircraft collision was a consideration in the original design. The documents indicate that a Boeing 707, the largest commercial aircraft at the time, flying at 600 mph was considered, and the analysis indicated that such collision would result in only local damage which could not cause collapse or substantial damage to the building and would not endanger the lives and safety of occupants not in the immediate area of impact. No documentary evidence of the aircraft impact analysis was available to review the criteria and methods used in the analysis of the aircraft impact into the WTC towers, or to provide details on the ability of the WTC towers to withstand such impacts.

Finding 12: The impact of a Boeing 767 engine at a speed of 500 mph on an exterior wall panel resulted in a complete penetration of the engine through the exterior wall and failure of impacted exterior columns.

Finding 13: Impact of an empty wing segment from approximately mid-span of the wing normal to the exterior wall produced significant damage to the exterior columns but not complete failure. Impact of the same wing section, but filled with fuel, resulted in extensive damage to the external panels of the tower, including complete failure of the exterior columns.

Finding 14: The response of the nonstructural building contents and the floor concrete slab to an aircraft engine impact was dominated by the mass of the workstations and the concrete slab, rather than by their strength.

Finding 15: The aircraft that impacted WTC 1 had a speed of 443±30 mph with a roll angle of 25±2 degrees (port wing downward). The vertical approach downward angle was 10.6±3 degrees and the lateral approach angle was close to being normal to the north wall of the tower. For WTC 2, the impacting aircraft had a speed of 542±24 mph with a roll angle of 38±2 degrees (port wing downward). The vertical approach downward angle was 6±2 degrees, and the lateral approach angle was 15±2 degrees clockwise from the south wall of the tower.

Finding 16: The aircraft impact on WTC 1 resulted in extensive damage to the north wall of the tower, which failed in the regions of the fuselage, engine, and fuel-filled wing section impacts. Damage to the exterior wall extended to the wing tips, but the exterior columns were not completely failed in the outer wing and vertical stabilizer impact regions. According to photographs, columns 112 to 144 along with column 151 were completely severed, while columns 145 to 148 were heavily damaged and columns 149 to 150 were moderately damaged (for reference, columns 101 and 159 are located on the west and east corner, respectively, of the north wall). The results of the impact analyses matched well with this damage pattern to the north wall. Photographic evidence also indicated that an exterior panel with columns 329, 330, and 331 on the south wall between floors 94 to 96 was dislodged. Failure of the exterior columns occurred both at the bolted connections between column ends and at various locations in the column depending on the local severity of the impact load and the proximity of the bolted connection to the impact. Subject to the uncertainties inherent in the models, the global impact simulations indicated that a total of three core columns were severed and four columns were heavily damaged in the base case, compared to six columns severed and three columns heavily damaged in the more severe case and one columns severed and two columns heavily damaged in the less severe case. In the analyses, the floor trusses, core beams, and floor slabs experienced significant impact-induced damage on floors 94 to 96, particularly in the path of the fuselage. The analyses indicated that the wing structures were completely fragmented due to the interaction with the exterior wall and as a result, aircraft fuel was dispersed on multiple floors. In addition, aircraft debris resulted in substantial damage to the nonstructural building contents (partitions and workstations) and also in dislodging of fireproofing. The bulk of the fuel and aircraft debris was deposited in floors 93 through 97, with the largest concentration on floor 94.

Finding 17: The aircraft impact on WTC 2 resulted in extensive damage to the south wall of the tower, which failed in the regions of the fuselage, engine, and fuel-filled wing section impacts. Damage to the exterior wall extended to the wing tips, but the exterior columns were not completely failed in the outer wing and vertical stabilizer impact regions. According to photographs, columns 410 to 436 and columns 438 to 439 were completely severed, while column 437 was heavily damaged (for reference, columns 401 and 459 are located on the east and west corner, respectively, of the south wall). The results of the impact analyses matched well with this damage pattern to the south wall. In addition, columns 407 to 409 were obscured by smoke, but the analysis results indicated that these columns were moderately damaged. Photographic evidence also indicated that columns 253, 254, 257, and 258 on the north wall were failed.

Failure of the exterior columns occurred both at the bolted connections between column ends and at various locations in the column depending on the local severity of the impact load and the proximity of the bolted connection to the impact. Subject to the uncertainties inherent in the models, the global impact simulations indicated that a total of five core columns were severed and four columns were heavily damaged in the base case, compared to ten columns severed and one column heavily damaged in the more severe case and three columns severed and two columns heavily damaged in the less severe case. In some cases, failure of the column splices located on floors 77, 80, and 83 contributed significantly to the failure of the core columns. In the analyses, the floor trusses, core beams, and floor slabs experienced significant impact-induced damage on floors 79 to 81, particularly in the path of the fuselage. The analyses indicated that the wing structures were completely fragmented due to the interaction with the exterior wall, and as a result, aircraft fuel was dispersed on multiple floors. In addition, aircraft debris resulted in substantial damage to the nonstructural building contents (partitions and workstations) and also in dislodging of fireproofing. The bulk of the fuel was concentrated on floors 79, 81, and 82, while the bulk of the aircraft debris was deposited in floors 78 through 80, with the largest concentration on floor 80.

Finding 18: Natural periods calculated from the reference global model of the WTC 1 tower matched well with those measured on the tower based on the analysis of data from accelerometers located atop WTC 1. The calculated period of oscillation in the N–S direction of the reference global model of WTC 2 matched well with the period estimated immediately after aircraft impact based on a detailed analysis of the building motion, which was captured in a video footage of the WTC 2 impact. This indicated that the overall lateral stiffness of the tower was not affected appreciably by the impact damage. The maximum deflection at the top of the tower after impact was estimated from the footage to be more than 1/3 of the drift resulting from the original design wind loads. This indicated that the tower still had reserve capacity after losing a number of columns and floor segments due to aircraft impact.

Finding 19: The towers sustained significant structural damage to the exterior walls, core columns, and floor systems due to aircraft impact. This structural damage contributed to the weakening of the tower structures, but did not, by itself, initiate building collapse. However, the aircraft impact damage contributed greatly to the subsequent fires and the thermal response of the tower structures that led ultimately to the collapse of the towers by: (1) dispersing jet fuel and igniting building contents over large areas, (2) creating large accumulations of combustible materials containing aircraft and building contents, and (3) increasing the air supply into the damaged buildings that permitted significantly higher energy release rates than would normally be seen in ventilation building fires, allowing the fires to spread rapidly on multiple floors.

Chapter 1
INTRODUCTION

1.1 BACKGROUND

As stated in the preface, the National Institute of Standards and Technology (NIST) investigation into the collapse of the World Trade Center (WTC) towers included eight interdependent projects (see Table P–1). The *Baseline Structural Performance and Aircraft Impact Damage Analysis* project had two primary tasks. These were:

1. To develop reference structural models of the towers and use these models to establish the baseline performance of each of the two towers under gravity and wind loads.

2. To estimate the damage to the towers due to aircraft impacts and establish the initial conditions for the fire dynamics modeling and the thermal-structural response and collapse initiation analyses.

This report presents the details of the studies related to both tasks. For each task, the report provides the following:

- Description of structural models: these include the reference structural models of the towers for the first task, and global impact models of the towers and a model of the aircraft for the second.

- Description of applied loads for analyses: these are gravity and wind load estimates for the first task, and aircraft impact initial conditions for the second.

- Analysis results: these include the baseline performance analyses of the towers for the first task, and a description of the impact-induced damage to the towers for the second.

The report is concluded by a set of findings (Chapter 8). The next sections provide the background, technical approach, and details for each task.

1.2 REFERENCE MODELS AND BASELINE PERFORMANCE ANALYSIS

The WTC towers used a structural system that, at the time of the design, incorporated a number of innovative features. Among these features were the use of a composite truss floor system to provide lateral stability and diaphragm action to the towers, the use of wind tunnel testing to estimate static and dynamic wind effects, and the use of viscoelastic dampers to reduce wind-induced vibrations. Wind loads were a governing factor in the design of the structural components that made up the frame-tube steel framing system. Wind load capacity is also a key factor in determining the overall strength of the towers and is important in determining not only the ability of the towers to withstand winds but also the reserve capacity of the towers to withstand unanticipated events such as a major fire or impact damage.

Accurate estimation of the wind load on tall buildings is a challenging task, given that wind engineering is still an evolving technology. For example, as is shown later, estimates of the wind-induced response presented in two recent independent studies of the WTC towers differed from each other by about 40 percent. The primary reasons for these differences appear to lie in the different approaches used in those studies to estimate extreme wind speeds, to estimate wind profiles, to integrate aerodynamic, dynamic, and extreme wind climatological information, and to combine wind effects in two orthogonal directions and in torsion. In this study, NIST developed refined estimates of wind effects using information provided in the two studies, a critical assessment of that information, and independent information concerning the wind climate. Furthermore, as shown in this study, the available prescriptive codes specify wind loads (pressures) on tall buildings that are significantly lower than wind tunnel-based loads. This case study provided an opportunity to assess effectively the current design practices and various code provisions on wind loads.

The baseline performance of the WTC towers under gravity and wind loads were established in order to assess the towers' ability to withstand those loads safely and to evaluate the reserve capacity of the towers to withstand unanticipated events. The baseline performance study provides a measure of the behavior of the towers under design loading conditions, specifically: (1) total and inter-story drift (the sway of the building under design wind loads); (2) floor deflections under gravity loads; (3) the stress demand-to-capacity ratio for primary structural components of the towers such as exterior walls, core columns, and floor framing; (4) performance of exterior walls under wind loading, including distribution of axial stresses and presence of tensile forces; (5) performance of connections between exterior columns; and (6) resistance of the towers to shear sliding and overturning at the foundation level.

For the purpose of establishing the baseline performance of the towers, various wind loads were considered in this study, including wind loads used in the original WTC design, wind loads based on two recent wind tunnel studies conducted in 2002 by Cermak Peterka Peterson, Inc. (CPP) and Rowan Williams Davis and Irwin, Inc. (RWDI) for a insurance litigation concerning the towers, and wind loads estimated by NIST by critically assessing information obtained from the CPP and RWDI reports and by bringing to bear state-of-the-art considerations.

In order to develop the reference models and perform the baseline performance analyses, the following steps were undertaken:

- Develop structural databases for the primary structural components of the WTC 1 and WTC 2 towers from the original computer printouts of the structural design documents.

- Develop reference structural analysis models that capture the intended behavior of each of the two towers using the generated databases. These reference models were used to establish the baseline performance of the towers and also served as a reference for more detailed models for aircraft impact damage analysis and thermal-structural response and collapse initiation analysis. The models included: (1) two global models (one for each tower) of the major structural components and systems of the towers, and (2) floor models of a typical truss-framed floor and a typical beam-framed floor.

- Develop estimates of design gravity (dead and live loads) and wind loads on each of the two towers for implementation into the reference structural models. The following three loading cases were considered:

  – *Original WTC design loads case.* Loads included dead and live loads as in original WTC design, in conjunction with original WTC design wind loads.

  – *State-of-the-practice case.* Loads included dead loads, current New York City Building Code (NYCBC 2001) live loads, and wind loads from the RWDI wind tunnel study, scaled in accordance with NYCBC 2001 wind speed.

  – *Refined NIST estimate case.* Loads included dead loads, live loads from the American Society of Civil Engineers (ASCE) 7-02 Standard (a national standard), and refined wind loads developed by NIST.

- Perform structural analyses to establish the baseline performance of each of the two towers under design gravity and wind loads.

The tasks outlined above were conducted by the firm of Leslie E. Robertson Associates, the firm responsible for the original structural engineering of the WTC towers, under contract to NIST for the development of the structural databases, reference structural models, and baseline performance analysis. NIST implemented a rigorous and comprehensive review procedure to ensure the integrity and objectivity of the output and results, including the structural databases, reference models, and baseline performance analysis. The review procedure included an in-house NIST review and a third-party review by the firm of Skidmore, Owings, and Merrill, under contract to NIST.

Chapters 2 through 4 provide a description of the structural modeling and analysis of the baseline performance of the towers. For further details, the reader is referred to NIST NCSTAR 1-2A.[1]

Chapter 2 presents the development of the reference structural models for WTC 1 and WTC 2, including the global tower models, typical floor models, and parametric studies conducted to support the development of the global models. The chapter provides a brief summary of the development of the structural databases. In addition, this chapter outlines the NIST and third-party review of the structural databases and reference models.

Chapter 3 provides a discussion on the loading cases used in the baseline performance analyses, and outlines the development of the gravity and wind loads on the global tower models. In this chapter, special emphasis is placed on the estimates of the wind load cases used in this study. These include the original design wind loads, the state-of-the-practice wind loads (the CPP and RWDI wind studies), and the refined NIST estimates. The chapter concludes with a comparison of the various wind studies.

Chapter 4 provides the results of the baseline performance analyses for the global tower models as well as the typical floor models. The results presented for the global models include total and inter-story drift, demand to capacity ratios for primary structural components of the towers, response of exterior walls

[1] This footnote is to one of the companion documents from this Investigation. A list of these documents appears in the Preface to this report.

under wind loading, performance of connections between exterior columns, and resistance of the towers to shear sliding and overturning. For the floor models, these results include floor mid-span deflections and demand to capacity ratios for primary floor framing members. The chapter also outlines the review process of the baseline performance analyses.

1.3 AIRCRAFT IMPACT DAMAGE ANALYSIS

Buildings are not specifically designed to withstand the impact of fuel-laden commercial aircraft, and building codes in the United States do not require building designs to consider aircraft impact. However, after the crash of a B-25 bomber into the Empire State Building in 1945, designers of high-rise buildings became aware of the potential of aircraft collision with buildings. Documents obtained from The Port Authority of New York and New Jersey (PANYNJ) indicated that the safety of the WTC towers and their occupants in an aircraft collision was a consideration in the original design. A three-page white paper "Salient points with regard to the structural design of the World Trade Center towers", February 1964, from the PANYNJ (see Appendix A) indicated that the impact of a Boeing 707 or DC 8 aircraft flying at a speed of 600 mph was analyzed during the design stage of the WTC towers. The paper also addressed the life safety considerations following such impact. The paper stated that "…The Buildings have been investigated and found to be safe in an assumed collision with a large jet airliner (Boeing 707 - DC 8) traveling at 600 miles per hour. Analysis indicates that such collision would result in only local damage which could not cause collapse or substantial damage to the building and would not endanger the lives and safety of occupants not in the immediate area of impact."

A three-page document "Period of Vibration due to plane crash at 80th floor," March 1964, from the PANYNJ included a calculation by the designer to estimate the period of vibration due to an aircraft impacting at the 80th floor of the towers. Although no conclusion was stated on the calculation sheet, it indicated that the design considered the possibility of aircraft impact on the towers. Aside from these two documents from the PANYNJ, no documentary evidence on the aircraft impact analysis was available to review the criteria and methods used in the analysis of the aircraft impact into the WTC towers or to provide details on the ability of the WTC towers to withstand such impacts.

The Federal Emergency Management Agency (FEMA) 403 (2002) report indicated that it was assumed in the 1960s design of the WTC towers that a Boeing 707 aircraft, lost in fog and seeking to land at a nearby airport, might strike the towers while low on fuel and at a landing speed of 180 mph.

A property risk assessment report, prepared for Silverstein Properties prior to leasing the WTC towers in 2001, identified the scenario of an aircraft striking a tower as one of the maximum foreseeable losses. The assessment states "This scenario is within the realm of the possible, but highly unlikely. In the event [of] such an unlikely occurrence, what might result? The structural designers of the towers have publicly stated that in their opinion that either of the Towers could withstand such an impact from a large modern passenger aircraft. The ensuing fire would damage the skin in this scenario, as the spilled fuel would fall to the Plaza level where it would have to be extinguished by the NYC Fire Department."

While the documents from the PANYNJ indicated that aircraft impact was considered in the design, there were two views expressed by the building designers during media interviews on whether the effects of the

subsequent fires and the implications on life safety were a consideration in the original design. One view[2] suggested that an analysis was done indicating that the biggest problem would be the fact that all the fuel would dump into the building and there would be horrendous fire. For implications on life safety, this view suggested that a lot of people would be killed, but the building structure would still be there. The other view[3] suggested that the fuel load and the subsequent fire damage may not have been considered in the design stage.

For the events of September 11, 2001, the aircraft impact damage to the exterior of the WTC towers could be visibly identified from the video and photographic records collected. However, no visible information could be obtained for the extent of damage to the interior of the towers, including the structural system (floors and core columns), partition walls, and interior building contents. Such information was needed for the subsequent fire dynamics simulations and post-impact structural analyses. In addition, for the fire dynamics modeling, the dispersion of the jet fuel and the location of combustible aircraft debris were required. The estimate of the extent of damage to the fireproofing on the structural steel in the towers due to impact was essential for the thermal and structural analyses. The aircraft impact damage analyses were the primary tool by which most of the information on the tower damage could be estimated.

The focus of the analysis was to analyze the aircraft impacts into each of the WTC towers to provide the following: (1) estimates of probable damage to structural systems, including exterior walls, floor systems, and interior core columns; (2) estimates of the aircraft fuel dispersion during the impact; and (3) estimates of debris damage to the building nonstructural contents, including partitions and workstations. The analysis results were to be used to estimate the damage to fireproofing based on the predicted path of the debris field inside the towers. This analysis thus estimated the condition of the two WTC towers immediately following the aircraft impacts and established the initial conditions for the fire dynamics modeling and the thermal-structural response and collapse initiation analysis. The impact analyses were conducted at various levels of complexity including: (1) the component level, (2) the subassembly level, and (3) the global level to estimate the probable damage to the towers due to aircraft impact.

The WTC aircraft impact analysis was a challenging task for the following reasons:

- The need to develop a comprehensive aircraft model that properly captured the stiffness and mass distributions of the aircraft, as well as the large scale fracture and fragmentation of the aircraft components. No such model was available at the beginning of the study. Associated with this task was the collection of information on the structure of the Boeing 767 aircraft from documentary aircraft structural information and data from measurements on a Boeing aircraft.

- The towers and aircraft included a variety of materials that exhibited highly nonlinear, rate-dependent behavior with failure that need to be included in the models. Also, the various joints and connections (bolts and weldments) in the tower and aircraft structures presented complex behavior and failure. The constitutive behavior of these materials and connections was included in the models based on testing of tower steels or from data available in the open literature.

[2] J. Skilling in 1993 from James Glanz and Eric Lipton, "*City in the Sky*," Times Books, 2003.

[3] L.E. Robertson in 2001 from "The Tower Builder" by John Seabrook, *The New Yorker*, November 19, 2001.

- The WTC towers and Boeing 767 aircraft were large and complex structural systems. To include all of the primary structural components and details of both the aircraft and towers using refined finite element meshes in the impact models was prohibitive. As a result, coarser meshes were used in the impact simulations. That presented a challenge, since a very fine mesh was needed to properly capture the failure and fracture of components in these analyses. A large array of impact simulations at the component level were conducted to calibrate the failure and fragmentation of coarsely meshed aircraft and tower components against those models with fine meshes.

- A significant portion of the weight of a Boeing 767 wing was from the fuel in its integral fuel tanks. Upon impact, this fuel was responsible for large distributed loads on the exterior columns of the WTC towers and subsequently on interior structures, as it was dispersed inside the building. Modeling of the fluid-structure interaction is complex, but was deemed necessary to predict the extent of damage and the fuel dispersion within the building and to help establish the initial conditions for the fire dynamics modeling. A number of modeling options were investigated for possible application in the global impact simulations.

- The impact analyses were subject to uncertainties in the input parameters such as initial impact conditions, material properties and failure criteria, aircraft mass and stiffness properties, connections response, the mass and strength of nonstructural contents, and modeling parameters. No information was available to determine *a priori* the sensitivity of the damage estimates to uncertainties in these parameters. Detailed sensitivity analyses using orthogonal factorial design were conducted at the component and subassembly levels to determine the most influential parameters that affect the damage estimates. The results of these analyses were used to provide a range of impact-induced damage estimates to the towers using the global models.

The analyses of the aircraft impacts performed for this investigation are believed to be the highest-fidelity simulations ever performed for this impact behavior using state-of-the art analysis methodologies. Wherever possible, the models were validated against observables or supporting test data developed by the WTC investigation.

In order to estimate the aircraft impact damage to the WTC towers, the following steps were undertaken:

- Constitutive relationships were developed to describe the actual behavior and failure of the materials under the dynamic impact conditions of the aircraft. These materials included the various grades of steels used in the exterior walls, core columns, and floor trusses of the towers, weldment metal, bolts, reinforced concrete, aircraft materials, and nonstructural contents.

- Global impact models were developed for the towers and aircraft: The tower models included the primary structural components of the towers in the impact zone, including exterior walls, floor systems, core columns, and connections, along with nonstructural building contents. A refined finite element mesh was used for the areas in the path of the aircraft, and a coarser mesh was used elsewhere. The aircraft model included the aircraft engines, wings, fuselage, empennage, and landing gear, as well as nonstructural components

of the aircraft. The aircraft model also included a representation of the fuel using the smooth particle hydrodynamics approach.

- Component and subassembly impact analyses were conducted to support the development of the global impact models: The primary objectives of these analyses were to (1) develop an understanding of the interactive failure phenomenon of the aircraft and tower components, and (2) develop the simulation techniques required for the global analysis of the aircraft impacts into the WTC towers, including variations in mesh density and numerical tools for modeling fluid-structure interaction for fuel impact and dispersion. The component and subassembly analyses were used to determine model simplifications for reducing the overall model size while maintaining fidelity in the global analyses.

- Initial conditions were estimated for the impact of the aircraft into the WTC towers: These included the aircraft speed at impact, aircraft orientation and trajectory, and impact location of the aircraft nose. The estimates also included the uncertainties associated with these parameters. This step utilized the videos and photographs that captured the impact event and subsequent damage to the exterior of the towers.

- Sensitivity analyses were conducted at the component and subassembly levels to assess the effect of uncertainties on the level of damage to the towers due to impact and to determine the most influential parameters that affect the damage estimates. The analyses were used to reduce the number of parameters that would be varied in the global impact simulations.

- Analyses of aircraft impact into WTC 1 and WTC 2 were conducted using the global tower and aircraft models: The analysis results included the estimation of the structural damage that degraded the towers' strength and the condition and position of nonstructural contents such as partitions, workstations, aircraft fuel, and other debris that influenced the behavior of the subsequent fires in the towers. The global analyses included, for each tower, a "base case" based on reasonable initial estimates of all input parameters. They also provided a range of damage estimates based on variations of the most influential parameters.

- Approximate analyses were conducted to provide guidance to the global finite element impact analyses: These included: (1) the analysis of the overall aircraft impact forces and assessment of the relative importance of the airframe strength and weight distribution, (2) the evaluation of the potential effects of the energy in the rotating engine components on the calculated engine impact response, (3) the influence of the static preloads in the towers on the calculated impact damage and residual strength predictions, and (4) the analysis of the load characteristics required to damage core columns compared to the potential loading from impact of aircraft components.

The tasks outlined above were conducted in collaboration with experts from Applied Research Associates, Inc. under contract to NIST. Chapters 5 through 7 provide a summary of this study. For further details, the reader is referred to NIST NCSTAR 1-2B.

Chapter 5 describes the global tower and aircraft impact models. The chapter provides the methodology used in the development for the models and the contents of the models, including geometry, element types and sizes, and boundary conditions. The chapter also includes a summary of the constitutive relationships

for the various materials used in the tower and aircraft models. Finally, the chapter provides a brief description of the components and subassembly models that were used to support and provide guidance to the development of the global models.

Chapter 6 presents the methodology used to estimate the initial aircraft impact conditions. These included, for each aircraft, the impact speed, horizontal and vertical angles of incidence, roll angle, and impact location of the aircraft nose. Uncertainties in each of these parameters were also quantified. The estimates were based on videos that captured the approach of the impacting aircraft and photographs of the damage to the exterior walls of the towers.

Chapter 7 presents the results of the global analyses of aircraft impact into WTC 1 and WTC 2 using the global tower and aircraft models. The global analyses included, for each tower, a "base case" based on reasonable initial estimates of all input parameters. They also provided a range of damage estimates of the towers due to aircraft impact. The chapter also provides a comparison between the simulation results and observables obtained from video and photographic evidence and eyewitness interviews, and a comparison of damage estimates from this study with those from prior studies.

Chapter 2
DEVELOPMENT OF REFERENCE STRUCTURAL MODELS

2.1 INTRODUCTION

This chapter outlines the development of the reference structural models of the World Trade Center (WTC) towers. The models were used (1) to establish the baseline performance of the towers under design gravity and wind loads, and (2) as a reference for more detailed models used in other phases of the National Institute of Standards and Technology (NIST) Investigation, including the aircraft impact analysis and the thermal-structural response and collapse initiation analysis. The reference models were developed to capture the intended behavior of the WTC towers under design loading conditions and included the following:

- A global model of the primary structural components and systems for each of the two towers.
- A model of a typical truss-framed floor (tenant floor) and a model of a typical beam-framed floor (mechanical level) within the impact and fire regions.

For the global models of the towers, the large amount of data required to construct the models dictated that a database of the primary structural components of the towers be developed from the original computer printouts of the structural design documents. The various databases, developed in Microsoft Excel format, were linked together using the relational database technique. The relational databases, developed using Microsoft Access, were generated in a format suitable for the development of the global finite element models of the towers.

For the floor models, typical truss-framed floors existed on tenant floors such as floors 10 to 24, 26 to 40, 50 to 58, 60 to 66, 68 to 74, 84 to 91, and 93 to 105 of WTC 1; and floors 14 to 24, 26 to 40, 50 to 58, 60 to 74, 84 to 91, and 93 to 106 of WTC 2. Typical beam-framed floors existed on mechanical floors (floors 7, 41, 75, and 108) and near mechanical floors (floors 9, 43, 77, 107, 110, and roof) of both towers.

Included in this chapter are descriptions of the reference structural models of the WTC towers, including the global and typical floor models. These models were linearly elastic and three-dimensional, and were developed using the Computers and Structures, Inc. SAP2000 Software (SAP2000 2002), Version 8. SAP2000 is a finite element software package that is customarily used for the analysis and design of building structures.

This chapter describes the work conducted by Leslie E. Robertson Associates (LERA), the firm responsible for the original structural engineering of the WTC towers under contract to NIST, for the development of the structural databases and reference structural models. This chapter also summarizes the review process for the structural databases and reference models, including the third-party review by the firm of Skidmore, Owings, and Merrill (SOM) under contract to NIST and the in-house review by NIST.

Section 2.2 presents an overview of the structural database development and contents. Section 2.3 describes the global models of the WTC 1 and WTC 2 towers. Sections 2.4 and 2.5 present the models for the typical truss-framed floor and beam-framed floor, respectively. Section 2.6 outlines the third-party review by SOM and the in-house review by NIST of the structural databases and reference models. Section 2.7 presents a summary of the chapter.

2.2 DEVELOPMENT OF STRUCTURAL DATABASES

The original structural drawings of the WTC towers were issued in two main formats: (1) large-size drawing sheets containing plan and elevation information, and (2) smaller book-sized drawings containing details and tabulated information of cross sectional dimensions and material properties. The large-size drawings referred to the structural drawing books in their notes, sections, and details. The structural databases, developed in Microsoft Excel file format, were generated from these drawing books and included modifications made after construction. The databases were generated for use in the development of the reference global models of the towers.

The structural databases primarily contained the computer and hand-tabulated data for the major structural components of the towers from the following drawing books:

- Drawing Book 1: exterior wall information, foundation to elevation 363 ft.
- Drawing Book 2: exterior wall information, elevation 363 ft to floor 9.
- Drawing Book 3: core column information.
- Drawing Book 4: exterior wall information, floor 9 to floor 110.
- Drawing Book 5: beam schedule.

Some additional information from Drawing Book 6 (core bracing schedule) and Drawing Book 9 (beams in the hat truss region) were included in the database files as it was utilized in the modeling of the towers. Modifications made after construction that were implemented in the structural databases included:

- Strengthening of a number of core columns: This included core columns 501, 508, 703, 803, 904, 1002, 1006, and 1007 from floors 98 to 106 in both towers. These columns were reinforced using steel plates welded to the wide flange core columns.
- Reinforcing of two corner core columns (508 and 1008) at floors 45 to 97 of WTC 2 due to the construction of a concrete vault at floor 97. The reinforcement consisted of plates welded to the flanges of the built-up box columns (floors 45 to 83) and the flanges of the rolled shape columns (floors 83 to 97).

The tasks that were undertaken to develop the structural databases included: (1) scanning and digitization of the original drawing books, (2) a four-step quality control procedure, (3) cross section property calculations, and (4) the development of the relational databases, using Microsoft Access, to link the generated database files into a format suitable for the development of the structural global models.

For further details on the development of the structural databases, refer to Chapter 2 of NIST NCSTAR 1-2A.

2.3 GLOBAL MODELS OF THE TOWERS

Three-dimensional models of the 110-story above-grade structure and 6-story below-grade structure within the footprint of each of the two towers were developed. The global models for the towers consisted of all primary structural elements in the towers, including exterior walls (exterior columns, spandrel beams, and bracings in the basement floors), core columns, hat trusses, and rigid and flexible diaphragms representing the floor systems.

For the development of the global models, each tower was divided into several sub-models that included:

- Exterior walls, which in turn was divided into
  - Exterior wall, foundation to floor 4
  - Exterior wall trees (floors 4 to 9)
  - Exterior wall, floors 9 to 106
  - Exterior wall, floors 107 to 110
- Core columns
- Hat truss

After these sub-models were assembled into a unified model, rigid and flexible diaphragms representing the floor systems, boundary conditions, gravity and wind loads, and masses were added to the unified model.

The development of the WTC 1 and WTC 2 models were separate and consecutive endeavors. The lessons learned in the assembly of the WTC 1 model were applied to the development of the WTC 2 model. While there were only minor differences in the basic structural systems of the two towers, there were significant differences in section and material properties, and additional column transfers at the basement levels in WTC 2 to create openings for the PATH subway line.

Isometric views of the complete WTC 1 model, with exterior walls, core columns, bracings, hat trusses, and flexible floor diaphragms, are shown in Fig. 2–1. Elevations of the complete WTC 2 model showing similar systems are shown in Fig. 2–2. A summary of the size of the global models of WTC 1 and WTC 2 is presented in Table 2–1. The following presents the details of each of the sub-models used in the development of the unified global models for WTC 1 and WTC 2.

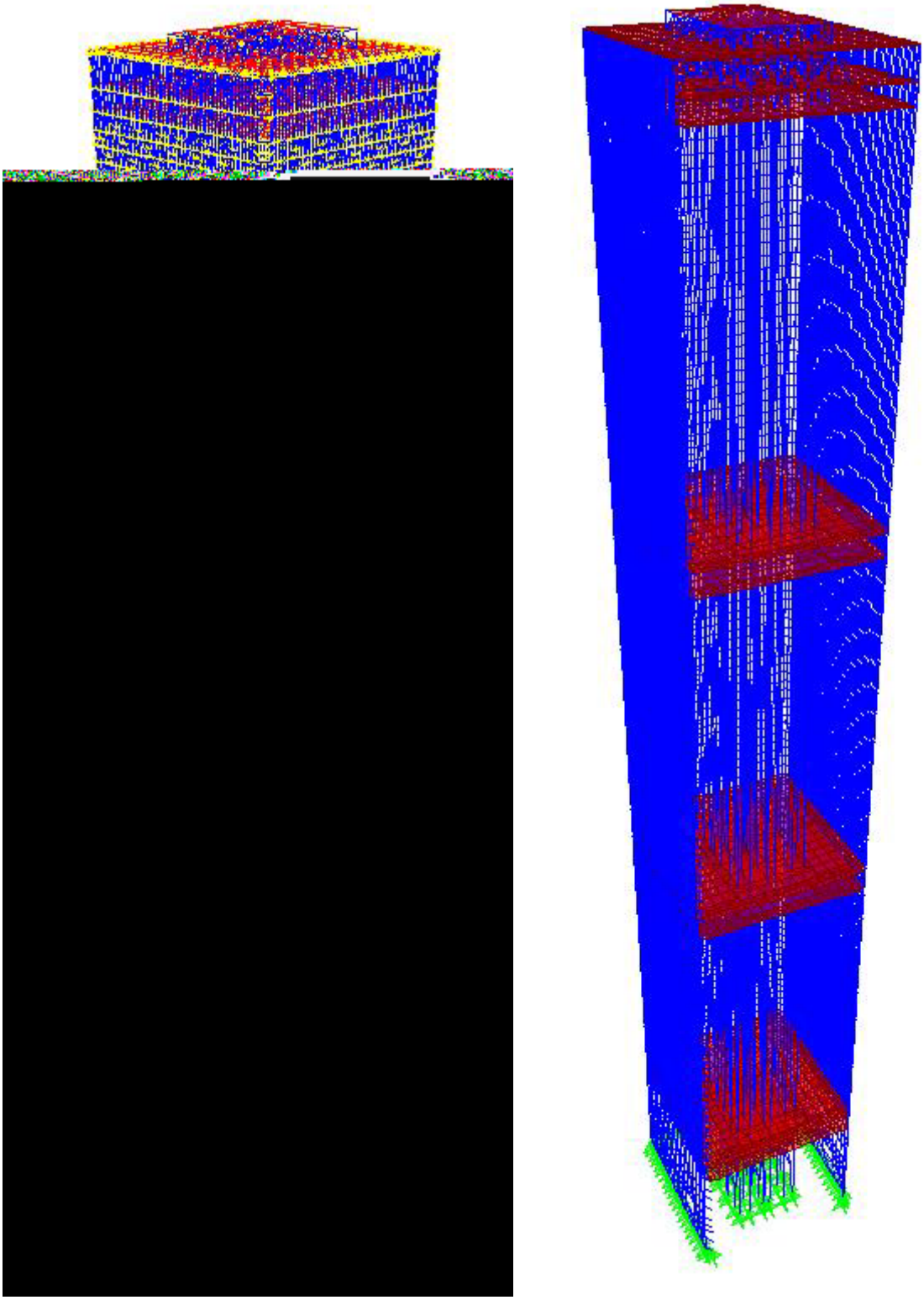

Figure 2–1. Rendered isometric views of the WTC 1 global model.

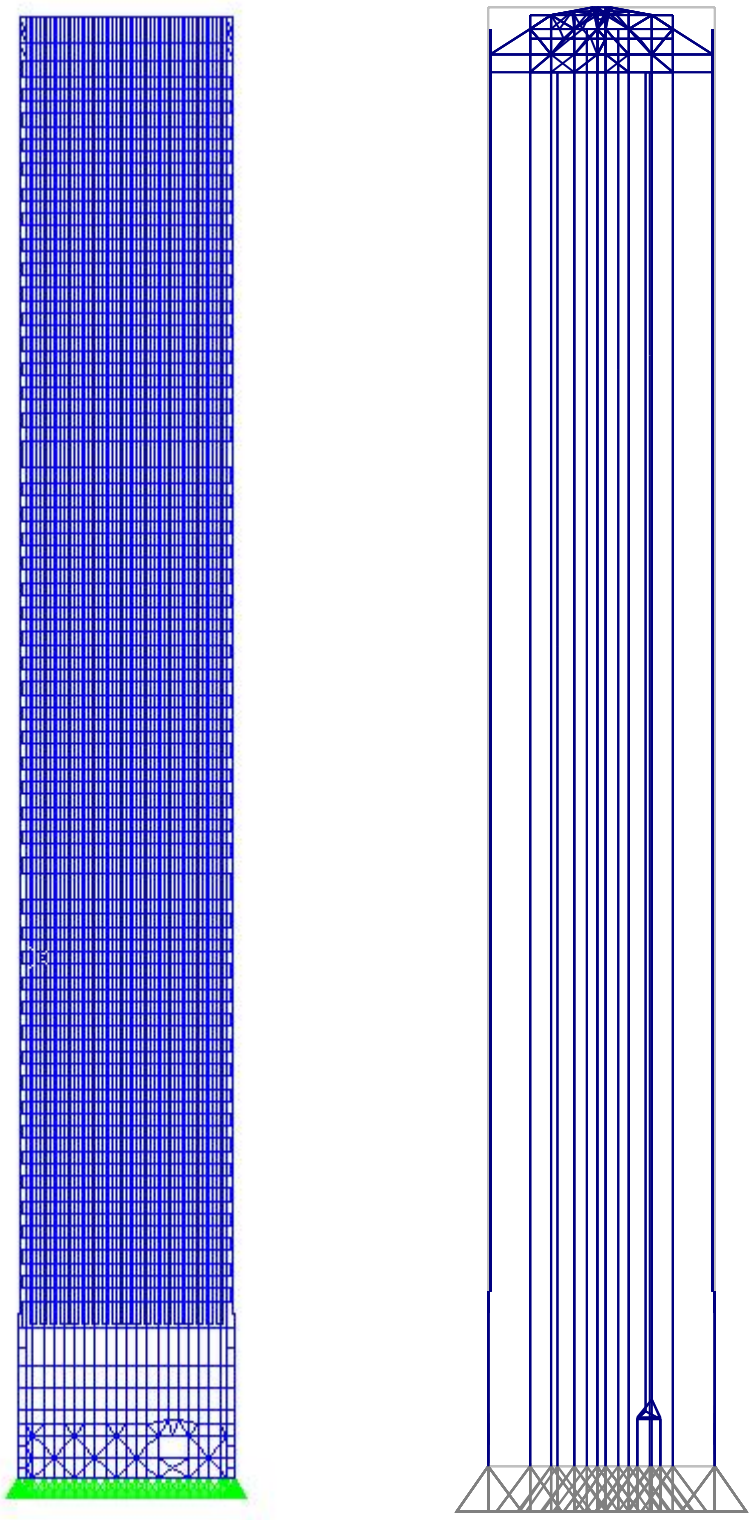

(a) (b)

Figure 2–2. Frame view of the WTC 2 model: (a) exterior wall elevation, and (b) interior section.

Table 2–1. Approximate size of the reference structural models (rounded).

Model	Number of Joints	Degrees of Freedom	Number of Frame Elements	Number of Shell Elements	Total Number of Elements
WTC 1 global model[a]	53,700	218,700	73,900	10,000	83,900
WTC 2 global model[a]	51,200	200,000	73,700	4,800	78,500
Typical truss-framed model	28,100	166,000	27,700	14,800	42,500
Typical beam-framed model	6,500	35,700	7,500	4,600	12,100

a. Model does not include floors except for flexible diaphragms at 17 floors as explained later.

2.3.1 Exterior Wall Modeling

The exterior walls of the WTC towers were intended to resist approximately 50 percent of the gravity loads and all of the lateral loads (primarily wind loads) on the towers. While the exterior wall between floors 9 to 106 represented repetitive typical panels, significant variations existed at the lower floors and the upper portion of the walls. The exterior wall columns from the foundation level up to elevation 363 ft were spaced 10 ft 0 in. on center. There were bracings in the plane of the exterior wall between the concourse level and the foundation. Between elevation 363 ft and floor 7, the single exterior wall columns spaced 10 ft 0 in. on center transitioned to three columns spaced at 3 ft 4 in. on center. The exterior wall columns above floor 7, that were spaced 3 ft 4 in. on center, were connected to each other by spandrel plates, typically 52 in. deep. The exterior columns and spandrels were pre-assembled into exterior wall panels, typically three-columns wide by three-stories high.

The exterior wall model for WTC 1 and WTC 2 consisted of prismatic and non-prismatic beam elements representing columns, spandrels, and bracings. The following describes the various parts of the exterior wall model.

Foundation to Floor 4

The sub-model of the exterior wall from the foundation level up to elevation 363 ft was developed using frame elements (also referred to as beam elements). Frame elements are typically used to model beams, columns, and truss members in planar and three-dimensional structures. They are modeled as straight lines connecting two nodes with six degrees of freedom (three translations and three rotations) at each node. The model was developed in a conventional manner, assigning joints and member connectivity as shown in the original WTC drawings. Below elevation 363 ft, columns were typically spaced at 10 ft and braced with spandrels and diagonals. Joints were defined at all locations where diagonals braced the columns. When coordinates were not given in the drawings, joint coordinates were determined based on the geometry of the diagonal. Structural details showed that the column-diagonal intersections were continuous.

Spandrel centerline elevations were generally used to define joint coordinates. The SAP2000 program allows assignment of rigid zone factors to frame end offsets to account for the overlap of cross sections. At the intersection of columns and spandrels, 100 percent rigidity for the column and the spandrels were assigned due to the large size of both columns and spandrels. Figure 2–3 shows a frame and a rendered view of the exterior wall from foundation to floor 9 of the WTC 1 model. The figure also shows the core columns and core bracings.

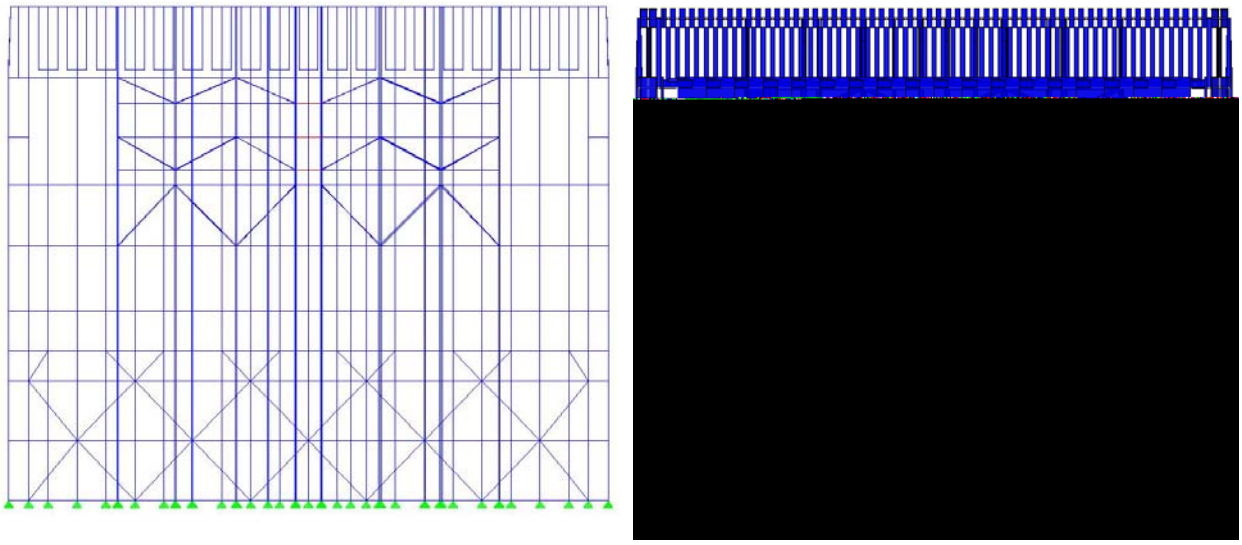

Figure 2–3. Frame view and rendered view of the WTC 1 model (foundation to floor 9).

Exterior Wall Trees (Floor 4 to 9)

The panels of the exterior walls between elevation 363 ft and elevation 418 ft 11 1/2 in. were called exterior wall trees. At the exterior wall trees, the typical exterior wall columns transitioned from a spacing of 10 ft to a spacing of 3 ft 4 in. A typical exterior wall tree panel was divided into five levels; level B, C, D, E, and F as shown in Fig. 2–4. For each panel in the model, the three exterior columns from above elevation 418 ft 11 1/2 in. continued down to level D. At that level, the three columns were connected by a horizontal rigid element to become one member, which extended down to elevation 363 ft.

Both prismatic and non-prismatic frame elements were used to model the exterior wall trees. Non-prismatic elements were used to accurately model the tapering columns as well as the complex geometry of the tress at the transition from three columns to a single column. For further details on the modeling details of the exterior wall trees, refer to Chapter 3 of NIST NCSTAR 1-2A. The final model of a typical tree is illustrated in Fig. 2–5.

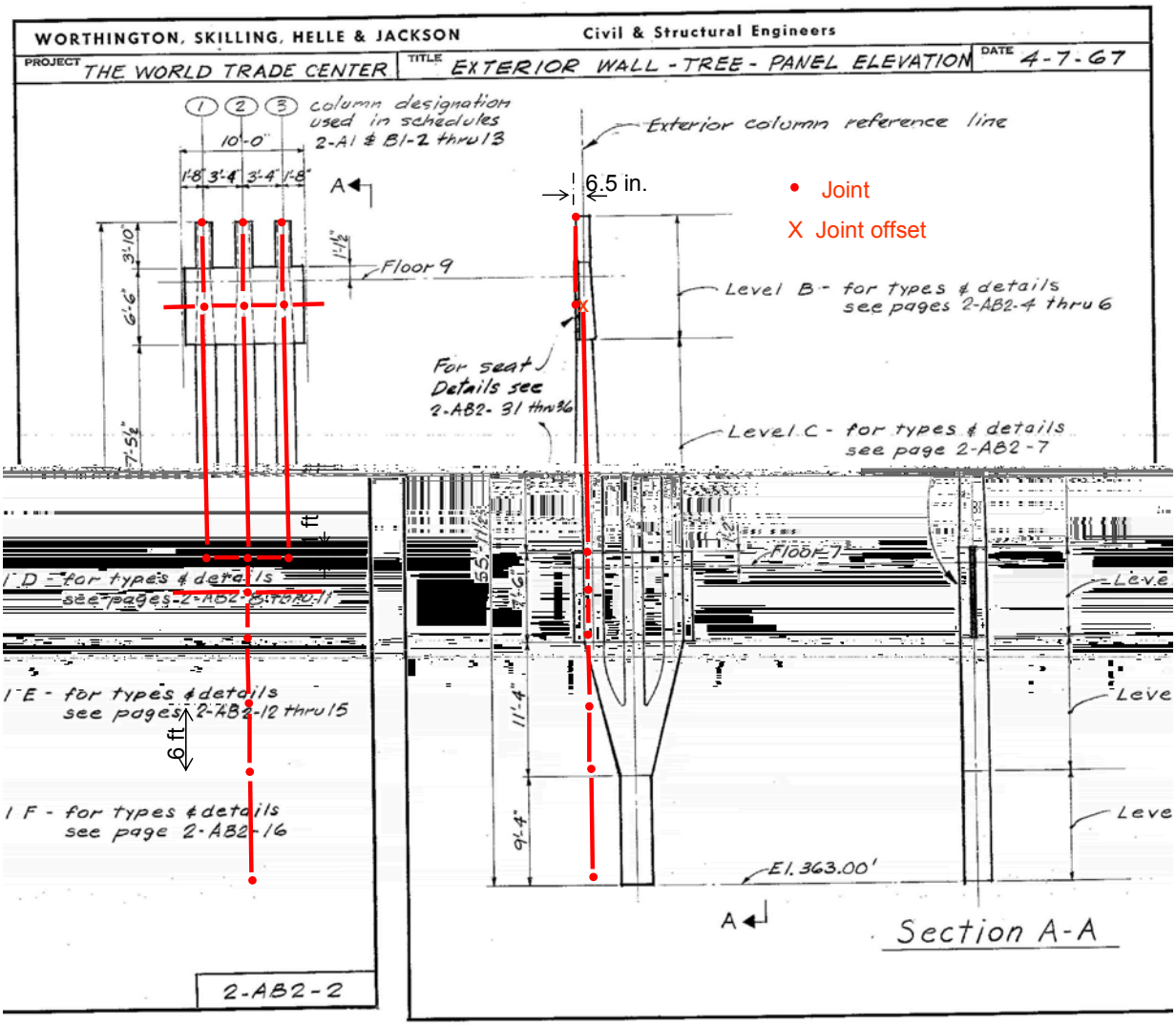

Source: Reproduced with permission of The Port Authority of New York and New Jersey. Enhanced by NIST.

Figure 2–4. Exterior wall tree panel (taken from Drawing Book 2, page 2-AB2-2).

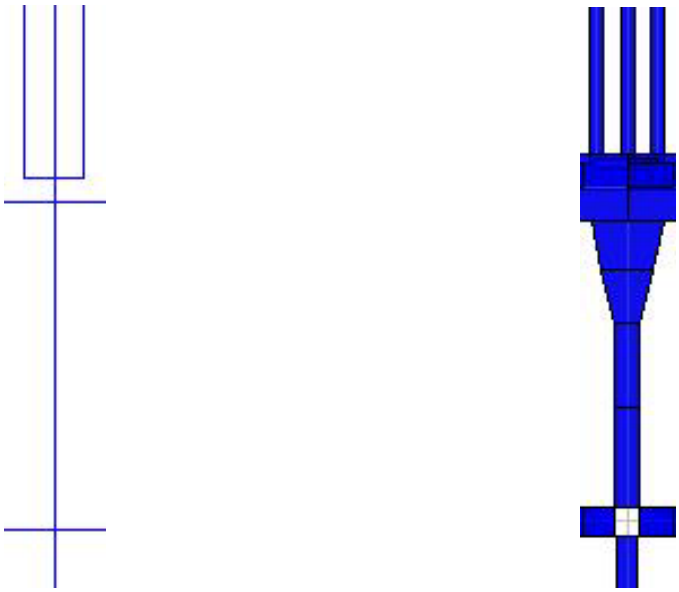

Figure 2–5. Frame and rendered view of an exterior wall tree.

Floor 9 to 106

The typical exterior panels were modeled using frame elements representing columns and spandrels. In plan, the columns and spandrels were joined at nodes located at the outside face of the spandrel, 6 1/2 in. from the exterior column reference line (Fig. 2–6). Thus the columns were offset horizontally, or 'inserted' at this node, using an insertion point located at the centerline of the interior plate 3 as shown in the figure. Insertion points were not adjusted for spandrel thickness. In elevation, the columns and spandrels were joined at the spandrel centerline, located typically 12 1/2 in. below the reference floor elevation (Fig. 2–6). The spandrels were then located correctly without the need for offsets to be defined.

As Fig. 2–6 indicates, nodes at five elevations were defined for a typical exterior wall panel. These included nodes at the three representative floor levels (defined at the spandrel centerlines), as well as the upper and lower column splices.

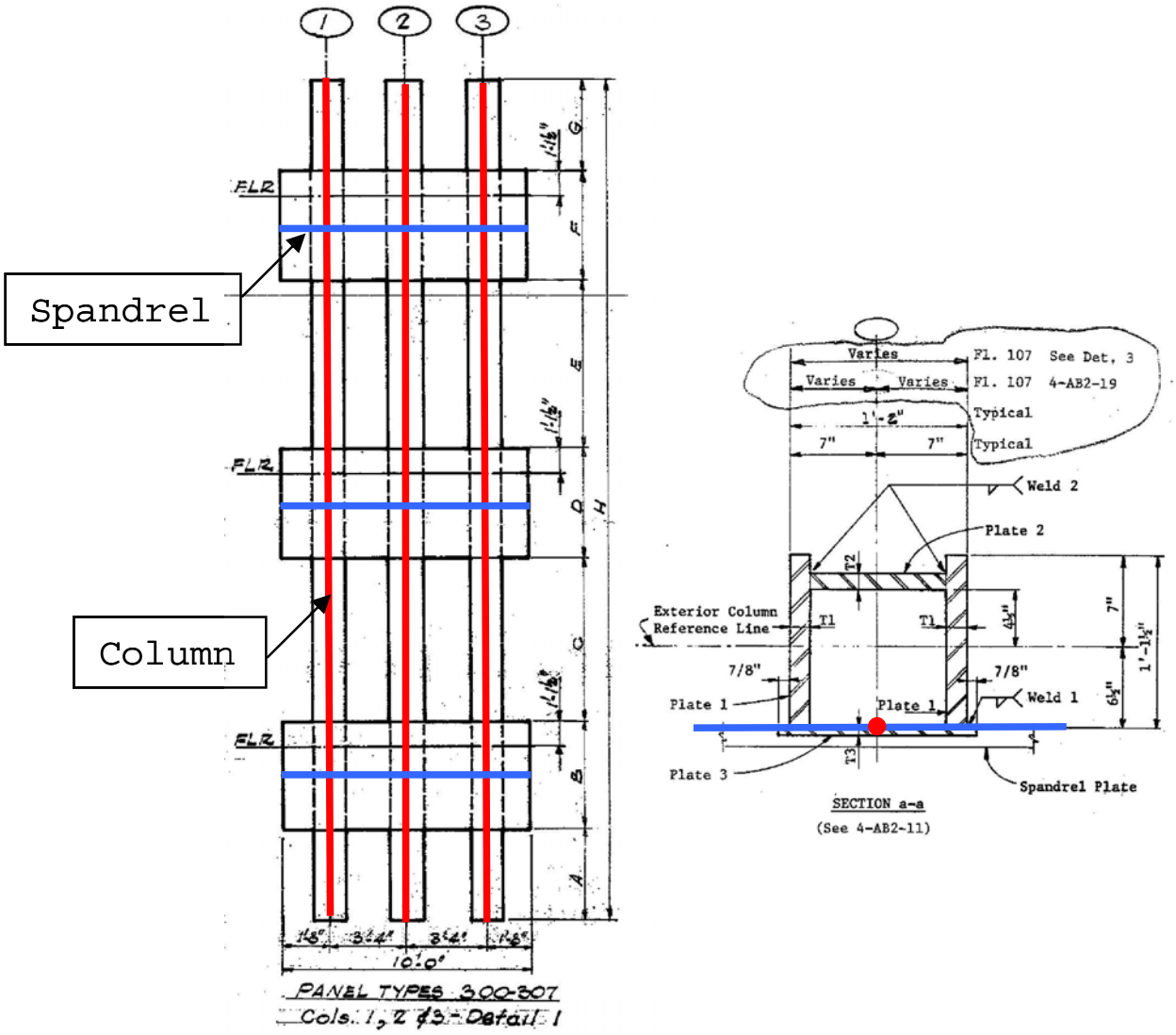

Source: Reproduced with permission of The Port Authority of New York and New Jersey. Enhanced by NIST.

Figure 2–6. Typical WTC tower exterior wall panel.

To develop a frame model of the exterior panel, a parametric study of typical three-column, three-spandrel exterior wall panels was performed using two modeling techniques (see Fig. 2–7). The first model was a detailed shell element model of the panel, and the second was a simplified frame element model similar to that used throughout the global models. Shell elements are typically used to model the plate and membrane behaviors in planar and three-dimensional structures. They can be used in a three- or four-node formulation with six degrees of freedom (three translations and three rotations) at each node. For the detailed shell element model, each plate of each column and spandrel was explicitly modeled, including internal column stiffeners.

The parametric study assumed that the detailed shell model best represented the as-built performance of the panel, and therefore, was used to tune the performance of the simplified frame model. The purposes of the parametric study were to (1) match the axial stiffness of the frame model with the detailed shell

model under gravity loads and (2) match the inter-story drift of the two models under lateral loads in the plane of the panel by modifying the rigidity of the column/spandrel intersections in the simplified frame model.

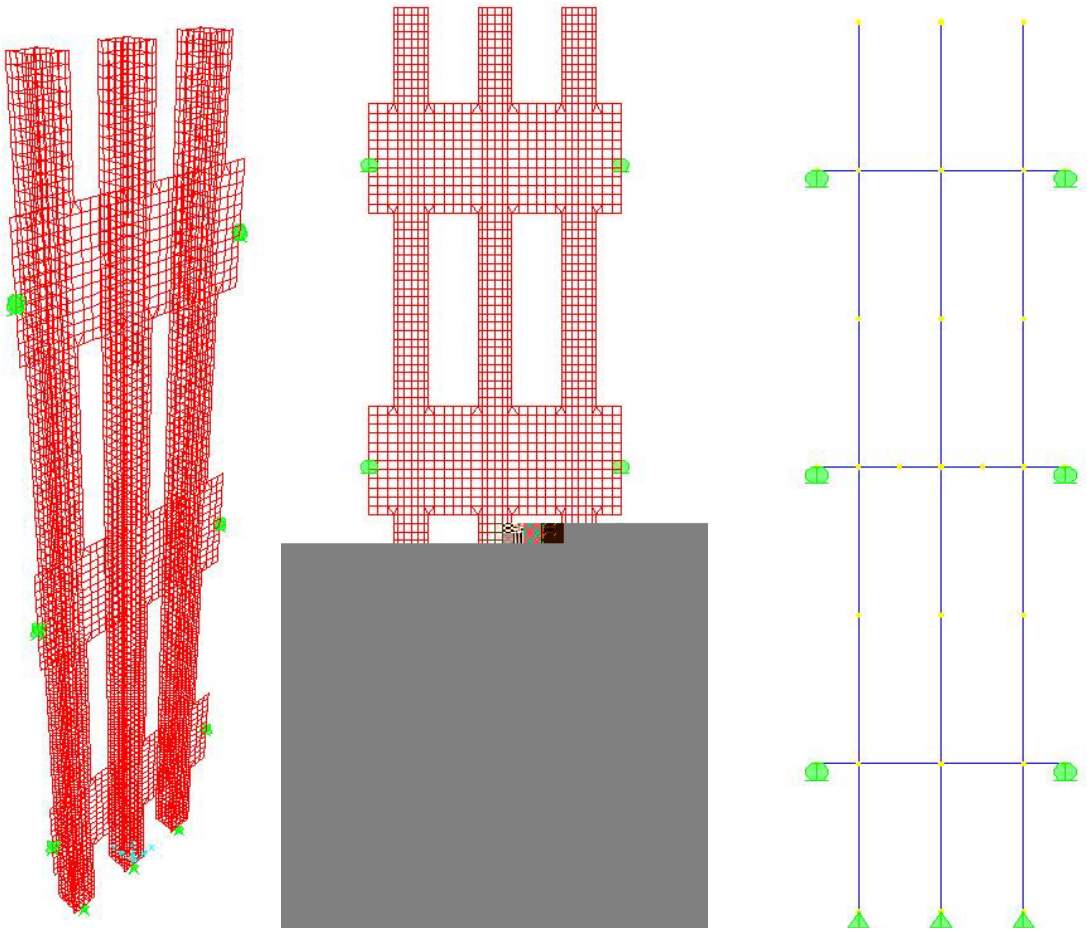

(a) (b) (c)

Figure 2–7. (a), (b) Shell element, and (c) frame element models of a typical exterior wall panel.

For comparing the axial stiffness of the simplified frame model of the panel with the detailed shell model, both models were loaded vertically by applying identical gravity loads to the three columns. The two models were simply supported at the bottom of the columns. The results indicated that the shell model was stiffer than the equivalent frame element model due to the contribution of the spandrel beams to the axial stiffness of the panel. This is due to the rigidity of the spandrel beams and the proximity between the columns. The parametric study on a wide range of panels over the height of the towers showed that the axial stiffness of the columns in the bottom third of the towers should be increased by a factor in the range of 25 percent to 28 percent, and the columns in the middle and upper thirds of towers should be increased by a factor in the range of 20 percent to 28 percent. Based on these figures, a 25 percent increase in the axial stiffness of exterior columns was selected as a reasonable representation for the panel vertical stiffness between floors 9 and 106. This was achieved using a frame property multiplier of 1.25 for the cross-sectional area of the exterior wall columns.

For studying the lateral deformation of the exterior panels, panel properties were taken from three different areas of the building at floors 79 to 82, 53 to 56, and 23 to 26. The deformations at points A, B, I, and II (Fig. 2–8) were studied for the three different panels. The top most columns were connected via a rigid link and loaded in the plane of the panel and perpendicular to the columns with a lateral load of 100 kip. The boundary conditions included roller supports at the spandrel ends and pin supports at the bottom of the columns as seen in Fig. 2–7.

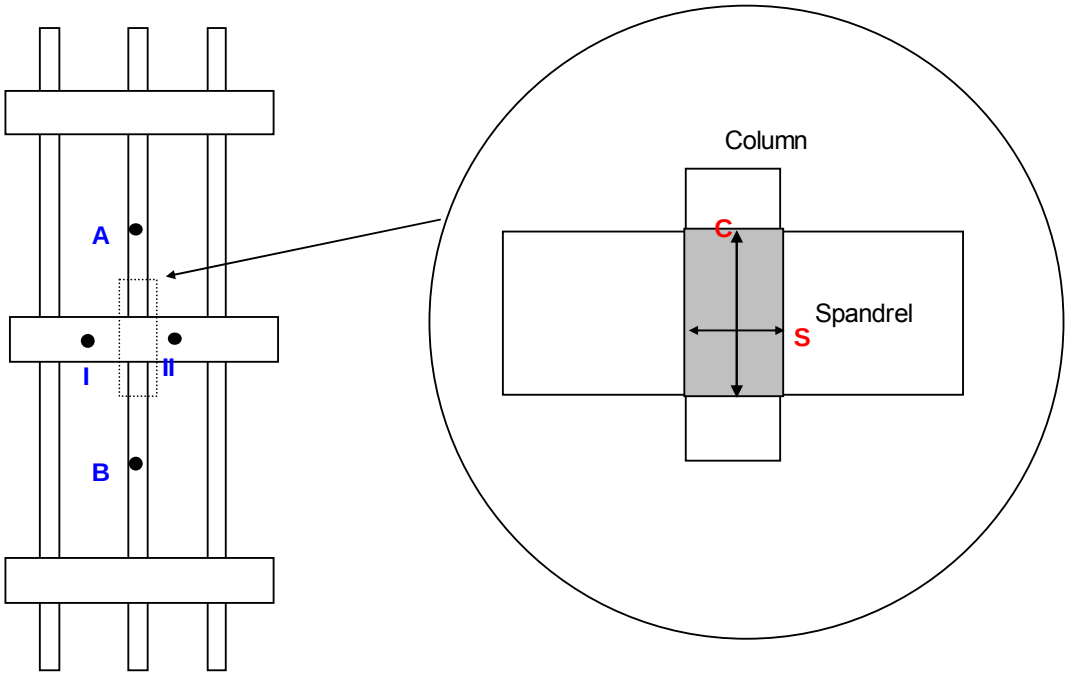

Figure 2–8. Selection of column and spandrel rigidity of typical exterior wall panel.

The lateral displacements calculated for the detailed shell and simplified frame models of typical exterior wall panels with varied column and spandrel intersection rigidities are shown in Table 2–2. The table indicates that using a column rigidity of 50 percent and a spandrel rigidity of 100 percent in the frame model produced deflection results consistent with the shell model. This was achieved in the global models by assigning 50 percent rigidity for the columns and 100 percent rigidity for the spandrels at the column-spandrel intersection.

A similar study was conducted for the corner exterior panels to develop a simplified frame model that matched the behavior of a detailed shell element model of the corner panels. These models are shown in Fig. 2–9. For details of the study, refer to NIST NCSTAR 1-2A. Based on the results of this parametric study, 25 percent rigidity for the columns and 50 percent rigidity for the spandrels were assigned to the exterior wall corner panels. Also, an area modifier was used to provide a 25 percent increase in the axial stiffness of the two continuous columns of the corner panels. No modifier was used for the intermittent columns at the corners.

Table 2–2. Lateral displacement (in.) for the shell and frame models of typical exterior wall panel with varied column and spandrel rigidities.

	Lateral displacement (in)			
	Floor 79-82			
	Shell model	Frame model (Rigidity)		
		No rigidity	C:50%, S:100%	C:100%, S:100%
A	0.60	1.04	0.59	0.35
B	0.28	0.52	0.29	0.18
I	0.45	0.78	0.44	0.26
II	0.45	0.78	0.44	0.26
	Floor 53-56			
	Shell model	Frame model (Rigidity)		
		No rigidity	C:50%, S:100%	C:100%, S:100%
A	0.26	0.43	0.27	0.18
B	0.12	0.22	0.14	0.11
I	0.19	0.32	0.2	0.15
II	0.19	0.32	0.2	0.15
	Floor 23-26			
	Shell model	Frame model (Rigidity)		
		No rigidity	C:50%, S:100%	C:100%, S:100%
A	0.21	0.37	0.21	0.12
B	0.1	0.18	0.1	0.06
I	0.16	0.28	0.16	0.09
II	0.16	0.28	0.16	0.09

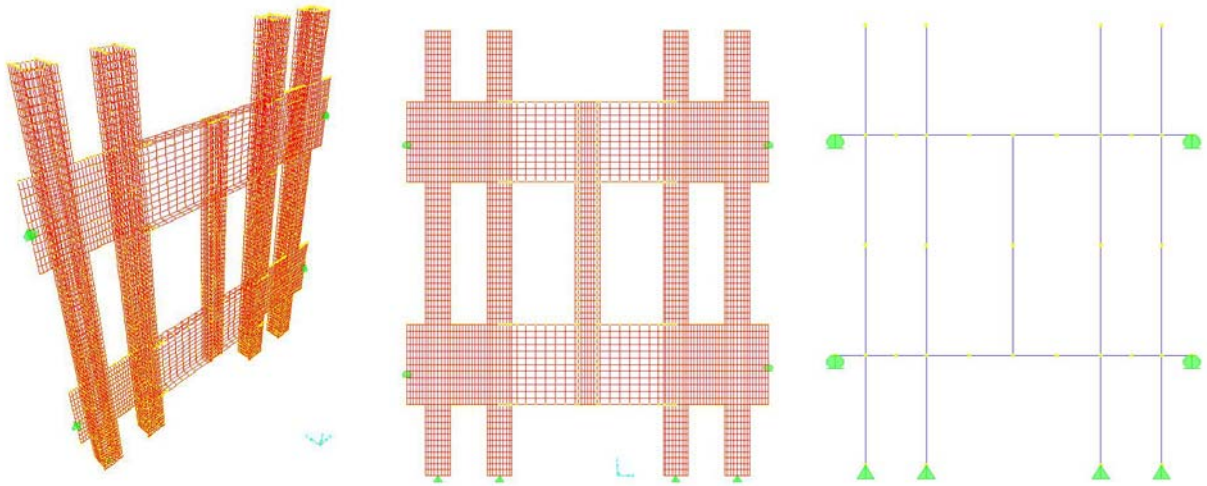

Figure 2–9. Shell element and frame models of typical exterior wall corner panel.

Floor 107 to 110

The exterior wall members from floors 107 to 110 were typically rolled shapes with a yield strength of 42 ksi or 50 ksi (where not shown in the drawings as 50 ksi, a yield strength of 42 ksi was used). Frame elements were used to model the columns and spandrels of the exterior walls at these floors. Spandrel depths varied at floors 108 and 110. A weighted average of spandrel depth was calculated in order to

define the average centerline elevation of the spandrels and, therefore, the node elevation for the entire floor.

2.3.2 Core Columns Modeling

The core columns were typically built-up box members at the lower floors and transitioned into rolled structural steel shapes at the upper floors for both towers. Core columns were modeled as frame elements spanning from node to node, defined at the representative floor elevations (centerline of spandrels). Splices in core columns occurred typically 3 ft above the floor level. In the models, however, the splice was considered to occur at the floor level, and nodes were only defined at these levels. Most three-story column pieces were unique. In the model, a section for each three-story piece was defined and assigned to each of the three frame members that represented that column.

Core column coordinates were tabulated based on the structural drawings. Column locations were typically referenced at their centerlines. However, columns on lines 500 and 1000 were located in plan drawings along most of their height according to the face of the column into which the floor trusses connected (i.e., WTC 1 north face for 500 series columns and south face for 1000 series columns). The centerline of these columns was based on their dimensions given in the drawing books. Where these column centerlines varied along the height of the towers (typically 1 1/2 in. between three-story pieces), a representative location was chosen to define the column node. Thus, the column coordinate at floor 106 was used as a constant along the tower height because at this level, these columns aligned with the hat truss above.

2.3.3 Hat Truss Modeling

In both WTC 1 and WTC 2, a truss system referred to as a ‘hat truss’ was constructed between floor 107 and the roof. The hat truss system was intended to support the load of the antenna on top of the tower and to interconnect the exterior walls to the core. Four trusses spanning perpendicularly to the long direction of the core and four trusses spanning perpendicularly to the short direction of the core were constructed atop the towers (refer to Figs. 2–10 and 2–11). The wide flange core columns represented the vertical members of the hat trusses. The diagonals were primarily wide flange rolled sections, with the exception of the end diagonals between the core and the exterior walls, which were built-up box sections. The majority of the horizontal members in the hat truss system were wide flange and built-up box section floor beams.

Members of the hat truss were modeled using frame elements. These frame elements between floors 107 and 110 were assigned to the model according to plan and elevation drawings of the hat truss. Node locations were set to coincide with the centerline of spandrels at the exterior wall. All columns and diagonals shown in the drawings were included in the model. Floor beams that did not participate in the hat truss system were not included in the model, unless they were used to transfer truss chords to the core columns. Flexible floor diaphragms (see Section 2.3.4) were used to represent the floors within the hat truss area.

In general, diagonals and columns of the hat truss were assumed to be non-composite, and floor beams were assumed to be composite. Hat truss diagonals, main chords, and main columns were modeled with continuous joints. However, hat truss beams had pinned ends.

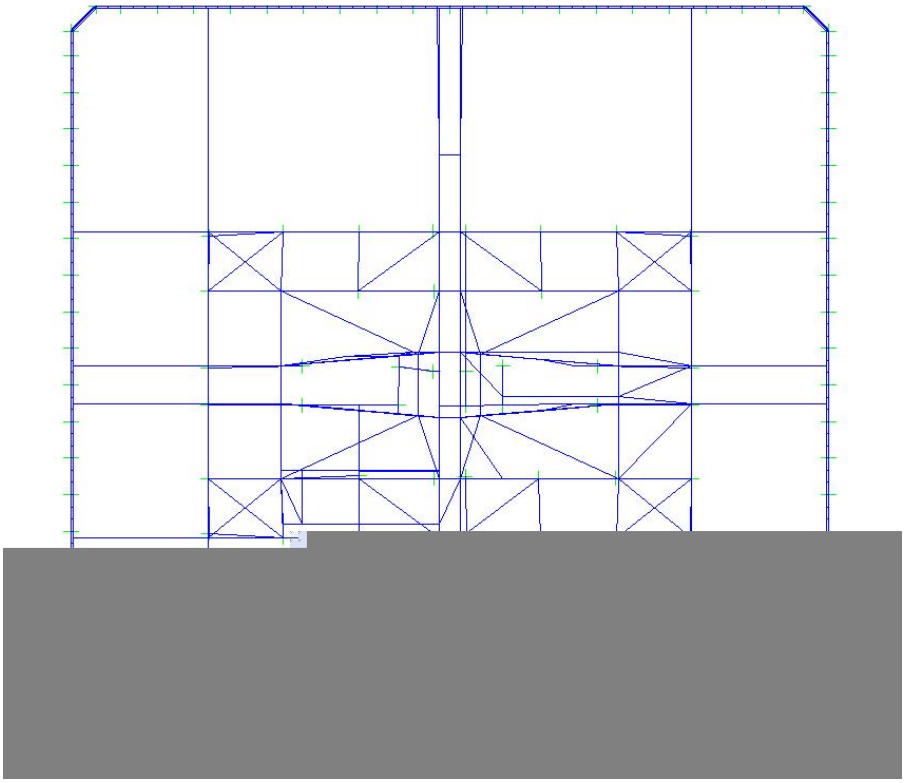

Figure 2–10. As-modeled plan of the WTC 1 hat truss.

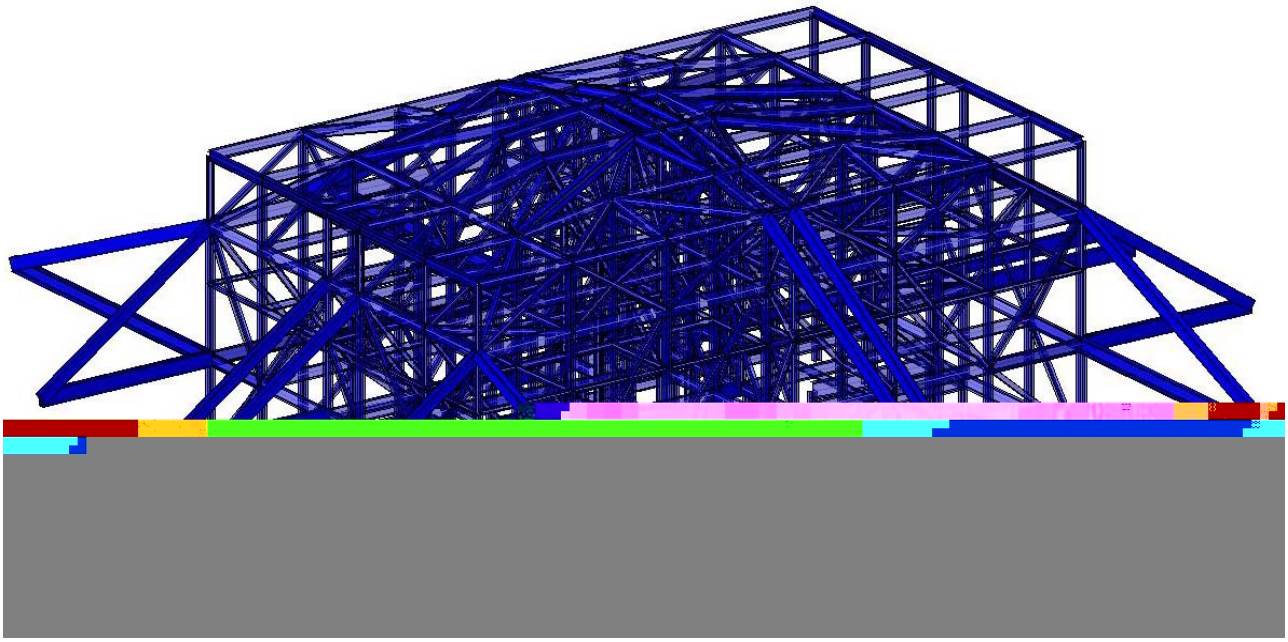

Figure 2–11. Rendered 3–D model of the WTC 1 hat truss.

2.3.4 Flexible and Rigid Floor Diaphragm Modeling

For floors with high in-plane stiffness, a rigid diaphragm constraint causes all of its constrained joints to move together as a planar diaphragm that is rigid against in-plane deformation. This is customarily done in practice for lateral force analyses to reduce the size of the building models. For most floors of the WTC towers, this constraint provided for a sufficiently accurate representation of the flow of forces and deformations for global structural response. Where the flow of forces and deformations would be significantly affected by the use of rigid diaphragms in the global models, the floors were modeled as flexible diaphragms.

Flexible diaphragms were used at the floors of the towers in the core of the atrium area, in the mechanical floors, and in the floors of the hat trusses. The floors modeled using flexible diaphragms included:

- Atrium levels: floors 3, 4, 5, 6, 7, and 9.
- Mechanical levels: floors 41, 42, 43, 75, 76, and 77.
- Hat truss levels: floors 107, 108, 109, 110, and roof.

The flexible floor diaphragms consisted of equivalent shell element floor models attached to all exterior wall columns and core columns.

The floor models developed as described in Sections 2.4 and 2.5 (see Fig. 2–12) were used to develop the flexible diaphragm stiffness used within the global models. For that purpose, parametric studies were conducted to compare the diaphragm stiffness of the two different floor models for both the typical truss-framed floor and the beam-framed floor. The simplified floor models duplicated the representation of the exterior wall columns and spandrels, core columns, and their boundary conditions. The difference between the detailed and simplified models was that the floor framing for the simplified models, both inside and outside the core, was replaced by a course mesh of shell elements (see Fig. 2–13). The material properties of the simplified shell model matched the properties of the concrete floor outside the core in the respective floor model.

The detailed and simplified floor models were loaded in the plane of the floors with a lateral load of 180 lb/ft on both the windward and leeward faces. The column base supports were released for the exterior wall columns along the loaded faces and for all core columns to allow lateral translation only in the direction of loading. The horizontal deflections of both floor models were calculated on both the windward and leeward sides of the model. Both the total horizontal deflection of the slab and the relative displacement between the windward and leeward sides were compared between the models. The shell thickness of the simplified model was modified to match the in-plane stiffness determined by the detailed floor models.

The deformations from the lateral load case using the 75th floor model of WTC 2 are illustrated in Fig. 2–12, while Fig. 2–13 shows the deformations of the simplified floor model. Figure 2–14 shows the lateral deflection of the north and south sides of the floor model under lateral load applied in the north direction using the detailed and equivalent floor models.

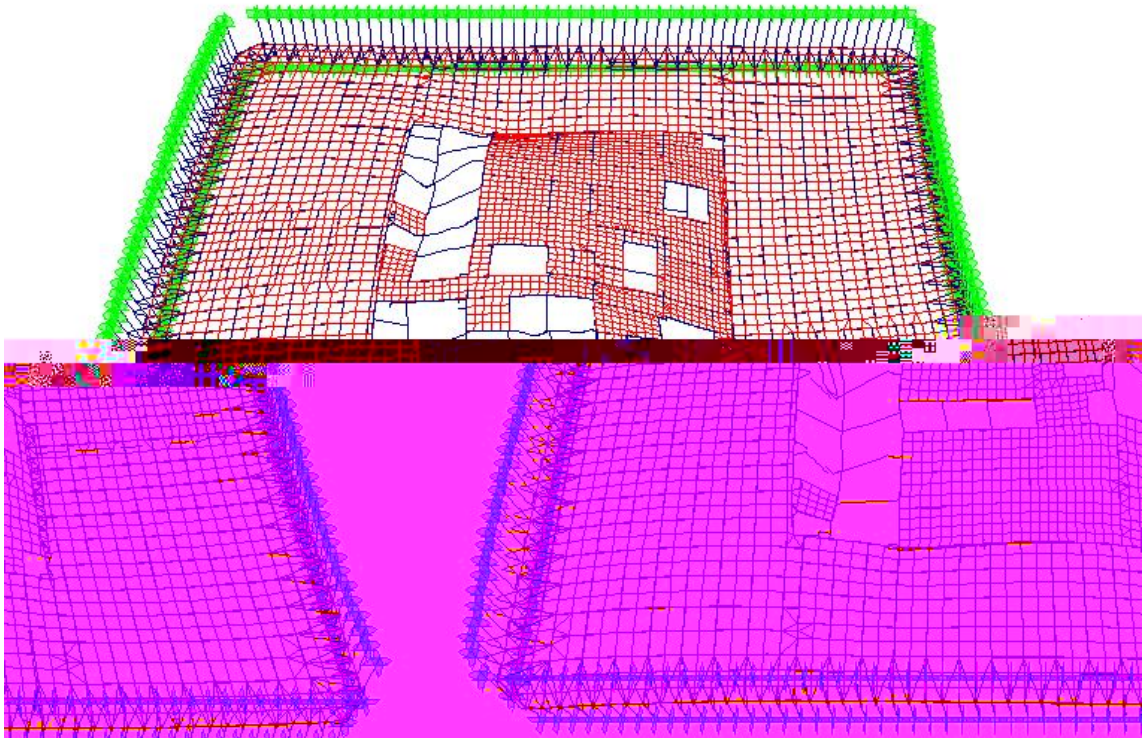

Figure 2–12. Deflection of typical beam-framed floor model due to lateral loading (exaggerated scale).

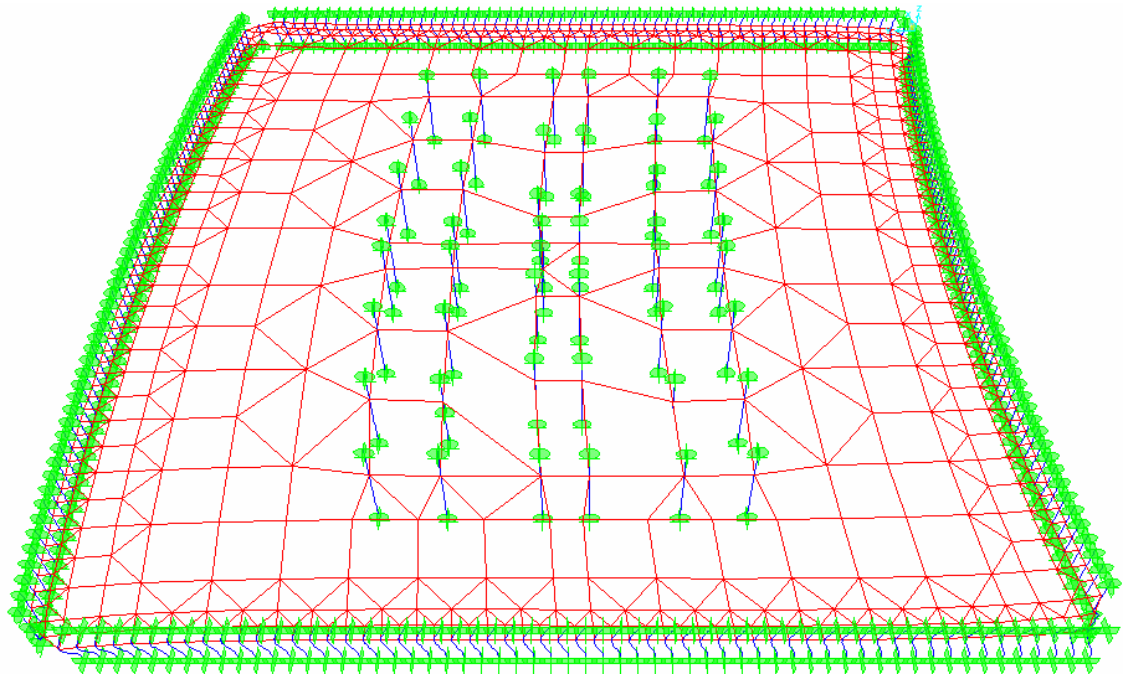

Figure 2–13. Deflection of equivalent floor model due to lateral loading (exaggerated scale).

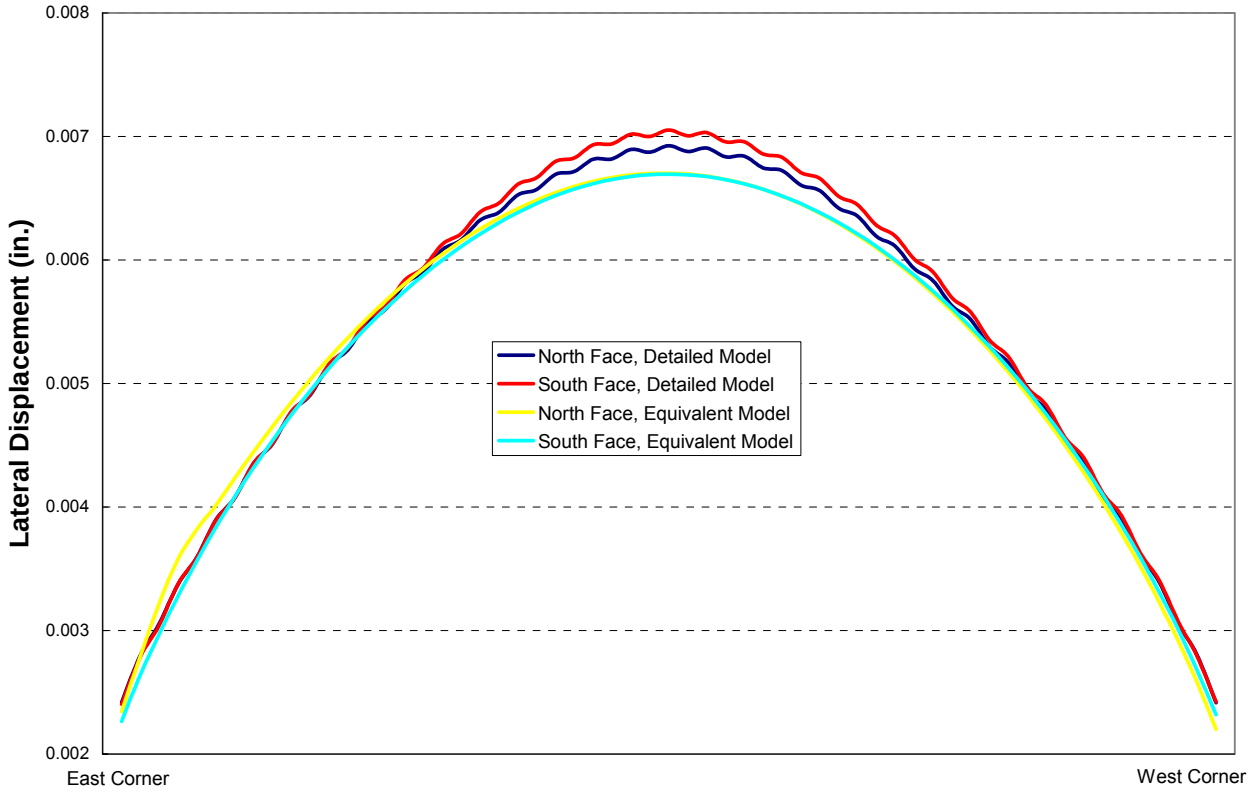

Figure 2–14. Deflections of the north and south faces of the floor for the detailed and equivalent floor models.

2.3.5 Boundary Conditions

The global models of the WTC 1 and WTC 2 towers were pin-supported at the bottom of the models, i.e., all translations were restrained and all rotations were permitted at the foundation level. No restraints were provided to account for the effect of floors at the basement levels outside the footprint of the towers.

2.3.6 Results of Modal Analysis

A modal analysis was conducted to estimate the natural frequencies of the WTC 1 and WTC 2 towers. The mass of the towers was estimated from the construction and superimposed dead loads only (see NIST NCSTAR 1-2A for further details). No live loads were used in estimating the floor masses for the modal analysis. The calculated first six periods and frequencies for WTC 1 and WTC 2 are presented in Table 2–3 without P-Δ effects and in Table 2–4 with P-Δ effects. P-Δ effects refer to secondary effects of column axial loads (designated P) and lateral deflection (designated Δ) on the moments in members, and hence the term P-Δ. Results of modal analysis without P-Δ effects are relevant for small-amplitude vibrations, while those with P-Δ effects are relevant for large-amplitude vibrations. As expected, the natural periods estimated with the P-Δ effects were longer than those without the P-Δ effects. The mode shapes can be found in Chapter 3 of NIST NCSTAR 1-2A.

Table 2–3. Calculated first six periods and frequencies without P-Δ effects.

Direction of Motion	WTC 1			WTC 2		
	Mode	Frequency (Hz)	Period (s)	Mode	Frequency (Hz)	Period (s)
N–S	1	0.088	11.4	2	0.093	10.7
E–W	2	0.093	10.7	1	0.088	11.4
Torsion	3	0.192	5.2	3	0.192	5.2
N–S	4	0.233	4.3	5	0.263	3.8
E–W	5	0.263	3.8	4	0.238	4.2
Torsion	6	0.417	2.4	6	0.417	2.4

Table 2–4. Calculated first six periods and frequencies with P-Δ effects.

Direction of Motion	WTC 1			WTC 2		
	Mode	Frequency (Hz)	Period (s)	Mode	Frequency (Hz)	Period (s)
N–S	1	0.083	12.1	2	0.089	11.2
E–W	2	0.088	11.3	1	0.083	12.1
Torsion	3	0.189	5.3	3	0.192	5.2
N–S	4	0.227	4.4	5	0.250	4
E–W	5	0.250	4	4	0.227	4.4
Torsion	8	0.455	2.2	8	0.455	2.2

Table 2–5 presents a comparison of the calculated first three natural frequencies and periods (N–S direction, E–W direction, and torsion) against measured frequencies and periods for WTC 1. These measurements were based on analyzing acceleration records obtained from accelerometers installed atop WTC 1. The measurements were taken during the period from 1978 through 1994 for wind speeds ranging from 11.5 mph to 41 mph. As the table indicates, the trend is for longer periods measured at larger wind speeds. The table also includes the values of the natural periods and frequencies predicted in the original design. The table shows good agreement between the calculated and measured periods, especially for the periods calculated without P-Δ effects (small amplitude vibrations). Thus, Table 2–5 indicates that the reference global model provided a reasonable representation of the actual structure.

Table 2–5. Comparison of measured and calculated natural frequencies and periods for WTC 1.

Data Source/ Event Date	Wind Speed & Direction	Frequency (HZ)			Period (s)		
		Direction of Motion			Direction of Motion		
		N-S	E-W	Torsion	N-S	E-W	Torsion
Historical Data							
October 11, 1978	11.5 mph, E/SE	0.098	0.105	0.211	10.2	9.5	4.7
January 24, 1979	33 mph, E/SE	0.089	0.093	0.203	11.2	10.8	4.9
March 21, 1980	41 mph, E/SE	0.085	0.092	0.201	11.8	10.9	5.0
December 11, 1992	-	0.087	0.092	-	11.5	10.9	-
February 2, 1993[1]	20 mph, NW	0.085	0.093	0.204	11.8	10.8	4.9
March 13, 1993[1]	32 mph, NW	0.085	0.094	0.199	11.8	10.6	5.0
March 10, 1994[1]	14 mph, W	0.094	0.094	0.196	10.6	10.6	5.1
December 25, 1994[2]	N	0.081	0.091	-	12.3	11.0	-
Average of Measured Data							
Average	-	0.088	0.094	0.202	11.4	10.6	4.9
Orginal Design - Predicted Values							
Theoretical Value	-	0.084	0.096	-	11.9	10.4	-
Reference Global Model							
LERA/NIST - WTC 1 without P-Delta		0.088	0.093	0.192	11.4	10.7	5.2
LERA/NIST - WTC 1 with P-Delta		0.083	0.088	0.189	12.1	11.3	5.3

Notes:

[1]Reported frequency value is the average of the SW corner, NE corner, and center core frequency measurements.

[2]Reported frequency is based on center core data only.

The period of oscillation in the N–S direction of WTC 2 was estimated immediately after aircraft impact based on a detailed analysis of the building motion, which was captured in video footage (Figure E–6 of Appendix E) of the WTC 2 impact (see NIST NCSTAR 1-5A). A frequency analysis of the displacement of the tower at the 70th floor, shown in Fig. 2–15, resulted in a fundamental mode in the N–S direction with a period of approximately 11.4 s, a torsional mode with a period of 5.3 s, and two higher translational modes with periods of 3.9 and 2.2 s. Periods were accurate to within ±0.1 s. The measured fundamental period of 11.4 s ±0.1 s was nearly identical to the calculated period from the model (11.2 s with P-Δ effects for large-amplitude vibrations). Also, the measured torsional period and the higher translational period were almost identical to the calculated periods from the model with P-Δ effects (5.2 s and 4.0 s for the torsional and higher translational modes, respectively).

The maximum displacement of the WTC 2 tower at floor 70 was measured to be about 12 in., while the maximum sway of the tower at the top was approximately 27 in. (NIST NCSTAR 1-5A).

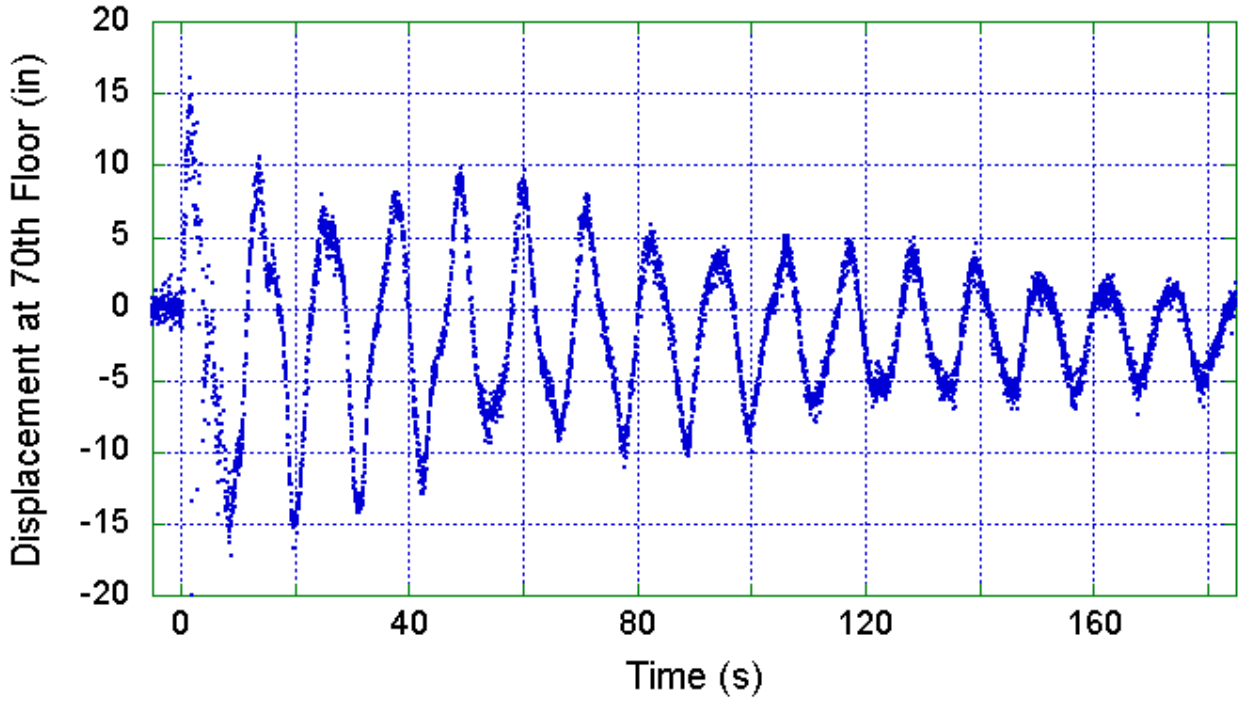

Figure 2–15. Displacement of floor 70 of WTC 2 after impact based on video analysis (NIST NCSTAR 1-5A).

The impact of the aircraft into WTC 2 caused the tower to sway back and forth for almost four minutes. The estimated period of oscillation was found to be nearly equal to the calculated first mode period of the undamaged structure, indicating that the overall lateral stiffness of the tower was not affected appreciably by the impact damage. The maximum deflection at the top of the tower was estimated to be more than 1/3 of the drift resulting from the original design wind loads (about 65 in. in the N–S direction) as calculated from the baseline analysis (see Chapter 4). Since the lateral stiffness of the building before and after impact was essentially the same, it can be concluded that the additional stresses in the columns due to this oscillation were roughly 1/3 of the column stresses resulting from the original design wind loads, assuming linear behavior and assuming that the oscillation mode shape and the static deflected shape under design wind loads were identical. The building demonstrated an ability to carry this additional load and therefore, still had reserve capacity. This was confirmed by the structural analysis of the damaged towers reported in NIST NCSTAR 1-6.

2.4 TYPICAL TRUSS-FRAMED FLOOR MODEL—FLOOR 96 OF WTC 1

The majority of the floors of the WTC towers were tenant floors, where the areas outside of the core were constructed of steel trusses acting in a composite fashion with concrete slabs cast over metal deck. The trusses consisted of double angle top and bottom chords with round bar webs that extended to the concrete slab to provide the composite action (shear knuckles). Two trusses were placed at every other exterior column line, resulting in a 6 ft 8 in. spacing between truss pairs. The typical floor consisted of three truss zones: a long span zone, a short span zone, and a two-way zone as shown in Fig. 2–16. The span of the trusses was about 36 ft in the short direction and 60 ft in the long direction. The two-way zone included trusses in the long span direction (primary trusses) as well as bridging trusses (secondary

trusses) normally found elsewhere. The secondary trusses had additional strength and connectivity to enable them to act in tandem with the long spanning trusses to form a two-way spanning truss grid. The floor trusses were pre-assembled into floor panels as defined in the contract drawings. The floor panels included primary trusses, bridging trusses, deck support angles, metal deck, and strap anchors. A typical composite beam and slab construction was used for the floors inside the core.

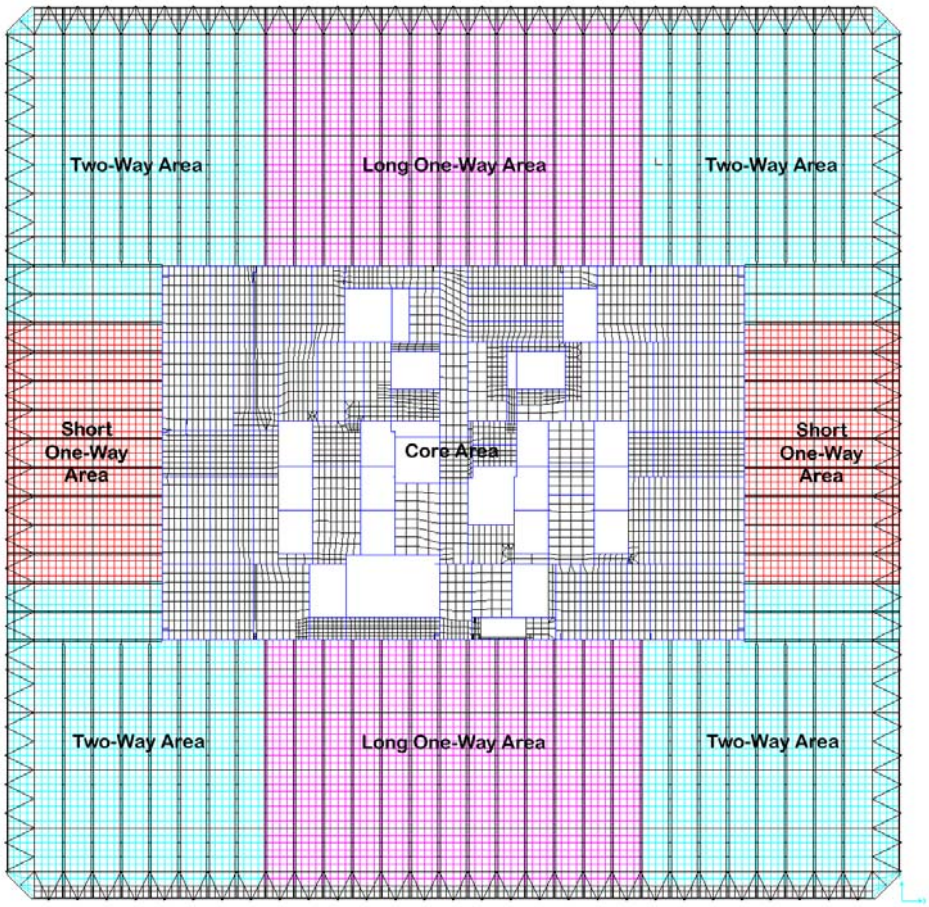

Figure 2–16. Typical floor truss framing zones.

In order to select the typical truss-framed floor within the expanded impact and fire zones of both towers, the drawings for floors 80 to 100 were reviewed to identify structural similarities. Appendix G of NIST NCSTAR 1-2A provides the details of this study. It was found that floor 96 of WTC 1 (96A) represented the typical truss-framed floor in the expanded impact and fire region for WTC 1 and WTC 2. An isometric view of the typical truss-framed floor model is shown in Fig. 2–17. Table 2–1 includes a summary of the size of the 96A floor model. The floor model consisted primarily of frame elements with the exception of the floor slabs, which were modeled using shell elements. The following summarizes the major components of the typical truss-framed floor model.

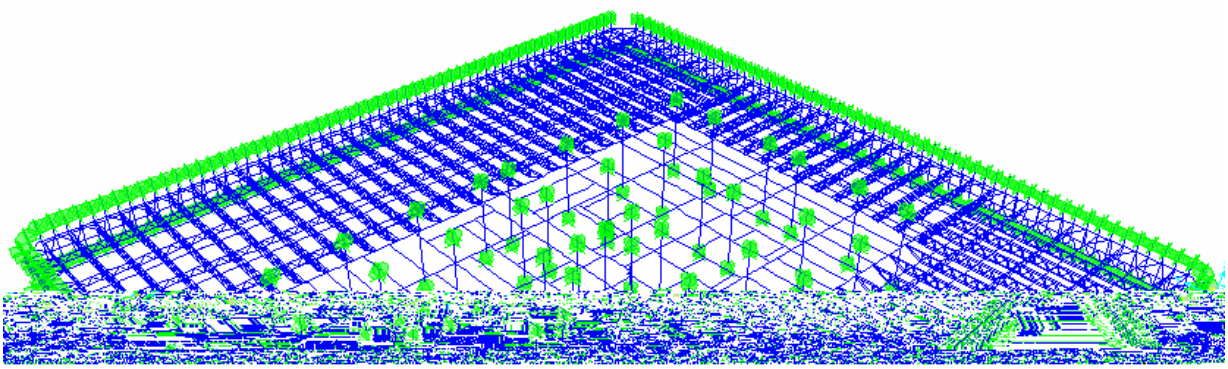

Figure 2–17. Typical truss-framed floor model (floor 96 of WTC 1), slab not shown.

2.4.1 Primary Trusses

The primary trusses consisted of double angle top and bottom chords, which were 29 in. out-to-out of the chords. The distance between the centroid of the two chords was 28.05 in. For a typical long-span truss, C32T1, the top chord consisted of two angles 2 in. by 1.5 in. by 0.25 in. and the bottom chord consisted of two angles 3 in. by 2 in. by 0.37 in.; both chords were short legs back-to-back. The top chords acted compositely with a 4 in. concrete slab on 1 1/2 in. metal deck. The distance from the centroid of the top chord to the neutral axis of the transformed composite slab with top chord was calculated to be 1.93 in. In the model, therefore, 30.0 in. (28.05 in. + 1.93 in. =29.98 in.) was assumed as the typical distance between the top and bottom chords for both short- and long-span primary trusses, see Fig. 2–18. The shell element representing the floor slab was located at the same level as the beam elements representing the top chord.

In the long-span truss zone, the two individual primary trusses, which were part of the same floor panel and attached to the same column, were separated, typically by a distance of 7 1/8 in. At the joint between panels, the distance between the abutting long-span trusses was 7 1/2 in. Therefore, in the model, 7 1/2 in. was used as the spacing between all long-span primary trusses. In the short-span truss zone, two individual trusses which attached to the same column were separated by a distance that varied between 4 7/8 in., 5 in., and 5 1/4 in. In the model, the typical spacing between all short-span double trusses was

5 in. The long span trusses in the two-way zone had an as-modeled length of 58 ft 10 in., while the long-span trusses in the one-way zone had an as-modeled length of 59 ft 8 in.

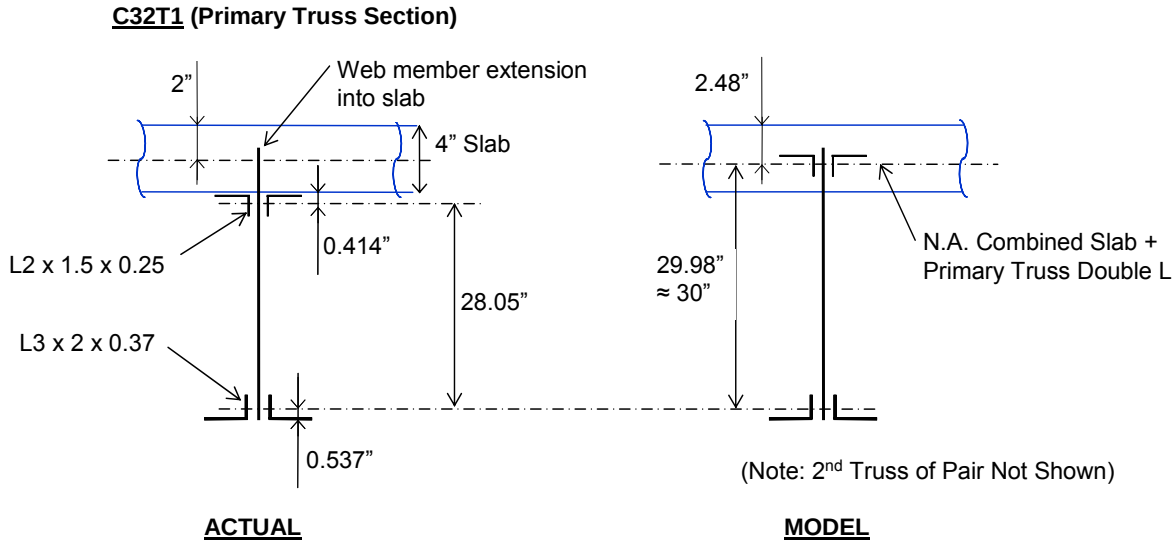

Figure 2–18. Typical primary truss cross-section, as-designed and as-modeled.

The diagonal web bars for the primary trusses were most often 1.09 in. diameter bars. Therefore, for double angle shapes in the primary trusses, 1.09 in. was taken as the distance between the two angles. This holds true for primary trusses where bar diameters varied between 0.92 in. and 1.14 in. The as-designed truss diagonals had end fixity, but were considered pinned in the model. Pinning the diagonals provided an upper bound of the gravity load stresses. To mitigate the effect of the pinned member approach, end length offsets were used for the truss diagonals to account for the difference between the as-built and the as-modeled unbraced length of the diagonal. A similar approach was used for the diagonals of the bridging trusses.

In 30 percent of the floor area, truss members were supplemented with cover plates. The members with additional plates included top chords, web members, and most typically bottom chords. The primary truss top chords were reinforced with an additional set of double angles at truss end connections. At these locations, the work points for the section were located at the centroid of the composite double angle and concrete slab. Plates 3/8 in. by 3 in. connected the bottom chord of the primary truss pairs together at each end and at the intersection with a bridging truss. These plates were included in the model.

2.4.2 Bridging Trusses

The bridging trusses were 24 in. deep, edge-to-edge, with double angle chords. For a typical bridging truss, 24T11, the top and bottom chords consisted of two angles 1.5 in. by 1.25 in. by 0.23 in. The distance between the centroid of the two chords was 23.26 in. The distance used as the offset between the top and bottom chords for all bridging trusses was taken as 23.25 in. (Fig. 2–19). The distance between the top chord of the bridging truss and the top chord of the primary trusses and equivalent slab plate for truss 24T11 was calculated to be 3.39 in. and was selected to be 3.375 in. for all bridging trusses. As in the as-designed structure, the bridging truss was not connected along its length to the slab shell elements

in the model. The intersection of the top chords of the primary and bridging trusses was modeled using vertical rigid links, connected in turn to the slab shell elements representing the concrete slab.

For bridging trusses in the model, a 0.75 in. angle gap was used for trusses with web bar diameters that varied between 0.75 in. and 0.98 in.

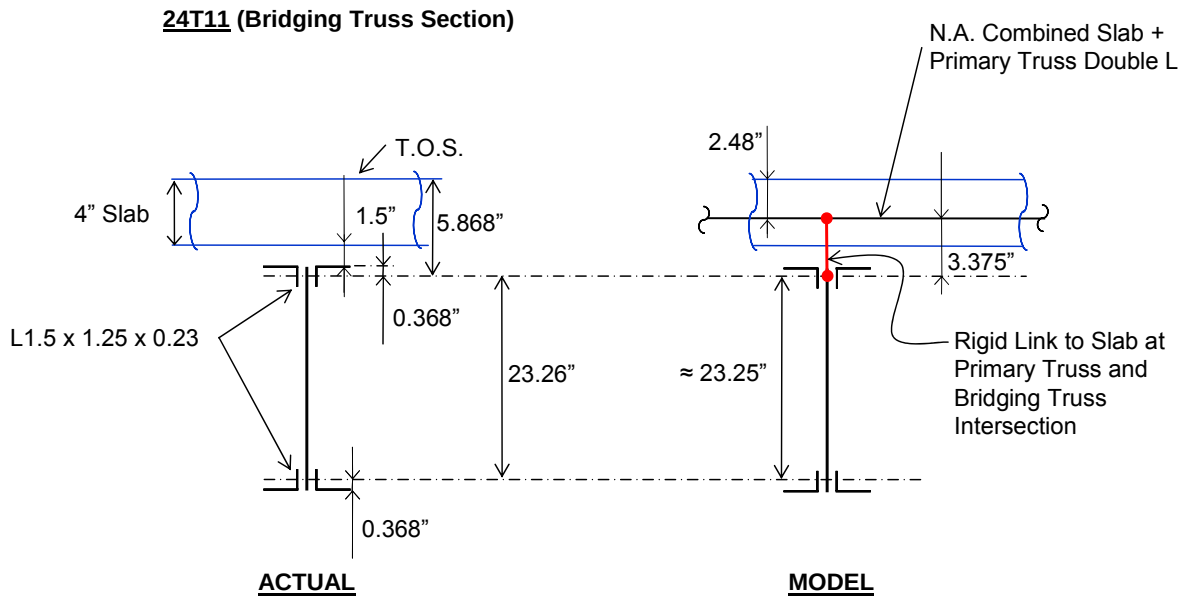

Figure 2–19. Typical bridging truss cross–section, as-designed and as-modeled.

2.4.3 Concrete Slab and Metal Deck

Outside the core, the primary trusses acted compositely with the 4 in. concrete slab on 1 1/2 in. metal deck. In the model, the average depth of the slab plus deck was modeled as 4.35 in. The concrete slab consisted of lightweight concrete with a self-weight of 100 pcf and a design compressive strength, f'_c= 3,000 psi. The concrete modulus of elasticity, E_c, was 1,810 ksi. These values were consistent with those included in the WTC Structural Design Criteria Book. In the as-designed structure, composite action was achieved by the shear connection provided by the web bar extending above the top chord and into the slab (shear knuckle). This composite action was modeled by assuming a rigid connection between the concrete slab and the top chord at the intersection with the diagonal (knuckle location).

Typically, inside the core, the beams acted compositely with a 4 1/2 in. formed concrete slab. The concrete slab consisted of normal weight concrete with a self-weight of 150 pcf and a design compressive strength, f'_c= 3,000 psi. The concrete modulus of elasticity, E_c, was 3,320 ksi. In the as-designed structure, composite action was achieved using shear stud connectors between the beam tops and the slab. This composite action was modeled by assuming a rigid connection between the concrete slab and the floor beams.

The floors of the WTC towers had an in-floor electrical distribution system of electrified metal deck and trench headers. The effects of the in-slab trench headers were included in the model by reducing the slab shell element thickness. A 1 ft 8 in. wide shell panel (the typical truss-floor shell mesh size) was reduced in thickness from 4.35 in. to 2.35 in. or 1.35 in. at the trench header locations.

2.4.4 Viscoelastic Dampers

Viscoelastic dampers were used to reduce the wind-induced vibrations and were located where the bottom chords of the long span, short span, and bridging trusses intersected the exterior columns. The dampers were defined in Drawing Book D. The dampers resisted static and quasi-static loads (such as gravity loads) at the time of load application. Immediately following load application, the dampers shed load until the stress in the dampers was dissipated. A placeholder element was located in the model at the damper location.

2.4.5 Strap Anchors

Exterior columns not supporting a truss or truss pair were anchored to the floor diaphragm by strap anchors. These strap anchors were connected to the columns by complete penetration welds. The strap anchors were then connected to the slab with shear stud connectors and to the top chords of the trusses by fillet welds. The straps were included in the model and located in the plane of the centroid of the composite top chord. Also, in the model the work points intersected with the centerline of the column and used a rigid link to attach back to the spandrel (see Fig. 2–20).

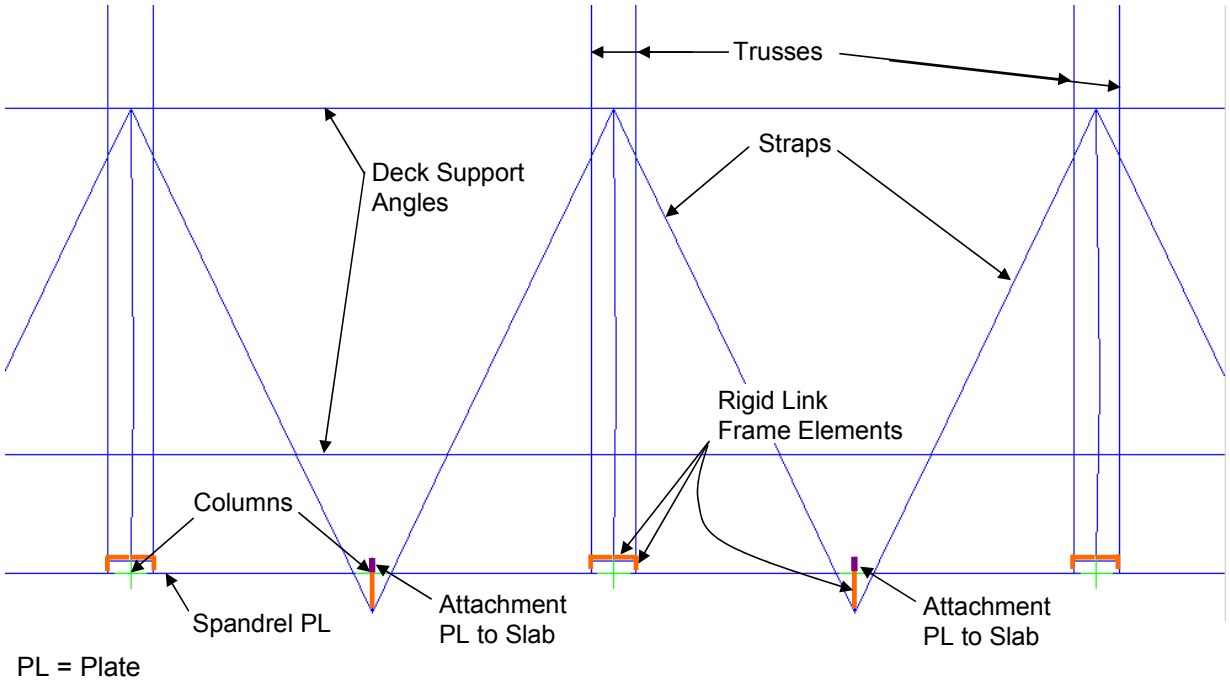

Figure 2–20. Strap anchors modeling, slab not shown.

2.5 TYPICAL BEAM-FRAMED FLOOR MODEL—FLOOR 75 OF WTC 2

Beam-framed floors were used for the mechanical floors within the towers. These floors were constructed using rolled structural steel shapes. The beam framing for the typical floor system consisted of W27 and W16 beams in the long- and short-span regions, respectively. Typical beam spacing was 6 ft 8 in. The steel beams acted in composite fashion with the normal weight concrete slab on metal deck. The deck spanned in the direction of the primary beams and was supported typically at 6 ft 8 in. intervals by a 4C5.4 deck support channel. A 2 in. concrete topping slab was placed on top of the structural slab.

The core area was framed similarly to the core of the truss-framed floors, but the steel beams were typically larger, and the concrete slab was 6 in. deep.

As described in Section 2.4 for truss-framed floors, the structural drawings were reviewed to identify structural similarities between the beam-framed floors within the expanded impact and fire zones of both towers (see Appendix G of NIST NCSTAR 1-2A). It was found that floor 75 of WTC 2 (75B) represented the typical beam-framed floor in the expanded impact zone for WTC 2 (floors 74B to 88B). There were no beam-framed floors within the expanded impact zone of WTC 1. An isometric view of the typical beam-framed floor model is presented in Fig. 2–21. Table 2–1 includes a summary of the size of the 75B floor model. The following presents the major structural systems and components of the beam-framed floor model.

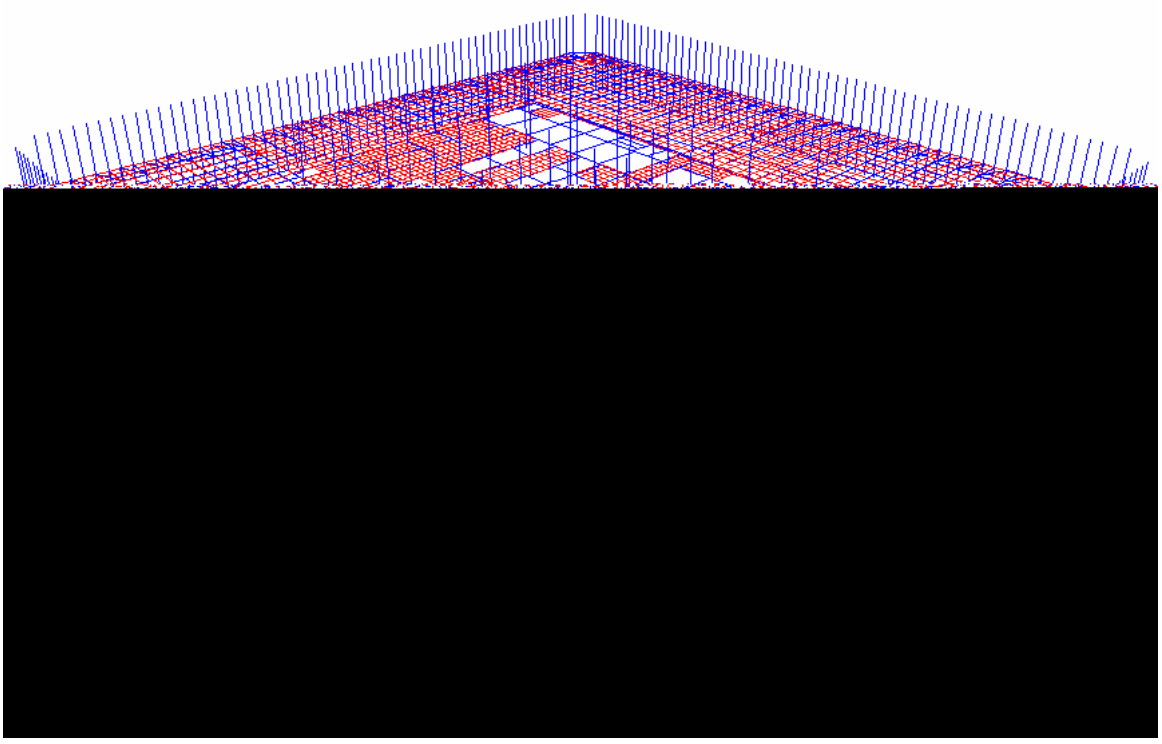

Figure 2–21. Typical beam-framed floor model (floor 75 of WTC 2).

2.5.1 Composite Beams

The beams in the model were located at the elevation of the centerline of the concrete slab. The insertion point for the beams was set at the beam top flange, and then the beam was offset down by one-half the thickness of the slab. The beam was rigidly linked with the slab to simulate the composite action. This option provided for accurate estimation of the composite stiffness of the floor.

2.5.2 Horizontal Trusses

Exterior columns that did not support a beam were connected to the floor for bracing purposes by horizontal trusses. These exterior horizontal trusses were anchored to the columns with complete joint penetration welds. The horizontal trusses were then connected with shear stud connectors to the slab.

The truss angles (typically 4 in. by 4 in. by 5/16 in.) were then connected to the top flange of the beams. In the model, the work points intersected with the centerline of the column and used a rigid link to attach back to the spandrel. The truss members were located in the plane of the centroid of the composite top chord (see Fig. 2–22).

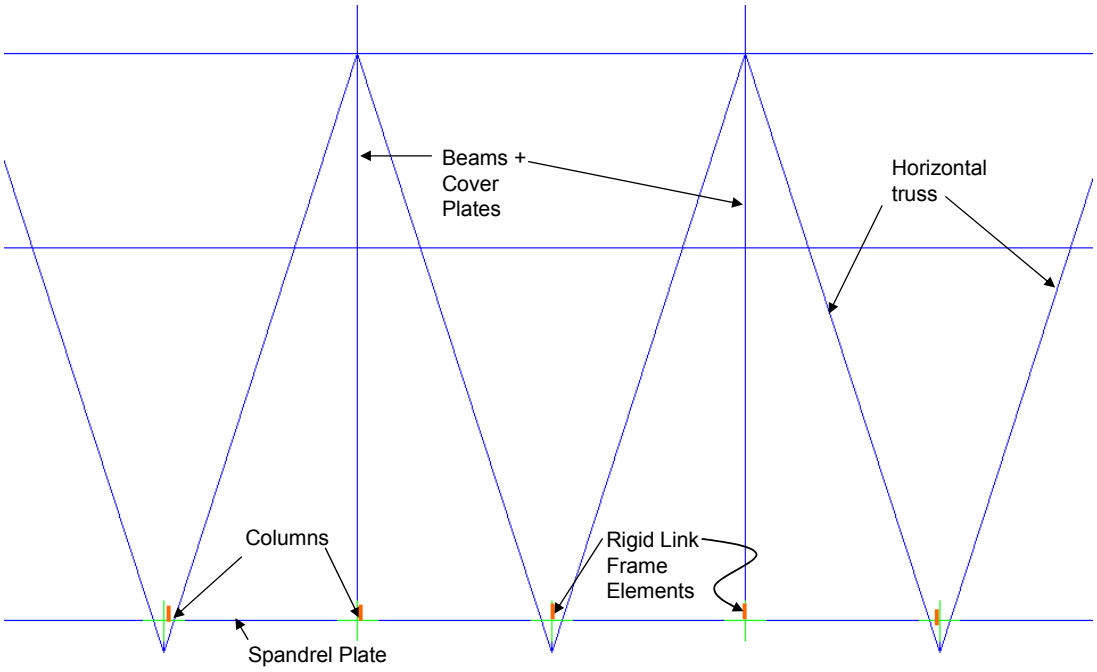

Figure 2–22. Horizontal truss modeling, slab not shown.

2.5.3 Concrete Slab and Metal Deck

Outside the core on the mechanical floors, the beams acted compositely with a 5 3/4 in. concrete slab on 1 1/2 in. metal deck. The average depth of the slab in the model was taken as 6.1 in. The concrete slab consisted of normal weight concrete with a self-weight of 150 pcf and a design compressive strength of typically f'_c= 3,000 psi. The concrete modulus of elasticity, E_c, was 3,320 ksi. Typically, inside the core, the beams acted compositely with a 6 in. formed concrete slab. The concrete slab consisted of normal weight concrete with the same properties as concrete outside the core.

The mechanical floors had a 2 in. maximum depth topping slab, both inside and outside the core. The topping slab stiffness was not included in the models, but this dead weight was accounted for in the baseline performance analyses.

2.5.4 Viscoelastic Dampers

Viscoelastic dampers were located below the bottom flange of the beams where the beams intersected the exterior columns. Similar to the typical truss-framed floor model, a placeholder element was located in the model at the damper location.

2.6 REVIEW OF THE STRUCTURAL DATABASES AND REFERENCE MODELS OF THE TOWERS

The following summarizes the results of the third-party review by the firm of SOM and the in-house NIST review for the developed structural databases and reference models.

2.6.1 Structural Databases

The third-party review by SOM included random checks of the digitized structural databases and cross section property calculations. The review indicated no discrepancies between the developed databases and the original drawing books. Also, for cross section property calculations, the review indicated good agreement (within 1 percent) between the properties in the developed databases and those estimated by SOM.

The in-house NIST review included the following steps: (1) line-by-line review of all database files, (2) random checks on the developed databases by the NIST investigator, and (3) calculation of all cross section properties and comparison with those in the developed databases. The review indicated minor discrepancies between the developed databases and the original drawing books. For cross section property calculations, good agreement was obtained between the properties in the developed databases and those estimated by NIST. The discrepancies between the developed databases and the original drawing books were reported to LERA, and they implemented the changes and modified the databases accordingly. Consequently, the structural databases were approved by NIST and were made available for other phases of the NIST investigation.

2.6.2 Reference Structural Models

The third-party review by SOM included: (1) random checks of the consistency of the developed reference models with the original structural drawings and drawing books, (2) verification and validation of the models (including reviewing assumptions and level of detail), and (3) performing analyses using various loading conditions to test the accuracy of the models. The review concluded that the developed models were consistent with the original design documents, and that, in general, the modeling assumptions and level of detail in the models were accurate and suitable for the purpose of the Investigation. The SOM review identified two areas where the models needed to be modified. The first was the effect of additional vertical stiffness of the exterior wall panels due to the presence of the spandrel beams (see Section 2.3.1). The second area was the modeling of the connections of the floor slab to the exterior columns of the 75B floor model (Section 2.5), where this connection appeared to be fixed while it would be appropriate to model it as pinned.

The in-house NIST review included: (1) checks on the consistency of the developed reference models with the original structural drawings and drawing books, (2) verification and validation of the models (including reviewing assumptions and level of detail), and (3) and performing analyses using various loading conditions to test the accuracy of the models. The review indicated minor discrepancies between the developed reference models and the original design documents. Similar to the third-party review, the in-house NIST review identified the proper modeling of the vertical stiffness of the exterior wall panels and the accurate modeling of the floor slab connections to the exterior columns in the 75B floor model as areas that needed to be modified in the models.

In addition, NIST conducted a workshop for NIST investigators and contractors to review the reference structural models developed by LERA. The workshop attendees included experts from LERA (two experts); SOM (two experts); Teng and Associates (one expert, contractors on probable structural collapse); Professor Kaspar Willam (contractor on thermal-structural analysis); Dr. David M. Parks (contractor on computational mechanics for aircraft impact analysis); Applied Research Associates (two experts, contractor on analysis of aircraft impact into the WTC towers), as well as all key investigators from NIST (17 experts). The purpose of the workshop was to discuss the methodology, assumptions, and details of the developed reference models. The feedback from the workshop was included in the final review of the models. The minutes of the workshop were made public.

The discrepancies between the developed models and the original design documents, as well as the areas identified by both the third-party and the NIST in-house review as needing modification, were reported to LERA, which implemented the changes and modified the models accordingly. Subsequently, the reference structural models were approved by NIST and were made available for use in other phases of the NIST investigation.

2.7 SUMMARY

This chapter described the development of the reference structural models for the WTC towers. These reference models were used to establish the baseline performance of the towers and also serve as a reference for more detailed models for the aircraft impact damage analysis and the thermal-structural response and collapse initiation analysis. The main types of the models developed were:

- Two global models of the towers, one each for WTC 1 and WTC 2. The models included all primary structural components in the towers, including exterior walls (columns and spandrel beams), core columns, exterior wall bracing in the basement floors, hat trusses, and rigid and flexible diaphragms representing the floor systems. To validate the global models, the calculated natural frequencies of WTC 1 were compared with those measured on the tower, and good agreement between the calculated and measured values was observed.

- One model each of a typical truss-framed floor (floor 96 of WTC 1) and a typical beam-framed floor (floor 75 of WTC 2) in the impact and fire zones in the two towers. The models included all primary structural components in the floor system, including primary and bridging trusses, beams, strap anchors and horizontal trusses, concrete slabs, and viscoelastic dampers. Both models were developed using frame elements, except for the concrete slabs which were modeled using shell elements with typical element sizes of 20 in. and 40 in. for the truss-framed floor and the beam framed floor, respectively.

Prior to the development of the reference models, databases of the primary structural components of the towers were developed from the original computer printouts of the structural design documents and modifications made after construction. These databases facilitated the development of the global models of the towers.

The structural databases and reference structural models were developed by LERA and were reviewed by SOM and NIST.

2.8 REFERENCES

SAP2000 (2002), Linear and Nonlinear Static and Dynamic Analysis and Design of Three-Dimensional Structures Basic Analysis Reference, Computers & Structures Inc., Berkeley, CA.

This page intentionally left blank.

Chapter 3
WIND LOADS ON THE WTC TOWERS[1]

3.1 INTRODUCTION

Wind loads were a governing factor in the design of the World Trade Center (WTC) towers' perimeter frame-tube system. The study of the wind loads on the WTC towers was required for evaluating: (1) the baseline performance of the towers under design loading conditions, (2) the towers' reserve capacity to withstand unanticipated events such as a major fire or impact damage, and (3) design practices and procedures.

The accurate estimation of the wind loads on tall buildings is challenging, since wind engineering is still an evolving technology. As is shown in this chapter, estimates of the wind-induced response presented in two recent independent studies of the WTC towers differed from each other by about 40 percent. This discrepancy is indicative of limitations of the current state of practice in wind engineering for tall buildings. Also, as will be shown later in this chapter, wind loads (pressures) specified in current prescriptive codes differ significantly from the loads estimated from wind tunnel-based studies. The study of the wind loads on the WTC towers provided an opportunity to assess current design practices and various code provisions on wind loads.

This chapter outlines the loading cases applied to the reference global models of the WTC towers (Section 2.3) to establish the towers' baseline performance. The following sources were used to develop the loads for the various loading cases:

- Design Criteria document of the WTC towers, prepared by Worthington, Skilling, Helle & Jackson (WSHJ) (henceforth referred to as Design Criteria).
- WTC architectural and structural drawings (henceforth WTC Dwgs).
- Wind reports prepared by WSHJ in the 1960s, describing the development of design wind loads for the WTC towers (henceforth WSHJ Wind Reports).
- Reports from two independent wind tunnel studies concerning the WTC towers, conducted in 2002 by Cermak Peterka Peterson, Inc. (henceforth CPP) and Rowan Williams Davis and Irwin, Inc. (henceforth RWDI) for insurance litigation.
- Current New York City Building Code (henceforth NYCBC 2001).
- Current American Society of Civil Engineers (ASCE 7) Standard (henceforth ASCE 7-02).

[1] This chapter was co-authored by Emil Simiu and Fahim Sadek of National Institute of Standards and Technology (NIST).

Three loading cases were considered for the baseline performance analysis. They included:

- *Original WTC design loads case:* Dead and live loads as in original WTC design in accordance with the Design Criteria, and original WTC design wind loads from WSHJ Wind Reports.

- *State-of-the-practice case:* Dead loads as in original design; NYCBC 2001 live loads; and wind loads from RWDI wind tunnel study, scaled in accordance with NYCBC 2001 wind speed. This wind load was considered to be a lower estimate state-of-the-practice case. As will be explained later, the CPP wind tunnel study produced larger wind loads and was, therefore, considered to be an upper estimate state-of-the-practice case.

- *Refined NIST estimate case:* Dead loads as in original design; live loads from American Society of Civil Engineers (ASCE) 7-02 (a national standard); and wind loads developed by NIST from a critical assessment of information obtained from the RWDI and CPP reports, and state-of-the-art considerations.

The purpose of considering the original WTC design loads case was to evaluate structural performance under original design loading conditions and ascertain whether those loads and the corresponding design were adequate given the knowledge available at the time of the design. In addition, this loading case was useful in evaluating the towers' reserve capacity to withstand unanticipated events such as those of September 11, 2001. The purpose of considering the state-of-the-practice case and the refined NIST estimate case was to better understand and assess the effects of successive changes in standards, codes, and practices on wind design for tall buildings, with a view to helping improve standard provisions for wind loads in the future. The study provided a unique opportunity to achieve this objective.

The gravity loads applied to the global WTC models consisted of dead loads and live loads (LLs), appropriately combined as stipulated in the Design Criteria. Dead loads were applied to the reference global models in two parts: construction dead loads (CDLs) and superimposed dead loads (SDLs), based on the WTC Dwgs and the Design Criteria.

- CDL is defined as the self-weight of the structural system, including floor slabs, beams, truss members, columns, spandrel beams, and so forth.

- SDL is defined as the added dead load associated with architectural, mechanical, electrical, and plumbing systems; such as curtain walls, ceilings, partitions, floor finishes, mechanical equipment and ducts, transformers, and so forth.

Three independent sets of live loads were combined with the dead loads:

- The first set was taken from the Design Criteria and was used with the original WTC design loads case.

- The second set was taken from NYCBC 2001 and was used for the state-of-the-practice case.

- The third set was taken from ASCE 7-02 and was used for the refined NIST estimate case. The live loads given in ASCE 7-02 are essentially identical to the NYCBC 2001 live loads.

For each live load set, live load reductions for column design were taken from their respective source. Refer to Chapter 4 of NIST NCSTAR 1-2A for further details on the estimation of gravity loads in the reference global models of WTC 1 and WTC 2.

Sections 3.2, 3.3, and 3.4 present, respectively, the original WTC design wind loads, the state-of-the-practice wind loads, and the refined NIST wind load estimates. Section 3.5 provides a comparison of the various wind loading cases.

3.2 ORIGINAL WTC DESIGN WIND LOADS

Wind loads were determined for the original design of the WTC towers through the development and implementation of a boundary-layer wind-tunnel study, which simulated the mean and fluctuating (turbulence) properties of the wind from ground to gradient height by using the knowledge and techniques available in the 1960s. Aeroelastic wind tunnel tests were conducted at a 1:500 scale at Colorado State University (CSU), and at a 1:400 scale at the National Physical Laboratory (NPL), Teddington, United Kingdom. Results from the tests conducted at NPL and CSU were in good qualitative and quantitative agreement. The original WTC wind loads were taken from summaries given in Part IV of the WSHJ Wind Reports. For further details, refer to NIST NCSTAR 1-1A.

Wind tunnel data were collected for each tower for wind approaching from 24 wind directions in 15 degree increments. Part IV of the WSHJ Wind Reports provided equations for the wind-induced shears and overturning moments in the towers at 21 elevations, z, along the building height, H, at increments of $0.05H$. For each wind direction, sets of coefficients were provided for use in these equations to obtain the static and the dynamic components of shear and overturning moment in the N–S and E–W directions. Coefficients were also provided for calculating torsional moments. Based on these equations, shears in the two orthogonal directions x and y, and torsions, were calculated for each wind direction. The equivalent effective static shear forces and overturning moments at each level consisted of sums of the respective static and dynamic components. For details see NIST NCSTAR 1-1. The wind speeds at 1,500 ft above ground averaged over 20 min, used in the original design, were assumed to be independent of direction and were estimated to be 98 mph.

Considering the 24 different wind directions and the four combinations of the static and dynamic parts of the N–S and E–W components of the building forces listed below, there were 96 different wind load cases for each tower.

N–S (Static + Dynamic) and E–W (Static + Dynamic)

N–S (Static + Dynamic) and E–W (Static – Dynamic)

N–S (Static – Dynamic) and E–W (Static + Dynamic)

N–S (Static – Dynamic) and E–W (Static – Dynamic)

The static and dynamic shears and overturning moments in the N–S and E–W directions were calculated for all 96 loading cases. In order to determine the most severe of the 96 loading cases for each tower, the wind-induced shears and overturning moments were compared, for each direction, at heights $z/H = 0.75$,

0.50, 0.25 and 0. The wind loading cases producing the maximum shears in either of the two orthogonal directions were identified for application to the global models.

To compare overturning moments for each loading case, the moments in the two orthogonal directions were combined vectorially (i.e., the magnitude of the resultant is equal to the square root of the sum of the squares of the components, and the direction β of the resultant is the arc whose tangent is equal to the ratio of the *y*- and *x*-components). The load cases were grouped by the angle β using increments of 45 degrees, resulting in eight groups of load cases. For each β group, at z/H = 0.75, 0.50, 0.25, and 0, the wind load cases that generated the maximum resultant moment were identified for application to the reference global models. Eight groups of maximum moment plus four directions of maximum shear at four heights in the towers would result in 48 different loading cases. Some individual wind load cases, however, produced a maximum resultant moment and/or a maximum shear at more than one elevation in the towers. As a result, 16 loading cases were identified for WTC 1, and 17 loading cases were identified for WTC 2.

For the floors modeled in the global models by rigid diaphragms, the wind forces were applied as concentrated loads at the geometric center of the building. The torsional moments were also taken into account. For the floors with flexible diaphragms (see Chapter 2), the forces based on tributary areas were resolved into point loads at the perimeter columns. At these floors, the torsional moment was represented by four identical concentrated forces applied parallel to the four faces of the tower at the center column of each face. For each loading case, the orthogonal wind forces were subdivided into windward and leeward forces based on the direction of the wind. The distribution of forces between the windward and leeward sides was based on Figure 6-6 of the ASCE 7-02 Standard (see Chapter 4 of NIST NCSTAR 1-2A for more details).

3.3 STATE-OF-THE-PRACTICE WIND LOADS

For the WTC towers, two wind tunnel tests and wind engineering studies based thereon were conducted in 2002 by independent laboratories as part of insurance litigation unrelated to the NIST investigation. The tests and studies were conducted by CPP and by RWDI. The results of both studies were made available to NIST. Since the CPP and RWDI studies are representative of current practices, their wind load estimates are considered "state-of-the-practice wind loads."

CPP study. The CPP wind tunnel tests modeled the terrain surrounding the WTC towers over an area with a radius of about 2,300 ft. Measurements were made only on the south tower. In one test the south tower was modeled by using a high-frequency force-balance (HFFB) device. In a second test the south tower was modeled aeroelastically. The test scale was 1:400, and testing was conducted for 36 wind directions at 10 degrees intervals. The wind-induced loads and responses were determined by combining the wind tunnel test data with (a) directional non-hurricane wind speed data recorded at three major airports in the New York area for periods of about 25 years, and (b) hurricane wind speed data (the source of the hurricane data was not indicated in the study). The directional wind tunnel and wind speed data were combined by using the sector-by-sector approach, described and assessed in Section 3.4 of this chapter. Wind effects corresponding to a damping ratio of 2.5 percent were provided for the south tower only, for nominal 50 year and 720 year mean recurrence intervals and consisted of peak shear force and bending moment components for two orthogonal directions and peak torsional moments. The peak components were combined in accordance with the "companion point-in-time" method, for example, by

using the full peak load in one direction and the loads in the other direction and in torsion at the time of occurrence of that peak. The CPP report considered 10 such combinations.

RWDI study. The RWDI wind tunnel tests modeled the terrain surrounding the WTC towers over an area with a radius of about 4,000 ft. The tests used an HFFB model for each of the towers and an aeroelastic model for the north tower only. The test scale was 1:500, and testing was conducted for 36 wind directions at 10 degree intervals. Corrections were made to account for the effects on the flow of the presence of building models (i.e., of wind tunnel blockage). Estimates of the full-scale wind effects and responses were obtained by combining the wind tunnel test data with a statistical model of winds for New York City, including surface wind measurements taken at three airports between 1948 and 1995 and proprietary simulated hurricane winds provided by Applied Research Associates (Raleigh, NC). The directional wind tunnel and wind speed data were combined by using an out-crossing approach developed by RWDI. Two sets of wind effects on the towers were developed by scaling the wind loads to the design wind speeds provided in the NYCBC 2001 and to the basic wind speeds specified by the ASCE 7-98 Standard. The wind effects were obtained, for a damping ratio of 2.5 percent, as peak shear forces and bending moments for two orthogonal directions, and peak torsional moments. The peak components were combined using the "principle of companion loads" entailing weighting combination factors based on engineering judgment. The RWDI report considered 24 such combinations.

Note. For both the CPP and RWDI studies, tests were conducted for the two-tower configuration and for a single tower configuration. For the purposes of this investigation, only the two-tower configuration was considered. As was mentioned earlier, the CPP study provided results for the south tower only, while the RWDI study provided wind load estimates for both towers. In the absence of CPP estimates for the north tower, the state-of-the-practice wind loads considered in the baseline study for the north and south towers were selected to be the RWDI wind loads scaled in accordance with a wind speed equivalent to the NYCBC 2001 wind speed. The latter was interpreted to be the 80 mph fastest-mile wind speed at 30 ft elevation over open terrain. In the baseline performance study, these wind loads were applied to the reference global models using the directional and torsional load combination factors presented in the RWDI reports. The application of the wind loads at each floor of the global models was similar for the lower-estimate state-of-the-practice case and for the original WTC design case.

The wind loads from RWDI were smaller than those obtained from CPP for WTC 2 (see Section 3.4). Therefore, RWDI loads may be viewed in this study as a “lower-estimate state-of-the-practice” case.

3.4 REFINED NIST ESTIMATE OF WIND EFFECTS

NIST completed an independent analysis to estimate the wind loads that would be appropriate for use in designing the towers. The analysis was based on results provided by CPP and RWDI, with refinements that drew on the state of the art in wind engineering. The objective of this analysis was to better understand and assess the effects of successive changes in standards, codes, and practices, not to assess the adequacy of the original design wind loads. The analysis yielded refined estimates of wind effects for the north and south WTC towers. These estimates made use of independent extreme wind climatological estimates developed by NIST (Appendix B), based on airport wind speed data obtained from the National Climatic Data Center, National Oceanic and Atmospheric Administration, and on the NIST hurricane wind speed database – the only such database publicly available at present (see Appendix B for details).

The estimates of wind-induced forces and moments provided in this report relied primarily on RWDI results, since no results for WTC 1 were available from CPP. However, the estimates took into account a comparative assessment of the RWDI and CPP results for WTC 2.

3.4.1 Summary Comparison by Weidlinger Associates, Inc., of CPP and RWDI Estimates

A useful summary comparison between CPP and RWDI estimates of maximum base moments and shear forces on WTC 2 induced by ASCE 7-98 wind loads is contained in a memorandum by Weidlinger and Associates.[2] As indicated in that memorandum, the values presented in Table 3–1 are based on nominal basic wind speeds (i.e., 500 yr speeds divided by square root of 1.5 for RWDI, and 720 yr loads divided by 1.6 for CPP).

Table 3–1. Approximate maximum base moments for WTC 2 induced by ASCE 7-98 standard wind loads.

Wind Tunnel Study	$\|M_y\|$ (lb-ft)	$\|M_x\|$ (lb-ft)
RWDI (Table 2a)	10.1e+9	11.1e+9
CPP (Upper Table, p. 21)	14.0e+9	15.5e+9

For the CPP results, the wind directions associated with the largest $|M_y|$ and $|M_x|$ moments were 205 degrees and 215 degrees, respectively (CPP report, Upper Table, p. 21; 0 degrees was defined as True North). Both RWDI and CPP results indicated that the critical base moments occurred for a wind direction of about 210 degrees. This agreement suggested that a comparison between those results was warranted in some detail for the 202.5 to 225 degree range. (The reason for the choice of this range was that hurricane data in the NIST database are provided for the 16 half-octants of the compass.) Such a comparison is presented in this report.

3.4.2 Review of CPP Estimates

Independent estimates by NIST of the 720 yr, 3 s peak gust speeds for the 202.5 degree and 225 degree angles were 104.1 mph and 91.1 mph, respectively (Appendix B, Fig. 1). Linear interpolation between these estimates yielded a 720 yr, 3 s peak gust speed of 99.8 mph for 210 degrees. CPP estimated the 720 yr peak 3 s peak gust speed at 210 degrees to be about 117.5 mph.[3] Therefore, the CPP results were modified through multiplication by the factor $(99.8/117.5)^2=1/1.386$. Owing to the dynamic character of the response, multiplication by the square of the ratio of the speeds is not rigorously correct, but in the absence of sufficiently detailed information it can serve as a useful approximation. A similar conclusion was reached in a letter by RWDI to NIST.[4]

---

[2] Memorandum on Comparison of RWDI and CPP Design Wind Loads, from N.N. Abboud and A. Jain, Weidlinger Associates, Inc., November 11, 2003.

[3] This is obtained through multiplication of the 93 mph speed (basis of design speeds for the 210 degree angle, CPP report, p. 10, upper curve) by the square root of 1.6.

[4] Letter on World Trade Center wind tunnel investigations, by P.A. Irwin, RWDI, November 7, 2003.

In addition to their multiplication by the factor 1/1.386, the CPP results were modified to account for the use by CPP of the sector-by-sector approach to integrating aerodynamic data and extreme-wind climatological data. The sector-by-sector approach is not valid from a physical point of view. This was also noted by RWDI.[5] In attempting to explain the differences between the CPP and RWDI estimates, RWDI assumed that the use of the sector-by-sector approach contributed to the overestimation of the response by CPP. This assumption was due to the difficulty of analyzing the CPP report. Such analysis required a special study by NIST, reported in Appendix C,[6] which concluded that, in fact, the sector-by-sector approach as applied by CPP underestimated the wind effects corresponding to a specified mean recurrence interval. According to preliminary estimates that would need to be confirmed by research using, e.g., Bonferroni bounds (see Appendix C), it was assumed that the underestimation was about 15 percent. Therefore, the CPP results, modified via multiplication by the factor 1/1.386, were further modified via multiplication by the factor 1.15. The reduction factor applied to the estimated CPP effects was, therefore, about $1.15/1.386 \approx 1/1.205$.

Conclusion. The CPP moments presented in Table 3–1 were reduced via application of the factor 1/1.205 from approximately 14.0e+9 lb-ft and 15.5e+9 lb-ft to approximately 11.62e+9 lb-ft and 12.86e+9 lb-ft, respectively. To within the limitations inherent in the information available for this investigation, and to within the approximations noted, these reduced values are reasonable estimates of the actual responses of interest.

3.4.3 Review of RWDI Estimates

According to the conclusion of Section 3.4.2 concerning the modified CPP results, the RWDI results underestimated the moments for the directions being considered. This conclusion is consistent with the fact that RWDI assumed wind profiles in hurricanes to be flatter (to increase more slowly with height) than wind profiles in non-hurricane winds. This assumption, and its effect on the RWDI estimates, were confirmed in the RWDI Response to NIST's Questions, September 2003.[7] The RWDI assumption regarding the relative flatness of hurricane wind profiles was based on a calculation of the ratio between wind speeds at 500 m and at 10 m over open terrain, based on the formula $V(500\text{ m})/V(10\text{ m}) = (500\text{ m}/10\text{ m})^{0.14} = 1.73$. In this calculation it was assumed that, in the power law model of the atmospheric boundary layer over open terrain, wind speeds increase monotonically up to an elevation of at least 1,640 ft (500 m). This assumption is not consistent with accepted practice, according to which in the power law model the mean speed increases with elevation only up to a gradient height which, for open terrain, is about 900 ft (275 m or so), rather than 1,640 ft (500 m) -- see, for example, the ASCE 7 Standard. An unconventional model such as the relatively flat hurricane profile model invoked by RWDI is not supported by measurements in the atmosphere. A recent article in *Nature* (Powell, Vickery, and Reinhold, 2003) indicated that the increase of hurricane wind speeds with height is consistent with the logarithmic law (see Figure 2 of the article). This is also true of extratropical storm winds. It is also noted that the ASCE 7 Standard does not differentiate between wind speed profiles in hurricane and non-

[5] Letter on Review of Wind Tunnel tests, RWDI Reference #02-1310 by P.A. Irwin to M. Levy of Weidlinger Associates, dated October 2, 2002.

[6] See also E. Simiu and J. J. Filliben, "Wind Tunnel Testing and the Sector-by-Sector Approach to Wind Directionality Effects," J. Struct. Eng., ASCE, July 2005, pp. 1143-1145.

[7] Responses to NIST's Questions on "Wind-Induced Structural Responses, World Trade Center, Project Number 02.1310A and 02.1310B, October 2002, by RWDI, Prepared for Hart-Weidlinger", Hart-Weidlinger, September 12, 2003.

hurricane winds, even though wind profiles affecting velocity pressures are defined therein up to 500 ft above ground, where the effect of wind profile differences would be significant.

In response to a NIST query,[8] the use of a ratio of approximately 1.1 between tower responses to 88 mph and 80 mph wind speeds (note 3 at the bottom of Tables 3b and 3c in the RWDI report) was ascribed to the assumption that hurricane wind profiles are relatively flat. This justification is not viewed as satisfactory for the reasons indicated in the preceding paragraph. In view of the current state of the art, according to which hurricane and non-hurricane wind profiles are substantially similar, a ratio of approximately $(88/80)^2=1.21$ is more appropriate than the ratio of approximately 1.1 used by RWDI.

Also, it is not clear that the weighting of hurricane wind speeds in proportion to their squares, as used by RWDI in the out-crossing method, is warranted. No justification was provided in the RWDI report for the weighting procedure based on squares of speeds, nor did RWDI list any reference pertaining to this approach. In the standard Peaks-Over-Threshold approach applied to extreme wind speeds by, among others, Simiu and Heckert (1996), all data above a threshold are affected by the weighting factor 1, while all the data below the threshold are weighted by the factor zero; the analysis is carried out for a large number of thresholds to ascertain the range of thresholds for which the estimates being sought are stable. The use of data lower than the lowest acceptable threshold results in the underestimation of the extreme wind effects being sought. Therefore, it can be expected that the use of such data, albeit weighted in accordance with the RWDI procedure, will have a similar effect. More generally, "concerns that the crossing-rate" (i.e., the out-crossing) "method may underestimate extreme wind-induced effects which depend upon both on wind speed and wind direction" were noted by Isyumov et al. (2003).

The University of Western Ontario (UWO) conducted an independent estimate of wind effects which by and large were reasonably close to the RWDI results.[9] It appears, however, that the assumptions used by UWO and RWDI with respect to hurricane wind profiles were the same or similar. According to UWO, the CPP directionality approach would appear to overestimate the 50 year response. This view is not consistent with the conclusions of Appendix C to this report.

A direct, full quantitative assessment and verification of the RWDI results was judged not to be possible given the information available. Nevertheless, as was shown earlier in connection with the wind profiles, a partial quantitative assessment was made, which indicated that the actual response would be higher than the RWDI estimated response. Given this assessment, and an estimate of the actual response based on the modified CPP estimates, the conclusion that the response was underestimated by RWDI by a factor of about 10 percent to 20 percent was judged to be warranted. The difference between the NIST estimate of the response and the RWDI estimate is smaller than the difference between the CPP estimate and the NIST estimate of the response.

Conclusion. Based on the discussion presented above, loads associated with the refined NIST estimates case and consistent with the design wind speed in the ASCE 7-98 and ASCE 7-02 Standards can be estimated approximately by using the RWDI results multiplied by a factor equal to the ratio of the modified CPP estimates (see Section 3.4.2) to the corresponding RWDI estimates. This factor varies

[8] Letter on Response to NIST Questions of March 30, 2004, by N.N. Abboud, Weidlinger Associates, Inc., April 6, 2004.

[9] Report Regarding the Review of the World Trade Center Twin Towers (NY) Wind Studies Carried Out by RWDI and CPP UWO File W020, cover letter to N. Abboud, Weidlinger Associates, dated November 3, 2003.

from (14.0e+9/1.205)/(10.1e+9) =1.15 to (15.5e+9/1.205)/(11.1e+9)=1.159. Therefore, the factor 1.15 was recommended for baseline analysis. However, the actual factor could be anywhere between, say, 1.10 and 1.20.

3.4.4 Comments by Third Party Reviewer (Skidmore, Owings & Merrill LLP – SOM) – Appendix D

SOM served as a third party reviewer for the wind load estimation by NIST. According to SOM, it would have been desirable for the measured fundamental period of vibration of the north tower to be used in lieu of the calculated periods for either tower. According to the RWDI report, for the south tower the fundamental periods for the *x*-direction (a) not accounting for P-Δ effects, and (b) accounting for P-Δ effects were 12.341 s and 13.292 s, respectively (Appendix A of RWDI report), the difference between them being about 7 percent. The respective estimated *x*-direction base shears in the RWDI report were 9.45e+06 lb and 9.71e+06 lb, respectively, the difference in this case being about 2.7 percent. In the *y*-direction, the differences between the respective shears were less than 1 percent. In view of the uncertainties in the measurement and calculation of the natural periods it is concluded that the differences between shears inherent in the differences between natural periods noted by SOM are not significant.

With respect to the NIST assessment of the CPP and RWDI results, SOM stated that the approach taken by NIST was reasonable, but that SOM was not able to confirm the precise values put forth in the NIST report. SOM noted that quantitative assessments and corrections were made by NIST to the CPP report, and that NIST made only qualitative assessments of the RWDI report. As was indicated in Section 3.4.3, this is indeed the case, except for the quantitative assessment related to wind profiles. No other quantitative assessments were possible, either by NIST or SOM. SOM's inability to confirm precise values is understandable in view of the lack of sufficient clarity in portions of the CPP and RWDI reports. NIST's intent was to recommend reasonable estimates, not precise values. The estimates may be somewhat larger or smaller than the non-attainable precise values. In NIST's judgment approximate bounds to these estimates are defined by the interval of about 1.1 to 1.2 (see Conclusion to Section 3.4.3).

SOM emphasized the urgent need to put order in the field of wind tunnel testing and the estimation of wind effects through standards developed by consensus. NIST fully agrees with this view. It also agrees with SOM's suggestion that the ASCE 7 Standard specify the use of an importance factor larger than unity for buildings representing a substantial hazard to human life in the event of failure. Currently, the ASCE 7 Standard specifies an importance factor larger than unity for buildings designed in accordance with the Standard's "analytical procedure." It does not require the use of the importance factor for buildings whose wind loads are estimated by the "wind tunnel procedure." In fact, neither the CPP nor the RWDI wind loads were augmented by the use of a 1.15 importance factor. It is also noted that even if an importance factor of 1.15 were required to augment wind effects estimated by the wind tunnel method, there could be some confusion over the definition of " buildings … where more than 300 people congregate in one area" (Table 1-1 of the ASCE 7 Standard), for which an importance factor of 1.15 is specified in the "analytical procedure." The question arises whether buildings like the WTC towers are included in that definition. This is not indicated clearly in the ASCE 7 Standard, in which the term "area" may be interpreted by some engineers as being restricted to, e.g., auditoria, rather than apartment buildings or other structures with an occupancy of more than 300 people. NIST also believes that the importance factor should be risk-based, rather than prescribed arbitrarily.

An increase of the wind pressures by an importance factor of 1.15 to account for the large population of some tall buildings (over 5,000 individuals) is specified in Table 1604.5 of the 2003 International Building Code (1BC 2003), which is otherwise mostly based on ASCE 7-02. A consensus should be reached on whether 5,000 is the appropriate threshold.

In addition, it does not appear appropriate for a tall building with significant dynamic effects to have the same load factor as an ordinary, rigid building: the tall building response depends on dynamic response parameters with uncertainties, including, in particular, uncertainty with respect to damping, that should affect the wind load factor applicable to the tall building. This is especially true of buildings designed in accordance with the "wind tunnel procedure." Therefore, research into differences between wind load factors for rigid and flexible buildings is warranted.

3.4.5 Summary

The lateral wind loads on the towers, consistent with the ASCE 7-98 and ASCE 7-02 design wind speed requirements, were estimated by using the effective static floor-by-floor wind loads presented in Table 5a (without P-Δ effects) or Table 5b (with P-Δ effects) of the RWDI report (north tower) for WTC 1 and Table 3a (without P-Δ effects) or Table 3b (with P-Δ effects) of the RWDI report (south tower) for WTC 2.[10] These effective static floor-by-floor wind loads were multiplied by the factor 1.15 (see Section 3.4.3) and by the factors indicated in footnote (3) to Tables 3 and 5 in RWDI to account for the ratio between the ASCE 7 and NYCBC wind speeds. The loads so obtained were applied to the reference global model of each tower using the load combinations presented in Table 6a of RWDI (north tower) and Table 4a of RWDI (south tower). The loads put forth in this section were used along with the load factors given in Section 2 of ASCE 7-02.

It would have been desirable to perform more elaborate calculations providing more comprehensive and precise results than those presented in this document. However, given the information available, this was not practicable.

3.5 COMPARISONS OF WIND LOADS, WIND SPEEDS, AND PRACTICES

The purpose of this section is to provide comparisons among wind loads and wind speeds applicable to the WTC towers in accordance with various codes, standards, and estimation procedures. Sections 3.5.1 and 3.5.2 present comparisons among wind loads and among wind speeds, respectively. Section 3.5.3 compares wind engineering features used to perform the response estimates for the original design and the CPP, RWDI, and NIST estimates.

3.5.1 Wind Loads

Tables 3–2 and 3–3 provide a summary of the wind-induced base shears and base moments[11] on WTC 1 and WTC 2, respectively, based on the 1938 and 1968 versions of the NYCBC, the RWDI study, the CPP study, the refined NIST estimates, and the original design. The wind loads are expressed in terms of two

[10] For the WTC 2 tower Tables 3b and 3c in the RWDI report (South Tower) were inadvertently switched. The loads accounting for P-Δ effects are in fact given in Table 3c of the report.

[11] All base moments presented in this chapter are calculated at the foundation level.

orthogonal components (N–S and E–W for base shears, and about N–S and about E–W for base moments), and of vectorial measures of the most unfavorable combined peaks. The vectorial measures are an indication of the relative conservatism of various methods for combining wind effects in the *x* and *y* directions, and were defined as the largest of a set of vectorial sums of *x* and *y* components, as follows:

- For the RWDI estimates, the set consisted of 24 vectorial sums, each corresponding to one of 24 *x* and *y* load combinations considered in the RWDI report. The combined *x* and *y* values were weighted as indicated in Section 3.3.

- For the CPP estimates, the set consisted of 10 vectorial sums, each sum corresponding to one of 10 *x* and *y* load combinations considered in the CPP report. The combined *x* and *y* values conformed to the "companion-load-in-time" approach described in Section 3.3.

- For the original WTC design estimates, the set consisted of 24 vectorial sums of peak *x* and *y* values, each corresponding to one of the 24 wind directions considered in the original design, as described in Section 3.2.

The NIST estimates were in all cases equal to 1.15 times the RWDI estimates based on the ASCE 7-98 Standard.

Table 3–4 is a summary of design base shears and base moments based on prescriptive provisions at the time of the design in the 1938 and 1968 New York City Building Codes, the 1964 New York State Code, the 1965 Building Officials and Code Administrators Basic Building Code (BOCA/BBC), and the 1967 Chicago Municipal Code.

Tables 3–2 and 3–3 indicate that the two orthogonal components of the original design wind load estimates exceeded in all cases their counterparts based on the New York City Building Code (a prescriptive code) prior to 1968, when the WTC towers were designed, and from 1968 to date. Table 3–4 shows that the design values were also higher than those required by other prescriptive building codes of the time, including the relevant national model building code. It is noted, however, that the prescriptive approach in these codes is oversimplified, and that these codes are therefore not appropriate for super-tall building design. In fact, wind effects obtained from three separate wind-tunnel-based studies (for the original WTC design, the CPP, and the RWDI studies) were in all cases higher than wind effects based on the prescriptive codes.

The two orthogonal base shear and base moment components used in the original design were in the majority of cases smaller than the CPP, RWDI, and NIST estimates. However, the vectorial measures of the most unfavorable combined peaks for the original design were larger, or smaller, by at most 10 percent or so, than those based on the CPP, RWDI, and NIST estimates. This is due to the conservative procedure used to combine the loads in the original design. For example, NIST estimates were higher by about 10 percent than the most unfavorable original design wind loads for WTC 1, and lower by about 5 percent than the most unfavorable original design loads for WTC 2.

Table 3–2. Comparison of wind load estimates for WTC 1 based on various sources.

Source	Year	Base Shear 10^3 kip			Base Moment 10^6 kip·ft		
		N–S	E–W	Most unfavorable combined peak	About N–S	About E–W	Most unfavorable combined peak
NYC Building Code	1938	5.3	5.3		4.2	4.2	
NYC Building Code	1968 to date	9.3	9.3		7.7	7.7	
RWDI / NYC Building Code	2002	11.4	10.5	13.0	10.1	10.5	12.2
RWDI / ASCE 7-98	2002	12.3	11.3	14.0	10.8	11.4	13.1
CPP / NYC Building Code	2002	NA	NA	NA	NA	NA	NA
CPP / ASCE 7-98	2002	NA	NA	NA	NA	NA	NA
NIST / third-party SOM review	2004	14.1	13.0	16.1	12.4	13.1	15.1
Original WTC Design	1960s	9.8	10.6	14.0	10.3	9.1	13.7

Table 3–3. Comparison of wind load estimates for WTC 2 based on various sources.

Source	Year	Base Shear 10^3 kip			Base Moment 10^6 kip·ft		
		N–S	E–W	Most unfavorable combined peak	About N–S	About E–W	Most unfavorable combined peak
NYC Building Code	1938	5.3	5.3		4.2	4.2	
NYC Building Code	1968 to date	9.3	9.3		7.6	7.6	
RWDI / NYC Building Code	2002	9.7	11.1	12.3	10.1	9.2	11.3
RWDI / ASCE 7-98	2002	10.6	12.2	13.5	11.1	10.1	12.4
CPP / NYC Building Code	2002	NA	NA	NA	NA	NA	NA
CPP / ASCE 7-98[a]	2002	15.1	15.3	17.1	15.5	14.0	17.0
NIST / third-party SOM review	2004	12.2	14.0	15.5	12.8	11.6	14.3
Original WTC Design	1960s	13.1	10.1	16.5	8.8	12.6	15.2

a. Using ASCE 7-98 Sections 6.5.4.1 and 6.6.

Table 3–4. Base shears and base moments due to wind loads based on various building codes.

Building Code	1938 NYC Code	1968 to data NYC Code	1964 NY State Code	1965 BOCA/BBC	1967 Chicago Municipal Code
Base Shear (10^3 kip)	5.3	9.3	9.5	9.8	8.7
Base Moment (10^6 kip·ft)	4.2	7.7	7.6	8.5	7.5

3.5.2 Wind Speeds

A comparison of wind speeds is presented in Table 3–5. The ASCE 7-02 Standard specifies a basic design wind speed for New York City of 104 mph at 33 ft above ground for open terrain exposure. This speed is equivalent to an 88 mph fastest-mile wind speed at 33 ft above ground. The wind speed specified by the NYCBC 2001 is 80 mph and is interpreted to be a fastest-mile wind speed at 33 ft above ground. For the original WTC design, a design wind speed of 98 mph averaged over 20 minutes at a height of 1,500 ft above ground was used. This speed is equivalent to a fastest-mile wind speed at 33 ft above

ground in open terrain of about 67 mph, based on wind tunnel measurements by CPP[12], and of about 75 mph, based on the National Building Code of Canada (NBC) provision for centers of large cities[13]. (A similar provision was deleted from ASCE 7 due to its uncertainty.) The 50 yr 3 s peak gust speed estimated by NIST for the three airports (La Guardia, Newark International Airport, and John F. Kennedy International airport), including hurricanes, was about 112 mph (see Figure 2 of Appendix B), regardless of direction. This speed is equivalent to a 96 mph fastest-mile wind speed. Note that the ASCE 7 basic wind speed does not correspond to a 50 yr event. Basic wind speeds in the ASCE 7 Standard are defined as wind speed estimates corresponding to a 500 year mean recurrence interval, divided by the square root of the load factor 1.5. For hurricane-prone regions, the ratio of 500 year speeds to 50 year speeds is typically larger than $\sqrt{1.5}$. Therefore, the mean recurrence intervals of basic speeds in hurricane-prone regions typically exceed 50 years. Table 3–5 shows that significant differences exist among various specified design wind speeds, just as significant differences were noted between, say, base shears and moments estimated by different laboratories for various wind directions. An evaluation of the wind speed specifications and the estimation of improved design wind speeds, as well as protocols for selection of site-specific wind speeds as functions of direction, are, therefore, in order.

[12] A 98 mph wind speed averaged over 20 minutes at a height of 1,500 ft above ground is equivalent to a wind speed averaged over 1 hr at 1,500 ft above ground at the building site, of 98/1.03=95 mph (see Fig. C6-2, ASCE 7-02 Commentary). By using the power law applied to centers of large cities, this speed is approximately equivalent to an hourly mean wind speed at 1,000 ft above ground at the building site of 95 $(1000/1500)^{0.4}$=81 mph. According to wind tunnel measurements in the CPP report, this is equivalent to a 3 s peak gust at 33 ft above ground in open terrain of about 81 mph, or to a fastest-mile wind speed at 33 ft above ground over open terrain of 81/1.26=64 mph. As a check, the averaging time for a 64 mph fastest-mile wind speed is 3,600/64=56 s. The ratio of wind speed averaged over 56 s to the hourly mean speed is 1.26 (ASCE 7-02 Commentary). The ratio of the 3 s speed to the hourly speed is about 1.525. The ratio of the 3 s speed to the fastest-mile speed averaged over 56 s is, therefore, about 1.21. Therefore, a 81/1.21= 67 mph fastest-mile wind speed at 33 ft above ground in open terrain corresponds approximately to a 98 mph 20-min speed at 1,500 ft elevation at the building site.

[13] The hourly wind speed at 1,700 ft above ground at the building site (gradient height for centers of large cities according to NBC Canada) is $(1,700/1,500)^{0.4}$ x 95=100 mph (gradient mean hourly speed). The nominal hourly mean speed at 33 ft above ground in open terrain is $(33/900)^{0.16}$ x 100=59 mph. The fastest-mile wind speed at 33 ft above ground in open terrain is, to a first approximation, 59 x 1.22=72 mph. As a check, the averaging time for a 72 mph fastest-mile wind speed is 3,600/72=50 s. The ratio of the fastest-mile speed to the mean hourly speed is 1.265. Therefore, 59x1.265=75 mph fastest-mile wind speed at 33 ft above ground in open terrain corresponds to a 98 mph 20-min speed at 1,500 ft elevation above the building site.

Table 3–5. Comparison between various design wind speeds.

Source	Wind Speed (fastest-mile at 33 ft above ground over open terrain)
ASCE 7-02	88 mph
NYCBC	80 mph[a]
Original WTC design	67 – 75 mph
NIST estimate	96 mph

a. This wind speed is assumed to be defined as a fastest-mile speed, even though no such definition is explicitly included in the NYCBC.

3.5.3 Wind Engineering Practices Pertaining to Tall Buildings

Table 3–3 shows that, for reasons explained in Section 3.4, the wind-induced loads on the towers estimated by CPP and RWDI differ by about 40 percent. Table 3–6 shows differences among wind engineering features of the original design, the CPP study, the RWDI study, and the refined NIST estimates.

Table 3–6. Comparison between the various wind studies.

Wind Study	Type of Wind Tunnel Testing	Wind Profile	Integration of Aerodynamics with Climatology
Original Design	Aeroelastic	Conventional hurricane wind profile	Extreme wind rosette assumed circular
CPP	HFFB and aeroelastic	Conventional hurricane wind profile	Sector-by-sector approach
RWDI	HFFB and aeroelastic	Hurricane profile flatter than conventional profile	Out-crossing based on sample including weighted low wind speeds
Refined NIST Estimates	Estimates based on RWDI and CPP tests	Conventional hurricane wind profile	Correction to sector-by-sector approach

Such differences highlight the limitations of the current state of practice in wind engineering for tall buildings and the need to put order in the field of wind tunnel testing and wind effects estimation.

The state of the practice with respect to wind loading and response is defined by the relevant assumptions, procedures, and methodologies accepted by professionals engaged in the design of super-tall buildings. Such professionals are structural engineers with unique experience in structural matters, but no special expertise in wind engineering. Therefore, they must rely for definitions of wind loading and response on specialized wind engineering practitioners. The state of practice is therefore *de facto* defined by the advice accepted by practicing structural engineers from wind engineering specialists.

North American structural engineers rely primarily on design wind loads estimated, from wind tunnel tests and extreme wind speed data, by three commercial wind engineering organizations: The Boundary

Layer Wind Tunnel of UWO (London, Ontario), RWDI (Guelph, Ontario), and CPP (Fort Collins, Colorado). Wind load estimates by these three organizations are not necessarily mutually compatible. Therefore, what the state of the practice depends largely upon the preferences structural engineers have for the practices implicit in the advice offered by these organizations, as well as upon prior experience in working with any of them, and wind-study cost considerations. Although some criteria for wind tunnel testing are available in Sect. 6. 6 of ASCE 7-02 and in the ASCE Manual *Wind Tunnel Studies of Buildings and Structures* (1999), they are not sufficient to guide these preferences.

No consensus exists on the wind loading estimates provided by the wind engineering experts. In addition, because, in general, the estimates are proprietary and confidential, no scrutiny of the technical basis of the estimates being provided is generally possible, nor are building inspectors equipped to offer such scrutiny. Finally, and most importantly, the basis for the estimates provided to the structural engineer is commonly presented in a manner that, according to some users, lacks clarity, transparency, and sufficient detail, so that not only the structural engineering user but even specialized wind engineering experts can have difficulty in following and checking key aspects of the calculations on which the estimates are based.

The state of the art in wind engineering for tall buildings is more advanced than the state of the practice. It offers the potential for developing a consensus of acceptable practices based on information and procedures representing the advanced knowledge currently available. Such consensus requires the use of publicly accessible data and methodologies. The realization that transparency and public scrutiny of wind engineering models is in the public interest is illustrated by the recent decision of the Florida Department of Insurance to forgo the use of mutually inconsistent "black box" models for which justifications are not available in any detail, in favor of the development of an open, public model of hurricane-induced losses.

For the reasons discussed in this section it is necessary that the following issues be considered:

- Methods for estimating wind effects with specified mean recurrence intervals that account for the directionality of extreme wind speeds, the aerodynamic response, and the dynamic response.
- Protocols for conducting wind tunnel tests.
- Criteria for flow structure modeling, including mean wind profiles and turbulence features, for various types of wind storms, including hurricanes.
- Protocols for site-specific estimation of extreme wind speeds from National Oceanic Atmospheric Administration (NOAA) and other sources of data for non-hurricane winds.
- Estimates of hurricane wind speeds for all U.S. hurricane-prone regions, similar to estimates currently performed for Florida by NOAA's Hurricane Research Division.
- Load combinations, and material-specific (e.g., steel, concrete, and composites) responses to peak loads.

Consensus standards need to be developed that would ensure that the current state of practice will be brought to a level consistent with the state of the art.

3.6 REFERENCES

ASCE 7-02: American Society of Civil Engineers, ASCE 7 Standard Minimum Design Loads for Buildings and Other Structures, Reston, VA, 2002.

BOCA/BBC 1965: BOCA Basic Building Code, Fourth Edition, Building Officials and Code Administrators, Chicago, IL.

CPP report: Data Report, Wind-Tunnel Tests – World Trade Center, Cermak Peterka Petersen, Inc. August 2002.

Design Criteria: Design Criteria document for the WTC towers developed by Worthington, Skilling, Helle & Jackson.

IBC 2003: International Building Code, International Code Council, Falls Church, VA, 2003.

Isyumov, N., Mikitiuk, M.J., Case, P.C., Lythe, G.R., and Welburn, A., (2003), "Predictions of Wind Loads and Responses from Simulated Tropical Storm Passages," *Proceedings of the Eleventh International Conference on Wind Engineering*, June 2-5 2003, Lubbock, TX, D.A. Smith and C.W. Letchford, eds, Texas Tech University, Lubbock, TX, USA.

Municipal Code of Chicago Relating to Buildings (as amended to and including January 1, 1967), 1967 Index Publishing Corp., Chicago, IL

New York State Building Code, 1964, State Building Construction Code Applicable to General Building Construction, Building Code Bureau, State of New York, New York, NY.

NYCBC 2001: Building Code of the City of New York, 2001 Edition, Gould Publications, Binghamton, NY.

Powell, M.D., Vickery, P.J., and Reinhold, T.A., (2003), "Reduced drag coefficients for high wind speeds in tropical cyclones, *Nature*, Vol. 422, pp. 279-283.

RWDI report: (South Tower) Final Report, Wind-Induced Structural Responses, World Trade Center – Tower 2, Rowan Williams Davis and Irwin, Inc., October 4, 2002.

RWDI report: (North Tower) Final Report, Wind-Induced Structural Responses, World Trade Center – Tower 1, Rowan Williams Davis and Irwin, Inc., October 4, 2002.

Simiu, E. and Heckert, N.A., (1996), "Extreme Wind Distribution Tails: A Peaks Over Threshold Approach," *J. Struct. Eng.* 122 539-547.

Wind Tunnel Studies of Buildings and Structures (1999), ASCE Manuals and Reports on Engineering Practice No. 67, N. Isyumov (ed.), American Society of Civil Engineers, Reston, VA.

WSHJ Wind Reports: A series of wind reports developed by Worthington, Skilling, Helle & Jackson, outlining the development of design wind loads for the WTC towers (see NIST NCSTAR 1-1).

WTC Dwgs: WTC architectural and structural drawings.

Chapter 4
BASELINE PERFORMANCE OF THE WTC TOWERS

4.1 INTRODUCTION

This chapter presents the results of the baseline performance analysis for the World Trade Center (WTC) towers. Results are presented for the global models under the three gravity and wind loading cases described in Chapter 3. These cases included the original WTC design load case (henceforth referred to as original design case), the lower-estimate state-of-the-practice case (henceforth SOP case), and the refined National Institute of Standards and Technology (NIST) estimate case (henceforth refined NIST case). Baseline performance results are also presented for the typical truss-framed and beam-framed floor models under gravity loads only. Baseline performance results include basic information about the towers' behavior under design loading conditions, pertaining to total and inter-story drift (the maximum sway of the building under design wind loads), floor deflections, demand/capacity ratios of primary structural components, exterior columns response (shear lag effects and presence of tensile forces), performance of connections, and resistance of the towers to shear sliding and overturning. The baseline performance analyses in this chapter were conducted under design loading conditions. Analyses under in-service loads of the towers before and after aircraft impact were conducted and reported in NIST NCSTAR 1-6.

This chapter reports on the work conducted by the firm of Leslie E. Robertson Associates (LERA) on the baseline performance analyses. The results were reviewed by Skidmore, Owings, and Merrill (SOM) and NIST. The reviews included checking the various load vectors, analysis procedure and results, and design parameters.

Section 4.2 presents the results of the baseline performance analysis for the global WTC 1 and WTC 2 models under the three loading cases. Similarly, Section 4.3 presents the baseline performance results for the two typical floor models. Section 4.4 outlines the third-party review by SOM and the in-house review by NIST of the baseline performance analyses. Section 4.5 presents a summary of the chapter.

4.2 BASELINE PERFORMANCE OF THE GLOBAL MODELS

4.2.1 Analysis Methodology

This section presents the details of the analysis procedure, including staged construction analysis, the load combinations, and method of estimation of the demand/capacity ratios (DCRs) for the structural components.

The global models were analyzed under the three loading cases identified in Chapter 3. For applying the gravity loads to the global models, the nonlinear staged construction analysis function in SAP2000 was used. The purpose of using the staged construction methodology in the analysis was to provide, at the top of the towers, a reasonably accurate distribution of dead loads between the core columns and the exterior walls. The hat truss system that was installed atop the towers distributed gravity and wind loads between the core and the exterior walls. The construction dead loads (CDLs) and superimposed dead loads

(SDLs), put in place prior to the completion of the hat truss system, were not distributed through the hat truss. In order reasonably to differentiate between those loads distributed through the hat truss system and those that were not, the construction sequence was considered in the analysis.

The global model of each tower was subdivided into two portions: floor 106 and below, and the area above floor 106 that included the hat truss. In the first stage, the lower portion of the global model was loaded with all of the CDL and SDL associated with floor 106 and below. In the second stage, the portion of the full model above floor 106 was activated, and the CDL and SDL associated with the upper floors were placed on the full computer model. Live loads on the whole model were applied to the full building with the hat truss engaged in the second stage. This methodology approximated well the way in which the towers were constructed.

For all analysis cases, the DCRs for structural components were estimated using the Allowable Stress Design (ASD) procedure as specified in the American Institute of Steel Construction (AISC) *Specification for Structural Steel Buildings – Allowable Stress Design and Plastic Design – 9th Edition, 1989.* The DCRs were calculated by dividing component demands by component capacities, taken at unfactored (working) loads and at working stresses, not at ultimate loads or yield stresses. These DCRs for the structural components were determined as follows:

1. The component demands were obtained from the results of the baseline performance analysis using the reference global models, and working loads based on the following load combinations:

    - For the original WTC design loading case and for the lower estimate, state-of-the-practice case, the load combinations were those specified by the AISC Specification (1989) and the New York City Building Code (NYCBC) 2001:

        Dead Load

        Dead Load + Live Load

        Dead Load + Live Load + Wind Load

        Dead Load + Wind Load

    - For the refined NIST estimate case, the load combinations were those specified by the American Society of Civil Engineers (ASCE 7-02) Standard:

        Dead Load

        Dead Load + Live Load

        Dead Load + Wind Load

        Dead Load + 0.75 x (Live Load + Wind Load)

        0.6 x Dead Load + Wind Load

2. The component capacities were based on the nominal steel strength as specified in the original design documents and using the AISC Specification (1989):

    - For the original design loading case and for the lower estimate, state-of-the-practice case (consistent with NYCBC 2001), a one-third increase in the allowable stress was

considered for load cases that included wind, as specified at the time of the design and as is currently specified in NYCBC 2001 and AISC Specification (1989).

- For the refined NIST estimate case, where loads were based on the ASCE 7-02 Standard, load combinations were taken from the ASCE 7-02 Standard, which does not allow the one-third increase in allowable stresses.

The interaction equation in AISC Specifications (1989) estimates the DCR as the larger of the following two equations for members subjected to both axial compression and bending stresses:

$$DCR = \frac{f_a}{F_a} + \frac{C_{mx} f_{bx}}{(1 - \frac{f_a}{F'_{ex}})F_{bx}} + \frac{C_{my} f_{by}}{(1 - \frac{f_a}{F'_{ey}})F_{by}}$$

$$DCR = \frac{f_a}{0.60F_y} + \frac{f_{bx}}{F_{bx}} + \frac{f_{by}}{F_{by}}$$

For the case when $f_a / F_a \leq 0.15$, the following equation is permitted in lieu of the previous two equations:

$$DCR = \frac{f_a}{F_a} + \frac{f_{bx}}{F_{bx}} + \frac{f_{by}}{F_{by}}$$

where the subscripts *x* and *y* indicate the axis of bending about which a particular stress or design property applies, and

F_a and F_b are the axial compressive stress and compressive bending stress, respectively, that would be permitted if axial force alone or if bending moment alone existed.

f_a and f_b are the computed axial stress and compressive bending stress at a given point, respectively.

F'_e is the Euler buckling stress divided by a factor of safety.

C_m is a coefficient that depends on column curvature caused by applied moment.

A review of the basic design equations and allowable stresses for combined axial and bending stresses for the 6th Edition of the AISC Specifications (1963), which was in effect at the time of the design, indicated that they are essentially identical to those of the 9th Edition (1989) design equations and allowable stresses. There are, however, some variations between the 6th and 9th Editions of the specification. The 1963 Specification did not specifically address biaxial bending in the combined stress equations. In addition, the allowable stress formulations for bending with lateral torsional buckling are somewhat different between the two design specifications.

For the original design loading case, the SAP2000 program was used directly to estimate the DCRs using the equations presented above. For the lower-estimate, state-of-the-practice case and the refined NIST estimate case, a second order analysis that accounted for P-Δ effects was used to estimate member

demands under the applied gravity and wind loads. The P-Δ analysis resulted in a moment magnification in the components of the global models; and as a result, the terms C_m and $(1 - f_a / F'_e)$ were assigned a unit value in the above equations to estimate component DCRs. For these cases, DCRs were calculated in Excel spreadsheets using results obtained by the SAP2000 computer program.

For further details, see Chapter 5 of NIST NCSTAR 1-2A.

4.2.2 Total and Inter-Story Drift

The calculated total drift of both WTC 1 and WTC 2 induced by the three loading cases is presented in Table 4–1. The table lists calculated total drift values at the top of the tower, in absolute terms and as a fraction of the height, H, from the foundation level to the roof (referred to in the table as the drift ratio). According to LERA, limiting total building drift under wind loads was not part of the original WTC design criteria (see NIST NCSTAR 1-2A). Instead, inter-story drifts were determined at the design stage and were compared with the ability of the architectural building systems such as the partitions and the exterior cladding, to accommodate these inter-story drifts. Accordingly, there is no project-specific data available to which the total drifts may be compared. Figure 4–1 presents the deflected shape of WTC 1 under the three loading cases. Similarly, Fig. 4–2 shows the inter-story drift distribution along the height of the tower, normalized to the story height. The plots are presented for the E–W and N–S directions for the wind load combination that produced the maximum cumulative drift for each case. Similar plots for WTC 2 can be found in Chapter 5 of NIST NCSTAR 1-2A.

Table 4–1. Total drift for WTC 1 and WTC 2 under the three loading cases.

Loading Case	WTC 1				WTC 2			
	E–W		N–S		E–W		N–S	
	Total Drift (in.)	Drift Ratio	Total Drift (in.)	Drift Ratio	Total Drift (in.)	Drift Ratio	Total Drift (in.)	Drift Ratio
Original design case	56.6	H/304	55.7	H/309	51.2	H/335	65.3	H/263
SOP case	56.8	H/303	68.1	H/253	59.7	H/287	56.1	H/306
Refined NIST case	70.6	H/244	83.9	H/205	75.6	H/227	71.0	H/242

Under the original WTC design loads, the cumulative drifts at the top of the WTC 1 tower were about 56.6 in. (H/304) and 55.7 in. (H/309) in the E–W and N–S direction, respectively. For WTC 2 the drifts were about 51.2 in. (H/335) in the E–W direction and 65.3 in. (H/263) in the N–S direction. For the state-of-the-practice case, the drifts for WTC 1 were larger than those from the original design case by about 0.5 percent and 22 percent for the E–W and N–S directions, respectively; for WTC 2 the drift was larger than that from the original design case by about 16 percent and 15 percent for the E-W and N–S drift, respectively. These differences are commensurate with those between the base shears for the two cases.

The drifts obtained from the refined NIST estimate case were about 25 percent larger than those from the state-of-the practice case for both towers.

As Fig. 4–2 indicates, the inter-story drift varied over the height of the tower. Under the original design loading case, the maximum inter-story drift was as high as h/225 and h/195 for WTC 1 and WTC 2, respectively, where h is the story height. Maximum inter-story drifts under the state-of-the practice case were about h/185 and h/200 for WTC 1 and WTC 2, respectively. For the refined NIST estimate case, these inter-story drifts were about 25 percent larger than those from the state-of-the practice case for both towers.

Currently no building codes specify a drift limit for wind design. The ASCE 7-02 Standard states in Section B.1.2 that the drift of structures due to wind effects shall not impair the serviceability of the structure. The commentary to this section of the standard indicates that drift limits in common usage for building design are on the order of 1/400 to 1/600 of the building (for total drift) or story height (for inter-story drift) to minimize damage to cladding and nonstructural walls and partitions. Structural engineers often use in their practice the criterion that total drift ratios should not exceed H/400 to H/500 for serviceability considerations and to enhance overall safety and stability (including P-Δ effects). Typical drift limits used in practice (H/400 to H/500) are superimposed on the drift plots shown as the shaded areas in Fig. 4–1. Reducing the drift of the WTC towers to the range of H/400 to H/500 (about 43 in. to 34 in.) would entail enhancing the stiffness and/or the damping capacity of the towers.

For inter-story drifts, structural engineers often use in their practice an inter-story drift limit in the range of h/300 to h/400. This is primarily done for serviceability considerations. Typical inter-story drift limits used in practice (h/300 to h/400) are superimposed on the inter-story drift plots shown as the shaded areas in Fig. 4–2. Similar to total drift, inter-story drifts of the towers were larger than what is generally used in practice today.

4.2.3 Demand/Capacity Ratios

The DCR statistics for WTC 1 obtained from the reference global model under the original WTC design loading case, the lower-estimate state-of-the-practice case, and the refined NIST estimate case are summarized in Tables 4–2, 4–3, and 4–4, respectively. The statistics include, for each member category, the total number of members, the mean value of the DCRs, their coefficient of variation (C.O.V.), the percentage of components with DCR greater than 1.0 and greater than 1.05, the number of components with a DCR greater than 1.05, and the maximum calculated DCR. The DCR statistics for WTC 2 under the three loading cases were comparable to those presented herein for WTC 1. See Chapter 5 of NIST NCSTAR 1-2A for details.

Fig. 4–3 shows the distribution of DCRs for the four exterior walls of WTC 1 under the original design load case. Close-up views are shown for the exterior walls below floor 9 in Fig. 4–4. DCRs for the WTC 1 core columns are provided in Fig. 4–5. Similar plots for WTC 2 DCRs can be found in Chapter 5 of NIST NCSTAR 1-2A.

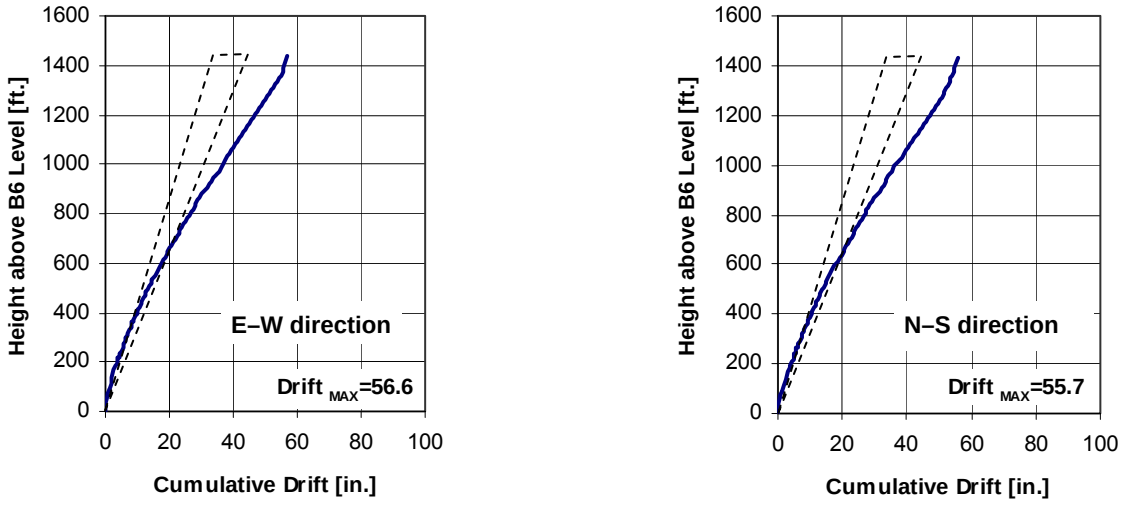

(a) Original WTC design wind loads

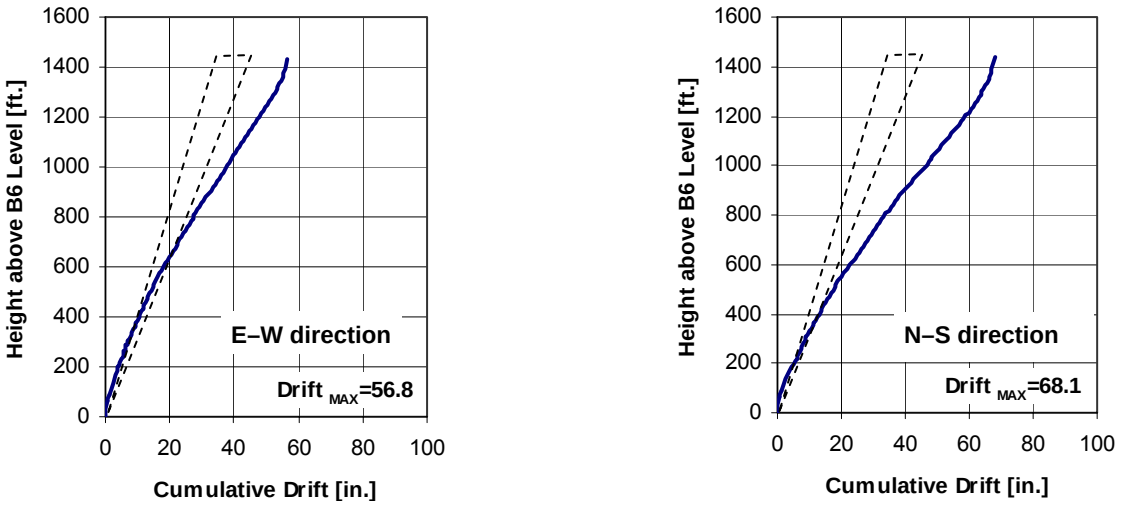

(b) Lower estimate, state-of-the-practice wind loads

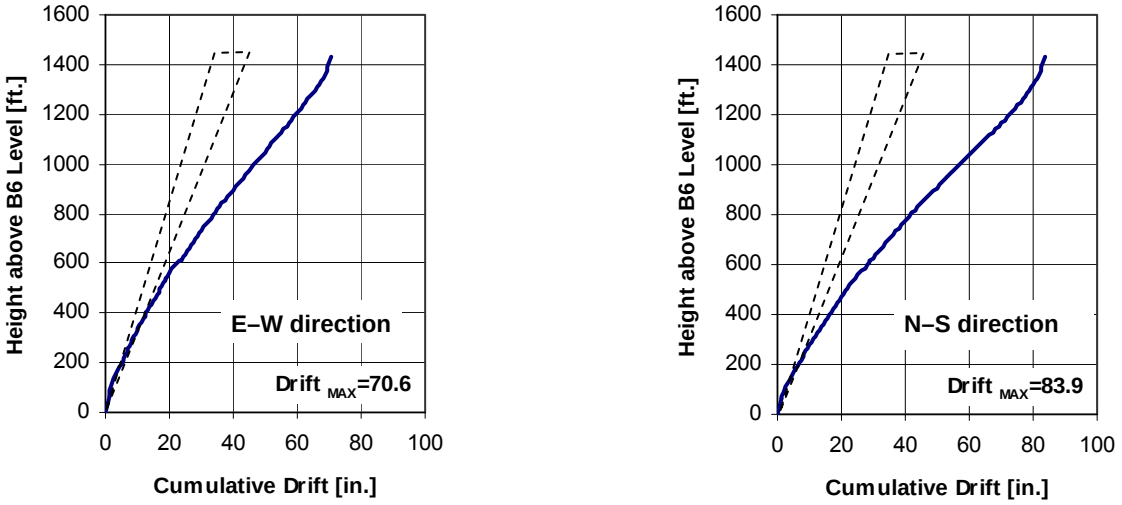

(c) Refined NIST wind loads

Figure 4–1. Cumulative drift diagrams for WTC 1 under the three wind loading cases.

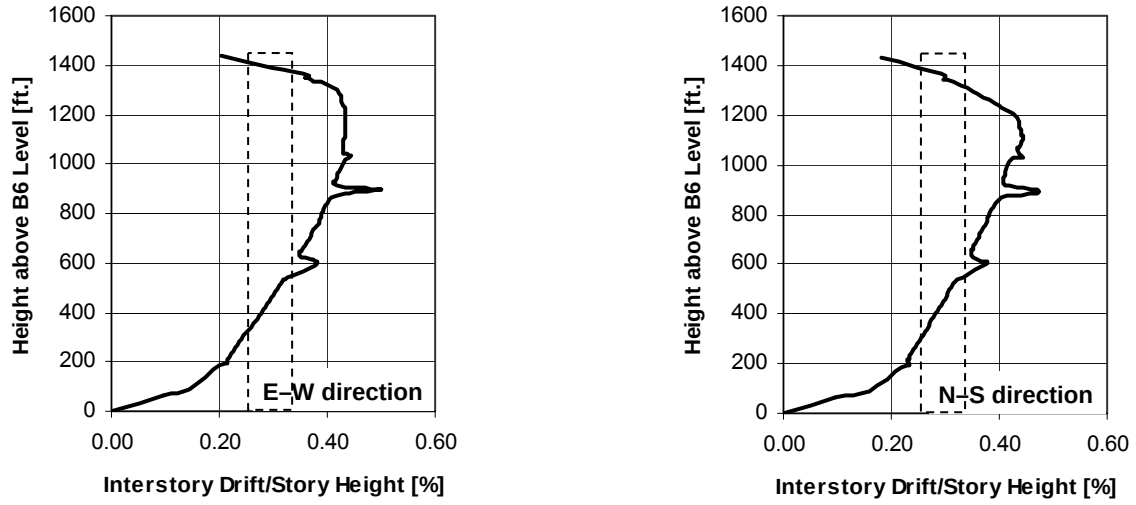

(a) Original WTC design wind loads

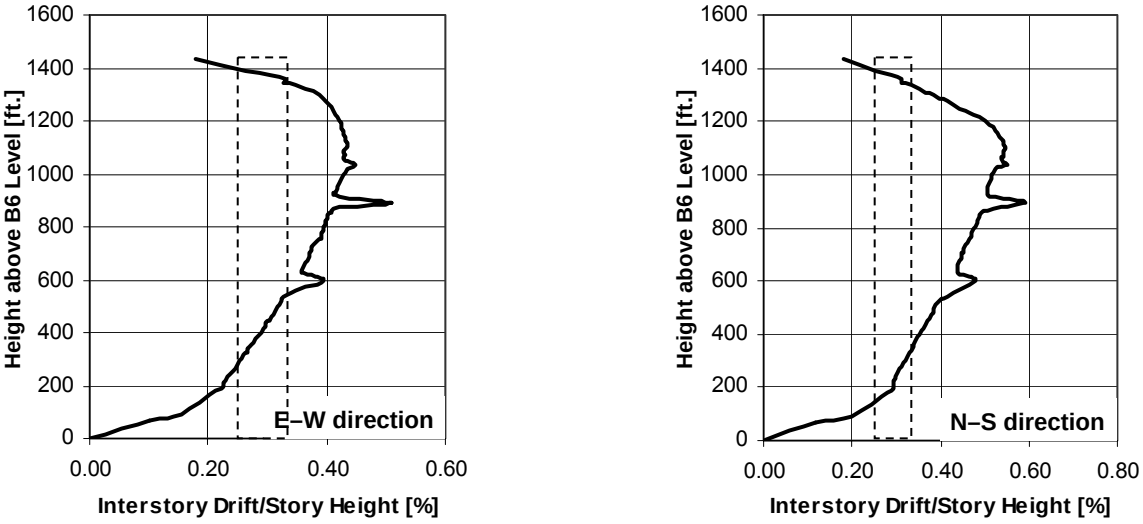

(b) Lower estimate, state-of-the-practice wind loads

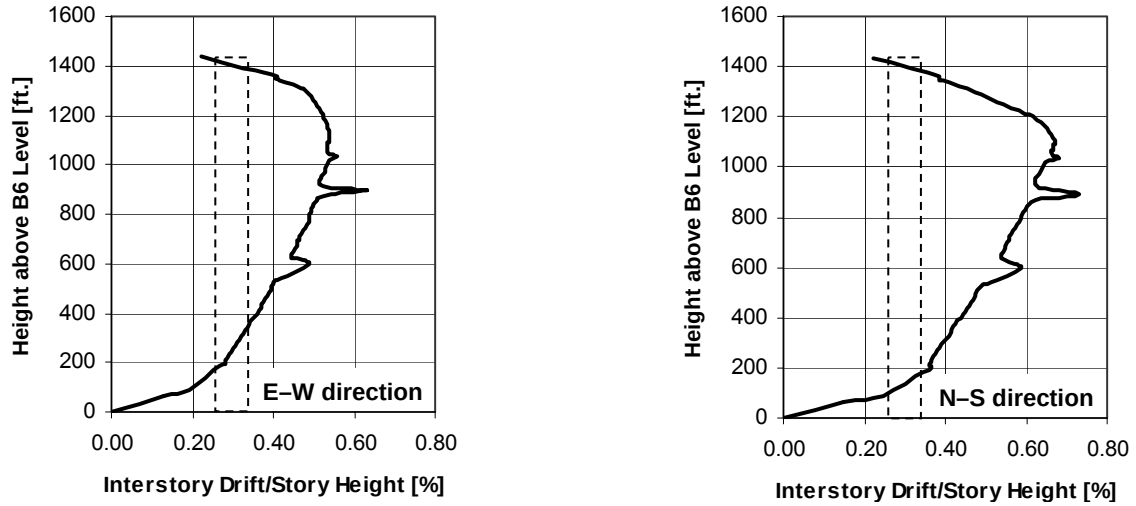

(c) Refined NIST wind loads

Figure 4–2. Inter-story drift diagrams for WTC 1 under the three wind loading cases.

Table 4–2 and Figures 4–3 through 4–5 indicate that under the original WTC design loading case, most structural members had a DCR of less than 1.0. A fraction of the structural members had DCRs in excess of 1.0. These were mainly observed in the exterior walls and core columns.

The types of members in the exterior walls that had DCRs larger than 1.0 were calculated for a combination of axial load and bending under the combination of gravity and wind loads. These included: (1) columns at the corners, (2) where the hat truss connected to the exterior wall, and (3) below floor 9. The members in these locations would be expected to experience a large degree of stress. The corner columns had some of the highest calculated forces under wind loading. The hat truss-to-exterior wall connections interconnected two major structural systems with large concentrated load transfers. The exterior wall below floor 9 was a highly variable and articulated structural system that had large calculated forces.

The core columns that had DCRs larger than 1.0 were calculated for axial stresses due to gravity loads and were generally located: (1) on the 600 column line between floors 80 and 106, and (2) at core perimeter columns 901 and 908 for much of their height. The gravity loads on these columns were affected significantly by assumptions about tributary areas, construction dead loads and superimposed dead loads, and the sequence of construction of the hat truss. According to LERA, the high degree of stress calculated at these core columns was likely associated with differences in these assumptions between the original and current computations.

The results indicated a number of members throughout the structures with DCRs larger than unity, which is inconsistent with the design requirements of the AISC, ASD Specification. One possible explanation may lie in the computer-based structural analysis and software techniques employed for this baseline performance study in comparison with those utilized in the original design nearly forty years ago. An example is the contribution of secondary moments in the various elements, which may have gone undetected in the original analysis and design. The exterior walls of the towers might have the potential for significant redistribution of the loads of members with large DCRs to adjacent members. Demand-capacity ratios greater than 1.0 detected in core columns and hat truss members are less easily resolved as the ability for redistribution may be limited.

While it is a normal design practice to achieve a DCR less than unity, the safety of the WTC towers on September 11, 2001, was most likely not affected by the fraction of members for which the demand exceeded capacity due to the following reasons:

- The allowable stress design method has an inherent factor of safety for structural components. The safety factor is about 1.67 and 1.92 for yielding and buckling, respectively, for components subjected primarily to gravity loads, such as core columns. The factor of safety is reduced by 1/3 for components subjected to wind loads, such as the exterior walls, due to the 1/3 increase in the allowable stresses.

- After reaching the yield strength, structural steel components continue to possess significant reserve capacity, thus allowing for load redistribution to other components that may still be in the elastic range.

- The DCRs presented herein were estimated using the design live loads. On September 11, 2001, the towers were subjected to in-service live loads, which are considered to be approximately 25 percent of the design live loads.

- On September 11, 2001, the wind loads were minimal, thus providing significantly more reserve capacity for the exterior walls.

A comparison between Tables 4–2 and 4–3 indicates that the DCRs estimated from the original WTC design load case were, in general, close to those obtained for the lower-estimate state-of-the practice case for WTC 1. Comparing Tables 4–2 through 4–4, it was found that the DCRs obtained for the refined NIST estimate loading case were higher than those from the original WTC design and the lower-estimate state-of-the-practice load cases, owing to the following reasons:

- The refined NIST estimated wind loads were higher than those used in the lower-estimate state-of-the-practice case by about 25 percent (about 10 percent difference between the RWDI loads scaled to the NYCBC 2001 wind speed and RWDI loads scaled to the ASCE 7-02 wind speed, in addition to the 15 percent increase estimated by NIST, Section 3.4). It is noted that the NIST estimated wind loads were about 20 percent smaller than those estimated by CPP (an upper-estimate state-of-the practice case, see Chapter 3).

- The original WTC design and the state-of-the-practice cases used NYCBC load combinations, which result in lower DCRs than the ASCE 7-02 load combinations used for the refined NIST case.

Similar observations and conclusions could be made for the DCRs estimated for WTC 2 for the three loading cases, see NIST NCSTAR 1-2A.

As part of the in-house NIST review into the baseline performance analyses, the DCRs were estimated using the Strength Design procedure as specified in the AISC Load & Resistance Factor Design (LRFD) Specification for Structural Steel Buildings (1993). The analysis was conducted for the exterior wall columns from floor 9 to floor 106, and for core columns of WTC 1 for the refined NIST estimate case. For this analysis, the load combinations were those specified by the ASCE 7-02 Standard:

1.4 Dead Load

1.2 Dead Load + 1.6 Live Load

1.2 Dead Load + 0.8 Wind Load

1.2 Dead Load + Live Load + 1.6 Wind Load

0.9 Dead Load + 1.6 Wind Load

The DCRs estimated using LRFD for the refined NIST case are presented in Table 4–5, along with the DCRs obtained from the ASD method. The results indicate that the mean DCRs estimated using the LRFD procedure were smaller than those using the ASD procedure by about 15 percent.

Table 4–2. Statistics of DCRs for WTC 1 under original design load case.

Member Type	Number of Members	Mean Calculated DCR	C.O.V. of DCR	Percentage of components with DCR > 1.0	Percentage of components with DCR > 1.05	Number of components with DCR > 1.05	Maximum Calculated DCR
Exterior Wall Columns							
Below floor 1	628	0.77	0.19	4.3	2.7	17	1.36
Floor 1 to 9	1,122	0.74	0.25	3.3	0.5	6	1.27
Floor 9 to 106	31,086	0.76	0.12	1.1	0.4	121	1.31
Above floor 106	578	0.73	0.31	12.3	10.0	58	1.46
Exterior Wall Spandrels							
Below floor 1	420	0.44	0.46	0.7	0.7	3	1.28
Floor 1 to 9	610	0.34	0.45	1.1	1.0	6	1.30
Floor 9 to 106	31,160	0.31	0.30	0	0	0	0.83
Above floor 106	836	0.35	0.69	1.9	1.7	14	1.55
Core Columns	5,219	0.86	0.14	10	5.3	278	1.36
Hat Truss System							
Columns	239	0.47	0.45	0.4	0.4	1	1.26
Beams	499	0.24	0.87	0.4	0.2	1	1.07
Braces	279	0.47	0.53	2.5	0.7	2	1.06
Exterior Wall Bracing							
Below floor 1	200	0.72	0.16	2	1	2	1.16
Above floor 106	12	0.40	0.52	0	0	0	0.75

Table 4–3. Statistics of DCRs for WTC 1 under the lower estimate, state-of-the practice case

Member Type	Number of Members	Mean Calculated DCR	C.O.V. of DCR	Percentage of components with DCR > 1.0	Percentage of components with DCR > 1.05	Number of components with DCR > 1.05	Maximum Calculated DCR
Exterior Wall Columns							
Below floor 1	628	0.77	0.19	6.1	4.0	25	1.30
Floor 1 to 9	1,122	0.78	0.26	13.1	5.2	58	1.15
Floor 9 to 106	31,086	0.78	0.13	2	0.9	281	1.44
Above floor 106	578	0.71	0.31	10.7	7.6	44	1.36
Exterior Wall Spandrels							
Below floor 1	420	0.49	0.46	4	2.4	10	1.26
Floor 1 to 9	610	0.37	0.45	1.3	1.1	7	1.22
Floor 9 to 106	31,160	0.32	0.29	0	0	0	0.80
Above floor 106	836	0.35	0.70	1.9	1.7	14	1.57
Core Columns	5,219	0.86	0.14	9.9	5.3	278	1.36
Hat Truss System							
Columns	239	0.45	0.50	0.4	0.4	1	1.26
Beams	499	0.23	0.93	0.2	0.2	1	1.07
Braces	279	0.41	0.60	1.1	0	0	1.03
Exterior Wall Bracing							
Below floor 1	200	0.76	0.16	2.5	2	4	1.18
Above floor 106	12	0.35	0.47	0	0	0	0.64

Table 4–4. Statistics of DCRs for WTC 1 under the refined NIST estimate case.

Member Type	Number of Members	Mean Calculated DCR	C.O.V. of DCR	Percentage of components with DCR > 1.0	Percentage of components with DCR > 1.05	Number of components with DCR > 1.05	Maximum Calculated DCR
Exterior Wall Columns							
Below floor 1	628	1.04	0.24	52.5	47.3	297	1.95
Floor 1 to 9	1,122	1.11	0.27	69.0	63.6	714	1.69
Floor 9 to 106	31,086	1.10	0.14	72.1	59.7	18572	2.05
Above floor 106	578	0.81	0.28	19.7	14.2	82	1.57
Exterior Wall Spandrels							
Below floor 1	420	0.81	0.46	22.1	21.4	90	2.05
Floor 1 to 9	610	0.61	0.45	8.0	4.3	26	2.03
Floor 9 to 106	31,160	0.52	0.29	0.5	0.3	109	1.32
Above floor 106	836	0.41	0.68	2.4	1.9	16	1.82
Core Columns	5219	0.84	0.15	8.9	5.2	270	1.40
Hat Truss System							
Columns	239	0.53	0.49	3.8	0.8	2	1.26
Beams	499	0.26	0.93	1.8	1.4	7	1.30
Braces	279	0.49	0.55	6.1	2.5	7	1.10
Exterior Wall Bracing							
Below floor 1	200	1.11	0.18	73.0	62.0	124	1.76
Above floor 106	12	0.52	0.42	0	0	0	0.90

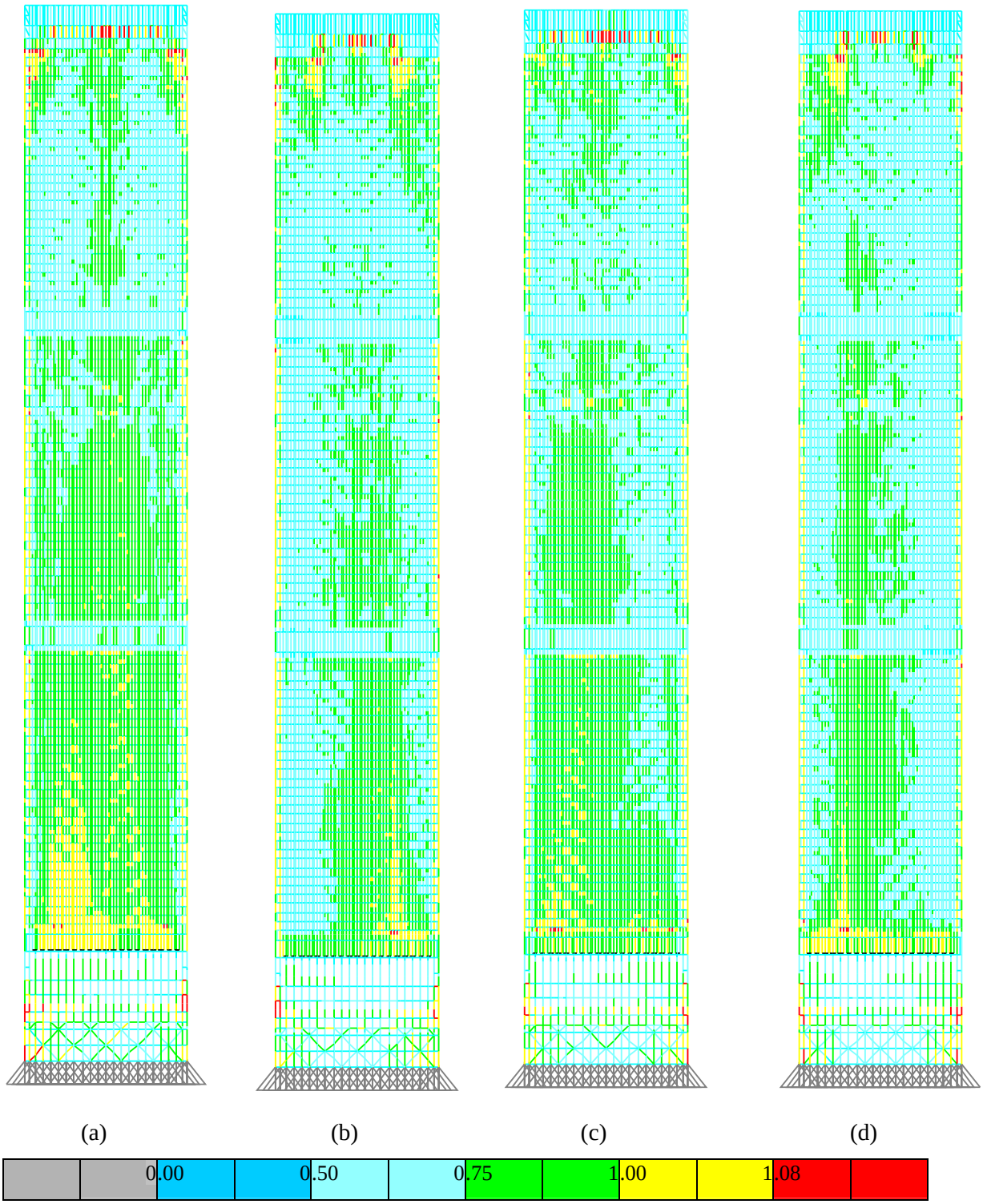

Figure 4–3. DCRs for the exterior walls of WTC 1 under original design case, (a) north elevation, (b) east elevation, (c) south elevation, and (d) west elevation.

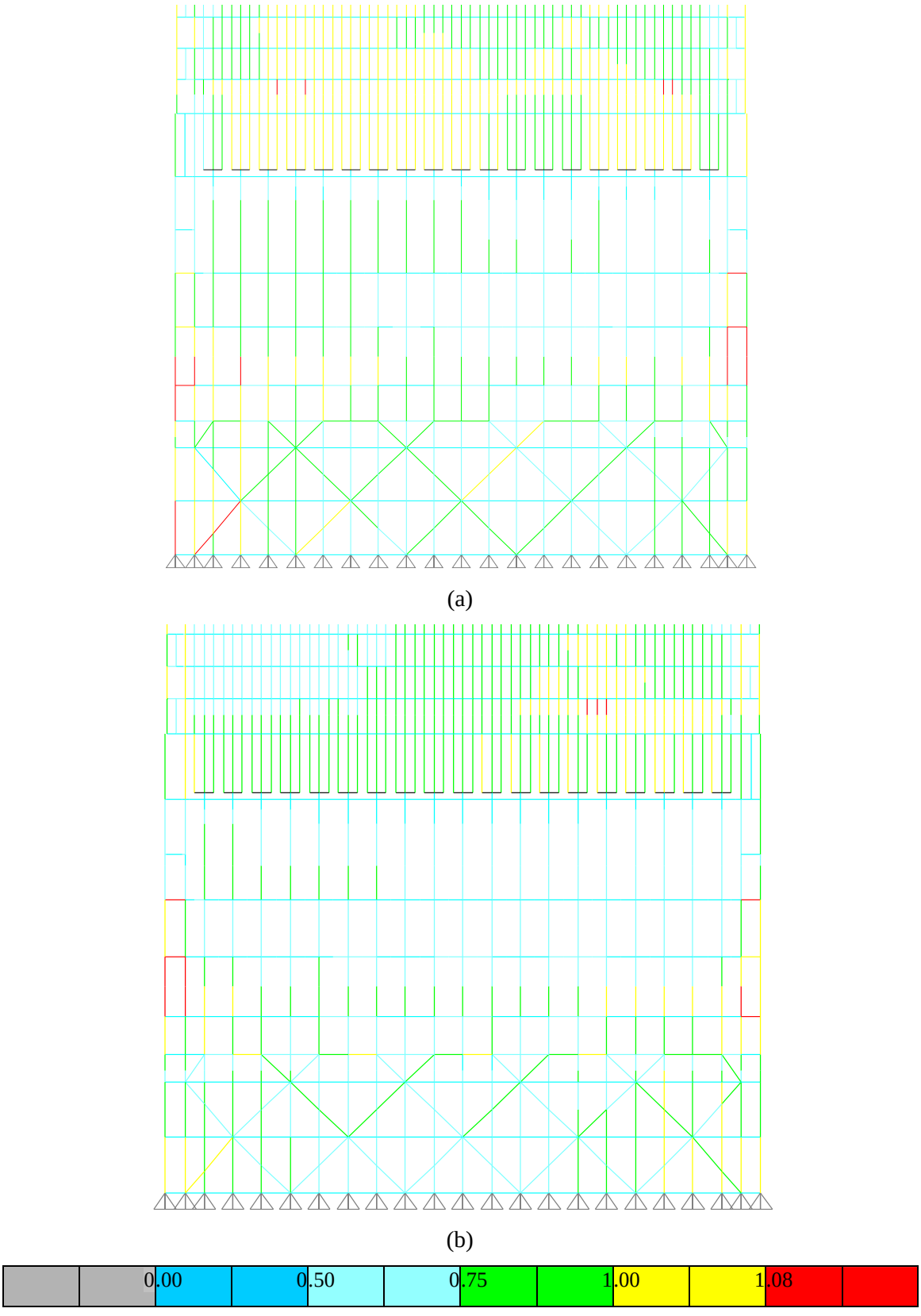

Figure 4–4. RCRs for WTC 1 under original design loads below floor 9, (a) north elevation, and (b) east elevation.

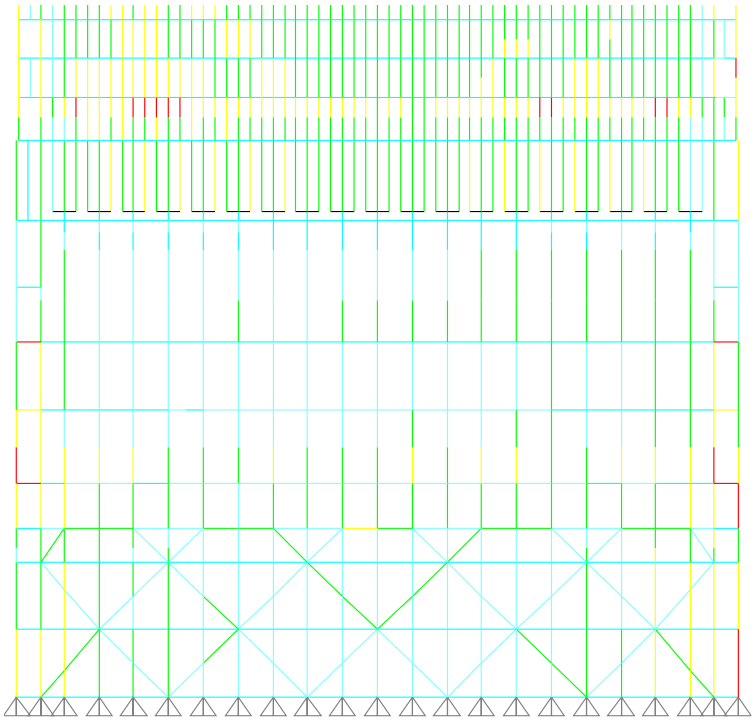

(c)

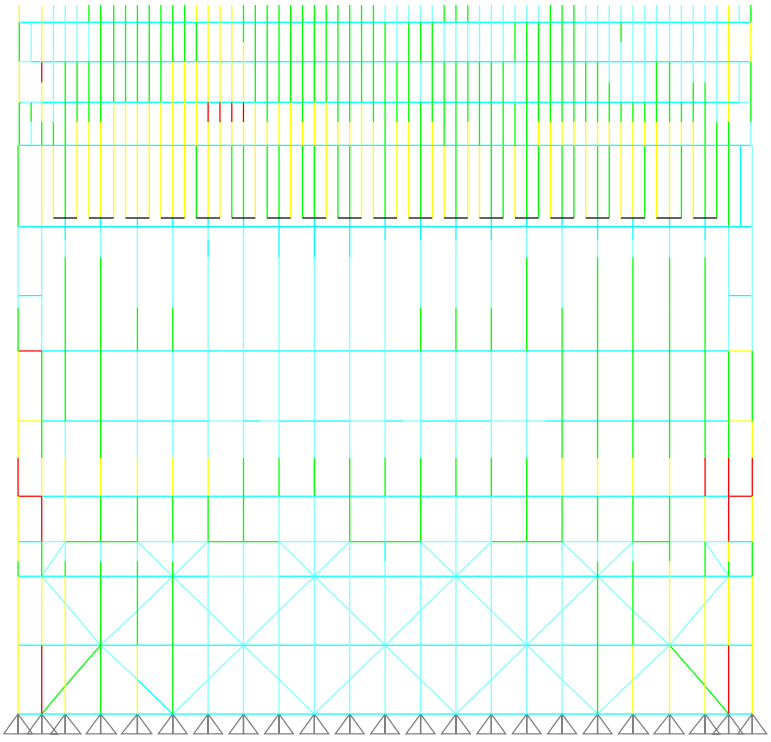

(d)

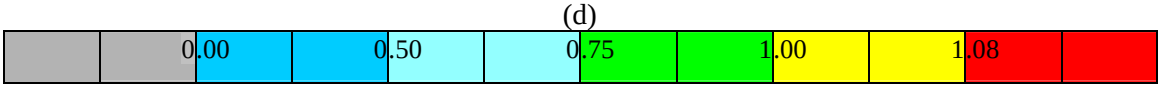

Figure 4–4. (c) south elevation, and (d) west elevation (continued).

LEVEL	TOWER A, DCR of CORE COLUMN 500's COLUMN NUMBER							
	501	502	503	504	505	506	507	508
106 FL	1.05	1.00	0.92	1.01	0.88	1.01	0.98	1.01
105 FL	0.85	1.09	0.99	0.85	0.96	1.09	1.07	0.83
104 FL	0.95	0.95	0.87	0.95	0.89	0.95	0.94	0.95
103 FL	1.02	1.02	0.93	1.02	0.95	1.01	1.01	1.02
102 FL	0.83	1.09	0.99	0.83	1.01	1.07	1.08	0.83
101 FL	0.90	0.92	0.85	0.90	0.93	0.88	0.90	0.90
100 FL	0.95	0.97	0.90	0.95	0.98	0.93	0.96	0.96
99 FL	1.01	1.03	0.95	1.01	1.04	0.97	1.01	1.01
98 FL	0.74	0.86	0.86	0.74	0.92	0.84	0.85	0.86
97 FL	0.78	0.91	0.91	0.78	0.96	0.88	0.90	0.90
96 FL	0.82	0.95	0.95	0.82	1.01	0.92	0.94	0.95
95 FL	0.73	0.84	0.84	0.73	0.88	0.81	0.83	0.73
94 FL	0.77	0.87	0.87	0.77	0.91	0.84	0.86	0.77
93 FL	0.80	0.91	0.91	0.80	0.95	0.87	0.90	0.80
92 FL	0.76	0.80	0.80	0.76	0.91	0.78	0.80	0.69
91 FL	0.79	0.83	0.83	0.79	0.95	0.81	0.83	0.71
90 FL	0.82	0.87	0.86	0.82	0.98	0.84	0.86	0.74
89 FL	0.70	0.78	0.77	0.70	0.86	0.75	0.83	0.70
88 FL	0.73	0.81	0.80	0.73	0.89	0.78	0.86	0.73
87 FL	0.75	0.83	0.83	0.75	0.92	0.81	0.89	0.75
86 FL	0.71	0.93	0.80	0.71	0.92	0.88	0.99	0.82
85 FL	0.73	0.96	0.82	0.73	0.95	0.90	1.02	0.85
84 FL	0.76	0.99	0.85	0.76	0.98	0.93	1.06	0.87
83 FL	0.83	0.91	0.90	0.83	0.89	0.87	0.94	0.83
82 FL	0.86	0.94	0.93	0.86	0.92	0.90	0.96	0.86
81 FL	0.89	0.97	0.95	0.89	0.94	0.93	0.99	0.89
80 FL	0.88	0.91	0.93	0.88	0.92	0.88	0.94	0.88
79 FL	0.91	0.94	0.96	0.91	0.95	0.90	0.97	0.91
78 FL	0.95	0.98	1.00	0.95	0.99	0.93	1.00	0.95
77 FL	0.66	0.67	0.68	0.66	0.67	0.65	0.69	0.66
76 FL	0.67	0.69	0.70	0.67	0.68	0.66	0.70	0.68
75 FL	0.83	0.84	0.85	0.83	0.89	0.84	0.86	0.84
74 FL	0.84	0.86	0.86	0.84	0.90	0.85	0.87	0.85
73 FL	0.86	0.87	0.88	0.86	0.92	0.87	0.89	0.87
72 FL	0.82	0.84	0.85	0.82	0.85	0.84	0.86	0.83
71 FL	0.84	0.85	0.87	0.84	0.87	0.85	0.88	0.85
70 FL	0.86	0.87	0.89	0.86	0.88	0.87	0.90	0.87
69 FL	0.81	0.80	0.83	0.81	0.85	0.82	0.83	0.82
68 FL	0.84	0.83	0.86	0.84	0.89	0.85	0.86	0.85
67 FL	0.85	0.84	0.87	0.85	0.89	0.85	0.87	0.86
66 FL	0.87	0.86	0.89	0.87	0.92	0.88	0.89	0.87
65 FL	0.88	0.87	0.91	0.88	0.93	0.89	0.91	0.89
64 FL	0.90	0.89	0.93	0.90	0.95	0.91	0.93	0.91
63 FL	0.86	0.87	0.89	0.86	0.92	0.88	0.88	0.86
62 FL	0.87	0.88	0.91	0.87	0.94	0.89	0.90	0.88
61 FL	0.89	0.90	0.92	0.89	0.96	0.91	0.91	0.89
60 FL	0.86	0.87	0.88	0.86	0.93	0.88	0.88	0.87
59 FL	0.88	0.88	0.89	0.88	0.95	0.89	0.89	0.88
58 FL	0.89	0.90	0.91	0.89	0.96	0.91	0.91	0.90
57 FL	0.86	0.85	0.88	0.86	0.91	0.87	0.86	0.87
56 FL	0.88	0.87	0.90	0.88	0.92	0.88	0.88	0.88
55 FL	0.89	0.88	0.91	0.89	0.94	0.89	0.89	0.89
54 FL	0.84	0.86	0.89	0.84	0.91	0.87	0.87	0.85
53 FL	0.85	0.88	0.90	0.85	0.93	0.89	0.89	0.86
52 FL	0.87	0.89	0.92	0.87	0.94	0.90	0.90	0.87
51 FL	0.85	0.86	0.88	0.85	0.92	0.87	0.87	0.86
50 FL	0.87	0.88	0.90	0.87	0.94	0.89	0.88	0.87
49 FL	0.88	0.89	0.91	0.88	0.95	0.90	0.90	0.88
48 FL	0.86	0.86	0.88	0.86	0.93	0.87	0.86	0.86
47 FL	0.87	0.87	0.89	0.87	0.94	0.88	0.87	0.87
46 FL	0.88	0.88	0.90	0.88	0.96	0.89	0.89	0.89
45 FL	0.80	0.80	0.83	0.80	0.89	0.83	0.80	0.81
44 FL	0.83	0.82	0.85	0.83	0.91	0.85	0.82	0.83
43 FL	0.63	0.62	0.64	0.63	0.69	0.63	0.63	0.64
42 FL	0.65	0.64	0.66	0.65	0.70	0.64	0.64	0.65
41 FL	0.84	0.85	0.87	0.84	0.95	0.86	0.86	0.85
40 FL	0.85	0.86	0.87	0.85	0.96	0.87	0.86	0.85
39 FL	0.84	0.84	0.86	0.84	0.94	0.85	0.85	0.84
38 FL	0.85	0.85	0.87	0.85	0.95	0.86	0.86	0.85
37 FL	0.86	0.86	0.88	0.86	0.96	0.87	0.87	0.86
36 FL	0.83	0.83	0.87	0.83	0.95	0.85	0.85	0.83
35 FL	0.84	0.85	0.88	0.84	0.96	0.86	0.86	0.85
34 FL	0.85	0.86	0.89	0.85	0.97	0.87	0.87	0.86
33 FL	0.84	0.84	0.87	0.84	0.95	0.85	0.85	0.85
32 FL	0.85	0.85	0.88	0.85	0.96	0.86	0.86	0.86
31 FL	0.86	0.86	0.89	0.86	0.97	0.87	0.87	0.87
30 FL	0.84	0.84	0.87	0.84	0.94	0.85	0.83	0.84
29 FL	0.85	0.85	0.88	0.85	0.95	0.86	0.84	0.85
28 FL	0.86	0.86	0.89	0.86	0.96	0.87	0.85	0.86
27 FL	0.85	0.84	0.85	0.85	0.95	0.85	0.83	0.85
26 FL	0.85	0.85	0.86	0.85	0.96	0.86	0.84	0.86
25 FL	0.86	0.86	0.87	0.86	0.97	0.87	0.85	0.87
24 FL	0.83	0.82	0.87	0.83	0.96	0.85	0.83	0.83
23 FL	0.84	0.83	0.88	0.84	0.97	0.86	0.84	0.84
22 FL	0.85	0.84	0.89	0.85	0.98	0.87	0.85	0.85
21 FL	0.84	0.82	0.87	0.84	0.94	0.85	0.83	0.84
20 FL	0.85	0.83	0.88	0.85	0.95	0.86	0.84	0.85
19 FL	0.86	0.84	0.89	0.86	0.96	0.87	0.85	0.86
18 FL	0.84	0.83	0.87	0.84	0.95	0.85	0.83	0.84
17 FL	0.85	0.83	0.88	0.85	0.96	0.86	0.84	0.85
16 FL	0.86	0.84	0.88	0.86	0.97	0.87	0.85	0.86
15 FL	0.85	0.83	0.87	0.85	0.96	0.86	0.83	0.85
14 FL	0.86	0.84	0.87	0.86	0.97	0.86	0.84	0.86
13 FL	0.87	0.85	0.88	0.87	0.98	0.87	0.85	0.87
12 FL	0.86	0.83	0.86	0.86	0.95	0.86	0.83	0.86
11 FL	0.86	0.84	0.87	0.86	0.96	0.87	0.84	0.87
10 FL	0.88	0.85	0.89	0.88	0.97	0.88	0.85	0.88
09 FL	0.92	0.83	0.92	0.92	1.04	0.90	0.89	0.84
08 FL	0.92	0.86	0.93	0.92	1.04	0.91	0.90	0.88
07 FL	0.78	0.76	0.78	0.78	0.81	0.77	0.75	0.78
06 FL	0.79	0.77	0.79	0.79	0.82	0.78	0.76	0.79
05 FL	0.79	0.77	0.79	0.79	0.82	0.78	0.77	0.79
04 FL	0.77	0.75	0.78	0.77	0.80	0.77	0.75	0.77
03 FL	0.84	0.81	0.83	0.84	0.87	0.82	0.81	0.84
02 FL	0.86	0.82	0.85	0.86	0.89	0.83	0.82	0.87
01 FL	0.83	0.83	0.86	0.83	0.90	0.84	0.83	0.83
B1 FL	0.82	0.82	0.85	0.82	0.90	0.84	0.82	0.82
B2 FL	0.83	0.83	0.86	0.83	0.91	0.85	0.83	0.83
B3 FL	0.83	0.81	0.83	0.83	0.89	0.80	0.80	0.84
B4 FL	0.89	0.86	0.88	0.89	0.95	0.85	0.85	0.91
B5 FL	0.90	0.86	0.89	0.90	0.96	0.86	0.86	0.91

(a)

LEVEL	TOWER A, DCR of CORE COLUMN 600's COLUMN NUMBER							
	601	602	603	604	605	606	607	608
106 FL	0.94	1.03	1.29	1.01	1.01	1.05	1.15	0.80
105 FL	1.03	1.10	1.36	1.11	1.09	1.13	1.23	0.92
104 FL	1.12	0.98	1.13	0.94	0.96	0.95	1.12	0.84
103 FL	1.04	1.03	1.18	1.01	1.03	1.01	1.18	0.93
102 FL	1.11	1.08	1.24	1.08	1.09	1.07	1.25	1.02
101 FL	1.19	1.06	1.05	0.88	0.99	1.07	1.05	1.09
100 FL	1.10	1.11	1.10	0.93	1.05	1.13	1.10	1.18
99 FL	1.16	1.16	1.15	0.99	1.10	1.20	1.15	1.27
98 FL	1.23	1.01	0.96	0.96	1.02	1.06	1.00	1.18
97 FL	1.18	1.06	1.00	1.01	1.07	1.12	1.04	1.25
96 FL	1.24	1.10	1.04	1.06	1.12	1.17	1.09	1.33
95 FL	1.31	0.97	0.93	0.98	1.05	1.05	0.96	1.12
94 FL	1.13	1.01	0.96	1.02	1.10	1.09	1.00	1.18
93 FL	1.18	1.04	0.99	1.07	1.13	1.14	1.04	1.24
92 FL	1.23	0.98	0.93	0.83	0.98	1.03	0.88	1.07
91 FL	1.08	1.02	0.95	0.86	1.02	1.07	1.01	1.12
90 FL	1.12	1.05	0.98	0.89	1.05	1.12	1.05	1.17
89 FL	1.17	0.95	0.89	0.93	0.92	1.02	0.94	1.03
88 FL	1.04	0.98	0.92	0.96	0.96	1.06	0.97	1.08
87 FL	1.08	1.01	0.94	1.00	0.99	1.10	1.00	1.12
86 FL	1.12	0.96	0.93	0.87	0.88	1.09	0.99	1.00
85 FL	1.15	0.98	0.95	0.90	0.90	1.13	1.02	1.04
84 FL	1.20	1.01	0.98	0.93	0.93	1.16	1.05	1.08
83 FL	1.25	0.93	0.90	0.96	0.96	0.99	0.96	1.11
82 FL	1.01	0.97	0.93	0.89	0.93	1.02	1.00	1.16
81 FL	1.04	1.02	0.99	1.04	1.03	1.07	1.05	1.21
80 FL	1.08	0.88	0.93	0.72	0.82	1.07	0.86	0.97
79 FL	1.04	0.90	0.96	0.74	0.84	1.09	0.88	1.01
78 FL	1.08	0.92	0.98	0.76	0.87	1.12	0.90	1.05
77 FL	0.76	0.63	0.66	0.62	0.68	0.65	0.66	0.85
76 FL	0.78	0.67	0.70	0.65	0.70	0.68	0.70	0.86
75 FL	0.97	0.84	0.89	0.82	0.91	0.86	0.86	1.00
74 FL	0.97	0.85	0.89	0.82	0.92	0.86	0.86	1.01
73 FL	1.00	0.86	0.91	0.84	0.93	0.88	0.88	1.04
72 FL	1.00	0.83	0.87	0.82	0.85	0.83	0.85	0.99
71 FL	1.03	0.84	0.88	0.83	0.86	0.84	0.88	1.02
70 FL	1.05	0.85	0.90	0.85	0.88	0.86	0.88	1.04
69 FL	0.80	0.78	0.82	0.80	0.84	0.83	0.83	0.86
68 FL	0.84	0.81	0.85	0.84	0.88	0.87	0.87	0.91
67 FL	0.83	0.80	0.85	0.84	0.87	0.86	0.86	0.90
66 FL	0.89	0.82	0.89	0.87	0.89	0.88	0.89	1.07
65 FL	0.90	0.82	0.89	0.87	0.89	0.88	0.89	1.09
64 FL	0.92	0.84	0.92	0.90	0.92	0.90	0.91	1.12
63 FL	0.90	0.81	0.89	0.86	0.88	0.87	0.88	0.99
62 FL	0.91	0.83	0.90	0.88	0.89	0.88	0.89	1.01
61 FL	0.93	0.84	0.92	0.89	0.91	0.89	0.91	1.03
60 FL	0.90	0.81	0.86	0.90	0.87	0.87	0.87	1.05
59 FL	0.91	0.82	0.87	0.91	0.89	0.88	0.88	1.07
58 FL	0.93	0.83	0.88	0.93	0.90	0.89	0.89	1.09
57 FL	0.90	0.81	0.86	0.90	0.87	0.86	0.86	1.05
56 FL	0.92	0.82	0.87	0.92	0.88	0.87	0.87	1.07
55 FL	0.93	0.83	0.88	0.93	0.89	0.88	0.88	1.08
54 FL	0.87	0.81	0.86	0.90	0.91	0.86	0.83	1.04
53 FL	0.88	0.82	0.87	0.91	0.92	0.87	0.84	1.06
52 FL	0.89	0.83	0.88	0.93	0.93	0.88	0.85	1.08
51 FL	0.87	0.81	0.86	0.90	0.90	0.86	0.83	1.04
50 FL	0.89	0.82	0.87	0.91	0.91	0.87	0.83	1.05
49 FL	0.90	0.83	0.88	0.92	0.93	0.88	0.84	1.07
48 FL	0.88	0.81	0.86	0.93	0.90	0.84	0.82	1.03
47 FL	0.89	0.82	0.87	0.94	0.91	0.85	0.83	1.05
46 FL	0.91	0.83	0.88	0.96	0.92	0.86	0.84	1.07
45 FL	0.83	0.77	0.81	0.86	0.84	0.80	0.75	0.92
44 FL	0.85	0.78	0.83	0.89	0.86	0.81	0.77	0.95
43 FL	0.64	0.56	0.60	0.65	0.65	0.61	0.58	0.70
42 FL	0.66	0.56	0.63	0.68	0.68	0.64	0.61	0.72
41 FL	0.85	0.77	0.83	0.88	0.90	0.84	0.81	0.92
40 FL	0.85	0.76	0.82	0.88	0.90	0.84	0.81	0.92
39 FL	0.84	0.77	0.82	0.88	0.88	0.84	0.80	0.90
38 FL	0.85	0.78	0.83	0.90	0.89	0.85	0.81	0.91
37 FL	0.87	0.79	0.84	0.91	0.90	0.86	0.82	0.93
36 FL	0.85	0.78	0.81	0.88	0.87	0.84	0.81	0.91
35 FL	0.86	0.79	0.82	0.89	0.88	0.85	0.82	0.92
34 FL	0.88	0.80	0.82	0.91	0.90	0.86	0.82	0.93
33 FL	0.84	0.77	0.81	0.89	0.87	0.83	0.80	0.92
32 FL	0.85	0.77	0.82	0.90	0.88	0.84	0.81	0.93
31 FL	0.86	0.78	0.83	0.91	0.89	0.85	0.82	0.94
30 FL	0.82	0.77	0.82	0.89	0.87	0.84	0.81	0.92
29 FL	0.83	0.78	0.82	0.90	0.88	0.85	0.82	0.94
28 FL	0.84	0.78	0.83	0.91	0.89	0.86	0.83	0.95
27 FL	0.83	0.77	0.82	0.89	0.88	0.83	0.80	0.93
26 FL	0.84	0.76	0.82	0.90	0.88	0.84	0.81	0.94
25 FL	0.85	0.79	0.83	0.91	0.89	0.85	0.82	0.95
24 FL	0.82	0.78	0.81	0.89	0.88	0.82	0.80	0.94
23 FL	0.83	0.78	0.81	0.90	0.89	0.82	0.81	0.95
22 FL	0.84	0.79	0.82	0.91	0.89	0.83	0.82	0.96
21 FL	0.82	0.78	0.81	0.92	0.88	0.82	0.81	0.94
20 FL	0.83	0.79	0.82	0.93	0.89	0.83	0.82	0.96
19 FL	0.84	0.79	0.83	0.94	0.90	0.83	0.83	0.97
18 FL	0.82	0.78	0.81	0.92	0.88	0.82	0.80	0.93
17 FL	0.83	0.79	0.82	0.93	0.89	0.82	0.80	0.94
16 FL	0.84	0.79	0.83	0.94	0.90	0.83	0.81	0.95
15 FL	0.81	0.77	0.80	0.93	0.90	0.81	0.80	0.93
14 FL	0.82	0.78	0.81	0.93	0.91	0.82	0.80	0.94
13 FL	0.83	0.79	0.82	0.94	0.92	0.82	0.81	0.95
12 FL	0.82	0.78	0.81	0.93	0.90	0.82	0.79	0.94
11 FL	0.83	0.78	0.82	0.94	0.91	0.82	0.79	0.95
10 FL	0.84	0.80	0.83	0.95	0.92	0.84	0.80	0.96
09 FL	0.92	0.76	0.90	1.04	1.01	0.97	0.87	1.03
08 FL	0.92	0.81	0.90	1.04	1.02	0.98	0.87	1.04
07 FL	0.57	0.53	0.56	0.62	0.60	0.60	0.55	0.61
06 FL	0.59	0.55	0.57	0.63	0.62	0.62	0.56	0.62
05 FL	0.59	0.55	0.58	0.64	0.63	0.63	0.57	0.62
04 FL	0.57	0.54	0.56	0.62	0.61	0.61	0.55	0.60
03 FL	0.66	0.61	0.64	0.71	0.70	0.69	0.63	0.69
02 FL	0.69	0.62	0.66	0.74	0.72	0.71	0.64	0.72
01 FL	0.80	0.79	0.82	0.92	0.90	0.88	0.79	0.88
B1 FL	0.79	0.78	0.81	0.91	0.89	0.87	0.79	0.88
B2 FL	0.81	0.79	0.82	0.93	0.90	0.88	0.80	0.89
B3 FL	0.77	0.75	0.81	0.89	0.87	0.87	0.78	0.84
B4 FL	0.79	0.83	0.89	0.99	0.97	0.95	0.86	0.95
B5 FL	0.80	0.83	0.90	1.00	0.98	0.96	0.87	0.96

(b)

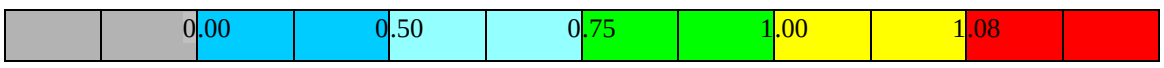

Figure 4–5. DCRs for WTC 1 core columns under original design loads, (a) 500 line, and (b) 600 line.

LEVEL	TOWER A, DCR of CORE COLUMN 700's COLUMN NUMBER							
	701	702	703	704	705	706	707	708
106 FL	0.78	0.99	0.86	0.05	0.32	0.50	0.78	0.82
105 FL	0.85	1.07	0.61	0.11	0.40	0.57	0.84	0.89
104 FL	1.00	0.99	0.78	0.16	0.40	0.58	0.79	0.79
103 FL	1.07	1.06	0.65	0.21	0.47	0.64	0.84	0.89
102 FL	1.14	1.13	0.51	0.26	0.53	0.70	0.89	0.91
101 FL	0.93	0.87	0.79	0.31	0.60	0.64	0.80	0.72
100 FL	0.99	0.91	0.85	0.36	0.66	0.69	0.84	0.76
99 FL	1.05	0.96	0.69	0.42	0.73	0.75	0.89	0.80
98 FL	0.82	0.85	0.75	0.35	0.79	0.69	0.84	0.71
97 FL	0.86	0.89	0.80	0.39	0.86	0.73	0.88	0.75
96 FL	0.90	0.93	0.84	0.44	0.93	0.78	0.92	0.79
95 FL	0.86	0.80	0.71	0.37	0.82	0.72	0.83	0.82
94 FL	0.90	0.84	0.75	0.41	0.87	0.77	0.87	0.86
93 FL	0.94	0.87	0.79	0.44	0.93	0.81	0.91	0.90
92 FL	0.80	0.80	0.74	0.42	0.89	0.75	0.83	0.76
91 FL	0.83	0.83	0.77	0.45	0.93	0.79	0.86	0.79
90 FL	0.87	0.86	0.80	0.48	0.96	0.83	0.90	0.82
89 FL	0.78	0.79	0.76	0.62	0.81	0.78	0.83	0.75
88 FL	0.81	0.82	0.79	0.65	0.85	0.81	0.86	0.78
87 FL	0.84	0.84	0.82	0.69	0.89	0.85	0.88	0.81
86 FL	0.77	0.80	0.76	0.66	1.07	0.83	0.85	0.76
85 FL	0.79	0.82	0.79	0.69	1.12	0.87	0.88	0.78
84 FL	0.82	0.85	0.82	0.73	1.16	0.90	0.91	0.81
83 FL	0.79	0.79	0.77	0.70	1.08	0.84	0.78	0.75
82 FL	0.81	0.82	0.80	0.73	1.12	0.87	0.81	0.78
81 FL	0.84	0.84	0.82	0.76	1.16	0.90	0.83	0.80
80 FL	0.78	0.87	0.85	0.65	1.06	0.94	0.94	0.84
79 FL	0.81	0.91	0.89	0.69	1.13	0.98	0.88	0.87
78 FL	0.84	0.94	0.92	0.73	1.19	1.02	1.01	0.91
77 FL	0.67	0.80	0.46	0.66	0.66	0.50	0.59	0.68
76 FL	0.69	0.65	0.53	0.55	0.61	0.57	0.64	0.70
75 FL	0.84	0.85	0.82	0.76	0.69	0.94	0.89	0.90
74 FL	0.85	0.84	0.83	0.75	0.70	0.94	0.90	0.91
73 FL	0.87	0.86	0.84	0.76	0.72	0.97	0.92	0.93
72 FL	0.85	0.81	0.79	0.72	0.69	0.92	0.87	0.91
71 FL	0.87	0.83	0.80	0.74	0.72	0.94	0.89	0.93
70 FL	0.89	0.84	0.81	0.75	0.74	0.97	0.91	0.95
69 FL	0.69	0.80	0.77	0.72	0.71	0.83	0.87	0.76
68 FL	0.72	0.85	0.80	0.77	0.78	0.89	0.92	0.79
67 FL	0.71	0.82	0.80	0.74	0.76	0.87	0.90	0.79
66 FL	0.87	0.84	0.81	0.75	0.78	0.89	0.92	0.93
65 FL	0.88	0.84	0.81	0.76	0.78	0.89	0.92	0.94
64 FL	0.90	0.86	0.83	0.78	0.83	0.93	0.95	0.97
63 FL	0.87	0.79	0.83	0.79	0.80	0.87	0.90	0.95
62 FL	0.89	0.81	0.84	0.81	0.82	0.88	0.92	0.96
61 FL	0.91	0.82	0.85	0.82	0.84	0.89	0.93	0.98
60 FL	0.86	0.83	0.81	0.78	0.81	0.84	0.86	0.95
59 FL	0.88	0.84	0.82	0.79	0.83	0.85	0.87	0.96
58 FL	0.89	0.86	0.83	0.80	0.85	0.86	0.88	0.98
57 FL	0.87	0.79	0.81	0.77	0.81	0.87	0.90	0.92
56 FL	0.89	0.80	0.82	0.78	0.83	0.88	0.91	0.94
55 FL	0.90	0.81	0.83	0.79	0.85	0.89	0.92	0.95
54 FL	0.88	0.82	0.80	0.76	0.83	0.84	0.84	0.91
53 FL	0.90	0.83	0.81	0.77	0.84	0.85	0.85	0.92
52 FL	0.91	0.84	0.82	0.78	0.86	0.87	0.86	0.93
51 FL	0.89	0.78	0.79	0.75	0.84	0.82	0.87	0.92
50 FL	0.91	0.79	0.80	0.76	0.85	0.83	0.88	0.93
49 FL	0.92	0.80	0.81	0.77	0.87	0.84	0.89	0.94
48 FL	0.90	0.81	0.78	0.74	0.84	0.85	0.82	0.92
47 FL	0.92	0.82	0.79	0.75	0.86	0.86	0.83	0.93
46 FL	0.93	0.83	0.80	0.77	0.88	0.88	0.85	0.94
45 FL	0.92	0.77	0.75	0.72	0.79	0.81	0.79	0.86
44 FL	0.95	0.80	0.76	0.75	0.82	0.83	0.81	0.89
43 FL	0.66	0.72	0.56	0.56	0.57	0.64	0.73	0.67
42 FL	0.68	0.76	0.59	0.60	0.60	0.69	0.77	0.69
41 FL	0.90	0.78	0.79	0.78	0.76	0.90	0.87	0.91
40 FL	0.90	0.77	0.79	0.77	0.76	0.89	0.87	0.90
39 FL	0.87	0.78	0.79	0.78	0.77	0.89	0.80	0.89
38 FL	0.88	0.79	0.79	0.79	0.79	0.90	0.81	0.91
37 FL	0.90	0.80	0.80	0.80	0.80	0.91	0.82	0.92
36 FL	0.87	0.73	0.78	0.77	0.78	0.89	0.83	0.90
35 FL	0.88	0.74	0.79	0.78	0.79	0.90	0.84	0.91
34 FL	0.89	0.75	0.79	0.78	0.80	0.91	0.85	0.92
33 FL	0.86	0.76	0.78	0.76	0.78	0.89	0.77	0.90
32 FL	0.87	0.77	0.79	0.77	0.80	0.90	0.78	0.91
31 FL	0.88	0.77	0.80	0.78	0.81	0.91	0.79	0.92
30 FL	0.85	0.77	0.78	0.76	0.79	0.88	0.80	0.91
29 FL	0.86	0.78	0.78	0.76	0.80	0.89	0.81	0.92
28 FL	0.87	0.78	0.79	0.77	0.82	0.90	0.82	0.93
27 FL	0.86	0.77	0.77	0.75	0.80	0.84	0.83	0.90
26 FL	0.87	0.77	0.77	0.76	0.81	0.85	0.84	0.92
25 FL	0.88	0.78	0.78	0.76	0.82	0.86	0.85	0.93
24 FL	0.86	0.77	0.76	0.74	0.80	0.81	0.83	0.91
23 FL	0.87	0.77	0.77	0.75	0.81	0.82	0.84	0.92
22 FL	0.88	0.78	0.78	0.76	0.83	0.83	0.85	0.93
21 FL	0.85	0.77	0.76	0.76	0.81	0.80	0.83	0.91
20 FL	0.86	0.76	0.77	0.77	0.82	0.81	0.83	0.92
19 FL	0.87	0.79	0.78	0.78	0.83	0.82	0.84	0.93
18 FL	0.86	0.77	0.76	0.76	0.78	0.79	0.81	0.89
17 FL	0.87	0.78	0.77	0.77	0.79	0.80	0.82	0.90
16 FL	0.88	0.78	0.77	0.77	0.80	0.81	0.83	0.91
15 FL	0.86	0.77	0.76	0.73	0.82	0.80	0.82	0.89
14 FL	0.87	0.78	0.77	0.73	0.83	0.80	0.82	0.89
13 FL	0.88	0.78	0.77	0.74	0.84	0.81	0.83	0.90
12 FL	0.86	0.77	0.74	0.75	0.78	0.80	0.81	0.88
11 FL	0.87	0.78	0.75	0.75	0.79	0.81	0.82	0.89
10 FL	0.88	0.79	0.76	0.77	0.81	0.82	0.84	0.90
09 FL	0.96	0.89	0.83	0.88	0.96	0.86	0.89	0.86
08 FL	0.97	0.90	0.84	0.89	0.99	0.89	0.75	0.87
07 FL	0.69	0.53	0.51	0.53	0.45	0.51	0.54	0.69
06 FL	0.71	0.54	0.53	0.56	0.46	0.53	0.55	0.71
05 FL	0.71	0.55	0.53	0.57	0.47	0.53	0.56	0.71
04 FL	0.68	0.54	0.52	0.56	0.46	0.52	0.55	0.69
03 FL	0.78	0.58	0.59	0.67	0.51	0.59	0.59	0.79
02 FL	0.81	0.59	0.60	0.69	0.52	0.60	0.61	0.81
01 FL	0.85	0.76	0.75	0.63	0.90	0.82	0.80	0.87
B1 FL	0.84	0.76	0.74	0.62	0.90	0.81	0.80	0.86
B2 FL	0.85	0.76	0.75	0.63	0.92	0.82	0.81	0.87
B3 FL	0.81	0.73	0.74	0.58	0.85	0.78	0.76	0.84
B4 FL	0.83	0.77	0.81	0.67	0.92	0.85	0.81	0.94
B5 FL	0.84	0.78	0.82	0.67	0.93	0.86	0.81	0.94

(c)

LEVEL	TOWER A, DCR of CORE COLUMN 800's COLUMN NUMBER						
	801	802	803	804	805	806	807
106 FL	0.86	0.95	0.54	0.37	0.59	0.74	0.90
105 FL	0.93	1.03	0.63	0.47	0.64	0.79	0.98
104 FL	0.82	0.89	0.59	0.48	0.58	0.73	0.90
103 FL	0.87	0.95	0.66	0.56	0.62	0.77	0.97
102 FL	0.93	1.01	0.47	0.64	0.66	0.81	1.04
101 FL	0.73	0.79	0.51	0.49	0.60	0.76	0.90
100 FL	0.77	0.82	0.55	0.55	0.64	0.80	0.95
99 FL	0.81	0.85	0.58	0.60	0.67	0.84	1.01
98 FL	0.85	0.80	0.55	0.62	0.53	0.75	0.74
97 FL	0.89	0.83	0.58	0.68	0.55	0.76	0.78
96 FL	0.94	0.86	0.61	0.73	0.58	0.81	0.82
95 FL	0.71	0.69	0.53	0.67	0.57	0.77	0.74
94 FL	0.73	0.71	0.56	0.72	0.59	0.80	0.78
93 FL	0.76	0.73	0.58	0.77	0.62	0.83	0.81
92 FL	0.71	0.65	0.54	0.70	0.57	0.75	0.77
91 FL	0.73	0.67	0.57	0.75	0.59	0.79	0.80
90 FL	0.75	0.69	0.59	0.79	0.61	0.80	0.83
89 FL	0.71	0.66	0.56	0.73	0.60	0.74	0.73
88 FL	0.73	0.67	0.58	0.77	0.62	0.76	0.76
87 FL	0.75	0.69	0.60	0.80	0.65	0.79	0.78
86 FL	0.74	0.71	0.70	0.76	0.73	0.72	0.73
85 FL	0.76	0.73	0.72	0.79	0.76	0.74	0.75
84 FL	0.78	0.75	0.75	0.82	0.78	0.76	0.78
83 FL	0.74	0.70	0.71	0.70	0.76	0.72	0.74
82 FL	0.76	0.72	0.73	0.73	0.79	0.74	0.76
81 FL	0.78	0.74	0.75	0.76	0.81	0.76	0.78
80 FL	0.84	0.64	0.80	0.79	0.84	0.78	0.80
79 FL	0.87	0.67	0.83	0.83	0.87	0.81	0.82
78 FL	0.90	0.69	0.86	0.87	0.90	0.83	0.85
77 FL	0.69	0.45	0.59	0.62	0.54	0.60	0.68
76 FL	0.70	0.49	0.58	0.65	0.61	0.57	0.71
75 FL	0.89	0.74	0.73	0.73	0.91	0.80	0.90
74 FL	0.90	0.74	0.74	0.73	0.91	0.80	0.91
73 FL	0.92	0.76	0.76	0.75	0.94	0.82	0.93
72 FL	0.89	0.72	0.73	0.73	0.85	0.78	0.87
71 FL	0.91	0.74	0.75	0.75	0.88	0.80	0.89
70 FL	0.93	0.76	0.77	0.77	0.90	0.82	0.91
69 FL	0.73	0.72	0.74	0.72	0.85	0.78	0.76
68 FL	0.76	0.77	0.78	0.79	0.92	0.83	0.79
67 FL	0.76	0.75	0.78	0.76	0.90	0.82	0.79
66 FL	0.90	0.77	0.80	0.78	0.86	0.83	0.93
65 FL	0.91	0.77	0.80	0.79	0.86	0.84	0.94
64 FL	0.93	0.80	0.84	0.82	0.90	0.87	0.97
63 FL	0.87	0.74	0.80	0.77	0.85	0.82	0.92
62 FL	0.89	0.76	0.82	0.79	0.86	0.84	0.94
61 FL	0.91	0.77	0.84	0.80	0.88	0.85	0.95
60 FL	0.88	0.79	0.81	0.79	0.82	0.79	0.93
59 FL	0.90	0.80	0.83	0.81	0.83	0.81	0.95
58 FL	0.92	0.82	0.85	0.83	0.85	0.82	0.97
57 FL	0.88	0.75	0.82	0.78	0.86	0.83	0.94
56 FL	0.89	0.77	0.84	0.80	0.87	0.85	0.95
55 FL	0.91	0.78	0.85	0.81	0.89	0.86	0.97
54 FL	0.87	0.80	0.83	0.80	0.83	0.79	0.92
53 FL	0.88	0.81	0.84	0.81	0.85	0.81	0.94
52 FL	0.90	0.82	0.86	0.83	0.86	0.82	0.95
51 FL	0.86	0.76	0.86	0.79	0.88	0.83	0.91
50 FL	0.87	0.76	0.88	0.80	0.89	0.85	0.92
49 FL	0.89	0.79	0.89	0.81	0.91	0.86	0.94
48 FL	0.87	0.80	0.87	0.76	0.85	0.80	0.91
47 FL	0.89	0.81	0.88	0.78	0.87	0.81	0.93
46 FL	0.91	0.83	0.90	0.79	0.88	0.82	0.94
45 FL	0.70	0.78	0.82	0.75	0.79	0.77	0.73
44 FL	0.73	0.80	0.85	0.78	0.82	0.80	0.76
43 FL	0.63	0.71	0.60	0.55	0.70	0.62	0.66
42 FL	0.65	0.75	0.62	0.58	0.74	0.64	0.68
41 FL	0.87	0.76	0.81	0.80	0.87	0.83	0.91
40 FL	0.87	0.75	0.81	0.79	0.86	0.83	0.91
39 FL	0.86	0.77	0.83	0.73	0.87	0.84	0.90
38 FL	0.87	0.76	0.84	0.75	0.89	0.85	0.91
37 FL	0.89	0.79	0.85	0.76	0.90	0.86	0.92
36 FL	0.87	0.80	0.82	0.77	0.81	0.79	0.89
35 FL	0.88	0.81	0.83	0.78	0.82	0.80	0.90
34 FL	0.89	0.82	0.85	0.79	0.83	0.81	0.91
33 FL	0.86	0.75	0.83	0.74	0.84	0.82	0.91
32 FL	0.88	0.76	0.84	0.75	0.86	0.83	0.92
31 FL	0.89	0.77	0.85	0.76	0.87	0.84	0.93
30 FL	0.86	0.78	0.84	0.78	0.87	0.85	0.90
29 FL	0.87	0.78	0.85	0.79	0.88	0.86	0.91
28 FL	0.88	0.79	0.86	0.80	0.89	0.87	0.92
27 FL	0.88	0.80	0.85	0.81	0.85	0.80	0.91
26 FL	0.89	0.81	0.86	0.82	0.86	0.80	0.92
25 FL	0.90	0.82	0.87	0.83	0.87	0.82	0.93
24 FL	0.88	0.81	0.84	0.78	0.86	0.83	0.91
23 FL	0.89	0.82	0.85	0.79	0.87	0.84	0.92
22 FL	0.90	0.83	0.86	0.80	0.88	0.85	0.93
21 FL	0.88	0.82	0.84	0.81	0.87	0.85	0.91
20 FL	0.89	0.83	0.85	0.82	0.88	0.86	0.92
19 FL	0.90	0.84	0.87	0.83	0.89	0.87	0.93
18 FL	0.88	0.82	0.85	0.79	0.86	0.84	0.89
17 FL	0.89	0.83	0.86	0.80	0.87	0.85	0.90
16 FL	0.90	0.84	0.87	0.81	0.88	0.86	0.91
15 FL	0.88	0.82	0.86	0.82	0.86	0.85	0.89
14 FL	0.89	0.83	0.87	0.83	0.87	0.86	0.90
13 FL	0.90	0.84	0.88	0.83	0.88	0.87	0.90
12 FL	0.88	0.83	0.87	0.79	0.87	0.85	0.91
11 FL	0.89	0.83	0.88	0.80	0.88	0.86	0.92
10 FL	0.91	0.85	0.90	0.82	0.89	0.88	0.93
09 FL	0.75	0.84	0.97	0.87	0.90	0.72	0.88
08 FL	0.80	0.85	0.97	0.88	0.91	0.78	0.88
07 FL	0.70	0.54	0.54	0.53	0.55	0.55	0.69
06 FL	0.72	0.56	0.56	0.54	0.57	0.56	0.71
05 FL	0.72	0.57	0.57	0.55	0.58	0.57	0.72
04 FL	0.70	0.56	0.55	0.54	0.56	0.57	0.69
03 FL	0.80	0.60	0.63	0.60	0.63	0.61	0.80
02 FL	0.83	0.62	0.65	0.62	0.65	0.62	0.83
01 FL	0.89	0.82	0.88	0.94	0.85	0.84	0.92
B1 FL	0.88	0.82	0.88	0.94	0.84	0.84	0.91
B2 FL	0.89	0.83	0.89	0.96	0.85	0.85	0.92
B3 FL	0.85	0.78	0.86	0.91	0.80	0.80	0.87
B4 FL	0.87	0.82	0.95	0.99	0.87	0.85	0.97
B5 FL	0.88	0.83	0.96	1.00	0.88	0.86	0.98

(d)

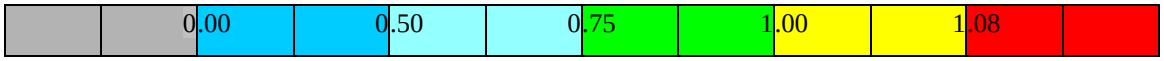

Figure 4–5. (c) 700 line, and (d) 800 line (continued).

LEVEL	TOWER A, DCR of CORE COLUMN 900's COLUMN NUMBER							
	901	902	903	904	905	906	907	908
106 FL	0.76	0.98	0.97	0.80	0.85	1.10	1.02	0.76
105 FL	0.82	1.05	1.02	0.71	0.91	1.16	1.08	0.80
104 FL	0.83	0.95	0.94	1.13	0.75	0.96	0.97	0.80
103 FL	0.92	1.01	0.98	1.21	0.80	1.01	1.02	0.89
102 FL	1.01	1.07	1.03	0.89	0.88	1.05	1.07	0.97
101 FL	0.87	0.96	0.86	0.98	0.76	0.89	0.98	0.84
100 FL	0.94	1.01	0.88	1.04	0.84	0.93	1.03	0.91
99 FL	1.01	1.05	0.91	1.10	0.90	0.97	1.08	0.98
98 FL	1.02	0.92	0.81	0.99	0.88	0.90	0.94	1.00
97 FL	1.09	0.96	0.83	1.05	0.93	0.93	0.98	1.06
96 FL	1.16	1.00	0.86	1.10	0.99	0.97	1.02	1.13
95 FL	0.91	0.84	0.81	0.88	0.86	0.86	0.90	1.08
94 FL	0.96	0.88	0.83	0.92	0.91	0.89	0.94	1.14
93 FL	1.00	0.91	0.85	0.96	0.95	0.92	0.97	1.20
92 FL	0.89	0.86	0.78	0.90	0.90	0.86	0.87	1.04
91 FL	0.93	0.89	0.80	0.94	0.94	0.89	0.90	1.09
90 FL	0.97	0.92	0.82	0.96	0.98	0.92	0.93	1.14
89 FL	1.01	0.84	0.76	0.84	0.84	0.83	0.85	1.00
88 FL	1.05	0.86	0.78	0.87	0.88	0.85	0.88	1.05
87 FL	1.09	0.89	0.80	0.90	0.91	0.88	0.90	1.09
86 FL	0.97	0.85	0.75	0.93	0.78	0.87	0.86	0.97
85 FL	1.01	0.87	0.77	0.96	0.81	0.89	0.88	1.00
84 FL	1.04	0.90	0.79	0.99	0.83	0.92	0.91	1.04
83 FL	1.07	0.79	0.73	0.86	0.79	0.87	0.80	1.07
82 FL	1.11	0.81	0.75	0.89	0.82	0.89	0.82	1.11
81 FL	1.15	0.83	0.77	0.92	0.84	0.91	0.84	1.14
80 FL	1.19	0.86	0.85	0.95	0.87	0.94	0.86	1.19
79 FL	1.25	0.89	0.88	0.99	0.91	0.97	0.89	1.24
78 FL	1.30	0.92	0.90	1.03	0.94	1.00	0.92	1.30
77 FL	0.84	0.67	0.62	0.71	0.60	0.56	0.55	0.85
76 FL	0.85	0.71	0.65	0.73	0.63	0.60	0.60	0.90
75 FL	0.98	0.85	0.84	0.94	0.76	0.85	0.88	1.05
74 FL	0.98	0.85	0.84	0.95	0.77	0.85	0.88	1.06
73 FL	1.01	0.87	0.86	0.97	0.79	0.87	0.90	1.09
72 FL	0.95	0.89	0.79	0.92	0.77	0.82	0.85	1.03
71 FL	0.98	0.91	0.81	0.94	0.79	0.85	0.87	1.06
70 FL	1.00	0.93	0.82	0.96	0.81	0.87	0.88	1.08
69 FL	0.81	0.81	0.79	0.91	0.77	0.82	0.84	0.88
68 FL	0.88	0.87	0.82	0.96	0.82	0.88	0.89	0.95
67 FL	0.86	0.85	0.82	0.96	0.81	0.86	0.87	0.92
66 FL	1.01	0.93	0.85	0.98	0.83	0.88	0.89	1.09
65 FL	1.03	0.93	0.85	0.98	0.83	0.89	0.89	1.11
64 FL	1.06	0.97	0.88	1.02	0.87	0.92	0.92	1.14
63 FL	1.00	0.91	0.83	0.97	0.82	0.94	0.88	1.07
62 FL	1.03	0.93	0.84	0.99	0.84	0.96	0.89	1.10
61 FL	1.05	0.95	0.85	1.01	0.85	0.99	0.91	1.12
60 FL	0.99	0.90	0.83	0.97	0.83	0.93	0.87	1.06
59 FL	1.01	0.92	0.84	0.99	0.85	0.95	0.88	1.08
58 FL	1.03	0.93	0.86	1.01	0.87	0.97	0.90	1.10
57 FL	1.06	0.88	0.84	1.01	0.85	0.93	0.84	1.04
56 FL	1.08	0.90	0.85	1.02	0.86	0.94	0.85	1.06
55 FL	1.10	0.91	0.86	1.04	0.88	0.96	0.87	1.09
54 FL	1.04	0.93	0.84	1.01	0.86	0.91	0.88	1.11
53 FL	1.06	0.94	0.85	1.02	0.87	0.93	0.89	1.13
52 FL	1.08	0.96	0.87	1.04	0.89	0.95	0.91	1.15
51 FL	1.03	0.89	0.85	0.99	0.86	0.97	0.83	1.09
50 FL	1.05	0.90	0.86	1.01	0.87	0.98	0.85	1.11
49 FL	1.07	0.91	0.87	1.03	0.89	1.00	0.86	1.13
48 FL	1.09	0.83	0.83	0.97	0.86	0.89	0.83	1.08
47 FL	1.12	0.85	0.85	0.98	0.87	0.92	0.85	1.11
46 FL	1.14	0.87	0.86	1.00	0.89	0.93	0.87	1.13
45 FL	0.85	0.78	0.77	0.76	0.83	0.84	0.79	0.88
44 FL	0.87	0.80	0.79	0.78	0.85	0.86	0.81	0.90
43 FL	0.75	0.61	0.60	0.69	0.63	0.66	0.62	0.77
42 FL	0.77	0.63	0.63	0.72	0.66	0.68	0.64	0.79
41 FL	1.00	0.85	0.83	0.94	0.86	0.90	0.86	1.00
40 FL	1.00	0.85	0.83	0.94	0.85	0.90	0.86	1.00
39 FL	0.98	0.83	0.84	0.94	0.84	0.89	0.84	1.01
38 FL	1.00	0.84	0.85	0.96	0.85	0.90	0.85	1.02
37 FL	1.01	0.85	0.86	0.97	0.86	0.92	0.86	1.04
36 FL	1.02	0.84	0.85	0.95	0.84	0.90	0.85	1.01
35 FL	1.03	0.85	0.86	0.96	0.85	0.91	0.86	1.03
34 FL	1.05	0.86	0.87	0.97	0.87	0.92	0.87	1.04
33 FL	1.02	0.84	0.85	0.94	0.84	0.90	0.85	1.02
32 FL	1.04	0.85	0.87	0.96	0.85	0.91	0.86	1.03
31 FL	1.05	0.86	0.88	0.97	0.86	0.92	0.87	1.04
30 FL	1.04	0.85	0.86	0.94	0.83	0.91	0.86	1.02
29 FL	1.05	0.86	0.87	0.95	0.84	0.92	0.87	1.03
28 FL	1.06	0.87	0.89	0.96	0.85	0.93	0.88	1.04
27 FL	1.17	0.86	0.87	0.97	0.84	0.91	0.86	1.02
26 FL	1.18	0.87	0.88	0.98	0.85	0.92	0.87	1.03
25 FL	1.07	0.88	0.89	0.99	0.86	0.93	0.88	1.05
24 FL	1.05	0.86	0.88	0.97	0.85	0.91	0.86	1.03
23 FL	1.06	0.87	0.89	0.98	0.86	0.92	0.86	1.04
22 FL	1.07	0.88	0.90	0.99	0.87	0.93	0.87	1.05
21 FL	1.05	0.87	0.89	0.97	0.86	0.92	0.86	1.06
20 FL	1.07	0.88	0.90	0.98	0.87	0.93	0.87	1.07
19 FL	1.08	0.89	0.91	0.99	0.87	0.94	0.88	1.09
18 FL	1.08	0.87	0.88	0.96	0.87	0.92	0.87	1.06
17 FL	1.10	0.88	0.89	0.97	0.88	0.93	0.88	1.08
16 FL	1.11	0.89	0.90	0.98	0.89	0.94	0.89	1.09
15 FL	1.09	0.86	0.89	0.99	0.86	0.93	0.87	1.08
14 FL	1.10	0.87	0.90	1.00	0.87	0.94	0.88	1.09
13 FL	1.11	0.88	0.91	1.01	0.86	0.95	0.89	1.10
12 FL	1.09	0.87	0.90	0.98	0.86	0.94	0.87	1.08
11 FL	1.11	0.88	0.91	0.99	0.87	0.95	0.88	1.09
10 FL	1.13	0.89	0.93	1.01	0.89	0.96	0.89	1.11
09 FL	0.91	0.86	0.89	0.97	0.99	1.03	0.97	1.06
08 FL	0.98	0.91	0.95	1.03	1.00	1.04	0.97	1.06
07 FL	0.63	0.60	0.61	0.62	0.67	0.59	0.59	0.62
06 FL	0.65	0.62	0.63	0.64	0.69	0.61	0.60	0.64
05 FL	0.65	0.63	0.64	0.65	0.70	0.62	0.61	0.64
04 FL	0.63	0.61	0.62	0.63	0.67	0.60	0.59	0.62
03 FL	0.72	0.69	0.71	0.72	0.80	0.68	0.67	0.71
02 FL	0.75	0.71	0.73	0.74	0.83	0.70	0.69	0.74
01 FL	1.07	0.89	0.92	1.01	1.00	0.96	0.90	1.07
B1 FL	1.06	0.88	0.91	1.00	0.98	0.94	0.88	1.06
B2 FL	1.08	0.89	0.92	1.01	0.99	0.96	0.90	1.08
B3 FL	1.02	0.85	0.89	0.97	0.93	0.92	0.86	1.01
B4 FL	1.05	0.87	0.98	1.07	1.05	1.00	0.94	1.13
B5 FL	1.06	0.88	0.99	1.08	1.06	1.01	0.95	1.14

(e)

LEVEL	TOWER A, DCR of CORE COLUMN 1000's COLUMN NUMBER							
	1001	1002	1003	1004	1005	1006	1007	1008
106 FL	0.93	1.12	1.07	0.82	0.95	1.23	1.02	0.96
105 FL	0.99	0.84	1.13	0.91	1.01	0.94	1.11	1.03
104 FL	0.87	1.07	1.01	0.84	0.90	1.10	1.03	0.90
103 FL	0.93	1.15	1.07	0.91	0.95	1.18	1.10	0.95
102 FL	1.00	1.00	1.12	0.98	1.00	1.25	0.97	1.01
101 FL	0.83	1.00	0.93	0.85	0.89	1.03	0.97	0.83
100 FL	0.88	1.06	0.98	0.91	0.93	1.09	1.02	0.89
99 FL	0.93	1.12	1.02	0.96	0.97	1.14	1.08	0.94
98 FL	0.74	0.84	0.89	0.90	0.88	0.78	0.91	0.74
97 FL	0.78	0.89	0.93	0.95	0.92	0.82	0.95	0.78
96 FL	0.82	0.93	0.97	1.00	0.96	0.86	1.00	0.82
95 FL	0.66	0.82	0.75	0.87	0.85	0.76	0.83	0.66
94 FL	0.69	0.86	0.77	0.91	0.88	0.79	0.87	0.70
93 FL	0.72	0.89	0.80	0.95	0.91	0.82	0.90	0.73
92 FL	0.69	0.79	0.72	0.91	0.78	0.74	0.80	0.69
91 FL	0.71	0.82	0.75	0.95	0.80	0.77	0.83	0.72
90 FL	0.74	0.85	0.77	0.98	0.83	0.80	0.86	0.74
89 FL	0.81	0.77	0.86	0.86	0.78	0.70	0.77	0.81
88 FL	0.84	0.79	0.88	0.89	0.80	0.73	0.80	0.84
87 FL	0.87	0.82	0.70	0.92	0.83	0.75	0.83	0.87
86 FL	0.82	0.92	0.76	0.91	0.78	0.81	0.93	0.82
85 FL	0.85	0.95	0.78	0.94	0.81	0.84	0.96	0.85
84 FL	0.87	0.98	0.80	0.97	0.83	0.86	0.99	0.88
83 FL	0.90	0.92	0.74	0.92	0.77	0.81	0.93	0.90
82 FL	0.93	0.95	0.76	0.94	0.79	0.83	0.96	0.93
81 FL	0.96	0.97	0.78	0.97	0.81	0.86	0.98	0.96
80 FL	0.91	1.01	0.70	1.00	0.87	0.88	1.02	0.91
79 FL	0.94	1.04	0.72	1.03	0.89	0.92	1.05	0.94
78 FL	0.98	1.09	0.75	1.08	0.92	0.95	1.10	0.98
77 FL	0.66	0.73	0.65	0.71	0.67	0.68	0.73	0.67
76 FL	0.68	0.74	0.67	0.70	0.72	0.70	0.75	0.68
75 FL	0.88	0.91	0.86	0.93	0.93	0.89	0.92	0.89
74 FL	0.89	0.92	0.86	0.95	0.94	0.90	0.93	0.90
73 FL	0.91	0.94	0.88	0.97	0.95	0.92	0.96	0.92
72 FL	0.87	0.89	0.84	0.91	0.89	0.87	0.91	0.87
71 FL	0.89	0.91	0.85	0.94	0.91	0.89	0.93	0.89
70 FL	0.91	0.93	0.87	0.96	0.93	0.91	0.95	0.91
69 FL	0.84	0.87	0.84	0.92	0.88	0.84	0.88	0.84
68 FL	0.87	0.90	0.87	0.96	0.91	0.87	0.92	0.87
67 FL	0.87	0.91	0.87	0.96	0.91	0.88	0.92	0.88
66 FL	0.91	0.93	0.86	0.99	0.95	0.90	0.95	0.91
65 FL	0.92	0.95	0.87	1.01	0.96	0.92	0.96	0.93
64 FL	0.94	0.97	0.89	1.03	0.98	0.94	0.98	0.94
63 FL	0.91	0.93	0.85	1.01	0.95	0.89	0.93	0.91
62 FL	0.93	0.95	0.86	1.03	0.96	0.91	0.95	0.93
61 FL	0.94	0.97	0.88	1.05	0.98	0.92	0.97	0.95
60 FL	0.91	0.93	0.83	1.01	0.94	0.89	0.93	0.91
59 FL	0.92	0.94	0.84	1.03	0.95	0.91	0.95	0.92
58 FL	0.94	0.96	0.86	1.05	0.97	0.92	0.97	0.94
57 FL	0.92	0.93	0.83	1.02	0.94	0.89	0.93	0.92
56 FL	0.93	0.94	0.84	1.04	0.95	0.90	0.95	0.93
55 FL	0.95	0.96	0.85	1.05	0.97	0.92	0.97	0.95
54 FL	0.89	0.93	0.82	1.03	0.94	0.89	0.93	0.89
53 FL	0.91	0.94	0.83	1.04	0.95	0.90	0.95	0.91
52 FL	0.92	0.96	0.84	1.06	0.96	0.91	0.96	0.92
51 FL	0.90	0.93	0.82	1.00	0.93	0.88	0.93	0.91
50 FL	0.92	0.94	0.83	1.02	0.95	0.89	0.95	0.92
49 FL	0.93	0.95	0.84	1.04	0.96	0.91	0.96	0.93
48 FL	0.89	0.90	0.80	1.01	0.90	0.85	0.89	0.89
47 FL	0.90	0.92	0.81	1.03	0.91	0.86	0.90	0.90
46 FL	0.91	0.93	0.82	1.05	0.93	0.87	0.92	0.91
45 FL	0.83	0.84	0.74	0.96	0.86	0.79	0.82	0.83
44 FL	0.85	0.86	0.76	0.99	0.88	0.81	0.84	0.85
43 FL	0.66	0.65	0.59	0.74	0.68	0.62	0.64	0.66
42 FL	0.68	0.66	0.60	0.75	0.70	0.63	0.65	0.68
41 FL	0.89	0.88	0.80	0.97	0.88	0.83	0.87	0.89
40 FL	0.89	0.88	0.80	0.98	0.89	0.83	0.88	0.90
39 FL	0.88	0.87	0.81	0.99	0.87	0.83	0.86	0.89
38 FL	0.89	0.88	0.82	1.01	0.88	0.84	0.87	0.90
37 FL	0.91	0.89	0.83	1.02	0.89	0.85	0.88	0.91
36 FL	0.89	0.87	0.81	0.97	0.87	0.83	0.85	0.90
35 FL	0.91	0.88	0.82	0.99	0.87	0.84	0.86	0.91
34 FL	0.92	0.89	0.83	1.00	0.88	0.85	0.88	0.92
33 FL	0.88	0.87	0.81	0.98	0.85	0.84	0.86	0.89
32 FL	0.89	0.88	0.82	1.00	0.86	0.85	0.87	0.90
31 FL	0.91	0.89	0.83	1.01	0.87	0.86	0.88	0.91
30 FL	0.90	0.85	0.79	0.99	0.85	0.84	0.84	0.90
29 FL	0.91	0.86	0.80	1.01	0.86	0.85	0.85	0.91
28 FL	0.92	0.87	0.81	1.02	0.87	0.86	0.86	0.92
27 FL	0.89	0.85	0.80	1.00	0.85	0.84	0.84	0.89
26 FL	0.90	0.86	0.81	1.01	0.86	0.85	0.85	0.90
25 FL	0.91	0.87	0.82	1.02	0.87	0.86	0.86	0.91
24 FL	0.88	0.85	0.80	0.99	0.85	0.84	0.84	0.88
23 FL	0.89	0.86	0.81	1.00	0.86	0.85	0.85	0.89
22 FL	0.90	0.87	0.82	1.01	0.87	0.86	0.86	0.90
21 FL	0.88	0.85	0.81	1.00	0.85	0.84	0.84	0.88
20 FL	0.89	0.86	0.81	1.01	0.86	0.85	0.85	0.89
19 FL	0.89	0.87	0.82	1.02	0.86	0.86	0.86	0.90
18 FL	0.87	0.85	0.81	1.01	0.84	0.83	0.84	0.87
17 FL	0.88	0.86	0.82	1.02	0.84	0.84	0.85	0.88
16 FL	0.89	0.87	0.83	1.03	0.85	0.85	0.86	0.89
15 FL	0.87	0.85	0.81	1.00	0.84	0.83	0.85	0.87
14 FL	0.88	0.86	0.82	1.01	0.85	0.84	0.85	0.88
13 FL	0.89	0.87	0.83	1.02	0.85	0.85	0.86	0.89
12 FL	0.88	0.85	0.82	1.01	0.84	0.84	0.85	0.88
11 FL	0.89	0.86	0.82	1.02	0.85	0.85	0.86	0.89
10 FL	0.90	0.87	0.84	1.04	0.86	0.86	0.87	0.90
09 FL	0.96	0.84	0.81	0.98	0.80	0.84	0.90	0.89
08 FL	0.96	0.87	0.85	1.03	0.83	0.87	0.91	0.93
07 FL	0.79	0.73	0.73	0.87	0.73	0.74	0.75	0.79
06 FL	0.80	0.74	0.74	0.88	0.74	0.76	0.76	0.81
05 FL	0.81	0.75	0.75	0.89	0.74	0.76	0.77	0.81
04 FL	0.79	0.73	0.73	0.86	0.73	0.74	0.75	0.79
03 FL	0.86	0.79	0.79	0.94	0.78	0.80	0.81	0.86
02 FL	0.88	0.80	0.80	0.96	0.79	0.81	0.82	0.88
01 FL	0.84	0.83	0.79	0.95	0.83	0.81	0.83	0.84
B1 FL	0.83	0.82	0.78	0.94	0.83	0.80	0.82	0.83
B2 FL	0.84	0.83	0.79	0.95	0.84	0.81	0.83	0.84
B3 FL	0.86	0.82	0.79	0.92	0.81	0.82	0.80	0.87
B4 FL	0.92	0.83	0.85	0.99	0.86	0.83	0.86	0.88
B5 FL	0.93	0.83	0.85	1.00	0.86	0.83	0.86	0.88

(f)

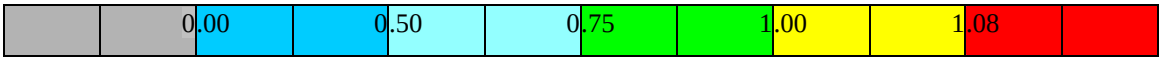

Figure 4–5. (e) 900 line, and (f) 1000 line (continued).

Table 4–5. Statistics of DCRs for WTC 1 under the refined NIST estimate case using LRFD and ASD.

Member Type	Number of Members	Mean Calculated DCR	C.O.V. of DCR	Percentage of components with DCR > 1.0	Percentage of components with DCR > 1.05	Number of components with DCR > 1.05	Maximum Calculated DCR
Exterior Wall Columns, floor 9-106							
LRFD	31,086	0.96	0.15	35.6	24.0	7,461	1.72
ASD	31,086	1.10	0.14	72.1	59.7	18,572	2.05
Core Columns							
LRFD	5,219	0.73	0.16	2.9	1.8	92	1.26
ASD	5,219	0.84	0.15	8.9	5.2	270	1.40

4.2.4 Exterior Columns Axial Loads and Stresses

The distribution of the normal stresses due to axial loads (axial column load divided by column cross sectional area) in the four exterior wall columns of WTC 1 due to wind loads only is presented in Fig. 4–6. The stresses are presented for the original design wind loads blowing from west to east and do not include the influence of gravity loads. The axial stresses are presented for the exterior wall columns at level B6 and floor 39. Fig. 4–7 shows a 3-dimensional plot of the same stresses at floors B6 and 39. The plots show both the tensile and compressive stresses on the columns induced by wind loading, where the shear lag effects can be observed. Similar plots were obtained for WTC 2 (NIST NCSTAR 1-2A).

At the B6 level, the plots indicate that there were significant differences in stresses between the two columns at a given corner. For example, at the southwest corner at level B6, the stresses at columns 359 (south wall) and 401 (east wall) were about 25 ksi and 15 ksi, respectively. This indicates significant deformations in the corner panels at the basement floors. Much smaller differences were observed in the stresses at the floor 39. This indicates that the behavior of the lower portion of the tower at the basement floors resembled that of a braced frame, while the behavior of the super-structure resembled that of a framed tube system.

A framed tube structure consists of closely spaced exterior columns tied together at each floor with deep spandrel beams, thereby creating a rigid wall-like structure around the building exterior (i.e., a hollow tube with perforated openings for windows) (Khan and Amin 1973; Taranath 1988). The behavior of the framed tube structure is hybrid, showing characteristics of both pure tube and pure frame behaviors. The overturning moments of the lateral loads are primarily resisted by the tube action, i.e., axial shortening (compression) and elongation (tension) of the columns on all sides of the tube. The shear from the lateral loads is primarily resisted by the frame action (in-plane bending of columns and spandrels) of the two sides of the building parallel to the direction of the lateral load (webs). Since the perimeter walls have a tendency to behave as a thin-walled tube structure, shear stresses and strains are large, and as a result the distribution of bending stresses is affected. Therefore, the bending stresses in the side walls (webs) are no longer proportional to the distance from the neutral axis and are larger near the flanges. The same large stresses occur in the flanges near the webs, and the stresses at the center of the flanges (normal to the lateral load) are reduced or ‘lag’ behind the stresses near the webs (parallel to load). Bending stresses in

the webs are also affected in a similar manner. This phenomenon is known as shear lag and can be clearly shown in Fig. 4–6(b). In the framed tube system, the floor diaphragms play a key role since they carry lateral forces to the side walls of the building, thereby allowing for the tube action to take place. In addition, floor diaphragms provide lateral support for the stability of the columns, and under torsion, they assure that the cross-sectional shape of the structure is maintained at each level by their in-plane shearing resistance.

An investigation into the behavior of the exterior wall columns indicated that under the original WTC design dead and wind loads (no live loads were considered), tension forces were developed in the exterior walls of the towers. The tension forces from the combination of dead and wind loads for the four exterior walls of WTC 1 are illustrated in Fig. 4–8. Similar plots for WTC 2 can be seen at Chapter 5 of NIST NCSTAR 1-2A. As the figure indicates, the tensile forces were largest at the base of the building and at the corners.

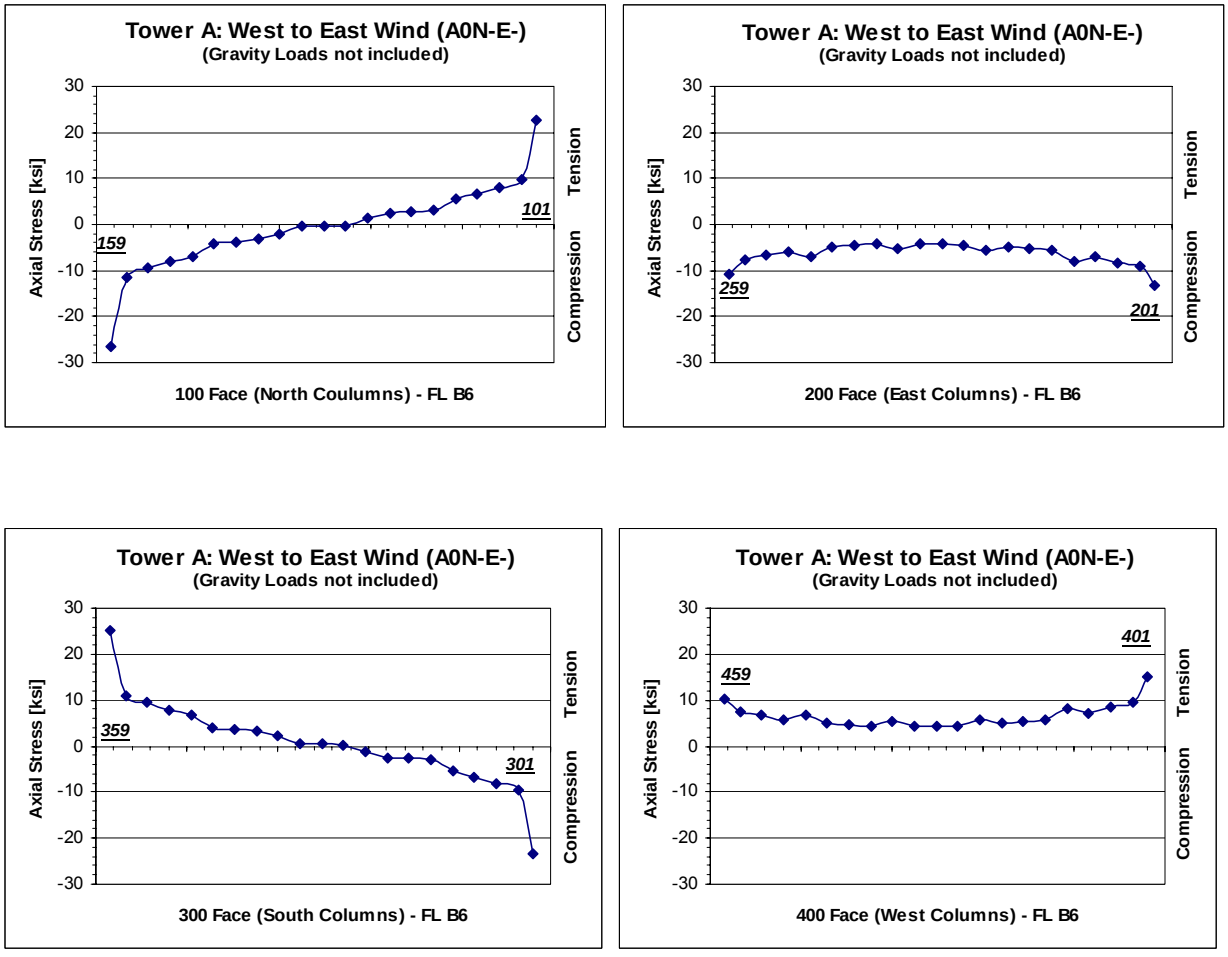

(a) Floor B6

Figure 4–6. Distribution of normal stresses in the exterior walls of WTC 1 due to original WTC wind loads only at (a) floor B6, and (b) floor 39.

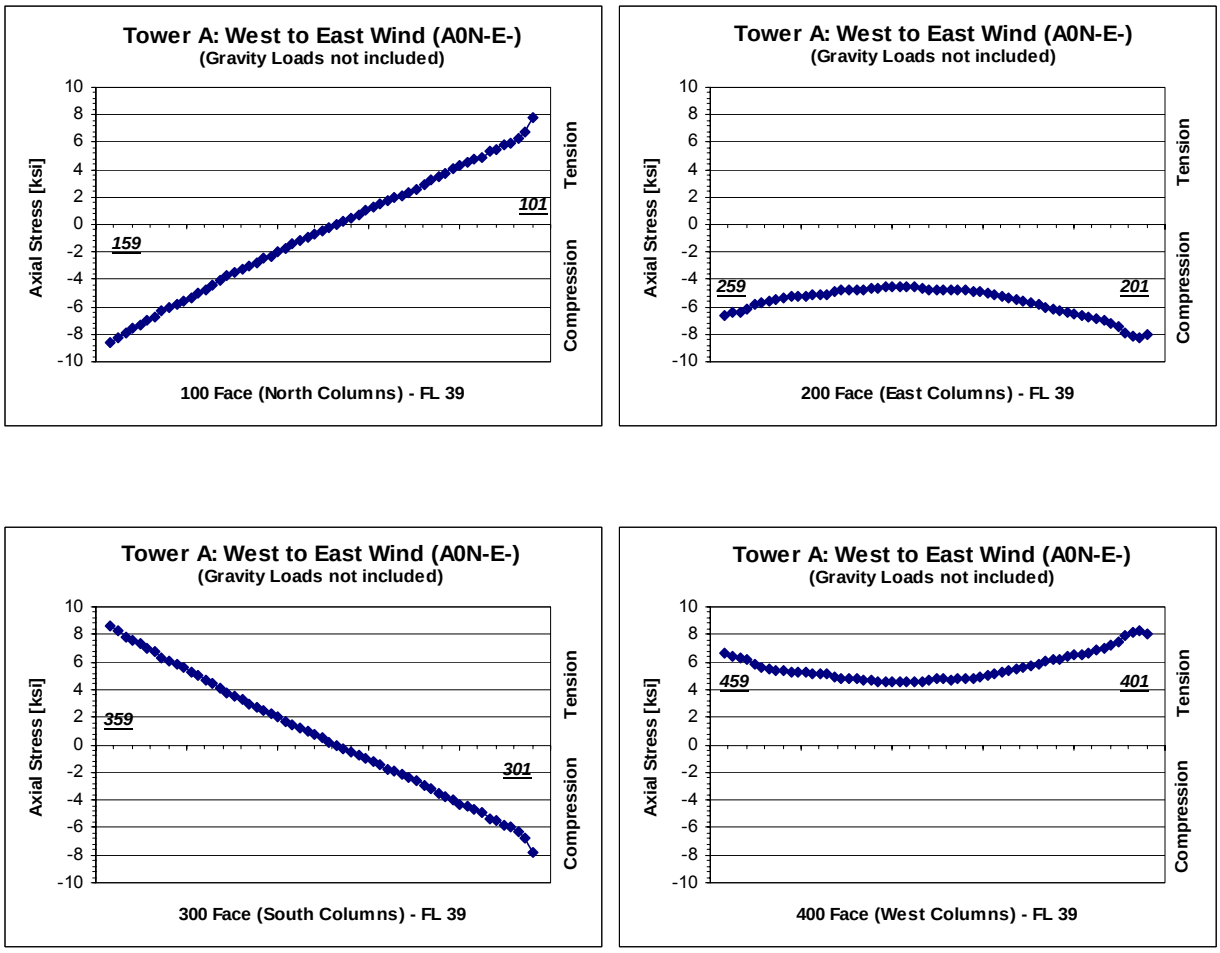

(b) Floor 39

Figure 4–6. Distribution of normal stresses in the exterior walls of WTC 1 due to original WTC wind loads only at (a) floor B6, and (b) floor 39 (continued).

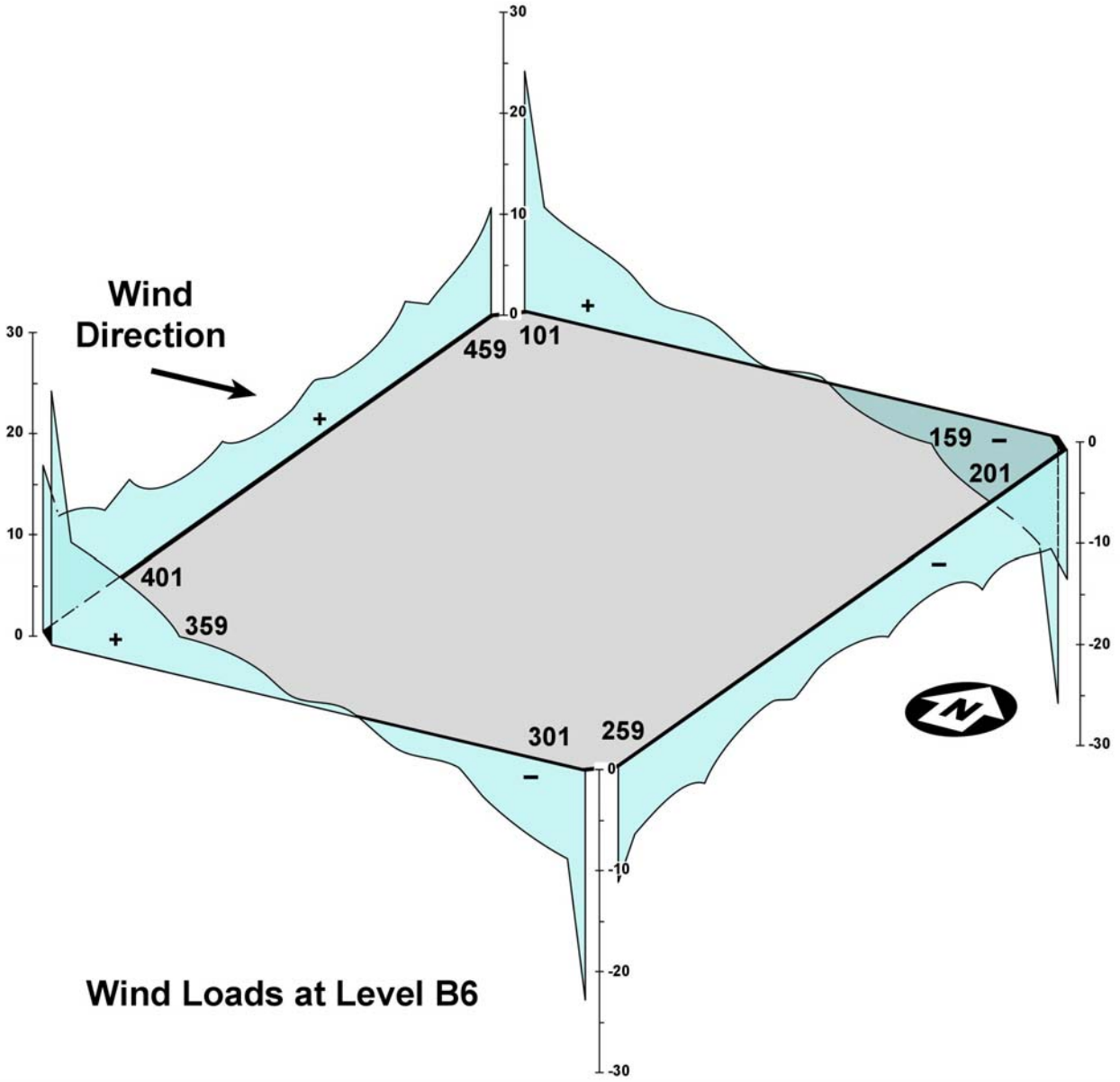

Figure 4–7. Three-dimensional distribution of normal stresses in the exterior walls of WTC 1 due to original WTC wind loads only at floors B6 and 39.

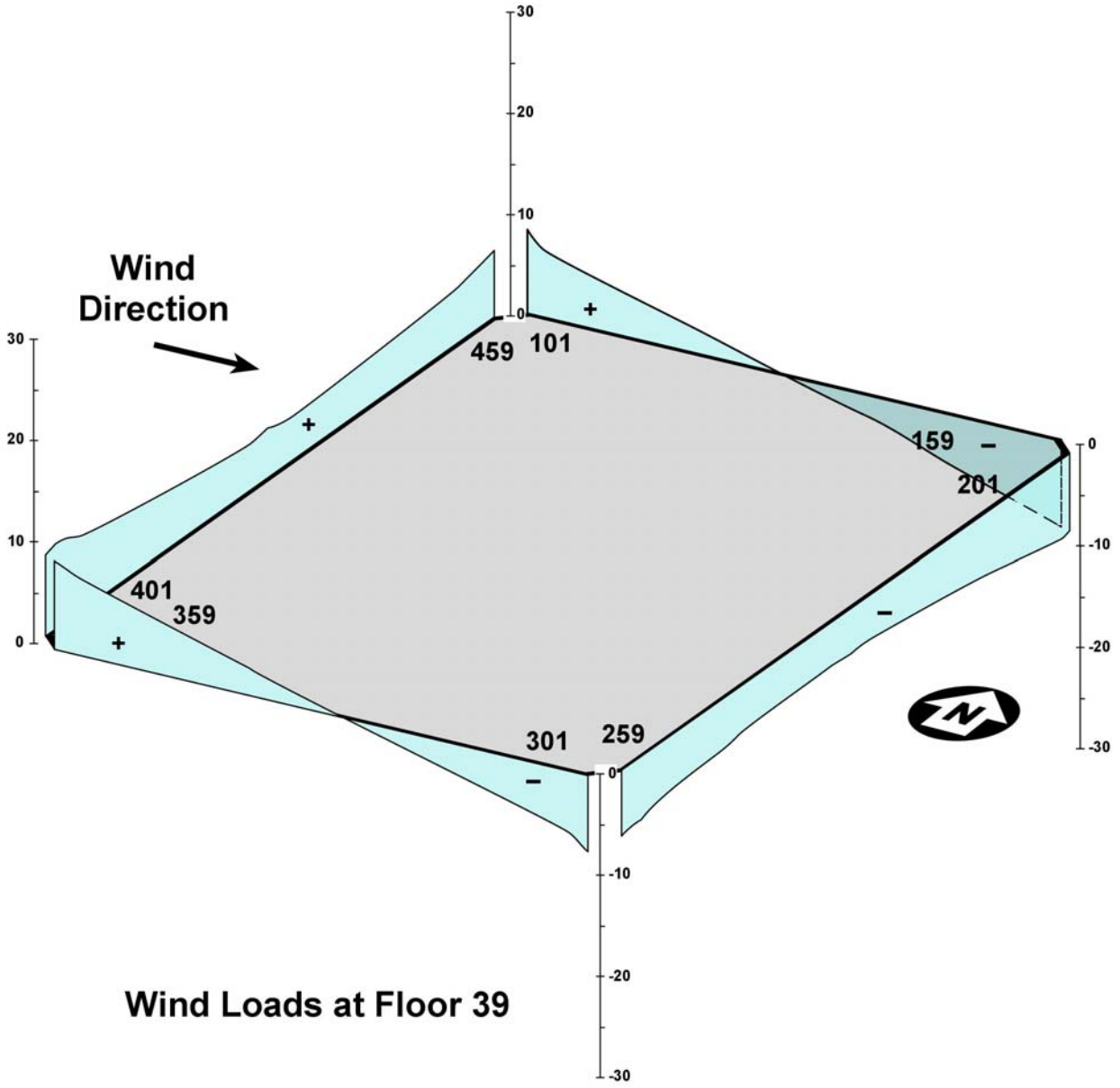

Figure 4–7. Three-dimensional distribution of normal stresses in the exterior walls of WTC 1 due to original WTC wind loads only at floors B6 and 39 (continued).

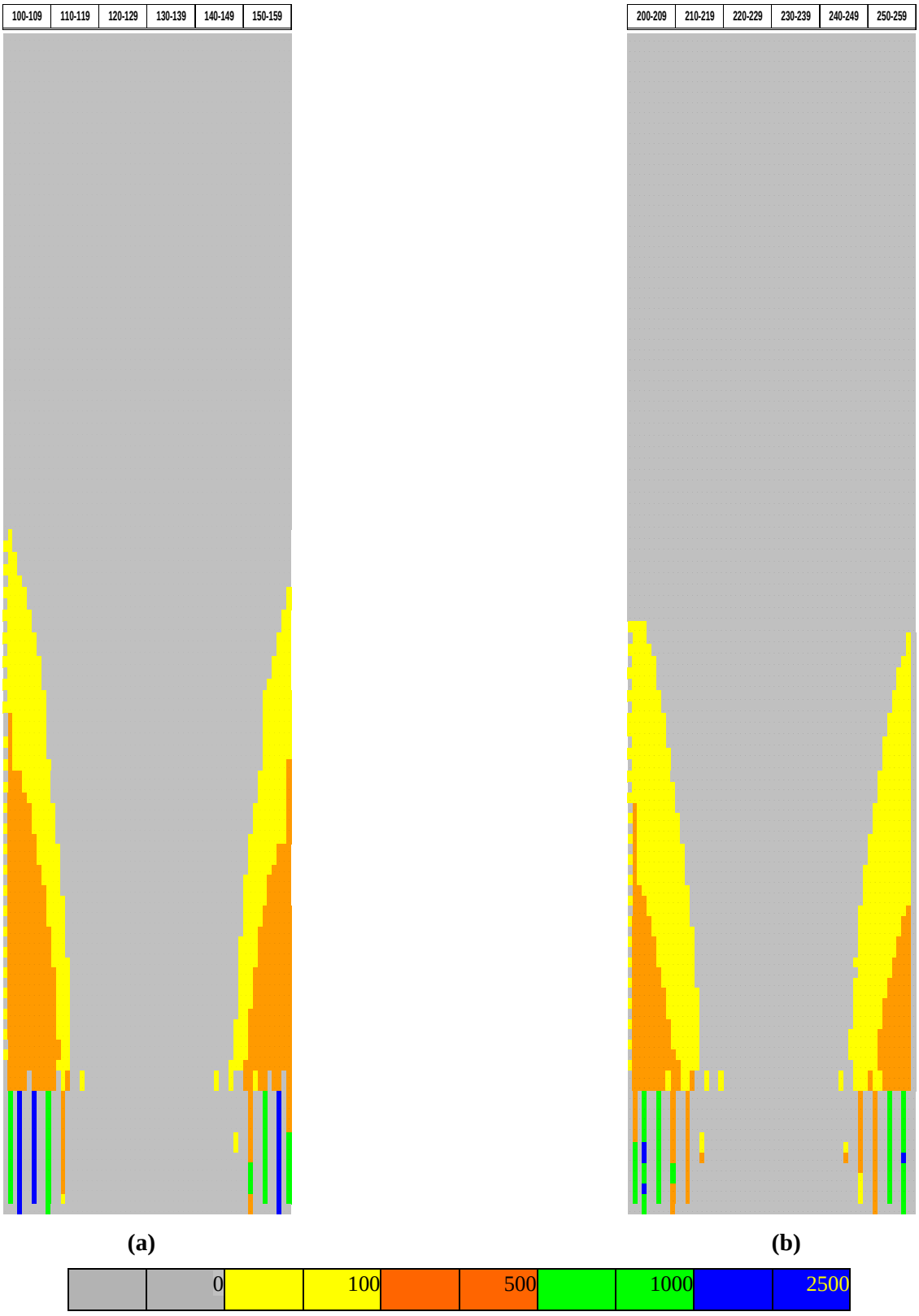

Figure 4–8. Tension force distribution (kip) in the exterior wall columns of WTC 1 under original design dead and wind loads (no live loads included), (a) 100 face (north), and (b) 200 face (east).

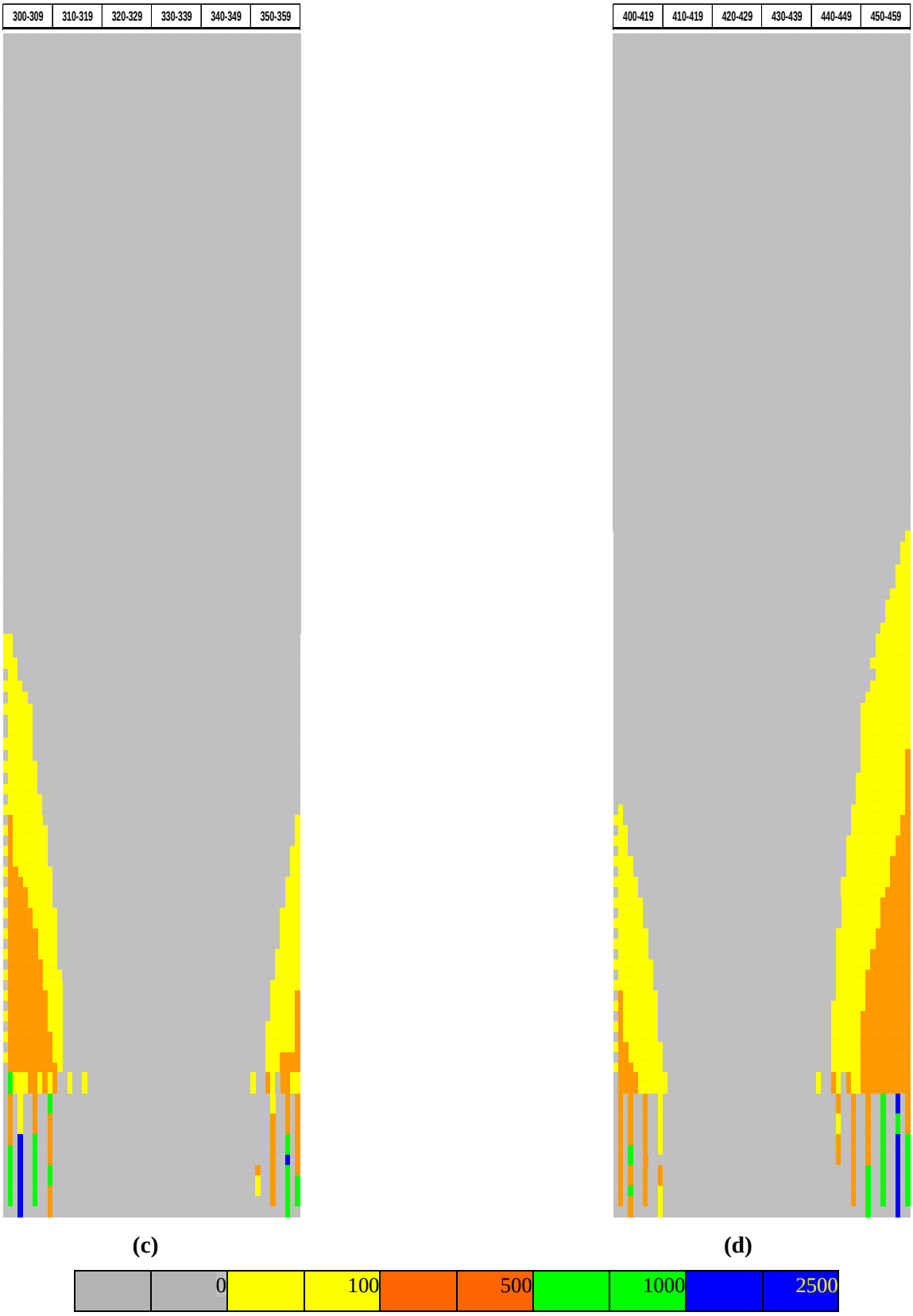

Figure 4–8. (c) 300 face (south), and (d) 400 face (west) (continued).

4.2.5 Exterior Columns Splice Connection

The axial tensile column loads estimated in Section 4.2.4 under dead and wind loads were transferred from one panel to another through the column splices. The exterior wall column splice capacities were calculated from the original details and compared to the tension forces for all four faces of WTC 1. The DCRs for the exterior wall splice connections for WTC 1 are summarized in Table 4–6. As can be observed from Table 4–6 and from a similar table for WTC 2 (NIST NCSTAR 1-2A), the DCRs were less than unity for all walls of both towers.

Table 4–6. Maximum calculated DCRs for exterior wall column splices for WTC 1 under original design dead and wind load case.

Exterior Wall Face	Exterior Wall Column Splices	Maximum Calculated DCR
100 Face (North)	Below floor 1	0.64
	Floor 1 to 9	0.31
	Floor 10 to 41	0.96
	Above floor 42	0.26
200 Face (East)	Below floor 1	0.53
	Floor 1 to 9	0.32
	Floor 10 to 41	0.63
	Above floor 42	0.14
300 Face (South)	Below floor 1	0.54
	Floor 1 to 9	0.26
	Floor 10 to 41	0.77
	Above floor 42	0.15
400 Face (West)	Below floor 1	0.59
	Floor 1 to 9	0.36
	Floor 10 to 41	0.84
	Above floor 42	0.26

4.2.6 Resistance of the Towers to Shear Sliding and Overturning Moment

The dead loads that acted on the exterior walls of the towers provided resistance to shear sliding and overturning induced by wind loads. Considering the resistance to shear sliding under wind loads, the factor of safety was estimated to be approximately 11.5 and 10 for WTC 1 and WTC 2, respectively. This was calculated by dividing the resisting force due to dead load on the exterior walls (a coefficient of friction of 0.7 was used) by the wind shear (maximum base shear) at the foundation level.

For the resistance of the towers to overturning due to wind loads, the factors of safety for WTC 1 were estimated to be approximately 2.3 and 2.6 for overturning about a north-south axis and an east-west axis, respectively. For WTC 2, these factors of safety were about 1.9 and 2.7 for overturning about a north-south axis and an east-west axis, respectively. These factors of safety were calculated by dividing the

resisting moment due to dead load on the exterior walls by the overturning moment due to wind loads taken at the foundation level (maximum base moments).

4.3 BASELINE PERFORMANCE OF THE TYPICAL FLOOR MODELS

This section presents the results of the baseline performance analysis for the typical floor models under gravity (dead and live) loads. These models included the typical truss-framed floor (floor 96 of WTC 1, see Section 2.4) and the typical beam-framed floor (floor 75 of WTC 2, see Section 2.5).

For application to the floor models, gravity loads were separated into three categories: CDLs, SDLs, and live loads (LLs). CDL is defined as the self-weight of the structural system, including floor trusses, floor beams, and concrete slabs. SDL is defined as the added dead load associated with architectural and mechanical/electrical/plumbing systems (curtain wall, floor finishes, mechanical equipment and ducts, transformers, etc.) The CDL and SDL were based on the WTC architectural and structural drawings and on the original WTC Design Criteria. For the estimation of the dead loads on the floor models, see Chapter 6 of NIST NCSTAR 1-2A.

Two independent sets of live loads were applied in combination with the dead loads. The first was taken from the original WTC Design Criteria and the second from the ASCE 7-02 Standard. The live loads in the NYCBC 2001 are essentially identical to the ASCE 7-02 live loads. Live load reductions were taken from the original WTC Design Criteria and from the ASCE 7-02 Standard, each for use with its respective live loads. For the typical beam-framed floor, it was found that the original WTC design criteria live loads, NYCBC 2001 loads, and the ASCE7-02 Standard loads were nearly identical. The only difference was that the live load for the corridors within the core was 100 psf in the original WTC design criteria, 75 psf in NYCBC 2001, and 80 psf in ASCE 7-02. As a result, only the original WTC design criteria loads were applied to the beam-framed floor model.

For the baseline performance analysis for the floor systems, DCRs for structural components were estimated using the ASD procedure as specified in the AISC Specification (1989), see Section 4.2.1.

4.3.1 Typical Truss-Framed Floor

For the CDL, SDL, and LL applied to this floor and for the selection of the design parameters for estimating the DCRs, see Chapter 6 of NIST NCSTAR 1-2A.

The maximum mid-span deflections for each of the long-span, short-span, and two-way zones for the original WTC Design Criteria and ASCE-7-02 total loads are provided in Table 4–7.

Table 4–7. Summary of maximum deflections for typical truss-framed floor under dead and live loads for areas outside of core.

Criteria	Two-Way Zone	Long Span	Short Span
WTC Design Criteria	1.44 in.	1.79 in. ≈ L/400	0.57 in. ≈ L/750
ASCE 7-02	1.14 in.	1.43 in. ≈ L/500	0.44 in. ≈ L/980

The Design Criteria for the towers specified that the floor trusses were to be cambered for construction dead loads and proportioned such that the deflection under SDL and LL did not exceed L/360. Table 4–7 clearly shows that this criterion was met.

For the components of the truss-framed floors, DCRs were calculated using the SAP2000 program. Calculations were made for the bottom chords, the diagonals and the verticals of the trusses, and for the beams and girders of the core.

DCR statistics for the truss-framed floor model are summarized in Table 4–8 for the original design loading case and in Table 4–9 for the ASCE 7-02 loading case. For the area outside the core, the DCRs for all floor trusses were less than 1.14 for the original WTC design loads and less than 0.86 for the ASCE 7-02 loading and (by comparison) for the NYCBC 2001 loading. Under the original WTC design loading, the DCR was less than 1.00 for 99.4 percent of the floor truss components. Inside the core, the DCRs for all floor beams were less than 1.08, and more than 99 percent of the members had a DCR of less than 1.0.

For the area outside the core, the average ratio of the DCRs estimated from the ASCE 7-02 loading to the DCRs from the original WTC design loading for all floor trusses was about 0.80.

Table 4–8. DCR statistics for the typical truss-framed floor under the original design load case.

Member Type	Number of Members	Mean Calculated DCR	C.O.V. of DCR	Percentage of components with DCR > 1.0	Percentage of components with DCR > 1.05	Number of components with DCR > 1.05	Maximum Calculated DCR
One-Way Long Span Zone							
Web members	1,792	0.44	0.61	3.7	1.28	23	1.14
Bottom chord members	1,038	0.74	0.26	0	0	0	0.99
One-Way Short Span Zone							
Web members	640	0.33	0.61	0	0	0	0.92
Bottom chord members	288	0.37	0.32	0	0	0	0.55
Two-Way Zone							
Web members	3,086	0.30	0.80	0.3	0.26	8	1.06
Bottom chord members	2,035	0.48	0.54	0	0	0	0.94
Bridging Trusses within One-Way Span Zones							
Web members	692	0.16	1.25	1	0	0	1.02
Bottom chord members	327	0.12	1.33	0	0	0	0.95
Core Beams							
Beams within core	1,361	0.33	0.67	0.9	0.3	4	1.07
Core perimeter channels	686	0.36	0.58	1.0	0.6	4	1.08

Table 4–9. DCR statistics for floor the typical truss-framed floor under the ASCE 7-02 loading case.

Member Type	Number of Members	Mean Calculated DCR	C.O.V. of DCR	Percentage of components with DCR > 1.0	Percentage of components with DCR > 1.05	Maximum Calculated DCR
One-Way Long Span Zone						
Web members	1,792	0.35	0.60	0	0	0.86
Bottom chord members	1,038	0.59	0.25	0	0	0.80
One-Way Short Span Zone						
Web members	640	0.26	0.65	0	0	0.69
Bottom chord members	288	0.30	0.33	0	0	0.43
Two-Way Zone						
Web members	3,086	0.24	0.79	0	0	0.78
Bottom chord members	2,035	0.38	0.55	0	0	0.74
Bridging Trusses within One-Way Span Zones						
Web members	692	0.11	1.55	0	0	0.95
Bottom chord members	327	0.09	1.44	0	0	0.81
Core Beams						
Beams within core	1,361	0.28	0.64	0.1	0.1	1.05
Core perimeter channels	686	0.28	0.61	0	0	0.86

4.3.2 Typical Beam-Framed Floor

For the CDL, SDL, and LL applied to this floor, see Chapter 6 of NIST NCSTAR 1-2A.

The maximum mid-span deflections of the long-span and short-span zones under the original WTC design loads were approximately 1.55 in. (≈ L/450) and 0.70 in. (≈ L/600), respectively. The Design Criteria for the towers specified that the floor beams be proportioned such that the deflection would not exceed L/360 under total load. If the beams were cambered for construction dead loads, the final deflection could not exceed L/360 under SDL + LL. The calculated deflections clearly showed that this criterion was met.

Using the SAP2000 computer program, DCRs were calculated for the components of the floor framing. Only two beams running in the east-west direction and cantilevering off of corner core columns 501 and 508 had DCRs larger than 1.0 under the original WTC design loading. For these two beams, the DCRs from the axial load and moment interaction equation were less than 1.0, while the DCRs in shear were 1.125 and 1.09.

Fig. 4–9 shows the distribution of DCRs for the floor framing. The figure shows the location of the two beams with DCR greater than 1.0. DCR statistics for the beam-framed floor model are summarized in Table 4–10 for the original design loading case. The statistics are provided for member groups that are shown in Fig. 4–10.

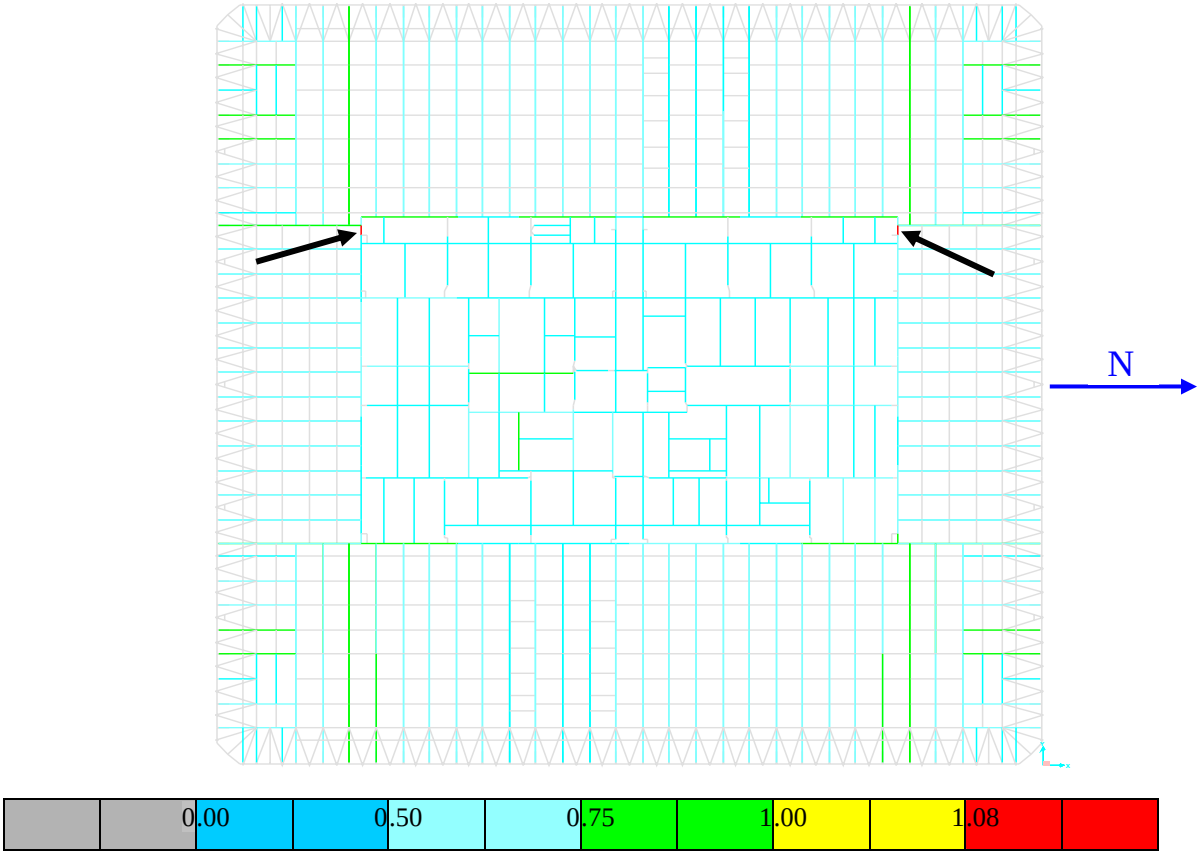

Figure 4–9. DCRs for the typical beam-framed floor under original WTC design criteria loading.

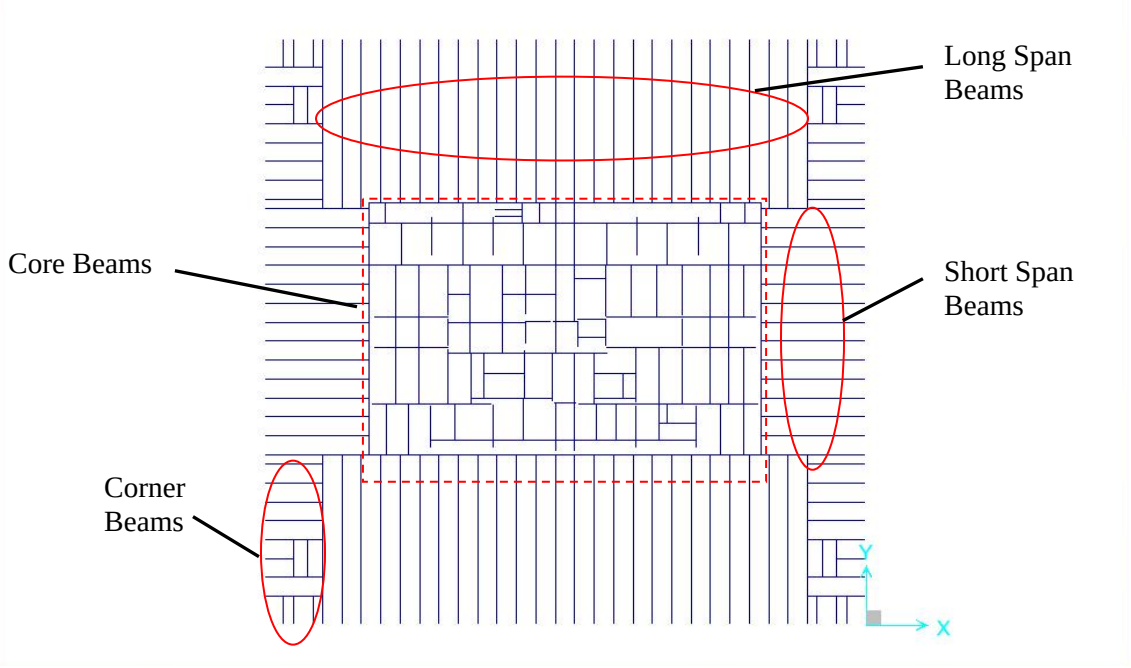

Figure 4–10. Beam-framed floor member groups.

Table 4–10. DCR statistics for the typical beam-framed floor under the original design loading case.

Member Type	Number of Members	Mean Calculated DCR	C.O.V. of DCR	Maximum Calculated DCR
Long Span Beams	156	0.64	0.16	0.83
Short Span Beams	84	0.65	0.12	0.89
Core Beams	156	0.31	0.77	1.13
Corner Beams	32	0.49	0.35	0.90

4.4 REVIEW OF BASELINE PERFORMANCE ANALYSES

As was the case for the structural databases and models, the baseline performance analyses outlined in this chapter for the global WTC models and the floor models were reviewed by SOM and NIST. The reviews included the following: (1) checks on the accuracy of load vectors (gravity and wind) as developed in Chapter 3; (2) reviews of the adequacy of the analysis procedures, including staged construction analysis, P-Δ effects, modal analysis, etc.; and (3) checks on the proper use of load combinations and component capacity estimates. The reviews indicated that the baseline performance analyses were appropriate. The reviews also included a thorough review of the report on baseline performance analysis, that resulted in substantial modifications to the report.

4.5 SUMMARY

This chapter presented the results of the baseline performance analysis for the WTC 1 and WTC 2 towers. For the global models of the towers, three gravity and wind loading cases were considered: (1) the

original WTC design load case, (2) the lower-estimate state-of-the-practices case, and (3) the refined NIST estimate case.

Under the original WTC design loads, the cumulative drifts at the top of the WTC towers ranged from H/263 to H/335. For the lower-estimate state-of-the-practice case, those drifts ranged from H/253 to H/306. The drifts obtained from the refined NIST estimate case were about 25 percent larger than those from the state-of-the practice case. While currently no building codes specify a drift limit for wind design, structural engineers often use in their practice the criterion that drift ratios should not exceed H/400 to H/500 for serviceability considerations and to enhance overall safety and stability (including P-Δ effects). Reducing the drift of the WTC towers to the range of H/400 to H/500 would entail enhancing the stiffness and/or damping characteristics of the buildings.

Structural engineers often use in their practice an inter-story drift limit in the range of h/300 to h/400 for serviceability considerations. Under design loading conditions, the maximum inter-story drift was as high as h/230 and h/200 for WTC 1 and WTC 2, respectively. Maximum inter-story drifts under the state-of-the practice case were about h/184 and h/200 for WTC 1 and WTC 2, respectively. For the refined NIST estimate case, these inter-story drifts were about 25 percent larger than those from the state-of-the practice case. Similar to total drift, inter-story drifts of the towers were larger than what is generally used in practice.

The DCRs were based on the allowable stress design (ASD) procedure and were estimated using the AISC Specifications (1989). The results indicated that DCRs estimated from the original WTC design load case were, in general, close to those obtained for the lower estimate state-of-the practice case. For both cases, a fraction of structural components had DCRs larger than 1.0. These were mainly observed in both towers at (1) the exterior walls at the columns around the corners, where the hat truss connected to the exterior walls, and below floor 9; and (2) the core columns on the 600 line between floors 80 and 106 and at core perimeter columns 901 and 908 for much of their height. The DCRs obtained for the refined NIST estimate case were higher than those from the original WTC design and the lower-estimate state-of-the-practice load cases, owing to the following reasons: (1) the NIST estimated wind loads were higher than those used in the state-of-the-practice case by about 25 percent, and (2) the original WTC design and the state-of-the-practice cases used NYCBC load combinations, which result in lower DCRs than the ASCE 7-02 load combinations used for the refined NIST case. The DCRs estimated using the load and resistance factor design (LRFD) procedure for exterior and core columns were, on average, smaller than those using the ASD procedure by about 15 percent.

While it is a normal design practice to achieve a DCR less than unity, the safety of the WTC towers on September 11, 2001, was most likely not affected by the fraction of members for which the demand exceeded capacity due to the following: (1) The inherent factor of safety in the allowable stress design method, (2) the load redistribution capability of ductile steel structures, and (3) on the day of the attack, the towers were subjected to in-service live loads (a fraction of the design live loads) and minimal wind loads.

Analysis of the axial stress distribution in the columns under lateral wind loads indicated that the behavior of the lower portion of the towers at the basement floors was that of a braced frame, while the behavior of the super-structure was that of a framed tube system. Under a combination of the original WTC design dead and wind loads, tension forces were developed in the exterior walls of both towers. The forces were largest at the base of the building and at the corners. These tensile column loads were transferred from

one panel to another through the column splices. The DCRs for the exterior wall splice connections under these tensile forces for both towers were shown to be less than 1.0.

The resistance of the towers to shear sliding and overturning due to wind was provided by the dead loads that acted on the exterior walls of the towers. Considering the resistance to shear sliding under wind load, the factor of safety was calculated to be between 10 and 11.5, while the factor of safety against overturning ranged from 1.9 to 2.7 for both towers.

Two typical floor models were each analyzed under gravity loads. The following is a summary of the results:

- For the typical truss-framed floor, the DCRs for all floor trusses were less than 1.14 for the original WTC design loads and less than 0.86 for the ASCE 7-02 loading. Under the original WTC design loads, the DCR was less than 1.00 for 99.4 percent of the floor truss components. Inside the core, the DCRs for all floor beams were less than 1.08, and more than 99 percent of the floor beams had a DCR of less than 1.0. The maximum mid-span deflections of the long-span and short-span zones under the original WTC design loads were approximately 1.79 in. (≈ L/400) and 0.57 in. (≈ L/750), respectively.

- For the typical beam-framed floor under the original WTC design loads, the DCRs for all floor beams were less than 1.0 except for two core beams where the DCRs in shear were 1.125 and 1.09. The maximum mid-span deflections of the long-span and short-span zones under the original design loads were approximately 1.55 in. (≈ L/450) and 0.70 in. (≈ L/600), respectively.

4.6 REFERENCES

AISC Specification (1989): American Institute of Steel Construction, Specification for Structural Steel Buildings – Allowable Stress Design and Plastic Design – 9th Edition, Chicago, IL, 1989.

AISC Specification (1993): American Institute of Steel Construction, Specification for Structural Steel Buildings – Load & Resistance Factor – 2nd Edition, Chicago, IL, 1993.

ASCE 7-02: American Society of Civil Engineers, ASCE 7 Standard Minimum Design Loads for Buildings and Other Structures, Reston, VA, 2002.

Khan, F.R., and Amin, N.R., (1973), "Analysis and Design of Framed Tube Structures for Tall Concrete Buildings," *The Structural Engineer*, 51(3), pp. 85-92.

NYCBC 2001: Building Code of the City of New York, 2001 Edition, Gould Publications, Binghamton, NY.

Taranath, B.S., (1988), *Structural Analysis & Design of Tall Buildings*, McGraw-Hill, Inc., New York, USA.

Chapter 5
DEVELOPMENT OF TOWER AND AIRCRAFT IMPACT MODELS

5.1 INTRODUCTION

This chapter describes the structural models used in the analysis of aircraft impact into the World Trade Center (WTC) towers. The WTC tower models for the impact analysis required considerably greater sophistication and detail than was required for the reference models described in Chapter 2. The reference models provided the basis for the more detailed models required for the impact simulations. The impact models of the towers, which utilized the structural databases described in Chapter 2 (see also NIST NCSTAR 1-2A), included the following refinements:

- The material properties used in the impact models accounted for the highly nonlinear behavior of the tower and aircraft materials, including softening and failure of components, and strain rate sensitivity.

- The impact simulations required a much higher level of detail than that in the reference global models. For instance, the impact analyses necessitated that the floors inside and outside the core in the impact region, as well as connections, be modeled in detail. In addition, structural components in the exterior walls and core of the towers were modeled using shell elements (instead of beam elements in the reference models) to properly capture the impact-induced damage to these components.

- The size of the impact models required a very large mesh (more than ten million degrees of freedom). The SAP2000 program cannot accommodate this model size.

- Contact and erosion algorithms were required for the impact analyses. That necessitated the use of appropriate software, specifically LS-DYNA (LS-DYNA 2003), for the development of the impact models.

Three separate models were developed for conducting the impact analyses. The first two were detailed models of the WTC 1 and WTC 2 towers in the impact region. The third model was a comprehensive model of the Boeing 767 aircraft. All models were developed for the LS-DYNA finite element code, which is a commercially available nonlinear explicit finite element code for the dynamic analysis of structures. The code has been used for a wide variety of crash, blast, and impact applications. The models were developed using the TrueGrid model generation program (TrueGrid Manual 2001). The input data for TrueGrid included a set of commands that defined the model geometry, material properties, boundary conditions, and mesh sizes. The output from TrueGrid was a complete LS-DYNA input file for the desired analysis.

One of the significant challenges in developing the tower and aircraft models for the global impact analyses was to minimize the model size while keeping sufficient fidelity in the impact zone to properly capture the characteristics of the impact response. The limitation was a model size that could be run on a 32-bit computer, since additional memory was needed to decompose a model with greater than ~

2.3 million nodes. Based on this limitation, each combined aircraft and tower model could not exceed 2.3 million nodes. These were distributed between the global WTC tower model and the aircraft so that the tower model would be about 1.5 million nodes and the aircraft about 0.8 million nodes. The approach used to meet this objective was to develop models for the various tower components at different levels of refinement. Components in the path of the impact and debris field were meshed with a higher resolution to capture the local impact damage and failure, while components outside the impact zone were meshed more coarsely to primarily capture their structural stiffness and inertial properties. As a result, an array of component and subassembly analyses were performed to optimize the finite element mesh densities and study the influence of a number of modeling options on the calculated response.

Section 5.2 and 5.3 provide the details and methodology used to develop the global tower and aircraft models, respectively, including constitutive relationships used for the various materials in the towers and aircraft. Section 5.4 provides a summary of the component level and subassembly analyses used to support the development of the global tower and aircraft models. Section 5.5 is a summary of the chapter.

5.2 DEVELOPMENT OF TOWER IMPACT MODELS

Given the complexity of the towers' structure, a key aspect of developing the global models was automating the mesh generation process. The component model generation files were developed in a parameterized format to support automated mesh generation. For that purpose, the electronic structural databases developed by the firm of Leslie E. Robertson Associates, R.L.L.P. under contract to NIST within the framework of Project 2, and reviewed and approved by NIST (see Chapter 2), were utilized. Visual Basic programs were developed to interface with the structural databases and to automatically write master level TrueGrid input files for mesh generation. These programs were used to generate the models for the core columns and exterior walls.

An example of such programs is presented in Figure 5–1, which shows the user interface for the program that generated the models of the exterior wall panels. In this program, the user identified the tower, upper and lower floor boundaries, and left and right (as viewed from outside the building) panel numbers. Additionally, the user could specify a fine mesh region, typically in the area of the aircraft impact. This program extracted information from the database and wrote a master TrueGrid file. Information not available in the database but included in the drawing books, such as the weld specifications, were included in the program. The automatically generated TrueGrid files included the geometry and material specification for the columns, butt plates, spandrels, welds, bolts, and spandrel splice plates. Node tolerance specifications (nodal merging commands) were also automatically generated to define the connectivity of adjacent parts in the model.

A summary of the model size and element types for the global tower models is presented in Table 5–1. The following sections provide the details of the various components used in the tower models.

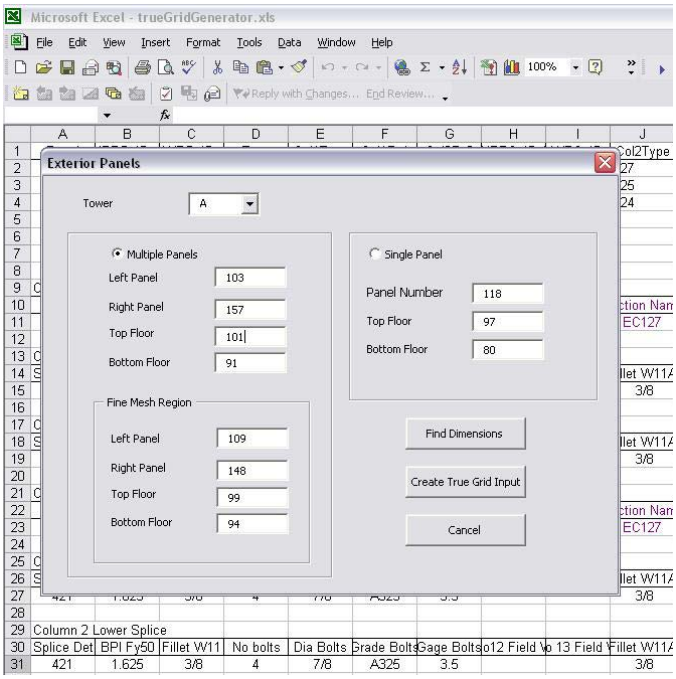

Figure 5–1. User interface for exterior panel generator.

Table 5–1. Summary of the size of the global impact tower models.

	WTC 1 Tower Model	WTC 2 Tower Model
Number of Nodes	1,300,537	1,312,092
Hughes-Liu Beam Elements	47,952	53,488
Belytschko-Tsay Shell Elements	1,156,947	1,155,815
Constant Stress Solid Elements	2,805	2,498

5.2.1 Exterior Wall Model Development

The exterior walls were constructed as an assembly of panels. The most common panel types on the exterior of the towers consisted of three columns and spans over three floors. The columns in each panel were attached together by spandrel plates, typically at each floor level. The construction of the exterior wall model required the generation of a parameterized model for each panel type that was located in the tower regions near the impact zones.

The complete exterior wall model in the impact zone for each tower was generated by placing the various panels in the actual locations with their dimensions and material specifications. The impact face for the global WTC 1 (north wall) and WTC 2 tower (south face) models are shown in Figure 5–2 and Figure 5–3, respectively. A refined mesh was used in the immediate impact zone for improved accuracy of the impact response, and a coarse mesh was used outside the impact zone for improved computational efficiency. All panels were primarily constructed from Belytschko-Tsay shell elements. The reader is

referred to the LS-DYNA Theoretical Manual for a complete description of this element type. For modeling the bolted column connection between columns, constant stress brick elements were used to model the butt plates in the refined panels, and Hughes-Liu beam elements were used for the bolts connecting the butt plates in the refined impact zone. Section 5.4.2 describes the details of the model for the exterior column connections. The column ends for the coarse far field exterior wall panels were merged together to create a perfect bond between column ends.

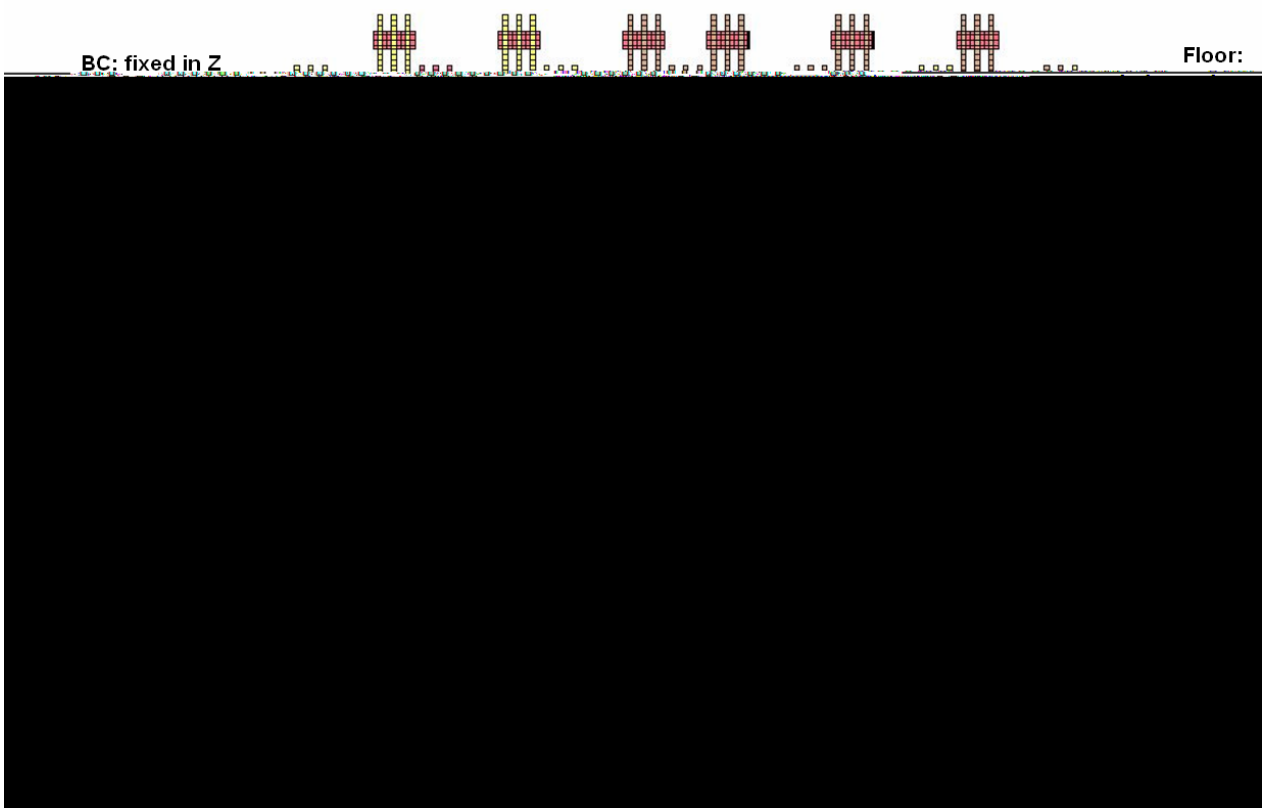

Figure 5–2. Impact face of the WTC 1 global model, floors 91–101.

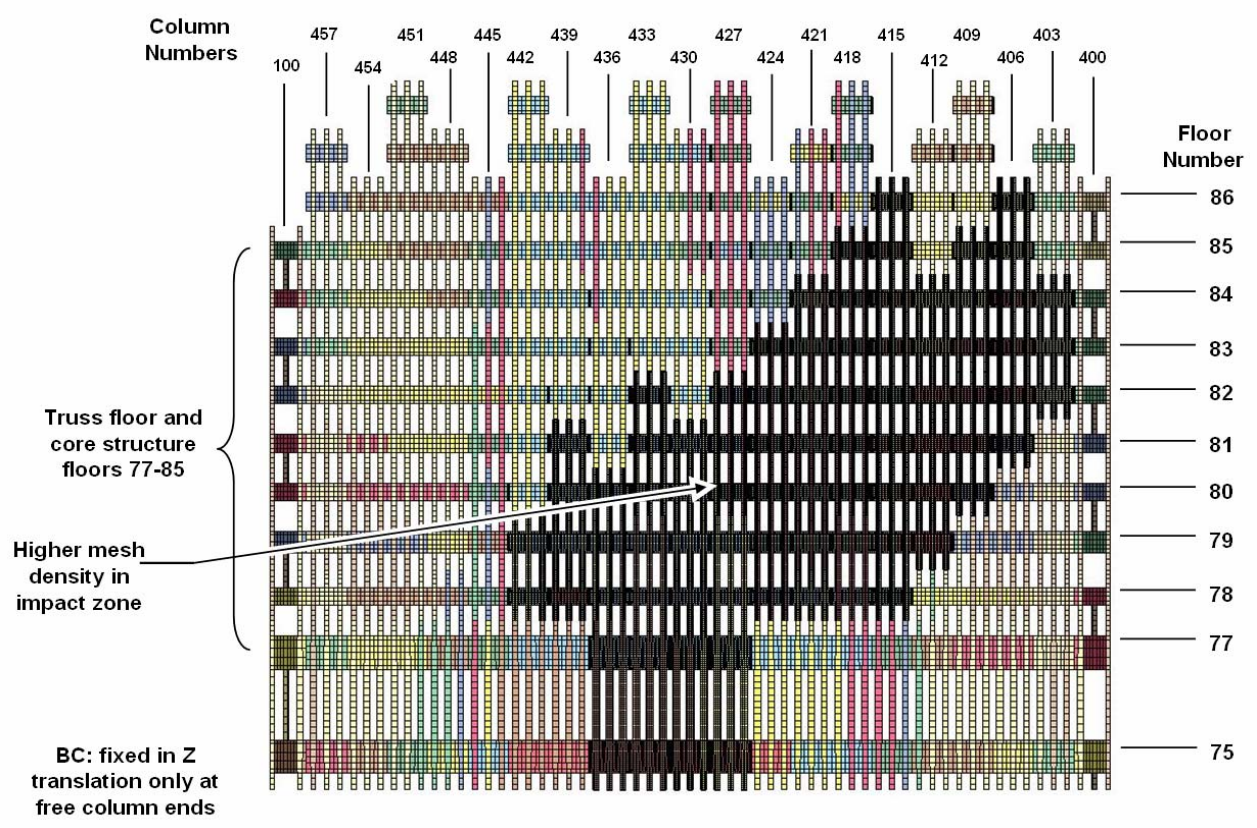

Figure 5–3. Impact face of the WTC 2 global model, floors 75–86.

The model of the spandrel splice plate connection is shown in Figure 5–4. Twelve nodes on the splice plate were attached to the spandrels using the spot weld tied node algorithm (LS-DYNA Type 7 tied interface). The spot weld approximated the connection of the individual bolts connecting the spandrel splice plates. Failure of these connections occurred through deformation of the splice plates and/or spandrel and ductile failure of the materials. The placement of the spandrel splice plates was limited to the higher resolution impact zone for the exterior wall. The far-field coarse panel models were merged together as shown in Figure 5–5. The influence of the spandrel splice connection on the impact response and exterior wall damage was investigated using engine component impact analyses (see Chapter 5 of NIST NCSTAR 1-2B).

Each three-column, three story panel in the impact zone contained 5,304 nodes, 5,202 shell elements, 78 brick elements, and 12 beam elements. The corresponding element sizes in the impact zone were a 1 in. element for the weld zone and 4 in. elements for the exterior column. A typical element dimension for the far field exterior panels was 14 in.

The boundary conditions at the top and bottom of the exterior wall were constrained vertical displacements. The lateral degrees of freedom and rotation about the vertical axis were not constrained. The free lateral displacements at the model boundary allowed for the tower model to have a rigid body velocity following the impact. Since the natural period of the tower was in the range of 10 to 11 s (see Chapter 2), the tower provided little structural resistance to the translation at the model boundary during the less than one second impact event.

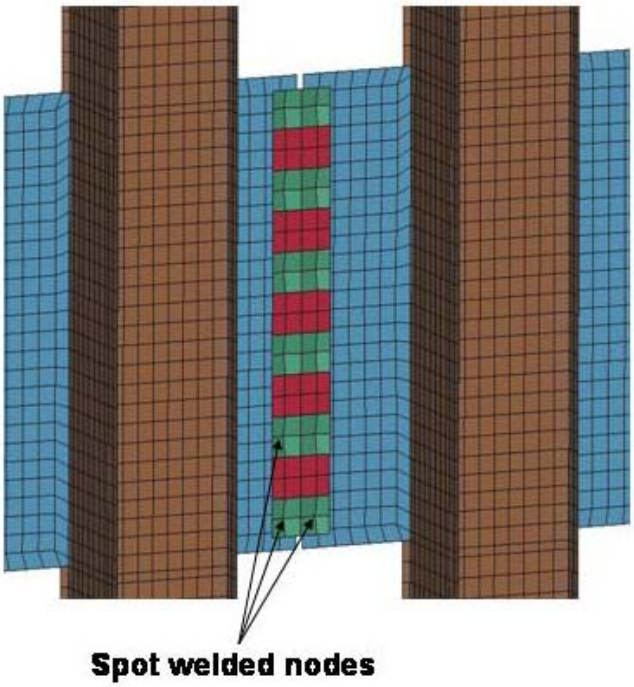

Figure 5–4. Model of the spandrel splice plate connection.

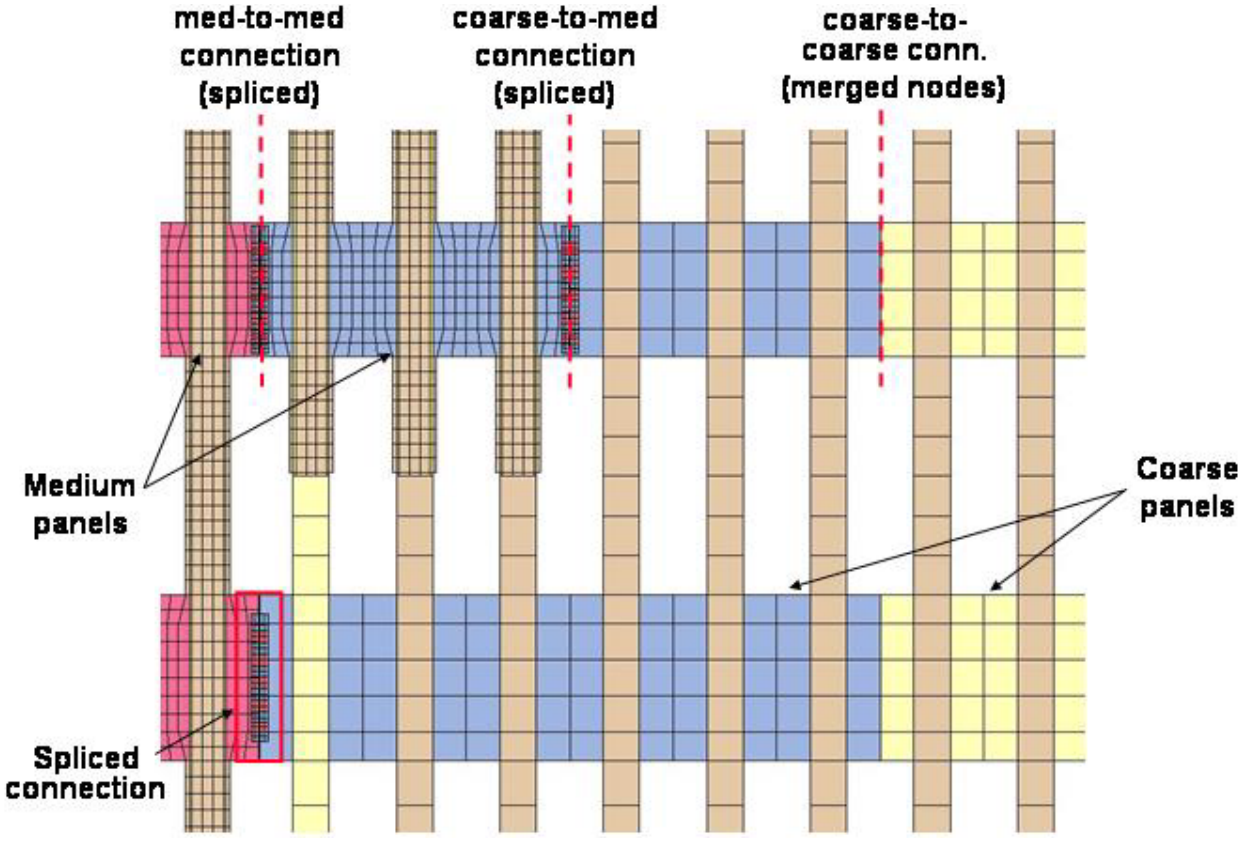

Figure 5–5. Placement of spandrel splice plates in the exterior wall model.

5.2.2 Core Columns and Floors Model Development

Core column models were generated as a group in single floor sections. Dimensions and material specifications were assigned automatically, as specified in the WTC structural databases. The boundary conditions at the top and bottom of the core model and the column splices were automatically generated. An example of the model of the WTC 1 core columns for floors 95 to 97 is shown in Figure 5–6. Different colors correspond to different material assignments for the various column sections.

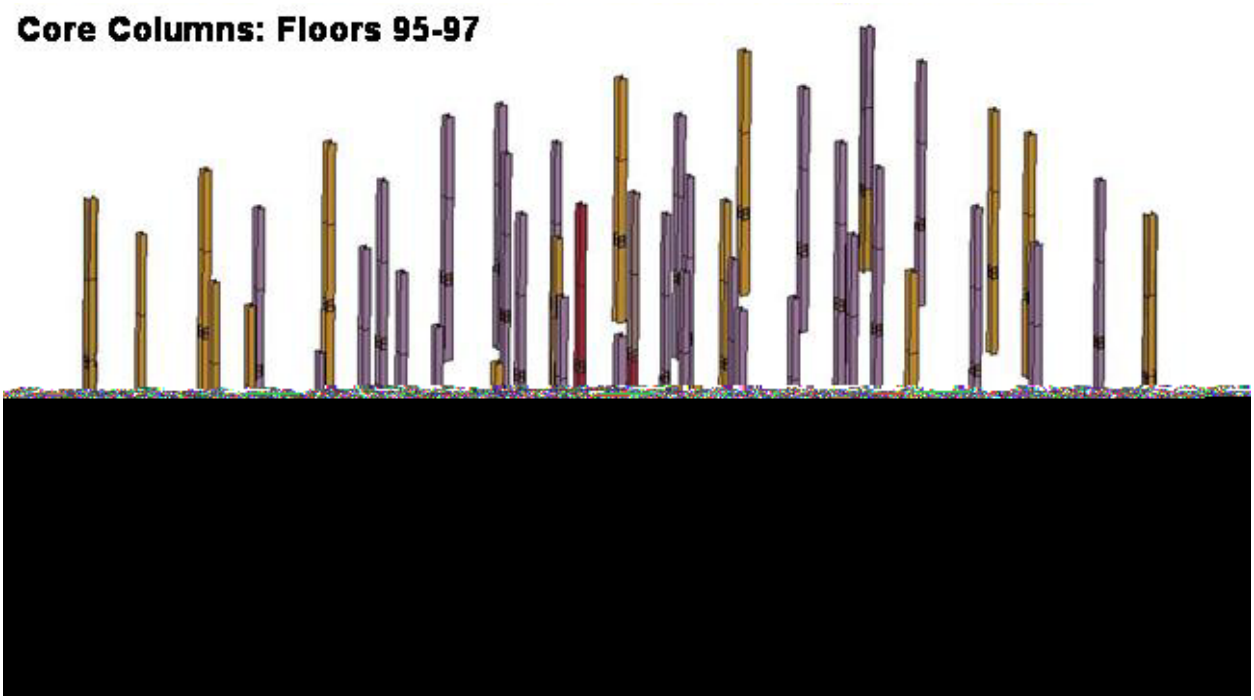

Figure 5–6. Model of the WTC 1 core columns and connections, floors 95–97.

Both wide flange and box core columns were modeled with Belytschko-Tsay shell elements. Two mesh densities were used in the model, a refined density in the direct impact area and a coarse far field density elsewhere. Typical element dimensions were 2 in. and 8 in. for the impact zone and far field, respectively. A single wide flange column in the impact zone had 552 shell elements and 600 nodes per floor, while a box column in the impact zone had 864 shell elements and 900 nodes per floor.

The wide flange-to-wide flange core column connections were modeled by splice plates placed on the outer side of each flange, as shown in Figure 5–7. The connection between the splice plate and column flange was modeled with a surface-to-surface tied interface without failure, which resulted in a perfect bond between the nodes of the splice plate and the flange of the adjacent column. If the columns were pulled apart, the elements at the splice plate spanning the gap between column ends would be stretched. Failure of the splice plate in the model resulted from ductile failure of the splice plate in the elements spanning the connection.

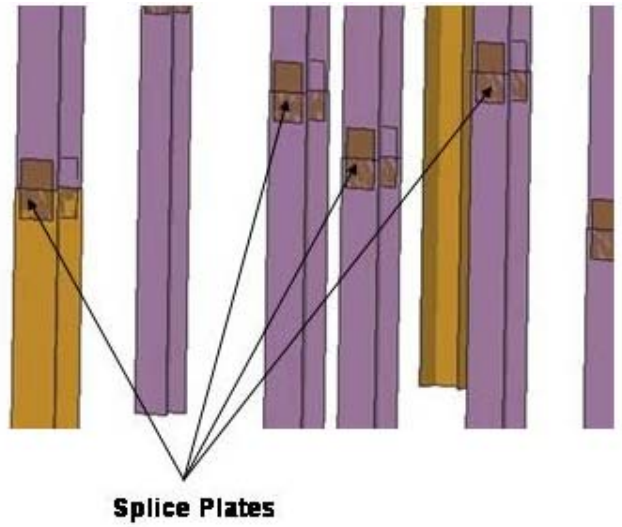

Figure 5–7. Detail of wide flange core columns splices

A typical box column-to-wide flange column connection is shown in Figure 5–8. The thick box column cap was modeled with shell elements and was perfectly merged into the lower box column. The connection between the wide flange column and the box column cap was an edge-to-surface tied interface without failure, which resulted in a perfect bond between the nodes of the wide flange column and the element segments of the box column cap plate. Failure of this connection would occur only when deformations and strains of this connection were sufficiently high to fail the elements in the columns adjacent to the joint.

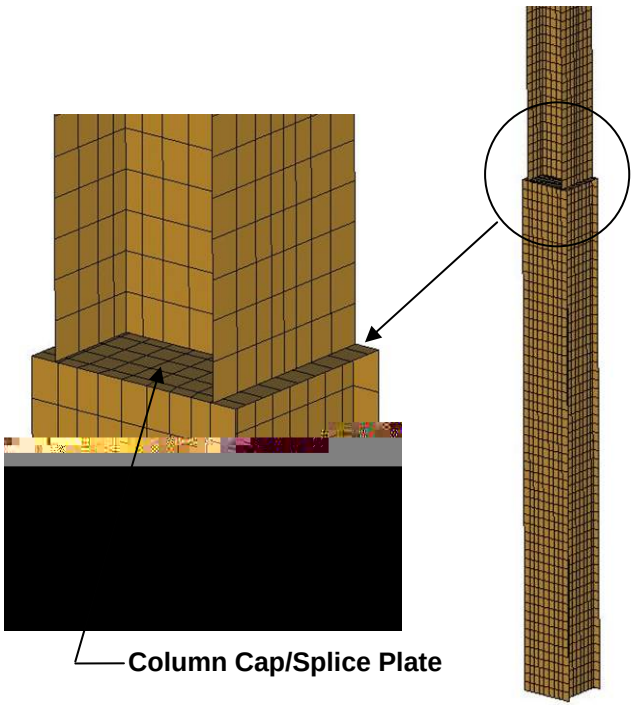

Figure 5–8. Detail of box column-to-wide flange core columns connection.

The approach for assembling the core floors in the global model was to generate models of typical floors in the impact zone and repeat them in the surrounding floors. For WTC 1, a model of floor 96 inside the core was developed and used for modeling floors 92 through 100. This approach was also used for floors 77 through 85 as the impact zone in WTC 2. Figure 5–9 shows the WTC 1 core prototype of the 96th floor with and without the concrete floor slab. The entire model was developed with Belytschko-Tsay shell elements. Mesh density was set independently from floor to floor to obtain higher accuracy in the impact zone and computational economy in the surrounding floors. A typical core floor with the higher impact zone mesh density had approximately 66,000 shell elements and 76,000 nodes. This included core floor slab, floor beams, connections, and core columns over a height of one floor.

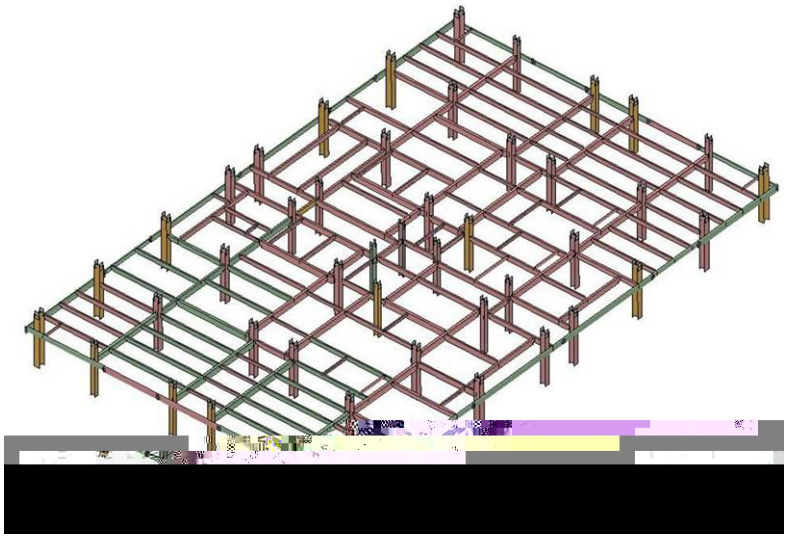

Figure 5–9. Model of the core of floor 96 of WTC 1 (with and without floor slab).

The various connection details between core beams are illustrated in Figure 5–10. Core perimeter beams were joined with splice plates in the same manner as the wide flange column end connections described above. Interior beams were connected with node-to-surface tied connections. This contact algorithm constrained the nodes to move with the same relative motions as the adjacent surface elements and was

appropriate for modeling a strong welded connection. An automatically generated model for the assembly of WTC 1 core floors 94 through 98 is shown in Figure 5–11.

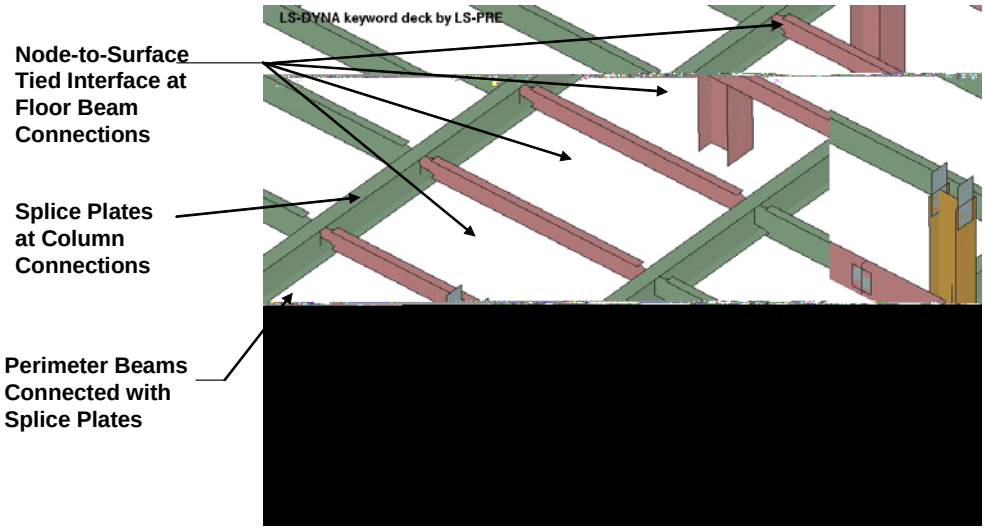

Figure 5–10. Model detail of core column and beam connections.

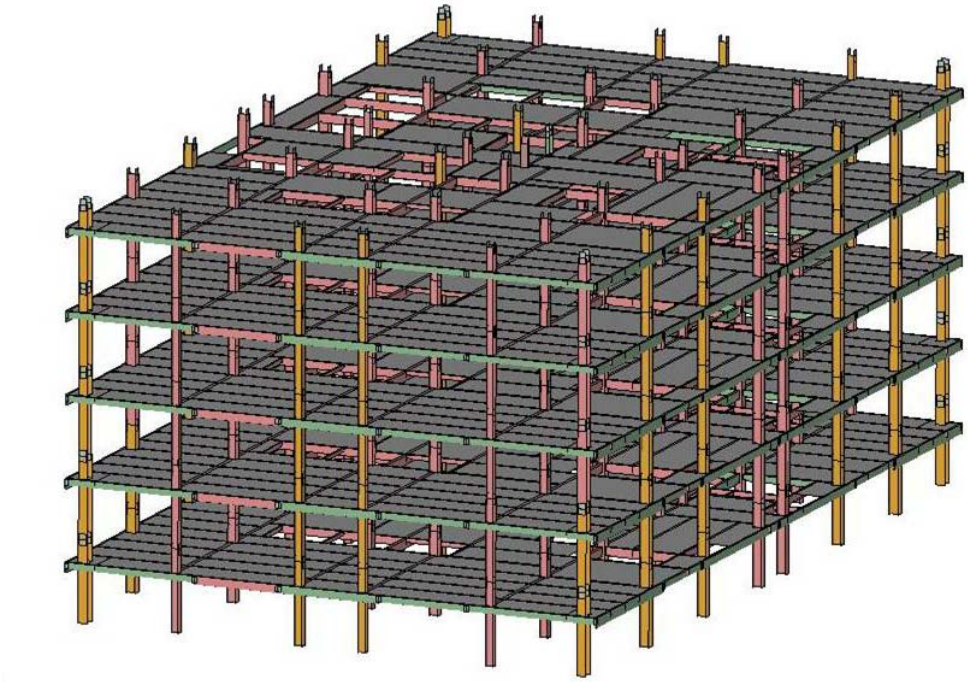

Figure 5–11. Model of the WTC 1 core, floors 94–98.

5.2.3 Truss Floor Model Development

The approach to the development of the truss floor model was very similar to other portions of the tower structure. Initially, parameterized component models were developed for segments of long-span trusses, short-span trusses, and corner two-way trusses. These parameterized models were then called repeatedly for generation and placement of the floor truss segments within the complete tower models. The

individual truss floor segments spanned the distance from the exterior wall to the core. An example of a truss floor segment used in the global model is shown in Figure 5–12. In the double truss sections, the two trusses were modeled explicitly with the proper dimensions.

Figure 5–12. Model of a truss floor segment.

The floor truss model was developed using a uniform layer of Belytschko-Tsay shell elements for the combined floor slab and metal decking, Belytschko-Tsay shell elements for the truss upper and lower chord components, and Hughes-Liu beam elements for the round bar truss diagonals. The upper chord was attached to the floor slab using a tied interface. This approach, using shell elements as opposed to solid brick elements for the floor slab, was adapted to reduce the model size requirements. Development of a model with matching mesh density in the slab and truss structures (nodal alignment for a merged connection) resulted in a much larger model size. Bridging trusses were modeled in a similar fashion to the primary trusses.

A series of dampers were installed in the WTC towers between the floor truss lower chord and the spandrel on the exterior wall. The primary function of these dampers was to reduce the vibration of the building under wind loading. These dampers, however, were of low mass and the arrangement of the damper and saddle (member attaching the damper to the bottom chord of the truss), along with their connections, had virtually no strength in the transverse direction. Under impact conditions, the aircraft applied transverse forces to the damper assembly due to the downward motion of the aircraft (see Chapter 6). Also, due to the short duration of the impact event (less then one second), damping was not included in the analyses. As a result, the dampers were considered to have sufficiently low mass and strength and were therefore not included in the impact analyses.

The mesh refinement used in this model for the truss floor would result in a very large global tower model size if used throughout the structure. The model for the long-span truss floor segment (Figure 5–12) contained 2,737 nodes, 362 beam elements, and 1,878 shell elements. Constructing a global impact tower model with these detailed floor segments was not practical due to model size limitations. A complete floor would result in approximately 200,000 nodes for a single truss floor structure. As a result, detailed floor segments were used only in the impact zone, and a simplified floor truss model was used elsewhere. The far-field floor truss was modeled with a significantly reduced mesh resolution, as shown in Figure 5–13, and provided the appropriate inertial properties and structural stiffness of the floor. The trusses were modeled with an effective shell element in place of the vertical truss structure and a beam element along the lower chord. These element dimensions were on the order of 30 in. and would not be able to accurately model a local collapse behavior of the trusses. The floor slab model was similar to the

floor slab in the impact zone, but with a typical element dimension of 30 in. compared to an element dimension of approximately 10 in. in the impact zone.

Figure 5–14 and Figure 5–15 show the truss floor connection details at the exterior and core, respectively. The models for the truss seat connections were developed using shell elements and attached using the tied interface algorithm. The failure of these seats occurred only as a result of exceeding the ductility of the seat or truss structures. A detailed model of floor 96 of WTC 1 is shown in Figure 5–16.

3-D View from Bottom

Figure 5–13. Simplified far field truss floor model.

Figure 5–14. Truss floor connection detail at exterior wall.

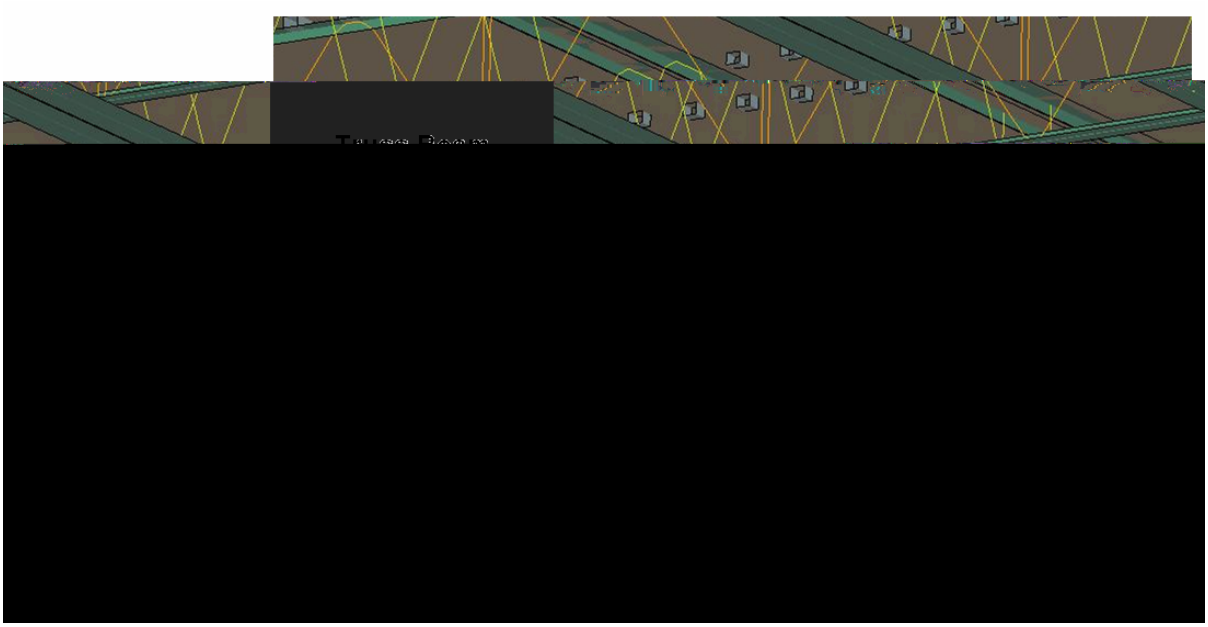

Figure 5–15. Truss floor connection detail at core perimeter.

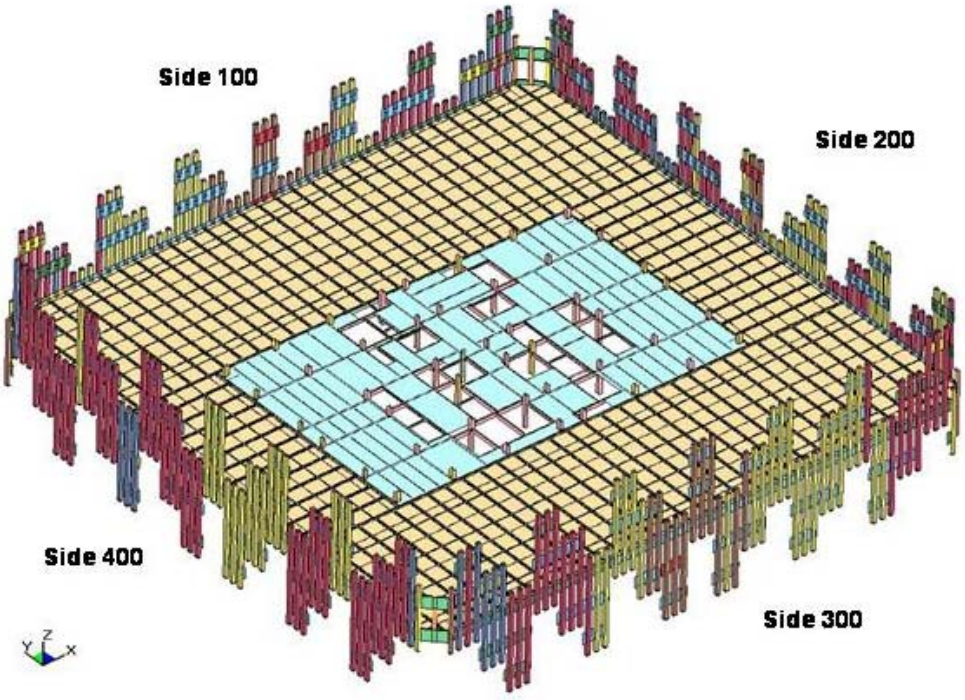

Figure 5–16. Detailed model of floor 96 of WTC 1.

5.2.4 Interior Contents Model Development

The interior nonstructural contents of the towers were modeled explicitly in the tower models used for the global impact analyses. The live load weight was distributed between gypsum walls and cubicle workstations that covered the truss floor area. The distribution of the gypsum walls was obtained from

architectural drawings and other information gathered as part of Project 5 of the NIST investigation (NIST NCSTAR 1-5). Similarly, data gathered by NIST for the floor layout plans in the impact zone were used to develop the approximate placement of workstations over the truss floor area. The resulting model of a floor with interior contents is shown in Figure 5–17.

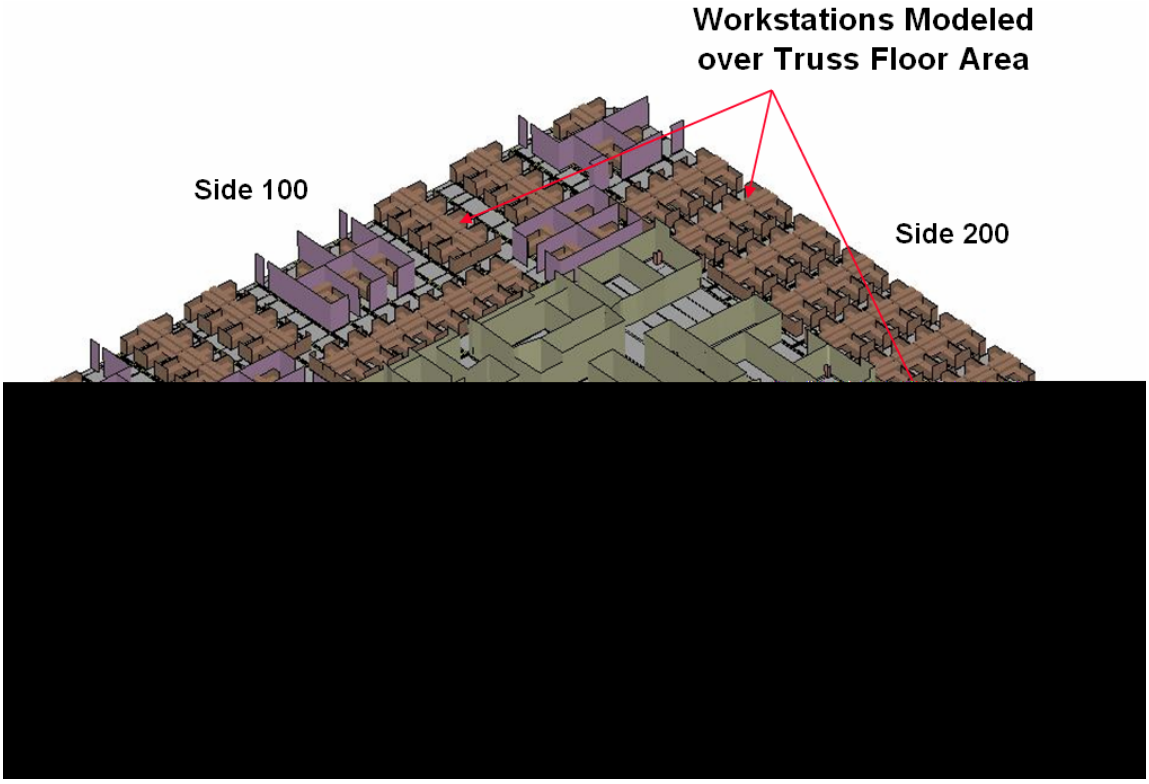

Figure 5–17. Model of floor 96 of WTC 1, including interior contents.

The densities of specific materials were scaled to obtain the desired magnitudes for the service live loads and superimposed dead loads. The densities of the tower contents (workstations and gypsum walls) were scaled by the appropriate ratios to obtain the desired distribution of live loads in the core and truss floor areas. The densities of all the remaining tower structural components were scaled proportionately to obtain the desired superimposed dead loads. These additional loads were important for obtaining an accurate mass distribution in the towers and inertial effects in the impact response. The in-service live load used was assumed to be 25 percent of the design live load on the floors inside and outside the core. The in-service live load was selected based on a survey of live loads in office buildings (Culver 1976) and on engineering judgment. The uncertainty in the amount of in-service live load was accounted for in the sensitivity analyses (Chapter 8 of NIST NCSTAR 1-2B) and in the global impact simulations (Chapter 7 of this report).

The partitions and workstations were modeled using shell elements. The model of the building contents (partitions and workstations) over a single floor, as shown in Figure 5–17, had 101,733 nodes and 97,284 shell elements. To include the complete distribution of the building contents over five floors in the global impact model would require approximately 500,000 nodes. As a result, the global models included the partitions and workstations only in the region of each floor directly in the path of the aircraft impact and debris. Using this approach significantly reduced the computational requirements needed to

include the building contents' inertial contributions. For example, the WTC 1 global impact model included only 160,410 nodes and 148,858 shell elements for the partitions and workstations in the impact path over five floors. These building content distributions for both tower models are shown in the following section.

5.2.5 Global Impact Models Assembly

The multiple floor global model of the impact zone in WTC 1 is shown in Figure 5–18. The model included the complete floors inside and outside the core, the exterior walls, and core structures for floors 92 through 100. The boundary conditions at the top and bottom of the exterior and core columns were constrained vertical displacements. This allowed for free translations of the tower structure in the longitudinal and lateral directions and rotation about the vertical axis. The higher resolution exterior wall panels in the impact zone can be seen on the impact face of the tower model (side 100).

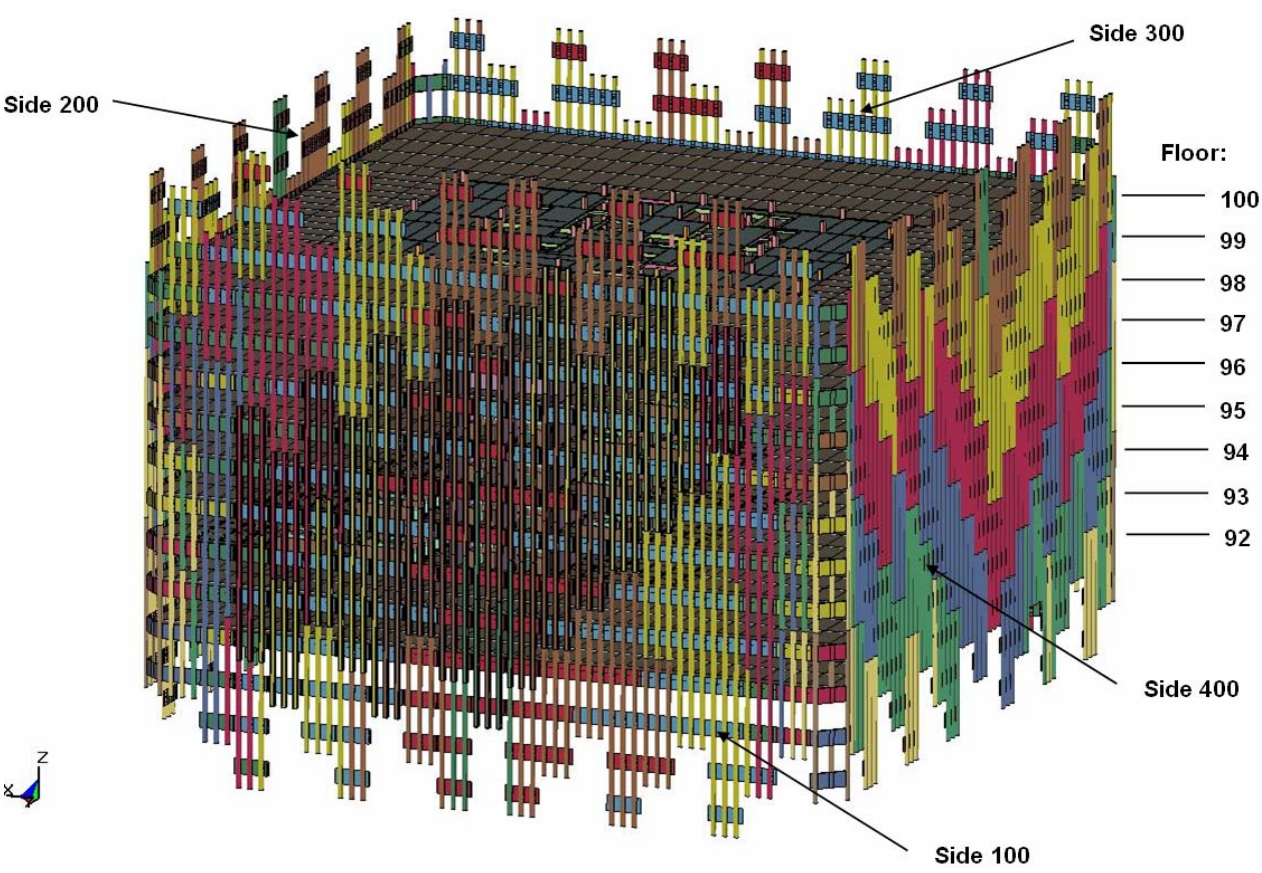

Figure 5–18. Global impact model of the WTC 1 tower.

The WTC 1 global impact model with the exterior wall removed is shown in Figure 5–19. The figure shows how the model was optimized to reduce mesh size and eliminate computational requirements outside of the immediate impact and damage zone. The nonstructural building contents (partitions and workstations) were modeled only in the path of the aircraft impact and debris cloud. These components are shown separately in Figure 5–20.

In the assembled global model, the core columns for floors 93 through 98 of WTC 1 were modeled with higher resolution than that in the floors above and below the direct impact zone. This higher mesh resolution was needed to capture the local damage that occurred from direct impact of aircraft structures and debris.

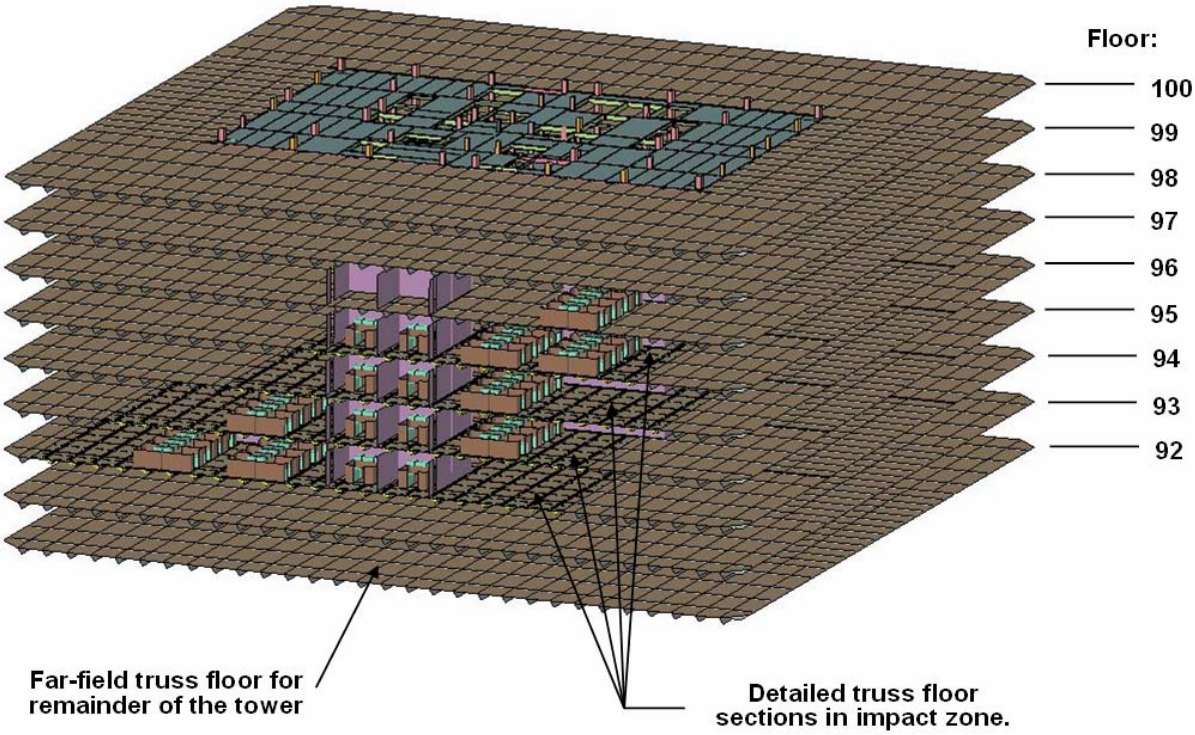

Figure 5–19. Interior structures and contents of the WTC 1 global impact model.

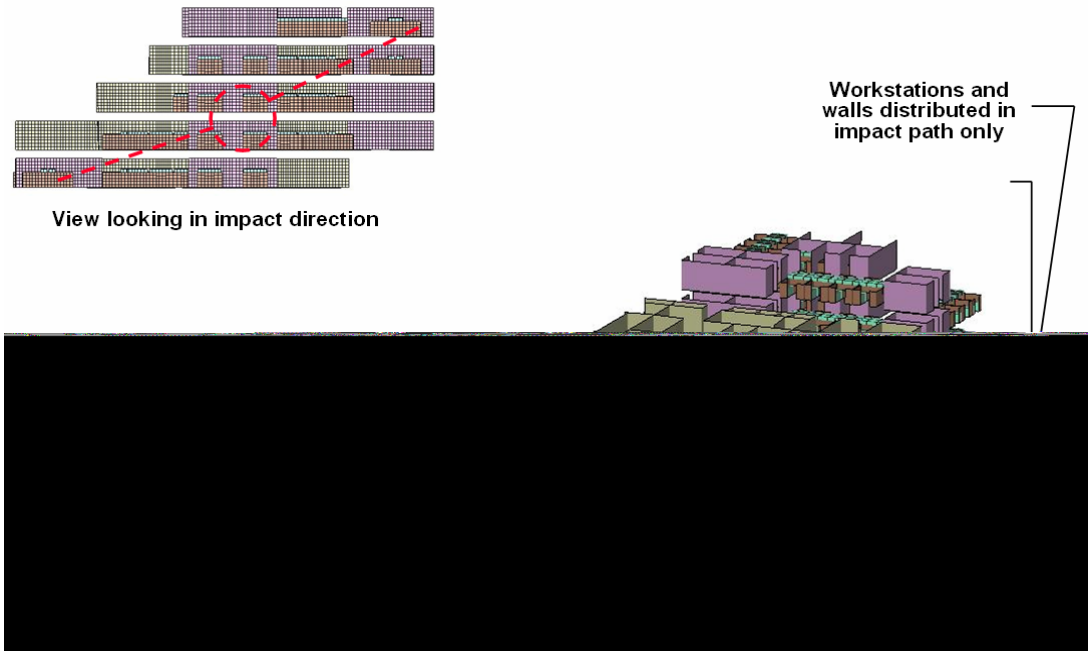

Figure 5–20. Nonstructural building contents in the WTC 1 global impact model.

The WTC 2 global impact model is shown in Figure 5–21. The model included the complete floor inside and outside the core for floors 77 through 85. The exterior wall panels at the bottom end of the model extended downward below floor 75. The boundary conditions at the top and bottom of the exterior and core columns were the same as those for the WTC 1 model. The higher resolution exterior wall panels in the impact zone can be seen on the impact face of the WTC 2 tower model (Side 400).

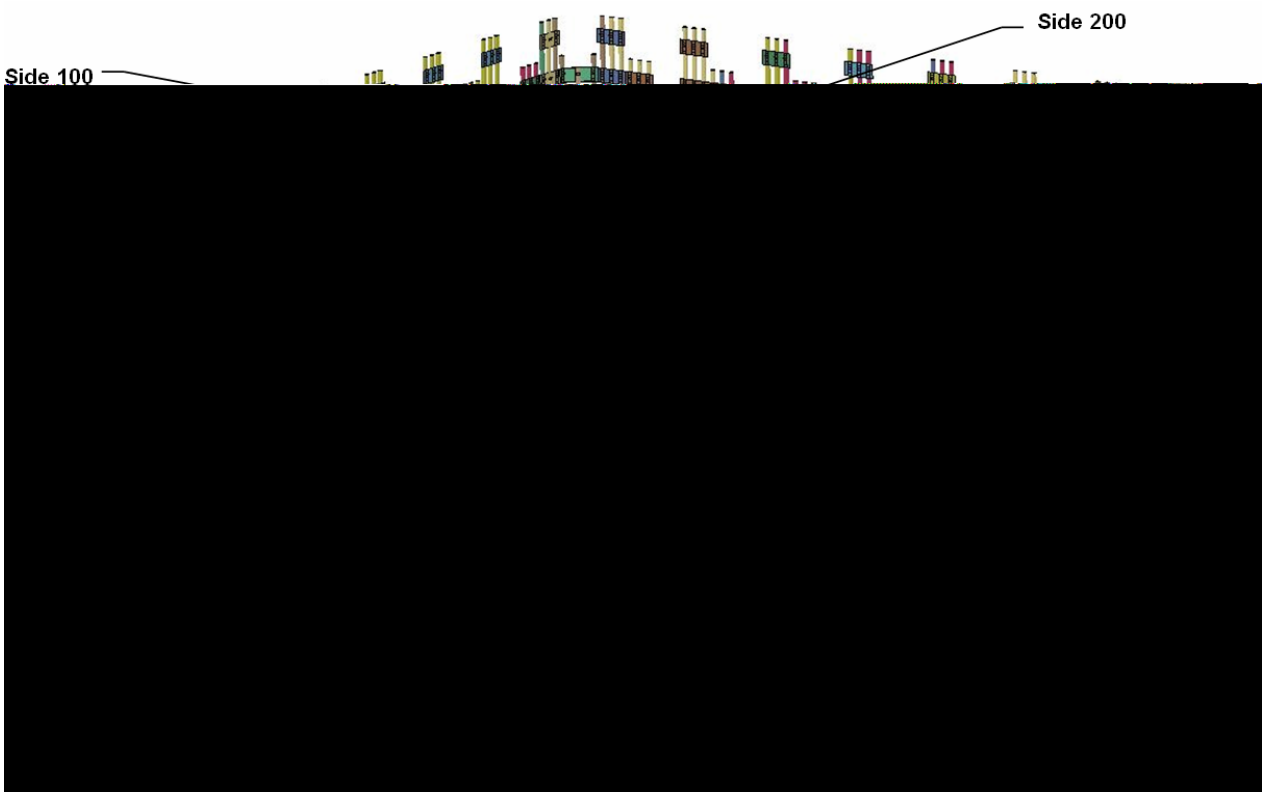

Figure 5–21. Global impact model of the WTC 2 tower.

The WTC 2 global impact model with the exterior wall removed is shown in Figure 5–22. The nonstructural building contents were again modeled only in the path of the aircraft impact and debris cloud. These components are shown separately in Figure 5–23. Similarly, the truss floor structures near the impact zone were modeled in greater detail as seen in Figure 5–22. These detailed sections of the truss floor were positioned adjacent to Side 400 (south face) for floors 78 through 81 and side 300 (east face) for floors 81 and 82. The surrounding truss floor structures were modeled with the far-field truss model.

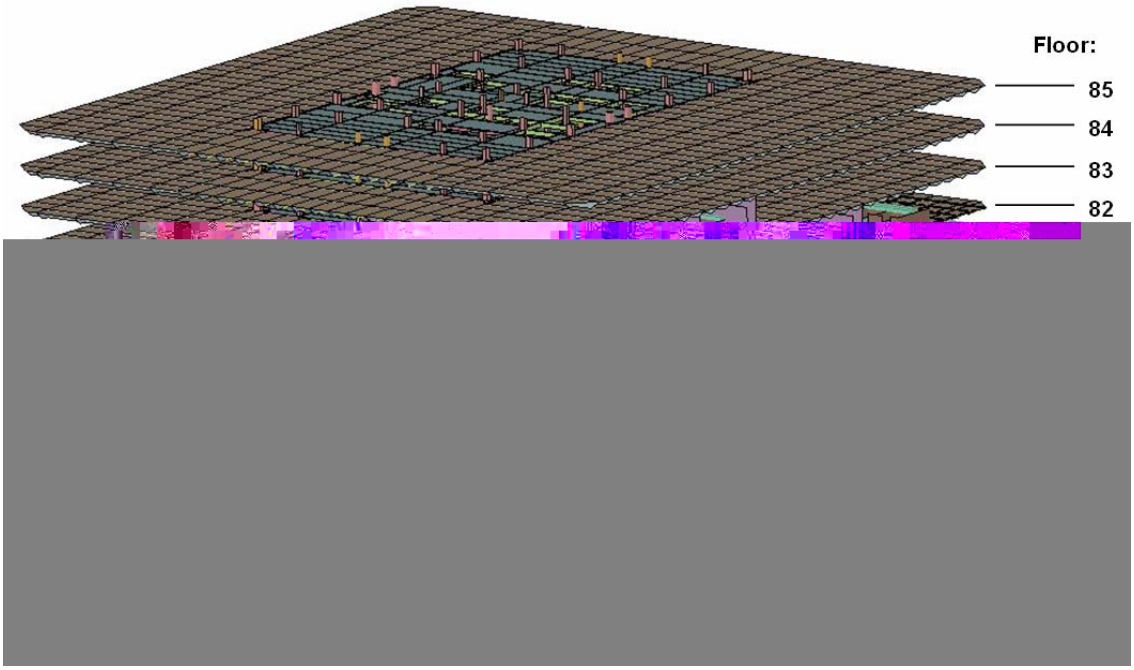

Figure 5–22. Interior structures and contents of the WTC 2 global impact model.

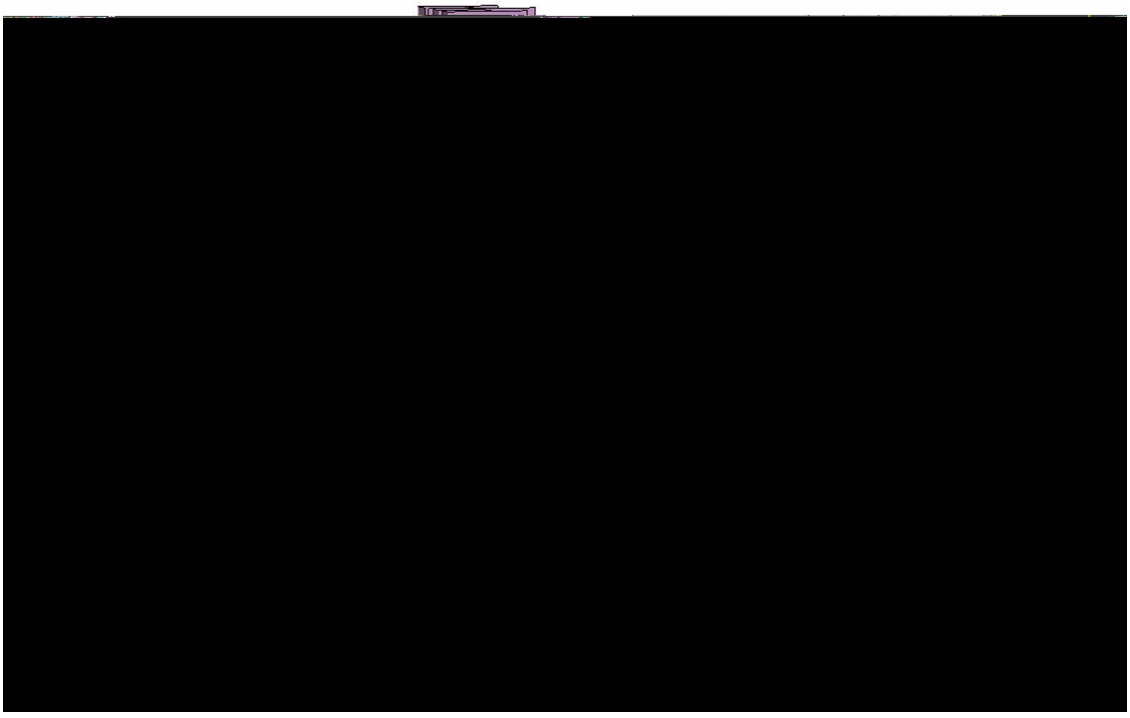

Figure 5–23. Nonstructural building contents in the WTC 2 global impact model.

5.2.6 Tower Material Constitutive Models

The development of constitutive models that properly captured the actual behavior of the WTC towers under the dynamic aircraft impact conditions was an important requirement for high fidelity simulation of

the aircraft impact damage. The primary materials that were considered included: (1) the several grades of steel used in the columns, spandrels, and floor trusses and beams of the WTC towers; (2) the concrete floor slabs; and (3) the nonstructural contents of the towers. These materials exhibit significant nonlinear rate-dependent deformation and failure behavior over the range of strain rates expected in the impact scenario. The following is a brief summary of the constitutive models used for these materials. Additional details can be found in Chapter 2 of NIST NCSTAR 1-2B, where constitutive models were described for bolt material and weldments. It also includes a discussion on the effect of mesh size on failure criteria.

WTC Tower Steel Constitutive Models

The primary constitutive model used for the several grades of the tower steels was the Piecewise Linear Plasticity model. This model is sufficient to model the nonlinear dynamic deformation and failure of steel structures. A tabular effective stress versus effective strain curve can be used in this model with various definitions of strain rate dependency. The constitutive model parameters for each grade of steel were based on engineering stress-strain data provided by the mechanical and metallurgical analysis of structural steels part of the NIST Investigation (see NIST NCSTAR 1-3D). Finite element analyses of the test specimens (ASTM Designation A 370 – 03a) were conducted with a fine and a medium mesh (similar to that used in the component level analysis) to capture the nonlinear material behavior up to failure, see Figure 5–24. The finite element analysis also provided a validation that the constitutive model parameters were defined accurately and that the model could reproduce the measured response for the test conditions.

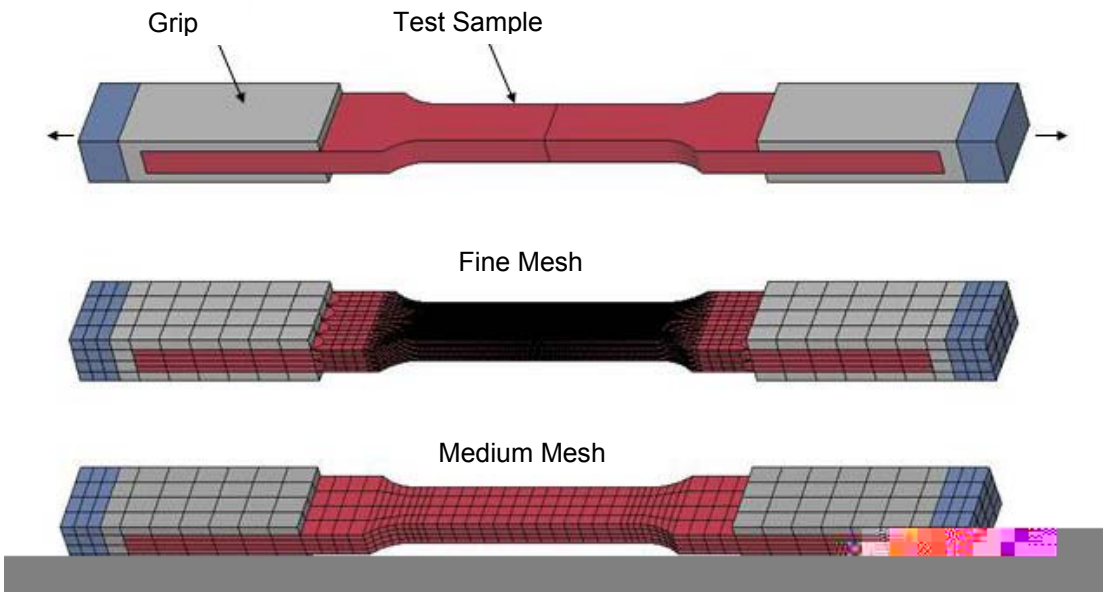

Figure 5–24. Finite element models of the ASTM 370 rectangular tensile specimen.

The first step in the constitutive model development process was to obtain a true stress-true strain curve. The typical approach was to select a representative test for each grade of steel and convert the engineering stress-strain curve to true stress-strain. The true stress-strain curve was extrapolated beyond the point of necking onset. This true stress-strain curve was then approximated by a piecewise linear curve in tabular

form, which was used to specify the mechanical behavior in the constitutive model. The final step was to simulate the tensile test (Figure 5–24). If necessary, the extrapolation of the true stress-strain behavior was adjusted until the simulation matched the measured engineering stress-strain response including necking and failure (the portion of the stress-strain curve beyond the maximum engineering stress). The true stress-strain curves used in the constitutive models for the various WTC tower steels are summarized in Figure 5–25.

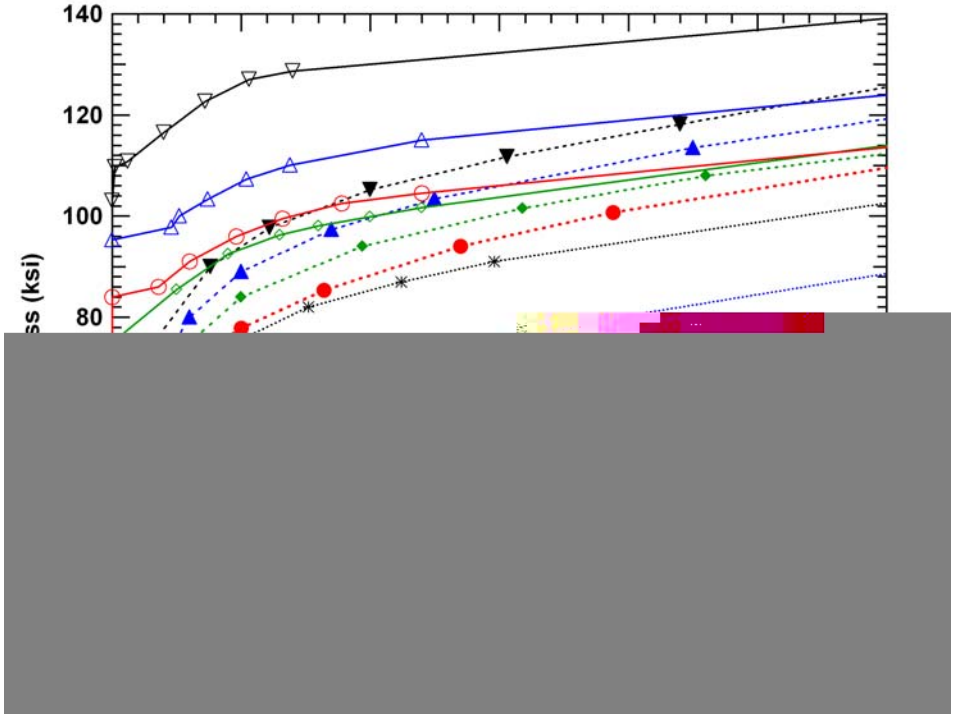

Figure 5–25. Tabular true stress-strain constitutive model curves for the tower steels.

Elevated strain rates can influence the strength and ductility of structural materials. For the materials and strain rates of the WTC tower impact analyses, these strain rate effects are expected to be somewhat small compared to the effects of the baseline (static) strength and failure modeling. Strain-rate effects on the steel yield strength were included in the constitutive model for tower steels with the Cowper and Symonds rate effect model. The functional form for the rate effects on strength is governed by the equation:

$$\sigma_y = \sigma_{y_0}[1 + (\frac{\dot{\varepsilon}}{C})^{1/p}]$$

where σ_y and σ_{y_0} are the yield strengths at strain rates of $\dot{\varepsilon}$ and zero, respectively. C and p are the Cowper and Symonds parameters.

A series of high-rate characterization tests was performed on tower steels by the mechanical and metallurgical analysis of structural steels part of the NIST Investigation (NIST NCSTAR 1-3D) at strain rates between 100 and 1000 s^{-1}. The Cowper and Symonds model parameters C

and *p* were then fit to the test data and were provided in the following functional form for a strain rate in s^{-1} and a yield strength in ksi:

- $\text{Log}(C) = -7.55 + 0.324\sigma_{yo} - 0.00153(\sigma_{yo})^2$
- $p = 6.7824$

The resulting rate effects used in the constitutive modeling of tower steels based on the Cowper and Symonds model are compared to the measured high rate test data for the 50 ksi, 75 ksi, and 100 ksi tower steels in Figure 5–26. The comparison shows that the Cowper and Symonds model was capable of reproducing the rate effects for the range of data available.

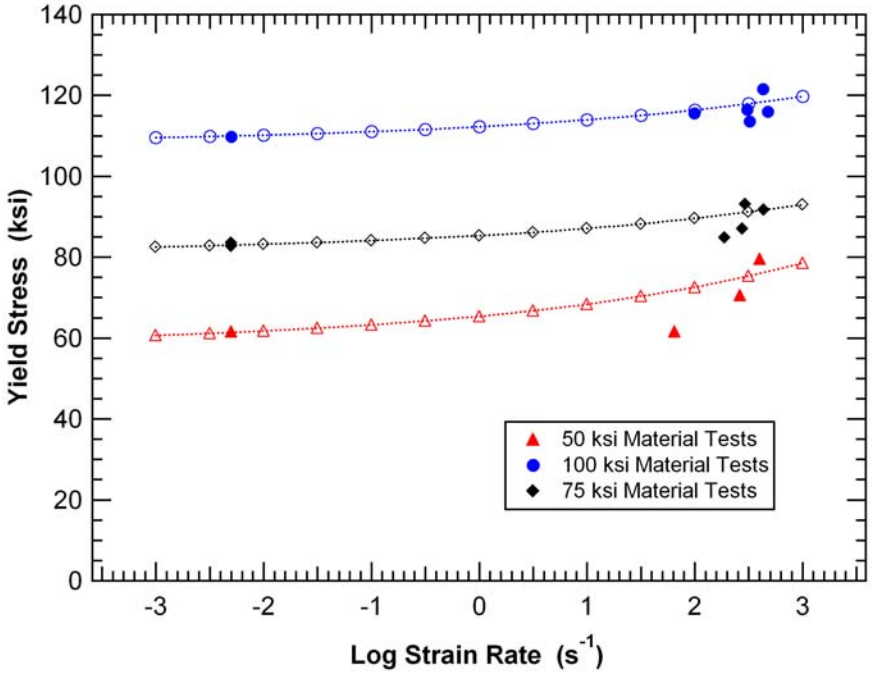

Figure 5–26. Comparison of rate effects model and test data.

Concrete Constitutive Models

The LS-DYNA material Type 16 (pseudo-tensor concrete model) was selected for modeling the concrete floor slabs due to its ability to accurately model the damage and softening of concrete, associated with low confinement. The model used two pressure-dependent yield functions and a damage-dependent function to migrate between curves. This allowed for implementation of tensile failure and damage scaling, which are more dominant material behaviors at low confinement. The pseudo-tensor model also accounted for the sensitivity of concrete to high strain rates. The reader is the reader is referred to the LS-DYNA user's manual (2003) for a detailed description of the model, and to NIST NCSTAR 1-2B for the model parameters used in the analysis.

Material constitutive parameters for the pseudo-tensor model were developed for both 3 ksi and 4 ksi compressive strength lightweight concrete. A simulation was performed of a standard unconfined concrete compression test to check the constitutive model behavior. The simulated behavior of the

concrete specimen is shown in Figure 5–27. The calculated compressive stress-strain response for the 3 ksi concrete was compared to measured compression data for 2.3 ksi and 3.8 ksi strength concretes in Figure 5–28 (Wischers 1978).

For subsequent global analyses, a 4 ksi concrete was used, instead of the 3 ksi concrete strength specified in the original design, to account for factors such as aging and the difference between specified nominal and actual concrete strength. The same material parameters were used for the concrete in both the core (normal weight concrete) and truss floor (lightweight concrete) areas.

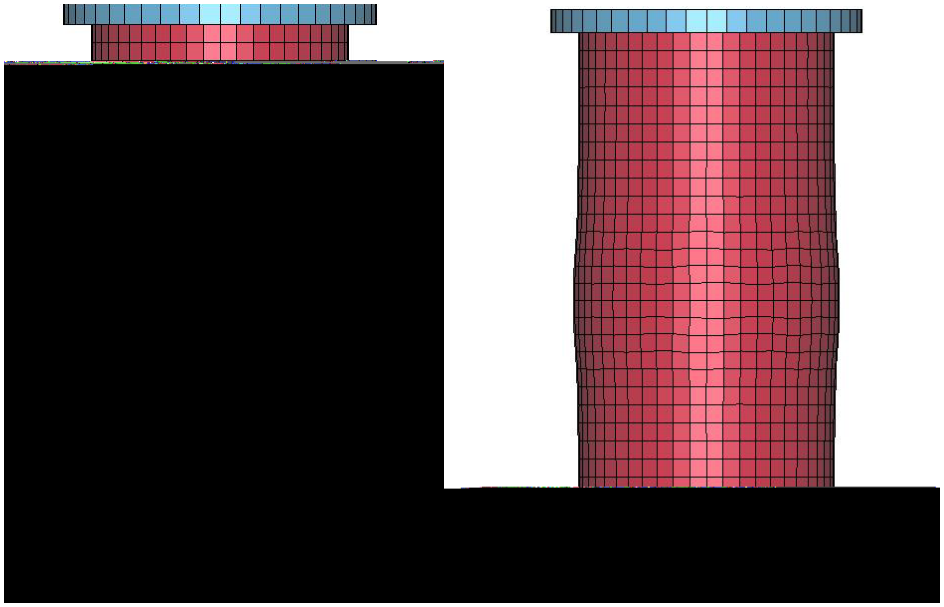

Initial configuration **2% compression**

Figure 5–27. Finite element analysis of the unconfined compression test.

Figure 5–28. Comparison of the calculated unconfined compression behavior with concrete compression test data.

Experimental characterization of the strain rate effects on concrete is difficult, and there is a wide scatter in data that is influenced by concrete type, strength, and the testing methods applied. In general, elevated strain rate loading has a greater influence on the tensile strength than on the compressive strength. However, in the aircraft impact response of the WTC towers, the majority of the high-rate damage occurs with impact and penetration of the floor slab by hard components such as the aircraft engine. As a result, the strain rate effects for compressive loading were used for the constitutive model. The strain rate effects were added to the model in tabular form. The rate effects curve used in the model is shown in Figure 5–29, based on the work of Bischoff and Perry (1991) and Ross et al. (1992). The curve was selected to provide a relatively smooth fit to the available compressive rate effects data on compressive strength.

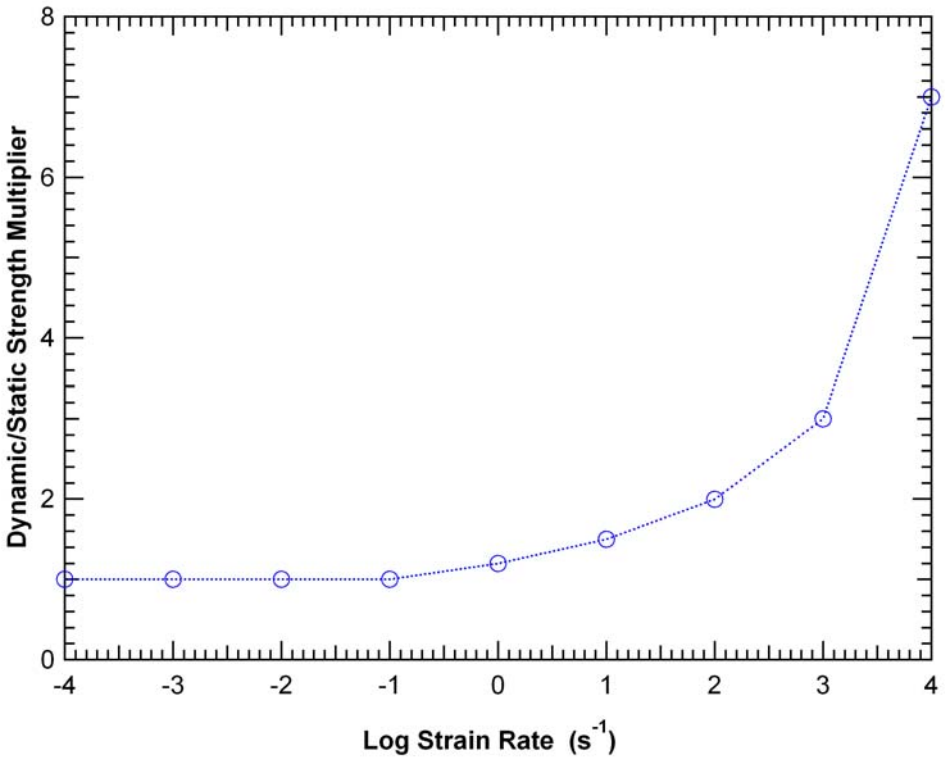

Figure 5–29. Tabular concrete strain rate effects curve.

Nonstructural Materials Constitutive Models

In general, the primary influence of the nonstructural components on the impact behavior was their inertial (mass) contribution. The effects of their strength were small. As a result, relatively simple approximations of their constitutive behavior were used. Typically, a simple elastic-plastic model was applied for these materials to allow for efficient modeling of deformation and subsequent erosion from the calculations as their distortions became large. The ability to include material failure and erosion of these soft materials was important for the stability of the impact analyses.

Based on a survey on the strength of various nonstructural building components (see Chapter 2 of NIST NCSTAR 1-2B), a bilinear elastic-plastic constitutive model with a yield strength of 500 psi and a failure strain of 60 percent was used. The large failure strain for these materials was used to prevent large scale erosion of the contents before the momentum transfer from the aircraft debris had occurred.

5.3 DEVELOPMENT OF AIRCRAFT MODEL

The finite element model of the Boeing 767-200ER aircraft was constructed through a three-step process: (1) data collection, (2) data interpretation and engineering analysis, and (3) meshing of the structure. A major focus of this effort was gathering sufficient structural data and including adequate detail in the aircraft model so that the mass and strength distribution of the aircraft and its contents were properly captured for implementation in the impact analyses. Structural data were collected for the Boeing 767-200ER aircraft from: (1) documentary aircraft structural information, and (2) data from measurements on Boeing 767 aircraft.

The objective of the aircraft model development was to properly simulate the impact damage and aircraft breakup, and their effects on the WTC towers. Key requirements were to simulate the mass distribution, dynamic impact response, fragmentation, and progress of the aircraft components and debris into and through the towers. The modeling approach was to model the airframe completely using shell elements as opposed to a shell element skin and beam elements for the airframe. Shell elements in the airframe provided higher fidelity simulation of the impact response and fragmentation behavior. As a result of the model size constraints, some of the details and smaller structural elements were not modeled explicitly. Where modeling simplifications were required, component analyses were applied to ensure that the impact strength and breakup behavior were maintained.

An example of this approach was the development of the wing model. A section of the aircraft wing structure was first modeled with a very fine mesh of the detailed wing structure to establish a baseline behavior for aircraft structural failure and fragmentation upon impacting the exterior wall of the WTC towers. A coarser and simplified version of the same wing section was subsequently developed, and the failure criteria were modified to obtain similar impact and fragmentation behavior to the fine, detailed version. Section 5.3.2 describes how this model was constructed and the methodology used for developing the coarsely meshed wing section. A similar mesh resolution and failure criteria were used throughout the rest of the aircraft model.

Similar to the global towers structural model, the LS-DYNA model of the aircraft was generated and meshed using the TrueGrid software (TrueGrid Manual 2001). The complete model for the Boeing 767-200ER is shown in Figure 5–30. A summary of the model size and weight parameters for the aircraft that impacted WTC 1 (American Airlines flight 11 [AA 11]) and the aircraft that impacted WTC 2 (United Airlines flight 175 [UAL 175]) is presented in Table 5–2. The weight cited for the unit load device (ULD) and seats included the empty weights plus the passenger or cargo weight. Carry on luggage and catering weight was distributed to the seats, and freight and cargo luggage weight was distributed to the ULD.

Fuel was distributed in the wings as shown in Figure 5–31, based on a detailed analysis of the fuel distribution in the aircraft wings at the time of impact (see Chapter 4 of NIST NCSTAR 1-2B for analysis details). The wings of the aircraft were also deflected from the surface model geometry to represent their in-flight condition, as shown in Figure 5–32. A cubic function of the wing span was used with a tip deflection of approximately 52 in., which was estimated from the impact pattern seen in photographs of the WTC towers and from the damage documented on the exterior panels.

The following sections outline the overall aircraft model developed for the impact analysis. Details in modeling each major component including the wings, engines, fuselage, empennage, and landing gear are provided.

Table 5–2. Boeing 767-200ER aircraft model parameters.

	AA 11	UAL 175
No. Brick Elements	70,000	70,000
No. Shell Elements	562,000	562,000
No. SPH Fuel Particles	60,672	60,672
Total Nodes	740,000	740,000
Total Weight (Empty)	183,500 lb	183,500 lb
ULD/Cargo Weight	12,420 lb	21,660 lb
Cabin Contents Weight	21,580 lb	10,420 lb
Fuel Weight	66,100 lb	62,000 lb
Total Weight (Loaded)	**283,600 lb**	**277,580 lb**

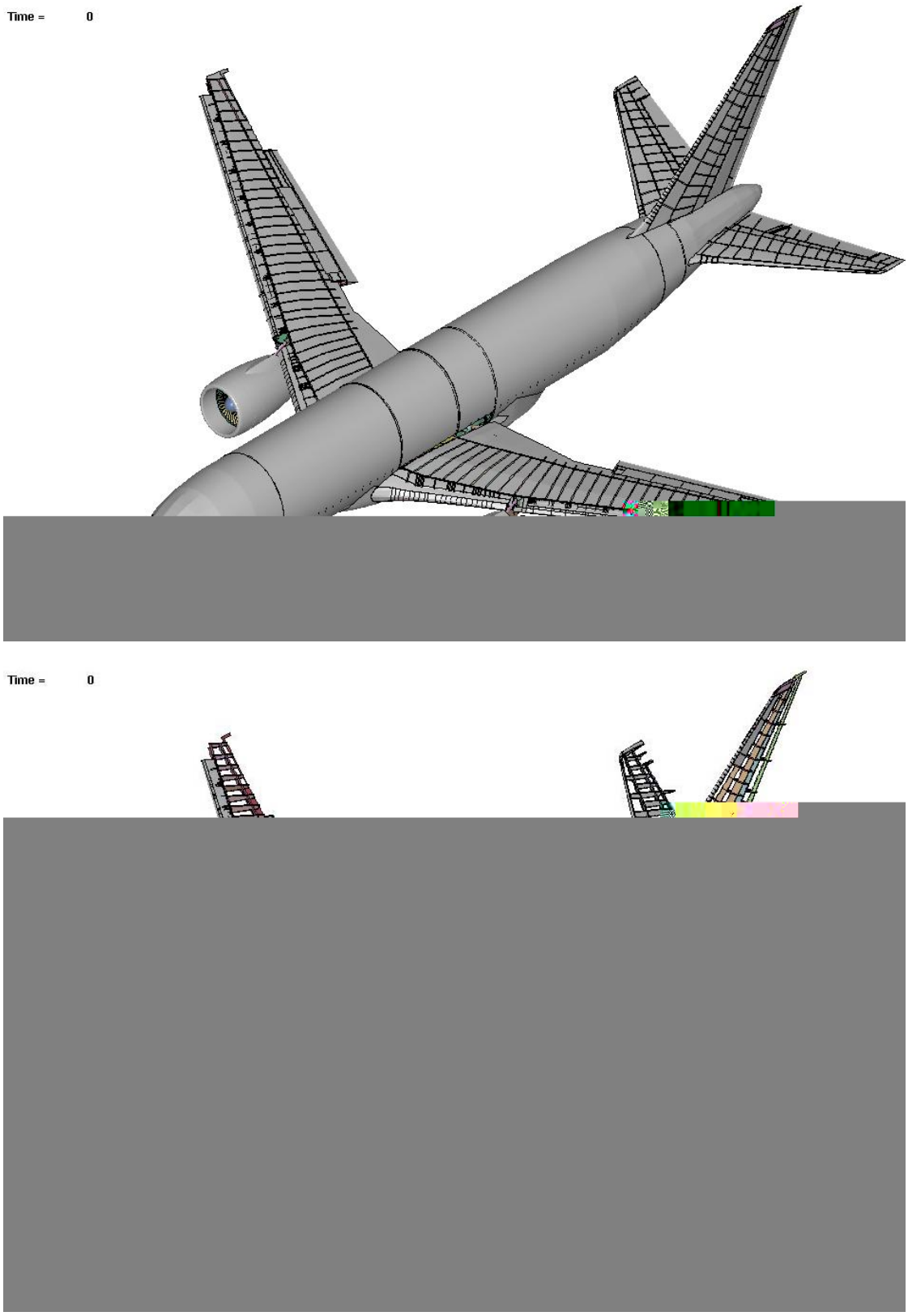

Figure 5–30. Finite element model of the Boeing 767-200ER.

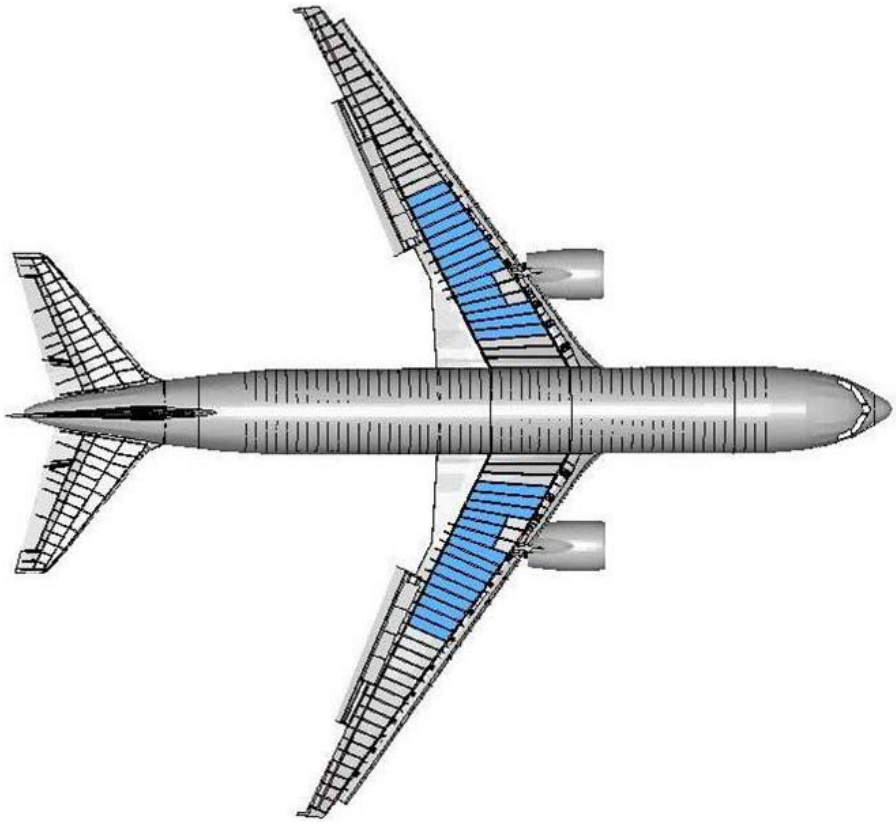

Figure 5–31. Boeing 767-200ER with fuel load at time of impact.

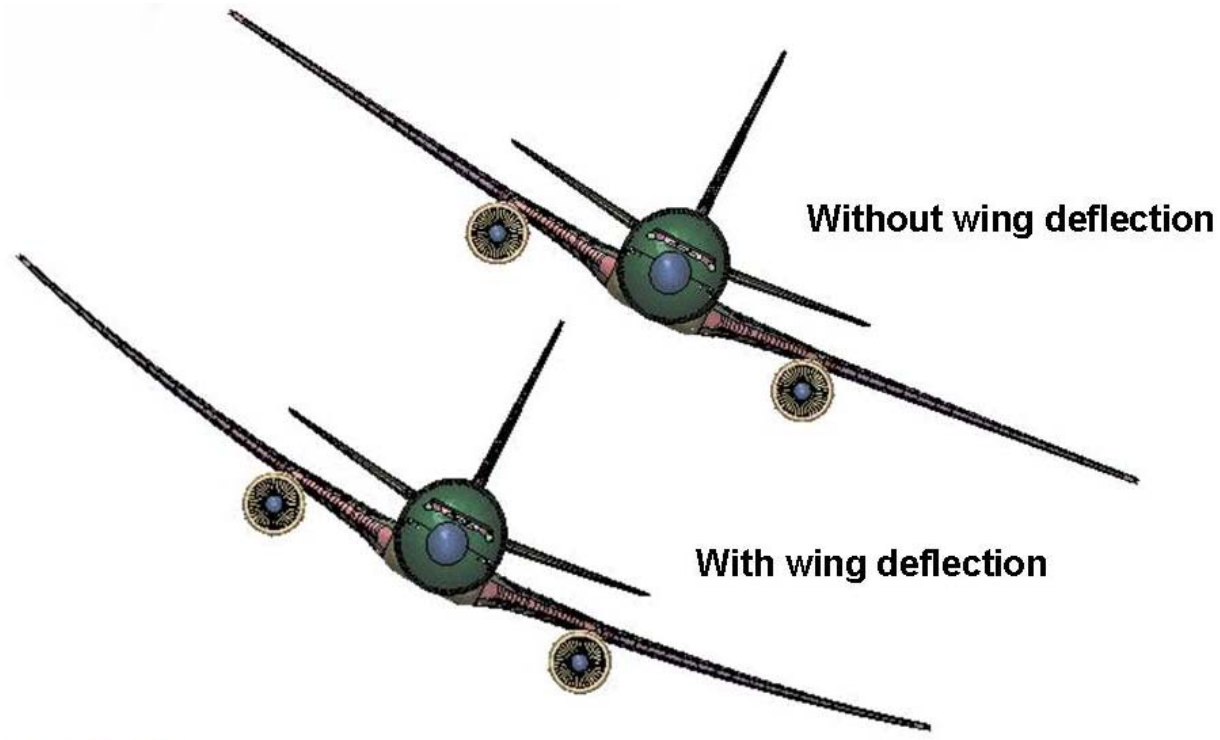

Figure 5–32. Boeing 767-200ER model wing deflections.

5.3.1 Airframe Model Development

The airframe model developed for the Boeing 767-200ER contained most of the significant structural components in the aircraft. The models of the fuselage, empennage, and wing structures were developed completely using Belytschko-Tsay shell elements. Models for the landing gear and engines were primarily developed using shell elements, but contained some brick elements as well. The model was developed in a parameterized form, where the mesh resolution was determined by a single element characteristic size parameter. This approach was selected early in the development to allow flexibility in the model size and resolution as the model development and impact analyses progressed. The objective was to develop a mesh with typical element dimensions between one and two in. for small components, such as spar or rib flanges, and element dimensions of three to four in. for large parts such as the wing or fuselage skin.

Detailed models of the empennage and landing gear are shown in Figure 5–33 and Figure 5–34, respectively. Ribs, spars, rudder, and elevator were all modeled in detail in the empennage. Tires and hubs, the main strut and truck, and support bracing were all included in the landing gear model. The underside of the airframe in the model is shown in Figure 5–35, illustrating the position of the retracted main landing gear in the wheel well. Also shown in the figure are the Unit Load Devices (ULDs shown in red with blue edges). The density of these containers was scaled to include the weight of the cargo.

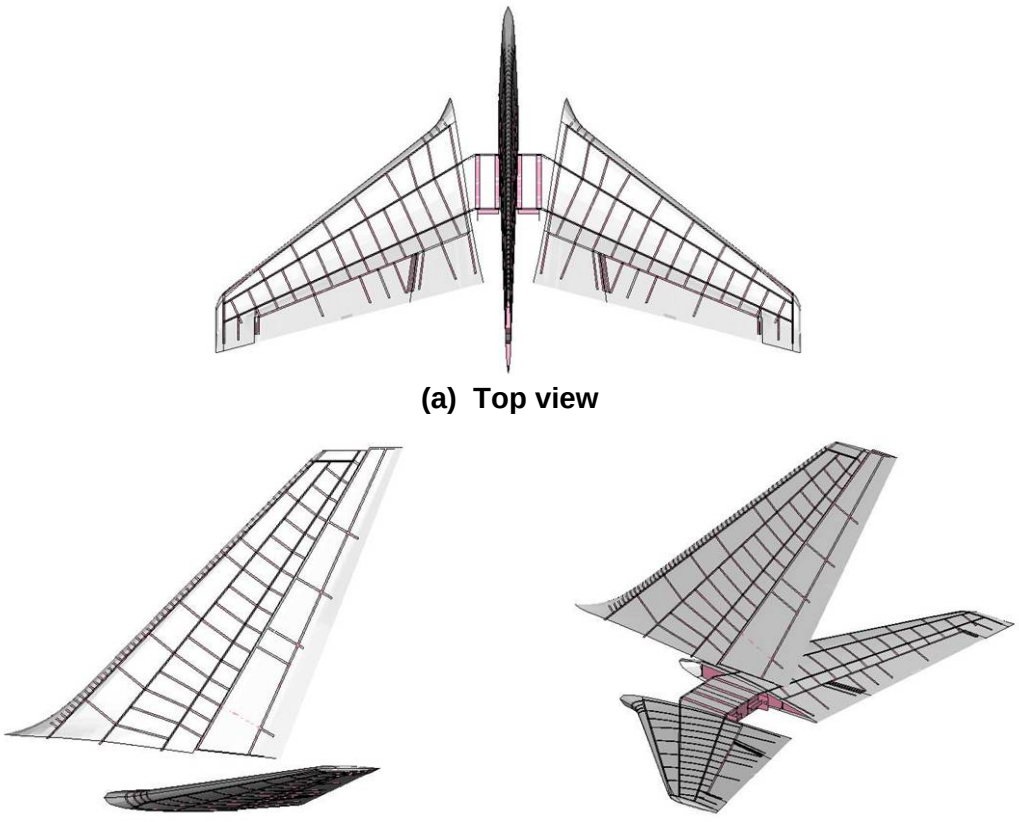

(a) Top view

(b) Side view **(c) Oblique view**

Figure 5–33. Empennage model of the 767-200ER aircraft.

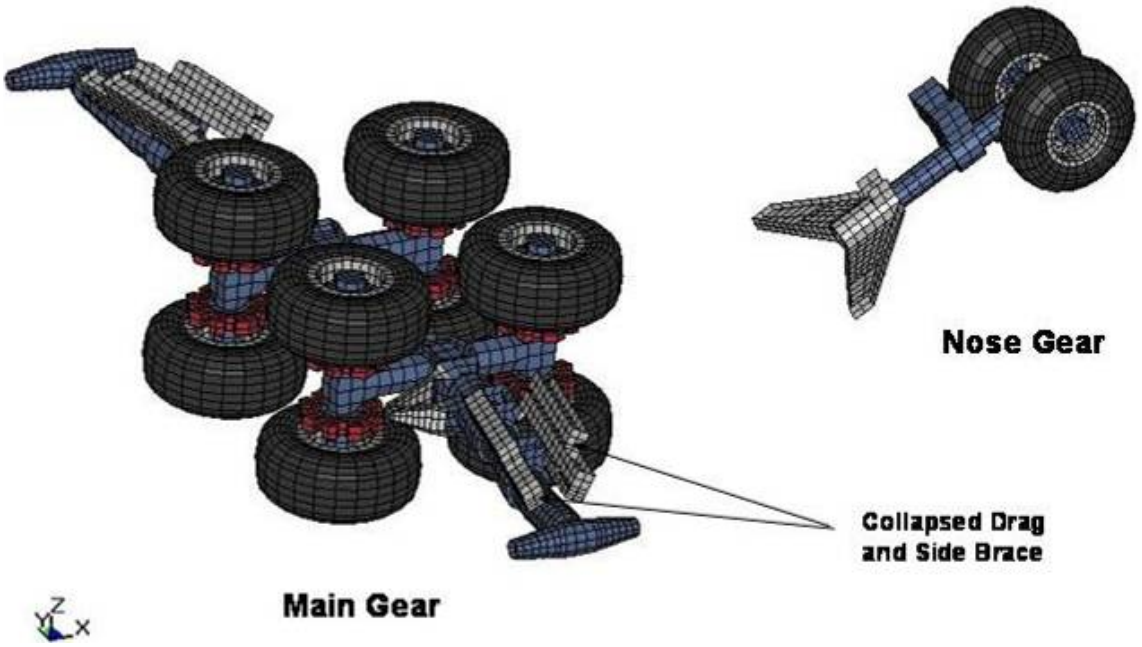

Figure 5–34. Retracted landing gear components for the 767-200ER aircraft model.

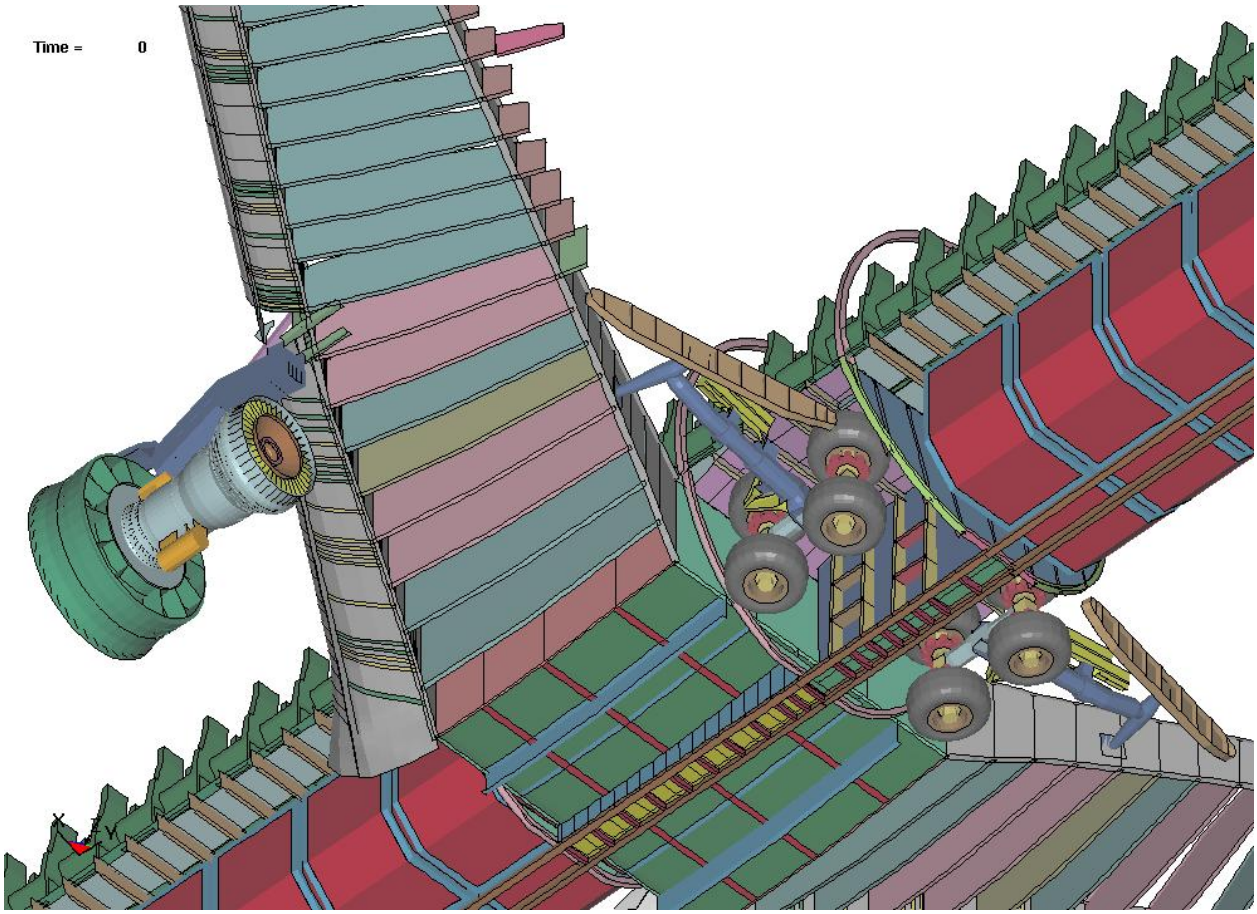

Figure 5–35. Underside of the 767 airframe model (skin removed) showing retracted landing gear, engine, and ULDs.

Figure 5–36 shows the model of the wing structure, including the center wing, which attaches the port and starboard wings. The wing stringers were not explicitly modeled to help reduce the size of the model. The stringers have a z-section geometry with typical dimensions of approximately one in. flanges and a two in. web with a thickness of approximately 1/8 in. These stringers run along the wing span over the top and bottom of the wing ribs. To account for the weight and strength of the riveted skin/stringer construction, an 'effective' wing skin was used, as discussed in Section 5.3.2.

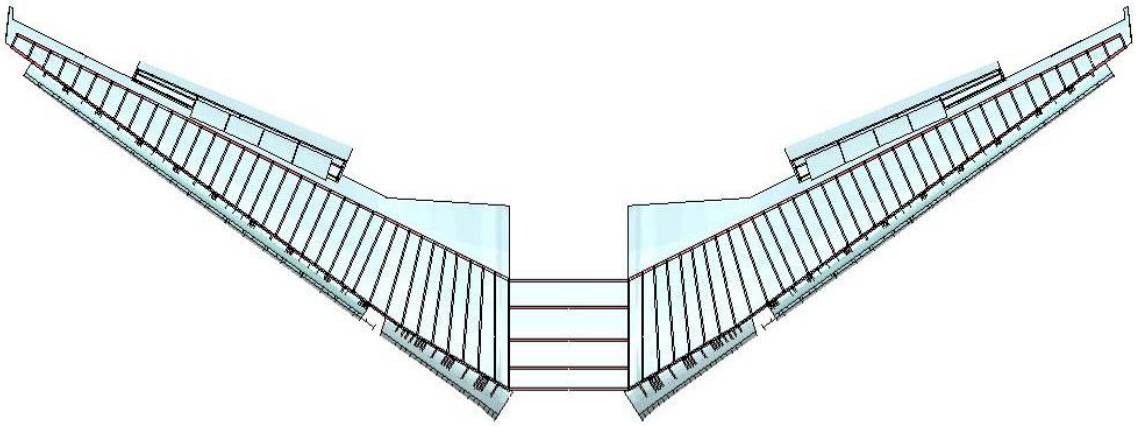

(a) Complete wing model

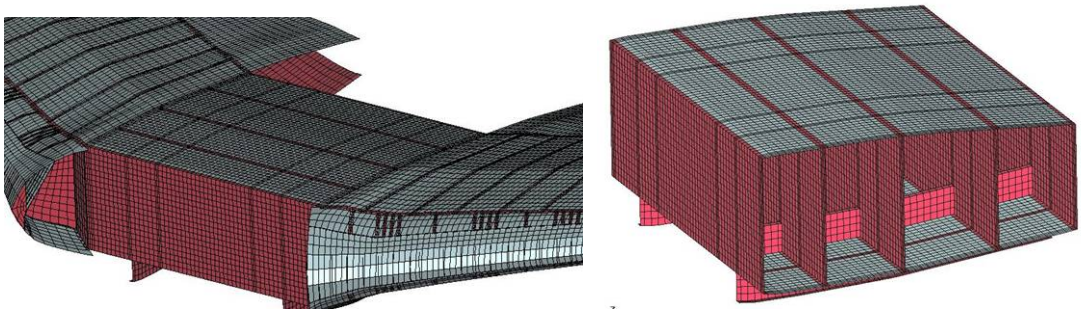

(b) Center wing structures

Figure 5–36. Complete wing structures for the 767 aircraft model.

A model of the fuselage was assembled with a stringer and frame construction supporting the external skin, as shown in Figure 5–37. A tied interface was used to connect the stringers to the frames and skin using the tied surface-to-surface algorithm in LS-DYNA, where nodes on a slave surface were constrained to nodes on a master surface, provided they were within a certain distance of the master surface node. This distance was a function of the element thickness or diagonal length. The wing was integrated into the fuselage structure through attachment of the center wing to the keel and front and rear spar bulkheads, as shown in Figure 5–38. These components were also attached using a tied interface. Due to model size constraints, the forward and aft portions of the fuselage were modeled without the detailed stringer/frame construction. Instead, the weight of these components was smeared into the skin by increasing the skin thickness and scaling down the strength by a factor of 40 percent, as described in the component analyses (see Chapter 4 of NIST NCSTAR 1-2B).

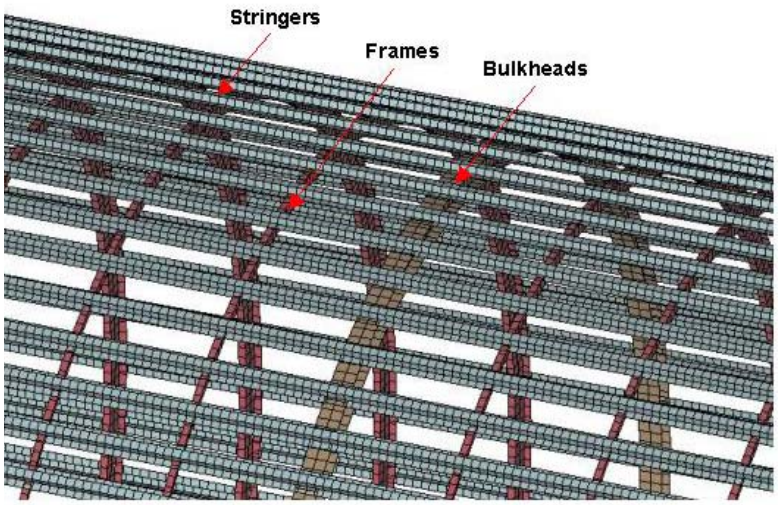

Figure 5–37. Model of fuselage interior frame and stringer construction.

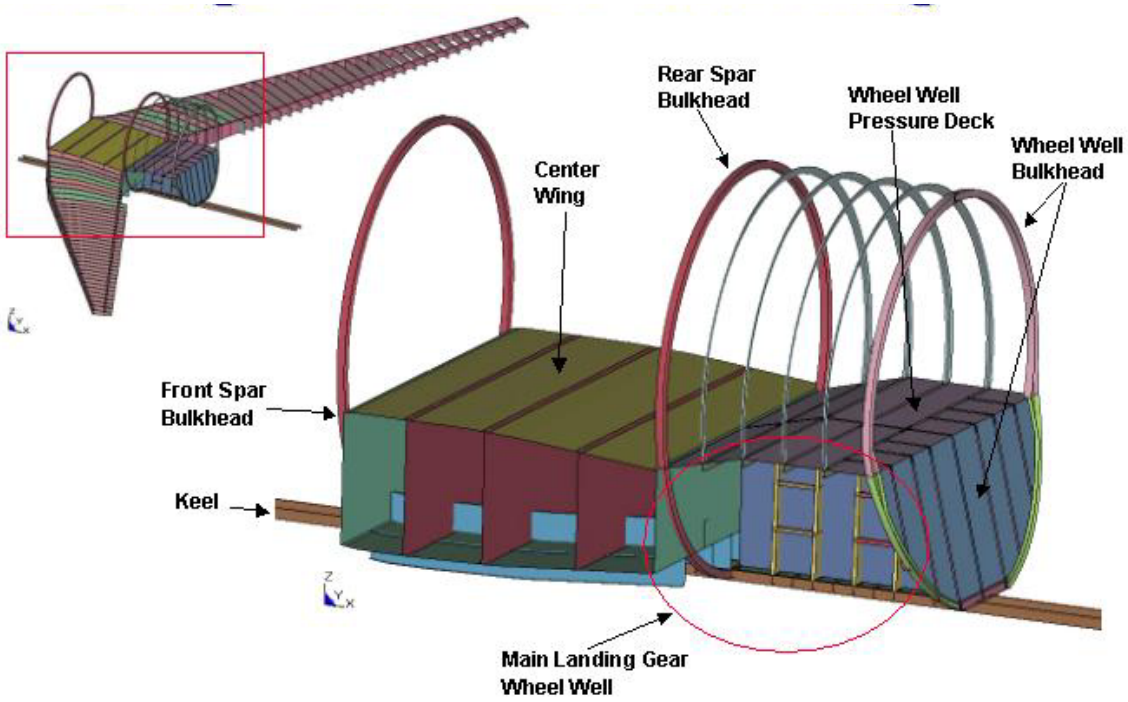

Figure 5–38. Integration of the fuselage and wing structures.

The density of various parts of the aircraft was increased to account for the mass of structural and nonstructural components not specifically modeled. Density scale factors and total weights for each major component are shown in Table 5–3. The difference in scale factors for flights AA 11 and UAL 175 were due to differences in passenger and cargo weight. In both cases, the weight of the cargo, passengers, and crew were incorporated in the ULD (cargo weight) and the seats (passenger, crew and carry on luggage weight). The weight of the modeled wings and empennage were doubled to account for the weight of small structural details, such as stiffeners, not specifically modeled, as well as hydraulic lines and fluid pumps, actuators, inboard flaps and outboard ailerons, flap and rudder connections, and other

nonstructural components. The weight of the landing gear was increased by a smaller amount (1.5) to account for hydraulic fluid and smaller structural components not included in the model. The weight of the fuselage was adjusted to match the published empty weight for the aircraft. That the scale factor for the fuselage was larger than for other components was reasonable as many heavy items in the fuselage were not specifically modeled (e.g. electronics, air conditioning, power units, ductwork, electronic wiring, cargo floor, actuator motors, insulation, hydraulics, galley and lavatories). These structural and non-structural components could not be modeled in detail due to the constraints on model size.

Table 5–3. Density scale factors and weights for aircraft components

Major Aircraft Component	Density Scale Factor (AA 11)	Total Weight (AA 11)	Density Scale Factor (UAL 175)	Total Weight (UAL 175)
Wings	2.0	37,000 lb	2.0	37,000 lb
Empennage	2.0	8,350 lb	2.0	8,350 lb
Fuselage	6.68	103,050 lb	6.68	103,050 lb
Landing Gear	1.5	8,400 lb	1.5	8,400 lb
Engines (with cowlings)	1.2	20,100 lb	1.2	20,100 lb
ULD	1.43	12,400 lb	2.50	21,650 lb
Seats	1.29	28,200 lb	0.78	17,050 lb
Fuel	1.0	66,100 lb	1.0	62,000 lb
Total Weight		283,600 lb		277,600 lb

5.3.2 Wing Section Component Model Development

A wing section model was developed to perform the component and subassembly level analyses (See Chapters 5 and 6, respectively, of NIST NCSTAR 1-2B). The full wing contained 35 ribs, with rib 1 closest to the fuselage and rib 35 near the wing tip. The wing section model described herein included the section of the wing from rib 14 to rib 18 and is shown in Figure 5–39.

The wing structure of the Boeing 767 contains a riveted stringer-skin construction between the front and rear spars. This part of the structure was not included in the wing model as it added significant complexity and size to the model. In order to reduce the size of the model for the global impact analysis, an ‘effective’ wing skin was developed to account for the weight and strength of the riveted skin/stringer construction. A simplified wing section model, containing a uniform stringer-skin construction and a simple rectangular cross-section, was also developed to determine the strength and weight of the effective skin. Both wing section component models utilized Belytschko-Tsay shell elements. The parameters of the effective wing skin model (39) were developed by calibrating this model against the simplified wing section model that included the main spars, wing ribs, leading edge ribs, nose beams, leading edge slats, and outboard flaps. Refer to Chapter 4 of NIST NCSTAR 1-2B for further details.

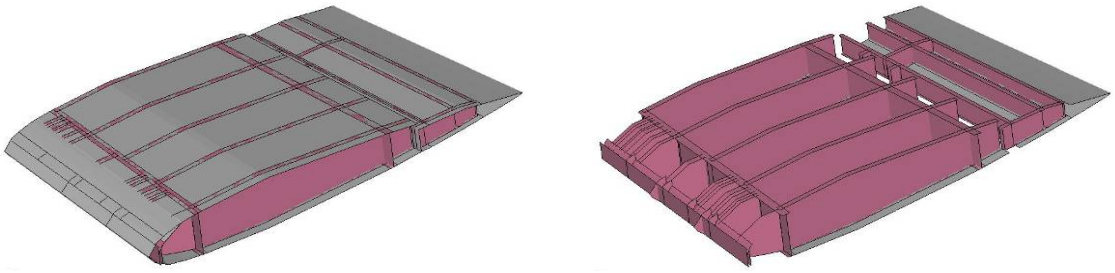

(a) Small wing section model **(b) Internal structure (skin removed)**

Figure 5–39. Wing section model for component level and subassembly analyses.

5.3.3 Engine Model Development

Initial sources indicated that the Pratt & Whitney PW4000 engine and the General Electric CF6-80 engine were on the aircraft that impacted the WTC towers (FEMA 2002). For this reason, the Engine Reference Manuals were obtained from Pratt & Whitney for the PW4000 turbofan engine. A detailed finite element model of the PW4000 engine was developed from these manuals.

After the engine model was developed, the engine types on each aircraft were clarified by the Aviation Safety Network (http://aviation-safety.net/). AA 11 was powered by two General Electric CF6-80A2 engines. UAL 175 was powered by two Pratt & Whitney JT9D-7R4D engines. However, careful review of these engines indicated that the PW4000 turbofan engine was very similar to the General Electric CF6-80A2 and the PW JT9D-7R4D engines. Comparisons of specific physical characteristics of the engines are given in Table 5–4. The JT9D-7R4D and PW4000-94 are almost identical as they are in the same family of Pratt & Whitney aircraft engines. The PW4000 was labeled the "new technology JT9D" when it began replacing the latter engine on 767s built after 1987. The PW4000-94 is 5.8 percent heavier than the JT9D-7R4 but produces up to 10 percent more thrust. Aside from an additional set of long stator blades and elongated exit nozzle, the CF6-80C2 is also of similar weight and dimensions to the PW4000. Due to these similarities, the PW4000 engine model was used for all impact simulations. Differences in the weights of aircraft components were accounted for in the uncertainty analyses.

Table 5–4. Boeing 767 Engine Comparison.

Engine	Pratt & Whitney PW4000-94	Pratt & Whitney JT9D-7R4[a,b]	General Electric CF6-80C2[c,d]
Fan Blade Diameter	94 (in.)	94 (in.)	93 (in.)[e]
Length	153 (in.)	153 (in.)	161-168 (in.)[f]
Dry Weight	9,400 (lb)	8,885 (lb)	9135-9860 (lb)

a. The JT9D-7R4 and PW4000-94 are almost identical: (1) They are in the same family of Pratt & Whitney aircraft engines, and (2) the PW4000 was labeled the "new technology JT9D" when it began replacing the latter engine on 767s built after 1987.
b. The PW4000-94 is 5.8 percent heavier than the JT9D-7R4 but produces up to 10 percent more thrust.
c. The CF6-80C2 has an additional set of long stator blades for the excess fan air that is not present in the PW4000.
d. The second stage compressor blades in the CF6-80C2 are closer to the central shaft than the PW4000 and do not appear to have counter weights.
e. Reference value of 106 in. also found – may include cowling.
f. The "tail" of the CF6-80C2 is much longer than the PW4000. This potentially accounts for the additional 15 in. in length.

Figure 5–40. The engine is an important component of the aircraft with the potential to produce significant damage to the WTC tower structures. As a result, special emphasis was given to the development of the engine model to include all the details of the engine construction.

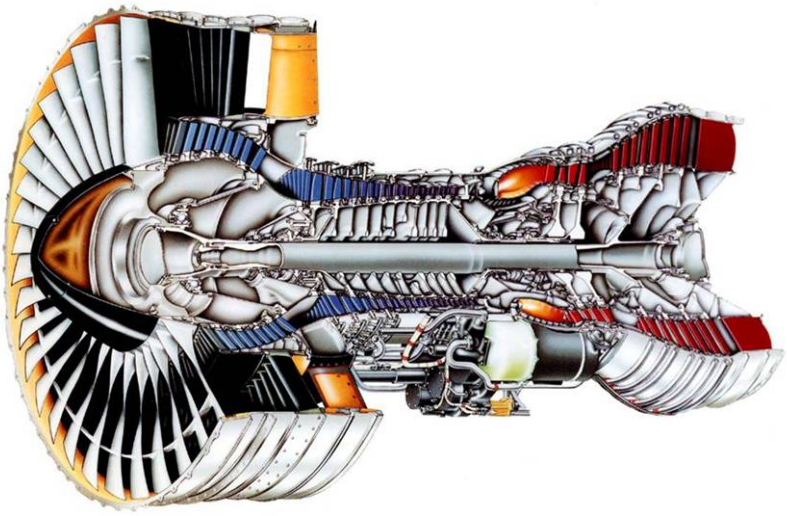

Used with Permission.

Figure 5–40. Pratt & Whitney PW4000 turbofan engine.

The approach used to capture the geometry of the engine was to start with a cross-sectional drawing provided by Pratt & Whitney that clearly showed many of the engine geometric details. In addition, the drawing had sufficient detail that the component thicknesses could be estimated. The primary structural components were identified and approximated with simplified geometry as illustrated in Figure 5–41. Known engine dimensions were used to determine the scale factor for the drawing. The simplified geometry of the engine structures could then be captured using a common digitization procedure.

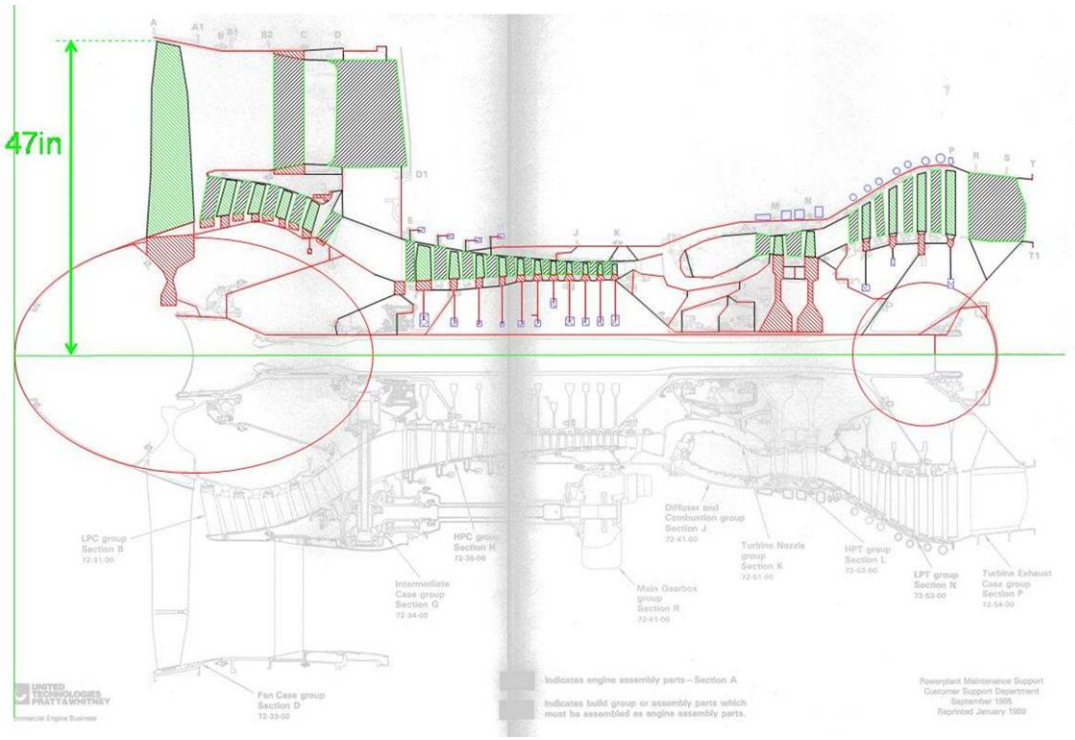

Used with Permission. Enhanced by NIST.

Figure 5–41. PW4000 engine cross-sectional geometry and simplification.

Once the engine internal geometry was captured, the digitized geometry was imported into TrueGrid and used to generate surface definitions and part geometries for the engine model. The engine model was developed using primarily shell elements with typical element dimensions between 1 in. and 2 in. Smaller element dimensions were required at many locations to capture details of the engine geometry. Brick elements were used for some of the thicker hubs and the roots of the compressor blades. The various components of the resulting engine model are shown in Figure 5–42. A summary of the elements used in the engine model is given in Table 5–5.

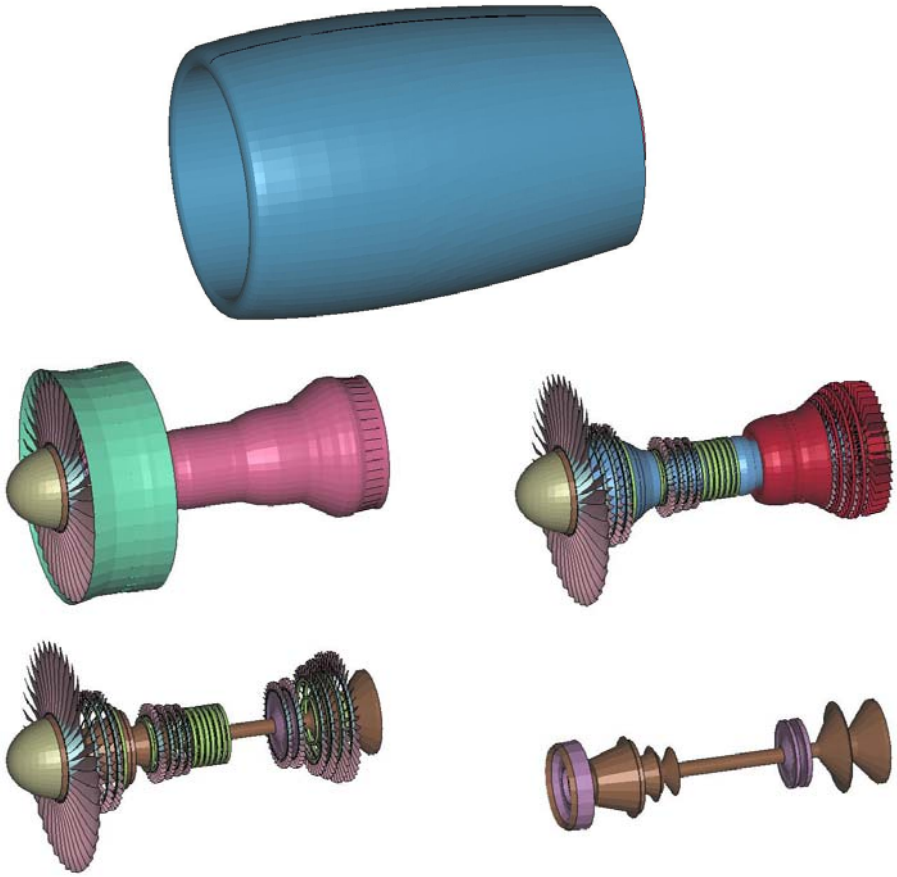

Figure 5–42. Pratt & Whitney PW4000 turbofan engine model.

Table 5–5. Engine model parameters.

	PW4000 Engine Model
No. Brick Elements	9,560
No. Shell Elements	54,788
Total Nodes	101,822
Preliminary Engine Model Weight	7,873 lb
Adjusted Engine Model Weight	9,447 lb

After the known primary structural components of the engine were included in the engine model, the weight of the model was calculated to be 7,873 lb. The dry weight of the PW4000 engine was listed at 9,400 lb and the JT9D-7R4 and CF6-80C2 engines weigh between 8,885 and 9,860 lb. These engine weights were approximately 20 percent larger than the initial model weight. The difference in weight potentially resulted from the nonstructural components (tubing, pumps, seals, bearings, etc.) that were not included in the model. To account for the difference, the density of all of the material models used for engine components was increased by 20 percent. This effectively smeared the missing mass in proportion to the original mass distribution in the model. The resulting adjusted engine model weight was 9,447 lb.

5.3.4 Aircraft Material Constitutive Models

The constitutive and failure properties for the aircraft materials were developed from data available in the open literature. The principal sources of data for the airframe materials were the Military Handbook (MIL-HDBK-5F), 1987 and the Aerospace Structural Metals Handbook [Brown, et al. 1991]. Additional sources of data were used to verify and supplement the information obtained from these primary data sources.

Complete engineering stress-strain curves were provided in the MIL-HDBK-5F for various 2024 and 7075 aluminum alloys that are commonly used in the construction of the Boeing 767 airframe. These curves were digitized for the various 2024 and 7075 alloys. Representative stress-strain curves were then converted into true stress and true strain and used to develop tabular curves for constitutive models. The calculated true stress-strain curves and tabular constitutive model fits are shown in Figure 5–43 and Figure 5–44, respectively. Appropriate failure criteria for the aircraft materials were developed using the fine and coarse wing component models, see NIST NCSTAR 1-2B. No rate sensitivity of the aircraft materials was considered.

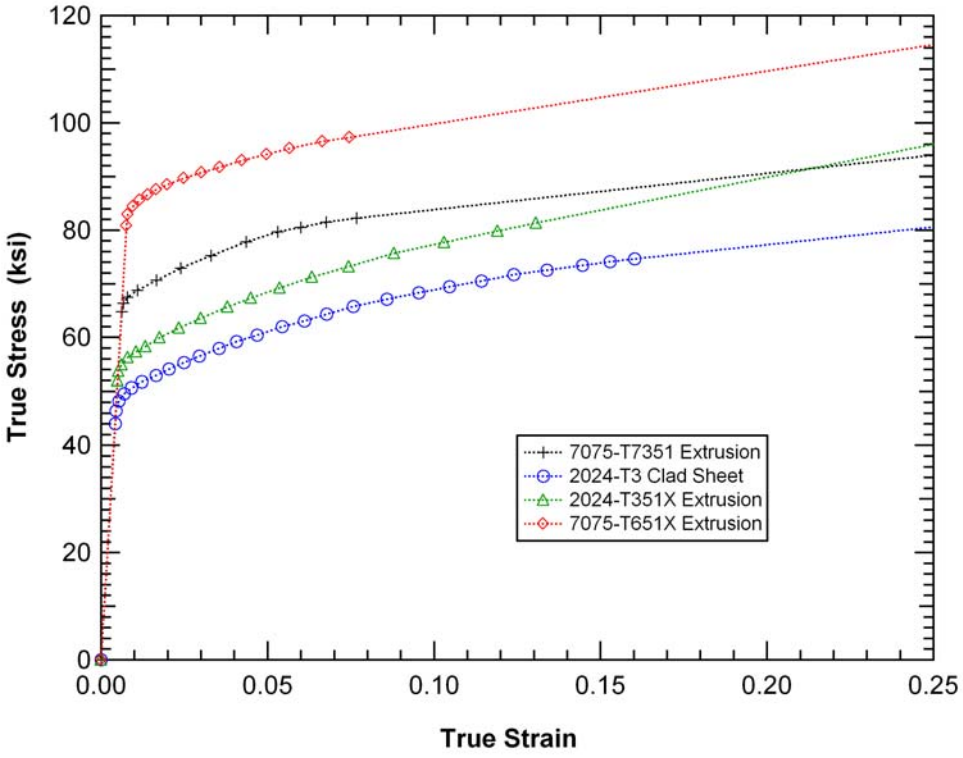

Figure 5–43. True stress-strain curves developed for various aircraft aluminum alloys.

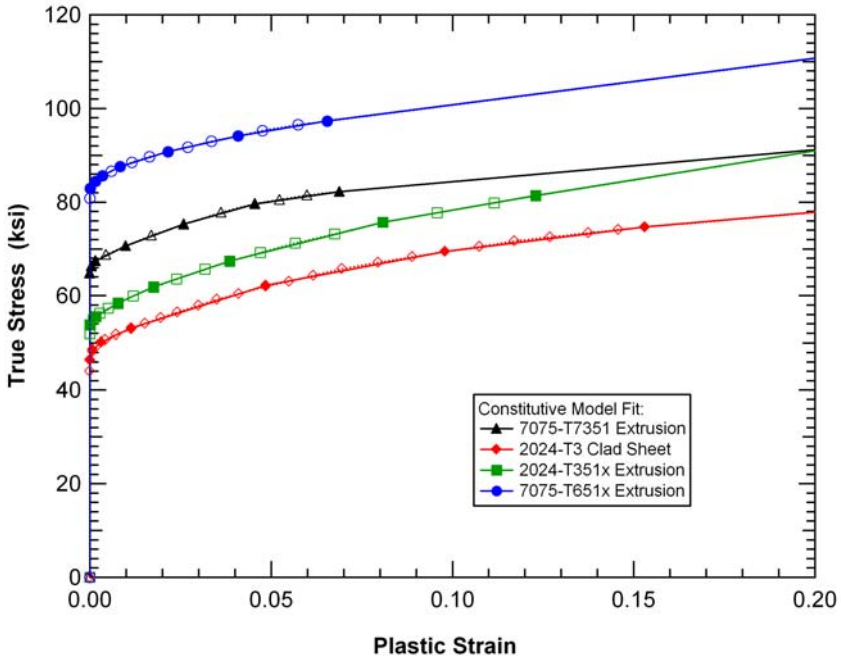

Figure 5–44. Tabular stress-strain curves developed for various aircraft aluminum alloys.

5.4 COMPONENT AND SUBASSEMBLY LEVEL ANALYSES

The primary objectives of the component modeling were to (1) develop understanding of the interactive failure phenomenon of the aircraft and tower components, and (2) develop the simulation techniques required for the global analysis of the aircraft impacts into the WTC towers. The approach taken for component modeling was to start with finely meshed, brick and shell element models of key components of the tower structure and progress to relatively coarsely meshed beam and shell element representations that were used for the global models. This was done to support the development of the reduced finite element global models appropriate for high fidelity global impact analyses, as modeling each component with fine details in the global models would be too demanding from a computational standpoint as was explained in Section 5.1. In addition to determining the optimal element size and type for global modeling, other key technical areas were addressed in the component modeling, including material constitutive modeling, treatment of connections, and modeling of aircraft fuel. The component analyses were also used in the uncertainty analyses to assess the effects of uncertainties associated with the aircraft and WTC towers on the level of damage to the towers after impact and to determine the most influential modeling parameters that affect the damage estimates (see Chapter 8 of NIST NCSTAR 1-2B).

The subassembly analyses were considered as a transition between the component analyses and the global impact analyses. The subassembly analyses were primarily used to investigate different modeling techniques and associated model size, run times, numerical stability, and impact response. The subassembly model was also used to investigate the sensitivity of the impact response to model parameters as well as for the uncertainty analyses (Chapter 8 of NIST NCSTAR 1-2B).

A large array of component and subassembly models were developed and used in the impact simulations. Examples of such analyses are included in this section. The reader is referred to Chapters 5 and 6 of NIST NCSTAR 1-2B for further details of the component and subassembly analyses, respectively.

5.4.1 Exterior Column Impacted with an Empty Wing

The objective of this analysis was to develop a model with a coarse mesh that could be applied to the global impact analyses and still capture the impact damage properly. The analysis used an empty wing section impacting an exterior wall column. The empty wing section model was selected to produce significant column damage at an impact speed of 470 mph without completely failing the column.

These calculations used a preliminary failure criterion. The exterior column modeled was constructed entirely with 55 ksi steel and the spandrel plates with 42 ksi steel. Both a model with a fine mesh of brick elements and a model with a coarser mesh of shell elements were developed. These models included a specific description of the weld geometry, with different properties. In the fine brick element model, the failure strain for the base metal, weld metal, and heat affected zone (HAZ) were all set at a uniform plastic strain of 64 percent, corresponding to the base metal ductility. Failure strains in the coarse shell element models were then adjusted until a similar impact damage and failure mechanism were obtained. A comparison of parameters for the two models is given in Table 5–6.

The calculated impact response is shown in Figure 5–45. The column model on the left has the fine mesh of brick elements, and the column model on the right has the coarse mesh of shell elements. Contours of resultant displacements are shown on the column components. The figure indicates that the overall response was similar in both magnitude and damage mode. The reduction in model refinement resulted in a significant reduction in run time from over 600 min to 9 min. This comparison demonstrated the significance of the mesh refinement on capturing local stress and strain concentrations and the resulting effect on the impact response.

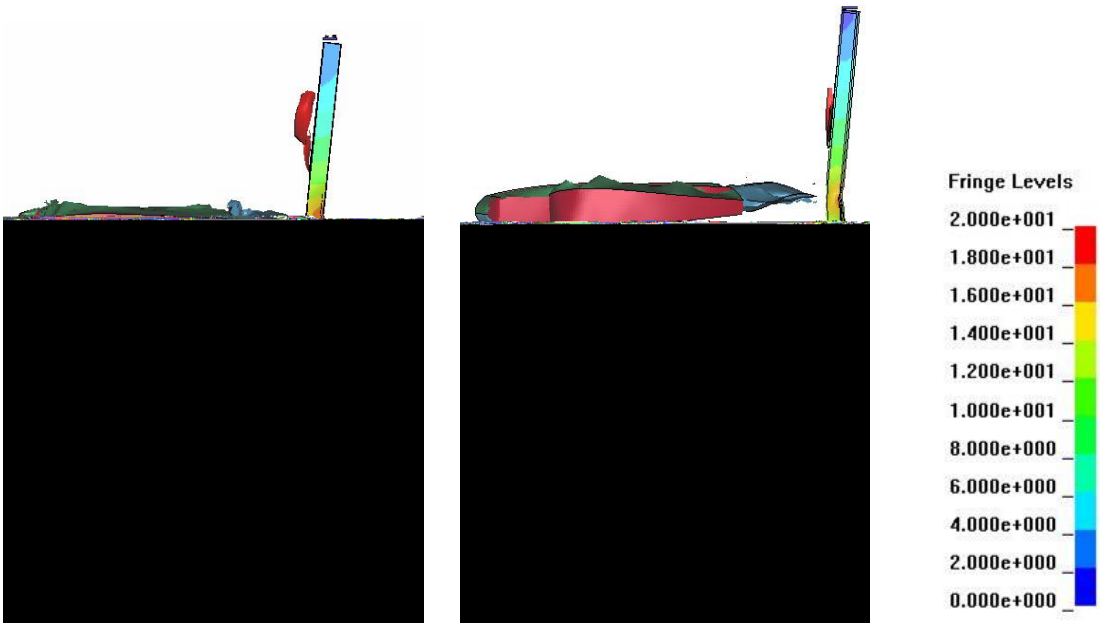

(a) Fine brick element column **(b) Coarse shell element column**

Figure 5–45. Exterior column response comparison, showing contours of the displacement magnitude (in.).

Table 5–6. Exterior column component analyses comparison.

Column Model Type	Fine Brick Model	Coarse Shell Model 1
Number of Brick Elements	473,208	352
Number of Shell Elements	0	9,192
Number of Beam Elements	0	8
Minimum Element Dimension	0.0625 in.	1.0 in.
Bulk Material Failure Strain	64 %	12 %
Weld Zone Failure Strain	64 %	2 %
Calculation Time (CPU)[a]	444 min	3 min
Elapsed Time	624 min	9 min

a. Simulation of 0.035 second duration impact response performed on 11 CPUs.

5.4.2 Bolted Connection Modeling

The objective of this analysis was to develop connection models for the global impact analyses that accurately captured the capacity and failure modes of the bolted connection between exterior columns. Component models of the exterior column butt plate connections are shown in Figure 5–46. The detailed model (a) included individual bolts and butt plates modeled with solid brick elements. The simplified model (b) used coarse brick element butt plates joined by beam elements representing the bolts. A dynamic analysis was carried out to calibrate the beam element bolt model. The loading condition was a dynamic separation of the two butt plates. The velocity profile used to separate the butt plates was a linearly increasing separation velocity between the butt plates with an initial velocity of zero and a velocity of 43 fps at a time of 5.0 ms, obtained from a preliminary engine impact analysis against the exterior wall.

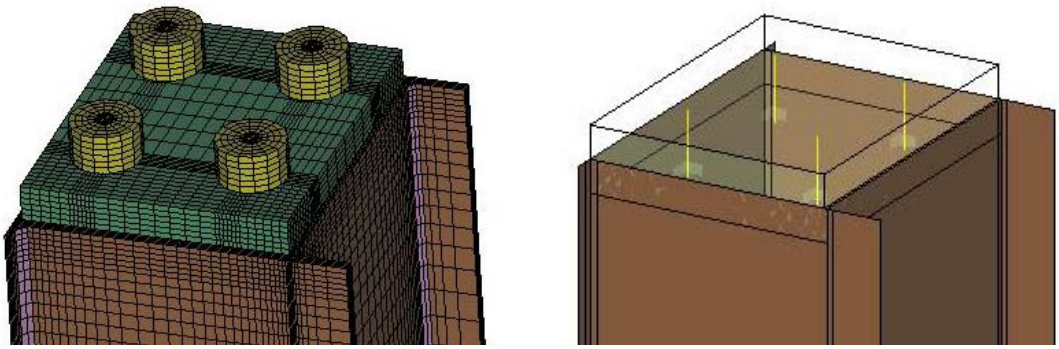

(a) Brick element bolts **(b) Beam element bolts (butt plates shown as transparent)**

Figure 5–46. Modeling of exterior column bolted connection.

Failure strain in the beam models was calibrated such that the beam bolts failed at the same time as the brick element bolts. Failure of the bolts occurred at a time of approximately 3.0 ms. These connection models were used in the corresponding brick and shell models of the exterior column component impact

analyses shown previously in Figure 5–45. Connection failure at the column ends was quite similar in both cases as shown in Figure 5–47. Failure of the connection is illustrated for both connection models at the same time, 35 ms, after impact with the empty wing segment. The primary failure mode for both models was a tensile failure of the bolts and subsequent separation of the column end butt plates.

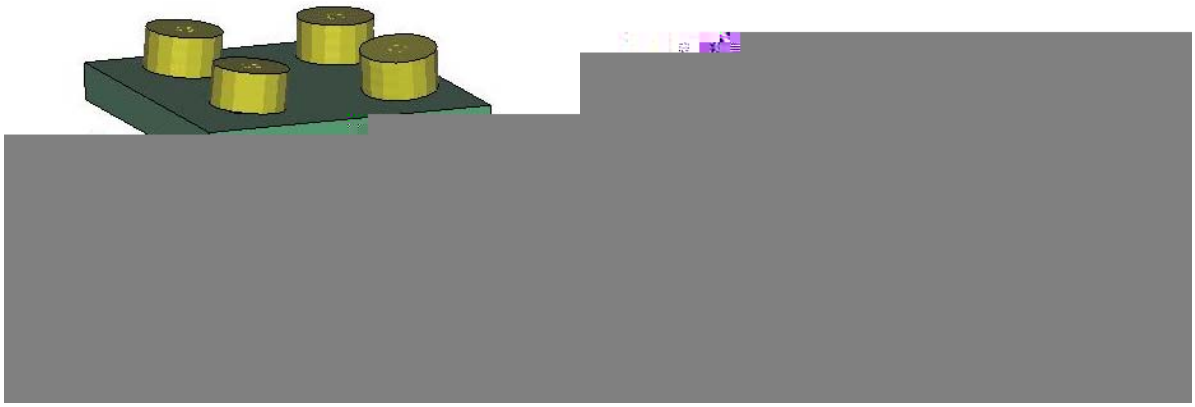

(a) Brick element bolts **(b) Beam element bolts**

Figure 5–47. Failure comparison of exterior column bolted connection treatments.

5.4.3 Floor Assembly Component Analysis

Floor truss impact analyses were carried out to develop a coarse representation of the truss floor, for use in the global impact simulations, that properly captured the impact response characteristics of the fine model of the floor system. For that purpose, detailed floor component models used a combination of brick elements for the concrete slab, beam elements for the truss round bar diagonals, and shell elements for the remainder of the structures, including the truss upper and lower chords and metal decking. This model is shown in Figure 5–48. A less-refined model, similar to that used in the global impact models, was then developed with coarser shell and beam elements as shown in Figure 5–49. This model reduced the size of the floor model by an order of magnitude and the run times by more than 80 percent (see the comparison in Table 5–7).

Table 5–7. Truss floor assembly component analyses comparison.

Model Type	Fine Brick Model	Coarse Shell Model
No. Beam Elements	6,928	3,440
No. Brick Elements	230,778	0
No. Shell Elements	148,256	39,000
Total Nodes	372,084	48,971
CPU Time	16,796 s (4.7 h)	2,482 s (0.7 h)
Elapsed Time	26,553 s (7.3 h)	4,454 s (1.2 h)

The concrete constitutive model used in the brick elements of the detailed floor model was the pseudo-tensor model described in Section 5.2.6. The coarse floor model used an effective material model for the

concrete and metal decking so that these parts would need to be meshed separately. As the pseudo-tensor model is developed for brick elements, and does not work for shell elements, a piecewise plasticity model was used for the effective slab-decking behavior. A tabular stress-strain curve was developed based on the rule of mixtures of the elastic-plastic metal decking with the unconfined compressive behavior for the concrete. The combined slab and decking stress-strain curve was compared to the concrete unconfined compressive behavior in Figure 5–50. The strength of the combined floor slab was dominated by the concrete strength at low strain levels (below 1 percent strain). However, as the concrete was fragmented and removed as debris, the residual strength was equivalent to that of the metal deck alone and remained ductile until a strain of 30 percent was reached. The strain rate effects used for the combined concrete slab and metal decking were those used for concrete as shown in Figure 5–29.

The impactor used in the component modeling was a simplified plow type impactor, which produced repeatable damage, not complicated by all the debris and randomness associated with an engine-floor impact. The weight of the plow impactor was comparable to an engine, and the impact speed was 500 mph, applied horizontally. An example analysis with a plow impactor and the fine mesh floor model is shown in Figure 5–51. The calculated impact damage with the coarser shell element floor system model is shown in Figure 5–52. This component impact configuration was useful for comparing the differences in response with changes in the modeling methods or refinement.

Figure 5–48. Detailed model of the truss floor system.

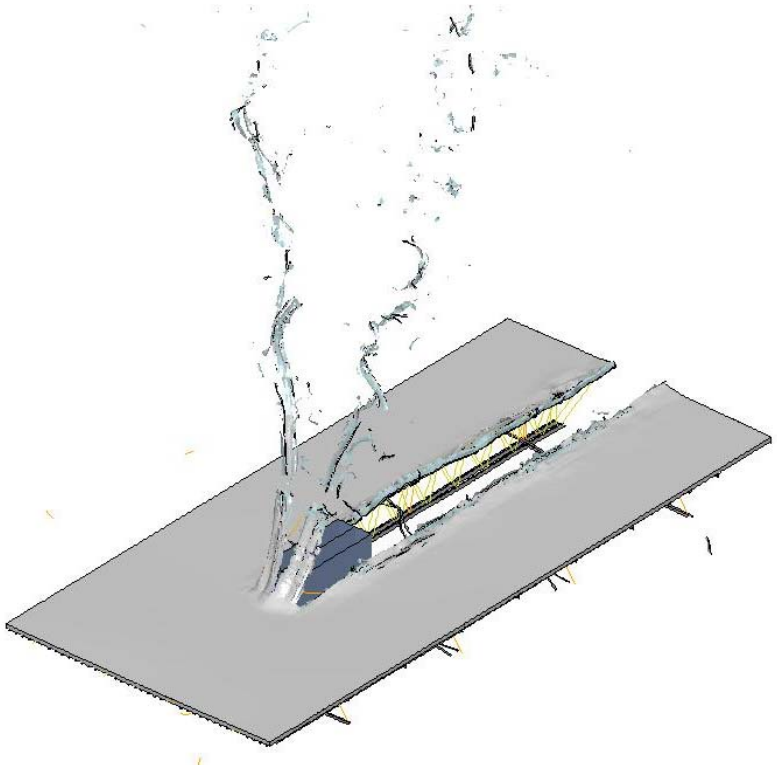

Impact response at 0.10 s

Figure 5–51. Floor assembly impact response with brick element concrete slab.

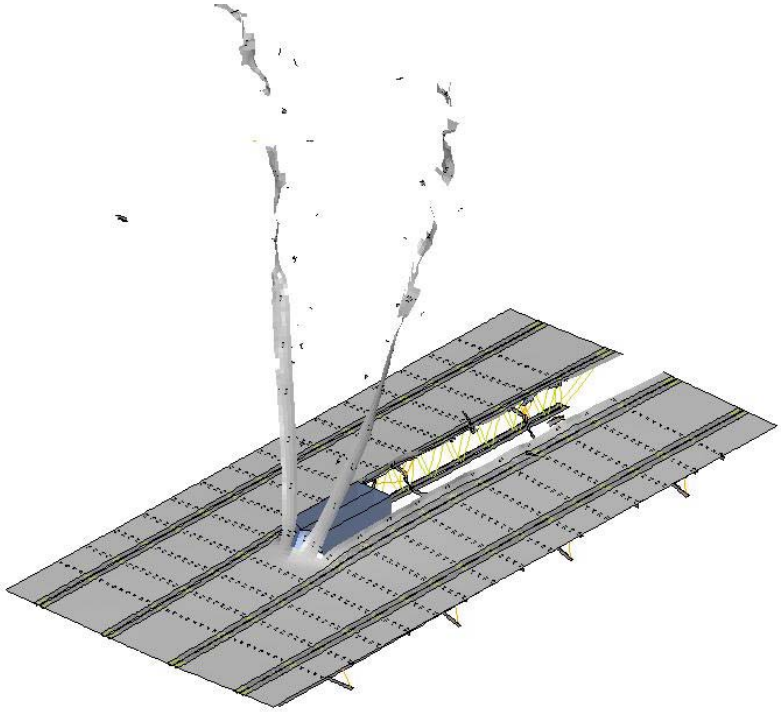

Impact response at 0.10 s

Figure 5–52. Floor assembly impact response with shell element concrete slab.

5.4.4 Modeling of Aircraft Wing Section Impact with Fuel

A significant portion of the weight of a Boeing 767 wing is from the fuel in its integral fuel tanks. At the time of impact, it is estimated that each aircraft had approximately 10,000 gal of fuel onboard. Upon impact, this fuel was responsible for large distributed loads on the exterior columns of the WTC towers and subsequently on interior structures, as it flowed into the building, potentially having a significant effect on the damage inflicted on the building structure. Modeling of the fluid-structure interaction was necessary to predict the extent of this damage and the fuel dispersion within the building to help establish the initial conditions for the fire dynamics modeling.

A number of approaches to solving fluid-structure interaction problems are available in LS-DYNA. One approach is the standard Lagrangian finite element analysis with erosion, where the fuel is modeled using a deformable mesh. This approach accounts for the inertial effects of the fuel, but does not simulate well the fuel flow during impact due to limitations on mesh distortion. The Arbitrary-Lagrangian-Eulerian (ALE) method was developed as a good approach to solve fluid and solid material interaction. With this methodology, fluids are modeled with an Eulerian mesh, which allows for materials to flow between mesh elements. Solid materials are modeled with a moving Lagrangian mesh. With ALE, both mesh types can interact. An alternative approach is to use mesh-free methods such as Smoothed Particle Hydrodynamics (SPH). SPH modeling for fuel effects has the advantage of a smaller mesh size and potentially much faster run times than ALE analyses. Both ALE and SPH methods were applied to the analysis of fuel impact and dispersion and are compared in this study.

A small wing segment was used for performing component level analyses of the wing with fuel. The segment was considered to be completely filled with fuel (approximately 850 gal). Figure 5–53 shows the wing section model with an SPH and ALE mesh for the fuel, shown in blue. The fuel was modeled with 6,720 SPH fuel particles and 110,825 ALE elements for the fuel and surrounding air region, shown in Figure 5–54. The impacted structures were two exterior wall panels as shown in Figure 5–54.

An ALE mesh, surrounding the wing segment and the panels, was needed for the fuel to flow into. In ALE analyses, material is advected from one element to the next so that a mesh is needed for initially "empty" regions. In this case, this mesh was filled with stationary air to interact with the fuel.

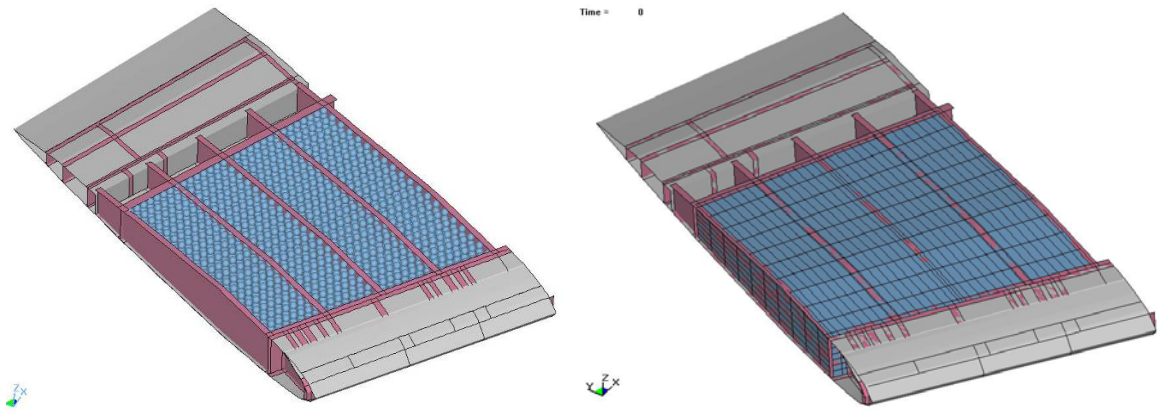

(a) SPH mesh **(b) ALE mesh**

Figure 5–53. SPH and ALE fuel models in the small wing segment.

The wing segment trajectory was that of a normal impact at 500 mph at mid-height between spandrels. The wing was oriented with no pitch, yaw, or roll. Therefore, the leading edge impacted the panels with the sweep angle of the wing relative to the fuselage. The two exterior panels were constrained rigidly at the butt plates and at the floor slab locations. Refer to Chapter 5 of NIST NCSTAR 1-2B for the fuel modeling parameters used in the ALE and SPH analyses.

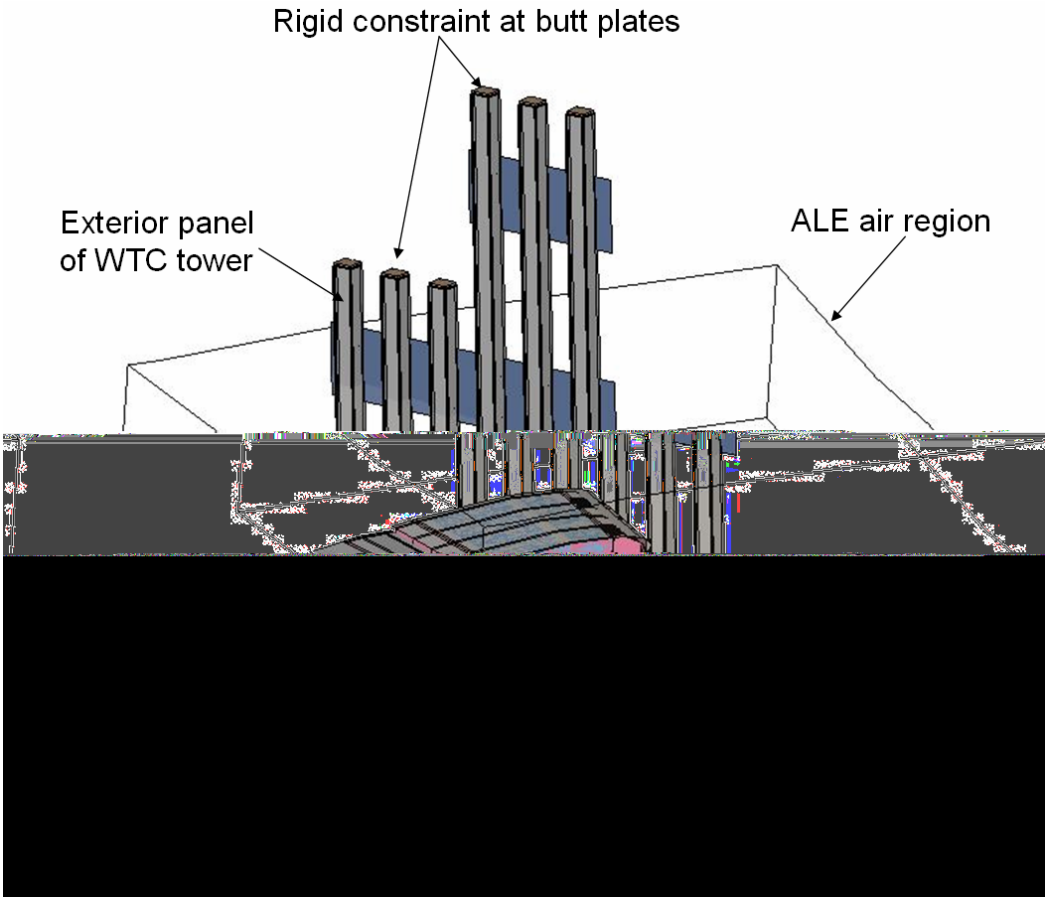

Figure 5–54. Wing segment, fuel, and exterior panel configuration.

Results of the impact analysis of the wing section using the ALE and SPH approaches are shown in Figure 5–55 and Figure 5–56, respectively. In both cases, the columns of the exterior panels were completely destroyed due to impact. Close-ups of the damage to the exterior panels are shown in Figure 5–57. Figure 5–58 and Figure 5–59 show close-up comparisons of the fuel dispersion and wing break up predicted by the two fuel modeling approaches. While both modeling approaches gave comparable results for the damage to the exterior wall panels, the SPH modeling method predicted greater fuel dispersion and wing break up than when using ALE, as can be shown clearly in the side views (Figure 5–59). Without experimental data, it is difficult to evaluate which method provides a more accurate solution.

Run-times from these component analyses clearly indicated that the SPH method was more practical for the global impact analyses. The SPH model ran about 10 times faster than the ALE method, as it required a smaller mesh and did not need to rezone after each time step, as was done in the ALE method. In

addition, the ALE method required a mesh for both the fuel region and the air zone into which the fuel could flow. Therefore, the SPH method was selected as the modeling technique for the global analyses.

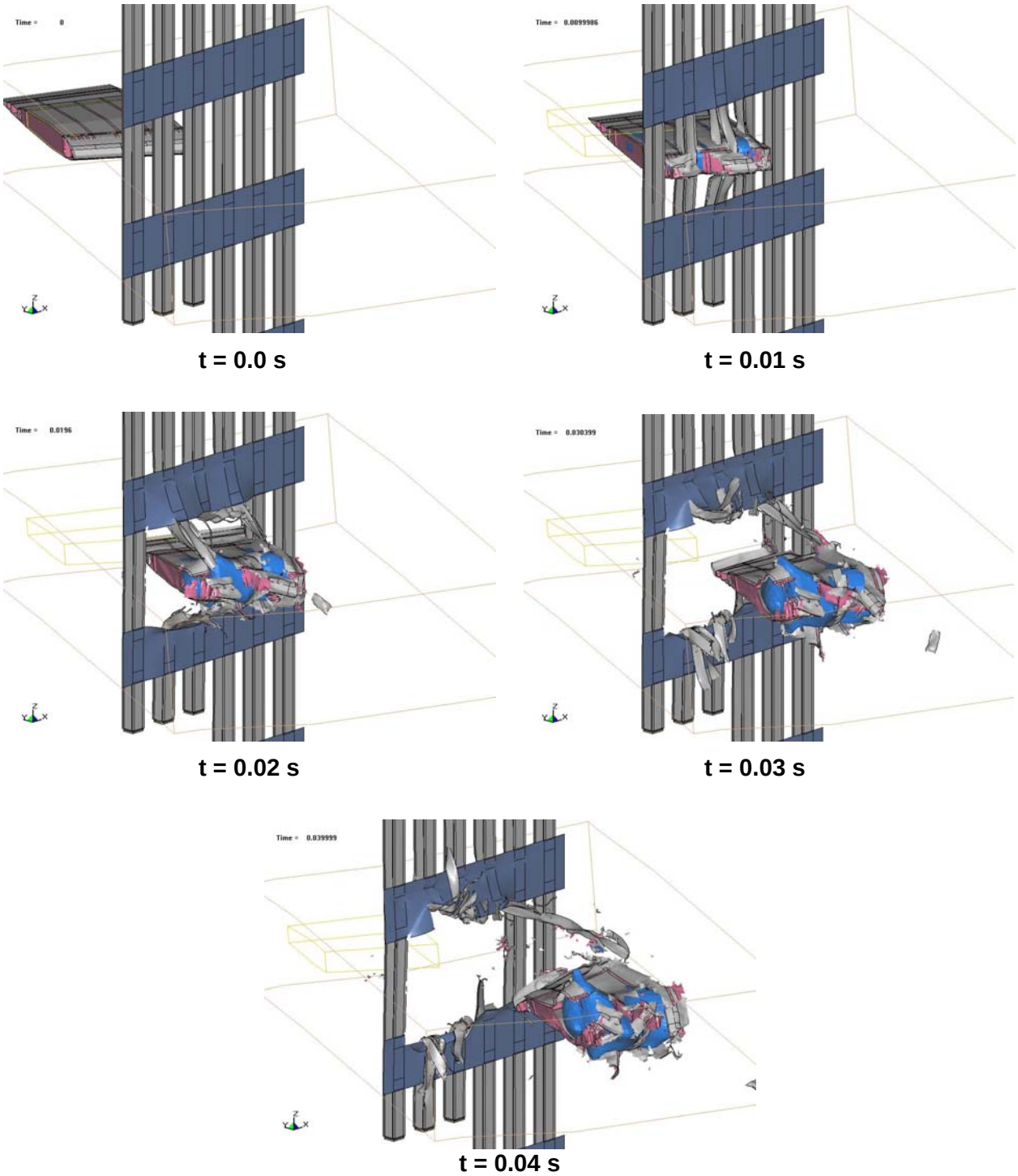

Figure 5–55. Impact response of a wing section laden with fuel modeled using ALE approach.

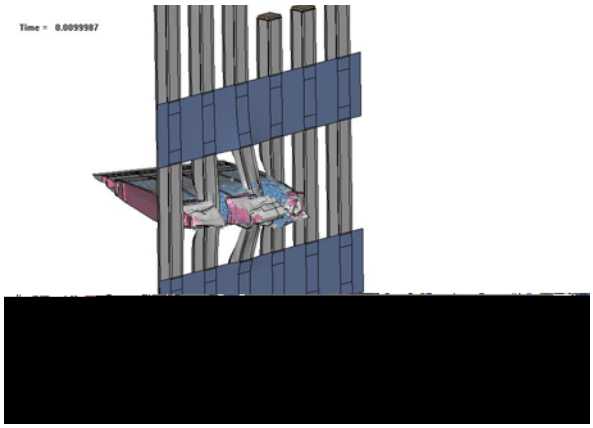

t = 0.0 s

t = 0.01 s

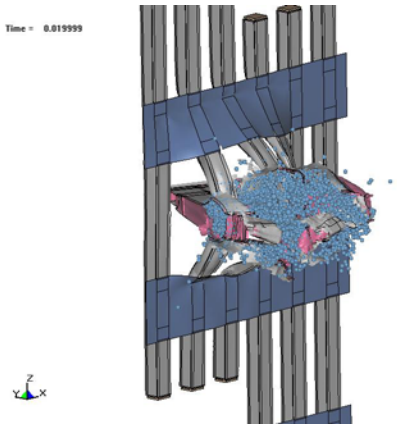

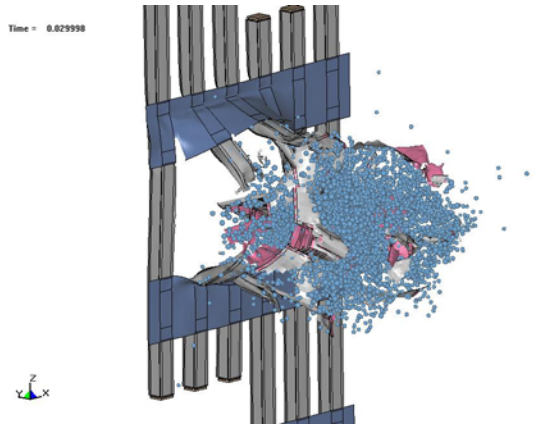

t = 0.02 s

t = 0.03 s

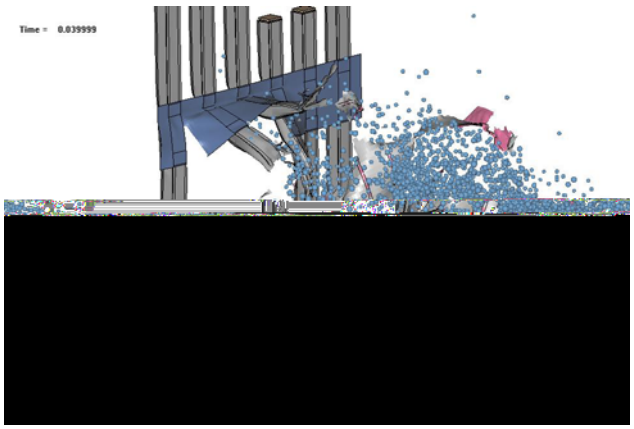

t = 0.04 s

Figure 5–56. Impact response of a wing section laden with fuel modeled using SPH approach.

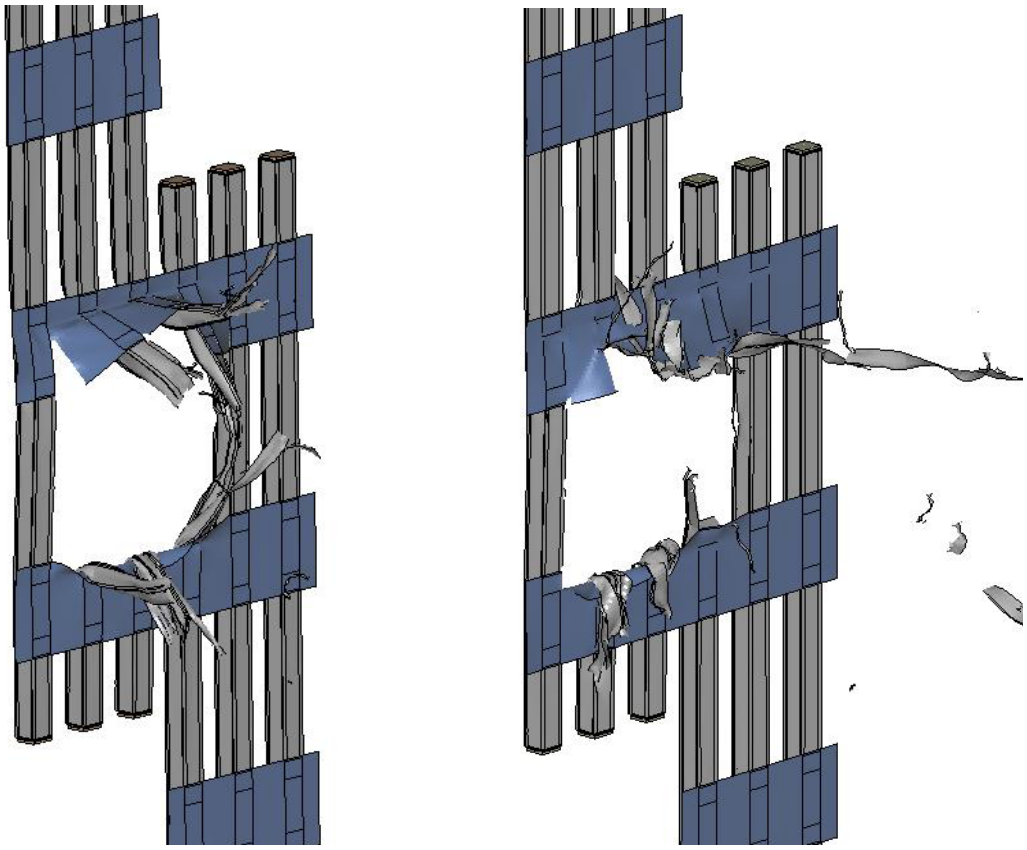

(a) With SPH approach **(b) With ALE appraoch**

Figure 5–57. Exterior panels after impact with a wing segment with fuel.

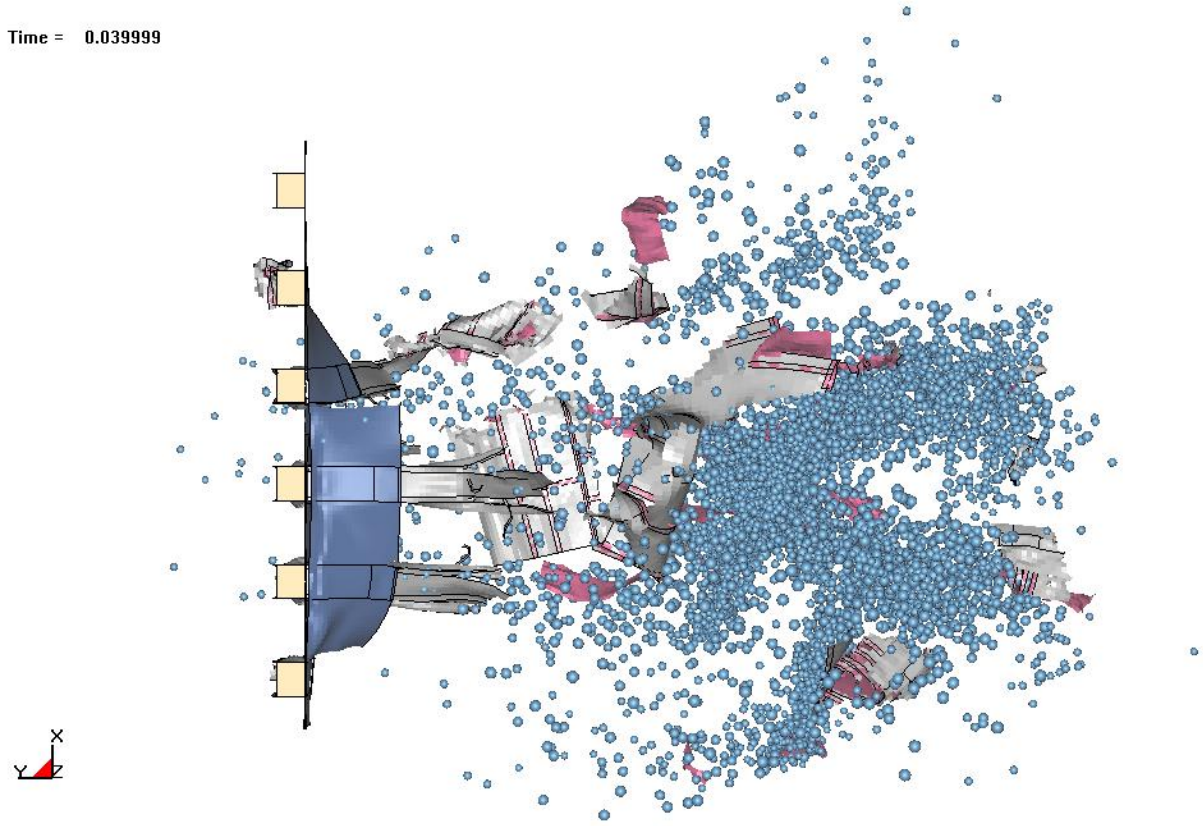

(a) SPH analysis

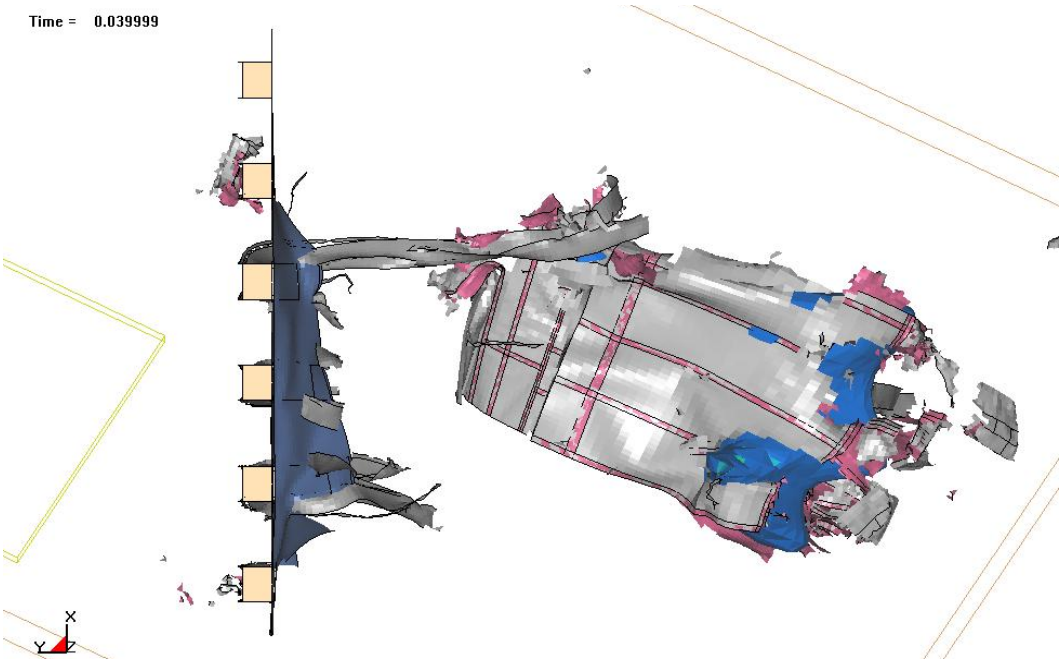

(b) ALE analysis

Figure 5–58. Top view of structural damage and fuel dispersion at 0.04 s.

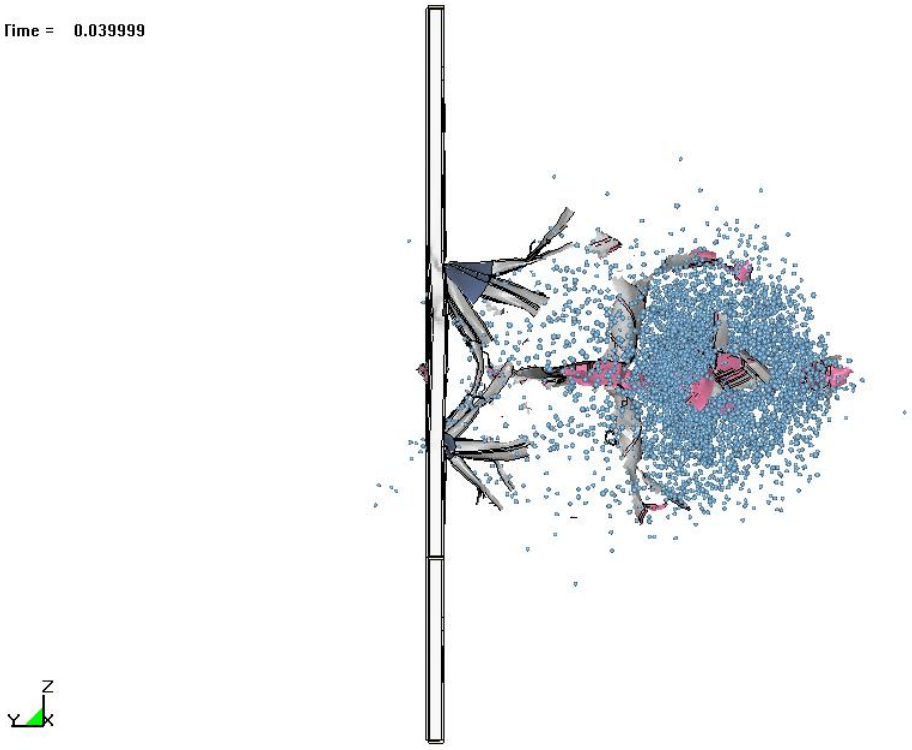

(a) SPH analysis

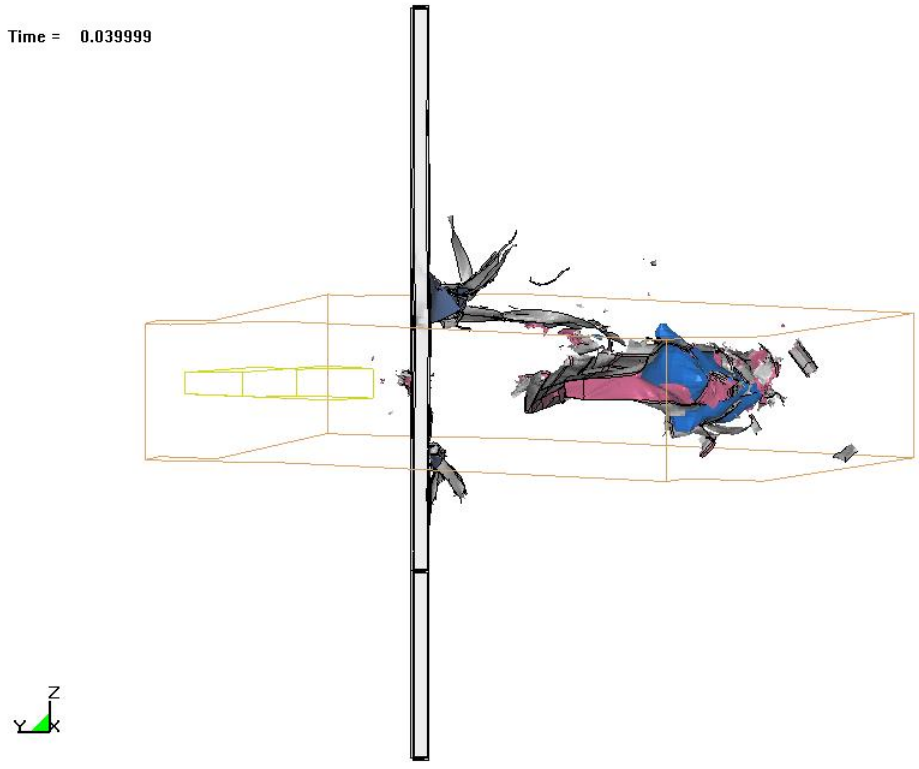

(b) ALE analysis

Figure 5–59. Side view of structural damage and fuel dispersion at 0.04 s.

5.4.5 Engine Impacts Subassembly Analyses

This subassembly model was developed using structural components from the impact zone on the north face of WTC 1. The model, shown in Figure 5–60, was used to evaluate the response of structural connections, material and failure models, and other issues affecting the global impact analyses. The model was three floors tall, spanning floors 95-97, three exterior panels wide, and extended from the exterior wall through to the first two rows of core columns. The exterior wall in the subassembly model included the exterior panels that extend into floors 95-97, as well as two panels above and below the panel, spanning all three floors. The structural components in the final subassembly model included the exterior panels, core framing, truss floor structures, and interior contents (workstations).

The vertical displacements were constrained at the top and bottom of the free ends of the core columns. For the exterior columns, a bolted connection was added to an adjacent butt plate for which the vertical motions were constrained. The lateral displacements were constrained at the free spandrel edges and at the sides of the truss floor structures.

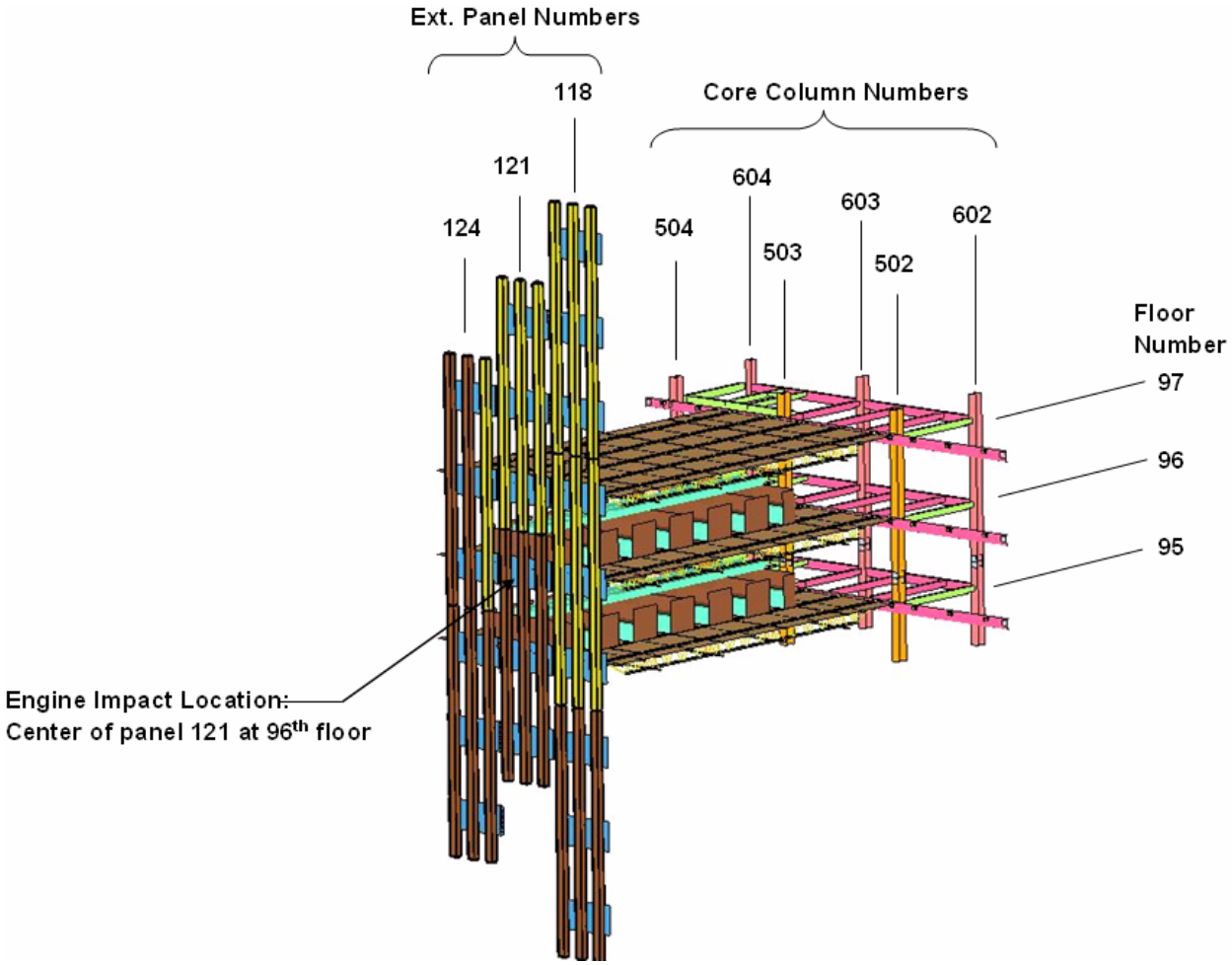

Figure 5–60. Tower subassembly model.

In this impact simulation, the engine had an initial speed of 413 mph and a trajectory with a lateral approach angle of 4 degrees from the exterior panel normal and vertical approach angle of 7.6 degrees

below the horizontal. The impact point was centered approximately 6 ft below the 97th floor so that the initial impact did engage a significant portion of the truss floor structures. The calculated impact response of the subassembly is shown in Figure 5–61. The engine penetrated the exterior wall and continued into the interior of the building along the initial downward trajectory. As the engine continued into the subassembly model, it plowed through the interior building contents (workstations) and eventually skipped off of the truss floor slab at floor 96.

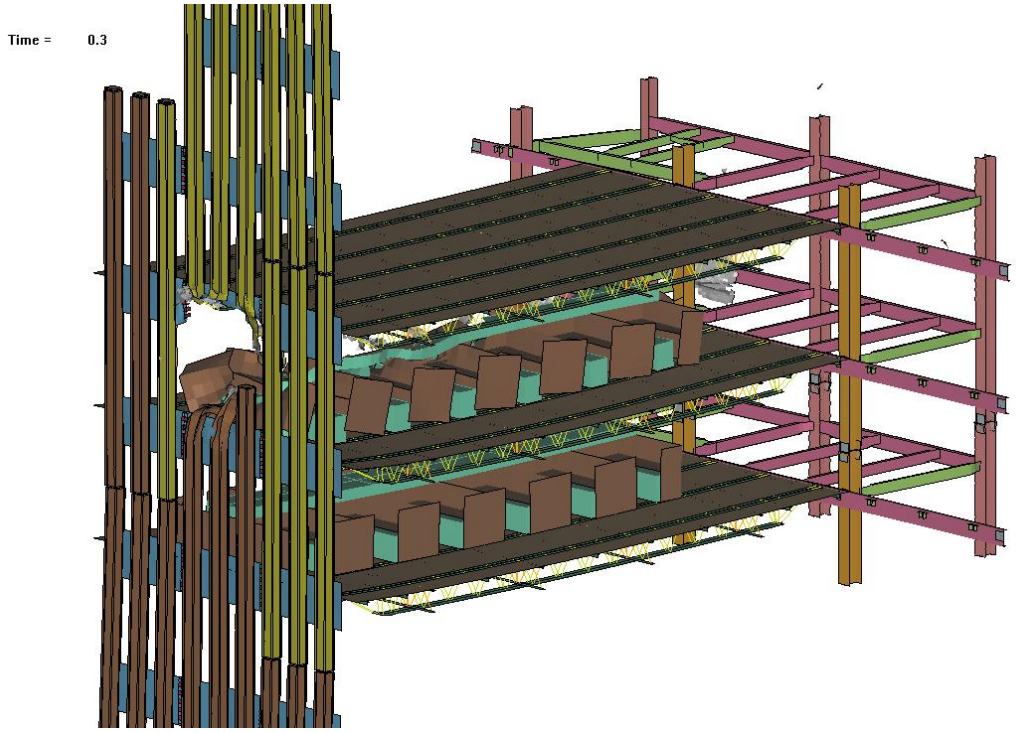

Figure 5–61. Response of the subassembly model to engine impact.

A side view of the impact behavior at different time instants during the response is shown in Figure 5–62. The engine penetrated the exterior wall following the initial downward trajectory. As the engine continued downward, it impacted the workstations and the truss floor structures of floor 96. The engine motion was redirected by the impact with the truss floor and continued its motion toward the core penetrating additional workstations. At a time of 0.25 s, the engine entered the core as shown in Figure 5–62(c). The impact conditions of this analysis resulted in a collision of the engine with core column 503. The speed-time history of the engine core in this impact analysis is shown in Figure 5–63. The deceleration that occurred in the first 5 ms was primarily from the penetration of the exterior wall and the floor slab and truss of floor 97.

(a) Time = 0.00 s

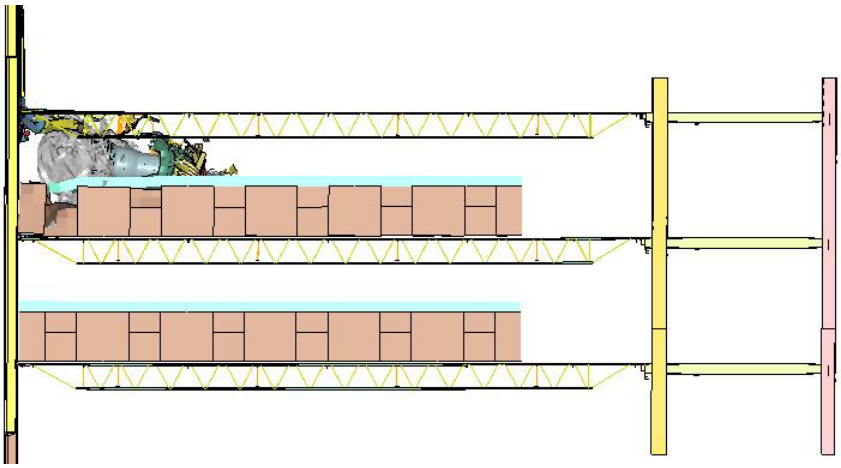

(b) Time = 0.05 s

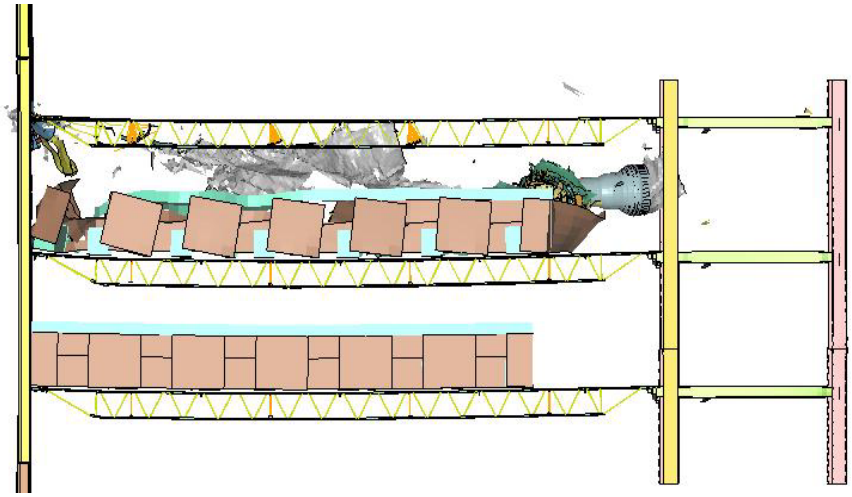

(c) Time = 0.25 s

Figure 5–62. Subassembly-engine impact and breakup response (side view).

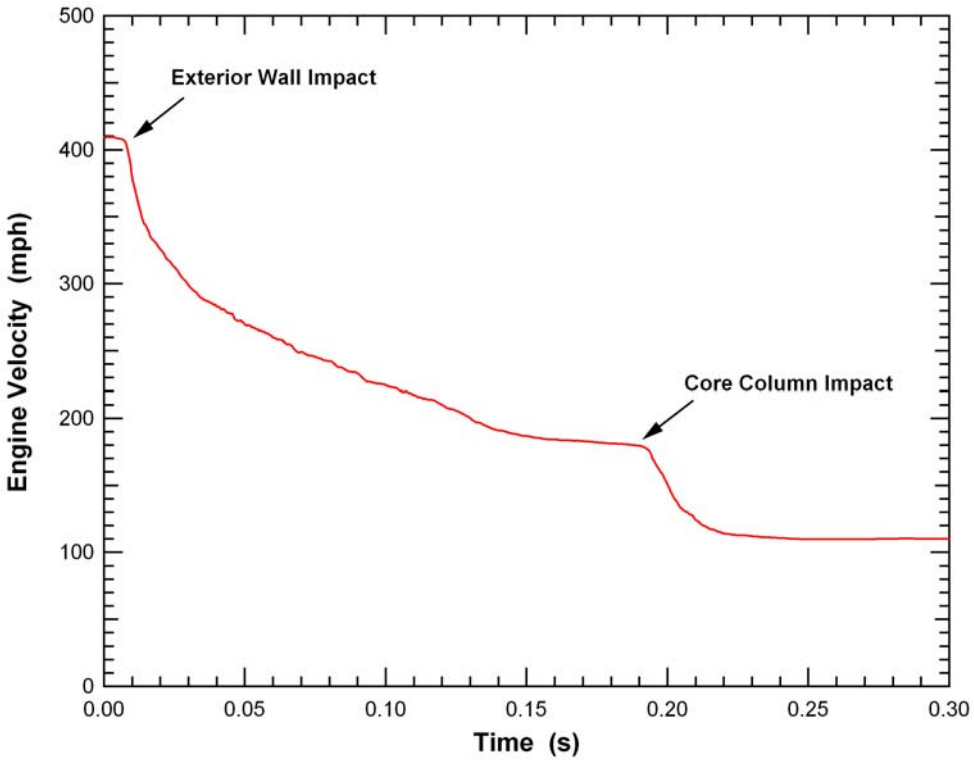

Figure 5–63. Speed history for the engine subassembly impact analysis.

This subassembly model was used to investigate the effect of a number of modeling parameters on the response and damage estimates. These parameters included the strength of the building nonstructural contents and the concrete slab strength. The reader is referred to Chapter 6 of NIST NCSTAR 1-2B for further details. The same configuration was also used to study the sensitivity of the response to 11 parameters as part of the uncertainty analysis, see Chapter 8 of NIST NCSTAR 1-2B.

5.5 SUMMARY

The towers were modeled primarily with shell elements with the exception of the exterior wall bolted connections (beam and brick elements) and the floor truss diagonals (beam elements). The WTC 1 model extended between floors 92 and 100, while the WTC 2 model extended between floors 77 and 85. The global impact models of the WTC towers included the following components:

- Exterior walls: The exterior columns and spandrels were modeled using shell elements with two mesh densities, a refined density in the immediate impact zone and a coarser far field density elsewhere. For the bolted connections between exterior panels in the refined mesh areas, brick elements were used to model the butt plates, and beam elements were used for the bolts.

- Core columns and floors: Core columns were modeled using shell elements with two mesh densities, a refined density in the direct impact area and a coarser far field density elsewhere. The spliced column connections were included in the model with proper failure criteria. The

floors within the core were modeled using shell elements representing the floor slabs and beams.

- Truss floor: In the direct impact area, the floor model included shell elements for the combined floor slab and metal decking, and for the upper and lower chords of the trusses. Beam elements were used for the truss diagonals. In the far field floor segments, simplified shell element representations were used for the floor slab and trusses.

- Interior building contents: The interior nonstructural contents of the towers were modeled explicitly. These included the partitions and workstations, which were modeled with shell elements in the path of the aircraft debris. The live load mass was distributed between the partitions and cubicle workstations.

The Boeing 767-200ER aircraft model was developed based on (1) documentary aircraft structural information, and (2) data from measurements on Boeing 767 aircraft. The airframe model contained most of the significant structural components in the aircraft. The models of the fuselage, empennage, and wing structures were developed completely using shell elements. Models for the landing gear and engines were primarily developed using shell elements, but contained some brick elements as well. The typical element dimensions were between 1 in. and 2 in. for small components, such as spar or rib flanges, and 3 in. to 4 in. for large parts such as the wing or fuselage skin.

Special emphasis was placed on modeling the aircraft engines due to their potential to produce significant damage to the tower components. The engine model was developed primarily with shell elements. The objective was to develop a mesh with typical element dimensions between 1 in. and 2 in. However, smaller element dimensions were required at many locations to capture details of the engine geometry. Brick elements were used for some of the thicker hubs and the roots of the compressor blades.

In support of the development of the global models of the towers and aircraft, a large array of component and subassembly models were developed and used in the impact simulations. Examples of such analyses included:

- Impact of a segment of an empty aircraft wing with an exterior column.

- Detailed and simplified modeling of exterior panel bolted connection under impact loading.

- Impact of a simplified plow type impactor with truss floor assembly.

- Impact of fuel-filled wing segment with exterior wall panels.

- Impact of an aircraft engine with a subassembly from the exterior wall though the core of the towers.

These component and subassembly analyses provided guidance on the optimal element size and type for global modeling, material constitutive modeling, treatment of connections, and modeling of aircraft fuel. They were also used for the sensitivity analyses conducted to assess the effects of uncertainties associated with various parameters on the level of damage to the towers and to determine the most influential modeling parameters that affect the damage estimates.

5.6 REFERENCES

"TrueGrid Manual, Version 2.1.0," XYZ Scientific Applications, Inc., September 2001.

"LS-DYNA Keyword User's Manual," Livermore Software Technology Corporation, Version 970, April 2003.

"LS-DYNA Theoretical Manual," Livermore Software Technology Corporation, May 1998.

ASTM Designation A 370 - 03a, "Standard Test Methods and Definitions for Mechanical Testing of Steel Products," Approved June 10, 2003.

Bischoff, P.H., Perry, S.H., "Compressive Behavior of Concrete at High Strain Rates," Materials and Structures, vol. 24, 1991, pp. 425-450.

Boeing Company, Aircraft Description of Boeing 767, Section 2, Document number D6-58328, www.boeing.com, 1989.

Brown, W. F. Jr., Mindlin, H., and Ho, C.Y., (Eds.), 1991, Aerospace Structural Metals Handbook, CINDAS/Purdue University Publishers, Volumes 3 & 4.

Culver, C.G., 1976, Survey Results for Fire Loads and Live Loads in Office Buildings, NBS Building Science Series, No. 85, National Bureau of Standards, Washington, DC.

FEMA 304, May 2002, World Trade Center Building Performance Study: Data Collection, Preliminary Observations, and Recommendations, Federal Emergency Management Agency.

Military Handbook, 1987, Metallic Materials and Elements for Aerospace Vehicle Structures, U.S. Dept. of Defense, MIL-HDBK-5F.

Ross, C.A., Kuennen, S.T., Tedesco, J.W., "Effects of Strain Rate on Concrete Strength," Session on Concrete Research in the Federal Government, ACI Spring Convention, Washington, D.C., March 1992.

Wischers, G., "Application of Effects of Compressive Loads on Concrete," Betontech, Berlin, Nos. 2 and 3, 1978.

Chapter 6
AIRCRAFT IMPACT INITIAL CONDITIONS

6.1 INTRODUCTION

In order to determine the impact loading on the World Trade Center (WTC) towers, the aircraft impact initial conditions needed to be estimated. These initial conditions included the aircraft speed, aircraft orientation and trajectory, and location of aircraft nose at impact. The estimates also included the uncertainties associated with these parameters. This chapter describes the estimation of the initial impact conditions of the aircraft which impacted the WTC towers from available records. These records included the videos that captured the two impact events and photographs of the damage to the exterior of both towers.

Two videos captured the approach and impact of the American Airlines Flight 11 (AA 11) aircraft that impacted the WTC 1 tower, and several videos captured the United Airlines Flight 175 (UAL 175) aircraft that impacted the WTC 2 tower. In addition, a large body of photographic evidence was available that could be used to determine the impact location and orientation relative to the towers. These videos and photographs were analyzed to estimate, with the best accuracy possible, the impact speed, horizontal and vertical angles of incidence, and roll angle of each aircraft during impact with each tower, as well as the location of impact.

The analysis of the initial aircraft impact conditions was performed in two steps. The first step was to perform an analysis of the video footage of the two impact events. This analysis compared the various videos and used visual references and known dimensions and positions of towers to determine the flight conditions prior to impact (Section 6.2). The second step was to use photographs of the impact damage to refine the details of the impact position, orientation, and trajectory (Section 6.3).

The impact orientation and trajectory parameters are defined in Figure 6–1. In this figure, two vectors were defined, one for the velocity vector of the aircraft (the trajectory) and one for the orientation of the aircraft. These two vectors may not be coincident. Both vectors were described in terms of a vertical angle around structure east, as shown in the figure, and a lateral angle, which was measured clockwise around the tower axis from structure north. The orientation was also described in terms of a wing-tip roll angle, as shown in the figure.

The resolution of the video footage was not sufficient to measure the wing deflections or impact points more accurately than within ± 6 ft. In the two videos that captured the WTC 1 impact, there also was not enough resolution to obtain an accurate orientation of the aircraft. Consequently, the impact point and roll angle of AA 11 were determined using only the still-frame photographs of the impact damage to the north wall of WTC 1. Since the UAL 175 impact was captured by several videos, the trajectory and orientation measurements could be made from the available video footage. Similar to WTC 1, the impact location was primarily determined from the still frame photography of the damaged WTC 2 south wall. The following sections describe the analysis methodologies used to determine the motion parameters and impact conditions.

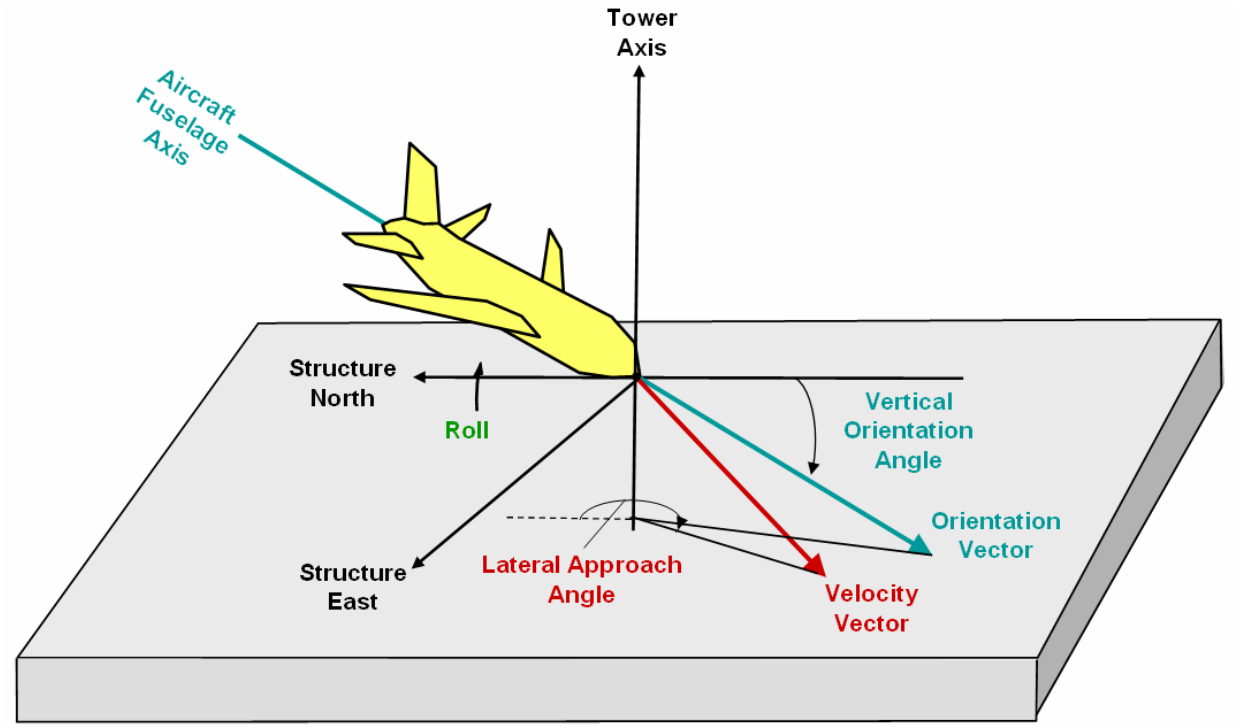

Figure 6–1. Definition of the aircraft impact parameters.

Section 6.2 of this chapter provides the details of the motion analysis methodology based on video footage of the two impact events. This included a complex and a simplified motion analysis. Section 6.3 presents the procedure used to refine the initial impact conditions obtained from the motion analysis based on the damage to exterior walls documented in photographs. Section 6.4 is a comparison between the impact conditions estimated from this study with those reported or estimated previously. Section 6.5 is a summary of the chapter.

6.2 MOTION ANALYSIS METHODOLOGY

6.2.1 Videos Used in the Analysis

The first task in the analysis of the aircraft impact conditions was to review and select appropriate videos and photographs that could be used for the estimation of the impact initial conditions. An extensive library of video and photographic evidence of the WTC tower impacts was collected by National Institute of Standards and Technology (NIST) (see NIST NCSTAR 1-5A). The available videos were reviewed to select the best video footage of the aircraft's approach and impact with each tower. The videos were digitized and stored in AVI files. The WTC 1 aircraft impact was captured in two videos, and both were used in the analysis. Several videos captured the aircraft impact into WTC 2 tower, and seven of them were selected for the analysis. The image coordinates of the aircraft nose, tail, wing tips, aileron, and several locations on the towers were measured in each frame of the videos. Adobe Photoshop was used to determine the image coordinates. Table 6–1 provides a summary of the videos used to analyze the impact initial conditions. Still images from each of these video records are provided in Appendix E.

Table 6–1. Videos used for the analysis of aircraft impact initial conditions.

Digitized Video File	Original Video Format	Tower Impact	Description
V1	NTSC	WTC 1	Footage taken at ground level at the corner of Church and Lispenard streets. Taken north and east of the towers.
V2	PAL	WTC 1	Footage taken from the entrance of the Brooklyn Battery Tunnel, heading west. Taken south and east of the towers.
V3	NTSC	WTC 2	Footage taken from a helicopter north and west of the towers.
V4	NTSC	WTC 2	Footage taken at ground level near the Castle Clinton National Monument. Footage taken south and east of the towers.
V5	NTSC	WTC 2	Footage taken from Brooklyn, south and east of the towers.
V6	NTSC	WTC 2	Footage taken from the 13th floor of a building in John Street, east of the towers.
V7	NTSC	WTC 2	Footage taken at ground level from the corner of Church and Liberty. Taken south and east of the towers.
V8	NTSC	WTC 2	Footage taken from a helicopter north of the towers.
V9	NTSC	WTC 2	Footage taken from a moving vehicle on FDR drive, heading west just before the Brooklyn Bridge. Footage taken north and east of the towers.

The second column in Table 6–1 lists the original format of the various videos that were analyzed. All the videos with the exception of one used the National Television System Committee (NTSC) video format, which is the standard television format in the United States. The V2 video used the Phase Alternating Line (PAL) video format, which is common in Europe and parts of Asia. Any image data from the interlaced field of the videos were neglected. It was also assumed that the digitized NTSC videos had a rate of 29.97 images per second, while the PAL videos had a rate of 25 images per second. The digitized images had sizes of 720x480 pixels (NTSC) and 720x576 pixels (PAL). The original video footage was assumed to have an aspect ratio of 1.33/1, so the X-values of the measured image coordinates were adjusted to account for the actual aspect ratio. The image coordinates were also shifted relative to the locations of fixed points in the field of view (corners of a tower) to eliminate the effects of movement and shaking of the camera.

6.2.2 Complex Motion Analysis

A complex motion analysis was the method originally used in this study to calculate the speed and the orientation and trajectory vectors of the aircraft. However, subsequent analysis methodologies, as discussed in the following sections, provided more accurate estimates of speed and orientation. The quality and limited video footage available produced larger uncertainty using the complex motion analysis methodology. Therefore, this analysis methodology was only used to define the aircraft trajectory. Following is a discussion on the complex motion analysis and an assessment of its accuracy.

The methodology used in this analysis to determine the aircraft impact conditions was previously developed for other applications (Cilke 1995). Figure 6–2 describes the analysis procedure. The image coordinates of the moving object (the aircraft) and two stationary positions on the structures within the field-of-view were triangulated with the known real-world positions of the structures and camera. The

camera was assumed to be a pin-hole type camera, i.e., all the light rays pass through a single focal point and project onto a flat surface that records the image. The result was the definition of the vector extending from the camera to the aircraft. However, the position of the aircraft along the vector was still unknown. The vector was then intersected with a surface defined by a set of vectors extending from a second camera to the measured object in multiple frames. The result was the real-world position of the aircraft at one instance in time. The global positions of other points on the aircraft and positions of the aircraft in multiple frames were then used to define the orientation and trajectory of the aircraft. Note that in ideal test conditions, where the video cameras and reference positions are precisely surveyed and the camera field-of-views are designed, the uncertainties in the measured object velocities range from 1 percent to 1.5 percent.

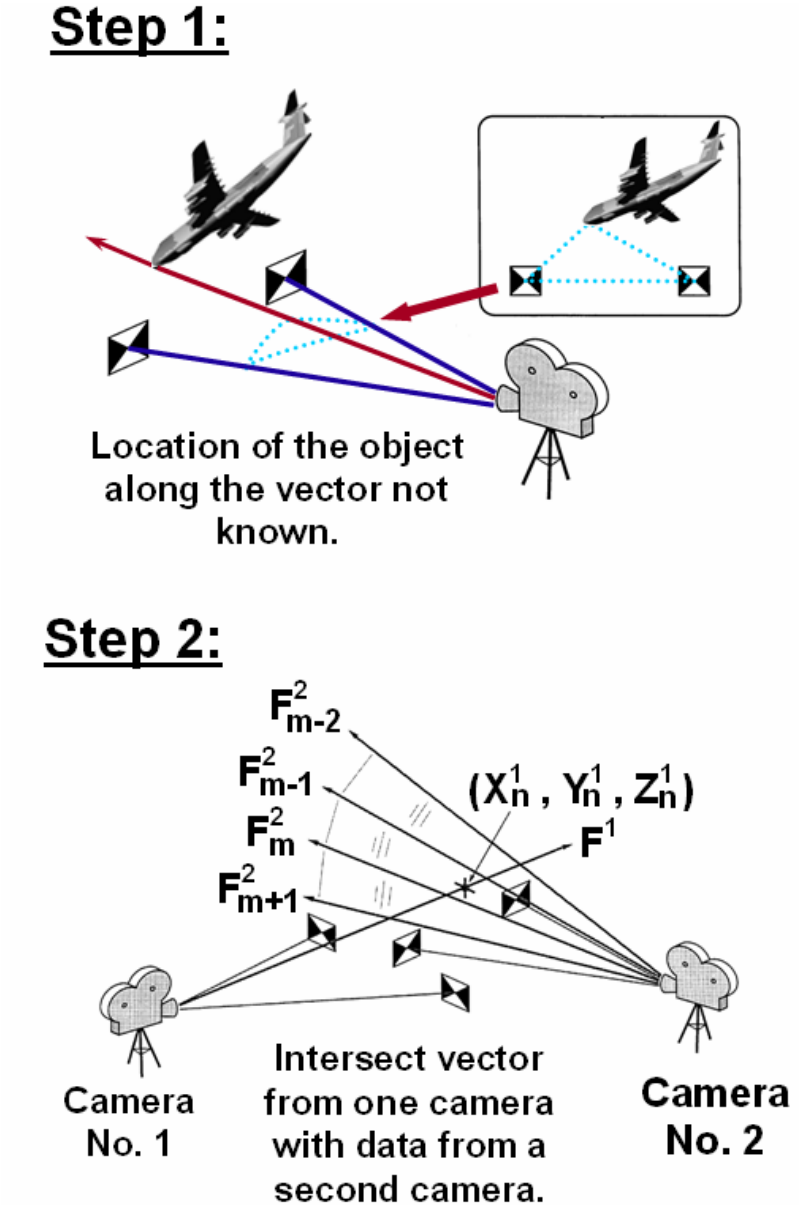

Figure 6–2. Complex motion analysis to measure object motions using multiple cameras.

For the WTC aircraft motion analysis, various locations on the two towers were used as fixed reference locations. The four corners of the towers at three floor levels were used, as they could be easily identified in the video footage. These three levels included the top floor and two mechanical floors. Additional points on the WTC 1 antenna were also used as reference locations. The tower reference positions were at the center of each beveled corner. The coordinates of the reference locations were determined by using the original construction drawings of the towers. While the locations on the structure could be determined with high fidelity, the coordinates of the cameras had to be estimated through an iterative process.

With the camera locations estimated, motion analyses were performed using the complex motion analysis technique. For the WTC 1 aircraft impact, image data from the V1 video were correlated with the data from the V2 video. The analysis produced a speed of 435 mph ± 30 mph for the WTC 1 aircraft at time of impact.

For the WTC 2 aircraft impact, data from each of the V4, V5, and V9 videos were correlated with the other two cameras to determine the motion of the aircraft prior to impact. The other cameras were less effective with this analysis technique (see Chapter 7 of NIST NCSTAR 1-2B for further details). Image data from the three videos converged to a tight set of trajectory angles and aircraft orientations (see Table 6–3). The uncertainties in the measured angles were derived from three components. First, there was a significant amount of scatter in the measured image coordinates. The perceived motion and orientation of the aircraft varied between frames, due to the relatively low resolution of the images and the motion of the camera fields-of-view. The scatter in the image data contributed to approximately ±2 degrees to ±4 degrees of the image uncertainty. The tips of the aircraft wings were more difficult to define accurately; the scatter in the wing measurements led to an estimated uncertainty of ±4 degrees in the roll angle. Second, the uncertainties in the camera locations contributed to the uncertainties in measured angles. Since there was more uncertainty in the cameras' horizontal positions than the vertical positions, the measured horizontal azimuths had larger uncertainties (±2 degrees). Third, the potential distortion in the field of view would distort the measured angles. The uncertainty of the measured angles due to image distortion was estimated to be ±1 degree.

The initial analyses using the complex motion methodology indicated the UAL 175 aircraft impact speed to be about 497 mph, which was heavily based on the V4 footage. However, subsequent analyses showed that the cameras did not provide an accurate aircraft impact speed due to three possible causes. First, the range of the camera could only be estimated. If the camera was close to the object motion, the range of the camera would have a significant effect on the perceived scale of the object in motion. Second, the scale of the image was determined from the dimensions of the towers in the field-of-view, which took up a relatively small portion of the field of view. As a result, the uncertainties in the measured image distances increased. Third, and most important, there were measurable distortions in the camera fields of view. For example, in the V5 video, the camera pans from left to right, tracking the aircraft as it approaches the south tower. The tower initially appears from the right edge of the image and moves to the center. The length of the aircraft (which remained in the center of the field-of view) appeared to decrease by 1.5 percent. However, the width of the south tower’s east edge appeared to decrease by 7 percent, indicating a significant distortion in the field of view. As a result, a simplified motion analysis procedure was used to determine the speed of the WTC 2 aircraft as described in the next section. The complex motion analysis was used only to define the aircraft orientation and trajectory vectors.

6.2.3 Simplified Motion Analysis

This procedure determined the impact speed by scaling the displacement of the aircraft within the field of view with the apparent fuselage length of the aircraft. Figure 6–3 depicts the simplified procedure to determine the aircraft speed. For several videos of the WTC tower impacts, linear regressions were performed for the image coordinates as functions of time. The displacements of the nose, tail, and wing tips were measured. The apparent length of the fuselage within each image was determined from the nose and tail regression lines, and the apparent displacement of the aircraft between images was normalized to the apparent length of the fuselage. Multiplying the result by the length of the aircraft determined the aircraft speed (there are constant time steps between frames). Finally, a geometric correction was made if the fuselage orientation and trajectory were not aligned.

The length of the fuselage of the Boeing 767-200ER aircraft is 155 ft (see Chapter 7 of NIST NCSTAR 1-2B). However, for the simplified motion analysis, the fuselage was assumed to have an apparent length of 153 ± 2 ft. The adjustment in apparent fuselage length was a result of the relatively low resolution of the video footage. As a sharp object entered a region captured by a single pixel, the background dominated the pixel color value until the object entered by a significant fraction. The low resolution could not accurately capture the shape of the aircraft nose and tail, and the aircraft nose in the videos appeared to be blunter than the actual nose of the Boeing 767-200ER. The average length of the fuselage in the videos analyzed was approximately 75 pixels (but varied depending on the footage). It was assumed that the resolution effect resulted in an apparent loss of approximately a half pixel at each end of the fuselage (one ft at each end of the fuselage). As a result, the apparent length of the fuselage in the video footage was approximately 2 ft less than the actual length.

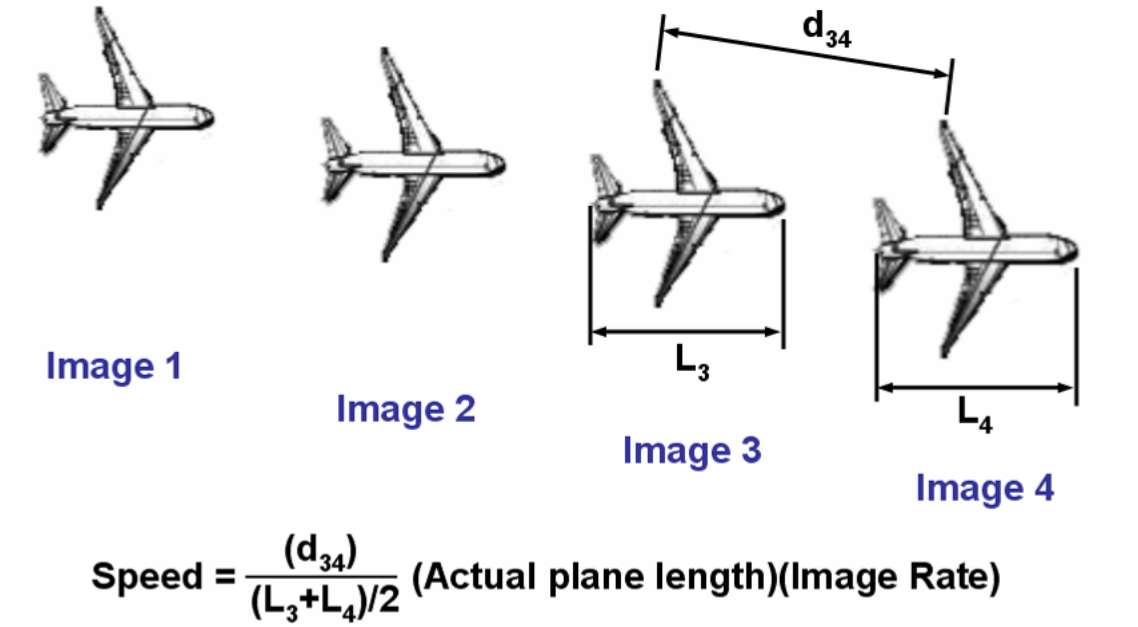

Figure 6–3. Simplified motion analysis procedure to determine aircraft speed.

The simplified motion analysis technique was used for the analysis of aircraft speed for both tower impacts. For the WTC 1 impact, only the V1 video could be used to determine the aircraft speed with this technique. The second video, V2, could not be used to obtain an accurate measure of speed as the aircraft

was traveling away from the camera. The simplified analysis produced a speed of 451 ± 30 mph, which was 16 mph higher than the value obtained from the complex motion analysis technique. Both of these values for the WTC 1 impact speed were within the uncertainties in the corresponding analyses. As a result, the WTC 1 aircraft impact speed provided in Table 6–3 was selected as the average of the two speeds obtained using the complex and simplified motion analysis methodologies.

Five videos with a viewing angle approximately perpendicular to the UAL 175 flight direction were used to estimate the aircraft speed at the time of impact. The results of the simplified motion analyses from each camera for UAL 175 are provided in Table 6–2. The uncertainties in the table were based on the scatter in the measured displacements, the aircraft length within the image, and uncertainty in the actual aircraft length as seen in the images due to unknown orientation. A systematic error in calculating the aircraft speed was introduced due to the lateral fuselage orientation relative to trajectory. The uncertainty in this value was due to the aircraft maneuvers during its approach. In calculating the uncertainty in the speed, an uncertainty of ±3 degrees in orientation was assumed.

A speed estimate was then calculated from the individual videos. A mean value was calculated using the weighted average of the mean values. The measurement precision (the reciprocal of the variance) was used as a weight factor on the mean values. If measurements were independent, the uncertainty in the mean could be calculated by summing the individual measurement precisions, giving 443 ± 21 mph for AA 11 and 542 ± 14 mph for UAL 175. However, some uncertainties were systematic and the actual bound on the uncertainty was larger as a result. Therefore, the uncertainty range was increased to ± 30 mph and ± 24 mph for AA 11 and UAL 175, respectively. A summary of the impact conditions derived from video analysis (both complex and simplified motion analyses) is presented in Table 6–3.

Table 6–2. Measured UAL 175 impact speeds using the simplified analysis methodology.

Video Reference	Calculated Aircraft Speed
V4	573 ± 55 mph
V5	556 ± 27 mph
V6	535 ± 23 mph
V7	523 ± 31 mph
V9	557 ± 53 mph
Best Estimate Speed	542 ± 24 mph

Table 6–3. Summary of measured aircraft impact conditions from video analysis.

	AA 11 (WTC 1)	UAL 175 (WTC 2)
Impact Speed (mph)	443 ± 30	542 ± 24
Vertical Approach Angle (Velocity vector)	10.6° ± 3° below horizontal (heading downward)	8° ± 4° below horizontal (heading downward)
Lateral Approach Angle (Velocity vector)	180.3° ± 4° clockwise from Structure North	19° ± 6° clockwise from Structure North
Vertical Fuselage Orientation from horizontal	—	3° ± 4° below horizontal (heading downward)
Lateral Fuselage Orientation from Structure North	—	8° ± 6° clockwise from Structure North[a]
Roll Angle (left wing downward)	25° ± 4°	38° ± 4°

a. Structure North is approximately 29 degrees clockwise from True North.

Initial results from the simplified motion analysis produced a mean speed for UAL 175 of 546 mph. This speed was therefore used in the global impact analysis, discussed in Chapter 7. Subsequent refinement of the analysis and associated uncertainties produced the slightly lower mean value of 542 mph as discussed above. Since this difference in speed was less than 1 percent and well within the uncertainty range, the speed used for the impact analysis was not modified.

6.3 REFINEMENT OF AIRCRAFT IMPACT CONDITIONS

Estimates of the aircraft impact locations, orientations, and trajectories were further refined based on the damage patterns documented on the exterior walls of the WTC towers. The general approach was to visualize the aircraft within the range of flight conditions estimated from the video analysis (Section 6.2) and project the impact points of the wings, fuselage, engines, and vertical stabilizer onto the exterior wall of each tower. A damage pattern was then estimated and compared to that obtained previously from analysis of the film and photographic evidence.

The estimated damage to the north face of WTC 1 is shown in Figure 6–4 along with approximate impact locations for various aircraft components of AA 11, including the wind tips, vertical stabilizer tip, and engines. For AA 11, it was found that the fuselage orientation needed to be 2 degrees above the vertical approach angle (2 degrees nose-up). The difference in the lateral approach angle and the fuselage orientation from structure north was 0°.

An example impact condition is shown in Figure 6–5, where the vertical approach angle was 10.6 degrees (fuselage orientation from horizontal = 8.6 degrees) and the lateral approach angle was 180° (fuselage orientation from structure north = 180 degrees). The position of the vertical stabilizer tip was the most critical factor in determining this relationship. The impact points of the wing tips were known to within approximately ±2 ft. This corresponded to an uncertainty in the roll angle of approximately ±2 degrees. Since no accurate orientation information could be derived from the video analysis, analysis of the damage pattern was critical in estimating the aircraft orientation at the time of impact.

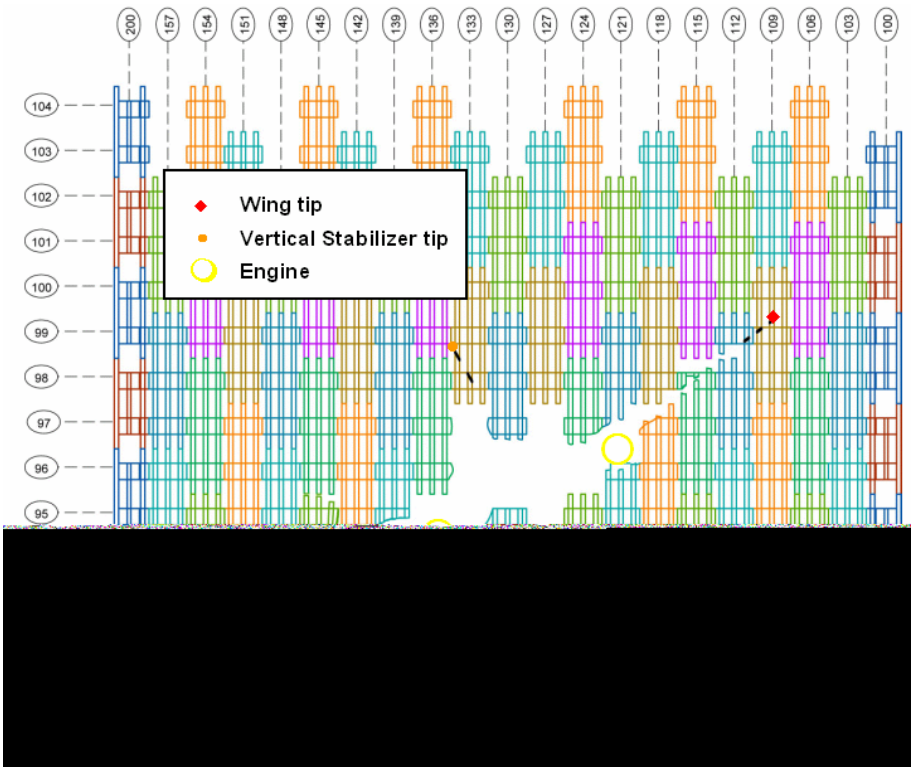

Figure 6–4. Estimated impact locations of aircraft components superimposed on the damaged face of WTC 1.

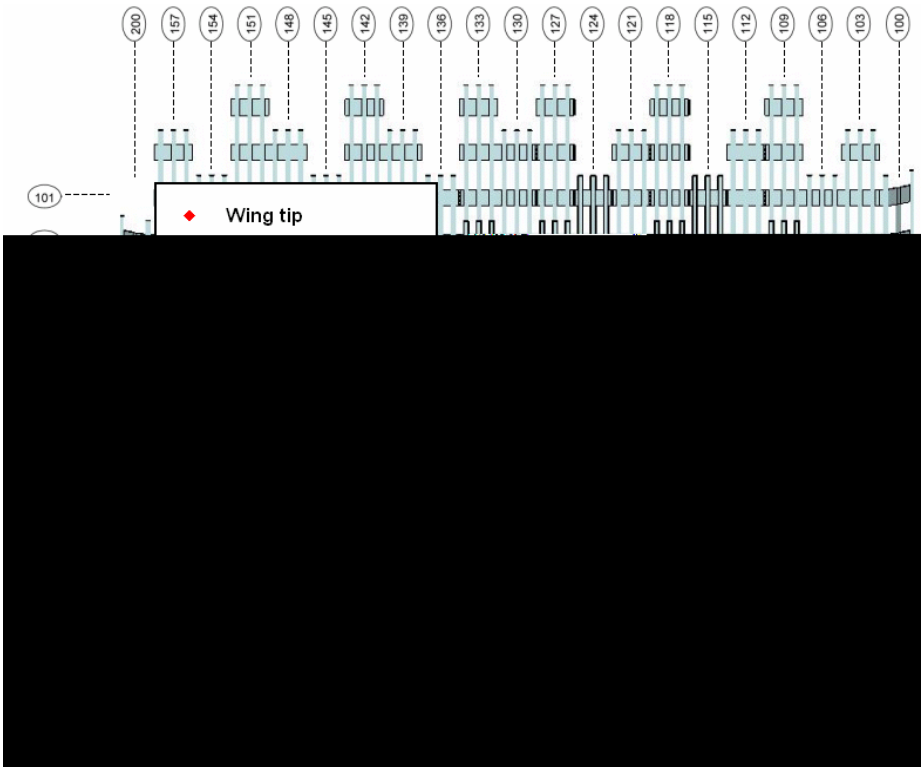

Figure 6–5. Orientation and trajectory of AA 11 that matched the impact pattern (vertical approach angle = 10.6°, lateral approach angle = 0°).

The estimated damage to the face of WTC 2 is shown in Figure 6–6, along with approximate impact locations for various aircraft components of UAL 175. From these impact locations, the combinations of flight conditions that were consistent with the observed impact damage could be estimated.

Figure 6–7 shows the south face of WTC 2 with the aircraft model positioned in the impact orientation and location estimated from the video analysis (Table 6–3). The viewpoint of the figure was along the trajectory axis so that the projection of each aircraft component onto the tower face represented its approximate impact location, assuming no significant structural deformation prior to impact with the building exterior. During the impact simulation, little structural deformation was observed in parts of the aircraft that had not yet impacted the towers. The vertical stabilizer, the last part of the aircraft to enter the building and the part that had the longest time to experience structural deformation, impacted close to this projected impact location.

The impact conditions shown in Figure 6–7, which were based on video analysis alone, would cause the starboard wing tip to miss the building and were, therefore, not physically possible. Also shown in the figure are the estimated impact locations for the wing tips, vertical stabilizer, and engines. These also did not align well with the observed impact damage. Translation of the aircraft alone did not account for the discrepancy in the impact point shown in the figure. Both a translation of 3.3 ft higher and 9.8 ft further west were needed, along with a specific relationship between the trajectory and orientation in order for the impact pattern to match. The final impact points, defined as the location where the nose of each aircraft initially contacted the towers, are provided in Table 6–5.

It was found that a strict relationship between the aircraft trajectory and orientation needed to be established in order to achieve an impact pattern consistent with the damage observed on the south wall of WTC 2. The fuselage orientation needed to be 1degree above the vertical approach angle (i.e., 1 degrees nose-up). The difference in the lateral approach angle and the fuselage orientation from structure north was 3 degrees as listed in Table 6–3. An example impact condition for UAL 175 is shown in Figure 6–8, where the vertical approach angle was 6 degrees (fuselage orientation from horizontal= 5 degrees) and the lateral approach angle was 13 degrees (fuselage orientation from structure north= 10 degrees). Larger or smaller angles resulted in projected impact points with the engines spaced too far horizontally or vertically or with the tip of the vertical stabilizer in the wrong location. Also, note that the impact point of the nose had been moved from original estimates, as previously discussed, and that the roll angle was maintained. A second example of an acceptable impact condition, this time with a lateral approach angle of 17 degrees, is shown in Figure 6–9.

The relationship between aircraft trajectory and orientation was then used to reduce the uncertainty of these parameters. The uncertainty in the vertical approach angle from the video analysis varied from 4 degrees to 12 degrees, as shown in Table 6–3, and the fuselage orientation from horizontal varied from –1 degrees to 7 degrees. As a 1 degree difference needed to be maintained in order for the impact pattern to match the observed damage, uncertainty in the vertical approach angle was reduced to 6 degrees ± 2 degrees and the fuselage orientation from horizontal to 4 degrees ± 1 degrees. Uncertainty in the lateral approach angle and the fuselage orientation from structure north was similarly reduced, as shown in Table 6–4. The impact points of the wing tips were known to within approximately ± 2 ft. This corresponded to an uncertainty in the roll angle of approximately ±2 degrees.

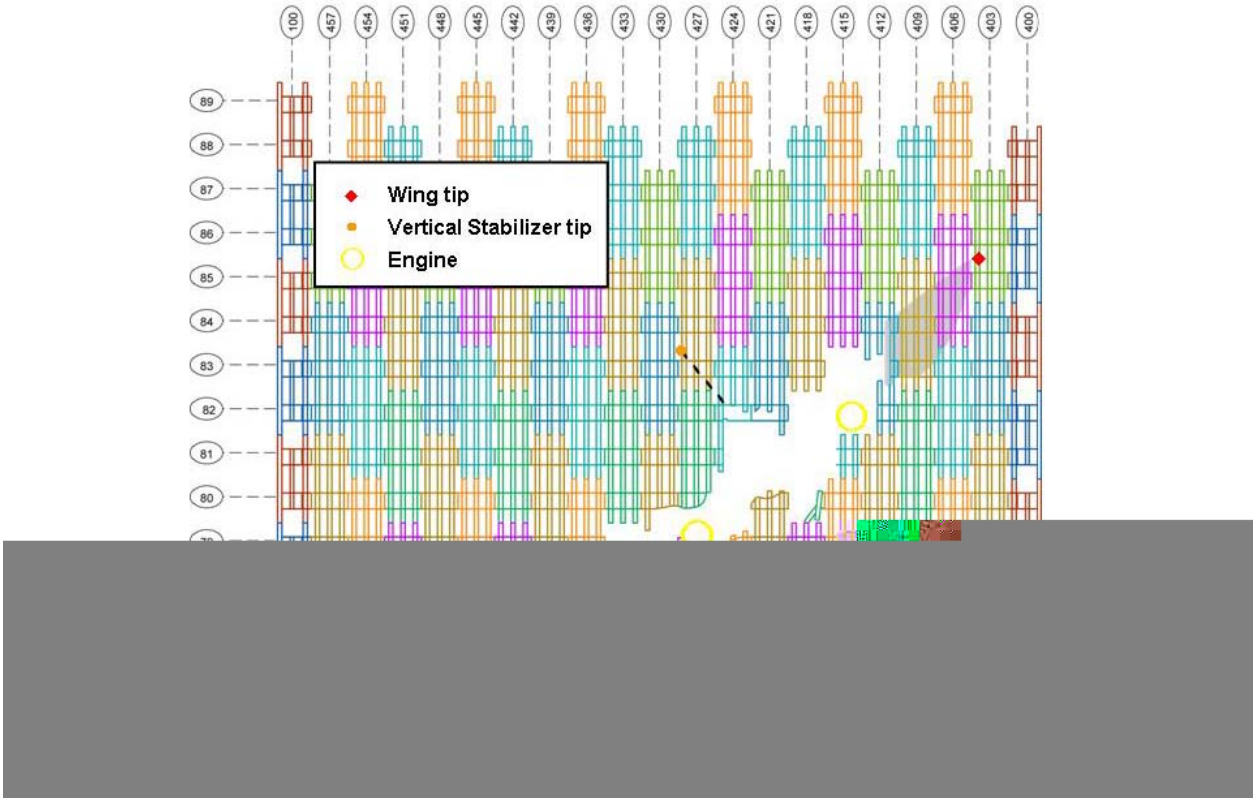

Figure 6–6. Estimated impact locations of aircraft components superimposed on the damaged face of WTC 2.

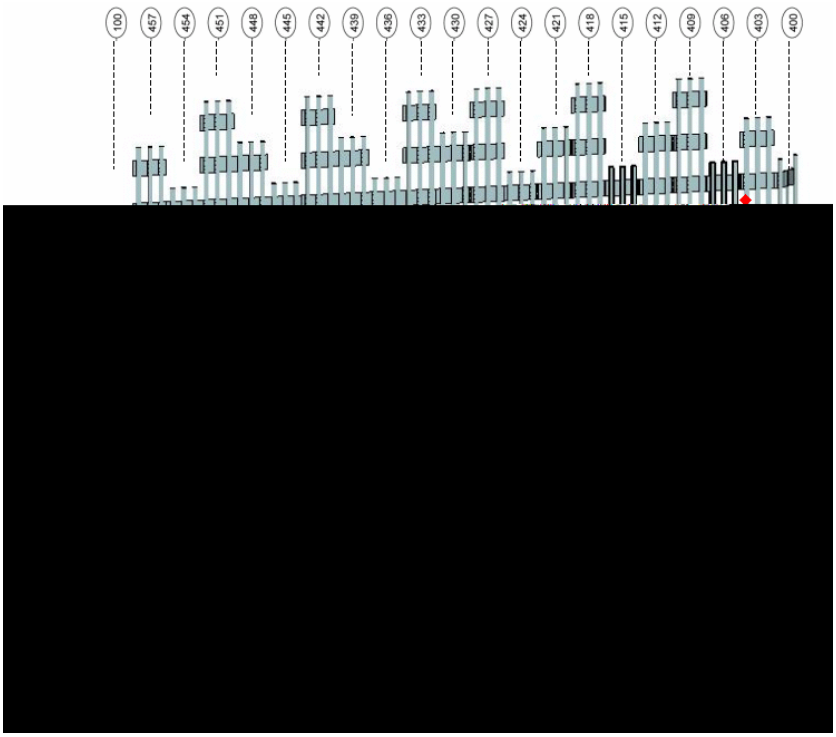

Figure 6–7. Orientation and Trajectory of UAL 175 from Video Analysis.

Table 6–4. Aircraft impact locations on the WTC towers.

	Horizontal Location	Vertical Location
AA 11 (WTC 1)	2.0 ± 3 ft west of tower centerline	1.6. ± 4 ft above floor 96
UAL 175 (WTC 2)	23.1 ± 3 ft east of tower centerline	0.6. ± 4 ft above floor 81

Table 6–5. Summary of refined aircraft impact conditions.

	AA 11 (WTC 1)	UAL 175 (WTC 2)
Impact Speed (mph)	443 ± 30	542 ± 24
Vertical Approach Angle (Velocity vector)	10.6° ± 3° below horizontal (heading downward)	6° ± 2° below horizontal (heading downward)
Lateral Approach Angle (Velocity vector)	180.3° ± 4° clockwise from Structure North	15° ± 2° clockwise from Structure North
Vertical Fuselage Orientation Relative to Trajectory	2° nose-up from the vertical approach angle	1° nose-up from the vertical approach angle
Lateral Fuselage Orientation Relative to Trajectory	0° clockwise from lateral approach angle	-3° clockwise from lateral approach angle
Roll Angle (left wing downward)	25° ± 2°	38° ± 2°

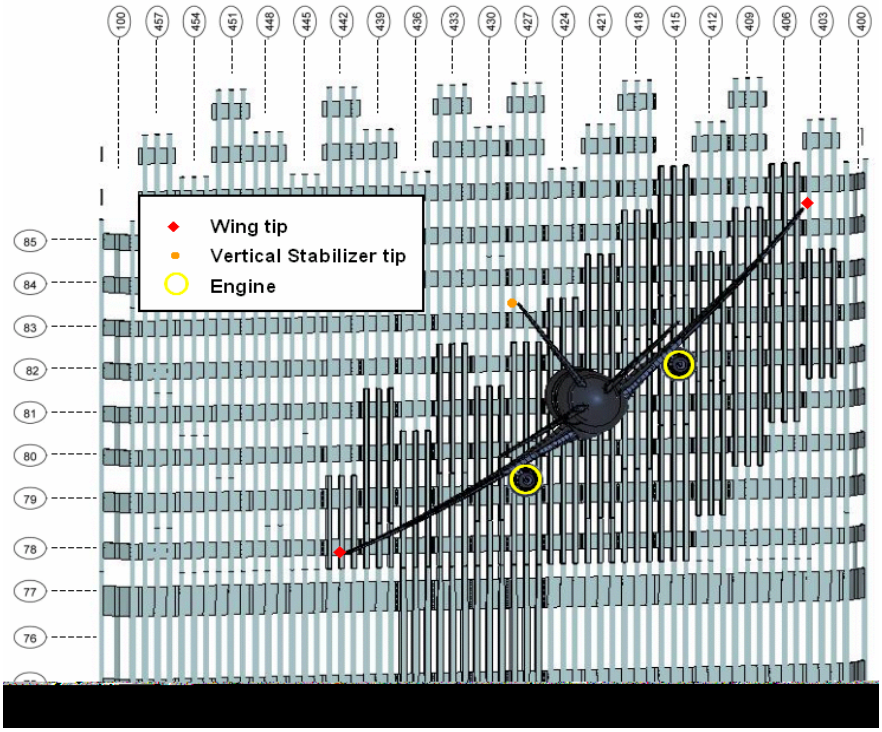

Figure 6–8. Orientation and trajectory of UAL 175 that matches the impact pattern (vertical approach angle = 6°, lateral approach angle = 13°).

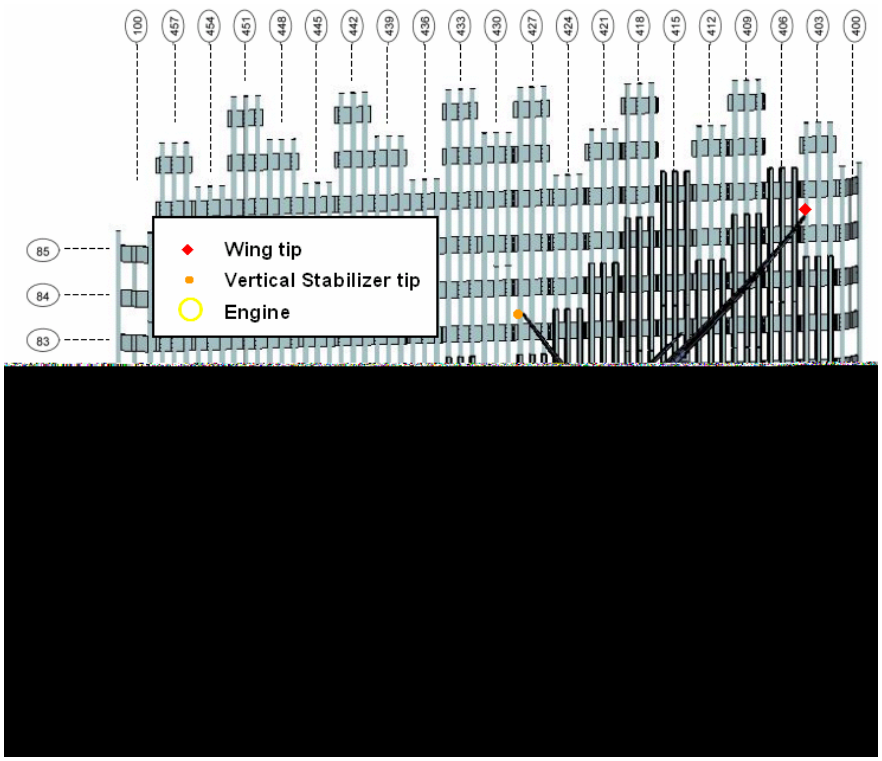

Figure 6–9. Orientation and trajectory of UAL 175 that matches the impact pattern (vertical approach angle = 6°, lateral approach angle = 17°).

Although the lateral approach angle of UAL 175 had a nominal value of 15 degrees, additional observable information was used to define the most probable flight condition. Figure 6–10 shows the top view of WTC 2 with the engines and landing gears in their pre-impact location. Also shown is the projected trajectory of the starboard engine of UAL 175, with an initial lateral approach trajectory of 13 degrees instead of 15 degrees, assuming the engine was not significantly deflected as it passed through the building. With this lateral trajectory, the starboard engine would exit the tower at the north east corner, consistent with the observables from video and photographic evidence. As a result, a lateral approach trajectory of 13 degrees was used for all WTC 2 impact simulations.

It is possible that the tower structure and/or contents could have deflected the engine from its initial lateral trajectory. The global simulations used a standard configuration for building contents similar to WTC 1. This configuration did not cause substantial deviation in the trajectory of the starboard engine. This lateral trajectory was, therefore, the most likely and was adopted for the global analyses.

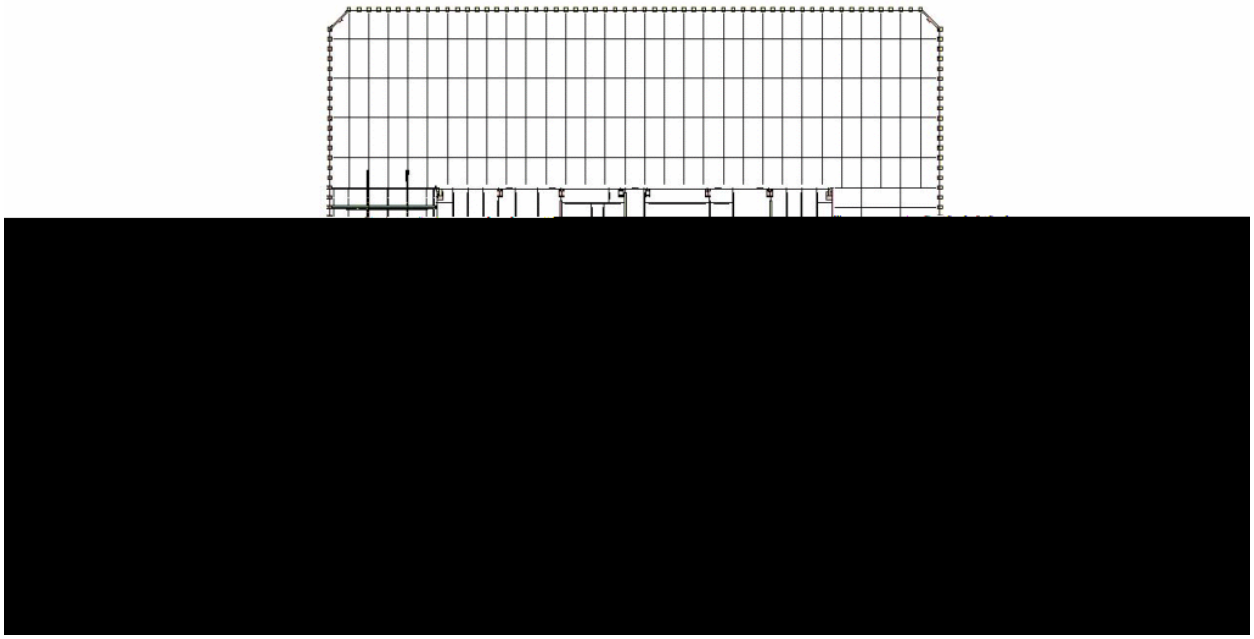

Figure 6–10. Projected trajectory of the starboard engine of UAL 175 with an initial lateral approach angle of 13°.

6.4 COMPARISON WITH PREVIOUS ESTIMATES OF AIRCRAFT IMPACT INITIAL CONDITIONS

Alternate analyses and values of the aircraft impact initial conditions were performed and reported by other studies. The objective of this chapter was to provide an independent assessment using the full database of video and photographic evidence collected and maintained by NIST. Many of these data sources may not have been available in the previous analyses. In this section, a comparison is presented between the aircraft impact conditions estimated in this study and those reported earlier. This comparison provides an opportunity to review the methodologies applied, as well as assists in the determination of the uncertainties in the impact conditions. The comparison includes estimates or analyses performed by the Federal Emergency Management Agency (FEMA), Federal Bureau of Investigation (FBI) (reported in the New York Times), Hart-Weidlinger, and MIT, and the analyses presented in this chapter (NIST). The analysis methodologies and data sources used for the FEMA and FBI estimates of the impact speeds were not available. As a result, an evaluation of those estimates of impact conditions and determination of their uncertainties could not be made. In addition, preliminary estimates of the speed based on a simplified analysis of a single video footage for each tower (V1 video for WTC 1 and V6 video for WTC 2) were conducted by Project 5 (NIST NCSTAR 1-5A) and are included in this comparison.

Table 6–6 compares the results of the motion analyses for the AA 11 impact. Both the Hart-Weidlinger and Massachusetts Institute of Technology (MIT) analyses utilized the Doppler shift of the engine noise to determine the aircraft speed. The Hart-Weidlinger velocity analysis was based on AA 11 approaching the north tower at an angle 4 degrees shallower than the analyses presented here (NIST analysis in Table 6–6). If the Hart-Weidlinger analysis had the aircraft approaching at a steeper angle, it would have reported a speed much closer to the MIT and NIST analyses. The difference between the speed estimated from this study and that from the simplified analysis (NIST NCSTAR 1-5A) was about 5 percent. However, both speeds were well within the uncertainty range. One significant difference in the analyses

of the AA 11 impact conditions was that none of the previous analyses had the opportunity to utilize the V2 video. This second video from a different location was very helpful to determine the motion parameters of the AA 11.

Table 6–6. AA 11 (WTC 1) aircraft impact analysis comparison.

	FEMA[a]	FBI[b]	Hart-Weidlinger[c]	MIT[d]	NIST Simplified Analysis[e]	NIST
Best Estimate Speed (mph)	470	494	500	429	466	443
Speed Error Estimate (mph)			+ 30 / - 50	± 51	± 34	± 30
Lateral Approach Angle (clockwise)			4.3º			0.3º ± 4º
Vertical Approach Angle (downward)			6.2º			10.6° ± 3°
Aircraft Roll (left wing down)			20.7º			25º± 2°

a. FEMA World Trade Center Building Performance Study, May 2002. Analysis methodology or data source not available.
b. Lipton, E. and J. Glanz, 2002, "First Tower to Fall Was Hit at Higher Speed, Study Finds," The New York Times, February 23
c. Levy, M. and Abboud N., 2002, "World Trade Center – Structural Engineering Investigation," Hart-Weidlinger.
d. The Towers Lost and Beyond, Massachusetts Institute of Technology, Eduardo Kausel.
e. NIST NCSTAR 1-5A.

Table 6–7 compares the results of the various motion analyses for the UAL 175 impact. The Hart-Weidlinger and the analyses presented here were consistent with the exception of the lateral approach angle. The MIT estimates of impact speed were low compared to the other analyses. However, assuming a lateral approach angle of 20 degrees would have increased the MIT estimate of the UAL 175 impact speed to about 524 mph. The simplified analysis (NIST NCSTAR 1-5A) yielded a speed that was very close to that obtained in this study.

Table 6–7. UAL 175 (WTC 2) aircraft impact analysis comparison.

	FEMA[a]	FBI[b]	Hart-Weidlinger[c]	MIT[d]	NIST Simplified Analysis[e]	NIST
Best Estimate Speed (mph)	590	586	550	503	545	542
Speed Error Estimate (mph)				± 38	± 18	± 24
Lateral Approach Angle (clockwise)			11.7º	15º		15° ± 2°
Vertical Approach Angle (downward)			2.7º	0º		6° ± 2°
Aircraft Roll (left wing down)			30.1º			38°± 2°

a. FEMA World Trade Center Building Performance Study, May 2002. Analysis methodology or data source not available.
b. Lipton, E. and J. Glanz, 2002, "First Tower to Fall Was Hit at Higher Speed, Study Finds," The New York Times, February 23
c. Levy, M. and Abboud N., 2002, "World Trade Center – Structural Engineering Investigation," Hart-Weidlinger.
d. The Towers Lost and Beyond, Massachusetts Institute of Technology, Eduardo Kausel.
e. NIST NCSTAR 1-5A.

6.5 SUMMARY

Three methods were used to estimate the impact conditions for the two aircraft that impacted the WTC towers. The initial impact conditions included aircraft speed, horizontal and vertical angles of incidence, roll angle of each aircraft, and the location of nose impact with each tower. The estimates also included the uncertainties associated with these parameters. The first method used a comparison of videos from different positions to calculate the three-dimensional trajectory of the aircraft. The second method used the relative frame-by-frame motion in a single video, scaled to the length of the aircraft in the video to calculate the impact speed. Finally, analysis of the impact damage on the face of each tower was used to refine the relative impact orientation and trajectory. This was done by matching the projected impact points of the wings, fuselage, engines, and vertical stabilizer onto the exterior wall of each tower to the observed damage pattern.

6.6 REFERENCES

Cilke, R.W., (1995), "Motion Picture Analysis Procedures for Impact Parameters of Air-Delivered Weapons," FCT-LR-95-6, prepared by Applied Research Associates, Inc., Letter Report to the Defense Nuclear Agency, June.

FEMA, May 2002, “World Trade Center Building Performance Study: Data Collection, Preliminary Observations and Recommendations,” FEMA 403.

Kausel, E., “The Towers Lost and Beyond,” Massachusetts Institute of Technology, May, 2002, http://web.mit.edu/civenv/wtc/index.html.

Levy, M. and Abboud N., August 1, 2002, “World Trade Center – Structural Engineering Investigation,” Hart-Weidlinger Technical Report, Prepared for Wachtell, Lipton, Rosen, and Katz.

Lipton, E. and J. Glanz, 2002, “First Tower to Fall Was Hit at Higher Speed, Study Finds,” The New York Times, February 23.

Chapter 7
AIRCRAFT IMPACT DAMAGE RESULTS

7.1 INTRODUCTION

This chapter presents the results of the analyses of the aircraft impacts into the two World Trade Center (WTC) towers. The analysis results include the estimation of the structural damage and the condition and position of nonstructural contents such as partitions, workstations, aircraft fuel, and other debris that influenced the behavior of the subsequent fires in the towers. These results were used to provide the initial conditions for the subsequent structural analyses (level of damage to columns and floor systems) and damage to fireproofing due to debris impact. The global impact simulations provided, for each tower, a range of damage estimates. These included the base case, based on reasonable initial estimates of all input parameters, along with a less severe and a more severe damage scenario. The less severe damage case did not meet two key observables: (1) no aircraft debris was calculated to exit the side opposite to impact and most of the debris was stopped prior to reaching that side, in contradiction to what was observed in photographs and videos of the impact event (see Section 7.10), and (2) the fire-structural and collapse initiation analyses of the damaged towers (NIST NCSTAR 1-6) indicated that the towers would not have collapsed had the less severe damage results been used. As a result, this chapter provides detailed description of the results of the analyses pertaining to the base case and the more severe case, which were used as the initial conditions for the fire dynamics simulations (NIST NCSTAR 1-5F), thermal analyses (NIST NCSTAR 1-5G), and fire-structural response and collapse initiation analyses (NIST NCSTAR 1-6). Only a brief description is provided for the less severe damage results for comparison purposes. The details of the less severe damage estimates can be found in National Institute of Standards and Technology (NIST) NCSTAR 1-2B.

Section 7.2 provides a description of the analysis methodology, including assumptions and limitations. Sections 7.3 and 7.4 provide detailed description of the impact analysis results for the base case and the more severe case, respectively for WTC 1. Sections 7.6 and 7.7 provide similar results for WTC 2. Sections 7.5 and 7.8 provide a brief description of the less severe case results for WTC 1 and WTC 2, respectively. The last three sections present different comparisons. Section 7.9 presents a comparison of the impact response between WTC 1 and WTC 2. Section 7.10 compares the simulation results with observables based on video and photographic evidence as well as eyewitness interviews. Section 7.11 presents a comparison between the damage estimates from this study with those from previous studies. A summary is provided in Section 7.12.

7.2 ANALYSIS METHODOLOGY, ASSUMPTIONS, AND LIMITATIONS

The impact analyses were performed using the LS-DYNA finite element code (LS-DYNA Version 971). LS-DYNA is a commercially available nonlinear explicit finite element code for the dynamic analysis of structures (LSTC 2003) and has been used for a wide variety of crash, blast, and impact applications. The impact analyses used a variety of capabilities and algorithms in LS-DYNA. A brief description of these capabilities is described in this section. A significantly detailed description of the analysis methods is provided in the LS-DYNA Theoretical Manual (1998).

The impact simulations used a nonlinear transient analysis with an explicit dynamics solver. This solver allows for simulating softening and failure of components in the analysis. The analysis solved the dynamic system of equations with a very small time increment ($\Delta T \approx 0.8$ μs), and with external loading defined as the initial conditions of the aircraft (velocity vector and location of the aircraft, see Chapter 6). Such analysis utilizes a number of capabilities that might not be customarily used in structural engineering applications. These include the following:

- Element erosion: Damage and failure of components were included in the models through the constitutive algorithms. Damage criteria (such as maximum plastic strain) were tracked for each element within the constitutive model evaluation, and elements were eroded when the failure criteria were exceeded. This allowed for a direct evaluation of damage and failure within the impact simulations. The eroded elements allow for the initiation and extension of fracture in the model. Eroded elements no longer supported any stress, and the strains in the eroded elements were no longer calculated. The associated mass of the elements remained with the nodes in the calculation. If adjacent elements did not reach the failure surface, the nodes remained attached to the structure. If all of the elements connected to a specific node failed, the node became a free particle. Free nodes can either be eliminated from the calculation or remain in the calculation with associated inertial properties and potential for impacts against other structural components (free nodes remain in contact algorithms).

- Contact behavior: A contact algorithm was used to detect contact between two bodies and to estimate the forces generated by this contact. Overall contact in the impact analyses was modeled using the automatic single surface contact algorithms in LS-DYNA. Interacting components were defined by a material list, and contact segments were automatically generated by LS-DYNA. This greatly simplified the specification of contact between various components in the aircraft and tower structures. The type 1 soft constraint option was used in the contact algorithm that determined the contact stiffness based on stability considerations, time step size, and nodal mass. This soft constraint option was found to be more robust than the default penalty formulation for modeling the complex contact behaviors in large impact and crash simulations.

- Complex failure modes: In specific applications, unique algorithms were required to introduce failure modes in the analysis. These were primarily used in modeling the response and failure of connections (see Chapter 5 for description of some of these connections). An example is the splice between core columns, where the connection between the splice plate and column flange was modeled with a surface-to-surface tied interface without failure. This resulted in a perfect bond between the nodes of the splice plate and the flange of the adjacent column. When columns were pulled apart, the elements at the splice plate spanning the gap between column ends would be stretched. Failure of the splice plate in the model resulted from ductile failure of the splice plate in the elements spanning the connection.

- Fluid-structure interaction: This was needed to model the fuel impact on the exterior wall and the subsequent dispersion inside the towers. The Smooth Particle Hydrodynamics (SPH), which utilizes a mesh free approach, was used to model the fuel in the impacting aircraft. In this approach, fuel was modeled as particles that were allowed to interact with the structure of the aircraft and tower.

The finite element meshes used in the impact analyses typically used elements with single point integration. The biggest disadvantage of the single point integration is the potential for hourglassing or zero energy modes. There are several methodologies for controlling hourglass modes in LS-DYNA. The typical approach used in the impact analyses was to apply a viscous hourglass control where a viscous damping was introduced that suppressed the formation of hourglass modes, but did not significantly influence the global modes.

As mentioned in Chapter 5, the global impact simulations were limited by the maximum finite element model size that could be executed on the available 32-bit computer clusters. The primary assumptions and limitations of the global impact analyses were the result of reducing the model size to meet this limitation, as well as to achieve a run time that allowed the global impact analyses to be completed within the duration of the investigation.

Although the analyses were performed on a 32 bit computer cluster, the precision used in the analyses can be controlled by the analysis software. Both single precision and double precision versions of LS-DYNA were available for the impact analyses. In general, single precision analyses are more efficient and the precision is sufficient for the type of impact simulation being performed. However, when the dimensions of the structure being analyzed are sufficiently large, the single precision analyses can introduce rounding errors in the analyses. The rounding errors occur since the analysis is resolving deformations or analyzing element penetrations on a local scale that is several orders of magnitude smaller than the controlling dimension.

In preliminary simulations, the coordinate system for the models of the tower structures was located near the base of the tower. As a result, the largest dimensions were the vertical position of the structures in the impact zone. This large vertical dimension controlled the size scale in the impact analyses and introduced rounding errors that were manifested as unstable element behaviors. To eliminate this precision problem, the tower model coordinate system was moved to be centered on the impact zone of the tower. The largest controlling dimension was therefore the distance across tower (significantly smaller than the height of the tower). After adjusting the coordinate location, the unstable element behaviors were no longer observed.

To confirm the adequacy of the single precision analysis, subassembly impact analyses (Section 5.4.5) were performed on the same model in both single and double precision. The comparison of the two analyses showed no substantial difference in the impact response and damage.

Specific assumptions and limitations introduced in the analyses to meet the computational and time constraints included:

- Tower structures away from the impact zone had a coarse mesh resolution, and as a result, damage in these regions may not have been accurately captured. An example is the potential damage to the exterior wall on the far side of the tower (opposite to impact). As debris passed through the building and struck a panel on the far side, the coarse mesh and merged boundary conditions at column ends (as opposed to bolted connections in the impact zone) underestimated the secondary impact damage.

- Tower contents (workstations and nonstructural walls) were only included in the expected path of the aircraft impact and subsequent debris cloud. Therefore, debris and fuel that

passed beyond this region could move more freely through the structure, only interacting with primary structural components. Also, the workstation layout from WTC 1 was used for WTC 2. That added an additional uncertainty to the nonstructural building contents for WTC 2.

- The analysis of the impact response of the aircraft fuel cloud had several limitations. Smooth Particle Hydrodynamics (SPH) was used to model the fuel in the impacting aircraft. The air in and around the towers was not modeled, so the deceleration of the fuel particles in the cloud by aerodynamic resistance was not included. The contact algorithm for the fuel particles and tower did not include a sticking or "wetting" behavior so the fuel particles would bounce off of components in the tower. The results of these limitations would spread the fuel cloud over a larger region in the simulation. Finally, the deflagration of the fuel was not modeled, and the resulting dynamic over-pressures in the tower from the combustion process were not included in the analysis.

- Windows were not modeled on the exterior of the tower. The open space between the exterior columns allowed fuel particles and small debris fragments from the aircraft and tower to escape that may have been contained if the windows were included. Note, however, that the weight of the windows was added to the columns as part of the superimposed dead loads.

- The rotational velocity of the spinning aircraft engine components was not modeled. The effects of the rotational kinetic energy, spin stabilization of the engine trajectory, or potential for engine thrust during impact were, therefore, not included in the analysis. An analysis was performed to estimate the magnitude of the effects of this assumption (see Chapter 10 of NIST NCSTAR 1-2B). The analysis indicated that the rotational kinetic energy of each engine was approximately one percent of the aircraft initial kinetic energy. In addition, much of this rotational energy was probably dissipated by internal deformations of the engine components following impact with the tower exterior. Therefore, this approximation should have had a small influence on the global impact damage.

- Aeroelastic forces were not applied to the aircraft wings since the resulting stresses were not expected to affect the impact response. A wing tip deflection of 52 in. was applied to the aircraft model based on photographic evidence.

- Gravitational acceleration was modeled during the impact analyses to include the gravity effects on debris movement and potential contributions to the collapse of the damaged truss floor regions. However, initial service loads (stresses) in the tower and aircraft were not included. The material internal energy associated with the elastic service loads were small compared to the material internal energy capacity. Therefore, their execution was not expected to have a significant influence on the dynamic impact response and deformation. Simplified analyses were performed to evaluate the magnitude of the effects of this assumption for the impact response of a core column (see Chapter 10 of NIST NCSTAR 1-2B). These analyses indicated that ignoring the static preload in the column had little influence on either the dynamic column deformations or the reserve capacity of the column.

- The impact analyses were subject to uncertainties in the input parameters, such as initial impact conditions, material properties and failure criteria, aircraft mass and stiffness properties, mass distribution inside the towers, the jet fuel distribution and dispersion, connections behavior, the presence of nonstructural building contents, etc. Sensitivity analyses were conducted as described in Chapter 8 of NIST NCSTAR 1-2B to assess the effects of these parameters on the damage estimates. The global analyses not only provided a "base case" based on reasonable initial estimates of all input parameters, but also provided a range of damage estimates based on variations of the most influential parameters, identified in the sensitivity analyses.

7.3 WTC 1 BASE CASE IMPACT ANALYSIS – CASE A

This case is referred to as Case A in the remainder of the WTC Investigation reports. This analysis provided an estimate of the impact damage based on reasonable initial estimates of all the variables obtained from photographic evidence, material testing, and data in the open literature. The combined aircraft and tower model used for the base case global impact conditions of WTC 1 is shown in Figure 7–1.

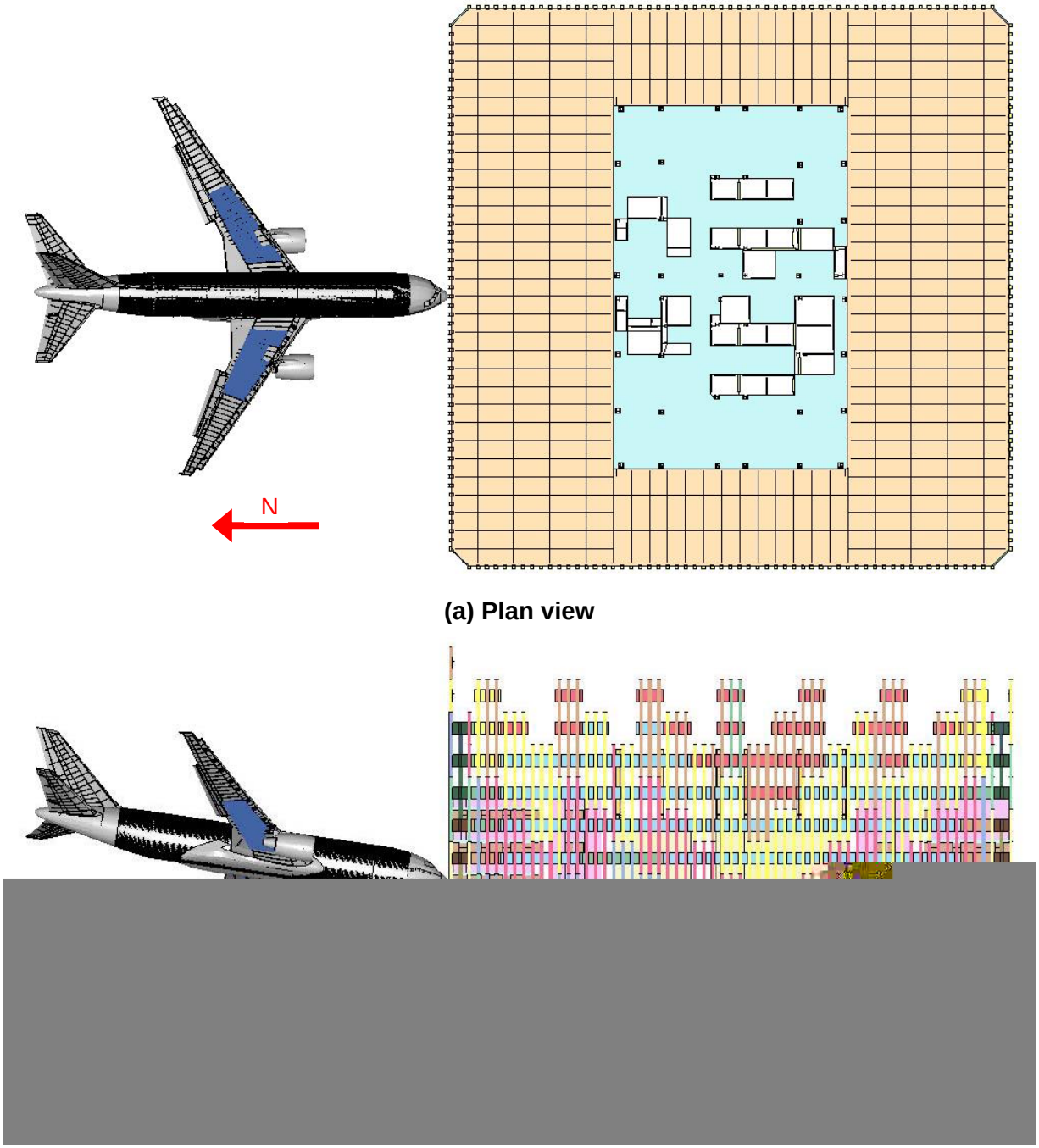

(a) Plan view

(b) Side view

Figure 7–1. WTC 1 global impact model.

The WTC 1 base case analysis was performed for a 0.715 s duration following initial impact of the aircraft nose with the north exterior wall. The analysis was performed on a computer cluster using twelve 2.8 GHz Intel Xeon processors, each on a separate node of the cluster. The run time for this analysis was approximately two weeks. The progress of the global impact simulations was monitored on average every two days. The calculations were terminated when the damage to the towers reached a steady state

and the motion of the debris was reduced to a level that was not expected to produce significant impact damage. The residual kinetic energy in the airframe components at the termination of the global impact simulation was less than one percent of the initial kinetic energy at impact.

7.3.1 Impact Response

The impact response of WTC 1 is shown in side and plan views in Figure 7–2 and Figure 7–3, respectively. The response is shown at intervals of 0.1 s from impact through the initial 0.5 s of the response. The initial 0.1 s of the response, shown in Figure 7–2(b) and Figure 7–3(b), was dominated by the impact, penetration, and fragmentation of the forward fuselage structures. The engines and wing sections were just starting to impact the exterior wall. The forward fuselage structures were severely damaged both from the penetration through the exterior columns and the interaction with the 96th floor slab that sliced the fuselage structures in half. The downward trajectory of the aircraft structures caused the airframe to collapse against the floor, and the subsequent debris motion was redirected inward along a more horizontal trajectory parallel to the floor.

By 0.2 s after impact, the wings completely penetrated the exterior wall, and only the tail structures were still outside the tower, as shown in Figure 7–2(c) and Figure 7–3(c). The wing structures were completely fragmented by the penetration through the exterior wall. The aircraft fuel cloud was starting to spread out but was still relatively dense, and the leading edge of the fuel was just reaching the tower core. The downward trajectory of the aircraft structures transferred sufficient vertical load that the truss floor structures on floors 95 and 96 were starting to collapse in the impact zone.

At 0.3 s after impact, the aircraft was completely inside of the tower (full penetration completed at approximately 0.25 s), as shown in Figure 7–2(d) and Figure 7–3(d). The airframe was mostly broken up, but some large sections of the aft fuselage and tail were still intact, having penetrated through the opening in the north wall created by the forward fuselage structures. The aircraft fuel cloud penetrated approximately half the distance through the core and was spreading out. However, the subsequent motion of the aircraft fragments and fuel debris cloud began to be noticeably slowed beyond this time. The fuel and debris did continue to spread through the tower, but at a much slower rate, as seen in the remaining images in Figure 7–2 and Figure 7–3.

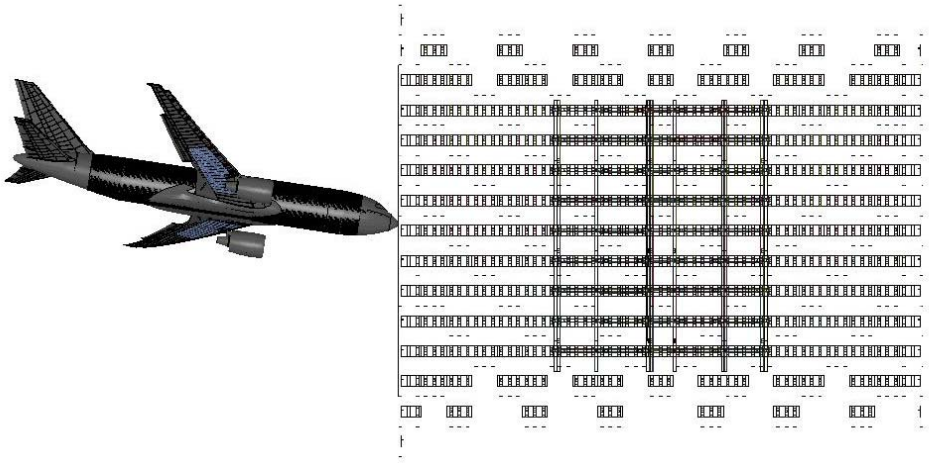

(a) Time=0.00 s

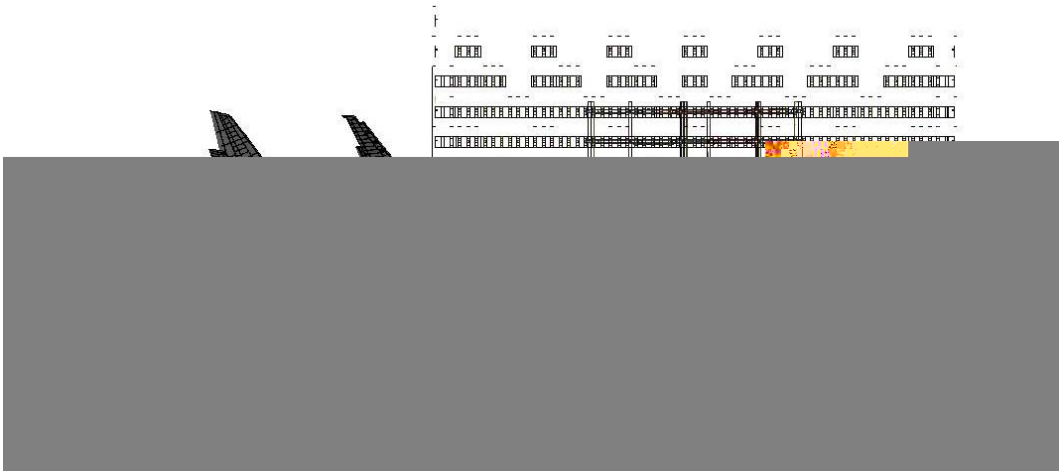

(b) Time=0.10 s

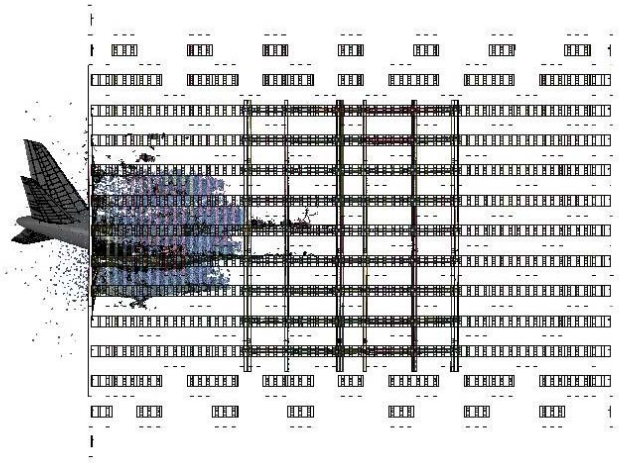

(c) Time=0.20 s

Figure 7–2. WTC 1 base case global impact analysis (side view).

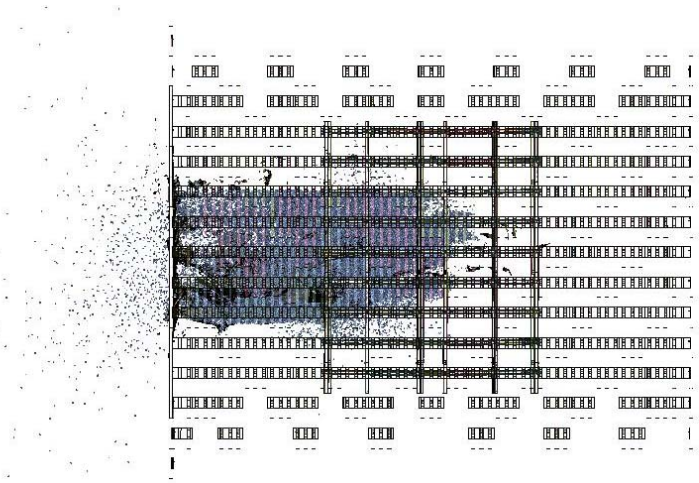

(d) Time=0.30 s

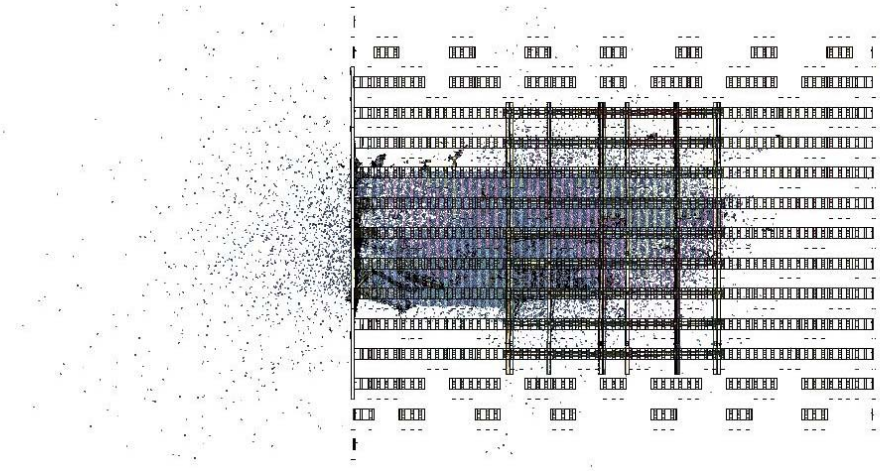

(e) Time=0.40 s

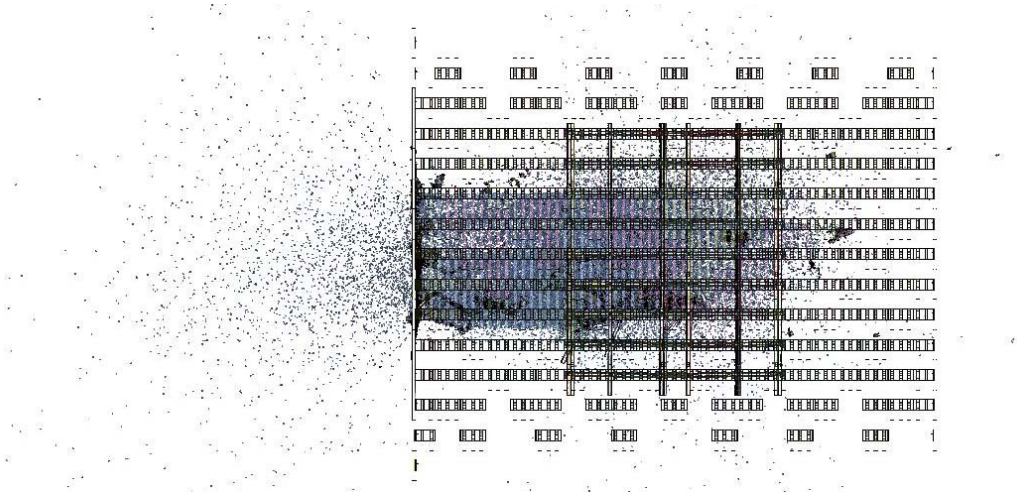

(f) Time=0.50 s

Figure 7–2. WTC 1 base case global impact analysis (side view) (continued).

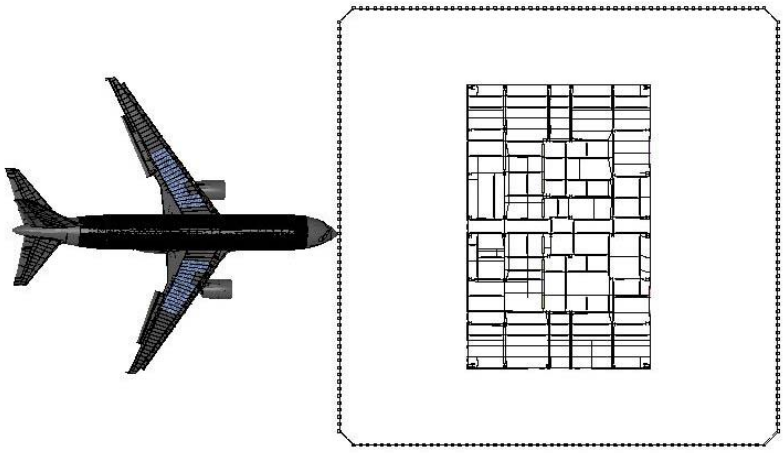

(a) Time=0.00 s

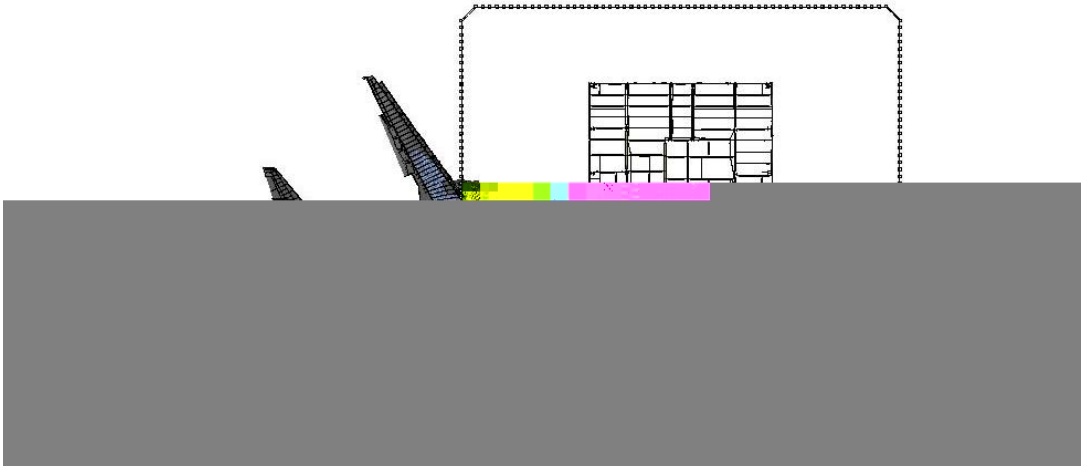

(b) Time=0.10 s

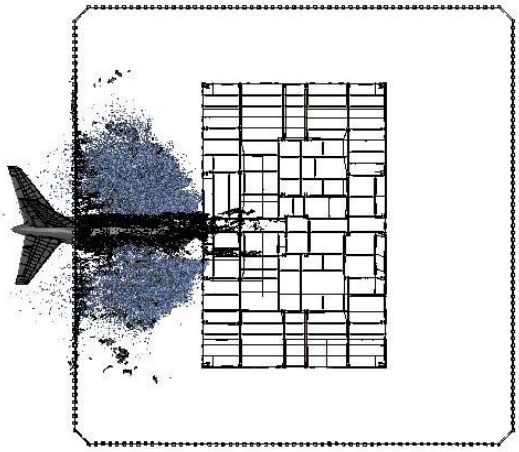

(c) Time=0.20 s

Figure 7–3. WTC 1 base case global impact analysis (plan view).

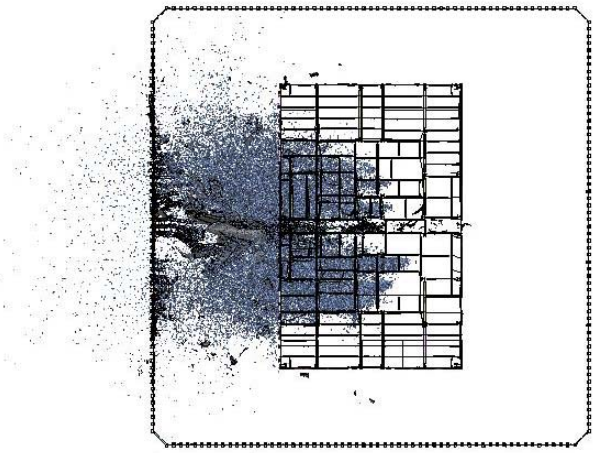

(d) Time=0.30 s

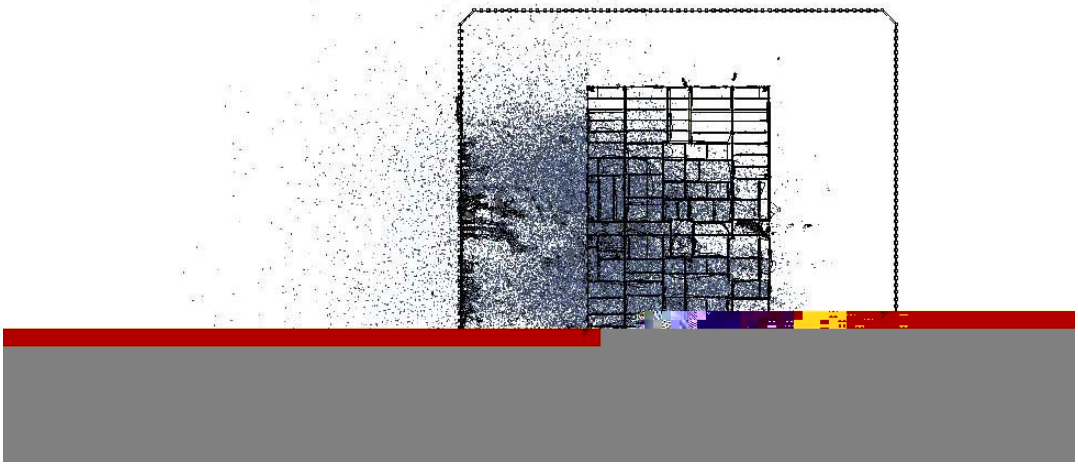

(e) Time=0.40 s

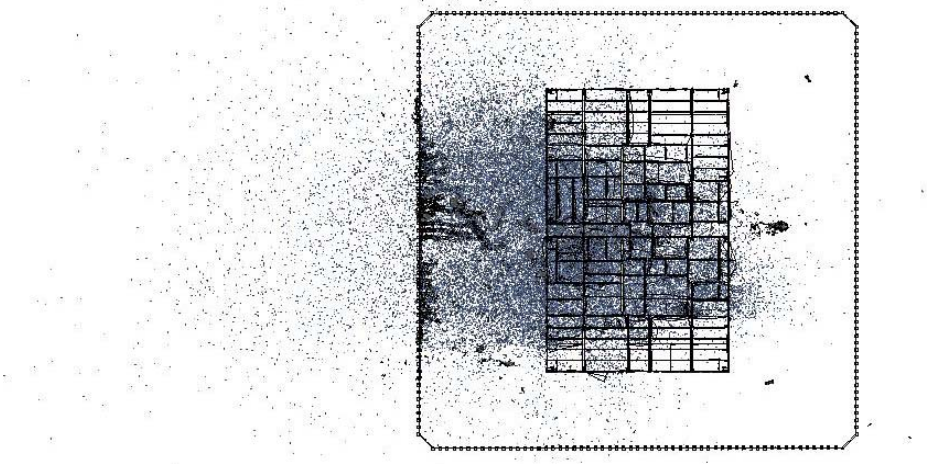

(f) Time=0.50 s

Figure 7–3. WTC 1 base case global impact analysis (plan view) (continued).

The load transfer of the aircraft impact can be described by the time-history of the aircraft momentum as shown in Figure 7–4. The momentum plotted was for all of the aircraft structures and contents (including fuel), normalized by the initial momentum magnitude. The curve illustrates an initial rate of load transfer during the first 0.1 s of impact as the forward fuselage penetrated the exterior wall and impacted the interior structures. Between 0.1 s and 0.25 s, a more rapid load transfer rate was observed as the area of the impact became larger (extending outward in the wing impact regions) and a higher percentage of the aircraft mass was impacting the interior structures. At 0.25 s, the aircraft completely penetrated the building and retained approximately 30 percent of its initial momentum. Beyond this time, the rate of load transfer was steadily decreasing with very little load transfer after approximately 0.5 s.

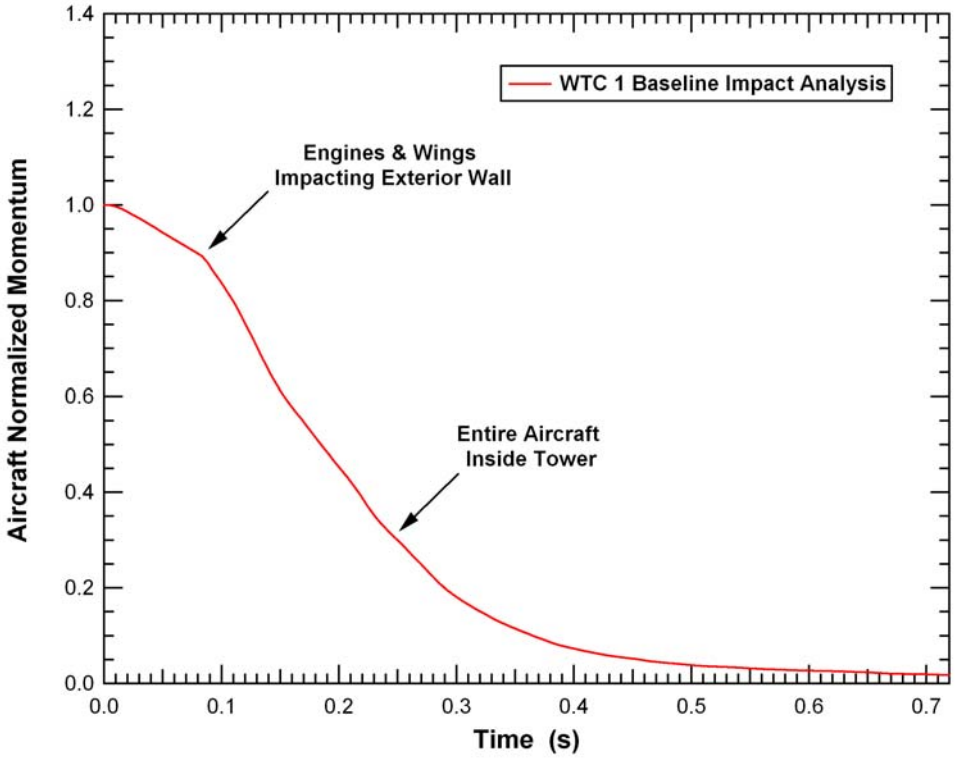

Figure 7–4. Normalized aircraft momentum for the WTC 1 base case impact.

The aircraft was severely broken into thousands of debris fragments of various sizes and mass as a result of the impact with the tower. Larger fragments occurred for specific components such as the engines. At the end of the simulation, the port engine was still inside the core, and the starboard engine was roughly one third of the distance from the core to the south exterior wall. Each engine had a speed of less than 50 mph.

7.3.2 Tower Structural Damage

The structural damage to the WTC 1 tower by the base case impact conditions is described in this section. The primary structural components of interest were the exterior wall, core columns and core framing components, and the floor structures and concrete floor slab. Only limited results are presented in this chapter. Refer to Chapter 9 of NIST NCSTAR 1-2B for further details.

Exterior Wall Damage

The exterior wall was the one structural system for which direct visual evidence of the impact damage was available. Therefore, the comparison of the calculated and observed exterior wall damage can provide a partial validation of the analysis methodologies used in the global impact analyses. A comparison of the north exterior wall observed and calculated damage from the base case WTC 1 global impact analysis is shown in Figure 7–5. The calculated impact damage to the exterior wall is shown with color fringes representing plastic strain magnitude, with undamaged sections in blue and strains at or above 5 percent shown in red. The schematic of observed damage was developed from inspections of the film and photographic data collected on the tower after impact. Both the observed and calculated damage wall regions illustrate a region of the exterior wall from column 108 to column 152, extending from floor 91 to floor 100 (spandrels at floors 92 through 100).

The comparison of the calculated and observed damage indicated that the geometry and location of the impact damage zone were in good agreement. This agreement in the position and shape of the impact damage served to validate the geometry of the aircraft model, including the aircraft orientation, trajectory, and flight distortions of the wings.

The comparison also indicated good agreement in the magnitude and mode of impact damage on the exterior wall. The exterior wall completely failed in the regions of the fuselage, engine, and fuel-filled wing section impacts. Damage to the exterior wall was observed all the way out to the wing tips, but the exterior columns were not completely failed in the outer wing and vertical stabilizer impact regions. Failure of the exterior columns occurred both at the bolted connections between column ends and at various locations in the column depending on the local severity of the impact load and the proximity of the bolted connection to the impact. The agreement of both the mode and magnitude of the impact damage served to partially validate the constitutive and damage modeling of the aircraft and exterior wall of the tower. Section 7.10.1 provides a detailed comparison of the calculated and observed damage mode and magnitude.

Core Structural Damage

The estimation of the damage to the core columns and core beams was important in determining the residual strength for the subsequent analyses of structural stability and collapse. The core had significant damage in the region close to the impact point. The columns in line with the aircraft fuselage failed on the impact side, and several of the core beams were also severely damaged or failed in the impact zone.

The calculated damage to the core columns by row is shown in Figure 7–6. The columns are shown with color fringes representing plastic strain magnitude, with undamaged sections in blue and strains at or above 5 percent shown in red. A summary of the column damage is listed in Table 7–1. The qualitative classification of the column damage levels is shown in Figure 7–7. This classification levels were light damage, moderate damage, heavy damage, and failed (severed). The light damage level was defined as having evidence of impact (low level plastic strains), but without significant structural deformations. The moderate damage level had visible local distortions of the column cross section (e.g. bending in a flange) but no lateral displacements of the column centerline. The heavy damage classification was for impacts that produced significant global deformation, resulting in a permanent deflection of the column centerline.

The severed columns were completely failed and could carry no residual load. The damage to the core floor framing for floors 95 and 96 is shown in Figure 7–8.

P–Δ effects generated due to the sway of the towers after impact, as observed in video evidence, were not expected to affect or impose additional damage to the core columns. The core columns were designed as axially loaded members without continuity of framing, and thus would not develop significant P–Δ moments (see Chapter 5 of NIST NCSTAR 1-2A).

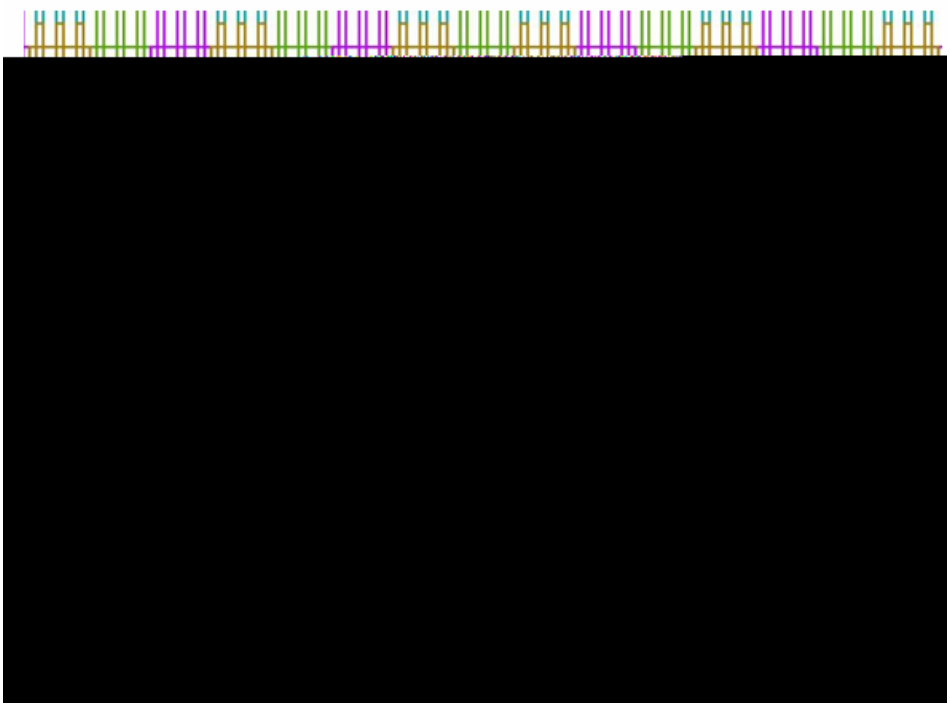

(a) Schematic of observed damage

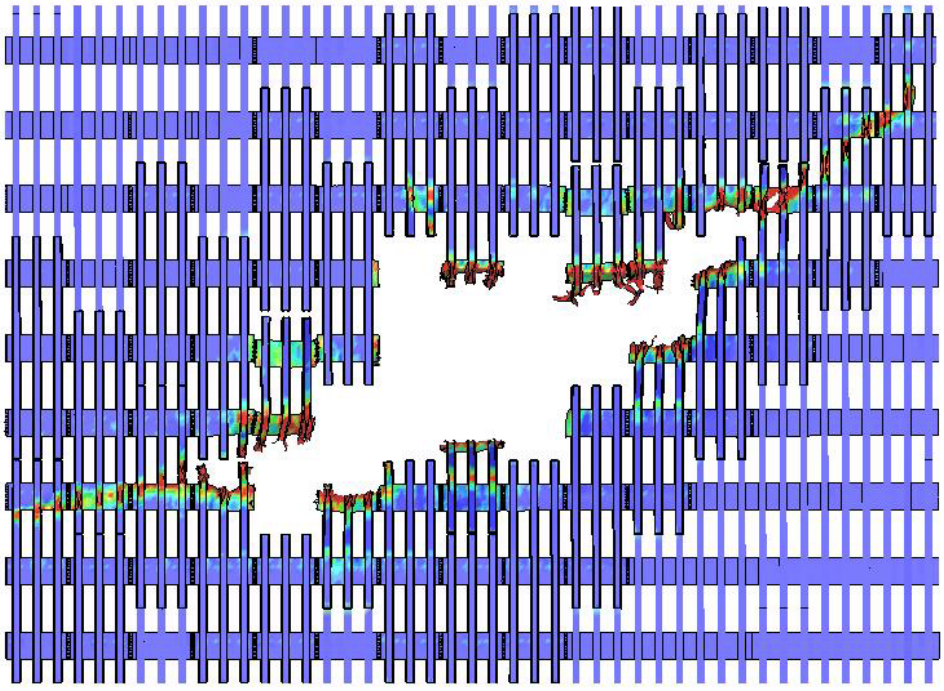

(b) Calculated damage

Figure 7–5. Base case impact damage to the WTC 1 exterior wall.

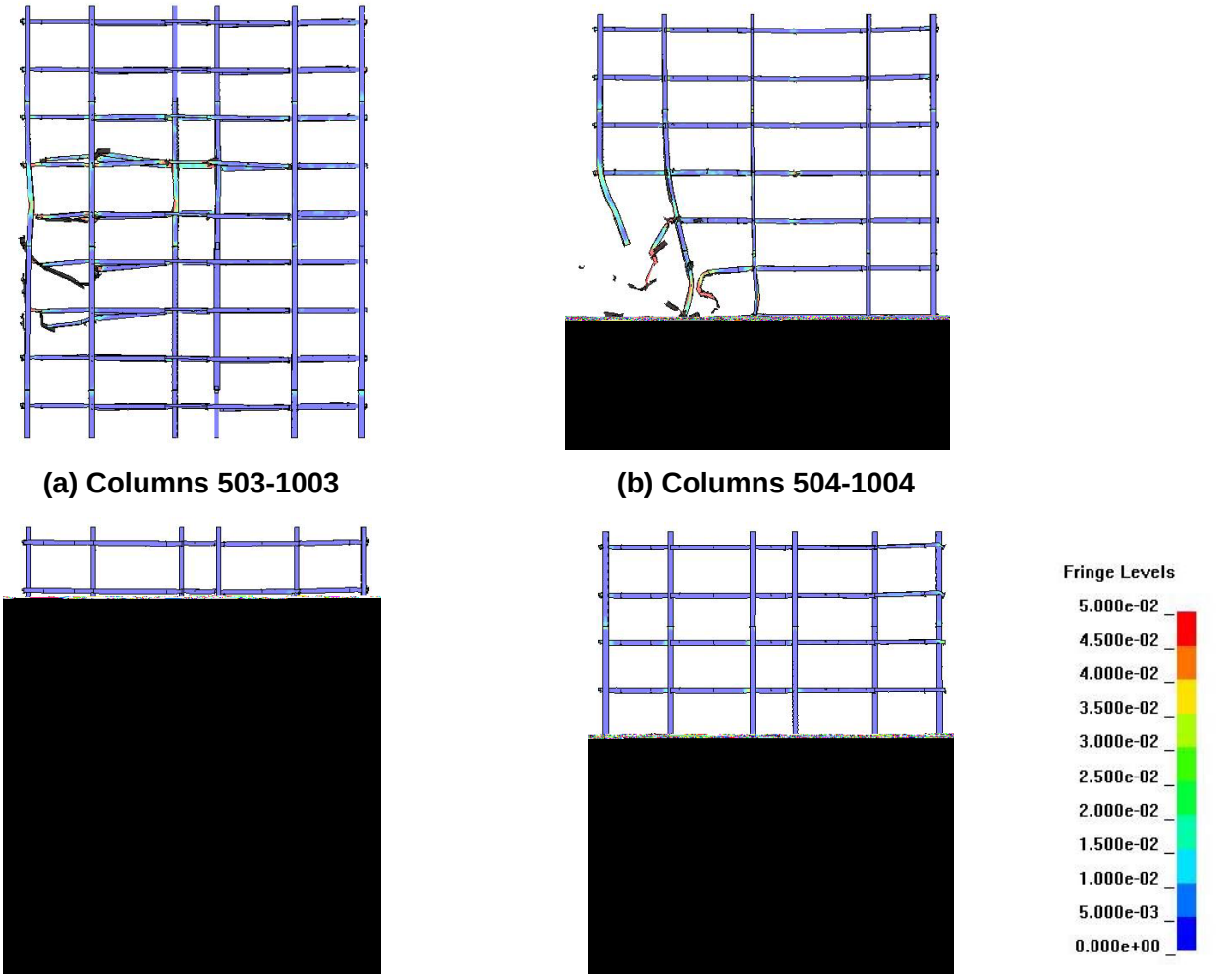

(a) Columns 503-1003 **(b) Columns 504-1004**

(c) Columns 505-1005 **(d) Columns 506-1006** **(e) Reference scale**

Figure 7–6. Base case impact damage to the WTC 1 core columns.

Table 7–1. Summary of core column damage for the base case WTC 1 impact.

Column	Location	Damage Level	Lateral Deflection of Column Centerline (in.)
Column 503	Floor 96	Heavy	18
Column 504	Floors 92-96	Severed	
Column 505	Floors 93-96	Heavy	20
Column 506	Floors 93-94	Heavy	10
Column 604	Floors 92-96	Severed	
Column 605	Floors 94-95	Moderate	
Column 702	Floor 96	Moderate	
Column 703	Floor 96	Moderate	
Column 704	Floor 94	Heavy	18
Column 705	Floor 95	Moderate	
Column 706	Floors 93-95	Severed	
Column 802	Floor 96	Moderate	
Column 805	Floor 94	Moderate	

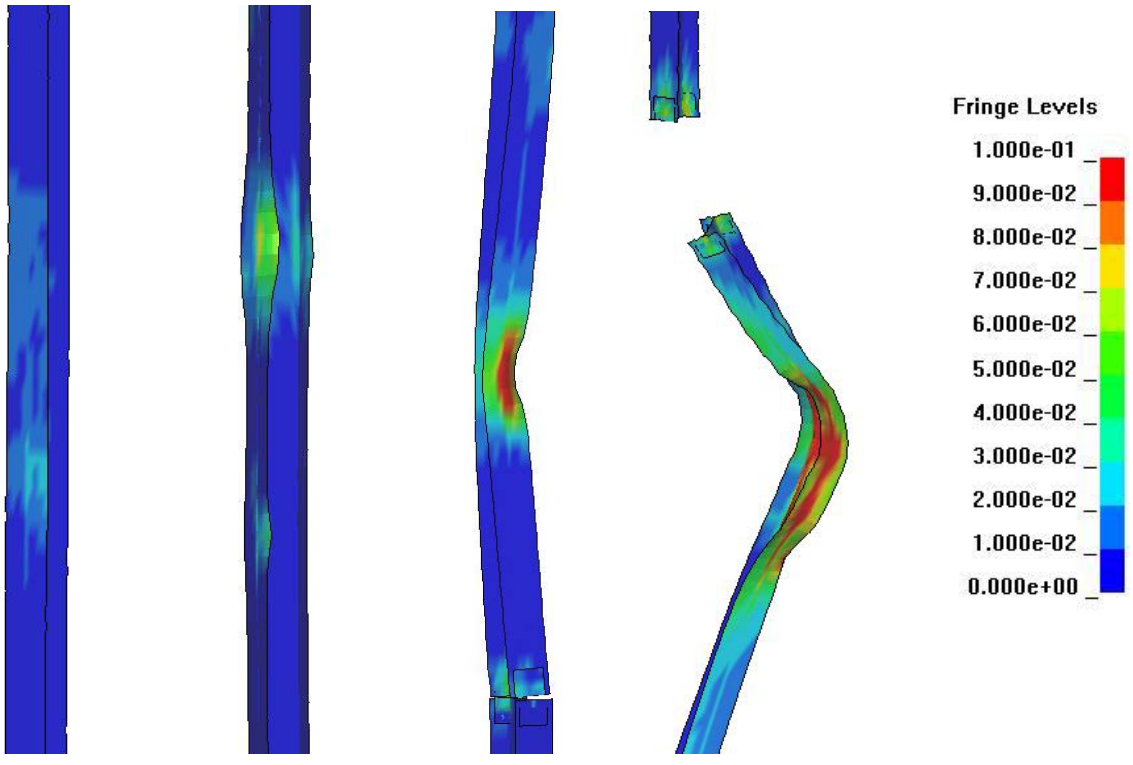

(a) Light **(b) Moderate** **(c) Heavy** **(d) Severed**

Figure 7–7. Classification of damage levels in core columns.

(a) Floor 95 Core Framing Damage **(b) Floor 96 Core Framing Damage**

Figure 7–8. Base case impact damage to the core beams of floors 95 and 96 of WTC 1.

Floor Truss and Slab Damage

An overall frontal view of the floor trusses in the impact zone along with the calculated impact damage to the floor trusses is shown in Figure 7–9. The figure shows that the trusses experienced significant damage and sagging in the impact zone. A plan view of the calculated damage to the trusses on floors 95 and 96 is shown in Figure 7–10. The calculated impact response produced severe damage to the truss structures in the primary impact path of the fuselage from the exterior wall to the core. The truss floor system on floors 94 through 96 were damaged and sagged downward as a result of the impact loading.

The calculated damage to the WTC 1 floor slab for floors 95 and 96 are shown in Figure 7–11. The fringes of damage were set such that the concrete slab failed in the regions colored red (2 percent plastic strain was used, corresponding to the zero strength strain limit for the concrete in unconfined compression). At these strain levels, the concrete slab was severely damaged and probably removed, exposing the supporting metal decking. Beyond 2 percent plastic strain, the strength of the floor slab was severely reduced in the analyses to model the residual strength of the metal deck after the concrete failure, breakup, and removal. At a plastic strain of 30 percent, corresponding to failure levels for the metal decking material, the elements were eroded (seen as holes ruptured in the floor slabs shown).

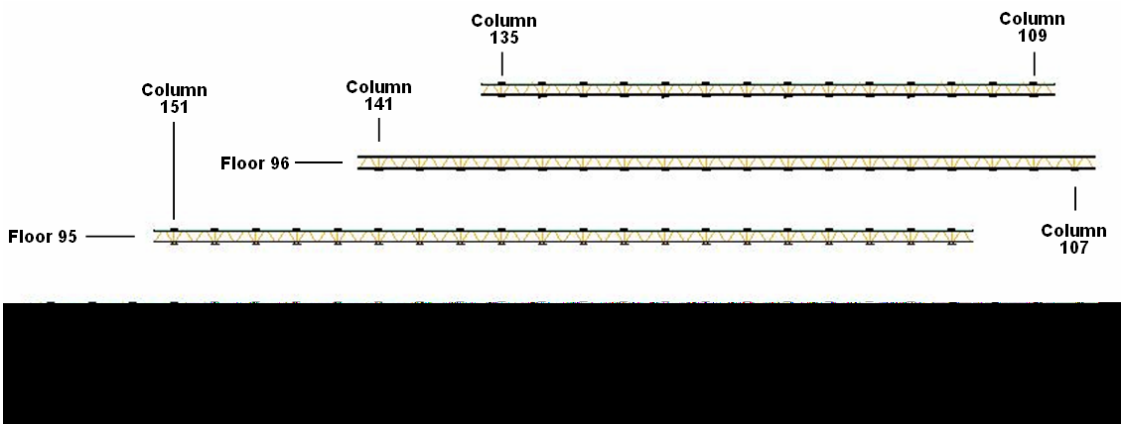

(a) Initial detailed truss structures

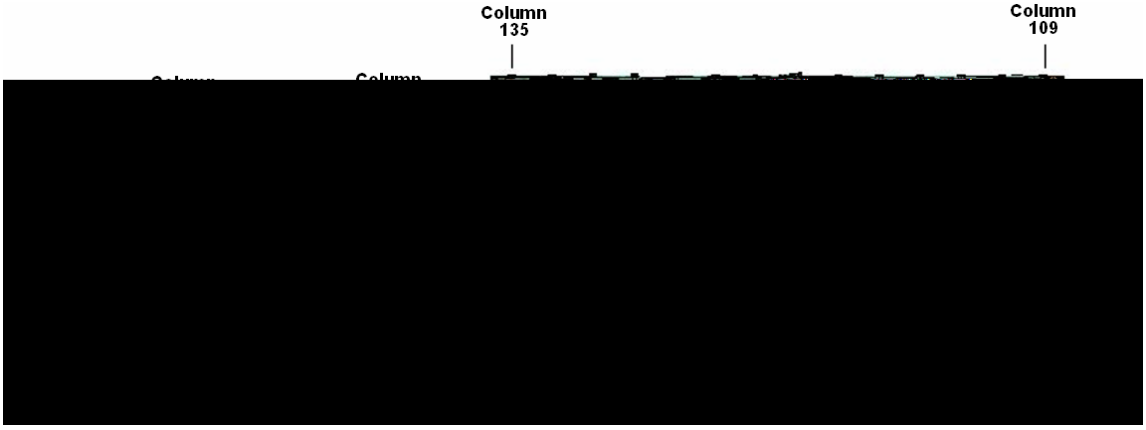

(b) Calculated damage

Figure 7–9. Base case impact damage to the WTC 1 floor trusses (front view).

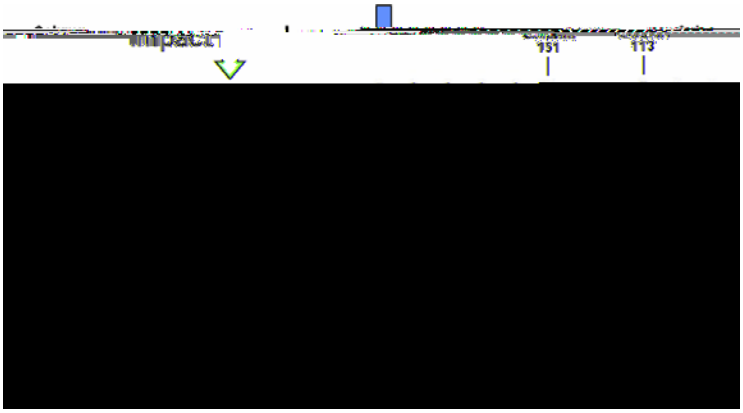

(a) Floor 95 truss damage

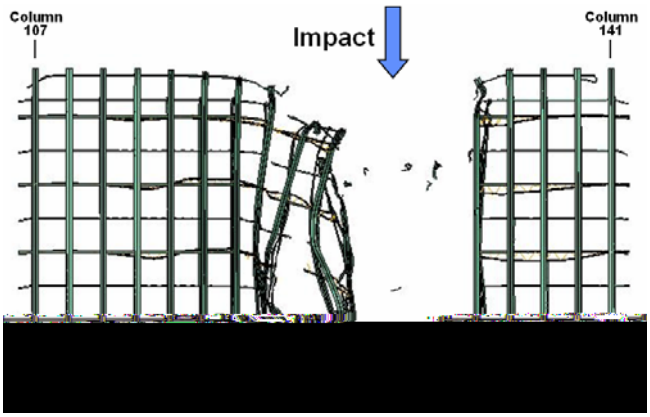

(b) Floor 96 truss damage

Figure 7–10. Base case impact damage to the trusses on floors 95 and 96 of WTC 1 (plan view).

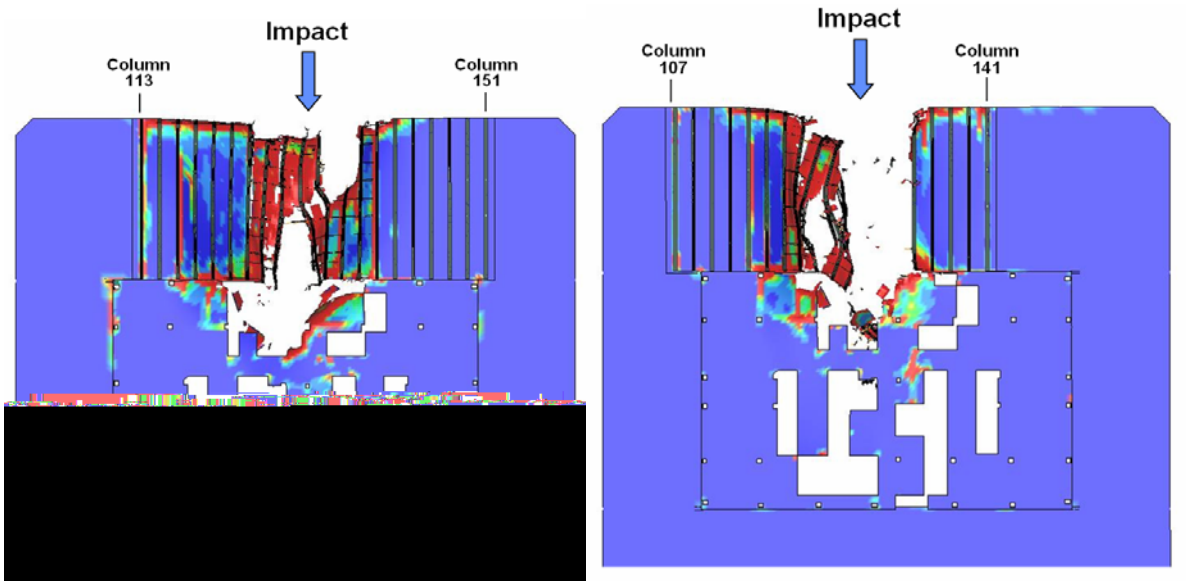

(a) Floor 95 slab damage **(b) Floor 96 slab damage**

Figure 7–11. Base Case impact damage to the slabs on floors 95 and 96 of WTC 1 (plan view).

Summary of Structural Damage

The impact-induced structural damage described above was used as the initial conditions for the post-impact fire-structural analyses. Figure 7–12 shows a summary of the structural damage to the core columns and floor systems at floors 93 through 97 of WTC 1 for the base case (Case A). The damage to the columns at the various levels is identified by the color of the circles, where red, blue, green, and yellow signify severed, heavily damaged, moderately damaged, and lightly damaged columns, respectively. The dotted boxes on the figures indicate areas where the impact created an opening in the floor. These were used to identify slab openings in the fire dynamics simulations (NIST NCSTAR 1-5F). The solid boxes indicate areas in the floor system that had severe structural damage. These areas were removed from the subsequent structural analyses (NIST NCSTAR 1-6).

Figure 7–13 presents the cumulative damage to WTC 1 on all affected floors and columns. The figure shows the damage to the exterior walls due to impact based on the photographs of the north wall. Note the panel that was severed in the south wall of the tower. While the analysis did not capture the failure of the connections at the ends of this panel due to the coarse mesh of the south wall, photographic evidence showed that this panel was knocked down by the impact (see Section 7.10.1). As a result, this panel was removed from the subsequent structural analyses (NIST NCSTAR 1-6).

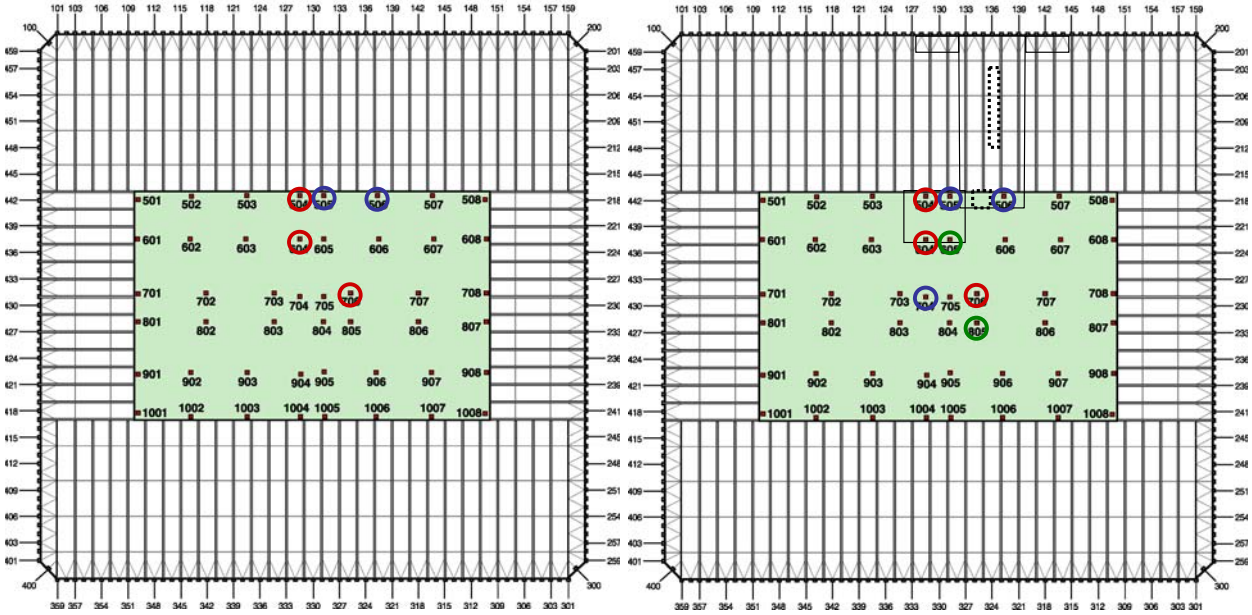

(a) Floor 93 (b) Floor 94

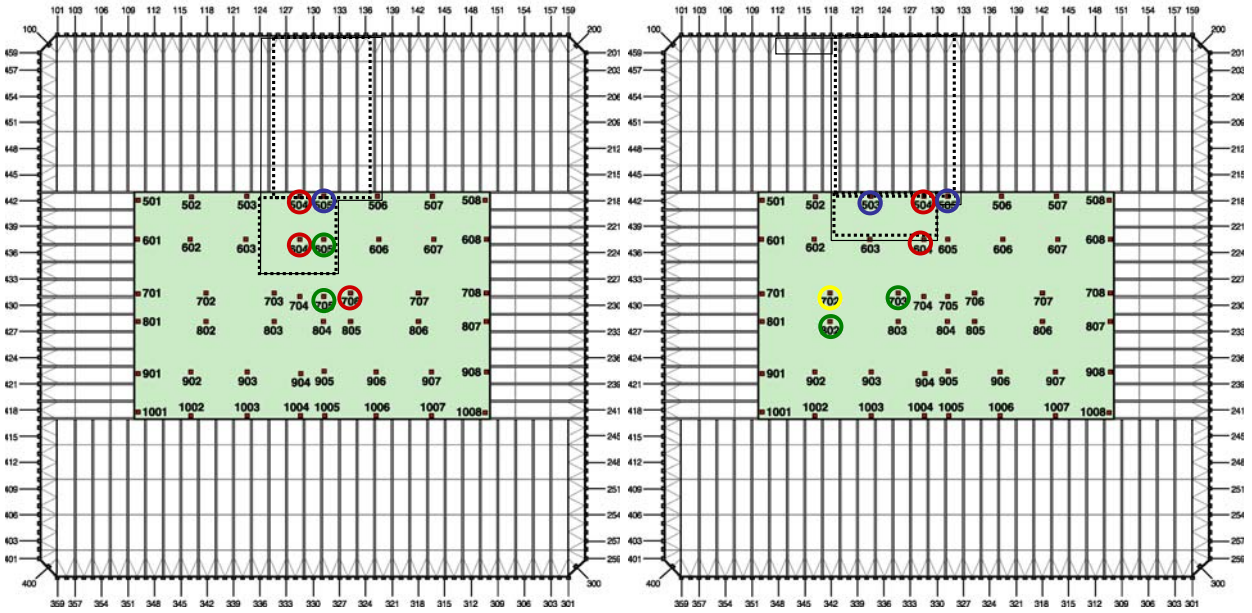

(c) Floor 95 (d) Floor 96

Figure 7–12. Summary of the floor-by-floor structural damage to the floors and columns of WTC 1 (base case).

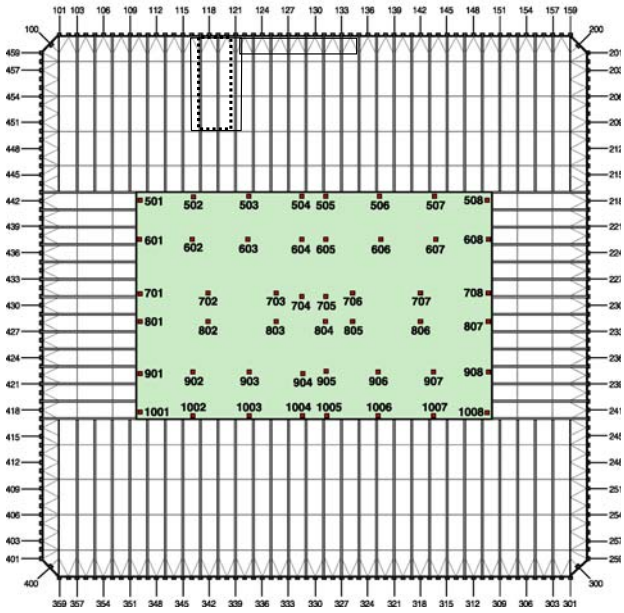

Severe Floor Damage

Floor system structural damage

Floor system removed

Column Damage

Severed

Heavy Damage

Moderate Damage

Light Damage

(e) Floor 97

Figure 7–12. Summary of the floor-by-floor structural damage to the floors and columns of WTC 1 (base case) (continued).

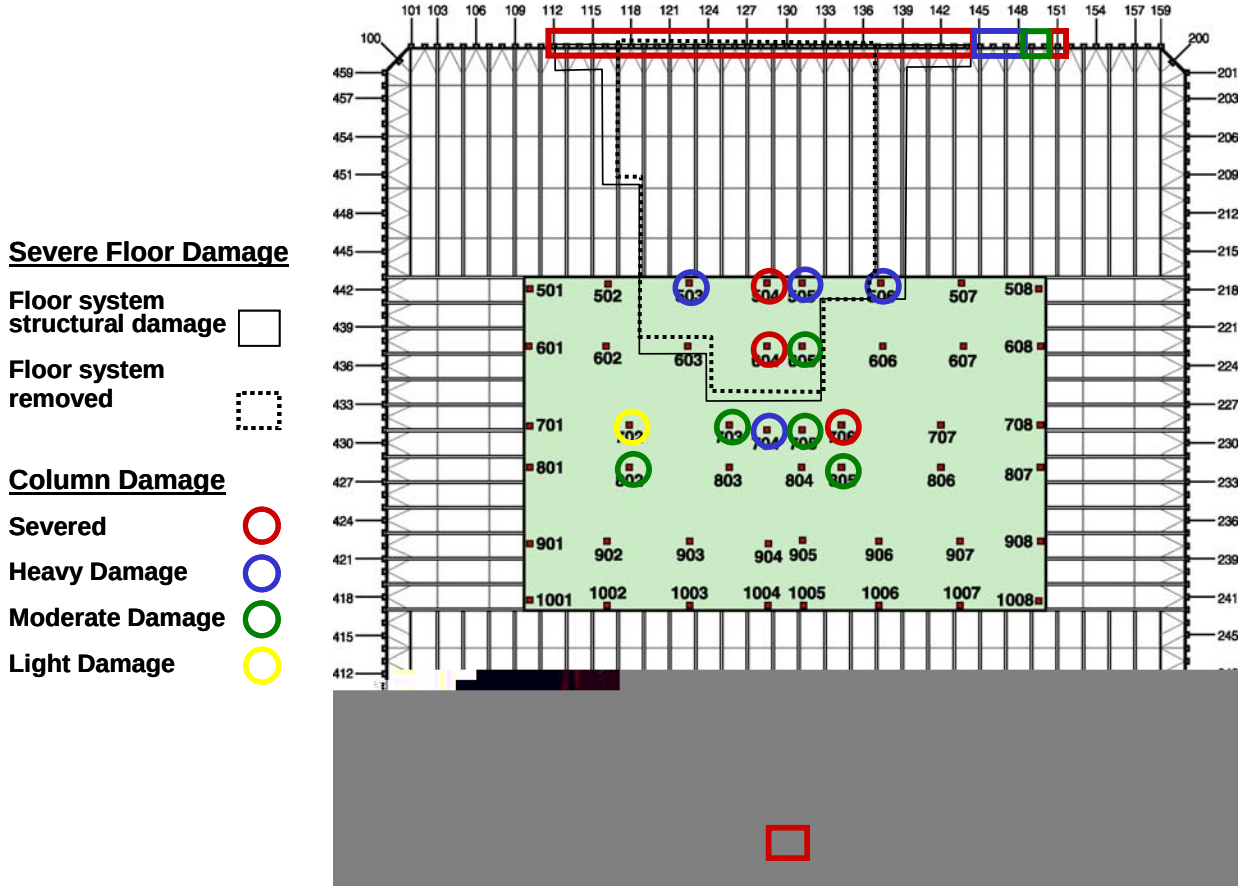

Severe Floor Damage

Floor system structural damage

Floor system removed

Column Damage

Severed

Heavy Damage

Moderate Damage

Light Damage

Figure 7–13. Cumulative structural damage to the floors and columns of WTC 1 (base case).

7.3.3 Fuel and Debris Distributions

The global impact results presented in this section include the distribution of the jet fuel inside the tower, the damage to the building contents (partition walls and workstations), and the aircraft debris distribution in the towers. For the base case WTC 1 global impact analysis, the calculated distribution of the fuel in the tower in a plan view and side view is shown in Figure 7–14. At the termination of the global impact analysis, the residual momentum of the jet fuel in the impact direction was less than one percent of the initial momentum, indicating that the fuel cloud was nearly at rest at about 0.715 s.

To more clearly present the calculated response of the structures that influenced the fire propagation, the structural components were removed from the visualization, with the exception that the core columns were maintained in the visualizations for reference positions. A plan view of the response of the remaining building contents and aircraft debris is shown in Figure 7–15. Similar plan views of floors 95 and 96 response of the building contents and debris field are provided in Figure 7–16 and Figure 7–17, respectively. The bulk of the aircraft debris and fuel were arrested prior to exiting the far side of the tower core. A small amount of aircraft debris was calculated to exit the south wall of the tower.

Plots of debris distribution and damage to tower contents at the end of the impact simulation similar to those in Figure 7–16(c) and Figure 7–17(c) were used to estimate the damage to fireproofing. The extent of dislodged fireproofing was estimated by considering fireproofing damage only to structural components in the direct path of debris. For details of the methodology and the extent of fireproofing damage, see NIST NCSTAR 1-6.

A quantitative characterization of the fuel and aircraft debris distribution was obtained by slicing the model at vertical floor locations and calculating the mass at each floor level. A summary of the floor-by-floor fuel and debris distributions is given in Table 7–2. The bulk of the fuel and aircraft debris was deposited in floors 93 through 97, with the greatest concentration on floor 94. Approximately 18,000 lb, or 7 percent, of aircraft mass was eliminated from the debris cloud at the final state as a result of the erosion in the aircraft structures due to impact and breakup. This mass was not accounted for in the fuel and debris distributions provided in Table 7–2. A first approximation would be to increase the airframe debris distribution proportionately to account for the eroded mass. This eroded mass was maintained in the calculation but was no longer included in the contact algorithm. As a result, any residual momentum at the time of erosion could not be subsequently transferred to the tower.

The calculated debris cloud included 17,400 lbs of debris and 6,700 lbs of aircraft fuel outside of the tower at the end of the impact analysis, either rebounding from the impact face (north wall) or passing through the tower (south wall). This amount might have been larger in the calculation, since the exterior walls were not modeled with windows that could contain the fuel cloud and small debris inside the towers. In addition, the impact behavior of the aircraft fuel cloud did not include the ability to stick to, or wet, interior components. Rather, the aircraft fuel SPH particles tended to bounce off of internal structures.

The physics of fuel impact and dispersion in this type of impact event is complex and no appropriate validation data could be found. The fuel starts as a continuous fluid within the tanks and ends up distributed both on the tower structures and as small droplets that interact with the atmosphere surrounding the impact zone. No single analysis technique is currently available that can analyze this full range of fuel dispersion without significant uncertainties.

Both the SPH and ALE analysis techniques (see Section 5.4.4) available for the analysis of the fuel impact and dispersion had limitations. Details of the fuel behavior such as the wetting of the fuel against tower structures and interior contents or the physics of the fuel breakup into droplets are not accurately reproduced in either analysis technique. However, the momentum transfer from the fuel to the tower structures and subsequent impact damage produced by the fuel can be modeled by both analysis techniques.

The detailed predictions of the fuel dispersion and distribution using SPH in the global impact analyses had significant uncertainties in the absence of improved validation testing. However, some aspects of the distribution had a higher confidence. The floors confined the vertical motion of the fuel, and the floor-by-floor distribution of fuel was controlled more by the geometry of the tower and impact conditions. As a result, this distribution by floor has a higher level of confidence. Similarly, the interior contents and partition walls, and the damage to these structures, controlled the spread of fuel.

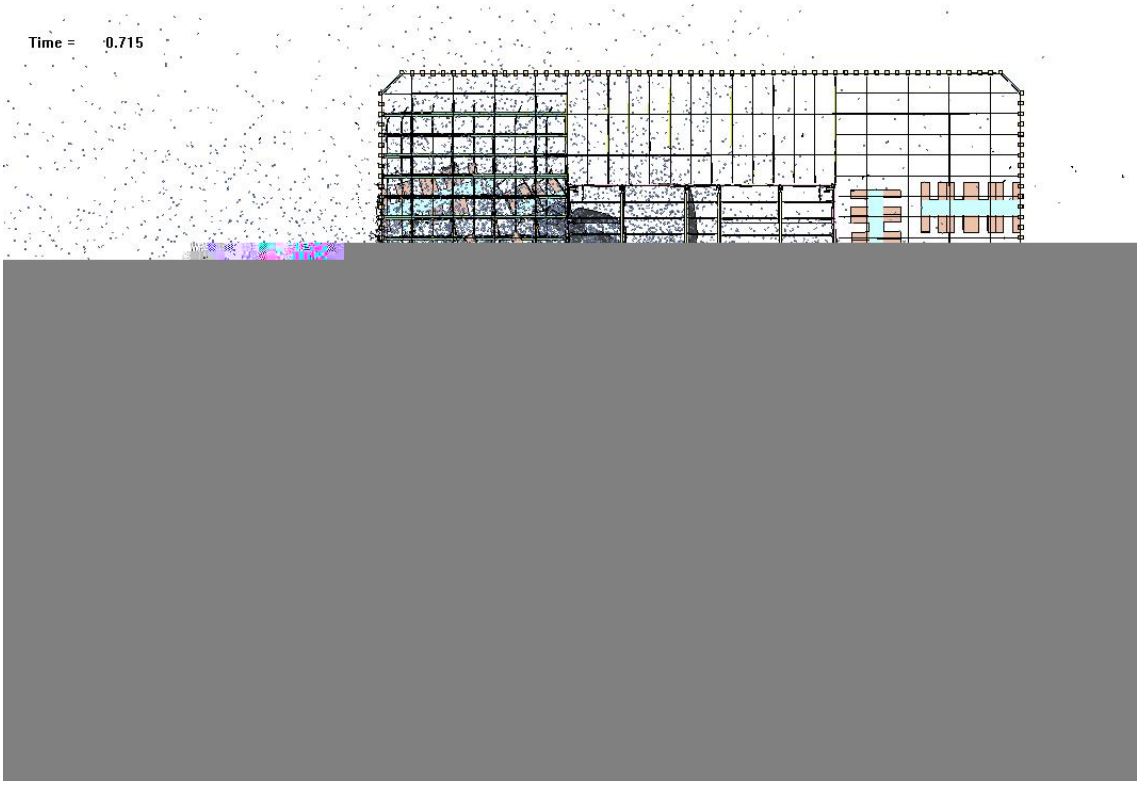

(a) Plan view (floor slab removed)

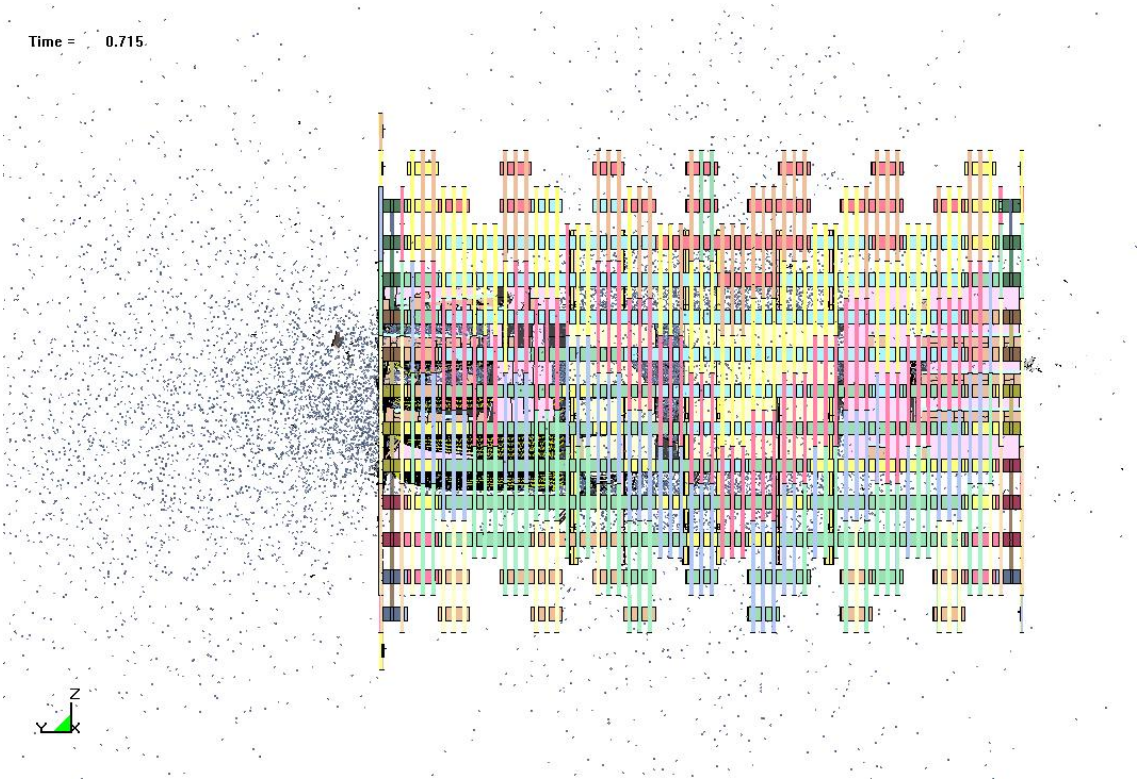

(b) Side view

Figure 7–14. Calculated fuel distribution in the base case WTC 1 analysis.

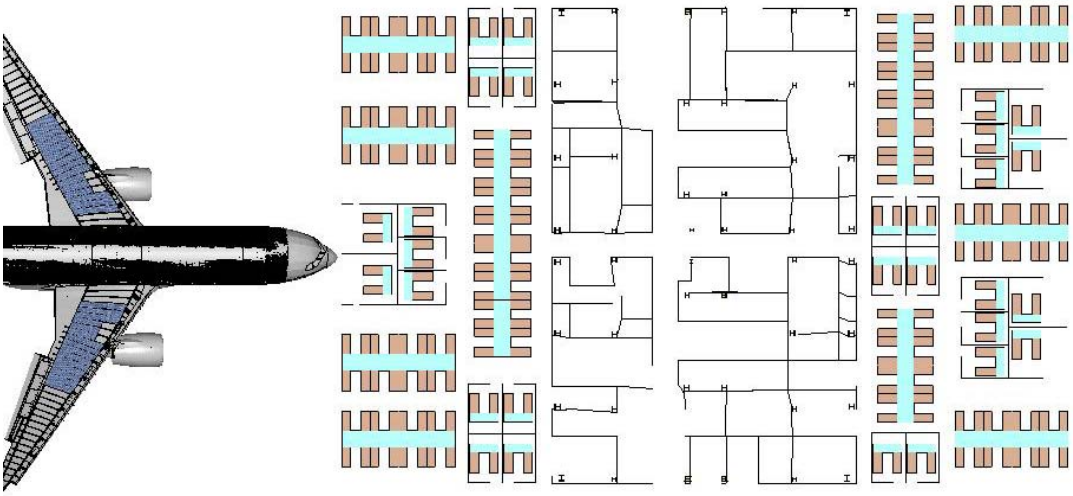

(a) Pre-impact configuration

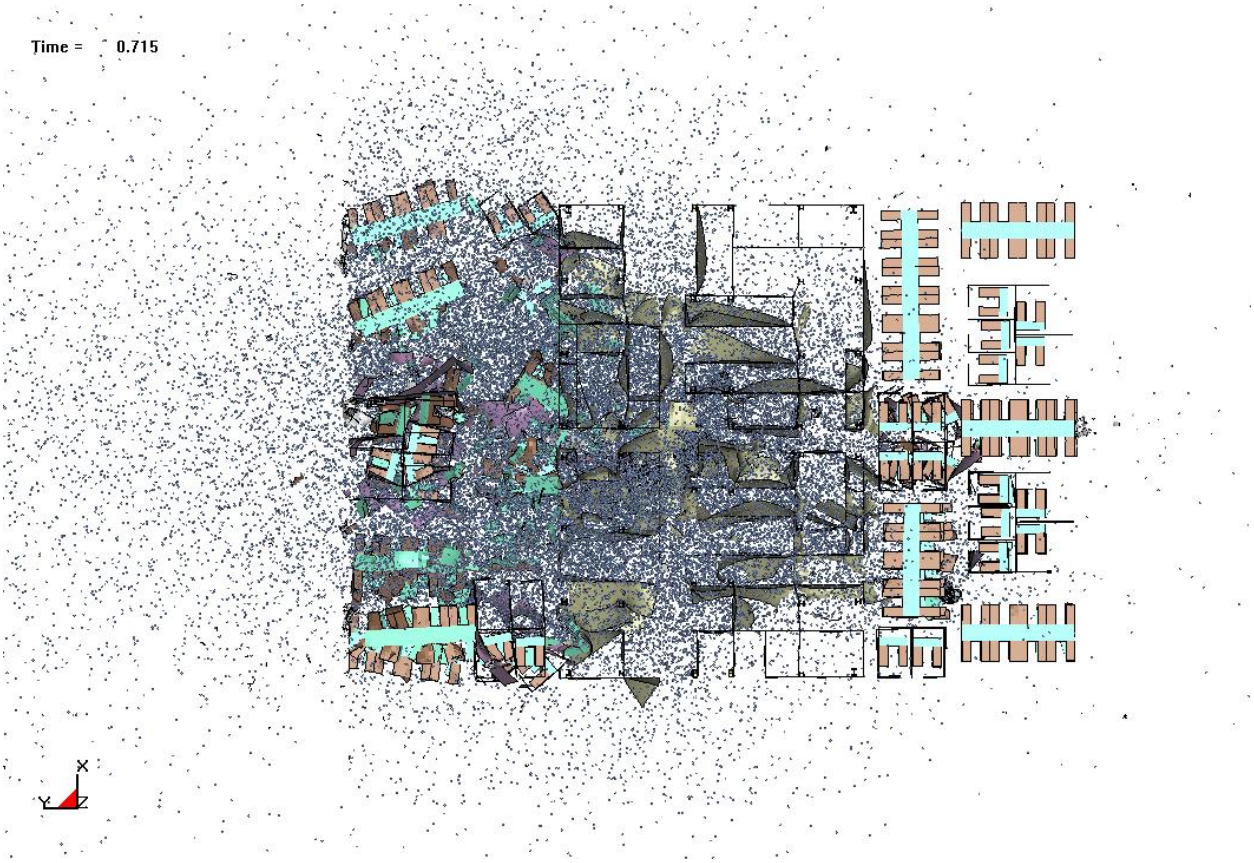

(b) Calculated impact response

Figure 7–15. Plan view of calculated WTC 1 building, fuel, and aircraft debris distribution for the base case.

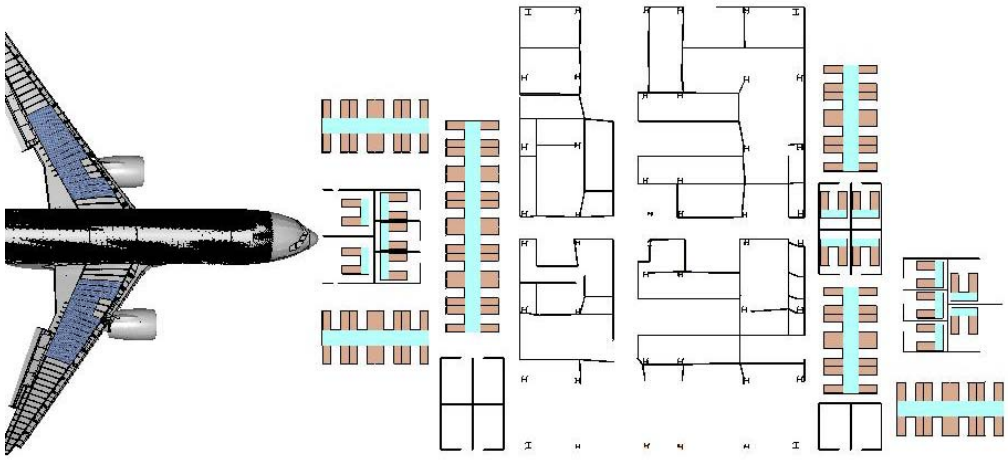

(a) Pre-impact configuration

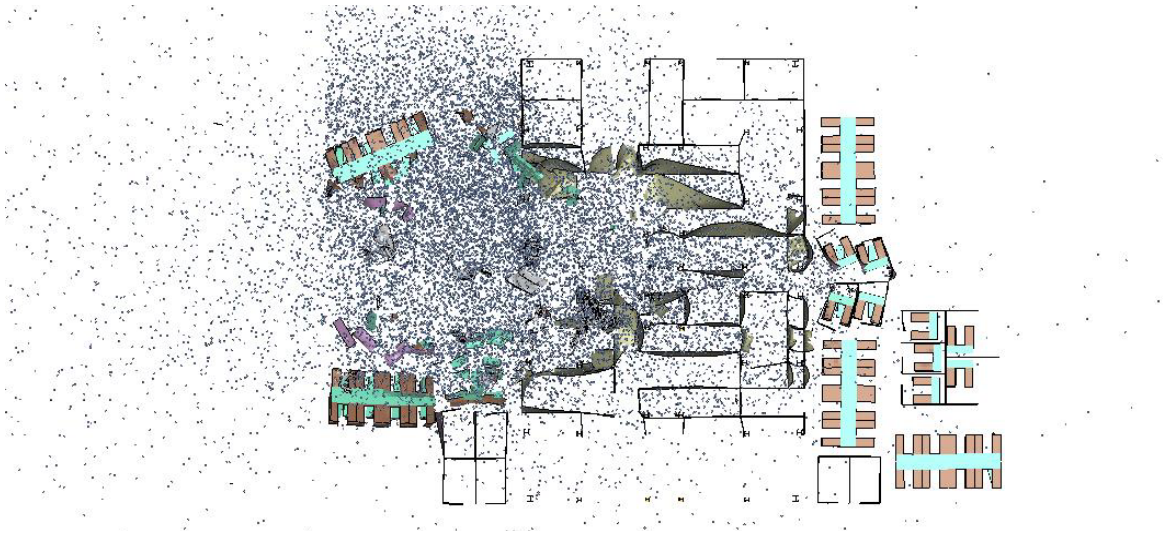

(b) Calculated impact response

(c) Calculated impact response (fuel removed)

Figure 7–16. Calculated floor 95 contents and fuel distribution (base case).

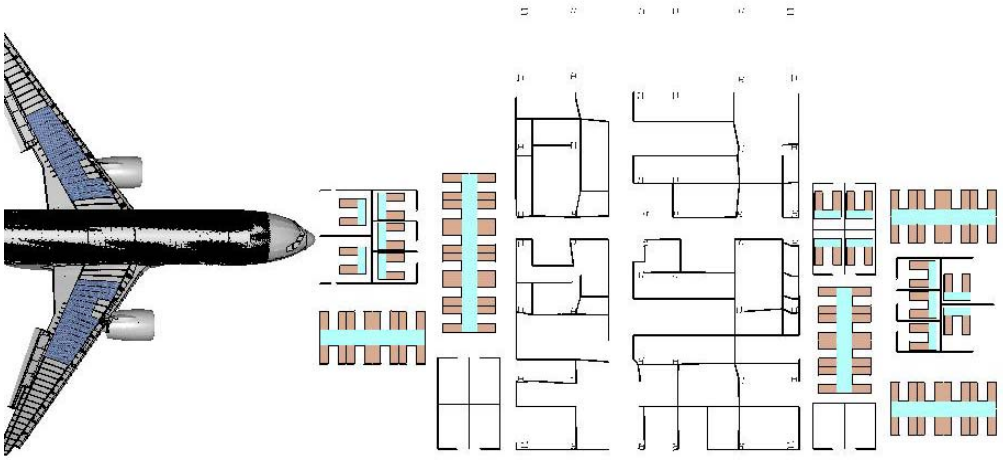

(a) Pre-impact configuration

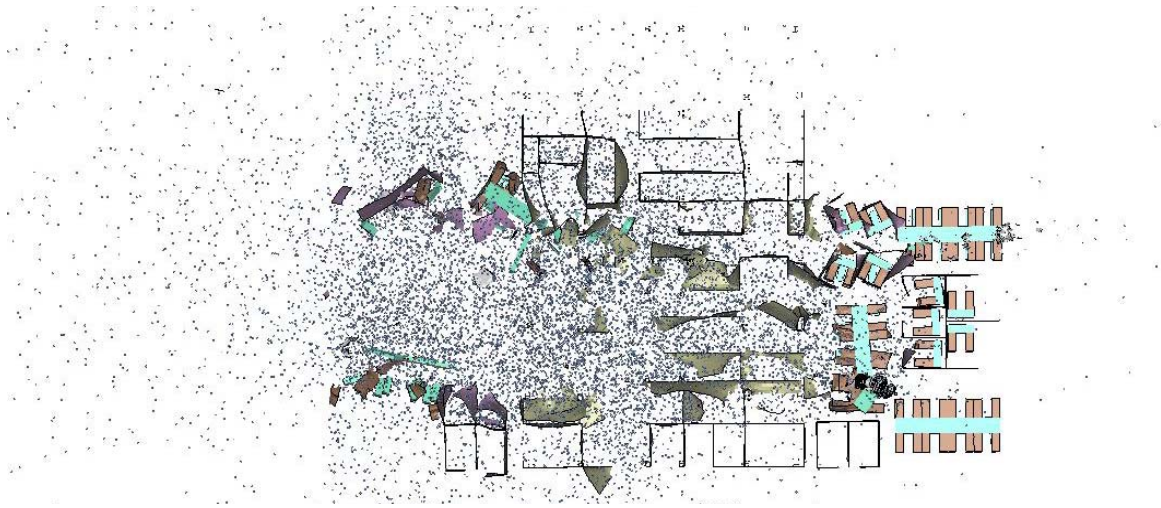

(b) Calculated impact response

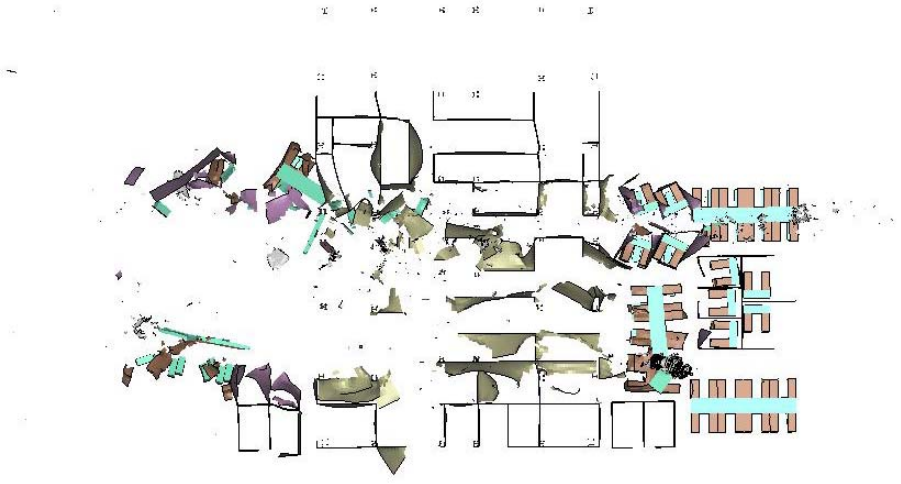

(c) Calculated impact response (fuel removed)

Figure 7–17. Calculated floor 96 contents and fuel distribution (base case).

Table 7–2. Fuel and aircraft debris distribution for the base case WTC 1 impact.

Tower Location	Aircraft Fuel	Aircraft Debris
Total Outside Tower	6,700 lb	17,400 lb
WTC 1 Floor 92	810 lb	260 lb
WTC 1 Floor 93	6,100 lb	22,600 lb
WTC 1 Floor 94	16,100 lb	96,000 lb
WTC 1 Floor 95	12,200 lb	28,000 lb
WTC 1 Floor 96	11,700 lb	19,400 lb
WTC 1 Floor 97	9,500 lb	6,000 lb
WTC 1 Floor 98	2,200 lb	6,000 lb
WTC 1 Floor 99	770 lb	90 lb
Total Weight	66,100 lb	196,000 lb

7.4 WTC 1 MORE SEVERE IMPACT ANALYSIS – CASE B

This case is referred to as Case B for the remainder of the WTC Investigation reports.

In addition to the base case impact analysis described in Section 7.3, two more impact analyses were performed for each tower to provide a range of calculated impact-induced damage. The variations in impact analysis parameters were developed based on the results of the sensitivity analyses and additional evaluations of the parameter uncertainties (see Chapter 8 of NIST NCSTAR 1-2B). These analyses included a more severe and a less severe case. Presented in this section is the more severe case.

The parameters for the more severe WTC 1 impact scenario are compared to the corresponding parameters in the base case analysis in Table 7–3. For the flight parameters, the impact speed was 472 mph in the more severe impact scenarios, which was the upper bound obtained from the analysis of aircraft impact conditions described in Chapter 6. The aircraft vertical trajectory angle was varied from 10.6 degrees in the base case to 7.6 degrees for the more severe impact case, which resulted in more impact energy directed inward toward the core. The lateral trajectory was not varied since the impact was close to being centered on the tower and normal to the north face of WTC 1. A small variation in the lateral approach angle would have had little effect on the energy of the aircraft debris entering the tower and core.

The parameters varied for the aircraft model were the weight of the aircraft and the ductility of the aircraft materials. A 5 percent increase in the total aircraft weight was considered for the more severe case. The failure strain was varied to be 125 percent of the baseline value. This relatively large variation in aircraft material ductility was used for multiple reasons. First, no material characterization testing of specimens cut from a 767 were performed as part of this Investigation. All of the material properties used for the aircraft was obtained from sources available in the open literature. Secondly, the variation in ductility was used as the single parameter in this analysis to evaluate the uncertainties in the energy absorption capacity of aircraft materials. An increase in aircraft material strength would have had a similar effect to an increase in material ductility for producing increased impact damage to the towers. Finally, the

material failure parameters were influenced by the resolution of the models in the impact analysis. The mesh refinement effects introduced an increased uncertainty on the failure strains in these analyses.

Table 7–3. Input parameters for the more and less severe WTC 1 impact analysis.

Analysis Parameters		Base Case	More Severe	Less Severe
Flight Parameters	**Impact speed**	443 mph	472 mph	414 mph
	Trajectory - pitch	10.6°	7.6°	13.6°
	Trajectory - yaw	0.0°	0.0°	0.0°
	Orientation - pitch	8.6°	5.6°	11.6°
	Orientation - yaw	0.0°	0.0°	0.0°
Aircraft Parameters	**Weight**	100 percent	105 percent	95 percent
	Failure Strain	100 percent	125 percent	75 percent
Tower Parameters	**Failure Strain**	100 percent	80 percent	120 percent
	Live Load Weight	25 percent	20 percent	25 percent

Finally, the parameters varied for the tower model were the ductility of the steel used in the tower construction and the weight of the contents inside the tower. A variation of 20 percent was used to account for the uncertainty in failure strain for the tower materials. The combination of increasing the aircraft material ductilities by 25 percent and reducing the tower material ductilites by 20 percent covered a wide range in relative aircraft and tower strength assumptions. The variations in internal tower contents (live load weight in Table 7–3) are specified as a percentage of the design live load.

Table 7–3 provides also the parameters used in the less severe damage case. As can be seen from the table, the parameters are selected to provide for a stronger tower and a weaker aircraft to yield less damage to the tower structure.

7.4.1 Impact Response

The impact response of WTC 1 for the more severe case is shown in side and plan views in Figure 7–18 and Figure 7–19, respectively. The response is shown at intervals of 0.1 s from impact through the initial 0.5 s of the response. Comparing the more severe impact response in Figure 7–18 and Figure 7–19 with the base case response in Figure 7–2 and Figure 7–3, it can be seen that the two responses were very similar with two exceptions. These were the slightly compressed time scale and the larger amount of debris exiting the south wall in the more severe case. These differences were due to the larger impact speed, the increased weight and material toughness of the aircraft, and the reduced contents mass and material toughness of the towers for the more severe case.

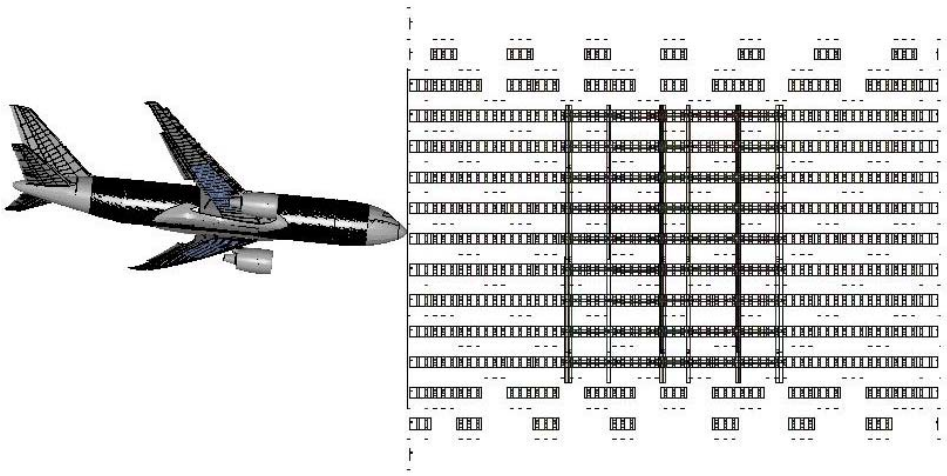

(a) Time=0.00 s

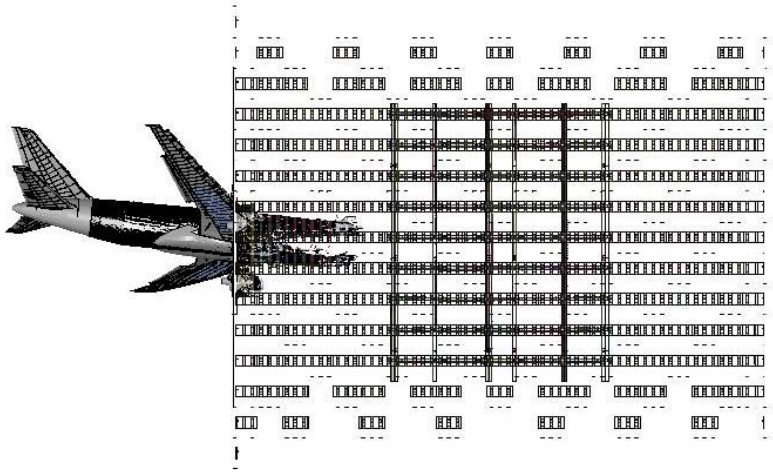

(b) Time=0.10 s

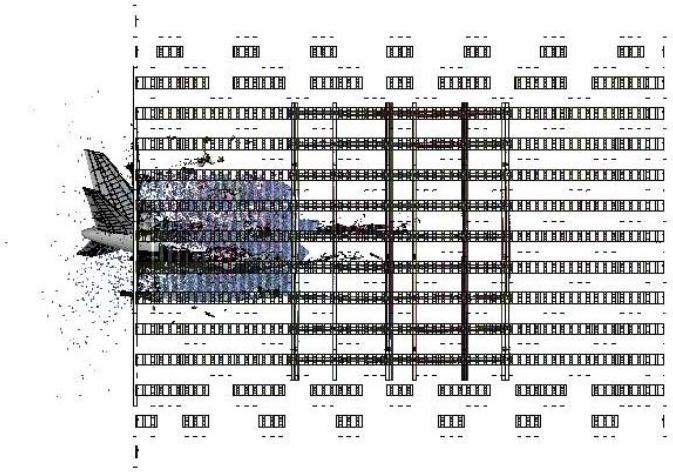

(c) Time=0.20 s

Figure 7–18. WTC 1 more severe global impact analysis (side view).

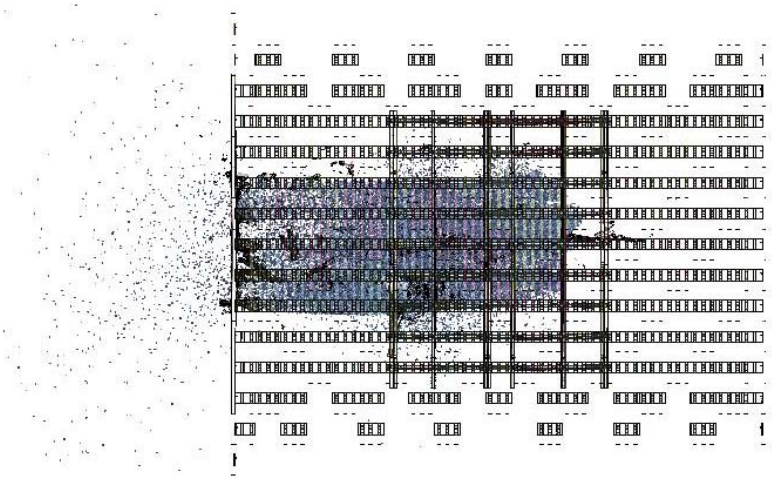

(d) Time=0.30 s

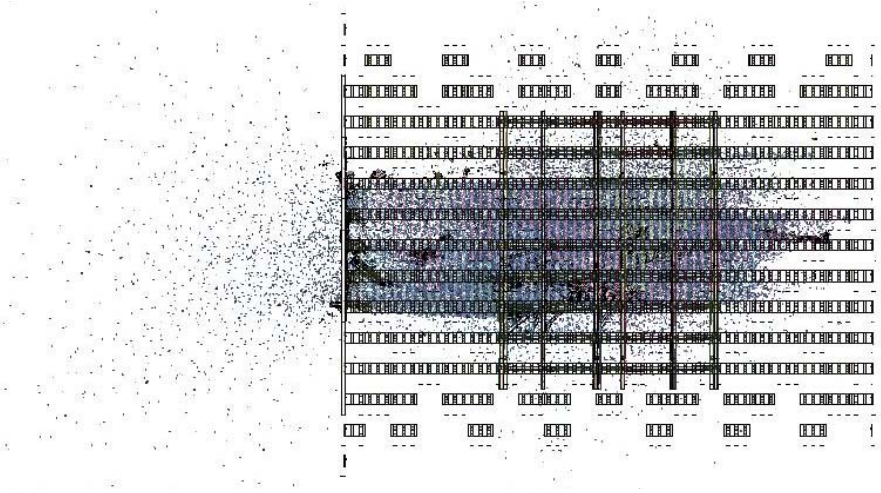

(e) Time=0.40 s

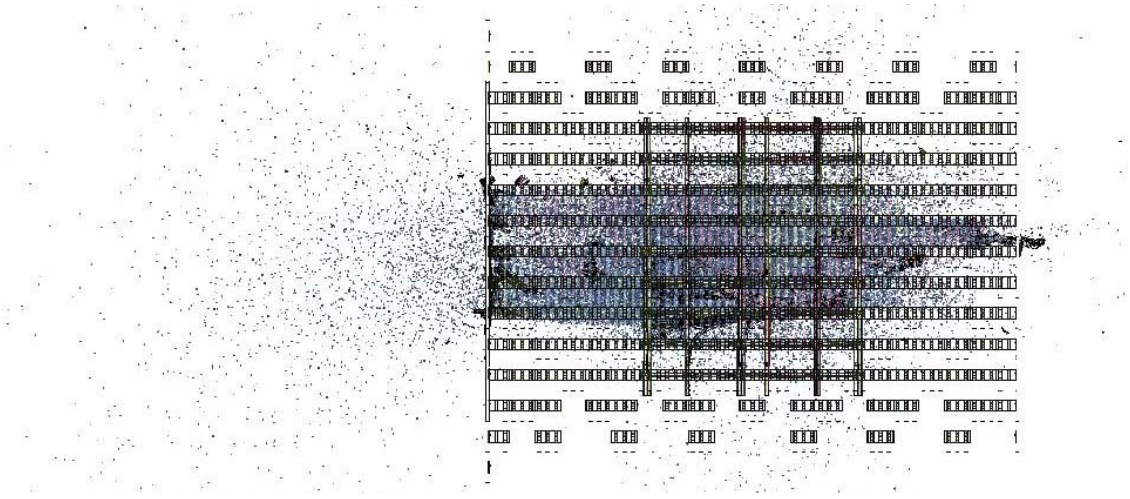

(f) Time=0.50 s

Figure 7–18. WTC 1 more severe global impact analysis (side view) (continued).

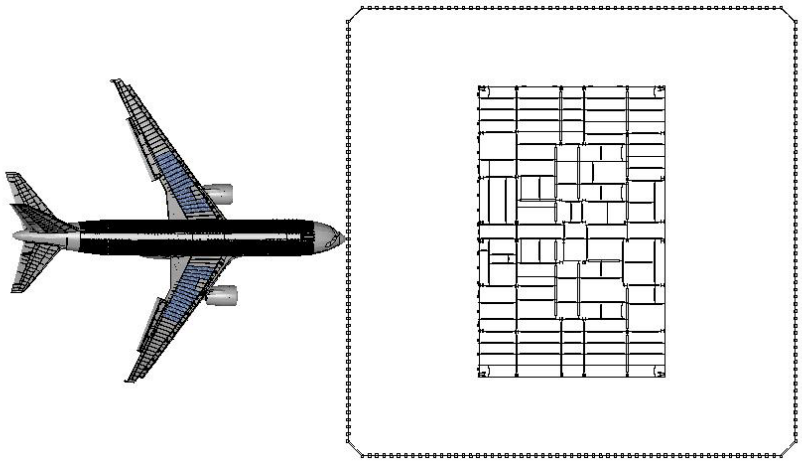

(a) Time=0.00 s

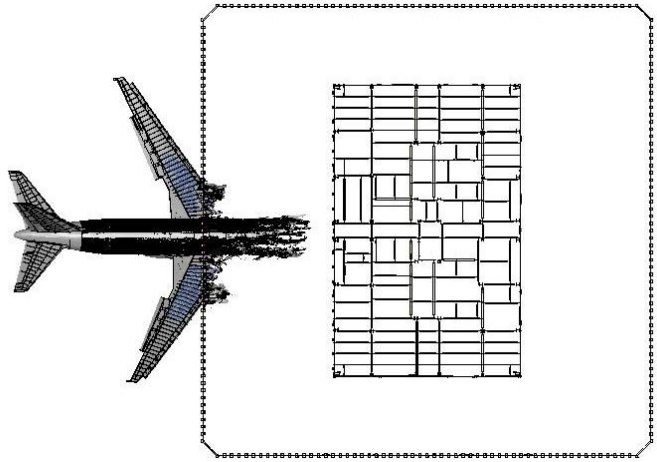

(b) Time=0.10 s

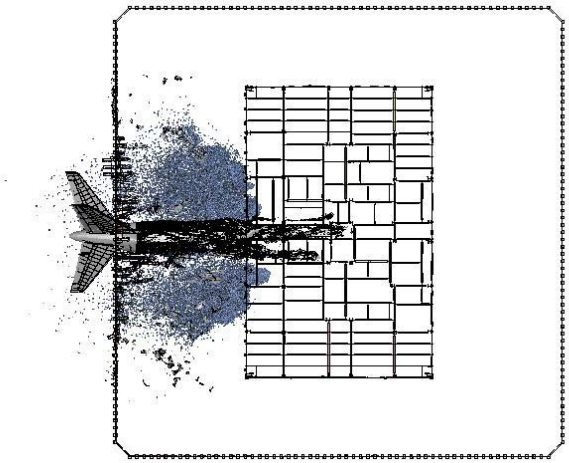

(c) Time=0.20 s

Figure 7–19. WTC 1 more severe global impact analysis (plan view).

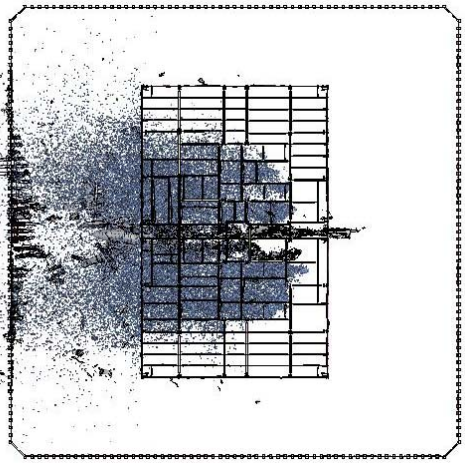

(d) Time=0.30 s

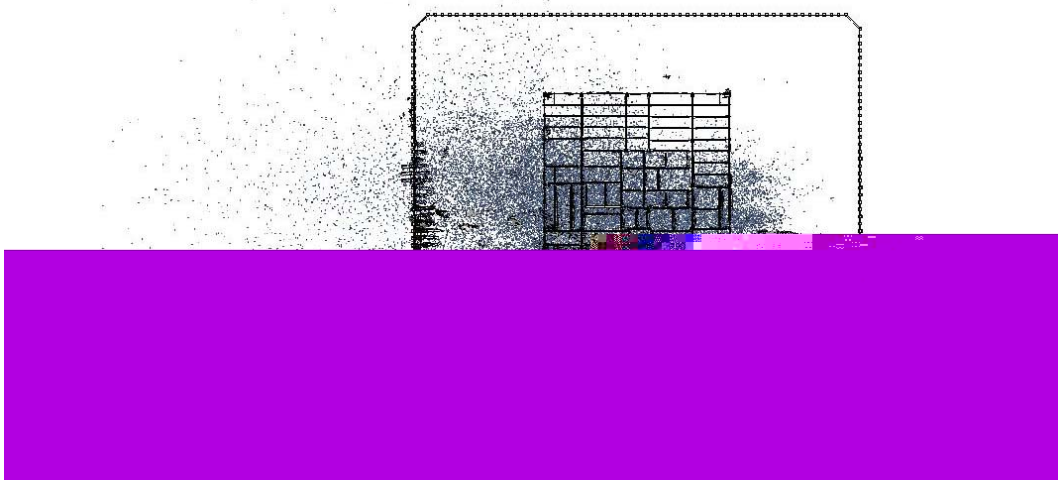

(e) Time=0.40 s

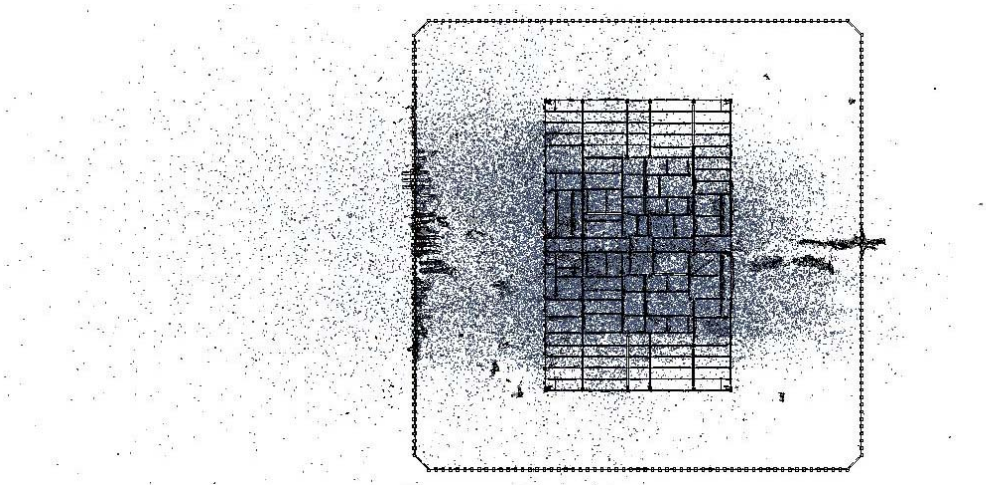

(f) Time=0.50 s

Figure 7–19. WTC 1 more severe global impact analysis (plan view) (continued).

7.4.2 Tower Structural Damage

Exterior Wall Damage

A comparison of the north exterior wall observed and calculated damage from the more severe WTC 1 global impact analysis is shown in Figure 7–20. The calculated and observed magnitude and mode of impact damage on the exterior wall were still in good agreement for the more severe impact analysis.

Comparing Figure 7–5 and Figure 7–20, it can be concluded that the overall agreement with the observed damage to the north wall was good for the base case and the more severe case, with the base case analysis providing the better match to the observed damage. The differences in apparent damage were largely due to panels that may have severed columns in one case and were removed at the connections in another. Toward the wing tips, where the columns and spandrels were not completely severed, the more severe impact damage analysis calculated higher damage to the exterior wall panels. These columns had the largest amount of material with plastic strains above 5 percent (shown in red in the figure). As would be expected, the base case analysis calculated less damage to the exterior wall than the more severe case near the wing tips.

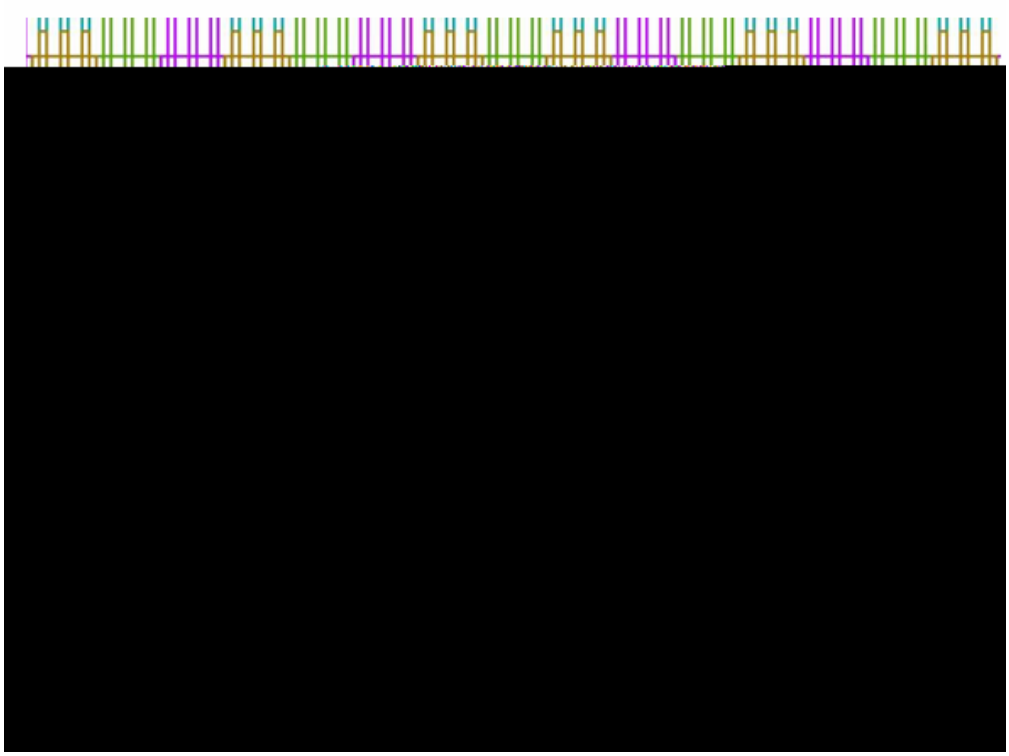

(a) Schematic of observed damage

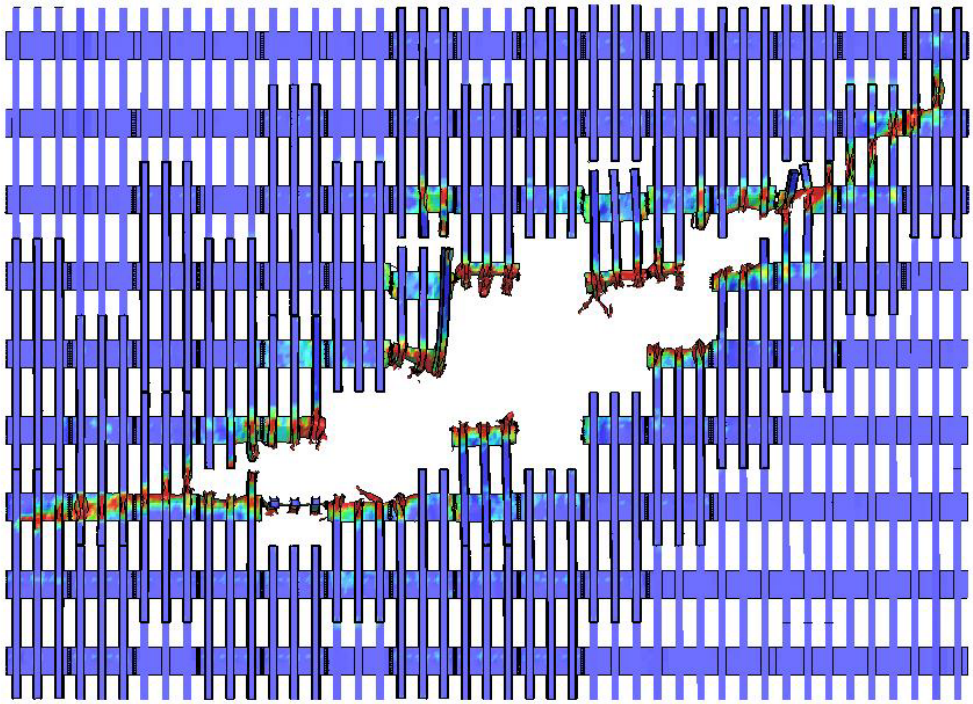

(b) Calculated Damage

Figure 7–20. More severe impact damage to the WTC 1 exterior wall.

Core Structural Damage

The core had extensive damage in the region close to the impact point. The columns in line with the aircraft fuselage failed on the impact side, and several of the core beams were also severely damaged or failed in the impact zone. In some cases, failure of the column splices located on floors 92, 95, and 98 contributed significantly to the failure of the core columns.

The calculated damage to the core columns by row is shown in Figure 7–21, and the damage to the core framing for floors 95 and 96 is shown in Figure 7–22. A summary of the core column damage is provided in Table 7–4, with the qualitative classification of the column damage levels provided previously in Figure 7–7. A total of six columns were severed, and three columns were heavily damaged in the more severe case, compared to three columns severed and four columns heavily damaged in the base case WTC 1 impact analysis. This shows a clear correlation between damage magnitude and impact severity.

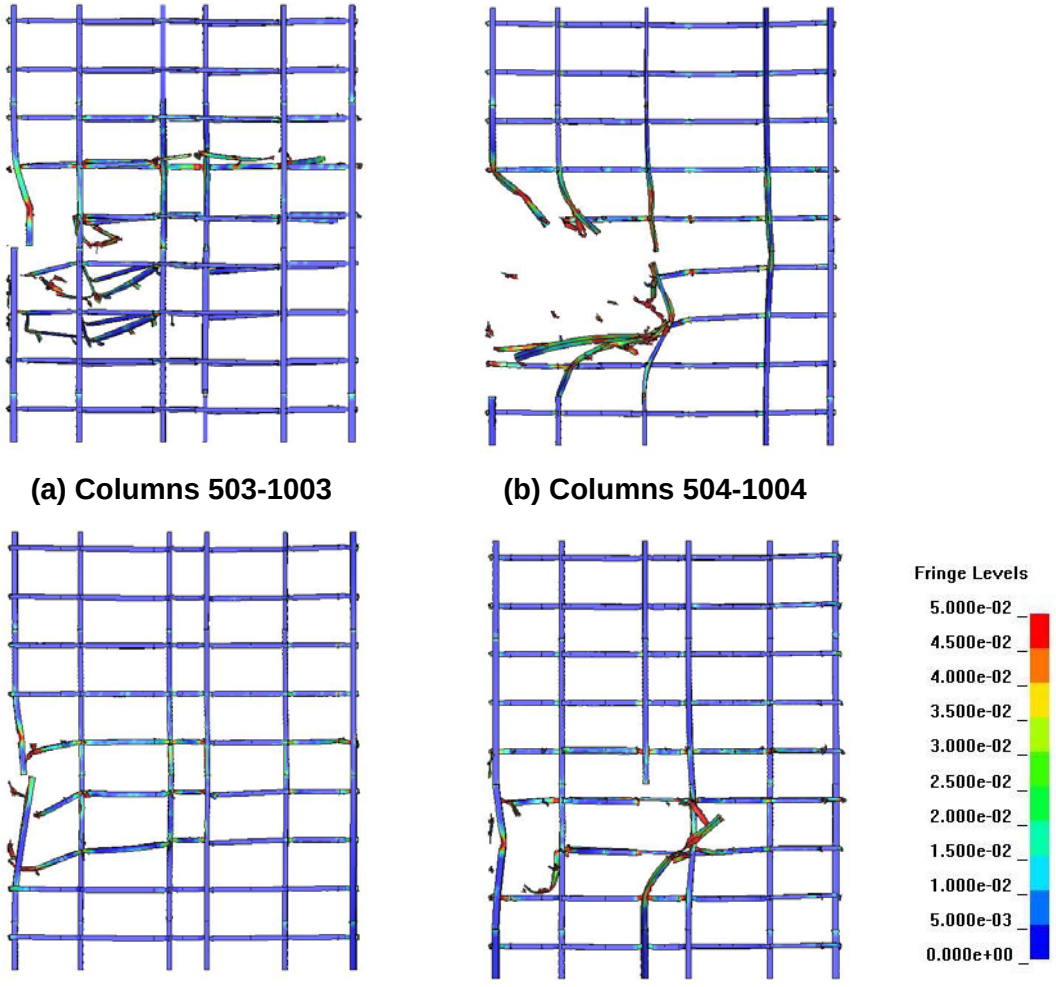

(a) Columns 503-1003 **(b) Columns 504-1004**

(c) Columns 505-1005 **(d) Columns 506-1006** **(e) Reference scale**

Figure 7–21. More severe impact response of the WTC 1 core columns.

(a) Floor 95 core framing damage (b) Floor 96 core framing damage

Figure 7–22. More severe impact damage to the core beams of floors 95 and 96 of WTC 1.

Table 7–4. Summary of core column damage for the more severe WTC 1 impact.

Column	Location	Damage Level	Lateral Deflection of Column Centerline (in.)
Column 503	Floor 95-96	Severed	
Column 504	Floors 92-96	Severed	
Column 505	Floors 93-96	Severed	
Column 506	Floors 93-95	Heavy	24
Column 603	Floors 96-97	Moderate	
Column 604	Floors 92-96	Severed	
Column 605	Floors 94-95	Moderate	
Column 606	Floors 94	Light	
Column 702	Floor 97	Light	
Column 703	Floor 96	Moderate	
Column 704	Floors 92-96	Severed	
Column 705	Floor 95	Moderate	
Column 706	Floors 93-95	Severed	
Column 802	Floor 96	Light	
Column 803	Floors 96-97	Moderate	
Column 804	Floor 94-96	Moderate	
Column 805	Floors 93-95	Heavy	20
Column 903	Floor 96	Light	
Column 904	Floors 95-96	Heavy	19
Column 905	Floor 95	Light	

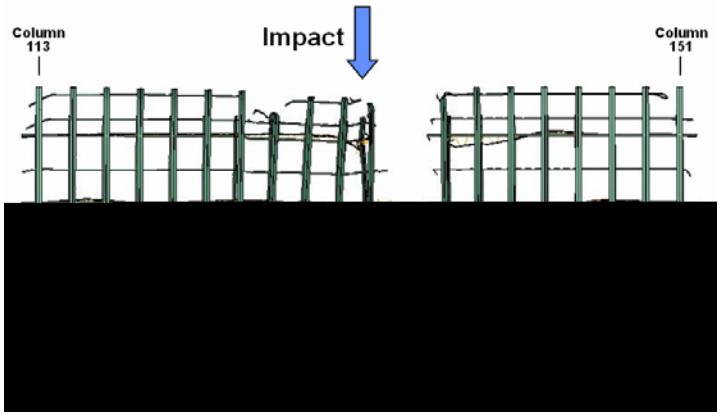

(a) Floor 95 truss damage

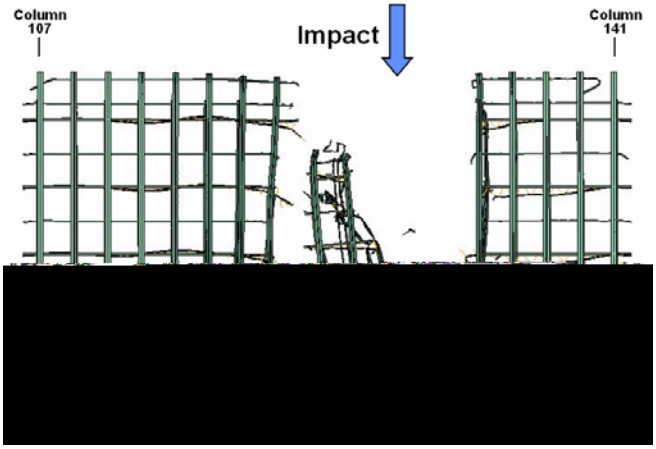

(b) Floor 96 truss damage

Figure 7–24. More severe impact damage to the trusses on floors 95 and 96 of WTC 1 (plan view).

The calculated more severe impact damage to the WTC 1 floor slab for floors 95 and 96 is shown in Figure 7–25. The magnitude of floor slab damage was, in general, very similar for the base case and more severe global impact analyses. When the floor-by-floor damage was compared for the two analyses, the damage appeared to be slightly less for the more severe impact analysis. Similar to the truss damage, the reduced damage in the floor slab is believed to be the result of the reduction in the downward impact trajectory angle from 10.6 to 7.6 degrees in the more severe impact analysis, reducing the normal downward force on the floor structures.

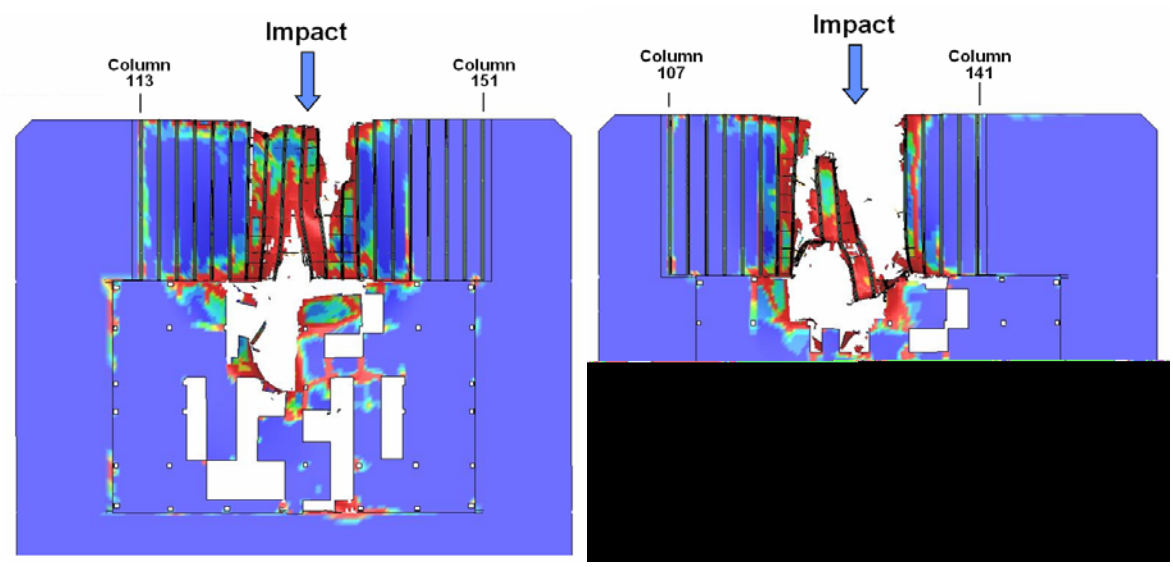

(a) Floor 95 slab damage **(b) Floor 96 slab damage**

Figure 7–25. More severe impact damage to the slabs on floors 95 and 96 of WTC 1 (plan view).

Summary of Structural Damage

Figure 7–26 shows a summary of the structural damage to the core columns and floor systems at floors 93 through 97 of WTC 1 for the more severe case (Case B). Figure 7–27 presents the cumulative damage to WTC 1 on all affected floors and columns.

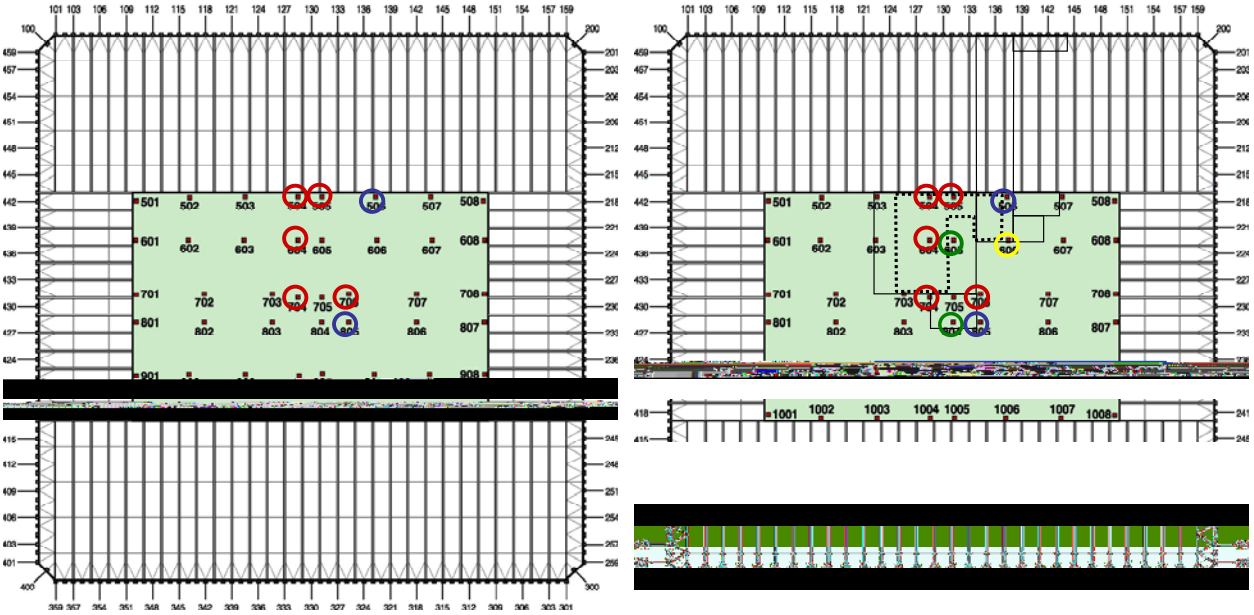

(a) Floor 93 (b) Floor 94

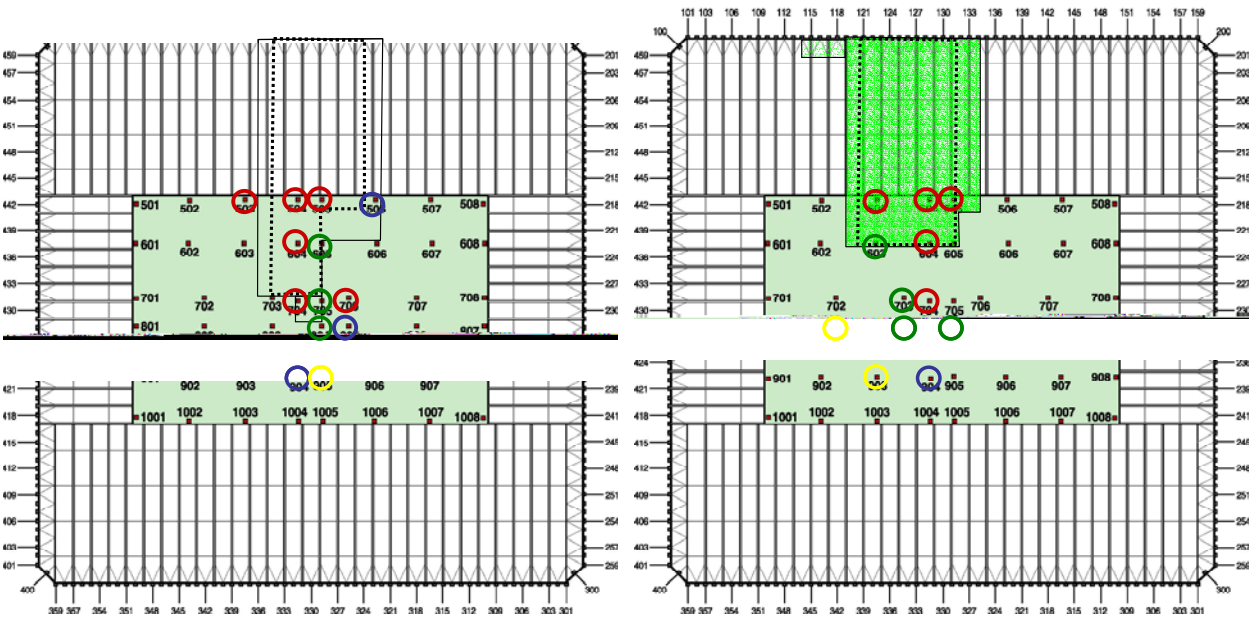

(c) Floor 95 (d) Floor 96

Figure 7–26. Summary of the floor-by-floor structural damage to the floors and columns of WTC 1 (more severe case).

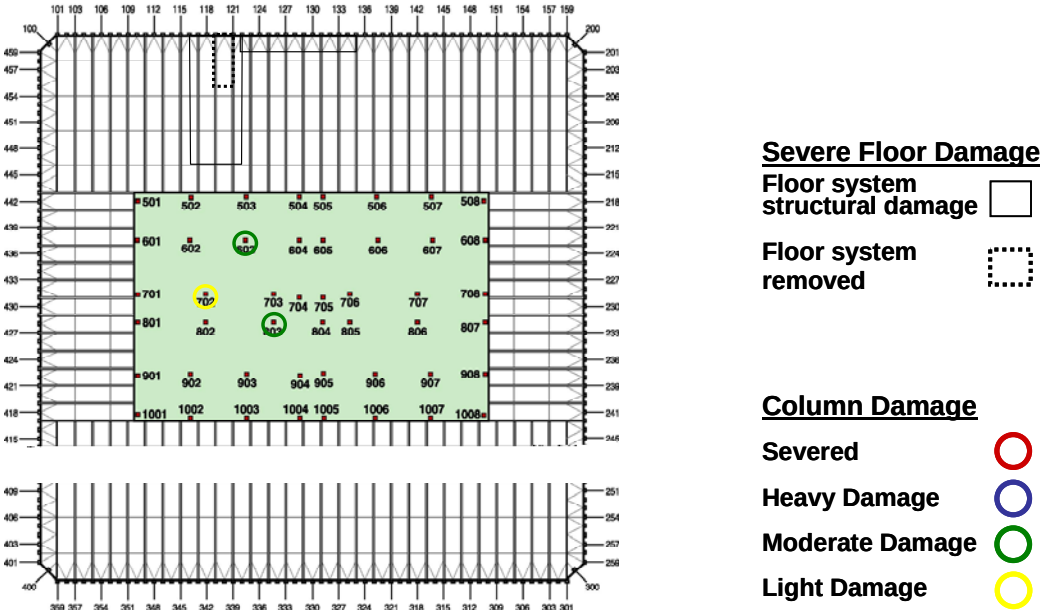

(e) Floor 97

Figure 7–26. WTC 1 more severe global impact analysis (plan view) (continued).

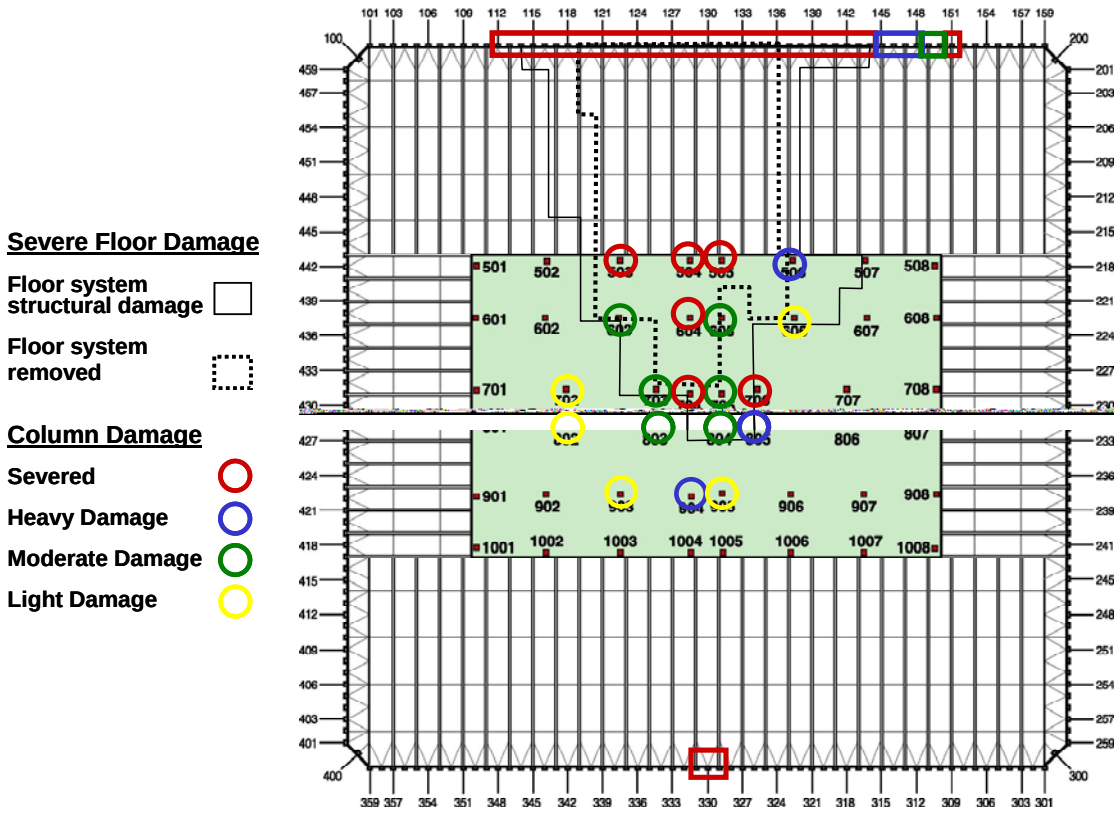

Figure 7–27. Cumulative structural damage to the floors and columns of WTC 1 (more severe case).

7.4.3 Fuel and Debris Distribution

The distribution of the fuel in the tower, calculated from the more severe case, in a plan view and side view is shown in Figure 7–28. At the termination of the global impact analysis, the residual momentum of the jet fuel was less than one percent of the initial momentum, indicating that the fuel cloud was nearly at rest. To more clearly present the calculated response of the structures that influenced the fire propagation, the structural components were removed from the visualization, with the exception that the core columns were maintained in the visualizations for reference positions. A plan view of the response of the remaining building contents and aircraft debris is shown in Figure 7–29.

The calculated damage to the WTC 1 contents for the more severe impact case is shown in plan views for floors 95 and 96 in Figure 7–30 and Figure 7–31, respectively. A comparison to the calculated damage for the base case WTC 1 impact analysis indicated that the content damage zone was very similar in width, but extended further south through the tower in the more severe impact. The more severe impact produced significantly greater content damage on the far side of the core and extended more fully through the tower.

A summary of the floor-by-floor fuel and debris distributions is given in Table 7–5. The bulk of the fuel and aircraft debris was deposited in floors 93 through 97, with the greatest concentration on floor 94. The calculated debris cloud included 46,800 lbs of debris and 7,500 lbs of aircraft fuel outside of the tower at the end of the impact analysis, either rebounding from the impact face (north wall) or passing through the tower (south wall). This amount might have been larger in the calculation due to the reasons mentioned previously for the base case impact (see Section 7.3.3). Comparing Figure 7–29 and Table 7–5 with Figure 7–15 and Table 7–2, it can be seen that the amount of debris exiting the south wall of the tower in the more severe case was much larger than that from the base case.

Table 7–5. Fuel and aircraft debris distribution for the more severe WTC 1 impact.

Tower Location	Aircraft Fuel	Aircraft Debris
Total Outside Tower	7,500 lb	46,800 lb
WTC 1 Floor 92	1.200 lb	15 lb
WTC 1 Floor 93	5,800 lb	39,100 lb
WTC 1 Floor 94	14,100 lb	59,900 lb
WTC 1 Floor 95	13,600 lb	22,500 lb
WTC 1 Floor 96	13,300 lb	21,500 lb
WTC 1 Floor 97	9,600 lb	5,200 lb
WTC 1 Floor 98	3,100 lb	7,300 lb
WTC 1 Floor 99	1,100 lb	400 lb
Total Weight	69,300 lb	202,700 lb

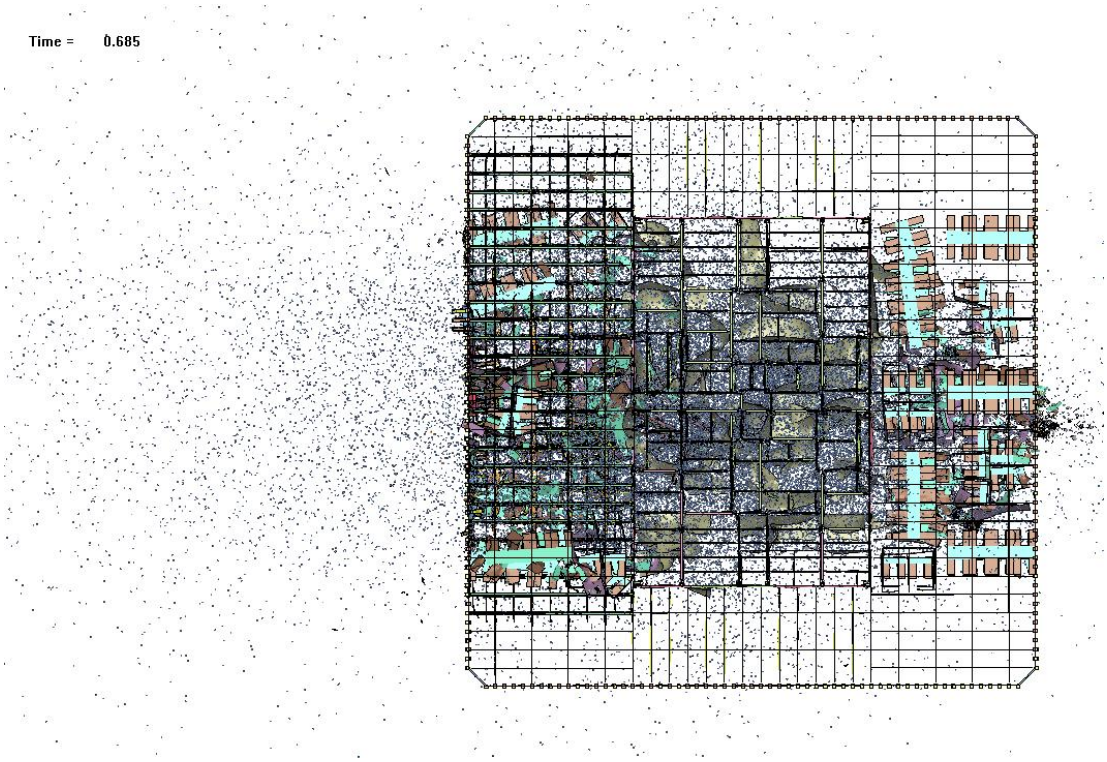

(a) Plan view (floor slab removed)

(b) Side view

Figure 7–28. Calculated fuel distribution in the more severe WTC 1 analysis.

(a) Pre-impact configuration

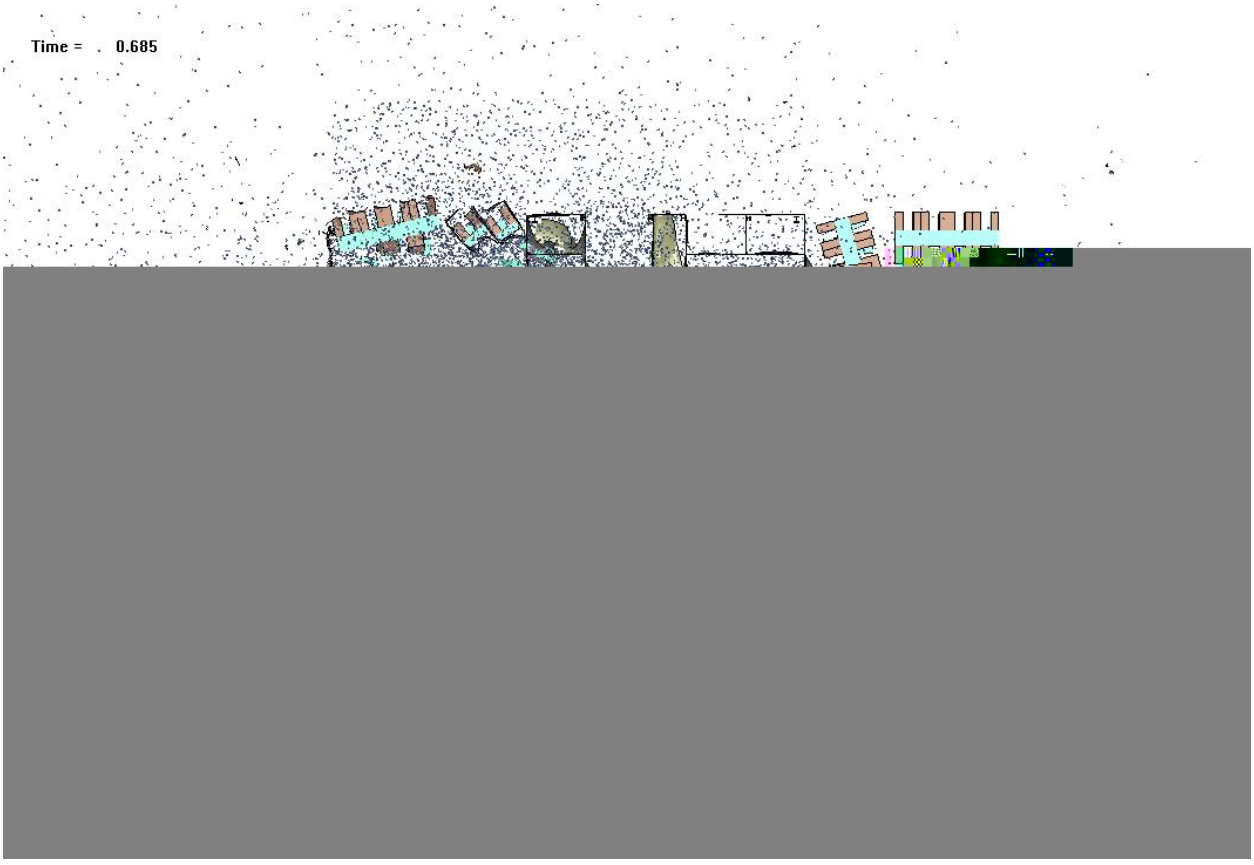

(b) Calculated impact response

Figure 7–29. Plan view of calculated WTC 1 building, fuel, and aircraft debris distribution for the more severe case.

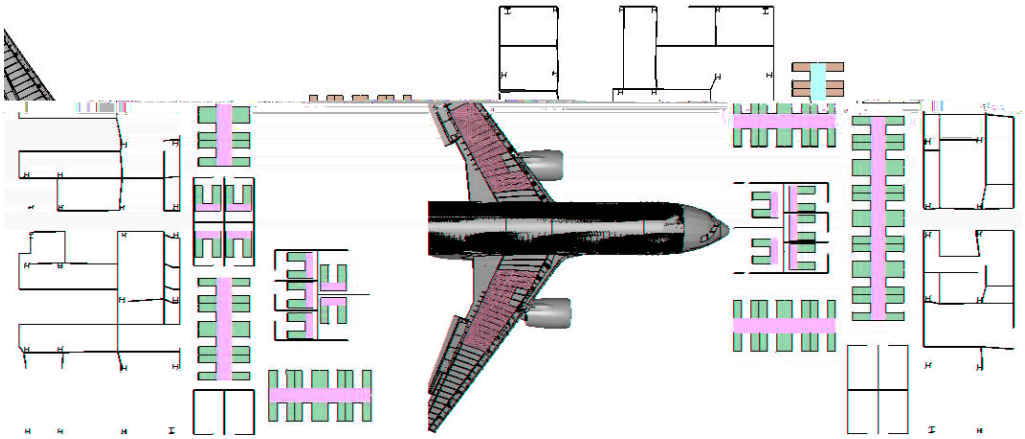

(a) Pre-impact configuration

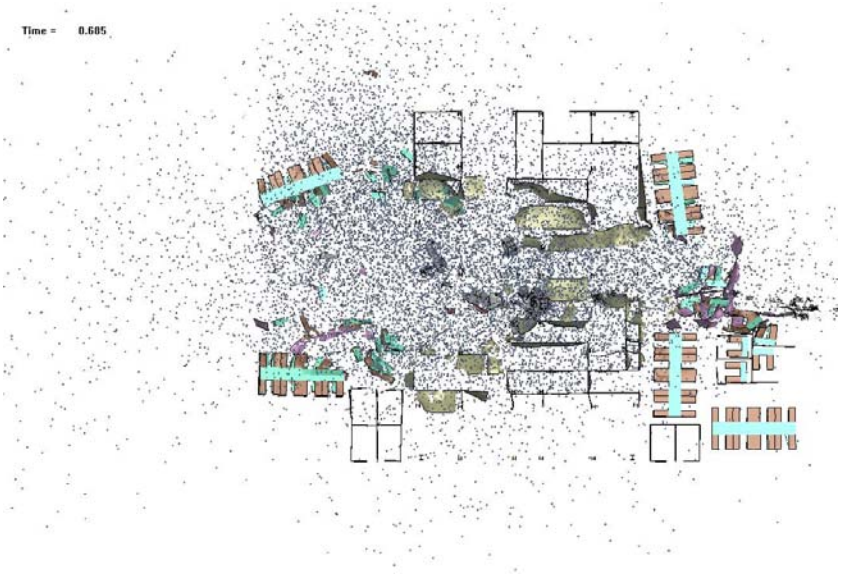

(b) Calculated impact response

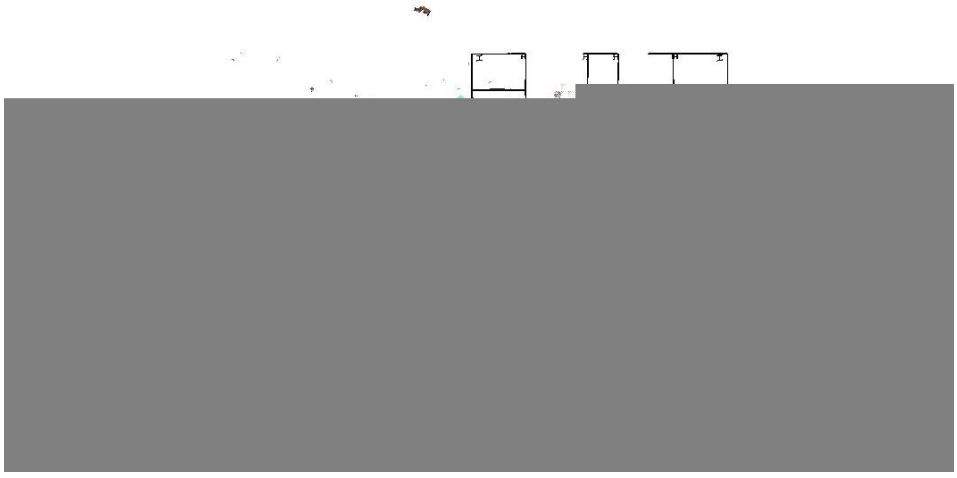

(c) Calculated impact response (fuel removed)

Figure 7–30. Calculated more severe WTC 1 impact response of floor 95 contents.

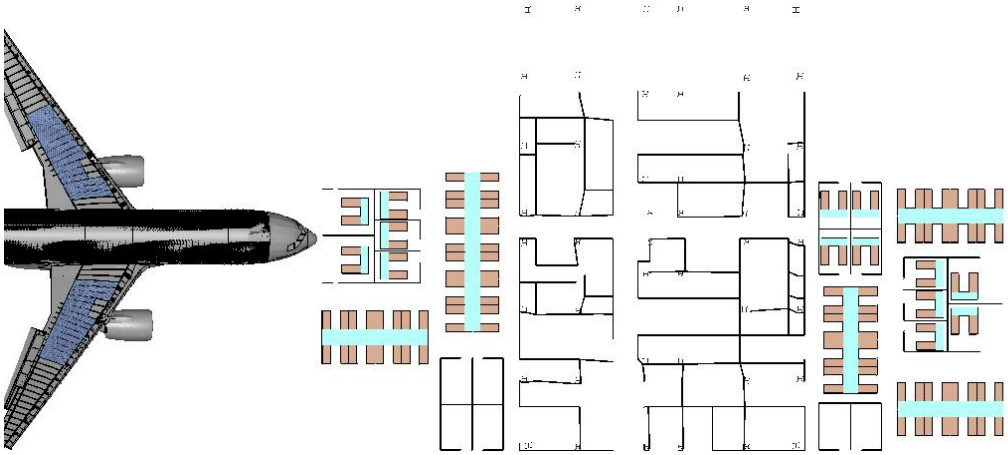

(a) Pre-impact configuration

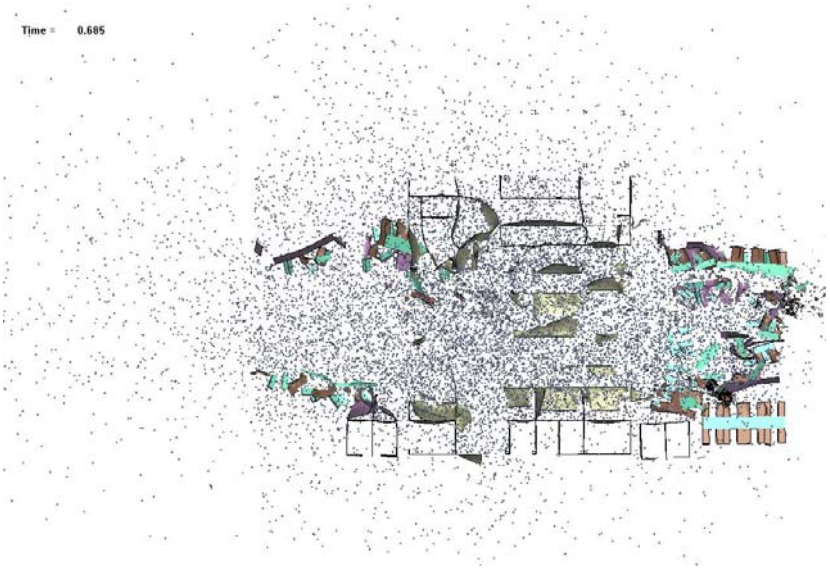

(b) Calculated impact response

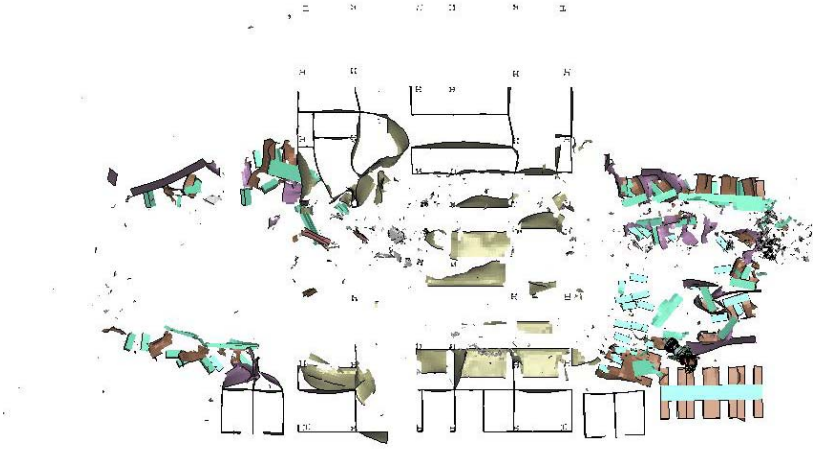

(c) Calculated impact response (fuel removed)

Figure 7–31. Calculated more severe WTC 1 impact response of floor 96 contents.

7.5 WTC 1 LESS SEVERE IMPACT ANALYSIS – BRIEF DESCRIPTION

This section presents a brief description of the results from the less severe damage case. The reader is referred to NIST NCSTAR 1-2B for further details.

For the north exterior wall of WTC 1, the magnitude and mode of impact damage were still in good agreement with the observed damage for the less severe impact scenario.

The core had a limited damage confined to the region nearest to the impact point. Only one column was severed, and two columns were heavily damaged for the less severe case, compared to three severed columns and four heavily damaged columns in the base case WTC 1 impact analysis. The failure of the column splices located on floors 92 and 95 contributed to the failure of the core column.

The floor trusses experienced significant damage in the impact zone. The calculated impact response produced severe damage to the truss structures in the primary impact path of the fuselage. The truss structures were severely damaged from the exterior wall to the core. The truss floor system on floors 94 through 96 were damaged and sagged downward as a result of the impact loading.

When compared with the base case, the magnitude of damage to the floor trusses and floor slabs was slightly increased for the less severe impact analysis. The parameters used in the less severe global impact analysis would primarily contribute to a reduced damage magnitude for the tower structures. However, the downward impact trajectory angle was increased from the 10.6 degree angle in the base case analysis to a 13.6 degree angle in the more severe impact analysis. This would have the effect of directing more of the impact energy downward, increasing the normal force on the floor structures in the impact zone. As a result, the combined effects of the analysis parameter variations produced a small increase in the damage to the truss structure in the less severe impact analysis scenario.

A comparison to the base case and less severe case indicated that the building contents damage zone was very similar in width but did not extend as far through the tower in the less severe impact. The less severe impact produced little content damage on the far side of the core and did not extend fully through the tower. Little or no debris penetration of the south wall of the tower was expected for the less severe impact condition.

7.6 WTC 2 BASE CASE IMPACT ANALYSIS – CASE C

This case is referred to as Case C for the remainder of the WTC Investigation reports. The combined aircraft and tower model used for the base case global impact conditions of WTC 2 is shown in Figure 7–32. The WTC 2 base case impact analysis was performed for a 0.62 s duration following initial impact of the aircraft nose with the south exterior wall.

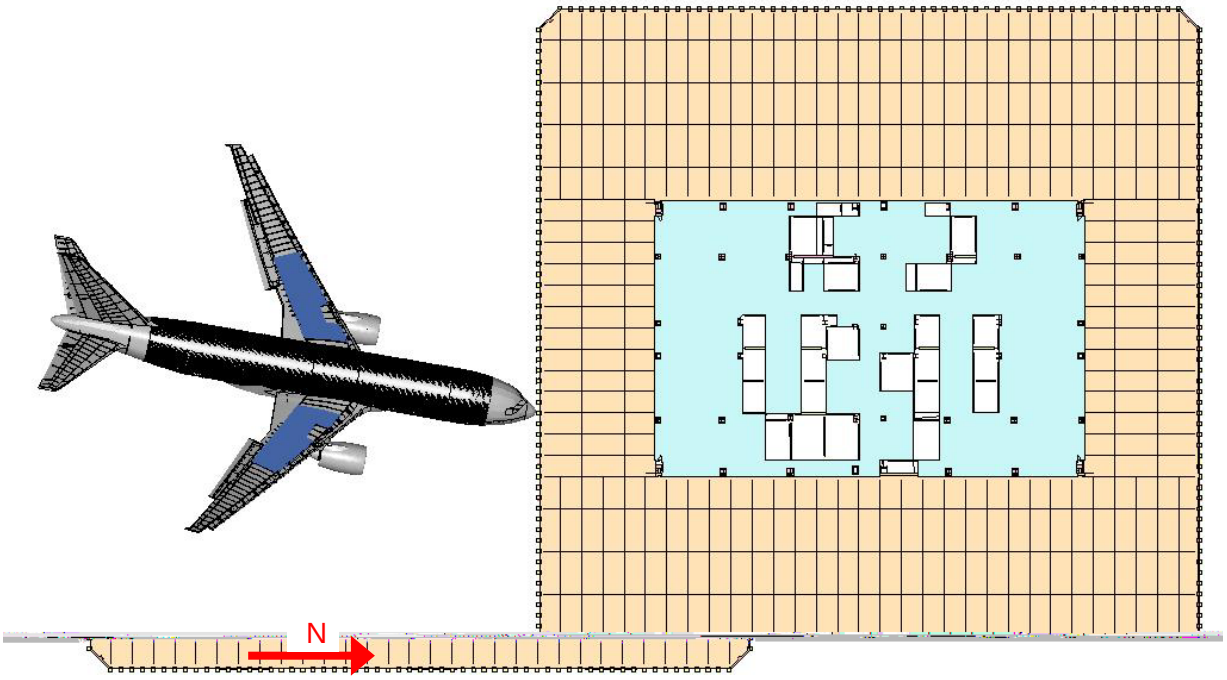

(a) Plan view

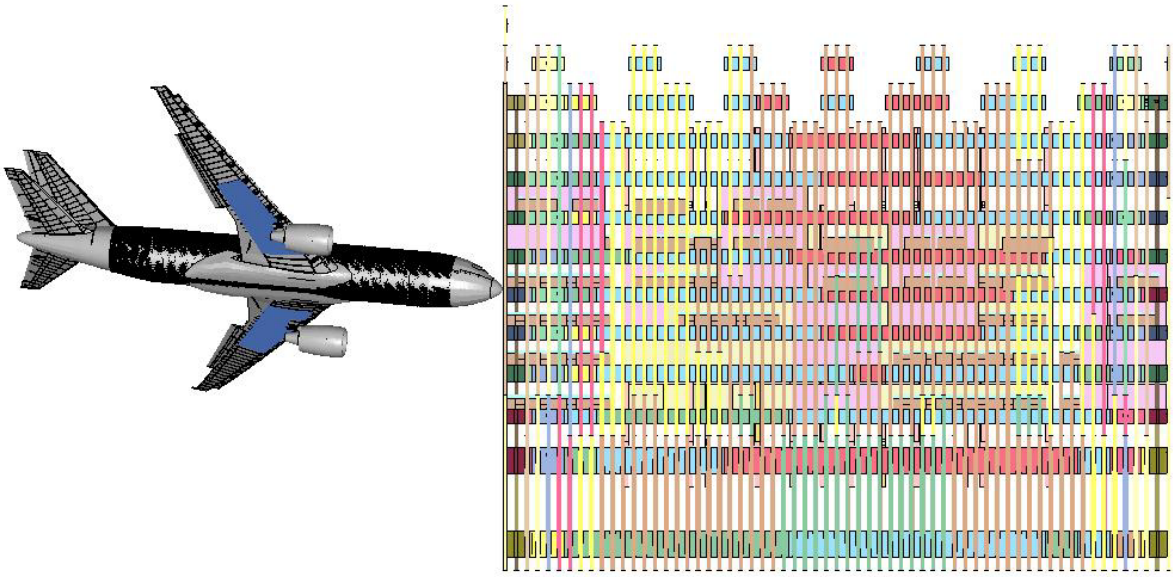

(b) Side view

Figure 7–32. WTC 2 global impact model.

7.6.1 Impact Response

The base case global aircraft impact response of WTC 2 is shown in side views and plan views in Figure 7–33 and Figure 7–34, respectively. The response is shown at intervals of 0.1 s from impact through the initial 0.5 s of the response. The initial 0.1 s of the base case global aircraft impact response, shown in Figure 7–33(b) and Figure 7–34(b), was dominated by the impact, penetration, and

fragmentation of the forward fuselage structures. The engines and leading portions of the wings penetrated the exterior wall. The forward fuselage structures were severely damaged both from the penetration through the exterior columns and the interaction with the 81st floor slab that sliced the fuselage structures in half. The downward trajectory of the aircraft structures caused the airframe to collapse against the floor, and the subsequent debris motion was redirected inward along a more horizontal trajectory parallel to the floor. The higher impact speed and short truss floor span in this impact orientation had the forward fuselage structures well into the tower core by this time.

By 0.2 s after impact, the full penetration of the aircraft into the tower was just completed, as shown in Figure 7–33(c) and Figure 7–34(c). The airframe was mostly broken up, but some large sections of the aft fuselage and tail were still intact, having penetrated through the opening in the south wall produced by the forward fuselage structures. The aircraft fuel cloud was starting to spread out, but was still relatively dense, and the leading edge of the fuel was approximately one-third through the tower core. By 0.2 s, the downward trajectory of the aircraft structures transferred sufficient vertical load that the truss floor structures on floors 80 and 81 were starting to collapse in the impact zone.

At 0.3 s after impact, the aircraft fuel cloud had penetrated approximately two-thirds the distance through the core and was spreading out, as shown in Figure 7–33(d) and Figure 7–34(d). However, the subsequent motion of the aircraft fragments and fuel debris cloud began to be noticeably slowed beyond this time. The fuel and debris continued to spread through the tower, but at a much slower rate, as seen in the remaining images in Figure 7–33 and Figure 7–34. The spread of the fuel and debris cloud was more rapid and extensive in the open truss floor regions than through the core as a result of the open volume above the workstations in the truss floor zone.

The load transfer of the base case WTC 2 aircraft impact can be described by the time-history of the aircraft momentum as shown in Figure 7–35. The curve illustrates an initial rate of load transfer during the first 0.1 s of impact as the forward fuselage penetrated the exterior wall and impacted the interior structures. Between 0.1 s and 0.2 s, a more rapid load transfer rate was observed as the area of the impact became larger (extending outward in the wing impact regions) and a higher percentage of the aircraft mass was impacting the interior structures. At 0.2 s, the aircraft completely penetrated the building and retained approximately 30 percent of its initial momentum. Beyond this time, the rate of load transfer was steadily decreasing, with very little load transfer after approximately 0.4 s. The behavior was very similar to that of the base case WTC 1 impact, shown in Figure 7–4, but with a slightly compressed time scale resulting from the higher impact speed on WTC 2.

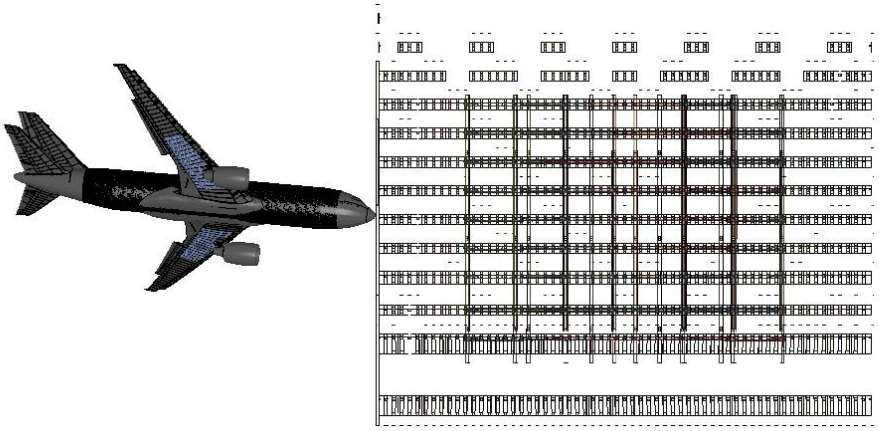

(a) Time=0.00 s

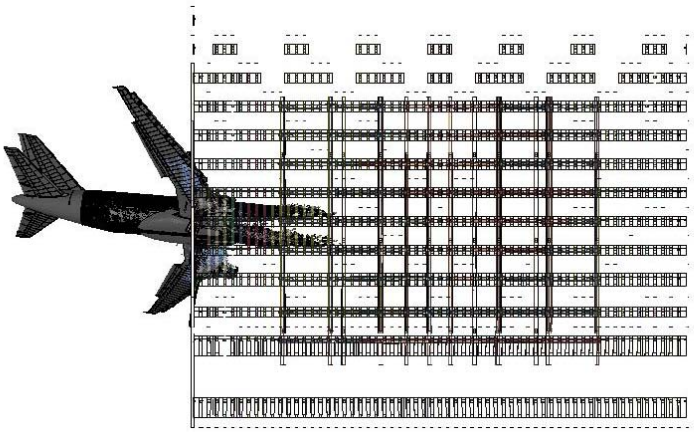

(b) Time=0.10 s

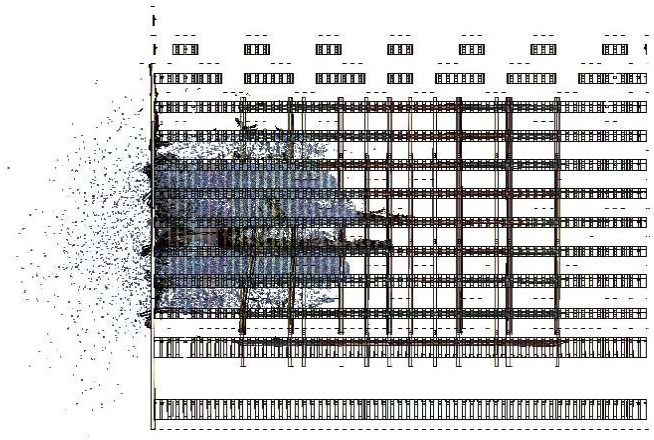

(c) Time=0.20 s

Figure 7–33. WTC 2 base case global impact analysis (side view).

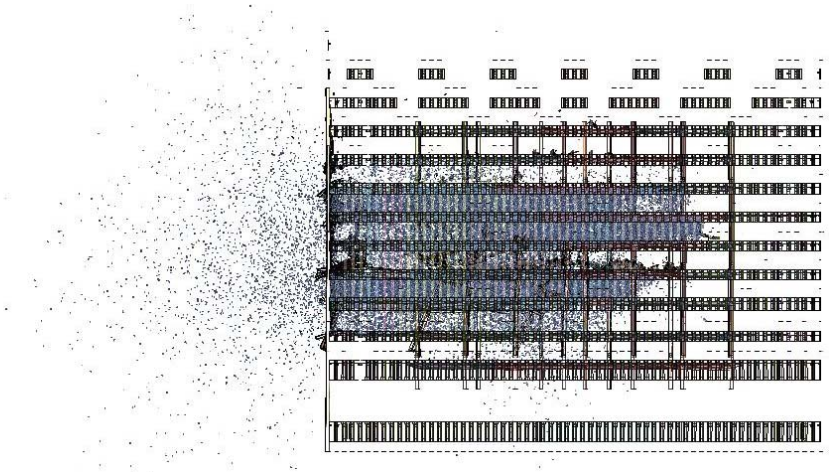

(d) Time=0.30 s

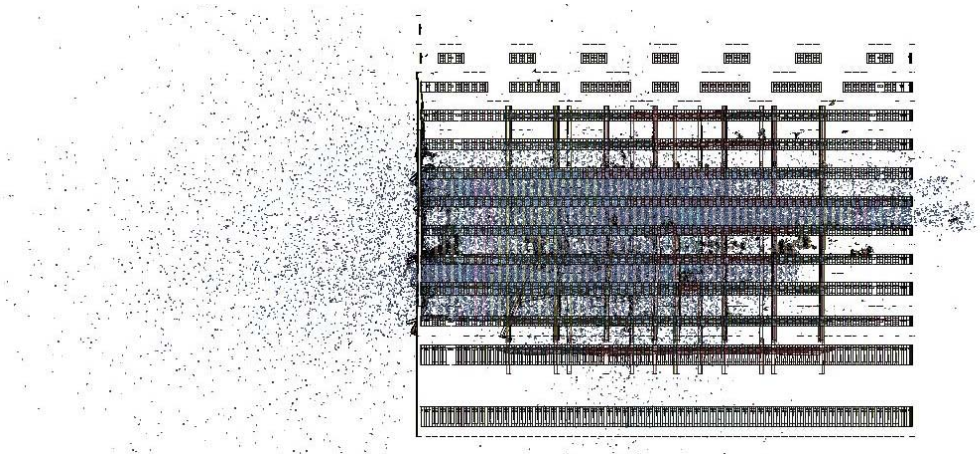

(e) Time=0.40 s

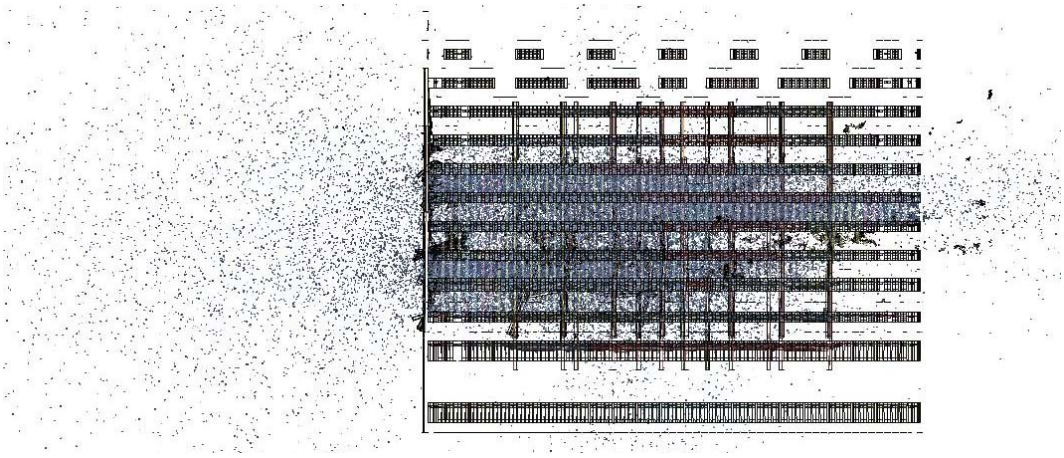

(f) Time=0.50 s

Figure 7–33. WTC 2 base case global impact analysis (side view) (continued).

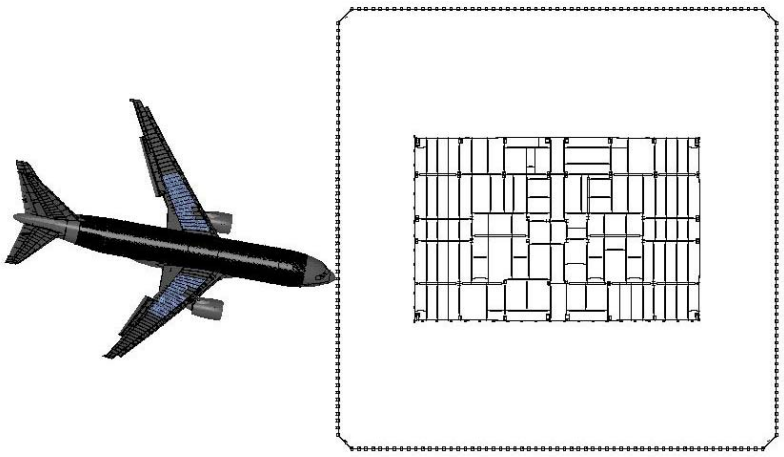

(a) Time=0.00 s

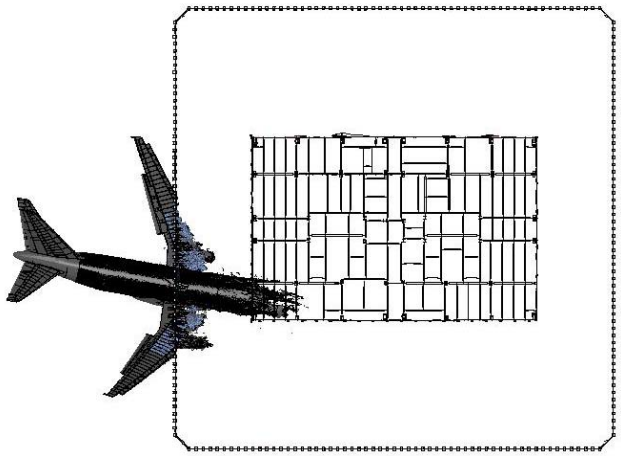

(b) Time=0.10 s

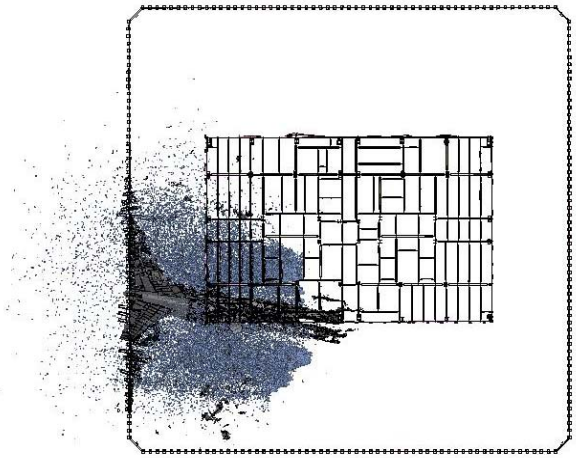

(c) Time=0.20 s

Figure 7–34. WTC 2 base case global impact analysis (plan view).

(d) Time=0.30 s

(e) Time=0.40 s

(f) Time=0.50 s

Figure 7–34. WTC 2 base case global impact analysis (plan view) (continued).

The exterior wall completely failed in the regions of the fuselage, engine, and fuel-filled wing section

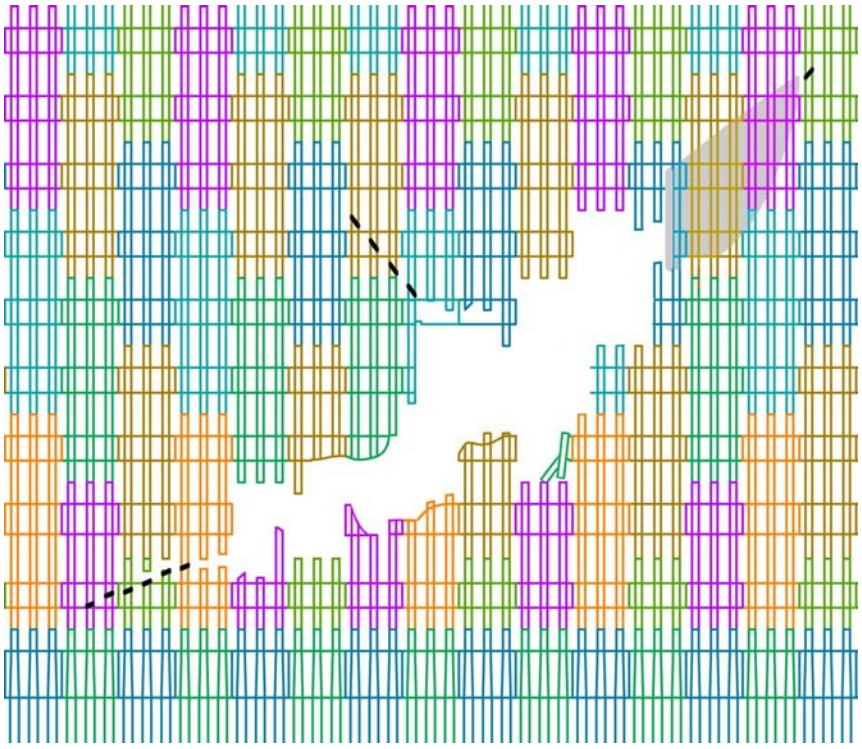

(a) Schematic of observed damage

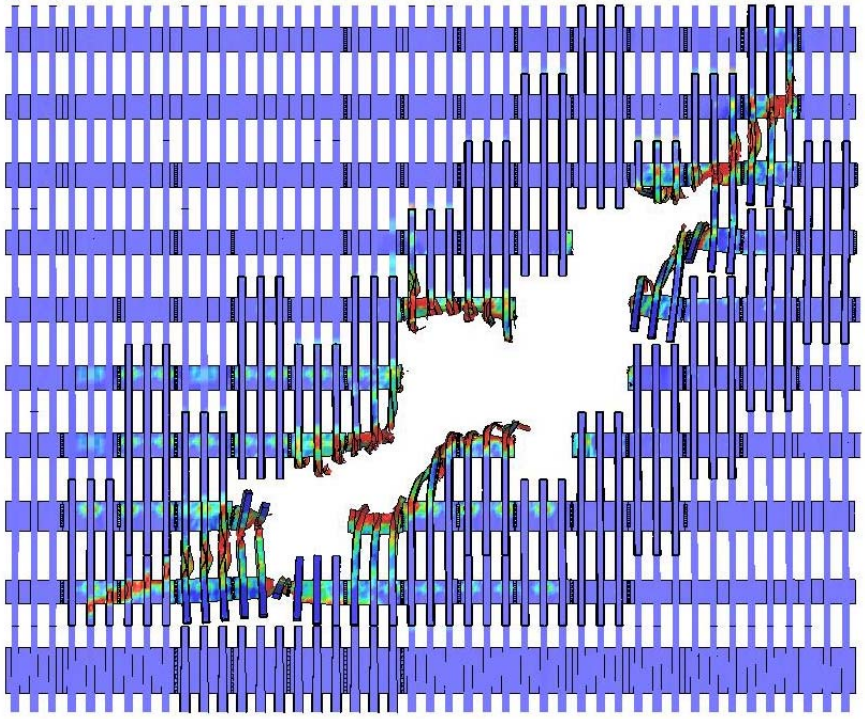

(b) Calculated damage

Figure 7–36. Base case impact damage to the WTC 2 exterior wall.

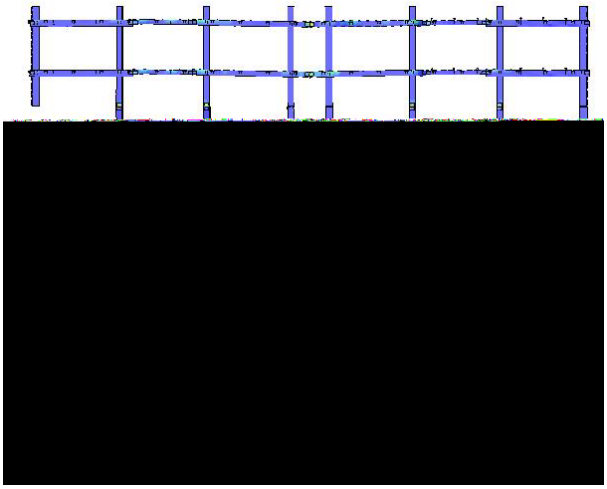

(a) Columns 1001-1008

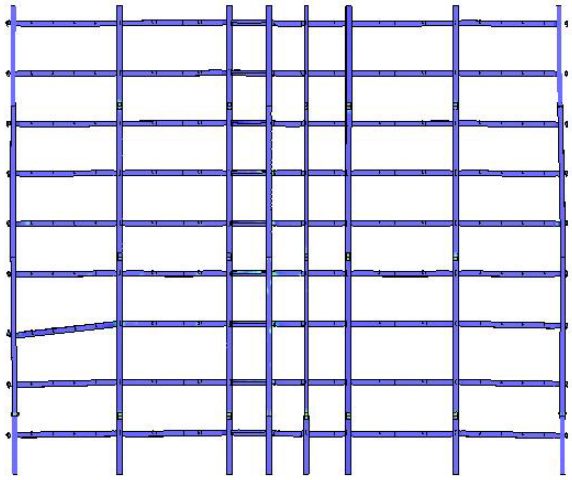

(b) Columns 901-908

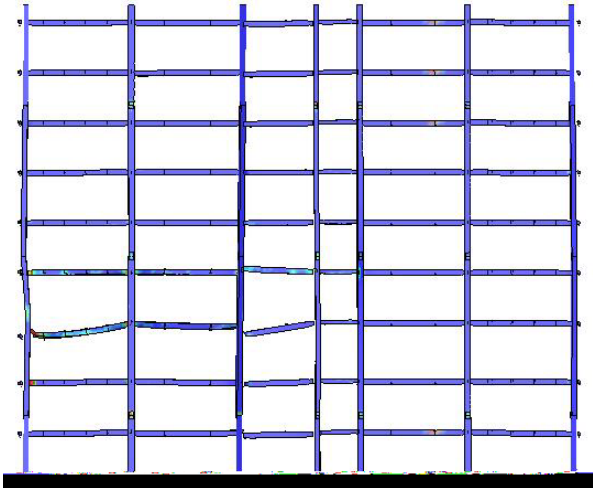

(c) Columns 801-807

(d) Columns 701-708

Figure 7–37. Base case impact damage to the WTC 2 core columns.

Floor Truss and Slab Damage

An overall frontal view for the floor truss structure in the WTC 2 impact zone, along with the calculated base case impact damage to the trusses, is shown in Figure 7–39. The figure shows that the trusses experienced significant damage in the impact zone, with the largest amount of damage on floor 81. A plan view of the calculated damage to the trusses on floors 80 and 81 is shown in Figure 7–40. The calculated impact response produced severe damage to the truss structures in the primary impact path of the fuselage. The truss structures were severely damaged from the exterior wall to the core. The truss floor system on floors 79 and 81 had sufficient damage from the impact that truss floor sections sagged downward as a result of the impact.

Table 7–6. Summary of core column damage for the base case WTC 2 impact.

Column	Location	Damage Level	Lateral Deflection of Column Centerline (in.)
Column 801	Floor 79	Heavy	10
Column 901	Floors 79-82	Severed	
Column 902	Floor 79	Heavy	32
Column 903	Floors 77-83	Severed	
Column 904	Floor 79	Moderate	
Column 905	Floor 79	Heavy	18
Column 1001	Floors 77-83	Severed	
Column 1002	Floors 79-81	Severed	
Column 1003	Floor 80	Severed	
Column 1004	Floor 80	Heavy	18

(a) Floor 80 core framing damage **(b) Floor 81 core framing damage**

Figure 7–38. Base case impact damage to the core beams of floors 80 and 81 of WTC 2.

(a) Initial detailed truss structures

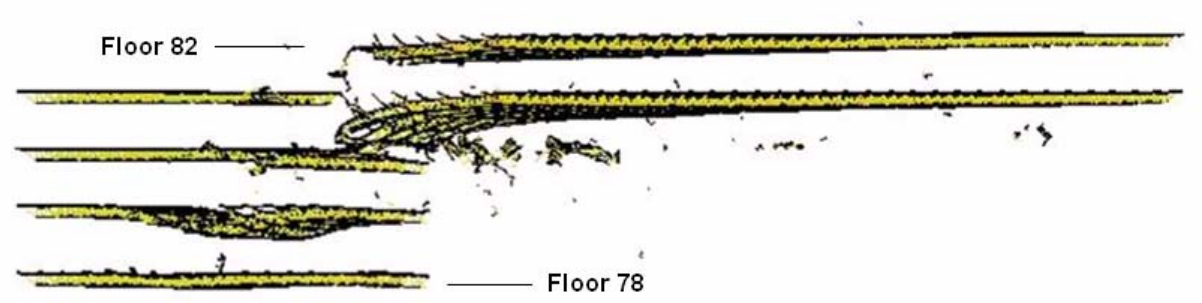

(b) Calculated damage

Figure 7–39. Base case impact damage to the WTC 2 floor trusses (front view).

The calculated damage to the WTC 2 floor slabs for floors 80 and 81 is shown in Figure 7–41. The fringes of damage were set such that the concrete failed in the regions colored red (2 percent plastic strain). In these regions, it is expected that the concrete had been severely damaged and potentially removed, exposing the supporting metal decking. The strength of the floor slab was severely reduced in the analysis beyond this strain to model the residual strength of the metal deck after the concrete failure, breakup, and removal. At a plastic strain of 30 percent, corresponding to failure levels for the metal decking material, the elements were eroded (seen as holes ruptured in the floor slab shown).

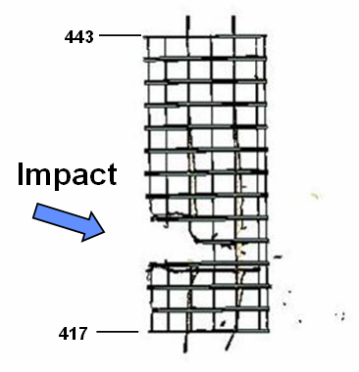

(a) Floor 80 truss damage

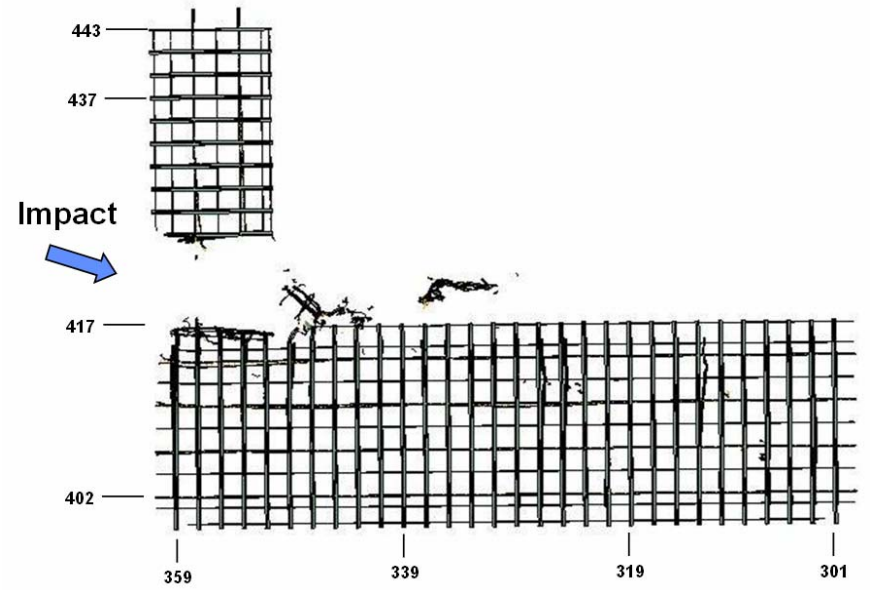

(b) Floor 81 truss damage

Figure 7–40. Base case impact damage to the trusses on floors 80 and 81 of WTC 2 (plan view).

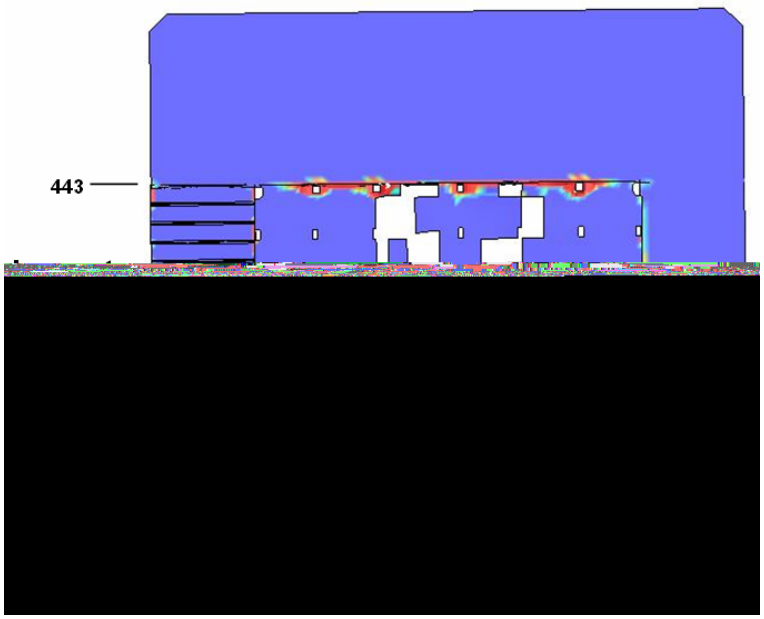

(a) Floor 80 slab damage

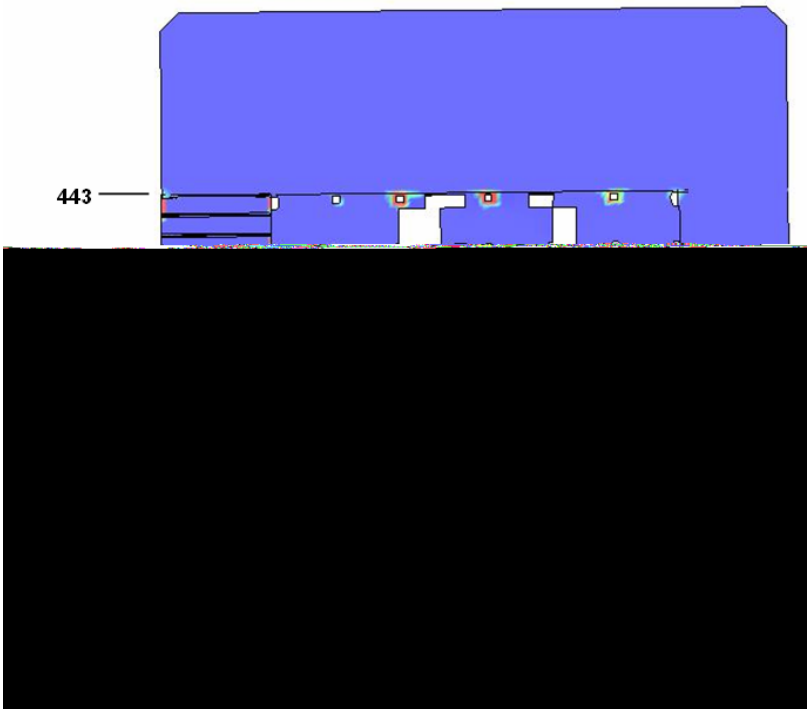

(b) Floor 81 slab damage

Figure 7–41. Base case impact damage to the slabs on floors 80 and 81 of WTC 2 (plan view).

Summary of Structural Damage

The impact-induced structural damage described above was used as the initial conditions for the post-impact fire-structural analyses. Figure 7–42 shows a summary of the structural damage to the core

columns and floor systems at floors 77 through 83 of WTC 2 for the base case (Case C). The damage to the columns at the various levels is identified by the color of the circles, where red, blue, green, and yellow signify severed, heavily damaged, moderately damaged, and lightly damaged columns, respectively. The dotted boxes on the figures indicate areas where the impact created an opening in the floor. These were used to identify openings in the floor slab in the fire dynamics simulations (NIST NCSTAR 1-5F). The solid boxes indicate areas in the floor system that had severe structural damage. These areas were removed from the subsequent structural analyses (NIST NCSTAR 1-6).

Figure 7–43 presents the cumulative damage to WTC 2 on all affected floors and columns. The figure shows the damage to the south exterior wall due to impact, based on photographs of the south walls. Note that damage to columns 407 through 409 was based on the analysis results, since this area was obscured by smoke in the photographs. Figure 7–43 also shows the damage to columns on the north perimeter wall, which the analysis did not capture due to the coarse mesh on the north wall. This damage was observed in photographs (see Section 7.10.2). As a result, this damage was accounted for in the subsequent structural analyses (NIST NCSTAR 1-6).

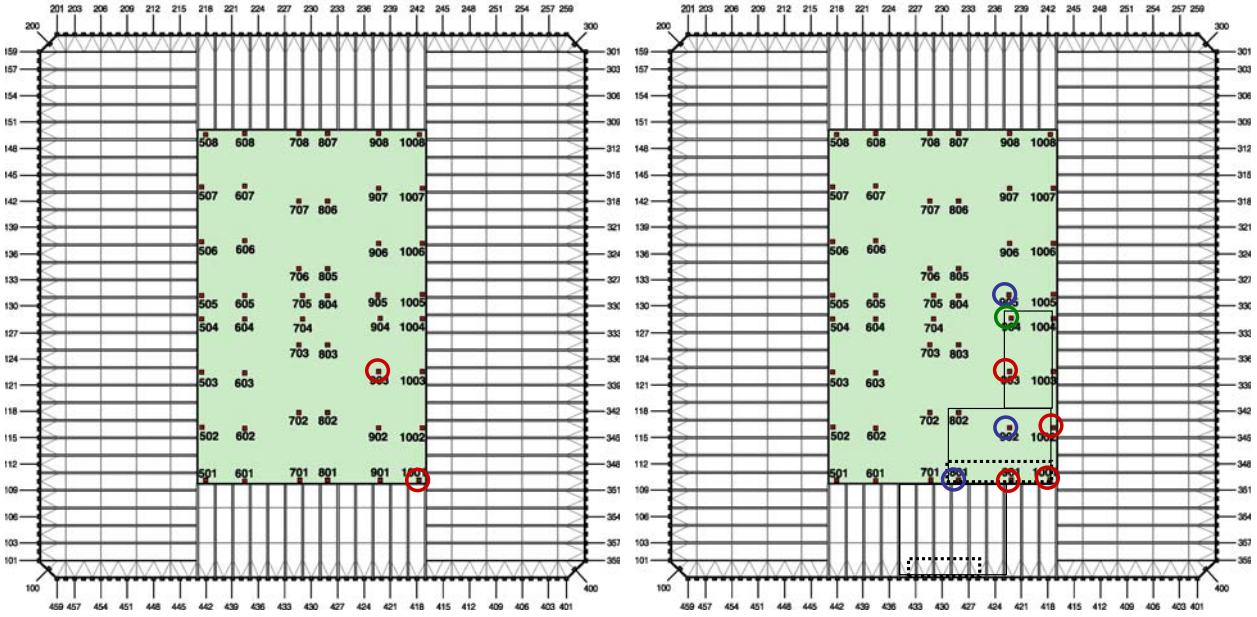

(a) Floors 77 and 78

(b) Floor 79

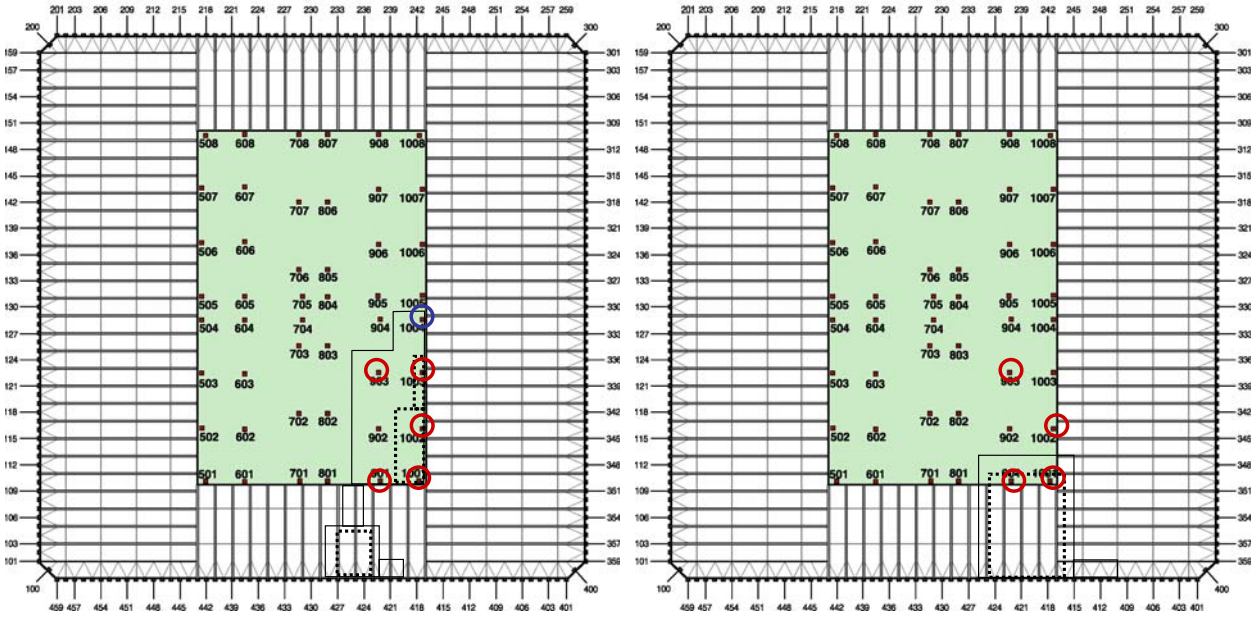

(c) Floor 80

(d) Floor 81

Figure 7–42. Summary of the floor-by-floor structural damage to the floors and columns of WTC 2 (base case).

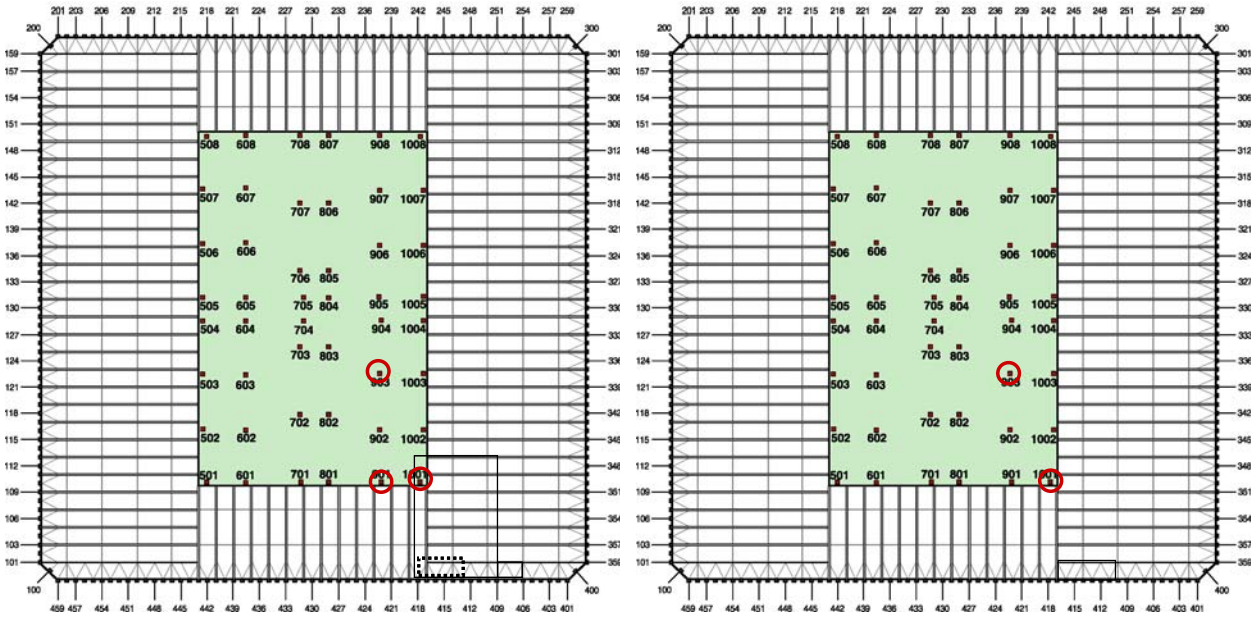

(c) Floor 82 (d) Floor 83

Severe Floor Damage

Floor system structural damage

Floor system removed

Column Damage

Severed

Heavy Damage

Moderate Damage

Light Damage

Figure 7–42. Summary of the floor-by-floor structural damage to the floors and columns of WTC 2 (base case) (continued).

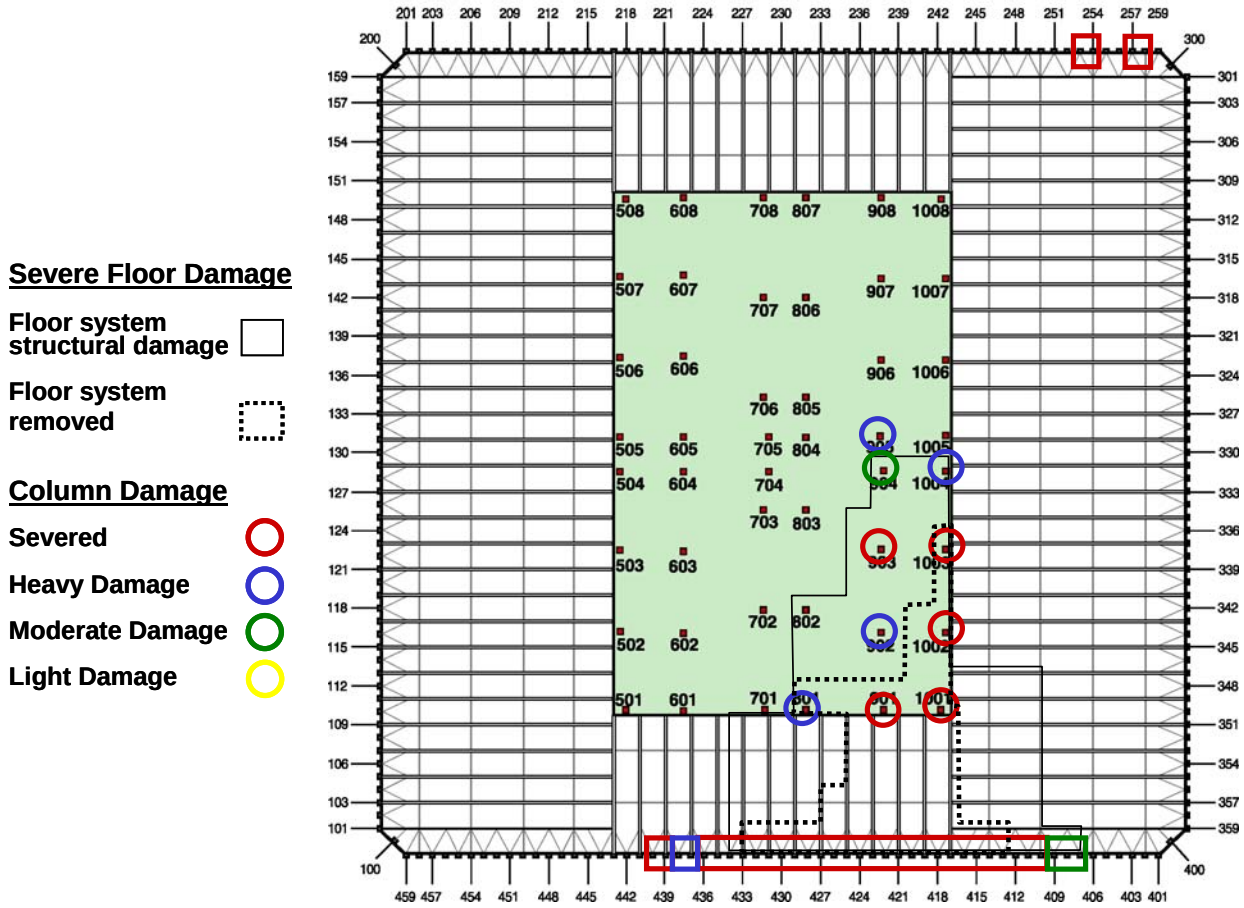

Figure 7–43. Cumulative structural damage to the floors and columns of WTC 2 (base case).

7.6.3 Fuel and Debris Distributions

The global impact results presented in this section include the distribution of the jet fuel and aircraft debris in the WTC 2 tower, and the damage to the building contents (partition walls and workstations). For the base case WTC 2 global impact analysis, the calculated distribution of the fuel in the tower and shape of the fuel cloud in a plan view and side view are shown in Figure 7–44. At the end of the analysis, the residual momentum of the jet fuel in the impact direction was less than one percent of the initial momentum, indicating that the fuel cloud was nearly at rest at about 0.62 s.

To more clearly present the calculated response of the structures that influenced the fire propagation, the structural components were removed from the visualization, with the exception that the core columns were maintained in the visualizations for reference positions. A plan view of the response of the remaining building contents and aircraft debris are shown in a plan view in Figure 7–45. Similar plan views of floor 80 and 81 slices through the building contents and debris field are provided in Figure 7–46 and Figure 7–47, respectively. The bulk of the aircraft debris and fuel was arrested prior to exiting the tower structures. However, a significant amount of aircraft debris was calculated to exit the north and east sides of the tower (Sides 300 and 200 of WTC 2).

Plots of debris distribution and damage to tower contents at the end of the impact simulation similar to those in Figure 7–46(c) and Figure 7–47(c), were used to estimate the damage to fireproofing. The extent of dislodged fireproofing was estimated by considering fireproofing damage only to structural components in the direct path of debris. For details of the methodology and the extent of fireproofing damage, see NIST NCSTAR 1-6.

A quantitative characterization of the fuel and aircraft debris distribution was obtained by slicing the model at vertical floor locations and calculating the mass at each floor level. A summary of the floor-by-floor fuel and debris distributions is given in Table 7–7. The bulk of the fuel and aircraft debris was deposited in floors 78 through 80, with the greatest concentration of aircraft debris on floor 80, and the largest concentration of aircraft fuel on floors 79, 81, and 82. Approximately 14,000 lb, or 5 percent, of the total aircraft mass was eliminated from the debris cloud in the final state as a result of the erosion in the aircraft structures due to impact and breakup. This eroded mass was maintained in the calculation but eliminated from consideration in the contact algorithm. As a result, any residual momentum at the time of erosion could not be subsequently transferred to the tower.

The calculated debris distribution included 55,800 lbs of debris and 10,600 lbs of aircraft fuel outside of the tower at the end of the impact analysis, either rebounding from the impact face or passing through the tower. These estimates of mass outside the tower were expected to be overestimated in the calculation since the exterior walls were not modeled with windows that could contain the fuel cloud and small debris inside the towers. In addition, the impact behavior of the aircraft fuel cloud did not include the ability to stick to, or wet, interior components. Rather the aircraft fuel SPH particles tended to bounce off of internal structures (see Section 7.3.3).

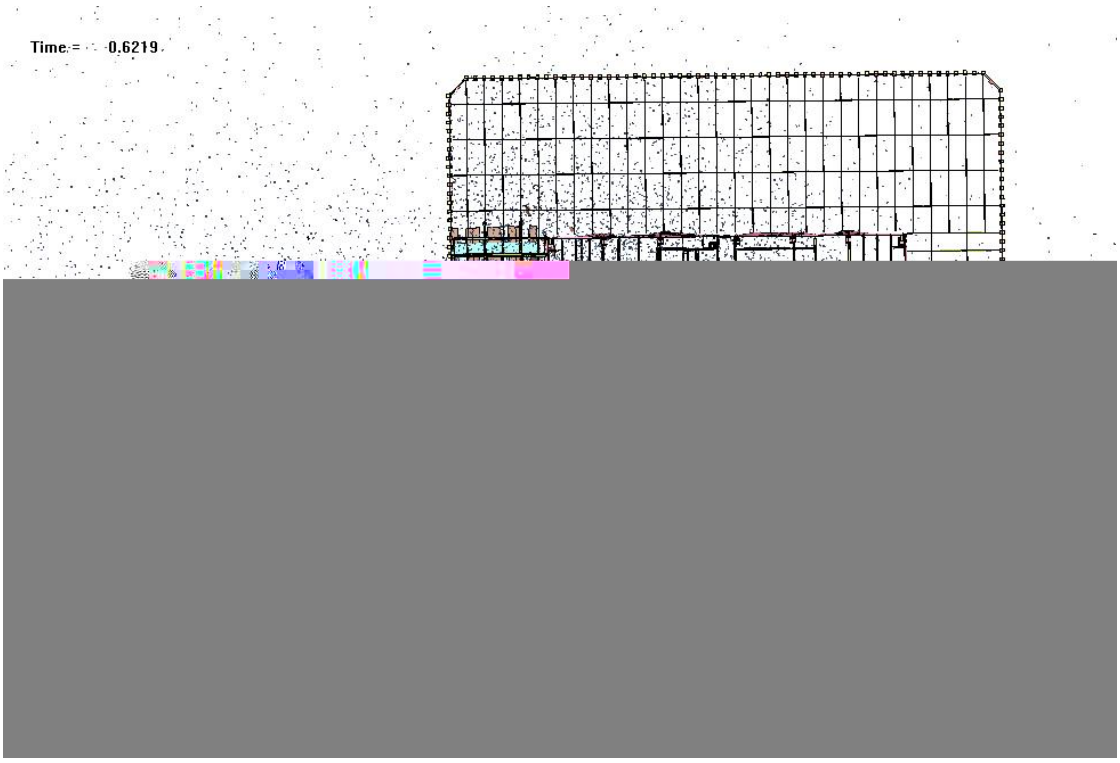

(a) Plan view (floor slab removed)

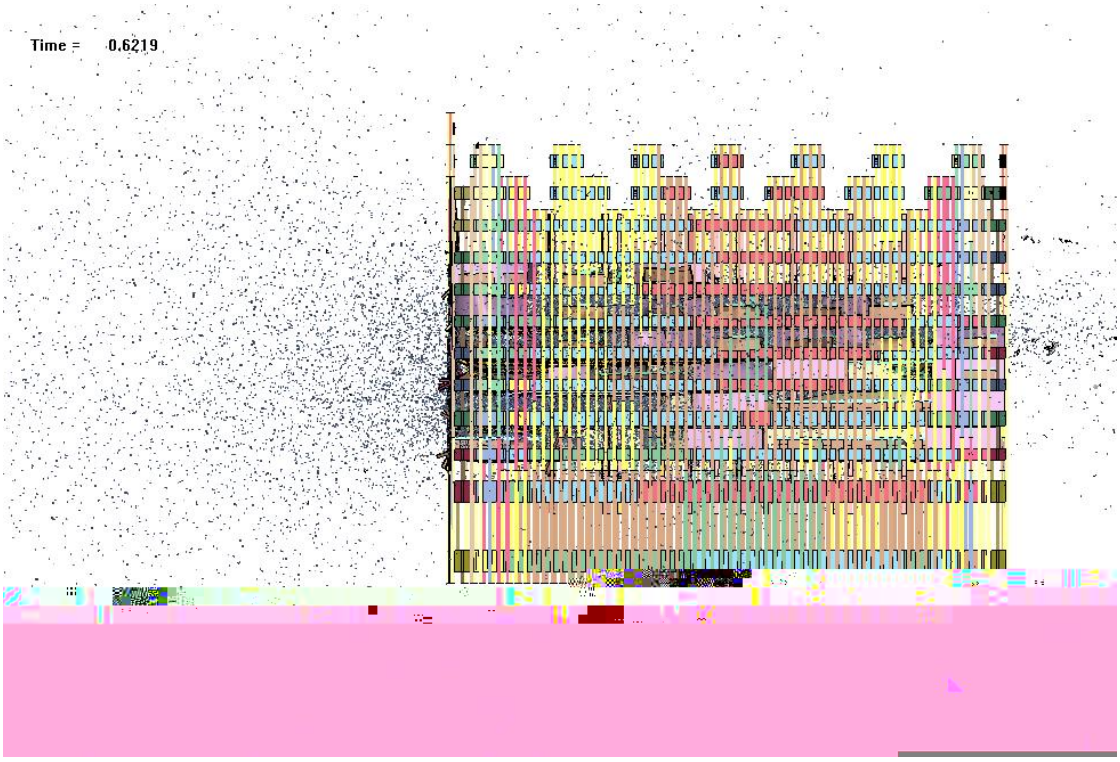

(b) Side view

Figure 7–44. Calculated fuel distribution in the base case WTC 2 analysis.

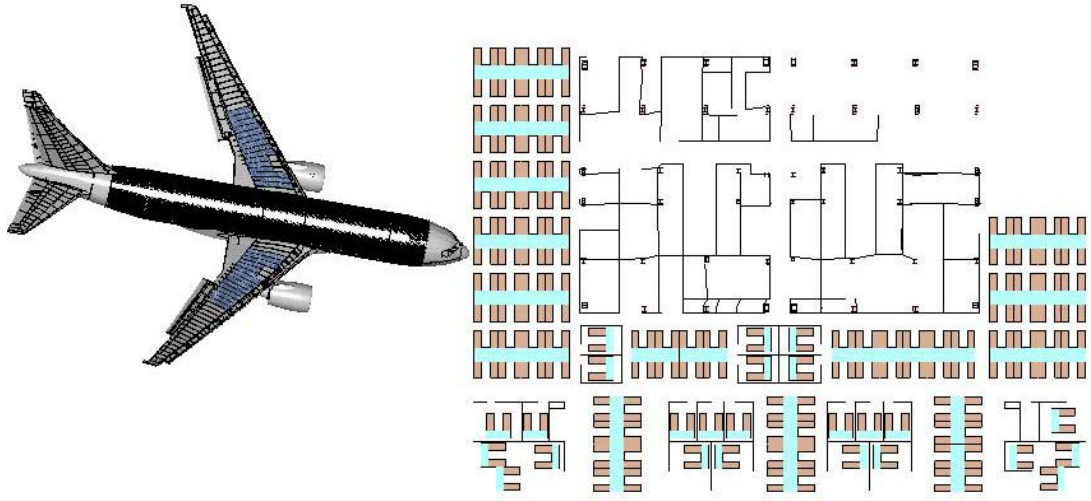

(a) Pre-impact configuration

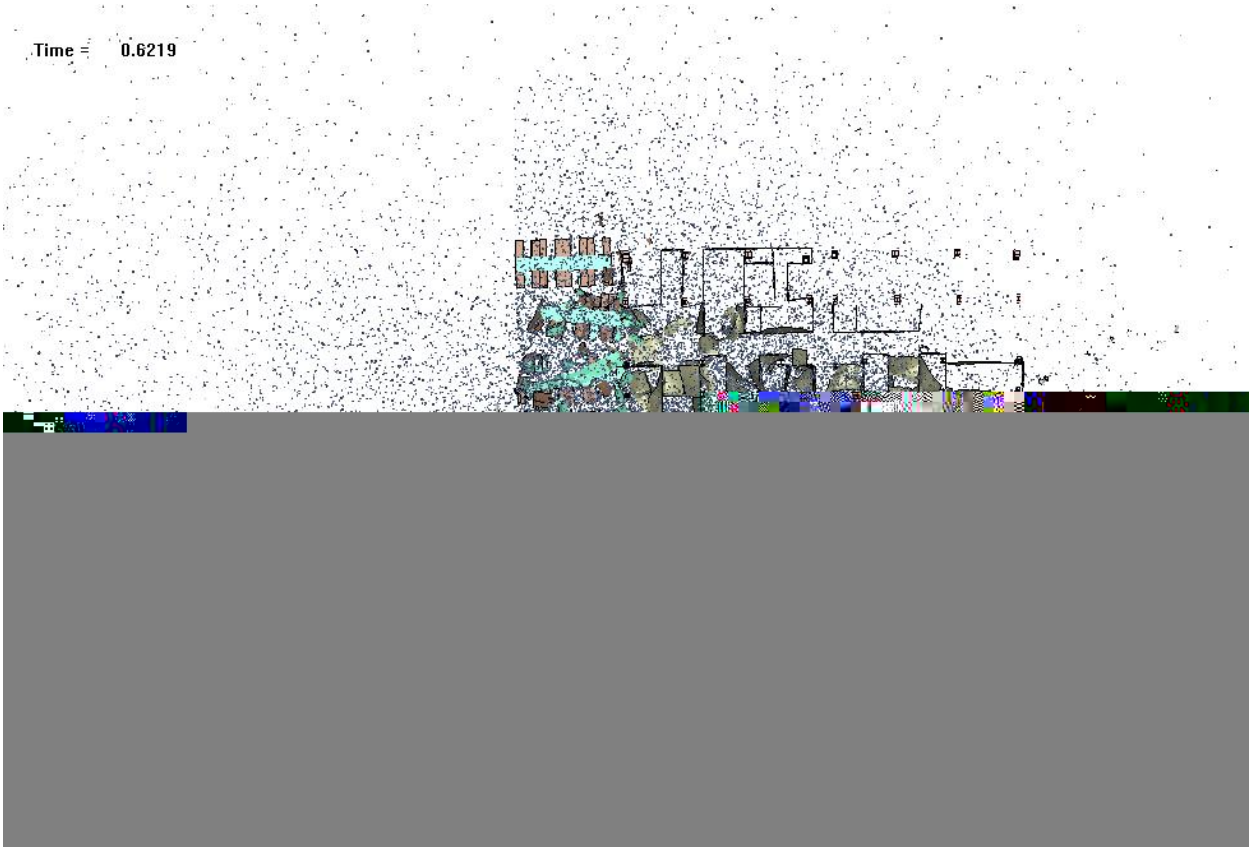

(b) Calculated impact response

Figure 7–45. Plan view of calculated WTC 2 building, fuel, and aircraft debris distribution for the base case.

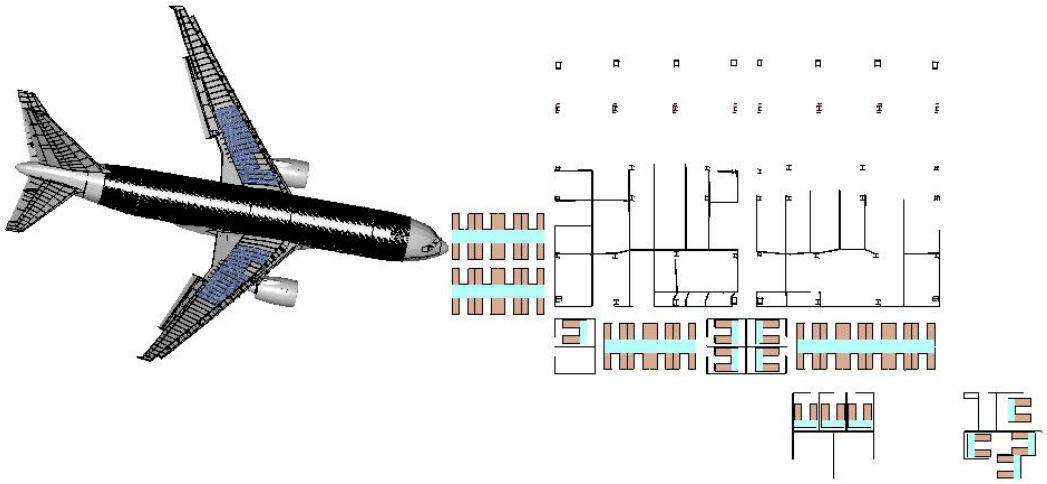

(a) Pre-impact configuration

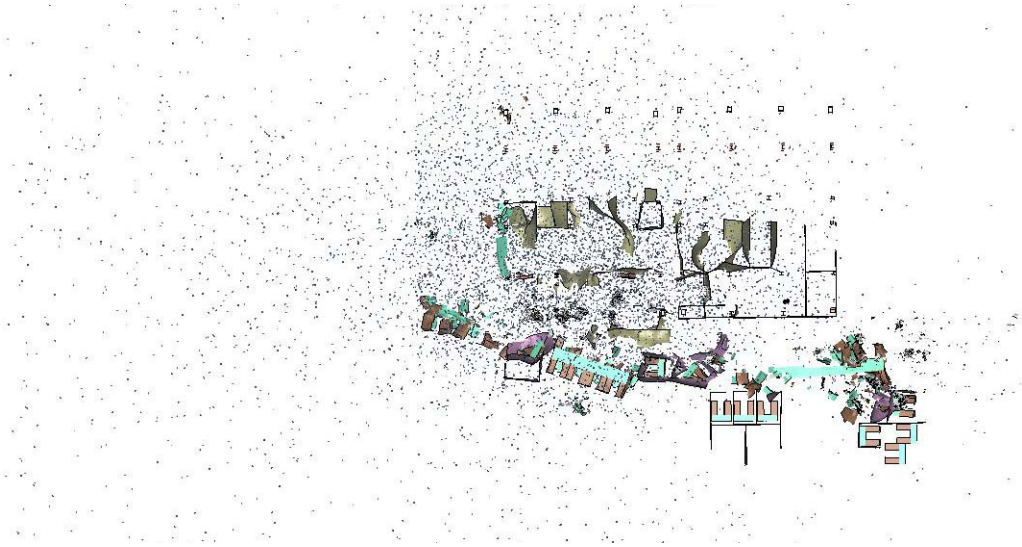

(b) Calculated impact response

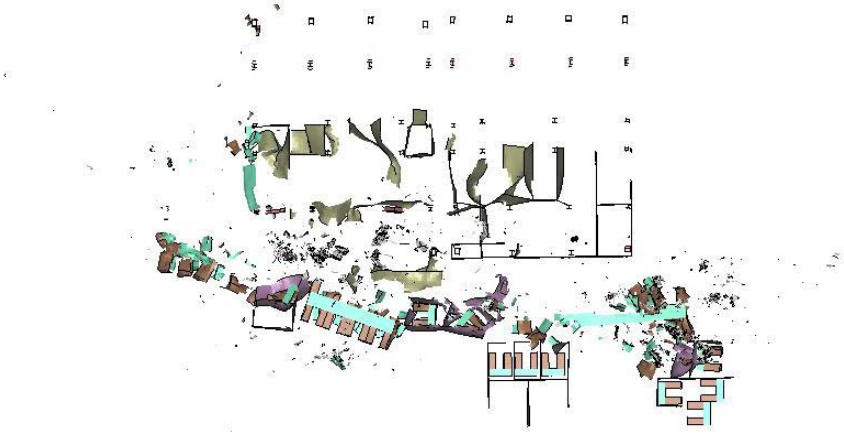

(c) Calculated impact response (fuel removed)

Figure 7–46. Calculated floor 80 contents, and fuel distribution (base case).

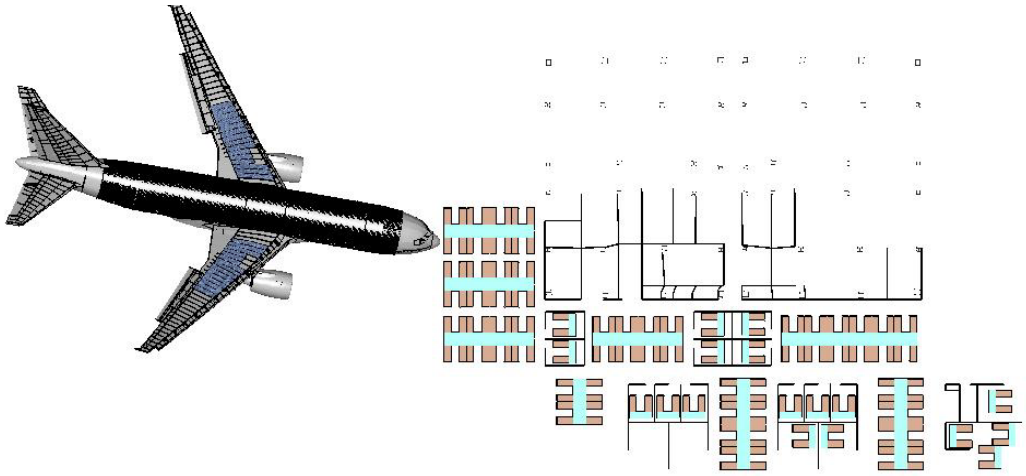

(a) Pre-impact configuration

(b) Calculated impact response

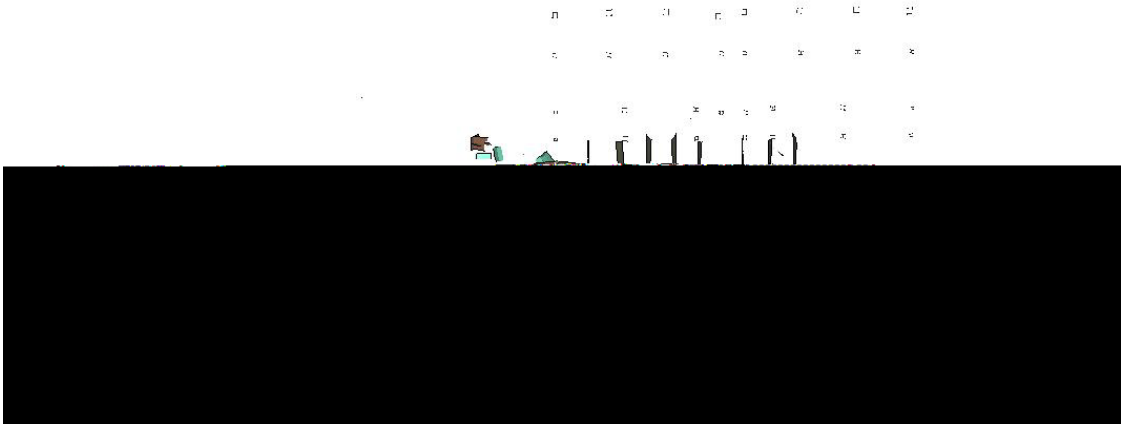

(c) Calculated impact response (fuel removed)

Figure 7–47. Calculated floor 81 contents and fuel distribution (base case).

Table 7–7. Fuel and aircraft debris distribution for the base case WTC 2 impact.

Tower Location	Aircraft Fuel	Aircraft Debris
Total Outside Tower	10,600 lb	55,800 lb
WTC 2 Floor 77	1,300 lb	400 lb
WTC 2 Floor 78	6,200 lb	4,800 lb
WTC 2 Floor 79	11,400 lb	16,200 lb
WTC 2 Floor 80	6,000 lb	83,800 lb
WTC 2 Floor 81	14,400 lb	27,300 lb
WTC 2 Floor 82	10,600 lb	3,600 lb
WTC 2 Floor 83	1,500 lb	4,300 lb
WTC 2 Floor 84	200 lb	500 lb
Total Weight	62,000 lb	197,600 lb

7.7 WTC 2 MORE SEVERE IMPACT ANALYSIS – CASE D

This case is referred to as Case D for the remainder of the WTC Investigation reports.

In addition to the base case impact analysis described in Section 7.6, two more impact analyses were performed for WTC 2 to provide a range of calculated impact-induced damage. The variations in impact analysis parameters were developed based on the results of the sensitivity analyses and additional evaluations of the parameter uncertainties (see Chapter 8 of NIST NCSTAR 1-2B). These analyses included a more severe and a less severe case. Presented herein is the more severe case only.

The parameters for the more severe impact scenario are compared to the corresponding parameters in the base case analysis in Table 7–8. For the flight parameters, the impact speed was 570 mph in the more severe impact scenario, which was the upper bound obtained from the analysis of aircraft impact conditions described in Chapter 6. The aircraft vertical trajectory angle was also varied from 6 degrees in the base case to 5 degrees for the more severe impact scenario, which resulted in more impact energy directed inward toward the core. The lateral trajectory was not varied in this analysis so that the starboard engine trajectory was aligned with exiting the northeast corner of the tower, as was observed from photographic evidence (see Section 7.10.2).

Table 7–8. Input parameters for the more severe WTC 2 impact analysis.

Analysis Parameters		Base Case	More Severe	Less Severe
Flight Parameters	**Impact Velocity**	546 mph	570 mph	521 mph
	Trajectory - pitch	6.0°	5.0°	8.0°
	Trajectory - yaw	13.0°	13.0°	13.0°
	Orientation - pitch	5.0°	4.0°	7.0°
	Orientation - yaw	10.0°	10.0°	10.0°
Aircraft Parameters	**Weight**	100 percent	105 percent	95 percent
	Failure Strain	100 percent	115 percent	75 percent
Tower Parameters	**Contents Strength**	100 percent	80 percent	100 percent
	Failure Strain	100 percent	90 percent	120 percent
	Live Load Weight	25 percent	20 percent	25 percent

For WTC 2, the variations in the parameters from the base case were similar to those for WTC 1 (see Table 7–3), with two exceptions. The first exception was the introduction of the strength of the building contents as a parameter. There was less information available about the layout of building contents in the WTC 2 impact zone and therefore a larger uncertainty associated with the contents was assumed (the workstation layout from WTC 1 was used for WTC 2). Thus, in the more severe case, the contents strength was reduced to 80 percent of the baseline value.

The second exception was the failure strains for the aircraft and tower materials. For the more severe WTC 1 analysis, 125 percent and 80 percent of the baseline values were used for the aircraft and tower failure strains, respectively. For the more severe WTC 2 analysis, 115 percent and 90 percent of the baseline values were used. The more severe WTC 2 analysis was the final global impact analysis performed. Based on the previous analyses, the variation in damage levels indicated that the WTC 2 more severe impact analysis would produce impact damage state that was not viable (e.g., the amount of debris exiting the north wall). To ensure that a viable damage state was obtained, the aircraft and tower materials were adjusted to the values presented in Table 7–8.

Table 7–8 provides also the parameters used in the less severe damage case. As can be seen from the table, the parameters are selected to provide for a stronger tower and a weaker aircraft to yield less damage to the tower structure.

7.7.1 Impact Response

The impact response of WTC 2 for the more severe case is shown in side and plan views in Figure 7–48 and Figure 7–49, respectively. The response is shown at intervals of 0.1 s from impact through the initial 0.5 s of the response. Comparing the more severe impact response in Figure 7–48 and Figure 7–49 with the base case response in Figure 7–33 and Figure 7–34, it can be seen that the two responses were very similar with two exceptions. These were the slightly compressed time scale and the larger amount of debris exiting the north wall in the more severe case. These differences were due primarily to the larger impact speed, the increased weight and material toughness of the aircraft, and the reduced contents mass and material toughness of the towers for the more severe case.

(a) Time=0.00 s

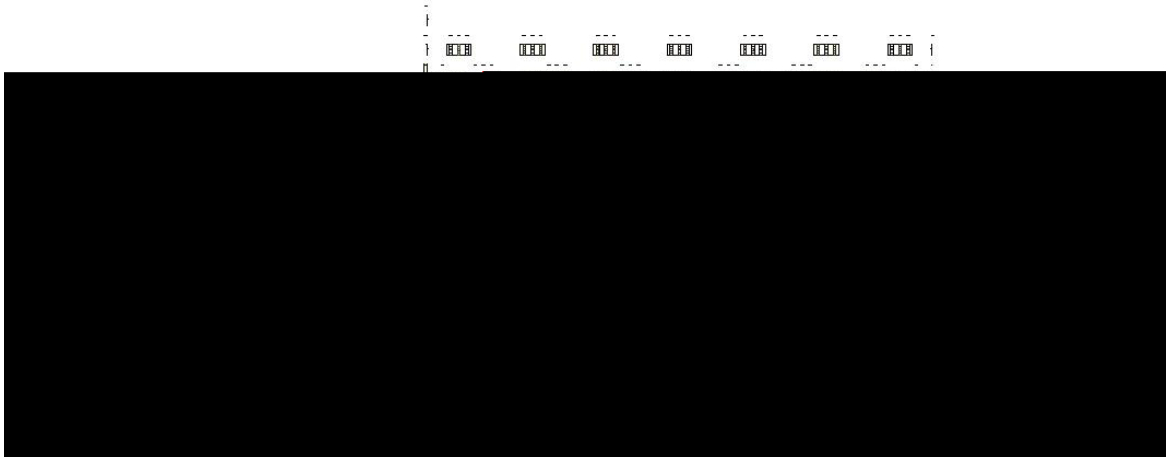

(b) Time=0.10 s

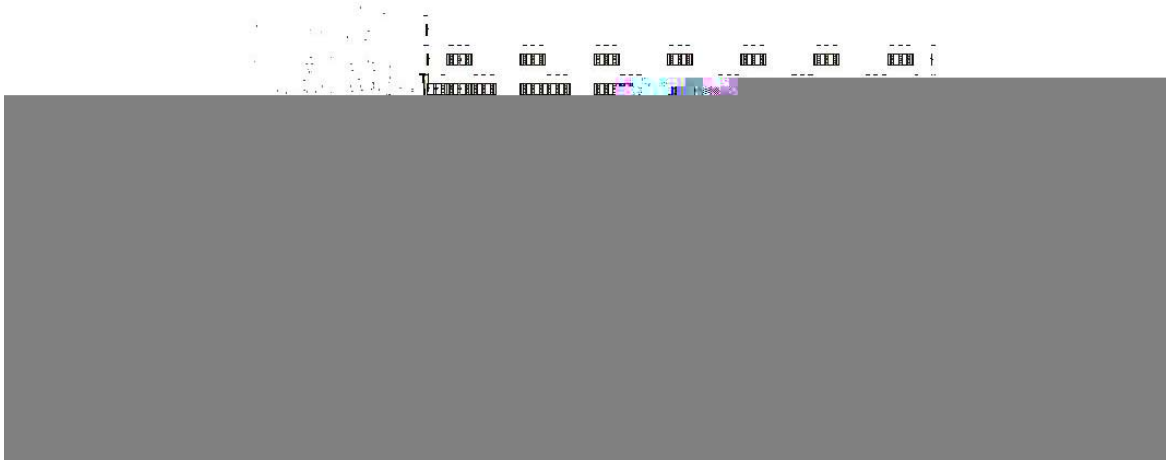

(c) Time=0.20 s

Figure 7–48. WTC 2 more severe global impact analysis (side view).

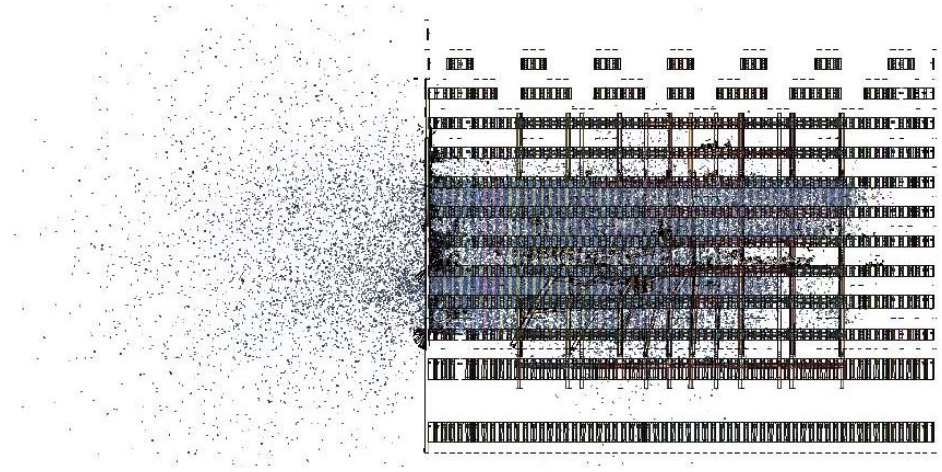

(d) Time=0.30 s

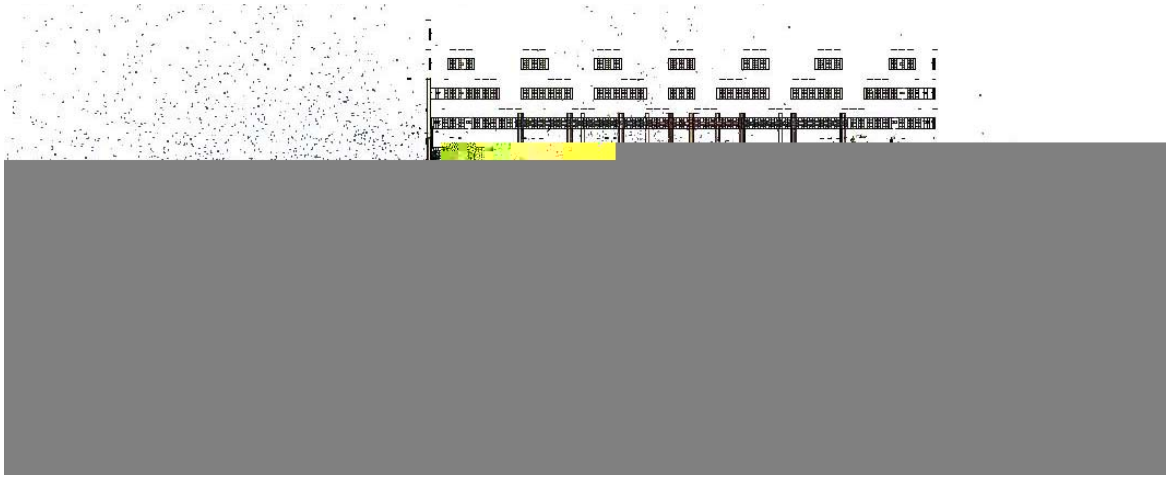

(e) Time=0.40 s

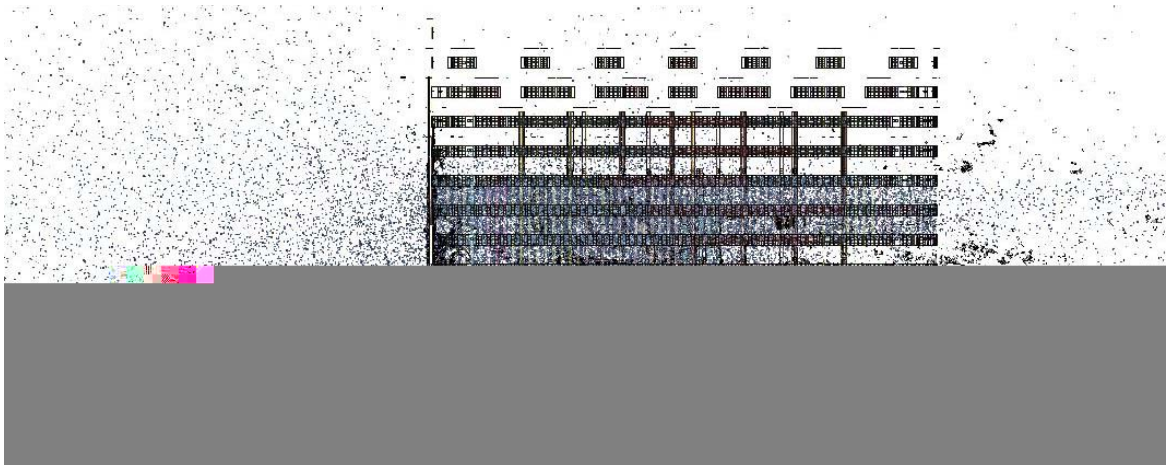

(f) Time=0.50 s

Figure 7–48. WTC 2 more severe global impact analysis (side view) (continued).

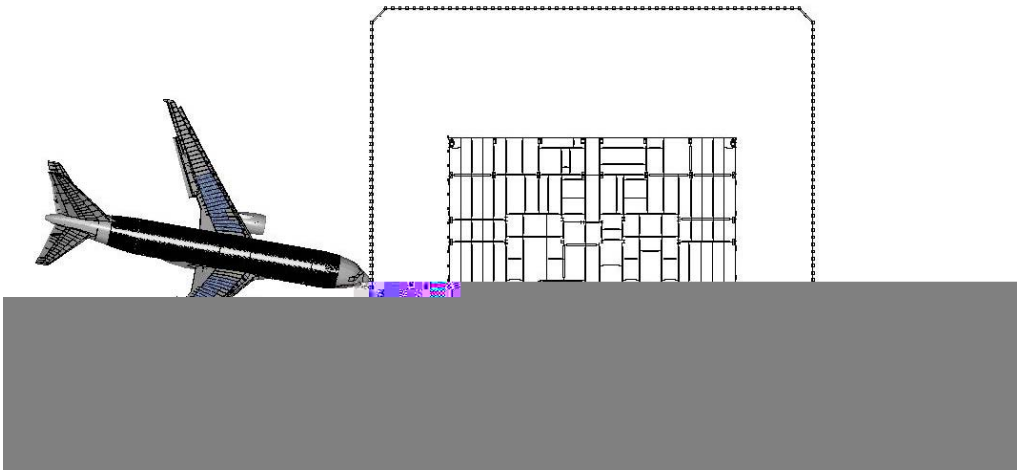

(a) Time=0.00 s

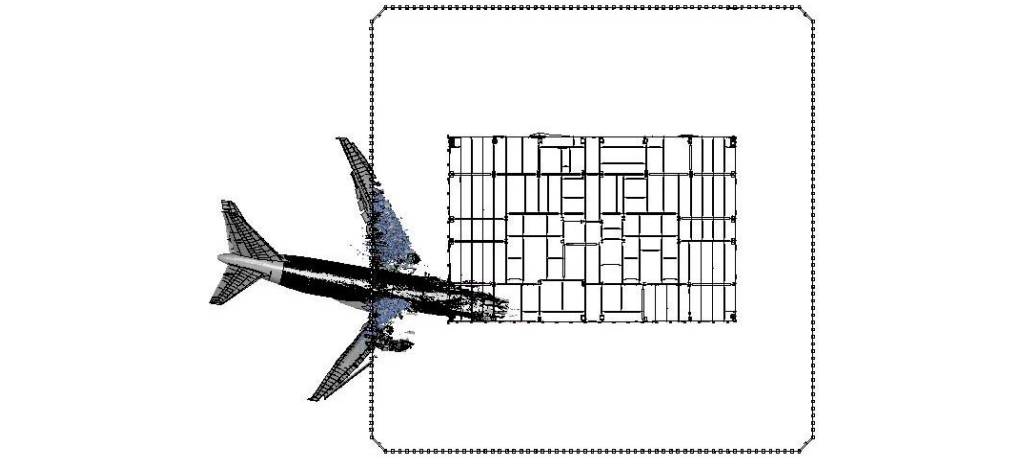

(b) Time=0.10 s

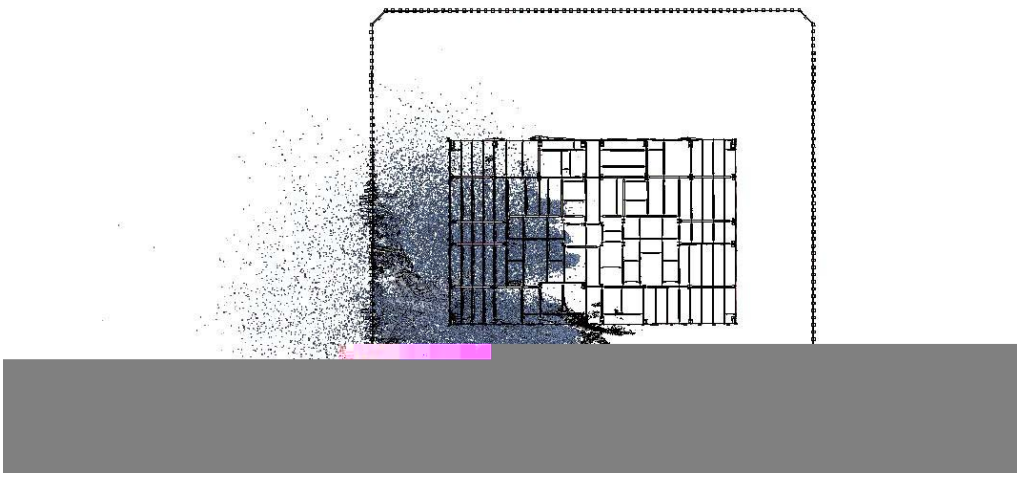

(c) Time=0.20 s

Figure 7–49. WTC 2 more severe global impact analysis (plan view).

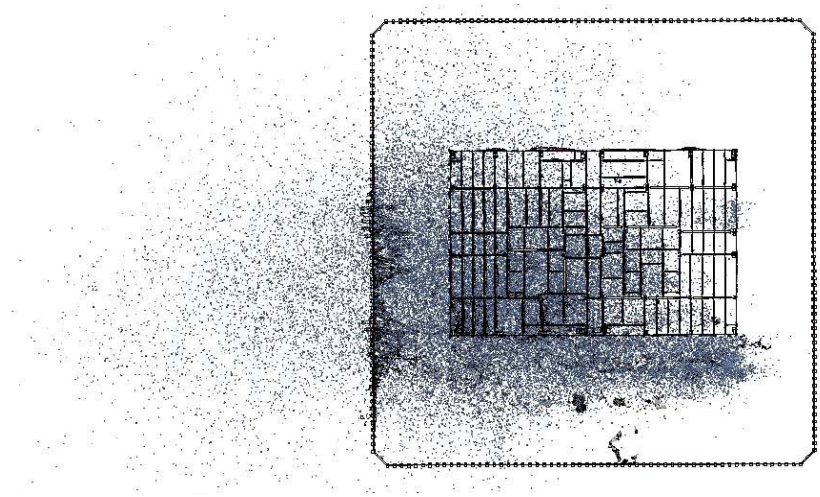

(d) Time=0.30 s

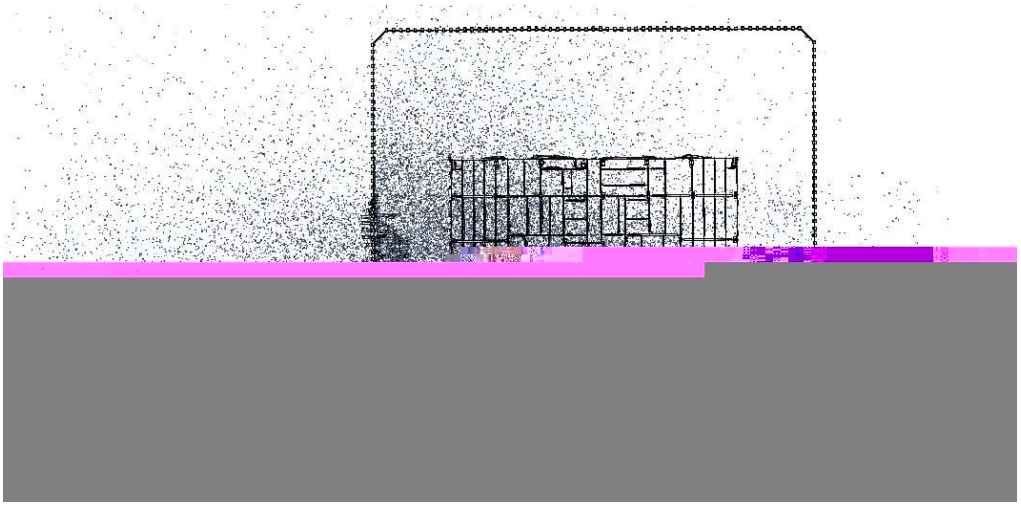

(e) Time=0.40 s

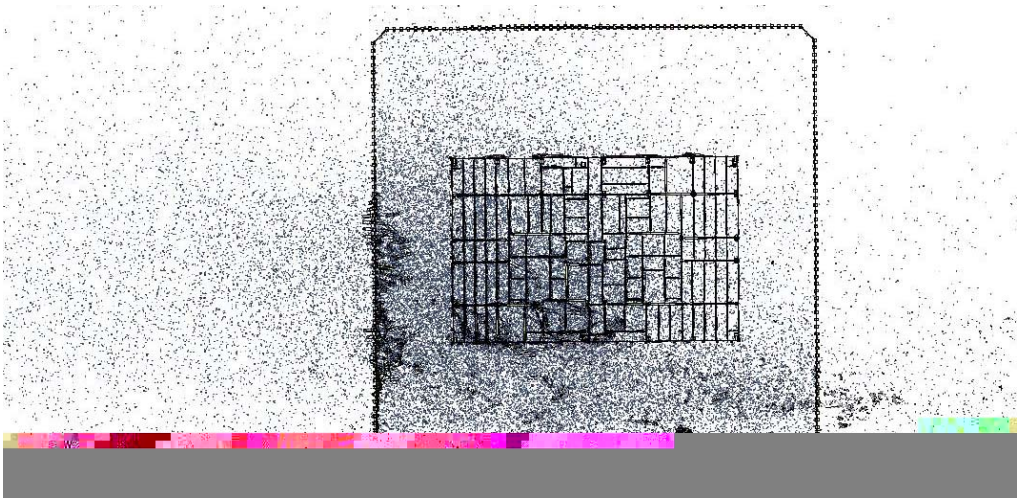

(f) Time=0.50 s

Figure 7–49. WTC 2 more severe global impact analysis (plan view) (continued).

7.7.2 Tower Structural Damage

Exterior Wall Damage

A comparison of the south exterior wall observed and calculated damage from the more severe WTC 2 global impact analysis is shown in Figure 7–50. The calculated impact damage to the exterior wall is shown with color fringes representing plastic strain magnitude, with undamaged sections in blue and strains at or above 5 percent shown in red. The mode and magnitude of the calculated and observed impact damage on the exterior wall were still in good agreement in this more severe impact analysis.

As was the case for WTC 1, there were small differences in the damage estimates for the south wall of WTC 2 from the base case and the more severe case scenarios (compare Figure 7–36 and Figure 7–50). Overall, the agreement with the observed damage from photographs was very good for both cases. The most obvious differences were largely due to portions of panels that may have severed columns in one case or have been removed at the connections in another.

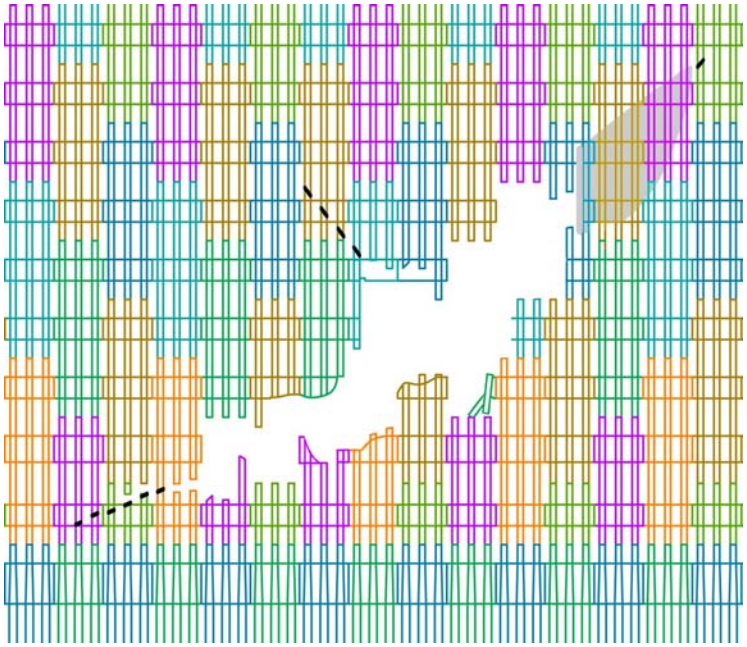

(a) Schematic of observed damage

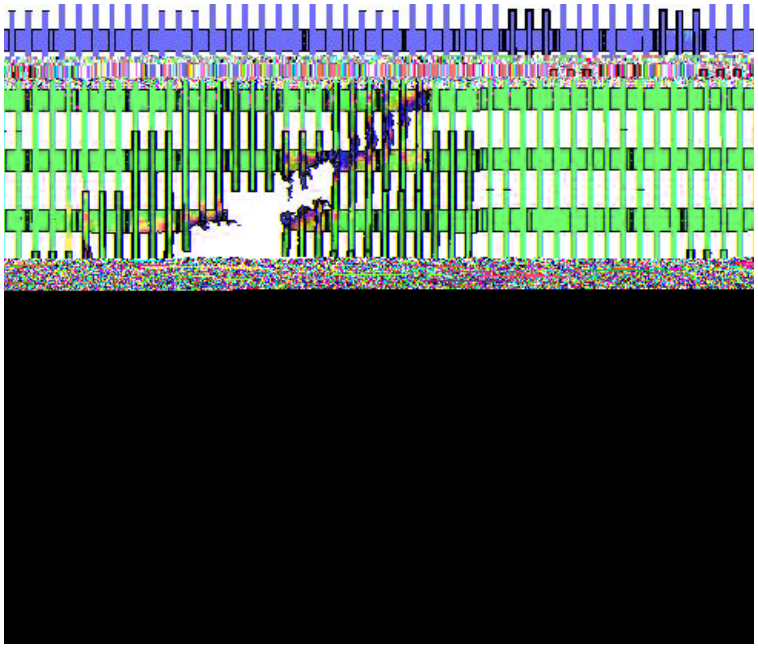

(b) Calculated damage

Figure 7–50. More severe impact damage to the WTC 2 exterior wall.

Core Structural Damage

The core had extensive damage in the region close to the impact point. The columns in line with the aircraft fuselage failed on the impact side, and several of the core beams were also severely damaged or failed in the impact zone. In some cases, failure of the column splices located on floors 77, 80, and 83 contributed significantly to the failure of the core columns.

The calculated damage to the core columns by row is shown in Figure 7–51, and the damage to the core framing at floors 80 and 81 is shown in Figure 7–52. A summary of the column damage is provided in Table 7–9, with the qualitative classification of the column damage levels provided previously in Figure 7–7. A total of ten columns were severed, and one column was heavily damaged in this WTC 2 more severe case, compared to five columns severed and four columns heavily damaged in the base case WTC 2 impact analysis.

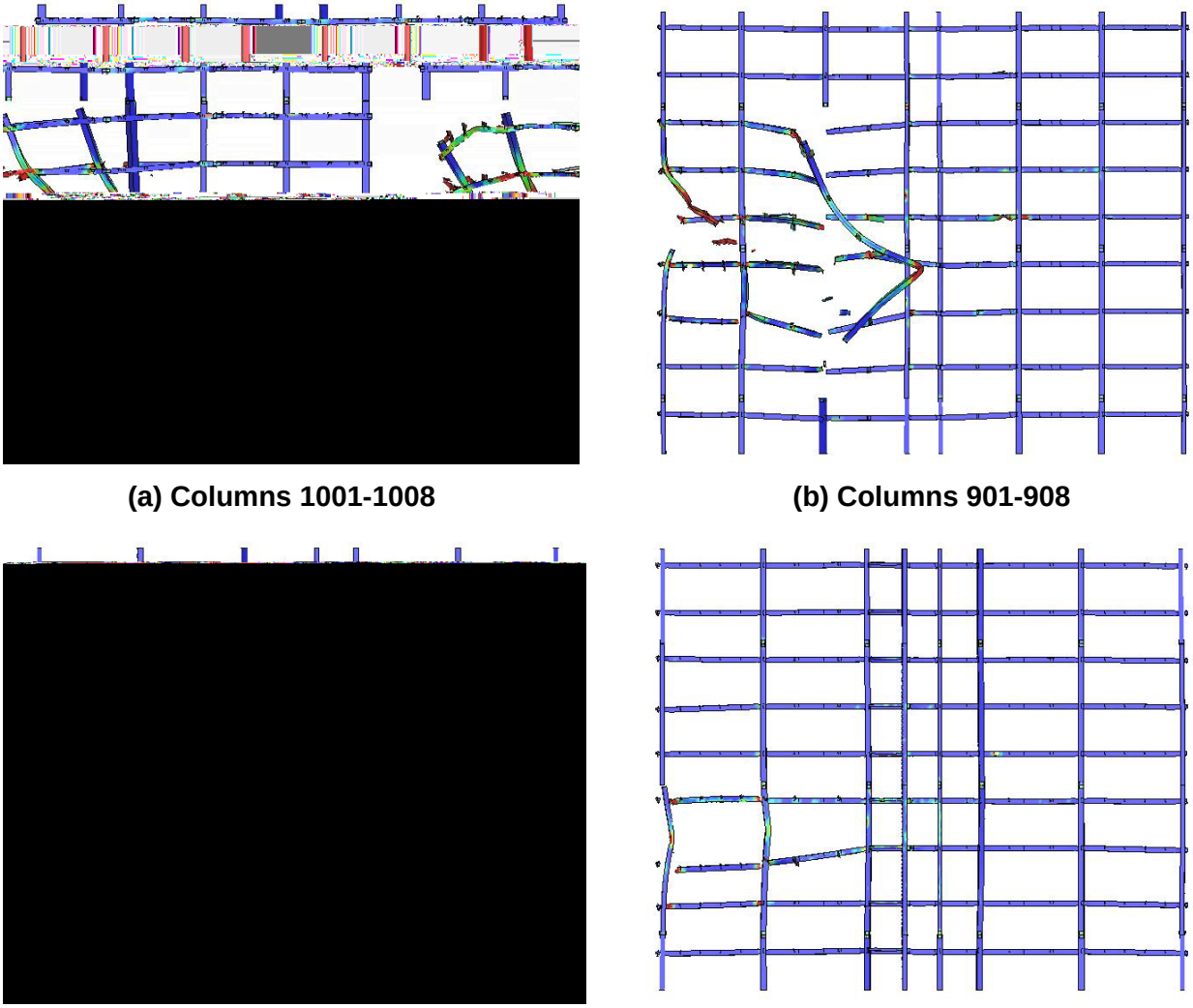

(a) Columns 1001-1008 **(b) Columns 901-908**

(c) Columns 801-807 **(d) Columns 701-708**

Figure 7–51. More severe impact damage to the WTC 2 core columns.

The strong correlation between the core damage and impact severity was expected. All of the parameter variations would be expected to produce an increase in core damage. The flight parameters had an increasing impact speed and a shallower impact angle, directing more energy toward the core. The aircraft had an increasing weight and higher material toughness. The tower had reduced mass in the contents and a reduced material toughness. All of these variations contributed toward the increased core damage with impact severity.

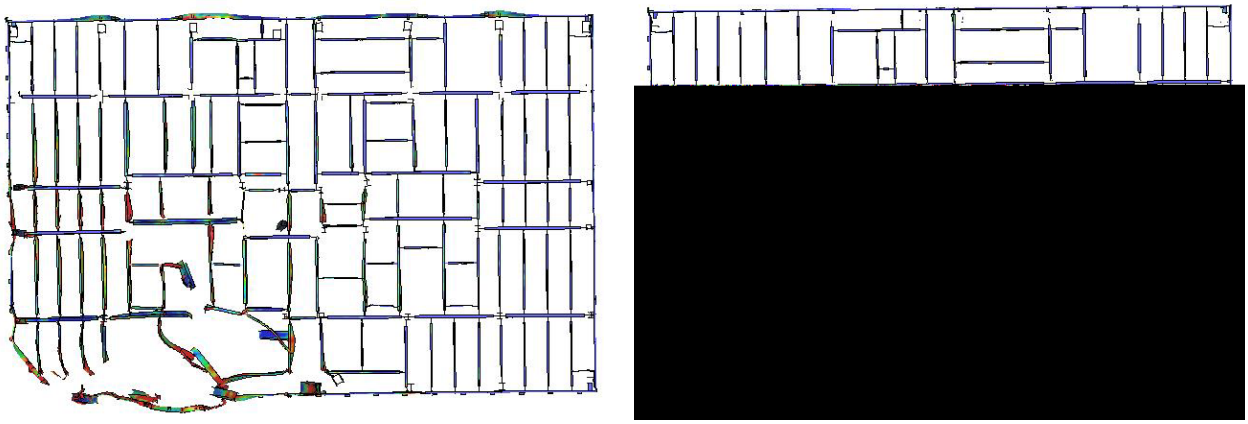

(a) Floor 80 core framing damage **(b) Floor 81 core framing damage**

Figure 7–52. More severe impact damage to the core beams of floors 80 and 81 of WTC 2.

Table 7–9. Summary of core column damage for the more severe WTC 2 impact.

Column	Location	Damage Level	Lateral Deflection of Column Centerline (in.)
Column 602	Floor 79	Moderate	
Column 605	Floor 79	Moderate	
Column 701	Floors 79-80	Severed	
Column 702	Floor 79	Heavy	16
Column 703	Floor 79	Moderate	
Column 704	Floor 79	Light	
Column 705	Floors 78-79	Light	
Column 705	Floor 78	Light	
Column 801	Floors 79-80	Severed	
Column 802	Floors 77-80	Severed	
Column 803	Floors 77-80	Severed	
Column 804	Floor 79	Light	
Column 901	Floors 80-81	Severed	
Column 902	Floor 79	Moderate	
Column 903	Floors 77-83	Severed	
Column 904	Floors 79-81	Moderate	
Column 905	Floors 79 & 81	Light	
Column 907	Floor 81	Light	
Column 1001	Floors 77-83	Severed	
Column 1002	Floors 79-83	Severed	
Column 1003	Floors 79-83	Severed	
Column 1004	Floors 79-83	Severed	
Column 1005	Floors 79-81	Moderate	

Floor Truss and Slab Damage

An overall frontal view for the floor truss structure in the WTC 2 impact zone, along with the calculated more severe impact damage to the trusses, is shown in Figure 7–53. The figure shows that the trusses experienced significant damage in the impact zone, with the heaviest damage on floor 81. A plan view of the calculated damage to the trusses on floors 80 and 81 is shown in Figure 7–54. The calculated impact response produced severe damage to the truss structures in the primary impact path of the fuselage. The truss structures were severely damaged from the exterior wall to the core. The truss floor system on floors 79 through 82 had sufficient damage from the impact that portions of the truss floor sections sagged downward as a result of the impact.

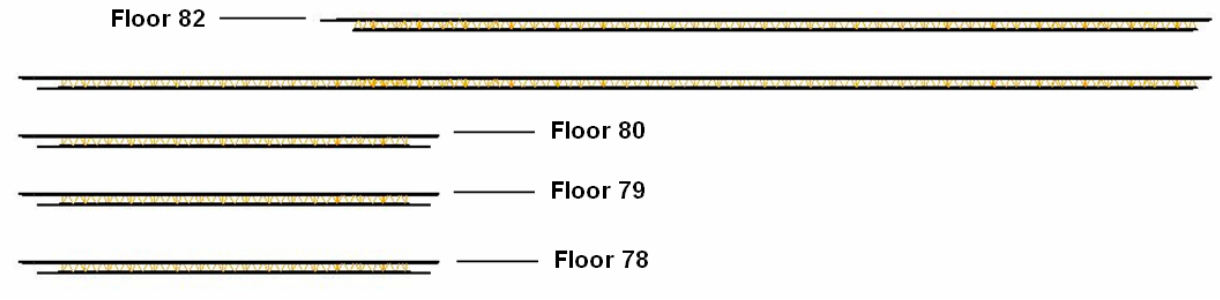

(a) Initial detailed truss structures

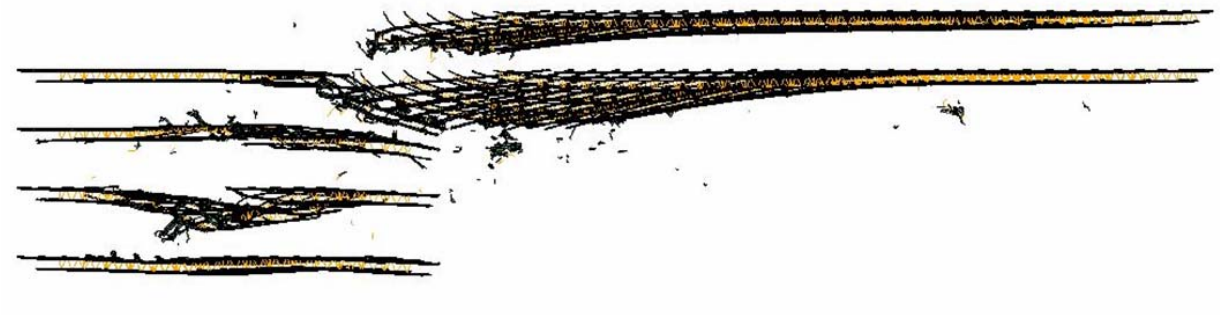

(b) Calculated damage

Figure 7–53. More severe impact damage to the WTC 2 floor trusses (front view).

The magnitude of truss floor damage was very similar for the base case and more severe global impact analyses. The parameters used in the more severe global impact analysis would primarily contribute to an increased damage for the tower structures. However, the downward impact trajectory angle was reduced from the 6 degree angle in the base case analysis to a 5 degree angle in the more severe impact analysis. This resulted in directing more of the impact energy inward toward the tower core, but reducing the normal downward force on the floor structures in the impact zone. As a result, the combined effects of the analysis parameter variations produced very similar damage to the truss structure.

The calculated damage to the WTC 2 floor slabs for floors 80 and 81 for the more severe impact is shown in Figure 7–55. The magnitude of floor slab damage was very similar for the base case and more severe global impact analyses due to the reasons explained above for the floor trusses.

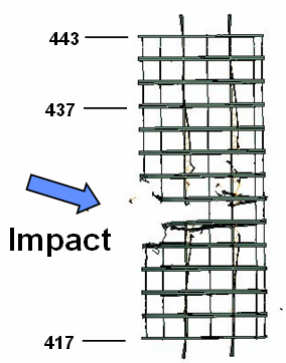

(a) Floor 80 truss damage

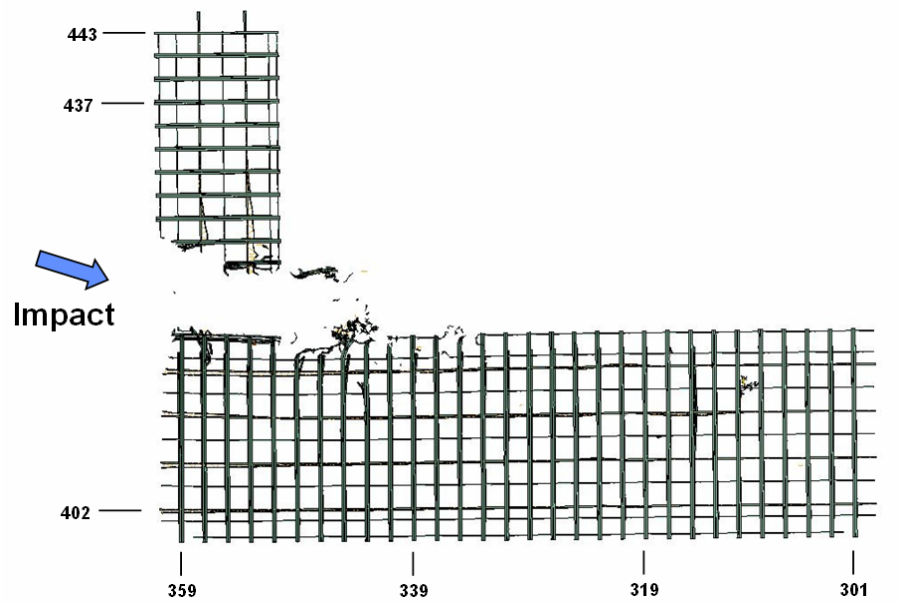

(b) Floor 81 truss damage

Figure 7–54. More severe impact damage to the trusses on floors 80 and 81 of WTC 2 (plan view).

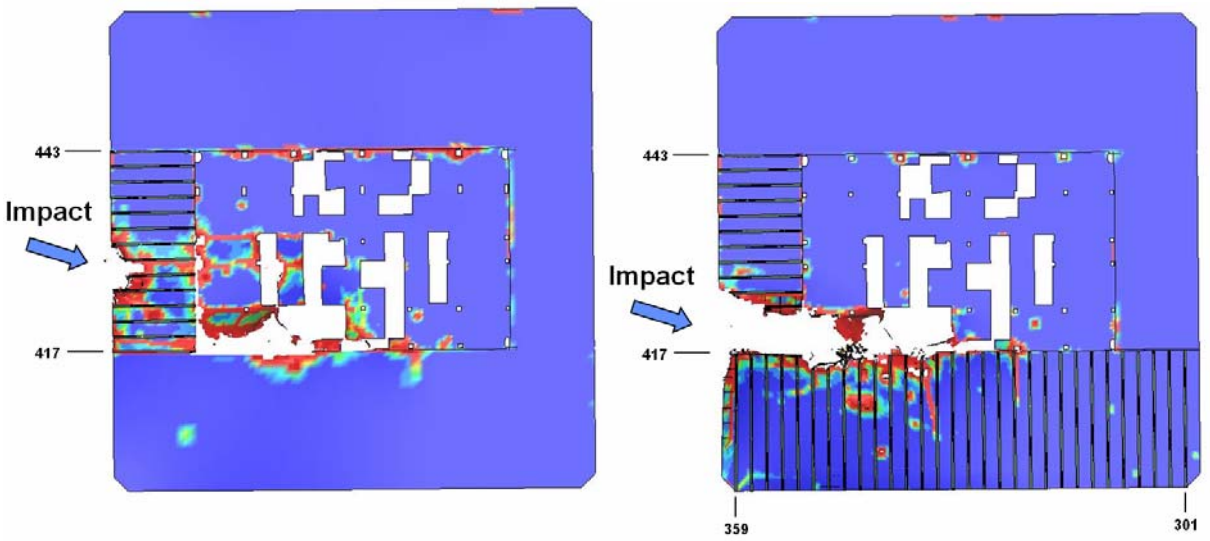

(a) Floor 80 slab damage **(b) Floor 81 slab damage**

Figure 7–55. More severe impact damage to the WTC 2 floor slab (plan view).

Summary of Structural Damage

Figure 7–56 shows a summary of the structural damage to the core columns and floor systems at floors 77 through 83 of WTC 2 for the more severe case (Case D). Figure 7–57 presents the cumulative damage to WTC 2 on all affected floors and columns.

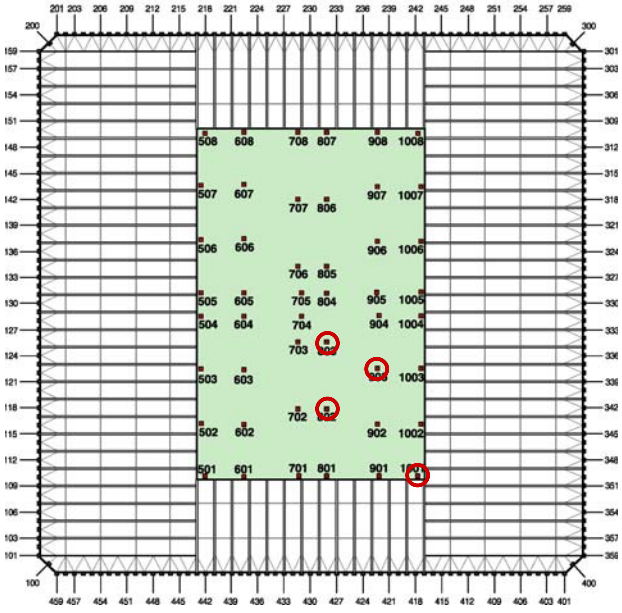

(a) Floors 77

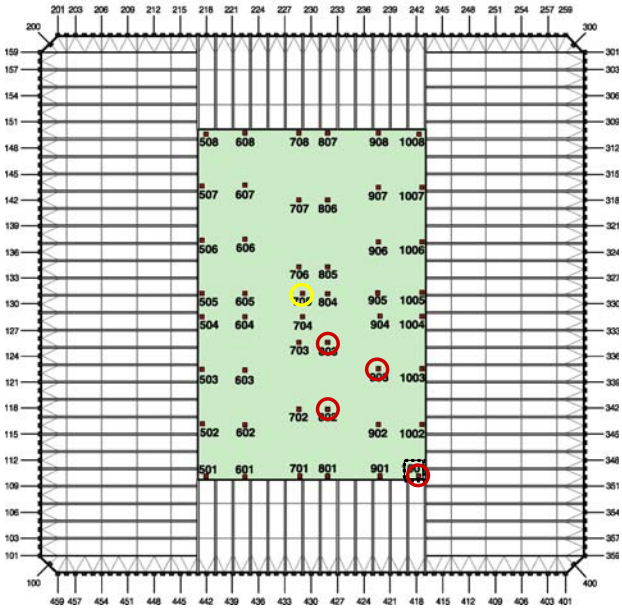

(b) Floor 78

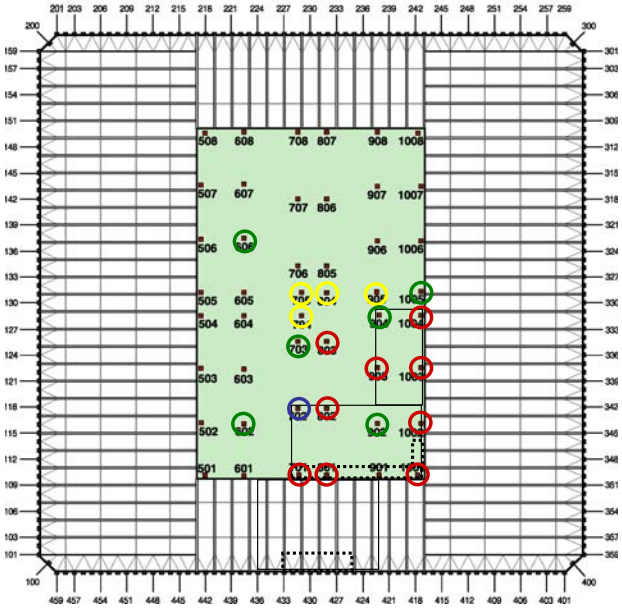

(c) Floor 79

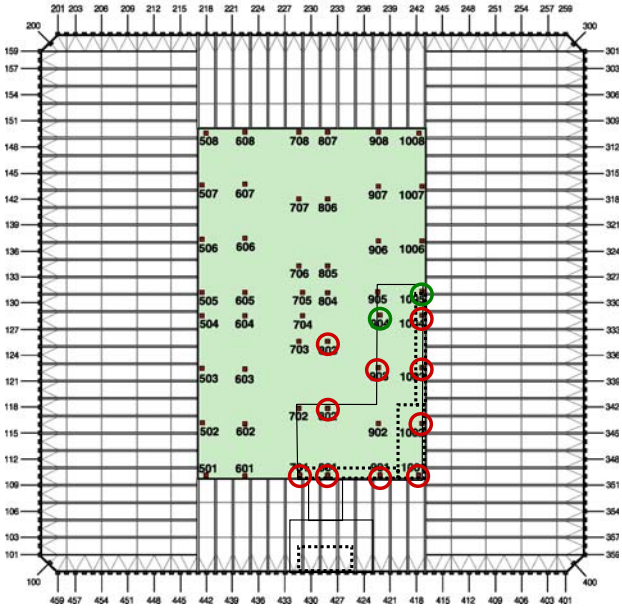

(d) Floor 80

Figure 7–56. Summary of the floor-by-floor structural damage to the floors and columns of WTC 2 (more severe case).

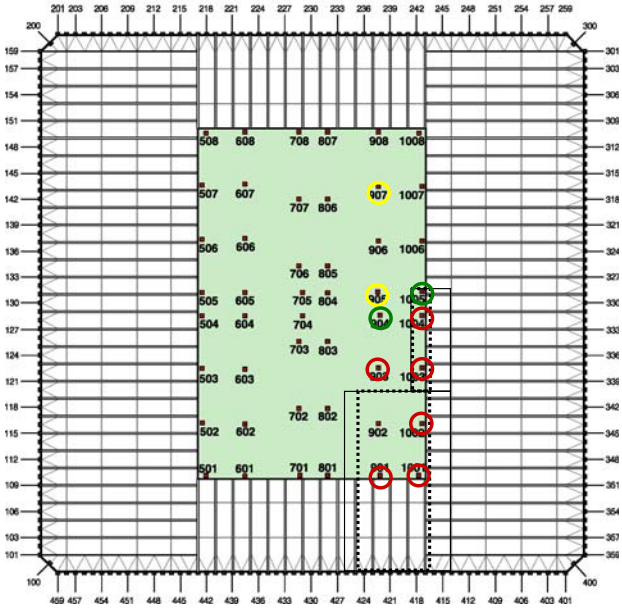

(e) Floor 81

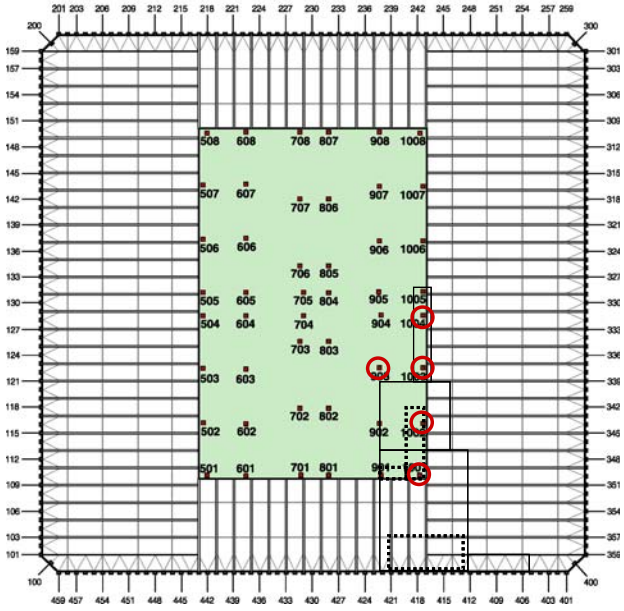

(f) Floor 82

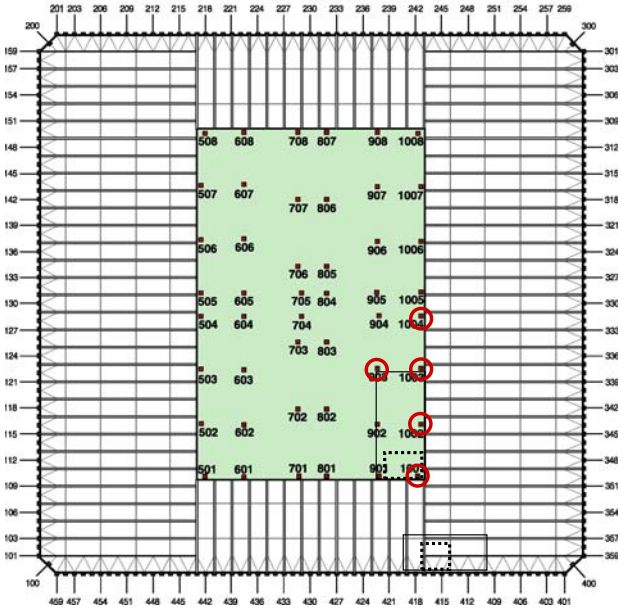

(g) Floor 83

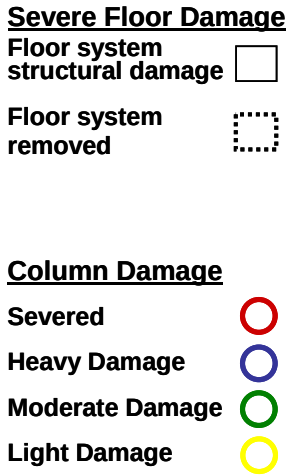

Figure 7–56. Summary of the floor-by-floor structural damage to the floors and columns of WTC 2 (more severe case) (continued).

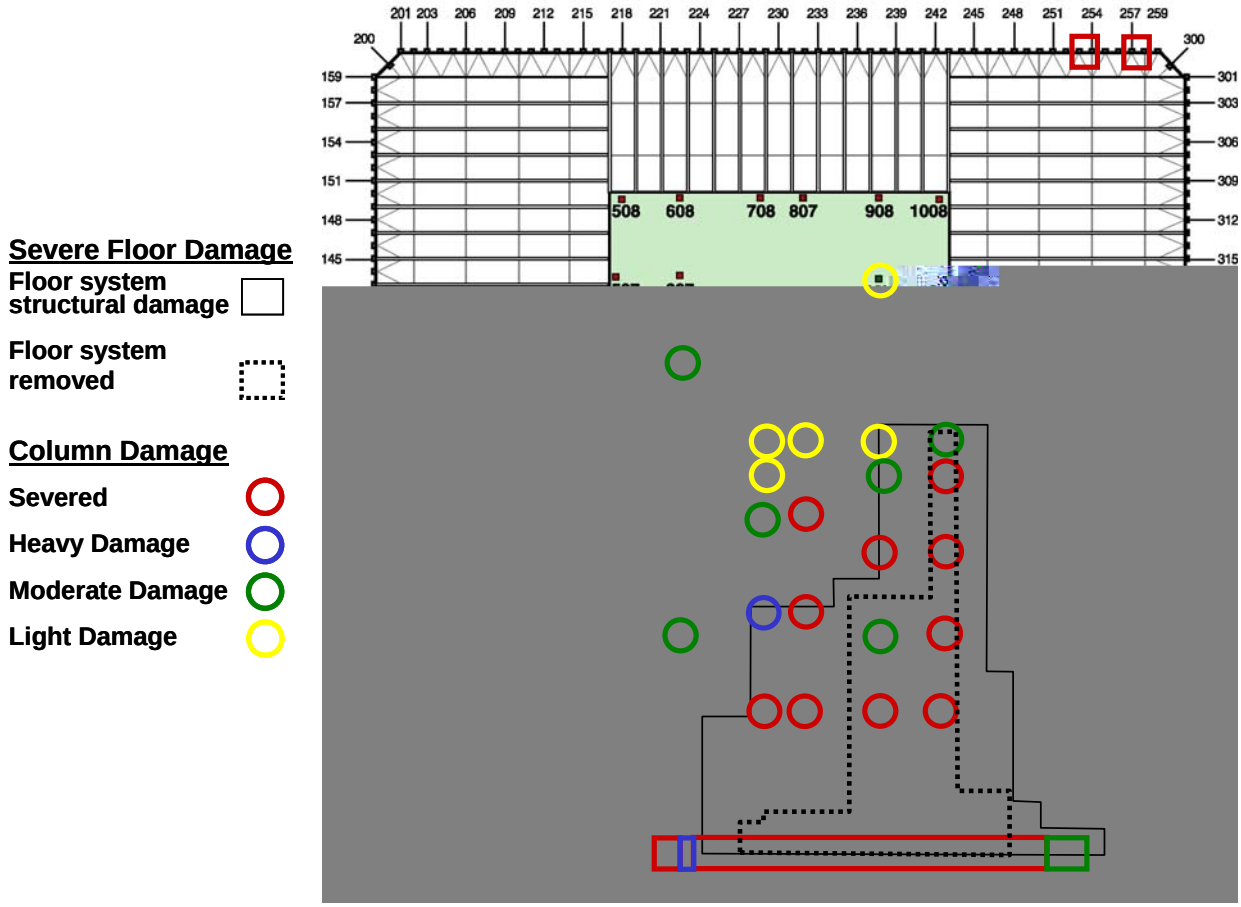

Figure 7–57. Cumulative structural damage to the floors and columns of WTC 2 (more severe case).

7.7.3 Fuel and Debris Distributions

The distribution of the fuel in the tower calculated from the more severe case in a plan view and side view is shown in Figure 7–58. At the termination of the global impact analysis, the residual momentum of the jet fuel was less than one percent of the initial momentum, indicating that the fuel cloud was nearly at rest. To more clearly present the calculated response of the structures that influenced the fire propagation, the structural components were removed from the visualization, with the exception that the core columns were maintained in the visualizations for reference positions. A plan view of the response of the remaining building contents and aircraft debris is shown in Figure 7–59.

The calculated damage to the WTC 2 contents for the more severe impact case is shown in plan views for floors 80 and 81 in Figure 7–60 and Figure 7–61, respectively. A comparison to the calculated damage for the base case WTC 2 impact analysis indicated that the tower contents damage zone was similar, with a slight increase in damage for the more severe impact.

A summary of the floor-by-floor fuel and debris distributions is given in Table 7–10. The bulk of the fuel and aircraft debris was deposited in floors 78 through 80, with the greatest concentration on floor 80. The calculated debris cloud included 121,000 lbs of debris and 14,800 lbs of aircraft fuel outside of the tower at the end of the impact analysis, either rebounding from the impact face (north wall) or passing through

the tower (south wall). This amount might have been larger in the calculation due to the reasons mentioned previously for the base case impact (see Section 7.3.3). Comparing Figure 7–59 and Table 7–10 with Figure 7–45 and Table 7–7, it can be seen that the amount of debris exiting the north wall of the tower in the more severe case was much larger than that from the base case.

Table 7–10. Fuel and aircraft debris distribution for the more severe WTC 2 impact.

Tower Location	Aircraft Fuel	Aircraft Debris
Total Outside Tower	14,800 lb	121,000 lb
WTC 2 Floor 77	1,300 lb	300 lb
WTC 2 Floor 78	7,400 lb	2,500 lb
WTC 2 Floor 79	12,500 lb	16,400 lb
WTC 2 Floor 80	7,200 lb	40,700 lb
WTC 2 Floor 81	10,000 lb	21,400 lb
WTC 2 Floor 82	10,200 lb	1,400 lb
WTC 2 Floor 83	1,400 lb	1,100 lb
WTC 2 Floor 84	300 lb	400 lb
Total Weight	65,100 lb	205,200 lb

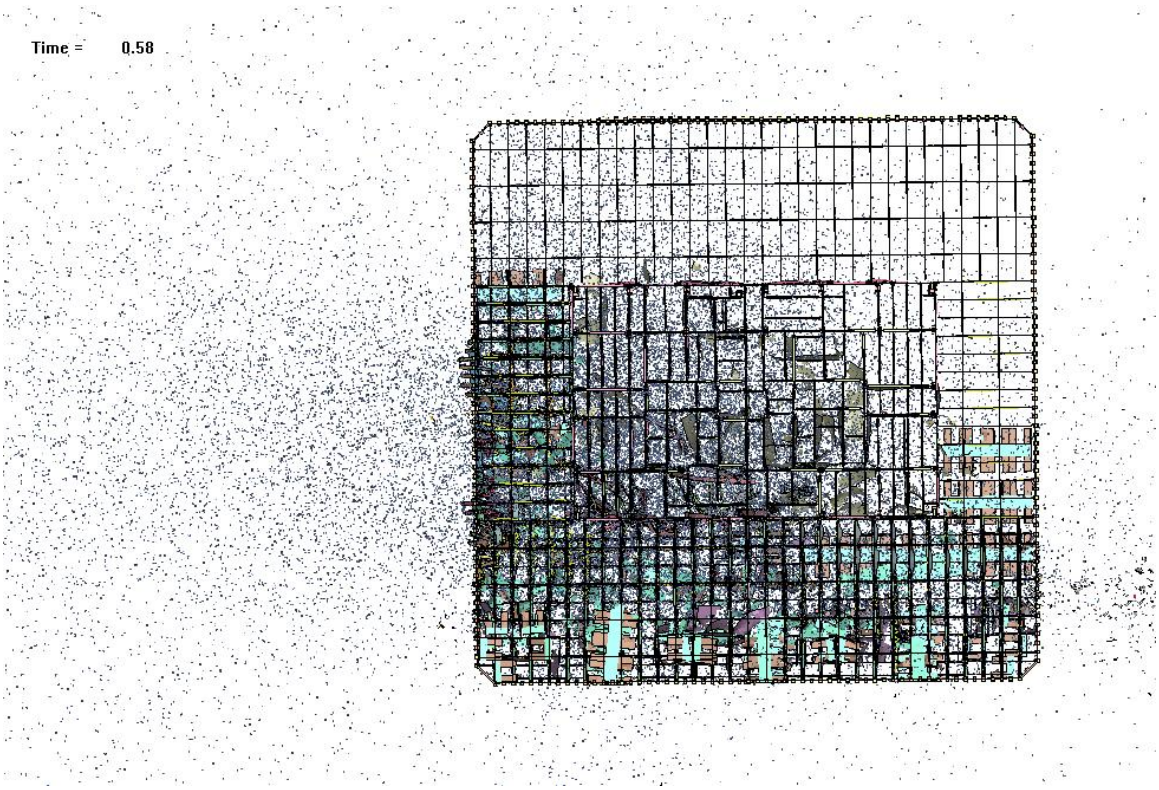

(a) Plan view (floor slab removed)

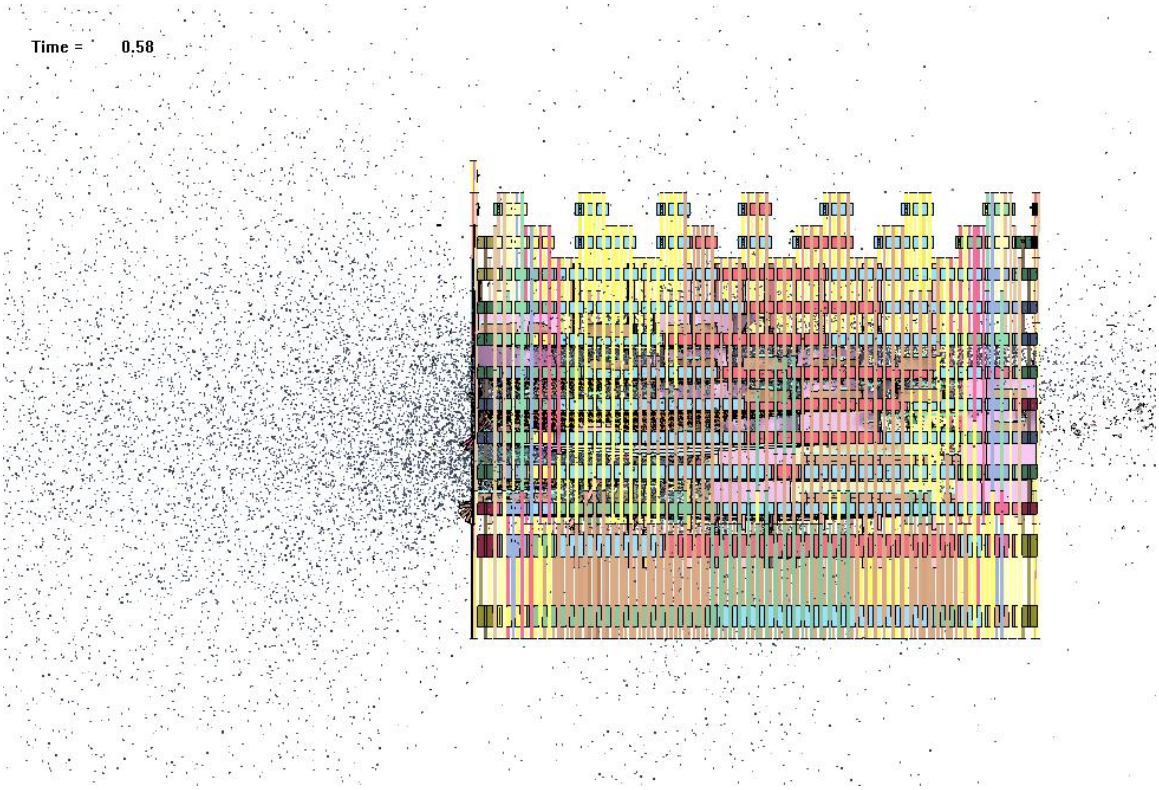

(b) Side view

Figure 7–58. Calculated fuel distribution in the more severe WTC 2 analysis.

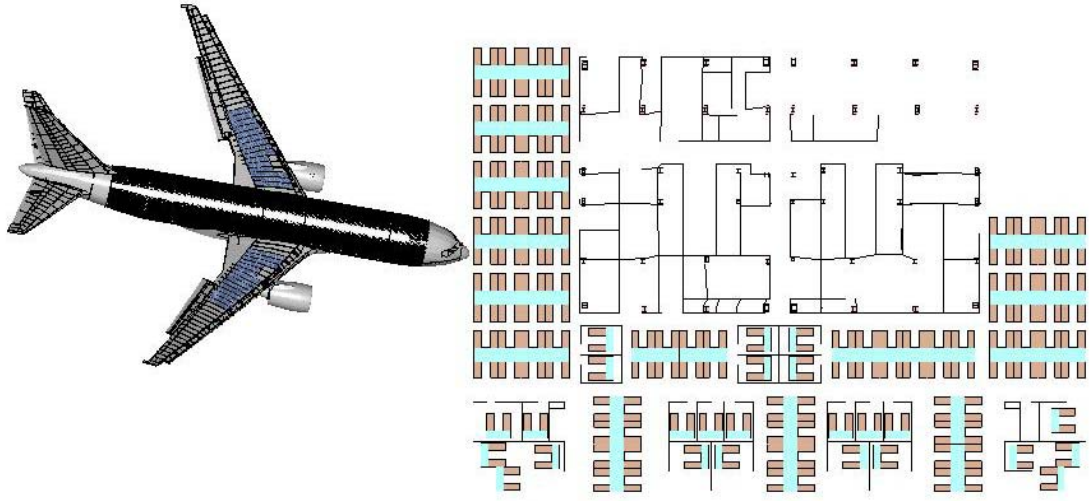

(a) Pre-impact configuration

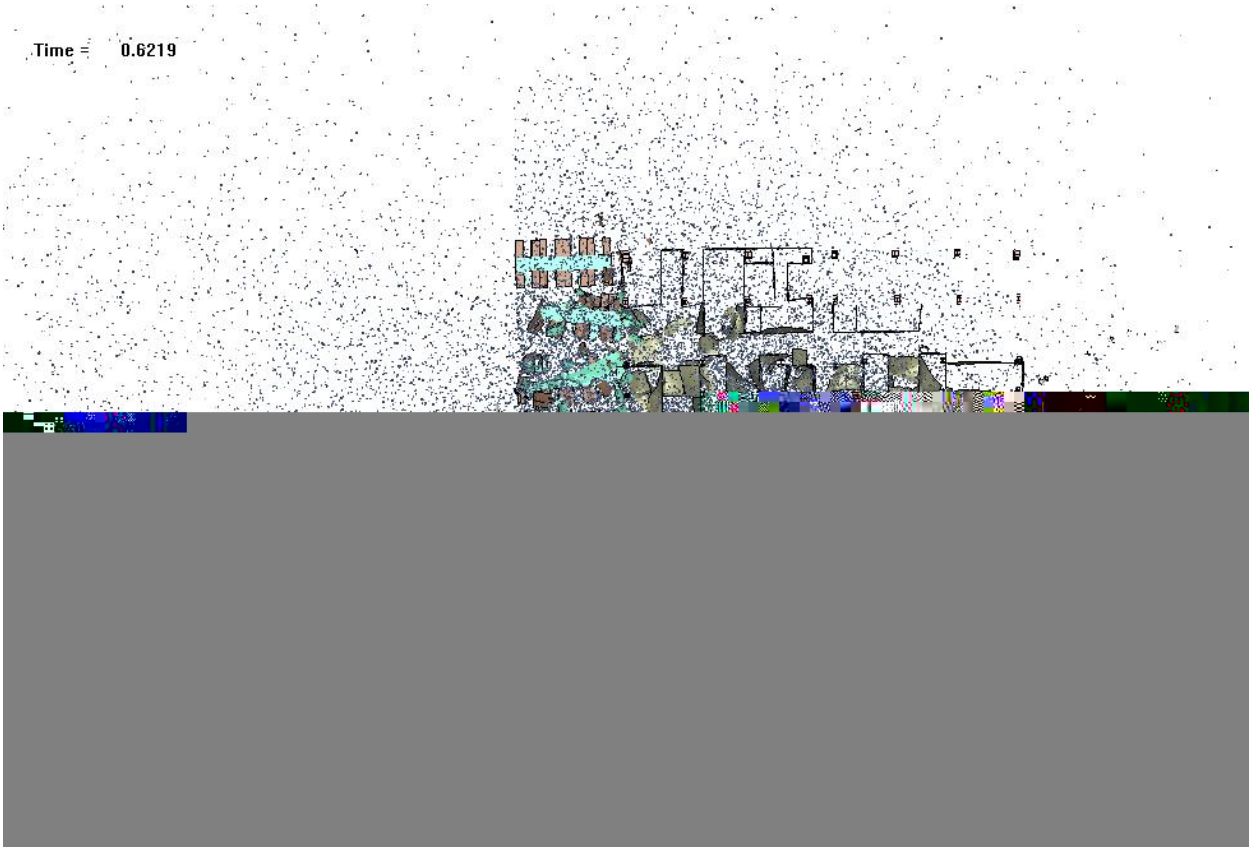

(b) Calculated impact response

Figure 7–59. Plan view of calculated more WTC 2 building, fuel, and aircraft debris distribution for the more severe case.

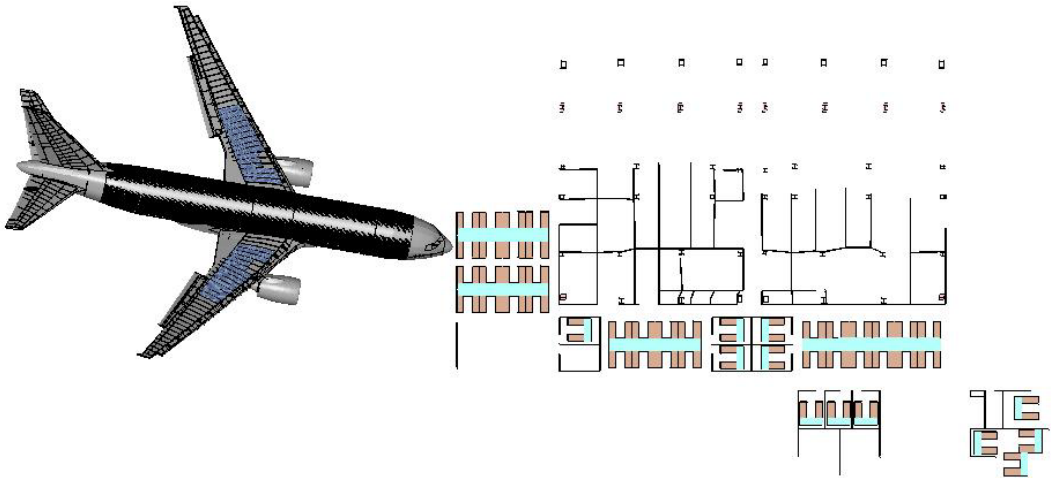

(a) Pre-impact configuration

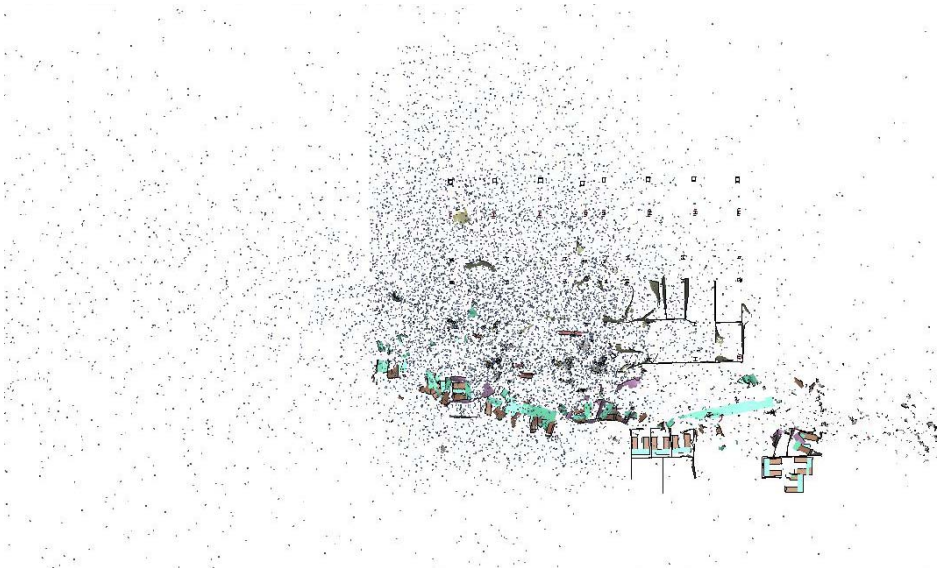

(b) Calculated impact response

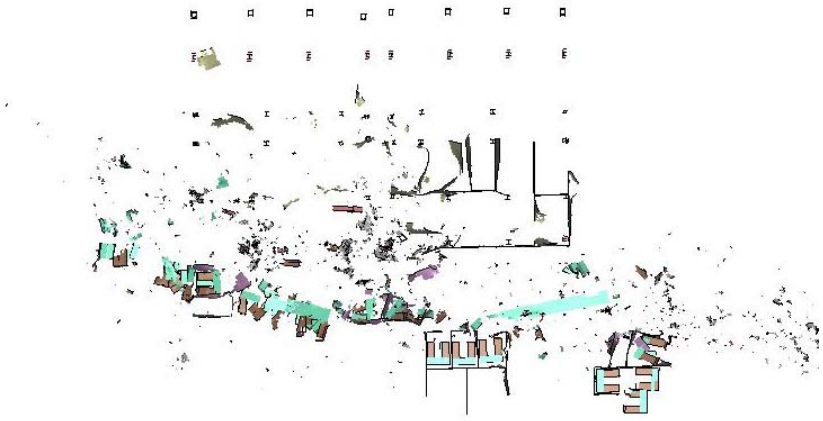

(c) Calculated impact response (fuel removed)

Figure 7–60. Calculated floor 80 contents and fuel distribution (more severe case).

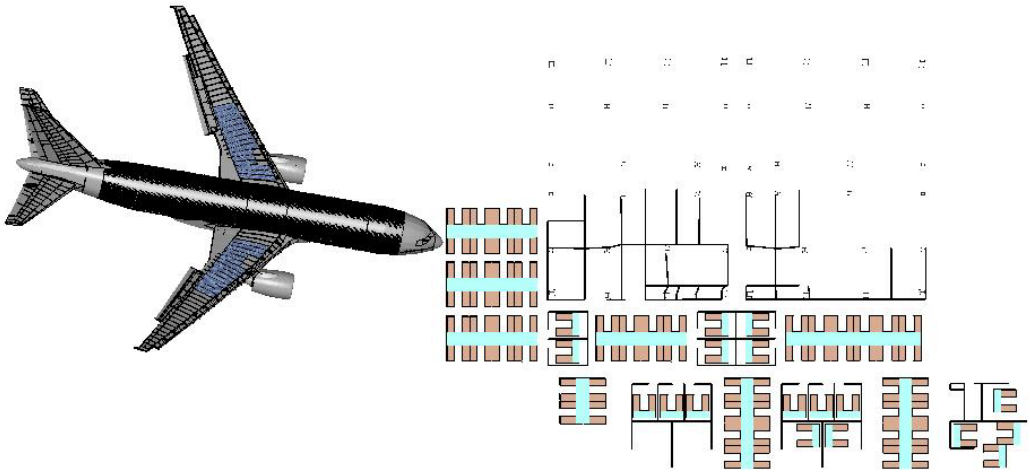

(a) Pre-impact configuration

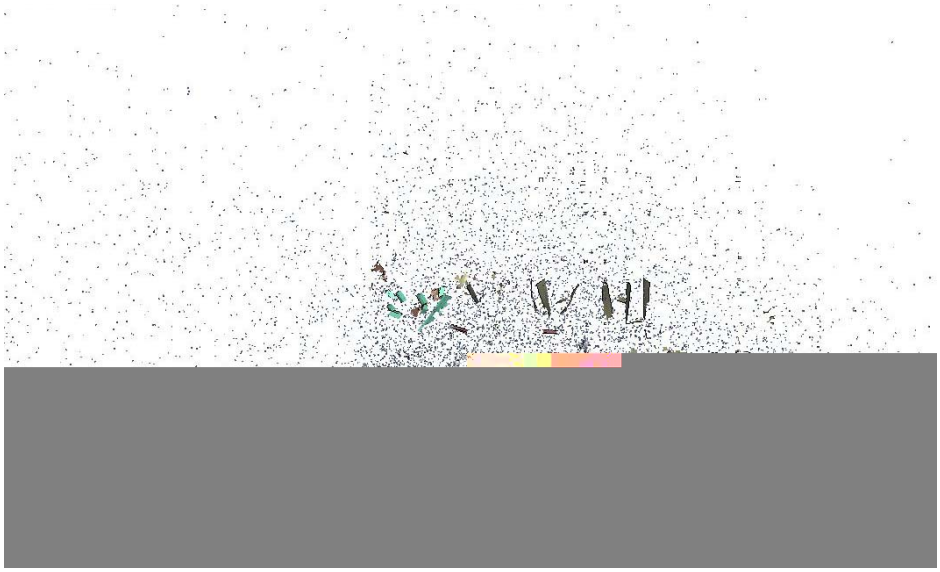

(b) Calculated impact response

(c) Calculated impact response (fuel removed)

Figure 7–61. Calculated floor 81 contents and fuel distribution (more severe case).

7.8 WTC 2 LESS SEVERE IMPACT ANALYSIS – BRIEF DESCRIPTION

This section presents a brief description of the results from the less severe damage case. The reader is referred to NIST NCSTAR 1-2B for further details.

For the south exterior wall of WTC 2, the magnitude and mode of impact damage were still in good agreement with the observed damage for the less severe impact scenario.

The core had significant damage in the region close to the impact point. The columns in line with the aircraft fuselage failed on the impact side, and several of the core beams were also severely damaged or failed in the impact zone. In some cases, failure of the column splices located on floors 77, 80, and 83 contributed significantly to the failure of the core columns. A total of three columns were severed, and two columns heavily damaged, compared to five severed columns and four heavily damaged columns in the base case WTC 2 impact analysis.

The truss floor system on floors 79 through 82 had sufficient damage from the impact that portions of the truss floor sections sagged downward as a result of the impact. The trusses experienced significant damage in the impact zone, with the heaviest damage on floor 81. The calculated impact response produced severe damage to the truss structures in the primary path of the fuselage. The truss structures were completely destroyed along the impact path on floor 81 from the exterior wall to the core.

When compared with the base case, the magnitude of damage to the floor trusses and floor slabs was slightly increased for the less severe impact analysis. The parameters used in the less severe global impact analysis would primarily contribute to a reduced damage magnitude for the tower structures. However, the downward impact trajectory angle was increased from the 6 degree angle in the base case analysis to an 8 degree angle in the less severe impact analysis. This would have the effect of directing more of the impact energy downward, increasing the normal force on the floor structures in the impact zone. As a result, the combined effects of the analysis parameter variations produced very similar damage to the truss structure.

A comparison to the base case and less severe case indicated that the building contents damage zone was similar, with a slight reduction in damage for the less severe impact.

7.9 COMPARISON BETWEEN WTC 1 AND WTC 2

The comparison of the aircraft impact response and resulting tower damage for WTC 1 and WTC 2 was complicated by the differences in the two impact scenarios. The base case WTC 1 impact was close to centered and perpendicular on the face of the tower, with the long-span trusses between the impact point and the core. The WTC 1 impact scenario resulted in a debris trajectory where almost all of the aircraft debris would pass through the core. The baseline impact conditions for WTC 1 were a 443 mph collision with a downward impact trajectory angle of 10.6 degrees. In contrast, the baseline WTC 2 impact was off center and angled away from the core, resulting in a significant fraction of the aircraft debris cloud outside (east) of the core. The WTC 2 impact had short-span trusses between the impact point and the core. Finally, the baseline impact conditions for WTC 2 were a 542 mph collision with a downward impact trajectory angle of 6 degrees.

7.9.1 Exterior Wall Damage

The calculated exterior wall damage for the base case WTC 1 and WTC 2 impacts are compared in Figure 7–62. Despite the differences in impact conditions, the mode and magnitude of damage to the exterior walls were quite similar in both towers. This was because the impact loads distributed over the majority of the aircraft structures were much larger than the exterior column rupture strength. The details of the failure mode (column deformation and rupture or failure and separation of bolted column end connections) were determined by the proximity of the floor slab and column joints to the impact point. For both impacts, the wing tip structures imparted damage, but did not completely fail the columns.

7.9.2 Core Column Damage

The calculated core column damage for the base case WTC 1 and WTC 2 impacts are compared in Figure 7–63. In the WTC 1 impact, there were three columns severed and four columns heavily damaged. The calculated region of significant core column damage appeared to extend three column rows deep into the core. In contrast, the calculated damage for the WTC 2 impact included five columns severed and four columns heavily damaged, and the region of significant core column damage appeared to extend four column rows deep. This increase in core damage was even more significant since the impact zone was 15 floors lower in WTC 2 (and therefore designed to carry more gravity loads), and as a result the core columns were heavier and more resistant to impact damage in the WTC 2 impact zone.

The differences in the core column damage between WTC 1 and WTC 2 can be explained by two primary factors. The first was that the WTC 2 impact speed was 23 percent higher (approximately 50 percent larger impact energy), and the shallower impact angle directed more impact energy inward toward the core. The second factor was that the orientation of the core relative to the impact was different in the two towers, as the core was closer to the impact point in WTC 2. As a result, WTC 2 had reduced energy absorbing capacity due to the shorter floor structures and less building contents between the impact point and the core.

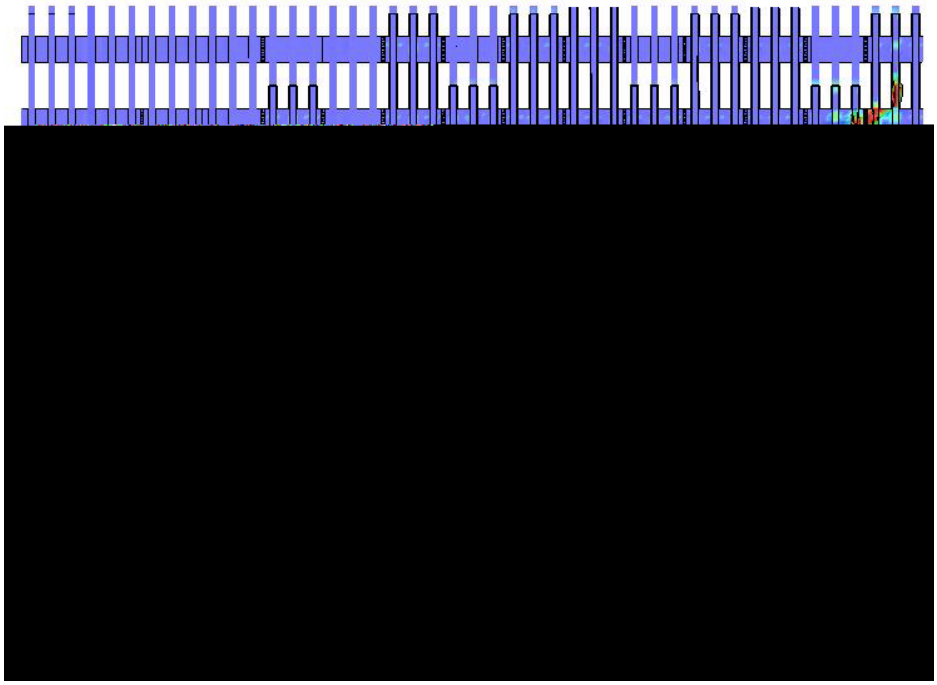

(a) WTC 1 calculated damage to the north wall

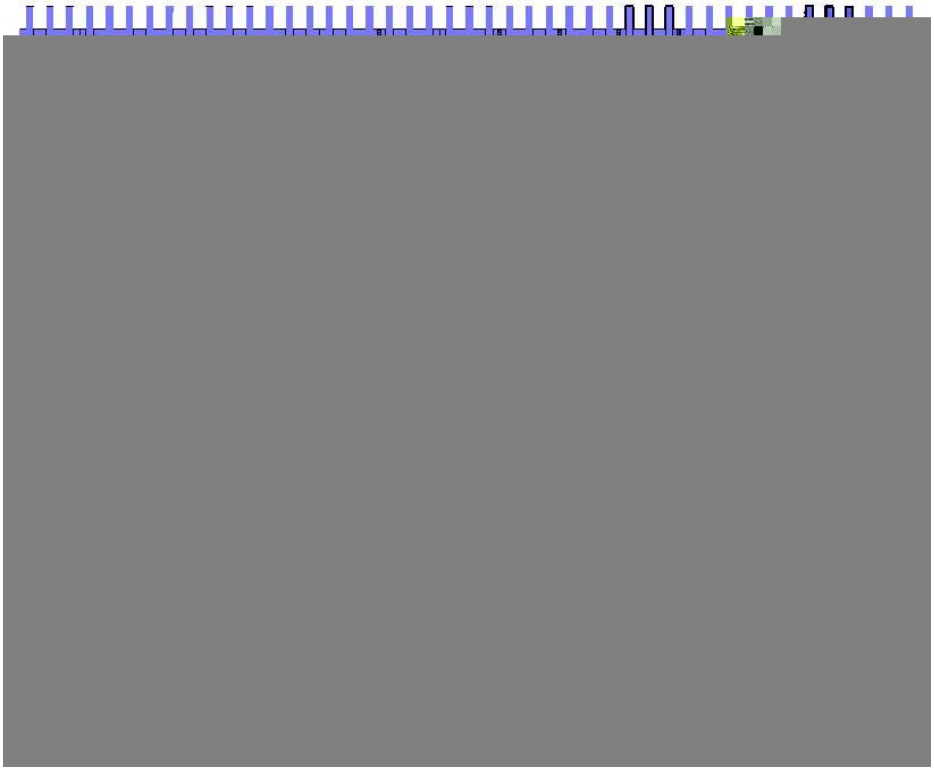

(b) WTC 2 calculated damage to the south wall

Figure 7–62. Comparison of base case impact damage to the exterior walls of WTC 1 and WTC 2.

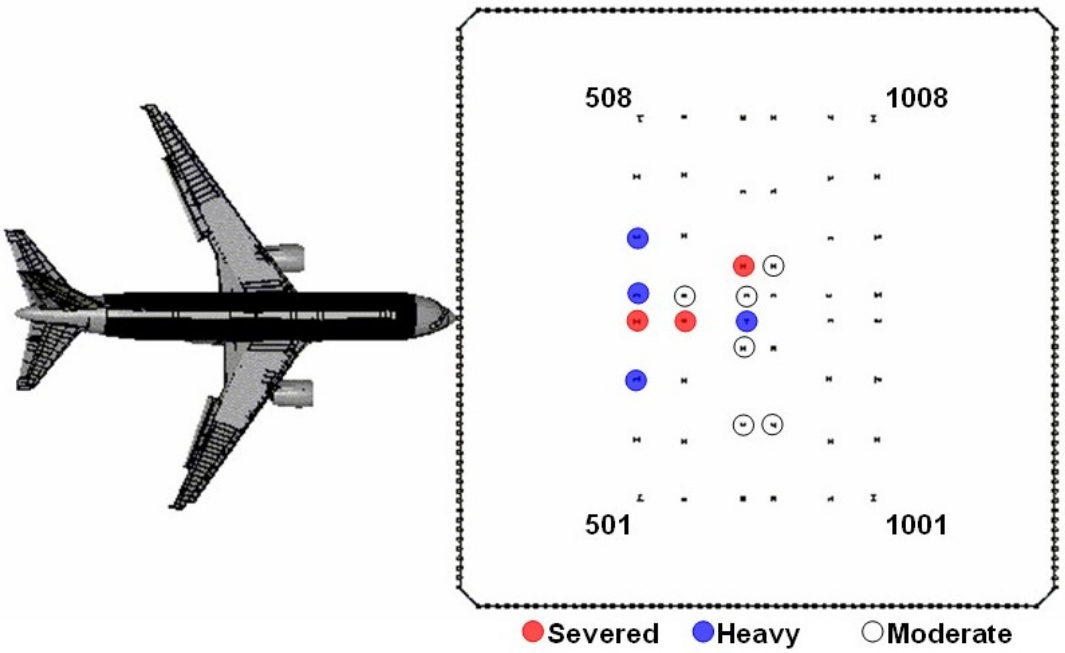

(a) WTC 1 calculated damage

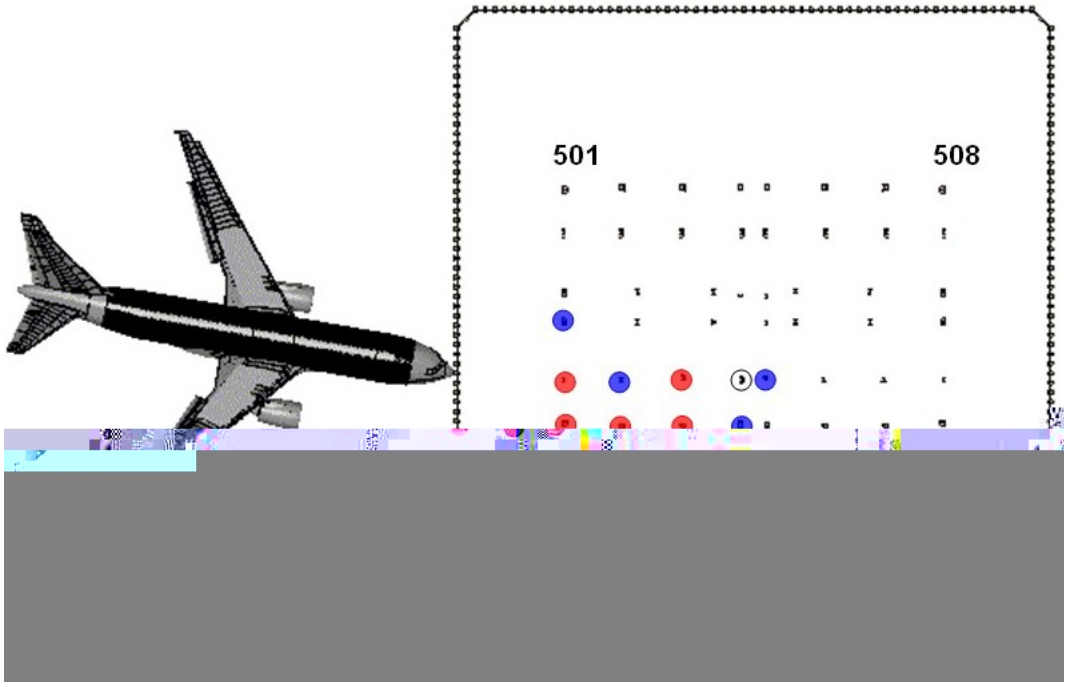

(b) WTC 2 calculated damage

Figure 7–63. Comparison of base case impact damage to the core columns of WTC 1 and WTC 2.

7.9.3 Floor Truss Damage

The calculated floor truss damage for the base case WTC 1 and WTC 2 impacts are compared in Figure 7–64. The comparison shows that the WTC 1 floor truss had greater damage and collapse of the truss floor despite the lower aircraft impact energy. The greater truss floor damage and deflection in WTC 1 can be explained by two factors. The primary factor was that the WTC 1 downward impact trajectory was nearly twice as steep as that of the WTC 2 impact. As a result, the steeper impact angle directed more impact energy normal to the floor slab. The vertical component of the impact load in WTC 1 was approximately 40 percent higher than in WTC 2. The secondary factor was that the damage to the long-span truss floors in the WTC 1 impact zone produced larger displacements than the corresponding damage level to the short-span truss region in WTC 2.

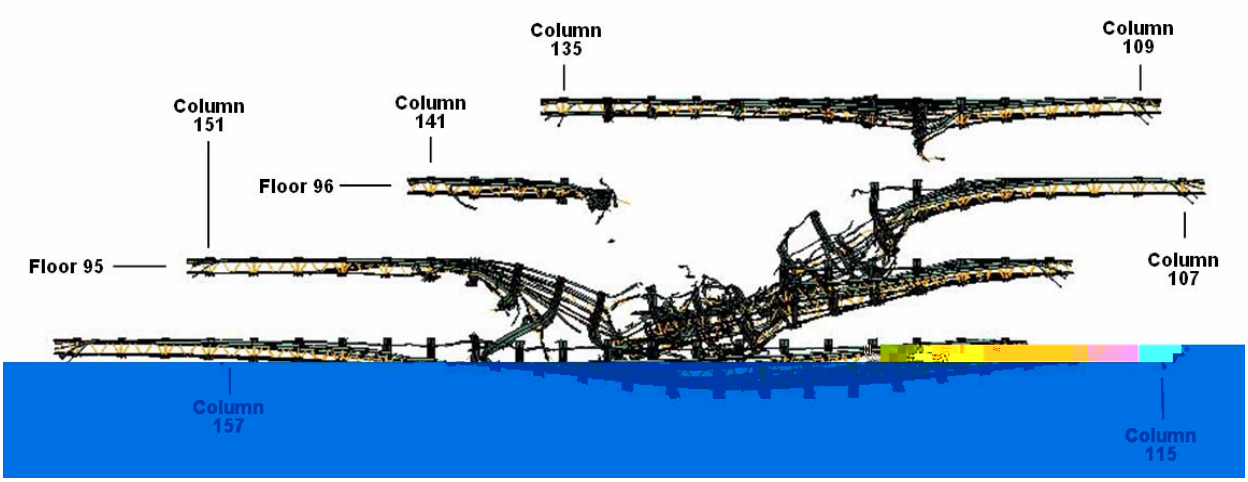

(a) WTC 1 calculated damage

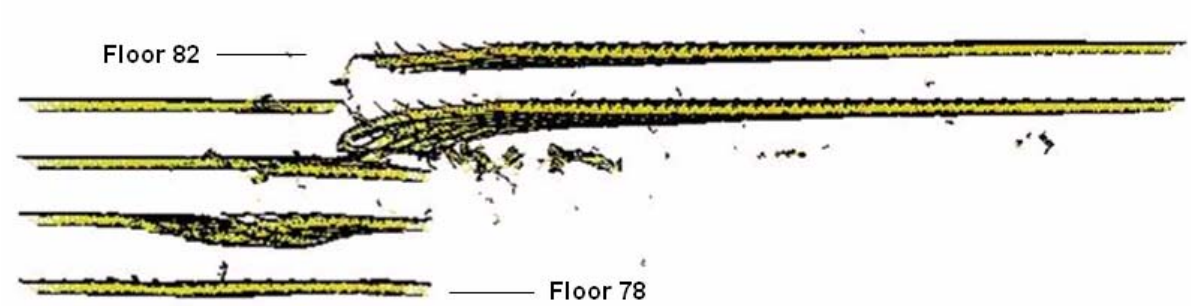

(b) WTC 2 calculated damage

Figure 7–64. Comparison of base case impact damage to floor trusses of WTC 1 and WTC 2.

7.10 COMPARISON WITH OBSERVABLES

The observable evidence available to help validate the global impact analyses included the following:

- Damage to the building exterior documented by photographic evidence.
- Floor damage visible from the building exterior documented by photographic evidence.

- Aircraft debris external to the towers as documented by photographic evidence.
- Eyewitness accounts from survivors who were inside portions of the buildings.

Another observable was that each tower remained standing after sustaining the impact-induced structural damage. Analyses of the structural response of the damaged towers immediately after impact, presented in NIST NCSTAR 1-6, showed that this observable was met for both towers. Sections 7.10.1 and 7.10.2 compare, for WTC 1 and WTC 2, respectively, these observables with the results of the simulations.

7.10.1 Comparison with Observables on WTC 1

Damage Comparison on the North Exterior Wall of WTC 1

The most valuable observable from a modeling standpoint was the damage to the impacted exterior wall of each tower. The impact damage to the exterior walls was well documented, and the impact response did not depend much on unknown parameters, such as the detailed office layout on each floor. Good agreement of the calculated and observed damage profile indicated that the geometric modeling of the aircraft and the initial trajectory and orientation of the aircraft were accurate. The agreement of both the mode and magnitude of the structural damage on the impact wall served to partially validate the constitutive and damage modeling of the aircraft and exterior wall structures of the tower. The agreement in exterior wall damage, based on the modeling methodologies described in this report, contributed to the confidence that the damage predictions for the interior of the towers were reasonably estimated.

Figure 7–65 provides the results of a detailed comparison between the observed and calculated damage (from the base case analysis) on the north wall of WTC 1. The comparison includes the mode, magnitude, and location of failure around the hole created by the aircraft impact. The color code included the following: (1) green circles indicating a proper match of the failure mode and magnitude between the observed and calculated damage; (2) yellow circles indicating a proper match in the failure mode, but not the magnitude; (3) red circles indicating that the failure mode and magnitude predicted by the calculation did not match that was observed; and (4) black circles indicating that the observed damage was obscured by smoke, fire, or other factors. The comparison shown in Figure 7–65 indicates that the overall agreement with the observed damage was very good.

Figure 7–65. Comparison of observable and calculated base case impact damage to the north wall of WTC 1.

Damage Comparison on the South Exterior Wall of WTC 1

The exterior panel from column 329 to 331 between floors 94 through 96 on the south face of WTC 1 was knocked free by landing gear and possibly other debris (see NIST NCSTAR 1-5A). These columns were located in the center of the south wall of the WTC 1. In both the base case and more severe damage global analyses, aircraft debris impacted the south face of the tower, as shown in Figure 7–66 and Figure 7–67, and exited the building. The figures also show the calculated landing gear debris for both simulations. None of the debris impacting the south wall happened to contain landing gear fragments. In the base case analysis, the debris impacted columns 328 to 330 at floor 96. In the more severe impact analysis, debris impacted columns 328 to 333 on both floors 95 and 96. In the base case analysis, very little damage was done to the exterior panels on the south wall. However, damage was heavy in the more severe damage analysis, as shown in Figure 7–68.

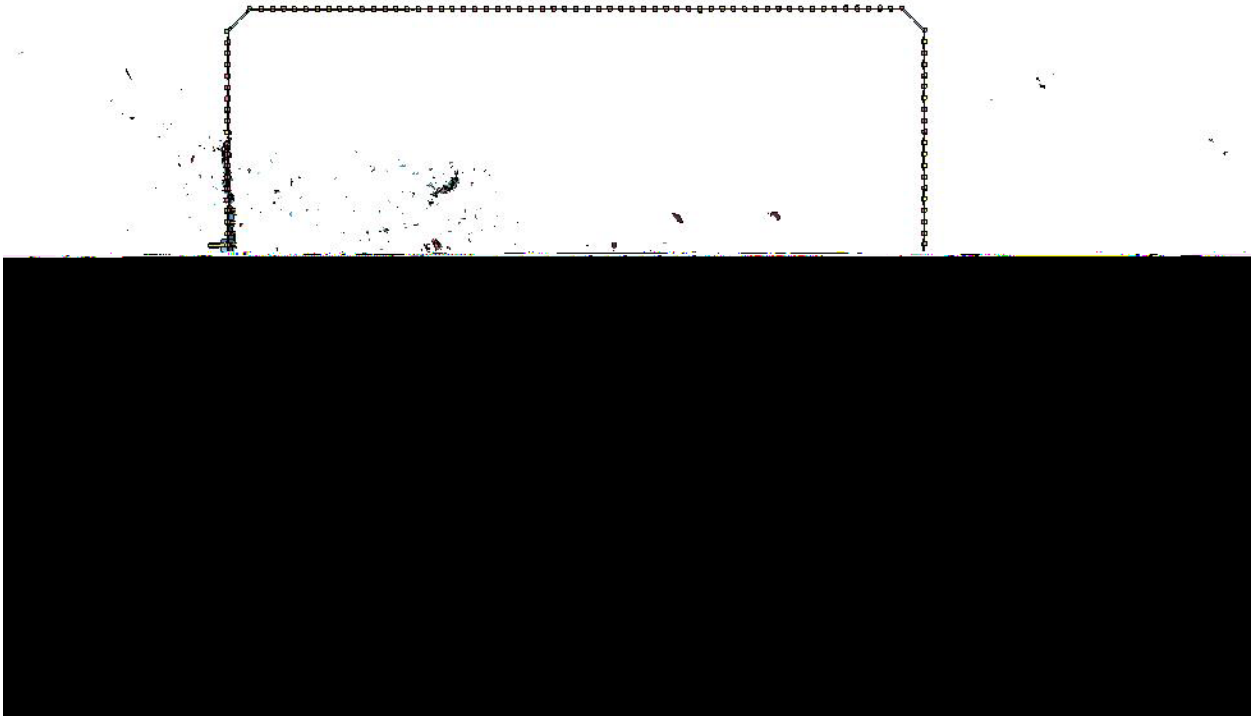

(a) Calculated aircraft debris (t = 0.685 s)

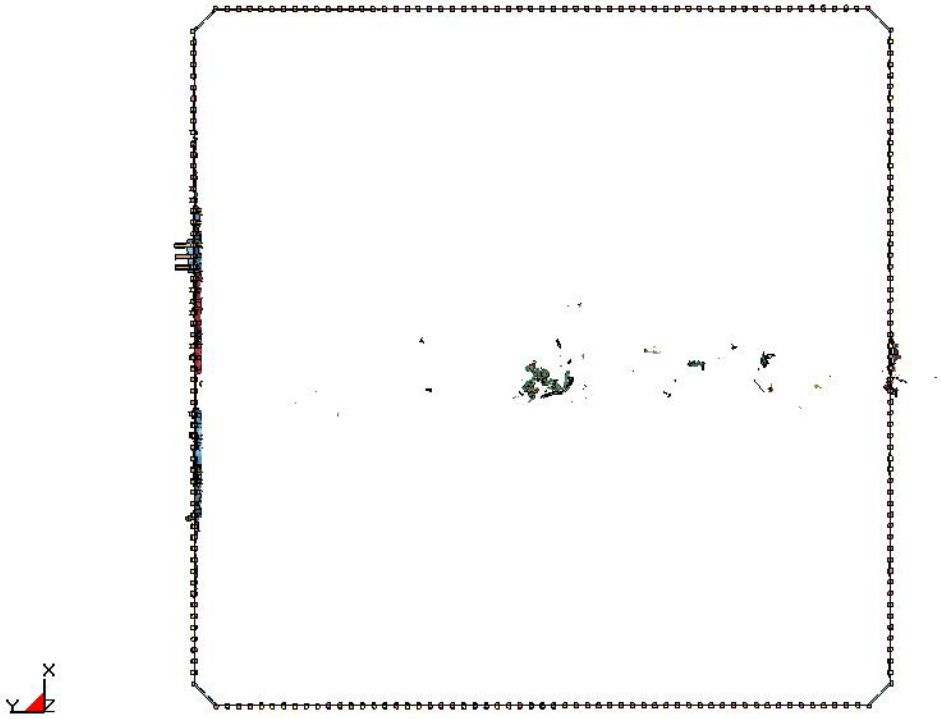

(b) Calculated landing gear debris (t = 0.685 s)

Figure 7–67. More severe damage aircraft debris distribution in WTC 1.

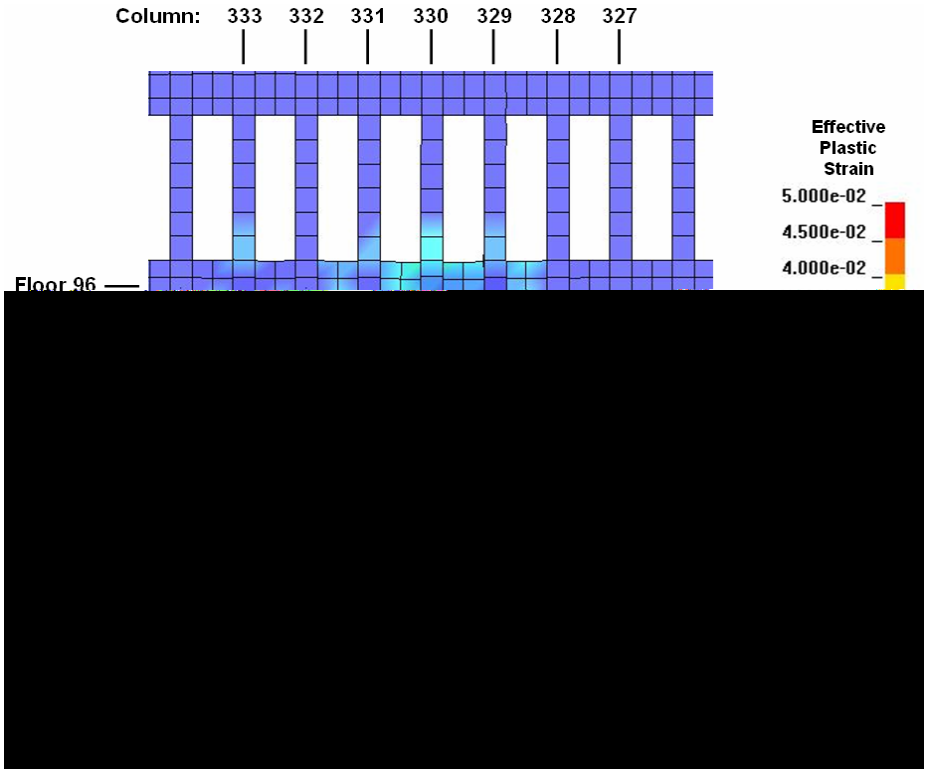

Figure 7–68. Damage to the south face of WTC 1 from the more severe damage global analysis.

Because of model size constraints, the panels on the south face of WTC 1 were modeled with a very coarse resolution. Neither the spandrel splice joints nor exterior column butt joints were modeled. Column ends and spandrel edges were merged together. The model therefore underestimated the damage to the tower on this face. The calculated damage produced by the more severe impact, shown in Figure 7–68, indicated that columns 329–331 on floors 94 through 96 sustained substantial damage. Had a fine mesh been used on these columns, it is likely that they would have failed on floor 95, and possibly on 94 and 96. Based on the failure modes observed on the north face and on the speed and mass of the debris, the panel would potentially be knocked free by failing at the connections.

Landing Gear Trajectory Comparison

A portion of the main landing gear of AA 11 exited WTC 1 at the 94th or 95th floor and landed at the corner of Rector St. and West St. The debris consisted of a tire, wheel, brake assembly and hub of a main landing gear, as shown in Figure 7–69. Based on the final position of the landing gear and assuming the landing gear to be a projectile with a horizontal initial velocity, the exit speed of the landing gear from the south wall of WTC 1 can be estimated to be about 105 mph. Note that there is a significant uncertainty in this estimate associated with the exit trajectory, aerodynamic effects, landing position rather than final resting position of debris, etc. Another piece of landing gear debris, shown in Figure 7–70, was found embedded in what is postulated to be the panel containing columns 329, 330, 331, running from the 93rd to the 96th floors. This panel was dislodged from the building and found at Cedar Street near its intersection with West Street. As little other damage had been documented on the south face of WTC 1,

it is postulated that the landing gear debris that landed at the corner of Rector St. and West St. also exited through this panel location.

The amount of aircraft debris found to exit WTC 1 in the global impact analyses varied, as shown in Figure 7–67 and Figure 7–68. However, no portion of the landing gear was observed to exit the tower in the simulations, but rather was stopped inside, or just outside, of the core. In order to simulate the trajectory of specific pieces of aircraft debris, a fairly precise knowledge of the internal configuration of the building was needed. This is especially true with components passing through the core of the building, where some of the most massive building contents and partition walls were present. Uncertainties regarding the internal layout of each floor, such as the location of hallways or walls, could make the difference between debris from a specific component passing through or being stopped inside the tower. In addition, modeling uncertainties and assumptions might play a role in not matching the observable.

Figure 7–69. Landing gear found at the corner of West and Rector Streets.

Figure 7–70. Landing gear found embedded in exterior panel knocked free from WTC 1.

Stairwell Disruption Comparison

According to eyewitness interviews, stairwells 1 (referred to also as stairwell A), 2 (stairwell C), and 3 (stairwell B) inside the core were impassable at floor 92 and possibly above after the impact of AA 11 (see NIST NCSTAR 1-7). The calculated base case stairwell disruption is shown in Figure 7–71 for floors 93 through 97. Stairwell positions are outlined with red boxes in the figure. No debris or disruption was observed to the core on floor 92 in the calculation, therefore, it is not shown in the figure. Recall that the global model for WTC 1 only contained partition walls in the core on floors 94 through 97. Therefore, the ability to ascertain damage and/or debris in the stairwell on floors 92 and 93 was limited. The floor slab was removed from the view on floors 94 through 97 so that debris is more visible.

Based on the calculated damage to, or debris in, the stairwells on floors 94 to 96, all three stairwells appear impassable. Given that falling debris in these areas would cause further subsequent damage to the floors below, as well as block passage on these floors, this result was reasonably consistent with the eyewitness accounts.

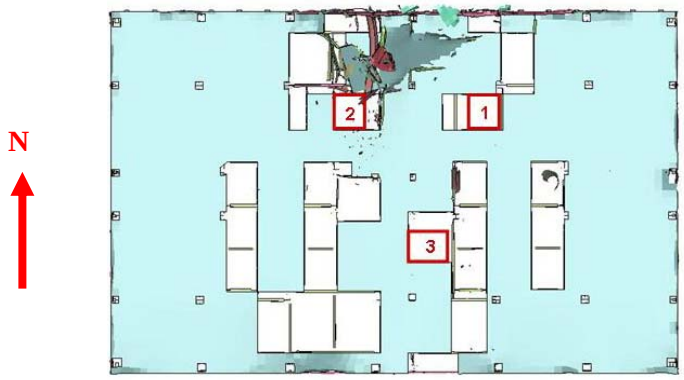

(a) Floor 93

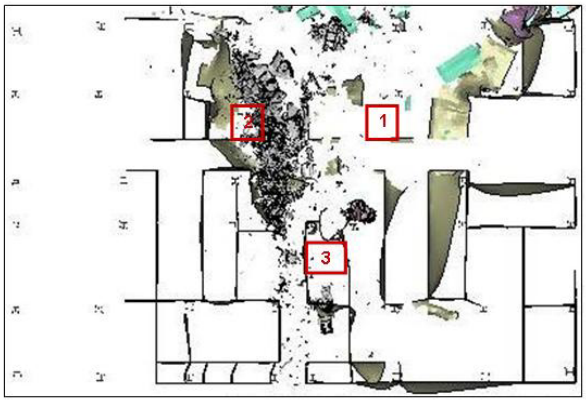

(b) Floor 94

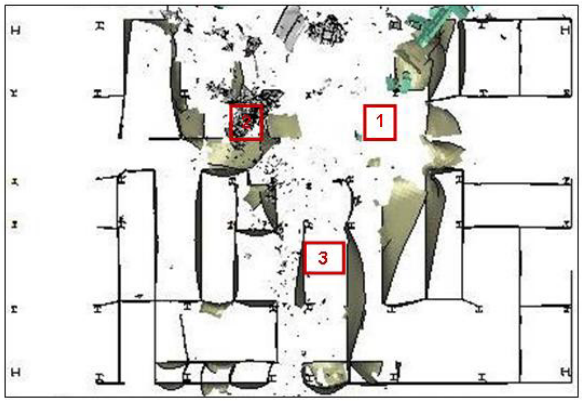

(c) Floor 95

(d) Floor 96

(e) Floor 97

Figure 7–71. Base case stairwell disruption in WTC 1.

Floor Damage Visible on the North Face of WTC 1

One location where the damage to the WTC 1 truss floors could be observed was through the opening in the tower exterior produced by the aircraft impact. A photograph of the impact damage on the north face of WTC 1 is shown in Figure 7–72(a). The magnitude of damage was difficult to quantify as a result of

the strong contrast in lighting between the tower interior and exterior and the smoke inside the building. However, the photograph shows that the truss floor was heavily damaged and/or removed in the primary impact zone. The depth of the floor damage extending into the tower could not be determined.

(a) Observed Damage

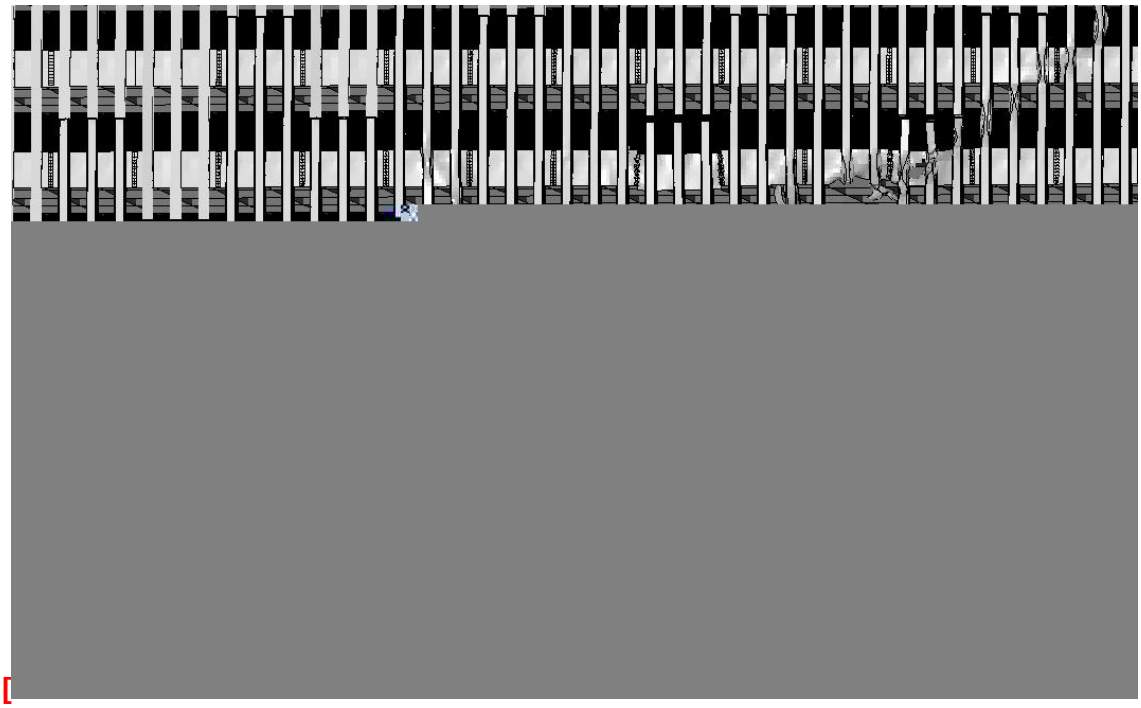

(b) Calculated damage

Figure 7–72. Observed and calculated WTC 1 damage (front view).

A corresponding image of the calculated damage to the tower structures is shown in Figure 7–65(b). The structures beyond the start of the core were removed and replaced with a black background for comparison with the photograph. Although a quantitative comparison of the calculated and observed damage could not be made from the available damage photographs, the truss floor damage appeared to be consistent.

7.10.2 Comparison with Observables on WTC 2

Damage Comparison on the South Wall of WTC 2

Figure 7–73 provides the results of a careful comparison between the observed and calculated damage (from the base case analysis) on the south wall of WTC 2. The comparison includes the mode, magnitude, and location of failure around the hole created by the aircraft impact. The comparison indicates that the overall agreement with the observed damage was very good.

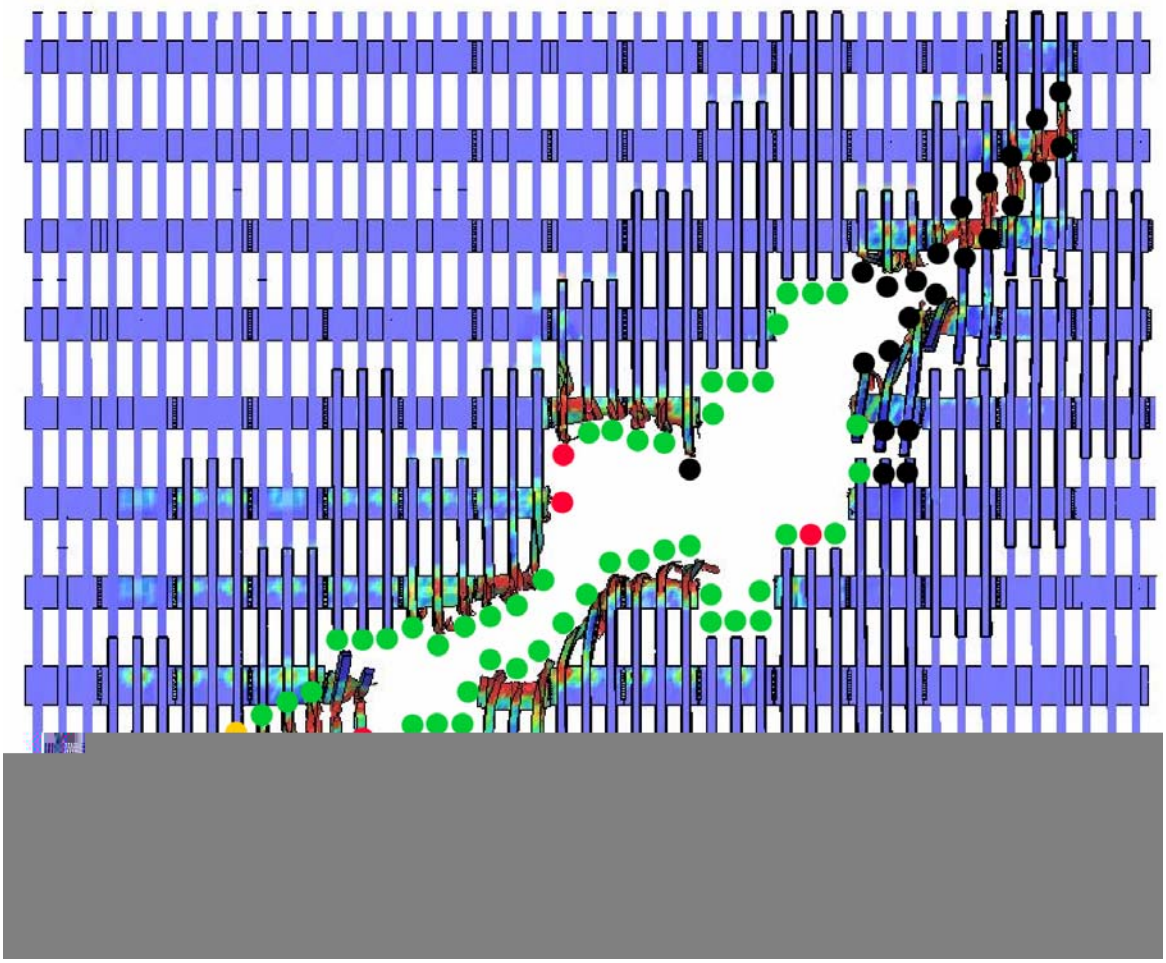

Figure 7–73. Comparison of observable and calculated base case impact damage to the south wall of WTC 2.

Damage Comparison on the North Wall of WTC 2

From photographic evidence, such as that shown in Figure 7–74, damage on the north wall at the northeast corner of WTC 2 was documented and is shown in Figure 7–75. As mentioned earlier, there was significant uncertainty as to the actual layout of the workstations and other building contents on the impacted floors of the towers. Recall that generic workstation configurations were used to model these building contents, as shown in the northeast corner of WTC 2 in Figure 7–76(a). Uncertainties regarding this layout, such as missing partition walls and workstations, could make the difference between debris from a specific component passing through or being stopped inside the structure. The base case impact response of the northeast corner of WTC 2 on the 81st floor is shown in Figure 7–76(b).

Figure 7–74. Impact damage to the northeast corner of the exterior wall of WTC 2.

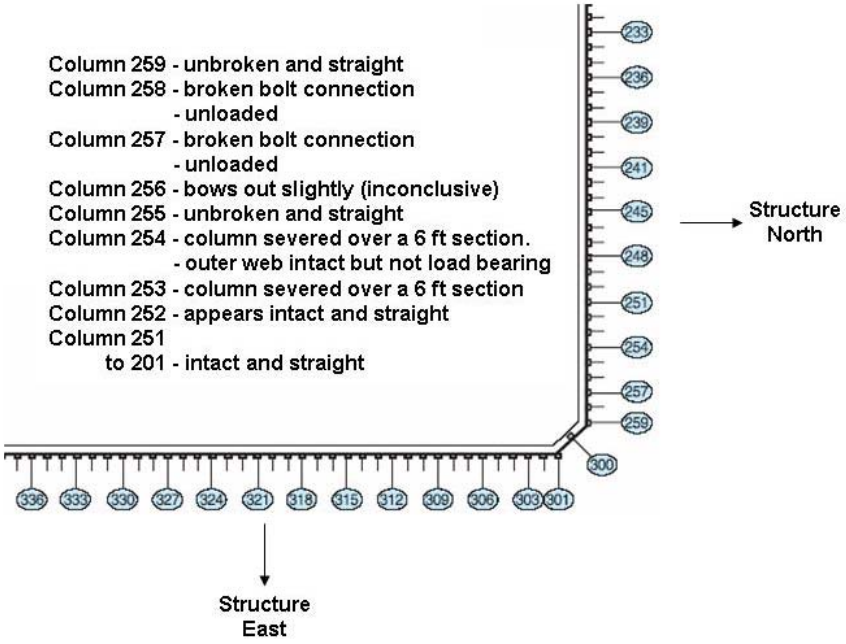

Figure 7–75. Documented damage to the northeast corner of floor 81 of WTC 2.

Aircraft debris on floor 81 of WTC 2 is shown in Figure 7–76(c), with the coloring depicting the residual speed of the debris field. Notice that some of the debris in this figure, weighing approximately 3,800 lb, was traveling at 110–150 mph and was projected to impact between columns 252 and 256. The leading debris was portions of the starboard main landing gear main strut and main landing gear beam. That significant debris was projected to impact in the region of significant damage shows positive agreement with damage evidence available for the north wall of WTC 2.

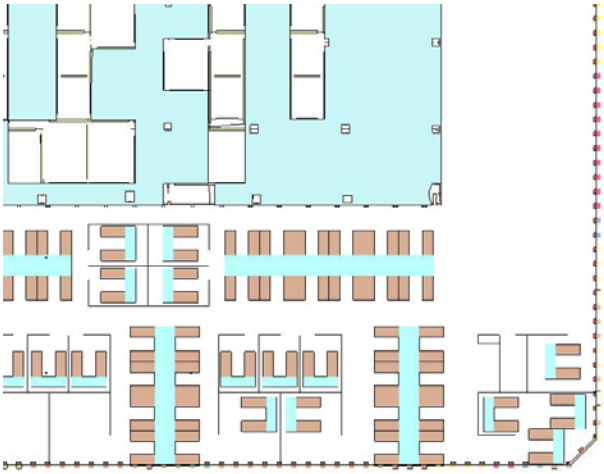

(a) Initial workstation configuration

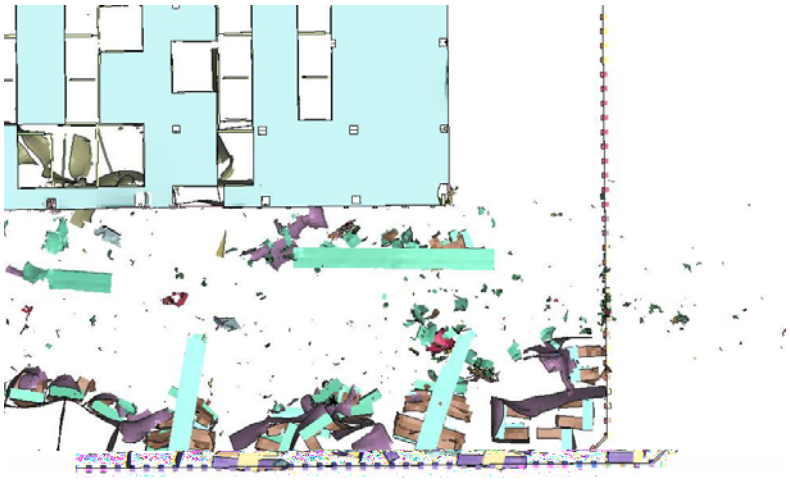

(b) Debris field at t = 0.62 s

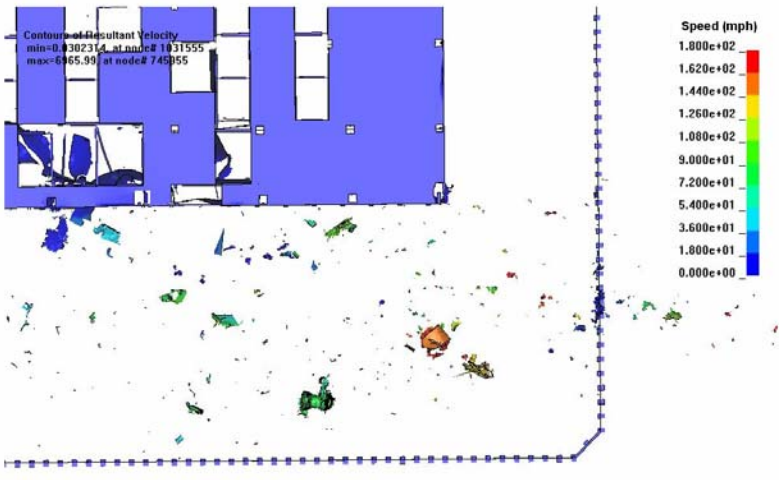

(c) Residual speed of aircraft debris (contours in mph)

Figure 7–76. Base case response on the northeast corner of floor 81 of WTC 2.

Stairwell Disruption Comparison

According to eyewitness interviews, stairwells 2 and 3 on floor 78 of WTC 2 were impassable (see NIST NCSTAR 1-7). Stairwell 1 (referred to also as stairwell A), which was located in the northwest corner of the core, was passable. The calculated base case stairwell disruption is shown in Figure 7–77. Stairwells 1 and 2 (stairwell C) on floor 78 of WTC 2 were outside of the core column region as is shown in the figure. These stairwells were not included in the WTC 2 model. Therefore, a good assessment could not be made for stairwell 2. However, disruption to stairwell 3 (stairwell B) is shown in Figure 7– 77. By the damage shown in the figure, the stairwell appears to be impassable. As no damage or debris was seen in the northwest corner of the tower, the top right in the figure, stairwell 1 in this area of the core was likely unaffected. Both of these assessments were consistent with the eyewitness accounts.

Figure 7–77. Base case stairwell disruption on floor 78 in WTC 2.

Landing Gear Trajectory Comparison

A portion of the landing gear of UAL 175 exited WTC 2 and landed on the roof of 45 Park Place (see FEMA 2002). No photographic evidence was available to document the size of the fragment and whether this was a nose or main landing gear. From the damage to the building, the landing gear fragment might have exited somewhere along the north wall between column 251 and the northeast corner on floor 81. Based on the final position of the landing gear and assuming the landing gear to be a projectile with a horizontal initial velocity, the exit speed of the landing gear from the north wall of WTC 2 can be estimated to be about 102 mph. Note that there is a significant uncertainty in this estimate associated with the exit trajectory, aerodynamic effects, landing position rather than final resting position of debris, etc.

The calculated aircraft debris distribution and landing gear and engine debris distributions for UAL 175 are shown in Figure 7–78 and Figure 7–79 for the base case and more severe case, respectively. A portion of the port main landing gear was seen to exit the building at approximately 230 mph in the more severe impact analysis, as shown in Figure 7–79(b). No landing gear debris exited the building in the base case. At the conclusion of the simulation, the base case analysis had a substantial piece of the starboard main landing gear still moving at approximately 130 mph that was expected to impact the northeast corner.

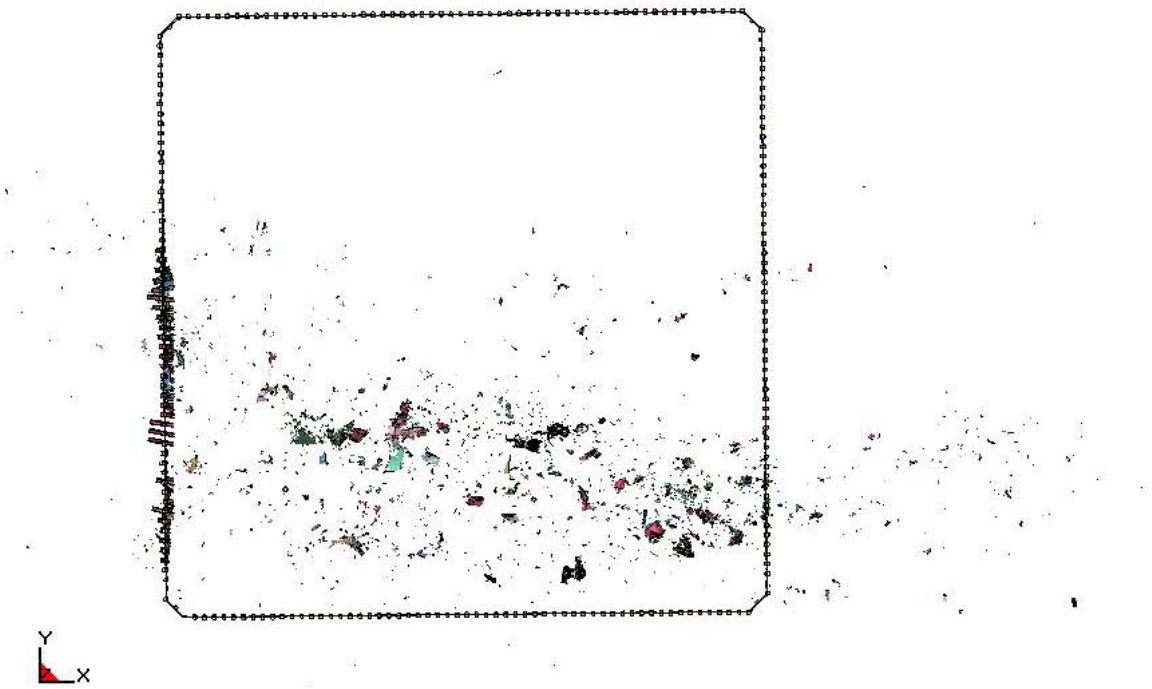

(a) Calculated aircraft debris (t = 0.62 s)

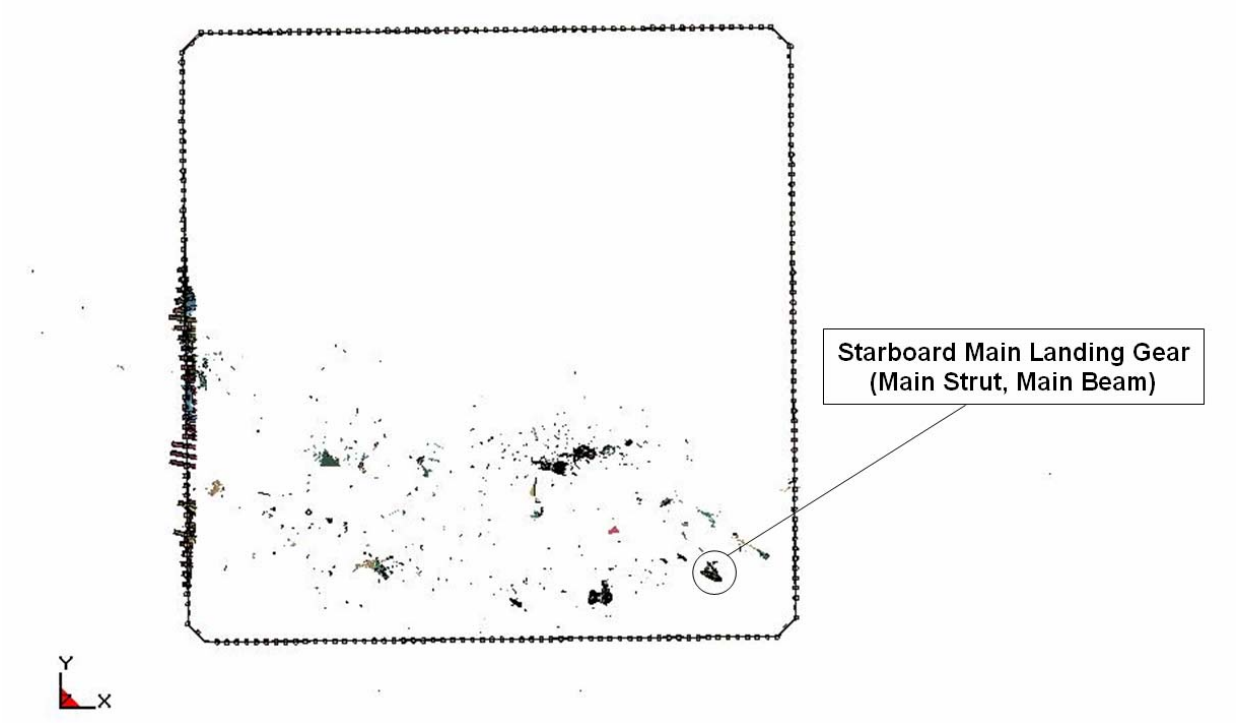

(b) Calculated engine and landing gear debris (t = 0.62 s)

Figure 7–78. Base case damage aircraft debris distribution in WTC 2.

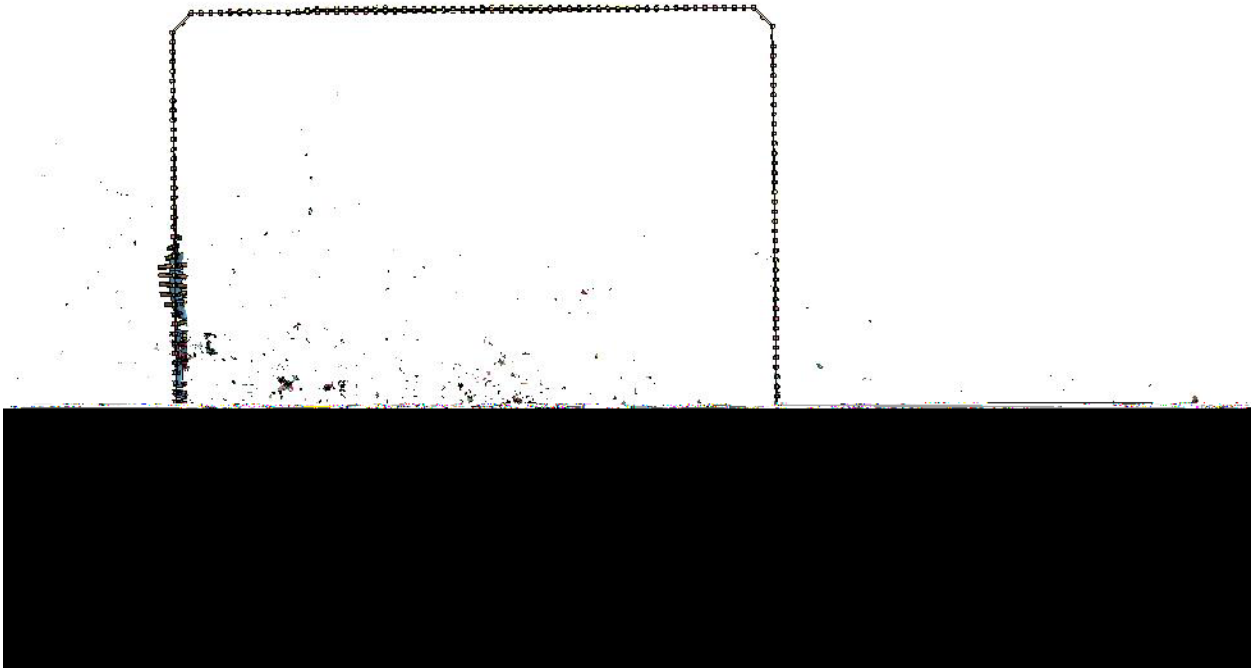

(a) Calculated aircraft debris (t = 0.58 s)

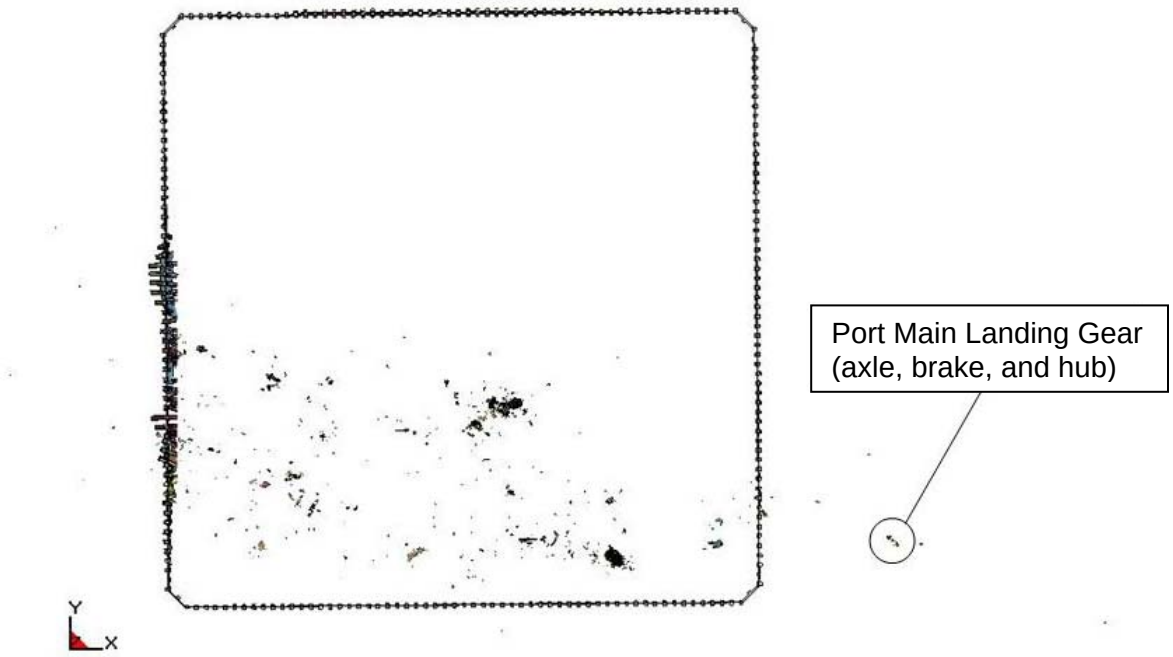

(b) Calculated engine and landing gear debris (t = 0.58 s)

Figure 7–79. Aircraft debris distribution in the more severe WTC 2 impact.

Engine Trajectory Comparison

A portion of an engine also exited the tower at the northeast corner of the building and was found at the intersection of Murray and Church Streets. From the damage to the building, it was believed that the engine exited the building in this corner of WTC 2. Based on this trajectory, it was estimated that the engine exited the building at approximately 120 mph. The engine trajectories predicted from the base case global analysis are shown in Figure 7–80, which indicates that the engine that exited from the northeast corner of the tower is likely the starboard engine. The dotted line indicates the extrapolated engine flight path based in the initial trajectory of the starboard engine. Notice that this trajectory would result in engine fragments exiting at the northeast corner. In the simulations, the engines were projected to stop short of this position, although they follow the extrapolated trajectory reasonably well.

Speed time-histories for the aft portion of the starboard engine are shown in Figure 7–81. The engine would typically breakup into smaller fragments from the forward section of the engine and a larger section from the aft end, as shown in Figure 7–82. In all simulations, the speed was seen to drop by approximately 200 mph due to impact with the exterior panel, floor slab, and floor truss. Interaction with these portions of the structure ended by approximately 0.12 s. This initial impact from the base case is shown in Figure 7–83. The engine debris then continued through the tenant space of the 81st floor, plowing through the workstations and contents. Whether or not the fragment passed over these contents, or if other debris and fuel removed the contents from the engine's path, affected the deceleration of the fragment. At the end of the simulation, the speed of the aft portion of the engine was below 80 mph, and it was more than 60 ft from the northeast corner of the building. For these calculations, it was estimated that the building contents would likely stop the engine fragment prior to impacting the northeast corner of the exterior wall.

None of the three WTC 2 global impact simulations resulted in a large engine fragment exiting the tower. However, the impact behavior suggests that only minor modifications would be required to achieve this response. For example, if the starboard engine impact location was lowered by 1 to 2 ft, which is within the aircraft impact geometry uncertainty range, the engine would likely have had a greater residual speed inside the tower, over 100 mph. In the global analyses performed, the engine impacted the underside of the 82nd floor, as shown in Figure 7–76. This resulted in a large reduction in speed of approximately 200 mph. In the component analyses, the engine speed decreased by roughly 60 mph when impacting an exterior panel alone. This additional speed would likely result in a large engine fragment exiting the northeast corner of the tower.

Other minor modifications to the model could also result in a large engine fragment exiting the building. As mentioned previously, there was significant uncertainty in the distribution of building contents on the floors of the impact area. If any portion of the east side of WTC 2 was relatively free of office materials, the engine fragment would have been free to move relatively unrestricted and would have experienced little loss of speed. After the engine entered the structure, and without office materials, the engine fragment would only slow due to friction with the floor slab and occasional interaction with floor trusses above. After initially entering the building, the engine did not further penetrate the floor slab. Removing much of the building contents from the east side would result in the starboard engine fragment impacting the northeast corner of the tower with sufficient speed to exit the building. Little or no difference in core damage would result, as debris in this area had no chance of impacting the core.

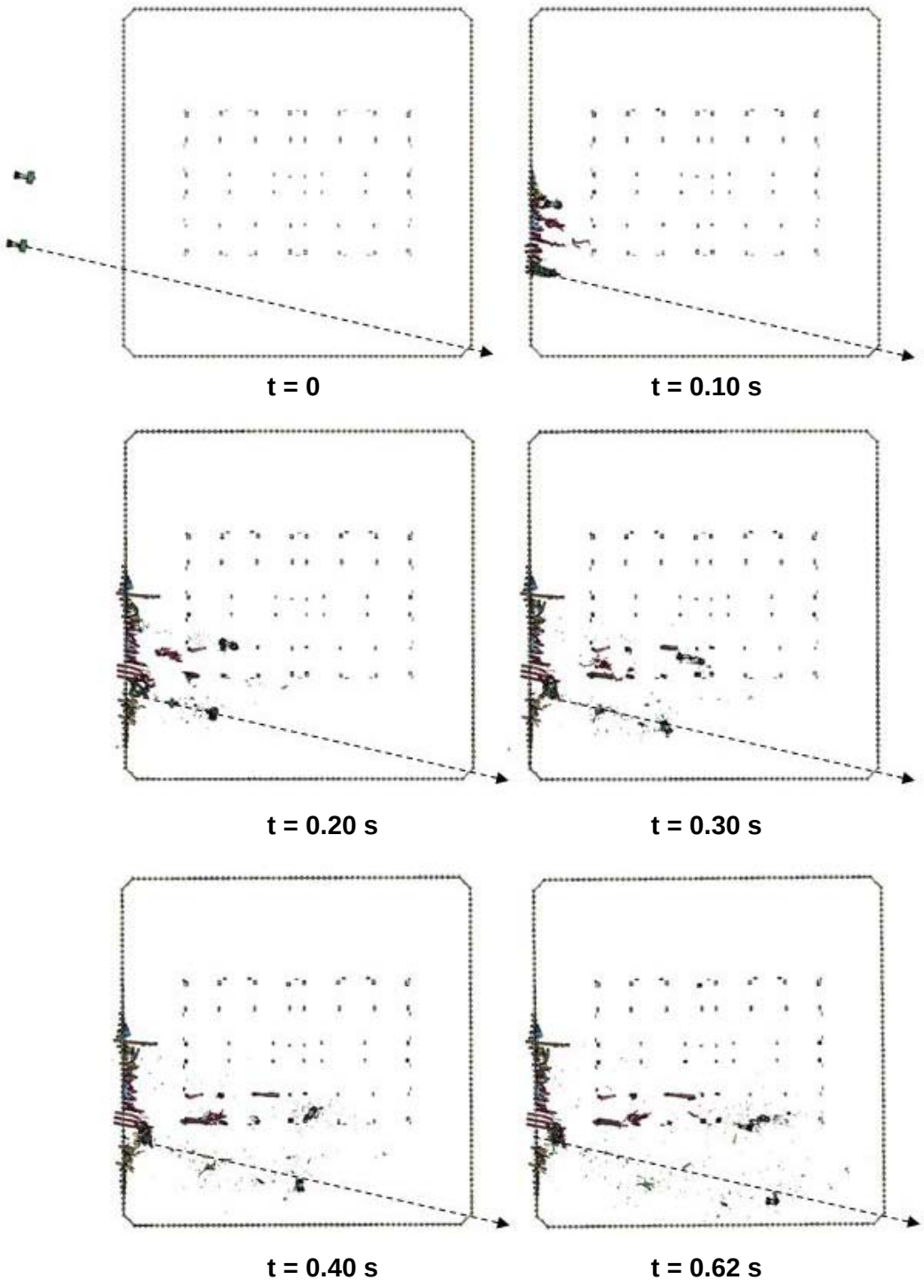

Figure 7–80. Starboard engine fragment trajectory in the base case global analysis of WTC 2.

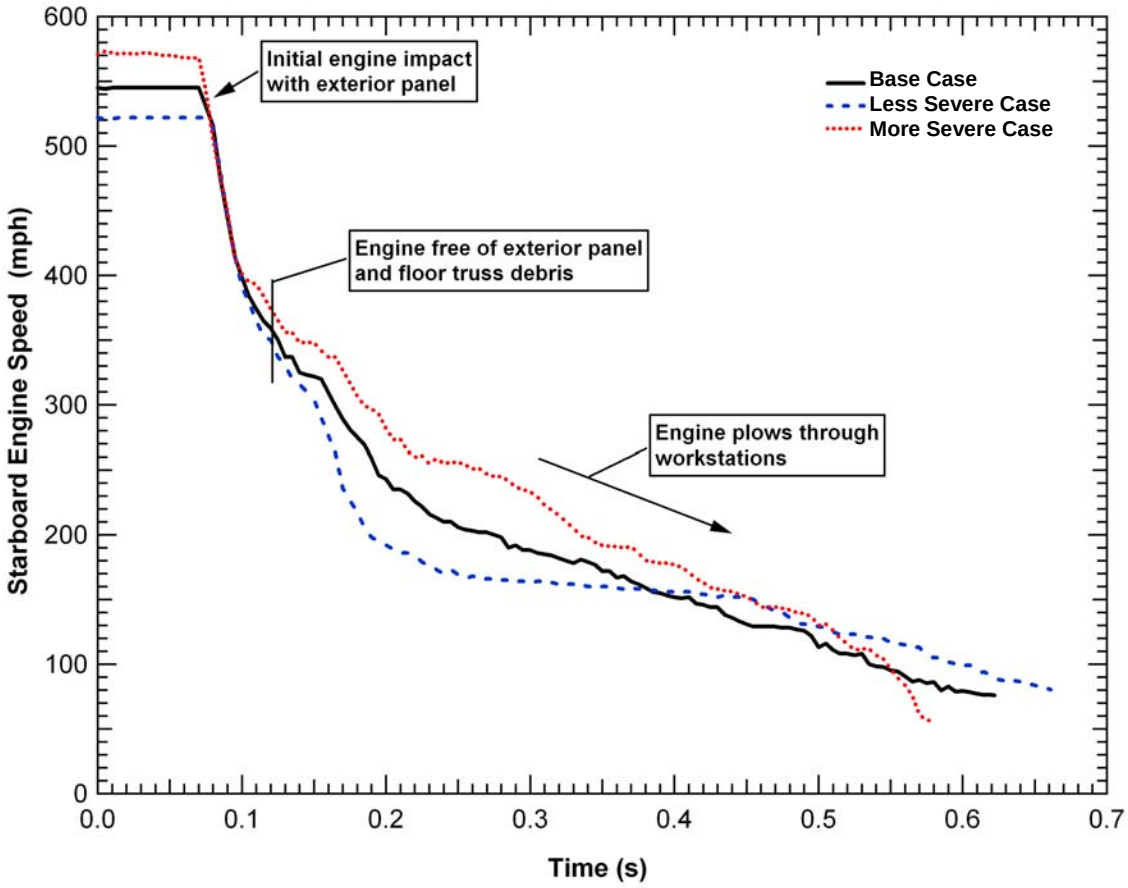

Figure 7–81. Speed of the aft portion of the starboard engine.

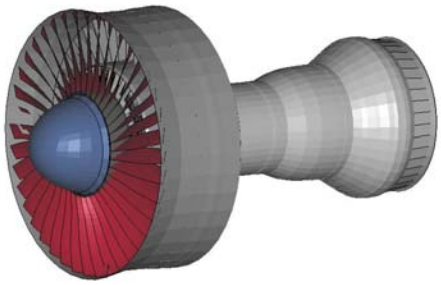

(a) Undamaged engine

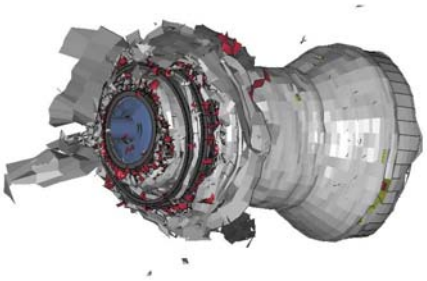

(b) Large engine fragment

(c) Engine fragment found at Murray and Church St.

Figure 7–82. Calculated and observed engine damage.

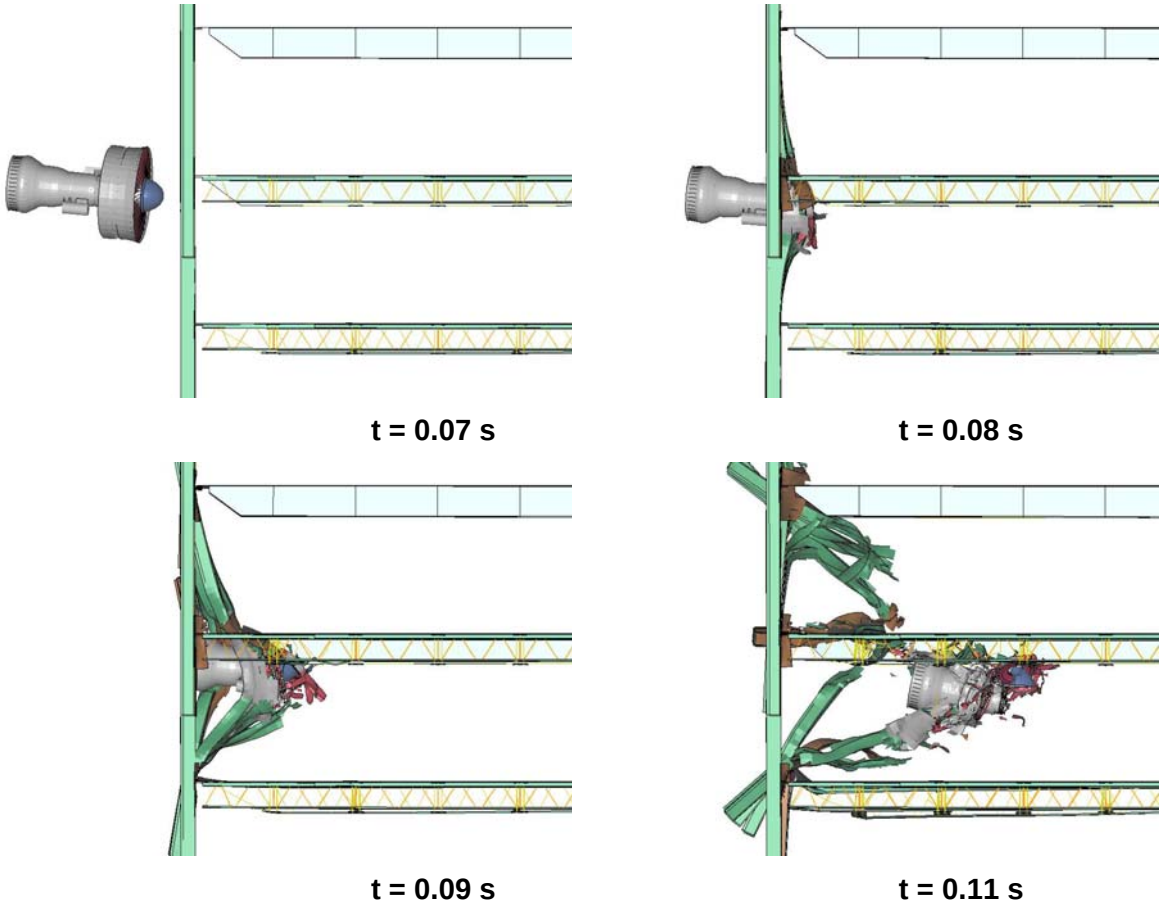

Figure 7–83. Starboard engine impact with the south face of WTC 2 in the base case global analysis.

Floor Damage Visible on the South Face of WTC 2

One location where the damage to the WTC 2 truss floor could be observed was through the opening in the tower exterior produced by the aircraft impact. A similar comparison for the WTC 1 truss floor damage was shown in Figure 7–72. The magnitude of damage was difficult to quantify as a result of the strong contrast in lighting between the tower interior and exterior and the smoke inside the building. This was worse for WTC 2, where the prevailing wind and fire conditions resulted in larger quantities of smoke exiting through the opening on the impact face. The partial photographic evidence did suggest that a similar level of truss floor damage in the impact zone occurred for WTC 2. The severity and the depth of the floor damage extending into the tower could not be determined. Although a quantitative comparison of the calculated and observed damage could not be made from the available damage photographs, the truss floor damage appeared to be consistent.

The 'Cold Spot' on the North Face of WTC 2

A 'cold spot' was observed on the north face of the tower between columns 238 and 250 on floors 80, 81, and 82. The cold spot was a region of the tower where no debris could be seen from the exterior of the tower and no significant fires were observed prior to tower collapse.

Much of the explanation for the cold spot was obtained from an analysis of the debris trajectory aligned with the cold spot. The debris path, obtained by projecting the width of the cold spot along the initial lateral impact trajectory of the aircraft, is shown in Figure 7–84 (13 degrees relative to the tower face normal). This region was aligned laterally with the left side of the fuselage and the port wing structures. Considering the baseline impact orientation and trajectory, shown in Figure 7–85, it can be seen that much of the wing debris impacted on floors lower than the observed cold spot. Only debris from very close to the fuselage would be expected on floor 80 or above. The debris from the port wing, including the majority of the aircraft fuel in the left side tanks, entered at floors 78 and 79.

The base case WTC 2 global analysis calculated a small amount of aircraft debris passing through the cold zone on floors 80 and 81. However, the building contents were not completely modeled over the entire path in this section. After clearing the core region, the debris in the calculation had primarily an open path to the cold spot on the north wall of WTC 2. If all of the internal contents had been included, it is likely that all of this debris would have been stopped before reaching the cold spot.

The comparison of the calculated and observed impact response cold spot is inconclusive. Much of the absence of damage and aircraft debris in this region is explained by the impact orientation and trajectory. Much of this region was not directly in the path of significant aircraft fuel and debris. In addition, the debris aligned with the cold spot would be required to pass through a significant portion of the core. A more accurate analysis of the impact mechanics leading to the formation of a cold spot would require a specific survey of the tenant layout, including both contents that acted as a barrier to the debris and walls that provided a barrier to subsequent fire propagation.

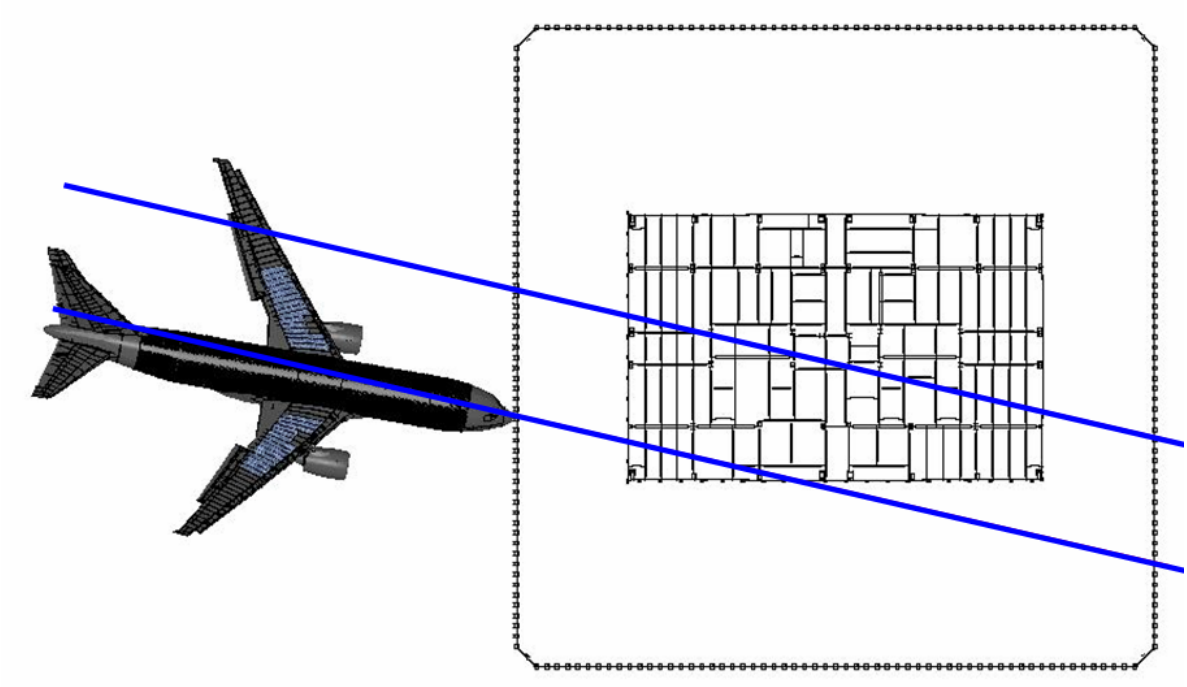

Figure 7–84. Projected debris path for the WTC 2 north face cold spot.

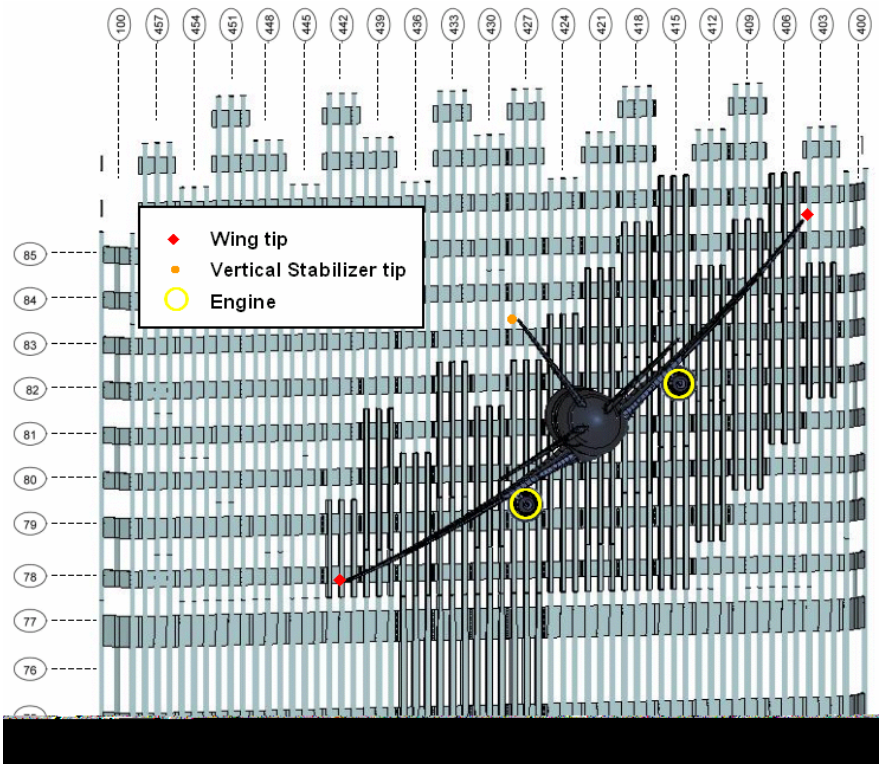

Figure 7–85. Base case WTC 2 impact orientation and trajectory (vertical approach angle = 6°. lateral approach angle = 13°).

7.10.3 Summary

In general, not all of these observables were perfectly matched by the impact simulations due to the uncertainties in exact impact conditions, the imperfect knowledge of the interior tower contents, the chaotic behavior of the aircraft breakup and subsequent debris motion, and the limitations of the models. In general, however, the results of the simulations matched these observables reasonably well. Examples where the simulations matched the observables included: (1) the damage to the exterior walls of both towers, (2) the disruption to the stairwells in both towers, (3) the landing gear trajectory and the cold spot on WTC 2.

7.11 COMPARISON WITH PREVIOUS STUDIES

Two previous studies were conducted to estimate the impact damage to the WTC towers. These studies were performed by Massachusetts Institute of Technology (MIT) (Wierzbicki, Xue, and Hendry-Brogan, 2002) and Weidlinger Associates, Inc. (WAI) (Levy and Abboud 2002). The MIT study used an energy balance approach to estimate damage to the core columns. Estimates were made for the initial kinetic energy of the impacting aircraft, and the internal energy absorbed in fragmentation of the aircraft and damage to the tower exterior columns, floor slab, and core columns. The energy absorbed by the core was used to estimate the number of failed core columns.

The WAI study used the FLEX finite element code to calculate the aircraft impact damage to both towers. The FLEX family of finite element modeling software (Vaughan 1997) was developed and maintained by WAI. FLEX is an explicit, nonlinear, large deformation transient analysis finite element code for the analysis of structures subjected to blast, impact, and shock loadings. The overall code architecture is similar to that of LS-DYNA, used to calculate the aircraft impact damage in this investigation.

In the WAI calculations, the aircraft and WTC towers models were composed of beam and shell elements. The aircraft model consisted of 27,000 shell elements and 23,000 beam elements. The aircraft fuel was included in the model by increasing the mass of the structures in the wing box. The tower models included the exterior wall on the impact face and the floor structures and the core frame for floors 91-101 and floors 76-86 for WTC 1 and WTC 2, respectively. The tower models had fixed boundary conditions at the top and bottom floors.

7.11.1 Comparison of Exterior Wall Damage

The calculated base case impact damage to the exterior north wall of WTC 1 from this study is compared to the impact damage calculated by WAI in Figure 7–86. The figure also shows a schematic of the damage observed in photographic evidence. Figure 7–87 shows a similar comparison for the south wall of WTC 2. In both towers, the base case impact damage estimated in this study closely matched the observed damage. The damage profiles in the WAI impact simulations had some noticeable differences. The first was that the damage profile included complete failure of the exterior columns over the entire length of the wings and to the top of the vertical stabilizer. The second difference was that the failure mode of the exterior walls was dominated more by local rupture of the columns adjacent to the impact point with less influence of the bolted connections on panel failure and removal.

The differences in the damage profiles in the two calculations most likely resulted from a variety of differences in the models. One major difference between the two studies was in the fidelity of the aircraft models. The WAI Boeing 767 model was based on their model of a Lockheed C-141B military transport. In the WAI model, the external geometry of the C-141B was modified to fit the dimensions of the 767, but the internal components, such as stiffener configuration, as well as material thicknesses and properties remained the same. The differences in the internal structure and materials could affect the way the aircraft responded to the impact. The aircraft model used in this study also contained an order of magnitude more elements (70,000 bricks, 562,000 shells, and 61,000 SPH particles) than the WAI model (27,000 shell elements and 23,000 beam elements). The higher resolution of the NIST model could also account for significant differences in the determination of the impact load distribution and resulting exterior damage. Additionally, the NIST model explicitly modeled the fuel. If the fuel mass in the WAI model was spread out further toward the wing tips as part of the wing structure, it would be expected that the calculated column damage would extend over a wider portion of the wings.

Secondary differences in the WAI and NIST impact analyses included, but were not limited to, variations in impact conditions (impact speed, orientation and trajectory, location, etc.), aircraft model differences (airframe geometry, component thicknesses, mass distribution, material properties, etc.) and tower model differences (material properties, geometry, joint modeling, number of elements, etc.).

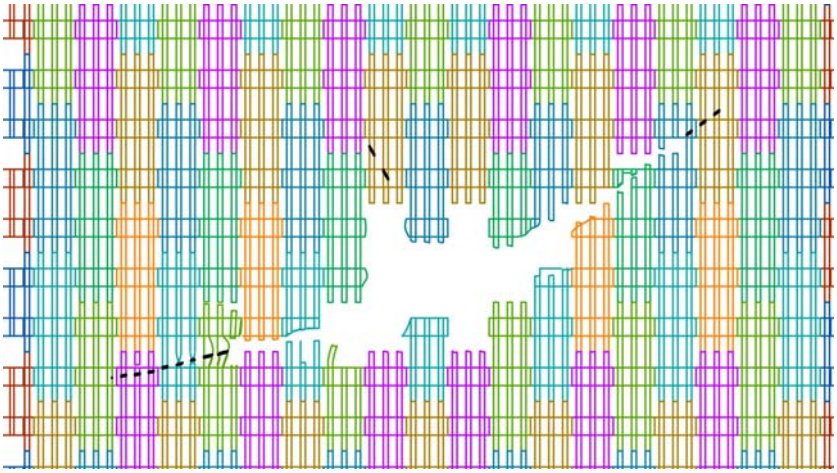

(a) Schematic of observed damage

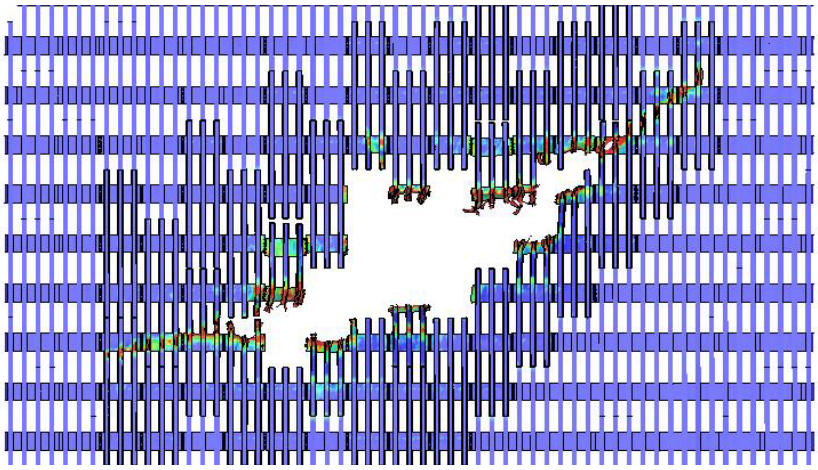

(b) NIST base case impact damage

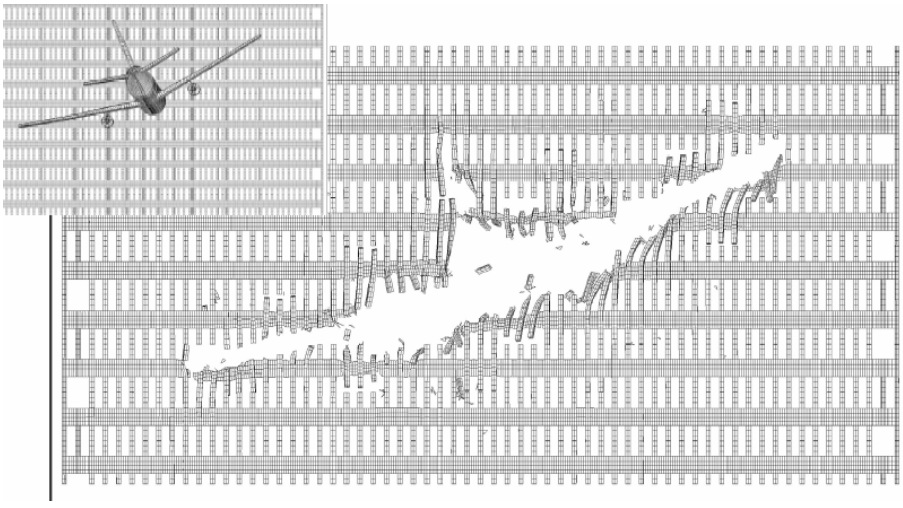

(c) WAI calculated damage (from Levy and Abboud, 2002)

Figure 7–86. Comparison of impact damage to the north wall of WTC 1.

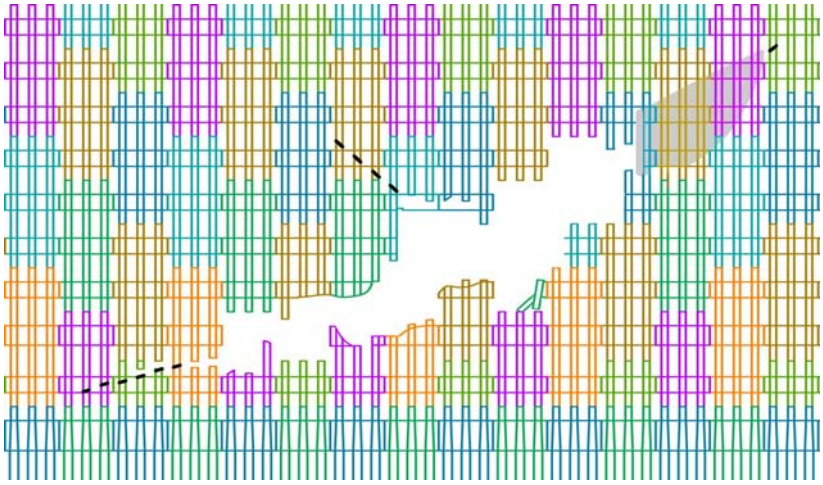

(a) Schematic of observed damage

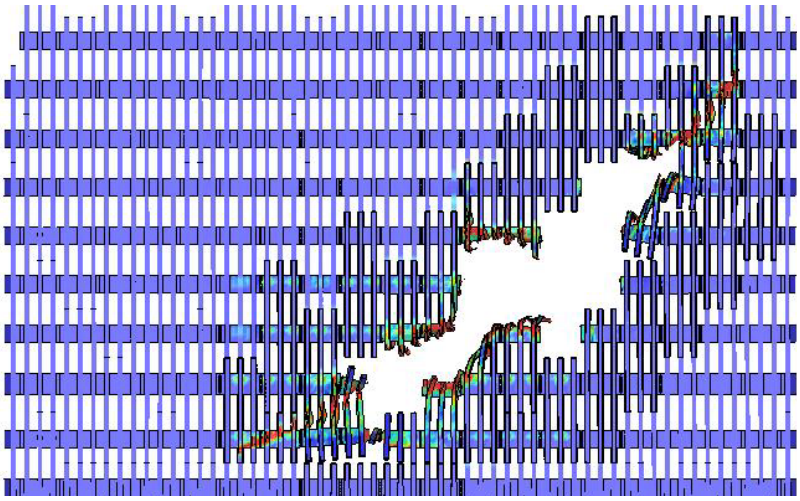

(b) NIST base case impact damage

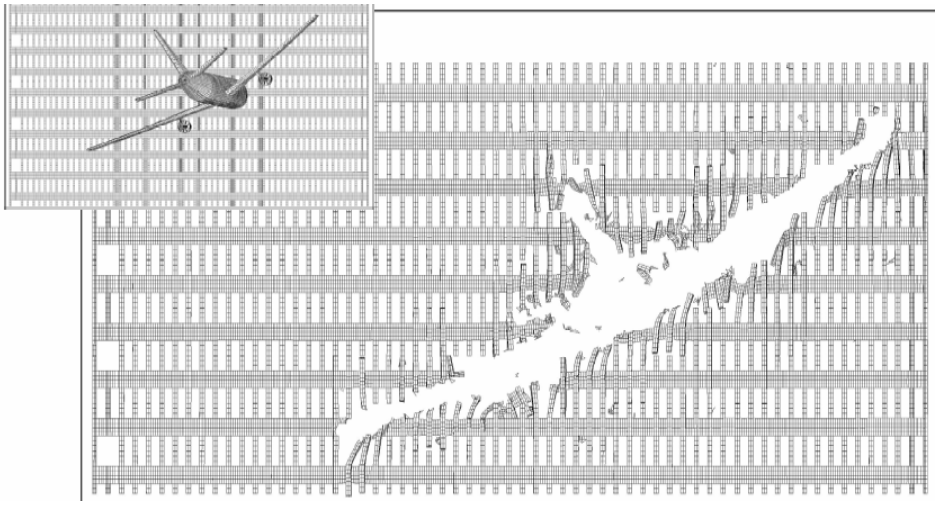

(c) WAI calculated damage (from Levy and Abboud, 2002)

Figure 7–87. Comparison of impact damage to the south wall of WTC 2.

7.11.2 Comparison of Core Column Damage

Table 7–11 compares the estimated core column damage from the various studies. For WTC 1, MIT (Wierzbicki, Xue, and Hendry-Brogan 2002) estimated that 4 to 12 core columns were failed. This MIT estimate of core columns was based on energy balance calculations and corresponded to a damage distribution ranging from four columns failed over a three-story length to 12 columns failed over a single floor length. The expected distribution of damage would fall between these bounds, with some columns damaged on a single floor and others with damage distributed on multiple floors. WAI gave two estimates for core column failure. The first estimate of 23 core columns failed and five damaged was obtained from the FLEX impact analysis. The second estimate of 20 failed columns was the number used in their collapse analysis. The NIST base case impact damage of three severed and four heavily damaged and less severe estimate of one severed and two heavily damaged fall below both the MIT and WAI estimates. The more severe estimate of six severed and three heavily damaged falls in the middle of the MIT range, but still well below the WAI estimates.

A similar trend in the predicted damage to the core columns was found in the WTC 2 analysis. MIT estimated seven to 20 columns failed (from seven columns failed over a three-story length to 20 columns failed over a single floor length). WAI calculated 14 core columns failed and another 10 damaged in their FLEX analysis, but reduced the number of failed columns to five for their collapse analysis. The NIST base case impact damage of five severed and four heavily damaged, as well as the more severe estimate of 10 severed and one heavily damaged fall in the middle of the range predicted by MIT. The less severe impact scenario predicted fewer columns severed and heavily damaged than the MIT and WAI studies.

The MIT prediction of the number of failed core columns agreed remarkably well with the NIST estimates using their simplified analysis. Differences may be a result of the estimates of material properties and structural geometry used (MIT did not have access to the detailed structural drawing of the WTC towers for their study), approximations in the estimates of damage mode and resulting energy absorption, as well as the fact that the MIT study did not include the energy absorbed by internal tower contents.

The WAI impact analysis predicted much greater core column failure and damage than the NIST estimates. One reason for the greater damage prediction may be the lack of internal tower contents in the WAI model, such as workstations and other live loads. This study found that the internal tower material absorbed a significant amount of the impact energy and, therefore, reduced the loads applied to the core columns. Another reason for the greater damage prediction in the WAI study could result from the aircraft model. As noted above, the WAI aircraft impact simulation overpredicted the extent of column damage and failure on the exterior wall. It is possible to assume that the aircraft model would also overpredict the damage to the core columns, especially that this damage configuration resulted in an unstable tower (Levy and Abboud, 2002).

In conducting a collapse analysis, WAI used engineering estimates to reduce the number of failed columns from that predicted by their FLEX model to stabilize the tower immediately after impact. Despite this adjustment, the WAI study still estimated significantly greater damage for WTC 1 than the MIT and NIST studies. For WTC 2 their adjusted estimate falls in line with the MIT and NIST studies.

In general, the MIT and WAI studies appear to over-predict the damage to the core columns compared to the NIST estimates.

Table 7–11. Comparison of damage to core columns from various studies

WTC Impact Study	WTC 1 Core Column Damage	WTC 2 Core Column Damage
MIT Impact Analysis	4–12 Severed	7–20 Severed
WAI Impact Analysis	23 failed & significantly damaged Plus 5 damaged	14 failed and significantly damaged Plus 10 damaged
WAI Collapse Analysis	20 Failed	5 Failed
NIST Base Case Impact Analysis	3 Severed Plus 4 Heavily Damaged	5 Severed Plus 4 Heavily Damaged
NIST More Severe Impact Analysis	6 Severed Plus 3 Heavily Damaged	10 Severed Plus 1 Heavily Damaged
NIST Less Severe Impact Analysis	1 Severed Plus 2 Heavily Damaged	3 Severed Plus 2 Heavily Damaged

7.12 SUMMARY

Presented in this chapter were estimates of damage to the WTC towers due to aircraft impact, calculated from the global impact simulations. The results indicated significant structural damage to the exterior walls, core columns, and floor systems in the affected floors. This structural damage contributed to the weakening of the tower structures, but did not, by itself, initiate building collapse. The aircraft impact damage, however, contributed greatly to the subsequent fires and the thermal response of the tower structures that led ultimately to the collapse of the towers by:

- Dispersing jet fuel and igniting building contents over large areas
- Creating large accumulations of combustible materials containing aircraft and building contents
- Increasing the air supply into the damaged buildings that permitted significantly higher energy release rates than would normally be seen in ventilation building fires, allowing the fires to spread rapidly on multiple floors (see NIST NCSTAR 1-5F)

Other effects of the impact on the towers were investigated in other projects of the Investigation based on the results reported herein. These included: (1) damage and dislodging of fireproofing from structural components in the direct path of the debris (see NIST NCSTAR 1-6), (2) damage to the sprinkler and water supply systems in the path of the aircraft debris (see NIST NCSTAR 1-4), and (3) damage to ceilings that enabled unabated heat transport over the floor-to-ceiling partition walls and to structural components (see NIST NCSTAR 1-5D).

7.13 REFERENCES

"LS-DYNA Keyword User's Manual," Livermore Software Technology Corporation, Version 970, April 2003.

FEMA, May 2002, "World Trade Center Building Performance Study: Data Collection, Preliminary Observations and Recommendations," FEMA 403.

Kausel, E., "The Towers Lost and Beyond," Massachusetts Institute of Technology, May, 2002, http://web.mit.edu/civenv/wtc/index.html.

Levy, M. and Abboud N., August 1, 2002, "World Trade Center – Structural Engineering Investigation," Hart-Weidlinger Technical Report, Prepared for Wachtel, Lipton, Rosen, and Katz.

Vaughan, D. K., FLEX User's Guide, Report UG8298, Weidlinger Associates, Los Altos, CA, May 1983 plus updates through 1997.

Wierzbicki, T., Xue, L., and Hendry-Brogan, M. (2002). "Aircraft impact damage of the World Trade Center towers." *Tech. Rep. No. 74*, Impact and Crashworthiness Lab, Massachusetts Institute of Technology, Cambridge, MA.

This page intentionally left blank

Chapter 8
FINDINGS

8.1 BASELINE PERFORMANCE ANALYSIS

8.1.1 Wind Loads on the World Trade Center Towers

Various wind load estimates for the World Trade Center (WTC) towers were considered in this study. These included: (1) wind loads used in the original WTC design, (2) wind loads based on two recent wind tunnel studies conducted in 2002 by Cermak Peterka Peterson, Inc. (CPP) and Rowan Williams Davis and Irwin, Inc. (RWDI) for insurance litigation concerning the towers, and (3) refined wind loads estimated by National Institute of Standards and Technology (NIST) by critically assessing information obtained from the CPP and RWDI reports and by bringing to bear state-of-the-art considerations. The following summarizes the study findings.

Finding 1: The original design wind loads on the towers exceeded those established in the prescriptive provisions of the New York City Building Code (NYCBC) prior to 1968, when the WTC towers were designed, and up to and including 2001. The original design load estimates were also higher than those required by other selected building codes of the time (Chicago and New York State), including the relevant national model building code, Building Officials and Code Administrators (BOCA). The prescriptive approach in these codes is oversimplified, and as a result, these codes are not necessarily appropriate for super-tall building design. This finding is supported by the fact that wind effects obtained from three separate wind-tunnel-based studies (the original WTC design, the CPP, and the RWDI studies) were in all cases higher than wind effects based on the prescriptive codes.

Finding 2: In the majority of the cases, each of the two orthogonal shear components and of the two orthogonal overturning moment components at the base of the towers used in the original wind design were smaller, than the CPP, RWDI, and refined NIST estimates. However, the most unfavorable combined peaks (resultant) from the original design were larger, or smaller by at most 15 percent, than estimates based on the CPP, RWDI, and NIST estimates. This is due to the conservative approach used to combine the loads in the original design. For example, the refined NIST estimates were higher by as much as 15 percent than the most unfavorable original design wind loads for WTC 1, and lower by about 5 percent than the most unfavorable original design loads for WTC 2.

Finding 3: The estimated wind-induced loads on the towers varied by as much as 40 percent between the wind tunnel/climatological studies conducted in 2002 by CPP and RWDI. The primary reason for these differences was the different approaches used in those studies to (1) estimate extreme wind speeds; (2) estimate wind profiles; (3) integrate aerodynamic, dynamic, and extreme wind climatological information; and (4) combine wind effects in two orthogonal directions and in torsion. Such disparity is indicative of the limitations and inconsistencies associated with the current state of practice in wind engineering for tall buildings. Among the issues that need to be considered are:

- Estimation methods for combining directional wind loads, integrating climatological (wind) and aerodynamic (wind tunnel) data.

- Evaluation of the wind speed specifications and the development of improved design wind speeds, as well as protocols for selection of site-specific wind speeds and directionality.
- Protocols for conducting the wind tunnel tests.
- Profiles of hurricane and non-hurricane winds.
- Load combinations, and material-specific responses to peak loads.

Finding 4: A comparison of wind speeds indicated significant differences among various specified design wind speeds. The basic wind speed specified in American Society of Civil Engineers (ASCE 7-02) for New York City is equivalent to an 88 mph fastest-mile wind speed at 33 ft above ground for open terrain exposure. The wind speed specified in the New York City Building Code (2001) is 80 mph and is interpreted to be a fastest-mile wind speed at 33 ft above ground. For the original WTC design, a design wind speed of 98 mph averaged over 20 minutes at a height of 1,500 ft above ground was used. This speed is equivalent to a fastest-mile wind speed at 33 ft above ground in open terrain of between 67 mph and 75 mph. The wind speed estimated by NIST for three airports (La Guardia, Newark International Airport, and John F. Kennedy International Airport), regardless of direction, was equivalent to 96 mph fastest-mile wind speed. An evaluation of the wind speed specifications and the development of improved design wind speeds, as well as protocols for selection of site-specific wind speeds and directionality, are, therefore, in order.

8.1.2 Baseline Performance of the Global Tower Models

The global models of the towers were analyzed under the following gravity and wind loading cases: (1) the original WTC design load case, (2) the lower-estimate state-of-the-practice case (NYCBC 2001 gravity loads plus wind loads from the RWDI study, scaled in accordance with NYCBC 2001 wind speed), and (3) the refined NIST estimate case (gravity loads from ASCE 7-02 plus refined wind loads developed by NIST). The following summarizes the findings from the analyses.

Finding 5: Under the original WTC design loads, the cumulative drifts at the top of the WTC towers ranged from H/263 to H/335, where H is the building height. For the lower-estimate state-of-the-practice case, those drifts ranged from H/253 to H/306. Under design loading conditions, the maximum inter-story drift was as high as h/230 and h/200 for WTC 1 and WTC 2, respectively, where h is the story height. Maximum inter-story drifts under the state-of-the practice case were about h/184 and h/200 for WTC 1 and WTC 2, respectively. For the refined NIST estimate case, the cumulative and inter-story drifts were about 25 percent larger than those from the state-of-the practice case. Currently no building codes specify a drift limit for wind design. The commentary to Section B.1.2 of the ASCE 7 Standard indicates that drift limits in common usage for building design are on the order of 1/400 to 1/600 of the building (for total drift) or story height (for inter-story drift) to minimize damage to cladding and nonstructural walls and partitions. Structural engineers often use in their practice the criterion that total drift ratios should not exceed H/400 to H/500 for serviceability considerations and to enhance overall safety and stability (including second order P-Δ effects). For inter-story drifts, structural engineers often use in their practice an inter-story drift limit in the range of h/300 to h/400. This is primarily done for serviceability considerations. Similar to total drift, inter-story drifts of the towers were larger than what is generally used in current practice.

Finding 6: The demand/capacity ratios (DCRs), based on the allowable stress design procedure, estimated from the original WTC design load case were in general close to those obtained for the lower-estimate state-of-the practice case. For both cases, a fraction of the structural components had DCRs larger than 1.0. These were mainly observed in the towers at (1) the exterior walls: (a) at the columns around the corners, (b) where the hat truss connected to the exterior walls, and (c) below floor 9; and (2) the core columns on the 600 line between floors 80 and 106 and at core perimeter columns 901 and 908 for much of their height. The DCRs obtained for the refined NIST estimate case were higher than those for the original WTC design and the lower-estimate state-of-the-practice load cases, owing to the following reasons: (1) the NIST estimated wind loads were larger than those used in the state-of-the-practice case by about 25 percent, and (2) the original WTC design and the state-of-the-practice cases used NYCBC load combinations, which result in lower DCRs than the ASCE 7-02 load combinations used for the refined NIST case.

Finding 7: The safety of the WTC towers on September 11, 2001 was most likely not affected by the fraction of members for which the demand exceeded allowable capacity due to: (1) the inherent factor of safety in the allowable stress design method, (2) the load redistribution capability of ductile steel structures, and (3) on the day of attack, the towers were subjected to in-service live loads (a fraction of the design live loads) and minimal wind loads.

Finding 8: The behavior of the lower portion of the towers at the basement floors resembled that of a braced frame, while the behavior of the super-structure resembled that of a framed tube system based on the analysis of the axial stress distribution in the columns under wind loads. Under a combination of the original WTC design dead and wind loads, tension forces developed in the exterior walls of both towers. The forces were largest at the base of the building at the corners. These tensile column loads were transferred from one panel to another through the column splices. The DCRs for the exterior wall splice connections under these tensile forces for both towers were shown to be less than 1.0.

Finding 9: For the towers' resistance to shear sliding under wind loads, the factor of safety was between 10 and 11.5, while the factor of safety against overturning ranged from 1.9 to 2.7 for both towers.

8.1.3 Baseline Performance of the Typical Floor Models

Finding 10: For the typical truss-framed floor under the original WTC design gravity loads, the DCRs for all floor trusses were less than unity for 99.4 percent of the floor truss components with a maximum of 1.14. Inside the core, the DCRs for all floor beams were less than 1.08, and more than 99 percent of floor beams had a DCR of less than 1.0. The maximum mid-span deflections of the long-span and short-span zones under the original design loads were approximately 1.79 in. (L/400) and 0.57 in. (L/750),

workstations. The global analyses included, for each tower, a "base case" based on reasonable initial estimates of all input parameters. They also provided a range of damage estimates of the towers due to aircraft impact. These included a more severe and a less severe damage estimates. The initial impact conditions were estimated based on a detailed analysis of video records that captured the approach and impact of the aircraft with the towers and the photographs of the exterior tower damage. The following summarizes the analyses findings:

Finding 15: The aircraft that impacted WTC 1 had a speed of 443±30 mph with a roll angle of 25±2 degrees (port wing downward). The vertical approach downward angle was 10.6±3 degrees, and the lateral approach angle was close to being normal to the north wall of the tower. For WTC 2, the impacting aircraft had a speed of 542±24 mph, with a roll angle of 38±2 degrees (port wing downward). The vertical approach downward angle was 6±2 degrees, and the lateral approach angle was 13±2 degrees clockwise from the south wall of the tower.

Finding 16: The aircraft impact on WTC 1 resulted in extensive damage to the north wall of the tower,

various locations in the column, depending on the local severity of the impact load and the proximity of the bolted connection to the impact. Subject to the uncertainties inherent in the models, the global impact simulations indicated that a total of five core columns were severed, and four columns were heavily damaged in the base case, compared to ten columns severed and one column heavily damaged in the more severe case and three columns severed and two columns heavily damaged in the less severe case. In some cases, failure of the column splices located on floors 77, 80, and 83 contributed significantly to the failure of the core columns. In the analyses, the floor trusses, core beams, and floor slabs experienced significant impact-induced damage on floors 79 to 81, particularly in the path of the fuselage. The analyses indicated that the wing structures were completely fragmented due to the interaction with the exterior wall and as a result, aircraft fuel was dispersed on multiple floors. In addition, aircraft debris resulted in substantial damage to the nonstructural buildings contents (partitions and workstations) and also in dislodging of fireproofing. The bulk of the fuel was concentrated on floors 79, 81, and 82, while the bulk of the aircraft debris was deposited in floors 78 through 80, with the largest concentration on floor 80.

Finding 18: Natural periods calculated from the reference global model of the WTC 1 tower matched well with those measured on the tower based on the analysis of data from accelerometers located atop WTC 1. The calculated period of oscillation in the N–S direction of the reference global model of WTC 2 matched well with the period estimated immediately after aircraft impact based on a detailed analysis of the building motion which was captured in a video footage of the WTC 2 impact. This indicated that the overall lateral stiffness of the tower was not affected appreciably by the impact damage. The maximum deflection at the top of the tower after impact was estimated from the footage to be more than 1/3 of the drift resulting from the original design wind loads. This indicated that the tower still had reserve capacity after losing a number of columns and floor segments due to aircraft impact.

Finding 19: The towers sustained significant structural damage to the exterior walls, core columns, and floor systems due to aircraft impact. This structural damage contributed to the weakening of the tower structures, but did not, by itself, initiate building collapse. However, the aircraft impact damage contributed greatly to the subsequent fires and the thermal response of the tower structures that led ultimately to the collapse of the towers by: (1) dispersing jet fuel and igniting building contents over large areas, (2) creating large accumulations of combustible materials containing aircraft and building contents, and (3) increasing the air supply into the damaged buildings that permitted significantly higher energy release rates than would normally be seen in ventilation building fires, allowing the fires to spread rapidly on multiple floors.

Appendix A
SALIENT POINTS WITH REGARD TO THE STRUCTURAL DESIGN OF THE WORLD TRADE CENTER TOWERS

Reproduced with permission of The Port Authority of New York and New Jersey.

Salient points with regard to the structural design of The World Trade Center towers:

1. The structural analysis carried out by the firm of Worthington, Skilling, Helle & Jackson is the most complete and detailed of any ever made for any building structure. The preliminary calculations alone cover 1,200 pages and involve over 100 detailed drawings.
2. The buildings have been designed for wind loads of 45 lbs. per square foot which is 2½ times the New York City Building Code requirements of 20 lbs. per square foot, the design load for the Empire State, Pan American and Chrysler Buildings. In addition to static wind loads, a complete dynamic analysis has been made to take into account extremely high velocity gusts.
3. The buildings have been investigated and found to be safe in an assumed collision with a large jet airliner (Boeing 707 - DC 8) travelling at 600 miles per hour. Analysis indicates that such collision would result in only local damage which could not cause collapse or substantial damage to the building and would not endanger the lives and safety of occupants not in the immediate area of impact.
4. Because of its configuration, which is essentially that of a beam 209' deep, the towers are actually far less daring structurally than a conventional building such as the Empire State where the spine or braced area of the building is far smaller in relation to the height.
5. The building as designed is sixteen times stiffer than a conventional structure. The design concept is so sound that the Structural Engineer has been able to be ultra-conservative in his design without adversely affecting the economics of the structure. This is not the case with conventional buildings where a more radical approach must be used if the building is to be constructed at reasonable cost.

6. The structural concept is new but the design principles, the stress analysis and the theories of mechanics upon which the design is based are well known and are in accordance with good engineering practice.

7. The design has been reviewed by some of the most knowledgeable people in the construction industry. In a letter to John Skilling, the Structural Engineer for The World Trade Center, the Chief Engineer of the American Bridge Division of U. S. Steel Corporation said:
"In reviewing this design with our Operating and Construction Departments, we are very optimistic that you have turned a new page in the design of structural steel. It is high time that some new thinking be applied in our industry. In the words of our General Manager of Operating, Lester Larison, he said - 'It was the best damn thing that he has seen come down the pike in his 46 years of experience. Imagine designing a 100-story building for under 30 pounds per square foot.'"

8. The Engineering News-Record of January 30th carries a series of quotations from people in the building industry with regard to The World Trade Center design.
   A. James Ruderman, one of the outstanding New York Structural Engineers says that "The structural design of the tower buildings shows a commendable job of rethinking, where ideas were given a lot of thought and not just treated routinely."
   B. Harold Bernhard, partner, Shreve, Lamb and Harmon Associates, Architects, says "It's a magnificent project."

9. In an editorial in the same issue of the Record is the comment:
"Thus, the PNYA will not build as high as permitted all over its property, despite the high-land [redacted]

Appendix B
ESTIMATION OF SECTORIAL EXTREME WIND SPEEDS[1]

Abstract

We present a procedure for estimating extreme wind speeds corresponding to a sector-by-sector approach to the estimation of extreme wind effects. We provide details of the data sets and their treatment, as well as details of the estimates themselves, in a manner intended to be thorough, clear, and transparent. Efforts in the direction of clarity and transparency are in our view necessary if estimates of extreme winds and their effects are to meet the need for effective scrutiny by users and building authorities, and if a solid technical basis for a consensus among practitioners, standards organizations, and professional organizations is to be created in the near future.

Introduction

The estimation of extreme wind speeds at a given site is, in principle, straightforward. However, in practice, for any given location, differences between approaches used by various wind engineers or other professionals can lead to widely divergent estimates. To assess any particular extreme wind speed estimates it is necessary to scrutinize with care the procedure on which that estimate is based. This requires, in turn, that the procedure, each of its steps, and the attendant calculations, be explained clearly, transparently, in sufficient detail, and in a manner that should be independently verifiable by users or building inspection authorities. For an example of detailed assessment of an extreme wind speed estimation methodology and attendant calculations, see (Coles and Simiu, 2003).

At this time no sufficient guidance is available in standards for (a) the estimation of extreme wind speeds on buildings subjected to wind tunnel testing and (b) the integration of those wind speeds with aerodynamic data. Several procedures are used by various practitioners, but no professional consensus appears to exist on how discrepancies between the respective estimates can be reconciled or how the various methods should be amended to avoid situations – which do occur in actual practice – wherein various estimates of wind effects corresponding to the same nominal mean recurrence interval can differ by as much as 50 percent.

Some wind engineering professionals perform estimates of structural responses corresponding to winds blowing from each of a number of *sectors.* The sectors we consider here are the half-octants bisected by the NNE, NE, ENE,….,N compass directions. Those winds are referred to as *sectorial* wind speeds. In this paper we describe the estimation of sectorial wind speeds.

[1] This appendix was co-authored by William P. Fritz and Emil Simiu of NIST.

This paper is intended to serve as a contribution to the professional debate that, in our opinion, is needed to create a robust basis for a consensus on extreme wind estimation. We present here a procedure for estimating sectorial extreme wind speeds in a region with both hurricane and non-hurricane winds, and show in some detail a numerical example illustrating the procedure. To fix the ideas we will consider a site close to New York City (NYC).

Extreme wind speed data

Hurricane wind speed data. We make use in this note of the NIST simulated hurricane wind speed database which, to our knowledge, is the only non-proprietary hurricane database currently in existence. The database is available online at the following link on the worldwide web: ftp://ftp.nist.gov/pub/bfrl/emil/hurricane/datasets/. This subdirectory contains the relevant data sets of simulated hurricane wind speeds in nautical miles per hour (nmi/hr) at 10 meters above ground in open terrain, averaged over 1-min. There are 55 files with data for locations ranging from milepost 150 (file2.dat; near Port Isabel, TX) to milepost 2850 (file56.dat; near Portland, ME), spaced at 50 mile intervals. The structure of each data file is as follows:

Line 1: Milepost identifier, plus other information not needed for the analysis program.

Line 2: Blank, usually. In some files, the milepost number is repeated here.

Line 3: URATE and NSTRMS. URATE is the estimated annual rate of occurrence of hurricanes at and near this milepost, and NSTRMS is the number of simulated storms used to create the data. For all data sets included in this subdirectory, NSTRMS=999.

Lines 4-1003: The wind speed data for each of the NSTRMS simulated storms. There are a total of 18 numbers on each line. The first 16 are the maximum wind speeds in 16 specified directions, beginning with NNE and moving clockwise to N. The 17^{th} number is the maximum wind speed for ANY direction (i.e., the largest of the previous speeds). The final number (18th) number in each line is the storm identifier.

The NIST data sets are based on the "highly regarded work of Batts et al. (1980)," (unpublished report prepared for Insurance Services Office, Inc., New York City, 1994 by Robert H. Simpson, former director of the National Hurricane Center and creator with Herbert Saffir of the well-known Saffir-Simpson hurricane intensity scale). A variety of other hurricane models are currently available, although the data based thereon are, to our knowledge, proprietary. Agreement between wind speeds near the coastline based on the NIST data sets and on data sets based on other models is very good. At milestone 2500 (one of the milestones tabulated in Simiu and Scanlan (1996, p. 117) that is closest to New York City), the estimated hurricane mean hourly speeds at 10 m above ground in open terrain according to Batts et al. (1980), Simiu, Heckert and Whalen (1996) (both based on the NIST database), Georgiou et al. (1983), and Vickery and Twisdale (1995) are, respectively, about 30 m/s, 30 m/s, 30 m/s, and 29 m/s for the 50-year speeds, and 45 m/s, 43 m/s, 47 m/s, and 45 m/s for the 2000-year speeds. In evaluating these differences it should be kept in mind that sampling errors in the estimation of hurricane wind speeds in the New York City area have estimated coefficients of variation of

roughly 10% for 50-year speeds and 20% for 500-year speeds (Coles and Simiu, 2003). Note that the sampling errors depend less on the number of simulated hurricanes in the database (999 in our case) than on the number of historical hurricanes (about 100) used to obtain statistics of the climatological parameters on which the simulations are based (i.e., radii of maximum wind speeds, atmospheric pressure defect, hurricane translation speed and direction, and so forth). Those statistics differ relatively little among the various simulation packages. It is the authors' understanding that hurricane wind speeds for the State of Florida, corresponding to various probabilities of exceedance, are currently being estimated by the NOAA Hurricane Research Division. In our opinion it would be desirable that this effort be expanded to cover all U.S. hurricane-prone regions.

Treatment of hurricane wind speed data. The data listed in the NIST database need to be rank-ordered for reasons explained subsequently in this note. The rank-ordered data for the location of interest (file 50, milestone 2550 – nearest to NYC – in the NIST database) and for the 202.5°and 225° sectors of interest are listed in Table 1. Note that for these sectors hurricane translation speeds and the relevant vortex speeds within the hurricanes at and near NYC are in many instances of opposite signs, resulting in relatively small and therefore negligible, or even vanishing, total hurricane wind speeds. It is therefore sufficient to show in the table only the largest 55 of the total of 999 data, while keeping in mind that all the 999 data should be accounted for in the calculations.

Table 1. Rank-ordered wind speeds (nmi/hr at 10m above ground in open terrain, averaged over 1-min) from NIST database for 202.5°and 225° sectors at milepost 2550.

Rank,*m*	SSW 202.5°	SW 225°	Rank,*m*	SSW 202.5°	SW 225°	Rank,*m*	SSW 202.5°	SW 225°
1	88.81	86.73	21	0	29.56	41	0	22.64
2	74.49	61.79	22	0	28.96	42	0	21.59
3	73.75	52.37	23	0	28.95	43	0	21.56
4	46.59	47.91	24	0	27.89	44	0	21.25
5	39.68	42.82	25	0	27.79	45	0	20.62
6	17.46	41.97	26	0	27.74	46	0	20.09
7	14.35	41.59	27	0	27.59	47	0	20.04
8	13.81	37.13	28	0	27.35	48	0	19.07
9	13.51	36.4	29	0	27.13	49	0	18.82
10	6.8	35.85	30	0	27.01	50	0	18.55
11	4.88	34.77	31	0	26.63	51	0	16.97
12	3.49	33.64	32	0	26.59	52	0	16.67
13	0	32.41	33	0	26.45	53	0	15.49
14	0	31.79	34	0	25.82	54	0	15.14
15	0	31.75	35	0	25.58	55	0	0
16	0	31.13	36	0	25.28			
17	0	30.64	37	0	24.16			
18	0	30.59	38	0	23.58			
19	0	30.01	39	0	23.04			
20	0	29.86	40	0	22.98			

Non-hurricane extreme wind speed data. In this paper we make use of wind speeds recorded using ASOS (Automated Surface Observing System) during the period 1983-2002, made available to NIST by the NOAA's National Climatic Center for three airports near NYC: La Guardia (LGA), Newark International Airport (EWR), and John F. Kennedy International Airport (JFK). The wind speed data sets include the peak 5-s gust speed multiplied by a factor of 10, for every hour within the period of record, in

m/s. The data were recorded at 20 ft (6.1m) above ground until May 1, 1996 at LGA and JFK and until July 1, 1996 at EWR. They were recorded at 10 m above ground thereafter.

Treatment of non-hurricane wind speed data. The results being sought are expressed in terms of 3-s peak gust speeds at 10 m above ground in open (airport) terrain. Therefore, all data need to be transformed from 5-s peak gust speeds to 3-s peak gust speeds. This can be done to within a sufficient approximation through multiplication of the 5-s speeds by a factor of 1.02 (see ASCE 7-02 Standard, Figure C6.2). The data not recorded at 10m must also be adjusted to correspond to a 10 m elevation above ground. This involves the use of the power law

$$V(z_1)/V(z_2)=(z_1/z_2)^{\hat{\alpha}} \quad (1)$$

where, for 3-s peak gust speeds, the exponent $\hat{\alpha}$ = 1/9.5 for Exposure C (see ASCE 7-02 Standard).

Note that in the data sets each wind speed is associated with the direction from which the wind is blowing. The directions from which the wind is blowing are measured in a clockwise direction from true north, and are recorded for 36 angles in 10 degree increments.

Data should be excluded from the analysis if (1) the record provides no direction for a recorded wind speed (this is the case for a relatively small number of speeds), and (2) if the data have a quality code other than 'good', as provided explicitly in the NOAA data set. Only one measurement at JFK (the maximum speed in the 50˚ sector in 1987) and two measurements at LGA (the maximum speeds in the 210˚ sector in 1983 and in the 200˚ sector in 1984) had a quality code other than 'good'.

Maximum wind speeds are extracted from an airport data set for each of the 36 wind directions for each year of record. For example, 20 years of maximum hourly wind speeds produce 36 × 20 values. The dates of major hurricanes of record for NYC during these 20 years should be checked against the dates of each tabulated maximum wind speed. Data recorded on September 27 and 28, 1985 (hurricane Gloria) and August 19 and 20, 1991 (hurricane Bob) (Neumann et al., 1993) should not be considered and the largest *non*-hurricane wind speeds in the records should be used instead.

The 36 directions are reduced through an appropriate scheme to 16 directions that match the NIST hurricane data. This can be accomplished by defining the wind speed data set associated with, say, the 22.5˚ sector as the set of maximum yearly wind speeds from the NOAA data sets for the 10˚, 20˚, 30˚ and 40˚ sectors. This definition is somewhat conservative, since the 22.5˚ sector is associated with the narrower sector 11.25˚ to 33.75˚, rather than the sector 5˚-45˚. However, in our opinion this conservatism is warranted by the fact that the data samples at our disposal are limited to 20 years. A longer than 20-year data set for the 11.25˚ to 33.75˚ sector may contain wind speeds that, during a 20-year interval, have actually blown within the small sectors 5˚ to 11.25˚ and 33.75˚ to 45˚. This minor conservatism affecting wind speeds is an empirical and

reasonable way of accounting for possible sampling errors with respect to the direction of extreme speeds, for which to our knowledge no applicable theory is available to date.

Estimates of extreme wind speeds

Estimation of extreme wind speeds regardless of whether they are associated with hurricanes or non-hurricane winds. Estimates of extreme wind speeds at 10 m above ground in open terrain at or near the site must take into account both hurricane and non-hurricane winds. We are interested in estimates of sectorial wind speeds, that is, wind speeds that occur in a specified sector defined by the azimuth of its bisector and the total angle swept by the sector. For specificity, in this note we illustrate our estimates of sectorial wind speeds for the 22.5° sectors defined by the bisectors with a 202.5° and a 225° azimuth (i.e., for the SSE and SE directions).

Let the probability of non-exceedance of the wind speed v be denoted by $P(V<v)$. This probability represents the probability that hurricane wind speeds do not exceed v *and* that non-hurricane wind speeds do not exceed v. Denoting the probability that hurricane wind speeds do not exceed v by $P_H(V<v)$ and the probability that non-hurricane speeds do not exceed v by $P_{NH}(V<v)$, and noting that the occurrences of hurricane and non-hurricane speeds are independent events, we have

$$P(V<v)= P_H(V<v)\, P_{NH}(V<v). \tag{2}$$

The corresponding mean recurrence interval of the wind speed V is, by definition,

$$N=1/[1-P(V<v)]. \tag{3}$$

Estimation of probabilities $P_H(V<v)$. For wind speeds blowing from any one of the 16 compass directions (corresponding to the 16 half-octants) the following procedure is used:

- Extract from the NIST database the hurricane mean rate of arrival (μ = 0.305/year) and, for the wind direction of interest, the 999 hurricane wind speed data for New York City (milestone 2550).
- Rank-order the 999 data. (This was done in Table 1.) If the hurricane mean arrival rate URATE (henceforth denoted in this paper by μ) was 1/year, the highest speed would have a 999-year (or approximately 1,000-year) mean recurrence interval. However, if μ <1, then the mean recurrence interval of the highest speed in the set is 999/ μ. (For example, if the mean arrival rate were one hurricane every two years (μ =0.5), then the mean recurrence interval of the highest speed in the set would be 999/0.5=1998, or about 2000 years.)
- The m-th largest speed in the set of 999 speeds corresponds to a mean recurrence interval N=999/(μ m). For example, if – as is the case for New York City area – the estimated mean rate of arrival is 0.305, the mean recurrence intervals of the first highest, second highest, and 65 highest speed are about 999/0.305=3275 years, 999/(0.305 x 2)=1640 years, and 999/(0.305 x 65)=50 years, respectively. Conversely, the hurricane wind speed with an N_H-year mean

recurrence interval corresponds to the *m*-th largest wind speed in the set, where $m=999/(\mu N_H)$.

- The probability that this wind speed does not exceed *v* is defined as follows:

$$P_H(V<v)=1-1/N_H. \quad (4)$$

Other estimation procedures are available, however to date there is no definitive consensus on which procedure is to be preferred. Some analysts believe that extreme value distributions are inadequate owing to their validity, strictly speaking, under asymptotic assumptions only; others believe that Weibull distributions are not appropriate since they are distributions of the smallest values, rather than distributions of the largest values. In spite of its theoretical non-optimality in terms of the precision of some estimates. the non-parametric approach used in this paper appears to be relatively non-controversial and appears to have been adopted by other analysts of hurricane wind speeds.

Estimation of probabilities $P_{NH}(V<v)$. The N_{NH}-year mean recurrence interval may be estimated by using techniques discussed in Simiu and Scanlan (1996, Appendix A1.7). Although other distributional models may be adopted, the least controversial model for extreme wind speeds of non-hurricane origin appears to date to be the Type I extreme value distribution. The mean recurrence interval associated with the non-hurricane wind speed *V* is then

$$N_{NH} = \exp\left[\frac{V-\bar{v}}{0.78s}+0.577\right] \quad (5)$$

The mean, $\bar{v}$, and standard deviation, *s*, are calculated from the yearly maximum wind 3-s peak gust speeds at 10 m above ground in open terrain for the sector of interest. The probability that the wind speed, *V*, does not exceed *v* is

$$P_{NH}(V<v)=1-1/N_{NH}. \quad (6)$$

The requisite probability $P(V<v)$ can be obtained from Eqs. 2, 4, and 6.

Numerical example

We seek the 50-, 500- and 720-year winds blowing from the sectors nominally associated with the 202.5˚ and 225˚ sectors for the area around New York City. We use 20 years of non-hurricane wind speed data measured at LGA and the NIST hurricane wind speed data for those sectors. The choice of the LGA data set is commented upon subsequently.

Let us first consider the 3-s peak gust speed V=100 mph at 10 m above ground in open terrain, and calculate its mean recurrence interval (Eq. 3). Recall that the estimated hurricane arrival rate at milepost 2550 is μ = 0.305/year. The 100 mph, 3-sec gust wind speed is divided by 1.525 (for conversion to mean hourly speeds), then divided by 1.15 (for conversion to nmi/hr) and finally multiplied by 1.25 (for conversion to 1-min

averaging time) (see ASCE 7-02 Standard, Figure C6.2). The 1-min speed at 10 m above ground in open terrain corresponding to the 100 mph peak 3-s speed is therefore 71.3 nmi/hr. This value ranks in Table 1 m = 3.1 and m=1.6 for the 202.5˚ and 225˚ sectors, respectively. The mean recurrence intervals of a 100 mph, 3-sec gust hurricane speed are therefore:

$$N_{H,202.5^\circ} = \frac{999}{0.305(3.1)} = 1057 \text{ years}$$

$$N_{H,225^\circ} = \frac{999}{0.305(1.6)} = 2047 \text{ years}$$

and the probability that the 100 mph, 3-sec wind does not exceed v is

$$P_{H,202.5^\circ}(100 \text{ mph}, 3\text{-s} < v) = 1 - \frac{1}{1057} = 0.99905$$

$$P_{H,225^\circ}(100 \text{ mph}, 3\text{-s} < v) = 1 - \frac{1}{2047} = 0.99951.$$

Note that if a Poisson-based approach to the estimation of the mean recurrence intervals was adopted, instead of the approach used in this paper, the results would be identical for practical purposes. The mean recurrence interval obtained by the Poisson-based approach is N=1/{1-exp{-μ[m/(999+1)]}}. This yields 1058 years for 202.5° sector and 2049 years for the 225° sector.

For non-hurricane winds, maximum hourly wind speeds at LGA airport are shown in Table 2 for the two directions considered and for each of 20 consecutive years (1983 to 2002). The original speeds in m/s, averaged over 5-sec, and affected by a scale factor of 10 from the NOAA data set are provided in Table 2 along with their converted values in 3-s peak gusts in mph at 10 meters. Also shown are the four directions of the NOAA data from which the maximum value is drawn for the 202.5˚ and 225˚ sectors. The mean ($\bar{v}$) and standard deviation (s) of each set of 20 values are also provided.

Table 2. Maximum non-hurricane wind speeds (mph, 3-s), LaGuardia (LGA).

	202.5˚		225˚	
	190˚,200˚,210˚,220˚		210˚,220˚,230˚,240˚	
Year	0.1m/s,5-sec	Mph,3-sec	0.1m/s,5-sec	mph,3-sec
1983	319	77	267	64
1984	268	65	268	65
1985	118	28	108	26
1986	113	27	103	25
1987	170	41	118	28
1988	154	37	134	32
1989	149	36	154	37
1990	154	37	113	27
1991	113	27	149	36
1992	138	33	118	28
1993	128	31	128	31
1994	118	28	128	31
1995	118	28	113	27
1996	154	37	103	24
1997	113	26	149	34
1998	118	27	118	27
1999	144	33	118	27
2000	134	31	113	26
2001	123	28	123	28
2002	123	28	123	28
mean		35.3		32.6
std		13.0		11.5

The mean recurrence interval of the 100 mph, 3-sec gust as a non-hurricane wind is therefore:

$$N_{NH,202.5^\circ} = \exp\left[\frac{100-35.3}{0.78(13.0)} + 0.577\right] = 1051 \text{ years}$$

$$N_{NH,225^\circ} = \exp\left[\frac{100-32.6}{0.78(11.5)} + 0.577\right] = 3265 \text{ years}$$

and the probability that a 100 mph, 3-sec wind does not exceed v is

$$P_{NH,202.5^\circ}(100 \text{ mph}, 3\text{-s} < v) = 1 - \frac{1}{1051} = 0.99905$$

$$P_{NH,225^\circ}(100 \text{ mph}, 3\text{-s} < v) = 1 - \frac{1}{3265} = 0.99969 .$$

In our opinion it would be desirable that a concerted effort be made that would engage NOAA on the one hand and wind and structural engineering professionals on the other, aimed at making wind speed observations archived by NOAA available in a suitable, user friendly format to the structural engineering community. The mean recurrence interval for the peak 3-s gust 100 mph speed, regardless of whether it is associated with hurricane or non-hurricane winds, is calculated using Eqs. 2, 4, and 6:

$$N_{202.5^\circ} = \frac{1}{1-P(100<v)} = \frac{1}{1-(0.99905)(0.99905)} = 527 \text{ years}$$

$$N_{225^\circ} = \frac{1}{1-P(100<v)} = \frac{1}{1-(0.99951)(0.99969)} = 1250 \text{ years.}$$

The procedure just described was followed for wind speeds between 60 and 105 mph. The mean recurrence interval of the wind speeds – regardless of whether they are associated with hurricane or non-hurricane winds – is plotted in Figure 1 for the two sectors. The mean recurrence intervals for the V=100 mph above are marked with a circle in the respective plots.

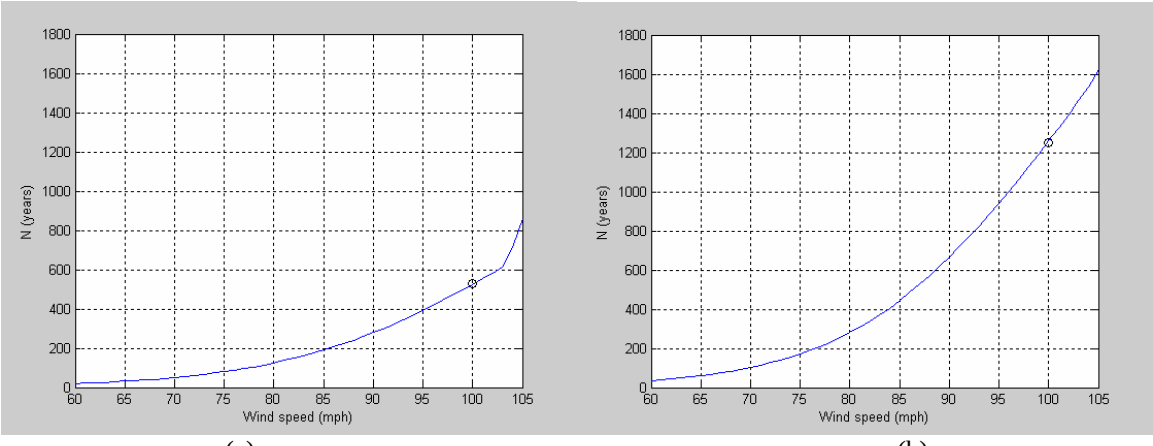

(a) (b)

Figure 1. Combined mean recurrence intervals as a function of peak 3-s gust wind speed for the (a) 202.5˚ and (b) 225˚ sectors.

Estimates of the 50-, 500- and 720-year, 3-s peak gust winds are obtained from Figure 1 and are shown in Table 3.

Table 3. Estimates of the NYC 50-, 500- and 720-year speeds, regardless of whether they are associated with hurricane or non-hurricane winds, at 10m above ground in open terrain for the 202.5˚ and 225˚ sectors.

	N-year wind (mph,3-s)		
Sector	50-yr	500-yr	720-yr
202.5˚	69.8	99.1	104.1
225˚	63.0	86.3	91.1

Choice of LGA sectorial data versus EWR and/or JFK sectorial data

The estimated sectorial wind speeds associated with the 202.5° and 225° directions were found to differ significantly for the LGA and EWR records, on the one hand, and the JFK record on the other. This may be due to relatively large sampling errors associated with wind directionality. In view of the uncertainties associated with sectorial wind speeds it appeared prudent to consider the LGA data above, whose variability for the sectors of interest is largest. Had the EWR data been considered instead, the final results would have been marginally lower. However, had the JFK results been used, the results would have been significantly smaller. This is due to the absence in the JFK record of some of the relatively high wind speeds that are present in the sectors of interest for LGA and EWR. This is an example of the occurrence of significant sampling errors in a sectorial wind speed record.

Rather than making use of the LGA data set alone, the analyst may be tempted to use a "super-station" comprising the data from the LGA, EWR, and JFK stations. However, in our opinion this consolidation of the three data sets into one larger data set would provide an inadequate basis for performing more precise estimates. The reason for this statement is that the three stations are relatively close to each other. The respective wind speed records are not necessarily independent, and gust speeds contain variabilities associated with turbulent fluctuations that may mask the actual correlations between the three records. In our opinion the issue of superstations constructed for stations that are geographically close needs to be researched in the future.

Comparison of extreme wind speed estimates at the three NYC airports

It was noted in the previous section that sectorial speeds can vary fairly significantly from station to station. It is of interest to compare extreme wind speed estimates at EWR, JFK and LGA without regard to wind direction. To do this, maximum wind speeds, regardless of their direction, are used in the procedure described earlier in lieu of sectorial wind speeds. That is, we consider hurricane winds from column 17 in file 50 of the NIST database and maximum yearly non-hurricane winds from the NOAA data set. Thus, non-hurricane data consist of 20 observations for each of the three NYC airports. Mean

recurrence intervals of wind speeds at each airport, regardless of whether they are associated with hurricane or non-hurricane winds, and regardless of their direction, are plotted in Figure 2. The 50-year 3-s peak gust speed at each airport, regardless of direction, is 112.2 mph.

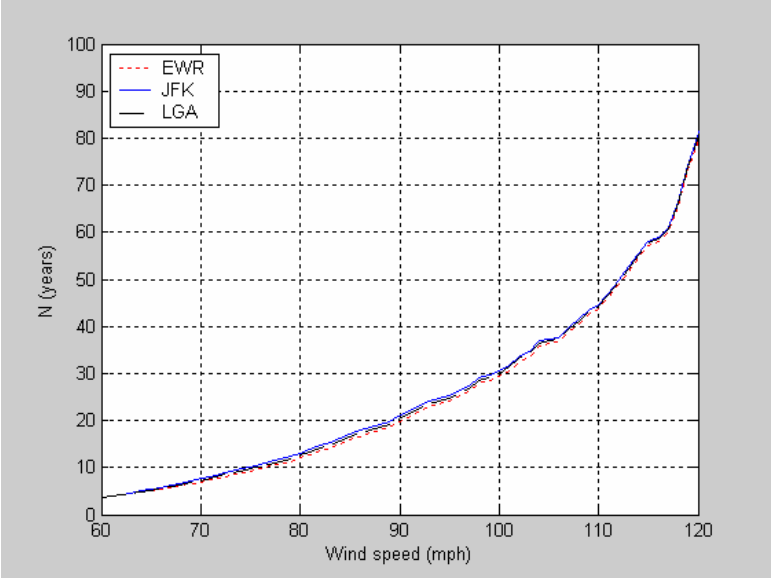

Figure 2. Mean recurrence intervals of wind speeds – regardless of whether they are associated with hurricanes or non-hurricane winds, and regardless of direction – for LGA, EWR, and JFK airports.

For any specified wind speed, the mean recurrence interval is generally shorter for winds regardless of their direction than for winds blowing from one sector only. The remarkable agreement between the estimates of extreme wind speeds at the three airports contrasts with the far less satisfactory agreement observed for the sectorial wind speeds. In other words, sectorial wind speeds appear to exhibit significant sampling errors for which, as mentioned earlier, no applicable theory or research appear to be available to date. This justifies, in our opinion, the use of the data set among the three available airport data sets that yields the most conservative results. In light of these remarks, we believe that caution is also warranted on the use of overly refined schemes for estimating extreme wind speeds for any one angular sector in approaches to wind directionality effects other than the sector-by-sector approach, e.g., the up-crossing approach.

Summary and conclusions

We presented a procedure for estimating extreme wind speeds corresponding to a sector-by-sector approach to the estimation of extreme wind effects. We provided details of the data sets and their treatment, as well as details of the estimates themselves, in a manner intended to be both clear and transparent. Efforts in the direction of clarity and transparency are in our view indispensable if estimates of extreme winds and their effects are to meet the need for effective scrutiny by users and building authorities, and if a solid technical basis for a consensus practitioners, standards organizations, and professional organizations is to be created in the near future.

In the authors' opinion it would be desirable (1) that the NOAA's Hurricane Research Division expand in the future its current efforts aimed at estimating hurricane wind speeds, with a view to covering all U.S. hurricane-prone regions, and (2) that NOAA's wind speed archives for non-hurricane wind speeds be made available to the wind and structural engineering communities in a suitable, user-friendly format to be agreed upon by NOAA and qualified representatives of those communities.

Acknowledgement

We wish to thank William Brown of the National Climatic Center (National Weather Service) for providing valuable help on the LaGuardia, Newark International Airport, and John F. Kennedy International Airport data sets, and information on the anemometer height history for those sets.

References

American Society of Civil Engineers. ASCE Standard ASCE 7-02, Minimum Design Loads for Buildings and Other Structures, American Society of Civil Engineers, Reston, Virginia, 2002.

Batts, M.E., Russell, L.R., and Simiu, E. (1980), "Hurricane Wind Speeds in the United States," Journal of the Structural Division, ASCE

then R would be attained under sectorial wind speeds $v_{j,50}$, rather than under the sectorial wind speed $v_{k,50}$, which would be contrary to the sectorial design criterion.)

Let $F_Q(Q \le R)$ denote the probability that the largest yearly wind effect Q, regardless of the direction from which the wind blows, does not exceed R. If the number of sectors were limited to one, then we would have, with notations similar to those used earlier,

$$F_Q(Q \le R) = \text{Prob}\,(v_1 \le v_{50}) = 1 - 1/50 = 0.98,$$

where v_1 denotes the wind speed inducing the effect Q. In this particular case the sectorial design criterion would be adequate.

For multi-directionally defined wind speeds and responses the following relation is consistent with the use of the sectorial design criterion:

$$F_Q(Q \le R) = \text{Prob}(v_1 \le v_{1,N1},\ v_2 \le v_{2,N2}, \ldots,\ v_8 \le v_{8,N8}) \qquad (1)$$

in which one of the indexes j=1, 2, .., 8 has the value k, to which there corresponds the sectorial speed $v_{k,Nk}$ with N_k=50 years, all other N_j's being larger than 50 years. Let us consider the following three cases: positively correlated speeds, independent speeds, and negatively correlated speeds. For each of these cases we will examine the probability $F(Q \le R)$. If it were true that $F(Q \le R)$=0.98, the sectorial design criterion design would be adequate. If $F(Q \le R)$<0.98, the design performed in accordance with the sectorial design criterion would be unconservative. If $F(Q \le R)$>0.98 the opposite would be the case.

Case 1. The speeds v_1, v_2,…, v_8 are *perfectly, positively correlated*. This means that for all $j \ne k$, we have $v_j = \alpha_j v_k$, where α_j are constants. Therefore,

$$F_Q(Q \le R) = \text{Prob}(v_k \le v_{k,50}) \qquad (2)$$

$$= 0.98.$$

Equation 2 is valid because, by the definition of the sectorial design criterion, the occurrence of the event $v_k \le v_{k,50}$ implies the occurrence of the events $v_j \le v_{j,Nj}$ for all j. It follows that in Case 1 the sectorial design criterion is adequate.

Case 2. The speeds v_1, v_2,…, v_8 are mutually *independent*. The mutual correlations of pairs of sectorial speeds then vanish. This implies

$$F_Q(Q \le R) = \text{Prob}(v_1 \le v_{1,N1}, v_2 \le v_{2,N2}, \ldots, v_8 \le v_{8,N8}) \quad (3a)$$

$$= \text{Prob}(v_1 \le v_{1,N1})\ \text{Prob}(v_2 \le v_{2,N2}) \ldots\ \text{Prob}(v_8 \le v_{8,N8}) \quad (3b)$$

$$\le 0.98, \quad (3c)$$

i.e., the mean recurrence interval of the event $Q \le R$ is equal to or less than 50 years. The inequality (3c) holds because in Eqs. 3, as in Eq. 1, one of the indexes j=1, 2, .., 8 has the value k, to which there corresponds the sectorial speed $v_{k,Nk}$ with N_k=50 years, and all other N_j's are equal to or larger than 50 years. Consider, for example, the case in which the effects from one of the sectors were dominant, that is, the mean recurrence interval of the event that winds from that sector would cause R to be exceeded would be 50 years, while for the other sectors the corresponding mean recurrence intervals would be much longer, say 250 years. Then, $F_Q(Q \le R) = (1 - 1/50) \times (1 - 1/250)^7 = 0.98 \times 0.996^7 \approx 0.95$, corresponding to a mean recurrence interval of the event $Q > R$ equal to 1/(1 - 0.95)=20 years. In other words, *the sectorial design criterion would lead to an underestimation of the wind effect.* It is reasonable to expect that this statement remains true even if the correlations do not vanish but are relatively small.

Case 3. The speeds v_1, v_2,…, v_8 have *negative correlations*. To illustrate the significance of this case from the point of view of the problem considered in this note, we consider the model consisting of one die with two sets of numbers, one in blue and one in

red, as follows. For faces 1, 2, 3, 4, 5, 6, the blue numbers are 1, 2, 3, 4, 5, 6, and the red numbers are 6, 5, 4, 3, 2, 1, respectively. The correlation coefficient between the red and blue outcomes is –1. The probability of the event of throwing a 4 or larger number, regardless of color, is 1 -- to which there corresponds a *mean recurrence interval of one throw*. (Blue and red numbers would correspond in our analogy to north and south winds, say.)

Instead the model just described, we now consider a model consisting of one die with two sets of numbers, one in blue and one in red, but with the following sets of numbers for faces 1, 2, 3, 4, 5, 6. Blue: 1, 2, 3, 4, 5, 6, and red: 1, 2, 3, 4, 5, 6, respectively. In this case the correlation coefficient between the red and blue outcomes is 1 (*perfect positive correlation*). The probability of throwing a 4 or larger number, regardless of color, is 1/2, to which there corresponds a *mean recurrence interval of two throws*, rather than one throw, as in the case of the die with negative correlation. If exceeding the critical value 4 is undesirable, it is seen that the case of negative correlation is more unfavorable than the case of positive correlation (the undesirable outcome occurs more frequently in the former than in the latter case).

It is of interest to also consider the case of throwing two ordinary dice, one with the blue numbers 1, 2, 3, 4, 5, and 6, and the other with red numbers 1, 2, 3, 4, 5, and 6. In this case *the correlation vanishes*, and the probability of getting in a throw of the two dice an outcome of 4 or larger is 27/36=0.75, i.e., *the mean recurrence interval of this outcome is 1.33 throws*. Again, this outcome occurs more frequently than in the case of positive perfect correlation, which is consistent with our earlier comparison between Case 1 and Case 2.

The preceding arguments suggest that *considering the case of strongly positive correlation when the correlation is in fact low or negative would overestimate the mean recurrence interval of the critical event*. This statement is valid not only for the cases of perfect positive correlation and negative or zero correlation. This can be checked by considering, for example: (a) Instead of a die with perfectly negatively correlated red and blue outcomes, one in which the blue and the red numbers are 1, 2, 3, 4, 5, 6, and 4, 3, 2, 2, 1, 1, respectively; for this die the correlation coefficient is -0.75, and the mean recurrence interval of an outcome of 4 or larger, regardless of color, is 1.5 throws. (b) Instead of the two dice considered earlier, two dice with blue and red numbers 1, 2, 3, 4, 5, 6, and 1, 1, 2, 2, 3, 4; in this case the correlation coefficient is again zero, and the mean recurrence interval of a blue or red outcome of at least four is 1.7 throws. (c) Instead of the die with perfectly positive correlation, one in which the blue and red numbers are 1, 2, 3, 4, 5, 6, and 1, 1, 2, 2, 3, 4, respectively; in this case the correlation coefficient is 0.86 and the mean recurrence interval of an outcome of 4 or larger, regardless of color, is 2 throws. Thus, the mean recurrence interval of this outcome is, again, shorter for both the uncorrelated case (1.7 throws) and the negatively correlated (1.5 throws) case that it is for the positively correlated case (2 throws).

Our choice of an intuitive argument is deliberate – it is intended to render our finding as clear as possible to practicing structural engineers, who may or may not have a theoretical probabilistic background. More basic probabilistic arguments are now adduced that strengthen and generalize our finding, without injecting unduly elaborate probabilistic manipulations.

Probabilistic approach. The advantage of a probabilistic argument is that is it more general. We invoke the definition of conditional probability:

$$P(E_1 \mid E_2) = \frac{P(E_1, E_2)}{P(E_2)} \tag{4a}$$

$$P(E_2 \mid E_1) = \frac{P(E_1, E_2)}{P(E_1)} \quad . \tag{4b}$$

from which it follows:

$$\begin{aligned} P(E_1, E_2) &= P(E_1 \mid E_2)P(E_2) \\ &= P(E_2 \mid E_1)P(E_1). \end{aligned} \tag{5a,b}$$

In Eqs. 4 and 5 $P(E_1,E_2)$ is the probability of occurrence of both events E_1 and E_2, $P(E_1|E_2)$ is the conditional probability of occurrence of event E_1 given that event E_2 has occurred, $P(E_2)$ is the probability of event E_2, and similar definitions hold for the second the above equalities. It follows from Eqs. 5 that

$$P(E_1,E_2) \leq \min\{P(E_1), P(E_2)\} \tag{6a}$$

For three events E_1, E_2, and E_3, it can be shown that

$$P(E_1,E_2, E_3) \leq \min\{P(E_1),P(E_2),\mathrm{P}(E_3)\}, \tag{7}$$

By induction, Eq. 7 may be extended for any number of events E_m (m=1,2,…).

Let the event $v_j \leq v_{j,50}$ be denoted by Ej. The application of the extension of Eq. 7 for 8 events E_j (i.e., to Eq. 1) shows that $F_Q(Q \leq R) \leq 0.98$.

Another, more intuitive way of conveying this result is the following. If the structure was strengthened so that it could fail only in direction k, the return period of the

exceedances of R would be 50 years. Hence for the unstrengthened structure the return period must be shorter.

CONCLUSION

We conclude that, except for the case of strong positive correlations between sectorial wind speed – a case that is rarely if ever encountered in nature, – designs based on the sectorial design criterion underestimate the 50-year wind-induced effects, and are therefore unconservative (on the unsafe side). Results of calculations based on Bonferroni bounds (Simiu et al., 1985, and Simiu, Leigh, and Nolan, 1986) are consistent with this conclusion. However, owing to combinatorial explosion issues those calculations could not be conducted to the degree of usefulness rendered possible by current computational capabilities. We believe similar calculations should be performed in the future by using such capabilities. Pending such calculations, the assumption of independence among sectorial wind speeds provides a lower bound of the actual mean return period of interest.

A rigorous estimation of probabilities $F_Q(Q \leq R)$ by reducing the multidirectional problem to a one-dimensional problem was described by Rigato, Chang, and Simiu (2001) for structures with no dynamic amplification effects. A similar solution applicable for structures exhibiting dynamic effects is in progress.

References

Rigato, A., Chang, P., and Simiu, E., "Database-assisted Design, Standardization, and Wind Direction Effects," *J. Struct. Eng.,* **127** 855-860 (2001).

Simiu, E., Hendrickson, E., Nolan, W., Olkin, I., and Spiegelman, C., "Multivariate Distributions of Directional Wind Speeds," *J. Struct. Eng.,* **111** 939-943 (1985).

Simiu, E., Leigh, S., and Nolan, W., "Environmental Load Direction and Reliability Bounds," *J. Struct. Eng.,* **112,** 1199-1203 (1986).

Appendix D
SOM PROJECT 2, PROGRESS REPORT NO. 3, WTC WIND LOAD ESTIMATES

SOM

NIST – World Trade Center Investigation

PROJECT 2: Baseline Structural Performance and Aircraft Impact Damage Analysis

Progress Report No. 3
WTC Wind Load Estimates

Outside Experts for Baseline Structural Performance

13 April 2004

Skidmore, Owings & Merrill LLP

Suite 1000, 224 South Michigan Avenue, Chicago, Illinois 60604
312 554-9090, Fax 312 360-4545, www.som.com

SOM

1.0 Table of Contents

2.0 Overview

2.1 Project Overview

The objectives for Project 2 of the WTC Investigation include the development of reference structural models and design loads for the WTC Towers. These will be used to establish the baseline performance of each of the towers under design gravity and wind loading conditions. The work includes expert review of databases and baseline structural analysis models developed by others as well as the review and critique of the wind loading criteria developed by NIST.

2.2 Report Overview

This report covers work on the development of wind loadings associated with Project 2. This task involves the review of wind loading recommendations developed by NIST for use in structural analysis computer models. The NIST recommendations are derived from wind tunnel testing/wind engineering reports developed by independent wind engineering consultants in support of insurance litigation concerning the WTC towers. The reports were provided voluntarily to NIST by the parties to the insurance litigation.

As the third party outside experts assigned to this Project, SOM's role during this task was to review and critique the NIST developed wind loading criteria for use in computer analysis models. This critique was based on a review of documents provided by NIST, specifically the wind tunnel/wind engineering reports and associated correspondence from independent wind engineering consultants and the resulting interpretation and recommendations developed by NIST.

3.0 NIST-Supplied Documents

3.1 Rowan Williams Davies Irwin (RWDI) Wind Tunnel Reports

Final Report
Wind-Induced Structural Responses
World Trade Center – Tower 1
New York, New York
Project Number: 02-1310A
October 4, 2002

Final Report
Wind-Induced Structural Responses
World Trade Center – Tower 2
New York, New York
Project Number:02-1310B
October 4, 2002

3.2 Cermak Peterka Petersen, Inc. (CPP) Wind Tunnel Report

Data Report
Wind-Tunnel Tests – World Trade Center
New York, NY
CPP Project 02-2420
August 2002

3.3 Correspondence

Letter dated October 2, 2002
From: Peter Irwin/RWDI
To: Matthys Levy/Weidlinger Associates
Re: Peer Review of Wind Tunnel Tests
World Trade Center
RWDI Reference #02-1310

Weidlinger Associates Memorandum dated March 19, 2003
From: Andrew Cheung
To: Najib Abboud
Re: ERRATA to WAI Rebuttal Report

Letter dated September 12, 2003
From: Najib N. Abboud/Hart-Weidlinger
To: S. Shyam Sunder and Fahim Sadek (sic)/NIST
Re: Responses to NIST's Questions on:
"*Wind-Induced Structural Responses, World Trade Center*, Project Number 02-1310A and 02-1310B October 2002, By RWDI, Prepared for Hart-Weidlinger"

Letter dated April 6, 2004
From: Najib N. Abboud /Weidlinger Associates
To: Fahim Sadek and Emil Simiu
Re: Response to NIST's question dated March 30, 2004 regarding "Final Report, Wind-Induced Structural Responses, World Trade Center – Tower 2, RWDI, Oct 4, 2002"

3.4 NIST Report

Estimates of Wind Loads on the WTC Towers
Emil Simiu and Fahim Sadek
April 7, 2004

4.0 Discussion and Comments

4.1 General

This report covers a review and critique of the NIST recommended wind loads derived from wind load estimates provided by two independent private sector wind engineering groups, RWDI and CPP. These wind engineering groups performed wind tunnel testing and wind engineering calculations for various private sector parties involved in insurance litigation concerning the destroyed WTC Towers in New York. There are substantial disparities (greater than 40%) in the predictions of base shears and base overturning moments between the RWDI and CPP wind reports. NIST has attempted to reconcile these differences and provide wind loads to be used for the baseline structural analysis.

4.2 Wind Tunnel Reports and Wind Engineering

The CPP estimated wind base moments far exceed the RWDI estimates. These differences far exceed SOM's experience in wind force estimates for a particular building by independent wind tunnel groups.

In an attempt to understand the basis of the discrepancies, NIST performed a critique of the reports. Because the wind tunnel reports only summarize the wind tunnel test data and wind engineering calculations, precise evaluations are not possible with the provided information. For this reason, NIST was only able to approximately evaluate the differences. NIST was able to numerically estimate some corrections to the CPP report but was only able to make some qualitative assessments of the RWDI report. **It is important to note that wind engineering is an emerging technology and there is not consensus on certain aspects of current practice.** Such aspects include the correlation of wind tunnel tests to full-scale (building) behavior, methods and computational details of treating local statistical (historical) wind data in overall predictions of structural response, and types of suitable aeroelastic models for extremely tall and slender structures. It is unlikely that the two wind engineering groups involved with the WTC assessment would agree with NIST in all aspects of its critique. This presumptive disagreement should not be seen as a negative, but reflects the state of wind tunnel practice. It is to be expected that well-qualified experts will respectfully disagree with each other in a field as complex as wind engineering.

SOM's review of the NIST report and the referenced wind tunnel reports and correspondence has only involved discussions with NIST; it did not involve direct communication with either CPP or RWDI. SOM has called upon its experience with wind tunnel testing on numerous tall building projects in developing the following comments.

4.2.1 CPP Wind Tunnel Report

The NIST critique of the CPP report is focused on two issues: a potential overestimation of the wind speed and an underestimation of load resulting from the method used for integrating the wind tunnel data with climatic data. NIST made an independent estimate of the wind speeds for a 720-year return period. These more rare wind events are dominated by hurricanes that are reported by rather broad directional sectors (22.5 degree). The critical direction for the towers is from the azimuth direction of 205 to 210 degrees. This wind direction is directly against the nominal "south" face of the towers (the plan north of the site is rotated approximately 30 degrees from the true north) and generates dominant cross-wind excitation from vortex shedding. The nearest sector data are centered on azimuth 202.5 (SSW) and 225 (SW). There is a substantial drop (12%) in the NIST wind velocity from the SSW sector to the SW sector. The change in velocity with direction is less dramatic in the CCP 720-year velocities or in the ARA hurricane wind roses included in the RWDI report. This sensitivity to directionality is a cause for concern in trying to estimate a wind speed for a particular direction. However, it should be noted that the magnitude of the NIST interpolated estimated velocity for the 210 azimuth direction is similar to the ARA wind rose. The reduction of forces has been estimated by NIST based on a square of the velocity, however, a power of 2.3 may be appropriate based on a comparison of the CPP 50-year (nominal) and 720-year base moments and velocities.

The NIST critique of the CPP use of sector by sector approach of integrating wind tunnel and climatic data is fairly compelling. The likelihood of some degree of underestimation

is high but SOM is not able to verify the magnitude of error (15%) which is estimated by NIST. This estimate would need to be verified by future research, as noted by NIST.

4.2.2 RWDI Wind Tunnel Report

The NIST critique of RWDI has raised some issues but has not directly estimated the effects. These concerns are related to the wind velocity profiles with height used for hurricanes and the method used for up-crossing.

NIST questioned the profile used for hurricanes and had an exchange of correspondence with RWDI. While RWDI's written response is not sufficiently quantified to permit a precise evaluation of NIST's concerns, significant numerical corroboration on this issue may be found in the April 6 letter (Question 2) from N. Abboud (Weidlinger Associates) to F. Sadek and E. Simiu (NIST).

NIST is also concerned about RWDI's up-crossing method used for integrating wind tunnel test data and climatic data. This method is computationally complex and verification is not possible because sufficient details of the method used to estimate the return period of extreme events are not provided.

4.2.3 Building Period used in Wind Tunnel Reports

SOM noted that both wind tunnel reports use fundamental periods of vibrations that exceed those measured in the actual (north tower) buildings. The calculation of building periods are at best approximate and generally underestimate the stiffness of a building thus overestimating the building period. The wind load estimates for the WTC towers are sensitive to the periods of vibration and often increase with increased period as demonstrated by a comparison of the RWDI base moments with and without P-Delta effects. Although SOM generally recommends tall building design and analysis be based on P-Delta effects, in this case even the first order period analysis (without P-Delta) exceeds the actual measurements. It would have been desirable for both RWDI and CPP to have used the measured building periods.

4.2.4 NYCBC Wind Speed

SOM recommends that the wind velocity based on a climatic study or ASCE 7-02 wind velocity be used in lieu of the New York City Building Code (NYCBC) wind velocity. The NYCBC wind velocity testing approach does not permit hurricanes to be accommodated by wind tunnel testing as intended by earlier ASCE 7 fastest mile versions because it is based on a method that used an importance factor to correct 50-year wind speeds for hurricanes. Because the estimated wind forces are not multiplied by an importance factor, this hurricane correction is incorporated in analytical methods of determining wind forces but is lost in the wind tunnel testing approach of determining wind forces.

4.2.5 Incorporating Wind Tunnel Results in Structural Evaluations

It is expected that ASCE 7 load factors will also be used for member forces for evaluating the WTC towers. Unfortunately, the use of ASCE 7 with wind tunnel-produced loadings is not straight forward. Neither wind tunnel report gives guidance on how to use the provided forces with ASCE 7 load factors.

The ASCE 7 load factors are applied to the nominal wind forces and, according to the ASCE 7 commentary, are intended to scale these lower forces up to wind forces associated with long return period wind speeds. The approach of taking 500-year return period wind speeds and dividing the speeds by the square root of 1.5 to create a nominal design wind speed; determining the building forces from these reduced nominal design wind speeds; and then magnifying these forces by a load factor (often 1.6) is, at best, convoluted. For a building that is as aerodynamically active as the WTC, an approach of directly determining the forces at the higher long return period wind speeds would be preferred. The CPP data did provide the building forces for their estimates of both 720-years (a load factor of 1.6) and the reduced nominal design wind speeds. A comparison of the wind forces demonstrates the potential error in using nominal wind speeds in lieu of directly using the underlying long period wind speeds.

It should also be noted that the analytical method of calculating wind forces in ASCE 7 provides an importance factor of 1.15 for buildings such as the WTC in order to provide more conservative designs for buildings with high occupancies. Unfortunately, no similar clear guidance is provided for high occupancy buildings where the wind loads are determined by wind tunnel testing. Utilizing methods provided in the ASCE 7 Commentary would suggest that a return period of 1800 years with wind tunnel-derived loads would be comparable to the ASCE 7 analytical approach to determining wind loads for a high occupancy building.

It would be appropriate for the wind tunnel private sector laboratories or NIST, as future research beyond the scope of this project, to address how to incorporate wind tunnel loadings into an ASCE 7-based design.

4.2.6 Summary

The NIST review is critical of both the CPP and RWDI wind tunnel reports. It finds substantive errors in the CPP approach and questions some of the methodology used by RWDI. It should be noted that boundary layer wind tunnel testing and wind engineering is still a developing branch of engineering and there is not industry-wide consensus on all aspects of the practice. For this reason, some level of disagreement is to be expected.

Determining the design wind loads is only a portion of the difficulty. As a topic of future research beyond the scope of this project, NIST or wind tunnel private sector laboratories should investigate how to incorporate these wind tunnel-derived results with the ASCE 7 Load Factors.

4.3 NIST Recommended Wind Loads

NIST recommends a wind load that is between the RWDI and CPP estimates. The NIST recommended values are approximately 83% of the CPP estimates and 115% of the RWDI estimates. SOM appreciates the need for NIST to reconcile the disparate wind tunnel results. It is often that engineering estimates must be done with less than the desired level of information. In the absence of a wind tunnel testing and wind engineering done to NIST specifications, NIST has taken a reasonable approach to estimate appropriate values to be used in the WTC study. However, SOM is not able to independently confirm the precise values developed by NIST.

The wind loads are to be used in the evaluation of the WTC structure. It is therefore recommended that NIST provide clear guidelines on what standards are used in the evaluations and how they are to incorporate the provided wind loads.

5.0 References

[1] American Society of Civil Engineers, *Minimum Design Loads for Buildings and Other Structures*, ANSI/ASCE 7-02, 2002.

[2] American Society of Civil Engineers, *Minimum Design Loads for Buildings and Other Structures*, ANSI/ASCE 7-93, 1993.

APPENDIX E
STILL IMAGES OF THE VIDEO RECORDS USED IN CHAPTER 6

This appendix provides still images of the video records (Figures E–1 through E–9) used to estimate the initial impact conditions of the aircraft that impacted World Trade Center (WTC) 1 and WTC 2 (see Chapter 6). A short description of each of these videos is provided in Table 6–1.

Figure E–1. Still image from Video V1 (WTC 1 impact).

Figure E–2. Still image from Video V2 (WTC 1 impact).

Figure E–3. Still image from Video V3 (WTC 2 impact).

Figure E–4. Still image from Video V4 (WTC 2 impact).

Figure E–5. Still image from Video V5 (WTC 2 impact).

Figure E–6. Still image from Video V6 (WTC 2 impact).

Figure E–7. Still image from Video V7 (WTC 2 impact).

Figure E–8. Still image from Video V8 (WTC 2 impact).

Figure E–9. Still image from Video V9 (WTC 2 impact).

This page intentionally left blank.

NIST NCSTAR 1-2A

Federal Building and Fire Safety Investigation of the World Trade Center Disaster

Reference Structural Models and Baseline Performance Analysis of the World Trade Center Towers

William J. Faschan
Richard B. Garlock

NIST National Institute of Standards and Technology • Technology Administration • U.S. Department of Commerce

NIST NCSTAR 1-2A

Federal Building and Fire Safety Investigation of the World Trade Center Disaster

Reference Structural Models and Baseline Performance Analysis of the World Trade Center Towers

William J. Faschan
Richard B. Garlock
Leslie E. Robertson Associates, R.L.L.P.

September 2005

U.S. Department of Commerce
Carlos M. Gutierrez, Secretary

Technology Administration
Michelle O'Neill, Acting Under Secretary for Technology

National Institute of Standards and Technology
William Jeffrey, Director

Disclaimer No. 1

Certain commercial entities, equipment, products, or materials are identified in this document in order to describe a procedure or concept adequately or to trace the history of the procedures and practices used. Such identification is not intended to imply recommendation, endorsement, or implication that the entities, products, materials, or equipment are necessarily the best available for the purpose. Nor does such identification imply a finding of fault or negligence by the National Institute of Standards and Technology.

Disclaimer No. 2

The policy of NIST is to use the International System of Units (metric units) in all publications. In this document, however, units are presented in metric units or the inch-pound system, whichever is prevalent in the discipline.

Disclaimer No. 3

Pursuant to section 7 of the National Construction Safety Team Act, the NIST Director has determined that certain evidence received by NIST in the course of this Investigation is "voluntarily provided safety-related information" that is "not directly related to the building failure being investigated" and that "disclosure of that information would inhibit the voluntary provision of that type of information" (15 USC 7306c).

In addition, a substantial portion of the evidence collected by NIST in the course of the Investigation has been provided to NIST under nondisclosure agreements.

Disclaimer No. 4

NIST takes no position as to whether the design or construction of a WTC building was compliant with any code since, due to the destruction of the WTC buildings, NIST could not verify the actual (or as-built) construction, the properties and condition of the materials used, or changes to the original construction made over the life of the buildings. In addition, NIST could not verify the interpretations of codes used by applicable authorities in determining compliance when implementing building codes. Where an Investigation report states whether a system was designed or installed as required by a code *provision*, NIST has documentary or anecdotal evidence indicating whether the requirement was met, or NIST has independently conducted tests or analyses indicating whether the requirement was met.

Use in Legal Proceedings

No part of any report resulting from a NIST investigation into a structural failure or from an investigation under the National Construction Safety Team Act may be used in any suit or action for damages arising out of any matter mentioned in such report (15 USC 281a; as amended by P.L. 107-231).

National Institute of Standards and Technology National Construction Safety Team Act Report 1-2A
Natl. Inst. Stand. Technol. Natl. Constr. Sfty. Tm. Act Rpt. 1-2A, 230 pages (September 2005)
CODEN: NSPUE2

U.S. GOVERNMENT PRINTING OFFICE
WASHINGTON: 2005

For sale by the Superintendent of Documents, U.S. Government Printing Office
Internet: bookstore.gpo.gov — Phone: (202) 512-1800 — Fax: (202) 512-2250
Mail: Stop SSOP, Washington, DC 20402-0001

ABSTRACT

This report establishes the baseline performance of the North and South World Trade Center Towers (WTC 1 and WTC 2) under design gravity and wind loading conditions. Baseline performance results include basic information about the towers behavior under design loading conditions. These include total and inter-story drift under wind loads, floor deflections under gravity loads, demand/capacity ratios for the primary structural components of the towers, exterior columns response (shear lag effects and presence of tensile forces), performance of connections, and resistance of the towers to shear sliding and overturning. The primary tasks that were undertaken to establish the baseline performance include the following:

- Development of structural databases of the primary components of WTC 1 and WTC 2 towers. These electronic databases were developed from original computer printouts of the structural design documents, including modifications made after construction. The task included the scanning and digitization of the original drawing books, a four-step quality control procedure, cross section property calculations, and development of the relational databases to link the generated database files into a format suitable for the development of the structural models.

- Development of reference structural analysis models that capture the intended behavior of each of the two towers using the generated databases. These reference models were used to establish the baseline performance of the towers and also serve as a reference for more detailed models for other phases of the investigation, including aircraft impact damage analysis, and thermal-structural response and collapse initiation analysis. The main types of models developed were:

  – Two global models of the major structural components and systems for the towers, one each for WTC 1 and WTC 2. The models included all primary structural components in the towers, including exterior walls (columns and spandrel beams), core columns, exterior wall bracing in the basement floors, core bracing at the mechanical floors, core bracing at the main lobby atrium levels, hat trusses, and rigid and flexible diaphragms representing the floor systems.

  – One model each of the typical truss-framed floor (floor 96 of WTC 1) and typical beam-framed floor (floor 75 of WTC 2). The models included all major structural components in the floor system, including primary and bridging trusses, beams, strap anchors and horizontal trusses, concrete slabs, and viscoelastic dampers.

  Parametric studies were performed to evaluate the behavior of typical portions of the structure and to develop simplified models for implementation into the global models. These parametric studies included detailed and simplified models of typical exterior and corner wall panels, and floor systems.

- Development of estimates of design gravity and wind loads on the towers for implementation into the reference structural models and use in the baseline performance analysis. Various wind load cases were considered in this study, including wind loads used in the original WTC design, wind loads based on two recent wind tunnel studies conducted in 2002 by Cermak Peterka Peterson, Inc. (CPP) and Rowan Williams Davies and Irwin, Inc. (RWDI) for insurance litigation concerning the towers, and refined wind load estimates developed by NIST from critical assessment of information obtained from the CPP and RWDI reports and state-of-the-art considerations. The following three loading cases were considered for the baseline performance analysis:

  – *Original WTC design loads case.* Loads included dead and live loads as in original WTC design in conjunction with original WTC design wind loads.

  – *State-of-the-practice case.* Loads included dead loads; current New York City Building Code (NYCBC 2001) live loads; and wind loads from the RWDI wind tunnel study, scaled in accordance with NYCBC 2001 wind speed.

  – *Refined NIST estimate case.* Loads included dead loads; live loads from the current American Society of Civil Engineers Standard Minimum Design Loads for Buildings and Other Structures (ASCE 7-02); and the refined wind load estimates developed by NIST.

The global tower models were analyzed using the various gravity and wind loading cases, and the baseline performance results were obtained. The results included:

- Total and inter-story drift under wind loads
- Demand/capacity ratios for the primary structural components of the towers
- Axial forces in the exterior columns, including shear lag effects and presence of tensile forces
- Performance of splice connections at the exterior walls
- Towers' resistance to shear sliding and overturning under wind loads.

Similarly, the typical floor models were analyzed under gravity loading conditions, and the baseline performance results were obtained. The results included:

- Floor mid-span deflections
- Demand/capacity ratios for the primary structural components of the floors.

Keywords: Columns, floor system, gravity load, load, model, structural, truss, wind load, World Trade Center.

TABLE OF CONTENTS

LIST OF FIGURES

This page intentionally left blank.

LIST OF TABLES

LIST OF ACRONYMS AND ABBREVIATIONS

Acronyms

AISC	American Institute of Steel Construction
AISI	American Iron and Steel Institute
ASCE	American Society of Civil Engineers
ASD	Allowable Stress Design
BOCA/BBC	Building Officials and Code Administrators Basic Building Code
CDL	construction dead load
CPP	Cermak Peterka Peterson, Inc.
DB	database
DCR	demand/capacity ratio
DL	dead load
E-W	East – West direction
GFI	Government Furnished Information
LERA	Leslie E. Robertson Associates, R.L.L.P.
LL	live load
LRFD	Load and Resistance Factor Design
MEP	mechanical, electrical, and plumbing
MER	mechanical equipment room
NIST	National Institute of Standards and Technology
N-S	North – South direction
NYCBC	New York City Building Code
OCR	Optical Character Recognition
PANYNJ	Port Authority of New York and New Jersey
RWDI	Rowan Williams Davies and Irwin, Inc.
SDL	superimposed dead load
SQL	Structured Query Language
WL	wind load
WSHJ	Worthington, Skilling, Helle & Jackson
WTC	World Trade Center

WTC 1	World Trade Center 1 (North Tower)
WTC 2	World Trade Center 2 (South Tower)
WTC 7	World Trade Center 7

Abbreviations

2D	two dimensional
3D	three dimensional
ft	foot
ft^2	square foot
F_y	yield strength
h	hour
in.	inch
kip	a force unit equal to 1,000 pounds
ksi	1,000 pounds per square inch
lb	pound
min	minute
pcf	pounds per cubic foot
psf	pounds per square foot
psi	pounds per square inch

PREFACE

Genesis of This Investigation

Immediately following the terrorist attack on the World Trade Center (WTC) on September 11, 2001, the Federal Emergency Management Agency (FEMA) and the American Society of Civil Engineers began planning a building performance study of the disaster. The week of October 7, as soon as the rescue and search efforts ceased, the Building Performance Study Team went to the site and began its assessment. This was to be a brief effort, as the study team consisted of experts who largely volunteered their time away from their other professional commitments. The Building Performance Study Team issued its report in May 2002, fulfilling its goal "to determine probable failure mechanisms and to identify areas of future investigation that could lead to practical measures for improving the damage resistance of buildings against such unforeseen events."

On August 21, 2002, with funding from the U.S. Congress through FEMA, the National Institute of Standards and Technology (NIST) announced its building and fire safety investigation of the WTC disaster. On October 1, 2002, the National Construction Safety Team Act (Public Law 107-231), was signed into law. The NIST WTC Investigation was conducted under the authority of the National Construction Safety Team Act.

The goals of the investigation of the WTC disaster were:

- To investigate the building construction, the materials used, and the technical conditions that contributed to the outcome of the WTC disaster.
- To serve as the basis for:
  - Improvements in the way buildings are designed, constructed, maintained, and used;
  - Improved tools and guidance for industry and safety officials;
  - Recommended revisions to current codes, standards, and practices; and
  - Improved public safety.

The specific objectives were:

1. Determine why and how WTC 1 and WTC 2 collapsed following the initial impacts of the aircraft and why and how WTC 7 collapsed;
2. Determine why the injuries and fatalities were so high or low depending on location, including all technical aspects of fire protection, occupant behavior, evacuation, and emergency response;
3. Determine what procedures and practices were used in the design, construction, operation, and maintenance of WTC 1, 2, and 7; and
4. Identify, as specifically as possible, areas in current building and fire codes, standards, and practices that warrant revision.

NIST is a nonregulatory agency of the U.S. Department of Commerce's Technology Administration. The purpose of NIST investigations is to improve the safety and structural integrity of buildings in the United States, and the focus is on fact finding. NIST investigative teams are authorized to assess building performance and emergency response and evacuation procedures in the wake of any building failure that has resulted in substantial loss of life or that posed significant potential of substantial loss of life. NIST does not have the statutory authority to make findings of fault nor negligence by individuals or organizations. Further, no part of any report resulting from a NIST investigation into a building failure or from an investigation under the National Construction Safety Team Act may be used in any suit or action for damages arising out of any matter mentioned in such report (15 USC 281a, as amended by Public Law 107-231).

Organization of the Investigation

The National Construction Safety Team for this Investigation, appointed by the then NIST Director, Dr. Arden L. Bement, Jr., was led by Dr. S. Shyam Sunder. Dr. William L. Grosshandler served as Associate Lead Investigator, Mr. Stephen A. Cauffman served as Program Manager for Administration, and Mr. Harold E. Nelson served on the team as a private sector expert. The Investigation included eight interdependent projects whose leaders comprised the remainder of the team. A detailed description of each of these eight projects is available at http://wtc.nist.gov. The purpose of each project is summarized in Table P–1, and the key interdependencies among the projects are illustrated in Fig. P–1.

Table P–1. Federal building and fire safety investigation of the WTC disaster.

Technical Area and Project Leader	Project Purpose
Analysis of Building and Fire Codes and Practices; Project Leaders: Dr. H. S. Lew and Mr. Richard W. Bukowski	Document and analyze the code provisions, procedures, and practices used in the design, construction, operation, and maintenance of the structural, passive fire protection, and emergency access and evacuation systems of WTC 1, 2, and 7.
Baseline Structural Performance and Aircraft Impact Damage Analysis; Project Leader: Dr. Fahim H. Sadek	Analyze the baseline performance of WTC 1 and WTC 2 under design, service, and abnormal loads, and aircraft impact damage on the structural, fire protection, and egress systems.
Mechanical and Metallurgical Analysis of Structural Steel; Project Leader: Dr. Frank W. Gayle	Determine and analyze the mechanical and metallurgical properties and quality of steel, weldments, and connections from steel recovered from WTC 1, 2, and 7.
Investigation of Active Fire Protection Systems; Project Leader: Dr. David D. Evans; Dr. William Grosshandler	Investigate the performance of the active fire protection systems in WTC 1, 2, and 7 and their role in fire control, emergency response, and fate of occupants and responders.
Reconstruction of Thermal and Tenability Environment; Project Leader: Dr. Richard G. Gann	Reconstruct the time-evolving temperature, thermal environment, and smoke movement in WTC 1, 2, and 7 for use in evaluating the structural performance of the buildings and behavior and fate of occupants and responders.
Structural Fire Response and Collapse Analysis; Project Leaders: Dr. John L. Gross and Dr. Therese P. McAllister	Analyze the response of the WTC towers to fires with and without aircraft damage, the response of WTC 7 in fires, the performance of composite steel-trussed floor systems, and determine the most probable structural collapse sequence for WTC 1, 2, and 7.
Occupant Behavior, Egress, and Emergency Communications; Project Leader: Mr. Jason D. Averill	Analyze the behavior and fate of occupants and responders, both those who survived and those who did not, and the performance of the evacuation system.
Emergency Response Technologies and Guidelines; Project Leader: Mr. J. Randall Lawson	Document the activities of the emergency responders from the time of the terrorist attacks on WTC 1 and WTC 2 until the collapse of WTC 7, including practices followed and technologies used.

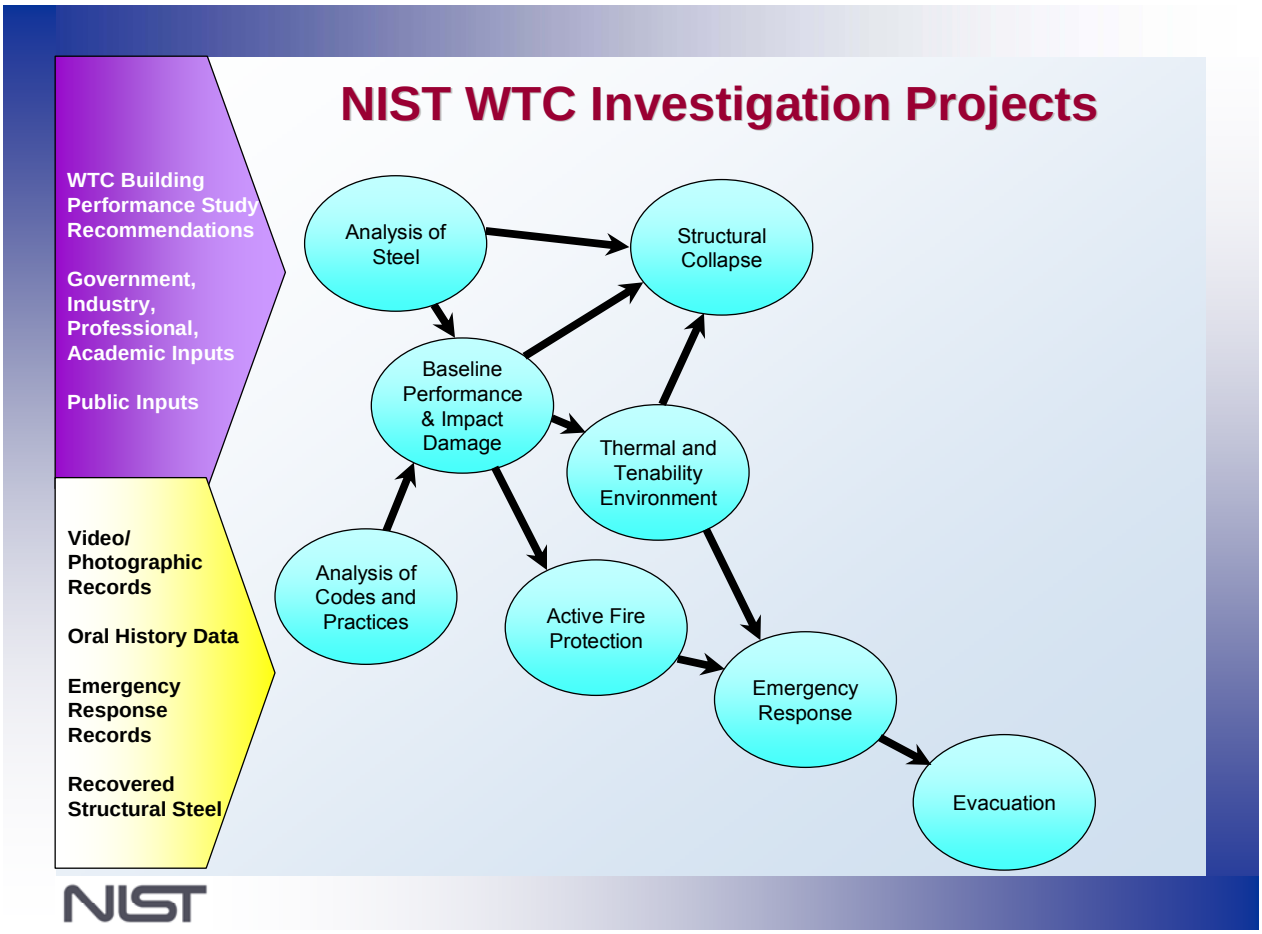

Figure P–1. The eight projects in the federal building and fire safety investigation of the WTC disaster.

National Construction Safety Team Advisory Committee

The NIST Director also established an advisory committee as mandated under the National Construction Safety Team Act. The initial members of the committee were appointed following a public solicitation. These were:

- Paul Fitzgerald, Executive Vice President (retired) FM Global, National Construction Safety Team Advisory Committee Chair
- John Barsom, President, Barsom Consulting, Ltd.
- John Bryan, Professor Emeritus, University of Maryland
- David Collins, President, The Preview Group, Inc.
- Glenn Corbett, Professor, John Jay College of Criminal Justice
- Philip DiNenno, President, Hughes Associates, Inc.

- Robert Hanson, Professor Emeritus, University of Michigan
- Charles Thornton, Co-Chairman and Managing Principal, The Thornton-Tomasetti Group, Inc.
- Kathleen Tierney, Director, Natural Hazards Research and Applications Information Center, University of Colorado at Boulder
- Forman Williams, Director, Center for Energy Research, University of California at San Diego

This National Construction Safety Team Advisory Committee provided technical advice during the Investigation and commentary on drafts of the Investigation reports prior to their public release. NIST has benefited from the work of many people in the preparation of these reports, including the National Construction Safety Team Advisory Committee. The content of the reports and recommendations, however, are solely the responsibility of NIST.

Public Outreach

During the course of this Investigation, NIST held public briefings and meetings (listed in Table P–2) to solicit input from the public, present preliminary findings, and obtain comments on the direction and progress of the Investigation from the public and the Advisory Committee.

NIST maintained a publicly accessible Web site during this Investigation at http://wtc.nist.gov. The site contained extensive information on the background and progress of the Investigation.

NIST's WTC Public-Private Response Plan

The collapse of the WTC buildings has led to broad reexamination of how tall buildings are designed, constructed, maintained, and used, especially with regard to major events such as fires, natural disasters, and terrorist attacks. Reflecting the enhanced interest in effecting necessary change, NIST, with support from Congress and the Administration, has put in place a program, the goal of which is to develop and implement the standards, technology, and practices needed for cost-effective improvements to the safety and security of buildings and building occupants, including evacuation, emergency response procedures, and threat mitigation.

The strategy to meet this goal is a three-part NIST-led public-private response program that includes:

- A federal building and fire safety investigation to study the most probable factors that contributed to post-aircraft impact collapse of the WTC towers and the 47-story WTC 7 building, and the associated evacuation and emergency response experience.
- A research and development (R&D) program to (a) facilitate the implementation of recommendations resulting from the WTC Investigation, and (b) provide the technical basis for cost-effective improvements to national building and fire codes, standards, and practices that enhance the safety of buildings, their occupants, and emergency responders.

Table P–2. Public meetings and briefings of the WTC Investigation.

Date	Location	Principal Agenda
June 24, 2002	New York City, NY	Public meeting: Public comments on the *Draft Plan* for the pending WTC Investigation.
August 21, 2002	Gaithersburg, MD	Media briefing announcing the formal start of the Investigation.
December 9, 2002	Washington, DC	Media briefing on release of the *Public Update* and NIST request for photographs and videos.
April 8, 2003	New York City, NY	Joint public forum with Columbia University on first-person interviews.
April 29–30, 2003	Gaithersburg, MD	NCST Advisory Committee meeting on plan for and progress on WTC Investigation with a public comment session.
May 7, 2003	New York City, NY	Media briefing on release of *May 2003 Progress Report.*
August 26–27, 2003	Gaithersburg, MD	NCST Advisory Committee meeting on status of the WTC investigation with a public comment session.
September 17, 2003	New York City, NY	Media and public briefing on initiation of first-person data collection projects.
December 2–3, 2003	Gaithersburg, MD	NCST Advisory Committee meeting on status and initial results and release of the *Public Update* with a public comment session.
February 12, 2004	New York City, NY	Public meeting on progress and preliminary findings with public comments on issues to be considered in formulating final recommendations.
June 18, 2004	New York City, NY	Media/public briefing on release of *June 2004 Progress Report.*
June 22–23, 2004	Gaithersburg, MD	NCST Advisory Committee meeting on the status of and preliminary findings from the WTC Investigation with a public comment session.
August 24, 2004	Northbrook, IL	Public viewing of standard fire resistance test of WTC floor system at Underwriters Laboratories, Inc.
October 19–20, 2004	Gaithersburg, MD	NCST Advisory Committee meeting on status and near complete set of preliminary findings with a public comment session.
November 22, 2004	Gaithersburg, MD	NCST Advisory Committee discussion on draft annual report to Congress, a public comment session, and a closed session to discuss pre-draft recommendations for WTC Investigation.
April 5, 2005	New York City, NY	Media and public briefing on release of the probable collapse sequence for the WTC towers and draft reports for the projects on codes and practices, evacuation, and emergency response.
June 23, 2005	New York City, NY	Media and public briefing on release of all draft reports for the WTC towers and draft recommendations for public comment.
September 12–13, 2005	Gaithersburg, MD	NCST Advisory Committee meeting on disposition of public comments and update to draft reports for the WTC towers.
September 13–15, 2005	Gaithersburg, MD	WTC Technical Conference for stakeholders and technical community for dissemination of findings and recommendations and opportunity for public to make technical comments.

- A dissemination and technical assistance program (DTAP) to (a) engage leaders of the construction and building community in ensuring timely adoption and widespread use of proposed changes to practices, standards, and codes resulting from the WTC Investigation and the R&D program, and (b) provide practical guidance and tools to better prepare facility owners, contractors, architects, engineers, emergency responders, and regulatory authorities to respond to future disasters.

The desired outcomes are to make buildings, occupants, and first responders safer in future disaster events.

National Construction Safety Team Reports on the WTC Investigation

A final report on the collapse of the WTC towers is being issued as NIST NCSTAR 1. A companion report on the collapse of WTC 7 is being issued as NIST NCSTAR 1A. The present report is one of a set that provides more detailed documentation of the Investigation findings and the means by which these technical results were achieved. As such, it is part of the archival record of this Investigation. The titles of the full set of Investigation publications are:

NIST (National Institute of Standards and Technology). 2005. *Federal Building and Fire Safety Investigation of the World Trade Center Disaster: Final Report on the Collapse of the World Trade Center Towers.* NIST NCSTAR 1. Gaithersburg, MD, September.

NIST (National Institute of Standards and Technology). 2008. *Federal Building and Fire Safety Investigation of the World Trade Center Disaster: Final Report on the Collapse of World Trade Center 7.* NIST NCSTAR 1A. Gaithersburg, MD, November.

Lew, H. S., R. W. Bukowski, and N. J. Carino. 2005. *Federal Building and Fire Safety Investigation of the World Trade Center Disaster: Design, Construction, and Maintenance of Structural and Life Safety Systems.* NIST NCSTAR 1-1. National Institute of Standards and Technology. Gaithersburg, MD, September.

Fanella, D. A., A. T. Derecho, and S. K. Ghosh. 2005. *Federal Building and Fire Safety Investigation of the World Trade Center Disaster: Design and Construction of Structural Systems.* NIST NCSTAR 1-1A. National Institute of Standards and Technology. Gaithersburg, MD, September.

Ghosh, S. K., and X. Liang. 2005. *Federal Building and Fire Safety Investigation of the World Trade Center Disaster: Comparison of Building Code Structural Requirements.* NIST NCSTAR 1-1B. National Institute of Standards and Technology. Gaithersburg, MD, September.

Fanella, D. A., A. T. Derecho, and S. K. Ghosh. 2005. *Federal Building and Fire Safety Investigation of the World Trade Center Disaster: Maintenance and Modifications to Structural Systems.* NIST NCSTAR 1-1C. National Institute of Standards and Technology. Gaithersburg, MD, September.

Grill, R. A., and D. A. Johnson. 2005. *Federal Building and Fire Safety Investigation of the World Trade Center Disaster: Fire Protection and Life Safety Provisions Applied to the Design and Construction of World Trade Center 1, 2, and 7 and Post-Construction Provisions Applied after Occupancy*. NIST NCSTAR 1-1D. National Institute of Standards and Technology. Gaithersburg, MD, September.

Razza, J. C., and R. A. Grill. 2005. *Federal Building and Fire Safety Investigation of the World Trade Center Disaster: Comparison of Codes, Standards, and Practices in Use at the Time of the Design and Construction of World Trade Center 1, 2, and 7*. NIST NCSTAR 1-1E. National Institute of Standards and Technology. Gaithersburg, MD, September.

Grill, R. A., D. A. Johnson, and D. A. Fanella. 2005. *Federal Building and Fire Safety Investigation of the World Trade Center Disaster: Comparison of the 1968 and Current (2003) New*

York City Building Code Provisions. NIST NCSTAR 1-1F. National Institute of Standards and Technology. Gaithersburg, MD, September.

Grill, R. A., and D. A. Johnson. 2005. *Federal Building and Fire Safety Investigation of the World Trade Center Disaster: Amendments to the Fire Protection and Life Safety Provisions of the New York City Building Code by Local Laws Adopted While World Trade Center 1, 2, and 7 Were in Use*. NIST NCSTAR 1-1G. National Institute of Standards and Technology. Gaithersburg, MD, September.

Grill, R. A., and D. A. Johnson. 2005. *Federal Building and Fire Safety Investigation of the World Trade Center Disaster: Post-Construction Modifications to Fire Protection and Life Safety Systems of World Trade Center 1 and 2*. NIST NCSTAR 1-1H. National Institute of Standards and Technology. Gaithersburg, MD, September.

Grill, R. A., D. A. Johnson, and D. A. Fanella. 2005. *Federal Building and Fire Safety Investigation of the World Trade Center Disaster: Post-Construction Modifications to Fire Protection, Life Safety, and Structural Systems of World Trade Center 7*. NIST NCSTAR 1-1I. National Institute of Standards and Technology. Gaithersburg, MD, September.

Grill, R. A., and D. A. Johnson. 2005. *Federal Building and Fire Safety Investigation of the World Trade Center Disaster: Design, Installation, and Operation of Fuel System for Emergency Power in World Trade Center 7*. NIST NCSTAR 1-1J. National Institute of Standards and Technology. Gaithersburg, MD, September.

Sadek, F. 2005. *Federal Building and Fire Safety Investigation of the World Trade Center Disaster: Baseline Structural Performance and Aircraft Impact Damage Analysis of the World Trade Center Towers.* NIST NCSTAR 1-2. National Institute of Standards and Technology. Gaithersburg, MD, September.

Faschan, W. J., and R. B. Garlock. 2005. *Federal Building and Fire Safety Investigation of the World Trade Center Disaster: Reference Structural Models and Baseline Performance Analysis of the World Trade Center Towers.* NIST NCSTAR 1-2A. National Institute of Standards and Technology. Gaithersburg, MD, September.

Kirkpatrick, S. W., R. T. Bocchieri, F. Sadek, R. A. MacNeill, S. Holmes, B. D. Peterson, R. W. Cilke, C. Navarro. 2005. *Federal Building and Fire Safety Investigation of the World Trade Center Disaster: Analysis of Aircraft Impacts into the World Trade Center Towers,* NIST NCSTAR 1-2B. National Institute of Standards and Technology. Gaithersburg, MD, September.

Gayle, F. W., R. J. Fields, W. E. Luecke, S. W. Banovic, T. Foecke, C. N. McCowan, T. A. Siewert, and J. D. McColskey. 2005. *Federal Building and Fire Safety Investigation of the World Trade Center Disaster: Mechanical and Metallurgical Analysis of Structural Steel.* NIST NCSTAR 1-3. National Institute of Standards and Technology. Gaithersburg, MD, September.

Luecke, W. E., T. A. Siewert, and F. W. Gayle. 2005. *Federal Building and Fire Safety Investigation of the World Trade Center Disaster: Contemporaneous Structural Steel Specifications.* NIST Special Publication 1-3A. National Institute of Standards and Technology. Gaithersburg, MD, September.

Banovic, S. W. 2005. *Federal Building and Fire Safety Investigation of the World Trade Center Disaster: Steel Inventory and Identification.* NIST NCSTAR 1-3B. National Institute of Standards and Technology. Gaithersburg, MD, September.

Banovic, S. W., and T. Foecke. 2005. *Federal Building and Fire Safety Investigation of the World Trade Center Disaster: Damage and Failure Modes of Structural Steel Components.* NIST NCSTAR 1-3C. National Institute of Standards and Technology. Gaithersburg, MD, September.

Luecke, W. E., J. D. McColskey, C. N. McCowan, S. W. Banovic, R. J. Fields, T. Foecke, T. A. Siewert, and F. W. Gayle. 2005. *Federal Building and Fire Safety Investigation of the World Trade Center Disaster: Mechanical Properties of Structural Steels.* NIST NCSTAR 1-3D. National Institute of Standards and Technology. Gaithersburg, MD, September.

Banovic, S. W., C. N. McCowan, and W. E. Luecke. 2005. *Federal Building and Fire Safety Investigation of the World Trade Center Disaster: Physical Properties of Structural Steels.* NIST NCSTAR 1-3E. National Institute of Standards and Technology. Gaithersburg, MD, September.

Evans, D. D., R. D. Peacock, E. D. Kuligowski, W. S. Dols, and W. L. Grosshandler. 2005. *Federal Building and Fire Safety Investigation of the World Trade Center Disaster: Active Fire Protection Systems.* NIST NCSTAR 1-4. National Institute of Standards and Technology. Gaithersburg, MD, September.

Kuligowski, E. D., D. D. Evans, and R. D. Peacock. 2005. *Federal Building and Fire Safety Investigation of the World Trade Center Disaster: Post-Construction Fires Prior to September 11, 2001.* NIST NCSTAR 1-4A. National Institute of Standards and Technology. Gaithersburg, MD, September.

Hopkins, M., J. Schoenrock, and E. Budnick. 2005. *Federal Building and Fire Safety Investigation of the World Trade Center Disaster: Fire Suppression Systems.* NIST NCSTAR 1-4B. National Institute of Standards and Technology. Gaithersburg, MD, September.

Keough, R. J., and R. A. Grill. 2005. *Federal Building and Fire Safety Investigation of the World Trade Center Disaster: Fire Alarm Systems.* NIST NCSTAR 1-4C. National Institute of Standards and Technology. Gaithersburg, MD, September.

Ferreira, M. J., and S. M. Strege. 2005. *Federal Building and Fire Safety Investigation of the World Trade Center Disaster: Smoke Management Systems.* NIST NCSTAR 1-4D. National Institute of Standards and Technology. Gaithersburg, MD, September.

Gann, R. G., A. Hamins, K. B. McGrattan, G. W. Mulholland, H. E. Nelson, T. J. Ohlemiller, W. M. Pitts, and K. R. Prasad. 2005. *Federal Building and Fire Safety Investigation of the World Trade Center Disaster: Reconstruction of the Fires in the World Trade Center Towers.* NIST NCSTAR 1-5. National Institute of Standards and Technology. Gaithersburg, MD, September.

Pitts, W. M., K. M. Butler, and V. Junker. 2005. *Federal Building and Fire Safety Investigation of the World Trade Center Disaster: Visual Evidence, Damage Estimates, and Timeline Analysis.* NIST NCSTAR 1-5A. National Institute of Standards and Technology. Gaithersburg, MD, September.

Hamins, A., A. Maranghides, K. B. McGrattan, E. Johnsson, T. J. Ohlemiller, M. Donnelly, J. Yang, G. Mulholland, K. R. Prasad, S. Kukuck, R. Anleitner and T. McAllister. 2005. *Federal Building and Fire Safety Investigation of the World Trade Center Disaster: Experiments and Modeling of Structural Steel Elements Exposed to Fire.* NIST NCSTAR 1-5B. National Institute of Standards and Technology. Gaithersburg, MD, September.

Ohlemiller, T. J., G. W. Mulholland, A. Maranghides, J. J. Filliben, and R. G. Gann. 2005. *Federal Building and Fire Safety Investigation of the World Trade Center Disaster: Fire Tests of Single Office Workstations.* NIST NCSTAR 1-5C. National Institute of Standards and Technology. Gaithersburg, MD, September.

Gann, R. G., M. A. Riley, J. M. Repp, A. S. Whittaker, A. M. Reinhorn, and P. A. Hough. 2005. *Federal Building and Fire Safety Investigation of the World Trade Center Disaster: Reaction of Ceiling Tile Systems to Shocks.* NIST NCSTAR 1-5D. National Institute of Standards and Technology. Gaithersburg, MD, September.

Hamins, A., A. Maranghides, K. B. McGrattan, T. J. Ohlemiller, and R. Anleitner. 2005. *Federal Building and Fire Safety Investigation of the World Trade Center Disaster: Experiments and Modeling of Multiple Workstations Burning in a Compartment.* NIST NCSTAR 1-5E. National Institute of Standards and Technology. Gaithersburg, MD, September.

McGrattan, K. B., C. Bouldin, and G. Forney. 2005. *Federal Building and Fire Safety Investigation of the World Trade Center Disaster: Computer Simulation of the Fires in the World Trade Center Towers.* NIST NCSTAR 1-5F. National Institute of Standards and Technology. Gaithersburg, MD, September.

Prasad, K. R., and H. R. Baum. 2005. *Federal Building and Fire Safety Investigation of the World Trade Center Disaster: Fire Structure Interface and Thermal Response of the World Trade Center Towers.* NIST NCSTAR 1-5G. National Institute of Standards and Technology. Gaithersburg, MD, September.

Gross, J. L., and T. McAllister. 2005. *Federal Building and Fire Safety Investigation of the World Trade Center Disaster: Structural Fire Response and Probable Collapse Sequence of the World Trade Center Towers.* NIST NCSTAR 1-6. National Institute of Standards and Technology. Gaithersburg, MD, September.

Carino, N. J., M. A. Starnes, J. L. Gross, J. C. Yang, S. Kukuck, K. R. Prasad, and R. W. Bukowski. 2005. *Federal Building and Fire Safety Investigation of the World Trade Center Disaster: Passive Fire Protection.* NIST NCSTAR 1-6A. National Institute of Standards and Technology. Gaithersburg, MD, September.

Gross, J., F. Hervey, M. Izydorek, J. Mammoser, and J. Treadway. 2005. *Federal Building and Fire Safety Investigation of the World Trade Center Disaster: Fire Resistance Tests of Floor Truss Systems.* NIST NCSTAR 1-6B. National Institute of Standards and Technology. Gaithersburg, MD, September.

Zarghamee, M. S., S. Bolourchi, D. W. Eggers, Ö. O. Erbay, F. W. Kan, Y. Kitane, A. A. Liepins, M. Mudlock, W. I. Naguib, R. P. Ojdrovic, A. T. Sarawit, P. R Barrett, J. L. Gross, and

T. P. McAllister. 2005. *Federal Building and Fire Safety Investigation of the World Trade Center Disaster: Component, Connection, and Subsystem Structural Analysis.* NIST NCSTAR 1-6C. National Institute of Standards and Technology. Gaithersburg, MD, September.

Zarghamee, M. S., Y. Kitane, Ö. O. Erbay, T. P. McAllister, and J. L. Gross. 2005. *Federal Building and Fire Safety Investigation of the World Trade Center Disaster: Global Structural Analysis of the Response of the World Trade Center Towers to Impact Damage and Fire.* NIST NCSTAR 1-6D. National Institute of Standards and Technology. Gaithersburg, MD, September.

Averill, J. D., D. S. Mileti, R. D. Peacock, E. D. Kuligowski, N. Groner, G. Proulx, P. A. Reneke, and H. E. Nelson. 2005. *Federal Building and Fire Safety Investigation of the World Trade Center Disaster: Occupant Behavior, Egress, and Emergency Communication.* NIST NCSTAR 1-7. National Institute of Standards and Technology. Gaithersburg, MD, September.

Fahy, R., and G. Proulx. 2005. *Federal Building and Fire Safety Investigation of the World Trade Center Disaster: Analysis of Published Accounts of the World Trade Center Evacuation.* NIST NCSTAR 1-7A. National Institute of Standards and Technology. Gaithersburg, MD, September.

Zmud, J. 2005. *Federal Building and Fire Safety Investigation of the World Trade Center Disaster: Technical Documentation for Survey Administration.* NIST NCSTAR 1-7B. National Institute of Standards and Technology. Gaithersburg, MD, September.

Lawson, J. R., and R. L. Vettori. 2005. *Federal Building and Fire Safety Investigation of the World Trade Center Disaster: The Emergency Response Operations.* NIST NCSTAR 1-8. National Institute of Standards and Technology. Gaithersburg, MD, September.

McAllister, T., R. G. Gann, J. D. Averill, J. L. Gross, W. L. Grosshandler, J. R. Lawson, K. B. McGrattan, H. E. Nelson, W. M. Pitts, K. R. Prasad, F. H. Sadek. 2008. *Federal Building and Fire Safety Investigation of the World Trade Center Disaster: Structural Fire Response and Probable Collapse Sequence of World Trade Center Building 7.* NIST NCSTAR 1-9. National Institute of Standards and Technology. Gaithersburg, MD, November.

MacNeill, R., S. Kirkpatrick, B. Peterson, and R. Bocchieri. 2008. *Federal Building and Fire Safety Investigation of the World Trade Center Disaster: Global Structural Analysis of the Response of World Trade Center Building 7 to Fires and Debris Impact Damage.* NIST NCSTAR 1-9A. National Institute of Standards and Technology. Gaithersburg, MD, November.

EXECUTIVE SUMMARY

E.1 INTRODUCTION

This report presents the work conducted to establish the baseline performance of the North and South World Trade Center Towers (WTC 1 and WTC 2) under design gravity and wind loading conditions. Baseline performance results include basic information about the behavior of the towers, such as total and inter-story drift under wind loads, floor deflections under gravity loads, demand/capacity ratios for primary structural components, exterior columns response (shear lag effects and presence of tensile forces), performance of connections, and the towers' resistance to shear sliding and overturning.

The primary tasks that were undertaken to establish the baseline performance included the following:

- To develop structural databases for the primary structural components of the WTC 1 and WTC 2 towers from the original computer printouts of the structural documents.
- To develop reference structural analysis models that capture the intended behavior of each of the two towers using the generated databases. These reference models were used to establish the baseline performance of the towers and also served as a reference for more detailed models for other phases of the National Institute of Standards and Technology (NIST) investigation.
- To develop estimates of design gravity (dead and live loads) and wind loads on each of the two towers for implementation into the reference structural models.
- To perform linear, static structural analyses to establish the baseline performance of each of the two towers under design gravity and wind loads.

E.2 DEVELOPMENT OF STRUCTURAL DATABASES FOR THE WTC TOWERS

This task included the development of structural databases of the primary components of the WTC 1 and WTC 2 towers. The electronic databases were developed from original computer printouts of the structural design documents, including modifications made after construction. The databases were generated for use in the development of the reference structural models of the towers.

The structural databases contained the computer and hand-tabulated data for the primary structural components of the towers from the original Drawing Books 1 through 5, including exterior walls, core columns, and beam schedule. In addition, some information from Drawing Book 6 (core bracing schedule) and Drawing Book 9 (beams in the hat truss region) were included in the database files as it was utilized in the modeling of the towers. Some modifications that were made to the towers were implemented in the databases, including strengthening of a number of core columns at floors 98 to 106 of both towers and reinforcing of two corner core column at floors 45 to 97 of WTC 2 due to the construction of a concrete vault at floor 97.

The task included the scanning and digitization of the original drawing books, a four-step quality control procedure, cross section property calculations, and development of the relational databases to link the generated database files into a format suitable for the development of the structural models.

E.3 DEVELOPMENT OF REFERENCE STRUCTURAL MODELS FOR THE WTC TOWERS

This task included the development of reference structural analysis models that capture the intended behavior of each of the two towers using the generated databases. These reference models were used to establish the baseline performance of the towers and also served as a reference for more detailed models for aircraft impact damage analysis and thermal-structural response and collapse initiation analysis. The main types of models developed were:

- Two global models of the major structural components and systems for the towers, one each for WTC 1 and WTC 2. The models included all primary structural components in the towers, including exterior walls (columns and spandrel beams), core columns, exterior wall bracing in the basement floors, core bracing at the mechanical floors, core bracing at the main lobby atrium levels, hat trusses, and rigid and flexible diaphragms representing the floor systems. To validate the global models, the calculated natural frequencies of WTC 1 were compared with those measured on the tower, and good agreement between the calculated and measured values was obtained.

- One model each of the typical truss-framed floor (floor 96 of WTC 1) and typical beam-framed floor (floor 75 of WTC 2). The models included all major structural components in the floor system, including primary and bridging trusses, beams, strap anchors and horizontal trusses, concrete slabs, and viscoelastic dampers. To validate the floor models, several studies were carried out to compare stresses and deflections estimated from the model with hand calculations for representative composite sections. Good agreement was obtained between the model results and hand calculations.

Parametric studies were performed to evaluate the behavior of typical portions of the structure and to develop simplified models for implementation into the global models. These parametric studies included detailed and simplified models of typical exterior and corner wall panels and floor systems.

E.4 GRAVITY AND WIND LOADS ON THE WTC GLOBAL MODELS

This task included the development of estimates of design gravity and wind loads on the towers for implementation into the reference structural models and use in the baseline performance analysis. Various wind loads were considered in this study, including wind loads used in the original WTC design, wind loads based on two recent wind tunnel studies conducted in 2002 by Cermak Peterka Peterson, Inc. (CPP) and Rowan Williams Davis and Irwin, Inc. (RWDI) for insurance litigation concerning the towers, and wind load estimates developed by NIST from critical assessment of information obtained from the CPP and RWDI reports and state-of-the-art considerations. The following three loading cases were considered for the baseline performance analysis:

- *Original WTC design loads case.* Loads included dead and live loads as in original WTC design in conjunction with original WTC design wind loads.

- *State-of-the-practice case.* Loads included dead loads; current New York City Building Code (NYCBC 2001) live loads; and wind loads from the RWDI wind tunnel study, scaled in accordance with NYCBC 2001 wind speed.

- *Refined NIST estimate case.* Loads included dead loads; live loads from the American Society of Civil Engineers (ASCE 7-02) Standard (a national standard); and wind loads developed by NIST.

The purpose of using the original WTC design loads was to evaluate the performance of the towers under original design loading conditions and ascertain whether those loads and the corresponding design were adequate given the knowledge available at the time of the design. The purpose of considering the state-of-the-practice and the refined NIST estimate cases was to better understand and assess the effects of successive changes in standards, codes, and practices on wind design practices for tall buildings.

The study indicated that the original WTC design wind load estimates exceeded those established by the NYCBC prior to 1968, when the WTC towers were designed, and up to and including 2001. The design values were also higher than those required by other prescriptive building codes of the time.

The two orthogonal base shear and base moment components used in the original design were in general smaller than the CPP, RWDI, and NIST estimates. However, the most unfavorable combined peaks from the original design were larger than, or smaller by at most 15 percent than, estimates based on the CPP, RWDI, and NIST estimates. This is due to the conservative procedure used to combine the loads in the original design.

The estimated wind-induced loads on the towers vary by as much as 40 percent between the wind tunnel/climatological studies conducted by CPP and RWDI in 2002, with CPP being the larger. Considering the differences between RWDI and CPP results, the RWDI loads may be viewed as a "lower-estimate, state-of-the-practice case."

E.5 BASELINE PERFORMANCE ANALYSIS OF THE WTC GLOBAL MODELS

The WTC 1 and WTC 2 global models were each analyzed under the three loading cases described above to establish their baseline performance. The following is a summary of the results:

- Under the original WTC design loads, the cumulative drifts at the top of the WTC 1 tower were about 56.6 in. (H/304) and 55.7 in. (H/309) in the E–W and N–S directions, respectively. These drifts were about 51.2 in. (H/335) in the E–W direction and 65.3 in. (H/263) in the N–S direction for WTC 2. For the lower estimate, state-of-the-practice case, the drifts for WTC 1 were larger than those from the original design case by about 0.5 percent and 22 percent for the E–W and N–S directions, respectively. For the lower estimate, state-of-the-practice case for WTC 2, the E–W drift was larger than that of the original design case by about 16 percent, and the N–S drift was smaller by about 15 percent. The drifts obtained from the refined NIST estimate case were about 25 percent larger than those from the state-

of-the practice case. These differences are consistent with the differences between the base shears for the three loading cases.

- The demand/capacity ratios (DCR) were based on the allowable stress design procedure and were estimated using the AISC Specifications (1989). The results indicated that DCRs estimated from the original WTC design load case were, in general, close to those obtained for the lower estimate, state-of-the practice case. For both cases, a small fraction of structural components had DCRs larger than 1.0. These were mainly observed in both towers at (1) the exterior walls at the columns around the corners, where the hat truss connected to the exterior walls, and below floor 9; and (2) the core columns on the 600 line between floors 80 and 106 and at core perimeter columns 901 and 908 for much of their height.

- The refined NIST case estimated DCRs were higher than those of the original WTC design estimates and the lower state-of-the-practice estimates for the following reasons: The NIST estimated wind loads were about 25 percent higher than those used in the lower state-of-the-practice estimate, and mixed, some higher and others lower than the original WTC design wind loads. It is noted that the NIST estimated wind loads are about 20 percent smaller than those estimated by CPP (an upper estimate, state-of-the practice case). In addition, the original WTC design and the state-of-the-practice cases used NYCBC load combinations, which result in lower DCRs than the ASCE 7-02 load combinations used for the refined NIST case.

- Under a combination of the original WTC design dead and wind loads, tension forces were observed in the exterior walls of both towers. The forces were largest at the base of the building and at the corners. These tensile column loads were transferred from one panel to another through the column splices. The DCR ratios for the exterior wall splice connections under the effect of the tensile forces for the two towers were shown to be less than 1.0.

- For the towers' resistance to shear sliding and overturning due to wind, the dead loads that acted on the perimeter walls of the towers provided resistance to shear sliding and overturning at the foundation level. Considering the resistance to shear sliding under wind load, the factor of safety was calculated to be between 10 and 11.5, while the factor of safety against overturning ranged from 1.9 to 2.7 for both towers.

E.6 BASELINE PERFORMANCE ANALYSIS OF THE TYPICAL FLOOR MODELS

The typical floor models were both analyzed under gravity loads. The following is a summary of the results:

- For the typical truss-framed floor (floor 96 of WTC 1), the DCRs for all floor trusses were less than 1.14 for the original WTC Design Criteria loads and less than 0.86 for the ASCE 7-02 loading. Under the original WTC Design Criteria loading, the DCR was less than 1.00 for 99.4 percent of the floor truss components. For the area outside the core, the average ratio of the DCRs under the ASCE 7-02 loading to the DCRs under the original WTC Design Criteria loading for all floor trusses was about 0.80. For the core area, the DCRs for all floor beams inside the core were less than 1.08, and more than 99 percent had a DCR of less than

1.0. Under the original WTC Design Criteria loading, the maximum floor deflections were 1.79 in., 0.57 in., and 1.44 in. for the long span one-way trusses, short span one-way trusses, and the two-way zone, respectively.

- For the typical beam-framed floor (floor 75 of WTC 2) under the original WTC Design Criteria loading, the DCRs for all floor beams were less than 1.0 except for two core beams where the shear DCRs were 1.125 and 1.09. The maximum mid-span deflections of the long span and short span zones under the original WTC Design Criteria loads were about 1.55 in. and 0.70 in., respectively.

This page intentionally left blank.

Chapter 1
INTRODUCTION

The objective of this analysis was to establish the baseline performance of the North and South World Trade Center Towers (WTC 1 and WTC 2) under design gravity and wind loading conditions. Baseline performance results provide basic information about the towers' behavior under design loading conditions, including total and inter-story drift under wind loads, floor deflections under gravity loads, demand/capacity ratios for the primary structural components of the towers, exterior columns response (shear lag effects and presence of tensile forces), performance of connections, and the towers' resistance to shear sliding and overturning. The primary tasks that were undertaken to establish the baseline performance include the following:

- To develop structural databases for the primary structural components of the WTC 1 and WTC 2 towers from the original computer printouts of the structural documents.
- To develop reference structural analysis models that capture the intended behavior of each of the two towers using the generated databases. These reference models were used to establish the baseline performance of the towers and also served as a reference for more detailed models for aircraft impact damage analysis and thermal-structural response and collapse initiation analysis.
- To develop estimates of design gravity (dead and live loads) and wind loads on each of the two towers for implementation into the reference structural models.
- To perform linear, static structural analyses to establish the baseline performance of each of the two towers under design gravity and wind loads.

Chapter 1 of this report presents an introduction and a brief description of the structural system of the towers. Chapter 2 presents an outline and description of the methodology used for the development of the structural databases for both towers, along with the relational databases that are used to link the generated databases for use in the development of the reference structural models. Chapter 3 presents the development of the reference structural analysis models for WTC 1 and WTC 2, including global tower models, typical floor models, and parametric studies conducted for the development of the global models. Chapter 4 provides a discussion on the loading cases used in the baseline performance analysis and outlines the development of the gravity and wind loads on the global tower models. Chapters 5 and 6 outline the results of the baseline performance analysis for the global tower models and floors models, respectively. A summary of the report is presented in Chapter 7.

1.1 DESCRIPTION OF WTC STRUCTURAL SYSTEM

1.1.1 Global Structural System

WTC 1 and WTC 2 each consisted of a 110-story above grade structure and a 6-story below grade structure. The buildings, which were each approximately 207 ft by 207 ft square in plan and with story

heights of typically 12 ft, rose to heights of 1,368 ft (WTC 1) and 1,362 ft (WTC 2) above ground. The exterior walls of the towers supported part of the gravity loads and all lateral loads, and were constructed of steel, closely spaced built-up columns and deep spandrels. The core contained columns that supported the remainder of the gravity loads of the towers. The core area was approximately 135 ft by 87 ft in plan (Fig. 1–1). The distances between the rectangular core and the square exterior wall were approximately 36 ft and 60 ft. The areas outside of the core were free of columns, and the floors were supported by truss-framing in the tenant areas and beam-framing in the mechanical rooms and other areas.

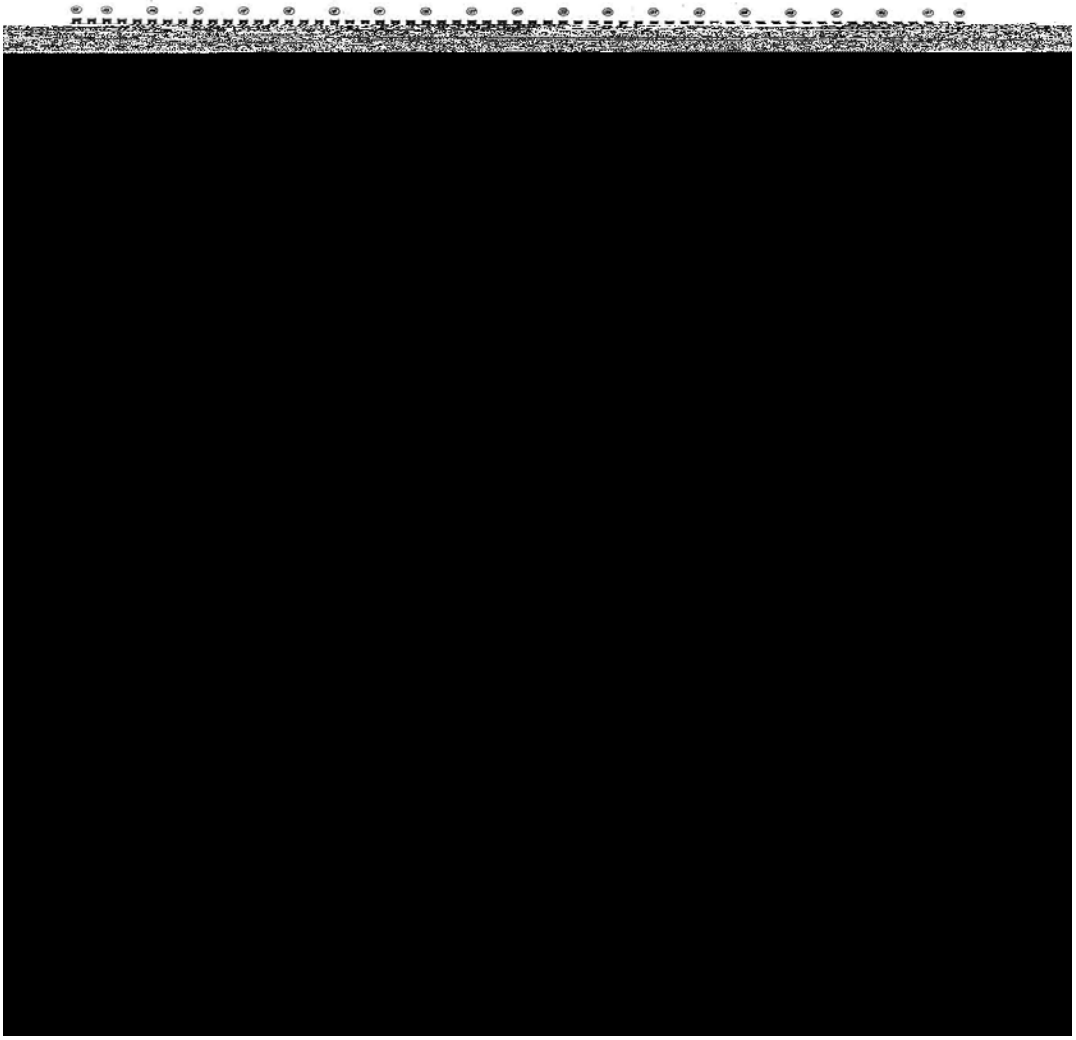

Source: Reproduced with permission of The Port Authority of New York and New Jersey.

Figure 1–1. Typical WTC tower architectural floor plan (floor 26, WTC 2).

The primary structural systems for the towers included exterior columns, spandrel beams, and bracing in the basement floors, core columns, core bracing at the mechanical floors, core bracing at the main lobby atrium levels, hat trusses, and the floor systems.

The exterior wall columns from the foundation level up to elevation 363 ft were spaced 10 ft 0 in. on center. They were built-up of steel plates and connected by deep spandrels. Bracings existed in the plane of the exterior wall between the Concourse level and the foundation (Fig. 1–2). Between elevation 363 ft

and floor 7, the single exterior wall columns spaced 10 ft 0 in. on center transitioned to three columns spaced at 3 ft 4 in. on center as shown in Fig. 1–2 (see also Fig. 3–6).

Source: Reproduced with permission of The Port Authority of New York and New Jersey.

Figure 1–2. Typical WTC exterior wall, foundation to floor 9.

The exterior wall columns above floor 7 that were spaced 3 ft 4 in. on center, were built-up of steel plates, and were connected to each other by spandrel plates, typically 52 in. deep. The exterior columns and spandrels were pre-assembled into exterior wall panels, typically 3-columns wide by 3-stories tall (refer to Fig. 3–9).

The core columns were typically built-up box members at the lower floors and transitioned into rolled structural steel shapes at the upper floors. The core columns were typically spliced at three-story intervals at 3 ft above floor level. Diagonal bracing of the core columns existed at the lobby atrium levels, the mechanical levels, and in the area of the hat truss.

At the top of each tower, hat trusses interconnected the core columns with the exterior wall panels and provided a base for the antennae. The vertical members of the hat trusses were wide flange core columns.

The diagonals were primarily wide flange rolled sections, with the exception of the end diagonals connecting the core to the exterior walls, which consisted of built-up box sections. The majority of the horizontal members in the hat truss system were wide flange and built-up box section floor beams. The members of the hat trusses were shown in the structural drawings SA/B-400 series elevations (see Fig. 1–3).

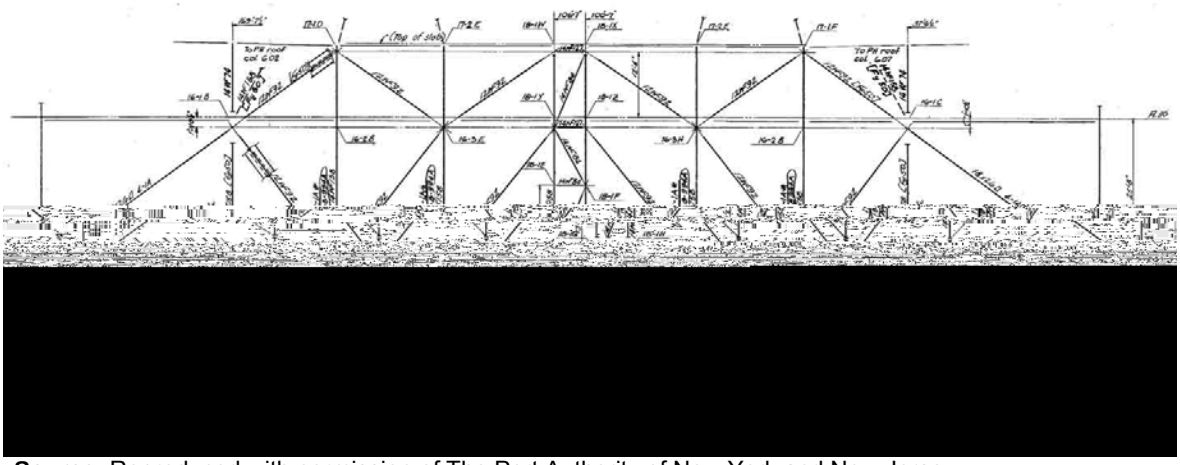

Source: Reproduced with permission of The Port Authority of New York and New Jersey.

Figure 1–3. Typical WTC tower hat truss elevation (Drawing SA 401).

1.1.2 Floor Structural System

In the typical WTC tower floor plan, the area inside the core was framed with rolled structural steel shapes acting in a composite fashion with formed concrete slabs. The area outside the core was framed either in trusses (typical on tenant floors) or in rolled structural steel shapes (typical on mechanical floors).

Truss-Framed Floors—The majority of the floors of the WTC towers were tenant floors where the areas outside of the core were constructed of steel trusses acting in a composite fashion with concrete slabs cast over metal deck. The trusses consisted of double angle top and bottom chords with round bar webs and were designed to act in a composite fashion with the concrete slab. Composite action was achieved by the shear connection provided by the web bar extending above the top chord and into the slab. Two trusses were placed at every other exterior column line, resulting in a 6 ft 8 in. spacing between truss pairs. The typical floor consisted of three truss zones: a long span zone, a short span zone, and a two-way zone (see Fig. 1–4).

The floor trusses were pre-assembled into floor panels as defined in the contract drawings. The span of the primary trusses was about 36 ft in the short direction and 60 ft in the long direction. The floor panels included primary trusses, bridging trusses, deck support angles, metal deck, and strap anchors, all of which were defined by the contract drawings and specifications. The two-way zone included trusses in the long-span direction (primary trusses) as well the bridging trusses (secondary trusses). The secondary trusses had additional strength and connectivity to enable them to act in tandem with the long spanning trusses to form a two-way spanning truss grid as shown in zones labeled two-way area in Fig. 1–4. Also; the short span truss at the corner of the core was heavier than the typical ones because it did support the long span trusses that framed to it.

Since the relative stiffness of the bridging trusses was significant in the two-way zone compared to that of the short span trusses, and since the corner of the floor was supported on two sides and the corner of the core, two directional structural behavior was developed. In the one-way zones, the bridging trusses were lighter and the floor was supported on only two sides (exterior wall spandrels and core perimeter beams), so only one-way behavior was dominant.

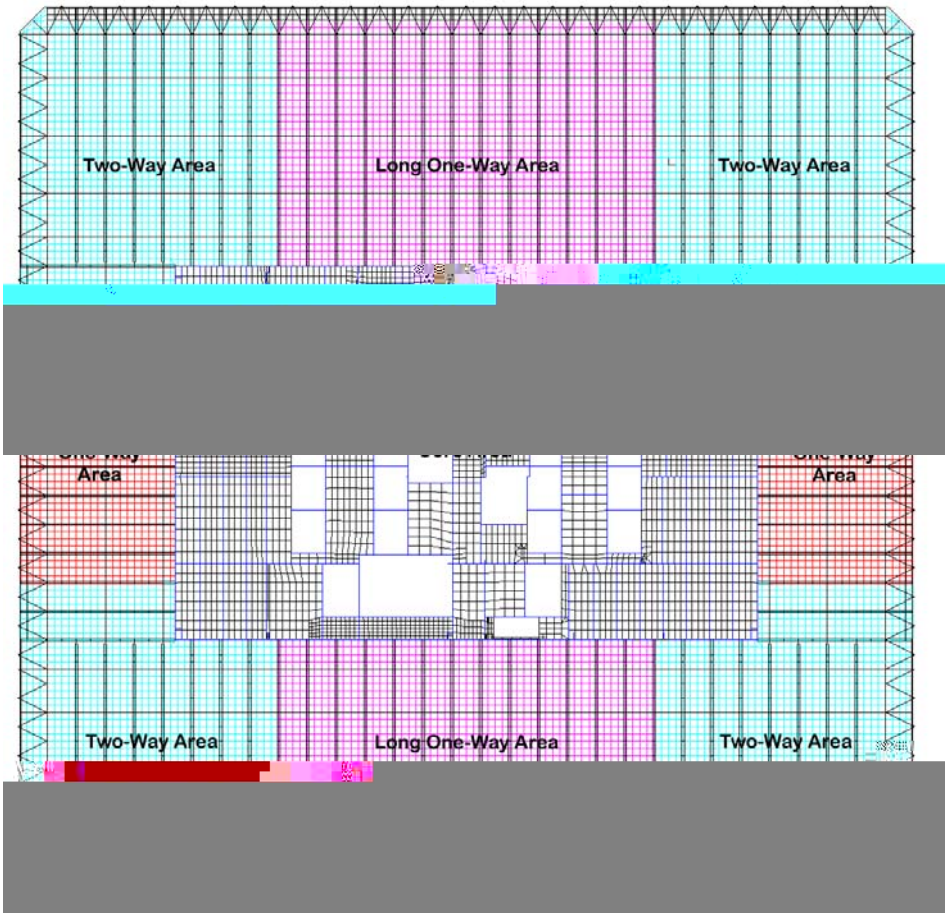

Figure 1–4. Typical WTC floor truss framing zones.

The floor truss panel types were indicated in the structural plans (Fig. 1–5). The plans refer in turn to Drawing Book 7 for information regarding the components of the floor truss panels, and to Drawing Book D for damper information (see Chapter 2 for more details). Drawing Book 7 provided panel by panel layout plans (Fig. 1–6) and elevations (Fig. 1–7) of each referenced truss. The section through a floor panel after the concrete was placed is illustrated in Fig. 1–8. Note that the dashed lines in Fig. 1–5 indicate power and telephone cells within the metal deck construction.

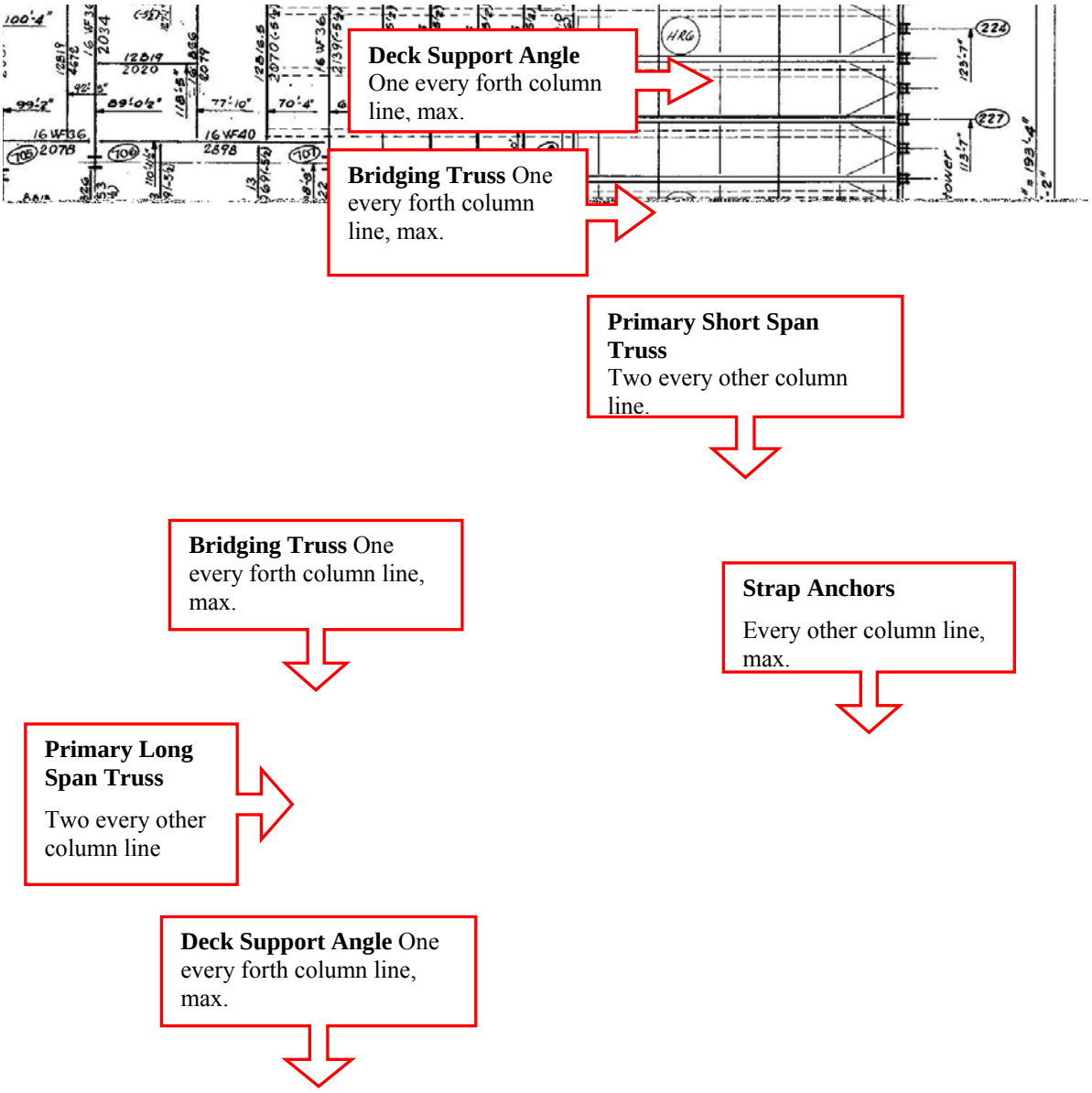

Source: Reproduced with permission of The Port Authority of New York and New Jersey. Enhanced by NIST.

Figure 1–5. Part plan of floor 96 of WTC 1 (Drawing SA-104), components of typical truss framing system.

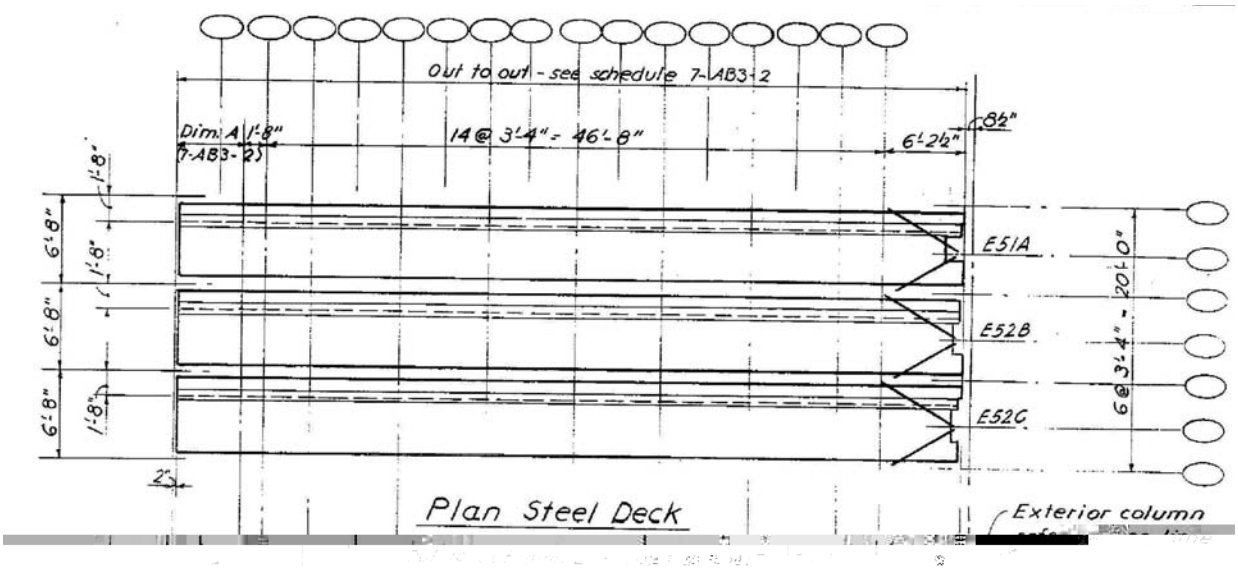

Source: Reproduced with permission of The Port Authority of New York and New Jersey.

Figure 1–6. Typical WTC floor panel layout plan.

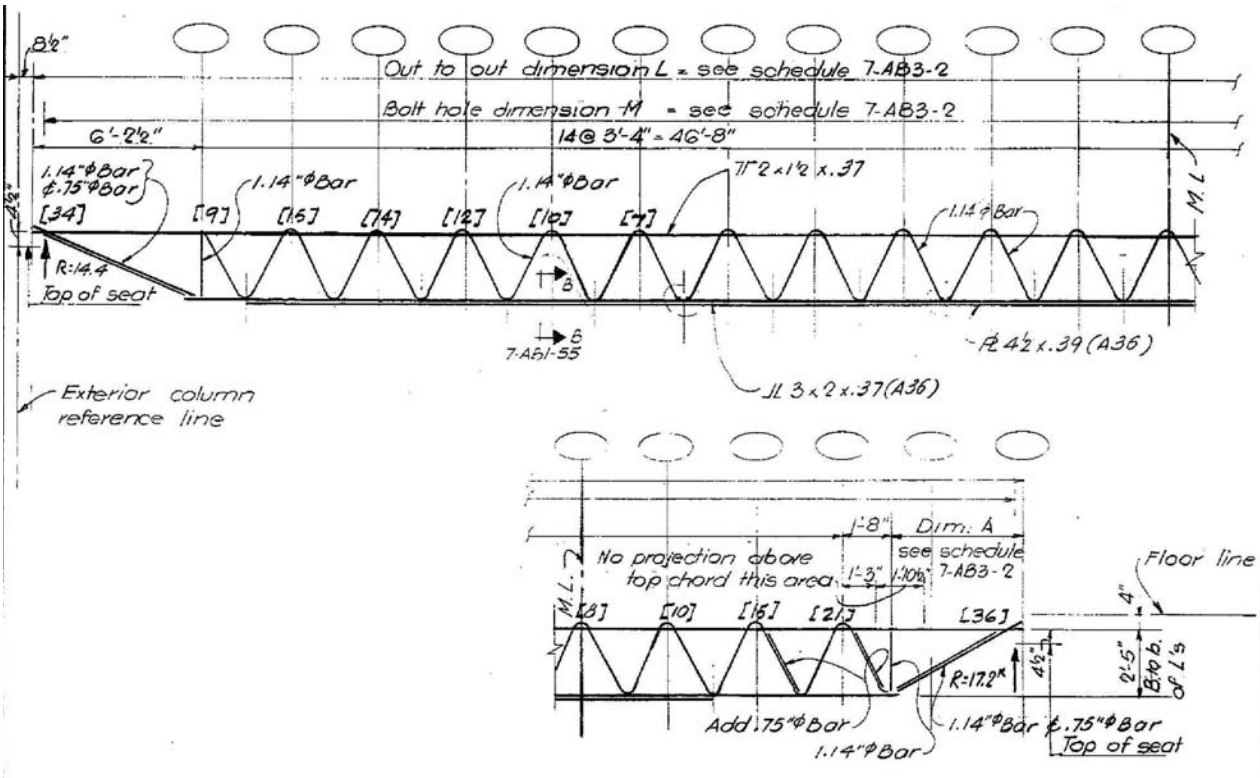

Source: Reproduced with permission of The Port Authority of New York and New Jersey.

Figure 1–7. Typical WTC floor truss elevation.

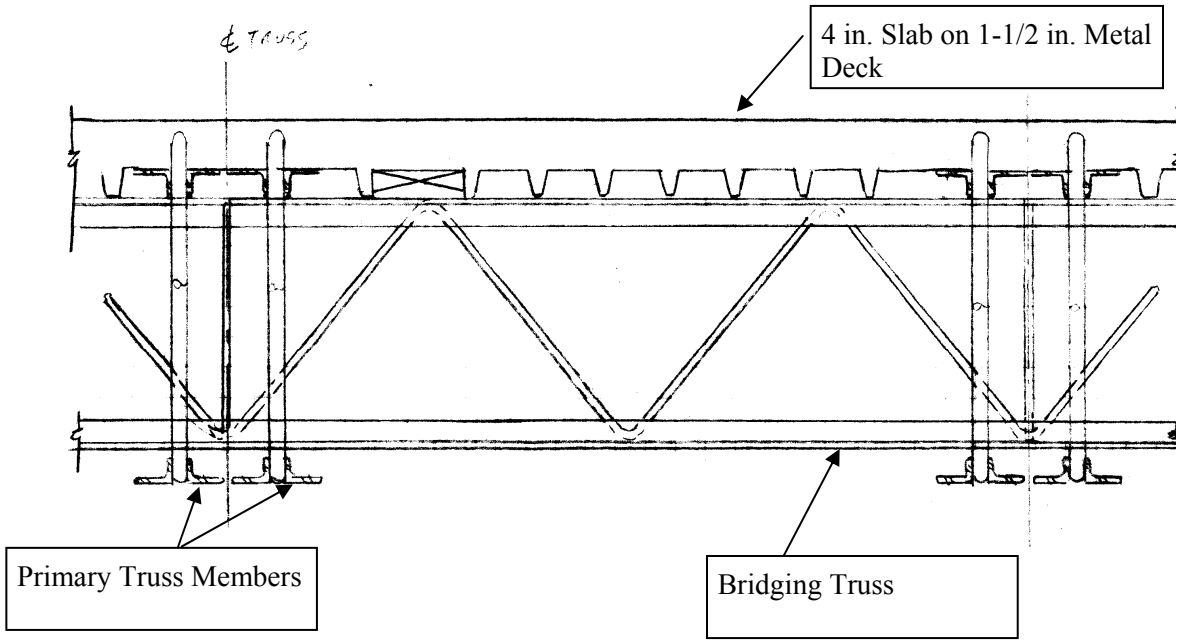

Source: Reproduced with permission of The Port Authority of New York and New Jersey. Enhanced by NIST.

Figure 1–8. Part section typical truss floor panel.

Viscoelastic damping units were used in the floor system to reduce the wind-induced vibrations of the towers. As the towers oscillated during wind excitations, part of the energy of oscillation was dissipated through shear deformations in the viscoelastic part of the damping unit. The dampers were located between the bottom chords of the floor trusses and the exterior wall columns as shown in Fig. 1–9 and the associated detail in Fig. 1–10. The figures show the construction of the dampers along with the plates, bolts, and viscoelastic material dimensions. The dampers were defined in Drawing Book D. For further details on the dampers design, construction, and testing, refer to NIST NCSTAR 1-1.[1]

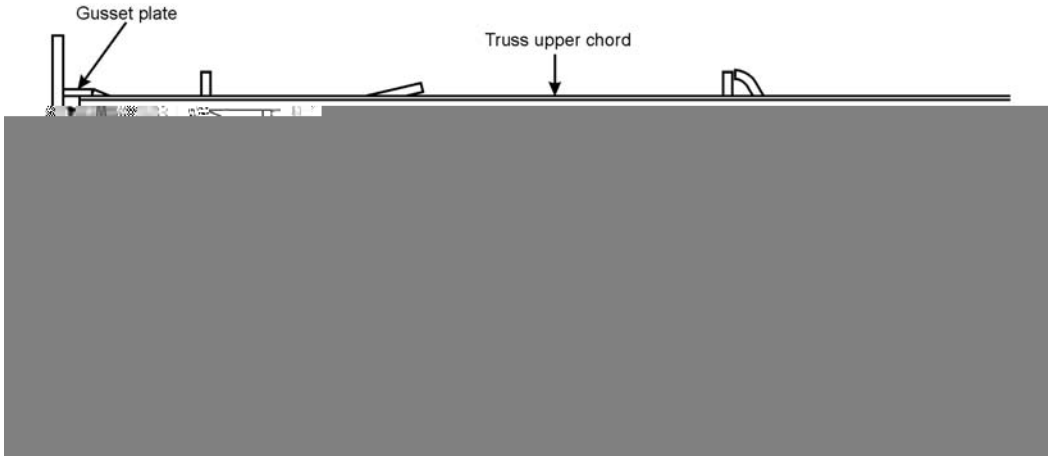

Source: Reproduced with permission of The Port Authority of New York and New Jersey. Enhanced by NIST.

Figure 1–9. Floor truss with exterior wall end detail.

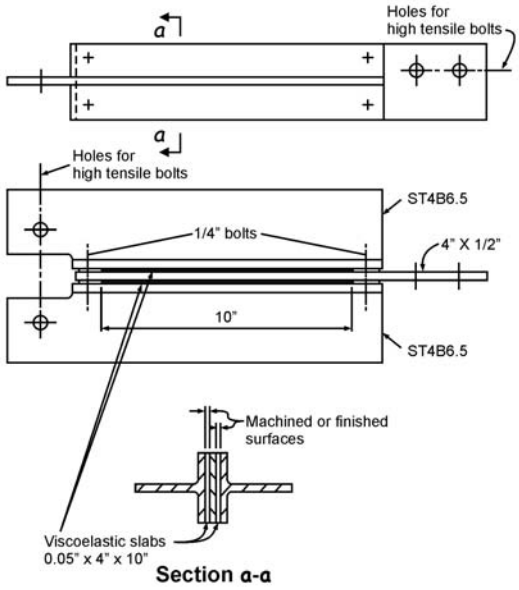

Source: Reproduced with permission of The Port Authority of New York and New Jersey. Enhanced by NIST.

Figure 1–10. Details of the damping unit used in the truss-framed floors.

[1] This reference is to one of the companion documents from this Investigation. A list of these documents appears in the Preface to this report.

Beam-Framed Floors—The typical locations of the beam-framed floors were the mechanical floors, the mechanical mezzanines, and the floors above the mezzanines (e.g., floors 41, 42, and 43). These floors were constructed using rolled structural steel shapes. The beam framing for the typical floor system consisted of W27 beams in the long span region and W16 beams in the short span region. Typical beam spacing was 6 ft 8 in. The steel beams acted in composite fashion with the normal weight concrete slab on metal deck.

The mechanical floors were 5 ¾ in. concrete slabs on 1 ½ in. metal deck outside the core. The deck spanned in the direction of the primary beams and was supported typically at 6 ft 8 in. intervals by a 4C5.4 deck support channel. A 2 in. concrete topping slab was placed on top of the structural slab. The core area was framed similarly to the core of the truss-framed floors, but the steel beams were typically larger, and the concrete slab was 6 in. deep. The beam-framed floors above the mechanical mezzanine had a 7 3/4 in. normal weight concrete slab on 1 1/2 in. metal deck, while the core slab was 8 in. normal weight concrete. The floor slabs were omitted from much of the mechanical mezzanines outside the core to provide double height space for the mechanical equipment.

Similar to the truss-framed floors, viscoelastic damping units were used in the beam-framed floors to reduce wind-induced vibrations. The dampers were located between the bottom flanges of the floor beams and the exterior wall columns as shown in Fig. 1–11. The dampers that were used in the beam-framed floors were slightly longer than those used in the truss-frames floors. Also the connections between the damping units and the floor trusses were different than those between the damping units and floor beams as can be seen from Fig. 1–9 and Fig. 1–11.

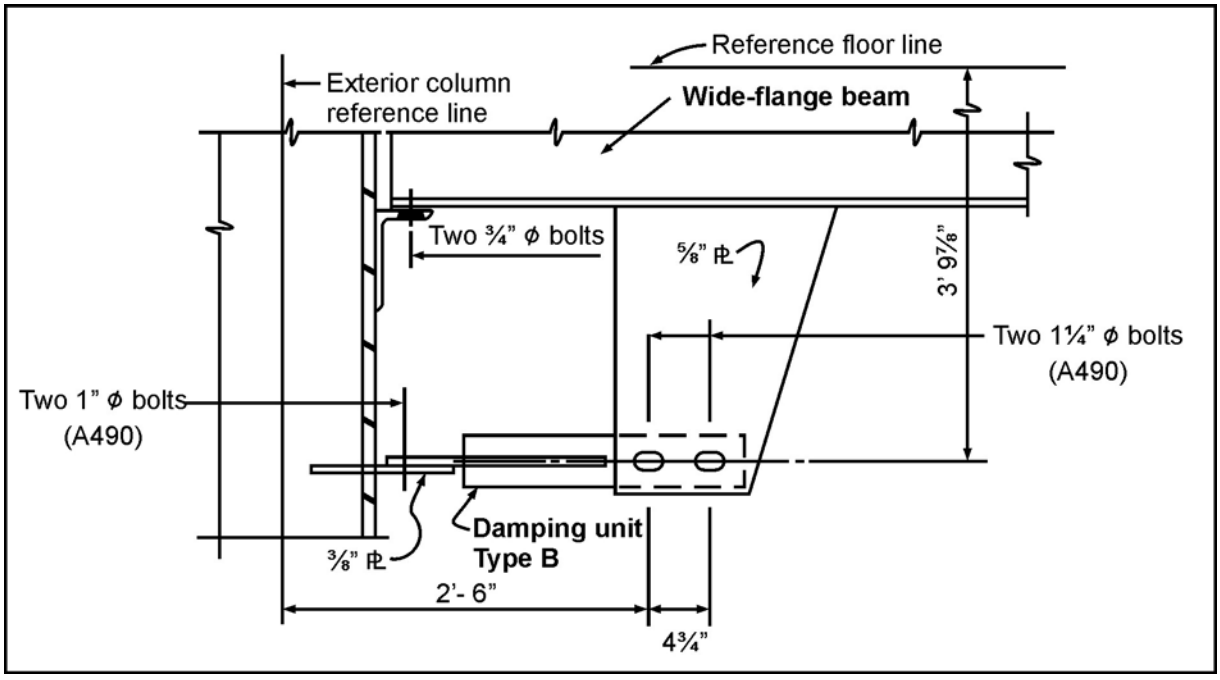

Figure 1–11. Damping unit used in the beam-framed floors.

Beam-framing was added to truss-framed floors at levels which supported escalators or stairs in the areas outside of the core. The escalator floors occurred typically in the two levels directly above the mechanical rooms.

Chapter 2
DEVELOPMENT OF STRUCTURAL DATABASES FOR THE WTC TOWERS

2.1 INTRODUCTION

The objective of this chapter is to describe the development of electronic structural databases for the primary structural components of the World Trade Center towers (WTC 1 and WTC 2) from the original computer printouts of the structural documents. These databases were generated for use in the development of the reference structural models of the towers (see Chapter 3).

Section 2.2 briefly describes the structural design documents of the towers. Section 2.3 presents an overview of the database development and contents, while Sec. 2.4 outlines the methodology used to develop the structural databases from the original computer printouts, and the relational databases used for the subsequent development of the reference structural analysis models of the towers (see Chapter 3). Section 2.5 describes the modifications made to elements of the database based on changes made to the primary structural components of the towers after construction. The calculation of cross section properties is presented in Sec. 2.6. Section 2.7 provides a summary of the chapter.

2.2 DESCRIPTION OF THE WTC STRUCTURAL DOCUMENTS

The WTC structural drawings were issued in two main formats: large-sized sheets containing plan and elevation information and smaller book-sized drawings containing details and tabulated information. Throughout the WTC drawings, Tower A or WTCA denotes WTC 1 (North Tower) and Tower B or WTCB denotes WTC 2 (South Tower). For WTC 1 and WTC 2, the large-size sheets are listed in Appendix A. These large-sized drawings always make reference to the structural drawing books in their notes, sections, and details. The structural drawing books for WTC 1 and WTC 2 contain the following materials:

- Book 1 contains exterior wall information to elevation 363 ft. (Dates: 02/1967 to 12/1968, Approx. 213 pages.)
- Book 2 contains exterior wall information elevation 363 ft to floor 9. (Dates: 04/1967 to 12/1967, Approx. 62 pages.)
- Book 3 contains core column information. (Dates: 03/1967 to 09/1969, Approx. 137 pages.)
- Book 4 contains exterior wall information floor 9 to floor 110. (Dates: 04/1967 to 10/1972, Approx. 1,080 pages.)
- Book 5 contains the beam schedule. (Dates: 05/1967 to 08/1969, Approx. 292 pages.)
- Book 6 contains connection details and core bracing. (Dates: 08/1967 to 05/1969, Approx. 1,060 pages.)

- Book 7 contains truss floor panel information. (Dates: 10/1967 to 07/1969, Approx. 345 pages.)
- Book 8 contains concrete notes and details. (Dates: 03/1968 to 07/1974, Approx. 926 pages.)
- Book 9 contains roof area column splice details. (Dates: 05/1970 to 04/1971, Approx. 440 pages.)
- Book 18 contains strap anchor and core truss seat information. (Dates: 10/1968 to 11/1969, Approx. 219 pages.)
- Book 19 contains revisions after fabrication. (Dates: 08/1968 to 05/1975, Approx. 374 pages.)
- Book 20 contains structural steel details. (Dates: 07/1968 to 03/1971, Approx. 41 pages.)
- Book D contains damper details. (Dates: 03/1969 to 09/1971, Approx. 43 pages.)

Books 10, 11, 12, and 13 contain information on the sub-grade structure. Books 14, 15, 16, and 17 were never used in the original design documents.

Until fabrication was begun, the drawings and drawing books listed above (with the exception of Book 19) were modified in keeping with requests for changes by contractor(s) and early tenant modifications. The drawings were modified up until such time as the fabrication of elements commenced. At that time, Book 19 was introduced. It contained the information regarding 'revisions after fabrication'.

Leslie E. Robertson Associates, R.L.L.P. (LERA) believes that the original structural drawings represent significantly accurate 'as-built' drawings for the towers. As tenant modification requests became large in scope, they became separate projects (e.g., the Fiduciary Trust Vault Project, see Sec. 2.5.2). Tenant structural modifications designed by LERA were then documented in a single book of quarter-size plans, referred to as the 'WTC Tenant Structural Modifications Book.' Later tenant modifications were mostly archived on a job-by-job basis without a central accounting for all the changes. In some instances (e.g., additions to the mechanical levels) modifications were made by The Port Authority of New York and New Jersey (PANYNJ) Engineering. In other instances, tenant modifications, such as adding floor openings, were made by other engineers. In these instances, LERA does not have record of the work completed. These modifications were considered to not significantly affect the member properties pertaining to the reference structural models and were not included in the WTC structural databases.

The few modifications made by LERA to the components compiled in the WTC structural databases that have an effect on the global behavior of the towers are listed in Table 2–1.

Drawing Book 19 has records of other modifications to structural elements of the WTC towers that were viewed as non-essential for the development of the reference models of the towers and as such were not included in the structural databases. These modifications are outlined in Appendix B.

Table 2–1. Modifications to members of the WTC database (WTC-DB).

Item	Description	Tower	Element	Floor	Element Effected	WTC-DB Modified	Archived
1	Core column reinforcing	WTC 1 and WTC 2	Numerous	98–106	Core columns	Book 3	Book 19
2	Fiduciary Bank Vault	WTC 2	Col. 508B and Col. 1008B	45–97	Core columns	Book 3	LERA P209
3	Bombing of 26 February 1993 repair	WTC 1	Col. 324, bracing G313A and G304A	B-2 level	Perimeter column and bracing	NA	LERA P1003118
4	EXCO stair	WTC 1	Col. 901A	26	Core column	NA	LERA P1003249

2.3 OVERVIEW OF THE WTC STRUCTURAL DATABASE (WTC-DB)

The original WTC design documents were devised to limit the need for repetition in documenting the data shared between different elements with similar characteristics. The drawing book schedules refer to subsequent tables for information common to several lines of the same schedule. In an effort to minimize the amount of repeated information, and thereby, the data checking of the digital WTC-DB, the drawing book data within the databases were linked in a similar manner. In order to accurately follow the original flow of the drawing book links, flowcharts of the drawing books to be digitized were developed. These flowcharts were used to organize the links of the digitized data within the relational database. The flowcharts are illustrated in Appendix C. An example of such flowcharts for Drawing Book 3 (core columns) is shown in Fig. 2–1.

The WTC-DB contained the computer and hand-tabulated data for the major structural components from original Drawing Books 1 through 5, including exterior walls, core columns, and beam schedule for the towers. Where information from Drawing Books 1 through 5 was modified by Drawing Book 19 and would affect the towers' modeling, the information was included in the database. In addition, some information from Drawing Book 6 (core bracing schedule) and Drawing Book 9 (beams in the hat truss region) was included in the database files as it was utilized in the finite element modeling of the towers.

The drawing book tables were first digitized and stored in Microsoft Excel format files. The Excel files included several worksheets that described the evolution of the data from the drawing book to the final database format, as well as additional information and notes for interpreting the data. Refer to Appendix D for the list of Excel format files.

The WTC relational database linked the Excel files and allowed users to view and select data through query commands. The primary benefit of the relational database format was the ability to programmatically query the database for data required in assembling the structural models of the towers. The query routine allowed multiple users the ability to review, extract, and export the basic data in any required form. The data can be manipulated using Structured Query Language (SQL) according to the desired output, for example the structure of the user's finite element model input file.

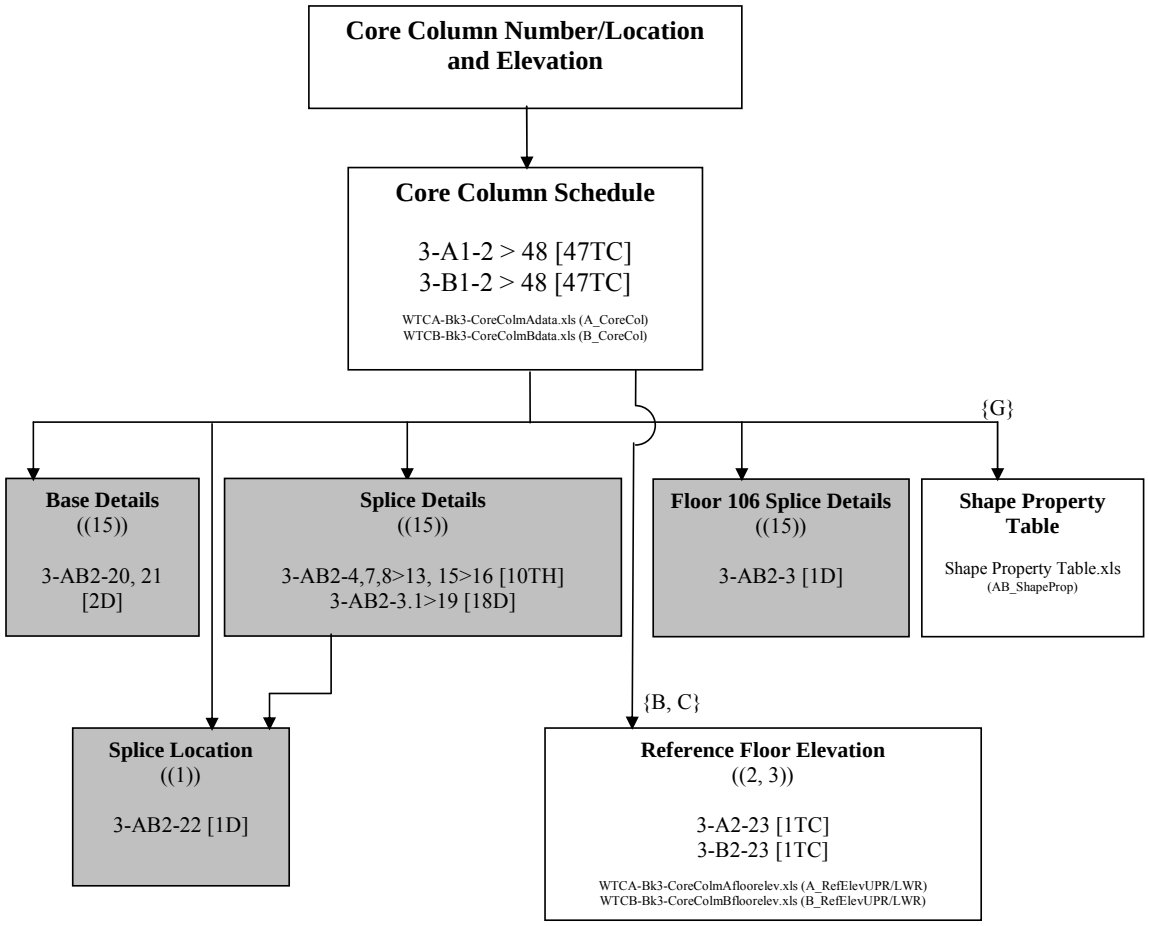

NOTES:
1. 4-AB-* Denotes Drawing Book 4, Tower A , B or AB, and page number
2. [*TC] Number of pages and type, where page types include:
   TC - Computer generated tables; TH - Hand written tables; D - Diagrams
3. *.xls Excel spreadsheet file name; (AB_***) database heading
4. ((*)) Reference note key from original Drawing Book information table.
5. {*} Relational database link (i.e. Excel column number) from previous *.xls file.
6. Figures of columns and panels are shown from inside of building looking out, unless otherwise noted.

Figure 2–1. Drawing Book 3 flowchart: WTC 1 and WTC 2 core columns, foundation to floor 106.

2.4 METHODOLOGY FOR THE WTC-DB DEVELOPMENT

2.4.1 Data Entry

The tabulated portions of WTC Drawing Books 1, 2, 3, 4, 5, 6, and 9 were first scanned and stored in Tagged Image File Format (TIFF) image files. The image files containing the tabulated information were then opened in an Optical Character Recognition (OCR) program that converted the information into a text file. The OCR program was modified to allow for the filtration of unnecessary characters during the document conversion process. In other words, the user could direct the program to block specific characters that were not on the actual page. As an example, if after reviewing a table, one recognizes that

axes, where applicable. The Section Designer function of SAP2000 Version 8 (SAP2000 2002) was used to calculate the cross section properties since it outlines the development of the models and enables the program to perform more precise code checks, as the dimensions of each plate element that was part of the section would be inputted in the finite element model.

The current rolled shape database in SAP2000 represents the modern day rolling practices. The rolled shapes used in the construction of the WTC towers were from a different era and, thus, had different properties in comparison to present day shapes. Therefore, a rolled shape database consistent with the time of construction was developed. See Sec. 2.6.5 for further discussion about the rolled shape database.

2.4.4 Relational Database Development

As discussed earlier, the original WTC drawing books were designed to avoid repeating identical information. The drawing book schedules, therefore, refer to other tables for information common to several lines of the same schedule. In keeping with the nature of the original drawing books and to minimize the data in the digital WTC-DB, the drawing book and section property data were linked using Microsoft Access.

The assembly of the relational database began with the mapping of the original WTC drawing book into flowcharts (see Fig. 2–1). The digitized drawing book data with the corresponding cross sectional member properties from the Excel-format files were then imported into the Microsoft Access database program and partitioned into tables. The tables were then joined using the links cataloged in the flowcharts. These tables were developed to provide the input files for the finite element modeling of the towers as illustrated in Chapter 3. The general Microsoft Access database files are listed in Appendix E. The relational database is described in the tutorial included in Appendix F.

2.5 MODIFICATIONS TO DATABASE ELEMENTS

Most original members and elements defined within the WTC-DB could be fully defined by the original data in the drawing books. As outlined in Table 2–1, however, some modifications were made, and these are described in the following sections. Of the items outlined in Table 2–1, items 1 and 2 were included within the database.

2.5.1 Core Column Reinforcing at Floors 98 to 106

A number of core columns in both WTC 1 and WTC 2 were reinforced at floors 98 to 106. Book 19,

The reinforcing plate data were tabulated and incorporated into the database in the same manner as the plates discussed in the previous section, except that a second length designation was added to differentiate the length of the plates on the north and south faces of the columns, i.e., the column designation "LN" refers to the length of the plates on the north face of the column. Again, when calculating the built-up column properties, the plate was assumed to be continuous along the floor-to-floor height of the column. When the length of the reinforcing plate shown in the drawing was greater than the floor height, the plate was attributed to the two column segments. Where the plate extended over the entire height of the segment, the length was tabulated as the height of the column segment. The remaining length of plate was attributed to the other column segment.

2.5.3 Repair Due to the Bombing of February 26, 1993

The 1993 bombing resulted in structural damage to WTC 1, centered at exterior column 324 (south wall), B-2 level. The face of the column toward the explosion was slightly bowed, and the splice in the column developed a hairline crack. The column was reinforced locally to account for the loss of steel area. The bracing on either side was replaced with equivalent sections and attached in a similar manner as the originals. No modification to the WTC-DB was made for this repair.

2.5.4 Tenant Alteration for an Interoffice Stair

A tenant alteration was provided for an interoffice stair between floors 25 and 26 in WTC 1. This work, adjacent to core column 901A, was performed by an engineering firm (other than LERA) and unknowingly resulted in the loss of a core column bracing strap (refer to Fig. 2–3), leaving the column unbraced about its minor axis for two stories. The PANYNJ alerted LERA to the issue, and asked LERA for a review. LERA found the column stability to be adequate. No modification to the WTC-DB has been made for this modification. The effect of removing the strap is accounted for in the global model of WTC 1; see Sec. 3.2.3.

2.5.5 Drawing Book Data Discrepancies

In the original WTC drawing book data, the following discrepancies were discovered by LERA:

- Book 1, page 1–B–15. For member number G311A, the inch portion of the length is listed as 3-1/18. Based on the comparison with similar bracing types in the area, this dimension was modified to be 3-1/8 in. in the WTC-DB.

- Book 3, page 3–A1–10. For core column 601A between floors 86 to 89 and 89 to 92, the column type is listed as 213. Type 213 is a column type which by definition has reinforcing plates, but for this location no plate data were provided in the schedule. This, in combination with comparisons with similar columns in plan, led to modifying the column type to 111. This also applies to column 601B, page 3–B1–10 between floors 86 to 89 and 89 to 92.

- Book 3, page 3–B1–48. For column 1008B between floors 63 to 66, the yield strength, F_y, is listed as 6 ksi in the table. Based on the yield strength of the columns above and below these floors, the yield strength was modified to be 36 ksi. For the same column number and floor segments, the lower splice detail number is listed as " 01G." Based on the lower splice detail

number of the columns above and below these floors, the number was modified to be "301G."

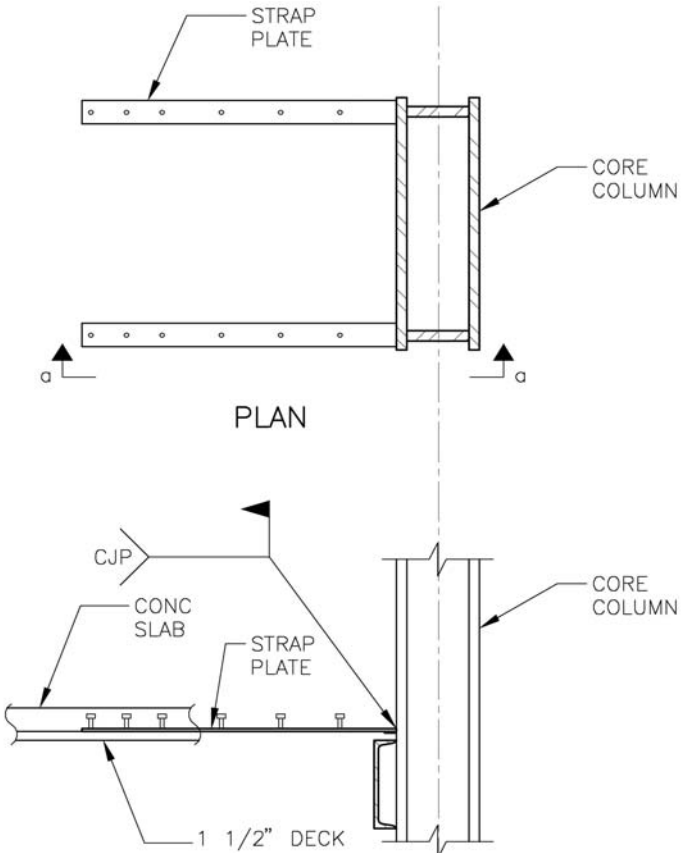

Source: Reproduced with permission of The Port Authority of New York and New Jersey. Enhanced by NIST.

Figure 2–3. Column section at original column strap detail (taken from drawing book 18, page 18–AB2–12).

- Book 3, page 3–B1–9. For core column 508B between floors 21 to 24, the length of plate 1, *W1*, is tabulated as 11.25 in. However, length *B* for this column is 22 in. and thickness *t2* is 5.5 in. *W1* equals *B* minus two times *t2* (see Fig. 2–4). Hence, assuming *t2* was listed correctly in the table, *W1* was modified to be 11 in.

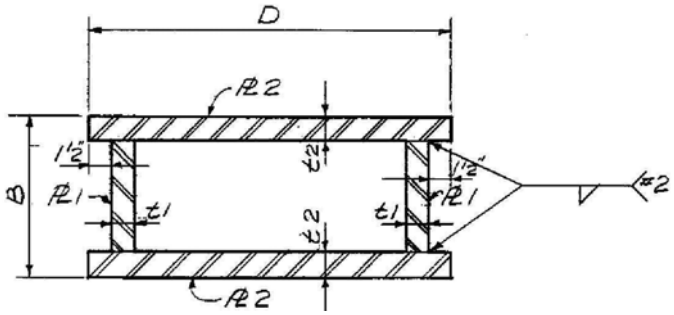

Source: Reproduced with permission of The Port Authority of New York and New Jersey. Enhanced by NIST.

Figure 2–4. Core column series 300.

- Book 1, page 1–B–23 and 1–B2–19. The details for column types 1024, 1025, 5024, and 6025 listed in the tables are not explicitly shown in the drawing book. For these members, column shapes were assumed to be as shown in the typical details in page 1–B–19 for the 1000 series columns, 1–B–24 for the 5000 series column, and the 1–B–27 for the 6000 series column.

- Book 3, page 3–AB2–6. The column type 216 does not appear to be assigned to any member in the drawing book.

2.6 SECTION PROPERTY CALCULATIONS

SAP2000 *Section Designer* was typically used to calculate section properties for built-up sections. The sections were "built-up" within SAP2000 by defining plate dimensions and offsets from 0-0 location. Section orientations were defined with the X-X axis horizontal to the bottom of the original drawing book page as the detail is shown in the drawing book.

During the process of calculating properties there was an exception to this orientation rule. Core column members CC1007A104L, CC1002A104L, CC703A106L, CC1007B104L, CC1002B104L, and CC703B106L consist of a wide flange shape and web reinforcing plates. These members were input into SAP2000 rotated 90 degrees from the orientation shown in the details to utilize the default orientation of the wide flange section in *Section Designer*. Once the properties were calculated, the sections were placed in the WTC-DB following the orientation of the detail (i.e., the axis was shifted back 90 degrees).

When rolled shapes were used to create built-up sections, the rolled shapes database developed for this analysis was used to build the sections in SAP2000 *Section Designer* as explained in Section 2.6.5. The 200 series core columns (wide flange rolled columns reinforced with plates) are examples of members whose properties were calculated in this manner.

2.6.1 Member Designations

For member section property calculations and assembly of the finite element models, the members were named using the following general member designations. The member designations are listed in the Microsoft Excel files.

First character:

- Book 1—below tree–B

- Book 2—exterior wall tree–T

- Book 3—core columns–C

- Book 4—exterior columns and spandrels–E

Second character:

- C—column
- S—spandrel and below grade exterior wall spandrel, strut, or bracing

Third to fifth character: (third to sixth character for 4 digit column e.g., 1004)

- Column number

Sixth character:

- A—WTC 1
- B—WTC 2

Seventh character and above:

- Upper splice level—for core columns
- U (upper), M (middle), or L (lower)—column segment where reinforcing plates are added
- T or B—top or bottom of nonprismatic columns
- Detail letter (lowercase)—(where more than one section is calculated)
- F or C—face or center of nonprismatic spandrel
- Elevation—below tree spandrel elevations

2.6.2 Column Member Multiple Section Property Calculation

In the database, the following three types of column members had different cross sections along the length of the members:

- Exterior wall tree at level C in Drawing Book 2 (two different cross sections)
- Exterior wall tree at level E in Drawing Book 2 (three different cross sections)
- Exterior column type 300 (floor 9 to 106) in Drawing Book 4 (two different cross sections)

For these three member types, the section properties of the different cross sections were calculated and listed in the database tables. In an effort to minimize repeated information, the raw input data for all sections were only shown in the rows that corresponded to the first cross section. For the second and third (if any) cross sections, the calculated data followed in the rows below. The constant raw data such as the column number were not repeated in these rows of the table, and thus, the corresponding cells were left blank. Since the column number was used as a link for the development of the relational database, only the row containing the raw input data and the first cross section properties were returned in a query,

and thus, the user must refer back to the Microsoft Access 'Tables' for the remaining section property information. The section names of the different cross sections along the member length were distinguished by the last one to two characters, which identified the cross sections where the section properties were calculated.

For example, exterior column EC339 (mechanical floors) tapers over a portion of the length of the member (refer to Fig. 2–5). The section properties above and below the spandrel were calculated. The column section above the spandrel was called EC339, while the column section below the spandrel was called EC339cc. The suffix 'cc' denoted the section below the spandrel. Note that the raw dimensional data for EC339cc were not shown in the table, as the information was the same as for EC339.

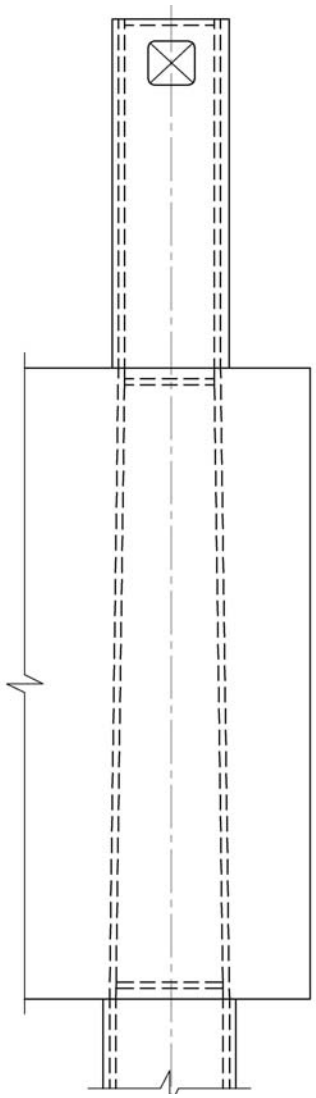

Source: Reproduced with permission of The Port Authority of New York and New Jersey. Enhanced by NIST.

Figure 2–5. Exterior column type 300, floor 9 to floor 106 (taken from drawing book 4, page 4–AB2–18).

2.6.3 Spandrel Member Multiple Section Property Calculation

In the database, the exterior columns below elevation 363 ft in column series 5000, 6000, and 7000 in Drawing Book 1 had corresponding spandrels shown in the details in Book 1. There were two types of spandrels for these members, tapered built-up box shapes and built-up I shapes. For the tapered built-up box shapes, the section properties of the different cross sections were calculated and listed in the database tables. The data were listed in the database files as described for columns with multiple cross sections. The section names of the different spandrel cross sections along the member length were distinguished by the last three to four characters, which identified the cross sections where the section properties were calculated.

For these exterior columns, there were spandrels at two elevations, 332 ft and 350 ft (see Fig. 2–6). At elevation 350 ft, the spandrels tapered, and as a result two cross section properties were calculated. The first section was at the face of the exterior column, and the corresponding section name had a Suffix F (face). The second section was at the center of the spandrel between two exterior columns, and the corresponding section name had a Suffix C (center). The elevations and locations of the cross sections of the spandrels were shown in the figures in the "Cross Section" worksheets in the database Excel files.

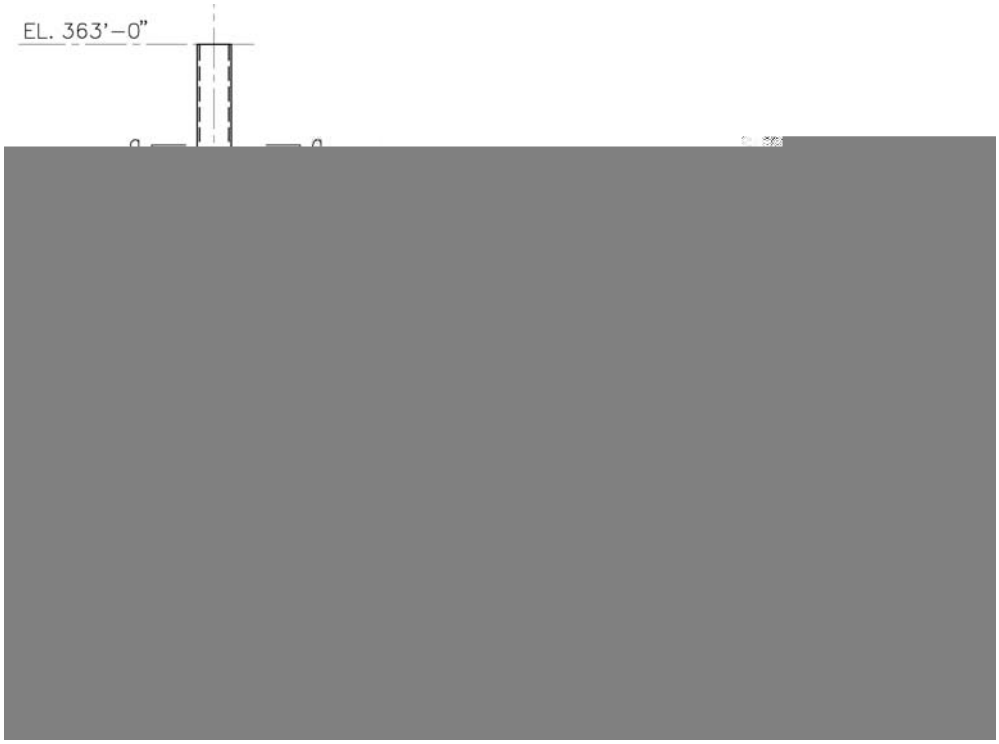

Source: Reproduced with permission of The Port Authority of New York and New Jersey. Enhanced by NIST.

Figure 2–6. Column type 6000 with tapered spandrel (taken from drawing book 1, pages 1–A2–27 and 28).

For example, four different section properties were calculated for exterior column 6009 in WTC 1. The first section was the exterior column itself, and the section name was BC6009A. The other three sections, BS6009AB332, BS6009AT350C, and BS6009AT350F were for the spandrel sections. The suffix B332 in BS6009AB332 denoted the bottom spandrel at elevation 332 ft. Suffixes T350C and T350F in

BS6009AT350C and BS6009AT350F, respectively, denoted the top spandrel at elevation 350 ft, and the "C" or "F" identified the location where the section properties were calculated, see Fig. 2–6.

2.6.4 Section Property Calculation Comparisons

For all the members whose section properties were included in the GFI database, the cross sectional properties in the GFI data were compared with the data contained within the WTC-DB. Most section property results differed between the GFI and the WTC-DB by no more than 1 percent. It was found that results from the calculations of the torsional constant, *J*, however, did vary. LERA in-house programs were then used to confirm the accuracy of the *J* calculation. For core columns in WTC 1, SAP2000 generated values used in the WTC-DB were on average 8 percent larger than *J* values calculated using the LERA in-house program, while the results provided by the GFI database were on average 13 percent greater than LERA in-house program *J* calculations.

The approximate equation used to calculate *J* values by the LERA in-house program for a built-up column or box section as shown in Fig. 2–7 is as follows:

$$J = \frac{2(bh)^2}{\frac{b}{t_f} + \frac{h}{t_w}} \qquad \text{(Eq. 2–1)}$$

It was found that for box sections, *J* values calculated by the above equation matched the *J* values given by SAP2000 *Tube Section*. However, for the same tube section, the *J* values given by SAP2000 *Section Designer* were greater than *J* given by SAP2000 *Tube Section*, even while all other properties were equivalent. According to Computers and Structures, Inc., the developer of SAP2000; the *J* values given by SAP2000 *Section Designer* are more accurate as SAP2000 *Section Designer* uses a finite element method to calculate the *J* values, while an approximate equation is used in SAP2000 *Tube Section*.

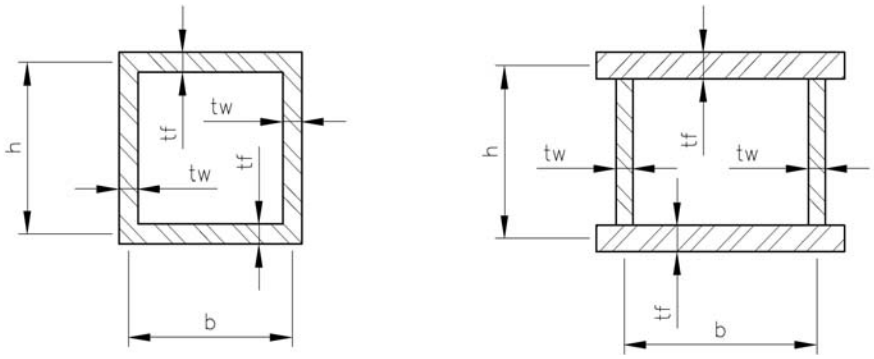

Figure 2–7. Box section and a built-up column.

In order to minimize the complexity of the model, where the member cross-section was of the type illustrated in Fig. 2–7 (a), box column members were defined in SAP2000 *Tube Section*. The remaining built-up box columns (similar to Fig. 2–7 b) were defined in SAP2000 *Section Designer*.

For members whose properties were not given in the GFI database, hand calculations or calculations by LERA in-house program were carried out to verify the results from SAP2000 *Section Designer* for at least one section for each member type.

In summary, it was found that SAP2000 *Section Designer* provided section properties in close agreement with calculated properties. In most cases these properties also closely matched with the properties listed in the GFI database. In the cases where SAP2000 results disagreed with the GFI database, the results were reviewed, and it was concluded that the SAP2000 calculation provided the correct properties. Therefore, the section property results calculated using SAP2000 were used in the WTC-DB and the development of the finite element models of the towers.

2.6.5 Rolled Shape Database

While the majority of the primary members of the WTC towers' super-structure were built-up members, rolled shapes were also used. The rolled shapes specified in the drawings in a number of cases are no longer produced and, consequently, are not included in the rolled shape database embedded within SAP2000. Therefore, a rolled shape database was developed using the old nomenclature and section properties. The result was a file named 'Shape Property Table.xls.' The file contains three worksheets: 'Database,' 'Excel Format,' and 'WF Shape Properties from SAP.' The following is a discussion of their contents.

Data contained in 'Database' and 'Excel Format'—Drawing Books 3, 4, and 5 include reference to specific rolled shapes. The referenced shape names were extracted from these books and assembled into a single reference database for rolled shapes. Most of the section properties were obtained from the Manual of Steel Construction, American Institute of Steel Construction (AISC), Sixth Edition, 1963 (AISC 6th Edition) with few exceptions where cross sections were not included in this edition. Examples of these exceptions include the following:

- Section properties of 14WF455 to 14WF730 were obtained from the Manual of Steel Construction–Load and Resistance Factor Design, American Institute of Steel Construction, Third Edition, 2001 (AISC-LRFD 3rd Edition).

- Section properties of 6CH12, 6CH15.1, 12CH40, 12CH45, and 12CH50 were obtained from the MC-shapes table in the AISC-LRFD 3rd Edition.

- Section properties of 18WF69 were obtained from the Iron and Steel Beams 1873 to 1952, the American Institute of Steel Construction, 1968. 16WF342 was assumed to have the same section properties of 16H342 tabulated in Iron and Steel Beams 1873 to 1952, the American Institute of Steel Construction, 1968.

- For 7x5 tube, Z_x, Z_y, and J were obtained from the AISC- Allowable Stress Design (ASD), 1989, 9th Edition.

- For 2L 3 1/2 in. × 3 in. × 1/2 in. long leg back to back, the combined properties were taken from SAP's embedded rolled shape database.

Data contained in 'WF Shape Properties from SAP'—For the rolled wide flange shapes, an additional database was created in SAP2000 based on the tabulated shape dimensions from the AISC Manuals as discussed above. Computers and Structures, Inc. provided an Microsoft Excel file named 'Proper.xls' with a macro that allowed the accurate calculation of the section properties for use within SAP2000. This information was then used by SAP2000 *Section Designer* to calculate section properties for built-up members comprised of wide flange sections and added plates.

For calculation of the properties with 'Proper.xls,' dimensions of the webs and flanges, as well as the size of the fillet, were input into the spreadsheet. The macro then calculated the section properties based on the input information. The results were shown to be in good agreement with the original tabulated properties.

2.7 SUMMARY

This chapter described the development of the electronic structural databases for the primary structural components of the WTC towers. These databases were developed from original computer printouts of the structural design documents, including modifications made after construction. The databases were generated for use in the development of the reference structural models of the towers.

The structural databases contained the computer and hand-tabulated data for the primary structural components of the towers from the original Drawing Books 1 through 5, including exterior walls, core columns, and beam schedule. In addition, some information from Drawing Book 6 (core bracing schedule) and Drawing Book 9 (beams in the hat truss region) were included in the database files as they were utilized in the modeling of the towers. Modifications to the towers that were implemented in the databases included strengthening of a number of core columns at floors 98 to 106 of both towers and reinforcing of two corner core columns at floors 45 to 97 of WTC 2 due to the construction of a concrete vault at floor 97.

The steps that were undertaken to develop the structural databases included: (1) the scanning and digitization of the original drawing books, (2) a four-step quality control procedure, (3) cross section property calculations, and (4) the development of the relational databases to link the generated database files into a format suitable for the development of the structural models.

Chapter 3
DEVELOPMENT OF REFERENCE STRUCTURAL MODELS FOR THE WTC TOWERS

3.1 INTRODUCTION

The objective of this chapter is to outline the development of the reference structural analysis models that capture the intended behavior of each of the two towers. The models were used to establish the baseline performance of the towers under gravity and wind loads. They also served as a reference for more detailed models used for other phases of the National Institute of Standards and Technology (NIST) Investigation, including aircraft impact analysis and thermal-structural response and collapse initiation analysis.

Included in this chapter are descriptions of the reference structural models, the modeling techniques, the parametric studies utilized in the development of the models, and the methodology used to export to the models the requisite data from the relational database (see Chapter 2). The main types of models developed are as follows:

- Two global models of the major structural components and systems for the towers, one each for World Trade Center (WTC) 1 and WTC 2.
- One model each of the typical truss-framed floor and typical beam-framed floor (mechanical level) within the impact and fire regions.

All models are linearly elastic and three-dimensional, and were developed using the Computers and Structures, Inc. SAP2000 Software, Version 8 (SAP2000 2002).

Section 3.2 describes the development, contents, and verification of the global models of WTC 1 and WTC 2. Sections 3.3 and 3.4 present the models for the typical truss-framed floor and beam-framed floor, respectively. Section 3.5 describes the parametric studies that were undertaken to facilitate the development of the global models. Section 3.6 presents a summary of the chapter.

3.2 GLOBAL MODELS OF THE TOWERS

A three-dimensional structural analysis computer model of the 110-story above-grade structure and 6-story below-grade structure for each of the two towers was developed. The global models for the towers consisted of the major structural components and systems required to establish the baseline performance of the towers under gravity and wind loads. In establishing the modeling techniques for the global models, parametric studies were performed to evaluate the behavior of typical portions of the structure and develop simplified models that could be implemented in the global models (see Sec. 3.5).

3.2.1 Components and Systems in the Towers' Global Models

The models included all primary structural elements in the towers, including exterior columns, interior (core) columns, exterior wall bracing in the basement floors, core bracing at the mechanical floors, core bracing at the main lobby atrium levels, spandrel beams, hat trusses, and rigid and flexible diaphragms representing the floor systems, as developed in Sec. 3.5 of this report. While the global models did not include the structural dampers in floor systems (see Secs. 3.3 and 3.4), the effect of the dampers on the wind load stresses is accounted for in the determination of equivalent static wind loads using a total damping ratio of 2.5 percent (see Chapter 4).

3.2.2 Coordinate System, Nomenclature, and Models Assembly Overview

The large amount of data required to assemble the tower models dictated that the relational database capability of the WTC-DB be used (see Sec. 2.4.4). The methodology for the development of the models using the relational database is described in this section.

Coordinate System—The coordinate system for the model geometry was based on the column layout from the original drawings. Figure 3–1 shows the location of the X and Y axes for the global models and the floor models. The Z coordinates were based on actual elevations of the towers. The original column numbers were used throughout the models for member identification.

Nomenclature—A standard nomenclature for joints, frame names, and section names for use in the models was established. The nomenclature enables the user to know quickly where in the building a section is located by viewing any given piece of the model. Joint names generally included the column number, tower letter, and floor level. Frame element names generally included the joint name at the 'j' end (second node). Section names were based on the section as described in the drawing book, and were repeated for each steel yield strength assigned for that section. Alternatively, where the section was unique to a particular member in the building, sections were named based on the frame member.

As an example, most nodes (or joints) in the tower models were named according to the following format:

- Column number
- Tower letter (A for WTC 1 and B for WTC 2)
- Floor level
- S for column splice nodes only
- J for spandrel splice nodes only

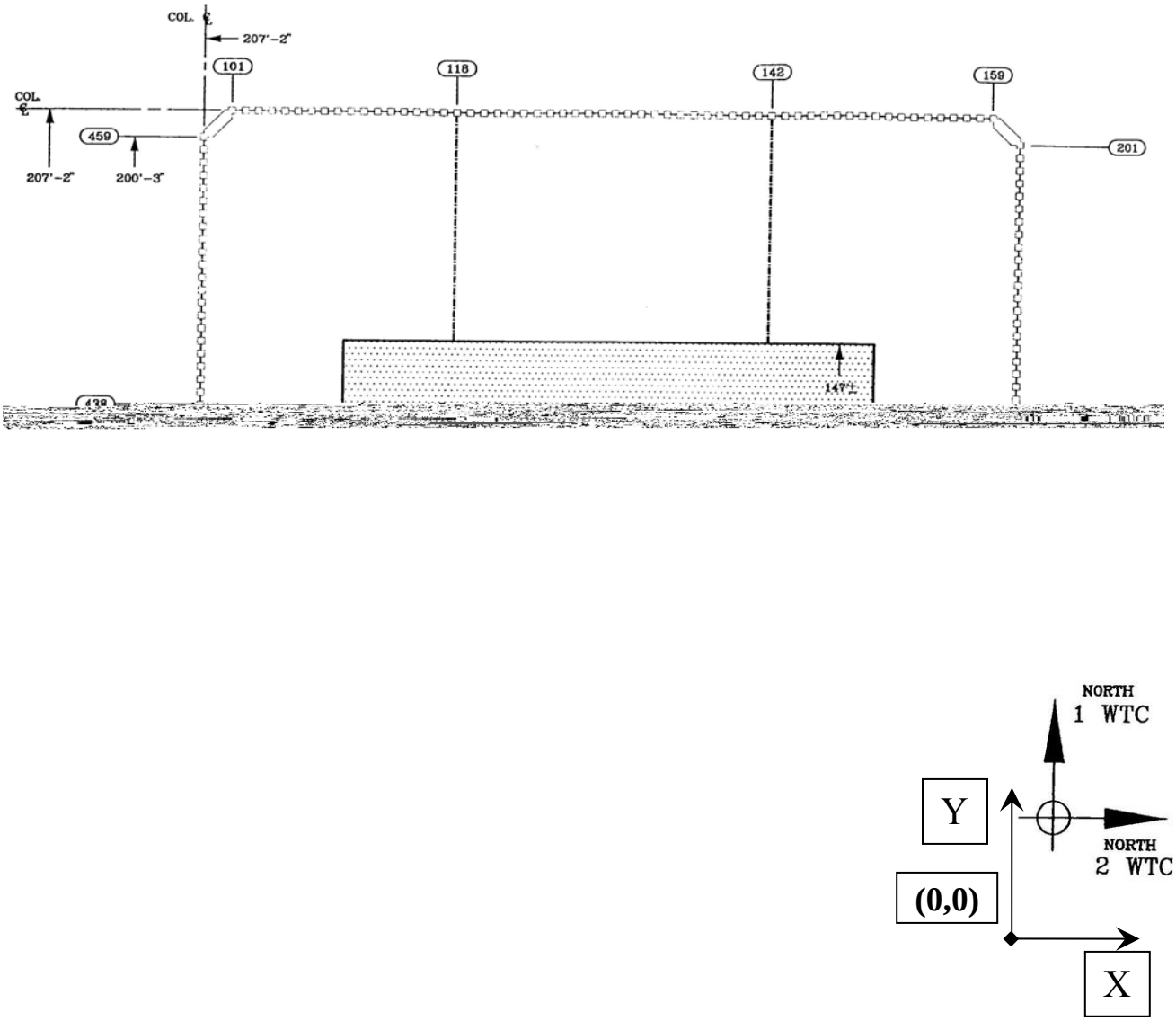

Source: Reproduced with permission from The Port Authority of New York and New Jersey. Enhanced by NIST.

Figure 3–1. Global model coordinate axis location.

Figure 3–2 illustrates the detailed frame and joint nomenclature for a typical exterior wall panel.

Model Assembly Overview—An overview of the assembly of the data into the tower model is described herein along with an expanded section on the programmatic assembly of the models.

Following a basic study of modeling techniques and testing of SAP2000, Version 8 input format and capabilities, it was determined that the best approach was to divide the model into six main parts and then assemble them into a unified model. Manipulation of these individual parts was more efficient than attempting to build the whole model simultaneously.

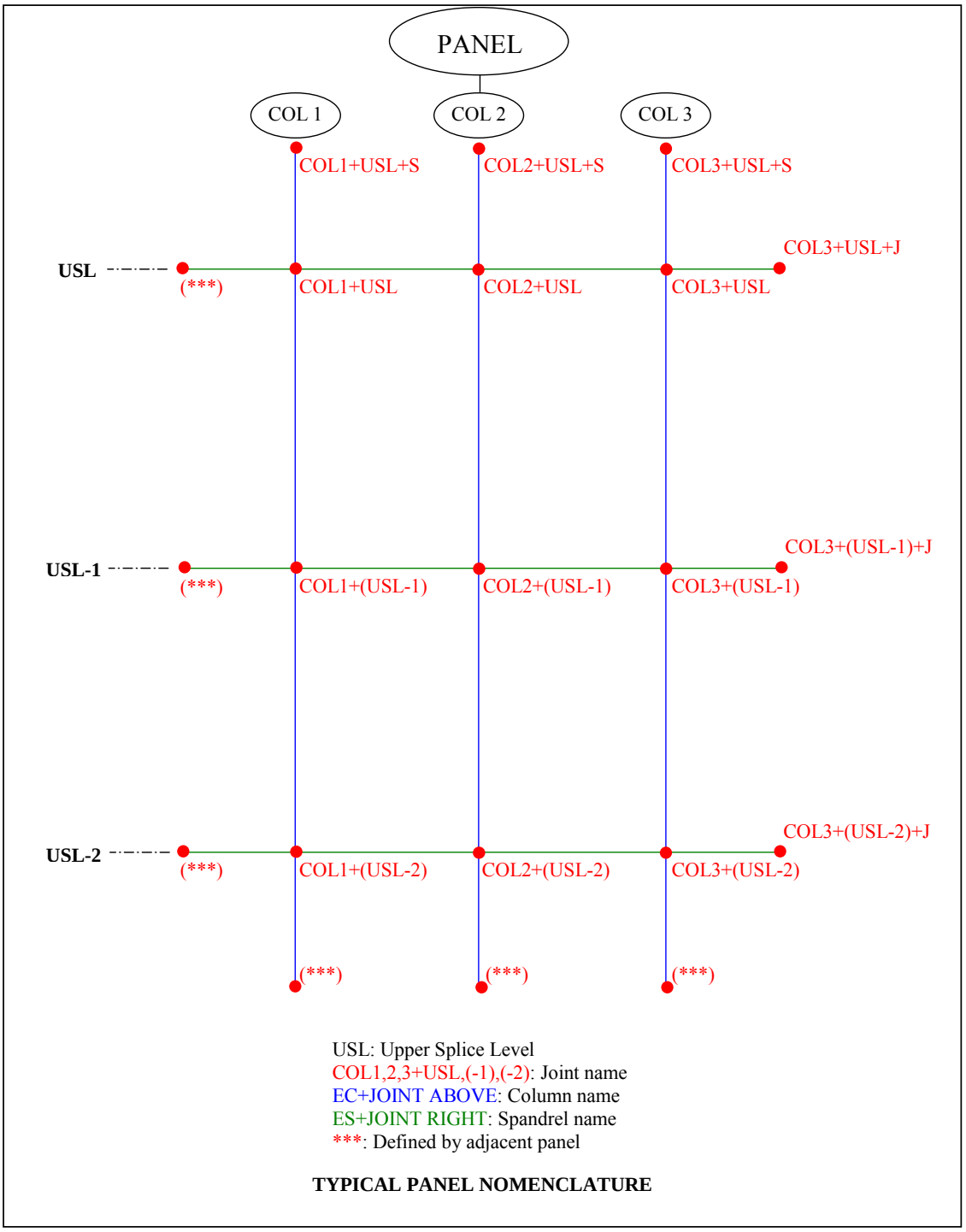

Figure 3–2. Typical exterior panel nomenclature.

The six initial models were:

- Core columns
- Exterior wall, foundation to floor 4
- Exterior wall trees (floors 4 to 9)
- Exterior wall, floors 9 to 106
- Exterior wall, floors 107 to 110
- Hat truss

For the core columns and exterior walls at floors 9 to 106, most of the analysis input files were generated from queries of the WTC-DB. The other four parts of the model were assembled primarily in a more conventional manner.

Core columns and exterior wall panels (floors 9 to 106) were the greatest data-intensive challenges in the model development. Both parts included a large number of frame members and section and material property variations. The query files were used to gather the necessary data, and then simple computer programming was used to convert the data into the SAP2000 input file format. Four main input tables for the SAP2000 input file were developed programmatically:

- Joint coordinates table
- Connectivity-frame/cable table
- Frame section properties tables
  - Frame section properties 1—general
  - Frame section properties 5—non-prismatic
  - Section designer properties 04—shape I/wide flange
  - Section designer properties 05—shape channel
  - Section designer properties 11—shape plate
- Frame assignments table
- Gravity and wind load assignments

The remaining data were added directly in the SAP2000 model:

- Material properties
- Frame local axis

- Joint restraint
- Insertion point
- Constraint

After the joint coordinates, connectivity, frame section properties, and frame assignments were complete for the six parts, the individual models were combined into a unified model. Rigid floor diaphragms, flexible floor diaphragms, core bracings, gravity loads, wind loads, and masses were then added to the unified model. After assembly of the model, the assignment of properties for selected model elements was spot-checked, and the model was executed to verify its performance.

The development of the WTC 1 and WTC 2 models were separate and consecutive endeavors. The lessons learned in the assembly of the WTC 1 model were applied to the development of the WTC 2 model. While there were only minor differences in the basic structural systems of the two towers, there were significant differences in section and material properties, and additional column transfers at the lower levels in WTC 2.

Isometric views of the complete WTC 1 model are shown in Fig. 3–3. Elevations of the complete WTC 2 model are shown in Fig. 3–4. A summary of the size of the global models of WTC 1 and WTC 2 is presented in Table 3–1. The following presents the details of each of the six parts used in the development of the unified global models for WTC 1 and WTC 2.

3.2.3 Core Columns Modeling

Core column coordinates were tabulated based on the structural drawings. Column locations were typically referenced at their centerlines. Columns on lines 500 and 1000, however, were located in plan drawings along most of their height according to the face of the column to which the floor trusses frame (i.e., WTC 1 north face for 500 columns and south face for 1000 columns). The centerline of these columns was based on their dimensions given in the drawing books. Where these column centerlines varied along the height of the towers (typically 1 1/2 in. between three-story pieces), a representative location was chosen to define the column node. Thus, the column coordinate at floor 106 was used as a constant along the tower height because at this level, these columns aligned with the hat truss above. Offsets were not used to shift the column locations because the floor framing needed to equilibrate such offsets was not included in the model.

The spandrel centerline elevation was selected as the representative floor elevation for exterior columns and used also for core columns. If there were no spandrels in exterior panels, reference elevations were used for the core columns. The reference elevations were defined in the original drawings and corresponded to the elevations of the top of the concrete floor.

There were over 5,000 nodes in the core column model. This amount of data required that the *Interactive Database* input table of SAP2000 be set up using a macro. These data were converted to text file format and later imported into SAP. Built-up sections were defined as *Section Designer* sections, and wide flange shapes were defined directly from "SectionWF1.pro" file (see Sec. 2.6.5). All section names were identical to those in the database. Around 1,280 *Section Designer* sections were defined in this model and imported through the *Interactive Database* function of SAP2000 to the model.

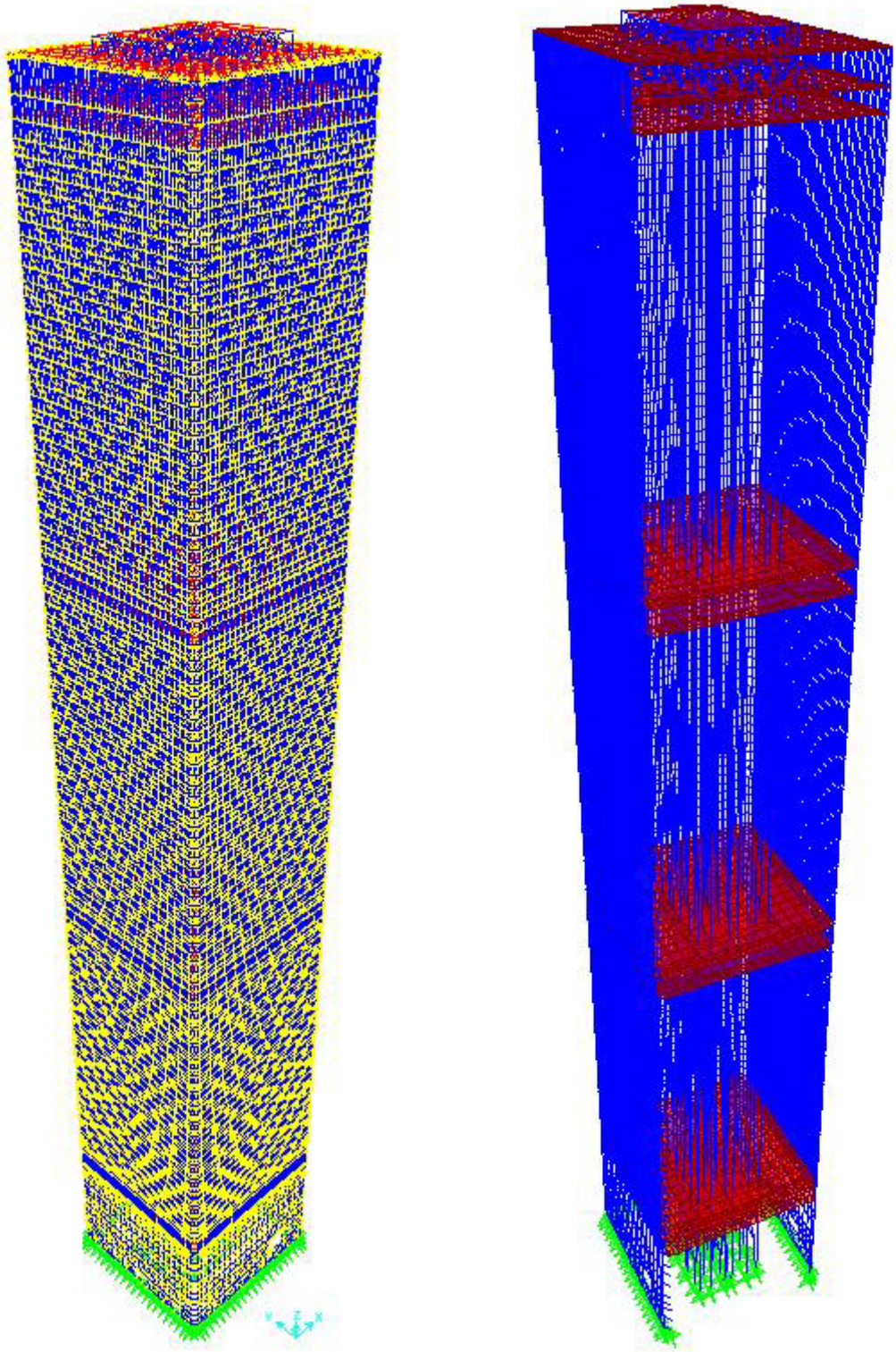

Figure 3–3. Rendered isometric views of the WTC 1 model.

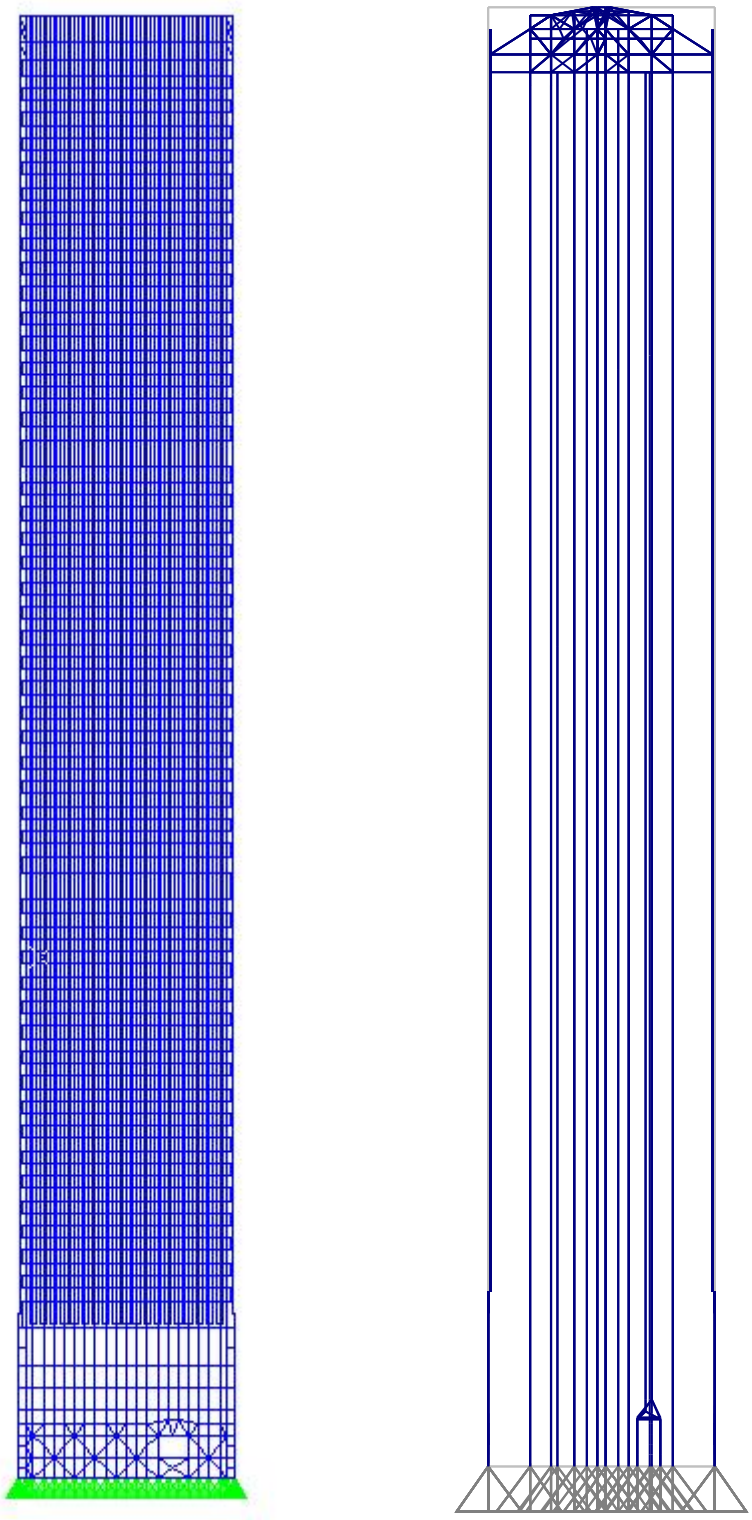

Figure 3–4. Frame view of the WTC 2 model: exterior wall elevation and interior section illustrating the core columns, core bracing, and hat truss.

Table 3–1. Approximate size of the reference structural models (rounded).

Model	Number of Joints	Degrees of Freedom	Number of Frame Elements	Number of Shell Elements	Total Number of Elements
WTC 1 global model[a]	53,700	218,700	73,900	10,000	83,900
WTC 2 global model[a]	51,200	200,000	73,700	4,800	78,500
Typical truss-framed model	28,100	166,000	27,700	14,800	42,500
Typical beam-framed model	6,500	35,700	7,500	4,600	12,100

a. Model does not include floors except for flexible diaphragms at 17 floors as explained later.

The core columns were defined as frame members spanning from node to node at the representative floor elevations. Splices in core columns occurred typically 3 ft above the floor level. In the models, however, the splice was considered to occur at the floor level, and nodes were only defined at these levels (i.e., typically at spandrel centerlines). Most three-story column pieces were unique, as tabulated in the WTC-DB (Drawing Book 3). A section for each three-story piece was defined and then assigned to each of the three frame members that made up that column. Using the SAP2000 shading feature to graphically show the section on the model, each frame was rotated to its proper orientation based on the structural drawings.

In the as-designed drawings, there were strap anchors connecting the core columns to the concrete floor slab to provide lateral bracing for the column. At floor 26 of WTC 1, the straps at column 901 were removed during a renovation project that was engineered by a firm other than Leslie E. Robertson Associates, R.L.L.P. (see Sec. 2.5.4). The loss of the straps at this location was included in the model by releasing the column from the diaphragm in the direction of the straps.

3.2.4 Exterior Wall, Foundation to Floor 4 Modeling

The models of the exterior wall up to elevation 363 ft were developed manually, assigning joints and members connectivity as shown in the drawings. The elevation drawings show that below elevation 363 ft, columns were typically spaced at 10 ft and braced with spandrels and diagonals. Joints were defined at all locations where diagonals braced the columns. However, when coordinates were not given in the drawings, joint coordinates were determined based on the geometry of the diagonal. Details in WTC Drawing Book 1 show that the column-diagonal intersections had continuity. Joints at elevation 253 ft (level B-5) were defined only where the diagonals connect to the columns, since the tower floor did not frame into the exterior spandrels at that floor.

Where noted in elevation drawings, spandrel centerline elevations were used to define joint coordinates. Additionally, joints were defined at the spandrel splice midway between two columns at elevation 350 ft 3 in. (floor 3) and at elevation 329 ft 3 in. (floor 2) to allow for section type transitions.

The majority of the elements at these levels were defined as *Section Designer* sections, except for box shapes, which were defined as "Box/Tube." Channel shapes were defined directly from the "SectionWF1.pro" file (see Sec. 2.6.5). All section names were identical to those in the database. Around 200 sections were defined in this model using the *Interactive Database* function of SAP2000, which was used to import data into the model.

Typical columns were connected from bottom to top, and typical spandrels were connected from left to right. The SAP2000 program allows assignment of rigid zone factors to frame end offsets to account for the overlap of cross sections. At the intersection of columns and spandrels, 100 percent rigidity for the column and the spandrels were assigned due to the large size of both columns and spandrels. Using the SAP2000 shading feature to graphically show the section on the model, each frame was rotated to its proper orientation based on the structural drawings.

Refer to Fig. 3–5 for a frame view and rendered view of the exterior wall (foundation to floor 9) of the WTC 1 model. The figure also shows the core columns and core bracings.

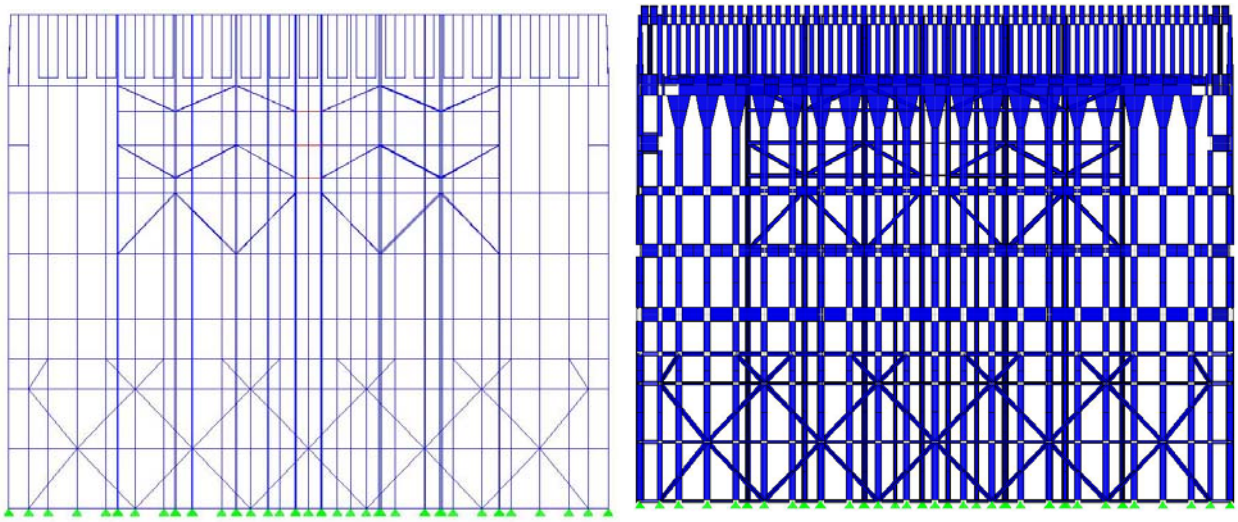

Figure 3–5. Frame view and rendered view of the WTC 1 model (foundation to floor 9).

3.2.5 Exterior Wall Trees (Floor 4 to 9) Modeling

The panels of the exterior wall between elevation 363 ft and elevation 418 ft 11 1/2 in. were called exterior wall trees. At the exterior wall trees, the typical exterior wall columns transitioned from a spacing of 10 ft to a spacing of 3 ft 4 in. A typical exterior wall tree panel is shown in Fig. 3–6, which indicates that each panel was divided into five different levels: B, C, D, E, and F. For each panel in the model, the three exterior columns from above elevation 418 ft 11 1/2 in. continued down to level D. At that level, the three columns were connected by a horizontal rigid element to become one member, which extended down to elevation 363 ft.

In the model, the tree was also the location where the column insertion point transitioned from the inside face (at the spandrel) of the upper column to the centerline of the lower column. Between levels B and D (see Fig. 3–6), the location of the spandrel transitioned from 6 1/2 in. offset from the exterior column reference line to the center of this reference line. Within the floor 9 spandrel, the exterior columns tapered; however, in the model, the tapering of the columns was not included because frame end length offsets were assigned to the columns to account for the rigidity of the spandrels.

Through the height of level C, the box-shaped columns tapered (Fig. 3–6). In the model, non-prismatic members were used to model the tapering columns. The columns started to taper at the bottom of the spandrel at level B, and ceased to taper at the top of the spandrel at level D. The dimensions of the

columns at the spandrel edges were defined in the drawing book. In the model, the column extended from the centerline of the spandrel at level B to 1 ft below the top of the spandrel at level D (see discussion for level D below). Therefore, in order to obtain the correct section properties along the length, the dimensions of the section at the joints were interpolated based on the dimensions of the section at the spandrel edges shown in the drawing book. The section properties of the tapering column were assumed to vary linearly between the two sections. Frame end length offsets were assigned to the columns to account for the rigidity of the spandrel at level B and the one foot dimension at level D.

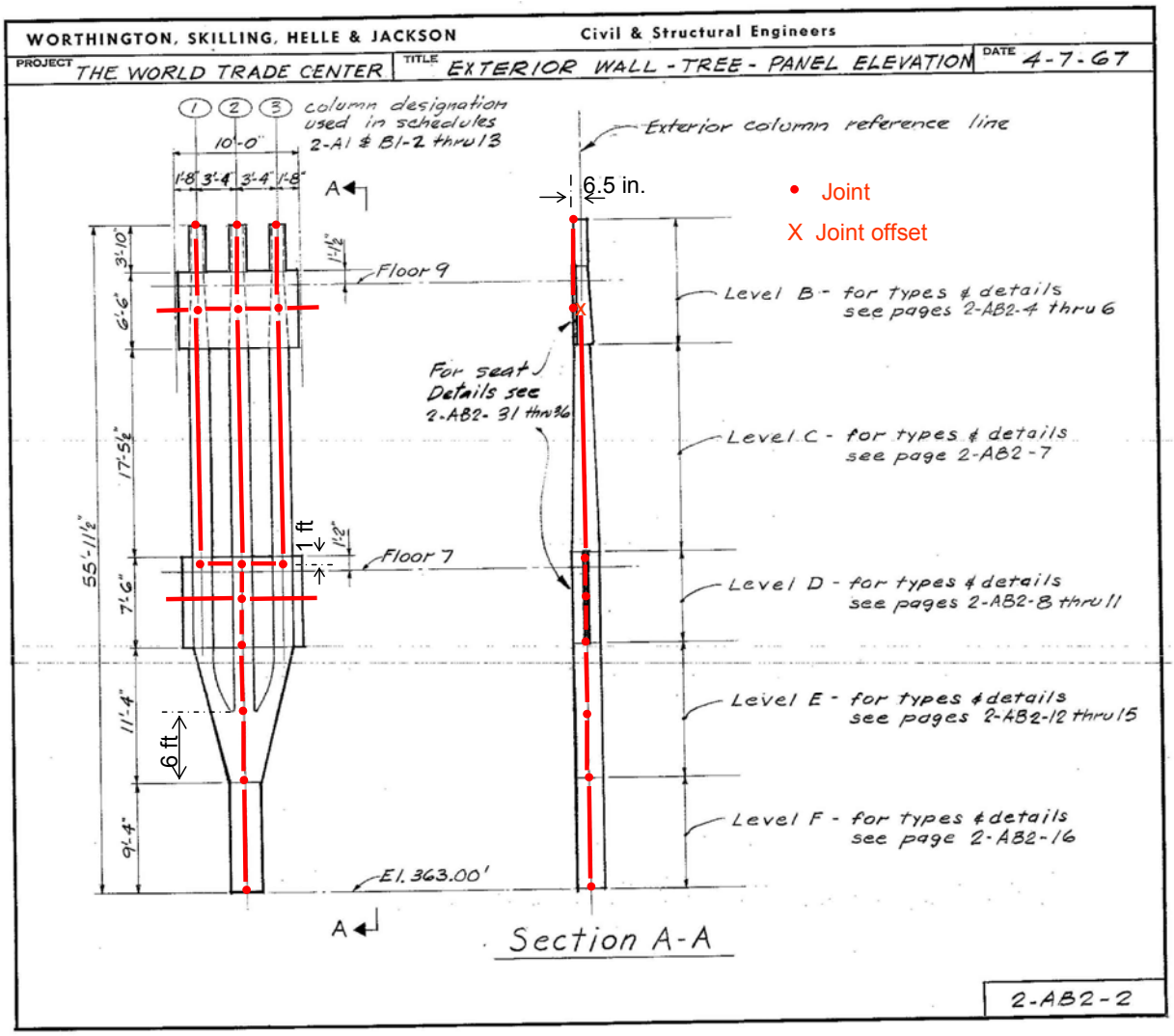

Source: Reproduced with permission of The Port Authority of New York and New Jersey. Enhanced by NIST.

Figure 3–6. Exterior wall tree panel (taken from Drawing Book 2, page 2-AB2-2).

At level D, two transitions occurred in the model. The first transition was for the exterior columns, where the three columns coming down from level C were connected by a horizontal rigid element to become one member at the bottom of the tree. This frame member consisted of the three exterior columns and the spandrel plate. Another horizontal member of the same section properties with the spandrel plate was also defined and connected between the neighboring exterior wall trees. This member connected the neighboring exterior wall trees and provided lateral bracing for the columns. Frame end length offsets

were assigned to the spandrel to account for the overlap of the spandrel plate with the frame member, which also included the spandrel plate. The transition of the three members into one member was assumed to occur at one foot below the top of the spandrel at level D to account for the fact that the spandrel becomes engaged with the exterior columns after being connected to the exterior columns for a certain distance. Hence, the joints were defined at one foot below the top of the spandrel at level D.

There was a second transition at level D (Fig. 3–6). The nodes for the exterior wall columns were typically defined at 6 1/2 in. offset from the exterior column reference line, but for the joints at and below level D in the exterior wall tree, the joint coordinates were defined along the exterior column reference line. As a result, for the column member that framed between the nodes at levels B and D, a rigid joint offset of 6 1/2 in. was assigned at the top of the member using a rigid body constraint, while no offset was assigned at the bottom. Therefore, the column remained a vertically straight element while being connected to nodes that were not aligned vertically.

At level E, the exterior columns tapered and had two different types of cross section (Fig. 3–7). For each panel, the exterior column transitioned from Section b–b in Fig. 3–7 into a box-shaped column (Sec. c–c in Fig. 3–7). The location of the transition between the different types of cross section varied for different column types from 5 ft 8 in. to 6 ft 4 in. measured from the bottom of level E. In the model, the transition was assumed to be at 6 ft measured from the bottom of level E. For each panel, the exterior column at level E was modeled as two non-prismatic members. The top section of the first non-prismatic member consisted of three box-shaped columns and a middle plate, while the bottom section was a box-shaped column (Sec. c–c in Fig. 3–7). The properties were assumed to vary linearly between the two sections. The second non-prismatic member was a tapering box shaped column (Sec. c-c in Fig. 3–7), and again, the properties were assumed to vary linearly between the two sections. At level F, the exterior wall tree columns were prismatic box-shaped columns.

The final model of a typical tree is illustrated in Fig. 3–8.

3.2.6 Exterior Wall (Floor 9 to 106) Modeling

In plan, column and spandrel members connected at nodes located at the outside face of the spandrel, 6 1/2 in. from the exterior column reference line (see Fig. 3–9). The columns were offset horizontally, or ‘inserted,’ at this node using an insertion point located at the centerline of plate 3. Insertion points were not adjusted for spandrel thickness. With this modeling, gravity and wind loads could be applied at the spandrel location.

In elevation, the columns and spandrel members connected at the spandrel centerline, typically 12 1/2 in. below the reference floor elevation (Fig. 3–9). The spandrels were then located correctly without the need for offsets to be defined. The effect of applying loads at both the spandrel centerlines and the reference floor elevations was studied, and it was found that it resulted in a negligible difference in spandrel stresses.

For typical exterior wall panels (i.e., three columns wide by three stories high), nodes at five elevations were defined. The models included nodes at the three representative floor levels (defined at the spandrel centerlines) as well as the upper and lower column splices. Diaphragms were assigned to all nodes at floor levels where concrete slabs existed to represent the high in-plane stiffness of the concrete floor slabs.

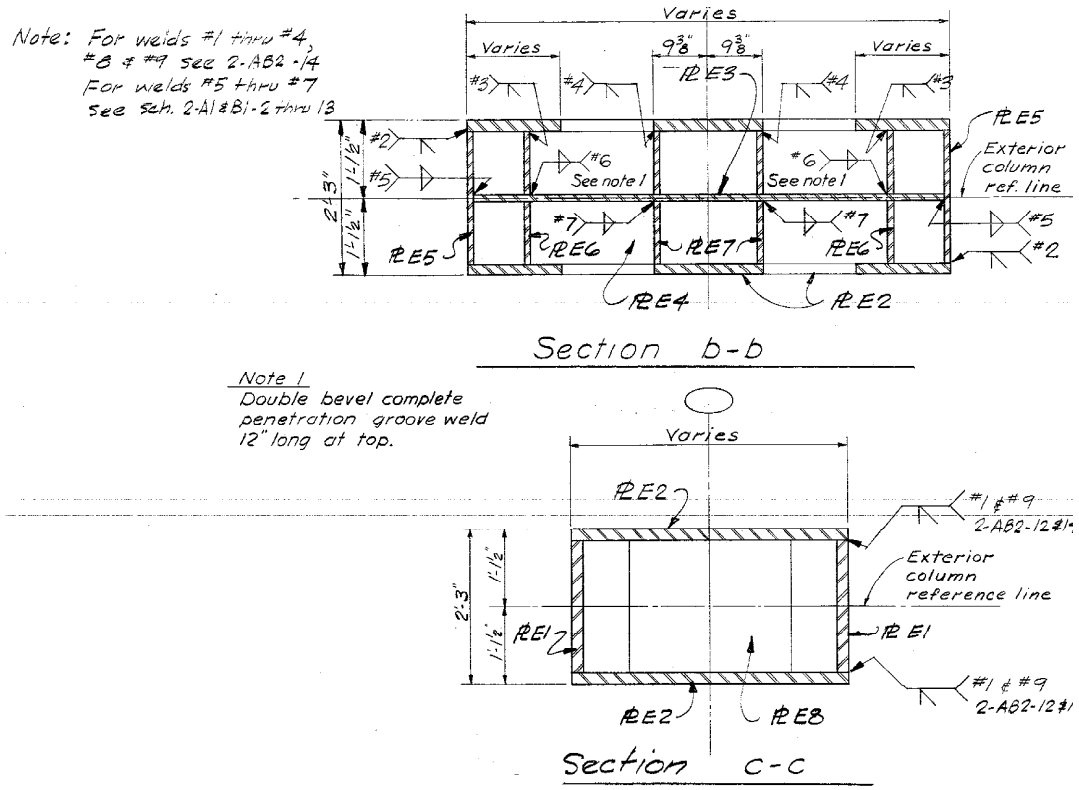

Source: Reproduced with permission of The Port Authority of New York and New Jersey.

Figure 3–7. Exterior wall tree: as-built cross sections for level E (taken from Drawing Book 2, page 2-AB2-13).

Figure 3–8. Frame view and rendered view of an exterior wall tree.

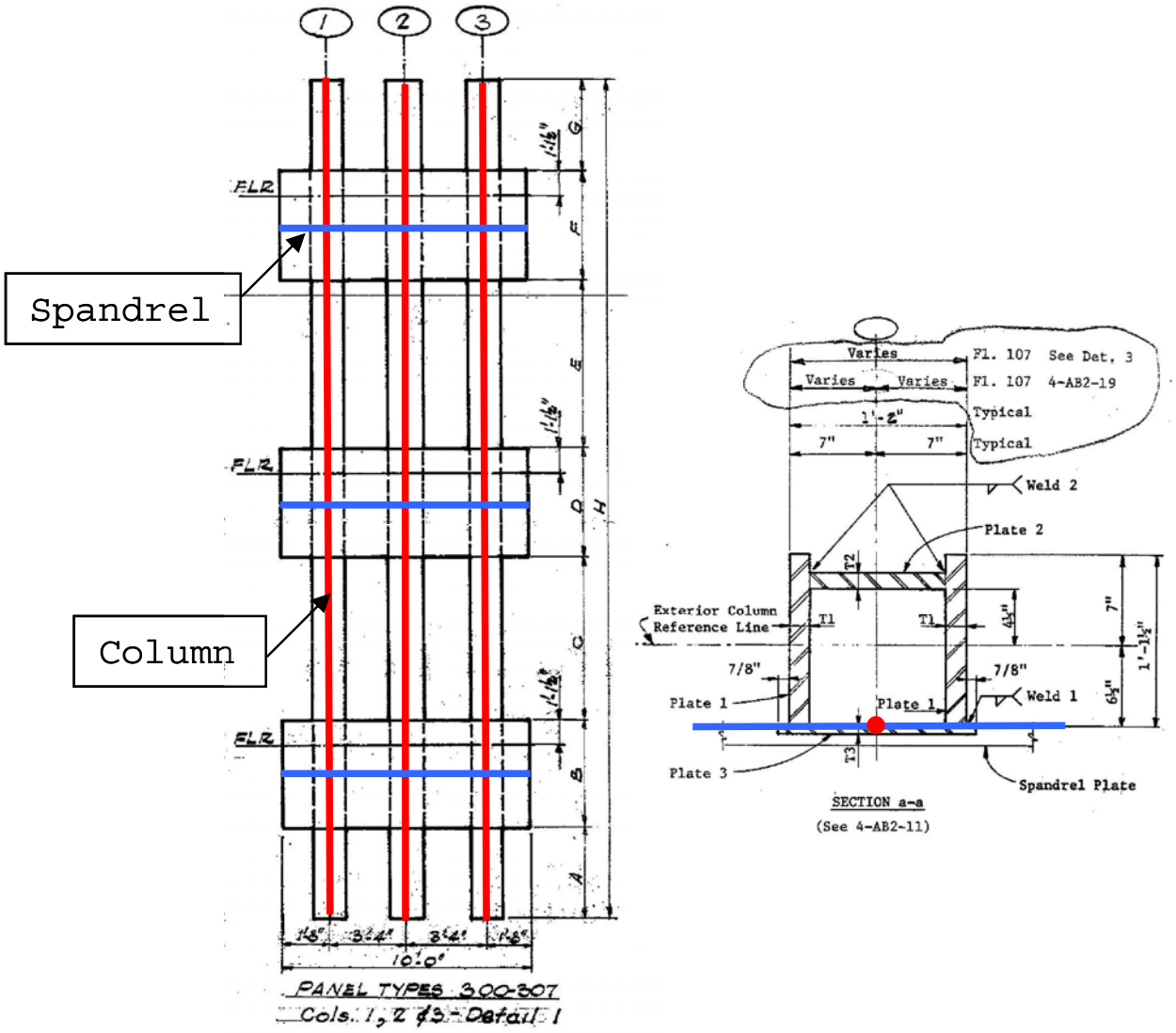

Source: Reproduced with permission of The Port Authority of New York and New Jersey. Enhanced by NIST.

Figure 3–9. Typical WTC tower exterior wall panel.

The SAP2000 program allows assignment of rigid zone factors to frame end offsets to account for the overlap of cross-sections. In the global model, 50 percent rigidity for the column and 100 percent rigidity for the spandrels were assigned for the typical exterior wall panels to match the lateral deflection of the detailed shell model of the panel based on the parametric study results (see Sec. 3.5.1). It was also found that, due to the relatively large depth of the spandrels and the close spacing between the columns, the spandrels contributed to the axial stiffness of the columns in the panels. This contribution was estimated to range from 20 percent to 28 percent increase in the vertical stiffness of the panels. Therefore, a frame property multiplier for the exterior wall column's cross-sectional area was used to provide a 25 percent increase in columns' axial stiffness (see Sec. 3.5.1).

For exterior wall corner panels, 25 percent rigidity for the columns and 50 percent rigidity for the spandrels were assigned based on the parametric study results (see Sec. 3.5.2). Also, an area modifier

was used to provide a 25 percent increase in the axial stiffness of the two continuous columns of the corner panels (Sec. 3.5.2). No modifier was used for the 100, 200, 300, and 400 series intermittent columns.

Exterior column types were defined in Drawing Book 4. A few types (100 series typical, 300 series at mechanical floors, and 400 to 500 series at corners) repeated extensively throughout the towers, with steel yield strengths that varied from 36 ksi to 100 ksi. Since SAP2000 does not allow for the assignment of material properties at the member assignment stage, the number of different steel strengths was determined for each exterior column type, and sections were defined for each. The section name included the section number and the yield strength as tabulated in the drawing books.

Typical spandrels and corner panels were defined as rectangular shape and *Section Designer* section with stiffener, respectively. The top and bottom stiffener of each corner spandrel were included in both the parametric study and the global models. The detail shows that the stiffeners were 6 in. plates of thickness matching plate 2 in the corner column.

3.2.7 Exterior Wall (Floor 107 to 110) Modeling

Spandrel depths varied at floors 108 and 110. A weighted average of spandrel depth was determined in order to define the average centerline elevation of the spandrels and therefore, the node elevation for the entire floor.

For the 7 × 5 structural tube sections that were used in these floors, sections from the current American Institute of Steel Construction (AISC) Manual were assigned, and modification factors of 1.04 were applied to the section properties. The modifiers were used to match the section properties from the 6th Edition AISC Manual.

The exterior wall members from floors 107 to 110 were typically rolled shapes with F_y =42 ksi or F_y =50 ksi. Where not shown in the drawings as F_y =50 ksi, F_y =42 ksi was used.

3.2.8 Hat Truss Modeling

In both WTC 1 and WTC 2, a truss system referred to as a ‘hat truss’ was constructed between floor 107 and the roof. The hat truss system was intended to support the load of the antenna on top of the tower and to interconnect the exterior walls to the core. The hat truss was made up of four trusses spanning perpendicularly to the long direction of the core and four trusses spanning perpendicularly to the short-direction of the core (refer to Figs. 3–10 and 3–11).

Frame members between floors 107 and 110 were assigned to the model according to plan and elevation drawings of the hat truss. Node locations were set to coincide with the centerline of spandrels at the exterior wall. Columns, diagonals, and beams were included in the model. All columns and diagonals shown in drawings SA/B–400 through SA/B-404 were included in the model. Floor beams that did not participate in the hat truss system were not included in the model, unless they were used to transfer truss chords or core columns. Flexible floor diaphragms were used in this area.

Coordinates were generally not given at floor 109, as this level did not contain a complete concrete floor slab. The geometry of the diagonals, columns, and beams was used to determine the location of the node where the diagonal would intersect floor 109. Unless otherwise noted in the drawings, diagonals and

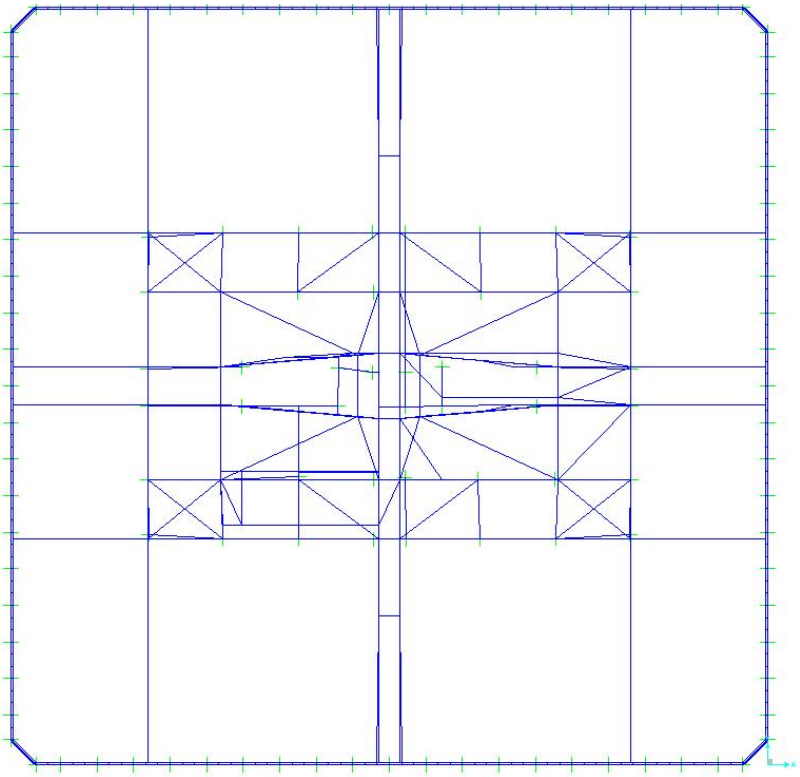

Figure 3–10. As-modeled plan of the WTC 1 hat truss.

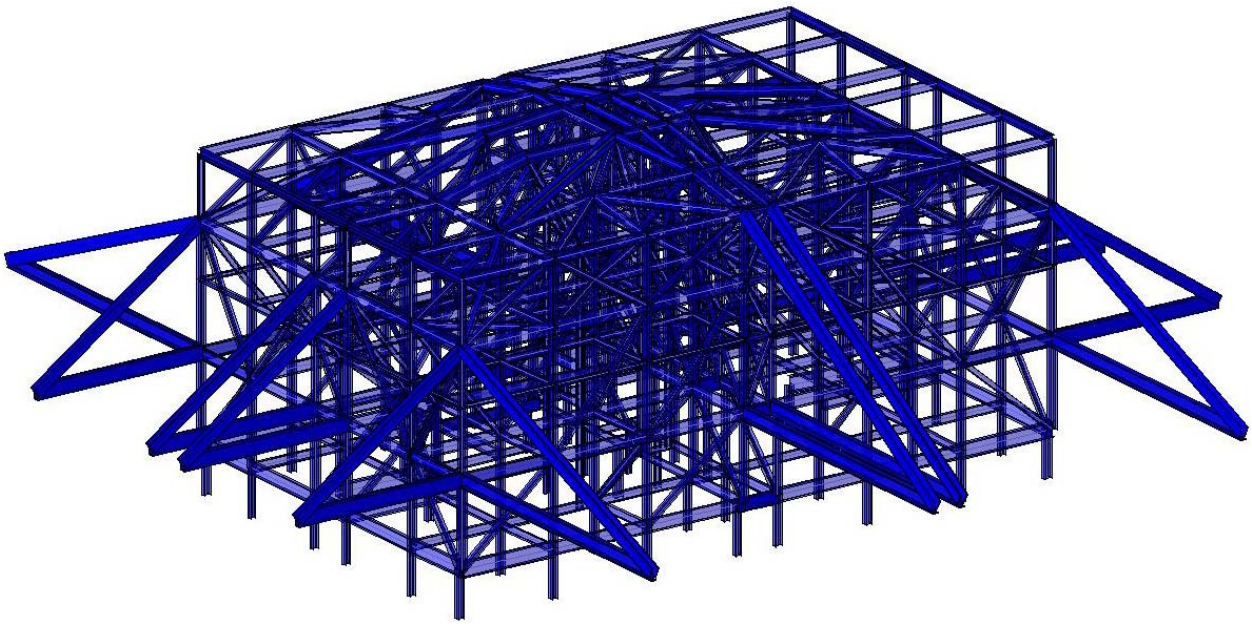

Figure 3–11. Rendered 3–D model of the WTC 1 hat truss (prior to assembly in the unified global model).

columns were assumed to be non-composite, and floor beams were assumed to be composite. Hat truss diagonals, main chords, and main columns were modeled with continuous joints. Hat truss beams, however, had pinned ends.

3.2.9 Flexible and Rigid Floor Diaphragm Modeling

For most floors, rigid diaphragms provide for a sufficiently accurate representation of the flow of forces and deformations for global structural response. This is a customary engineering practice for lateral force analyses. In cases where the flow of forces and deformations would be affected significantly by the use of rigid diaphragms, the floors were modeled as flexible diaphragms.

The floor models described in Secs. 3.3 and 3.4 were used to develop the flexible diaphragm stiffness utilized within the global models. Section 3.5.3 outlines the study for the determination of the in-plane diaphragm stiffness of the detailed floor models, using that in-plane stiffness to arrive at an equivalent shell element floor model. The equivalent shell element floor was used to represent the in-plane floor stiffness in the global model. The shell elements attached to all exterior wall columns and core columns.

Flexible diaphragms were used at the floors of the towers in the core of the atrium area, in the mechanical floors, and in the floors of the hat trusses. The floors modeled using flexible diaphragms were floors 3, 4, 5, 6, 7, 9 (atrium levels); 41, 42, 43, 75, 76, 77 (mechanical levels); 107, 108, 109, 110, and roof (hat truss region) of both towers. For the floors of the hat trusses, the stiffness of the flexible diaphragms was reduced by a factor of twenty, which resulted in diaphragm forces that were consistent with the diaphragm strength. This was done to achieve a reasonable agreement between the as-modeled stiffness of the floor diaphragm and the strength of the diaphragm to resist the forces it attracts. In the case of concrete floor slabs at the top and bottom chords of outrigger trusses or hat trusses, it has been found consistently that floor slabs modeled at nominal uncracked stiffness attract forces completely out of scale with the strength of the slabs. Based on parametric studies for a series of major high rise buildings, it became a customary engineering practice to reduce the stiffness of such floor slabs. This reduction factor was found, based on the parametric studies, to be about twenty. This reduction accounts for cracking and other factors that are consistent with the expected behavior of the floor diaphragms.

3.2.10 Verification of Global Models

Several steps were taken to verify the model input. SAP2000 Version 8 offers a ‘shading’ option once a model has been built with frame section assignments. This allows the user to view the members as the program interpreted their input. The shading option was helpful for using section-designed shapes, and for verifying the orientation (i.e., local axes) of members. Note that shading is not correct when two *Section Designer* sections are used in non-prismatic members, so orientations for these sections were verified by reviewing their local axis member properties. The work was independently reviewed by engineers not associated with the initial model development.

Once the models were completed, checks for gravity and wind loads were performed. The overall performance of the tower models under these loads was found to be reasonable by checking deformations, stresses, reactions, etc.

3.2.11 Results of Modal Analysis

Verification of the global models also included comparing the calculated natural frequencies with frequencies measured from accelerometers placed atop WTC 1. The natural frequencies for WTC 1 and WTC 2 global models were estimated using modal analysis. The mass of the towers was estimated from the construction and superimposed dead loads only (see Chapter 4 for further details). No live loads were used in estimating the floor masses for the modal analysis. The calculated first six periods and frequencies for WTC 1 and WTC 2 are presented in Table 3–2 without P-Δ effects and in Table 3–3 with P-Δ effects. The first three mode shapes are presented in Fig. 3–12.

Table 3–2. Calculated first six periods and frequencies without P-Δ effects for the WTC towers.

Direction of Motion	WTC 1			WTC 2		
	Mode	Frequency (Hz)	Period (s)	Mode	Frequency (Hz)	Period (s)
N–S	1	0.088	11.4	2	0.093	10.7
E–W	2	0.093	10.7	1	0.088	11.4
Torsion	3	0.192	5.2	3	0.192	5.2
N–S	4	0.233	4.3	5	0.263	3.8
E–W	5	0.263	3.8	4	0.238	4.2
Torsion	6	0.417	2.4	6	0.417	2.4

Table 3–3. Calculated first six periods and frequencies with P-Δ effects for the WTC towers.

Direction of Motion	WTC 1			WTC 2		
	Mode	Frequency (Hz)	Period (s)	Mode	Frequency (Hz)	Period (s)
N–S	1	0.083	12.1	2	0.089	11.2
E–W	2	0.088	11.3	1	0.083	12.1
Torsion	3	0.189	5.3	3	0.192	5.2
N–S	4	0.227	4.4	5	0.250	4
E–W	5	0.250	4	4	0.227	4.4
Torsion	8	0.455	2.2	8	0.455	2.2

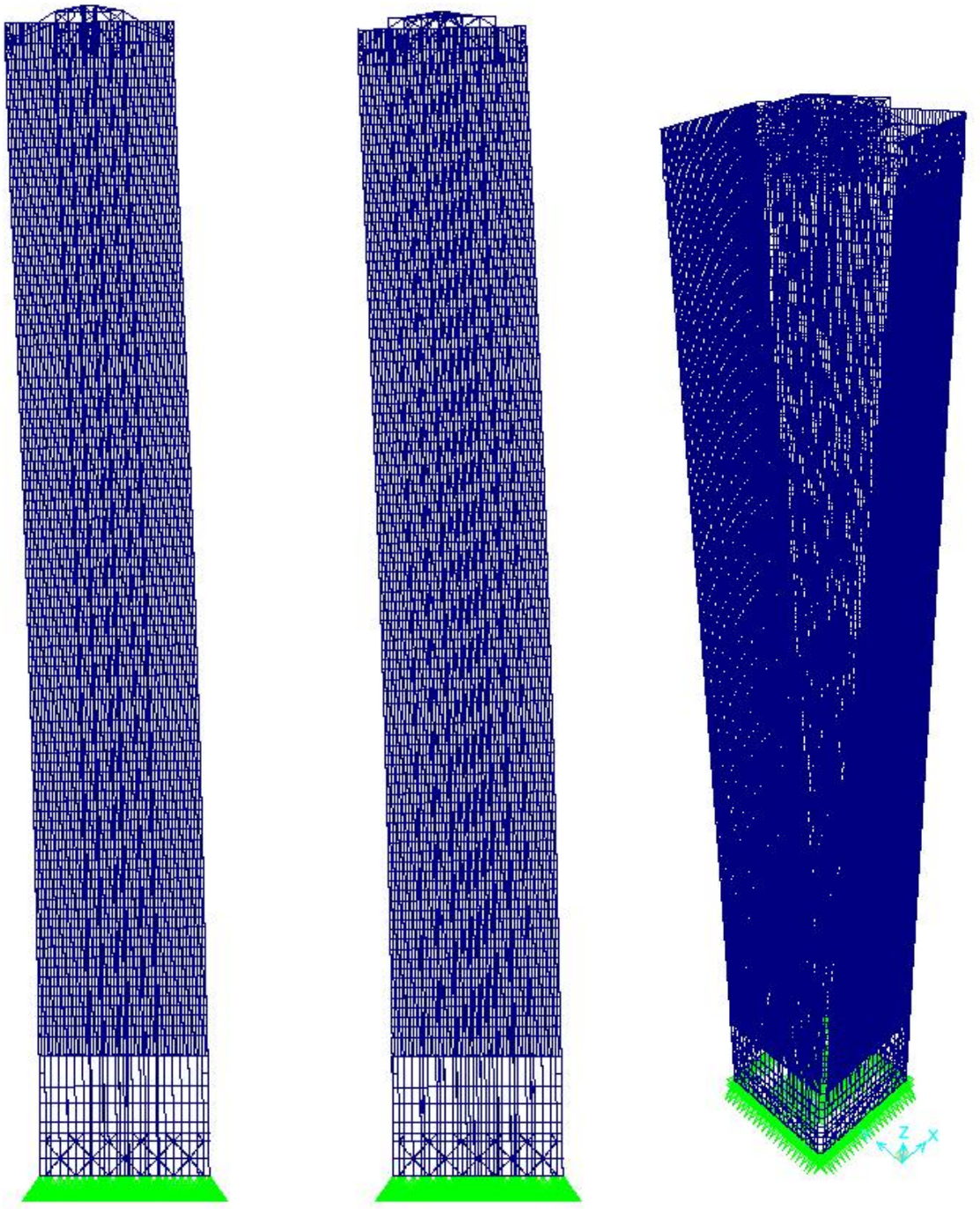

(a) **(b)** **(c)**

Figure 3–12. Mode shapes of WTC 1 (exaggerated): (a) first mode shape (E-W), (b) second mode shape (N-S), (c) Third mode shape (torsion).

Table 3–4 presents a comparison of the calculated first three natural frequencies and periods (N–S direction, E–W direction, and torsion) against measured frequencies and periods obtained from WTC 1 based on analyzing acceleration records obtained from accelerometers installed on the top of WTC 1. The table also includes the values of the natural periods and frequencies predicted in the original design. The table shows good agreement between the calculated and measured periods, especially for the periods estimated without P-Δ effects, thus indicating that the reference global model is a reasonable representation of the actual structure. No measured periods or frequencies were available for WTC 2.

Table 3–4. Comparison of measured and calculated first two natural frequencies and periods for WTC 1.

Data Source/ Event Date	Wind Speed & Direction	Frequency (HZ)			Period (s)		
		Direction of Motion			Direction of Motion		
		N-S	E-W	Torsion	N-S	E-W	Torsion
Historical Data							
October 11, 1978	11.5 mph, E/SE	0.098	0.105	0.211	10.2	9.5	4.7
January 24, 1979	33 mph, E/SE	0.089	0.093	0.203	11.2	10.8	4.9
March 21, 1980	41 mph, E/SE	0.085	0.092	0.201	11.8	10.9	5.0
Decmber 11, 1992	-	0.087	0.092	-	11.5	10.9	-
February 2, 1993[1]	20 mph, NW	0.085	0.093	0.204	11.8	10.8	4.9
March 13, 1993[1]	32 mph, NW	0.085	0.094	0.199	11.8	10.6	5.0
March 10, 1994[1]	14 mph, W	0.094	0.094	0.196	10.6	10.6	5.1
December 25, 1994[2]	N	0.081	0.091	-	12.3	11.0	-
Average of Measured Data							
Average	-	0.088	0.094	0.202	11.4	10.6	4.9
Orginal Design - Predicted Values							
Theoretical Value	-	0.084	0.096	-	11.9	10.4	-
Reference Global Model							
LERA/NIST - WTC 1 without P-Delta		0.088	0.093	0.192	11.4	10.7	5.2
LERA/NIST - WTC 1 with P-Delta		0.083	0.088	0.189	12.1	11.3	5.3

Notes:

[1]Reported frequency value is the average of the SW corner, NE corner and center core frequency measurements.

[2]Reported frequency is based on center core data only.

3.3 TYPICAL TRUSS-FRAMED FLOOR MODEL—FLOOR 96A

In order to select the typical truss-framed floor within the expanded impact and fire zones of both towers, the drawings for floors 80 to 100 were reviewed to identify structural similarities. The summary of this review is provided in Appendix G, which shows a summary of the construction type and space usage for each floor, along with a categorization and description of floor types for both towers. It was found that floor 96 of WTC 1 (96A) represented the typical truss-framed floor in the expanded impact and fire

region for WTC 1 (floors 89A to 103A). The only exception in this region of WTC 1 was floor 92, which had an increased dead load capacity required for the support of secondary water lines.

Floor 96A was also representative of the typical truss-framed floor in the expanded region for WTC 2 (floors 74B–88B). Specifically, floor 96A was similar to the truss framing at floor 74B and floors 84B through 88B. Floors 78B and 79B were sky lobby and upper escalator floors, respectively. Both contained long span trusses, which were similar to floor 96A, but also contained beam-framed floor construction in the entire short span area (where the escalators were located). Floors 80B through 83B had beam framing in place of a single truss panel in the short span area, while the remaining area contained trusses which were similar to floor 96A.

Based on the above analysis, floor 96 of WTC 1 was selected as the overall representative truss-framed floor for the majority of the expanded impact and fire zone in both towers and is described in the following sections (see Fig. 3–13). An isometric view of the typical truss-framed floor model is shown in Fig. 3–14. Table 3–1 includes a summary of the size of the 96A floor model. The following presents the major structural systems and components of the truss-framed floor model.

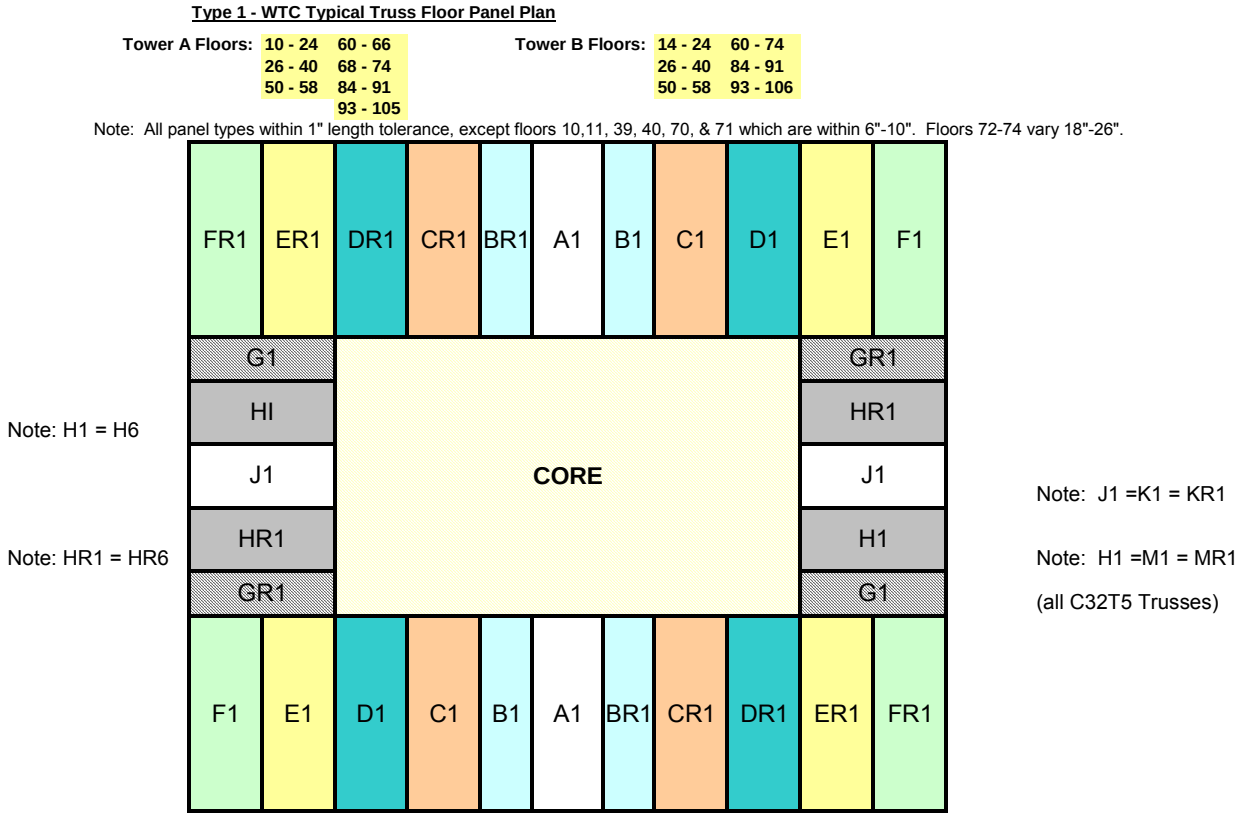

Figure 3–13. Typical truss-framed floor panels arrangement.

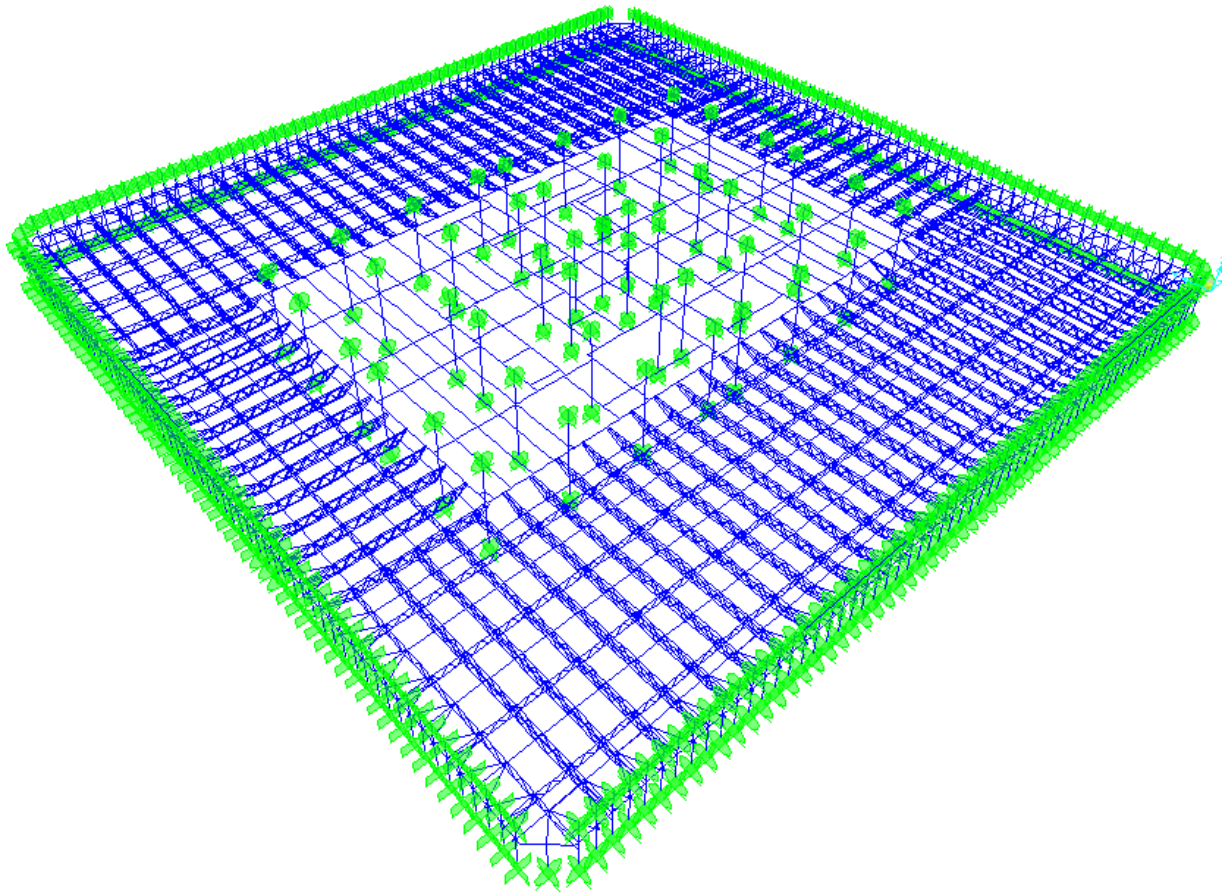

Figure 3–14. Typical truss-framed floor model (floor 96A), slab not shown.

3.3.1 Primary Trusses

The primary trusses consisted of double angle top and bottom chords, which were 29 in. out-to-out of the chords. The trusses acted compositely with a 4 in. concrete slab on 1 1/2 in. metal deck. For a typical long-span truss, C32T1, the top chord consisted of two angles 2 in. by 1.5 in. by 0.25 in., short legs back-to-back (SLB), and the bottom chord consisted of two angles 3 in. by 2 in. by 0.37 in., SLB. The distance between the centroid of the two chords was calculated to be 28.05 in. The distance from the centroid of the top chord to the neutral axis of the transformed composite slab with top chord was calculated to be 1.93 in. The sum of the distances, thus, was 28.05 + 1.93 = 29.98 in. (Fig. 3–15). Dimensions for the short-span trusses were essentially identical to those for the long-span trusses. Therefore, in the model, 30.0 in. was taken as the typical distance between the top and bottom chords for both short- and long-span primary trusses.

In the long-span truss zone, the two individual primary trusses, which were part of the same floor panel and attached to the same column, were separated (typically) by a distance of 7 1/8 in. At the joint between panels, the distance between the abutting long-span trusses was 7 1/2 in. Therefore, in the model, 7 1/2 in. was used as the spacing between all long-span primary trusses. In the short-span truss zone, two individual trusses which attached to the same column were separated by a distance that varied between 4 7/8 in., 5 in., and 5 1/4 in. In the model, the typical spacing between all short-span double

trusses was 5 in. The long span trusses in the two-way zone had an as-modeled length of 58 ft 10 in., while the long span trusses in the one-way zone had an as-modeled length of 59 ft 8 in.

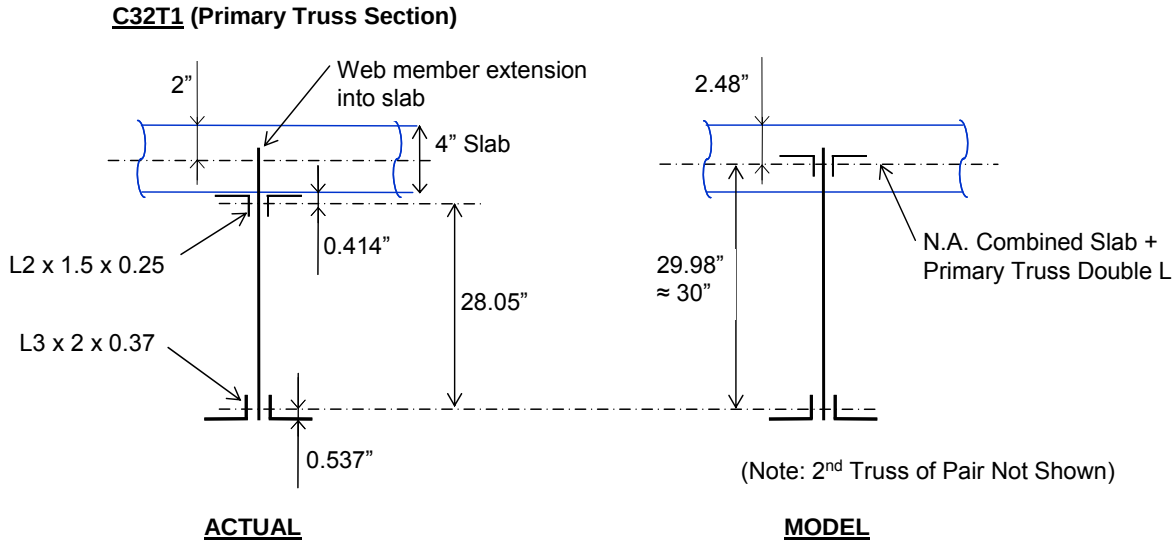

Figure 3–15. Typical primary truss cross-section, as-built and as-modeled transformed truss work points.

The diagonal web bars for the primary trusses were most often 1.09 in. diameter bars. Therefore, for double angle shapes in the primary trusses, 1.09 in. was taken as the distance between the two angles. This holds true for primary trusses where bar diameters varied between 0.92 in. and 1.14 in.

The as-built truss diagonals had end fixity, but were considered pinned for the analysis. Pinning the diagonals is conservative and provides an upper bound of the gravity load stresses. To mitigate the effect of the pinned member approach, end length offsets were used for the truss diagonals to compensate for the difference in the as-built diagonal unbraced length and the model unbraced length. The as-built unbraced length for a typical diagonal in a primary truss was 32.4 in., while the modeled member length was 36.05 in., and therefore, an end offset of 1.8 in. was used at both ends. Similarly, for the bridging trusses, the actual unbraced length for a typical diagonal of a bridging truss was 29 in., while the modeled length was 30.66 in. Therefore, an end offset of 0.83 in. was used at both ends. A rigid zone factor of 100 percent was used for all offset zones.

In the model, the deck support angles, typically 3 in. by 2 in. by 0.75 in. were located in the same plane as the combined truss top chord and composite slab centroid.

3.3.2 Bridging Trusses

The bridging trusses were 24 in. deep, edge-to-edge, with double angle chords. For a typical bridging truss, 24T11, the top and bottom chords consisted of two angles 1.5 in. by 1.25 in. by 0.23 in., SLB. The distance between the centroid of the two chords was 23.26 in. The distance used as the offset between the top and bottom chords for all bridging trusses was taken as 23.25 in. (Fig. 3–16). The distance between the work points of the top chord of the bridging truss and the top chord of the primary trusses and equivalent slab plate for truss 24T11 was calculated to be 3.39 in. This distance was selected for all

bridging trusses to be 3.375 in. As in the as-built structure, the bridging truss was not connected along its length to the slab shell elements in the model. At the intersection of the top chords of the primary and the bridging trusses, the intersection was modeled using vertical rigid links, connected in turn to the slab shell elements representing the concrete slab.

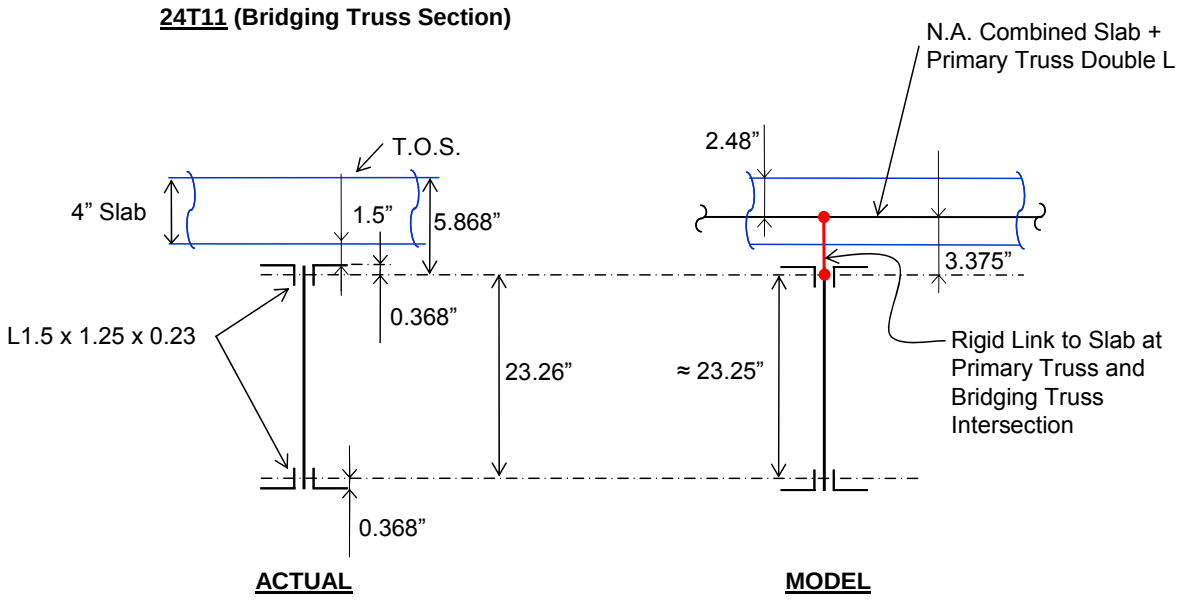

Figure 3–16. Typical bridging truss cross–section, as-built and as-modeled transformed truss work points.

The original contract drawings indicated that the bottom chord of the primary trusses was connected to the bottom chord of the bridging trusses along the length of the primary trusses only on column lines 111, 149, 311, and 349. The connection consisted of double angles 2 in. by 1 1/2 in. by 0.25 in. welded to both primary and bridging truss lower chord members as shown in Fig. 3–17. These connection angles were included in the model. The Laclede (the manufacturer of the floor truss panels) shop drawings indicated that the bottom chords of the primary trusses were similarly connected to the bottom chords of the bridging trusses at all their intersections for construction purposes. These were conservatively not included in the models.

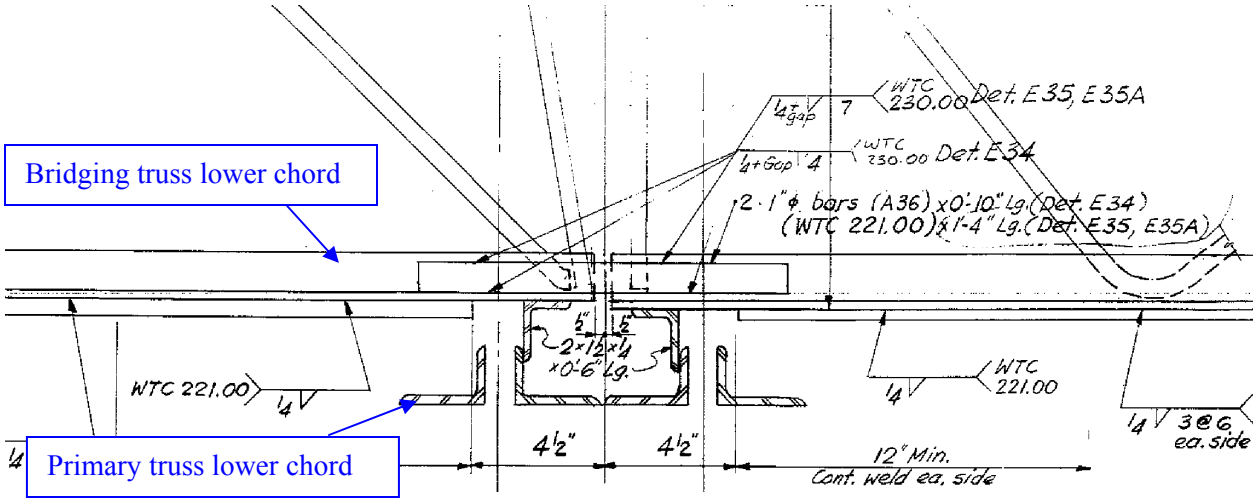

Source: Reproduced with permission of The Port Authority of New York and New Jersey. Enhanced by NIST.

Figure 3–17. Connection between bottom chords of primary and bridging trusses.

For bridging trusses in the model, a 0.75 in. angle gap was used for trusses with web bar diameters that varied between 0.75 in. and 0.98 in.

3.3.3 Truss Member Cover Plates

In 30 percent of the floor area, truss members were supplemented with cover plates. The members with additional plates included top chords, web members, and most typically bottom chords. Section properties were calculated with SAP2000 *Section Designer*. The primary truss top chords were reinforced with an additional set of double angles at truss end connections. At these locations, the work points for the section were located at the centroid of the composite double angle and concrete slab.

The Laclede shop drawings indicated plates 3/8 in. by 3 in. connecting the bottom chord of the primary truss pairs together at each end and where intersected by a bridging truss. These plates were included in the model.

3.3.4 Viscoelastic Dampers

Viscoelastic dampers were located where the bottom chords of the long span, short span, and bridging trusses intersected the exterior columns (see Chapter 1 for description and details). The dampers resisted static and quasi-static loads (such as gravity loads) at the time of load application. Immediately following load application, the dampers shed load until the stress in the dampers was dissipated. A placeholder element was located in the model at the damper location.

3.3.5 Strap Anchors

Exterior columns not supporting a truss or truss pair were anchored to the floor diaphragm by strap anchors. These strap anchors were connected to the columns by complete penetration welds. The strap anchors were then connected to the slab with shear stud connectors and to the top chords of the trusses by fillet welds. The straps were included in the model and located in the plane of the centroid of the

composite top chord. Also, in the model the work points intersected with the centerline of the column and used a rigid link to attach back to the spandrel (see Fig. 3–18).

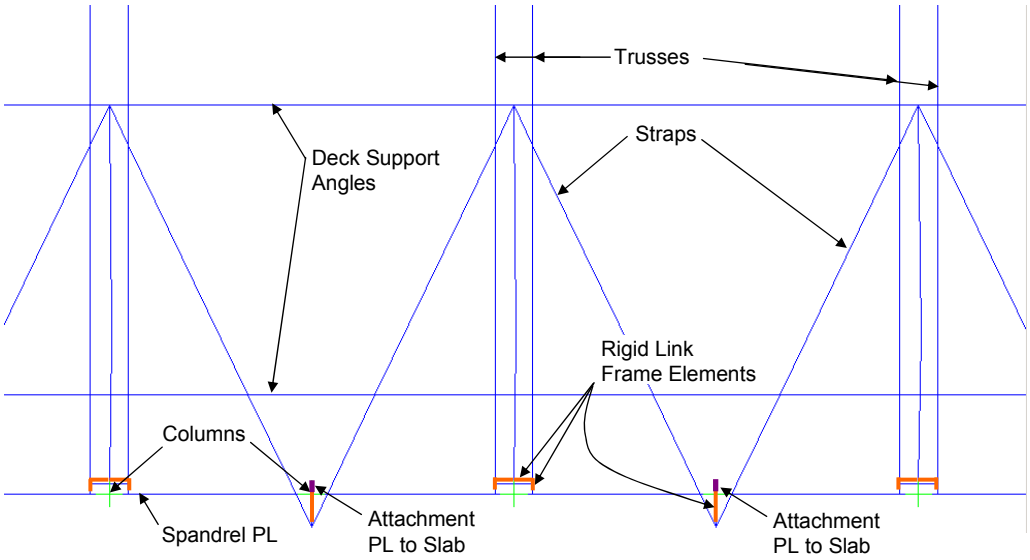

Key: PL, Plate.
Note: Slab not shown.

Figure 3–18. Strap anchors modeling.

3.3.6 Concrete Slab and Metal Deck

Outside the core, the primary trusses acted compositely with the 4 in. concrete slab on 1 1/2 in. metal deck. In the model, the average depth of the slab plus deck was modeled as 4.35 in. The concrete slab consisted of lightweight concrete with a self-weight of 100 pcf and a design compressive strength, f'_c= 3,000 psi. The concrete modulus of elasticity, E_c, used for modeling was 1,810 ksi, and the calculated modular ratio, $n=E_s/E_c$, was taken as 16, where E_s is the steel modulus of elasticity. These values are consistent with those included in the WTC Structural Design Criteria Book.

Typically, inside the core, the beams acted compositely with a 4 1/2 in. formed concrete slab. The concrete slab consisted of normal weight concrete with a self-weight of 150 pcf and a design compressive strength, f'_c= 3000 psi. The concrete modulus of elasticity, E_c, used for modeling was 3,320 ksi, and the calculated n ratio, E_s/E_c, was taken as 8.7.

The floors of the WTC towers had an in-floor electrical distribution system of electrified metal deck and trench headers. The effects of the in-slab trench headers were accommodated in the model by reducing the slab shell element thickness. A 1 ft 8 in. wide shell panel (the typical truss-floor shell mesh size) was reduced in thickness from 4.35 in. to 2.35 in. or 1.35 in. at the trench header locations per drawing SCA–109 (Floor 96A Structural Concrete Floor Plan).

3.3.7 Verification of the 96th Floor Model

Several steps were taken to verify the model input. SAP2000 Version 8 offers a ‘shading’ option once a model has been built with frame section assignments. This allows the user to view the members as the program has interpreted their input. The shading option was helpful for using section designed shapes,

and for verifying the orientation (i.e., local axes) of members. The work was independently reviewed by engineers not associated with the initial model development.

Once the model was completed, checks were performed for gravity loads. All superimposed dead loads and live loads included in the model were based on WTC Design Criteria; self weight was m accounted for by SAP2000. To justify the modeling assumptions, several studies were performed to compare stress results to hand calculations for representative composite sections. Hand calculations were used to estimate deflections and member stresses for a simply supported composite truss under gravity loading. For the composite truss sections, the steel stress results were within 4 percent of those calculated by SAP2000 for the long-span truss and 3 percent for the short-span truss. Deflections for the beams and trusses matched hand calculations within 5 percent to 15 percent.

3.4 TYPICAL BEAM-FRAMED FLOOR MODEL—FLOOR 75B

As described in Section 3.3 for truss-framed floors, the structural drawings were reviewed to identify structural similarities between the beam-framed floors within the expanded impact and fire zones of both towers (see Appendix G). It was found that floor 75 of WTC 2 (75B) represented the typical beam-framed floor in the expanded impact zone for WTC 2 (floors 74B to 88B). There were no beam-framed floors within the expanded impact zone of WTC 1.

Floors 75 and 76 of WTC 2, lower and upper mechanical equipment room (MER) floors, respectively, were typical of the lower three MER floor pairs in both towers (floors 7 and 8, 41 and 42, and 75 and 76 for both WTC 1 and WTC 2). Floor 77 of WTC 2, a lower escalator floor, was a beam-framed floor similar to the lower floor of the MER floor pairs, i.e., floor 75B.

Based on the above analysis, floor 75 of WTC 2 was selected as the overall representative beam-framed floor for the expanded impact and fire zone in both towers and is described in the following sections (see Fig. 3–19). An isometric view of the typical beam-framed floor model is illustrated in Fig. 3–20. Table 3–1 includes a summary of the size of the 75B floor model. The following presents the major structural systems and components of the beam-framed floor model.

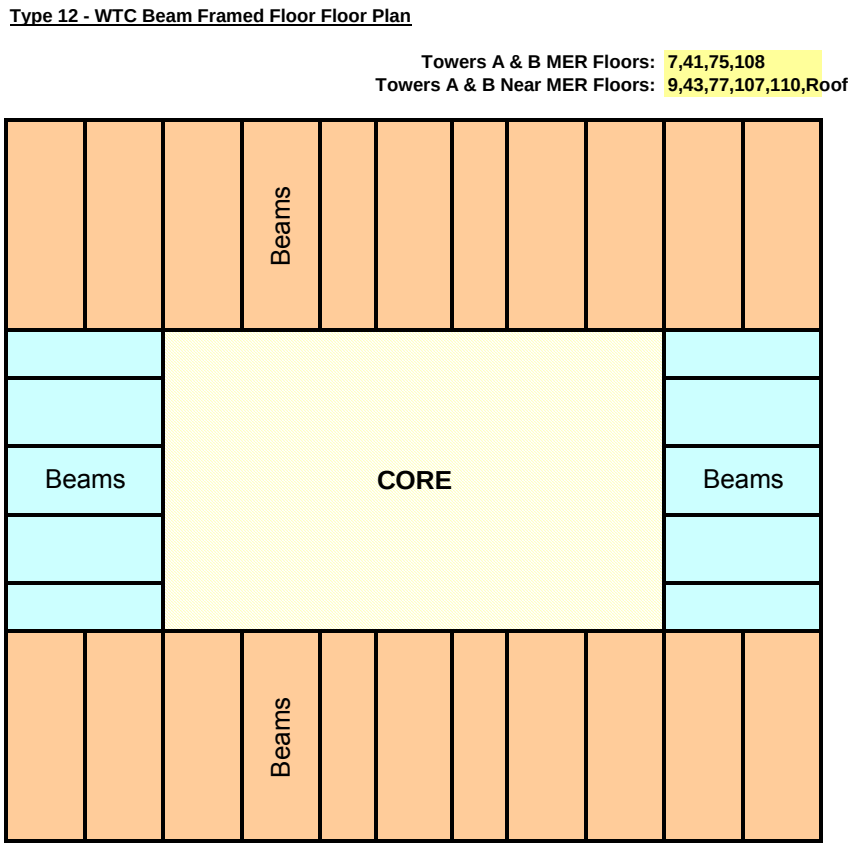

Figure 3–19. Typical beam-framed floor arrangement.

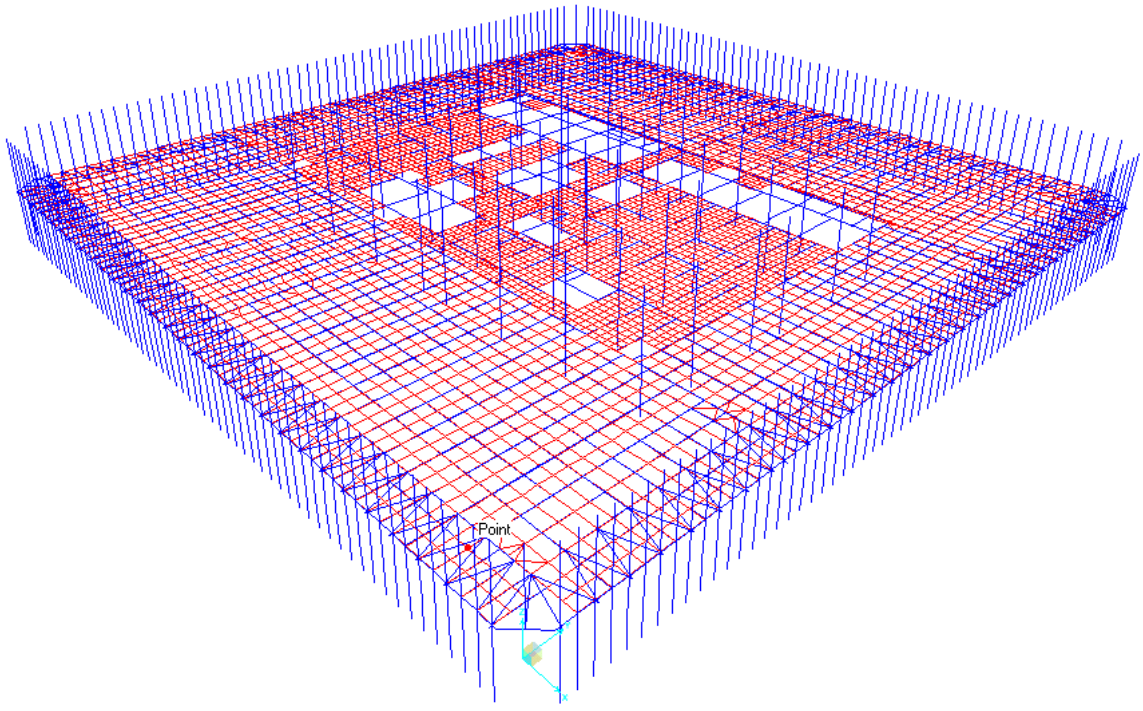

Figure 3–20. Typical beam-framed floor model (floor 75B).

3.4.1 Composite Beams

The beams in the model were located at the elevation of the centerline of the concrete slab. The insertion point for the beams was set at the beam top flange, and then the beam was offset down by one-half the thickness of the slab. The beam was rigidly linked with the slab to simulate the composite action. This option provided for accurate estimation of the composite stiffness of the floor.

For beams with cover plates, the properties were calculated by SAP2000 *Section Designer*, and the slab, beam, and reinforcing plates were rigidly linked.

3.4.2 Horizontal Trusses

Exterior columns which did not support a beam were connected to the floor for bracing purposes by horizontal trusses. These exterior horizontal trusses were anchored to the columns with complete joint penetration welds. The horizontal trusses were then connected with shear stud connectors to the slab. The truss angles (typically 4 in. by 4 in. by 5/16 in.) were then field welded to the top flange of the beams. In the model, the work points intersected with the centerline of the column and used a rigid link to attach back to the spandrel. The truss members were located in the plane of the centroid of the composite top chord (see Fig. 3–21).

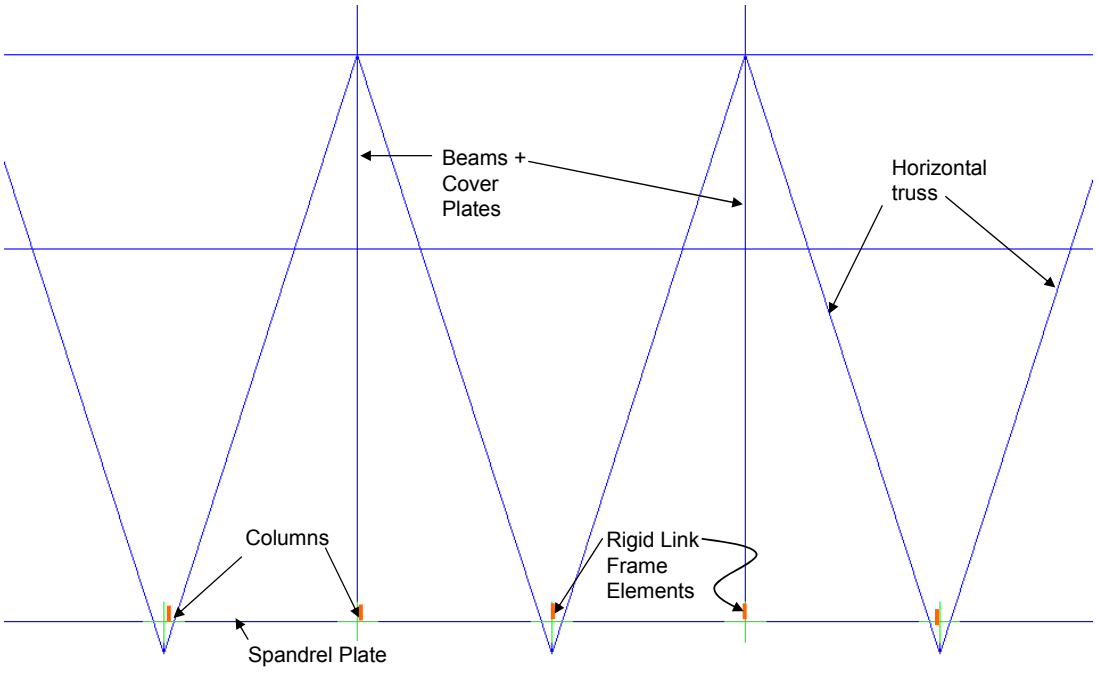

Figure 3–21. Horizontal truss modeling, slab not shown.

3.4.3 Concrete Slab and Metal Deck

Outside the core on the mechanical floors, the beams acted compositely with a 5 3/4 in. concrete slab on 1 1/2 in. metal deck. The average cross-sectional depth of the slab in the model was taken as 6.1 in. The

deck spanned between channels that, in turn, spanned between the floor beams. The concrete slab consisted of normal weight concrete with a self-weight of 150 pcf and a design compressive strength of typically f'_c= 3,000 psi. The concrete modulus of elasticity, E_c, used for modeling was 3,320 ksi and the calculated modular ratio, n, was taken as 8.7.

Typically, inside the core, the beams acted compositely with a 6 in. formed concrete slab. The concrete slab consisted of normal weight concrete with the same properties as concrete outside the core.

The mechanical floors had a 2 in. maximum depth topping slab both inside and outside the core. The topping slab stiffness was not included in the models, but the weight was accounted for in the baseline performance analysis.

3.4.4 Viscoelastic Dampers

Viscoelastic dampers were located below the bottom flange of the beams where the beams intersected the exterior columns (see Chapter 1 for description). Similar to floor 96A model, a placeholder element was located in the model at the damper location.

3.4.5 Verification of the 75th Floor Model

Similar to the 96th floor model, the 'shading' option in SAP2000 was used to view the members as the program interpreted their input. The shading option was helpful for using section designed shapes, and for verifying the orientation (i.e., local axes) of members. The work was independently reviewed by engineers not associated with the initial model development.

Once the model was completed, checks were performed for gravity loads. All superimposed dead loads and live loads included in the model were based on WTC Design Criteria; self-weight is accounted for by SAP2000. To justify the modeling assumptions, several studies were performed to compare stress results to hand calculations for representative composite sections. Hand calculations were used to estimate deflections and member stresses for a simply supported composite beam under gravity loading. The model yielded accurate steel stress results compared to hand calculations—around 1 percent for both short- and long-span beams. Where the beams were built-up with reinforcing plates, it was found that SAP2000 *Section Designer* shapes were not calculating the stresses correctly, so instead, separate beam and plate elements drawn over each other were inserted. This method yielded very accurate steel stress results—between 1 percent and 2 percent for both short- and long-span beams.

3.5 PARAMETRIC STUDIES

Modeling techniques employed in the development of the global models of WTC 1 and WTC 2 were consistent with, but often more advanced than, the techniques typically employed in the analysis and design of high-rise buildings. As such, building components were idealized so that overall performance was replicated while appropriately reducing the computational requirements. The following describes the studies undertaken to establish the idealizations used in the models, including typical exterior wall panels, exterior corner panels, and flexible floor diaphragms.

3.5.1 Exterior Wall Columns/Spandrel Typical Panels (Floors 9 to 106)

A parametric study of typical three-column, three-spandrel exterior wall panels from the faces of the towers (floors 9 to 106) was performed using two modeling methods (see Fig. 3–22). The first model was a detailed shell model, where each plate of each column or spandrel was specifically modeled, and the second was a simplified frame model. Internal column stiffeners were included in the shell model. The parametric study assumed that the shell model best represented the as-built panel performance, and therefore, it was used to tune the performance of the frame model, which was used throughout the global model (see Sec. 3.2.6). The objectives of the study were to (1) match the axial stiffness of the frame model with the detailed shell model under gravity load and (2) match the inter-story drift of the two models by modifying the rigidity of the column/spandrel intersections in the frame model.

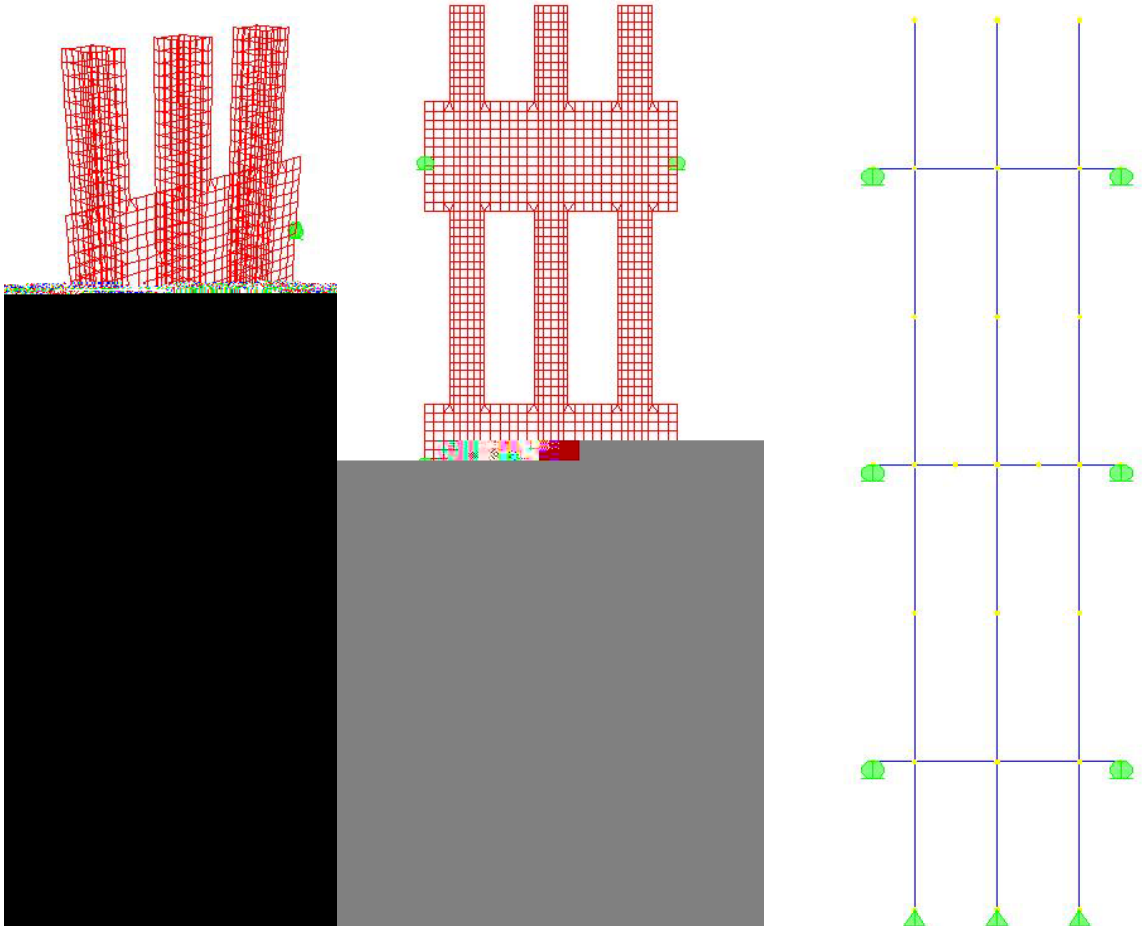

Figure 3–22. Shell element and frame models of typical exterior wall panel.

For comparing the axial stiffness of the simplified frame model of the panel with the detailed shell model, both models were loaded vertically while pin-supported at the bottom of the columns. The results indicated that the shell model was stiffer than the equivalent beam model due to the contribution of the spandrel beams to the columns' axial stiffness. This was due to the rigidity of the spandrel beams and the proximity between the columns. The parametric study on a wide range of panels over the height of the

towers showed that the vertical stiffness of the columns in the bottom third of the towers should be increased by a factor in the range of 25 percent to 28 percent, and the columns in the middle and upper thirds of towers should be increased by a factor in the range of 20 percent to 28 percent. Based on these results, 25 percent increase of the axial stiffness of exterior columns was selected as a reasonable representation for the panel vertical stiffness over the height of the towers between floors 9 and 106 (see Sec. 3.2.6).

For studying the lateral deformation of the exterior panels, panel properties were taken from three different areas of the building. These included floors 79 to 82, 53 to 56, and 23 to 26. The deformations at points A, B, I, and II (see Fig. 3–23) were studied for three different panel locations and their respective spandrel and column thickness. The topmost columns were connected via a rigid link and loaded in the plane of the panel and perpendicular to the column with a 100 kip-load. The boundary conditions were as shown in Fig. 3–22.

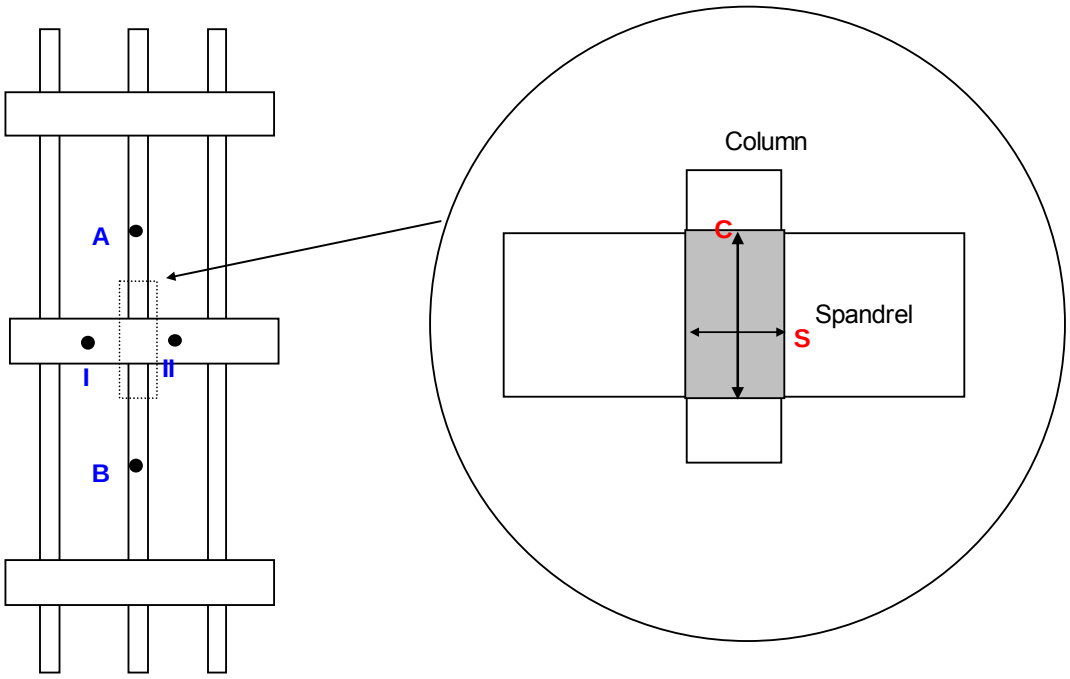

Figure 3–23. Selection of column and spandrel rigidity of typical exterior wall panel.

The lateral displacements found for the shell and frame models of typical exterior wall panels with varied column and spandrel intersection rigidities are reported in Table 3–5. The study found that 50 percent column rigidity and 100 percent spandrel rigidity in the frame model produced deflection results consistent with the shell model.

Table 3–5. Lateral displacement (in.) for the shell and frame models of typical exterior wall panel with varied column and spandrel rigidities.

	Lateral displacement (in)			
	Floor 79-82			
	Shell model	Frame model (Rigidity)		
		No rigidity	C:50%, S:100%	C:100%, S:100%
A	0.60	1.04	0.59	0.35
B	0.28	0.52	0.29	0.18
I	0.45	0.78	0.44	0.26
II	0.45	0.78	0.44	0.26
	Floor 53-56			
	Shell model	Frame model (Rigidity)		
		No rigidity	C:50%, S:100%	C:100%, S:100%
A	0.26	0.43	0.27	0.18
B	0.12	0.22	0.14	0.11
I	0.19	0.32	0.2	0.15
II	0.19	0.32	0.2	0.15
	Floor 23-26			
	Shell model	Frame model (Rigidity)		
		No rigidity	C:50%, S:100%	C:100%, S:100%
A	0.21	0.37	0.21	0.12
B	0.1	0.18	0.1	0.06
I	0.16	0.28	0.16	0.09
II	0.16	0.28	0.16	0.09

3.5.2 Exterior Wall Columns/Spandrel Corner Panels (Floors 9 to 106)

A parametric study was performed of an exterior wall corner panel typical over each corner of the towers from floors 9 to 106. Similar to the exterior typical panels, to account for the contribution of the spandrels into the axial stiffness of the columns, it was found that an area modifier to provide a 25 percent increase in the axial stiffness of the two continuous columns of the corner panels was suitable for modeling the columns' axial stiffness. No modifiers were needed for the intermittent columns.

The panel from floor 53 to 56 was selected to be representative, with two additional columns attached on either side. The objective of the study was to match the inter-story drift of a detailed shell model and a simplified frame model of the corner panel by modifying the rigidity of the column/spandrel intersections in the frame model. For this parametric study, the panel was straightened to simplify the study and to isolate the behavior of interest (see Fig. 3–24). The deformations at points T1, T2, B1, B2, and M2 (Fig. 3–25) were studied for representative column and spandrel plate dimensions. The topmost columns were connected via a rigid link and loaded in the plane of the panel and perpendicular to the column with a 100 kip load.

The lateral displacements calculated for the shell and frame models of the typical exterior wall corner panel with varied column and spandrel rigidities are reported in Table 3–6. The study indicated that 25 percent column rigidity and 50 percent spandrel rigidity in the frame model produced deflection results consistent with the shell model.

Figure 3–24. Shell element and frame models of typical exterior wall corner panel.

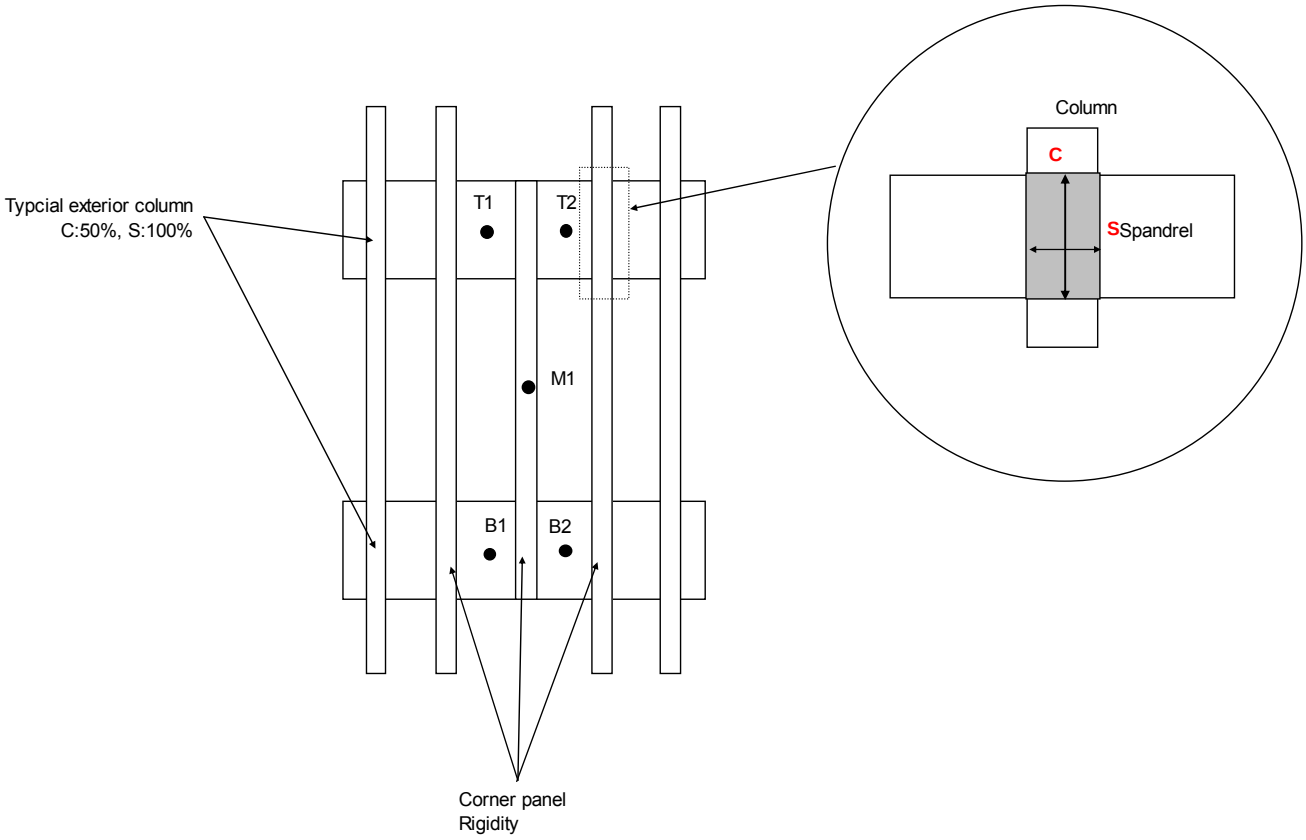

Figure 3–25. Selection of column and spandrel rigidity of typical exterior wall corner panel.

Table 3–6. Lateral displacement (in.) for the shell and frame models of typical exterior wall corner panel with varied column and spandrel rigidities.

	Floor 53-56			
	Shell model	Corner panel rigidity		
		No rigidity	C:25%, S:50%	C:100%, S:100%
T1	0.227	0.236	0.222	0.152
T2	0.227	0.236	0.222	0.152
M1	0.149	0.154	0.149	0.102
B1	0.084	0.072	0.077	0.053
B2	0.084	0.072	0.077	0.053

As part of the in-house NIST review of the reference structural models (see NIST NCSTAR 1-2), a detailed shell element model of original corner panel (not straightened) was analyzed under lateral loads to test the accuracy of the simplified frame model with 25 percent column rigidity and 50 percent spandrel rigidity calculated above. Both the detailed and simplified models were loaded as shown in Fig. 3–26. The deflections calculated from the frame model were consistent with those estimated from the shell model, indicating that the rigidities estimated using the straight model (Fig. 3–25) accurately represented the actual corner panel behavior.

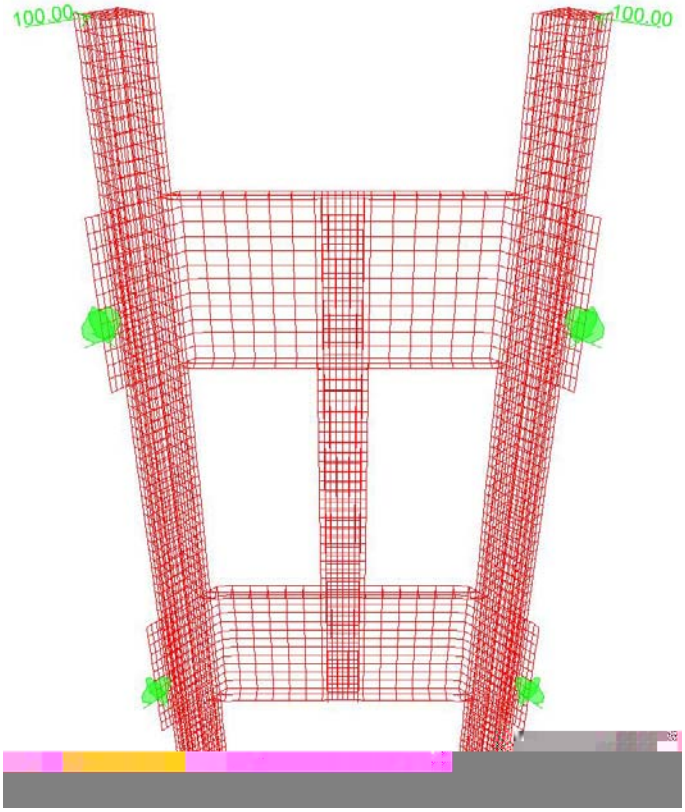

Figure 3–26. Detailed and simplified model of the exterior wall corner panel.

3.5.3 Flexible Floor Diaphragm

The floor models developed as described in Secs. 3.3 and 3.4 were used to develop the flexible diaphragm stiffness used within the WTC 1 and WTC 2 global models. The in-plane diaphragm stiffness of the

detailed floor models was determined and used to arrive at an equivalent shell element floor model. This flexible shell element floor model was then inserted in the global models at specific floors to capture the in-plane flow of forces and deformations. These flexible diaphragms were not used throughout, as the rigid diaphragms in the majority of floors provided for a sufficiently accurate representation of the flow of forces and deformations while keeping manageable the model's computational requirements. In the global models, flexible diaphragms were used at the beam-framed floors 3, 4, 5, 6, 7, 9, 41, 42, 43, 75, 76, 77, 107, 108, 109, 110, and roof of both towers. For floors 107, 108, 109, 110, and roof, the stiffness of the flexible diaphragms was reduced to prevent these diaphragms from attracting large forces incompatible with the strength of the slabs (see Sec. 3.2.9).

Parametric studies were performed to compare the diaphragm stiffness of two different floor models for both the typical truss-framed floor and the beam-framed floor. The typical floor models were compared with simplified equivalent models that duplicated the representation of the exterior wall columns, exterior wall spandrels, core columns, and their boundary conditions. The floor framing, both inside and outside the core, was replaced by shell elements. The material properties of the shell model matched the properties of the concrete floor outside the core in the respective floor model.

The comparative floor models were loaded in the plane of the floors with a lateral load of 180 lb/ft (equivalent to 15 psf over the 12 ft story height) on both the windward and leeward faces. The column base supports were released for the exterior wall columns along the loaded faces and for all core columns to allow lateral translation only in the direction of loading.

The comparative models were executed to assess the horizontal deflection of the floor on both the windward and leeward sides of the model and for the case where the lateral loads were applied non-concurrently along the 100 face and 200 face of the tower. Both the total horizontal deflection of the slab and the relative displacement between the windward and leeward sides were compared between the models. The shell thickness was modified to match the in-plane stiffness determined by the detailed floor models.

The deformations from the lateral load case using the 75th floor model of WTC 2 are illustrated in Fig. 3–27, while Fig. 3–28 shows the deformations of the simplified floor model. Fig. 3–29 shows the lateral deflection of the north and south sides of the floor model under lateral load applied in the north direction using the detailed and equivalent floor models.

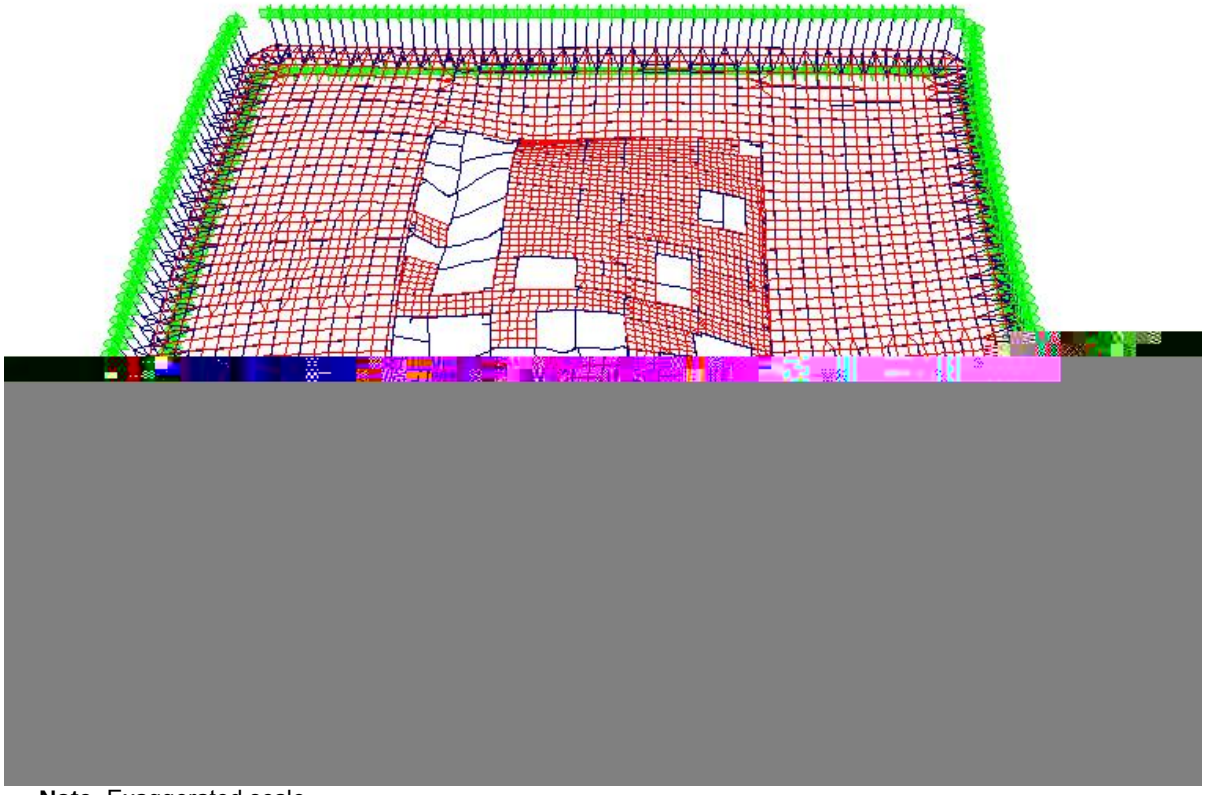

Note: Exaggerated scale.

Figure 3–27. Deflection of typical beam-framed floor model due to lateral loading.

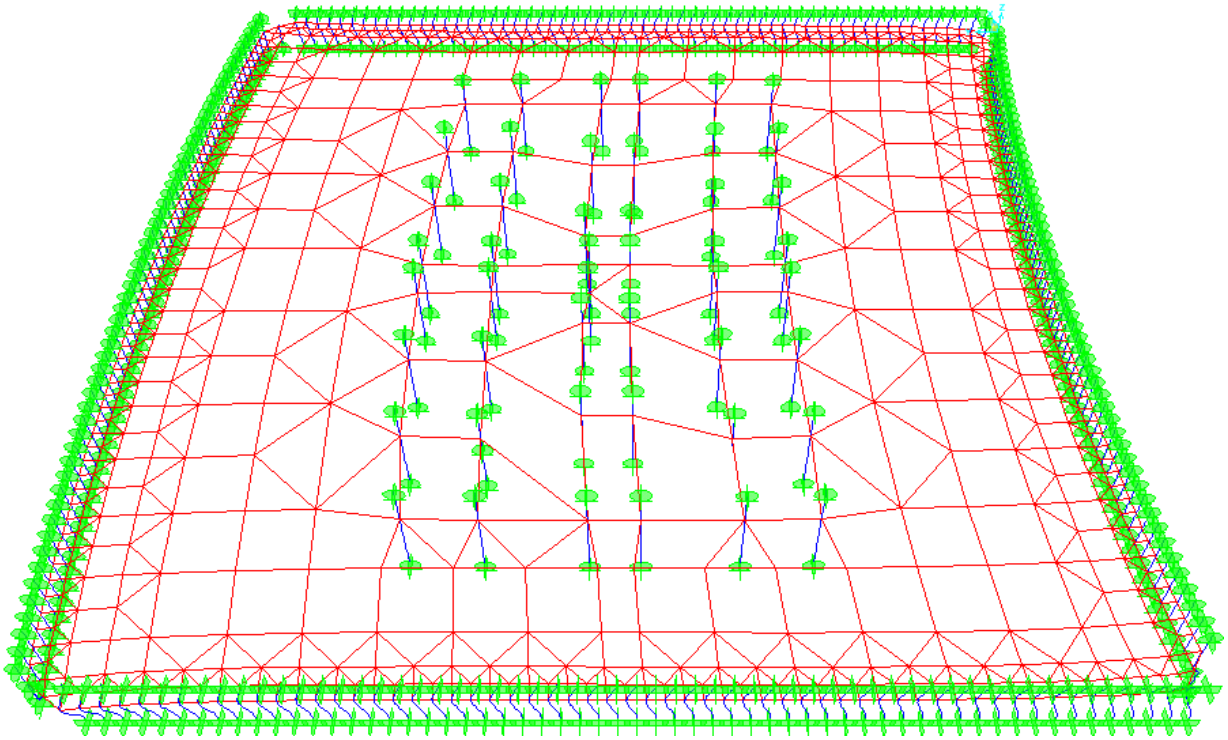

Note: Exaggerated scale.

Figure 3–28. Deflection of equivalent floor model due to lateral loading.

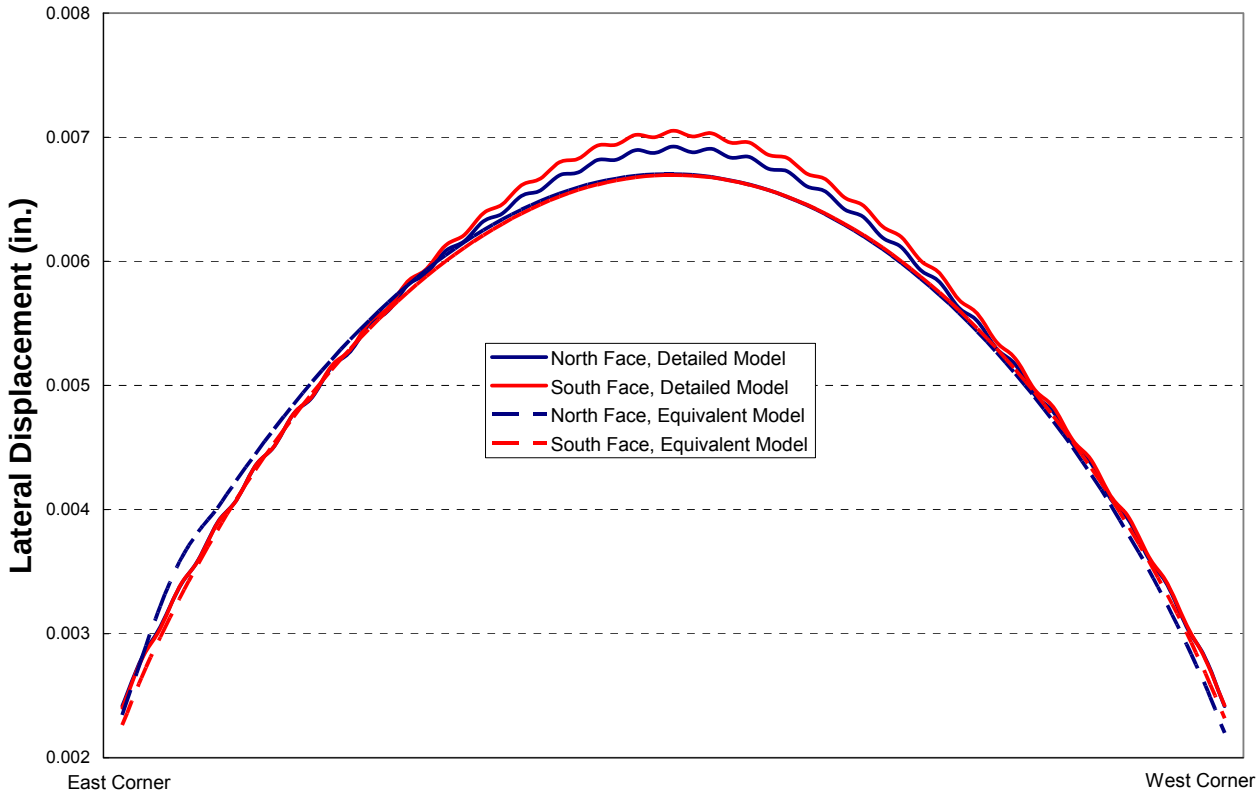

Figure 3–29. Deflections of the north and south faces of the floor for the detailed and equivalent floor models.

3.6 SUMMARY

This chapter described the development of the reference structural models for the WTC towers. These reference models were used to establish the baseline performance of the towers and also served as a reference for more detailed models for aircraft impact damage analysis and thermal-structural response and collapse initiation analysis. The main types of models developed were:

- Two global models of the towers, one each for WTC 1 and WTC 2. The models included all primary structural components in the towers, including exterior walls (columns and spandrel beams), core columns, exterior wall bracing in the basement floors, core bracing at the mechanical floors, core bracing at the main lobby atrium levels, hat trusses, and rigid and flexible diaphragms representing the floor systems. The models were developed using the electronic databases described in Chapter 2. To validate the global models, the calculated natural frequencies of WTC 1 were compared with those measured on the tower and good agreement between the calculated and measured values was obtained.

- One model each of a typical truss-framed floor (floor 96 of WTC 1) and a typical beam-framed floor (floor 75 of WTC 2) in the impact and fire zones in the two towers. The models included all primary structural components in the floor system, including primary and bridging trusses, beams, strap anchors and horizontal trusses, concrete slabs, and viscoelastic dampers. To validate the floor models, several studies were carried out to compare stresses

and deflections estimated from the model with hand calculations for representative composite sections. Good agreement was obtained between the model results and hand calculations.

Parametric studies were performed to evaluate the behavior of typical portions of the structure and to develop simplified models that could be implemented in the global models. These parametric studies included detailed and simplified models of typical exterior and corner wall panels, and floor systems.

This page intentionally left blank.

Chapter 4
GRAVITY AND WIND LOADS ON THE WTC GLOBAL MODELS

4.1 INTRODUCTION

This chapter outlines the estimation of the gravity and wind loads applied to the global models of the World Trade Center (WTC) towers to establish their baseline performance. The following sources were used to develop the loads for the various loading cases considered in this study:

- Design Criteria document of the WTC towers, prepared by Worthington, Skilling, Helle & Jackson (henceforth referred to as Design Criteria).
- WTC architectural and structural drawings (henceforth WTC Dwgs.).
- Wind reports prepared by Worthington, Skilling, Helle & Jackson, describing the development of design wind loads for the WTC towers (henceforth WSHJ Wind Reports).
- Reports from two independent wind tunnel studies concerning the WTC towers, conducted in 2002 for insurance litigation by Cermak Peterka Peterson, Inc. (henceforth CPP) and Rowan Williams Davies and Irwin, Inc. (henceforth RWDI).
- Current New York City Building Code (henceforth NYCBC 2001).
- Current American Society of Civil Engineers (ASCE 7) Standard (henceforth ASCE 7-02).

Three loading cases were considered for the baseline performance analysis. They included:

- *Original WTC design loads case.* Loads were as follows: Dead and live loads as in original WTC design in accordance with Design Criteria, used in conjunction with original WTC design wind loads from WSHJ Wind Reports.
- *State-of-the-practice case.* Loads were as follows: Dead loads as in original design; NYCBC 2001 live loads; and wind loads from RWDI wind tunnel study, scaled in accordance with NYCBC 2001 wind speed. This wind load is considered as a lower estimate state of the practice since, as will be explained later, the CPP wind tunnel study produced larger wind loads on the towers and is considered as an upper estimate state-of-the-practice case.
- *Refined NIST estimate case.* Loads were as follows: Dead loads as in original design; live loads from ASCE 7-02 (a national standard); and wind loads developed by National Institute Standards and Technology (NIST) from critical assessment of information obtained from the RWDI and CPP reports and state-of-the-art considerations.

The purpose of using the original WTC design loads was to evaluate the performance of the towers under original design loading conditions, and ascertain whether those loads and the corresponding design were adequate given the knowledge available at the time of the design. The purpose of considering the state-

of-the-practice case and the refined NIST estimate case was to better understand and assess the effects of successive changes in standards, codes, and practices on wind design practices for tall buildings.

Section 4.2 of this chapter presents the gravity loads on the towers, including: dead loads and live loads used in the original design, and in accordance with NYCBC 2001 and ASCE 7-02. Section 4.3 presents and compares the wind loads used in the original design, state-of-the-practice wind loads, and wind load estimates developed by NIST.

4.2 GRAVITY LOADS

The gravity loads applied to the global WTC models consisted of dead loads (DL) and live loads (LL), appropriately combined as stipulated in the Design Criteria. Dead loads were applied to the global system computer models in two parts: construction dead loads (CDL) and superimposed dead loads (SDL), based on the WTC Dwgs and the Design Criteria.

- CDL is defined as the self-weight of the structural system, including floor slabs, beams, truss members, columns, spandrel beams, etc.

- SDL is defined as the added dead load associated with architectural, mechanical, electrical, and plumbing systems; such as curtain walls, ceilings, partitions, floor finishes, mechanical equipment and ducts, transformers, etc.

Three independent sets of live loads were combined with the dead loads:

- The first set was taken from the Design Criteria and was used with the original WTC design loads case.

- The second set was taken from NYCBC 2001 and was used for the state-of-the-practice case.

- The third set was taken from ASCE 7-02 and was used for the refined NIST estimates case. The live loads given in ASCE 7-02 are essentially identical to the NYCBC 2001 live loads.

For each live load set, live load reductions for column design were taken from their respective source. The live load reductions in NYCBC 2001 are essentially identical to those of the Design Criteria.

Gravity loads were applied to the global system computer models using three methods:

- The self-weight of the structural steel frame for the exterior wall, core columns, and hat truss was applied using the SAP2000 self-weight feature.

- The loads from areas outside the core of the typical truss-framed and beam-framed floors were taken from the reactions of the typical floor computer models (see Sec. 4.2.1) and were applied to the global models as concentrated loads on the columns.

- Since the occupancy, opening layout, and floor framing in the core area varied among floors, the loads within the core area, from floor B5 to the roof, were calculated using a spreadsheet (see Sec. 4.2.2) and were applied to the global models as concentrated loads on the columns.

4.2.1 Gravity Loads from Areas Outside of Core

The loads from areas outside the core area of the typical truss-framed floor were based on the reactions from the typical floor computer model (floor 96 of WTC 1). The Design Criteria live load for areas outside of core was 100 psf. The reduced applied loads for the typical truss-framed floor for use in the global system computer models are summarized in Table 4–1, which shows the original WTC design criteria for gravity loads. The partition allowance from the original WTC Design Criteria was also used as the partition allowance for the NYCBC 2001 and the ASCE 7-02. The live load of 50 psf is the same for the original design criteria, the NYCBC 2001, and ASCE 7-02.

Table 4–1. Original WTC design criteria loads for floor 96A model for the design of columns (typical truss floor).[a]

Floor Area	CDL[b] (psf)	SDL[c] (psf)	Total DL (psf)	LL (psf)
Long Span	3.5	14	17.5	50
Short Span	3.5	14	17.5	50
Two-Way Zone	3.5	16	19.5	50
Core[d]	None	None	None	None

a. The self-weight of interior and exterior columns, exterior spandrels, core frame members, and core floor slabs is not included in the tabulated loads and is not applied to the floor computer model.
b. The self-weight of the concrete slab and of the structural steel members in the floor system, as computed by SAP2000, is added to these loads.
c. Includes a 6 psf allowance for partitions.
d. Since the loads inside the core are applied separately to the global system computer models, the live loads, superimposed dead loads on the core area, and core frame members are reduced to zero in the floor computer models.

Live load reductions for columns for the original WTC design live loads were taken from the Design Criteria and were identical to those specified in NYCBC 2001. Live load reductions for the ASCE 7-02 live loads follow the ASCE 7-02 tributary area provisions. For the ASCE 7-02 loads, at the exterior walls live load reductions were calculated using an influence factor coefficient of two as defined in ASCE 7-02. The influence area for exterior wall columns was calculated using a 45 degree spread for the distribution of loads among the columns located below the loading point.

In the floor model, the self-weights of the exterior columns and spandrels, the interior core columns, and interior core beams (not including those of the core perimeter) were not included in the analysis, since these weights were already accounted for in the global models. For this purpose, the zero self-weight frame property modifier in SAP2000 was used. Appropriate portions of the core slab section definition were also modified by using a zero self-weight property modifier. In addition, since the loads inside the core were applied separately to the global models, the live loads and superimposed dead loads on the core area elements and core frame members were reduced to zero in the floor computer models.

For calculating the loads outside the core, three typical floors (floor 96, 75, and 43) were selected to be representative of all of the floors in the tower except for the roof, the floors at and below floor 2, and the mezzanine floors. Models of floors 75 and 96 were developed as discussed previously in Chapter 3, and floor 43 was used as a representative of the beam-framed floors that were not mechanical floors (floor 75 model with modified loads was used to simulate this floor). Based on the column reactions from the typical floor computer models, gravity loads on columns at other floors were generated by applying

conversion factors to the results from these floor computer models. The conversion factors were based on unit area loading differences between floors. These calculations were performed in a spreadsheet.

The conversion factors were calculated for CDL, SDL, and LL. For CDL and SDL, the conversion factors were calculated for any given floor by dividing the overall floor CDL and SDL by their counterparts at the representative typical floor. For LL, the conversion factors were similarly calculated, except that the factors included also the appropriate live load reduction factor. The overall floor CDL and SDL were compiled using a weighted average based on the floor area for each of the floor zones: long-span, short-span, and two-way zone.

Loads on columns outside of the core at the roof, floors at and below floor 2, and the mezzanine floors were calculated by spreadsheet.

4.2.2 Gravity Loads from Areas Inside of Core

For the floor areas inside the core from floor B5 to the roof, gravity loads were calculated for individual columns on the basis of tributary areas using a spreadsheet. The calculations were based on the WTC Dwgs and the original Design Criteria.

The floor framing information was obtained from the structural drawings. Occupancies and opening layouts (elevator and shaft layout) for each floor inside the core were obtained from the architectural drawings. Floors with similar occupancy, opening layout, and floor framing were grouped together and were represented by a typical floor in the group. Floors with special occupancies, opening layouts, or floor framing were calculated individually.

The core column loads for each of the typical floors and special floors below floor 107 were calculated in spreadsheets. The NYCBC 2001 loads are essentially identical to, and were used for the ASCE 7-02 loads. In the worksheet, the tributary area of a core column was divided into four regions. For each region, the area was calculated from the coordinates of the core columns in the computer models, then modified for each type of floor according to the opening layout specific to that floor.

For each region, the dominant occupancy specified in the architectural plan was used. For the loads corresponding to each occupancy, the floor worksheet referenced the *Load* worksheet in the same Excel file. For each occupancy, the *Load* worksheet tabulated the CDL of the concrete slab, the SDL, and the LL.

Dead loads

In addition to the weight of the concrete slab (including reinforcing steel and metal deck), the CDL of the floor framing consisted of the weight of the structural steel beams. The floor computer models were used to calculate the weight of the steel floor framing averaged over the floor area. The weight of the steel floor framing was calculated to be 6 psf and 7 psf at floors 96 and 75, respectively.

The floor framing CDL calculated for floor 96 was applied to all floors except the mechanical floors, where the floor 75 CDL was applied. For typical occupancies inside the core, such as corridors and elevator lobbies, the concrete slab CDL was based on the structural drawings and was listed in the *Load* worksheet. For special floors, the concrete slab CDL for these typical occupancies was overwritten in the *Floor* worksheet to reflect the actual thickness of the concrete slab specified in the structural drawings.

Where a load was not listed in the *Load* worksheet, the concrete slab CDL was included in the *Floor* worksheet.

The SDL includes the weights of partitions, beam fireproofing, ductwork, electrical conduit and piping, floor finish, ceiling, and mechanical equipment. The types of floor finish and ceiling applied to each occupancy were obtained from the architectural plans and from the finish schedule in the architectural drawings. The weight of finishes was obtained from the Design Criteria (Sheet BC-1-7). In accordance with the original WTC Design Criteria, for equipment rooms on the mechanical floors an SDL of 75 psf was used.

Partition layouts and types were obtained from the architectural drawings, and the partition weights were taken from the Design Criteria (Sheets BC-1-7 and BC-1-8). As shown in Figs. 4–1 and 4–2, partition loads per gross area were calculated for seven typical opening/occupancy configurations. A partition weight of 20 psf per gross area was assumed for the return plenums and for areas where the occupancy was not specified in the architectural drawings. A partition weight of 6 psf, taken over the gross area, was used for tenant space. For occupancies that included an additional 75 psf in SDL for equipment weight, a partition weight was not added.

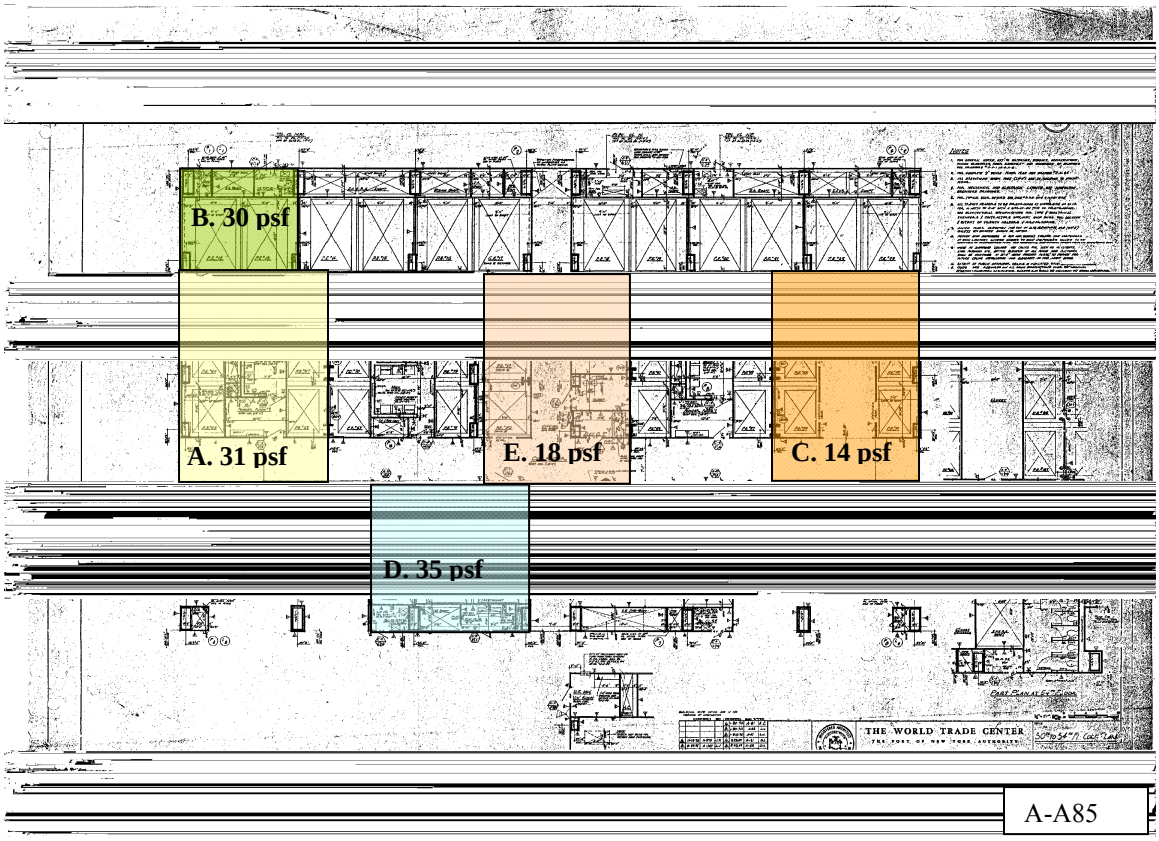

Source: Reproduced with permission of The Port Authority of New York and New Jersey. Enhanced by NIST.

Figure 4–1. Partition groups A, B, C, D, and E.

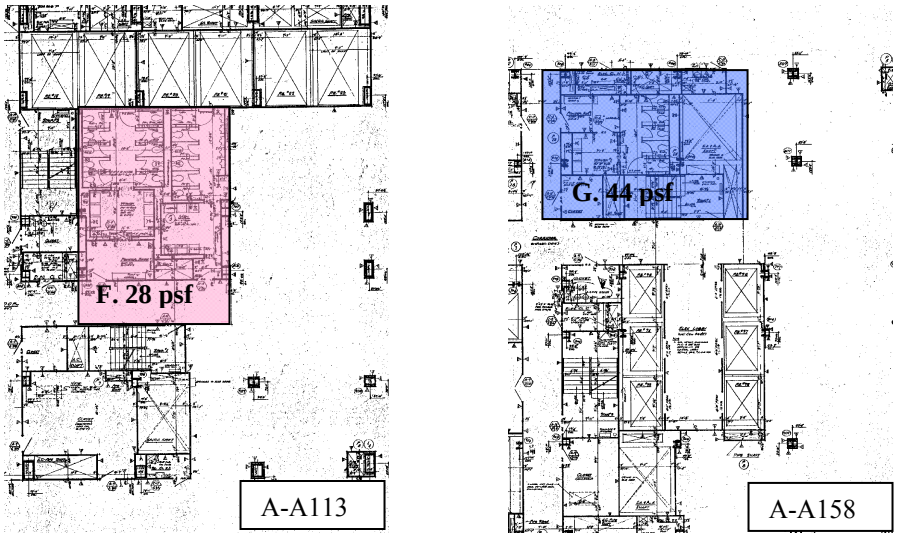

Source: Reproduced with permission of The Port Authority of New York and New Jersey. Enhanced by NIST.

Figure 4–2. Partition groups G and F.

Weights of concrete beam encasements were taken from the structural drawings and the Design Criteria. At floors 77, 43, 9 to B3, and B5, most of the core beams were concrete-encased. For the entire core, a 20 psf uniformly distributed load taken on the gross tributary area was added to the dead load. See below for the concrete encasement weights assumed for floors in the hat truss region. For all other floors, the concrete beam encasement loads were applied directly to the columns to which concrete-encased beams were connected.

The loads due to the construction of the Fiduciary Trust vault in WTC 2 (see Sec. 2.5.2) were added to the dead loads of the original construction.

Live Loads

The original WTC live loads for occupancies inside the core were taken from the Design Criteria (Sheets CC-1-2 and CC-1-3). For a few occupancies not explicitly listed in the Design Criteria, the live load listed for the most similar occupancy was used.

ASCE7-02 live loads were taken from Table 4–1 of the standard. Where a WTC occupancy was not listed in ASCE7-02, the Design Criteria live load was used. NYCBC 2001 live loads are essentially identical to the ASCE 7-02 live loads and were not tabulated separately.

Live Load Reduction

For use with the corresponding live loads, live load reductions for column design were based on the original WTC Design Criteria and on ASCE 7-02.

The live load reduction factors in the original WTC design were taken from sheets DC1-3 of the Design Criteria. NYCBC 2001 live load reductions are essentially identical to the original WTC Design Criteria and were not tabulated separately.

For the core columns, the ASCE7-02 live load reductions were calculated in accordance with the tributary area provisions of ASCE7-02. Core columns were divided into three column groups based on their tributary areas:

- Columns 704, 705, 805, and 904
- Columns at the perimeter of the core
- All other core columns

A single set of live load reduction factors was applied to all the columns within the same column group.

Hat Truss Floors

Except for floor 107, for the floor areas tributary to the hat truss framing, gross tributary areas were calculated by hand. Openings were subtracted from gross tributary areas, and the resulting net areas were entered into an Excel spreadsheet. Except for columns 704B106Z, 704B107, 705B106Z, 803B107, 804AB107, and 804B106Z, where gross and net areas were calculated directly, for floor 107, the net areas were taken from floor 106.

CDL, SDL, and LL were based on the Design Criteria sheets BF1-11A, BF1-12, BF1-13, and BF1-14. These sheets assign uniform loads throughout entire floors (both outside and inside the core). For floor 109 (mechanical floor), sheet BC1-3 indicates LL = 150 psf. However, for consistency with the design criteria for other mechanical floors, this live load was applied in two parts, as LL = 75 psf and additional SDL = 75 psf.

For some occupancies in the core for floors 107 to the roof, the occupancy-specific live load given elsewhere in the WTC Design Criteria exceeded the uniform live load specified for the entire floor. For these occupancies, the higher live load was applied to the computer model. These occupancies are summarized below:

- Stair: LL=100 psf (instead of the uniform LL=75 psf)
- Corridors: LL= 100 psf per WTC Design Criteria or 80 psf per ASCE 7-02 (instead of the uniform LL=75 psf)
- Service room: LL= 100 psf (instead of the uniform LL=75 psf)
- Window washer storage LL=125 psf (instead of 75 psf)

Note that beams, girders, and diagonals that were part of the hat truss system were included in the global models and that their self weights were calculated by SAP2000 and added to the CDL. In addition, a 20 psf uniform load at every level (floor 107 to roof) was used to account for the weight of structural steel that was not modeled and the weight of concrete encasement. The ASCE 7-02 loads were essentially identical to and were used for the NYCBC 2001 loads.

The antenna gravity loads were also considered in the WTC 1 global model.

4.2.3 Construction Sequence Loading Effects

Located between floor 107 and the roof in both towers, the hat truss interconnected the core columns and the columns of the exterior walls. The hat truss system distributed both gravity loads and wind loads between the core and the exterior walls. However, the CDL and SDL put in place prior to the completion of the hat truss system were not distributed through the hat truss. In order reasonably to differentiate between those loads distributed through the hat truss system and those that were not, the construction sequence was considered in the computer models.

The effects of construction sequence on the distribution of gravity loads was modeled using the nonlinear staged construction analysis function in SAP2000. The primary purpose of this step in the analysis was to provide, at the top of the towers, a reasonably accurate distribution of construction and superimposed dead loads between the core columns and the exterior wall. Accordingly, the global system computer model was subdivided into two portions: floor 106 and below, and the area above floor 106. In the first stage, the lower portion of the full computer model was loaded with all of the CDL and SDL associated with floor 106 and below. In the second stage, the portion of the full model above floor 106 was activated, and the CDL and SDL associated with the upper floors were placed on the full computer model. Live loads on the whole model were applied to the full building with the hat truss engaged in the second stage. This methodology approximates well the way in which the towers were built.

4.3 WIND LOADS

The investigation of wind loads and wind effects presented in this report has two objectives. The first is to ascertain the adequacy of the original wind loads and the corresponding structural design given the knowledge available at the time of the design. The second objective is better to understand and assess the effects on design practices of successive changes in standards, codes, and practices, with a view to helping improve standard provisions for wind loads in the future. This case study provides an opportunity to achieve this objective with unique effectiveness.

To achieve these objectives, three independent sets of wind loads were applied to the global tower models as explained in Sec. 4.1. These sets are further described as follows:

4.3.1 Original WTC Design Wind Loads

Wind loads were determined for the original design of the WTC towers through the development and implementation of a boundary-layer wind-tunnel study which simulated the mean and fluctuating (turbulence) properties of the wind from ground to gradient height by using the knowledge and techniques available in the 1960s. The original WTC wind loads were taken from summaries given in Part IV of the WSHJ Wind Reports. From among the loading cases, the most severe were determined by comparisons of diagrams of wind-induced shear and overturning moment.

In the original WTC wind tunnel studies, wind tunnel data were collected for each tower for wind approaching from 24 wind directions, α, in 15 degree increments. Part IV of the WSHJ Wind Reports provides equations for the wind-induced shears and overturning moments in the towers at 21 elevations, z, along the building height, H, at increments of $0.05H$. For each wind direction, the reports provided sets of coefficients to be used in these equations to obtain the static and the dynamic components of shear and

overturning moment in the N-S and E-W directions. Coefficients were also provided for calculating torsional moments. The torsional moments are associated with eccentricity of the global wind excitation of the building with respect to the building center of rigidity. Based on these equations, shears and torsions were calculated for each wind direction for the two orthogonal directions. The equivalent effective static shear forces, *S*, and overturning moments, *M*, at each level were comprised of static and dynamic components:

$$S = \overline{S} + S'$$
$$M = \overline{M} + M' \tag{4–1}$$

where the first and second terms indicate, respectively, the mean or steady-state components and dynamic components. The static components of the shears and moments were calculated from the following equations:

$$\overline{S}(z) = \frac{1}{2}\rho \overline{V}_o^2 DHC_S(z)$$
$$\overline{M}(z) = \frac{1}{2}\rho \overline{V}_o^2 DHC_M(z) \tag{4–2}$$

where:

ρ = design air density = 0.0023 slug/ft^3

$\overline{V}_o$ = mean (or equivalent) design wind speed, determined to be 98 mph averaged over 20 min at a height of 1,500 ft above ground.

C_S and C_M = shear force and overturning moment coefficients, respectively, obtained from wind tunnel tests and provided in tabular form

D and H = dimension in plan and height of the tower

The dynamic components of the shear forces and overturning moments at any height z were obtained from the following equations:

$$S'(z) = 4\pi^2 n_o^2 A \int_z^H m(z)\mu(z)dz$$
$$M'(z) = \int_z^H S'(z)dz \tag{4–3}$$

where:

n_o = natural frequency of oscillation of the tower

A = amplitude of oscillation at the top of the tower corresponding to the mean design wind speed

$m(z)$ = mass per unit height of the tower

$\mu(z)$ = amplitude of fundamental vibration mode at height *z* for unit amplitude at the top of the tower.

The wind loads were calculated on the basis of 2.5 percent total damping. This value includes the intrinsic damping of the structural systems plus the supplemental damping provided by the dampers.

The differential static and dynamic shears between successive levels were calculated and distributed using two different methods:

- The static wind load to be applied to each floor was determined from the shear diagram.
- The dynamic wind load to be applied to each floor was based on the distribution of mass over the tower height, the fundamental mode shape, and the dynamic component of the lateral wind-induced sway at the roof.

Note that for $\alpha = 90$ degrees, coefficients were not found in the microfilm of the WSHJ Wind Reports for calculating the static component of the wind forces for WTC 1. Accordingly, the static coefficients were deduced from data for the $\alpha = 270$ degrees, for WTC 2. By observation of the static coefficient data, it was determined that the basic data for the two towers is shifted by 180 degrees.

Considering the 24 different wind directions and the four combinations of the static and dynamic components of the N-S and E-W components of the building forces listed below, there were 96 different wind load cases for each tower.

N-S (Static + Dynamic) and E-W (Static + Dynamic)

N-S (Static + Dynamic) and E-W (Static – Dynamic)

N-S (Static – Dynamic) and E-W (Static + Dynamic)

N-S (Static – Dynamic) and E-W (Static – Dynamic)

The static and dynamic shears in the N-S and E-W directions were calculated for all 96 loading cases, and the overturning moments were calculated from the shears. In order to determine the most severe of the 96 loading cases for each tower, the wind-induced shears and overturning moments were compared, for each direction, at heights $z/H = 0.75$, 0.50, 0.25 and 0. The wind loading cases producing the maximum shears in either of the two orthogonal directions were identified for application to the global models.

To compare overturning moments for each loading case, the moments in the two orthogonal directions were combined vectorially (i.e., the magnitude of the resultant is equal to the square root of the sum of the squares of the components, and the direction β of the resultant moment is the arctangent of the ratio of the

y- and *x*-components). The load cases were grouped by the angle β using an increment of 45 degrees, resulting in 8 groups of load cases. For each β group, at $z/H = 0.75$, 0.50, 0.25 and 0, the wind load cases that generated the maximum resultant moment were identified for application to the computer global system models. Eight groups of maximum moment plus four directions of maximum shear at four heights in the towers would result in 48 different loading cases. However, some individual wind load cases produced a maximum resultant moment and/or a maximum shear at more than one elevation in the towers. As a result, for WTC 1, 16 loading cases were identified, and for WTC 2, 17 loading cases were identified.

For cases where an intermediate floor did not provide lateral support for the exterior wall, the wind load was distributed to the floors above and below, omitting the intermediate floor wind load.

For the floors modeled in the global model by rigid diaphragms, the wind forces in the N-S and E-W directions were applied as concentrated loads at the geometric center of the building. The torsional moments were also taken into account. For the floors with flexible diaphragms (see Chapter 3), the forces, based on tributary areas, were resolved into point loads at the perimeter columns. Both windward and leeward forces were applied. At these floors, the torsional moment was represented by four identical concentrated forces applied parallel to the four faces of the tower at the center columns of each face. The simplified method used for applying the torsional loads at floors with flexible diaphragms did not have any noticeable effects on the analysis results. For each loading case, the orthogonal wind forces were subdivided into windward and leeward forces based on the direction of the wind. For this purpose, the 24 wind directions α (discussed previously) were divided into 8 groups as given in Table 4–2. The wind direction for $\alpha = 0$ is for wind blowing from north to south.

Table 4–2. Grouping of the wind directions.

Group	α
1	$337.5 \le \alpha \le 22.5$
2	$22.5 < \alpha < 67.5$
3	$67.5 \le \alpha \le 112.5$
4	$112.5 < \alpha < 157.5$
5	$157.5 \le \alpha \le 202.5$
6	$202.5 < \alpha < 247.5$
7	$247.5 \le \alpha \le 292.5$
8	$292.5 < \alpha < 337.5$

For groups 1, 3, 5, and 7 (orthogonal or near-orthogonal wind directions), the wind forces were distributed in accordance with Fig. 4–3a. For groups 2, 4, 6, and 8 (diagonal or near-diagonal wind directions), the wind forces were distributed in accordance with Fig. 4–3b. The factors shown in Fig. 4–3 were based on Figure 6-6 of ASCE 7-02 Standard.

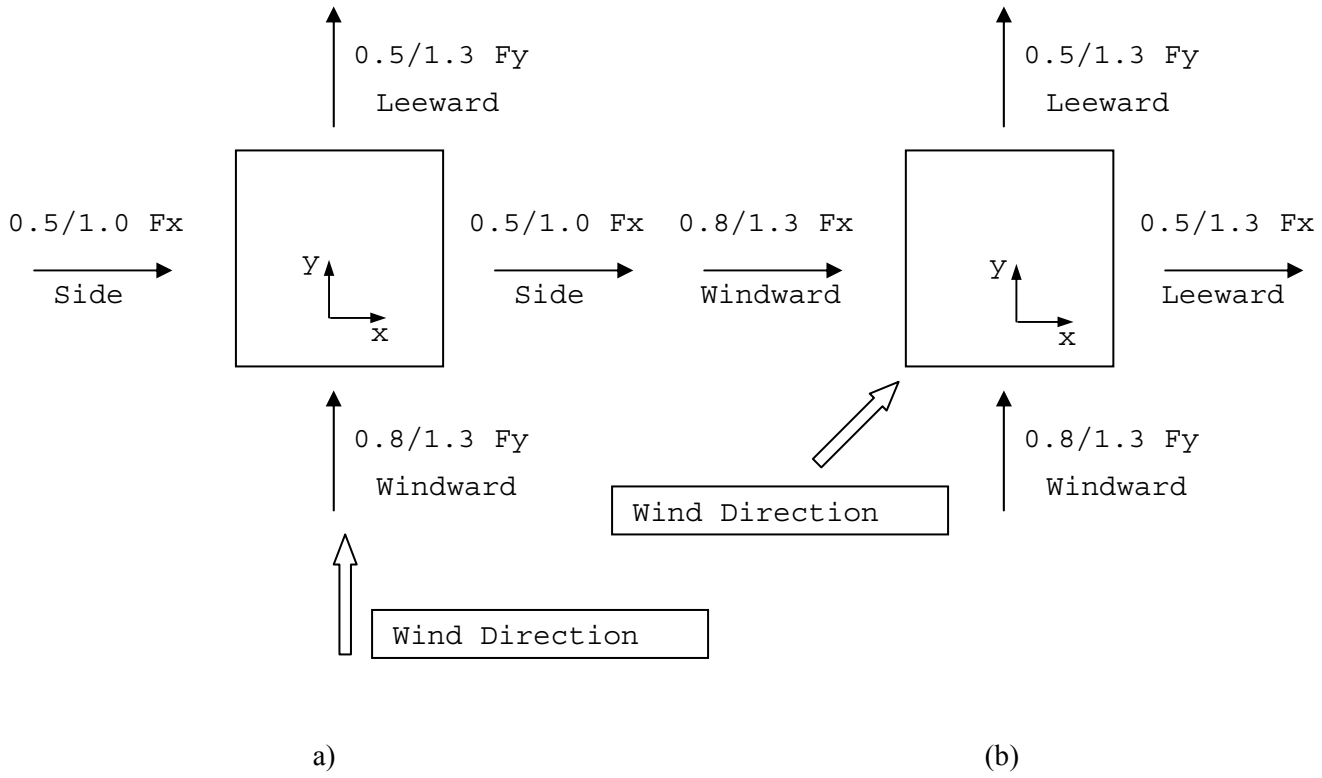

Figure 4–3. Windward and leeward distribution for (a) orthogonal and (b) diagonal wind directions.

4.3.2 State-of-the-Practice Wind Loads

For the WTC towers, two wind tunnel tests and wind engineering studies based thereon were conducted in 2002 by independent laboratories as part of insurance litigation unrelated to the NIST investigation. The tests and studies were conducted by Cermak Peterka Peterson, Inc. (CPP) and by RWDI. The results of both studies were made available to NIST; see NIST NCSTAR 1-2 for more details.

For the purpose of the baseline analysis, the state-of-the-practice wind load case consisted of the wind load estimates provided by RWDI, scaled in accordance with a wind speed equivalent to the NYCBC 2001 wind speed (interpreted to be the 80 mph fastest-mile wind speed at 30 ft elevation over open terrain). These wind loads were applied to the global models using the directional and torsional load combination factors presented in the RWDI reports.

The wind loads from RWDI are smaller than those obtained from CPP for WTC 2 (see Sec. 4.3.4). Considering the differences between RWDI and CPP results, RWDI practice may be viewed as a "lower-estimate, state-of-the-practice case."

The state-of-the-practice wind loads were distributed in the global system computer models in a manner similar to that described in connection with the original design wind loads.

4.3.3 Refined NIST Estimates

NIST completed an independent analysis to estimate the wind loads that would be appropriate for use in designing the towers based on state-of-the-art considerations. The analysis was based on results provided by CPP and RWDI, with modifications that draw on recently developed knowledge in wind engineering. The objective of this analysis was not to assess the adequacy of the original design wind loads, but rather to better understand and assess the effects of successive changes in standards, codes, and practices.

Wind loads based on recently developed knowledge and consistent with the design wind speed in ASCE 7-98 Standard (which is the same as in the ASCE 7-02 Standard) were estimated by NIST using the RWDI results scaled in accordance with a wind speed equivalent to the ASCE 7-02 Standard wind speed and then multiplied by a factor of 1.15. This number was recommended by NIST for the refined NIST baseline analysis. For details on how these wind loads were obtained see NIST NCSTAR 1-2.

The lateral wind loads on the towers, consistent with the ASCE 7-98 and ASCE 7-02 design wind speed requirements, were estimated by using the effective static floor-by-floor wind loads presented in Table 5a (without P-Δ effects) or Table 5b (with P-Δ effects) of the RWDI report (north tower) for WTC 1 and Table 3a (without P-Δ effects) or Table 3b (with P-Δ effects) of the RWDI report (south tower) for WTC 2.[2] These effective static floor-by-floor wind loads were multiplied by the factor 1.15 and by the factors indicated in note (3) provided at the bottom of Tables 3 and 5 in RWDI. The loads so obtained were applied to the global model of each tower using the load combinations presented in Table 6a of RWDI (north tower) and Table 4a of RWDI (south tower).

4.3.4 Comparisons of Wind Loads

Tables 4–3 and 4–4 provide a summary of the wind-induced base shears and base moments on WTC 1 and WTC 2, respectively. The values in Tables 4–3 and 4–4 are based on the 1938 and 1968 versions of the NYCBC, the RWDI study, the CPP study, the refined NIST estimates, and the original design. The wind loads are expressed in terms of two orthogonal components and of measures of the most unfavorable combined peaks obtained by various methods, as follows:

- RWDI: Most unfavorable peak is calculated as vector sum of weighted *x* and *y* peaks, with weighting factors approximately consistent with the "principle of companion loads," the approximations being based on engineering judgment and in-house experience.

- CPP: Most unfavorable peak is calculated as vector sum of *x* peak and companion point-in-time *y*-response, or *y* peak and companion point-in-time *x*-response, whichever is larger.

- Original WTC design: Most unfavorable peak is calculated as vector sum of *x* and *y* peaks corresponding to most unfavorable wind direction. These *x* and/or *y* peaks may be smaller for that most unfavorable direction than the *x* peaks and *y* peaks corresponding to wind normal to a building face (see Sec. 4.3.1).

[2] For the WTC 2 tower Tables 3b and 3c in the RWDI report (South Tower) were inadvertently switched. The loads accounting for P-Δ effects are in fact given in Table 3c of the report.

Table 4–3. A comparison of wind load estimates for WTC 1 from various sources.

Source	Year	Base Shear 103 kip			Base Moment 106 kip·ft		
		N-S	E-W	Most unfavorable combined peak	About N-S	About E-W	Most unfavorable combined peak
NYC Building Code	1938	5.3	5.3		4.2	4.2	
NYC Building Code	1968 to date	9.3	9.3		7.7	7.7	
RWDI / NYC Building Code	2002	11.4	10.5	13.0	10.1	10.5	12.2
RWDI / ASCE 7-98	2002	12.3	11.3	14.0	10.8	11.4	13.1
CPP / NYC Building Code	2002	NA	NA	NA	NA	NA	NA
CPP / ASCE 7-98	2002	NA	NA	NA	NA	NA	NA
NIST / third-party SOM review	2004	14.1	13.0	16.1	12.4	13.1	15.1
Original WTC Design	1960's	9.8	10.6	14.0	10.3	9.1	13.7

Table 4–4. Comparison of wind load estimates for WTC 2 from various sources.

Source	Year	Base Shear 103 kip			Base Moment 106 kip·ft		
		N-S	E-W	Most unfavorable combined peak	About N-S	About E-W	Most unfavorable combined peak
NYC Building Code	1938	5.3	5.3		4.2	4.2	
NYC Building Code	1968 to date	9.3	9.3		7.6	7.6	
RWDI / NYC Building Code	2002	9.7	11.1	12.3	10.1	9.2	11.3
RWDI / ASCE 7-98	2002	10.6	12.2	13.5	11.1	10.1	12.4
CPP / NYC Building Code	2002	NA	NA	NA	NA	NA	NA
CPP / ASCE 7-98[a]	2002	15.1	15.3	17.1	15.5	14.0	17.0
NIST / third-party SOM review	2004	12.2	14.0	15.5	12.8	11.6	14.3
Original WTC Design	1960's	13.1	10.1	16.5	8.8	12.6	15.2

a. Using ASCE 7-98 Sections 6.5.4.1 and 6.6.

Table 4–5 presents a summary of design base shears and base moments based on various building codes at the time of the design. Note that the base moments presented in Tables 4–3 to 4–5 are calculated at the foundation level (rather than at the street level).

Table 4–5. Base shears and base moments due to wind loads from different building codes.

Building Code	1938 NYC Building Code	1968 to Date NYC Building Code	1964 NY State Code	1965 BOCA/BBC	1967 Chicago Municipal Code
Base Shear (10^3 kip)	5.3	9.3	9.5	9.8	8.7
Base Moment (10^6 kip·ft)	4.2	7.7	7.6	8.5	7.5

Tables 4–3 and 4–4 indicate that the original design wind load estimates exceed in all cases those established by the NYCBC (a prescriptive minimum requirements code) prior to 1968, when the WTC towers were designed, and up to and including 2001. Table 4–5 shows that the design values are also higher than those required by other prescriptive building codes of the time, including the 1964 New York State Code, the 1965 Building Officials and Code Administrators Basic Building Code (BOCA/BBC), and the 1967 Chicago Municipal Code. It is noted also that wind effects obtained from various wind-tunnel-based studies are in all cases higher than wind effects based on prescriptive codes and standards.

The two orthogonal base shear and base moment components used in the original design are in general smaller than the CPP, RWDI, and refined NIST estimates. However, the most unfavorable combined peaks from the original design are larger than, or smaller, by at most 15 percent than estimates based on the CPP, RWDI, and NIST estimates. This is due to the conservative procedure used to combine the loads in the original design. (For example, NIST estimates are higher by about 15 percent than the most unfavorable original design wind loads for WTC 1, and lower by about 5 percent than the most unfavorable original design loads for WTC 2.)

Tables 4–3 and 4–4 indicate that the estimated wind-induced loads on the towers vary by as much as 40 percent between the wind tunnel/climatological studies conducted in 2002 by CPP and RWDI, with CPP being the larger. Thus, CPP loads are considered as an upper estimate, state of the-practice, while RWDI loads are considered as a lower estimate, state of the-practice.

4.4 REFERENCES

ASCE 7-02: American Society of Civil Engineers, ASCE 7 Standard Minimum Design Loads for Buildings and Other Structures, Reston, VA, 2002.

CPP report: Data Report, Wind-Tunnel Tests – World Trade Center, Cermak Peterka Petersen, Inc. August 2002.

Design Criteria: Design Criteria document for the WTC towers developed by Worthington, Skilling, Helle & Jackson.

NYCBC 2001: Building Code of the City of New York, 2001 Edition, Gould Publications, Binghamton, NY.

RWDI report: (north tower) Final Report, Wind-Induced Structural Responses, World Trade Center – Tower 1, Rowan Williams Davies and Irwin, Inc., October 4, 2002.

(south tower) Final Report, Wind-Induced Structural Responses, World Trade Center – Tower 2, Rowan Williams Davies and Irwin, Inc., October 4, 2002.

SAP2000 (2002), Linear and Nonlinear Static and Dynamic Analysis and Design of Three-Dimensional Structures Basic Analysis Reference, Computers & Structures Inc., Berkeley, CA.

WSHJ Wind Reports: A series of wind reports developed by Worthington, Skilling, Helle & Jackson, outlining the development of design wind loads for the WTC towers (see NIST NCSTAR 1-1).

WTC Dwgs: WTC architectural and structural drawings.

Chapter 5
BASELINE PERFORMANCE ANALYSIS OF THE WTC GLOBAL MODELS

5.1 INTRODUCTION

This chapter presents the results of the baseline performance analysis for the World Trade Center (WTC) 1 and WTC 2 global models under the three gravity and wind loading cases described in Chapter 4. These cases include the original WTC design load case, the lower-estimate state-of-the-practice case, and the refined National Institute of Standards and Technology (NIST) estimate case. Baseline performance results include basic information about the behavior of the towers under design loading conditions, pertaining to total and inter-story drift, demand/capacity ratios of primary structural components, exterior columns response (shear lag effects and presence of tensile forces), performance of connections, and the towers' resistance to shear sliding and overturning.

Section 5.2 describes the estimation of the demand/capacity ratios and the selection of the design parameters for their estimation. Section 5.3 presents the results of the baseline performance analysis for WTC 1 under the three loading cases. Similarly, Sec. 5.4 presents the results for WTC 2. Section 5.5 presents a summary of the results. For both towers, detailed baseline performance results are provided for the original WTC design loading case, while a brief summary of the results is provided for the state-of-the-practice and refined NIST estimate cases.

5.2 CALCULATION OF DEMAND/CAPACITY RATIOS

For all analysis cases, the demand/capacity ratios (DCRs) for structural components were estimated using the Allowable Stress Design (ASD) procedure as specified in the American Institute of Steel Construction (AISC) *Specification for Structural Steel Buildings – Allowable Stress Design and Plastic Design – 9th Edition, 1989.* The DCRs were calculated by dividing component demands by component capacities, taken at unfactored (working) loads and at working stresses, not at ultimate loads or yield stresses. These DCRs for the structural components were determined as follows:

1. The component demands were obtained from the results of the baseline performance analysis using the reference global models (see Sec. 3.2) and working loads based on the following load combinations:

    - For the original WTC design loading case and for the state-of-the-practice case, the load combinations were those specified by the AISC Specification (1989) and the New York City Building Code (NYCBC) 2001:

        Dead Load

        Dead Load + Live Load

        Dead Load + Live Load + Wind Load

Dead Load + Wind Load

- For the refined NIST estimate case, the load combinations were those specified by the American Society of Civil Engineers (ASCE 7-02) Standard:

  Dead Load

  Dead Load + Live Load

  Dead Load + Wind Load

  Dead Load + 0.75 × (Live Load + Wind Load)

  0.6 × Dead Load + Wind Load

2. The component capacities were based on the nominal steel strength as specified in the original design documents and using the AISC Specification (1989):

   - For the original design loading case and for the state-of-the-practice case (consistent with NYCBC 2001), a one-third increase in the allowable stress was considered for load cases that included wind, as specified at the time of the design and as is currently specified in NYCBC 2001 and AISC Specification (1989).

   - For the refined NIST estimate case, where loads were based on the ASCE 7-02 Standard, load combinations were taken from the ASCE 7-02 Standard, which does not allow the one-third increase in allowable stress.

The interaction equation in AISC Specifications (1989) estimates the DCR as the larger of the following two equations for members subjected to both axial compression and bending stresses:

$$DCR = \frac{f_a}{F_a} + \frac{C_{mx} f_{bx}}{(1 - \frac{f_a}{F'_{ex}})F_{bx}} + \frac{C_{my} f_{by}}{(1 - \frac{f_a}{F'_{ey}})F_{by}}$$

$$DCR = \frac{f_a}{0.60F_y} + \frac{f_{bx}}{F_{bx}} + \frac{f_{by}}{F_{by}} \qquad \text{(Eq. 5–1)}$$

For the case when $f_a / F_a \leq 0.15$, the following equation is permitted in lieu of the previous two equations:

$$DCR = \frac{f_a}{F_a} + \frac{f_{bx}}{F_{bx}} + \frac{f_{by}}{F_{by}} \qquad \text{(Eq. 5–2)}$$

where the subscripts *x* and *y* indicate the axis of bending about which a particular stress or design property applies, and

F_a and F_b are the axial compressive stress and compressive bending stress, respectively, that would be permitted if axial force alone or if bending moment alone existed.

f_a and f_b are the computed axial stress and compressive bending stress at a given point, respectively.

F'_e is the Euler buckling stress divided by a factor of safety.

C_m is a coefficient that depends on column curvature caused by applied moment.

A review of the basic design equations and allowable stresses for combined axial load and bending for the 6th Edition of the AISC Specifications (1963), which was in effect at the time of the design, indicates that they are essentially identical to those of the 9th Edition (1989) design equations and allowable stresses. There are, however, some variations between the 6th and 9th Editions of the specification. The 1963 Specification did not specifically address biaxial bending in the combined stress equations. In addition, the allowable stress formulations for bending with lateral torsional buckling are somewhat different between the two design specifications.

For the original design loading case, the SAP2000 program was used directly to estimate the DCRs using the above equations. For the lower-estimate state-of-the-practice case and the refined NIST estimate case, a second order analysis that accounted for P-Δ effects was used to estimate member demands under the applied gravity and wind loads. The P-Δ analysis results in a moment magnification in the components of the global models; as a result, the terms C_m and $(1 - f_a / F'_e)$ were assigned a unit value in the above equations to estimate component DCRs. For these cases, DCRs were calculated in Excel spreadsheets, using results obtained by the SAP2000 computer program. The calculations were spot-checked for accuracy and to verify that the correct design information was being applied. For most of the component calculations that were checked, the SAP2000/Microsoft Excel spreadsheet calculations were found to be acceptable. When errors were detected, the design parameters were corrected to provide for an acceptable calculation.

5.2.1 Selection of Global Models Design Parameters

For estimating the DCRs of the structural components under the various loading conditions, the following design parameters were used in the global models of WTC 1 and WTC 2 to yield accurate results:

- The effective length factors, K factors, for ASD column design were selected by comparing the actual column end conditions with the theoretical end conditions depicted in Table C-C2.1 in the Commentary of the 9th Edition of the AISC ASD Manual.

- Virtually all core columns were designed originally as axially loaded members without significant eccentric loads and without continuity of framing that would generate significant P-Δ moments. The details of construction are consistent with this design approach. Accordingly, in order to eliminate erroneous bending stresses in the interaction equations, allowable bending stresses for core columns were increased sufficiently to reduce the bending term in the interaction equation to less than 0.01.

- The cross-section of the intermittent corner columns of the tower included a web plate that extended beyond the flanges. The web plate extensions effectively, but inappropriately, reduced the section modulus of the cross-section by significantly limiting the allowable stress in the flange. To correct for this inappropriate reduction, the allowable bending stress for in-plane bending was increased.

- For the floor 107, 108, and 110 spandrel beams, for bending in the plane of the slab, the slab would resist the tendency for the spandrels to bend preventing significant bending stresses from developing in the spandrels. To achieve this behavior in the model, the spandrels' allowable bending stress was increased sufficiently to limit the bending term in the interaction equation to less than 0.01, eliminating erroneous bending stresses.

- For the floor 7 spandrels, the actual span length was insignificant due to the actual geometry of the spandrel plate construction. Since the as-modeled spandrels had a significant span and would otherwise develop erroneous bending stresses, the allowable bending stress was increased sufficiently to limit the bending term in the interaction equation to less than 0.01.

- At the exterior wall between floors 1 and 10TT1Tm he s

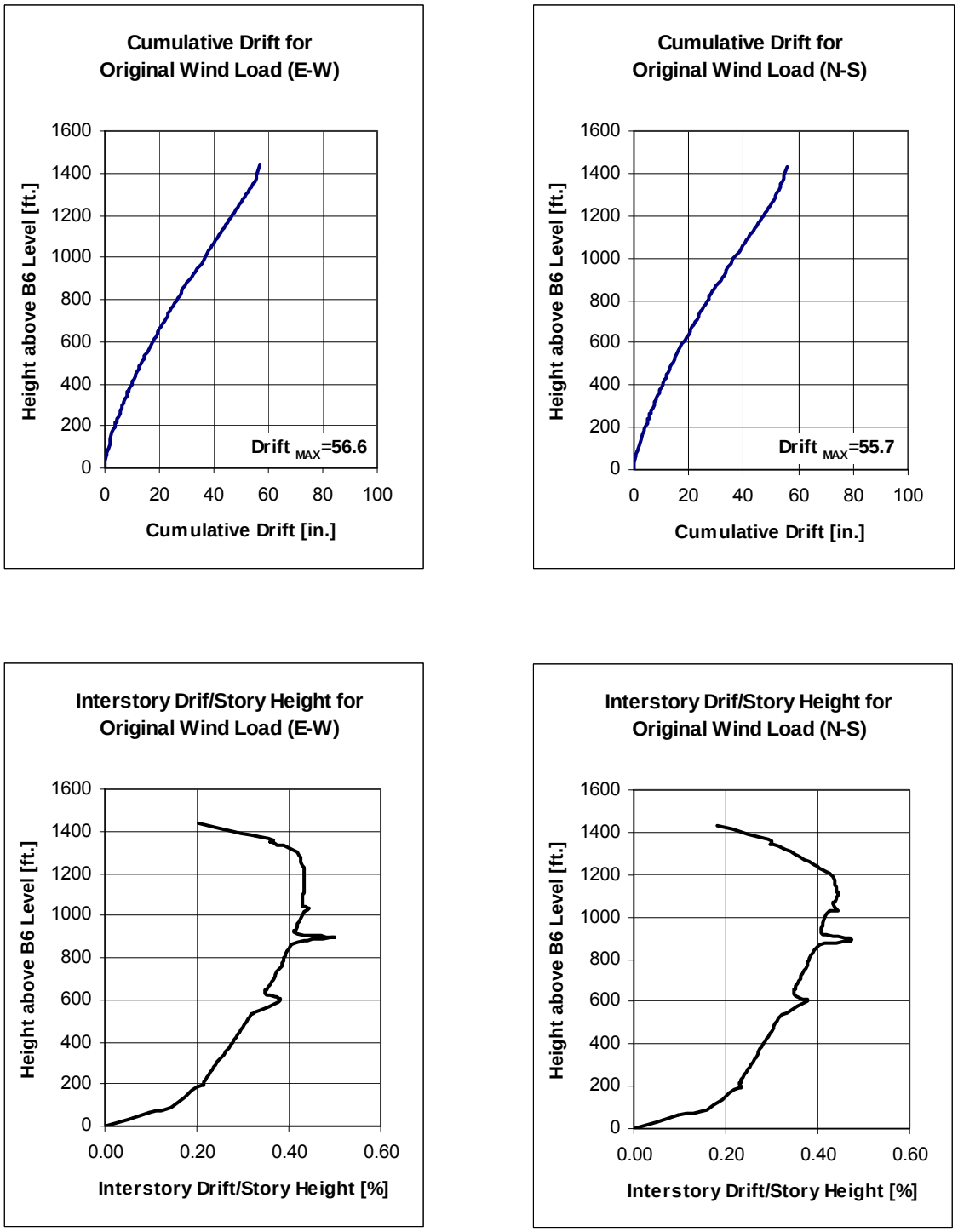

Figure 5–1. Drift diagrams of WTC 1 due to original WTC wind loads, (a) A0N-E- and (b) A75N+E-.

Table 5–1. Statistics of demand/capacity ratios for WTC 1 under original design load case.

Member Type	Number of Members	Mean Calculated DCR	C.O.V. of DCR	Percentage of Components with DCR > 1.0	Percentage of Components with DCR > 1.05	Number of Components with DCR > 1.05	Maximum Calculated DCR
Exterior Wall Columns							
Below floor 1	628	0.77	0.19	4.3	2.7	17	1.36
Floor 1 to 9	1,122	0.74	0.25	3.3	0.5	6	1.27
Floor 9 to 106	31,086	0.76	0.12	1.1	0.4	121	1.31
Above floor 106	578	0.73	0.31	12.3	10.0	58	1.46
Exterior Wall Spandrels							
Below floor 1	420	0.44	0.46	0.7	0.7	3	1.28
Floor 1 to 9	610	0.34	0.45	1.1	1.0	6	1.30
Floor 9 to 106	31,160	0.31	0.30	0	0	0	0.83
Above floor 106	836	0.35	0.69	1.9	1.7	14	1.55
Core Columns	5,219	0.86	0.14	10	5.3	278	1.36
Hat Truss System							
Columns	239	0.47	0.45	0.4	0.4	1	1.26
Beams	499	0.24	0.87	0.4	0.2	1	1.07
Braces	279	0.47	0.53	2.5	0.7	2	1.06
Exterior Wall Bracing							
Below floor 1	200	0.72	0.16	2	1	2	1.16
Above floor 106	12	0.40	0.52	0	0	0	0.75

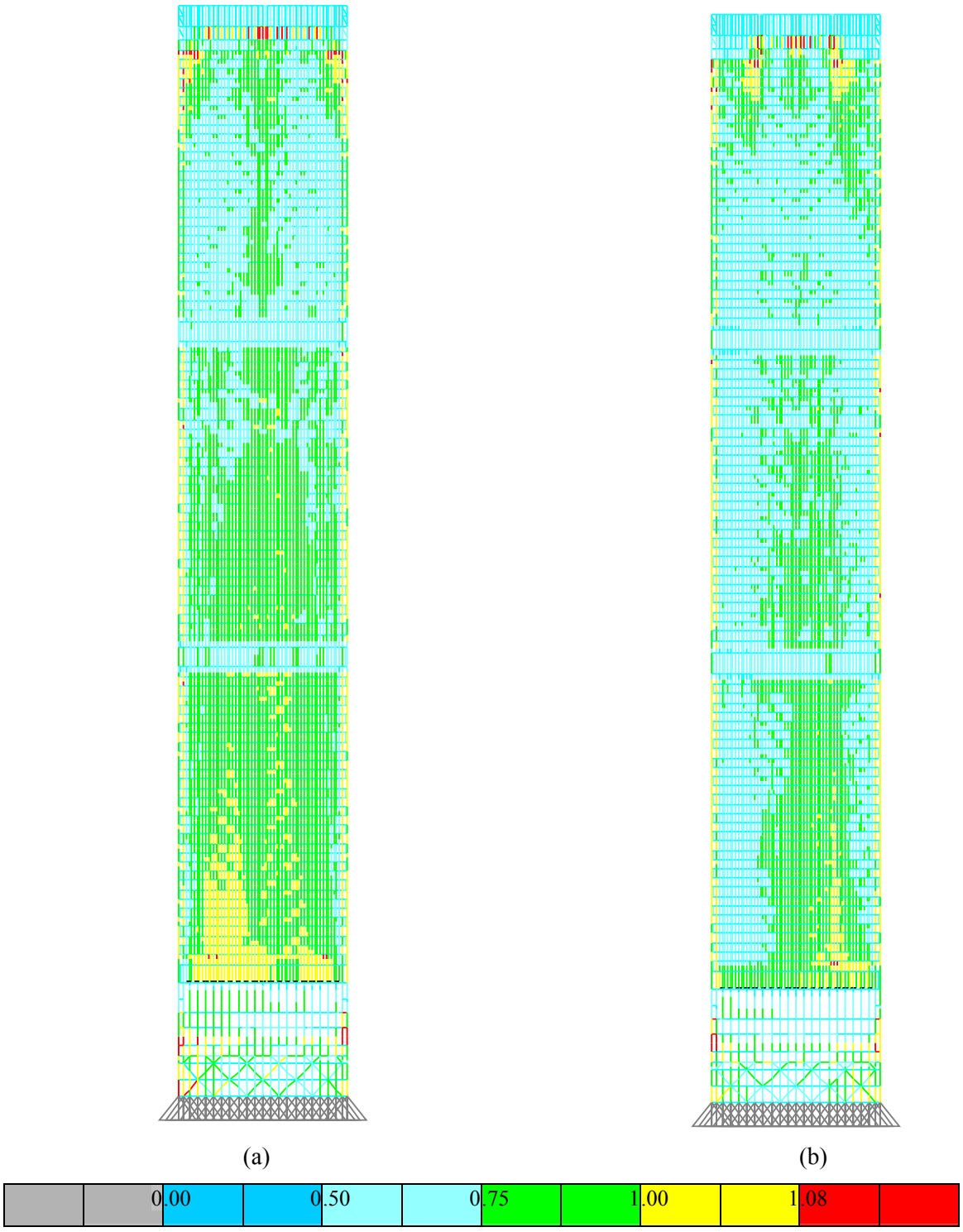

Figure 5–2. Demand/capacity ratios for WTC 1 under original design loads, (a) north elevation and (b) east elevation.

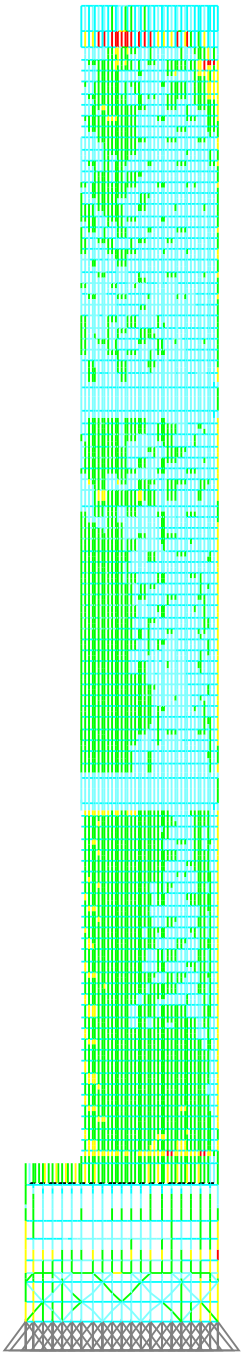

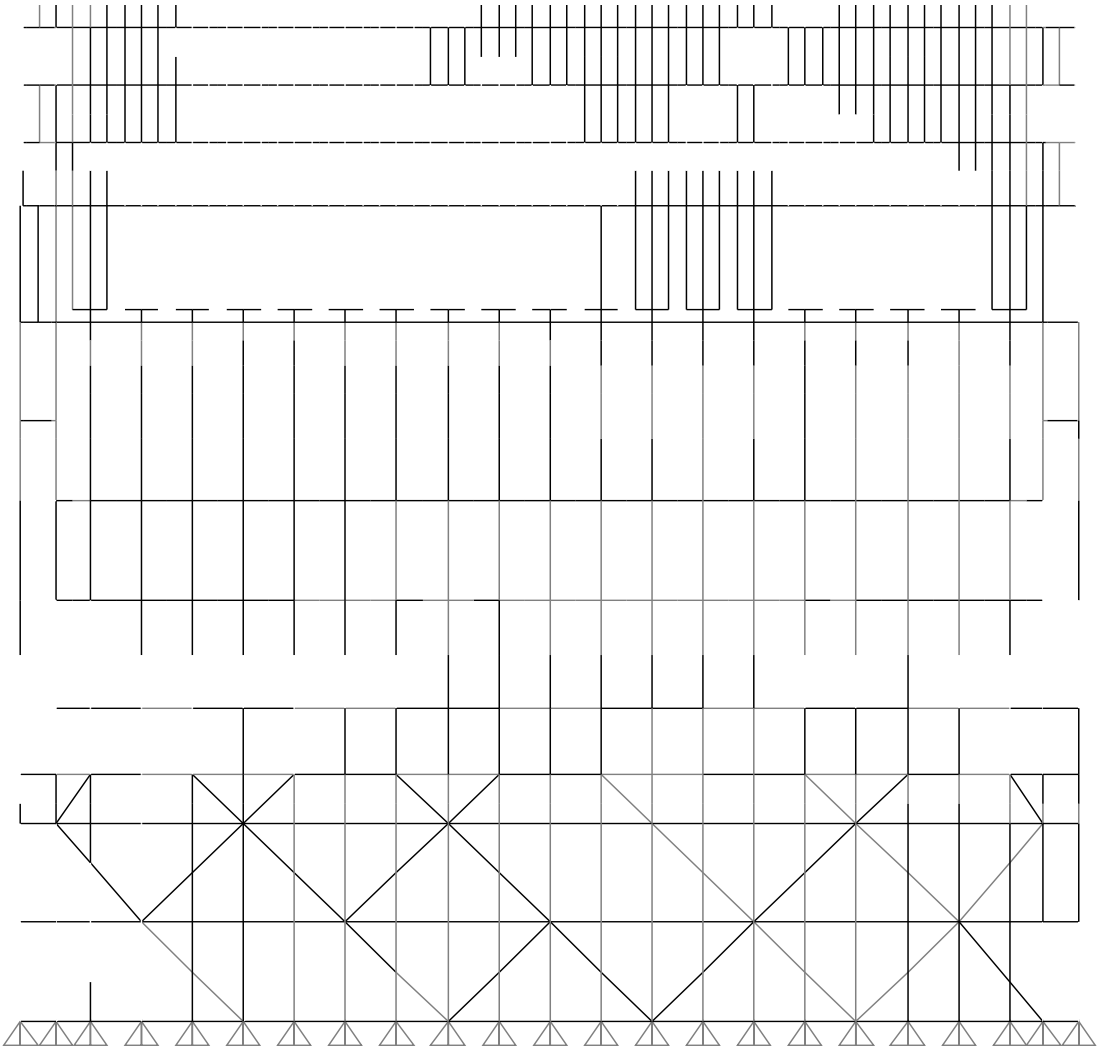
0
.50
0

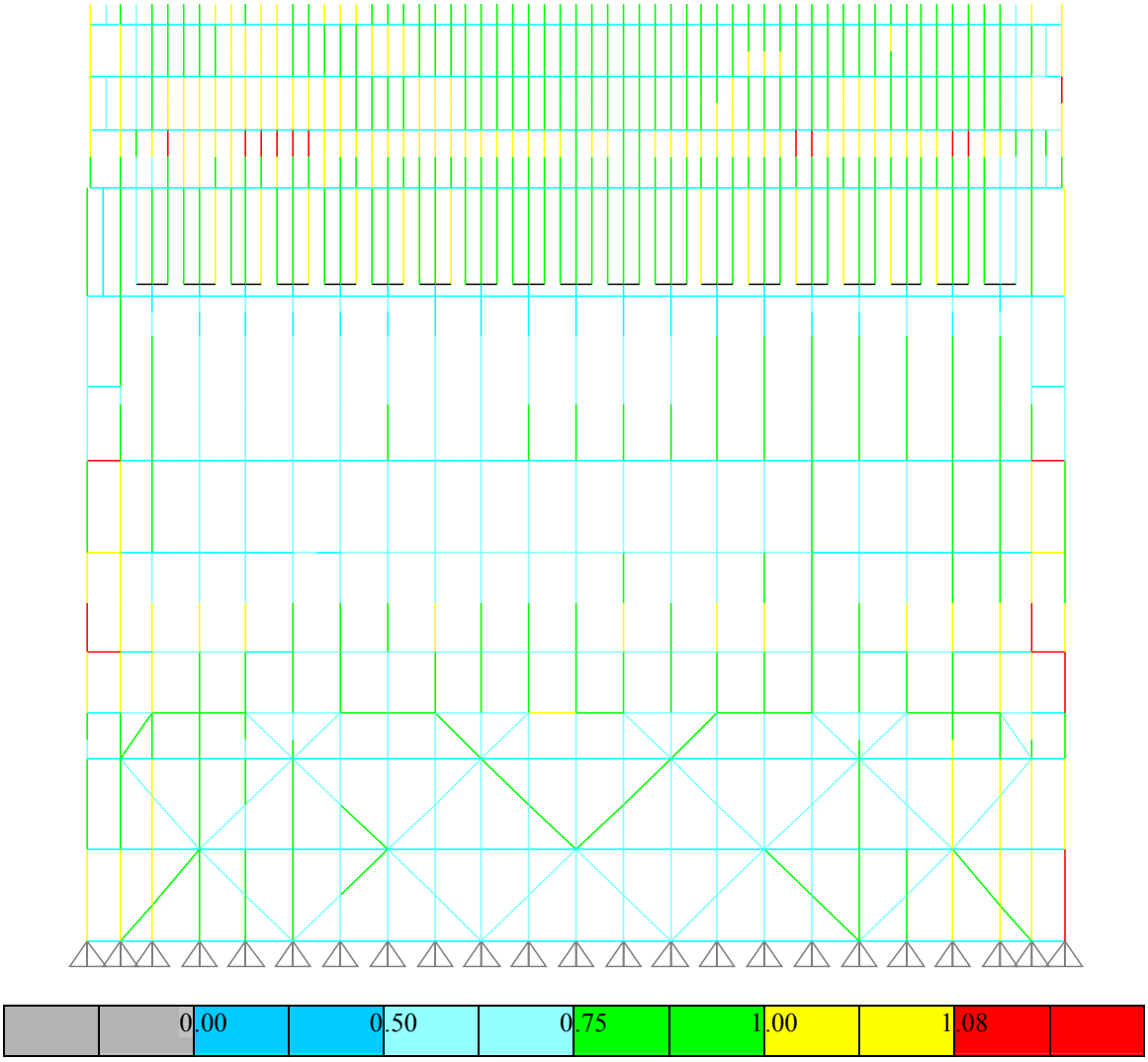

(c)

Figure 5–3. Demand/capacity ratios for WTC 1 under original design loads (c) south elevation below floor 9 (continued).

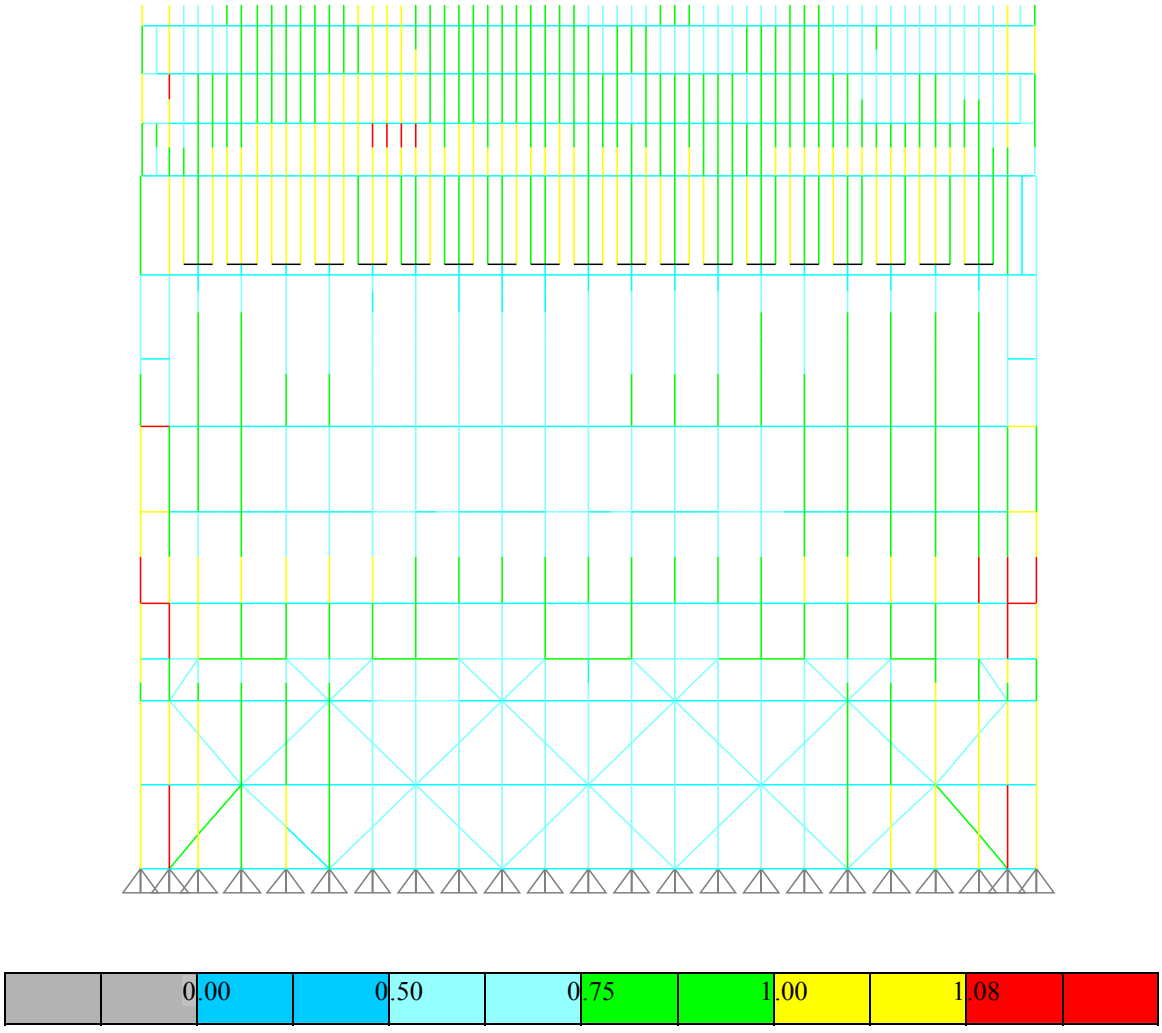

(d)

Figure 5–3. Demand/capacity ratios for WTC 1 under original design loads, (d) west elevation below floor 9 (continued).

LEVEL	TOWER A, DCR of CORE COLUMN 500's COLUMN NUMBER							
	501	502	503	504	505	506	507	508
106 FL	1.05	1.00	0.92	1.01	0.88	1.01	0.98	1.01
105 FL	0.85	1.09	0.99	0.85	0.96	1.09	1.07	0.83
104 FL	0.95	0.95	0.87	0.95	0.89	0.95	0.94	0.95
103 FL	1.02	1.02	0.93	1.02	0.95	1.01	1.01	1.02
102 FL	0.83	1.09	0.99	0.83	1.01	1.07	1.08	0.83
101 FL	0.90	0.92	0.85	0.90	0.93	0.88	0.90	0.90
100 FL	0.95	0.97	0.90	0.95	0.98	0.93	0.96	0.96
99 FL	1.01	1.03	0.95	1.01	1.04	0.97	1.01	1.01
98 FL	0.74	0.86	0.86	0.74	0.92	0.84	0.86	0.86
97 FL	0.78	0.91	0.91	0.78	0.96	0.88	0.90	0.90
96 FL	0.82	0.95	0.95	0.82	1.01	0.92	0.94	0.95
95 FL	0.73	0.84	0.84	0.73	0.88	0.81	0.83	0.73
94 FL	0.77	0.87	0.87	0.77	0.91	0.84	0.86	0.77
93 FL	0.80	0.91	0.91	0.80	0.95	0.87	0.90	0.80
92 FL	0.76	0.80	0.80	0.76	0.91	0.78	0.80	0.69
91 FL	0.79	0.83	0.83	0.79	0.95	0.81	0.83	0.71
90 FL	0.82	0.87	0.86	0.82	0.99	0.84	0.86	0.74
89 FL	0.70	0.78	0.77	0.70	0.86	0.75	0.83	0.70
88 FL	0.73	0.81	0.80	0.73	0.89	0.78	0.86	0.73
87 FL	0.75	0.83	0.83	0.75	0.92	0.81	0.89	0.75
86 FL	0.71	0.93	0.80	0.71	0.92	0.88	0.98	0.82
85 FL	0.73	0.96	0.82	0.73	0.95	0.90	1.02	0.85
84 FL	0.76	0.99	0.85	0.76	0.98	0.93	1.06	0.87
83 FL	0.83	0.91	0.90	0.83	0.89	0.87	0.94	0.83
82 FL	0.86	0.94	0.93	0.86	0.92	0.90	0.96	0.86
81 FL	0.88	0.97	0.95	0.88	0.94	0.93	0.99	0.88
80 FL	0.88	0.91	0.93	0.88	0.92	0.88	0.94	0.88
79 FL	0.91	0.94	0.96	0.91	0.95	0.90	0.97	0.91
78 FL	0.95	0.98	1.00	0.95	0.99	0.93	1.00	0.95
77 FL	0.66	0.67	0.68	0.66	0.67	0.65	0.69	0.66
76 FL	0.67	0.69	0.70	0.67	0.68	0.66	0.70	0.68
75 FL	0.83	0.84	0.85	0.83	0.89	0.84	0.86	0.84
74 FL	0.84	0.86	0.86	0.84	0.90	0.85	0.87	0.85
73 FL	0.86	0.87	0.88	0.86	0.92	0.87	0.89	0.87
72 FL	0.82	0.84	0.85	0.82	0.85	0.84	0.86	0.83
71 FL	0.84	0.85	0.87	0.84	0.87	0.85	0.88	0.85
70 FL	0.86	0.87	0.89	0.86	0.88	0.87	0.90	0.87
69 FL	0.81	0.80	0.83	0.81	0.85	0.82	0.83	0.82
68 FL	0.84	0.83	0.86	0.84	0.89	0.85	0.86	0.85
67 FL	0.85	0.84	0.87	0.85	0.89	0.85	0.87	0.86
66 FL	0.87	0.86	0.89	0.87	0.92	0.88	0.89	0.87
65 FL	0.88	0.87	0.91	0.88	0.93	0.89	0.91	0.89
64 FL	0.90	0.89	0.93	0.90	0.95	0.91	0.93	0.91
63 FL	0.86	0.87	0.89	0.86	0.92	0.88	0.88	0.86
62 FL	0.87	0.88	0.91	0.87	0.94	0.89	0.90	0.88
61 FL	0.89	0.90	0.92	0.89	0.96	0.91	0.91	0.89
60 FL	0.86	0.87	0.88	0.86	0.93	0.88	0.88	0.87
59 FL	0.88	0.88	0.89	0.88	0.95	0.89	0.89	0.88
58 FL	0.89	0.90	0.91	0.89	0.96	0.91	0.91	0.90
57 FL	0.86	0.85	0.88	0.86	0.91	0.87	0.86	0.87
56 FL	0.88	0.87	0.90	0.88	0.92	0.88	0.88	0.88
55 FL	0.89	0.88	0.91	0.89	0.94	0.89	0.89	0.89
54 FL	0.84	0.86	0.89	0.84	0.91	0.87	0.87	0.85
53 FL	0.85	0.88	0.90	0.85	0.93	0.89	0.89	0.86
52 FL	0.87	0.89	0.92	0.87	0.94	0.90	0.90	0.87
51 FL	0.85	0.86	0.88	0.85	0.92	0.87	0.87	0.86
50 FL	0.87	0.88	0.90	0.87	0.94	0.89	0.88	0.87
49 FL	0.88	0.89	0.91	0.88	0.95	0.90	0.90	0.88
48 FL	0.86	0.86	0.88	0.86	0.93	0.87	0.86	0.86
47 FL	0.87	0.87	0.89	0.87	0.94	0.88	0.87	0.87
46 FL	0.88	0.88	0.90	0.88	0.96	0.89	0.89	0.89
45 FL	0.80	0.80	0.83	0.80	0.89	0.83	0.80	0.81
44 FL	0.83	0.82	0.85	0.83	0.91	0.85	0.82	0.83
43 FL	0.63	0.62	0.64	0.63	0.69	0.63	0.63	0.64
42 FL	0.65	0.64	0.66	0.65	0.70	0.64	0.64	0.65
41 FL	0.84	0.85	0.87	0.84	0.95	0.86	0.86	0.85
40 FL	0.85	0.86	0.87	0.85	0.96	0.87	0.86	0.85
39 FL	0.84	0.84	0.86	0.84	0.94	0.85	0.85	0.84
38 FL	0.85	0.85	0.87	0.85	0.95	0.86	0.86	0.85
37 FL	0.86	0.86	0.88	0.86	0.96	0.87	0.87	0.86
36 FL	0.83	0.83	0.87	0.83	0.95	0.85	0.85	0.83
35 FL	0.84	0.85	0.88	0.84	0.96	0.86	0.86	0.85
34 FL	0.85	0.86	0.89	0.85	0.97	0.87	0.87	0.86
33 FL	0.84	0.84	0.87	0.84	0.95	0.85	0.85	0.85
32 FL	0.85	0.85	0.88	0.85	0.96	0.86	0.86	0.86
31 FL	0.86	0.86	0.89	0.86	0.97	0.87	0.87	0.87
30 FL	0.84	0.84	0.87	0.84	0.94	0.85	0.83	0.84
29 FL	0.85	0.85	0.88	0.85	0.95	0.86	0.84	0.85
28 FL	0.86	0.86	0.89	0.86	0.96	0.87	0.85	0.86
27 FL	0.85	0.84	0.85	0.85	0.95	0.85	0.83	0.85
26 FL	0.85	0.85	0.86	0.85	0.96	0.86	0.84	0.86
25 FL	0.86	0.86	0.87	0.86	0.97	0.87	0.85	0.87
24 FL	0.83	0.82	0.87	0.83	0.96	0.85	0.83	0.83
23 FL	0.84	0.83	0.88	0.84	0.97	0.86	0.84	0.84
22 FL	0.85	0.84	0.89	0.85	0.98	0.87	0.85	0.85
21 FL	0.84	0.82	0.87	0.84	0.94	0.85	0.83	0.84
20 FL	0.85	0.83	0.88	0.85	0.95	0.86	0.84	0.85
19 FL	0.86	0.84	0.89	0.86	0.96	0.87	0.85	0.86
18 FL	0.84	0.83	0.87	0.84	0.95	0.85	0.83	0.84
17 FL	0.85	0.83	0.88	0.85	0.96	0.86	0.84	0.85
16 FL	0.86	0.84	0.88	0.86	0.97	0.87	0.85	0.86
15 FL	0.86	0.83	0.87	0.86	0.96	0.86	0.83	0.85
14 FL	0.86	0.84	0.87	0.86	0.97	0.86	0.84	0.86
13 FL	0.87	0.85	0.88	0.87	0.98	0.87	0.85	0.87
12 FL	0.86	0.83	0.86	0.86	0.95	0.86	0.83	0.86
11 FL	0.86	0.84	0.87	0.86	0.96	0.87	0.84	0.87
10 FL	0.88	0.85	0.89	0.88	0.97	0.88	0.85	0.88
09 FL	0.92	0.83	0.92	0.92	1.04	0.90	0.89	0.84
08 FL	0.92	0.86	0.93	0.92	1.04	0.91	0.90	0.88
07 FL	0.78	0.76	0.78	0.78	0.81	0.77	0.75	0.78
06 FL	0.79	0.77	0.79	0.79	0.82	0.78	0.76	0.79
05 FL	0.79	0.77	0.79	0.79	0.82	0.78	0.77	0.79
04 FL	0.77	0.75	0.78	0.77	0.80	0.77	0.75	0.77
03 FL	0.84	0.81	0.83	0.84	0.87	0.82	0.81	0.84
02 FL	0.86	0.82	0.85	0.86	0.89	0.83	0.82	0.87
01 FL	0.83	0.83	0.86	0.83	0.90	0.84	0.83	0.83
B1 FL	0.82	0.82	0.85	0.82	0.90	0.84	0.82	0.82
B2 FL	0.83	0.83	0.86	0.83	0.91	0.85	0.83	0.83
B3 FL	0.83	0.81	0.83	0.83	0.89	0.80	0.80	0.84
B4 FL	0.89	0.86	0.88	0.89	0.95	0.85	0.86	0.91
B5 FL	0.90	0.86	0.89	0.90	0.96	0.86	0.86	0.91

(a)

LEVEL	TOWER A, DCR of CORE COLUMN 600's COLUMN NUMBER							
	601	602	603	604	605	606	607	608
106 FL	0.94	1.03	1.20	1.01	1.01	1.05	1.15	0.80
105 FL	1.03	1.19	1.36	1.11	1.09	1.19	1.23	0.92
104 FL	1.12	0.98	1.13	0.94	0.96	0.95	1.12	0.84
103 FL	1.04	1.03	1.18	1.01	1.03	1.01	1.18	0.93
102 FL	1.11	1.08	1.24	1.08	1.09	1.07	1.25	1.02
101 FL	1.19	1.06	1.05	0.88	0.99	1.07	1.05	1.09
100 FL	1.10	1.11	1.10	0.93	1.05	1.13	1.10	1.18
99 FL	1.16	1.18	1.15	0.99	1.10	1.20	1.16	1.27
98 FL	1.23	1.01	0.96	0.96	1.02	1.06	1.00	1.18
97 FL	1.18	1.06	1.00	1.01	1.07	1.12	1.04	1.25
96 FL	1.24	1.10	1.04	1.06	1.12	1.17	1.09	1.33
95 FL	1.31	0.97	0.93	0.98	1.05	1.05	0.96	1.12
94 FL	1.13	1.01	0.96	1.02	1.10	1.09	1.00	1.18
93 FL	1.18	1.04	0.99	1.07	1.14	1.14	1.04	1.24
92 FL	1.23	0.98	0.93	0.83	0.98	1.03	0.98	1.07
91 FL	1.08	1.02	0.95	0.86	1.02	1.07	1.01	1.12
90 FL	1.12	1.05	0.98	0.89	1.05	1.10	1.05	1.17
89 FL	1.17	0.95	0.89	0.93	0.92	1.02	0.94	1.03
88 FL	1.04	0.98	0.92	0.96	0.96	1.06	0.97	1.08
87 FL	1.08	1.01	0.94	1.00	0.99	1.10	1.00	1.12
86 FL	1.12	0.96	0.93	0.87	0.88	1.09	0.99	1.00
85 FL	1.15	0.99	0.95	0.90	0.90	1.13	1.02	1.04
84 FL	1.20	1.01	0.98	0.93	0.93	1.16	1.05	1.08
83 FL	1.25	0.93	0.90	0.96	0.96	0.99	0.96	1.11
82 FL	1.01	0.97	0.93	0.99	0.99	1.02	1.00	1.16
81 FL	1.04	1.02	0.99	1.04	1.03	1.07	1.05	1.21
80 FL	1.08	0.88	0.93	0.72	0.82	1.07	0.86	0.97
79 FL	1.04	0.90	0.96	0.74	0.84	1.09	0.88	1.01
78 FL	1.08	0.92	0.98	0.76	0.87	1.12	0.90	1.05
77 FL	0.76	0.63	0.66	0.62	0.68	0.65	0.66	0.85
76 FL	0.78	0.67	0.70	0.65	0.70	0.68	0.70	0.86
75 FL	0.97	0.84	0.89	0.82	0.91	0.86	0.86	1.00
74 FL	0.97	0.85	0.89	0.82	0.92	0.86	0.86	1.01
73 FL	1.00	0.86	0.91	0.84	0.93	0.88	0.88	1.04
72 FL	1.00	0.83	0.87	0.82	0.85	0.83	0.85	0.99
71 FL	1.03	0.84	0.88	0.83	0.86	0.84	0.86	1.02
70 FL	1.05	0.85	0.90	0.85	0.88	0.86	0.88	1.04
69 FL	0.80	0.78	0.82	0.80	0.84	0.83	0.83	0.86
68 FL	0.84	0.81	0.85	0.84	0.88	0.87	0.87	0.91
67 FL	0.83	0.80	0.85	0.84	0.87	0.86	0.86	0.90
66 FL	0.89	0.82	0.89	0.87	0.89	0.88	0.89	1.07
65 FL	0.90	0.82	0.89	0.87	0.89	0.86	0.89	1.09
64 FL	0.92	0.84	0.92	0.90	0.92	0.90	0.91	1.12
63 FL	0.90	0.81	0.89	0.86	0.88	0.87	0.88	0.99
62 FL	0.91	0.83	0.90	0.88	0.89	0.88	0.89	1.01
61 FL	0.93	0.84	0.92	0.89	0.91	0.89	0.91	1.03
60 FL	0.90	0.81	0.86	0.90	0.87	0.87	0.87	1.05
59 FL	0.91	0.82	0.87	0.91	0.89	0.88	0.88	1.07
58 FL	0.93	0.83	0.88	0.93	0.90	0.89	0.89	1.08
57 FL	0.90	0.81	0.86	0.90	0.87	0.86	0.86	1.05
56 FL	0.92	0.82	0.87	0.92	0.88	0.87	0.87	1.07
55 FL	0.93	0.83	0.88	0.93	0.89	0.88	0.88	1.08
54 FL	0.87	0.81	0.86	0.90	0.91	0.86	0.83	1.04
53 FL	0.88	0.82	0.87	0.91	0.92	0.87	0.84	1.06
52 FL	0.89	0.83	0.88	0.93	0.93	0.88	0.85	1.08
51 FL	0.87	0.81	0.86	0.90	0.90	0.86	0.83	1.04
50 FL	0.89	0.82	0.87	0.91	0.91	0.87	0.83	1.05
49 FL	0.90	0.83	0.88	0.92	0.93	0.88	0.84	1.07
48 FL	0.88	0.81	0.86	0.93	0.90	0.84	0.82	1.03
47 FL	0.89	0.82	0.87	0.94	0.91	0.85	0.83	1.05
46 FL	0.91	0.83	0.88	0.96	0.92	0.86	0.84	1.07
45 FL	0.83	0.77	0.81	0.86	0.84	0.80	0.75	0.92
44 FL	0.85	0.78	0.83	0.89	0.86	0.81	0.77	0.95
43 FL	0.64	0.56	0.60	0.65	0.65	0.61	0.58	0.70
42 FL	0.66	0.56	0.63	0.68	0.68	0.64	0.61	0.72
41 FL	0.85	0.77	0.83	0.88	0.90	0.84	0.81	0.92
40 FL	0.85	0.76	0.82	0.88	0.90	0.84	0.81	0.92
39 FL	0.84	0.77	0.82	0.88	0.88	0.84	0.80	0.90
38 FL	0.85	0.78	0.83	0.90	0.89	0.85	0.81	0.91
37 FL	0.87	0.79	0.84	0.91	0.90	0.86	0.82	0.93
36 FL	0.85	0.78	0.81	0.88	0.87	0.84	0.81	0.91
35 FL	0.86	0.79	0.82	0.89	0.88	0.85	0.82	0.92
34 FL	0.88	0.80	0.82	0.91	0.90	0.86	0.82	0.93
33 FL	0.84	0.77	0.81	0.89	0.87	0.83	0.80	0.92
32 FL	0.85	0.77	0.82	0.90	0.88	0.84	0.81	0.93
31 FL	0.86	0.78	0.83	0.91	0.89	0.85	0.82	0.94
30 FL	0.82	0.77	0.82	0.89	0.87	0.84	0.81	0.92
29 FL	0.83	0.78	0.82	0.90	0.88	0.85	0.82	0.94
28 FL	0.84	0.78	0.83	0.91	0.89	0.86	0.83	0.95
27 FL	0.83	0.77	0.82	0.89	0.88	0.85	0.80	0.93
26 FL	0.84	0.78	0.82	0.90	0.88	0.84	0.81	0.94
25 FL	0.85	0.79	0.83	0.91	0.89	0.85	0.82	0.95
24 FL	0.82	0.78	0.81	0.89	0.88	0.82	0.80	0.94
23 FL	0.83	0.78	0.81	0.90	0.89	0.82	0.81	0.95
22 FL	0.84	0.79	0.82	0.91	0.89	0.83	0.82	0.96
21 FL	0.82	0.78	0.81	0.92	0.88	0.82	0.81	0.94
20 FL	0.83	0.79	0.82	0.93	0.89	0.83	0.82	0.96
19 FL	0.84	0.79	0.83	0.94	0.90	0.83	0.83	0.97
18 FL	0.82	0.78	0.81	0.92	0.88	0.82	0.80	0.93
17 FL	0.83	0.79	0.82	0.93	0.89	0.82	0.80	0.94
16 FL	0.84	0.79	0.83	0.94	0.90	0.83	0.81	0.95
15 FL	0.81	0.77	0.80	0.93	0.90	0.81	0.80	0.93
14 FL	0.82	0.78	0.81	0.93	0.91	0.82	0.80	0.94
13 FL	0.83	0.79	0.82	0.94	0.92	0.82	0.81	0.95
12 FL	0.82	0.78	0.81	0.93	0.90	0.82	0.79	0.94
11 FL	0.83	0.78	0.82	0.94	0.91	0.82	0.79	0.95
10 FL	0.84	0.80	0.83	0.95	0.92	0.84	0.80	0.96
09 FL	0.92	0.76	0.90	1.04	1.01	0.97	0.87	1.03
08 FL	0.92	0.81	0.90	1.04	1.02	0.98	0.87	1.04
07 FL	0.57	0.53	0.56	0.62	0.60	0.60	0.55	0.61
06 FL	0.59	0.55	0.57	0.63	0.62	0.62	0.56	0.62
05 FL	0.59	0.55	0.58	0.64	0.63	0.63	0.57	0.62
04 FL	0.57	0.54	0.56	0.62	0.61	0.61	0.55	0.60
03 FL	0.66	0.61	0.64	0.71	0.70	0.69	0.63	0.69
02 FL	0.69	0.62	0.66	0.74	0.72	0.71	0.64	0.72
01 FL	0.80	0.79	0.82	0.92	0.90	0.88	0.79	0.88
B1 FL	0.79	0.78	0.81	0.91	0.89	0.87	0.79	0.88
B2 FL	0.81	0.79	0.82	0.93	0.90	0.88	0.80	0.89
B3 FL	0.77	0.75	0.81	0.89	0.87	0.87	0.78	0.84
B4 FL	0.79	0.83	0.89	0.99	0.97	0.95	0.86	0.95
B5 FL	0.80	0.83	0.90	1.00	0.98	0.96	0.87	0.92

(b)

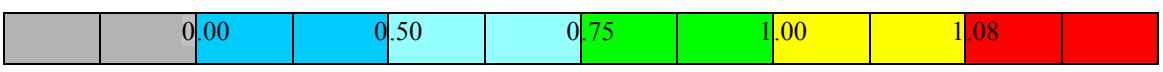

Figure 5–4. Demand/capacity ratios for WTC 1 core columns under original design loads, (a) 500 line and (b) 600 line.

LEVEL	TOWER A, DCR of CORE COLUMN 700's COLUMN NUMBER							
	701	702	703	704	705	706	707	708
106 FL	0.78	0.99	0.86	0.05	0.32	0.50	0.78	0.82
105 FL	0.85	1.07	0.61	0.11	0.40	0.57	0.84	0.89
104 FL	1.00	0.99	0.78	0.16	0.40	0.58	0.79	0.79
103 FL	1.07	1.06	0.85	0.21	0.47	0.64	0.84	0.85
102 FL	1.14	1.13	0.51	0.26	0.53	0.70	0.89	0.91
101 FL	0.93	0.87	0.79	0.31	0.60	0.64	0.80	0.72
100 FL	0.99	0.91	0.85	0.36	0.66	0.69	0.84	0.76
99 FL	1.05	0.96	0.89	0.42	0.73	0.75	0.89	0.80
98 FL	0.82	0.85	0.76	0.35	0.79	0.69	0.84	0.71
97 FL	0.86	0.89	0.80	0.39	0.86	0.73	0.88	0.75
96 FL	0.90	0.93	0.84	0.44	0.93	0.78	0.92	0.79
95 FL	0.86	0.80	0.71	0.37	0.82	0.72	0.83	0.82
94 FL	0.90	0.84	0.75	0.41	0.87	0.77	0.87	0.86
93 FL	0.94	0.87	0.79	0.44	0.93	0.81	0.91	0.90
92 FL	0.80	0.80	0.74	0.42	0.89	0.75	0.83	0.76
91 FL	0.83	0.83	0.77	0.45	0.93	0.79	0.86	0.79
90 FL	0.87	0.86	0.80	0.48	0.98	0.83	0.90	0.82
89 FL	0.78	0.79	0.76	0.62	0.81	0.78	0.83	0.75
88 FL	0.81	0.82	0.79	0.65	0.85	0.81	0.86	0.78
87 FL	0.84	0.84	0.82	0.69	0.89	0.85	0.88	0.81
86 FL	0.77	0.80	0.76	0.66	1.07	0.83	0.85	0.76
85 FL	0.79	0.82	0.79	0.69	1.12	0.87	0.88	0.78
84 FL	0.82	0.85	0.82	0.73	1.16	0.90	0.91	0.81
83 FL	0.79	0.79	0.77	0.70	1.08	0.84	0.78	0.75
82 FL	0.81	0.82	0.80	0.73	1.12	0.87	0.81	0.78
81 FL	0.84	0.84	0.82	0.76	1.16	0.90	0.83	0.80
80 FL	0.78	0.87	0.85	0.65	1.06	0.94	0.94	0.84
79 FL	0.81	0.91	0.89	0.69	1.13	0.98	0.98	0.87
78 FL	0.84	0.94	0.92	0.73	1.18	1.02	1.01	0.91
77 FL	0.67	0.60	0.46	0.46	0.66	0.50	0.59	0.68
76 FL	0.69	0.65	0.53	0.55	0.61	0.57	0.64	0.70
75 FL	0.84	0.85	0.82	0.76	0.69	0.94	0.89	0.90
74 FL	0.85	0.84	0.83	0.75	0.70	0.94	0.90	0.91
73 FL	0.87	0.86	0.84	0.76	0.72	0.97	0.92	0.93
72 FL	0.85	0.81	0.79	0.72	0.69	0.92	0.87	0.91
71 FL	0.87	0.83	0.80	0.74	0.72	0.94	0.89	0.93
70 FL	0.89	0.84	0.81	0.75	0.74	0.97	0.91	0.95
69 FL	0.69	0.80	0.77	0.72	0.71	0.83	0.87	0.76
68 FL	0.72	0.85	0.80	0.77	0.78	0.89	0.92	0.79
67 FL	0.71	0.82	0.80	0.74	0.76	0.87	0.90	0.79
66 FL	0.87	0.84	0.81	0.75	0.78	0.89	0.92	0.93
65 FL	0.88	0.84	0.81	0.76	0.78	0.89	0.92	0.94
64 FL	0.90	0.86	0.83	0.78	0.83	0.93	0.95	0.97
63 FL	0.87	0.79	0.83	0.79	0.80	0.87	0.90	0.95
62 FL	0.89	0.81	0.84	0.81	0.82	0.88	0.92	0.96
61 FL	0.91	0.82	0.85	0.82	0.84	0.89	0.93	0.98
60 FL	0.86	0.83	0.81	0.78	0.81	0.84	0.86	0.95
59 FL	0.88	0.84	0.82	0.79	0.83	0.85	0.87	0.96
58 FL	0.89	0.86	0.83	0.80	0.85	0.86	0.88	0.98
57 FL	0.87	0.79	0.81	0.77	0.81	0.87	0.90	0.92
56 FL	0.89	0.80	0.82	0.78	0.83	0.88	0.91	0.94
55 FL	0.90	0.81	0.83	0.79	0.85	0.89	0.92	0.95
54 FL	0.88	0.82	0.80	0.76	0.83	0.84	0.84	0.91
53 FL	0.90	0.83	0.81	0.77	0.84	0.85	0.85	0.92
52 FL	0.91	0.84	0.82	0.78	0.86	0.87	0.86	0.93
51 FL	0.89	0.76	0.79	0.75	0.84	0.82	0.87	0.92
50 FL	0.91	0.79	0.80	0.76	0.85	0.83	0.88	0.93
49 FL	0.92	0.80	0.81	0.77	0.87	0.84	0.89	0.94
48 FL	0.90	0.81	0.78	0.74	0.84	0.85	0.82	0.92
47 FL	0.92	0.82	0.79	0.75	0.86	0.86	0.83	0.93
46 FL	0.93	0.83	0.80	0.77	0.88	0.88	0.85	0.94
45 FL	0.92	0.77	0.75	0.72	0.79	0.81	0.79	0.86
44 FL	0.95	0.80	0.76	0.75	0.82	0.83	0.81	0.89
43 FL	0.66	0.72	0.56	0.56	0.57	0.64	0.73	0.67
42 FL	0.68	0.76	0.59	0.60	0.60	0.69	0.77	0.69
41 FL	0.90	0.78	0.79	0.78	0.76	0.90	0.87	0.91
40 FL	0.90	0.77	0.79	0.77	0.76	0.89	0.87	0.90
39 FL	0.87	0.78	0.79	0.78	0.77	0.89	0.80	0.89
38 FL	0.88	0.79	0.79	0.79	0.79	0.90	0.81	0.91
37 FL	0.90	0.80	0.80	0.80	0.80	0.91	0.82	0.92
36 FL	0.87	0.73	0.78	0.77	0.78	0.89	0.83	0.90
35 FL	0.88	0.74	0.79	0.78	0.79	0.90	0.84	0.91
34 FL	0.89	0.75	0.79	0.78	0.80	0.91	0.85	0.92
33 FL	0.86	0.76	0.78	0.76	0.78	0.89	0.77	0.90
32 FL	0.87	0.77	0.79	0.77	0.80	0.90	0.78	0.91
31 FL	0.88	0.77	0.80	0.78	0.81	0.91	0.79	0.92
30 FL	0.85	0.77	0.78	0.76	0.79	0.88	0.80	0.91
29 FL	0.86	0.78	0.78	0.76	0.80	0.89	0.81	0.92
28 FL	0.87	0.78	0.79	0.77	0.82	0.90	0.82	0.93
27 FL	0.86	0.77	0.77	0.75	0.80	0.84	0.83	0.90
26 FL	0.87	0.77	0.77	0.76	0.81	0.85	0.84	0.92
25 FL	0.88	0.78	0.78	0.76	0.82	0.86	0.85	0.93
24 FL	0.86	0.77	0.76	0.74	0.80	0.81	0.83	0.91
23 FL	0.87	0.77	0.77	0.75	0.81	0.82	0.84	0.92
22 FL	0.88	0.78	0.78	0.76	0.83	0.83	0.85	0.93
21 FL	0.85	0.77	0.76	0.76	0.81	0.80	0.83	0.91
20 FL	0.86	0.78	0.77	0.77	0.82	0.81	0.83	0.92
19 FL	0.87	0.79	0.78	0.78	0.83	0.82	0.84	0.93
18 FL	0.86	0.77	0.76	0.76	0.79	0.79	0.87	0.89
17 FL	0.87	0.78	0.77	0.77	0.79	0.80	0.82	0.90
16 FL	0.88	0.78	0.77	0.77	0.80	0.81	0.83	0.91
15 FL	0.86	0.77	0.76	0.73	0.82	0.80	0.82	0.89
14 FL	0.87	0.78	0.77	0.73	0.83	0.80	0.82	0.89
13 FL	0.88	0.78	0.77	0.74	0.84	0.81	0.83	0.90
12 FL	0.86	0.77	0.74	0.75	0.78	0.80	0.81	0.88
11 FL	0.87	0.78	0.75	0.75	0.79	0.81	0.82	0.89
10 FL	0.88	0.79	0.76	0.77	0.81	0.82	0.84	0.90
09 FL	0.96	0.89	0.83	0.88	0.98	0.88	0.86	0.86
08 FL	0.97	0.90	0.84	0.89	0.99	0.89	0.75	0.87
07 FL	0.69	0.53	0.51	0.53	0.45	0.51	0.54	0.69
06 FL	0.71	0.54	0.53	0.56	0.46	0.53	0.55	0.71
05 FL	0.71	0.55	0.53	0.57	0.47	0.53	0.56	0.71
04 FL	0.68	0.54	0.52	0.56	0.46	0.52	0.55	0.69
03 FL	0.78	0.58	0.59	0.67	0.51	0.59	0.59	0.79
02 FL	0.81	0.59	0.60	0.69	0.52	0.60	0.61	0.81
01 FL	0.85	0.78	0.75	0.63	0.90	0.82	0.80	0.87
B1 FL	0.84	0.76	0.74	0.62	0.90	0.81	0.80	0.86
B2 FL	0.85	0.76	0.75	0.63	0.92	0.82	0.81	0.87
B3 FL	0.81	0.73	0.74	0.58	0.85	0.78	0.76	0.84
B4 FL	0.83	0.77	0.81	0.67	0.92	0.85	0.81	0.94
B5 FL	0.84	0.76	0.82	0.67	0.93	0.86	0.81	0.94

(c)

LEVEL	TOWER A, DCR of CORE COLUMN 800's COLUMN NUMBER						
	801	802	803	804	805	806	807
106 FL	0.86	0.95	0.54	0.37	0.59	0.74	0.90
105 FL	0.93	1.03	0.63	0.47	0.64	0.79	0.98
104 FL	0.82	0.89	0.59	0.48	0.58	0.73	0.90
103 FL	0.87	0.95	0.66	0.56	0.62	0.77	0.97
102 FL	0.93	1.01	0.47	0.64	0.66	0.81	1.04
101 FL	0.73	0.79	0.51	0.49	0.60	0.76	0.90
100 FL	0.77	0.82	0.55	0.55	0.64	0.80	0.95
99 FL	0.81	0.85	0.58	0.60	0.67	0.84	1.01
98 FL	0.85	0.80	0.55	0.62	0.53	0.75	0.74
97 FL	0.89	0.83	0.58	0.68	0.55	0.78	0.78
96 FL	0.94	0.86	0.61	0.73	0.58	0.81	0.82
95 FL	0.71	0.69	0.53	0.67	0.57	0.77	0.74
94 FL	0.73	0.71	0.56	0.72	0.59	0.80	0.78
93 FL	0.76	0.73	0.58	0.77	0.62	0.83	0.81
92 FL	0.71	0.65	0.54	0.70	0.57	0.75	0.77
91 FL	0.73	0.67	0.57	0.75	0.59	0.78	0.80
90 FL	0.75	0.69	0.59	0.79	0.61	0.80	0.83
89 FL	0.71	0.66	0.56	0.73	0.60	0.74	0.73
88 FL	0.73	0.67	0.58	0.77	0.62	0.76	0.76
87 FL	0.75	0.69	0.60	0.80	0.65	0.79	0.78
86 FL	0.74	0.71	0.70	0.76	0.73	0.72	0.73
85 FL	0.76	0.73	0.72	0.79	0.76	0.74	0.75
84 FL	0.78	0.75	0.75	0.82	0.78	0.76	0.78
83 FL	0.74	0.70	0.71	0.70	0.76	0.72	0.74
82 FL	0.76	0.72	0.73	0.73	0.79	0.74	0.76
81 FL	0.78	0.74	0.75	0.76	0.81	0.76	0.78
80 FL	0.84	0.64	0.80	0.79	0.84	0.78	0.80
79 FL	0.87	0.67	0.83	0.83	0.87	0.81	0.82
78 FL	0.90	0.69	0.86	0.87	0.90	0.83	0.85
77 FL	0.69	0.45	0.56	0.62	0.54	0.50	0.68
76 FL	0.70	0.49	0.58	0.65	0.61	0.57	0.71
75 FL	0.89	0.74	0.73	0.73	0.91	0.80	0.90
74 FL	0.90	0.74	0.74	0.73	0.91	0.80	0.91
73 FL	0.92	0.76	0.76	0.75	0.94	0.82	0.93
72 FL	0.89	0.72	0.73	0.73	0.85	0.78	0.87
71 FL	0.91	0.74	0.75	0.75	0.88	0.80	0.89
70 FL	0.93	0.76	0.77	0.77	0.90	0.82	0.91
69 FL	0.73	0.72	0.74	0.72	0.85	0.78	0.76
68 FL	0.76	0.77	0.78	0.79	0.92	0.83	0.79
67 FL	0.76	0.75	0.78	0.76	0.90	0.82	0.79
66 FL	0.90	0.77	0.80	0.78	0.86	0.83	0.93
65 FL	0.91	0.77	0.80	0.79	0.86	0.84	0.94
64 FL	0.93	0.80	0.84	0.82	0.90	0.87	0.97
63 FL	0.87	0.74	0.80	0.77	0.85	0.82	0.92
62 FL	0.89	0.76	0.82	0.79	0.88	0.84	0.94
61 FL	0.91	0.77	0.84	0.80	0.88	0.85	0.95
60 FL	0.88	0.79	0.81	0.79	0.82	0.79	0.93
59 FL	0.90	0.80	0.83	0.81	0.83	0.81	0.95
58 FL	0.92	0.82	0.85	0.83	0.85	0.82	0.97
57 FL	0.88	0.75	0.82	0.78	0.86	0.83	0.94
56 FL	0.89	0.77	0.84	0.80	0.87	0.85	0.95
55 FL	0.91	0.78	0.85	0.81	0.89	0.86	0.97
54 FL	0.87	0.80	0.83	0.80	0.83	0.79	0.92
53 FL	0.88	0.81	0.84	0.81	0.85	0.81	0.94
52 FL	0.90	0.82	0.86	0.83	0.86	0.82	0.95
51 FL	0.86	0.76	0.86	0.79	0.88	0.83	0.91
50 FL	0.87	0.78	0.88	0.80	0.89	0.85	0.92
49 FL	0.89	0.79	0.89	0.81	0.91	0.86	0.94
48 FL	0.87	0.80	0.87	0.76	0.85	0.80	0.91
47 FL	0.89	0.81	0.88	0.78	0.87	0.81	0.93
46 FL	0.91	0.83	0.90	0.79	0.88	0.82	0.94
45 FL	0.70	0.78	0.82	0.75	0.79	0.77	0.73
44 FL	0.73	0.80	0.85	0.78	0.82	0.80	0.76
43 FL	0.63	0.71	0.60	0.55	0.70	0.62	0.66
42 FL	0.65	0.75	0.62	0.58	0.74	0.64	0.68
41 FL	0.87	0.76	0.81	0.80	0.87	0.83	0.91
40 FL	0.87	0.75	0.81	0.79	0.86	0.83	0.91
39 FL	0.86	0.77	0.83	0.73	0.87	0.84	0.90
38 FL	0.87	0.78	0.84	0.75	0.89	0.85	0.91
37 FL	0.89	0.79	0.85	0.76	0.90	0.86	0.92
36 FL	0.87	0.80	0.82	0.77	0.81	0.79	0.89
35 FL	0.88	0.81	0.83	0.78	0.82	0.80	0.90
34 FL	0.89	0.82	0.85	0.79	0.83	0.81	0.91
33 FL	0.86	0.75	0.83	0.74	0.84	0.82	0.91
32 FL	0.88	0.76	0.84	0.75	0.86	0.83	0.92
31 FL	0.89	0.77	0.85	0.76	0.87	0.84	0.93
30 FL	0.86	0.78	0.84	0.78	0.87	0.85	0.90
29 FL	0.87	0.78	0.85	0.79	0.88	0.86	0.91
28 FL	0.88	0.79	0.86	0.80	0.89	0.87	0.92
27 FL	0.88	0.80	0.85	0.81	0.85	0.80	0.91
26 FL	0.89	0.81	0.86	0.82	0.86	0.80	0.92
25 FL	0.90	0.82	0.87	0.83	0.87	0.82	0.93
24 FL	0.88	0.81	0.84	0.78	0.86	0.83	0.91
23 FL	0.89	0.82	0.85	0.79	0.87	0.84	0.92
22 FL	0.90	0.83	0.86	0.80	0.88	0.85	0.93
21 FL	0.88	0.82	0.84	0.81	0.87	0.85	0.91
20 FL	0.89	0.83	0.85	0.82	0.88	0.86	0.92
19 FL	0.90	0.84	0.87	0.83	0.89	0.87	0.93
18 FL	0.88	0.82	0.85	0.79	0.86	0.84	0.89
17 FL	0.89	0.83	0.86	0.80	0.87	0.85	0.90
16 FL	0.90	0.84	0.87	0.81	0.88	0.86	0.91
15 FL	0.88	0.82	0.86	0.82	0.86	0.85	0.89
14 FL	0.89	0.83	0.87	0.83	0.87	0.86	0.90
13 FL	0.90	0.84	0.88	0.83	0.88	0.87	0.90
12 FL	0.88	0.83	0.87	0.79	0.87	0.85	0.91
11 FL	0.89	0.83	0.88	0.80	0.88	0.86	0.92
10 FL	0.91	0.85	0.90	0.82	0.89	0.88	0.93
09 FL	0.75	0.84	0.97	0.87	0.90	0.72	0.89
08 FL	0.80	0.85	0.97	0.88	0.91	0.78	0.88
07 FL	0.70	0.54	0.54	0.53	0.55	0.55	0.69
06 FL	0.72	0.56	0.56	0.54	0.57	0.56	0.71
05 FL	0.72	0.57	0.57	0.55	0.58	0.57	0.72
04 FL	0.70	0.56	0.55	0.54	0.56	0.57	0.69
03 FL	0.80	0.60	0.63	0.60	0.63	0.61	0.80
02 FL	0.83	0.62	0.65	0.62	0.65	0.62	0.83
01 FL	0.89	0.62	0.88	0.94	0.85	0.84	0.92
B1 FL	0.88	0.82	0.88	0.94	0.84	0.84	0.91
B2 FL	0.89	0.83	0.89	0.96	0.85	0.85	0.92
B3 FL	0.85	0.78	0.86	0.91	0.80	0.80	0.87
B4 FL	0.87	0.82	0.95	0.99	0.87	0.85	0.97
B5 FL	0.88	0.83	0.96	1.00	0.88	0.86	0.98

(d)

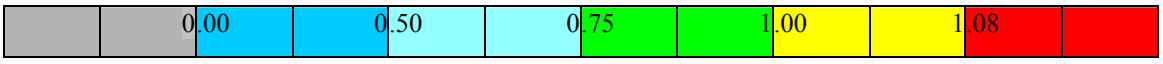

Figure 5–4. Demand/capacity ratios for WTC 1 core columns under original design loads, (c) 700 line and (d) 800 line (continued).

LEVEL	TOWER A, DCR of CORE COLUMN 900's COLUMN NUMBER							
	901	902	903	904	905	906	907	908
106 FL	0.76	0.98	0.97	0.80	0.85	1.10	1.02	0.76
105 FL	0.82	1.05	1.02	0.71	0.91	1.16	1.08	0.80
104 FL	0.83	0.95	0.94	1.15	0.75	0.96	0.97	0.80
103 FL	0.92	1.01	0.98	1.21	0.80	1.01	1.02	0.89
102 FL	1.01	1.07	1.03	0.89	0.88	1.05	1.07	0.97
101 FL	0.87	0.96	0.86	0.98	0.78	0.89	0.98	0.84
100 FL	0.94	1.01	0.88	1.04	0.84	0.93	1.03	0.91
99 FL	1.01	1.05	0.91	1.10	0.90	0.97	1.08	0.98
98 FL	1.02	0.92	0.81	0.99	0.88	0.90	0.94	1.00
97 FL	1.03	0.96	0.83	1.05	0.93	0.93	0.98	1.06
96 FL	1.16	1.00	0.86	1.10	0.99	0.97	1.02	1.13
95 FL	0.91	0.84	0.81	0.88	0.86	0.86	0.90	1.08
94 FL	0.96	0.88	0.83	0.92	0.91	0.89	0.94	1.14
93 FL	1.00	0.91	0.85	0.96	0.95	0.92	0.97	1.20
92 FL	0.89	0.86	0.78	0.90	0.90	0.86	0.87	1.04
91 FL	0.93	0.89	0.80	0.94	0.94	0.89	0.90	1.09
90 FL	0.97	0.92	0.82	0.98	0.98	0.92	0.93	1.14
89 FL	1.01	0.84	0.76	0.84	0.84	0.83	0.85	1.00
88 FL	1.05	0.86	0.78	0.87	0.88	0.85	0.88	1.05
87 FL	1.09	0.89	0.80	0.90	0.91	0.88	0.90	1.09
86 FL	0.97	0.85	0.75	0.93	0.78	0.87	0.86	0.97
85 FL	1.01	0.87	0.77	0.96	0.81	0.89	0.88	1.00
84 FL	1.04	0.90	0.79	0.99	0.83	0.92	0.91	1.04
83 FL	1.07	0.79	0.73	0.86	0.79	0.87	0.80	1.07
82 FL	1.14	0.81	0.75	0.89	0.82	0.89	0.82	1.11
81 FL	1.15	0.83	0.77	0.92	0.84	0.91	0.84	1.14
80 FL	1.19	0.86	0.85	0.95	0.87	0.94	0.86	1.19
79 FL	1.25	0.89	0.88	0.99	0.91	0.97	0.89	1.24
78 FL	1.30	0.92	0.90	1.03	0.94	1.00	0.92	1.30
77 FL	0.84	0.67	0.62	0.71	0.60	0.56	0.55	0.88
76 FL	0.85	0.71	0.65	0.73	0.63	0.60	0.60	0.90
75 FL	0.96	0.85	0.84	0.94	0.76	0.85	0.88	1.05
74 FL	0.96	0.85	0.84	0.95	0.77	0.85	0.88	1.06
73 FL	1.01	0.87	0.86	0.97	0.79	0.87	0.90	1.09
72 FL	0.95	0.89	0.79	0.92	0.77	0.82	0.85	1.03
71 FL	0.98	0.91	0.81	0.94	0.79	0.85	0.87	1.06
70 FL	1.00	0.93	0.82	0.96	0.81	0.87	0.88	1.08
69 FL	0.81	0.81	0.79	0.91	0.77	0.82	0.84	0.88
68 FL	0.88	0.87	0.82	0.96	0.82	0.88	0.89	0.95
67 FL	0.86	0.85	0.82	0.96	0.81	0.86	0.87	0.92
66 FL	1.01	0.93	0.85	0.98	0.83	0.88	0.89	1.09
65 FL	1.03	0.93	0.85	0.98	0.83	0.89	0.89	1.11
64 FL	1.06	0.97	0.88	1.02	0.87	0.92	0.92	1.14
63 FL	1.00	0.91	0.83	0.97	0.82	0.94	0.88	1.07
62 FL	1.03	0.93	0.84	0.99	0.84	0.96	0.89	1.10
61 FL	1.05	0.95	0.85	1.01	0.85	0.99	0.91	1.12
60 FL	0.99	0.90	0.83	0.97	0.83	0.93	0.87	1.06
59 FL	1.01	0.92	0.84	0.99	0.85	0.95	0.88	1.08
58 FL	1.03	0.93	0.86	1.01	0.87	0.97	0.90	1.10
57 FL	1.06	0.88	0.84	1.01	0.85	0.93	0.84	1.04
56 FL	1.08	0.90	0.85	1.02	0.86	0.94	0.85	1.06
55 FL	1.10	0.91	0.86	1.04	0.88	0.96	0.87	1.09
54 FL	1.04	0.93	0.84	1.01	0.86	0.91	0.88	1.11
53 FL	1.06	0.94	0.85	1.02	0.87	0.93	0.89	1.13
52 FL	1.08	0.96	0.87	1.04	0.89	0.95	0.91	1.15
51 FL	1.03	0.89	0.85	0.99	0.86	0.97	0.83	1.09
50 FL	1.05	0.90	0.86	1.01	0.87	0.98	0.85	1.11
49 FL	1.07	0.91	0.87	1.03	0.89	1.00	0.86	1.13
48 FL	1.09	0.83	0.83	0.97	0.86	0.89	0.83	1.08
47 FL	1.12	0.85	0.85	0.98	0.87	0.92	0.85	1.11
46 FL	1.14	0.87	0.86	1.00	0.89	0.93	0.87	1.13
45 FL	0.85	0.78	0.77	0.76	0.83	0.84	0.79	0.88
44 FL	0.87	0.80	0.79	0.78	0.85	0.86	0.81	0.90
43 FL	0.75	0.61	0.60	0.69	0.63	0.66	0.62	0.77
42 FL	0.77	0.63	0.63	0.72	0.66	0.68	0.64	0.79
41 FL	1.00	0.85	0.83	0.94	0.86	0.90	0.86	1.00
40 FL	1.00	0.85	0.83	0.94	0.85	0.90	0.86	1.00
39 FL	0.98	0.83	0.84	0.94	0.84	0.89	0.84	1.01
38 FL	1.00	0.84	0.85	0.96	0.85	0.90	0.85	1.02
37 FL	1.01	0.85	0.86	0.97	0.86	0.92	0.86	1.04
36 FL	1.02	0.84	0.85	0.95	0.84	0.90	0.85	1.01
35 FL	1.03	0.85	0.86	0.96	0.85	0.91	0.86	1.03
34 FL	1.05	0.86	0.87	0.97	0.87	0.92	0.87	1.04
33 FL	1.02	0.84	0.85	0.94	0.84	0.90	0.85	1.02
32 FL	1.04	0.85	0.87	0.96	0.85	0.91	0.86	1.03
31 FL	1.05	0.86	0.88	0.97	0.86	0.92	0.87	1.04
30 FL	1.04	0.85	0.86	0.94	0.83	0.91	0.86	1.02
29 FL	1.05	0.86	0.87	0.95	0.84	0.92	0.87	1.03
28 FL	1.06	0.87	0.89	0.96	0.85	0.93	0.88	1.04
27 FL	1.17	0.86	0.87	0.97	0.84	0.91	0.86	1.02
26 FL	1.16	0.87	0.88	0.98	0.85	0.92	0.87	1.03
25 FL	1.07	0.88	0.89	0.99	0.86	0.93	0.88	1.05
24 FL	1.05	0.86	0.88	0.97	0.85	0.91	0.85	1.03
23 FL	1.06	0.87	0.89	0.98	0.86	0.92	0.86	1.04
22 FL	1.07	0.88	0.90	0.99	0.87	0.93	0.87	1.05
21 FL	1.05	0.87	0.89	0.97	0.86	0.92	0.86	1.06
20 FL	1.07	0.88	0.90	0.98	0.87	0.93	0.87	1.07
19 FL	1.08	0.89	0.91	0.99	0.87	0.94	0.88	1.09
18 FL	1.08	0.87	0.88	0.96	0.87	0.92	0.87	1.06
17 FL	1.10	0.88	0.89	0.97	0.88	0.93	0.88	1.08
16 FL	1.11	0.89	0.90	0.98	0.89	0.94	0.89	1.09
15 FL	1.09	0.86	0.89	0.99	0.86	0.93	0.87	1.08
14 FL	1.10	0.87	0.90	1.00	0.87	0.94	0.88	1.09
13 FL	1.11	0.88	0.91	1.01	0.88	0.95	0.89	1.10
12 FL	1.09	0.87	0.90	0.98	0.86	0.94	0.87	1.08
11 FL	1.11	0.88	0.91	0.99	0.87	0.95	0.88	1.09
10 FL	1.13	0.89	0.93	1.01	0.89	0.96	0.89	1.11
09 FL	0.91	0.86	0.89	0.97	0.99	1.03	0.97	1.06
08 FL	0.98	0.91	0.95	1.03	1.00	1.04	0.97	1.06
07 FL	0.63	0.60	0.61	0.62	0.67	0.59	0.59	0.62
06 FL	0.65	0.62	0.63	0.64	0.69	0.61	0.60	0.64
05 FL	0.65	0.63	0.64	0.65	0.70	0.62	0.61	0.64
04 FL	0.63	0.61	0.62	0.63	0.67	0.60	0.59	0.62
03 FL	0.72	0.69	0.71	0.72	0.80	0.68	0.67	0.71
02 FL	0.75	0.71	0.73	0.74	0.83	0.70	0.69	0.74
01 FL	1.07	0.89	0.92	1.01	1.00	0.96	0.90	1.07
B1 FL	1.06	0.88	0.91	1.00	0.98	0.94	0.88	1.06
B2 FL	1.08	0.89	0.92	1.01	0.99	0.96	0.90	1.08
B3 FL	1.02	0.85	0.89	0.97	0.93	0.92	0.86	1.01
B4 FL	1.05	0.87	0.98	1.07	1.05	1.00	0.94	1.13
B5 FL	1.06	0.88	0.99	1.08	1.06	1.01	0.95	1.14

(e)

LEVEL	TOWER A, DCR of CORE COLUMN 1000's COLUMN NUMBER							
	1001	1002	1003	1004	1005	1006	1007	1008
106 FL	0.93	1.12	1.07	0.82	0.95	1.23	1.02	0.86
105 FL	0.99	0.84	1.12	0.91	1.01	0.94	1.15	1.03
104 FL	0.87	1.07	1.01	0.84	0.99	1.10	1.03	0.99
103 FL	0.93	1.15	1.07	0.91	0.95	1.18	1.10	0.95
102 FL	1.00	1.00	1.12	0.98	1.00	1.25	0.97	1.01
101 FL	0.83	1.00	0.93	0.85	0.89	1.03	0.97	0.83
100 FL	0.88	1.06	0.98	0.91	0.93	1.08	1.02	0.89
99 FL	0.93	1.12	1.02	0.96	0.97	1.16	1.08	0.94
98 FL	0.74	0.84	0.89	0.90	0.88	0.78	0.91	0.74
97 FL	0.78	0.89	0.93	0.95	0.92	0.82	0.95	0.78
96 FL	0.82	0.93	0.97	1.00	0.96	0.86	1.00	0.82
95 FL	0.66	0.82	0.75	0.87	0.85	0.76	0.83	0.66
94 FL	0.69	0.86	0.77	0.91	0.88	0.79	0.87	0.70
93 FL	0.72	0.89	0.80	0.95	0.91	0.82	0.90	0.73
92 FL	0.69	0.79	0.72	0.91	0.78	0.74	0.80	0.69
91 FL	0.71	0.82	0.75	0.95	0.80	0.77	0.83	0.72
90 FL	0.74	0.85	0.77	0.98	0.83	0.80	0.86	0.74
89 FL	0.81	0.77	0.66	0.86	0.78	0.70	0.77	0.81
88 FL	0.84	0.79	0.68	0.89	0.80	0.73	0.80	0.84
87 FL	0.87	0.82	0.70	0.92	0.83	0.75	0.83	0.87
86 FL	0.82	0.92	0.76	0.91	0.78	0.81	0.93	0.82
85 FL	0.85	0.95	0.78	0.94	0.81	0.84	0.96	0.85
84 FL	0.87	0.98	0.80	0.97	0.83	0.86	0.99	0.88
83 FL	0.90	0.92	0.74	0.92	0.77	0.81	0.93	0.90
82 FL	0.93	0.95	0.76	0.94	0.79	0.83	0.96	0.93
81 FL	0.96	0.97	0.78	0.97	0.81	0.86	0.98	0.96
80 FL	0.91	1.01	0.70	1.00	0.87	0.88	1.02	0.91
79 FL	0.94	1.04	0.72	1.03	0.89	0.92	1.05	0.94
78 FL	0.98	1.09	0.75	1.08	0.92	0.95	1.10	0.98
77 FL	0.66	0.73	0.65	0.71	0.67	0.68	0.73	0.67
76 FL	0.68	0.74	0.67	0.70	0.72	0.70	0.75	0.68
75 FL	0.88	0.91	0.86	0.93	0.93	0.89	0.92	0.89
74 FL	0.88	0.92	0.86	0.95	0.94	0.90	0.93	0.90
73 FL	0.91	0.94	0.88	0.97	0.95	0.92	0.96	0.92
72 FL	0.87	0.89	0.84	0.91	0.89	0.87	0.91	0.87
71 FL	0.89	0.91	0.85	0.94	0.91	0.89	0.93	0.89
70 FL	0.91	0.93	0.87	0.96	0.93	0.91	0.95	0.91
69 FL	0.84	0.87	0.84	0.92	0.88	0.84	0.88	0.84
68 FL	0.87	0.90	0.87	0.96	0.91	0.87	0.92	0.87
67 FL	0.87	0.91	0.87	0.96	0.91	0.88	0.92	0.88
66 FL	0.91	0.93	0.86	0.99	0.95	0.90	0.95	0.91
65 FL	0.92	0.95	0.87	1.01	0.96	0.92	0.96	0.93
64 FL	0.94	0.97	0.89	1.03	0.98	0.94	0.98	0.94
63 FL	0.91	0.93	0.85	1.01	0.95	0.89	0.93	0.91
62 FL	0.93	0.95	0.86	1.03	0.96	0.91	0.95	0.93
61 FL	0.94	0.97	0.88	1.05	0.98	0.92	0.97	0.95
60 FL	0.91	0.93	0.83	1.01	0.94	0.89	0.93	0.91
59 FL	0.92	0.94	0.84	1.03	0.95	0.91	0.95	0.92
58 FL	0.94	0.96	0.86	1.05	0.97	0.92	0.97	0.94
57 FL	0.92	0.93	0.83	1.02	0.94	0.89	0.93	0.92
56 FL	0.93	0.94	0.84	1.04	0.95	0.90	0.95	0.93
55 FL	0.95	0.96	0.85	1.05	0.97	0.92	0.97	0.95
54 FL	0.89	0.90	0.82	1.03	0.94	0.89	0.93	0.89
53 FL	0.91	0.94	0.83	1.04	0.95	0.90	0.95	0.91
52 FL	0.92	0.96	0.84	1.06	0.96	0.91	0.96	0.92
51 FL	0.90	0.93	0.82	1.00	0.93	0.88	0.93	0.91
50 FL	0.92	0.94	0.83	1.02	0.95	0.89	0.95	0.92
49 FL	0.93	0.95	0.84	1.04	0.96	0.91	0.96	0.93
48 FL	0.89	0.90	0.80	1.01	0.90	0.85	0.89	0.89
47 FL	0.90	0.92	0.81	1.03	0.91	0.86	0.90	0.90
46 FL	0.91	0.93	0.82	1.05	0.93	0.87	0.92	0.91
45 FL	0.83	0.84	0.74	0.96	0.86	0.79	0.82	0.83
44 FL	0.85	0.86	0.76	0.99	0.88	0.81	0.84	0.85
43 FL	0.66	0.65	0.59	0.74	0.68	0.62	0.64	0.66
42 FL	0.68	0.66	0.60	0.75	0.70	0.63	0.65	0.68
41 FL	0.89	0.88	0.80	0.97	0.88	0.83	0.87	0.89
40 FL	0.89	0.88	0.80	0.98	0.89	0.83	0.88	0.90
39 FL	0.88	0.87	0.81	0.99	0.87	0.83	0.86	0.89
38 FL	0.89	0.88	0.82	1.01	0.88	0.84	0.87	0.90
37 FL	0.91	0.89	0.83	1.02	0.89	0.85	0.88	0.91
36 FL	0.89	0.87	0.81	0.97	0.87	0.83	0.85	0.90
35 FL	0.91	0.88	0.82	0.99	0.87	0.84	0.86	0.91
34 FL	0.92	0.89	0.83	1.00	0.88	0.85	0.88	0.92
33 FL	0.88	0.87	0.81	0.98	0.85	0.84	0.86	0.89
32 FL	0.89	0.88	0.82	1.00	0.86	0.85	0.87	0.90
31 FL	0.91	0.89	0.83	1.01	0.87	0.86	0.88	0.91
30 FL	0.90	0.85	0.79	0.99	0.85	0.84	0.84	0.90
29 FL	0.91	0.86	0.80	1.01	0.86	0.85	0.85	0.91
28 FL	0.92	0.87	0.81	1.02	0.87	0.86	0.86	0.92
27 FL	0.89	0.85	0.80	1.00	0.85	0.84	0.84	0.89
26 FL	0.90	0.86	0.81	1.01	0.86	0.85	0.85	0.90
25 FL	0.91	0.87	0.82	1.02	0.87	0.86	0.86	0.91
24 FL	0.88	0.85	0.80	0.99	0.85	0.84	0.84	0.88
23 FL	0.89	0.86	0.81	1.00	0.86	0.85	0.85	0.89
22 FL	0.90	0.87	0.82	1.01	0.87	0.86	0.86	0.90
21 FL	0.88	0.85	0.81	1.00	0.85	0.84	0.84	0.88
20 FL	0.89	0.86	0.81	1.01	0.86	0.85	0.85	0.89
19 FL	0.89	0.87	0.82	1.02	0.86	0.86	0.86	0.90
18 FL	0.87	0.85	0.81	1.01	0.84	0.83	0.84	0.87
17 FL	0.88	0.86	0.82	1.02	0.84	0.84	0.85	0.88
16 FL	0.89	0.87	0.83	1.03	0.85	0.85	0.86	0.89
15 FL	0.87	0.85	0.81	1.00	0.84	0.83	0.85	0.87
14 FL	0.88	0.86	0.82	1.01	0.85	0.84	0.85	0.88
13 FL	0.89	0.87	0.83	1.02	0.85	0.85	0.86	0.89
12 FL	0.88	0.85	0.82	1.01	0.84	0.84	0.85	0.88
11 FL	0.88	0.86	0.82	1.02	0.85	0.85	0.86	0.89
10 FL	0.90	0.87	0.84	1.04	0.86	0.86	0.87	0.90
09 FL	0.96	0.84	0.81	0.98	0.80	0.84	0.90	0.89
08 FL	0.96	0.87	0.85	1.03	0.83	0.87	0.91	0.93
07 FL	0.79	0.73	0.73	0.87	0.73	0.74	0.75	0.79
06 FL	0.80	0.74	0.74	0.88	0.74	0.76	0.76	0.81
05 FL	0.81	0.75	0.75	0.89	0.74	0.76	0.77	0.81
04 FL	0.79	0.73	0.73	0.86	0.73	0.74	0.75	0.79
03 FL	0.86	0.79	0.79	0.94	0.78	0.80	0.81	0.86
02 FL	0.88	0.80	0.80	0.96	0.79	0.81	0.82	0.88
01 FL	0.84	0.83	0.79	0.95	0.83	0.81	0.83	0.84
B1 FL	0.83	0.82	0.78	0.94	0.83	0.80	0.82	0.83
B2 FL	0.84	0.83	0.79	0.95	0.84	0.81	0.83	0.84
B3 FL	0.86	0.82	0.79	0.92	0.81	0.82	0.80	0.87
B4 FL	0.92	0.83	0.85	0.99	0.86	0.83	0.86	0.86
B5 FL	0.93	0.83	0.85	1.00	0.86	0.83	0.86	0.88

(f)

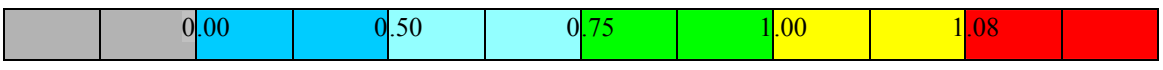

Figure 5–4. Demand/capacity ratios for WTC 1 core columns under original design loads, (e) 900 line and (f) 1000 line (continued).

The types of members in the exterior wall that had DCRs larger than 1 were calculated for a combination of axial load and bending under a combination of gravity and wind loads and were generally found in three types of location:

1. Columns at the corners;
2. Where the hat truss connects to the exterior wall; and
3. Below floor 9.

The members in these locations would be expected to experience large forces. The corner columns had some of the highest calculated forces under wind loads. The hat truss-to-exterior wall connections interconnected two major structural systems with large concentrated load transfers. The exterior wall below floor 9 was a highly variable and articulated structural system that had large calculated forces. Given the extraordinary difficulty of replicating with precision a set of engineering calculations performed almost forty years ago with relatively rudimentary computational tools, DCRs in excess of one were observed in the analysis at locations of highest forces and at locations where there was significant complexity of system behavior.

The core columns that had DCRs larger than 1 were calculated for axial stresses due to gravity loads and were generally located on the 600 column line between floors 80 and 106 and at core perimeter columns 901 and 908 for much of their height. The gravity loads on these columns were affected significantly by assumptions about tributary areas, unit construction dead loads and superimposed dead loads, and the sequence of construction of the hat truss. The high degree of stress calculated at these core columns is likely associated with differences in these assumptions between the original and current computations.

Figure 5–5 presents the distribution of the normal stresses due to axial loads (axial column load divided by columns cross sectional area) in the columns of the four exterior walls due to wind loads only (gravity loads are not included in these plots). The axial stresses are presented at three levels along the height of the tower: B6, 39, and 73. The plots show both the tensile and compressive stresses on the columns induced by wind loading, where shear lag effects can be observed. For corner columns 101, 159, 301, and 359 at floor 73, Fig. 5–5(c) indicates that their stresses are smaller than their neighboring columns. This is likely due to the influence of the special corner framing at that floor, i.e., the discontinuous columns and chamfered plan layout of the exterior wall framing.

The results of the baseline performance analyses indicated that tension forces were developed in the exterior walls of WTC 1 under the original WTC design dead and wind loads. The tension forces from the combination of dead and wind loads for all faces are illustrated in Fig. 5–6. The figure indicates that tensile forces are largest at the base of the building and at the corners.

These axial tensile column loads were transferred from one panel to another through the column splices. The exterior wall column splice capacities were calculated from the original details and compared to the tension forces for all four faces of WTC 1. The DCR ratios for the exterior wall splice connections for WTC 1 are summarized in Table 5–2.

For the tower resistance to shear sliding and overturning due to wind, the dead loads that acted on the perimeter walls of the tower provided resistance to shear sliding and overturning at the foundation level.

Considering the resistance to shear sliding under wind load, the factor of safety was estimated to be approximately 11.5. This was calculated by dividing the resisting force due to dead load on the perimeter wall (a coefficient of friction of 0.7 was used) by the wind shear at the foundation level. Considering resistance to overturning due to wind load, the factors of safety were estimated to be approximately 2.3 and 2.6 for overturning about a north-south axis and for an east-west axis, respectively. This was calculated by dividing the resisting moment due to dead load on the perimeter wall by the overturning moment due to wind load taken at the foundation level.

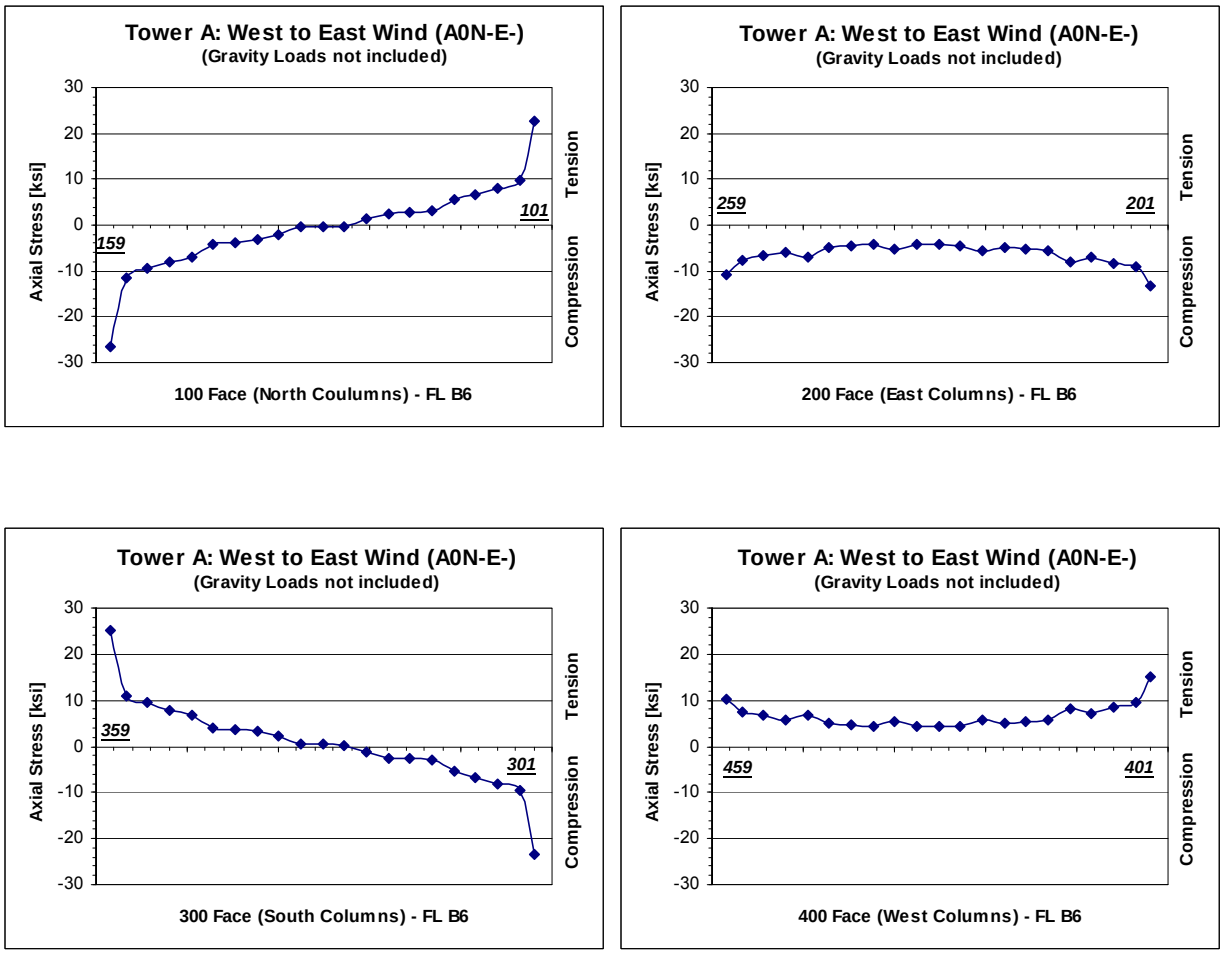

(a)

Figure 5–5. Shear lag diagrams of WTC 1 due to original WTC wind loads at (a) floor B6, (b) floor 39, and (c) floor 73.

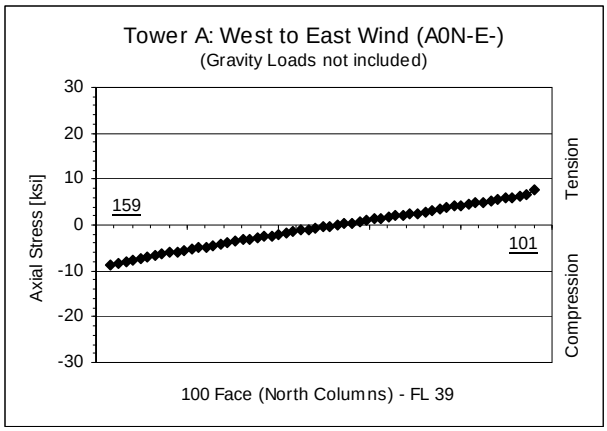
Tower A: West to East Wind (A0N-E-)
(Gravity Loads not included)
30
20
10
0
-10
-20
-30
Axial Stress [ksi]
159
101
Tension
Compression
100 Face (North Columns) - FL 39

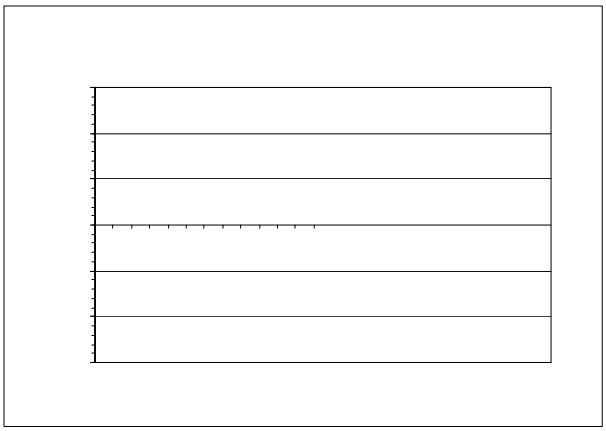

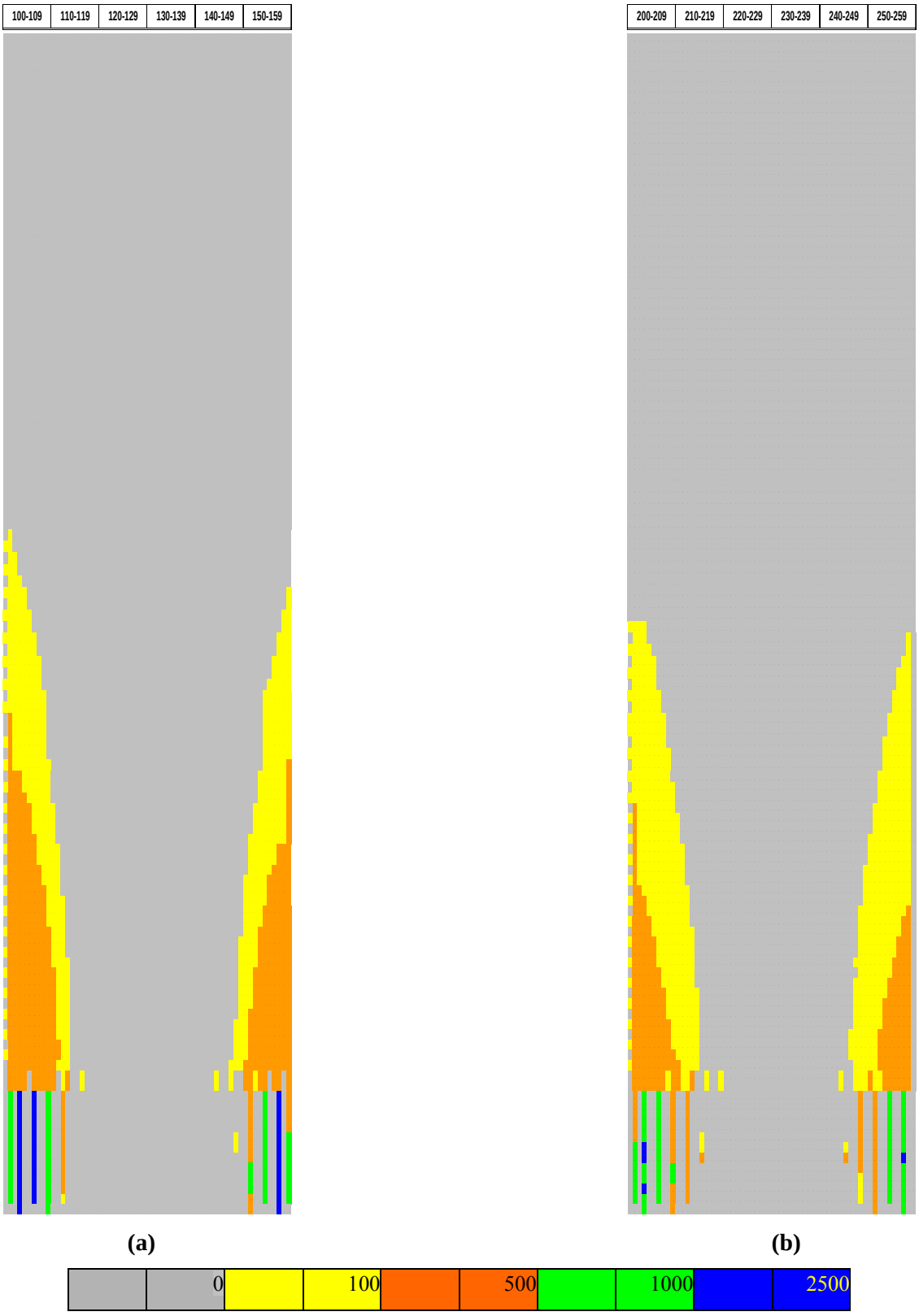

Figure 5–6. Tension force distribution (kip) in the exterior wall columns of WTC 1 under original design dead and wind loads, (a) 100 face (north) and (b) 200 face (east).

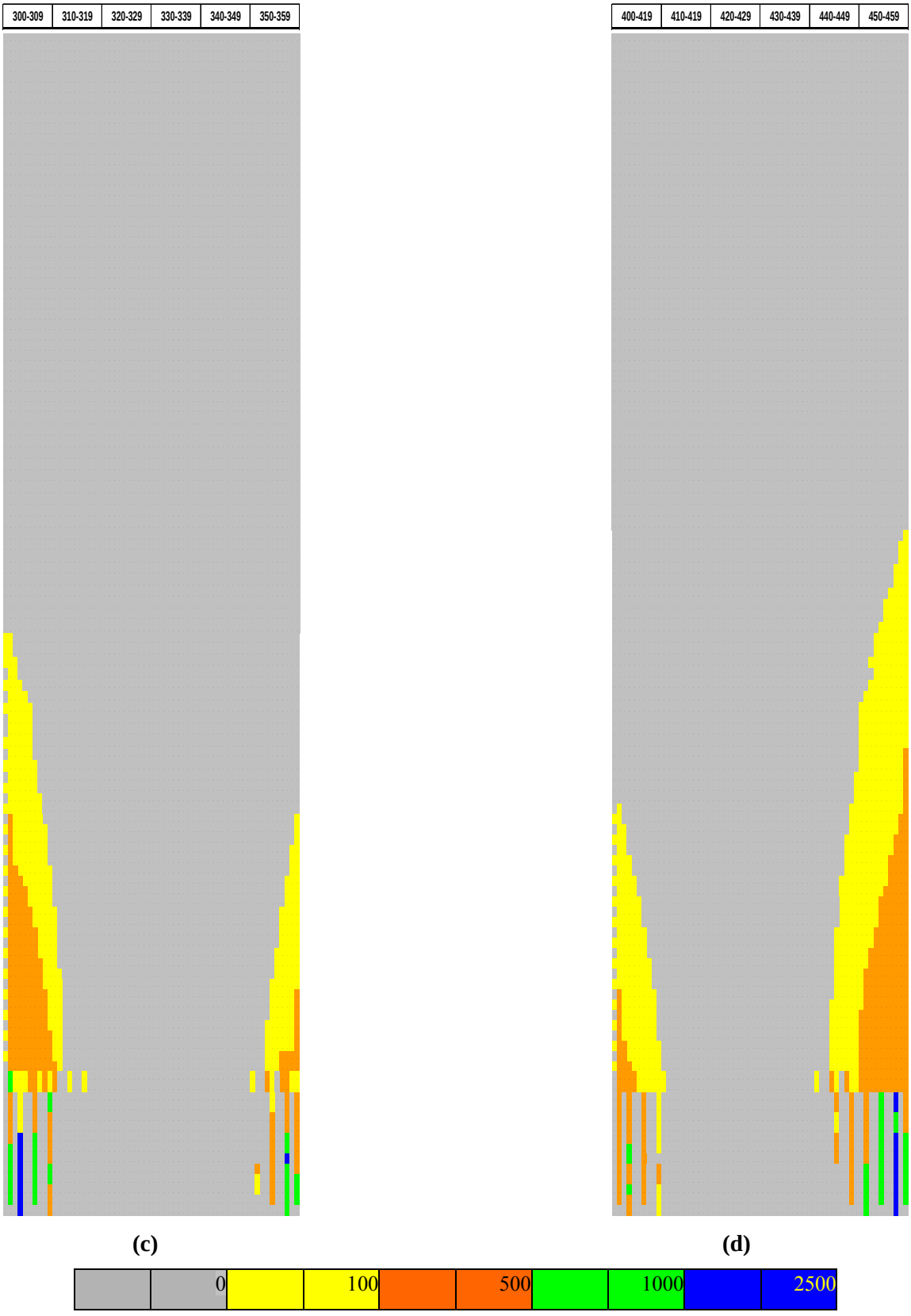

Figure 5–6. (c) 300 face (south) and (d) 400 face (west) (continued).

Table 5–2. Maximum calculated demand/capacity ratios (DCRs) for exterior wall column splices for WTC 1 under original design dead and wind load case.

Exterior Wall Face	Exterior Wall Column Splices	Maximum Calculated DCR
100 Face (North)	Below floor 1	0.64
	Floor 1 to 9	0.31
	Floor 10 to 41	0.96
	Above floor 42	0.26
200 Face (East)	Below floor 1	0.53
	Floor 1 to 9	0.32
	Floor 10 to 41	0.63
	Above floor 42	0.14
300 Face (South)	Below floor 1	0.54
	Floor 1 to 9	0.26
	Floor 10 to 41	0.77
	Above floor 42	0.15
400 Face (West)	Below floor 1	0.59
	Floor 1 to 9	0.36
	Floor 10 to 41	0.84
	Above floor 42	0.26

5.3.2 State-of-the-Practice Case

The WTC 1 global model was analyzed using the lower estimate, state-of-the-practice loading case, as described in Chapter 4 (see also NIST NCSTAR 1-2). This loading case included dead loads, live loads according to the NYCBC 2001, and wind loads from the Rowan Williams Davies and Irwin, Inc. (RWDI) wind tunnel study, scaled in accordance with NYCBC 2001 wind speed.

The calculated total drift of WTC 1 induced by the lower estimate, state-of-the-practice case was approximately 56.8 in. (4 ft 8.8 in.) in the E–W direction and 68.1 in. (5 ft 8.1 in.) in the N–S direction. The drifts are equivalent to about H/303 and H/253 in the E–W and N–S directions, respectively. Figure 5–7 presents the deflected shape (cumulative drift) and the inter-story drifts normalized by the story height for WTC 1 under the state-of-the-practice case. The plots are presented for the E-W and N-S directions for the load combinations producing the maximum cumulative drift.

DCR statistics for WTC 1 global system components under the lower estimate, state-of-the-practice loading case are summarized in Table 5–3. A comparison of the mean values of the DCRs estimated from the original design case (Table 5–1) with those from the state-of-the-practice case (Table 5–3) indicated that the results are very similar. Also, the distribution of the DCRs and the locations of members with DCRs greater than 1.0 were very similar between the original design case and the state-of-the-practice case.

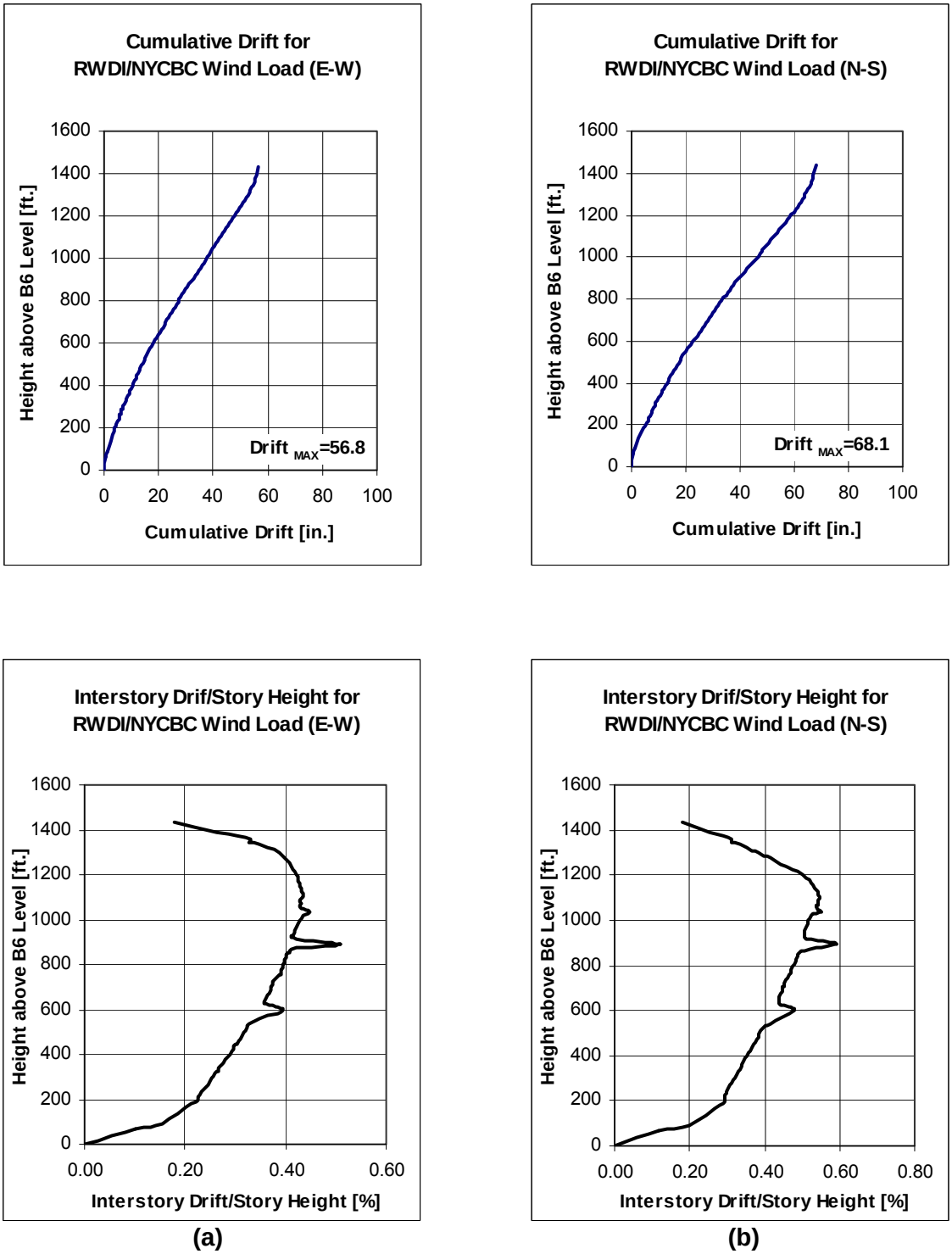

Figure 5–7. Drift diagrams of WTC 1 due to the lower estimate, state-of-the-practice loads, (a) 1R14PDN and (b) 1R8PDN.

Table 5–3. Statistics of demand/capacity ratios (DCRs) for WTC 1 under the lower estimate, state-of-the practice case.

Member Type	Number of Members	Mean Calculated DCR	C.O.V. of DCR	Percentage of Components with DCR > 1.0	Percentage of Components with DCR > 1.05	Number of Components with DCR > 1.05	Maximum Calculated DCR
Exterior Wall Columns							
Below floor 1	628	0.77	0.19	6.1	4.0	25	1.30
Floor 1 to 9	1,122	0.78	0.26	13.1	5.2	58	1.15
Floor 9 to 106	31,086	0.78	0.13	2	0.9	281	1.44
Above floor 106	578	0.71	0.31	10.7	7.6	44	1.36
Exterior Wall Spandrels							
Below floor 1	420	0.49	0.46	4	2.4	10	1.26
Floor 1 to 9	610	0.37	0.45	1.3	1.1	7	1.22
Floor 9 to 106	31,160	0.32	0.29	0	0	0	0.80
Above floor 106	836	0.35	0.70	1.9	1.7	14	1.57
Core Columns	5,219	0.86	0.14	9.9	5.3	278	1.36
Hat Truss System							
Columns	239	0.45	0.50	0.4	0.4	1	1.26
Beams	499	0.23	0.93	0.2	0.2	1	1.07
Braces	279	0.41	0.60	1.1	0	0	1.03
Exterior Wall Bracing							
Below floor 1	200	0.76	0.16	2.5	2	4	1.18
Above floor 106	12	0.35	0.47	0	0	0	0.64

5.3.3 The Refined NIST Estimate Case

The WTC 1 global model was analyzed using the refined NIST estimate case, as described in Chapter 4 (see also NIST NCSTAR 1-2). This loading case included dead loads, live loads in accordance with the ASCE 7-02 Standard, and wind loads developed by NIST based on critical assessment of information obtained from RWDI and CPP reports and state-of-the-art considerations in wind engineering.

The calculated total drift of WTC 1 induced by the refined NIST estimate case was approximately 70.6 in. (5 ft 10.6 in.) in the E–W direction and 83.9 in. (6 ft 11.9 in.) in the N–S direction. These drifts are equivalent to about H/244 and H/205 in the E–W and N–S directions, respectively. Figure 5–8 presents the deflected shape (cumulative drift) and the inter-story drifts normalized by the story height for WTC 1 under the refined NIST wind loads. The plots are presented for the E-W and N-S directions for the load combination producing the maximum cumulative drift.

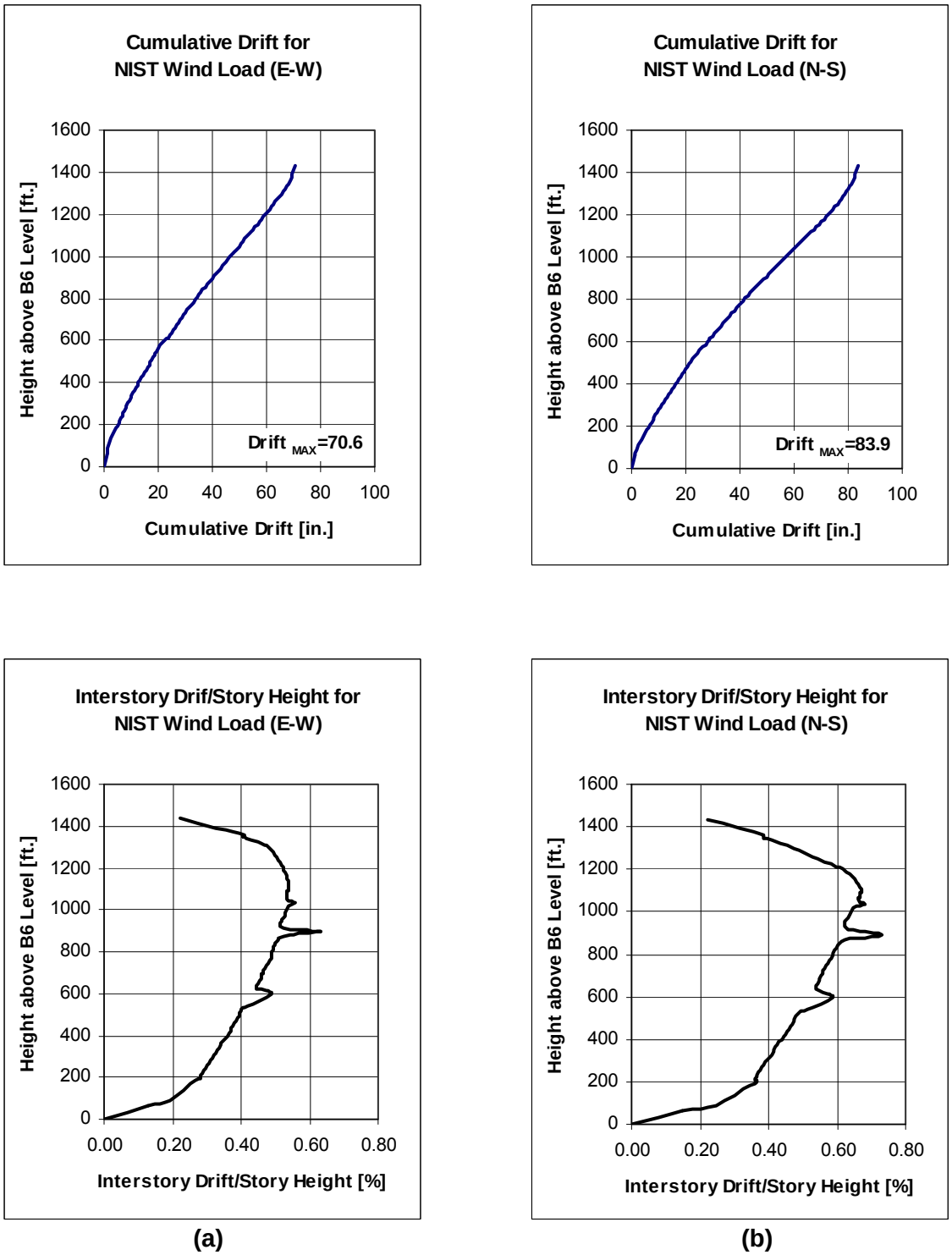

Figure 5–8. Drift diagrams of WTC 1 due to refined NIST estimate wind loads, (a) 1R14PD and (b) 1R8PD.

DCR statistics for WTC 1 global systems components under the refined NIST estimate case are summarized in Table 5–4. The DCRs for the core columns and hat truss members estimated from the original design and the state-of-the-practice cases (Tables 5–1 and 5–3, respectively) are generally close to those estimated from the refined NIST estimate case (Table 5–4). This is due to the fact that core columns and hat truss members do not significantly contribute to wind load resistance. The DCRs for the exterior walls, including columns, spandrels, and bracings calculated from the refined NIST estimate case are larger than those estimated from the original design and the state-of-the-practice cases. For example, for the exterior walls, the ratio of the mean DCRs from the refined NIST estimate case to the mean DCRs from the original design case ranged from 1.84 to 1.11. The ratio of the mean DCRs from the refined NIST estimate case to the mean DCRs from the lower estimate, state-of-the-practice case ranged from 1.65 to 1.14.

Table 5–4. Statistics of demand/capacity ratios (DCRs) for WTC 1 under the refined NIST estimate case.

Member Type	Number of Members	Mean Calculated DCR	C.O.V. of DCR	Percentage of Components with DCR > 1.0	Percentage of Components with DCR > 1.05	Number of Components with DCR > 1.05	Maximum Calculated DCR
Exterior Wall Columns							
Below floor 1	628	1.04	0.24	52.5	47.3	297	1.95
Floor 1 to 9	1,122	1.11	0.27	69.0	63.6	714	1.69
Floor 9 to 106	31,086	1.10	0.14	72.1	59.7	18572	2.05
Above floor 106	578	0.81	0.28	19.7	14.2	82	1.57
Exterior Wall Spandrels							
Below floor 1	420	0.81	0.46	22.1	21.4	90	2.05
Floor 1 to 9	610	0.61	0.45	8.0	4.3	26	2.03
Floor 9 to 106	31,160	0.52	0.29	0.5	0.3	109	1.32
Above floor 106	836	0.41	0.68	2.4	1.9	16	1.82
Core Columns	5,219	0.84	0.15	8.9	5.2	270	1.40
Hat Truss System							
Columns	239	0.53	0.49	3.8	0.8	2	1.26
Beams	499	0.26	0.93	1.8	1.4	7	1.30
Braces	279	0.49	0.55	6.1	2.5	7	1.10
Exterior Wall Bracing							
Below floor 1	200	1.11	0.18	73.0	62.0	124	1.76
Above floor 106	12	0.52	0.42	0	0	0	0.90

5.4 BASELINE PERFORMANCE ANALYSIS OF WTC 2

The baseline performance analysis of the global model of WTC 2 was performed on a Pentium 4 personal computer with a CPU speed of 3.06 GHz and 1.0 GB of RAM. The duration of the analysis was about 15 h. The following summarizes the results under the three loading cases.

5.4.1 Original WTC Design Load Case

The analysis reported in this section used the gravity and wind loads used in the original design of the towers, as explained in Chapter 4.

The results of the analysis indicated that for the dead and live loads used in the original WTC design, the core columns and the exterior walls of WTC 2 carried approximately 53 percent and 47 percent, respectively, of the total gravity load at the basement (B6) level.

The calculated total drift of WTC 2 induced by the original WTC design wind loads was approximately 51.2 in. (4 ft 3.2 in.) in the E–W direction and 65.3 in. (5 ft 5.3 in.) in the N–S direction. These drifts are equivalent to about H/335 and H/263 in the E–W and N–S directions, respectively. Similar to WTC 1, building drift under wind loads was not a design criterion and accordingly, no historical project-specific data is available to which the total drifts may be compared. Fig. 5–9 presents the deflected shape (cumulative drift) and the inter-story drifts normalized by the story height for WTC 2 under the original design loads. The plots are presented for the E-W and N-S directions for the cases producing the maximum cumulative drift (wind azimuth 180 and 90 degrees for the E–W and N–S directions, respectively, where azimuth 0 indicates tower north).

DCRs were calculated using the SAP2000 computer program. As was done for WTC 1, the calculations were spot checked for accuracy and to verify that the correct design information was being applied, and the calculations were found to be acceptable. The DCR statistics for WTC 2 global systems components under the original WTC design loading are summarized in Table 5–5. Figure 5–10 shows the distribution of the DCRs for the four exterior walls of WTC 2 under the original design loads. Close-up views are provided for the exterior walls below floor 9 in Fig. 5–11. DCRs for the core columns are illustrated in Fig. 5–12.

The types of members in the exterior wall that had DCRs larger than 1 were calculated for a combination of axial load and bending under a combination of gravity and wind loads and were generally found in three types of location:

1. Columns at the corners;
2. Where the hat truss connects to the exterior wall; and
3. Below floor 9.

The members in these locations would be expected to experience large forces. The corner columns had some of the highest calculated forces under wind loads. The hat truss-to-exterior wall connections interconnected two major structural systems with large concentrated load transfers. The exterior wall below floor 9 was a highly variable and articulated structural system that had large calculated forces. Given the extraordinary difficulty of replicating with precision a set of engineering calculations performed almost 40 years ago with relatively rudimentary computational tools, DCRs in excess of one were observed in the analysis at locations of highest forces and at locations where there was significant complexity of system behavior.

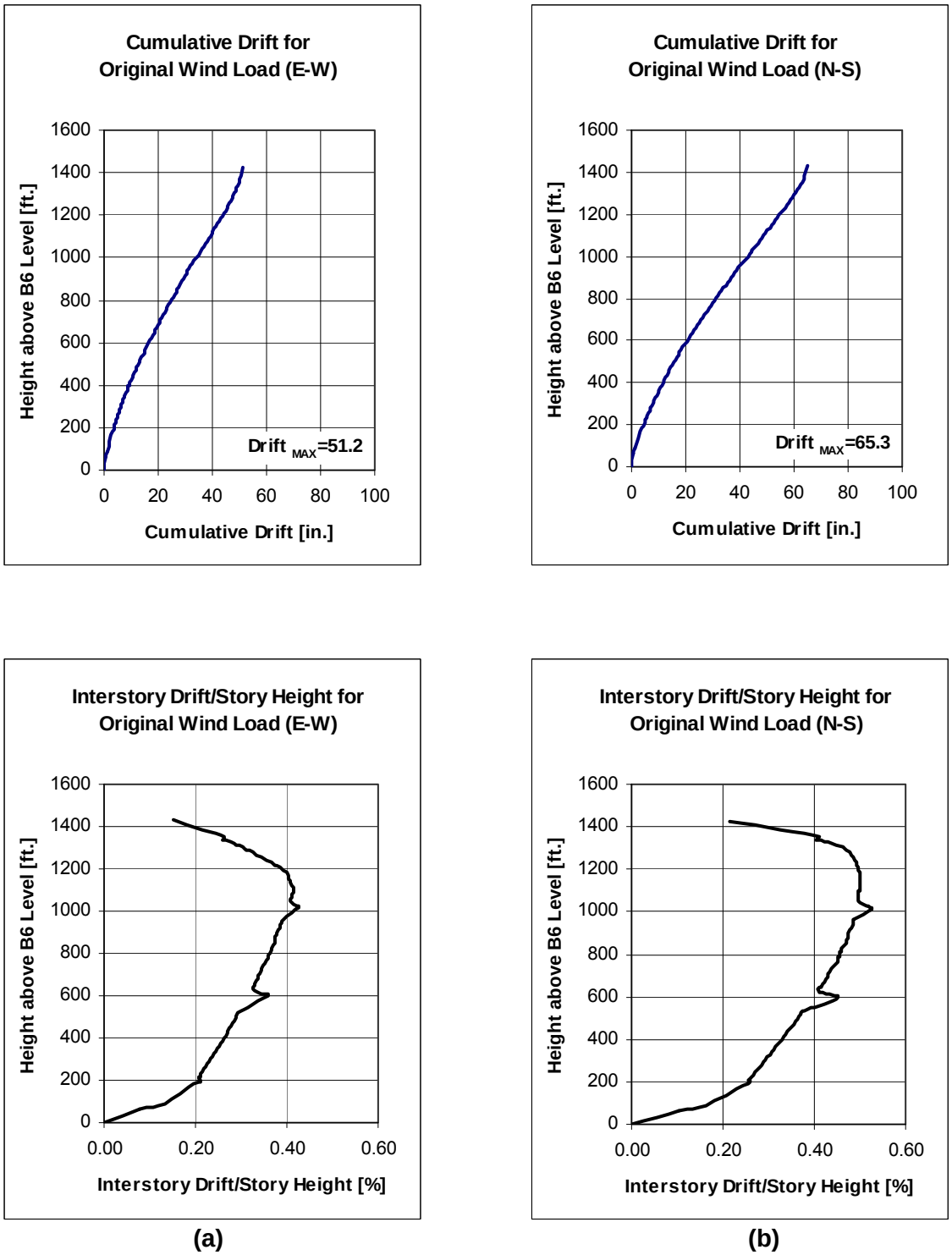

Figure 5–9. Drift diagrams of WTC 2 due to original WTC wind loads, (a) B180N+E- and (b) B90N-E+.

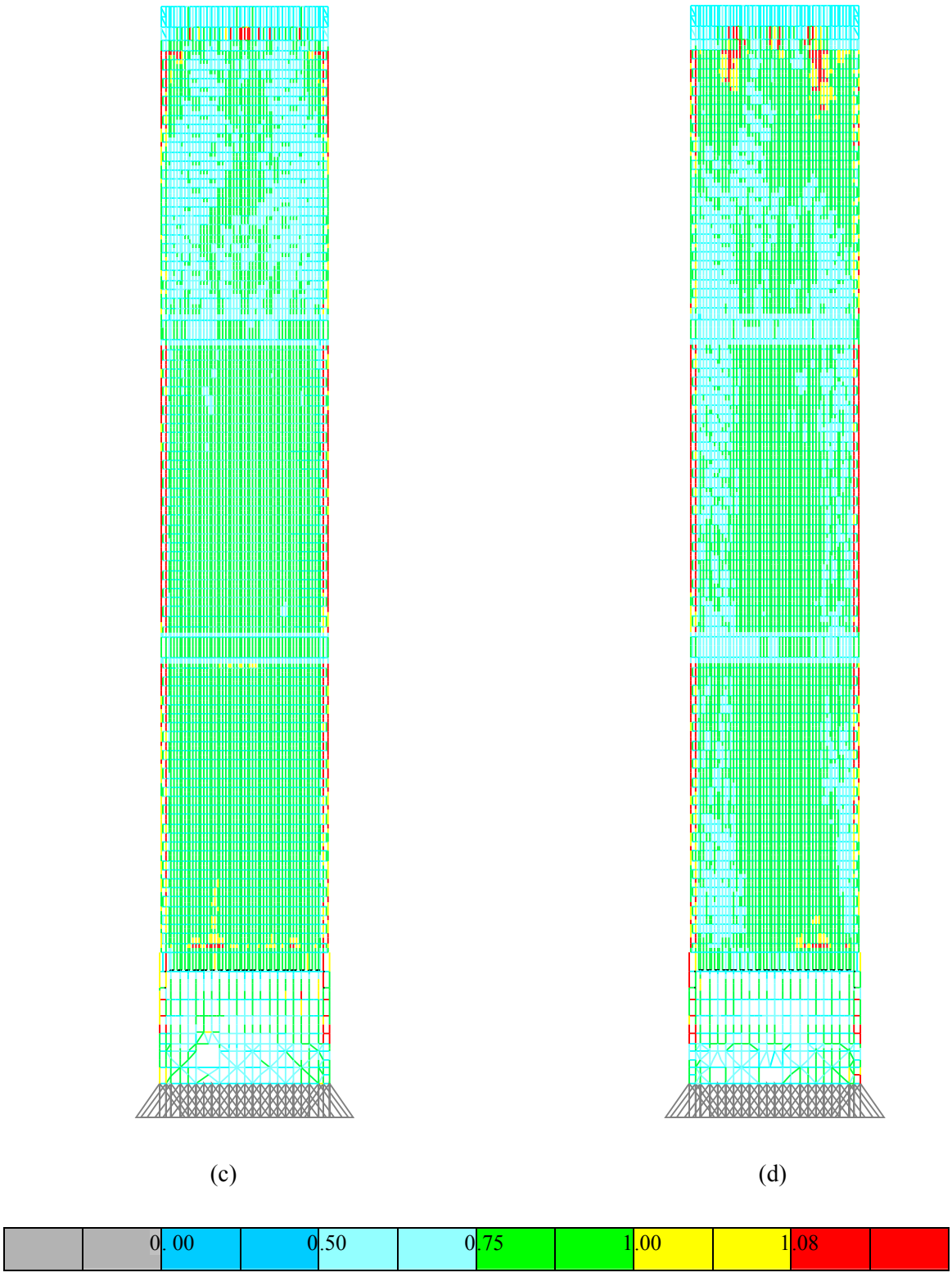

Figure 5–10. (c) east elevation and (d) south elevation (continued).

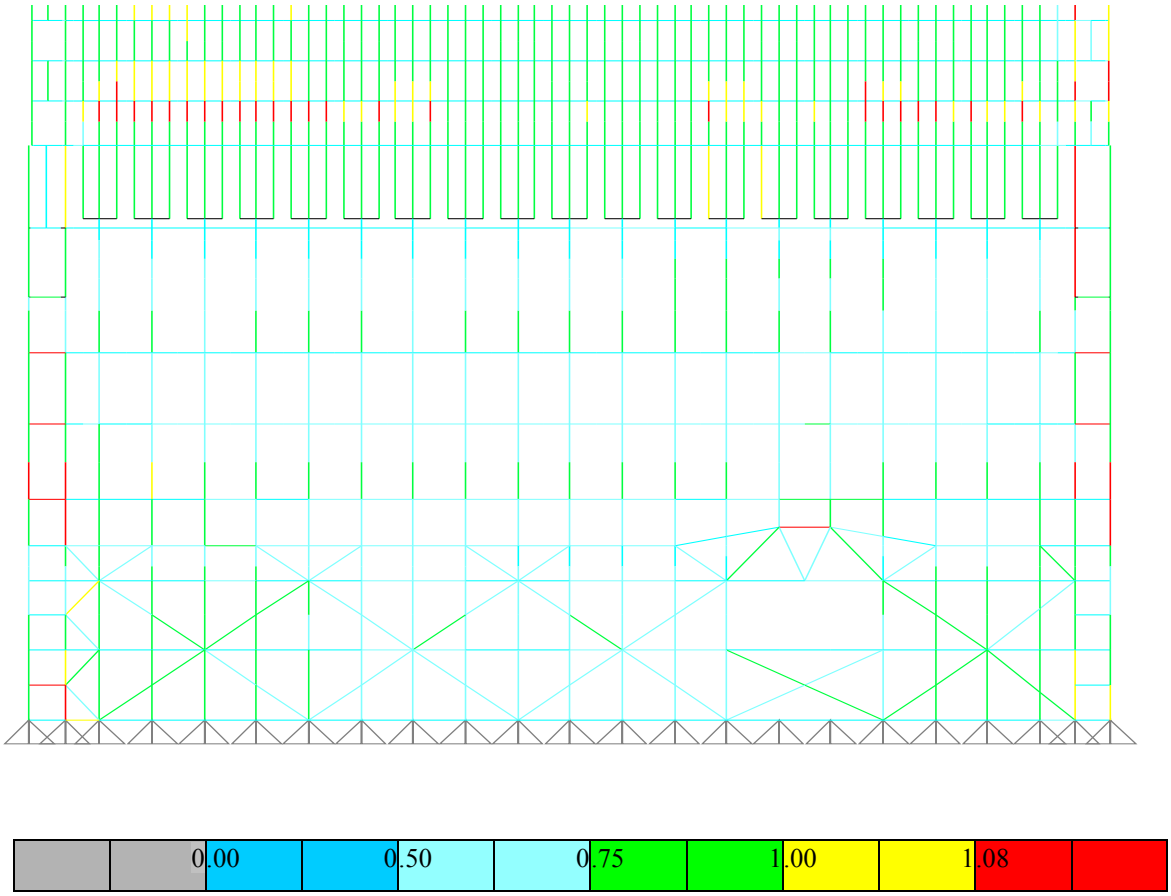

(a)

Figure 5–11. Demand/capacity ratios for WTC 2 under original design load case, (a) west elevation below floor 9.

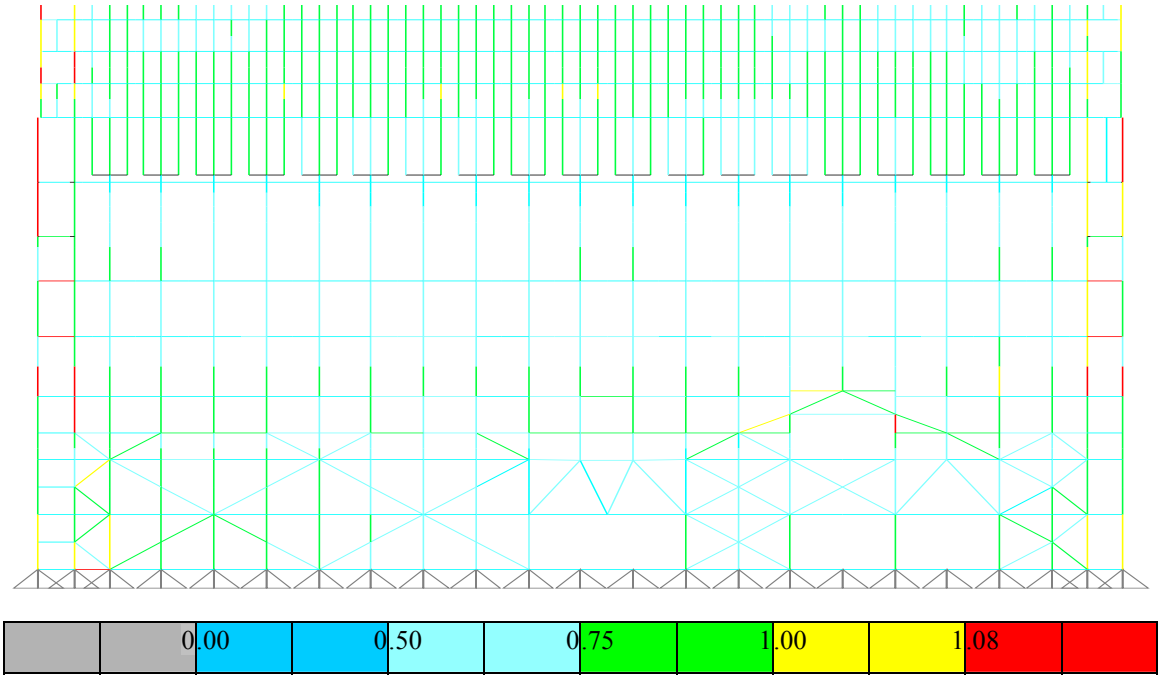

(b)

Figure 5–11. Demand/capacity ratios for WTC 2 under original design load case, (b) north elevation below floor 9 (continued).

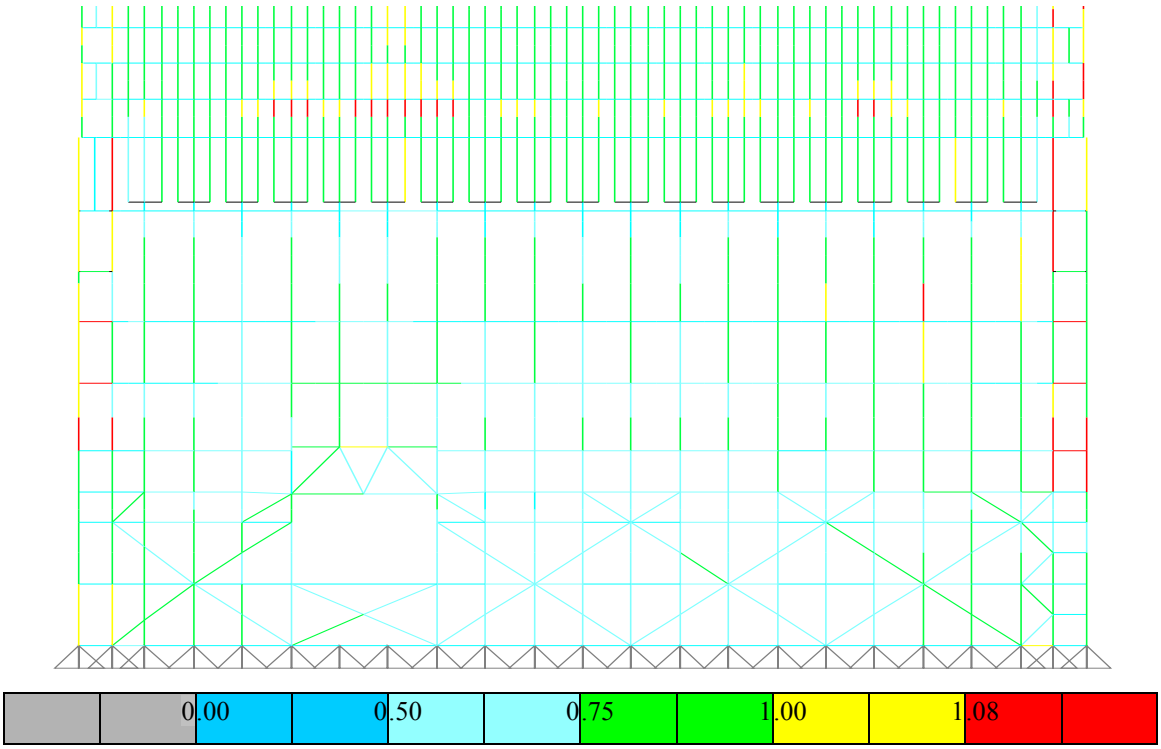

(c)

Figure 5–11. Demand/capacity ratios for WTC 2 under original design load case, (c) east elevation below floor 9 (continued).

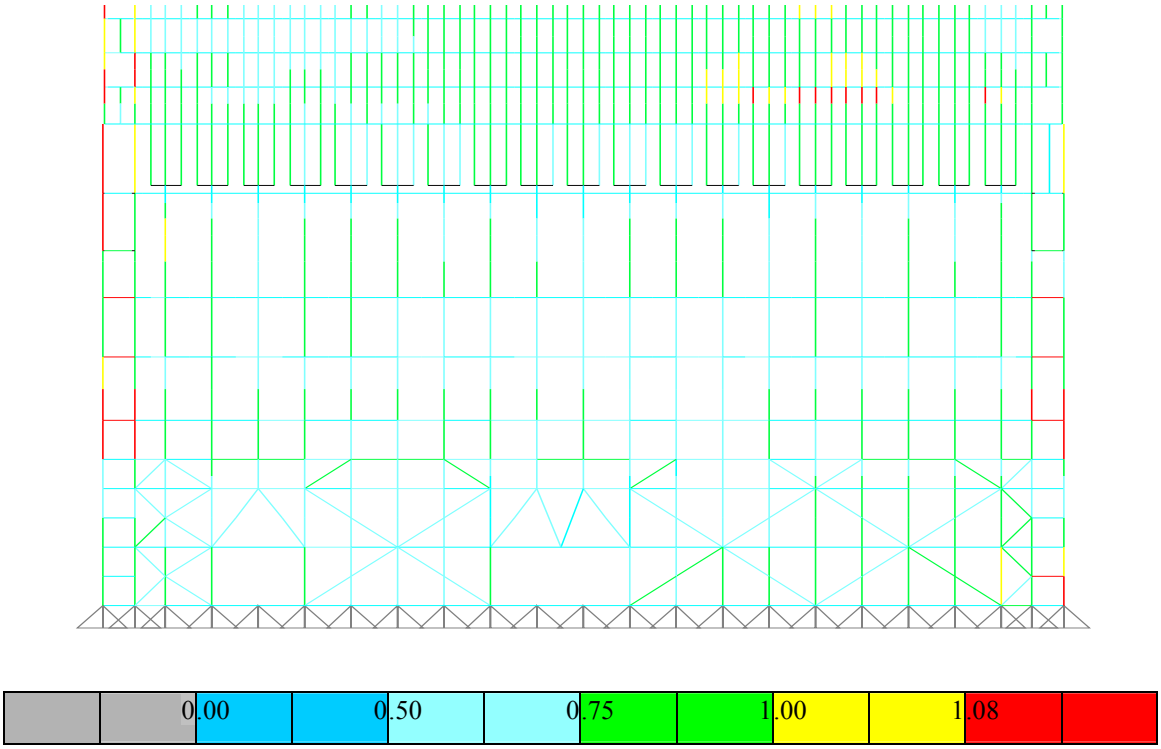

(d)

Figure 5–11. Demand/capacity ratios for WTC 2 under original design load case, (d) south elevation below floor 9 (continued).

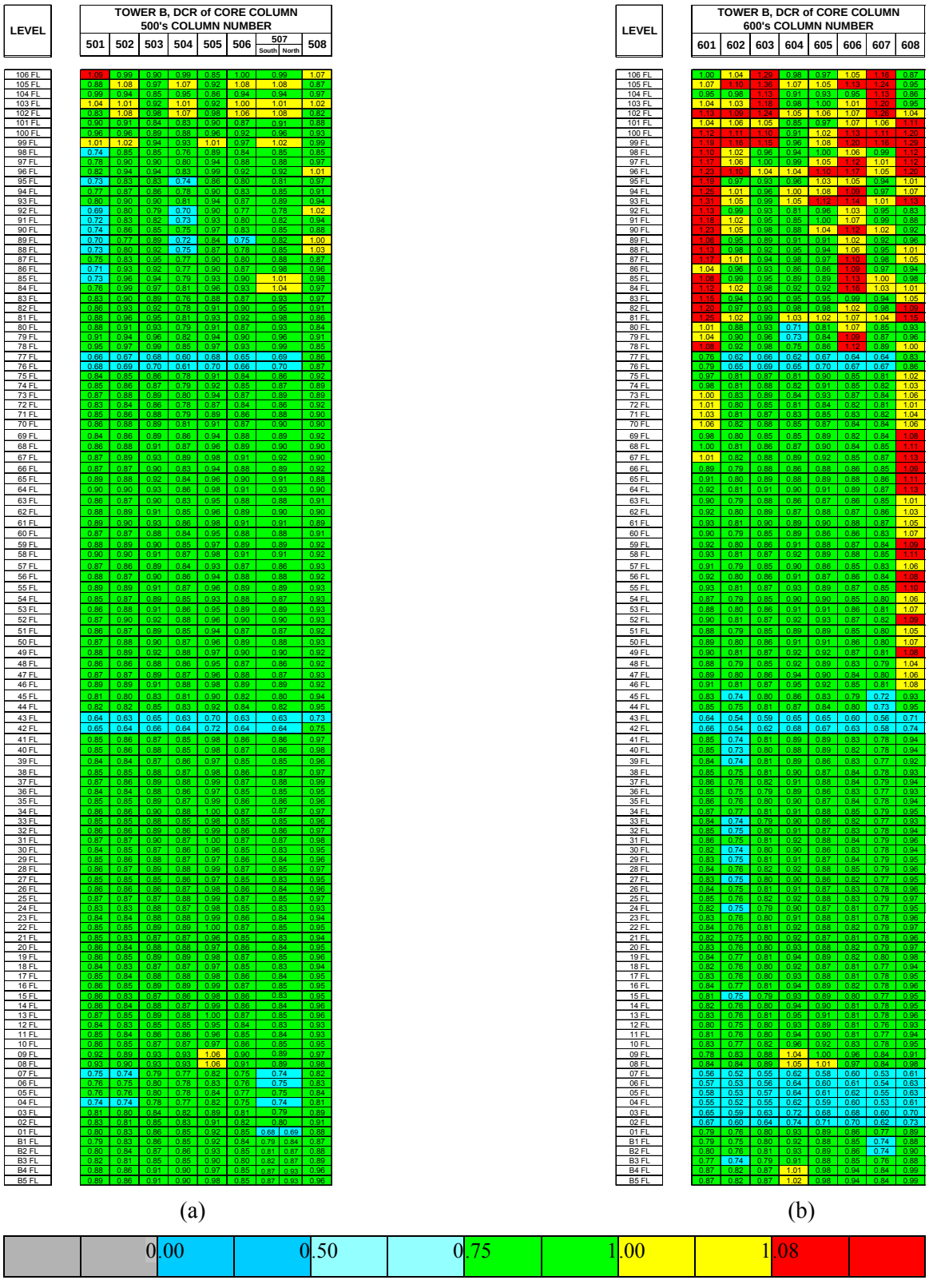

Figure 5–12. Demand/capacity ratios for WTC 2 core columns under original design loads, (a) 500 line and (b) 600 line.

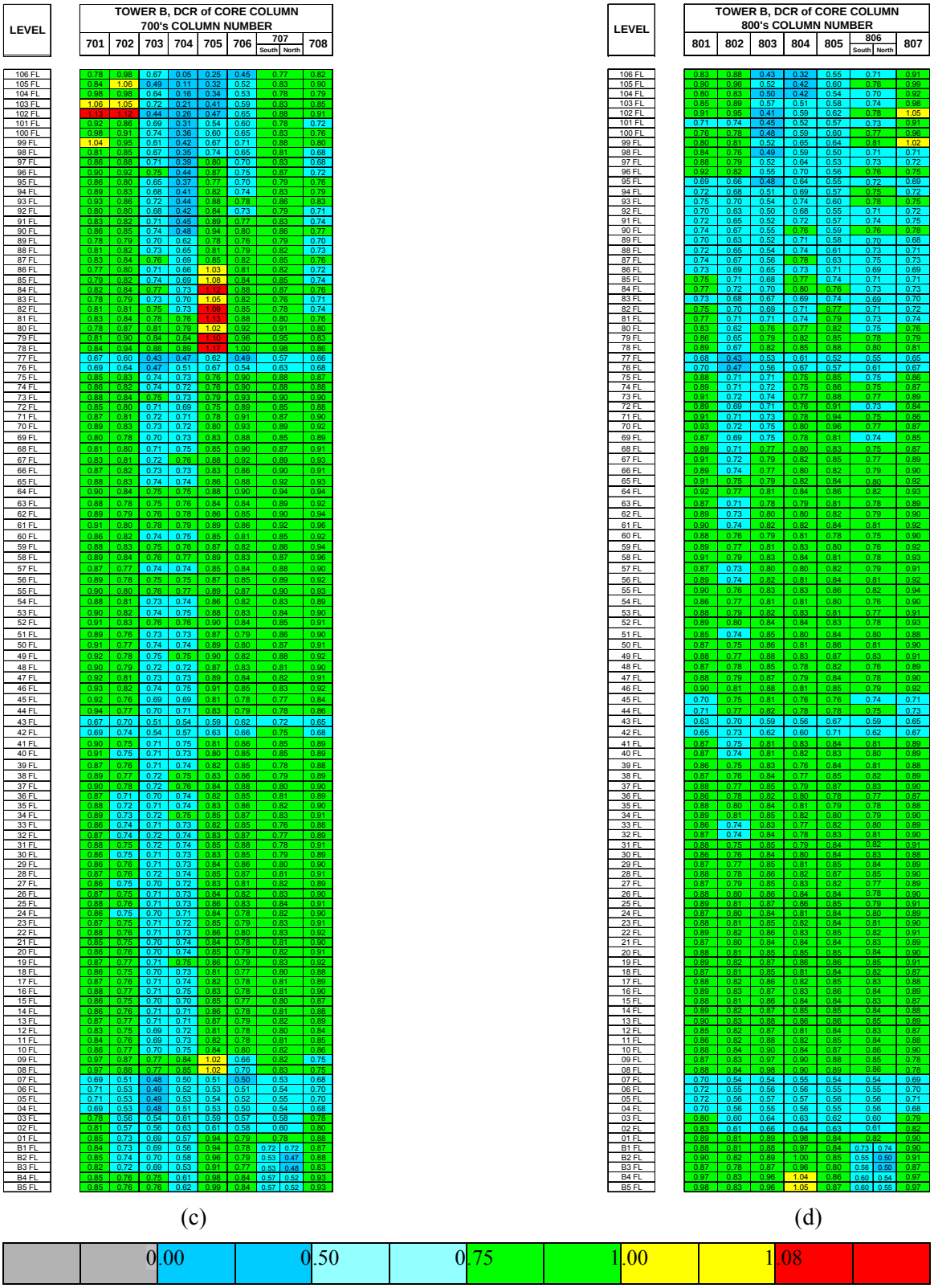

LEVEL	TOWER B, DCR of CORE COLUMN 700's COLUMN NUMBER							
	701	702	703	704	705	706	707 South	707 North	708
106 FL	0.78	0.98	0.67	0.05	0.25	0.45	0.77	0.82
105 FL	0.84	1.06	0.49	0.11	0.32	0.52	0.83	0.90
104 FL	0.98	0.98	0.64	0.16	0.34	0.53	0.78	0.79
103 FL	1.06	1.05	0.72	0.21	0.41	0.59	0.83	0.85
102 FL	1.13	1.12	0.44	0.26	0.47	0.65	0.88	0.91
101 FL	0.92	0.86	0.69	0.31	0.54	0.60	0.78	0.72
100 FL	0.98	0.91	0.74	0.36	0.60	0.65	0.83	0.76
99 FL	1.04	0.95	0.61	0.42	0.67	0.71	0.88	0.80
98 FL	0.91	0.85	0.67	0.35	0.74	0.65	0.81	0.68
97 FL	0.86	0.88	0.71	0.39	0.80	0.70	0.83	0.68
96 FL	0.90	0.92	0.75	0.44	0.87	0.75	0.87	0.72
95 FL	0.86	0.80	0.65	0.37	0.77	0.70	0.79	0.76
94 FL	0.89	0.83	0.68	0.41	0.82	0.74	0.83	0.79
93 FL	0.93	0.86	0.72	0.44	0.88	0.78	0.86	0.83
92 FL	0.80	0.80	0.68	0.42	0.84	0.73	0.79	0.71
91 FL	0.83	0.82	0.71	0.45	0.89	0.77	0.83	0.74
90 FL	0.86	0.85	0.74	0.48	0.94	0.80	0.86	0.77
89 FL	0.78	0.79	0.70	0.62	0.78	0.76	0.79	0.70
88 FL	0.81	0.82	0.73	0.65	0.81	0.79	0.82	0.73
87 FL	0.83	0.84	0.76	0.69	0.85	0.82	0.85	0.76
86 FL	0.77	0.80	0.71	0.66	1.03	0.81	0.82	0.72
85 FL	0.79	0.82	0.74	0.69	1.08	0.84	0.85	0.74
84 FL	0.82	0.84	0.77	0.73	1.12	0.88	0.87	0.76
83 FL	0.78	0.79	0.73	0.70	1.05	0.82	0.76	0.71
82 FL	0.81	0.81	0.75	0.73	1.09	0.85	0.78	0.74
81 FL	0.83	0.84	0.78	0.76	1.13	0.88	0.80	0.76
80 FL	0.78	0.87	0.81	0.79	1.02	0.92	0.91	0.80
79 FL	0.81	0.90	0.84	0.84	1.10	0.96	0.95	0.83
78 FL	0.84	0.94	0.88	0.89	1.17	1.00	0.98	0.86
77 FL	0.67	0.60	0.43	0.47	0.62	0.49	0.57	0.66
76 FL	0.69	0.64	0.47	0.51	0.67	0.54	0.63	0.68
75 FL	0.85	0.83	0.74	0.73	0.76	0.90	0.88	0.87
74 FL	0.86	0.82	0.74	0.72	0.76	0.90	0.88	0.88
73 FL	0.88	0.84	0.75	0.73	0.79	0.93	0.90	0.90
72 FL	0.85	0.80	0.71	0.69	0.75	0.89	0.85	0.88
71 FL	0.87	0.81	0.72	0.71	0.78	0.91	0.87	0.90
70 FL	0.89	0.83	0.73	0.72	0.80	0.93	0.89	0.92
69 FL	0.80	0.78	0.70	0.73	0.83	0.88	0.85	0.89
68 FL	0.81	0.80	0.71	0.75	0.85	0.90	0.87	0.91
67 FL	0.83	0.81	0.72	0.76	0.88	0.92	0.89	0.93
66 FL	0.87	0.82	0.73	0.73	0.83	0.86	0.90	0.91
65 FL	0.88	0.83	0.74	0.74	0.86	0.88	0.92	0.93
64 FL	0.90	0.84	0.75	0.75	0.88	0.90	0.94	0.94
63 FL	0.88	0.78	0.75	0.76	0.84	0.84	0.89	0.92
62 FL	0.89	0.79	0.76	0.78	0.86	0.85	0.90	0.94
61 FL	0.91	0.80	0.78	0.79	0.89	0.86	0.92	0.96
60 FL	0.86	0.82	0.74	0.75	0.85	0.81	0.85	0.92
59 FL	0.88	0.83	0.75	0.76	0.87	0.82	0.86	0.94
58 FL	0.89	0.84	0.76	0.77	0.89	0.83	0.87	0.96
57 FL	0.87	0.77	0.74	0.74	0.85	0.84	0.88	0.90
56 FL	0.89	0.78	0.75	0.75	0.87	0.85	0.89	0.92
55 FL	0.90	0.80	0.76	0.77	0.89	0.87	0.90	0.93
54 FL	0.88	0.81	0.73	0.74	0.86	0.82	0.83	0.89
53 FL	0.90	0.82	0.74	0.75	0.88	0.83	0.84	0.90
52 FL	0.91	0.83	0.76	0.76	0.90	0.84	0.85	0.91
51 FL	0.89	0.76	0.73	0.73	0.87	0.79	0.86	0.90
50 FL	0.91	0.77	0.74	0.74	0.89	0.80	0.87	0.91
49 FL	0.92	0.78	0.75	0.75	0.90	0.82	0.88	0.92
48 FL	0.90	0.79	0.72	0.72	0.87	0.83	0.81	0.90
47 FL	0.92	0.81	0.73	0.73	0.89	0.84	0.82	0.91
46 FL	0.93	0.82	0.74	0.75	0.91	0.85	0.83	0.92
45 FL	0.92	0.76	0.69	0.69	0.81	0.78	0.77	0.84
44 FL	0.94	0.77	0.70	0.71	0.83	0.79	0.78	0.86
43 FL	0.67	0.70	0.51	0.54	0.59	0.62	0.72	0.65
42 FL	0.69	0.74	0.54	0.57	0.63	0.66	0.75	0.68
41 FL	0.90	0.75	0.71	0.75	0.81	0.86	0.85	0.89
40 FL	0.91	0.75	0.71	0.73	0.80	0.85	0.85	0.89
39 FL	0.87	0.76	0.71	0.74	0.82	0.85	0.78	0.88
38 FL	0.89	0.77	0.72	0.75	0.83	0.86	0.79	0.89
37 FL	0.90	0.78	0.72	0.76	0.84	0.88	0.80	0.90
36 FL	0.87	0.71	0.70	0.74	0.82	0.85	0.81	0.89
35 FL	0.88	0.72	0.71	0.74	0.83	0.86	0.82	0.90
34 FL	0.89	0.73	0.72	0.75	0.85	0.87	0.83	0.91
33 FL	0.86	0.74	0.71	0.73	0.82	0.85	0.76	0.88
32 FL	0.87	0.74	0.72	0.74	0.83	0.87	0.77	0.89
31 FL	0.88	0.75	0.72	0.74	0.85	0.88	0.78	0.91
30 FL	0.86	0.75	0.71	0.73	0.83	0.85	0.79	0.89
29 FL	0.86	0.76	0.71	0.73	0.84	0.86	0.80	0.90
28 FL	0.87	0.76	0.72	0.74	0.85	0.87	0.81	0.91
27 FL	0.86	0.75	0.70	0.72	0.83	0.81	0.82	0.89
26 FL	0.87	0.75	0.71	0.73	0.84	0.82	0.83	0.90
25 FL	0.88	0.76	0.71	0.73	0.86	0.83	0.84	0.91
24 FL	0.86	0.75	0.70	0.71	0.84	0.78	0.82	0.90
23 FL	0.87	0.75	0.71	0.72	0.85	0.79	0.83	0.91
22 FL	0.88	0.76	0.71	0.73	0.86	0.80	0.83	0.92
21 FL	0.85	0.75	0.70	0.74	0.84	0.78	0.81	0.90
20 FL	0.86	0.76	0.70	0.74	0.85	0.79	0.82	0.91
19 FL	0.87	0.77	0.71	0.75	0.86	0.79	0.83	0.92
18 FL	0.86	0.75	0.70	0.73	0.81	0.77	0.80	0.88
17 FL	0.87	0.76	0.71	0.74	0.82	0.78	0.81	0.89
16 FL	0.88	0.77	0.71	0.75	0.83	0.78	0.81	0.90
15 FL	0.86	0.75	0.70	0.70	0.85	0.77	0.80	0.87
14 FL	0.86	0.76	0.71	0.71	0.86	0.78	0.81	0.88
13 FL	0.87	0.77	0.71	0.71	0.87	0.79	0.82	0.89
12 FL	0.83	0.75	0.69	0.72	0.81	0.78	0.80	0.84
11 FL	0.84	0.76	0.69	0.73	0.82	0.78	0.81	0.85
10 FL	0.86	0.77	0.70	0.75	0.84	0.80	0.82	0.86
09 FL	0.97	0.87	0.77	0.84	1.02	0.66	0.82	0.75
08 FL	0.97	0.88	0.77	0.85	1.02	0.70	0.83	0.75
07 FL	0.69	0.51	0.48	0.50	0.51	0.50	0.53	0.68
06 FL	0.71	0.53	0.49	0.52	0.53	0.51	0.54	0.70
05 FL	0.71	0.53	0.49	0.53	0.54	0.52	0.55	0.70
04 FL	0.69	0.53	0.48	0.51	0.53	0.50	0.54	0.68
03 FL	0.78	0.56	0.54	0.61	0.59	0.57	0.58	0.78
02 FL	0.81	0.57	0.56	0.63	0.61	0.58	0.60	0.80
01 FL	0.85	0.73	0.69	0.57	0.94	0.79	0.78	0.88
B1 FL	0.84	0.73	0.69	0.56	0.94	0.78	0.72	0.72	0.87
B2 FL	0.85	0.74	0.70	0.58	0.96	0.79	0.53	0.47	0.88
B3 FL	0.82	0.72	0.69	0.53	0.91	0.77	0.53	0.48	0.83
B4 FL	0.85	0.76	0.75	0.61	0.98	0.84	0.57	0.52	0.93
B5 FL	0.85	0.76	0.76	0.62	0.99	0.84	0.57	0.52	0.93

(c)

LEVEL	TOWER B, DCR of CORE COLUMN 800's COLUMN NUMBER						
	801	802	803	804	805	806 South	806 North	807
106 FL	0.83	0.88	0.43	0.32	0.55	0.71	0.91
105 FL	0.90	0.90	0.52	0.42	0.60	0.76	0.99
104 FL	0.80	0.83	0.50	0.42	0.54	0.70	0.92
103 FL	0.85	0.89	0.57	0.51	0.58	0.74	0.98
102 FL	0.91	0.95	0.41	0.59	0.62	0.78	1.05
101 FL	0.71	0.74	0.45	0.52	0.57	0.73	0.91
100 FL	0.76	0.78	0.48	0.59	0.60	0.77	0.96
99 FL	0.80	0.81	0.52	0.65	0.64	0.81	1.02
98 FL	0.84	0.78	0.49	0.59	0.50	0.71	0.71
97 FL	0.88	0.79	0.52	0.64	0.53	0.73	0.72
96 FL	0.92	0.82	0.55	0.70	0.56	0.76	0.75
95 FL	0.69	0.66	0.48	0.64	0.55	0.72	0.69
94 FL	0.72	0.68	0.51	0.69	0.57	0.75	0.72
93 FL	0.75	0.70	0.54	0.74	0.60	0.78	0.75
92 FL	0.70	0.63	0.50	0.68	0.55	0.71	0.72
91 FL	0.72	0.65	0.52	0.72	0.57	0.74	0.75
90 FL	0.74	0.67	0.55	0.76	0.59	0.76	0.78
89 FL	0.70	0.63	0.52	0.71	0.58	0.70	0.68
88 FL	0.72	0.65	0.54	0.74	0.61	0.73	0.71
87 FL	0.74	0.67	0.56	0.78	0.63	0.75	0.73
86 FL	0.73	0.69	0.65	0.73	0.71	0.69	0.69
85 FL	0.75	0.71	0.68	0.77	0.74	0.71	0.71
84 FL	0.77	0.72	0.70	0.80	0.76	0.73	0.73
83 FL	0.73	0.68	0.67	0.69	0.74	0.69	0.70
82 FL	0.75	0.70	0.69	0.71	0.77	0.71	0.72
81 FL	0.77	0.71	0.71	0.74	0.79	0.73	0.74
80 FL	0.83	0.62	0.76	0.77	0.82	0.75	0.76
79 FL	0.86	0.65	0.79	0.82	0.85	0.78	0.79
78 FL	0.89	0.67	0.82	0.85	0.88	0.80	0.81
77 FL	0.68	0.43	0.53	0.61	0.52	0.55	0.65
76 FL	0.70	0.47	0.56	0.67	0.57	0.61	0.67
75 FL	0.88	0.71	0.71	0.75	0.85	0.75	0.89
74 FL	0.89	0.71	0.72	0.75	0.86	0.75	0.87
73 FL	0.91	0.72	0.74	0.77	0.88	0.77	0.89
72 FL	0.89	0.69	0.71	0.76	0.91	0.73	0.84
71 FL	0.91	0.71	0.73	0.78	0.94	0.75	0.86
70 FL	0.93	0.72	0.75	0.80	0.96	0.77	0.87
69 FL	0.87	0.69	0.75	0.78	0.81	0.74	0.85
68 FL	0.89	0.71	0.77	0.80	0.83	0.75	0.87
67 FL	0.91	0.72	0.79	0.82	0.85	0.77	0.89
66 FL	0.89	0.74	0.77	0.80	0.82	0.79	0.90
65 FL	0.91	0.75	0.79	0.82	0.84	0.80	0.92
64 FL	0.92	0.77	0.81	0.84	0.86	0.82	0.93
63 FL	0.87	0.71	0.78	0.79	0.81	0.78	0.89
62 FL	0.89	0.73	0.80	0.80	0.82	0.79	0.90
61 FL	0.90	0.74	0.82	0.82	0.84	0.81	0.92
60 FL	0.88	0.76	0.79	0.81	0.78	0.75	0.90
59 FL	0.89	0.77	0.81	0.83	0.80	0.76	0.92
58 FL	0.91	0.79	0.83	0.84	0.81	0.78	0.93
57 FL	0.87	0.73	0.80	0.80	0.82	0.79	0.91
56 FL	0.89	0.74	0.82	0.81	0.84	0.81	0.92
55 FL	0.90	0.76	0.83	0.83	0.86	0.82	0.94
54 FL	0.86	0.77	0.81	0.81	0.80	0.76	0.90
53 FL	0.88	0.79	0.82	0.83	0.81	0.77	0.91
52 FL	0.89	0.80	0.84	0.84	0.83	0.78	0.93
51 FL	0.85	0.74	0.85	0.80	0.84	0.80	0.88
50 FL	0.87	0.75	0.86	0.81	0.86	0.81	0.90
49 FL	0.88	0.77	0.88	0.83	0.87	0.83	0.91
48 FL	0.87	0.78	0.85	0.78	0.82	0.76	0.89
47 FL	0.88	0.79	0.87	0.79	0.84	0.78	0.90
46 FL	0.90	0.81	0.88	0.81	0.85	0.79	0.92
45 FL	0.70	0.75	0.81	0.76	0.76	0.74	0.71
44 FL	0.71	0.77	0.82	0.78	0.78	0.75	0.73
43 FL	0.63	0.70	0.59	0.56	0.67	0.59	0.65
42 FL	0.65	0.73	0.62	0.60	0.71	0.62	0.67
41 FL	0.87	0.75	0.81	0.83	0.84	0.81	0.89
40 FL	0.87	0.74	0.81	0.82	0.83	0.80	0.89
39 FL	0.86	0.75	0.83	0.76	0.84	0.81	0.88
38 FL	0.87	0.76	0.84	0.77	0.85	0.82	0.89
37 FL	0.88	0.77	0.85	0.79	0.87	0.83	0.90
36 FL	0.86	0.78	0.82	0.80	0.78	0.77	0.87
35 FL	0.88	0.80	0.84	0.81	0.79	0.78	0.88
34 FL	0.89	0.81	0.85	0.82	0.80	0.79	0.90
33 FL	0.86	0.74	0.83	0.77	0.82	0.80	0.89
32 FL	0.87	0.74	0.84	0.78	0.83	0.81	0.90
31 FL	0.88	0.75	0.85	0.79	0.84	0.82	0.91
30 FL	0.86	0.76	0.84	0.80	0.84	0.83	0.88
29 FL	0.87	0.77	0.85	0.81	0.85	0.84	0.89
28 FL	0.88	0.78	0.86	0.82	0.87	0.85	0.90
27 FL	0.87	0.79	0.85	0.83	0.82	0.77	0.89
26 FL	0.88	0.80	0.86	0.84	0.84	0.78	0.90
25 FL	0.89	0.81	0.87	0.86	0.85	0.79	0.91
24 FL	0.87	0.80	0.84	0.81	0.84	0.80	0.89
23 FL	0.88	0.81	0.85	0.82	0.84	0.81	0.90
22 FL	0.89	0.82	0.86	0.83	0.85	0.82	0.91
21 FL	0.87	0.80	0.84	0.84	0.84	0.83	0.89
20 FL	0.88	0.81	0.85	0.85	0.85	0.84	0.90
19 FL	0.89	0.82	0.87	0.86	0.86	0.85	0.91
18 FL	0.87	0.81	0.85	0.81	0.84	0.82	0.87
17 FL	0.88	0.82	0.86	0.82	0.85	0.83	0.88
16 FL	0.89	0.83	0.87	0.83	0.86	0.84	0.89
15 FL	0.88	0.81	0.86	0.84	0.84	0.83	0.87
14 FL	0.89	0.82	0.87	0.85	0.85	0.84	0.88
13 FL	0.90	0.83	0.88	0.86	0.86	0.85	0.89
12 FL	0.85	0.82	0.87	0.81	0.84	0.83	0.87
11 FL	0.86	0.82	0.88	0.82	0.85	0.84	0.88
10 FL	0.88	0.84	0.90	0.84	0.87	0.86	0.90
09 FL	0.87	0.83	0.97	0.90	0.88	0.85	0.78
08 FL	0.88	0.84	0.98	0.90	0.89	0.86	0.78
07 FL	0.70	0.54	0.54	0.55	0.54	0.54	0.69
06 FL	0.72	0.55	0.56	0.56	0.55	0.55	0.70
05 FL	0.72	0.56	0.57	0.57	0.56	0.56	0.71
04 FL	0.72	0.56	0.55	0.56	0.55	0.56	0.68
03 FL	0.80	0.60	0.64	0.63	0.62	0.60	0.79
02 FL	0.83	0.61	0.66	0.64	0.63	0.61	0.82
01 FL	0.89	0.81	0.89	0.98	0.84	0.82	0.90
B1 FL	0.88	0.81	0.88	0.97	0.84	0.73	0.74	0.90
B2 FL	0.90	0.82	0.89	1.00	0.85	0.55	0.50	0.91
B3 FL	0.87	0.78	0.87	0.96	0.80	0.56	0.50	0.87
B4 FL	0.97	0.83	0.96	1.04	0.86	0.60	0.54	0.97
B5 FL	0.98	0.83	0.96	1.05	0.87	0.60	0.55	0.97

(d)

Figure 5–12. Demand/capacity ratios for WTC 2 core columns under original design loads, (c) 700 line and (d) 800 line (continued).

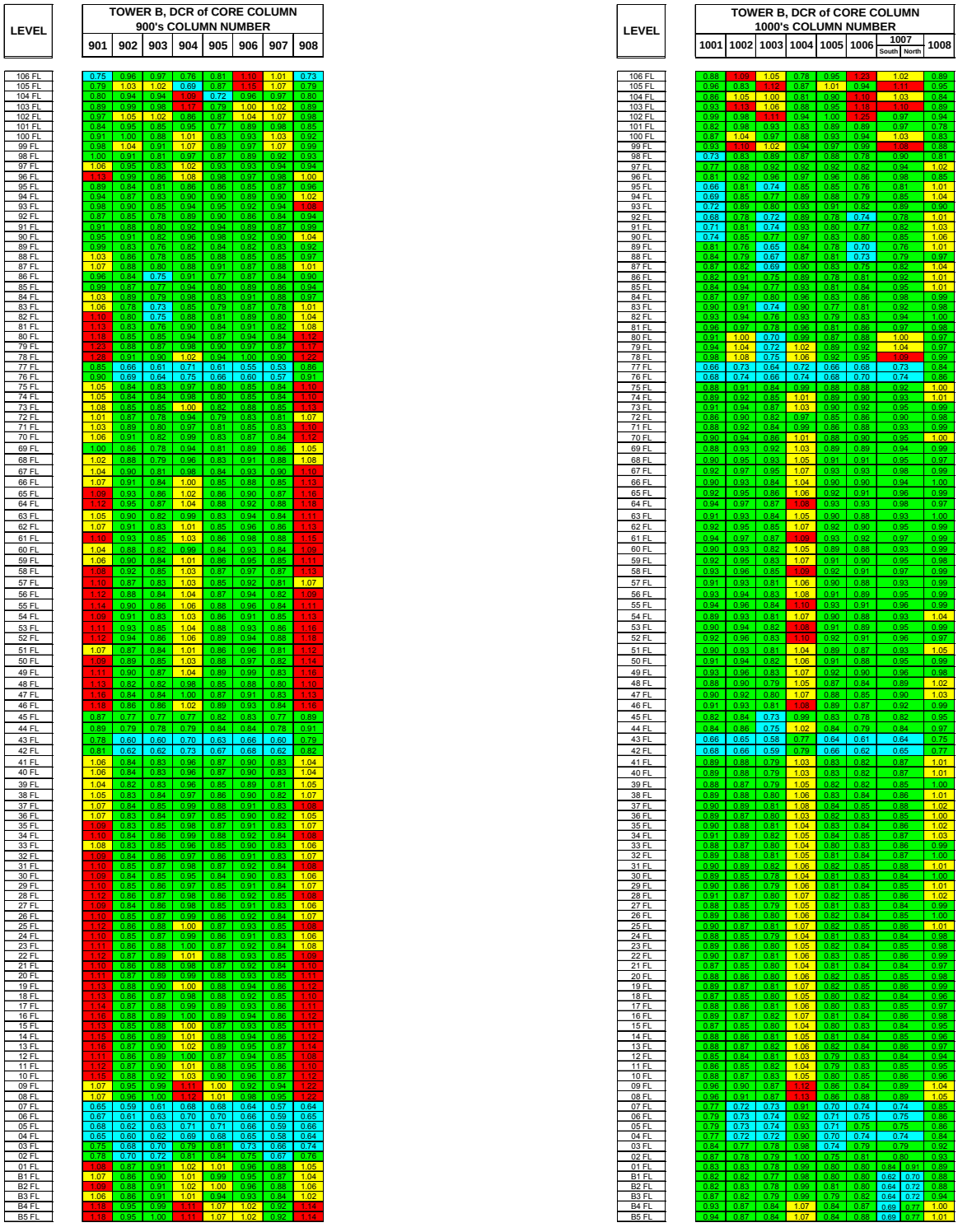

Figure 5–12. Demand/capacity ratios for WTC 2 core columns under original design loads, (e) 900 line and (f) 1000 line (continued).

The core columns that have DCRs>1 were calculated for axial stresses due to gravity loads and were generally located on the 600 column line between floors 80 and 106 and at columns 901 and 908 for much of their height. The gravity loads on these columns were affected significantly by assumptions about tributary areas, unit construction dead loads and superimposed dead loads, and the sequence of construction of the hat truss. The high degree of stress calculated at these core columns is likely associated with differences in these assumptions between the original and current computations.

Figure 5–13 presents the distribution of the normal stresses due to axial loads (axial column load divided by columns cross sectional area) in the columns of the four exterior walls due to wind loads only (gravity loads are not included in these plots). The axial stresses are presented at three levels along the height of the tower: B6, 39, and 73. The plots show both the tensile and compressive stresses on the columns induced by wind loading, where shear lag effects can be observed. For corner columns 101, 159, 301, and 359 at floor 73, Fig. 5–13(c) indicates that their stresses are smaller than their neighboring columns. This is likely due to the influence of the special corner framing at that floor, i.e. the discontinuous columns and chamfered plan layout of the exterior wall framing.

The results of the baseline performance analysis indicated that tension forces were developed in the exterior walls of WTC 2 under the original WTC design dead and wind loads. The tension forces from the combination of dead and wind loads for all faces are illustrated in Fig. 5–14. The figure indicates that forces are largest at the base of the building and at the corners.

These axial tensile column loads were transferred from one panel to another through the column splices. The exterior wall column splice capacities were calculated from the original details and compared to the tension forces for all four faces of WTC 2. The DCR ratios for the exterior wall splice connections for WTC 2 are summarized in Table 5–6.

For the tower resistance to shear sliding and overturning due to wind, the dead loads that acted on the perimeter walls of the tower provided resistance to shear sliding and overturning at the foundation level. Considering the resistance to shear sliding under wind load, the factor of safety was calculated to be approximately 10. Considering resistance to overturning due to wind load, the factors of safety were calculated to be approximately 1.9 and 2.7 for overturning about a north-south axis and for an east-west axis, respectively.

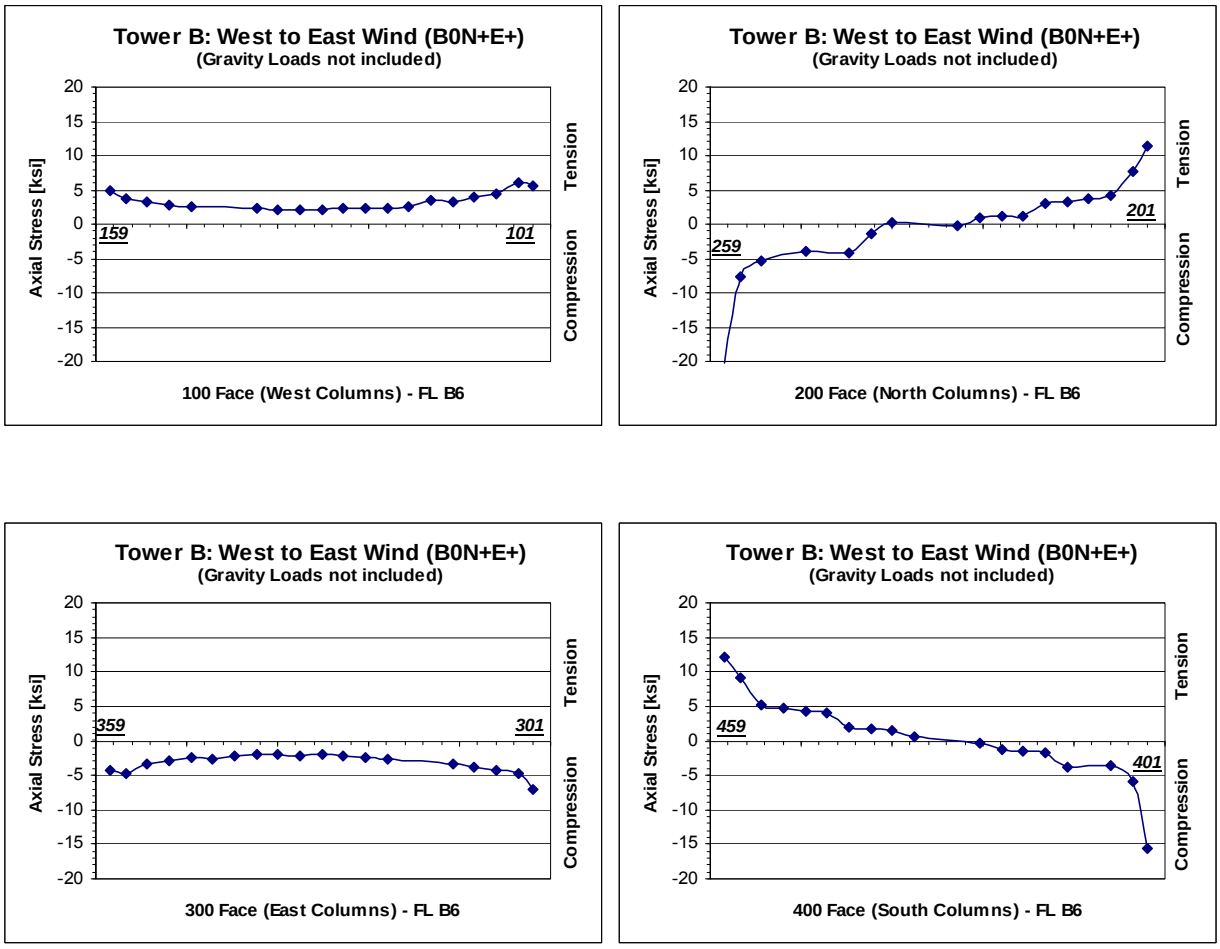

(a)

Figure 5–13. Shear lag diagrams of WTC 2 due to original WTC wind loads at (a) floor B6, (b) floor 39, and (c) floor 73.

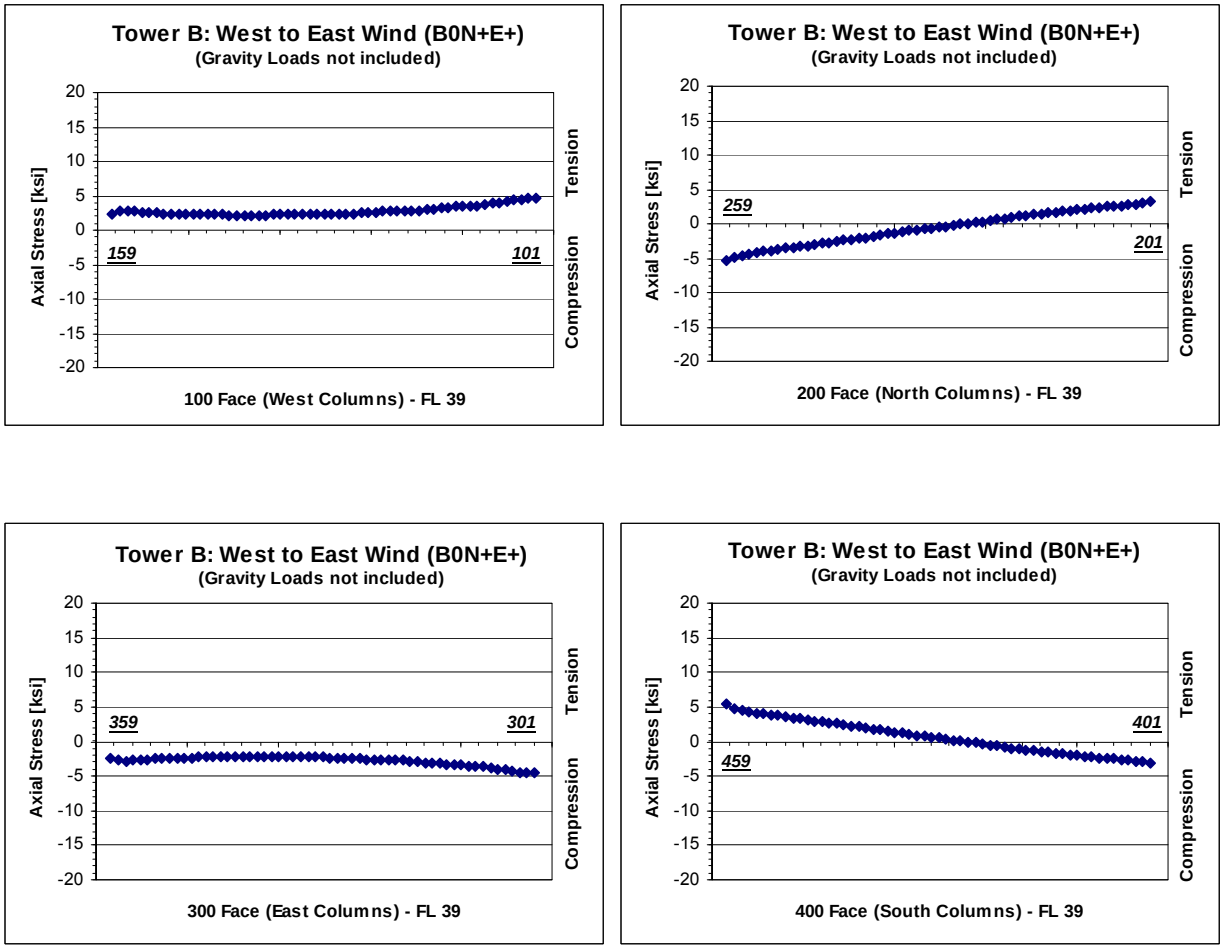

(b)

Figure 5–13. Shear lag diagrams of WTC 2 due to original WTC wind loads at (a) floor B6, (b) floor 39, and (c) floor 73 (continued).

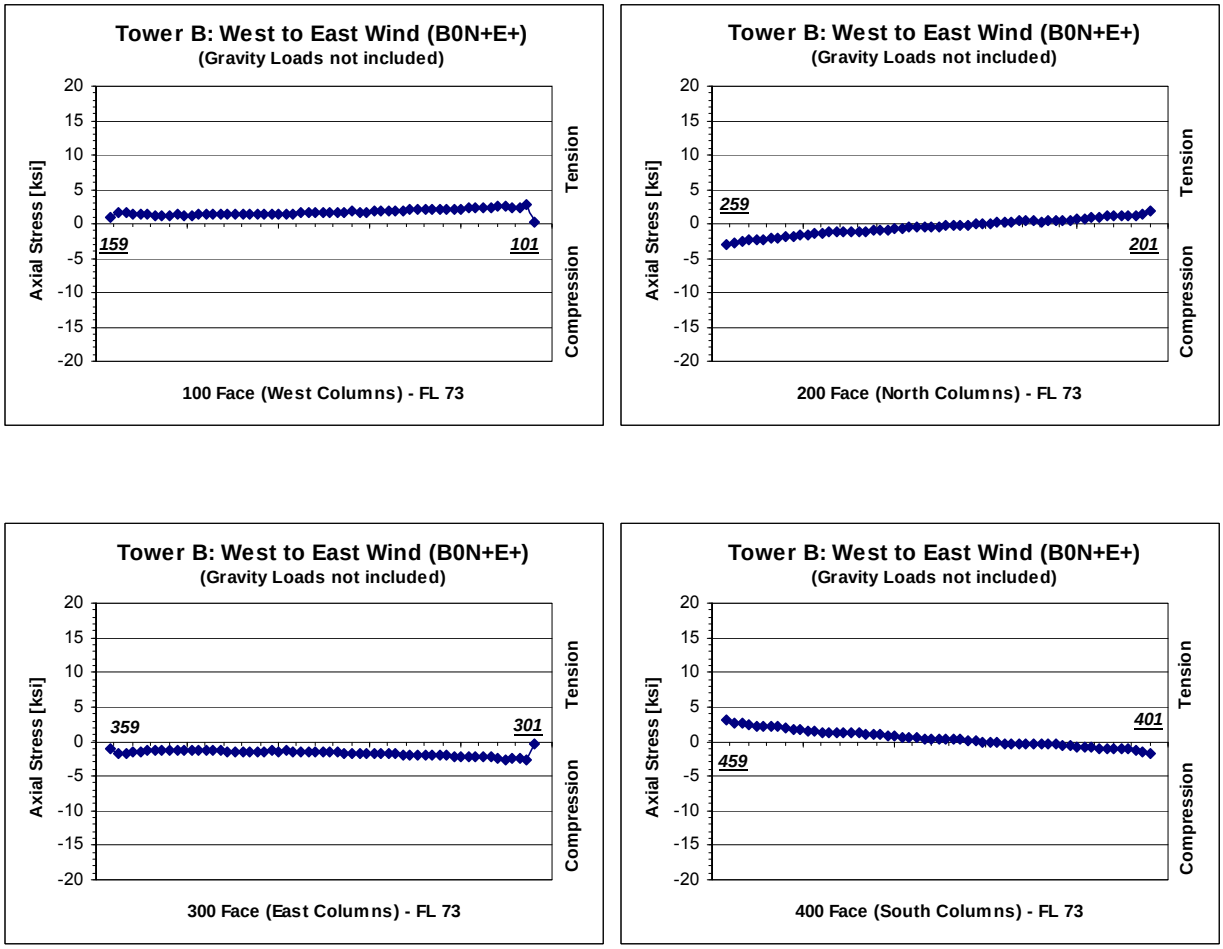

(c)

Figure 5–13. Shear lag diagrams of WTC 2 due to original WTC wind loads at (a) floor B6, (b) floor 39, and (c) floor 73 (continued).

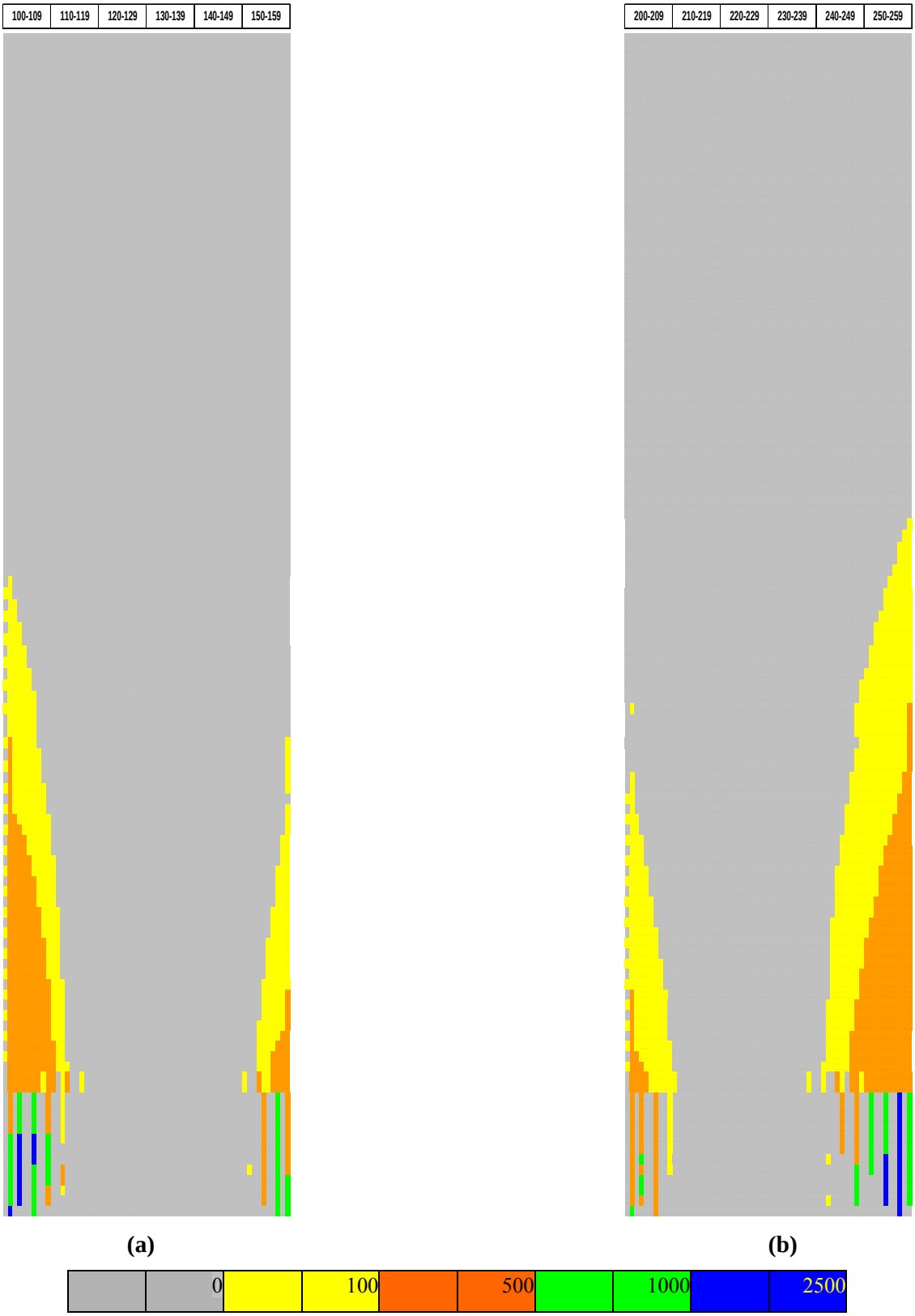

Figure 5–14. Tension force distribution (kip) in the exterior wall columns of WTC 2 under original design dead and wind loads, (a) 100 face (west) and (b) 200 face (north).

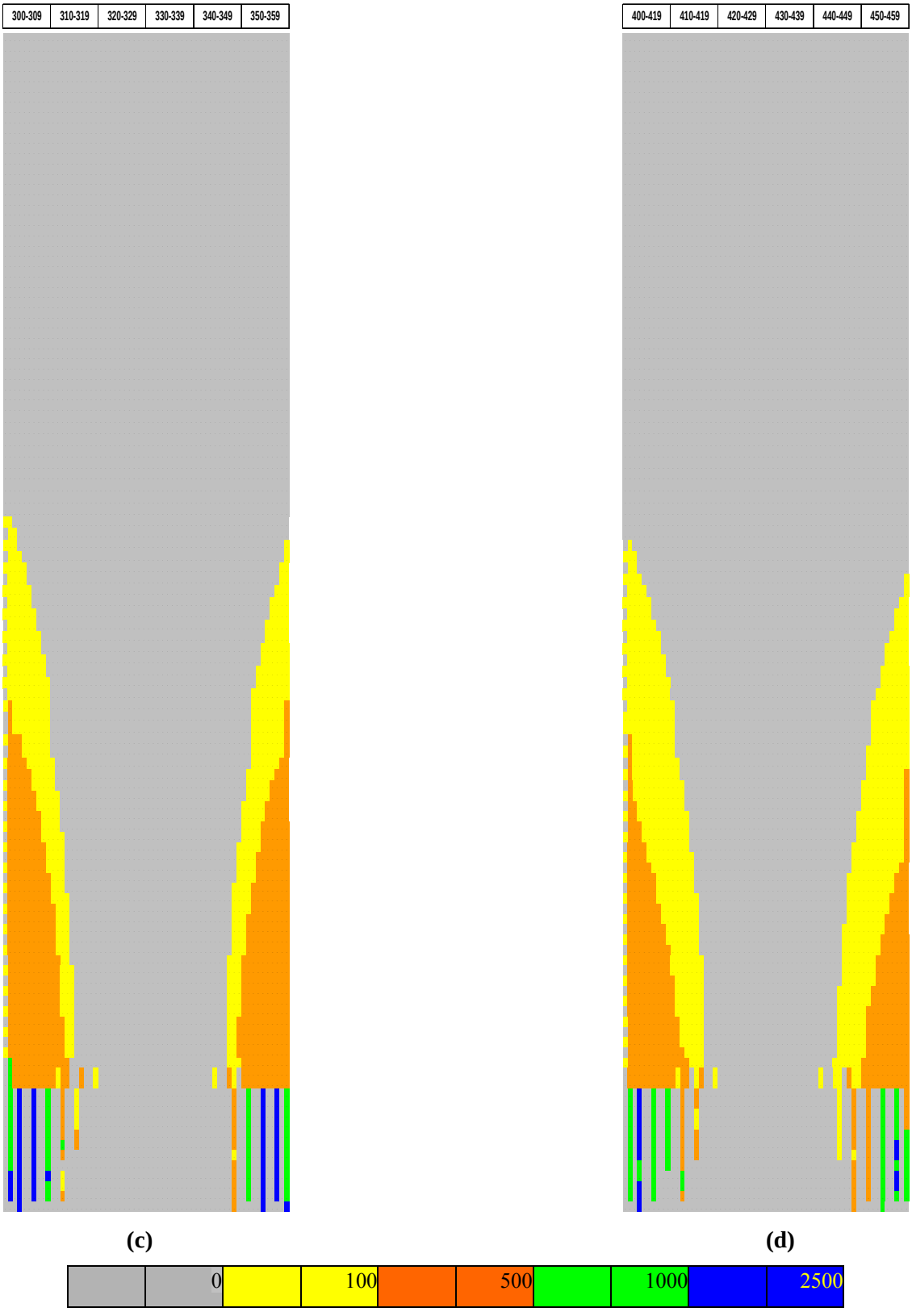

Figure 5–14. (c) 300 face (east) and (d) 400 face (south) (continued).

Table 5–6. Maximum calculated demand/capacity ratios (DCRs) for exterior wall column splices for WTC 2 under original design dead and wind load case.

Exterior Wall Face	Exterior Wall Column Splice	Maximum Calculated DCR
100 Face (West)	Below floor 1	0.64
	Floor 1 to 9	0.25
	Floor 10 to 41	0.83
	Above floor 42	0.10
200 Face (North)	Below floor 1	0.70
	Floor 1 to 9	0.36
	Floor 10 to 41	0.99
	Above floor 42	0.13
300 Face (East)	Below floor 1	0.75
	Floor 1 to 9	0.35
	Floor 10 to 41	0.96
	Above floor 42	0.16
400 Face (South)	Below floor 1	0.60
	Floor 1 to 9	0.33
	Floor 10 to 41	0.84
	Above floor 42	0.21

5.4.2 State-of-the-Practice Case

The WTC 2 global model was analyzed using the lower estimate, state-of-the-practice loading case, as described in Chapter 4 (see also NIST NCSTAR 1-2). This loading case included dead loads, live loads according to the NYCBC 2001, and wind loads from RWDI wind tunnel study, scaled in accordance with the NYCBC 2001 wind speed.

The calculated total drift of WTC 2 induced by the lower estimate, state-of-the-practice case was approximately 59.7 in. (4 ft 11.7 in.) in the E–W direction and 55.9 in. (4 ft 8.1 in.) in the N–S direction. These drifts are equivalent to about H/287 and H/307 in the E–W and N–S directions, respectively. Figure 5–15 presents the deflected shape (cumulative drift) and the inter-story drifts normalized by the story height for WTC 2 under the lower estimate, state-of-the-practice case. The plots are presented for the E–W and N–S directions for the load combinations producing the maximum cumulative drift.

DCR statistics for WTC 2 global systems components under the lower estimate, state-of-the-practice loading case are summarized in Table 5–7. A comparison of the mean values of the DCRs estimated from the original design case (Table 5–5) with those from the state-of-the-practice case (Table 5–7) indicated that the results are very similar. Also the distribution of the DCRs and the locations of members with DCRs greater than 1.0 were very similar between the original design case and the state-of-the-practice case.

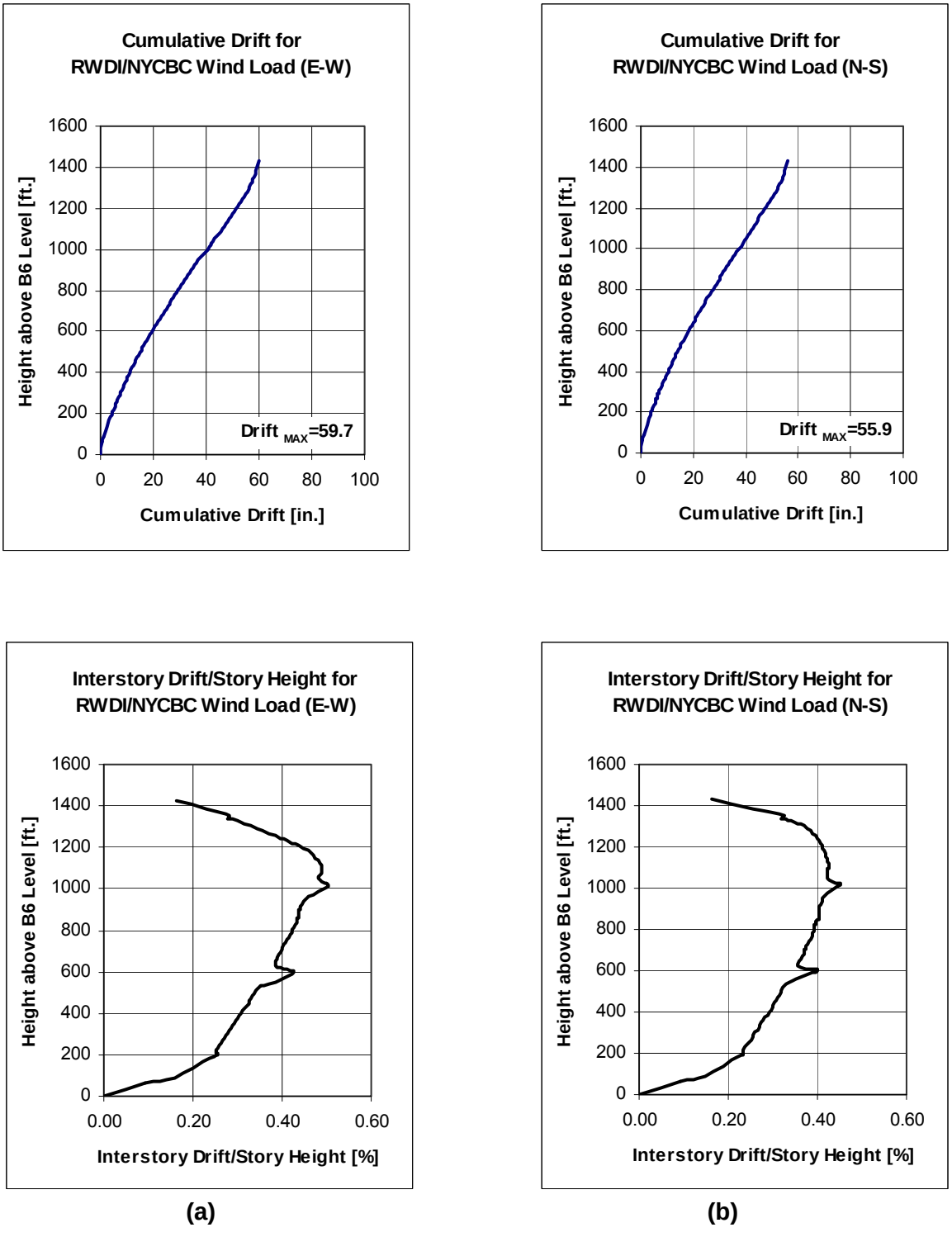

Figure 5–15. Drift diagrams of WTC 2 due to the lower estimate, state-of-the-practice case, (a) 2R4PDN and (b) 2R11PDN.

Table 5–7. Statistics of demand/capacity ratios (DCRs) for WTC 2 under the lower estimate, state-of-the practice case.

Member Type	Number of Members	Mean Calculated DCR	C.O.V. of DCR	Percentage of Components with DCR > 1.0	Percentage of Components with DCR > 1.05	Number of Components with DCR > 1.05	Maximum Calculated DCR
Exterior Wall Columns							
Below floor 1	577	0.70	0.20	3.1	1.4	8	1.30
Floor 1 to 9	1,122	0.72	0.26	2.2	1.1	12	1.16
Floor 9 to 106	31,086	0.77	0.13	1.8	0.6	189	1.21
Above floor 106	578	0.71	0.30	8.7	5.4	31	1.40
Exterior Wall Spandrels							
Below floor 1	408	0.45	0.47	1.7	0.7	3	1.15
Floor 1 to 9	594	0.37	0.44	0.7	0.7	4	1.19
Floor 9 to 106	31,160	0.31	0.27	0	0	0	0.73
Above floor 106	836	0.33	0.70	1.7	1.4	12	1.47
Core Columns	5,245	0.86	0.15	10.8	6.6	345	1.36
Hat Truss System							
Columns	238	0.48	0.57	3.8	2.5	6	1.35
Beams	504	0.23	0.82	0.2	0	0	1.01
Braces	283	0.40	0.57	0.7	0	0	1.04
Exterior Wall Bracing							
Below floor 1	227	0.69	0.17	0.9	0.4	1	1.13
Above floor 106	12	0.27	0.31	0	0	0	0.41

5.4.3 The Refined NIST Estimate Case

The WTC 2 global model was analyzed using the refined NIST estimate case as described in Chapter 4 (see also NIST NCSTAR 1-2). This loading case included dead loads, live loads in accordance with the current ASCE 7-02 Standard, and wind loads developed by NIST based on critical assessment of information obtained from RWDI and CPP reports and state-of-the-art considerations in wind engineering.

The calculated total drift of WTC 2 induced by the refined NIST estimate case was approximately 75.6 in. (6 ft 3.6 in.) in the E–W direction and 70.8 in. (5 ft 11 in.) in the N–S direction. These drifts are equivalent to about H/227 and H/242 in the E–W and N–S directions, respectively. Fig. 5–16 presents the deflected shape (cumulative drift) and the inter-story drifts normalized by the story height for WTC 2 under the refined NIST wind loads. The plots are presented for the E–W and N–S directions for the load combinations producing the maximum cumulative drift.

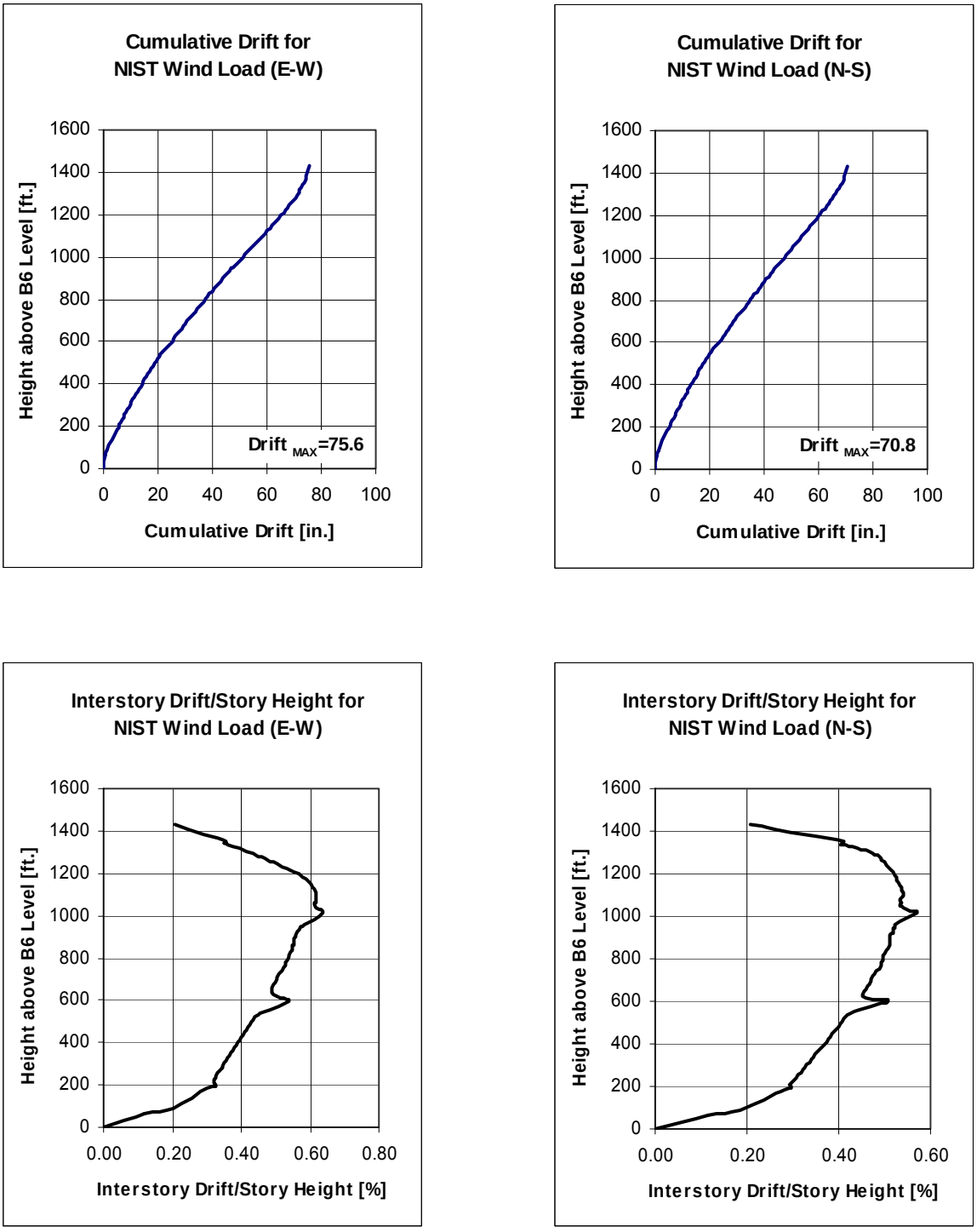

(a) **(b)**

Figure 5–16. Drift diagrams of WTC 2 due to refined NIST estimate wind loads, (a) 2R4PD and (b) 2R11PD.

DCR statistics for WTC 2 global systems components under the refined NIST estimate case are summarized in Table 5–8. The DCRs for the core columns and hat truss members estimated from the original design and the state-of-the-practice cases (Tables 5–5 and 5–7, respectively) are generally close to those estimated from the refined NIST estimate case (Table 5–8). This is due to the fact that core columns and hat truss members do not significantly contribute to wind load resistance. The DCRs for the exterior walls, including columns, spandrels, and bracings estimated from the refined NIST estimate case are larger than those estimated from the original design and the state-of-the-practice cases. For example, for the exterior wall, the ratio of the mean DCRs from the refined NIST estimate case to the mean DCRs from the original design case ranged between 1.60 and 1.11. The ratio of the mean DCRs from the refined NIST estimate case to the mean DCRs from the lower estimate, state-of-the-practice case ranged between 1.65 and 1.17.

Table 5–8. Statistics of demand/capacity ratios (DCRs) for WTC 2 under the refined NIST estimate case.

Member Type	Number of Members	Mean Calculated DCR	C.O.V. of DCR	Percentage of Components with DCR > 1.0	Percentage of Components with DCR > 1.05	Number of Components with DCR > 1.05	Maximum Calculated DCR
Exterior Wall Columns							
Below floor 1	577	0.96	0.25	42	41.1	229	1.95
Floor 1 to 9	1,122	1.04	0.27	63.7	58.0	651	1.69
Floor 9 to 106	31,086	1.09	0.14	73.5	60.9	18,941	1.78
Above floor 106	578	0.83	0.28	19.6	15.1	87	1.66
Exterior Wall Spandrels							
Below floor 1	408	0.73	0.46	15.9	13.7	56	1.78
Floor 1 to 9	594	0.61	0.44	7.7	5.2	31	2.02
Floor 9 to 106	31,160	0.51	0.28	0.4	0.2	61	1.21
Above floor 106	836	0.39	0.68	2.0	1.9	16	1.73
Core Columns	5,245	0.83	0.16	10.6	6.0	315	1.42
Hat Truss System							
Columns	238	0.59	0.59	14.3	10.5	25	1.95
Beams	504	0.28	0.82	1.0	0.8	4	1.12
Braces	283	0.49	0.52	3.9	2.8	8	1.09
Exterior Wall Bracing							
Below floor 1	227	1.01	0.18	48.0	38.8	88	1.04
Above floor 106	12	0.43	0.31	0	0	0	0.64

5.5 SUMMARY

This chapter presented the results of the baseline performance analysis for the WTC 1 and WTC 2 global models under three gravity and wind loading cases: (1) the original WTC design load case, (2) the lower-estimate, state-of-the-practices case, and (3) the refined NIST estimate case. The baseline performance

results included total and inter-story drift, demand/capacity ratios, exterior columns behavior (shear lag effects and presence of tensile forces), behavior of exterior wall splice connections, and the towers' resistance to shear sliding and overturning.

Under the original WTC design loads, the cumulative drifts at the top of the WTC 1 tower were about 56.6 in. (H/304) and 55.7 in. (H/309) in the E–W and N–S direction, respectively. These drifts were about 51.2 in. (H/335) in the E–W direction and 65.3 in. (H/263) in the N–S direction for WTC 2. For the lower estimate, state-of-the-practice case, the drifts for WTC 1 were larger than those from the original design case by about 0.5 percent and 22 percent for the E–W and N–S directions, respectively. For the lower estimate, state-of-the-practice case for WTC 2, the E–W drift was larger than that from the original design case by about 16 percent, while the N–S drift was smaller by about 15 percent. These differences are consistent with the differences between the base shears for the two cases (see Tables 4–3 and 4–4 of Chapter 4). The drifts obtained from the refined NIST estimate case were about 25 percent larger than those from the state-of-the practice case.

The demand/capacity ratios (DCR) were based on the allowable stress design procedure and were estimated using the AISC Specifications (1989). The results indicated that DCRs estimated from the original WTC design load case were, in general, close to those obtained for the lower estimate, state-of-the practice case. For both cases, a small fraction of structural components had DCRs larger than 1.0. These were mainly observed in both towers at (1) the exterior walls: at the columns around the corners, where the hat truss connected to the exterior walls, and below floor 9; and (2) the core columns on the 600 line between floors 80 and 106 and at core perimeter columns 901 and 908 for much of their height.

The DCRs obtained for the refined NIST estimate case were higher than those from the original WTC design and the lower estimate, state-of-the-practice load cases, owing to the following reasons:

- The NIST estimated wind loads were higher than those used in the lower estimate, state-of-the-practice case by about 25 percent (about 10 percent difference between the RWDI loads scaled to the NYCBC 2001 wind speed and RWDI loads scaled to the ASCE 7-02 wind speed, in addition to the 15 percent increase estimated by NIST, see Sec. 4.4.3). It is noted that the NIST estimated wind loads were about 20 percent smaller than those estimated by CPP (an upper estimate state-of-the practice case, see Chapter 4).

- The original WTC design and the state-of-the-practice cases used NYCBC load combinations, which result in lower DCRs than the ASCE 7-02 load combinations used for the refined NIST case.

Under a combination of the original WTC design dead and wind loads, tension forces were developed in the exterior walls of WTC 1 and WTC 2. The forces were largest at the base of the building and at the corners. These tensile column loads were transferred from one panel to another through the column splices. The DCR ratios for the exterior wall splice connections under these tensile forces for both towers were shown to be less than 1.0.

For the towers' resistance to shear sliding and overturning due to wind, the dead loads that acted on the perimeter walls of the towers provided resistance to shear sliding and overturning at the foundation level. Considering the resistance to shear sliding under wind load, the factor of safety was calculated to be

between 10 and 11.5, while the factor of safety against overturning ranged from 1.9 to 2.7 for both towers.

5.6 REFERENCES

AISC Specification 1989: American Institute of Steel Construction, Specification for Structural Steel Buildings – Allowable Stress Design and Plastic Design – 9th Edition, Chicago, IL, 1989.

ASCE 7-02: American Society of Civil Engineers, ASCE 7 Standard Minimum Design Loads for Buildings and Other Structures, Reston, VA, 2002.

NYCBC 2001: Building Code of the City of New York, 2001 Edition, Gould Publications, Binghamton, NY.

Chapter 6
BASELINE PERFORMANCE ANALYSIS OF TYPICAL FLOOR MODELS

6.1 INTRODUCTION

This chapter presents the results of the baseline performance analysis for the typical floor models discussed in Chapter 3. These models included the typical truss-framed floor (floor 96 of World Trade Center [WTC] 1, see Sec. 3.3) and the typical beam-framed floor (floor 75 of WTC 2, see Sec. 3.4).

For application to the floor models, gravity loads were separated into three categories: construction dead loads (CDL), superimposed dead loads (SDL), and live loads (LL). CDL is defined as the self-weight of the structural system. The self-weight of the floor trusses, floor beams, and concrete slabs were automatically generated in SAP2000. SDL is defined as the added dead load associated with architectural and mechanical/electrical/plumbing systems (curtain wall, floor finishes, mechanical equipment and ducts, transformers, etc.) The CDL and SDL were based on the WTC architectural and structural drawings and on the original WTC Design Criteria.

Two independent sets of live loads were applied in combination with the dead loads. The first was taken from the original WTC Design Criteria and the second from the American Society of Civil Engineers (ASCE 7-02) Standard. The live loads in the New York City Building Code (NYCBC 2001) are essentially identical to the American Society of Civil Engineers (ASCE) 7-02 live loads. Live load reductions were taken from the original WTC Design Criteria and from the ASCE 7-02 Standard, each for use with its respective live loads.

For the baseline performance analysis for the floor systems, demand/capacity ratios (DCRs) for structural components were estimated using the Allowable Stress Design (ASD) procedure as specified in the American Institute of Steel Construction (AISC) Specification (1989), see Chapter 5. The DCRs were calculated by dividing component demands by component capacities, taken at unfactored (working) loads and at working stresses, not at ultimate loads or yield stresses. These DCRs for the structural components were determined as follows:

1. The component demands were taken from the results of the baseline performance analysis using the reference floor models, making use of working loads.

2. The component capacities were determined based on the nominal steel strength as specified in the original design documents and using the AISC Specification (1989).

This chapter reports on the results of the baseline performance analysis for the floor systems under gravity loading. Sections 6.2 and 6.3 present the loading and baseline performance analysis results for the truss-framed floor and the beam-framed floor, respectively.

6.2 TYPICAL TRUSS-FRAMED FLOOR

The analysis of the typical truss-framed floor was performed on the computer model of floor 96 of WTC 1 (see Sec. 3.3). This section describes the gravity loads applied to the model along with the results of the baseline performance analysis.

6.2.1 Gravity Loads

Areas Outside Core

The CDL was calculated based on the member's geometry and material properties. The SDL allowance was typically 11.5 psf to 13.5 psf outside the core. Figure 6–1 shows the WTC Design Criteria reduced live load for the floor design. Table 6–1 provides a comparison between the live loads from the WTC Design Criteria, NYCBC 2001, and the ASCE 7-02 Standard.

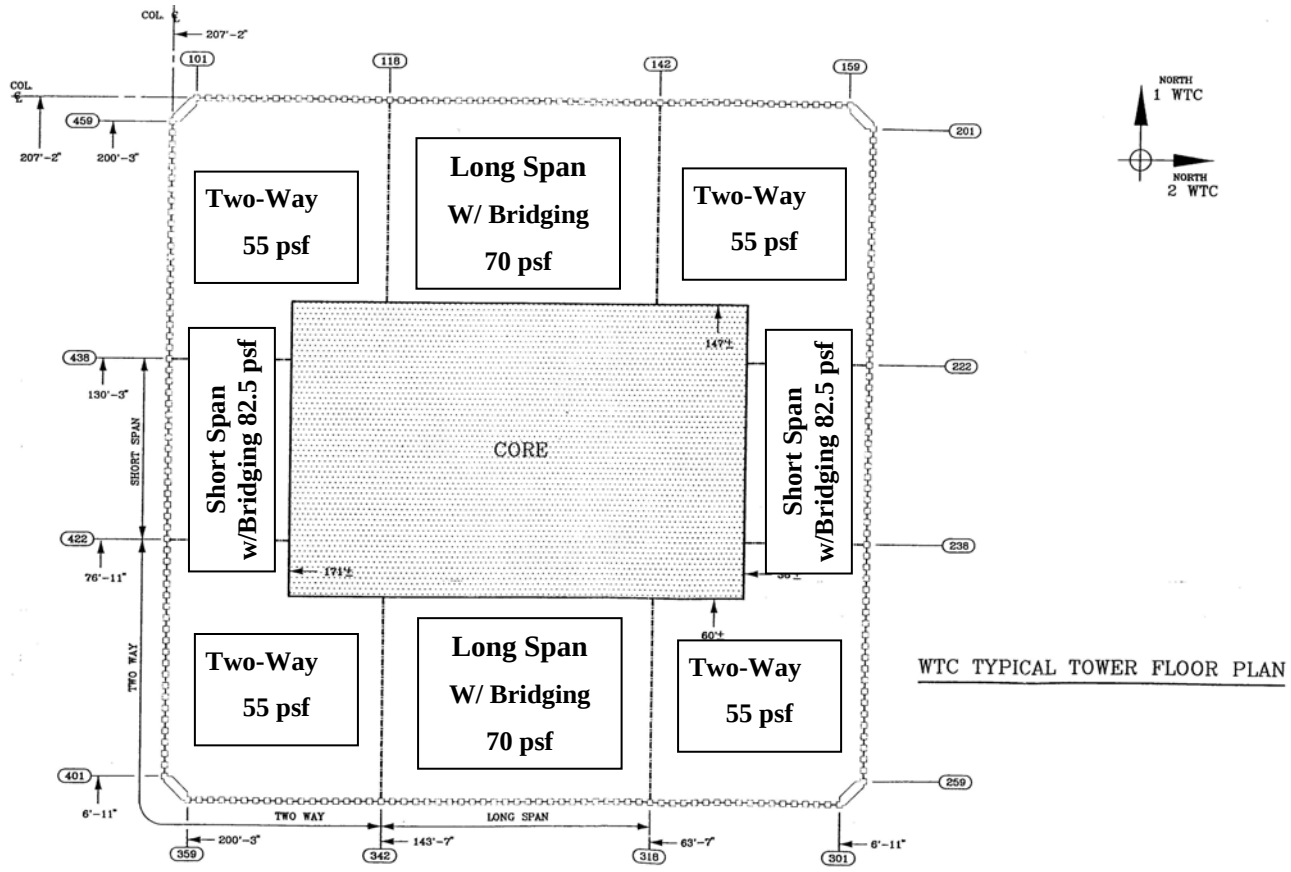

Source: Reproduced with permission of The Port Authority of New York and New Jersey. Enhanced by NIST.

Figure 6–1. Summary of WTC-design criteria reduced live loads for floor design: design load of 100 psf - partition load is included in LL allowance.

Table 6–1. Summary of typical truss-framed floor live loads and (reduced live loads) for areas outside of core.

Criteria	Design	Two-Way Zone	Long Span	Short Span	Partition
WTC Design Criteria	Floor	100 psf (55 psf)	100 psf (70 psf)	100 psf (82.5 psf)	Included in LL
NYC Building Code	Floor	50 psf (25 psf)	50 psf (39 psf)	50 psf (47 psf)	6 psf
ASCE 7-02	Floor	50 psf (25 psf)	50 psf (39 psf)	50 psf (47 psf)	6 psf

Areas Inside Core

Table 6–2 shows the CDL and SDL used inside the core area along with the live loads from the WTC Design Criteria, NYCBC 2001, and the ASCE 7-02 Standard. Loads are shown for the various occupancies within the core area.

Table 6–2. Area inside core: loading floor 96, WTC 1.

Area	Loading (psf)				
			Live Load for Floor Design		
	CDL	SDL	WTC Design Criteria	ASCE 7-02	NYCBC 2001
Tenant Space	Varies See Original Structural Drawings	33	100	50	50
Toilets		49	40	40	40
Stair, Service, Closet		29	100	100	100
Elevator Lobby, Corridor		41	75	80	80
Telephone, Electric Closet		29	75	75	75

6.2.2 Results of Baseline Analysis

The maximum mid-span deflections for each of the long-span, short-span, and two-way zones for the original WTC Design Criteria and ASCE 7-02 total loads are provided in Table 6–3.

Table 6–3. Summary of maximum deflections for typical truss-framed floor under DL + LL for areas outside of core.

Criteria	Two-Way Zone	Long Span	Short Span
WTC Design Criteria	1.44 in.	1.79 in.	0.57 in.
NYCBC ASCE 7-02	1.14 in.	1.43 in.	0.44 in.

For the components of the truss-framed floors, DCRs were calculated using the SAP2000 program. Calculations were made for the top and bottom chords, the diagonals and the verticals of the primary and bridging trusses, and for the beams and girders of the core. Since the top chords consisted of a pair of steel angles plus the concrete slab, the capacity of the concrete slab predominated and was much greater than the capacity of the top chord; therefore, a calculation of the stress in the slab seemed irrelevant and would have required significant intervention to SAP's post-processor to establish a proper design calculation.

DCRs were not calculated for the following elements in this computer model:

- Strap elements
- Damper elements
- Frame connections assigned as "plate" elements and similar connectors
- Rigid links
- Core columns, spandrels, and exterior columns
- Deck support angles
- Core perimeter channel members within close proximity to supports

The calculations were spot checked for accuracy and to verify that the correct design information was applied. For most of the component calculations checked, the standard SAP2000-generated calculations were found to be acceptable; however, for some components, the computer model did not accurately represent the actual construction, and for other components, the standard SAP2000 calculations yielded erroneous results. As a result, for estimating the DCRs of the structural components, the following adjustments to the design parameters were applied to the floor model to yield accurate results:

- Length factors were assigned to truss web members to reflect the length of the actual constructed member. For example, in the model, to account for the participation of the composite slab, the distance between the top and bottom chord of the primary floor trusses was taken as 30 in. However, this distance was actually 28 in. Therefore, a length modifier was applied to the primary truss diagonals to account for the actual length of the diagonal. In general, the length modifier was determined by measuring the diagonal distance from the underside of the top chord to the centerline of the bottom chord (see Fig. 6–2).

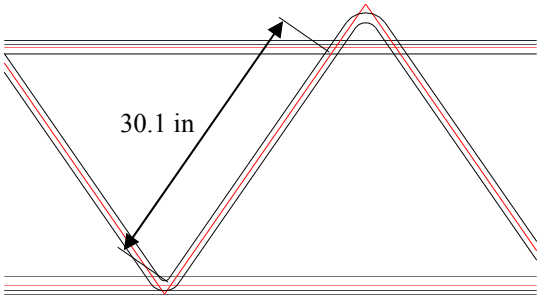

Theoretical unbraced length = 30.1 inches, measured from the face of top chord to the centerline of the bottom chord.

The unbraced length is adjusted in the SAP2000 computer model by a factor of 30.1″ / 36.0″ = 0.84

Figure 6–2. Unbraced length of truss diagonal.

- Significant out-of-plane bending is not expected in the members of planar trusses subjected to concentric vertical loading. However, due to the complexity of the floor model, significant out-of-plane (i.e., minor axis) bending moments were observed in some truss diagonals and bottom chord members. As a result, the allowable minor axis bending stress was substantially increased to effectively eliminate these bending moments from the DCR calculation.

- The allowable shear stress for truss diagonals with additional bar reinforcement was substantially increased since for these members, the SAP2000 program computed an erroneous shear area.

For the area outside the core, the DCRs for all floor trusses were less than 1.14 for the original WTC Design Criteria and less than 0.86 for the ASCE 7-02 loading and (by comparison) for the NYCBC 2001 loading. Under the original WTC Design Criteria loading, the DCR was less than 1.00 for 99.4 percent of the floor truss components. For the core area, the DCRs for all floor beams inside the core were less than 1.08 and more than 99 percent had a DCR of less than 1.0.

DCR statistics for the truss-framed floor model are summarized in Table 6–4 for the original design loading case and in Table 6–5 for the ASCE 7-02 loading case. For the area outside the core, the average ratio of the DCRs estimated from the ASCE 7-02 loading to the DCRs from the original WTC Design Criteria loading for all floor trusses was about 0.80.

Table 6–4. Statistics of demand/capacity ratios for floor 96 under original design load case.

Member Type	Number of Members	Mean Calculated DCR	C.O.V. of DCR	Percentage of Components with DCR > 1.0	Percentage of Components with DCR > 1.05	Number of Components with DCR > 1.05	Maximum Calculated DCR
One-Way Long Span Zone							
Web members	1,792	0.44	0.61	3.7	1.28	23	1.14
Bottom chord members	1,038	0.74	0.26	0	0	0	0.99
One-Way Short Span Zone							
Web members	640	0.33	0.61	0	0	0	0.92
Bottom chord members	288	0.37	0.32	0	0	0	0.55
Two-Way Zone							
Web members	3,086	0.30	0.80	0.3	0.26	8	1.06
Bottom chord members	2,035	0.48	0.54	0	0	0	0.94
Bridging Trusses within One-Way Span Zones							
Web members	692	0.16	1.25	1	0	0	1.02
Bottom chord members	327	0.12	1.33	0	0	0	0.95
Core Beams							
Beams within core	1,361	0.33	0.67	0.9	0.3	4	1.07
Core perimeter channels	686	0.36	0.58	1.0	0.6	4	1.08

Table 6–5. Statistics of demand/capacity ratios (DCRs) for floor 96 under the ASCE 7-02 loading case.

Member Type	Number of Members	Mean Calculated DCR	C.O.V. of DCR	Percentage of Components with DCR > 1.0	Percentage of Components with DCR > 1.05	Maximum Calculated DCR
One-Way Long Span Zone						
Web members	1,792	0.35	0.60	0	0	0.86
Bottom chord members	1,038	0.59	0.25	0	0	0.80
One-Way Short Span Zone						
Web members	640	0.26	0.65	0	0	0.69
Bottom chord members	288	0.30	0.33	0	0	0.43
Two-Way Zone						
Web members	3,086	0.24	0.79	0	0	0.78
Bottom chord members	2,035	0.38	0.55	0	0	0.74
Bridging Trusses within One-Way Span Zones						
Web members	692	0.11	1.55	0	0	0.95
Bottom chord members	327	0.09	1.44	0	0	0.81
Core Beams						
Beams within core	1,361	0.28	0.64	0.1	0.1	1.05
Core perimeter channels	686	0.28	0.61	0	0	0.86

6.3 TYPICAL BEAM-FRAMED FLOOR

The analysis of the typical beam-framed floor was performed on the model of floor 75 of WTC 2 (see Sec. 3.4). This section describes the gravity loads applied to the model along with the results of the baseline performance analysis.

6.3.1 Gravity Loads

Comparing the live loads from the original WTC design criteria, NYCBC 2001, and the ASC E7-02 Standard for this floor, it was found that the three sets of loads were nearly identical. The only difference was that the live load for the corridor within the core was 100 psf in the original WTC design criteria, 75 psf in NYCBC 2001, and 80 psf in ASCE 7-02. As a result, only the original WTC design criteria loads were applied to the computer model.

In the areas outside of the core, the superimposed dead load was taken from the original design criteria as 141 psf, including 75 psf for equipment loads, and the live load was 75 psf.

Table 6–6 shows the CDL and SDL used inside the core area along with the live loads from the WTC Design Criteria, NYCBC 2001, and the ASCE 7-02 Standard. Loads are shown for the various occupancies within the core area.

Table 6–6. Beam-framed core area: loading floor 75, WTC 2.

Area	Loading (psf)				
	CDL	SDL	Live Load for Floor Design		
			WTC-DC	ASCE 7-02	NYCBC 2001
Return Air Plenum	Varies See Original Structural Drawings	66	75	75	75
Toilets		66	40	40	40
Stair, Service, Closet		25	100	100	100
Corridor		66	100	80	75
Motor Generator Room		141	75	75	75
Pump Platform		141	75	75	75
Electric Sub-Station		141	75	75	75
Mail Room		141	75	75	75
Secondary Motor Room		141	75	75	75
Unassigned Space		66	75	75	75

6.3.2 Results of Baseline Analysis

The maximum mid-span deflections of the long-span and short-span zones under the original WTC Design Criteria loads were approximately 1.55 in. and 0.70 in., respectively.

Using the SAP2000 computer program, DCRs were calculated for the components of the floor framing. The calculations were spot checked for accuracy and to verify that the correct design information was being applied. For most of the component calculations checked, the SAP2000 calculations were found to be acceptable.

DCRs were not calculated for the bridging members and anchor straps as they were not a part of the primary floor framing system. Also, DCRs were not calculated for the spandrels and columns as their DCRs were calculated in the global systems computer models.

Except for the two 30WF116 beams running in the east-west direction and cantilevering from the core columns 501 and 508 (see Fig. 6–3), the DCRs for all beam-framed floor components were less than 1.0 for the original WTC design criteria loading. For the two beams cited above, the DCRs from the axial load and moment interaction equation were less than 1.0, while the shear DCRs were 1.125 and 1.09. These shear DCRs occurred in the section of the 30WF116 beams located near the support between beam 30×10 ½ WF[3] and the centerline of the column.

[3] This beam designation was used in original contract drawings to indicate a 30 in. deep wide flange beam with cover plates and is used here for consistency.

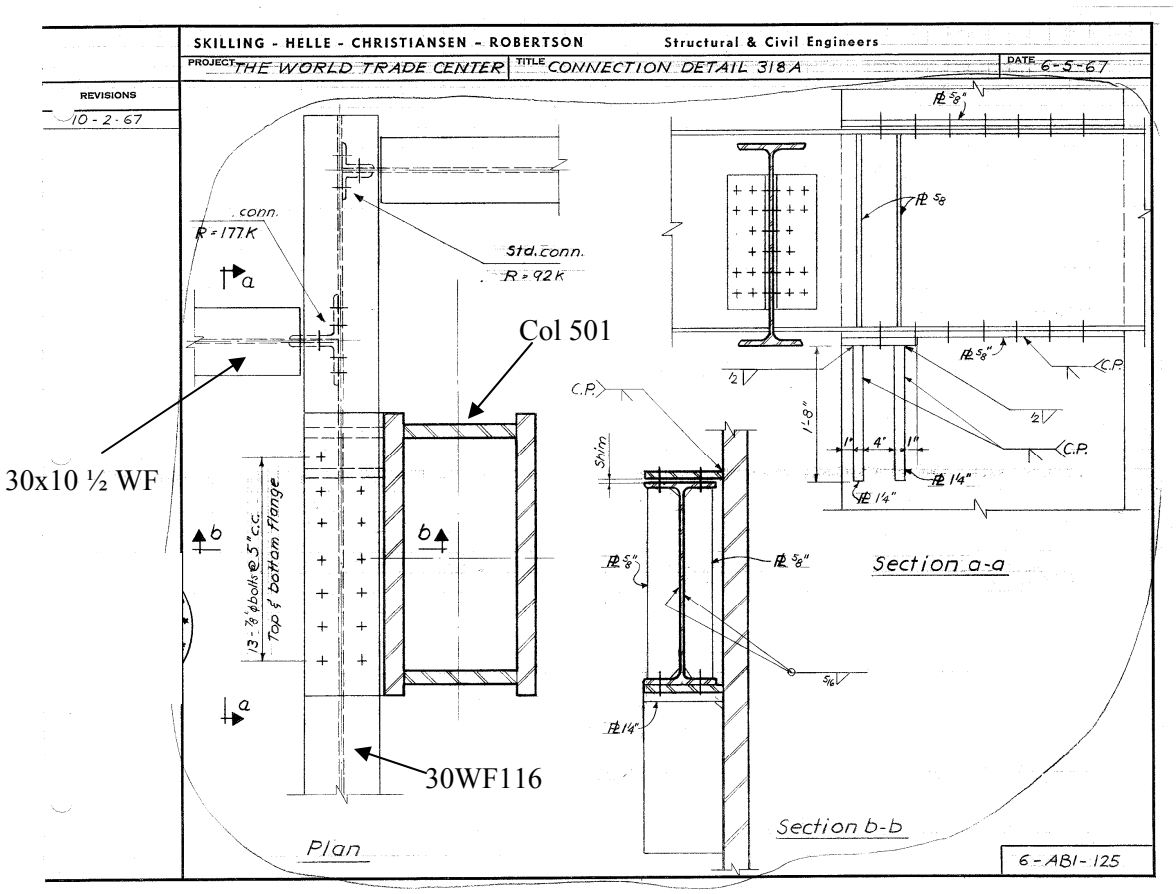

Source: Drawing reproduced with permission of The Port Authority of New York and New Jersey. Enhanced by NIST.

Figure 6–3. Connection detail for beam 30WF116, floor 75 of WTC 2.

Figure 6–4 shows the distribution of DCRs for the floor framing. The figure shows the location of the two beams with DCR greater than 1.0. DCR statistics for the beam-framed floor model are summarized in Table 6–7 for the original design loading case. The statistics are provided for member groups that are shown in Fig. 6–5.

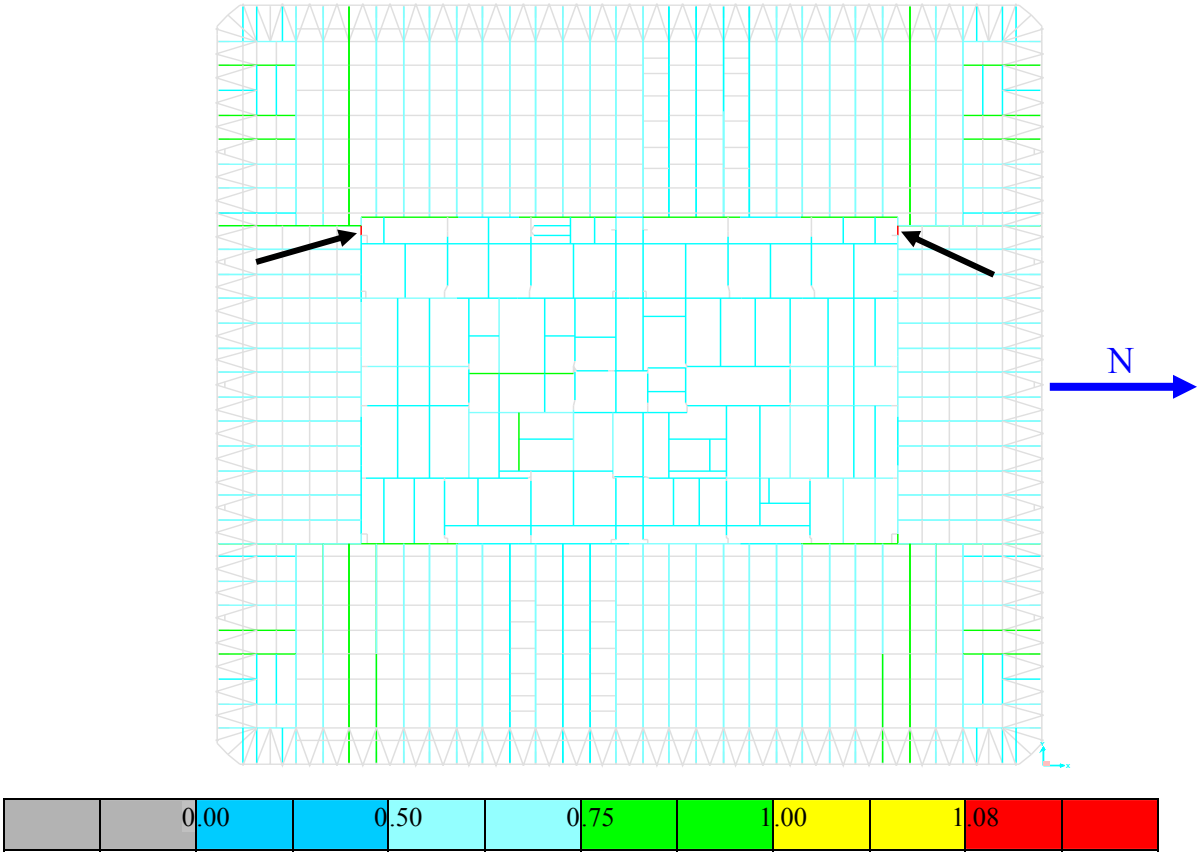

Figure 6–4. Demand/capacity ratios for floor 75, WTC 2: original WTC design criteria loading.

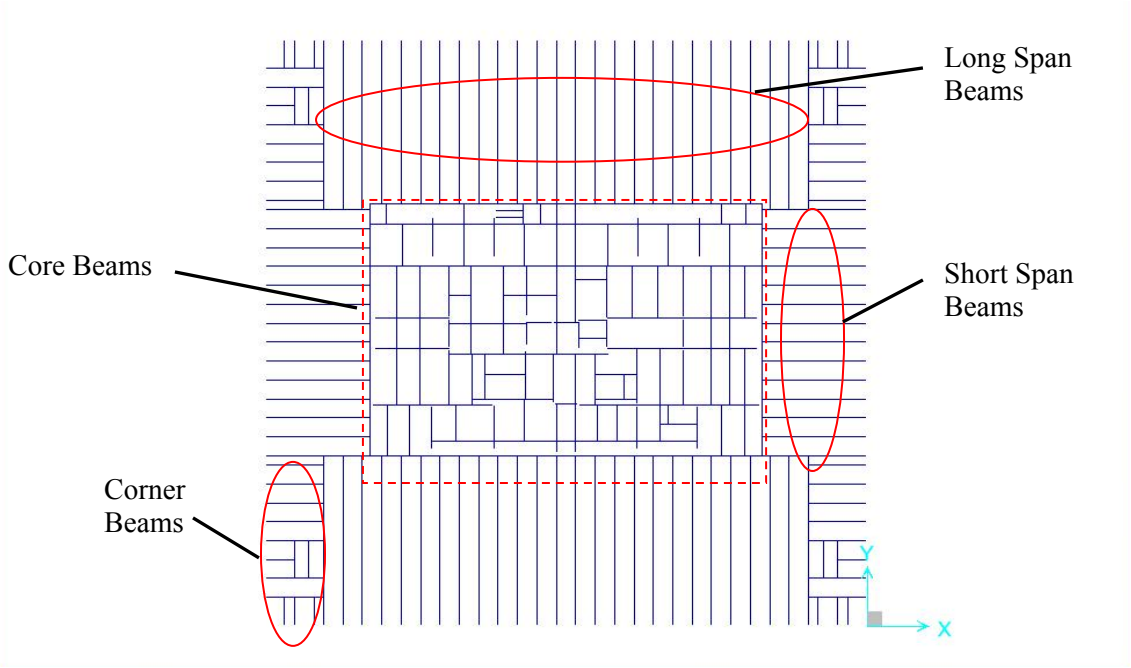

Figure 6–5. Beam-framed floor member groups.

Table 6–7. Statistics of demand/capacity ratios for floor 75 under the original design loading case.

Member Type	Number of Members	Mean Calculated DCR	C.O.V. of DCR	Maximum Calculated DCR
Long Span Beams	156	0.64	0.16	0.83
Short Span Beams	84	0.65	0.12	0.89
Core Beams	156	0.31	0.77	1.13
Corner Beams	32	0.49	0.35	0.90

Chapter 7
SUMMARY

This report presented the work conducted to establish the baseline performance of the North and South World Trade Center Towers (WTC 1 and WTC 2) under design gravity and wind loading conditions. Baseline performance results include basic information about the behavior of the towers, such as total and inter-story drift under wind loads, floor deflections under gravity loads, demand/capacity ratios for primary structural components, exterior columns response (shear lag effects and presence of tensile forces under a combination of dead and wind loads), performance of connections, and the towers' resistance to shear sliding and overturning.

The following tasks were undertaken to allow performing the baseline performance analyses of the towers:

- Development of structural databases of the primary components of the WTC 1 and WTC 2 towers. The electronic databases were developed from original computer printouts of the structural design documents, including modifications made after construction. The task included the scanning and digitization of the original drawing books, a four-step quality control procedure, cross-section property calculations, and development of the relational databases to link the generated database files into a format suitable for the development of the structural models.

- Development of reference structural analysis models that captured the intended behavior of each of the two towers using the generated databases. These reference models were used to establish the baseline performance of the towers and also served as a reference for more detailed models for aircraft impact damage analysis and thermal-structural response and collapse initiation analysis. The main types of models developed were:

  - Two global models of the major structural components and systems for the towers, one each for WTC 1 and WTC 2. The models included all primary structural components in the towers, including exterior walls (columns and spandrel beams), core columns, exterior wall bracing in the basement floors, core bracing at the main lobby atrium levels, hat trusses, and rigid and flexible diaphragms representing the floor systems. To validate the global models, the calculated natural frequencies of WTC 1 were compared with those measured on the tower, and good agreement between the calculated and measured values was obtained.

  - One model each of the typical truss-framed floor (floor 96 of WTC 1) and typical beam-framed floor (floor 75 of WTC 2) in the impact and fire zone of the towers. The models included all major structural components in the floor system, including primary and bridging trusses, beams, strap anchors and horizontal trusses, concrete slabs, and viscoelastic dampers. To validate the floor models, several studies were carried out to compare stresses and deflections estimated from the model with hand calculations for

representative composite sections. Good agreement was obtained between the model results and hand calculations.

Parametric studies were performed to evaluate the behavior of typical portions of the structure and to develop simplified models for implementation into the global models. These parametric studies included detailed and simplified models of typical exterior and corner wall panels and floor systems.

- Development of estimates of design gravity and wind loads on the towers for implementation into the reference structural models and use in the baseline performance analysis. Various wind load cases were considered in this study, including wind loads used in the original WTC design, wind loads based on two recent wind tunnel studies conducted in 2002 by Cermak Peterka Peterson, Inc. (CPP) and Rowan Williams Davies and Irwin, Inc. (RWDI) for insurance litigation concerning the towers, and wind load estimates developed by NIST from critical assessment of information obtained from the CPP and RWDI reports and state-of-the-art considerations. The following three loading cases were considered for the baseline performance analysis:

  – *Original WTC design loads case.* Loads included dead and live loads as in original WTC design, in conjunction with original WTC design wind loads.

  – *State-of-the-practice case.* Loads included dead loads; New York City Building Code (NYCBC) 2001 live loads; and wind loads from the RWDI wind tunnel study, scaled in accordance with NYCBC 2001 wind speed.

  – *Refined NIST estimate case.* Loads included dead loads; live loads from the American Society of Civil Engineers (ASCE 7-02) Standard; and wind loads developed by NIST.

  The purpose of using the original WTC design loads was to evaluate the performance of the towers under original design loading conditions and ascertain whether those loads and the corresponding design were adequate given the knowledge available at the time of the design. The purpose of considering the state-of-the-practice case and the refined NIST estimate case was to better understand and assess the effects of successive changes in standards, codes, and practices on wind design practices for tall buildings.

  The study indicated that the original WTC design wind load estimates exceeded those established by the NYCBC prior to 1968, when the WTC towers were designed, and up to and including 2001. The design values were also higher than those required by other prescriptive building codes of the time.

  The two orthogonal base shear and base moment components used in the original design were, in general, smaller than the CPP, RWDI, and NIST estimates. However, the most unfavorable combined peaks from the original design were larger, or smaller by at most 15 percent, than estimates based on the CPP, RWDI, and NIST estimates. This is due to the conservative procedure used to combine the loads in the original design.

  The estimated wind-induced loads on the towers varied by as much as 40 percent between the wind tunnel/climatological studies conducted by CPP and RWDI in 2002.

The WTC 1 and WTC 2 global models were each analyzed under the three loading cases described above to establish their baseline performance. The following is a summary of the results:

- Under the original WTC design loads, the cumulative drifts at the top of the WTC 1 tower were about 56.6 in. (H/304) and 55.7 in. (H/309) in the E–W and N–S direction, respectively. These drifts were about 51.2 in. (H/335) in the E–W direction and 65.3 in. (H/263) in the N–S direction for WTC 2. For the lower estimate, state-of-the-practice case, the drifts for WTC 1 were larger than those from the original design case by about 0.5 percent and 22 percent for the E–W and N–S directions, respectively. For the lower estimate, state-of-the-practice case for WTC 2, the E–W drift was larger than that from the original design case by about 16 percent, and the N–S drift was smaller by about 15 percent. The drifts obtained from the refined NIST estimate case were about 25 percent larger than those from the state-of-the practice case. These differences are consistent with the differences among the base shears for the three loading cases.

- The demand/capacity ratios (DCRs) were based on the allowable stress design procedure and were estimated using the American Institute of Steel Construction (AISC) Specifications (1989). The results indicated that DCRs estimated from the original WTC design load case were, in general, close to those obtained for the lower estimate, state-of-the practice case. For both cases, a small fraction of structural components had DCRs larger than 1.0. These were mainly observed in both towers at (1) the exterior walls: at the columns around the corners, where the hat truss connected to the exterior walls, and below floor 9; and (2) the core columns on the 600 line between floors 80 and 106 and at core perimeter columns 901 and 908 for much of their height.

- The refined National Institute of Standards and Technology (NIST) case estimated DCRs were higher than those of the original WTC design estimates and the lower state-of-the-practice estimates for the following reasons: The NIST estimated wind loads were about 25 percent higher than those used in the lower state-of-the-practice estimate, and mixed, some higher and others lower than the original WTC design wind loads. It is noted that the NIST estimated wind loads are about 20 percent smaller than those estimated by CPP (an upper estimate, state-of-the practice case). In addition, the original WTC design and the state-of-the-practice cases used NYCBC load combinations, which result in lower DCRs than the ASCE 7-02 load combinations used for the refined NIST case.

- Under a combination of the original WTC design dead and wind loads, tension forces were developed in the exterior walls of WTC 1 and WTC 2. The forces were largest at the base of the building and at the corners. These tensile column loads were transferred from one panel to another through the column splices. The DCR ratios for the exterior wall splice connections under the effect of the tensile forces for the two towers were shown to be less than 1.0.

- For the towers' resistance to shear sliding and overturning due to wind, the dead loads that acted on the perimeter walls of the tower provided resistance to shear sliding and overturning at the foundation level. Considering the resistance to shear sliding under wind load, the factor of safety was calculated to be between 10 and 11.5, while the factor of safety against overturning ranged from 1.9 to 2.7 for both towers.

Two typical floor models were each analyzed under gravity loads. The following is a summary of the results:

- For the typical truss-framed floor (floor 96 of WTC 1), the DCRs for all floor trusses were less than 1.14 for the original WTC Design Criteria loads and less than 0.86 for the ASCE 7-02 loading. Under the original WTC Design Criteria loading, the DCR was less than 1.00 for 99.4 percent of the floor truss components. For the area outside the core, the average ratio of the DCRs under the ASCE 7-02 loading to the DCRs under the original WTC Design Criteria loading for all floor trusses was about 0.80. For the core area, the DCRs for all floor beams inside the core were less than 1.08, and more than 99 percent had a DCR of less than 1.0. Under the original WTC Design Criteria loading, the maximum floor deflections were 1.79 in., 0.57 in., and 1.44 in. for the long-span one-way trusses, short-span one-way trusses, and the two-way zone, respectively.

- For the typical beam-framed floor (floor 75 of WTC 2) under the original WTC Design Criteria loading, the DCRs for all floor beams were less than 1.0 except for two core beams where the shear DCRs were 1.125 and 1.09. The maximum mid-span deflections of the long-span and short-span zones under the original WTC Design Criteria loads were about 1.55 in. and 0.70 in., respectively.

Appendix A
WTC TOWER STRUCTURAL DRAWINGS INDEX FOR LARGE-SIZE SHEETS

WTC TOWER A STRUCTURAL STEEL DRAWING INDEX - (18-MAY-73)

Drawing No.	Drawing Title	Latest Revision Date
LA-1	Foundation loading plan	27-Apr-67
SA-1	Foundation plan	29-Aug-68
SA-2	Plan sub-level 5 EL.242	09-Apr-69
SA-3	Framing plan sub-level 4	09-Apr-69
SA-4	Framing plan sub-level 3 EL.264	07-Oct-68
SA-5	Framing plan sub-level 2 EL.274	17-Jul-68
SA-6	Framing plan sub-level 1 EL.284	07-Oct-68
SA-7	Framing plan service level EL.294	17-Jul-68
SA-8	Framing plan floor 1	17-Jul-68
SA-9	Framing plan intermediate level	17-Jul-68
SA-10	Framing plan floor 2	17-Jul-68
SA-11	Framing plan floor 3	17-Jul-68
SA-12	Framing plan floor 4	17-Jul-68
SA-13	Framing plan floor 5	17-Jul-68
SA-14	Framing plan floor 6	17-Jul-68
SA-15	Framing plan floor 7	17-Jul-68
SA-16	Framing plan floor 8	17-Jul-68
SA-17	Framing plan floor 9	17-Jul-68
SA-18	Framing plan floors 10-11	09-Oct-68
SA-19	Not used	
SA-20	Framing plan floors 12-16	09-Oct-68
SA-21	Not used	
SA-22	Not used	
SA-23	Not used	
SA-24	Not used	
SA-25	Framing plan floor 17	09-Oct-68
SA-26	Framing plan floor 18	09-Oct-68
SA-27	Framing plan floor 19	09-Oct-68
SA-28	Framing plan floor 20	09-Oct-68
SA-29	Framing plan floors 21-23	09-Oct-68
SA-30	Not used	

Drawing No.	Drawing Title		Latest Revision Date
SA-31	Not used		
SA-32	Framing plan floor	24	09-Oct-68
SA-33	Framing plan floor	25	09-Oct-68
SA-34	Framing plan floor	26	09-Oct-68
SA-35	Framing plan floor	27	09-Oct-68
SA-36	Framing plan floors	28-31	09-Oct-68
SA-37	Not used		
SA-38	Not used		
SA-39	Not used		
SA-40	Framing plan floor	32	09-Oct-68
SA-41	Framing plan floor	33	09-Oct-68
SA-42	Framing plan floor	34	09-Oct-68
SA-43	Framing plan floor	35	09-Oct-68
SA-44	Framing plan floors	36-38	09-Oct-68
SA-45	Not used		
SA-46	Not used		
SA-47	Framing plan floor	39	09-Oct-68
SA-48	Framing plan floor	40	09-Oct-68
SA-49	Framing plan floor	41	10-Jan-69
SA-50	Framing plan floor	42	10-Jan-69
SA-51	Framing plan floor	43	10-Jan-69
SA-52	Framing plan floor	44	01-Sep-70
SA-53	Framing plan floor	45	01-Sep-70
SA-54	Framing plan floor	46	10-Jan-69
SA-55	Framing plan floor	47	10-Jan-69
SA-56	Framing plan floor	48	22-Nov-68
SA-57	Framing plan floor	49	22-Nov-68
SA-58	Framing plan floor	50	22-Nov-68
SA-59	Framing plan floors	51-54	22-Nov-68
SA-60	Not used		
SA-61	Not used		
SA-62	Not used		
SA-63	Framing plan floor	55	22-Nov-68
SA-64	Framing plan floor	56	22-Nov-68
SA-65	Framing plan floor	57	22-Nov-68
SA-66	Framing plan floor	58	22-Nov-68
SA-67	Framing plan floor	59	22-Nov-68
SA-68	Framing plan floor	60	22-Nov-68
SA-69	Framing plan floor	61	22-Nov-68

Drawing No.	Drawing Title		Latest Revision Date
SA-70	Framing plan floor	62	22-Nov-68
SA-71	Framing plan floor	63	22-Nov-68
SA-72	Framing plan floor	64	22-Nov-68
SA-73	Framing plan floor	65	22-Nov-68
SA-74	Framing plan floor	66	12-Dec-69
SA-75	Framing plan floor	67	12-Dec-69
SA-76	Framing plan floor	68	12-Dec-69
SA-77	Framing plan floor	69	22-Nov-68
SA-78	Framing plan floor	70	22-Nov-68
SA-79	Framing plan floor	71	22-Nov-68
SA-80	Framing plan floor	72	22-Nov-68
SA-81	Framing plan floor	73	22-Nov-68
SA-82	Framing plan floor	74	22-Nov-68
SA-83	Framing plan floor	75	25-Sep-68
SA-84	Framing plan floor	76	25-Sep-68
SA-85	Framing plan floor	77	25-Sep-68
SA-86	Framing plan floor	78	18-Aug-69
SA-87	Framing plan floor	79	01-Aug-69
SA-88	Framing plan floor	80	01-Aug-69
SA-89	Framing plan floor	81	27-Nov-68
SA-90	Framing plan floor	82	01-Aug-69
SA-91	Framing plan floor	83	01-Aug-69
SA-92	Framing plan floor	84 -86	01-Aug-69
SA-93	Not used		
SA-94	Not used		
SA-95	Framing plan floor	87	01-Aug-69
SA-96	Framing plan floor	88	01-Aug-69
SA-97	Framing plan floor	89	01-Aug-69
SA-98	Framing plan floor	90,91	01-Aug-69
SA-99	Not used		
SA-100	Framing plan floor	92	01-Aug-69
SA-101	Framing plan floor	93	01-Aug-69
SA-102	Framing plan floor	94	01-Aug-69
SA-103	Framing plan floor	95	01-Aug-69
SA-104	Framing plan floor	96	01-Aug-69
SA-105	Framing plan floor	97-100	01-Aug-69
SA-106	Not used		
SA-107	Not used		
SA-106	Not used		

Drawing No.	Drawing Title	Latest Revision Date
SA-107	Not used	
SA-108	Not used	
SA-109	Framing plan floor 101	01-Aug-69
SA-110	Framing plan floor 102	01-Aug-69
SA-111	Framing plan floor 103	01-Aug-69
SA-112	Framing plan floor 104	01-Aug-69
SA-113	Framing plan floor 105	07-Jan-71
SA-114	Framing plan floor 106	16-Jun-72
SA-115	Framing plan floor 107	16-Jun-72
SA-116	Framing plan floor 107 upper	Void
SA-117	Framing plan floor 108	20-Oct-70
SA-118	Framing plan floor 109	20-Oct-70
SA-119	Framing plan floor 110	02-Jul-71
SA-120	Framing plan p.h. roof	07-May-71
SA-121	Not used	
SA-122	Floor panel fireproofing plan	Hold
SA-123	Not used	
SA-124	Floor panel schedule	06-Jan-69
SA-125	Ext. wall to 9th - elevation wall 100	07-Apr-67
SA-126	Ext. wall to 9th - elevation wall 200	08-May-67
SA-127	Ext. wall to 9th - elevation wall 300	07-Apr-67
SA-128	Ext. wall to 9th - elevation wall 400	08-May-67
SA-129	129 thru 139 not used	
SA-140	Ext. wall above 9th - elevation wall 100	08-Sep-69
SA-141	Ext. wall above 9th - elevation wall 200	08-Sep-69
SA-142	Ext. wall above 9th - elevation wall 300	08-Sep-69
SA-143	Ext. wall above 9th - elevation wall 300	08-Sep-69
SA-144	144 thru 150 not used	
SA-151	Grillage details	29-Aug-68
SA-152	Grillage details	15-Nov-67
SA-153	Not used	
SA-154	Not used	
SA-155	Not used	

For SA-156 and above see Tower A & B Index

SA-401	T/V mast support el. lines 500, 600 & 700	12-Oct-70
SA-402	T/V mast support el. lines 800, 900 & 1000	12-Oct-70
SA-403	T/V mast support el. lines 001, 002, 003 &004	10-Jul-70
SA-404	T/V mast support el. lines 005, 006, 007 &008	10-Jul-70

WTC Tower A Structural Concrete Drawing Index - (18-May-73)

SCA-1	Concrete plan sub level 5 el.242	18-Dec-68
SCA-2	Concrete plan sub level 4 el.253	10-Dec-68
SCA-3	Concrete plan sub level 3 el.264 - core	17-Jan-69
SCA-4	Concrete plan sub level 3 el.264 - floor	23-Jan-69
SCA-5	Concrete plan sub level 2 el.274 - core	22-Jan-69
SCA-6	Concrete plan sub level 2 el.274 - floor	22-Jan-69
SCA-7	Concrete plan sub level 1 el.284 - core	28-Jan-69
SCA-8	Concrete plan sub level 1 el.284 - floor	28-Jan-69
SCA-9	Concrete plan service level el.294 - core	03-Feb-69
SCA-10	Concrete plan service level el.294 - floor	03-Feb-69
SCA-11	Concrete plan floor 1 el.310 - core	10-Dec-68
SCA-12	Concrete plan floor 1 el.310 - floor	19-Mar-69
SCA-13	Concrete plan intermediate level	02-Dec-69
SCA-14	Concrete plan floor 2 - core	17-Jan-69
SCA-15	Concrete plan floor 2 - floor	04-Oct-71
SCA-16	Concrete plan floor 3-6 - floor	02-Dec-69
SCA-17	Concrete plan floor 7 - core	02-Dec-69
SCA-18	Concrete plan floor 7 - floor	26-May-69
SCA-19	Concrete plan floor 8 - core	16-Mar-70
SCA-20	Concrete plan floor 9 - core	16-Mar-70
SCA-21	Concrete plan floor 9 - floor	11-Feb-69
SCA-22	Not used	
SCA-23	Concrete plan floors 10-40 - floor	19-Mar-70
SCA-24	Concrete plan floors 10-16 - core	19-Mar-70
SCA-25	Not used	
SCA-26	Not used	
SCA-27	Not used	
SCA-28	Not used	
SCA-29	Not used	
SCA-30	Concrete plan floor 17 - core	15-Apr-70
SCA-31	Concrete plan floor 18 - core	15-Apr-70
SCA-32	Concrete plan floor 19 - core	15-Apr-70
SCA-33	Concrete plan floor 20 - core	15-Apr-70
SCA-34	Concrete plan floors 21-23 - core	15-Apr-70
SCA-35	Not used	
SCA-36	Not used	
SCA-37	Concrete plan floor 24 - core	12-Mar-69
SCA-38	Concrete plan floor 25 - core	15-Apr-70
SCA-39	Concrete plan floor 26 - core	15-Apr-70

SCA-40	Concrete plan floor 27 - core	15-Apr-70
SCA-41	Concrete plan floors 28-31 - core	15-Apr-70
SCA-42	Not used	
SCA-43	Not used	
SCA-44	Not used	
SCA-45	Concrete plan floor 32 - core	12-Mar-69
SCA-46	Concrete plan floor 33 - core	15-Apr-70
SCA-47	Concrete plan floor 34 - core	15-Apr-70
SCA-48	Concrete plan floor 35 - core	15-Apr-70
SCA-49	Concrete plan floors 36-40 - core	15-Apr-70
SCA-50	Not used	
SCA-51	Not used	
SCA-52	Not used	
SCA-53	Not used	
SCA-54	Concrete plan floor 41 - core	10-Aug-70
SCA-55	Concrete plan floor 41 - floor	10-Aug-70
SCA-56	Concrete plan floor 42 - core	10-Aug-70
SCA-57	Concrete plan floor 43 - core	24-Oct-69
SCA-58	Concrete plan floor 43 - floor	20-Feb-70
SCA-59	Concrete plan floor 44 - core	24-Oct-69
SCA-60	Concrete plan floor 44 - floor	20-Feb-70
SCA-61	Concrete plan floor 45 - core	10-Aug-70
SCA-62	Concrete plan floor 45 - floor	10-Aug-70
SCA-63	Concrete plan floor 46 - core	10-Aug-70
SCA-64	Concrete plan floors 46,47,48 - floor	10-Aug-70
SCA-65	Concrete plan floor 47 - core	18-Sep-70
SCA-66	Concrete plan floor 48 - core	10-Aug-70
SCA-67	Not used	
SCA-68	Concrete plan floors 49-74 - floor	10-Aug-70
SCA-68	Alt concrete plan floors 49-74 -floor	04-May-70
SCA-69	Concrete plan floors 57,58 -core	10-Aug-70
SCA-70	Not used	
SCA-71	Not used	
SCA-72	Not used	
SCA-73	Not used	
SCA-74	Concrete plan floor 54 - core	03-Nov-69
SCA-75	Concrete plan floor 55 - core	10-Aug-70
SCA-76	Concrete plan floor 56 - core	10-Aug-70
SCA-77	Concrete plan floors 57,58 -core	10-Aug-70
SCA-78	Not used	
SCA-79	Concrete plan floor 59 - core	03-Nov-69

SCA-80	Concrete plan floor 60 - core	10-Aug-70
SCA-81	Concrete plan floor 61 - core	03-Nov-69
SCA-82	Concrete plan floor 62 - core	10-Aug-70
SCA-83	Concrete plan floor 63 - core	10-Aug-70
SCA-84	Concrete plan floor 64 - core	10-Aug-70
SCA-85	Concrete plan floor 65 - core	10-Aug-70
SCA-86	Concrete plan floor 66 - core	01-May-70
SCA-87	Concrete plan floor 67 - core	15-May-70
SCA-88	Concrete plan floor 68 - core	15-May-70
SCA-89	Concrete plan floor 69 - core	24-Aug-70
SCA-90	Concrete plan floors 70-73 - core	24-Aug-70
SCA-91	Not used	
SCA-92	Not used	
SCA-93	Not used	
SCA-94	Concrete plan floor 74 - core	24-Aug-70
SCA-95	Concrete plan floor 75 - core	01-May-70
SCA-96	Concrete plan floor 75 - floor	25-Aug-70
SCA-97	Concrete plan floor 76 - core	25-Aug-70
SCA-98	Concrete plan floor 77 - core	25-Aug-70
SCA-99	Concrete plan floor 77 - floor	25-Aug-70
SCA-100	Concrete plan floor 78 - core	25-Aug-70
SCA-101	Concrete plan floor 78 - floor	25-Aug-70
SCA-102	Concrete plan floor 79 - core	25-Aug-70
SCA-103	Concrete plan floor 79 - floor	13-Jul-70
SCA-104	Concrete plan floor 80 - core	25-Aug-70
SCA-105	Concrete plan floors 80,81,82 - floor	13-Jul-70
SCA-106	Concrete plan floor 81 - core	25-Aug-70
SCA-107	Concrete plan floor 82 - core	25-Aug-70
SCA-108	Concrete plan floor 106A - floor	16-Jun-72
SCA-109	Concrete plan floors 83-103A- 83-104B-floor	01-Sep-70
SCA-109	Alt Concrete plan floors 83-103A- 83-104B-floor	04-May-70
SCA-110	Concrete plan floors 104-105A-105-106A-floor	01-Sep-70
SCA-111	Concrete plan floor 83-core	25-Aug-70
SCA-112	Concrete plan floors 84-86 - core	25-Aug-70
SCA-113	Not used	
SCA-114	Concrete plan floor 87 - core	25-Aug-70
SCA-115	Concrete plan floor 88 - core	25-Aug-70
SCA-116	Concrete plan floors 89,90,91 - core	25-Aug-70
SCA-117	Not used	
SCA-118	Not used	
SCA-119	Concrete plan floor 92 - core	25-Aug-70

SCA-120	Concrete plan floor 93 - core	11-Aug-70
SCA-121	Concrete plan floor 94 - core	15-Mar-71
SCA-122	Concrete plan floor 95 - core	15-Mar-71
SCA-123	Concrete plan floors 96-99A-96-1008-core	15-Mar-71
SCA-124	Not used	
SCA-125	Not used	
SCA-126	Not used	
SCA-127	Concrete plan floor 100 - core	01-May-70
SCA-128	Concrete plan floor 101 - core	15-Mar-71
SCA-129	Concrete plan floor 102 - core	15-Mar-71
SCA-130	Concrete plan floor 103 - core	01-Dec-70
SCA-131	Concrete plan floor 104 - core	01-Mar-71
SCA-132	Concrete plan floors 105 - core	15-May-72
SCA-133	Concrete plan floors 106 - core	07-Jul-72
SCA-134	Concrete plan floor 107 - floor	16-Jun-72
SCA-135	Concrete plan floor 107 - core	16-Jun-72
SCA-136	Concrete plan floor 108 - core	15-May-72
SCA-137	Concrete plan floor 108 - floor	01-Mar-71
SCA-138	Concrete plan floor 109 - core	30-Jul-71
SCA-139	Concrete plan floor 110 - core	15-May-72
SCA-140	Concrete plan floor 110 - floor	28-Jul-71
SCA-141	Concrete plan penthouse roof - core	02-Sep-71
SCA-142	Concrete plans secondary levels	01-Dec-70
SCA-143	Concrete plan sub stations, escalator pits	01-Dec-70
SCA-145	Concrete plan el.264, post tension	Void
SCA-146	Concrete plan penthouse roof lower level	12-Jul-71
SCA-147	Concrete plan penthouse roof upper level	01-Oct-71
SCA-148	Concrete plan raised floor 107 - core	07-Jul-72
SCA-149	Concrete plan raised floor 107 -floor	16-Jun-72
SCA-150	Concrete plan raised floor 106 - floor	16-Jun-72

WTC TOWER B STRUCTURAL STEEL DRAWING INDEX - (18-MAY-73)

SB-L1	Tower B foundation loading plan	21-Mar-68
SB-1	Foundation plan	06-Sep-68
SB-2	Plan sub-level 5 el.242	25-Sep-68
SB-3	Framing plan sub-level 4 el.253	25-Sep-68
SB-4	Framing plan sub-level 3 el.264	07-Oct-68
SB-5	Framing plan sub-level 2 el.274	17-Jul-68
SB-6	Framing plan sub-level 1 el.284	07-Oct-68
SB-7	Framing plan service level el.294	28-May-69
SB-8	Framing plan floor 1	17-Jul-68
SB-9	Framing plan intermediate level	17-Jul-68
SB-10	Framing plan floor 2	17-Jul-68
SB-11	Framing plan floor 3	17-Jul-68
SB-12	Framing plan floor 4	17-Jul-68
SB-13	Framing plan floor 5	17-Jul-68
SB-14	Framing plan floor 6	17-Jul-68
SB-15	Framing plan floor 7	13-Mar-69
SB-16	Framing plan floor 8	17-Jul-68
SB-17	Framing plan floor 9	17-Aug-68
SB-18	Framing plan floor 10	19-Mar-69
SB-19	Framing plan floor 11	19-Mar-69
SB-20	Framing plan floor 12	19-Mar-69
SB-21	Framing plan floor 13	19-Mar-69
*SB-22	Framing plan floors 14-16	09-Oct-68
SB-23	Not used	
SB-24	Not used	
*SB-25	Framing plan floor 17	09-Oct-68
*SB-26	Framing plan floor 18	09-Oct-68
*SB-27	Framing plan floor 19	09-Oct-68
*SB-28	Framing plan floor 20	09-Oct-68
*SB-29	Framing plan floors 21-23	09-Oct-68
SB-30	Not used	
SB-31	Not used	
SB-32	Framing plan floor 24	09-Oct-68
*SB-33	Framing plan floor 25	09-Oct-68
*SB-34	Framing plan floor 26	09-Oct-68
*SB-35	Framing plan floor 27	09-Oct-68
*SB-36	Framing plan floors 28-31	09-Oct-68
SB-37	Not used	
SB-38	Not used	

SB-39	Not used		
SB-40	Framing plan floor	32	09-Oct-68
*SB-41	Framing plan floor	33	09-Oct-68
*SB-42	Framing plan floor	34	09-Oct-68
*SB-43	Framing plan floor	35	09-Oct-68
*SB-44	Framing plan floors	36-38	09-Oct-68
SB-45	Not used		
SB-46	Not used		
*SB-47	Framing plan floor	39	09-Oct-68
*SB-48	Framing plan floor	40	09-Oct-68
*SB-49	Framing plan floor	41	10-Jan-69
*SB-50	Framing plan floor	42	10-Jan-69
*SB-51	Framing plan floor	43	10-Jan-69
SB-52	Framing plan floor	44	01-Sep-70
*SB-53	Framing plan floor	45	22-Nov-68
*SB-54	Framing plan floor	46	22-Nov-68
*SB-55	Framing plan floor	47	22-Nov-68
*SB-56	Framing plan floor	48	22-Nov-68
*SB-57	Framing plan floor	49	22-Nov-68
*SB-58	Framing plan floor	50	22-Nov-68
*SB-59	Framing plan floors	51-54	22-Nov-68
SB-60	Not used		
SB-61	Not used		
SB-62	Not used		
*SB-63	Framing plan floor	55	22-Nov-68
*SB-64	Framing plan floor	56	22-Nov-68
*SB-65	Framing plan floor	57	22-Nov-68
*SB-66	Framing plan floor	58	22-Nov-68
*SB-67	Framing plan floor	59	22-Nov-68
*SB-68	Framing plan floor	60	22-Nov-68
*SB-69	Framing plan floor	61	22-Nov-68
*SB-70	Framing plan floor	62	22-Nov-68
*SB-71	Framing plan floor	63	22-Nov-68
*SB-72	Framing plan floor	64	22-Nov-68
*SB-73	Framing plan floors	65,66	22-Nov-68
SB-74	Not used		
SB-75	Framing plan floor	67	22-Nov-68
SB-76	Framing plan floor	68	22-Nov-68
SB-77	Framing plan floor	69	22-Nov-68
*SB-78	Framing plan floor	70	22-Nov-68
*SB-79	Framing plan floor	71	22-Nov-68

*SB-80	Framing plan floor	72	22-Nov-68
*SB-81	Framing plan floor	73	22-Nov-68
*SB-82	Framing plan floor	74	22-Nov-68
*SB-83	Framing plan floor	75	27-Nov-68
*SB-84	Framing plan floor	76	01-Aug-69
*SB-85	Framing plan floor	77	27-Nov-68
*SB-86	Framing plan floor	78	18-Mar-69
*SB-87	Framing plan floor	79	01-Aug-69
*SB-88	Framing plan floor	80	01-Aug-69
*SB-89	Framing plan floor	81	27-Nov-68
*SB-90	Framing plan floor	82	27-Nov-68
*SB-91	Framing plan floor	83	01-Aug-69
*SB-92	Framing plan floor	84-86	27-Nov-68
SB-93	Not used		
SB-94	Not used		
*SB-95	Framing plan floor	87	01-Aug-69
*SB-96	Framing plan floor	88	01-Aug-69
*SB-97	Framing plan floor	89	01-Aug-69
*SB-98	Framing plan floor	90,91,93	01-Sep-70
SB-99	Not used		
*SB-100	Framing plan floor	92	27-Nov-68
SB-101	Not used		
*SB-102	Framing plan floor	94	01-Aug-69
*SB-103	Framing plan floor	95	01-Aug-69
*SB-104	Framing plan floor	96	01-Aug-69
*SB-105	Framing plan floors	97-100	01-Aug-69
SB-106	Not used		
SB-107	Not used		
SB-108	Not used		
*SB-109	Framing plan floor	101	01-Aug-69
*SB-110	Framing plan floor	102	01-Aug-69
*SB-111	Framing plan floor	103	01-Aug-69
*SB-112	Framing plan floor	104	01-Aug-69
*SB-113	Framing plan floor	105	10-Dec-69
*SB-114	Framing plan floor	106	10-Dec-69
*SB-115	Framing plan floor	107	05-Mar-71
*SB-116	Framing plan floor	107 upper	void
*SB-117	Framing plan floor	108	05-Mar-71
*SB-118	Framing plan floor	109	05-Mar-71
*SB-119	Framing plan floor	110	02-Jul-71
SB-120	Framing plan p.h. roof upper level		27-Sep-71

SB-121	Framing plan p.h. roof lower level	27-Sep-71
SB-122	Not used	
SB-123	Framing plan truck ramp	void
SB-124	Floor panel schedule	28-Mar-69
SB-125	Ext. wall to 9th -elevation wall 100	15-Feb-68
SB-126	Ext. wall to 9th -elevation wall 200	15-Feb-68
SB-127	Ext. wall to 9th -elevation wall 300	15-Feb-68
SB-128	Ext. wall to 9th -elevation wall 400	15-Feb-68
SB-129	129 thru 139 not used	
SB-140	Ext. wall above 9th -elevation wall 100	08-Sep-69
SB-141	Ext. wall above 9th -elevation wall 200	08-Sep-69
SB-142	Ext. wall above 9th -elevation wall 300	08-Sep-69
SB-143	Ext. wall above 9th -elevation wall 400	08-Sep-69
SAB-144	144 thru 150 not used	
SB-151	Grillage details	08-Sep-69
SB-151.1	Anchor Bolt Details	08-Sep-69
SB-151.2	Anchor Bolt Details	08-Sep-69
SB-151.3	Anchor Bolt Details	08-Sep-69
SB-152	Grillage details	09-Feb-68
SB-153	Grillage details	15-Nov-67
SB-154	Grillage details	13-Dec-67
SB-155	Not used	
SB-401	TV mast support elev. Lines 500,600,700	05-Mar-71
SB-402	TV mast support elev. Lines 800,900,1000	05-Mar-71
SB-403	TV mast support elev. Lines 001,002,003,004	05-Mar-71
SB-404	TV mast support elev. Lines 005,006,007,008	14-Dec-70

** formerly included with tower A*

WTC TOWER B STRUCTURAL CONCRETE DRAWING INDEX - (18-MAY-73)

SCB-1	Concrete plan sub level 5 el.242	02-Jan-70
SCB-2	Concrete plan sub level 4 el.253	11-Apr-69
SCB-3	Concrete plan sub level 3 el.264 - core	05-Aug-69
SCB-4	Concrete plan sub level 3 el.264 - floor	05-Aug-69
SCB-5	Concrete plan sub level 2 el.274 - core	05-Aug-69
SCB-6	Concrete plan sub level 2 el.274 - floor	05-Aug-69
SCB-7	Concrete plan sub level 1 el.284 - core	05-Aug-69
SCB-8	Concrete plan sub level 1 el.284 - floor	05-Aug-69
SCB-9	Concrete plan service level el.294 - core	10-Jul-69
SCB-10	Concrete plan service level el.294 - floor	10-Jul-69
SCB-11	Concrete plan floor 1 el.310 - core	11-Jul-69
SCB-12	Concrete plan floor 1 el.310 - floor	11-Jul-69
SCB-13	Concrete plan intermediate level	see SCA-13
*SCB-14	Concrete plan floor 2 - core	06-Dec-69
SCB-15	Concrete plan floor 2 - floor	see SCA-15
SCB-16	Concrete plan floors 3-6 - core	see SCA-16
SCB-17	Concrete plan floor 7 - core	see SCA-17
SCB-18	Concrete plan floor 7 - floor	02-Dec-69
SCB-19	Concrete plan floor 8 - core	see SCA-19
SCB-20	Concrete plan floor 9 - core	see SCA-20
SCB-21	Concrete plan floor 9 - floor	16-Mar-70
SCB-22	Concrete plan floor 10 - floor	19-Mar-70
*SCB-23	Concrete plan floor 10 - core	19-Mar-70
*SCB-24	Concrete plan floor 11 - core	19-Mar-70
SCB-25	Concrete plan floor 11 - floor	19-Mar-70
SCB-26	Concrete plan floor 12 - floor	19-Mar-70
SCB-27	Concrete plan floor 12 - core	19-Mar-70
SCB-28	Concrete plan floor 13 - floor	19-Mar-70
SCB-29	Not used	
SCB-30	Concrete plan floor 17 - core	see SCA-30
SCB-31	Concrete plan floor 18 - core	see SCA-31
SCB-32	Concrete plan floor 19 - core	see SCA-32
SCB-33	Concrete plan floor 20 - core	see SCA-33
SCB-34	Concrete plan floor 21-23 - core	see SCA-34
SCB-35	Not used	
SCB-36	Not used	
SCB-37	Concrete plan floor 24 - core	15-Apr-70
SCB-38	Concrete plan floor 25 - core	see SCA-38
SCB-39	Concrete plan floor 26 - core	see SCA-39

SCB-40	Concrete plan floor 27 - core	see SCA-40
SCB-41	Concrete plan floor 28-31 - core	see SCA-41
SCB-42	Not used	
SCB-43	Not used	
SCB-44	Not used	
SCB-45	Concrete plan floor 32 - core	15-Apr-70
SCB-46	Concrete plan floor 33 - core	see SCA-46
SCB-47	Concrete plan floor 34 - core	see SCA-47
SCB-48	Concrete plan floor 35 - core	see SCA-48
SCB-49	Concrete plan floor 36-40 - core	see SCA-49
SCB-50	Not used	
SCB-51	Not used	
SCB-52	Not used	
SCB-53	Not used	
SCB-54	Concrete plan floor 41 - core	see SCA-54
SCB-55	Concrete plan floor 41 - floor	see SCA-55
SCB-56	Concrete plan floor 42 - core	see SCA-56
SCB-57	Concrete plan floor 43 - core	10-Aug-70
SCB-58	Concrete plan floor 43 - floor	10-Aug-70
SCB-59	Concrete plan floor 44 - core	24-Sep-70
SCB-60	Concrete plan floor 44 - floor	24-Sep-70
SCB-61	Concrete plan floor 45 - core	see SCA-61
SCB-62	Concrete plan floor 45 - floor	see SCA-62
SCB-63	Concrete plan floor 46 - core	see SCA-63
SCB-64	Concrete plan floors 46-48 - floor	see SCA-64
SCB-65	Concrete plan floor 47 - core	see SCA-65
SCB-66	Concrete plan floor 48 - core	see SCA-66
SCB-67	Not used	
SCB-68	Concrete plan floors 49-74 - floor	see SCA-68
SCB-69	Concrete plan floors 49-54 - core	see SCA-69
SCB-70	Not used	
SCB-71	Not used	
SCB-72	Not used	
SCB-73	Not used	
SCB-74	Not used	
SCB-75	Concrete plan floor 55 - core	see SCA-75
SCB-76	Concrete plan floor 56 - core	see SCA-76
SCB-77	Concrete plan floors 57-58 - core	see SCA-77
SCB-78	Not used	
SCB-79	Concrete plan floor 59 - core	see SCA-79
SCB-80	Concrete plan floor 60 - core	see SCA-80

SCB-81	Concrete plan floor 61 - core	10-Aug-70
SCB-82	Concrete plan floor 62 - core	see SCA-82
SCB-83	Concrete plan floor 63 - core	see SCA- 83
SCB-84	Concrete plan floor 64 - core	see SCA-84
SCB-85	Concrete plan floor 65 - core	see SCA-85
SCB-86	Concrete plan floor 66 - core	24-Aug-70
SCB-87	Concrete plan floor 67 - core	24-Aug-70
SCB-88	Concrete plan floor 68 - core	24-Aug-70
SCB-89	Concrete plan floor 69 - core	see SCA-89
SCB-90	Concrete plan floors 70-73 - core	see SCA-90
SCB-91	Not used	
SCB-92	Not used	
SCB-93	Not used	
SCB-94	Concrete plan floor 74 - core	see SCA-94
SCB-95	Concrete plan floor 75 - core	see SCA-95
SCB-96	Concrete plan floor 75 - floor	see SCA-96
SCB-97	Concrete plan floor 76 - core	see SCA-97
SCB-98	Concrete plan floor 77 - core	see SCA-98
SCB-99	Concrete plan floor 77 - floor	see SCA-99
SCB-100	Concrete plan floor 78 - core	see SCA-100
SCB-101	Concrete plan floor 78 - floor	see SCA-101
SCB-102	Concrete plan floor 79 - core	see SCA-102
SCB-103	Concrete plan floor 79 - floor	see SCA-103
SCB-104	Concrete plan floor 80 - core	see SCA-104
SCB-105	Concrete plan floor 80-82 - floor	see SCA-105
SCB-106	Concrete plan floor 81 - core	see SCA-106
SCB-107	Concrete plan floor 82 - core	see SCA-107
SCB-108	Not used	
SCB-109	Concrete plan floors 83-106 - floor	see SCA-109
SCB-110	Not used	
SCB-111	Concrete plan floor 83 - core	see SCA-111
SCB-112	Concrete plan floor 84-86 - core	see SCA-112
SCB-113	Not used	
SCB-114	Concrete plan floor 87 - core	see SCA-114
SCB-115		see SCA-115
SCB-116	Concrete plan floors 89,90,91 - core	see SCA-116
SCB-117	Not used	
SCB-118	Not used	
SCB-119	Concrete plan floor 92 - core	see SCA-119
SCB-120	Concrete plan floor 93 - core	15-Mar-71
SCB-121	Concrete plan floor 94 - core	see SCA-121

SCB-122	Concrete plan floor 95 - core	see SCA-122
SCB-123	Concrete plan floors 96-100 - core	see SCA-123
SCB-124	Not used	
SCB-125	Not used	
SCB-126	Not used	
SCB-127	Not used	
SCB-128	Concrete plan floor 101 - core	see SCA-128
SCB-129	Concrete plan floor 102 - core	see SCA-129
SCB-130	Concrete plan floor 103 - core	see SCA-130
SCB-131	Concrete plan floor 104 - core	15-Mar-71
SCB-132	Concrete plan floor 105 - core	18-Jun-71
SCB-133	Concrete plan floor 106 - core	18-Jun-71
SCB-134	Concrete plan floor 107 - floor	30-Jul-71
SCB-135	Concrete plan floor 107 - core	30-Jul-71
SCB-136	Concrete plan floor 108 - core	30-Jul-71
SCB-137	Concrete plan floor 108 - floor	01-Dec-71
SCB-138	Concrete plan floor 109 - core	see SCA-138
SCB-139	Concrete plan floor 110 - core	03-Sep-71
SCB-140	Concrete plan floor 110 - floor	03-Sep-71
SCB-141	Concrete plan penthouse roof - core	10-Apr-72
SCB-142	Concrete plans secondary levels	see SCA-142
SCB-143	Concrete plan sub stations, escalator pits	see SCA-143
SCB-144	Sections, truck ramp el.284	11-Jul-69
SCB-145	Concrete plan el.264, post tension	Void
SCB-146	Concrete plan penthouse low roof - floor	26-Mar-73
SCB-147	Concrete plan penthouse high roof - floor	22-Sep-72
SCB-148	Core plan observation deck	08-Mar-73

** Formerly included with Tower A*

Note- Tower B Concrete plan floors 14-40 - floor see SCA-23

Tower B Concrete plans floors 13-16 - core see SCA-24

WTC TOWER A & B STRUCTURAL STEEL DECK DRAWING INDEX – (18-MAY-73)

SA-156	Steel deck plan floor	7	28-Mar-69
SA-157	Steel deck plan floor	9	28-Mar-69
SA-158	Steel deck plan floors	19-40	28-Mar-69
SA-159	Steel deck plan floor	41	17-Jun-68
SA-160	Steel deck plan floor	43	27-Aug-69
SB-160	Steel deck plan floor	43	27-Aug-69
SAB-161	Steel deck plan floor	45	17-Jun-68
SA-162	Steel deck plan floor	44	27-Aug-69
SB-162	Steel deck plan floor	44	27-Aug-69
SAB-163	Steel deck plan floors	46-49	11-6-67, 6-17-68
SAB-164	Steel deck plan floors	50-58	17-Jun-68
SAB-165	Steel deck plan floors	59-62	17-Jun-68
SAB-166	Steel deck plan floors	63-66	12-Dec-69
SAB-167	Steel deck plan floors	67-70	12-Dec-69
SAB-168	Steel deck plan floors	71-74	17-Jun-68
SAB-169	Steel deck plan floors	65-69	17-Jun-68
SB-169			
SAB-170	Steel deck plan floor	75	17-Jun-68
SAB-171	Steel deck plan floor	77	17-Jun-68
SAB-172	Steel deck plan floors	78-79	18-Mar-69
SAB-173	Steel deck plan floors	80-81	17-Jun-68
SAB-174	Steel deck plan floors	82-83	17-Jun-68
SAB-175	Steel deck plan floors	84-89	17-Jun-68
SAB-176	Steel deck plan floors	90-94	17-Jun-68
SAB-177	Steel deck plan floors	95-101	17-Jun-68
SAB-178	Steel deck plan floors	102-106	02-Jul-71
SA-179	Steel deck plan floor	107	08-Sep-70
SB-179	Steel deck plan floor	107	01-Oct-70
SA-180	Steel deck plan floor	108	08-Sep-70
SB-180	Steel deck plan floor	108	01-Oct-70
SA-181	Steel deck plan floor	110	08-Sep-70
SB-181	Steel deck plan floor	110	29-Jan-72
SB-182	Steel deck plan floor	7	28-Mar-69
SB-183	Steel deck plan floor	9	28-Mar-69
SB-184	Steel deck plan floor	10	28-Mar-69
SB-185	Steel deck plan floor	11	28-Mar-69
SB-186	Steel deck plan floor	12	28-Mar-69
SB-187	Steel deck plan floor	13	07-Nov-69

Miscellaneous

SX-105	Framing plan-typical office floor	21-Dec-70
SX-144	Sewer ejector & sump pits	20-Mar-69
SX-146	Closure tieback anchorage perimeter	24-Jun-68
?SAB-240	Floor plan el.229 *(original print missing)	12-Sep-66

Appendix B
DRAWING BOOK 19 MODIFICATIONS FOR STRUCTURAL ELEMENTS NOT INCLUDED IN THE DATABASE

The following is a table of Drawing Book 19 (Revisions After Fabrication) changes not included in the database because they were considered to not significantly affect the member properties pertaining to the reference structural models. The listed modifications only pertain to tower modifications. Modifications outside of the towers are not included.

Drawing Number(s)	Title	Date	Description
19–B–913	Detail 913	10/9/68	½ in. by 1 in. shim plates for p/t cells.
19–A–914	Detail 914	11/20/68	Clip angle location changed for seated connection.
19–A–918	Detail 918	1/15/69	Additional studs and flange plates for beam in beam framed between core and exterior wall in WTC 1, elevation 274 ft.
19–A–921	Detail 921	1/27/69	Additional flange plate for beam in core framing in WTC 1, elevation 284 ft.
19–B–975	Beam repair det. Floor 59 and 92	10/28/70	Beam reinforcing for conduits passing through core channel.
19–A–982.1, 982.2	Floor 106 beam cover plate	1/17/71	Beam cover plates Floor 106.
19–B–994	Column splice repair Floor 107	3/15/71	Column Splice Repair Floor 107
19–A–1001, 19–AB–1002, 1003	245 A 12-9 Seat detail	6/5/69	Truss seat modifications Floor 10–12, Column 246, WTC 1 and seat detail dimensional modifications Floor 10–107, WTC 1 and WTC 2.
19–AB-1004.1, 1004.2	Column splice repair procedure	6/20/69	Additional weld for exterior wall column splice connections.
19–B–2100.1 – 2100.4	Modification to pent house roof framing plan	9/27/71	Raised girder using stubs on roof level framing.

This page intentionally left blank.

Appendix C
WTC DRAWING BOOK FLOWCHARTS

This Appendix presents the drawing books flowcharts that illustrate the flow of the drawing book links. These flowcharts were used to organize the links of the electronic databases within the relational database. For the flowcharts presented in Figs. C–1 through C–9, the following notes are common:

- "4-AB-*" denotes Drawing Book 4, Tower A , B or AB, and page number
- [*TC] denotes number of pages and type, where page types include:
- TC: computer generated tables; TH: hand written tables; and D: diagrams
- *.xls denotes Microsoft Excel spreadsheet file name; and (AB_***) denotes database heading
- ((*)) denotes reference note key from original Drawing Book information table.
- {*} denotes relational database link (i.e. Microsoft Excel column number) from previous *.xls file.
- Figures of columns and panels are shown from inside of building looking out, unless otherwise noted.

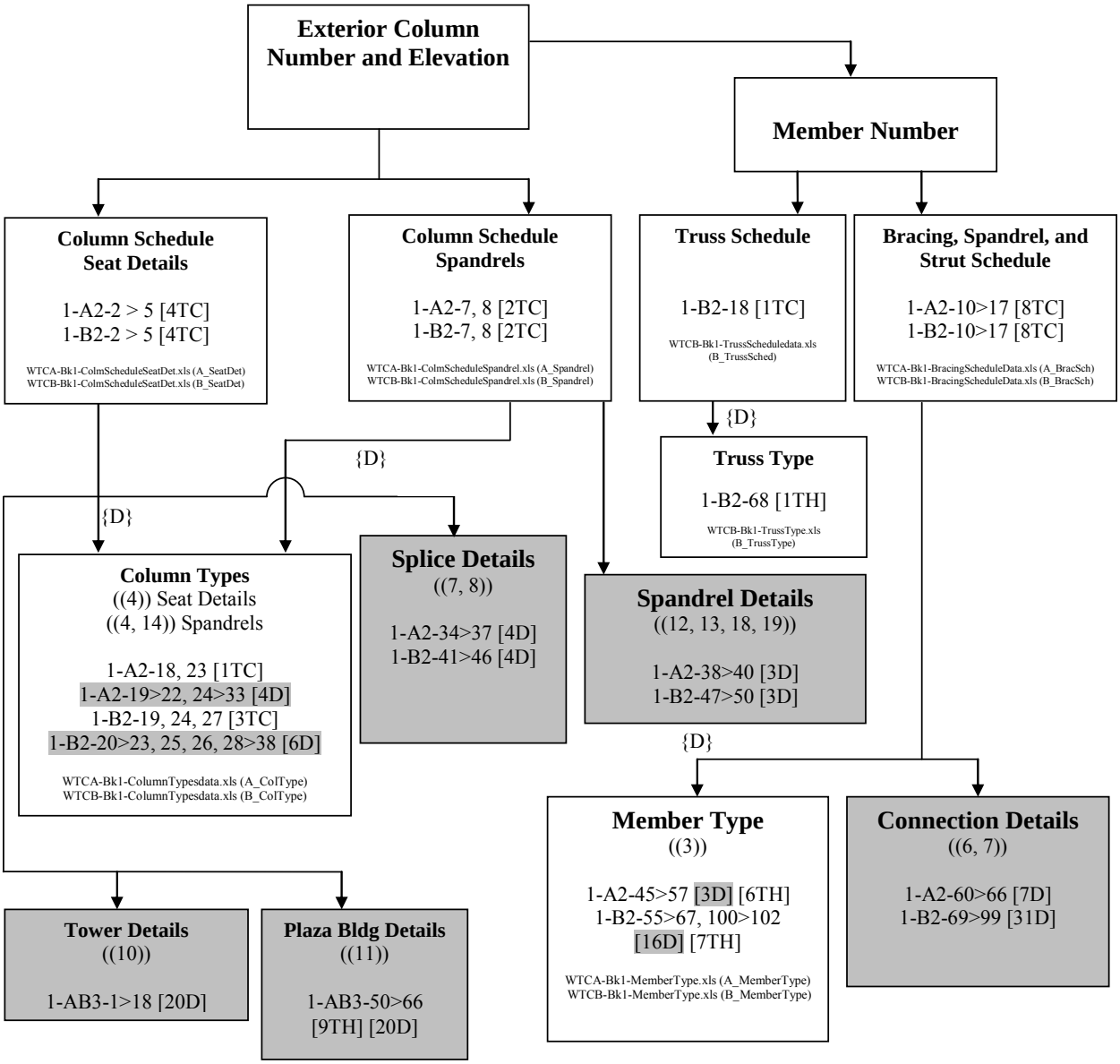

Figure C–1. Drawing Book 1 – WTC 1 and WTC 2 exterior wall to elevation 363 ft.

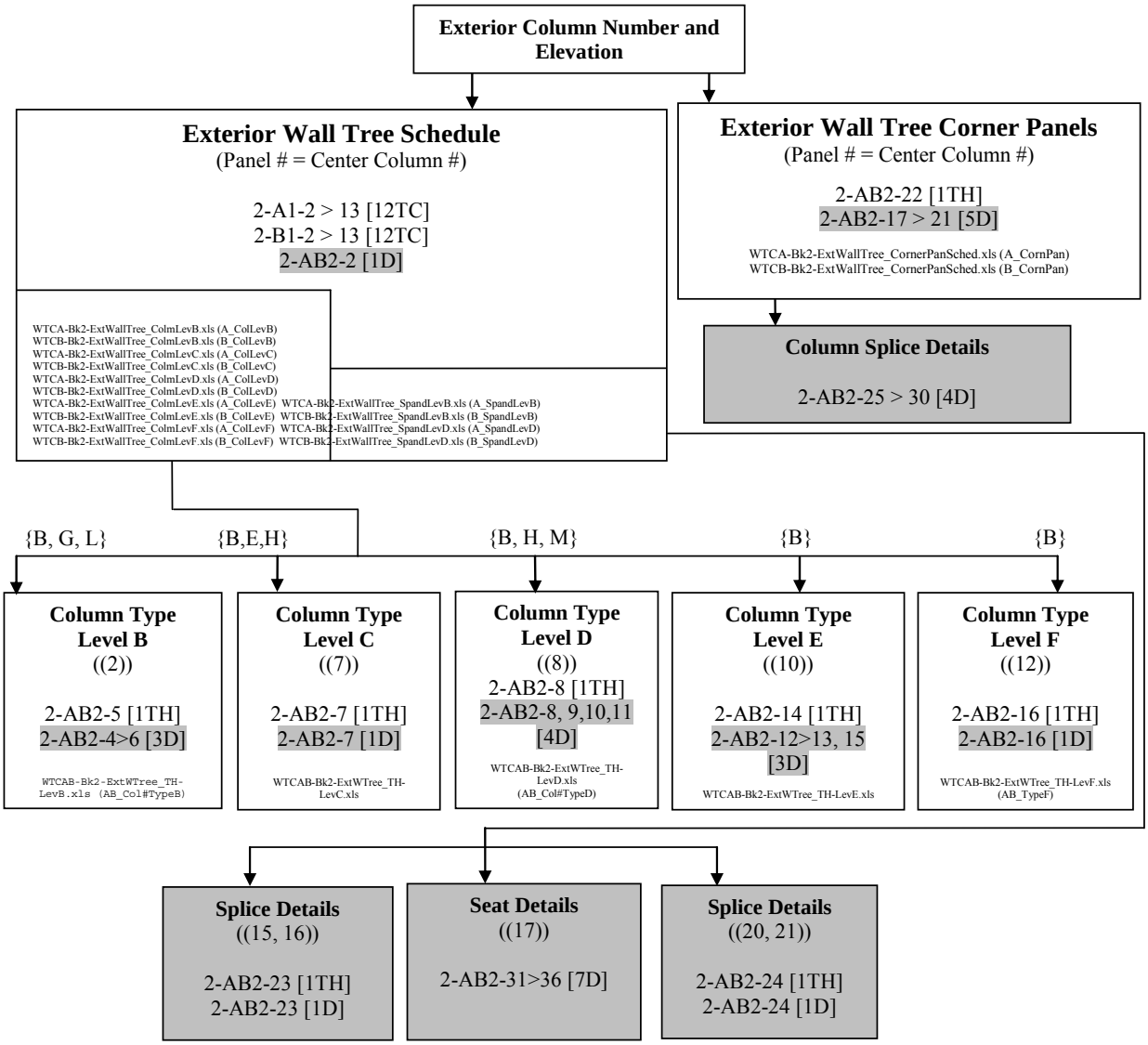

Figure C–2. Drawing Book 2 – WTC 1 and WTC 2 exterior wall tree, elevation 363 ft to floor 9.

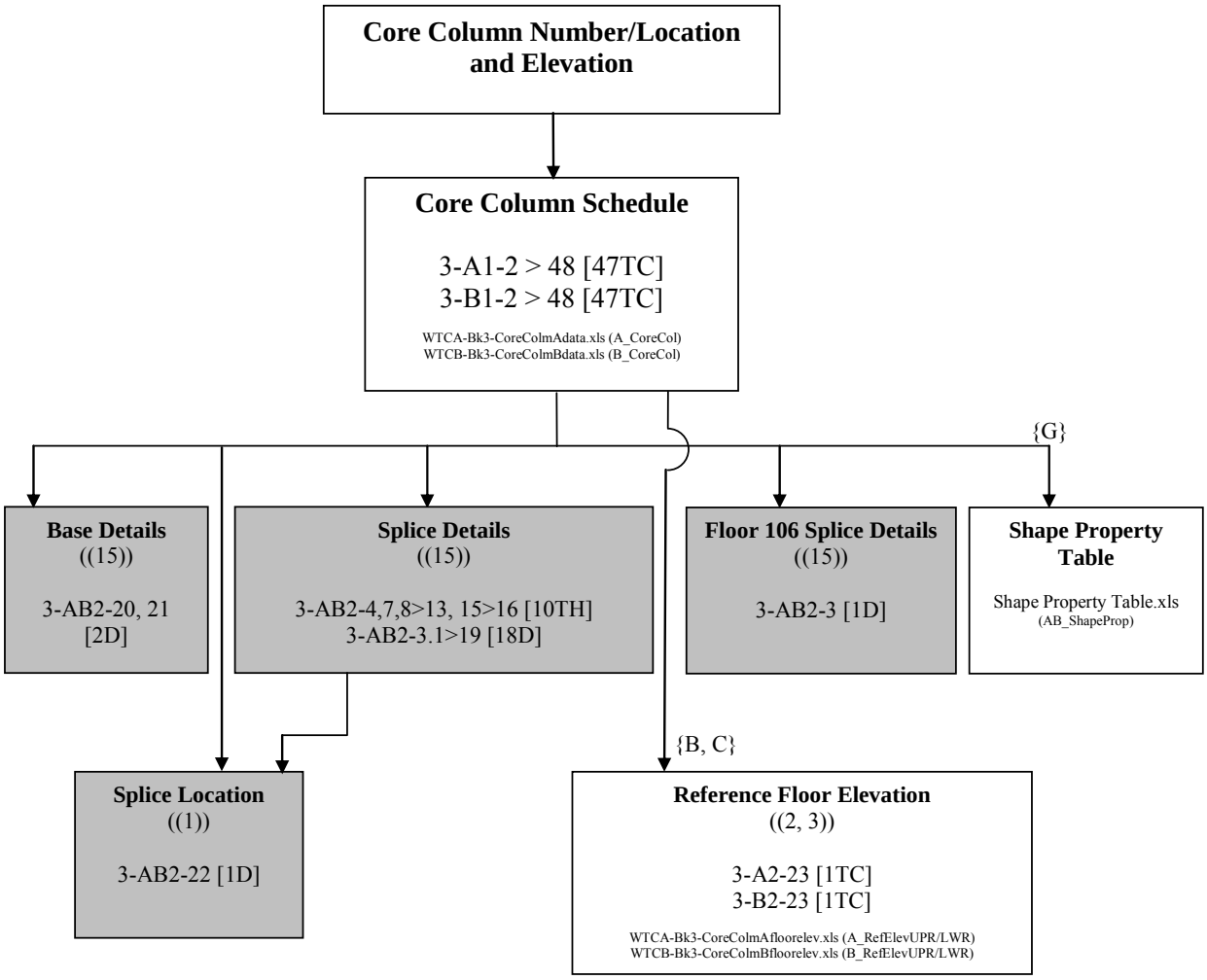

Figure C–3. Drawing Book 3 – WTC 1 and WTC 2 core columns, foundations to floor 106.

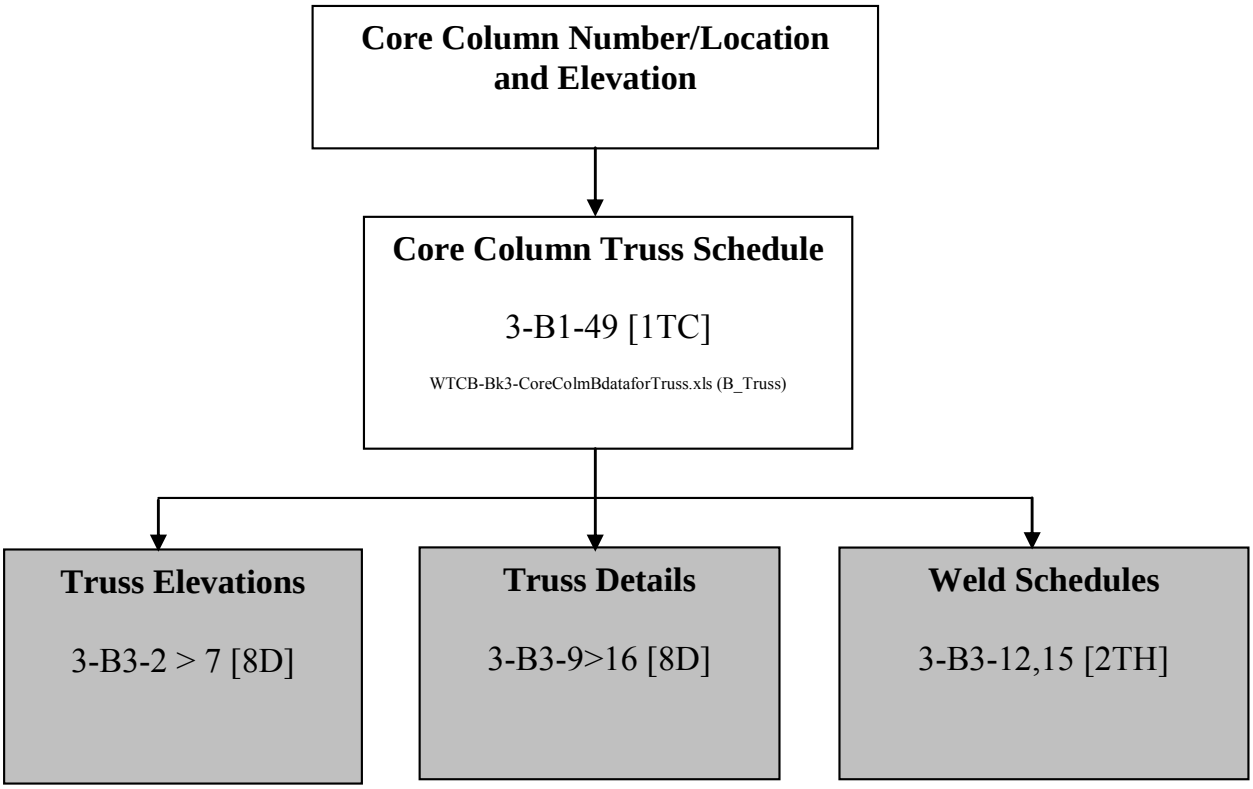

Figure C–4. Drawing Book 3 – WTC 1 and WTC 2 core column trusses.

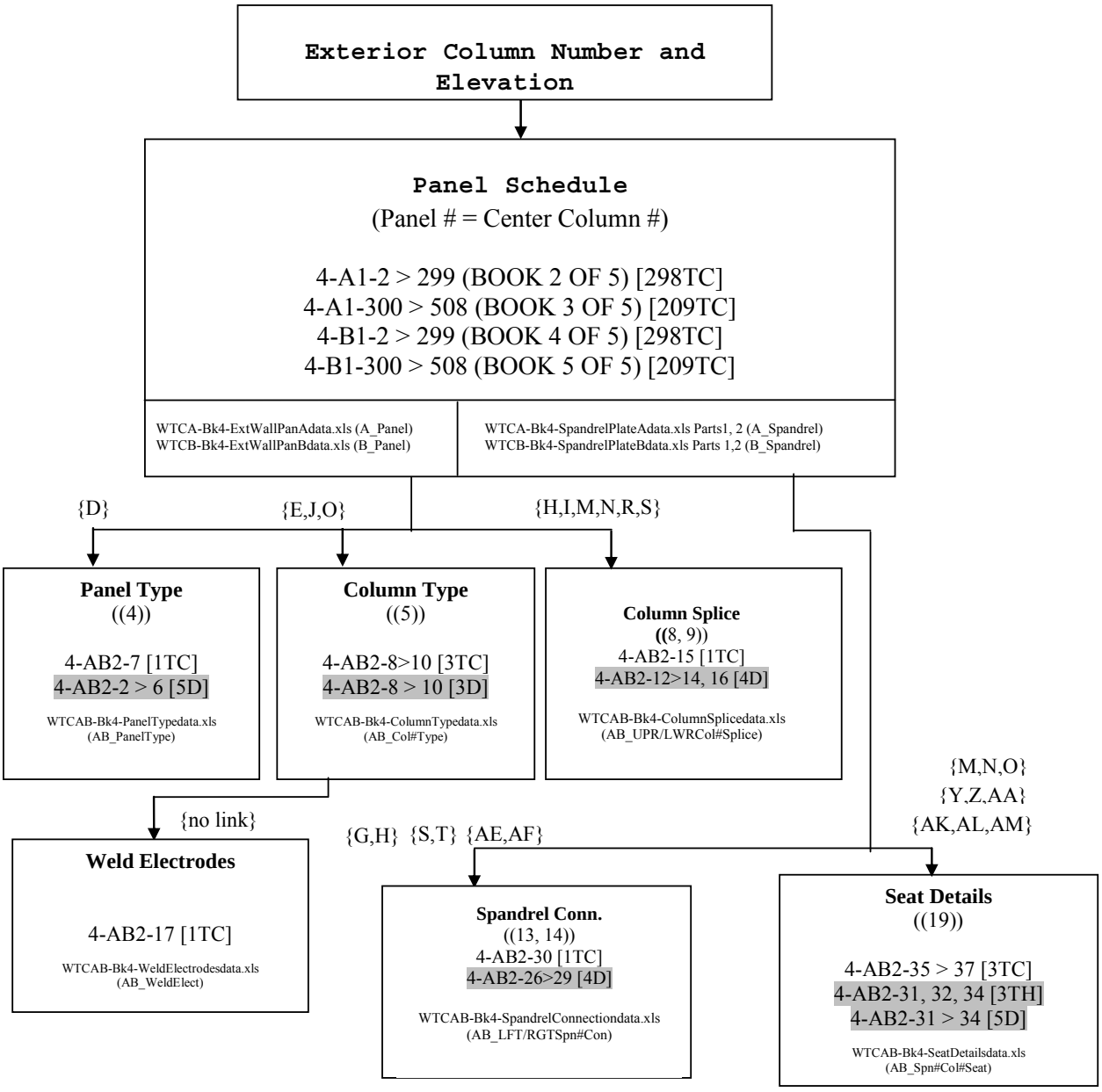

Figure C–5. Drawing Book 4 – WTC 1 and WTC 2 exterior wall, floors 9 to 106.

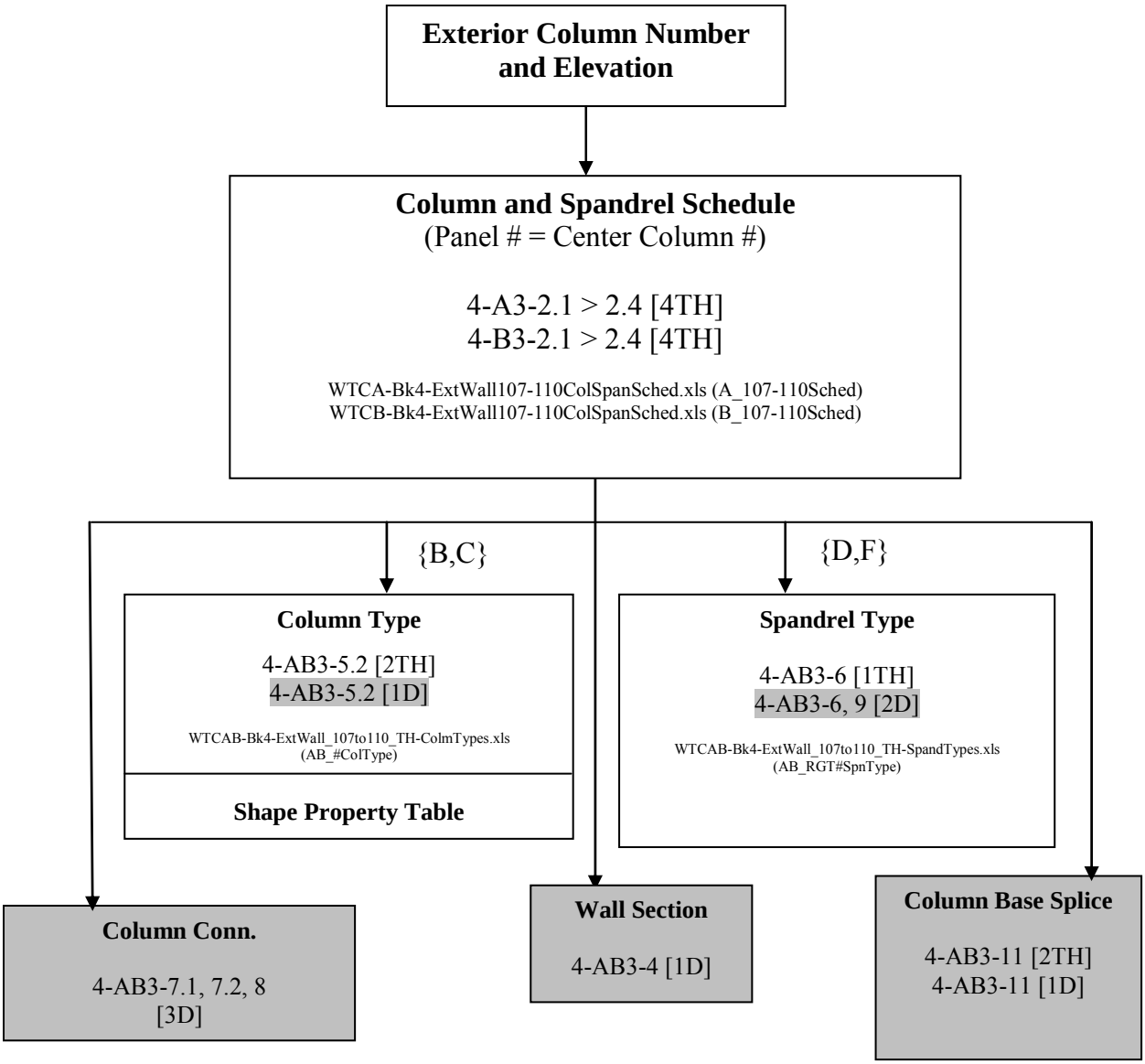

Figure C–6. Drawing Book 4 – WTC 1 and WTC 2 exterior wall, floors 107 to 110.

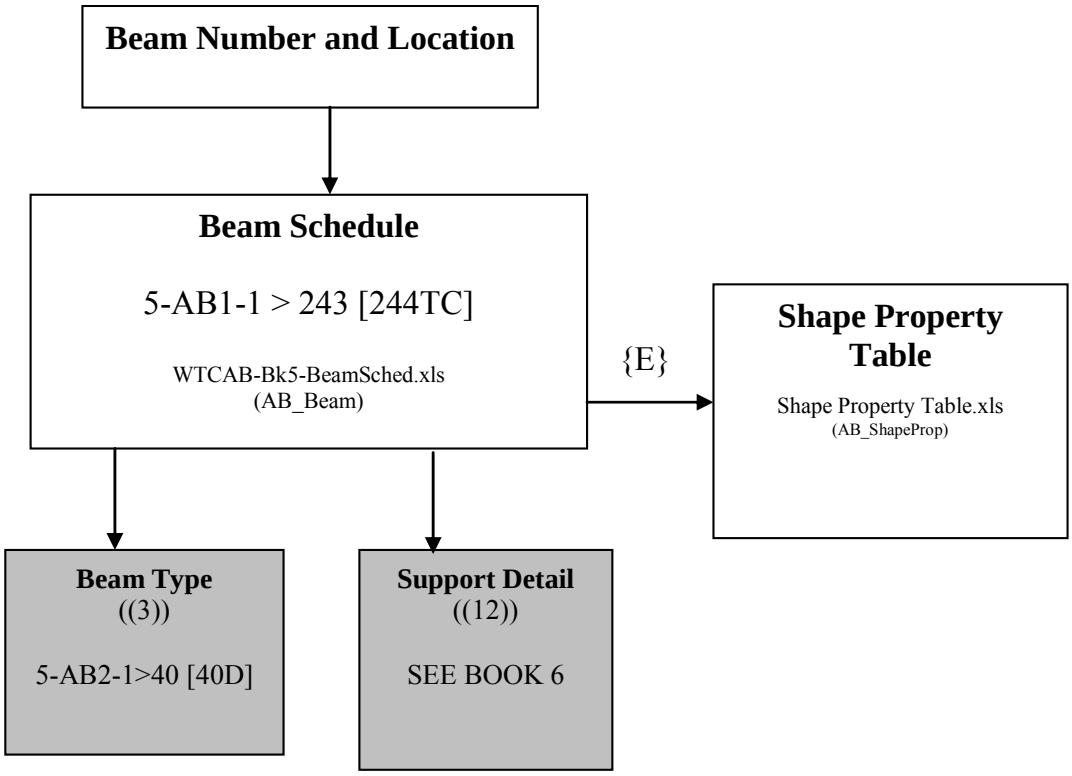

Figure C–7. Drawing Book 5 – WTC 1 and WTC 2 beam schedule and types.

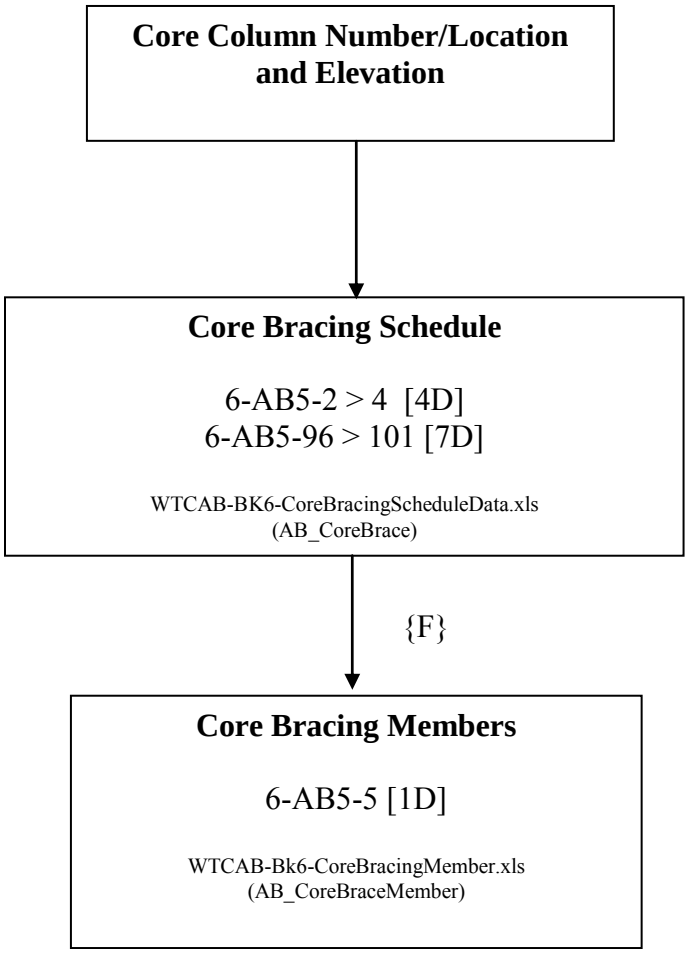

Figure C–8. Drawing Book 6 – WTC 1 and WTC 2 core bracing schedule and types.

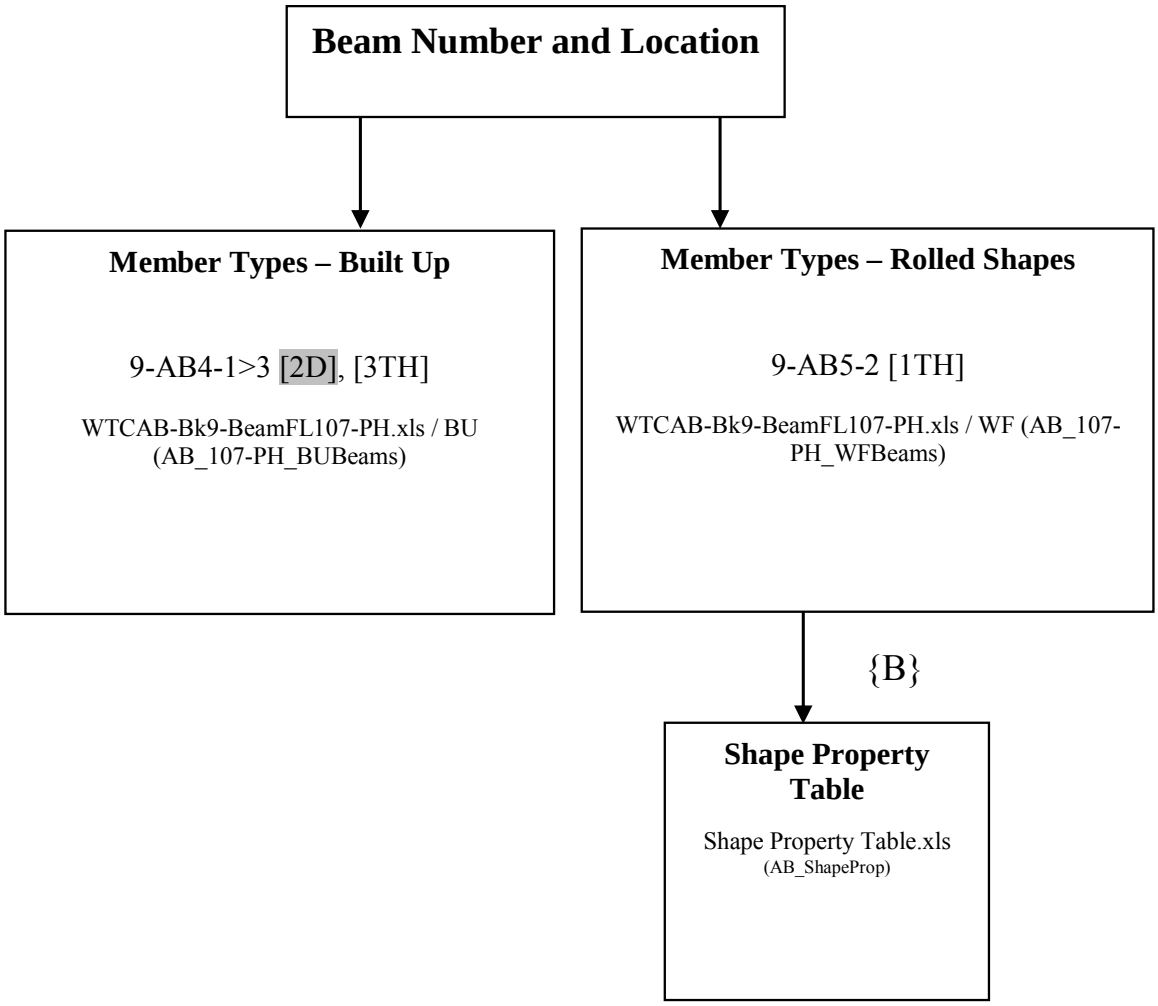

Figure C–9. Drawing Book 9 – WTC 1 and WTC 2 floor 107 to penthouse beam schedule.

Appendix D
EXCEL FILE LIST AND DESCRIPTION

Files with (♣) include section property calculations
Files with (♠) include multiple section properties calculations for some members

Drawing Book 1

WTCA-Bk1-ColumnTypesdata.xls♣ ♠
WTC Drawing Book 1: Tower A Exterior Wall to EL 363' Column Types

WTCA-Bk1-BracingScheduleData.xls
WTC Drawing Book 1: Tower A Exterior Wall to EL 363' Bracing, Spandrel and Strut Schedule

WTCA-Bk1-ColmScheduleSeatDet.xls
WTC Drawing Book 1: Tower A Exterior Wall to EL 363' Column Schedule - Seat Details

WTCA-Bk1-ColmScheduleSpandrel.xls
WTC Drawing Book 1: Tower A Exterior Wall to EL 363' Column Schedule - Spandrels

WTCA-Bk1-MemberTypes.xls♣
WTC Drawing Book 1: Tower A Exterior Wall to EL 363' Member Type

WTCB-Bk1-ColumnTypesdata.xls♣ ♠
WTC Drawing Book 1: Tower B Exterior Wall to EL 363' Column Types

WTCB-Bk1-BracingScheduledata.xls
WTC Drawing Book 1: Tower B Exterior Wall to EL 363' Bracing, Spandrel and Strut Schedule

WTCB-Bk1-ColmScheduleSeatDet.xls
WTC Drawing Book 1: Tower B Exterior Wall to EL 363' Column Schedule - Seat Details

WTCB-Bk1-ColmScheduleSpandrel.xls
WTC Drawing Book 1: Tower B Exterior Wall to EL 363' Column Schedule - Spandrels

WTCB-Bk1-MemberTypes.xls♣
WTC Drawing Book 1: Tower B Exterior Wall to EL 363' Member Type

WTCB-Bk1-TrussScheduledata.xls♣
WTC Drawing Book 1: Tower B Exterior Wall to EL 363' Truss Schedule

WTCB-Bk1-TrussType.xls
WTC Drawing Book 1: Tower B Exterior Wall to EL 363' Truss Type

Drawing Book 2

WTCAB-Bk2-ExtWTree_TH-LevB.xls♣
WTC Drawing Book 2: Tower A and B Exterior Wall Tree EL 363' to Floor 9 - Column Type at Level B

WTCAB-Bk2-ExtWTree_TH-LevC.xls♣ ♠
WTC Drawing Book 2: Tower A and B Exterior Wall Tree EL 363' to Floor 9 - Column Type at Level C

WTCAB-Bk2-ExtWTree_TH-LevD.xls♣
WTC Drawing Book 2: Tower A and B Exterior Wall Tree EL 363' to Floor 9 - Column Type at Level D

WTCAB-Bk2-ExtWTree_TH-LevE.xls♣ ♠
WTC Drawing Book 2: Tower A and B Exterior Wall Tree EL 363' to Floor 9 - Column Type at Level E

WTCAB-Bk2-ExtWTree_TH-LevF.xls♣
WTC Drawing Book 2: Tower A and B Exterior Wall Tree EL 363' to Floor 9 - Column Type at Level F

WTCA-Bk2-ExtWallTree_ColmLevB.xls
WTC Drawing Book 2: Tower A Exterior Wall Tree EL 363' to Floor 9 - Exterior Wall Tree Schedule at Level B

WTCA-Bk2-ExtWallTree_ColmLevC.xls
WTC Drawing Book 2: Tower A Exterior Wall Tree EL 363' to Floor 9 - Exterior Wall Tree Schedule at Level C

WTCA-Bk2-ExtWallTree_ColmLevD.xls
WTC Drawing Book 2: Tower A Exterior Wall Tree EL 363' to Floor 9 - Exterior Wall Tree Schedule at Level D

WTCA-Bk2-ExtWallTree_ColmLevE.xls
WTC Drawing Book 2: Tower A Exterior Wall Tree EL 363' to Floor 9 - Exterior Wall Tree Schedule at Level E

WTCA-Bk2-ExtWallTree_ColmLevF.xls
WTC Drawing Book 2: Tower A Exterior Wall Tree EL 363' to Floor 9 - Exterior Wall Tree Schedule at Level F

WTCA-Bk2-ExtWallTree_CornerPanSched.xls♣ ♠
WTC Drawing Book 2: Tower A Exterior Wall Tree EL 363' to Floor 9 - Exterior Wall Tree Corner Panel Schedule

WTCA-Bk2-ExtWallTree_SpandLevB.xls
WTC Drawing Book 2: Tower A Exterior Wall Tree EL 363' to Floor 9 - Exterior Wall Tree Spandrel Schedule at Level B

WTCA-Bk2-ExtWallTree_SpandLevD.xls

WTC Drawing Book 2: Tower A Exterior Wall Tree EL 363' to Floor 9 - Exterior Wall Tree Spandrel Schedule at Level D

WTCB-Bk2-ExtWallTree_ColmLevB.xls
WTC Drawing Book 2: Tower B Exterior Wall Tree EL 363' to Floor 9 - Exterior Wall Tree Schedule at Level B

WTCB-Bk2-ExtWallTree_ColmLevC.xls
WTC Drawing Book 2: Tower B Exterior Wall Tree EL 363' to Floor 9 - Exterior Wall Tree Schedule at Level C

WTCB-Bk2-ExtWallTree_ColmLevD.xls
WTC Drawing Book 2: Tower B Exterior Wall Tree EL 363' to Floor 9 - Exterior Wall Tree Schedule at Level D

WTCB-Bk2-ExtWallTree_ColmLevE.xls
WTC Drawing Book 2: Tower B Exterior Wall Tree EL 363' to Floor 9 - Exterior Wall Tree Schedule at Level E

WTCB-Bk2-ExtWallTree_ColmLevF.xls
WTC Drawing Book 2: Tower B Exterior Wall Tree EL 363' to Floor 9 - Exterior Wall Tree Schedule at Level F

WTCB-Bk2-ExtWallTree_CornerPanSched.xls♣ ♠
WTC Drawing Book 2: Tower B Exterior Wall Tree EL 363' to Floor 9 - Exterior Wall Tree Corner Panel Schedule

WTCB-Bk2-ExtWallTree_SpandLevB.xls
WTC Drawing Book 2: Tower B Exterior Wall Tree EL 363' to Floor 9 - Exterior Wall Tree Spandrel Schedule at Level B

WTCB-Bk2-ExtWallTree_SpandLevD.xls
WTC Drawing Book 2: Tower B Exterior Wall Tree EL 363' to Floor 9 - Exterior Wall Tree Spandrel Schedule at Level D

Drawing Book 3

WTCA-Bk3-CoreColmAdata.xls♣
WTC Drawing Book 3: Tower A Core Columns Foundation to Floor 106 - Core Column Schedule

WTCA-Bk3-CoreColmAfloorelev.xls
WTC Drawing Book 3: Tower A Core Columns Foundation to Floor 106 Reference Floor Elevation

WTCB-Bk3-CoreColmBdata.xls♣
WTC Drawing Book 3: Tower B Core Columns Foundation to Floor 106 - Core Column Schedule

WTCB-Bk3-CoreColmBdataforTruss.xls♣
WTC Drawing Book 3: Tower B Core Columns Foundation to Floor 106 - Core Column Truss Schedule

WTCB-Bk3-CoreColmBfloorelev.xls
WTC Drawing Book 3: Tower B Core Columns Foundation to Floor 106 Reference Floor Elevation

Drawing Book 4

WTCAB-Bk4-ColumnTypedata.xls♣ ♠
WTC Drawing Book 4: Tower A and B Exterior Wall above 9th Floor (To 106th Floor) Column Type

WTCAB-Bk4-PanelTypedata.xls
WTC Drawing Book 4: Tower A and B Exterior Wall above 9th Floor (To 106th Floor) Panel Type

WTCAB-Bk4-SeatDetailsdata.xls
WTC Drawing Book 4: Tower A and B Exterior Wall above 9th Floor (To 106th Floor) Seat Details

WTCAB-Bk4-SpandrelConnectiondata.xls
WTC Drawing Book 4: Tower A and B Exterior Wall above 9th Floor (To 106th Floor) Spandrel Connection

WTCAB-Bk4-WeldElectrodesdata.xls
WTC Drawing Book 4: Tower A and B Exterior Wall above 9th Floor (To 106th Floor) Weld Electrodes

WTCAB-Bk4-ColumnSplicedata.xls
WTC Drawing Book 4: Tower A and B Exterior Wall above 9th Floor (To 106th Floor) Column Spice

WTCA-Bk4-ExtWallPanAdata.xls
WTC Drawing Book 4: Tower A Exterior Wall above 9th Floor (To 106th Floor) Panel Schedule

WTCA-Bk4-SpandrelPlateAdata_part1.xls
WTC Drawing Book 4: Tower A Exterior Wall above 9th Floor (To 106th Floor) Spandrel Schedule Part 1

WTCA-Bk4-SpandrelPlateAdata_part2.xls
WTC Drawing Book 4: Tower A Exterior Wall above 9th Floor (To 106th Floor) Spandrel Schedule Part 2

WTCB-Bk4-ExtWallPanBdata.xls
WTC Drawing Book 4: Tower B Exterior Wall above 9th Floor (To 106th Floor) Panel Schedule

WTCB-Bk4-SpandrelPlateBdata_part1.xls
WTC Drawing Book 4: Tower B Exterior Wall above 9th Floor (To 106th Floor) Spandrel Schedule Part 1

WTCB-Bk4-SpandrelPlateBdata_part2.xls
WTC Drawing Book 4: Tower B Exterior Wall above 9th Floor (To 106th Floor) Spandrel Schedule Part 2

WTCAB-Bk4-ExtWall_107to110_TH-ColmTypes.xls♣
WTC Drawing Book 4: Tower A and B Exterior Wall Floors 107 to 110 Column Type

WTCAB-Bk4-ExtWall_107to110_TH-SpandTypes.xls♣
WTC Drawing Book 4: Tower A and B Exterior Wall Floors 107 to 110 Spandrel Type

WTCA-Bk4-ExtWall107-110ColSpanSched.xls
WTC Drawing Book 4: Tower A Exterior Wall Floors 107 to 110 Column and Spandrel Schedule

WTCB-Bk4-ExtWall107-110ColSpanSched.xls
WTC Drawing Book 4: Tower B Exterior Wall Floors 107 to 110 Column and Spandrel Schedule

Drawing Book 5

WTCAB-Bk5-BeamSched.xls
WTC Drawing Book 5: Tower A and B Beam Schedule

Drawing Book 6

WTCAB-Bk6-CoreBracingMember.xls♣
WTC Drawing Book 6: Tower A and B Core Bracing Members

WTCAB-Bk6-CoreBracingScheduleData.xls
WTC Drawing Book 6: Tower A and B Core Bracing Schedule

Drawing Book 9

WTCAB-Bk9-BeamFL107-PH.xls♣
WTC Drawing Book 9: Tower A and B Floors 107 to Penthouse Beam Member Types

Included outside of the Drawing Book folders:

Shape Property Table.xls
Shape Property Table

This page intentionally left blank.

Appendix E
RELATIONAL DATABASE FILE LIST AND DESCRIPTION

(Files with (♣) include section property calculations)
(Files with (♠) include multiple section properties calculations for some members)

WTCA_DBk1.mdb♣ ♠
WTC Drawing Book 1: Tower A Exterior Wall to EL. 363'

WTCB_DBk1.mdb♣ ♠
WTC Drawing Book 1: Tower B Exterior Wall to EL. 363'

WTCA_DBk2.mdb♣ ♠
WTC Drawing Book 2: Tower A Exterior Wall Tree EL. 363' to Floor 9

WTCB_DBk2.mdb♣ ♠
WTC Drawing Book 2: Tower B Exterior Wall Tree EL. 363' to Floor 9

WTCA_DBk3_col_foundation.mdb♣
WTC Drawing Book 3: Tower A Core Columns Foundations to Floor 106

WTCB_DBk3_col_foundation.mdb♣
WTC Drawing Book 3: Tower B Core Columns Foundations to Floor 106

WTCB_DBk3_col_truss.mdb♣
WTC Drawing Book 3: Tower B Core Column Trusses

WTCA_DBk4_9-106.mdb♣ ♠
WTC Drawing Book 4: Tower A Exterior Wall above 9th Floor (To 106th Flr)

WTCB_DBk4_9-106.mdb♣ ♠
WTC Drawing Book 4: Tower B Exterior Wall above 9th Floor (To 106th Flr)

WTCA_DBk4_107-110.mdb♣
WTC Drawing Book 4: Tower A Exterior Wall Floor 107 to Floor 110

WTCB_DBk4_107-110.mdb♣
WTC Drawing Book 4: Tower B Exterior Wall Floor 107 to Floor 110

WTCAB_DBk5.mdb
WTC Drawing Book 5: Tower A and B Beam Schedules and Types

WTCAB_DBk6.mdb♣
WTC Drawing Book 6: Tower A and B Core Bracing Schedules and Types

WTCAB_DBk9.mdb♣

WTC Drawing Book 9: Tower A and B Floor 107 to Penthouse Beam Schedules

Appendix F
RELATIONAL DATABASE TUTORIAL

Database Structure:

The relational database was developed using Microsoft Access 2002. Each database was set up based on the WTC Drawing Book flowcharts (refer to Appendix C). Each flowchart has a separate database for WTC 1 and WTC 2. The arrows in the flowcharts depict the links or common threads between tables. The relational database allows the data to be viewed and exported based on the user's preferences and communicated to the database via a query (a type of filter). Note: All screen views and examples below are based on the Drawing Book 2, WTC 1 database (WTC_DBk2_TWRA.mdb).

Viewing Tables:

To view a database table, first make sure that the tables are listed in the database window. To do this, click on "Tables" under Objects in the upper left box. The list of database tables should appear in the right hand box. (Fig. F–1) Note that the table names are listed in the flowcharts of Appendix C.

Double-click on the desired table to open it. The table will look similar to an Excel spreadsheet with columns and rows of data.

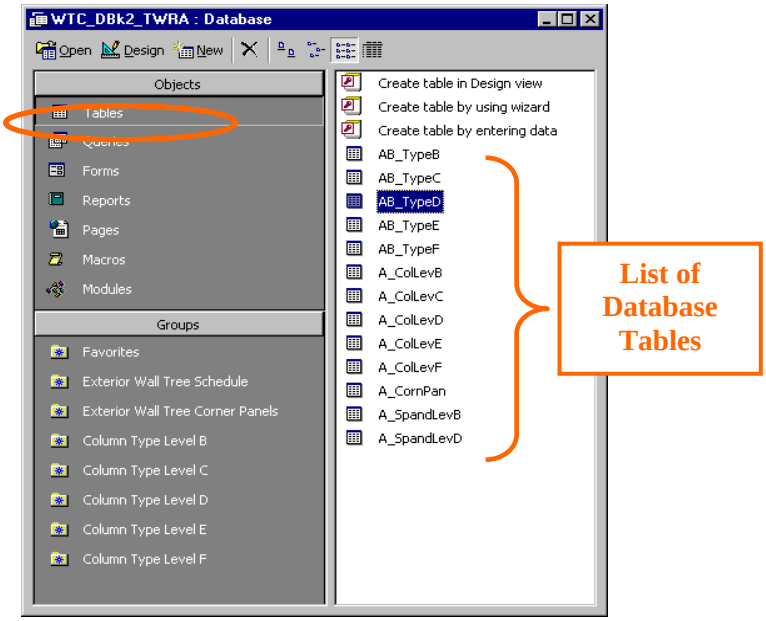

Figure F–1. List of database tables.

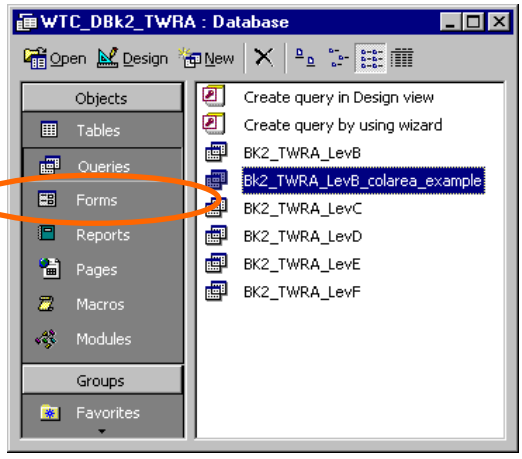

Figure F–2. List of database queries.

Running Queries:

To run a query, open up the query view from the main Database window by clicking on "Queries" under the Objects title in the upper left corner of the window. (Fig. F–2) A list of queries will be displayed in the box on the right.

Double-click on the desired query to run the query.

Note: All of the resident queries contain the established links between different tables. These queries list all data from all linked tables. To include only desired data in a query, see "Creating Custom Queries" below.

Creating Custom Queries:

Note: All custom queries must be created from one of the original queries as the links between tables have already been established in these queries. Any new query would not contain these links and would require these links to be created manually.

Start by saving a new version of the query to be edited. Right-click on the query to be edited and select "Save As…" from the sub-menu that appears. (Fig. F–3)

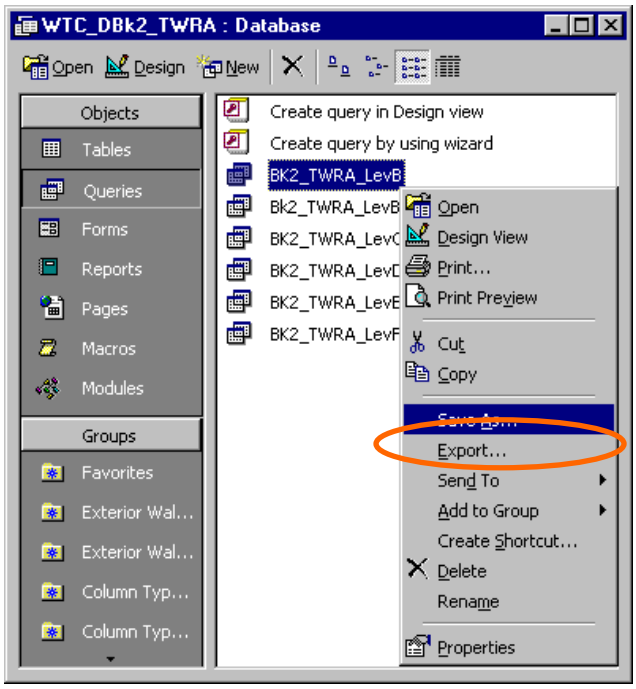

Figure F–3. Copying a query.

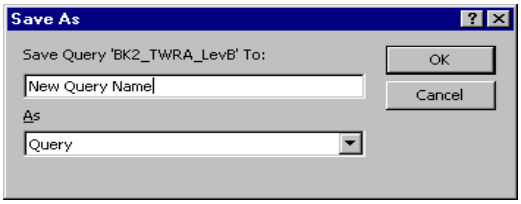

Figure F–4. Naming new query.

In the pop-up window, type in a name for the new query. Make sure that "Query" is selected in the "As" select-box. (Fig. F–4)

To edit the query, select the newly copied query and click on the "Design" button on the upper left corner of the database window (Fig. F–5). The query will appear in design (edit) view.

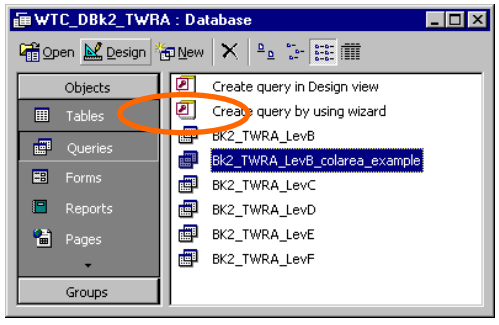

Figure F–5. Selecting design view for a query.

The design view shows all table associations (depicted by arrows) for this query. The first box (from left) shows the main table. The tables to the right are the ones that are linked from the main table. The arrows show where the association is made. For example, "Col1Type" in the main table (table A_ColLevB) links to "Column" in the AB_Col1TypeB table. The lower part of the view shows the query selections that will be displayed when the query is run. (Fig. F–6)

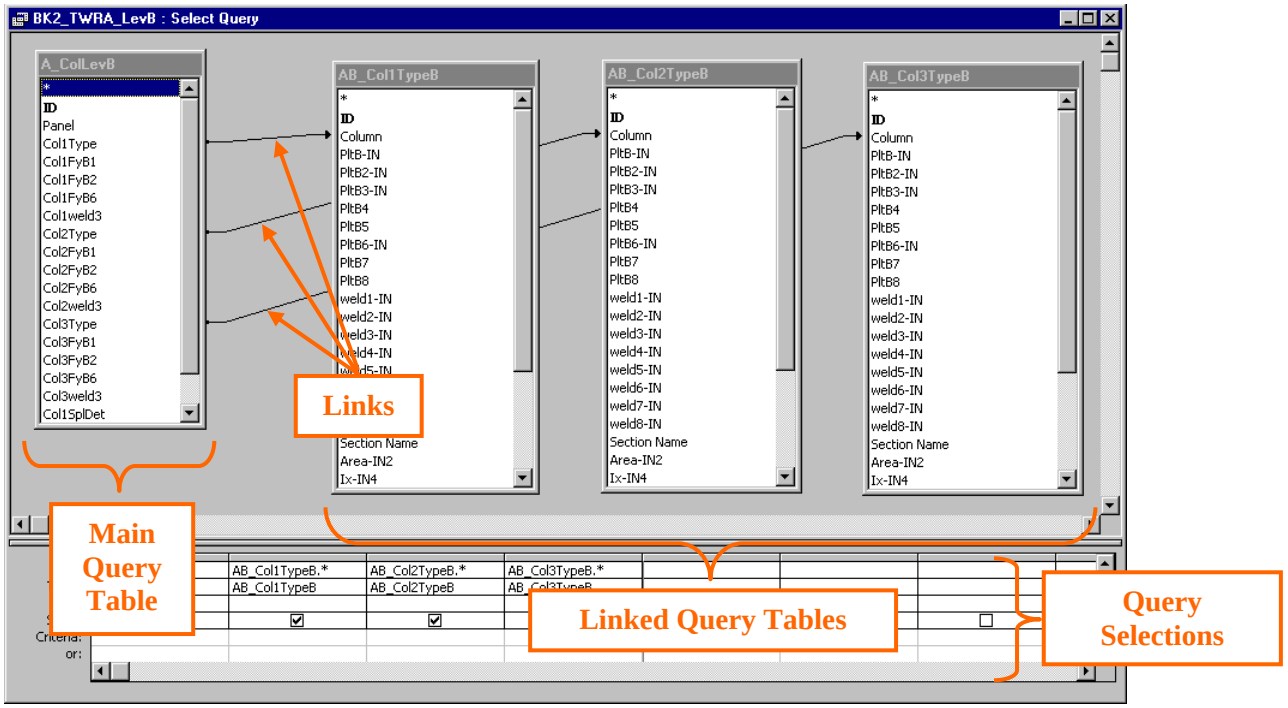

Figure F–6. Query design view.

First delete all the present query selections by clicking on the top row of each query selection (Fig. F–7) and pressing the delete key on the keyboard. Do this until all text is deleted from the query selections (the boxes themselves will not disappear)

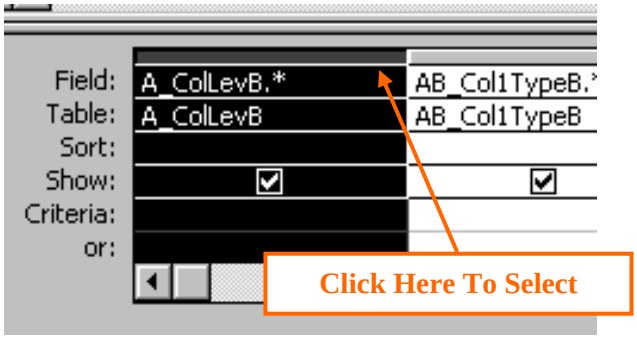

Figure F–7. Selecting query selection.

Double-click on the data to be included in your query (see example below).

Note: Selecting the asterisk (*) at the top of each table will list all fields in that table.

Example: How to include the panel, the three column types, as well as their associated areas in one table.

Note: This example is an example query called "Bk2_TWRA_LevB_colarea_example" in the WTC Book 2 Tower A database.

Once the original query selections are deleted, select the "Panel" field from the main table (table A_ColLevB) by double-clicking on it. It should appear as a query selection below (Fig. F–8).

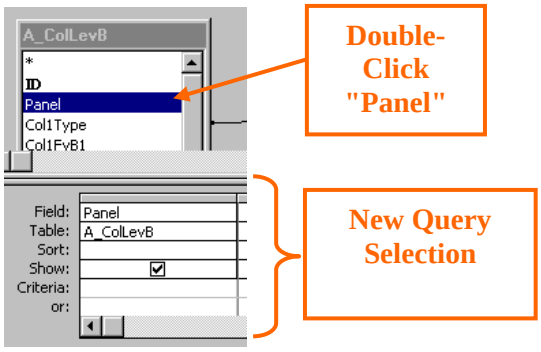

Figure F–8. Select panel field.

Select "Col1Type" from the main table. Then, select the "Area-IN2" field from the AB_Col1TypeB table. For the second column, select "Col2Type" from the main table and "Area-IN2" from the AB_Col2TypeB table. Repeat this for the third column, choosing the last table for the area of the column. There should now be 7 fields displaying in the Query Selection.

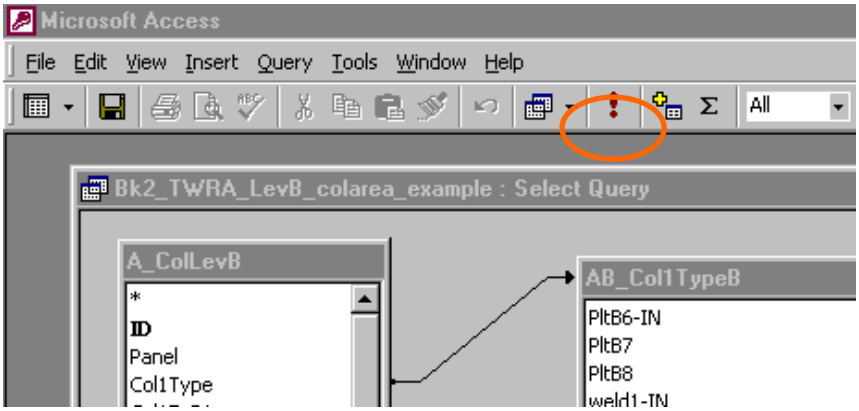

To run this query, click on the exclamation mark – Run button - on the middle top bar of the MS Access window. (Fig. F–9).

Note: To save the query, either click on the save button, or go to File Menu – Save.

Figure F–9. Run query button.

Exporting Data:

Data can be exported from any query or table into a number of formats, including text and Excel formats. To export a query, open the query and select File Menu – Export. Select the location, name, and the type to save as (from the drop-down menu) and click "Save All".

Appendix G
CATEGORIZATION OF FLOOR CONSTRUCTION TYPES FOR AREAS OUTSIDE OF CORE

The structural drawings for the floors in both towers were reviewed to identify structural similarities within the areas outside the core. Table G–1 summarizes the construction types and space usage for each floor for both towers. Information regarding the categorization and description of floor construction types are provided in Figs. G–1 through G–4. Based on this review, the typical truss-framed and beam-framed floors were selected for modeling.

Table G–1. Representative categorizations of floor construction types outside of core.

Tower A Floor Framing

Floor	Space Usage	Const. Type
PH Roof	Roof	Type 12
110	TV/Storage	Type 12
109	Upper Mech Fl	Type 13
108	Lower Mech Fl	Type 12
107	Restaurant	Type 12
106	Tenant	Type 10
105	Tenant	Type 1
104	Tenant	Type 1
103	Tenant	Type 1
102	Tenant	Type 1
101	Tenant	Type 1
100	Tenant	Type 1
99	Tenant	Type 1
98	Tenant	Type 1
97	Tenant	Type 1
96	Tenant	Type 1
95	Tenant	Type 1
94	Tenant	Type 1
93	Tenant	Type 1
92	Tenant	Type 2
91	Tenant	Type 1
90	Tenant	Type 1
89	Tenant	Type 1
88	Tenant	Type 1
87	Tenant	Type 1
86	Tenant	Type 1
85	Tenant	Type 1
84	Tenant	Type 1
83	Tenant	Type 9
82	Tenant	Type 9
81	Tenant	Type 9
80	Tenant	Type 9
79	Upper Escalator	Type 8
78	Sky Lobby	Type 7
77	Lower Escalator	Type 12
76	Upper Mech Fl	Type 13
75	Lower Mech Fl	Type 12
74	Tenant	Type 1
73	Tenant	Type 1
72	Tenant	Type 1
71	Tenant	Type 1
70	Tenant	Type 1
69	Tenant	Type 1
68	Tenant	Type 1
67	Tenant	Type 6
60-66	Tenant	Type 1
59	Tenant	Type 2
50-58	Tenant	Type 1
49	Tenant	Type 3
48	Tenant	Type 3
47	Tenant	Type 3
46	Tenant	Type 3
45	Upper Escalator	Type 5
44	Sky Lobby	Type 4
43	Lower Escalator	Type 12
42	Upper Mech	Type 13
41	Lower Mech	Type 12
27-40	Tenant	Type 1
26	Tenant	Type 1
25	Tenant	Type 2
14-24	Tenant	Type 1
13	Tenant	Type 1
12	Tenant	Type 1
11	Tenant	Type 1
10	Tenant	Type 1
9	Tenant	Type 12
8	Upper Mech	Type 13
7	Lower Mech	Type 12
3-6	Core Only (Storage)	NA
2	Plaza - Lobby	Type 15
1	Concourse	Type 14
B1	EL. 294	Type 14

Tower B Floor Framing

Floor	Space Usage	Const. Type
PH Roof	Observation	Type 12
110	Storage	Type 12
109	Upper Mech Fl	Type 13
108	Lower Mech Fl	Type 12
107	Observation	Type 12
106	Tenant	Type 1
105	Tenant	Type 1
104	Tenant	Type 1
103	Tenant	Type 1
102	Tenant	Type 1
101	Tenant	Type 1
100	Tenant	Type 1
99	Tenant	Type 1
98	Tenant	Type 1
97	Tenant	Type 1
96	Tenant	Type 1
95	Tenant	Type 1
94	Tenant	Type 1
93	Tenant	Type 1
92	Tenant	Type 2
91	Tenant	Type 1
90	Tenant	Type 1
89	Tenant	Type 1
88	Tenant	Type 1
87	Tenant	Type 1
86	Tenant	Type 1
85	Tenant	Type 1
84	Tenant	Type 1
83	Tenant	Type 9
82	Tenant	Type 9
81	Tenant	Type 9
80	Tenant	Type 9
79	Upper Escalator	Type 8
78	Sky Lobby	Type 7
77	Lower Escalator	Type 12
76	Upper Mech Fl	Type 13
75	Lower Mech Fl	Type 12
74	Tenant	Type 1
73	Tenant	Type 1
72	Tenant	Type 1
71	Tenant	Type 1
70	Tenant	Type 1
69	Tenant	Type 1
68	Tenant	Type 1
67	Tenant	Type 1
60-66	Tenant	Type 1
59	Tenant	Type 2
50-58	Tenant	Type 1
49	Tenant	Type 3
48	Tenant	Type 3
47	Tenant	Type 3
46	Tenant	Type 3
45	Upper Escalator	Type 5
44	Sky Lobby	Type 4
43	Lower Escalator	Type 12
42	Upper Mech	Type 13
41	Lower Mech	Type 12
27-40	Tenant	Type 1
26	Tenant	Type 1
25	Tenant	Type 2
14-24	Tenant	Type 1
13	Tenant	Type 11
12	Tenant	Type 11
11	Tenant	Type 11
10	Tenant	Type 11
9	Tenant	Type 12
8	Upper Mech	Type 13
7	Lower Mech	Type 12
3-6	Core Only (Storage)	NA
2	Plaza - Lobby	Type 15
1	Concourse	Type 14
B1	EL. 294	Type 14

Expanded Zone

Impact Zone

Combined Zones

Refer to Fig. G–1 through G–4 for description of floor system categories

Figure G–1. Floor construction types 1 through 4.

Figure G–2. Floor construction types 5 through 8.

Figure G–3. Floor construction types 9 through 11.

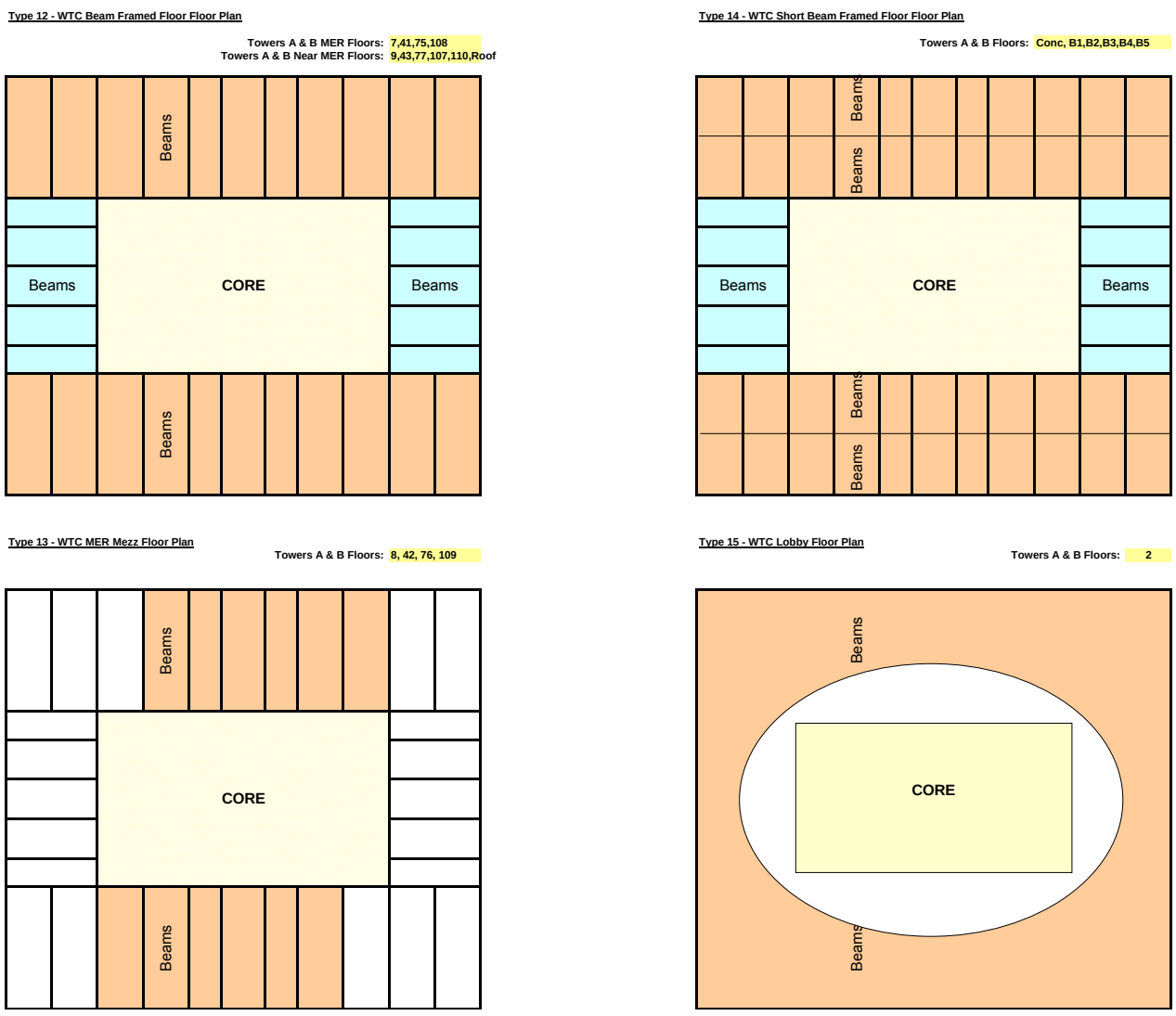

Figure G–4. Floor construction types 12 through 15.

NIST NCSTAR 1-2B

Federal Building and Fire Safety Investigation of the World Trade Center Disaster

Analysis of Aircraft Impacts into the World Trade Center Towers

Steven W. Kirkpatrick
Robert T. Bocchieri
Fahim Sadek
Robert A. MacNeill
Samuel Holmes
Brian D. Peterson
Robert W. Cilke
Claudia Navarro

NIST National Institute of Standards and Technology • Technology Administration • U.S. Department of Commerce

NIST NCSTAR 1-2B

Federal Building and Fire Safety Investigation of the World Trade Center Disaster

Analysis of Aircraft Impacts into the World Trade Center Towers

Steven W. Kirkpatrick
Robert T. Bocchieri
Applied Research Associates

Fahim Sadek
Building and Fire Research Laboratory
National Institute of Standards and Technology

Robert A. MacNeill
Samuel Holmes
Brian D. Peterson
Robert W. Cilke
Claudia Navarro
Applied Research Associates

September 2005

U.S. Department of Commerce
Carlos M. Gutierrez, Secretary

Technology Administration
Michelle O'Neill, Acting Under Secretary for Technology

National Institute of Standards and Technology
William Jeffrey, Director

Disclaimer No. 1

Certain commercial entities, equipment, products, or materials are identified in this document in order to describe a procedure or concept adequately or to trace the history of the procedures and practices used. Such identification is not intended to imply recommendation, endorsement, or implication that the entities, products, materials, or equipment are necessarily the best available for the purpose. Nor does such identification imply a finding of fault or negligence by the National Institute of Standards and Technology.

Disclaimer No. 2

The policy of NIST is to use the International System of Units (metric units) in all publications. In this document, however, units are presented in metric units or the inch-pound system, whichever is prevalent in the discipline.

Disclaimer No. 3

Pursuant to section 7 of the National Construction Safety Team Act, the NIST Director has determined that certain evidence received by NIST in the course of this Investigation is "voluntarily provided safety-related information" that is "not directly related to the building failure being investigated" and that "disclosure of that information would inhibit the voluntary provision of that type of information" (15 USC 7306c).

In addition, a substantial portion of the evidence collected by NIST in the course of the Investigation has been provided to NIST under nondisclosure agreements.

Disclaimer No. 4

NIST takes no position as to whether the design or construction of a WTC building was compliant with any code since, due to the destruction of the WTC buildings, NIST could not verify the actual (or as-built) construction, the properties and condition of the materials used, or changes to the original construction made over the life of the buildings. In addition, NIST could not verify the interpretations of codes used by applicable authorities in determining compliance when implementing building codes. Where an Investigation report states whether a system was designed or installed as required by a code *provision*, NIST has documentary or anecdotal evidence indicating whether the requirement was met, or NIST has independently conducted tests or analyses indicating whether the requirement was met.

Use in Legal Proceedings

No part of any report resulting from a NIST investigation into a structural failure or from an investigation under the National Construction Safety Team Act may be used in any suit or action for damages arising out of any matter mentioned in such report (15 USC 281a; as amended by P.L. 107-231).

National Institute of Standards and Technology National Construction Safety Team Act Report 1-2B
Natl. Inst. Stand. Technol. Natl. Constr. Sfty. Tm. Act Rpt. 1-2B, 496 pages (September 2005)
CODEN: NSPUE2

U.S. GOVERNMENT PRINTING OFFICE
WASHINGTON: 2005

For sale by the Superintendent of Documents, U.S. Government Printing Office
Internet: bookstore.gpo.gov — Phone: (202) 512-1800 — Fax: (202) 512-2250
Mail: Stop SSOP, Washington, DC 20402-0001

ABSTRACT

The objective of this report was to analyze the aircraft impacts into each of the World Trade Center (WTC) towers to provide the following: (1) estimates of probable damage to structural systems due to aircraft impact, including exterior walls, floor systems, and interior core columns; (2) estimates of the aircraft fuel dispersal during the impact; (3) estimates of debris damage to the interior tower contents, including partitions and workstations. Thus, this analysis established the initial conditions for the fire dynamics modeling and the thermal-structural response and collapse initiation analysis.

The impact analyses were conducted at various levels of complexity including: (1) the component level, (2) the subassembly level, and (3) the global level to estimate the probable damage to the towers due to aircraft impact. Simplified analyses were also used to support the development of the global finite element models. Analysis of uncertainties using the component and subassembly analyses were conducted to assess the effects of variability associated with various input parameters and identify the most influential parameters that affect the damage estimates using orthogonal factorial design. Based on the results of the sensitivity analyses, the most influential parameters identified were varied in the global models to provide a range of damage estimates for WTC 1 and WTC 2.

As part of the tower and aircraft models, constitutive relationships describing the actual behavior of the structures under the dynamic impact conditions of the aircraft were developed based on test results of the tower steels and from the open literature for other materials. Various grades of steels used in the exterior walls and core columns of the towers, weldment metal, bolts, reinforced concrete, aircraft materials, and nonstructural contents were considered. The constitutive relationships included high strain-rate effects and failure criteria for the various materials.

The tower models used in the global impact analyses were developed based on the original WTC drawings and the structural databases of the towers developed within the framework of the baseline structural performance analysis. The tower models included the primary structural components of the towers in the impact zone, including exterior walls, floor systems, core columns, and connections. A refined finite element mesh was used for the areas in the path of the aircraft and a coarser mesh was used elsewhere. The models also included the nonstructural building contents, such as partitions and workstations, in the path of the aircraft debris.

The Boeing 767 aircraft model was developed based on information gathered from documentary aircraft structural information, and data from measurements on a Boeing 767 aircraft. The model included the aircraft engines, wings, fuselage, empennage, and landing gear, as well as nonstructural components of the aircraft. A detailed analysis was carried out to estimate the fuel distribution in the aircraft wings at the time of impact.

The WTC towers and Boeing 767 aircraft are complex structural systems. In the global model development process, the objective was to include all of the primary structural components and details of both the aircraft and towers. This approach, however, results in very large models. The component and subassembly analyses were used to determine model simplifications to reduce the overall model size while maintaining fidelity in the analysis. Therefore, a series of component impact and subassembly

analyses were performed. The primary objectives of the component and subassembly modeling were to (1) develop an understanding of the interactive failure phenomenon of the aircraft and tower components and (2) develop the simulation techniques required for the global analysis of the aircraft impacts into the WTC towers, including variations in mesh density and numerical tools for modeling fluid-structure interaction for fuel impact and dispersion. The approach taken for component modeling was to start with finely meshed models of key components of the tower and aircraft structures and progress to relatively coarsely meshed beam and shell element representations that were used for the global models. An example of component level analysis is the analysis of exterior wall panels impacted by a segment of an aircraft wing with and without fuel. An example of the subassembly analysis is an aircraft engine impacting a strip from the exterior wall to the core of the tower.

The initial conditions of the impact of the aircraft into the WTC towers were estimated. This task utilized the two videos that captured the approach and impact of the American Airlines flight 11, which impacted WTC 1, and the several videos that captured United Airlines flight 175, that impacted WTC 2. In addition, a large body of photographic evidence was used to determine the impact location and orientation relative to the towers. These videos and photographs were analyzed to estimate, with the best accuracy possible, the speed, horizontal and vertical angles of incidence, and roll angle of each aircraft. Uncertainties in each of these parameters were also quantified.

The analysis of aircraft impact into the WTC towers is subject to large uncertainties in the input parameters such as the initial conditions of the impact, material properties, mass properties of aircraft and building contents, connection behavior, modeling uncertainties, etc. Sensitivity analyses were performed at the component and subassembly levels. The objectives of these analyses were to assess the effect of uncertainties on the level of damage to the towers after impact and to determine the most influential parameters that affect the damage estimates.

The primary objective of this analysis was to determine the condition of the WTC towers immediately following the aircraft impacts using the global tower and aircraft models. This assessment included the estimation of the structural damage that degraded their strength and the condition and position of nonstructural contents such as partitions, workstations, aircraft fuel, and other debris that influenced the behavior of the subsequent fires in the towers. The global impact analyses were the primary method by which the damage to the towers was estimated. The global analyses included, for each tower, a “base case” based on a best estimate of all input parameters. They also provided more and less severe damage estimates based on variations of the most influential parameters. These more and less severe damage scenarios provided a range of damage estimates of the towers due to aircraft impact. Comparisons between the simulation results and observables obtained from video and photographic evidence as well as eyewitness interviews were also conducted. Not all of these observables were perfectly matched by the simulations due to the uncertainties in exact impact conditions, the imperfect knowledge of the interior tower contents, the chaotic behavior of the aircraft break up and subsequent debris motion, and the limitations of the models. In general, however, the results of the simulations matched these observables reasonably well. A comparison with prior estimates of the damage obtained from other studies was also provided.

Approximate impact analyses were carried out to provide guidance to the global finite element impact analyses. These included: (1) the analysis of the overall aircraft impact forces and assessment of the relative importance of the airframe strength and weight distribution, (2) the evaluation of the potential effects of the energy in the rotating engine components on the calculated engine impact response, (3) the influence of the static preloads in the towers on the calculated impact damage and residual strength predictions, and (4) the analysis of the load characteristics required to damage core columns compared to the potential loading from impact of aircraft components.

Keywords: Aircraft impact, aircraft model, dynamic analysis, failure, finite element analysis, fuel dispersion, structural dynamics, World Trade Center.

This page intentionally left blank.

TABLE OF CONTENTS

This page intentionally left blank.

LIST OF FIGURES

This page intentionally left blank.

LIST OF TABLES

LIST OF ACRONYMS AND ABBREVIATIONS

Acronyms

AA	American Airlines
ALE	Arbitrary-Lagrangian-Eulerian
ARA	Applied Research Associates, Incorporated
ASTM	American Society for Testing and Materials
CPU	central processing unit
FEMA	Federal Emergency Management Agency
HAZ	heat affected zone
LERA	Leslie E. Robertson Associates
LSTC	Livermore Software Technology Corporation
MIT	Massachusetts Institute of Technology
MDF	medium density fiberboard
NIST	National Institute of Standards and Technology
SPH	Smoothed Particle Hydrodynamics
UAL	United Airlines
ULD	unit load device
WTC	World Trade Center
WTC 1	World Trade Center 1 (North Tower)
WTC 2	World Trade Center 2 (South Tower)
WTC 7	World Trade Center 7

Abbreviations

±	plus or minus
ft	foot
ft^2	square foot
ft^3	cubic foot
gal	gallon
GHz	gigahertz
in.	inch

kip	a force equal to 1,000 pounds
ksi	1,000 pounds per square inch
lb	pound
min	minute
mph	miles per hour
ms	millisecond
psf	pounds per square foot
psi	pounds per square inch
s	second

PREFACE

Genesis of This Investigation

Immediately following the terrorist attack on the World Trade Center (WTC) on September 11, 2001, the Federal Emergency Management Agency (FEMA) and the American Society of Civil Engineers began planning a building performance study of the disaster. The week of October 7, as soon as the rescue and search efforts ceased, the Building Performance Study Team went to the site and began its assessment. This was to be a brief effort, as the study team consisted of experts who largely volunteered their time away from their other professional commitments. The Building Performance Study Team issued its report in May 2002, fulfilling its goal "to determine probable failure mechanisms and to identify areas of future investigation that could lead to practical measures for improving the damage resistance of buildings against such unforeseen events."

On August 21, 2002, with funding from the U.S. Congress through FEMA, the National Institute of Standards and Technology (NIST) announced its building and fire safety investigation of the WTC disaster. On October 1, 2002, the National Construction Safety Team Act (Public Law 107-231), was signed into law. The NIST WTC Investigation was conducted under the authority of the National Construction Safety Team Act.

The goals of the investigation of the WTC disaster were:

- To investigate the building construction, the materials used, and the technical conditions that contributed to the outcome of the WTC disaster.
- To serve as the basis for:
  - Improvements in the way buildings are designed, constructed, maintained, and used;
  - Improved tools and guidance for industry and safety officials;
  - Recommended revisions to current codes, standards, and practices; and
  - Improved public safety.

The specific objectives were:

1. Determine why and how WTC 1 and WTC 2 collapsed following the initial impacts of the aircraft and why and how WTC 7 collapsed;
2. Determine why the injuries and fatalities were so high or low depending on location, including all technical aspects of fire protection, occupant behavior, evacuation, and emergency response;
3. Determine what procedures and practices were used in the design, construction, operation, and maintenance of WTC 1, 2, and 7; and
4. Identify, as specifically as possible, areas in current building and fire codes, standards, and practices that warrant revision.

NIST is a nonregulatory agency of the U.S. Department of Commerce's Technology Administration. The purpose of NIST investigations is to improve the safety and structural integrity of buildings in the United States, and the focus is on fact finding. NIST investigative teams are authorized to assess building performance and emergency response and evacuation procedures in the wake of any building failure that has resulted in substantial loss of life or that posed significant potential of substantial loss of life. NIST does not have the statutory authority to make findings of fault nor negligence by individuals or organizations. Further, no part of any report resulting from a NIST investigation into a building failure or from an investigation under the National Construction Safety Team Act may be used in any suit or action for damages arising out of any matter mentioned in such report (15 USC 281a, as amended by Public Law 107-231).

Organization of the Investigation

The National Construction Safety Team for this Investigation, appointed by the then NIST Director, Dr. Arden L. Bement, Jr., was led by Dr. S. Shyam Sunder. Dr. William L. Grosshandler served as Associate Lead Investigator, Mr. Stephen A. Cauffman served as Program Manager for Administration, and Mr. Harold E. Nelson served on the team as a private sector expert. The Investigation included eight interdependent projects whose leaders comprised the remainder of the team. A detailed description of each of these eight projects is available at http://wtc.nist.gov. The purpose of each project is summarized in Table P–1, and the key interdependencies among the projects are illustrated in Fig. P–1.

Table P–1. Federal building and fire safety investigation of the WTC disaster.

Technical Area and Project Leader	Project Purpose
Analysis of Building and Fire Codes and Practices; Project Leaders: Dr. H. S. Lew and Mr. Richard W. Bukowski	Document and analyze the code provisions, procedures, and practices used in the design, construction, operation, and maintenance of the structural, passive fire protection, and emergency access and evacuation systems of WTC 1, 2, and 7.
Baseline Structural Performance and Aircraft Impact Damage Analysis; Project Leader: Dr. Fahim H. Sadek	Analyze the baseline performance of WTC 1 and WTC 2 under design, service, and abnormal loads, and aircraft impact damage on the structural, fire protection, and egress systems.
Mechanical and Metallurgical Analysis of Structural Steel; Project Leader: Dr. Frank W. Gayle	Determine and analyze the mechanical and metallurgical properties and quality of steel, weldments, and connections from steel recovered from WTC 1, 2, and 7.
Investigation of Active Fire Protection Systems; Project Leader: Dr. David D. Evans; Dr. William Grosshandler	Investigate the performance of the active fire protection systems in WTC 1, 2, and 7 and their role in fire control, emergency response, and fate of occupants and responders.
Reconstruction of Thermal and Tenability Environment; Project Leader: Dr. Richard G. Gann	Reconstruct the time-evolving temperature, thermal environment, and smoke movement in WTC 1, 2, and 7 for use in evaluating the structural performance of the buildings and behavior and fate of occupants and responders.
Structural Fire Response and Collapse Analysis; Project Leaders: Dr. John L. Gross and Dr. Therese P. McAllister	Analyze the response of the WTC towers to fires with and without aircraft damage, the response of WTC 7 in fires, the performance of composite steel-trussed floor systems, and determine the most probable structural collapse sequence for WTC 1, 2, and 7.
Occupant Behavior, Egress, and Emergency Communications; Project Leader: Mr. Jason D. Averill	Analyze the behavior and fate of occupants and responders, both those who survived and those who did not, and the performance of the evacuation system.
Emergency Response Technologies and Guidelines; Project Leader: Mr. J. Randall Lawson	Document the activities of the emergency responders from the time of the terrorist attacks on WTC 1 and WTC 2 until the collapse of WTC 7, including practices followed and technologies used.

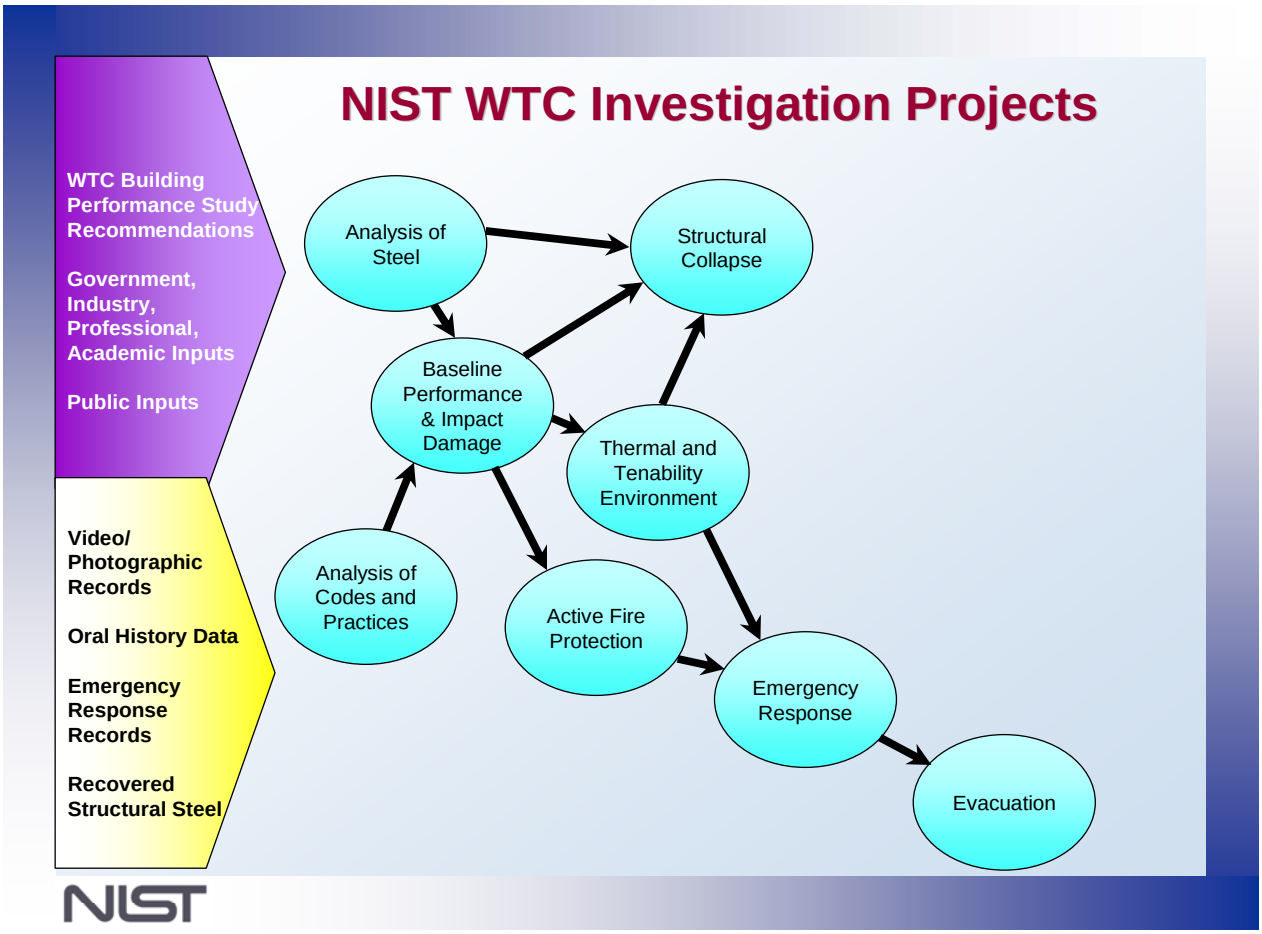

Figure P–1. The eight projects in the federal building and fire safety investigation of the WTC disaster.

National Construction Safety Team Advisory Committee

The NIST Director also established an advisory committee as mandated under the National Construction Safety Team Act. The initial members of the committee were appointed following a public solicitation. These were:

- Paul Fitzgerald, Executive Vice President (retired) FM Global, National Construction Safety Team Advisory Committee Chair
- John Barsom, President, Barsom Consulting, Ltd.
- John Bryan, Professor Emeritus, University of Maryland
- David Collins, President, The Preview Group, Inc.
- Glenn Corbett, Professor, John Jay College of Criminal Justice
- Philip DiNenno, President, Hughes Associates, Inc.

- Robert Hanson, Professor Emeritus, University of Michigan
- Charles Thornton, Co-Chairman and Managing Principal, The Thornton-Tomasetti Group, Inc.
- Kathleen Tierney, Director, Natural Hazards Research and Applications Information Center, University of Colorado at Boulder
- Forman Williams, Director, Center for Energy Research, University of California at San Diego

This National Construction Safety Team Advisory Committee provided technical advice during the Investigation and commentary on drafts of the Investigation reports prior to their public release. NIST has benefited from the work of many people in the preparation of these reports, including the National Construction Safety Team Advisory Committee. The content of the reports and recommendations, however, are solely the responsibility of NIST.

Public Outreach

During the course of this Investigation, NIST held public briefings and meetings (listed in Table P–2) to solicit input from the public, present preliminary findings, and obtain comments on the direction and progress of the Investigation from the public and the Advisory Committee.

NIST maintained a publicly accessible Web site during this Investigation at http://wtc.nist.gov. The site contained extensive information on the background and progress of the Investigation.

NIST's WTC Public-Private Response Plan

The collapse of the WTC buildings has led to broad reexamination of how tall buildings are designed, constructed, maintained, and used, especially with regard to major events such as fires, natural disasters, and terrorist attacks. Reflecting the enhanced interest in effecting necessary change, NIST, with support from Congress and the Administration, has put in place a program, the goal of which is to develop and implement the standards, technology, and practices needed for cost-effective improvements to the safety and security of buildings and building occupants, including evacuation, emergency response procedures, and threat mitigation.

The strategy to meet this goal is a three-part NIST-led public-private response program that includes:

- A federal building and fire safety investigation to study the most probable factors that contributed to post-aircraft impact collapse of the WTC towers and the 47-story WTC 7 building, and the associated evacuation and emergency response experience.
- A research and development (R&D) program to (a) facilitate the implementation of recommendations resulting from the WTC Investigation, and (b) provide the technical basis for cost-effective improvements to national building and fire codes, standards, and practices that enhance the safety of buildings, their occupants, and emergency responders.

Table P–2. Public meetings and briefings of the WTC Investigation.

Date	Location	Principal Agenda
June 24, 2002	New York City, NY	Public meeting: Public comments on the *Draft Plan* for the pending WTC Investigation.
August 21, 2002	Gaithersburg, MD	Media briefing announcing the formal start of the Investigation.
December 9, 2002	Washington, DC	Media briefing on release of the *Public Update* and NIST request for photographs and videos.
April 8, 2003	New York City, NY	Joint public forum with Columbia University on first-person interviews.
April 29–30, 2003	Gaithersburg, MD	NCST Advisory Committee meeting on plan for and progress on WTC Investigation with a public comment session.
May 7, 2003	New York City, NY	Media briefing on release of *May 2003 Progress Report.*
August 26–27, 2003	Gaithersburg, MD	NCST Advisory Committee meeting on status of the WTC investigation with a public comment session.
September 17, 2003	New York City, NY	Media and public briefing on initiation of first-person data collection projects.
December 2–3, 2003	Gaithersburg, MD	NCST Advisory Committee meeting on status and initial results and release of the *Public Update* with a public comment session.
February 12, 2004	New York City, NY	Public meeting on progress and preliminary findings with public comments on issues to be considered in formulating final recommendations.
June 18, 2004	New York City, NY	Media/public briefing on release of *June 2004 Progress Report.*
June 22–23, 2004	Gaithersburg, MD	NCST Advisory Committee meeting on the status of and preliminary findings from the WTC Investigation with a public comment session.
August 24, 2004	Northbrook, IL	Public viewing of standard fire resistance test of WTC floor system at Underwriters Laboratories, Inc.
October 19–20, 2004	Gaithersburg, MD	NCST Advisory Committee meeting on status and near complete set of preliminary findings with a public comment session.
November 22, 2004	Gaithersburg, MD	NCST Advisory Committee discussion on draft annual report to Congress, a public comment session, and a closed session to discuss pre-draft recommendations for WTC Investigation.
April 5, 2005	New York City, NY	Media and public briefing on release of the probable collapse sequence for the WTC towers and draft reports for the projects on codes and practices, evacuation, and emergency response.
June 23, 2005	New York City, NY	Media and public briefing on release of all draft reports for the WTC towers and draft recommendations for public comment.
September 12–13, 2005	Gaithersburg, MD	NCST Advisory Committee meeting on disposition of public comments and update to draft reports for the WTC towers.
September 13–15, 2005	Gaithersburg, MD	WTC Technical Conference for stakeholders and technical community for dissemination of findings and recommendations and opportunity for public to make technical comments.

- A dissemination and technical assistance program (DTAP) to (a) engage leaders of the construction and building community in ensuring timely adoption and widespread use of proposed changes to practices, standards, and codes resulting from the WTC Investigation and the R&D program, and (b) provide practical guidance and tools to better prepare facility owners, contractors, architects, engineers, emergency responders, and regulatory authorities to respond to future disasters.

The desired outcomes are to make buildings, occupants, and first responders safer in future disaster events.

National Construction Safety Team Reports on the WTC Investigation

A final report on the collapse of the WTC towers is being issued as NIST NCSTAR 1. A companion report on the collapse of WTC 7 is being issued as NIST NCSTAR 1A. The present report is one of a set that provides more detailed documentation of the Investigation findings and the means by which these technical results were achieved. As such, it is part of the archival record of this Investigation. The titles of the full set of Investigation publications are:

NIST (National Institute of Standards and Technology). 2005. *Federal Building and Fire Safety Investigation of the World Trade Center Disaster: Final Report on the Collapse of the World Trade Center Towers.* NIST NCSTAR 1. Gaithersburg, MD, September.

NIST (National Institute of Standards and Technology). 2008. *Federal Building and Fire Safety Investigation of the World Trade Center Disaster: Final Report on the Collapse of World Trade Center 7.* NIST NCSTAR 1A. Gaithersburg, MD, November.

Lew, H. S., R. W. Bukowski, and N. J. Carino. 2005. *Federal Building and Fire Safety Investigation of the World Trade Center Disaster: Design, Construction, and Maintenance of Structural and Life Safety Systems.* NIST NCSTAR 1-1. National Institute of Standards and Technology. Gaithersburg, MD, September.

Fanella, D. A., A. T. Derecho, and S. K. Ghosh. 2005. *Federal Building and Fire Safety Investigation of the World Trade Center Disaster: Design and Construction of Structural Systems.* NIST NCSTAR 1-1A. National Institute of Standards and Technology. Gaithersburg, MD, September.

Ghosh, S. K., and X. Liang. 2005. *Federal Building and Fire Safety Investigation of the World Trade Center Disaster: Comparison of Building Code Structural Requirements.* NIST NCSTAR 1-1B. National Institute of Standards and Technology. Gaithersburg, MD, September.

Fanella, D. A., A. T. Derecho, and S. K. Ghosh. 2005. *Federal Building and Fire Safety Investigation of the World Trade Center Disaster: Maintenance and Modifications to Structural Systems.* NIST NCSTAR 1-1C. National Institute of Standards and Technology. Gaithersburg, MD, September.

Grill, R. A., and D. A. Johnson. 2005. *Federal Building and Fire Safety Investigation of the World Trade Center Disaster: Fire Protection and Life Safety Provisions Applied to the Design and Construction of World Trade Center 1, 2, and 7 and Post-Construction Provisions Applied after Occupancy*. NIST NCSTAR 1-1D. National Institute of Standards and Technology. Gaithersburg, MD, September.

Razza, J. C., and R. A. Grill. 2005. *Federal Building and Fire Safety Investigation of the World Trade Center Disaster: Comparison of Codes, Standards, and Practices in Use at the Time of the Design and Construction of World Trade Center 1, 2, and 7.* NIST NCSTAR 1-1E. National Institute of Standards and Technology. Gaithersburg, MD, September.

Grill, R. A., D. A. Johnson, and D. A. Fanella. 2005. *Federal Building and Fire Safety Investigation of the World Trade Center Disaster: Comparison of the 1968 and Current (2003) New*

York City Building Code Provisions. NIST NCSTAR 1-1F. National Institute of Standards and Technology. Gaithersburg, MD, September.

Grill, R. A., and D. A. Johnson. 2005. *Federal Building and Fire Safety Investigation of the World Trade Center Disaster: Amendments to the Fire Protection and Life Safety Provisions of the New York City Building Code by Local Laws Adopted While World Trade Center 1, 2, and 7 Were in Use*. NIST NCSTAR 1-1G. National Institute of Standards and Technology. Gaithersburg, MD, September.

Grill, R. A., and D. A. Johnson. 2005. *Federal Building and Fire Safety Investigation of the World Trade Center Disaster: Post-Construction Modifications to Fire Protection and Life Safety Systems of World Trade Center 1 and 2*. NIST NCSTAR 1-1H. National Institute of Standards and Technology. Gaithersburg, MD, September.

Grill, R. A., D. A. Johnson, and D. A. Fanella. 2005. *Federal Building and Fire Safety Investigation of the World Trade Center Disaster: Post-Construction Modifications to Fire Protection, Life Safety, and Structural Systems of World Trade Center 7*. NIST NCSTAR 1-1I. National Institute of Standards and Technology. Gaithersburg, MD, September.

Grill, R. A., and D. A. Johnson. 2005. *Federal Building and Fire Safety Investigation of the World Trade Center Disaster: Design, Installation, and Operation of Fuel System for Emergency Power in World Trade Center 7*. NIST NCSTAR 1-1J. National Institute of Standards and Technology. Gaithersburg, MD, September.

Sadek, F. 2005. *Federal Building and Fire Safety Investigation of the World Trade Center Disaster: Baseline Structural Performance and Aircraft Impact Damage Analysis of the World Trade Center Towers.* NIST NCSTAR 1-2. National Institute of Standards and Technology. Gaithersburg, MD, September.

Faschan, W. J., and R. B. Garlock. 2005. *Federal Building and Fire Safety Investigation of the World Trade Center Disaster: Reference Structural Models and Baseline Performance Analysis of the World Trade Center Towers.* NIST NCSTAR 1-2A. National Institute of Standards and Technology. Gaithersburg, MD, September.

Kirkpatrick, S. W., R. T. Bocchieri, F. Sadek, R. A. MacNeill, S. Holmes, B. D. Peterson, R. W. Cilke, C. Navarro. 2005. *Federal Building and Fire Safety Investigation of the World Trade Center Disaster: Analysis of Aircraft Impacts into the World Trade Center Towers*, NIST NCSTAR 1-2B. National Institute of Standards and Technology. Gaithersburg, MD, September.

Gayle, F. W., R. J. Fields, W. E. Luecke, S. W. Banovic, T. Foecke, C. N. McCowan, T. A. Siewert, and J. D. McColskey. 2005. *Federal Building and Fire Safety Investigation of the World Trade Center Disaster: Mechanical and Metallurgical Analysis of Structural Steel.* NIST NCSTAR 1-3. National Institute of Standards and Technology. Gaithersburg, MD, September.

Luecke, W. E., T. A. Siewert, and F. W. Gayle. 2005. *Federal Building and Fire Safety Investigation of the World Trade Center Disaster: Contemporaneous Structural Steel Specifications.* NIST Special Publication 1-3A. National Institute of Standards and Technology. Gaithersburg, MD, September.

Banovic, S. W. 2005. *Federal Building and Fire Safety Investigation of the World Trade Center Disaster: Steel Inventory and Identification.* NIST NCSTAR 1-3B. National Institute of Standards and Technology. Gaithersburg, MD, September.

Banovic, S. W., and T. Foecke. 2005. *Federal Building and Fire Safety Investigation of the World Trade Center Disaster: Damage and Failure Modes of Structural Steel Components.* NIST NCSTAR 1-3C. National Institute of Standards and Technology. Gaithersburg, MD, September.

Luecke, W. E., J. D. McColskey, C. N. McCowan, S. W. Banovic, R. J. Fields, T. Foecke, T. A. Siewert, and F. W. Gayle. 2005. *Federal Building and Fire Safety Investigation of the World Trade Center Disaster: Mechanical Properties of Structural Steels.* NIST NCSTAR 1-3D. National Institute of Standards and Technology. Gaithersburg, MD, September.

Banovic, S. W., C. N. McCowan, and W. E. Luecke. 2005. *Federal Building and Fire Safety Investigation of the World Trade Center Disaster: Physical Properties of Structural Steels.* NIST NCSTAR 1-3E. National Institute of Standards and Technology. Gaithersburg, MD, September.

Evans, D. D., R. D. Peacock, E. D. Kuligowski, W. S. Dols, and W. L. Grosshandler. 2005. *Federal Building and Fire Safety Investigation of the World Trade Center Disaster: Active Fire Protection Systems.* NIST NCSTAR 1-4. National Institute of Standards and Technology. Gaithersburg, MD, September.

Kuligowski, E. D., D. D. Evans, and R. D. Peacock. 2005. *Federal Building and Fire Safety Investigation of the World Trade Center Disaster: Post-Construction Fires Prior to September 11, 2001.* NIST NCSTAR 1-4A. National Institute of Standards and Technology. Gaithersburg, MD, September.

Hopkins, M., J. Schoenrock, and E. Budnick. 2005. *Federal Building and Fire Safety Investigation of the World Trade Center Disaster: Fire Suppression Systems.* NIST NCSTAR 1-4B. National Institute of Standards and Technology. Gaithersburg, MD, September.

Keough, R. J., and R. A. Grill. 2005. *Federal Building and Fire Safety Investigation of the World Trade Center Disaster: Fire Alarm Systems.* NIST NCSTAR 1-4C. National Institute of Standards and Technology. Gaithersburg, MD, September.

Ferreira, M. J., and S. M. Strege. 2005. *Federal Building and Fire Safety Investigation of the World Trade Center Disaster: Smoke Management Systems.* NIST NCSTAR 1-4D. National Institute of Standards and Technology. Gaithersburg, MD, September.

Gann, R. G., A. Hamins, K. B. McGrattan, G. W. Mulholland, H. E. Nelson, T. J. Ohlemiller, W. M. Pitts, and K. R. Prasad. 2005. *Federal Building and Fire Safety Investigation of the World Trade Center Disaster: Reconstruction of the Fires in the World Trade Center Towers.* NIST NCSTAR 1-5. National Institute of Standards and Technology. Gaithersburg, MD, September.

Pitts, W. M., K. M. Butler, and V. Junker. 2005. *Federal Building and Fire Safety Investigation of the World Trade Center Disaster: Visual Evidence, Damage Estimates, and Timeline Analysis.* NIST NCSTAR 1-5A. National Institute of Standards and Technology. Gaithersburg, MD, September.

Hamins, A., A. Maranghides, K. B. McGrattan, E. Johnsson, T. J. Ohlemiller, M. Donnelly, J. Yang, G. Mulholland, K. R. Prasad, S. Kukuck, R. Anleitner and T. McAllister. 2005. *Federal Building and Fire Safety Investigation of the World Trade Center Disaster: Experiments and Modeling of Structural Steel Elements Exposed to Fire.* NIST NCSTAR 1-5B. National Institute of Standards and Technology. Gaithersburg, MD, September.

Ohlemiller, T. J., G. W. Mulholland, A. Maranghides, J. J. Filliben, and R. G. Gann. 2005. *Federal Building and Fire Safety Investigation of the World Trade Center Disaster: Fire Tests of Single Office Workstations.* NIST NCSTAR 1-5C. National Institute of Standards and Technology. Gaithersburg, MD, September.

Gann, R. G., M. A. Riley, J. M. Repp, A. S. Whittaker, A. M. Reinhorn, and P. A. Hough. 2005. *Federal Building and Fire Safety Investigation of the World Trade Center Disaster: Reaction of Ceiling Tile Systems to Shocks.* NIST NCSTAR 1-5D. National Institute of Standards and Technology. Gaithersburg, MD, September.

Hamins, A., A. Maranghides, K. B. McGrattan, T. J. Ohlemiller, and R. Anleitner. 2005. *Federal Building and Fire Safety Investigation of the World Trade Center Disaster: Experiments and Modeling of Multiple Workstations Burning in a Compartment.* NIST NCSTAR 1-5E. National Institute of Standards and Technology. Gaithersburg, MD, September.

McGrattan, K. B., C. Bouldin, and G. Forney. 2005. *Federal Building and Fire Safety Investigation of the World Trade Center Disaster: Computer Simulation of the Fires in the World Trade Center Towers.* NIST NCSTAR 1-5F. National Institute of Standards and Technology. Gaithersburg, MD, September.

Prasad, K. R., and H. R. Baum. 2005. *Federal Building and Fire Safety Investigation of the World Trade Center Disaster: Fire Structure Interface and Thermal Response of the World Trade Center Towers.* NIST NCSTAR 1-5G. National Institute of Standards and Technology. Gaithersburg, MD, September.

Gross, J. L., and T. McAllister. 2005. *Federal Building and Fire Safety Investigation of the World Trade Center Disaster: Structural Fire Response and Probable Collapse Sequence of the World Trade Center Towers.* NIST NCSTAR 1-6. National Institute of Standards and Technology. Gaithersburg, MD, September.

Carino, N. J., M. A. Starnes, J. L. Gross, J. C. Yang, S. Kukuck, K. R. Prasad, and R. W. Bukowski. 2005. *Federal Building and Fire Safety Investigation of the World Trade Center Disaster: Passive Fire Protection.* NIST NCSTAR 1-6A. National Institute of Standards and Technology. Gaithersburg, MD, September.

Gross, J., F. Hervey, M. Izydorek, J. Mammoser, and J. Treadway. 2005. *Federal Building and Fire Safety Investigation of the World Trade Center Disaster: Fire Resistance Tests of Floor Truss Systems.* NIST NCSTAR 1-6B. National Institute of Standards and Technology. Gaithersburg, MD, September.

Zarghamee, M. S., S. Bolourchi, D. W. Eggers, Ö. O. Erbay, F. W. Kan, Y. Kitane, A. A. Liepins, M. Mudlock, W. I. Naguib, R. P. Ojdrovic, A. T. Sarawit, P. R Barrett, J. L. Gross, and

T. P. McAllister. 2005. *Federal Building and Fire Safety Investigation of the World Trade Center Disaster: Component, Connection, and Subsystem Structural Analysis.* NIST NCSTAR 1-6C. National Institute of Standards and Technology. Gaithersburg, MD, September.

Zarghamee, M. S., Y. Kitane, Ö. O. Erbay, T. P. McAllister, and J. L. Gross. 2005. *Federal Building and Fire Safety Investigation of the World Trade Center Disaster: Global Structural Analysis of the Response of the World Trade Center Towers to Impact Damage and Fire.* NIST NCSTAR 1-6D. National Institute of Standards and Technology. Gaithersburg, MD, September.

Averill, J. D., D. S. Mileti, R. D. Peacock, E. D. Kuligowski, N. Groner, G. Proulx, P. A. Reneke, and H. E. Nelson. 2005. *Federal Building and Fire Safety Investigation of the World Trade Center Disaster: Occupant Behavior, Egress, and Emergency Communication.* NIST NCSTAR 1-7. National Institute of Standards and Technology. Gaithersburg, MD, September.

Fahy, R., and G. Proulx. 2005. *Federal Building and Fire Safety Investigation of the World Trade Center Disaster: Analysis of Published Accounts of the World Trade Center Evacuation.* NIST NCSTAR 1-7A. National Institute of Standards and Technology. Gaithersburg, MD, September.

Zmud, J. 2005. *Federal Building and Fire Safety Investigation of the World Trade Center Disaster: Technical Documentation for Survey Administration.* NIST NCSTAR 1-7B. National Institute of Standards and Technology. Gaithersburg, MD, September.

Lawson, J. R., and R. L. Vettori. 2005. *Federal Building and Fire Safety Investigation of the World Trade Center Disaster: The Emergency Response Operations.* NIST NCSTAR 1-8. National Institute of Standards and Technology. Gaithersburg, MD, September.

McAllister, T., R. G. Gann, J. D. Averill, J. L. Gross, W. L. Grosshandler, J. R. Lawson, K. B. McGrattan, H. E. Nelson, W. M. Pitts, K. R. Prasad, F. H. Sadek. 2008. *Federal Building and Fire Safety Investigation of the World Trade Center Disaster: Structural Fire Response and Probable Collapse Sequence of World Trade Center Building 7.* NIST NCSTAR 1-9. National Institute of Standards and Technology. Gaithersburg, MD, November.

MacNeill, R., S. Kirkpatrick, B. Peterson, and R. Bocchieri. 2008. *Federal Building and Fire Safety Investigation of the World Trade Center Disaster: Global Structural Analysis of the Response of World Trade Center Building 7 to Fires and Debris Impact Damage.* NIST NCSTAR 1-9A. National Institute of Standards and Technology. Gaithersburg, MD, November.

ACKNOWLEDGMENTS

Applied Research Associates, Inc. (ARA) supported the National Institute of Standards and Technology (NIST) World Trade Center (WTC) Investigation by performing analyses of aircraft impacts into the WTC towers. A collaborative relationship was developed among the NIST Investigation Team that greatly contributed to the success of this effort. The high level of commitment and cooperation of all the Investigation participants both at NIST and their various contractors was greatly appreciated by ARA.

The results presented in this report are from the analysis efforts at ARA in collaboration with Dr. Fahim Sadek of NIST, Leader of Project 2 of the NIST Investigation. The authors would like to acknowledge several investigation team members that participated directly to the success of this project. Leslie E. Robertson Associates (LERA) developed the structural databases in an electronic format that were crucial in the development of the WTC tower models for the impact analyses. Several NIST investigators, including Dr. William Luecke, Dr. Richard Fields, Dr. Frank Gayle, Dr. Tim Foecke, and Dr. Stephen Banovic contributed to the development of the WTC tower material models by providing invaluable materials test data.

The development of the aircraft model could not have been completed without the support of Dr. Peter Dunn (ARA) who contributed to the data collection effort on the Boeing 767 structure. Similarly, Dr. Matthew Koebbe of GADAB engineering provided significant support in the development of the finite element mesh for the Boeing 767 model.

The methodologies used in the uncertainty analyses were developed by Dr. Justin Wu, Marsh Hardy, and Dr. Youngwon Shin of ARA. The authors also want to thank Dr. James Filliben of NIST for his guidance in the performance of the uncertainty analyses. Dr. Filliben contributed significantly to the methodologies that allowed a large reduction in the total number of analyses required and to the presentation of the probabilistic analyses.

Several other NIST investigators made important contributions to this effort. In particular, Dr. Therese McAllister provided guidance throughout the Investigation and contributed to the characterization and presentation of the WTC tower damage states in the impact analyses. In addition, Dr. William Pitts provided considerable assistance in the interpretation of the video and photographic data collected by NIST. This visual data was used as the basis of both the analysis of the aircraft impact conditions and the comparison of calculated impact response to observables.

This page intentionally left blank.

EXECUTIVE SUMMARY

E.1 INTRODUCTION

As part of the National Institute of Standards and Technology (NIST) Investigation into the collapse of the World Trade Center (WTC) towers, under contract from NIST, Applied Research Associates, Inc. (ARA) conducted the analysis of the aircraft impacts into the WTC towers. The objective of this effort was to analyze the aircraft impacts to determine the following: (1) estimates of probable damage to structural systems, including the exterior walls, floor systems, and interior core columns; (2) estimates of the aircraft fuel dispersal during the impact; and (3) estimates of debris damage to the interior tower contents, including partitions and workstations to be used for estimating damage to fire proofing and to the mechanical and architectural systems inside the towers. Thus, this analysis established the initial conditions for the fire dynamics modeling and the thermal-structural response and collapse initiation analysis of the NIST Investigation.

The WTC aircraft impact analysis is very complex, with large scale fracture and fragmentation of both tower and aircraft structures, nonlinear rate-dependent material behaviors, and the fluid-structure interaction of the aircraft fuel. The analyses of the aircraft impacts performed for this investigation are believed to be the highest-fidelity simulations ever performed for this impact behavior using state-of-the art analysis methodologies. Wherever possible, the models were validated against observables or supporting test data developed by the WTC Investigation.

The impact analyses were conducted at various levels of complexity including: (1) the component level, (2) the subassembly level, and (3) the global level to estimate the probable damage to the towers due to aircraft impact. Analysis of uncertainties using the component, subassembly, and global analyses were also conducted to assess the effect of uncertainties associated with various parameters on the damage estimates and to identify the most influential parameters that affect the impact response.

E.2 MATERIAL CONSTITUTIVE MODELING

An important requirement for high fidelity simulation of the aircraft impact damage was the development of constitutive models that represent the actual behavior of the WTC towers and aircraft under the dynamic impact conditions. The materials that were considered included: (1) the several grades of steel used in the columns, spandrels, and floor trusses and beams of the WTC towers, (2) the concrete floor slabs, (3) the various aluminum and titanium alloys used in the aircraft, and (4) the nonstructural contents of the towers. These materials exhibit significant nonlinear rate-dependent deformation and failure behavior that need to be represented in the constitutive relationship. The following is a brief summary of the constitutive models used for these materials.

WTC Tower Steel Constitutive Models

The primary constitutive model that was used for the tower steels was the Piecewise Linear Plasticity model in LS-DYNA. This model is sufficient to model the nonlinear rate-dependent deformation and failure of the steel structures. A tabular effective stress versus effective strain curve was used in this

model with various definitions of strain rate dependency. The constitutive model parameters for each grade of steel were based on engineering stress-strain data obtained from the mechanical and metallurgical analysis of the NIST Investigation. Finite element analyses of the test specimens were conducted with a fine and a medium mesh (similar to that used in the component level analysis) to capture the nonlinear material behavior up to failure (Figure E–1). The finite element analysis provided a validation that the constitutive model parameters were defined accurately and that the model could reproduce the measured response for the test conditions.

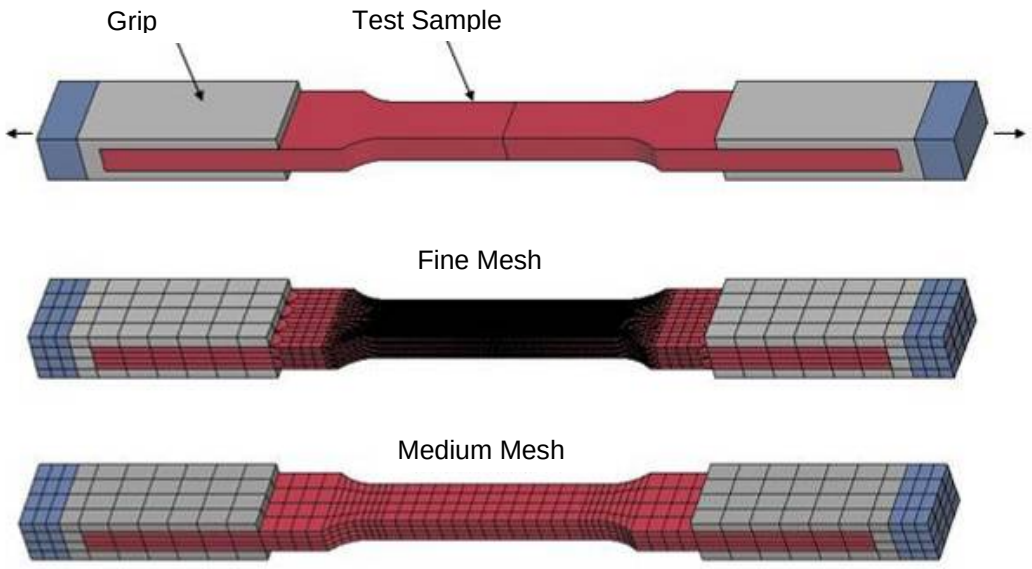

Figure E–1. Finite element models of the ASTM 370 rectangular tensile specimen.

The first step in the constitutive model development process was to obtain a true stress-true strain curve. The typical approach was to select a representative test for each grade of steel and convert the engineering stress-strain curve to true stress-strain. The true stress-strain curve was extrapolated beyond the point of necking onset. This curve was the input used to specify the mechanical behavior in the simulation of the tensile test (Figure E–1). If necessary, the extrapolation of the true stress-strain behavior was adjusted until the simulation matched the measured engineering stress-strain response, including necking and failure. A summary of the true stress-strain curves used in the constitutive models for the various WTC tower steels are summarized in Figure E–2.

Strain-rate effects on the steel yield strength were included in the constitutive model for tower steels with the Cowper and Symonds rate effect model. The resulting rate effects used in the constitutive modeling of tower steels based on this model are compared to the measured high rate test data for the 50 ksi, 75 ksi, and 100 ksi tower steels in Figure E–3. In the figure, the dashed lines with open symbols are the fits using the Cowper and Symonds model, while the corresponding solid symbols are the experimental data. The comparison showed that the Cowper and Symonds model was capable of reproducing the rate effects for the range of data available.

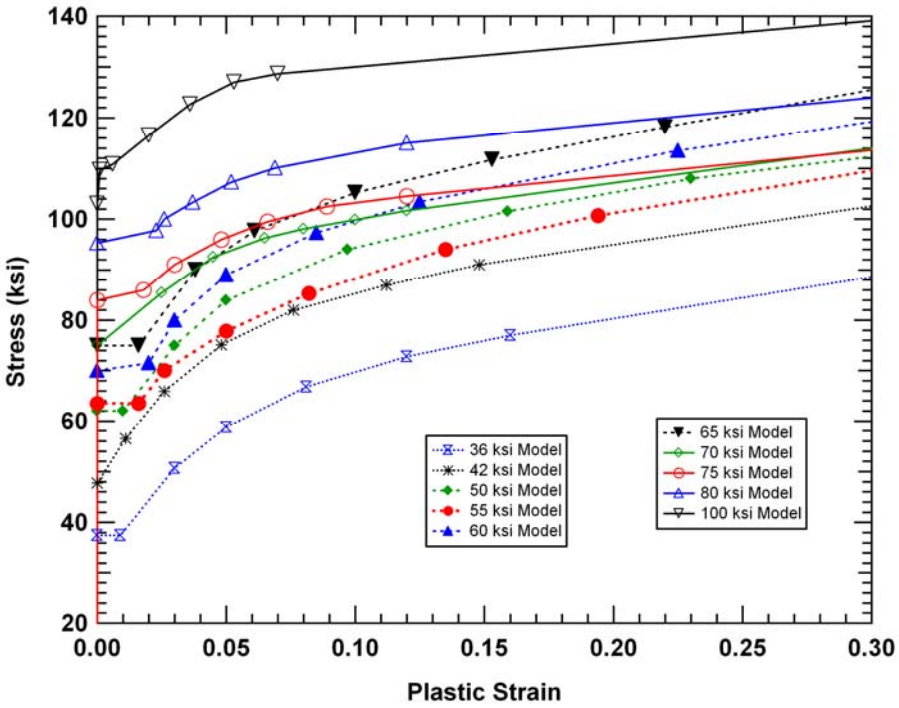

Figure E–2. Tabular true stress-strain constitutive model curves for the tower steels.

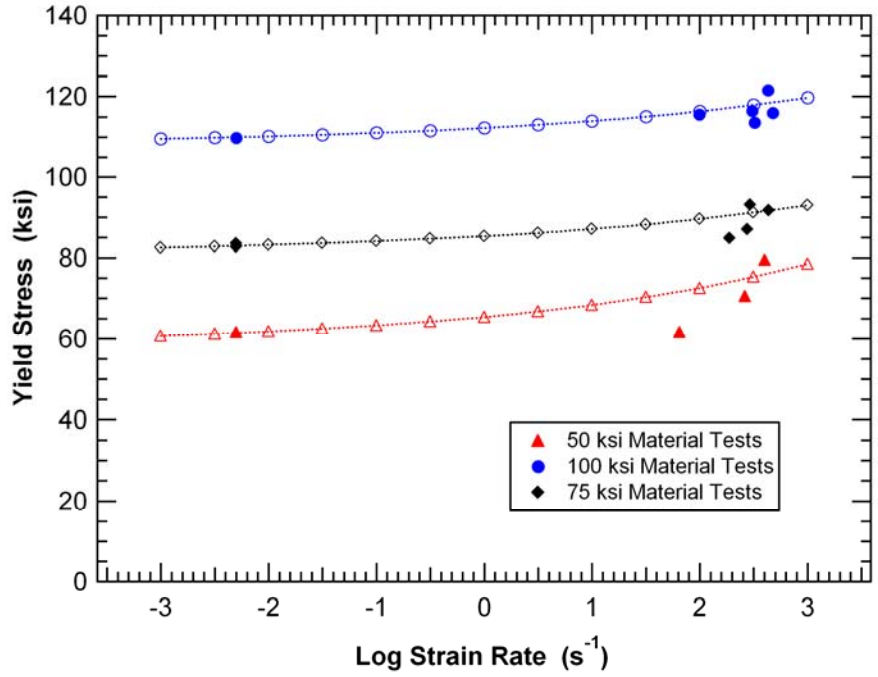

Figure E–3. Comparison of rate effects model and test data.

Concrete Constitutive Models

The LS-DYNA material Type 16 (pseudo-tensor concrete model) was selected for modeling the concrete floor slabs due to its ability to accurately model the damage and softening behavior of concrete associated with low confinement conditions. The model uses two pressure-dependent yield functions and a damage-dependent function to migrate between curves. This allows for implementation of tensile failure and damage scaling, which are more dominant material behaviors at low confinement. The pseudo-tensor model also accounts for the sensitivity of concrete to high strain-rates. Material constitutive parameters for the pseudo-tensor model were developed. A simulation was performed of a standard unconfined concrete compression test to check the constitutive model behavior. The simulated behavior of the concrete specimen is shown in Figure E–4. The calculated compressive stress-strain response for the 3 ksi concrete was compared to measured compression data for 2.3 ksi and 3.8 ksi strength concretes in Figure E–5.

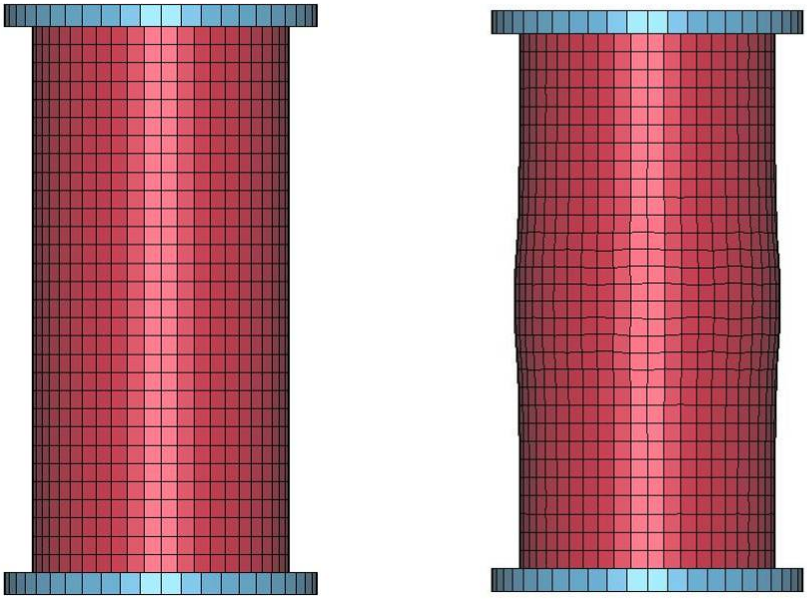

Initial configuration 2% compression

Figure E–4. Finite element analysis of the unconfined compression test.

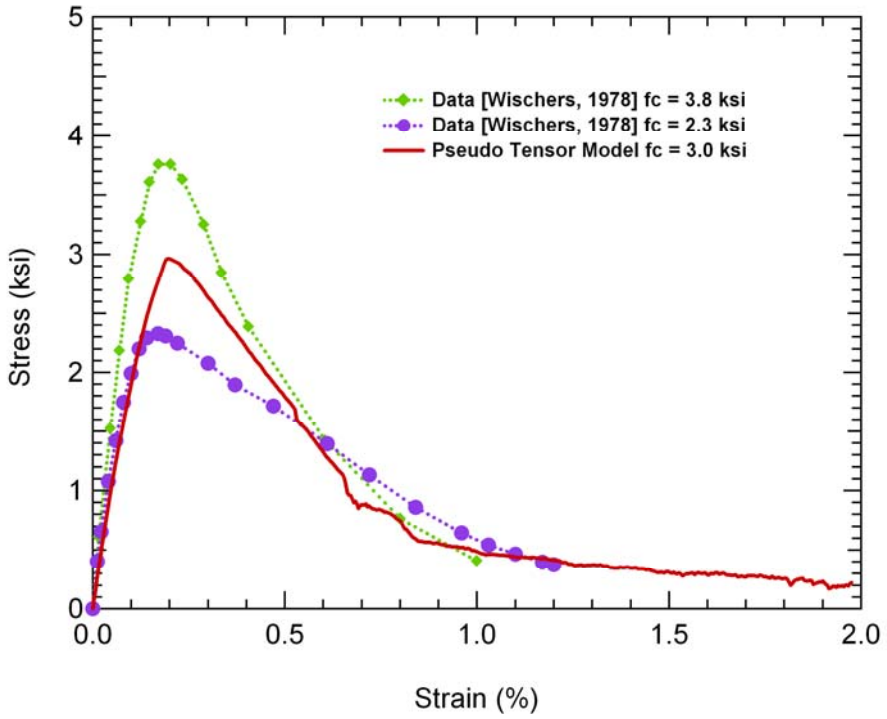

Figure E–5. Comparison of the calculated unconfined compression behavior with concrete compression test data.

Aircraft Materials Constitutive Models

The constitutive and failure properties for the aircraft materials were developed from data available in the open literature. Complete engineering stress-strain curves were obtained for various 2024 and 7075 aluminum alloys that are commonly used in the construction of the Boeing 767 airframe structures. These curves were digitized for the various aluminum alloys. Representative stress-strain curves were then converted into true stress and true strain and used to develop tabular curves for constitutive models. The tabular constitutive model fits are shown in Figure E–6. No rate sensitivity of the aircraft materials was considered.

Nonstructural Materials Constitutive Models

The primary influence of the nonstructural components on the impact behavior is their inertial contribution. The effects of their strength are small. As a result, relatively simple approximations of their constitutive behavior were used. Typically, a bilinear elastic-plastic constitutive model was applied for these materials to allow for efficient modeling of deformation and subsequent erosion from the calculations as their distortions become large. The ability to include material failure and erosion of these soft materials was important for the stability of the impact analyses.

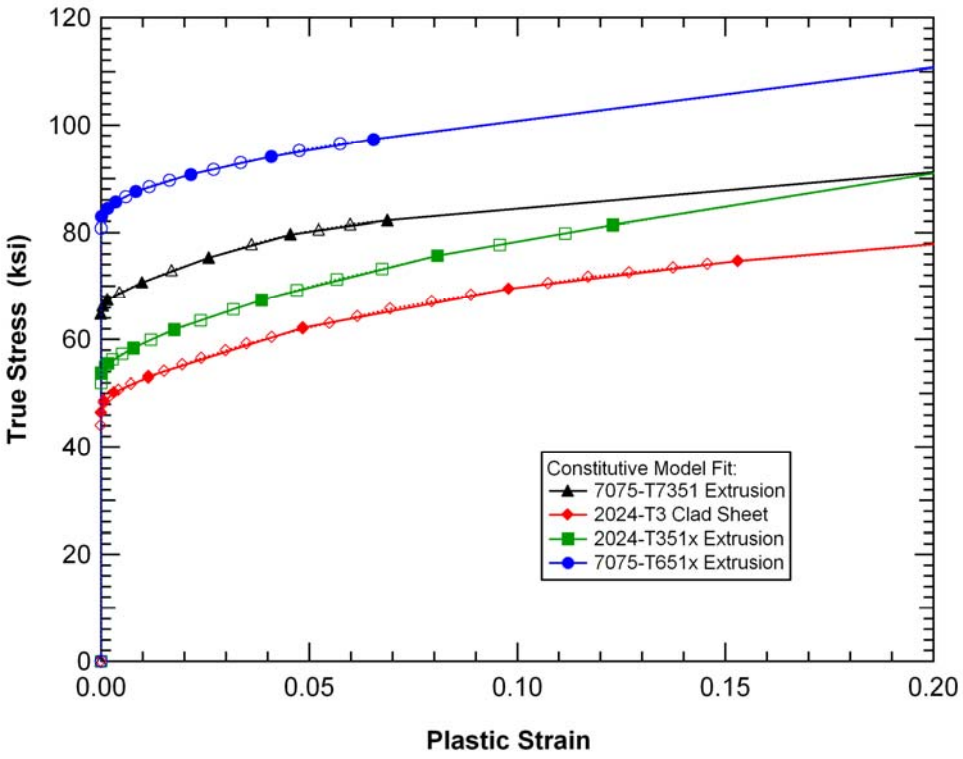

Figure E–6. True stress-strain curves developed for various aircraft aluminum alloys.

E.3 TOWER MODEL DEVELOPMENT

One of the significant challenges in developing the tower and aircraft models for the global impact analyses was to minimize the model size while keeping sufficient fidelity in the impact zone to capture the deformations and damage distributions. The limitation was that the combined aircraft and tower models should not exceed approximately 2.3 million nodes. These were distributed between the global WTC tower model and the aircraft so that the tower model would be about 1.5 million nodes and the aircraft about 0.8 million nodes. The approach used to meet this objective was to develop models for the various tower components at different levels of refinement. Components in the path of the impact and debris field were meshed with a higher resolution to capture the local impact damage and failure, while components outside the impact zone were meshed more coarsely to primarily capture their structural stiffness and inertial properties.

A summary of the size of the global impact models of both towers is presented in Table E–1. As the table indicates, the towers were modeled primarily with shell elements with the exception of the exterior wall bolted connections (beam and brick elements) and the floor truss diagonals (beam elements). The WTC 1 model extended between floors 92 and 100, while the WTC 2 model extended between floors 85 and 77.

Table E–1. Summary of the global impact models for the WTC towers.

	WTC 1 Tower Model	WTC 2 Tower Model
Number of Nodes	1,300,537	1,312,092
Hughes-Liu Beam Elements	47,952	53,488
Belytschko-Tsay Shell Elements	1,156,947	1,155,815
Constant Stress Solid Elements	2,805	2,498

The global impact models of the WTC towers included the following components:

- Core columns and floors: Core columns were modeled using shell elements with two mesh densities, a refined density in the direct impact area and a coarser far field density elsewhere. The spliced column connections were included in the model with proper failure criteria. The floors within the core were modeled using shell elements representing the floor slabs and beams. A generated model for the core of WTC 1 between floors 94 and 98 is shown in Figure E–7.

- Exterior walls: The exterior columns and spandrels were modeled using shell elements with two mesh densities, a refined density in the immediate impact zone and a coarser far field density elsewhere. For the bolted connections between exterior panels in the refined mesh areas, brick elements were used to model the butt plates and beam elements were used for the bolts. The model of the impact face of WTC 1 is shown in Figure E–8.

- Truss floor: In the direct impact area, the floor model included shell elements for the combined floor slab and metal decking, and for the upper and lower chords of both the primary and bridging trusses. Beam elements were used for the truss diagonals. In the far field floor segments, simplified shell element representations were used for the floor slab and trusses. A model assembled for the entire 96th floor of WTC 1 is shown in Figure E–9.

- Interior building contents: The interior nonstructural contents of the towers were modeled explicitly. These included the partitions and workstations, which were modeled with shell elements in the path of the aircraft debris. The live load mass was distributed between the partitions and cubicle workstations. The resulting model of a floor with interior contents is shown in Figure E–10.

Figure E–11 shows the assembled global impact model of WTC 1.

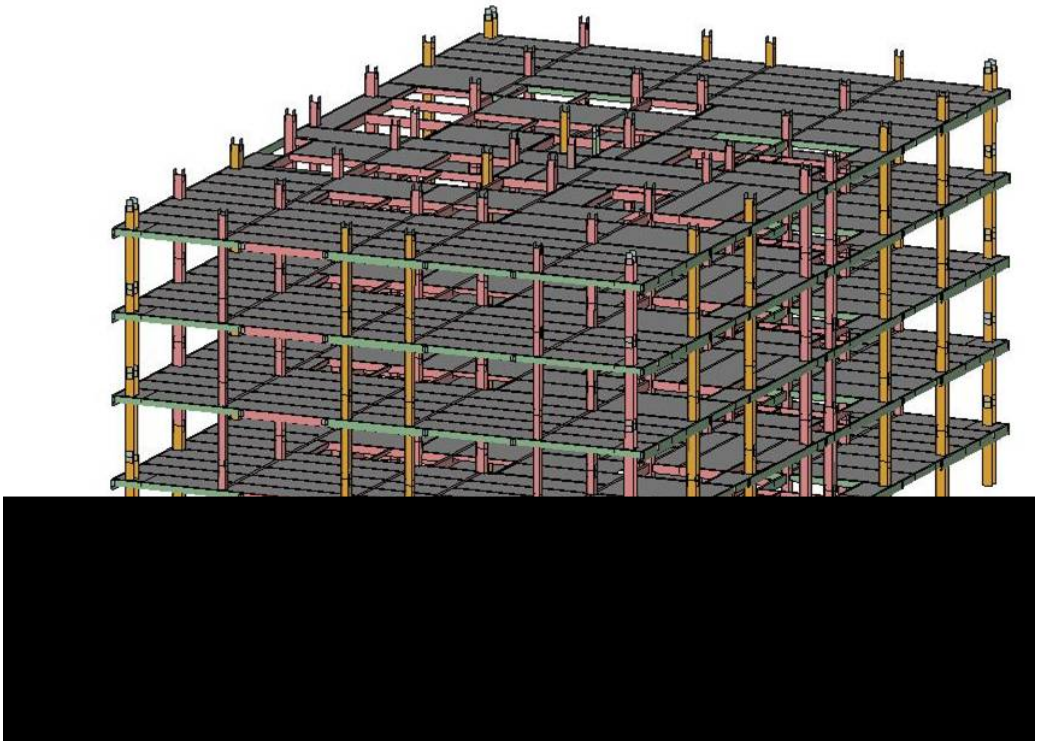

Figure E–7. Model of the WTC 1 core, floors 94–98.

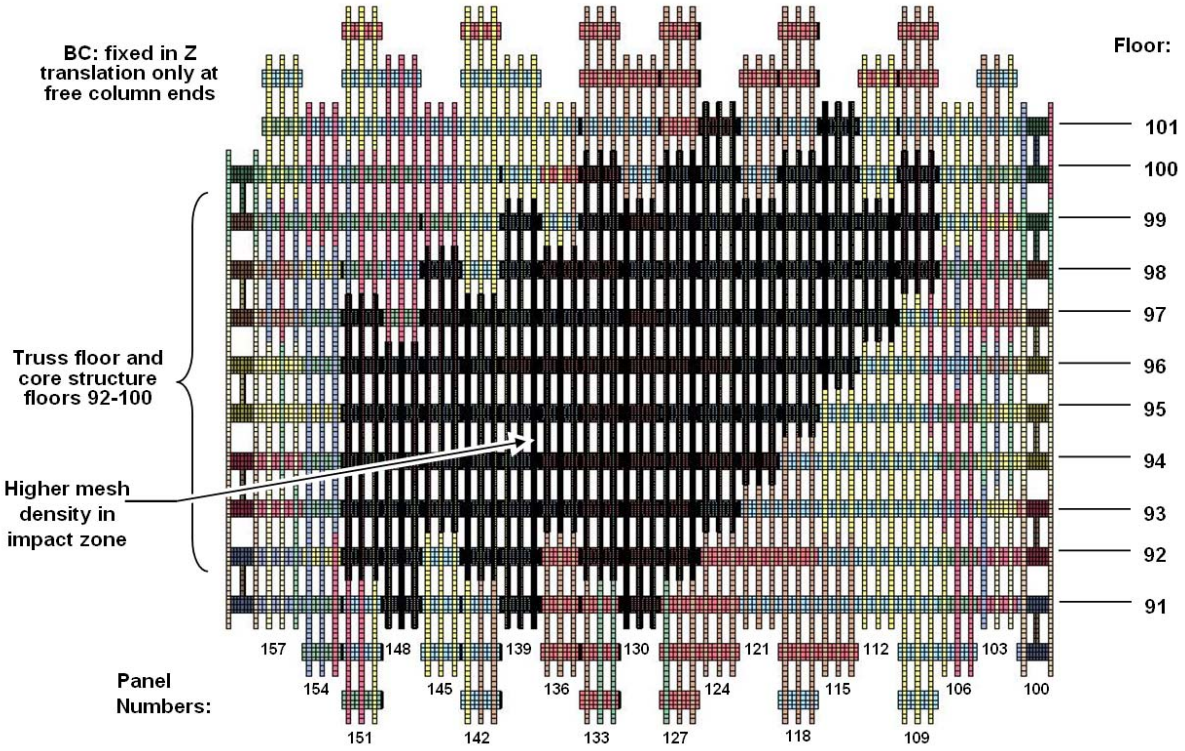

Figure E–8. Impact face of the WTC 1 model, floors 91–101.

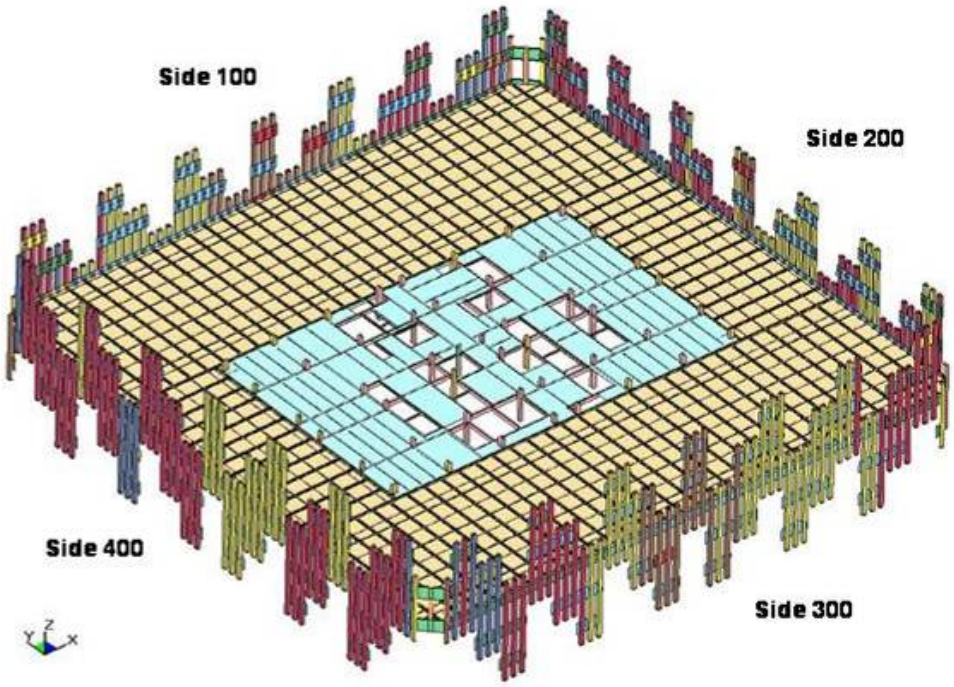

Figure E–9. Model of the 96th floor of WTC 1.

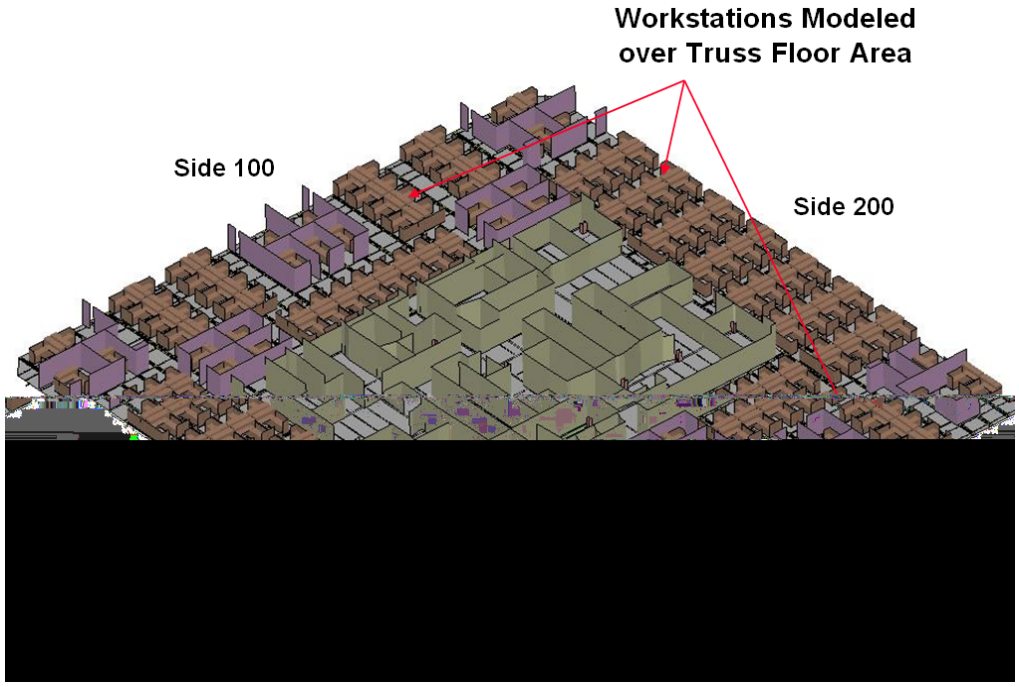

Figure E–10. Model of the 96th floor of WTC 1, including interior contents.

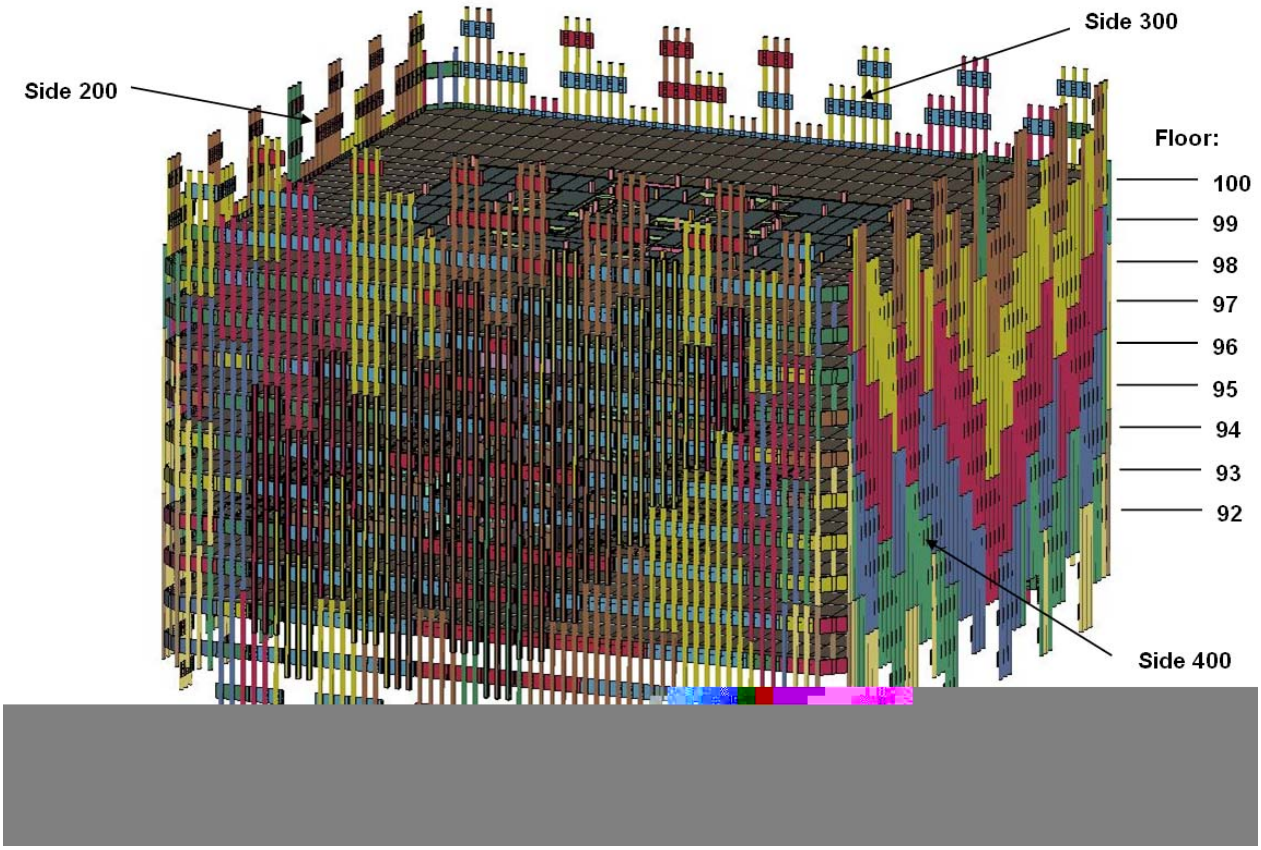

Figure E–11. Multi-floor global impact model of the WTC 1 tower.

E.4 AIRCRAFT MODEL DEVELOPMENT

The finite element model for the Boeing 767-200ER aircraft was constructed through a three-step process: (1) data collection, (2) data interpretation and engineering analysis, and (3) meshing of the structure. The focus of this effort was on gathering sufficient structural data and including adequate detail in the aircraft model so that the mass and strength distribution of the aircraft and contents were properly captured for implementation in the impact analyses. Structural data were collected for the Boeing 767-200ER aircraft from (1) documentary aircraft structural information and (2) data from measurements on Boeing 767 aircraft.

The complete model of the Boeing 767-200ER is shown in Figure E–12. A summary of the aircraft model size and parameters is presented in Table E–2 for American Airlines 11 (AA 11) and United Airlines 175 (UAL 175) that impacted WTC 1 and WTC 2, respectively. The airframe model contained most of the significant structural components in the aircraft. The models of the fuselage, empennage, and wing structures were developed completely using shell elements. Models for the landing gear and engines were developed primarily using shell elements, but contained some brick elements as well. The typical element dimensions were between 1 in. and 2 in. for small components, such as spar or rib flanges, and 3 in. to 4 in. for large parts such as the wing or fuselage skin.

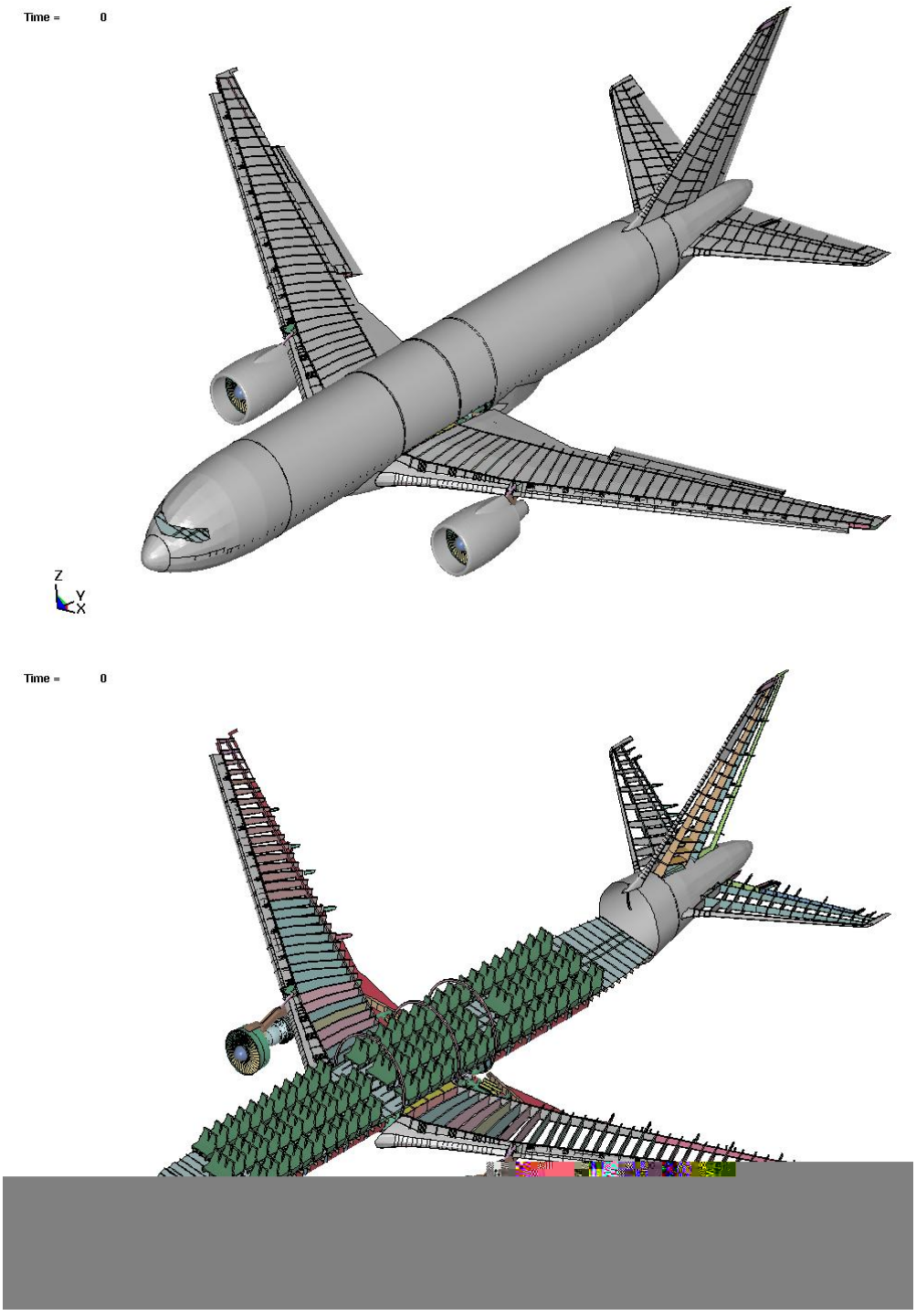

Figure E–12. Finite element model of the Boeing 767-200ER.

Table E–2. Boeing 767-200ER aircraft model parameters.

	AA 11	UAL 175
No. Brick Elements	70,000	70,000
No. Shell Elements	562,000	562,000
No. SPH Fuel Particles	60,672	60,672
Total Nodes	740,000	740,000
Total Weight (Empty)	183,500 lb	183,500 lb
ULD/Cargo Weight	12,420 lb	21,660 lb
Cabin Contents Weight	21,580 lb	10,420 lb
Fuel Weight	66,100 lb	62,000 lb
Total Weight (Loaded)	283,600 lb	277,580 lb

Special emphasis was placed on modeling the aircraft engines due to their potential to produce significant damage to the tower components. The engine model was developed primarily with shell elements. The objective was to develop a mesh with typical element dimensions between 1 in. and 2 in. However, smaller element dimensions were required at many locations to capture details of the engine geometry. Brick elements were used for some of the thicker hubs and the roots of the compressor blades. The various components of the resulting engine model are shown in Figure E–13. Fuel was distributed in the wing as shown in Figure E–14 based on a detailed analysis of the fuel distribution at the time of impact.

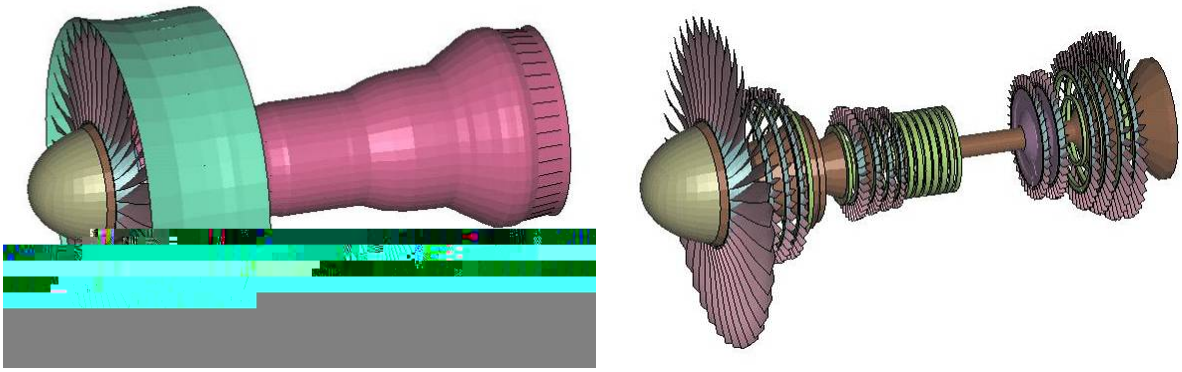

Figure E–13. Pratt & Whitney PW4000 turbofan engine model.

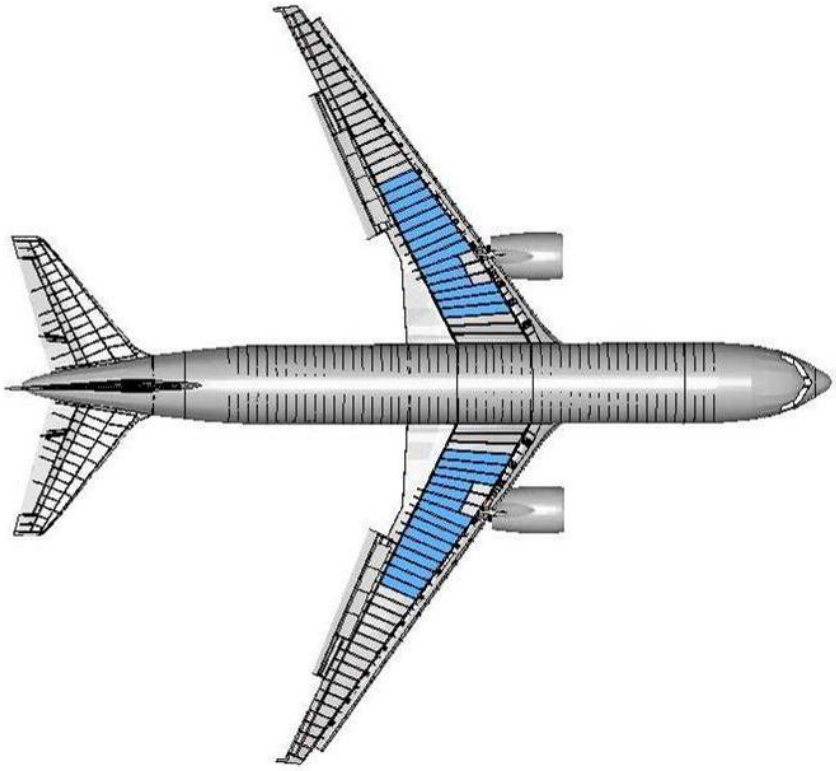

Figure E–14. Boeing 767-200ER with fuel load at time of impact.

E.5 COMPONENT LEVEL ANALYSES

A series of component impact analyses were performed using models of tower core and exterior columns impacted by models for a wing section and an engine. The primary objectives of the component modeling were to (1) develop understanding of the interactive failure phenomenon of the aircraft and tower components and (2) develop the simulation techniques required for the global analysis of the aircraft impacts into the WTC towers. The approach taken for component modeling was to start with finely meshed, brick and shell element models of key components of the tower and aircraft structures and progress to relatively coarsely meshed beam and shell element representations used in the global models. In addition to determining the optimal element size and type for global modeling, other key technical areas were addressed in the component modeling, including material constitutive modeling, treatment of connections, and modeling of aircraft fuel. Examples of the component impact analyses included:

- Impact of a segment of an aircraft wing with an exterior column.
- Impact of a segment of an aircraft wing with a core column.
- Detailed and simplified modeling of exterior panel bolted connection under impact loading and modeling of the bolted spandrel connection.
- Impact of an aircraft engine with exterior wall panels (Figure E–15).
- Impact of a simplified plow type impactor with truss floor assembly.

- Impact of an empty wing segment with exterior wall panels (Figure E–16).
- Impact of fuel-filled wing segment with exterior wall panels (Figure E–17).

The following results were obtained from the component impact analyses:

- A 500 mph engine impact against an exterior wall panel resulted in a penetration of the exterior wall and failure of impacted exterior columns. If the engine did not impact a floor slab, the majority of the engine core would remain intact through the exterior wall penetration with a reduction in speed between 10 percent and 20 percent. The residual velocity and mass of the engine after penetration of the exterior wall was sufficient to fail a core column in a direct impact condition. Interaction with additional interior building contents prior to impact or a misaligned impact against the core column could change this result.
- A normal impact of the exterior wall by an empty wing segment from approximately mid-span of the wing produced significant damage to the exterior columns but not complete failure. Impact of the same wing section, but filled with fuel, resulted in extensive damage to the external panels of the tower, including complete failure of the exterior columns. The resulting debris propagating into the building maintained the majority of its initial momentum prior to impact.
- Three different numerical techniques were investigated for modeling impact effects and dispersion of fuel: (1) standard Lagrangian finite element analysis with erosion, (2) Smoothed Particle Hydrodynamics (SPH) analysis, and (3) Arbitrary-Lagrangian-Eulerian (ALE) analysis. Of these approaches, use of the SPH offered the best viable option due to its computational efficiency.

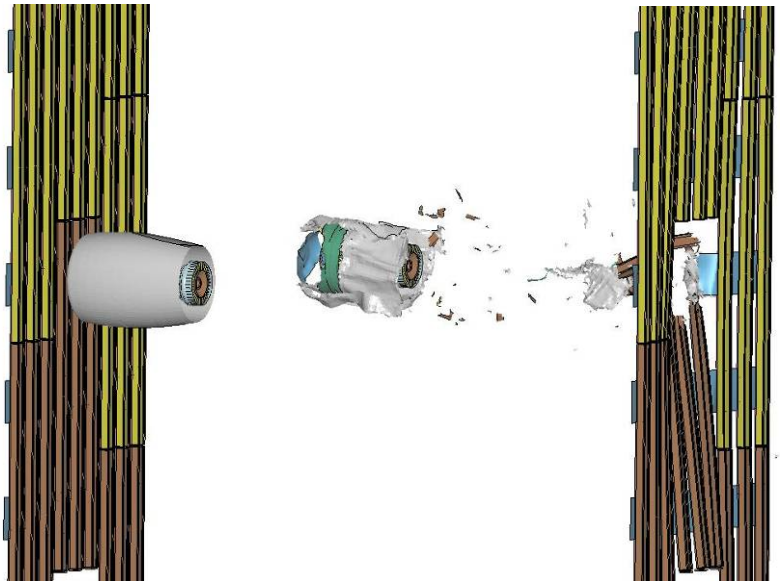

(a) Initial configuration **(b) Impact response at 80 ms**

Figure E–15. Example engine impact analysis with exterior columns.

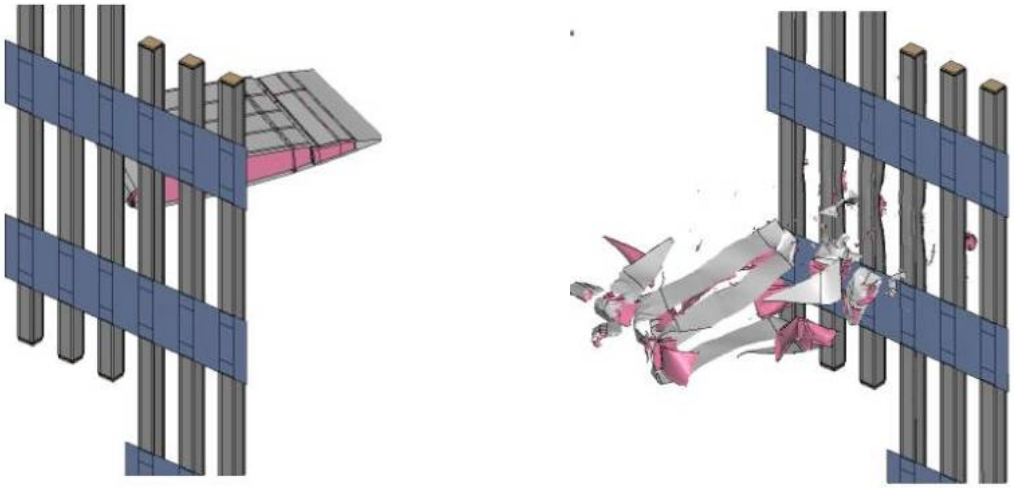

t = 0.0 s t = 0.04 s

Figure E–16. Calculated impact of a fine-mesh empty wing section with two exterior panels at 442 mph.

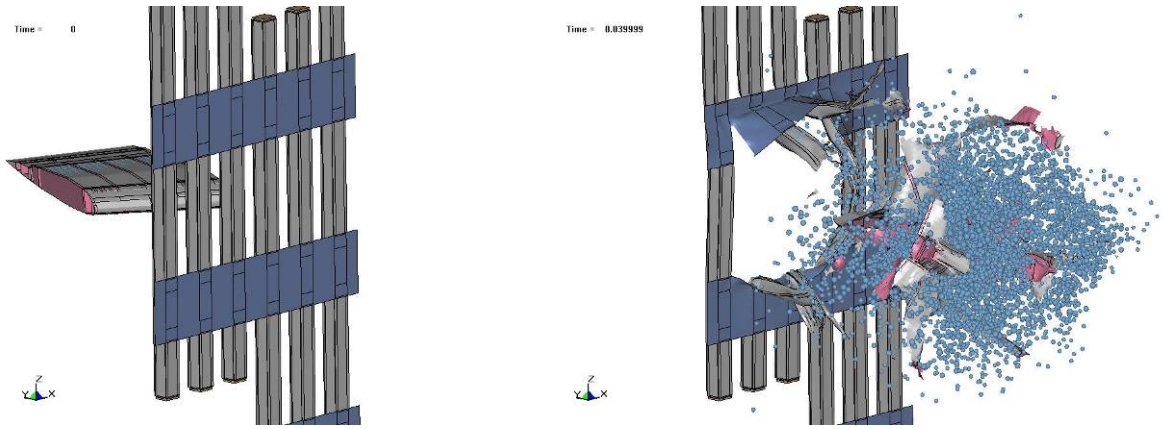

t = 0.0 s t = 0.04 s

Figure E–17. Calculated impact of a coarse mesh wing section laden with fuel modeled using SPH particles.

E.6 SUBASSEMBLY IMPACT ANALYSES

The subassembly analyses were used as a transition between the component level analyses and the global impact analyses. With the subassembly analyses, more complex structural behavior not captured in the component analyses could be investigated with significantly shorter run times than required for the global analyses. The subassembly analyses were primarily used to investigate different modeling techniques and associated model size, run times, numerical stability, and impact response. The final subassembly model used structural components from the impact zone on the north face of WTC 1. The structural components in the final subassembly model included the exterior panels, core framing, truss floor structures, and interior contents (workstations), Figure E–18.

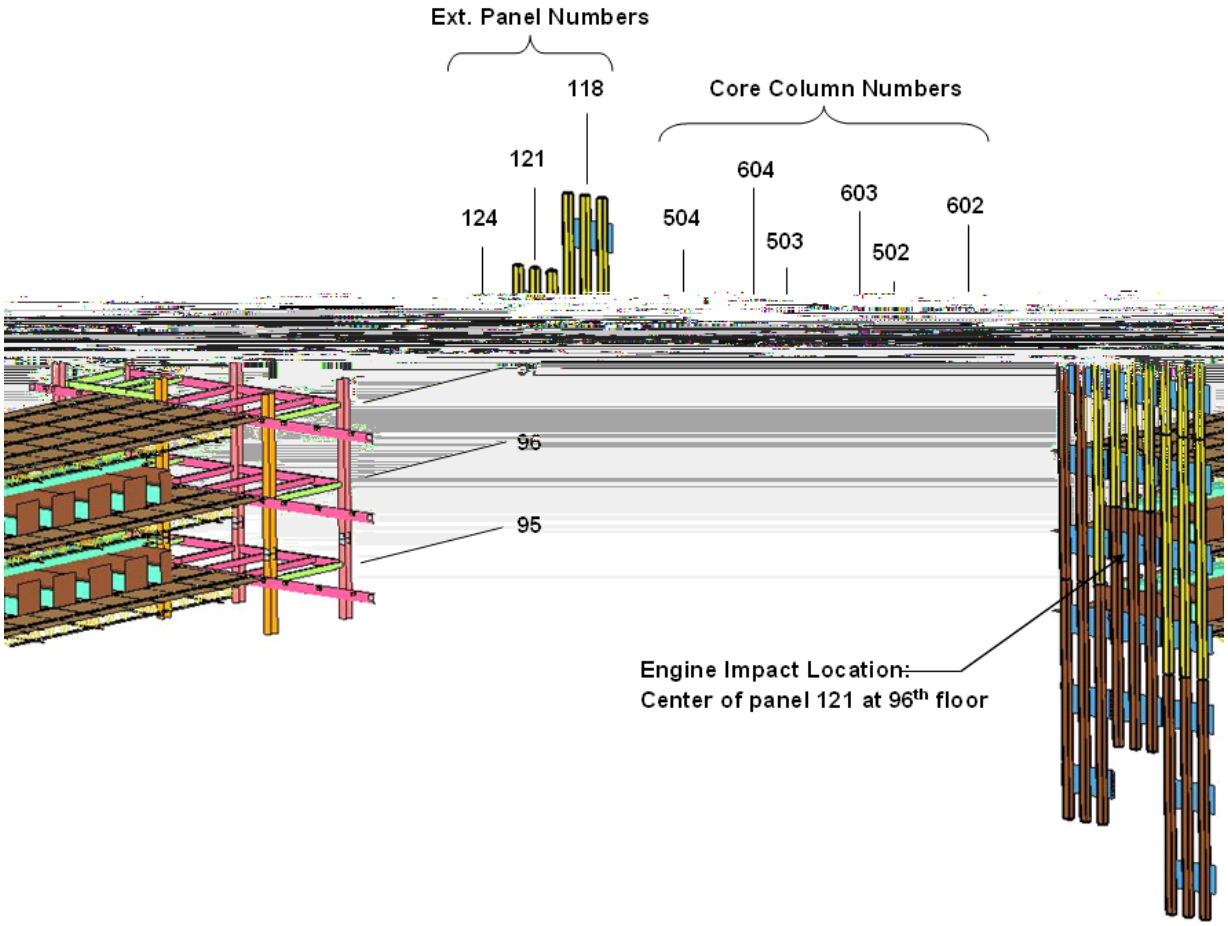

Figure E–18. Final WTC tower subassembly model.

The subassembly model was impacted by an aircraft engine and by a segment of a fuel-filled wing. The response of the structure to the engine impact is shown in Figure E–19 and to the wing impact in Figure E–20. The subassembly model was used to investigate the effect of a number of modeling parameters on the response and damage estimates. For the engine impact simulations, these parameters included the strength of the building nonstructural contents and the concrete slab strength. For the wing impact simulations, the effect of the ductility of the exterior column weldment on the impact response was investigated. The results of these parametric studies indicated the following:

The deceleration profile of the impacting engine indicated that the response of the nonstructural building contents was dominated by the mass of the workstations, rather than by their strength.

Varying the strength of the floor concrete slab from 4 ksi to 3 ksi did not result in significant change in the impact response. It appears that the mass of the concrete slab had a greater effect on the engine deceleration and damage to the floor than did the concrete strength.

Varying the ductility of the weld zone in the exterior columns from 8 percent to 1 percent did not result in any noticeable difference in the damage pattern (Figure E–21) or the energy absorbed by the exterior panels, indicating that the weld ductility had a negligible effect on the impact response.

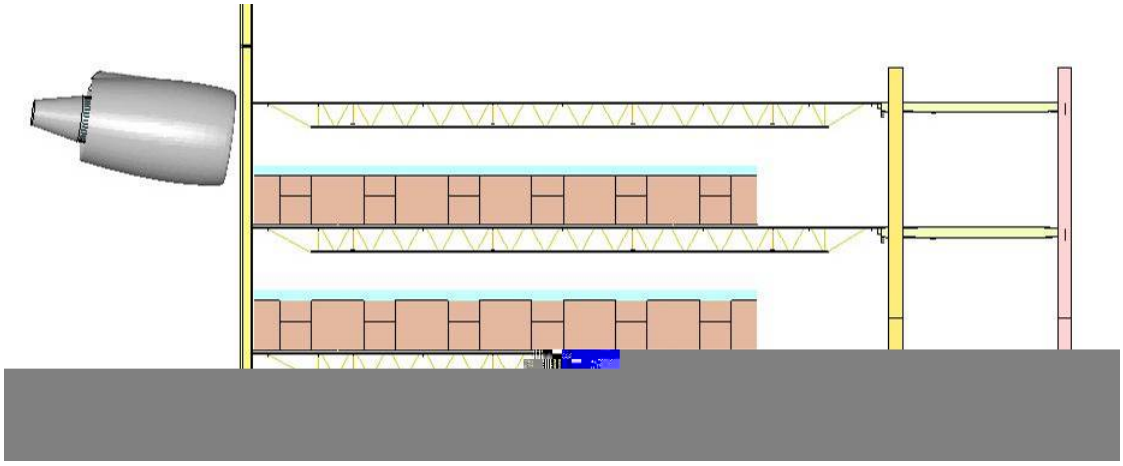

(a) Time = 0.00 s

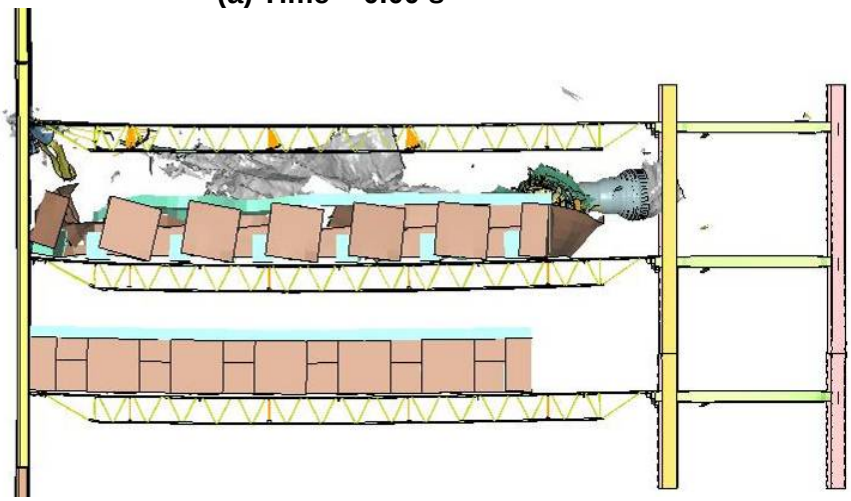

(b) Time = 0.25 s

Figure E–19. Engine impact and break up behavior (side view).

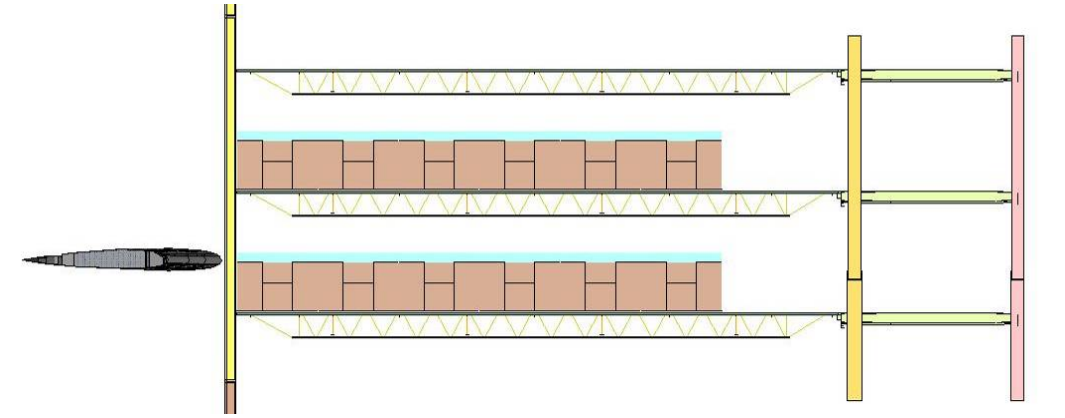

(a) Time = 0.00 s

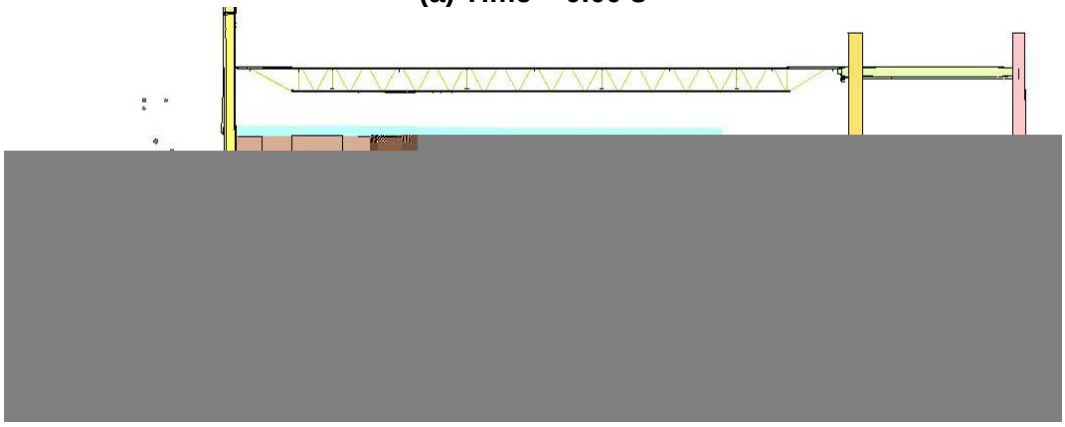

(b) Time = 0.05 s

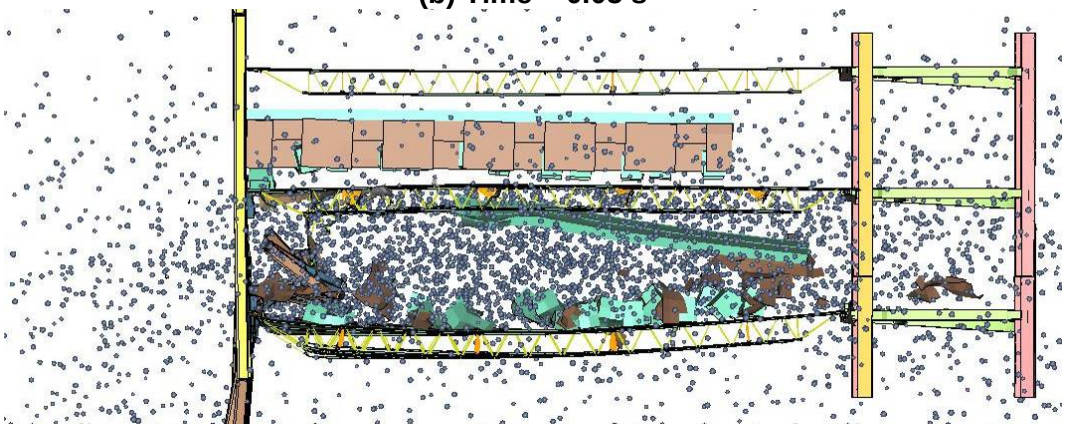

(c) Time = 0.25 s

Figure E–20. Wing section impact and break up behavior (side view).

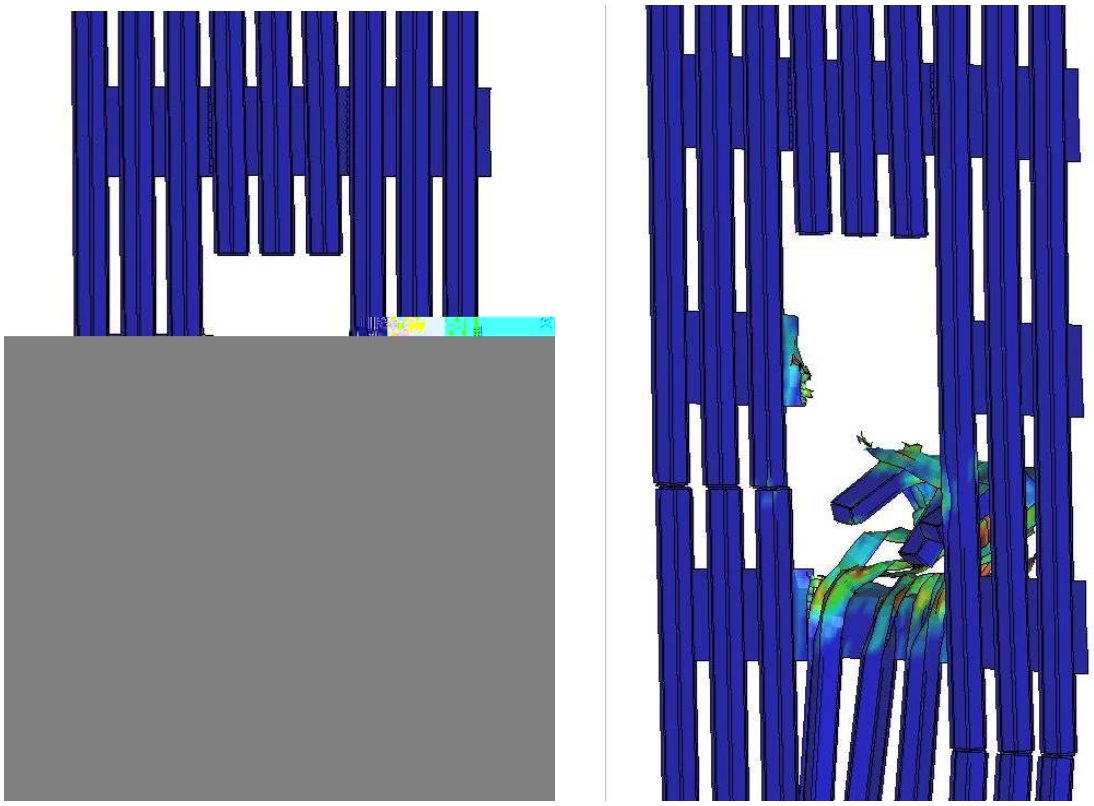

(a) 8 percent weld ductility **(b) 1 percent weld ductility**

Figure E–21. Exterior wall damage for the wing section impact analyses.

E.7 ANALYSIS OF AIRCRAFT IMPACT CONDITIONS

Three different methods were applied to determine the impact conditions for the two aircraft that impacted the towers. The first method used a comparison of videos from different positions to calculate the three-dimensional trajectory of the aircraft. The second method used the relative frame-by-frame motion in a single video scaled to the length of the aircraft in the video to calculate the impact speed. Finally, analysis of the impact damage on the face of each tower was used to refine the relative impact orientation and trajectory.

The aircraft impact conditions matching the observed exterior wall damage are shown in Figure E–22 and Figure E–23 for WTC 1 and WTC 2, respectively. The aircraft and exterior wall models were used to visualize the impact scenario in the figures, and the view shown was aligned with the aircraft trajectory. Matching the projected impact points of the wings, fuselage, engines, and vertical stabilizer onto the exterior wall of each tower to the observed damage pattern was an important constraint in the determination of impact conditions. The final set of impact conditions from the analyses are summarized in Table E–3.

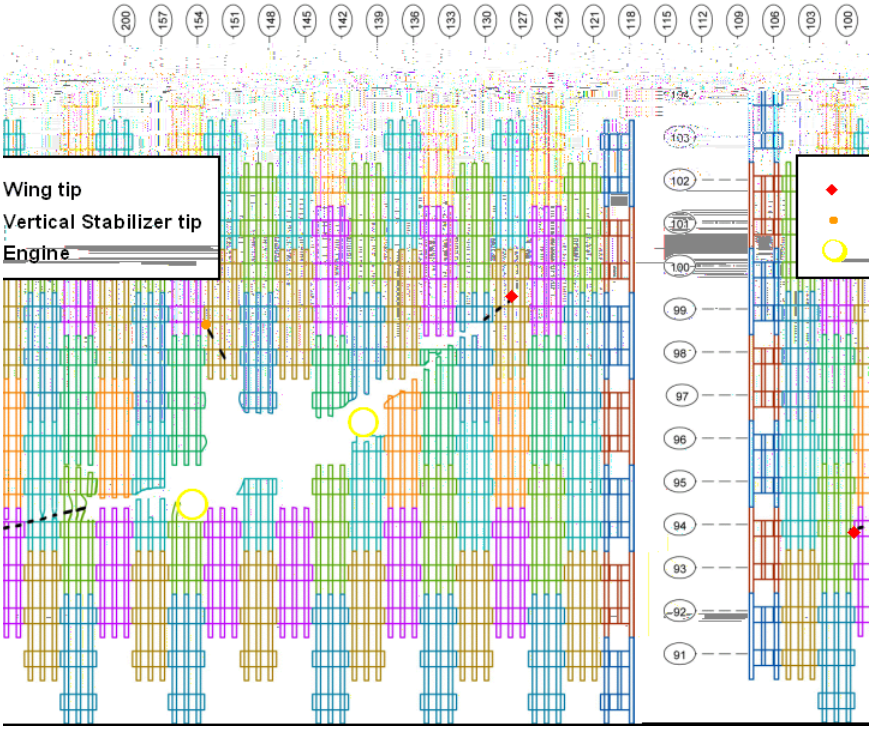

(a) Impact damage

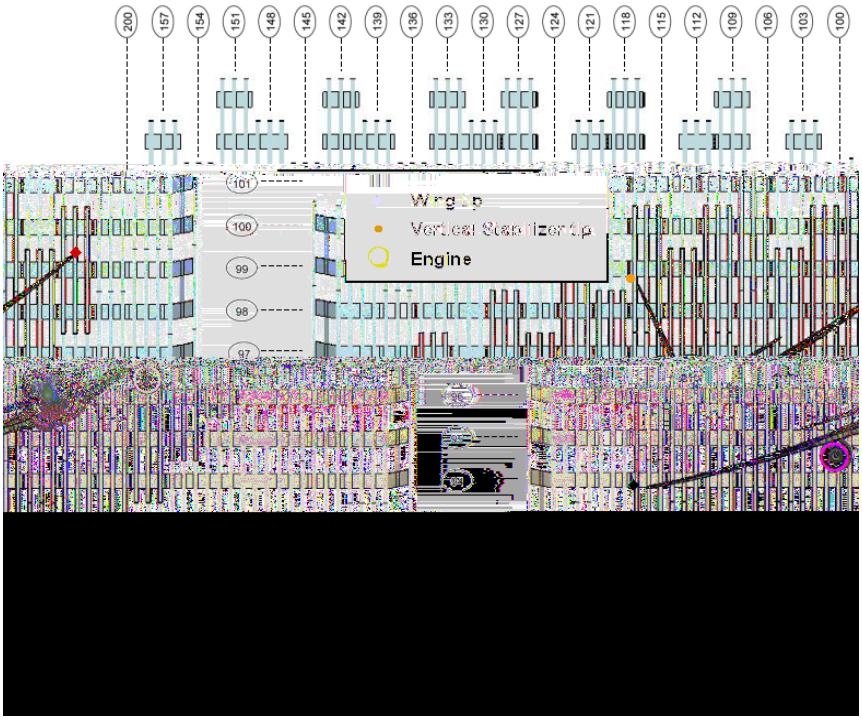

(b) Impact conditions (vertical angle = 10.6°, lateral angle = 0°)

Figure E–22. WTC 1 impact damage and impact conditions.

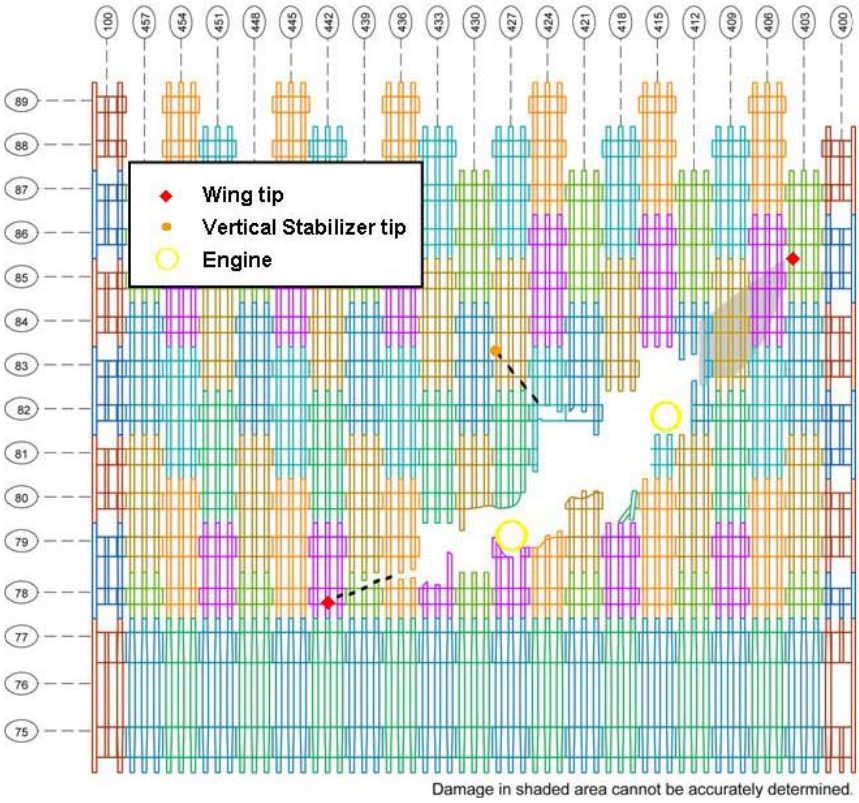

(a) Impact damage

(b) Impact conditions (vertical angle = 6°, lateral angle = 13°)

Figure E–23. WTC 2 impact damage and impact conditions.

Table E–3. Summary of refined aircraft impact conditions.

	AA 11 (WTC 1)	UAL 175 (WTC 2)
Impact Speed (mph)	443 ± 30	542 ± 24
Vertical Approach Angle (Velocity vector)	10.6° ± 3° below horizontal (heading downward)	6° ± 2° below horizontal (heading downward)
Lateral Approach Angle (Velocity vector)	180.3° ± 4° clockwise from Structure North[a]	15° ± 2° clockwise from Structure North[a]
Vertical Fuselage Orientation Relative to Trajectory	2° nose-up from the vertical approach angle	1° nose-up from the vertical approach angle
Lateral Fuselage Orientation Relative to Trajectory	0° clockwise from lateral approach angle	-3° clockwise from lateral approach angle
Roll Angle (left wing downward)	25° ± 2°	38° ± 2°

a. Structure North is approximately 29 degrees clockwise from True North.

E.8 UNCERTAINTY ANALYSES

The objectives of the uncertainty analyses were to assess the effect of uncertainties associated with the aircraft and WTC towers parameters on the level of damage to the towers after impact and to determine the most influential modeling parameters that affect the damage estimates. Uncertainty arises in these analyses from the following key parameters:

- Aircraft impact parameters: aircraft speed, horizontal and vertical angles of incidence, orientation, and location of impact.
- Material properties: high strain rate material constitutive behavior and failure criteria for the towers and the aircraft.
- Aircraft mass and stiffness properties, and the jet fuel distribution in the aircraft.
- Tower parameters: structural strength and mass distribution, connection and joint positions relative to impact and joint failure behavior.
- Nonstructural building contents that may share in absorbing energy imparted by the aircraft impact.

An important source of uncertainty that is not listed in these key parameters is the inaccuracy associated with mathematical or numerical models. The inaccuracies of models, also known as modeling errors, are deterministic in nature, but are often treated as random variables to characterize the effects of the analysis methodologies on the calculated response. All of these variables did not necessarily have a significant effect on the estimated impact damage to the WTC towers.

Because of the complexity of the problem and the limited number of parameters that could be varied in the global analyses, it was necessary to down-select a refined list of uncertainty parameters from all of the possible parameters. Therefore, variable screening was conducted using design of experiments methodology. Screening was first conducted at component and subassembly levels using orthogonal factorial design techniques in order to identify the most influential parameters and reduce the number of

parameters to a more manageable number for the global impact analyses. The sensitivity analyses included engine impacts against core columns, wing section impacts against exterior panels, and engine-impact subassembly analyses.

Based on the three sensitivity analyses, the set of influential modeling parameters was reduced. The following parameters were selected for variation in the global impact analyses:

- Impact speed.
- Vertical approach angle of the aircraft.
- Lateral approach angle of the aircraft.
- Total aircraft weight.
- Aircraft materials failure strain.
- Tower materials failure strain.
- Building contents weight.

The impact speed and vertical approach angle were selected as significant parameters in the global analyses due to their importance in the component and subassembly impact response. The vertical approach angle played a primary role in the magnitude of the vertical impact loads on the truss floor structures. Lateral approach angle was also selected as this parameter dictated to a large extent where aircraft debris traveled and what part of the core was affected by this debris.

Variations in the strength and ductility (failure strain) of materials had a similar effect on the amount of absorbed energy. An increase in yield strength or an increase in failure strain resulted in an increase in the energy absorbing capacity of the structure. The yield strength of materials was typically known more accurately than the failure strains. This was particularly true within the finite element analyses where the value of the failure strain needed to be assigned based on the model resolution and failure criteria used. As a result, only the uncertainties in the material failure strain were used as a material uncertainty parameter for both the aircraft and the towers in the subsequent global impact analyses.

The uncertainty in the weights associated with building contents (corresponding to service live loads) was found to be of secondary importance in the engine-subassembly impact analysis. In the global impact analyses, the live load contents were expected to play a more significant role in confining the fuel and debris dispersion. In addition, the partition walls were significant for controlling the subsequent spread of fire through the towers. As a result, the uncertainty in building contents weight was included as an uncertainty parameter in the global analyses.

E.9 GLOBAL IMPACT ANALYSES

The primary objective of this analysis was to determine the condition of the two WTC towers immediately following the aircraft impacts. This assessment included the estimation of the structural damage that degraded their strength and the condition and position of nonstructural contents such as

partitions, workstations, aircraft fuel, and other debris that influenced the behavior of the subsequent fires in the towers. The global impact analyses were the primary method by which the damage to the towers was estimated.

E.9.1 WTC 1 Base Case Global Impact Analysis

The combined aircraft and tower model for the base case WTC 1 global impact analysis is shown in Figure E–24. The base case impact analysis was performed for a 0.715 second duration following initial impact of the aircraft nose with the north exterior wall. The analysis was performed on a computer cluster using twelve 2.8 GHz Intel Xeon processors, each on a separate node of the cluster. The run time for this analysis was approximately two weeks. The progress of the global impact simulations was monitored on average every two days. The calculations were terminated when the damage to the towers reached a steady state and the motion of the debris was reduced to a level that was not expected to produce any significant increase in the impact damage. The residual kinetic energy of the airframe components at the termination of a global impact simulation was typically less than 1 percent of the initial kinetic energy at impact.

A side view of the base case WTC 1 global impact response is shown in Figure E–25. In the figure, the tower interior contents were removed, and the tower structures were shown as transparent so that the impact response in the tower interior could be seen. A corresponding top view of the impact response is shown in Figure E–26. The aircraft impact response was dominated by the impact, penetration, and fragmentation of the airframe structures. The entire aircraft fully penetrated the tower at approximately 0.25 s. The fuselage structures were severely damaged both from the penetration through the exterior columns and the penetration of the 96th floor slab that sliced the fuselage structures in half. The downward trajectory of the aircraft structures caused the airframe to collapse against the floor, and the subsequent debris motion was redirected inward along a more horizontal trajectory parallel to the floor. The downward trajectory of the aircraft structures transferred sufficient vertical load such that the truss floor structures on the 95th and 96th floors collapsed in the impact zone.

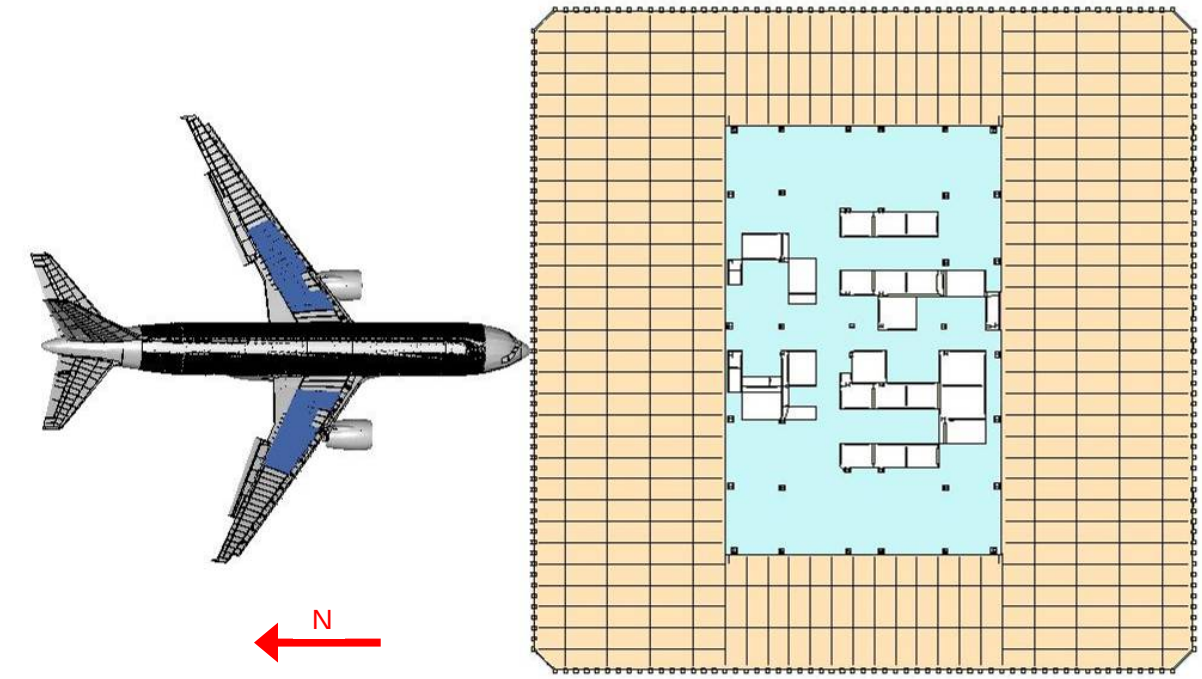

(a) Top view

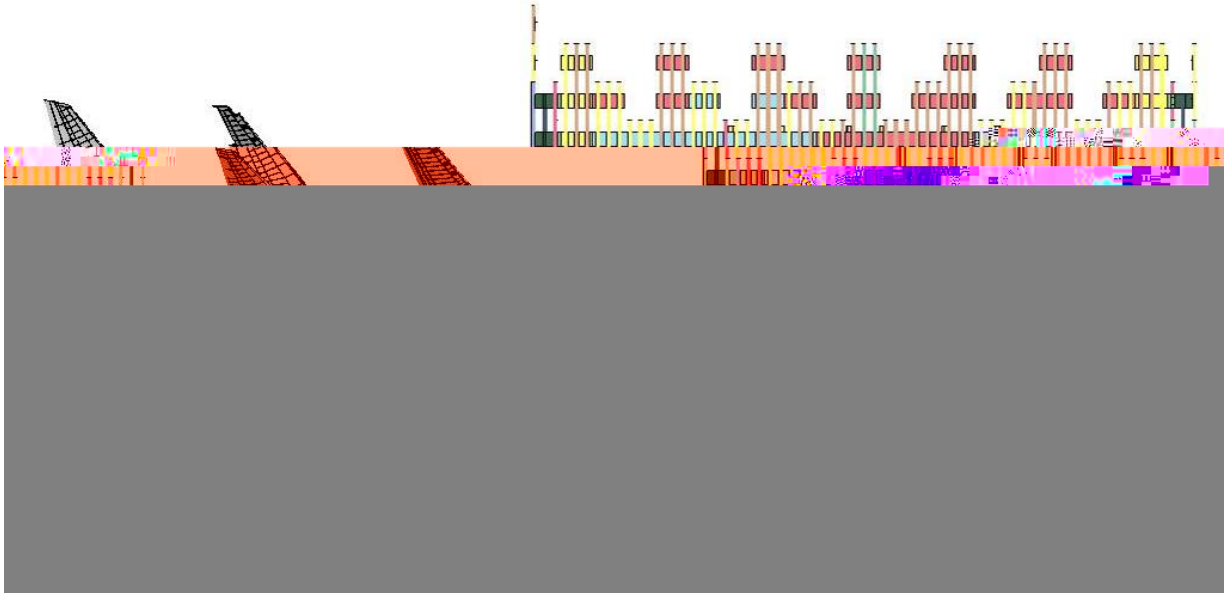

(b) Side view

Figure E–24. WTC 1 global impact model.

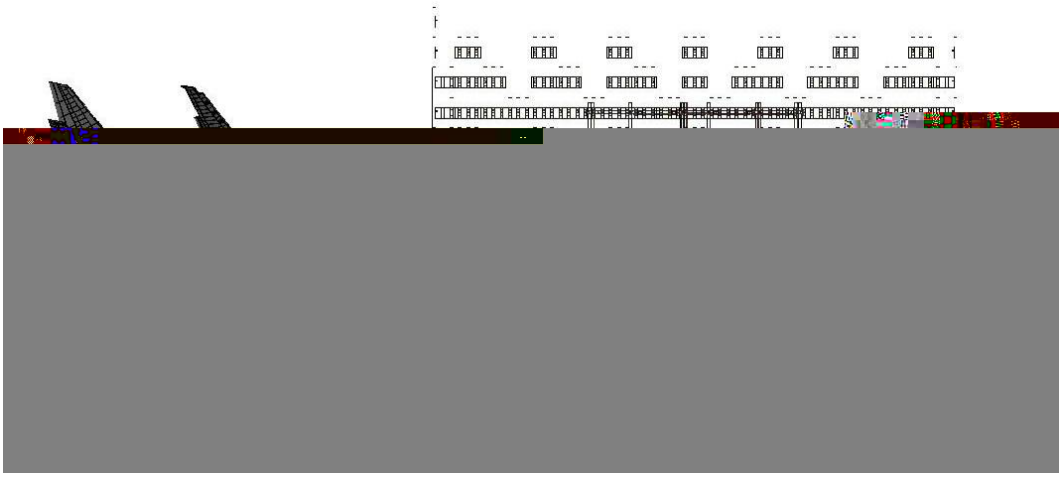

(a) Time=0.00 s

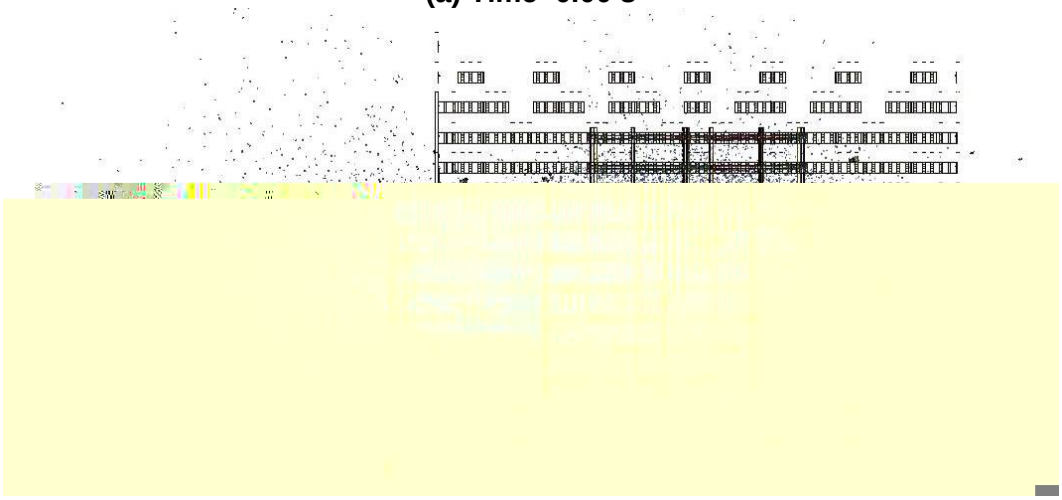

(b) Time=0.50 s

Figure E–25. WTC 1 base case global impact analysis – side view.

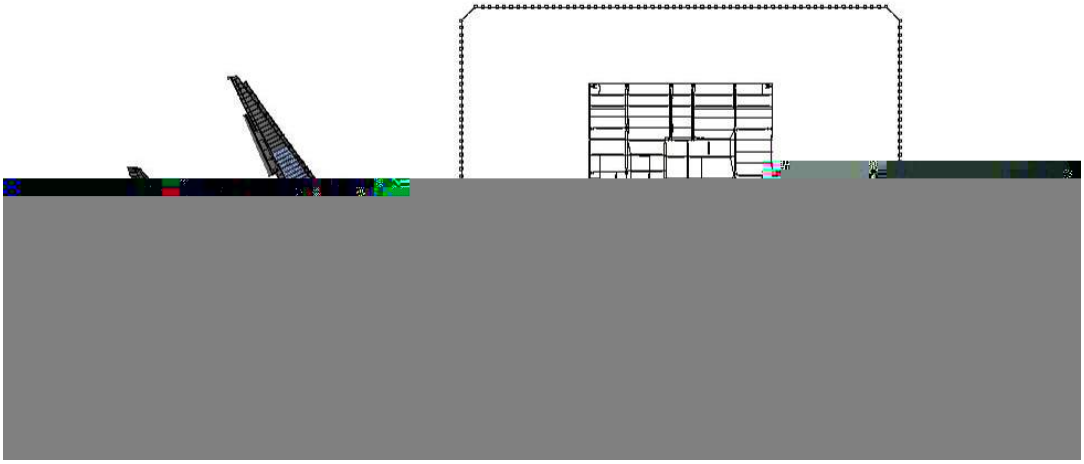

(a) Time=0.00 s

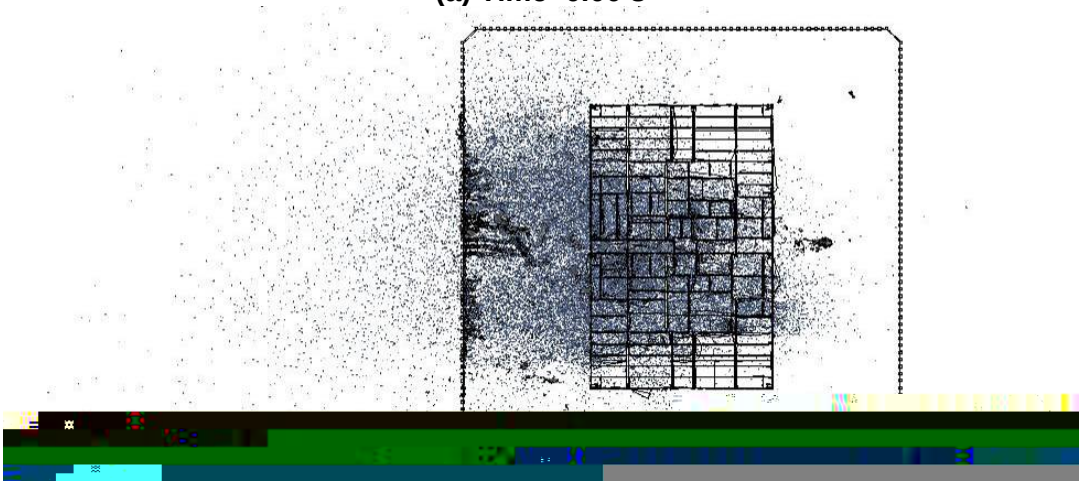

(b) Time=0.50 s

Figure E–26. WTC 1 base case global impact analysis – top view.

The wing structures were completely fragmented by the exterior wall. The aircraft fuel cloud began to spread out after impact but remained relatively dense until the leading edge of the fuel reached the tower core. The aircraft fuel and debris cloud eventually penetrated most of the distance through the core before their motion was halted.

Load transfer of the aircraft momentum into the tower structure is shown in Figure E–27. The momentum plotted was for all of the aircraft structures and contents (including fuel) and was normalized by the initial momentum magnitude. During the first 0.1 s of impact, the forward fuselage penetrated the exterior wall and impacted the interior structures. Between 0.1 s and 0.25 s a more rapid load transfer rate was observed as the area of the impact was larger (extending outward in the wing impact regions) and a higher percentage of the aircraft mass was impacting the interior structures. At 0.25 s, as indicated in Figure E–27, the aircraft completely penetrated the building and retained approximately 30 percent of its initial momentum. Beyond this time, the rate of load transfer steadily decreased with very little load transfer after approximately 0.5 s.

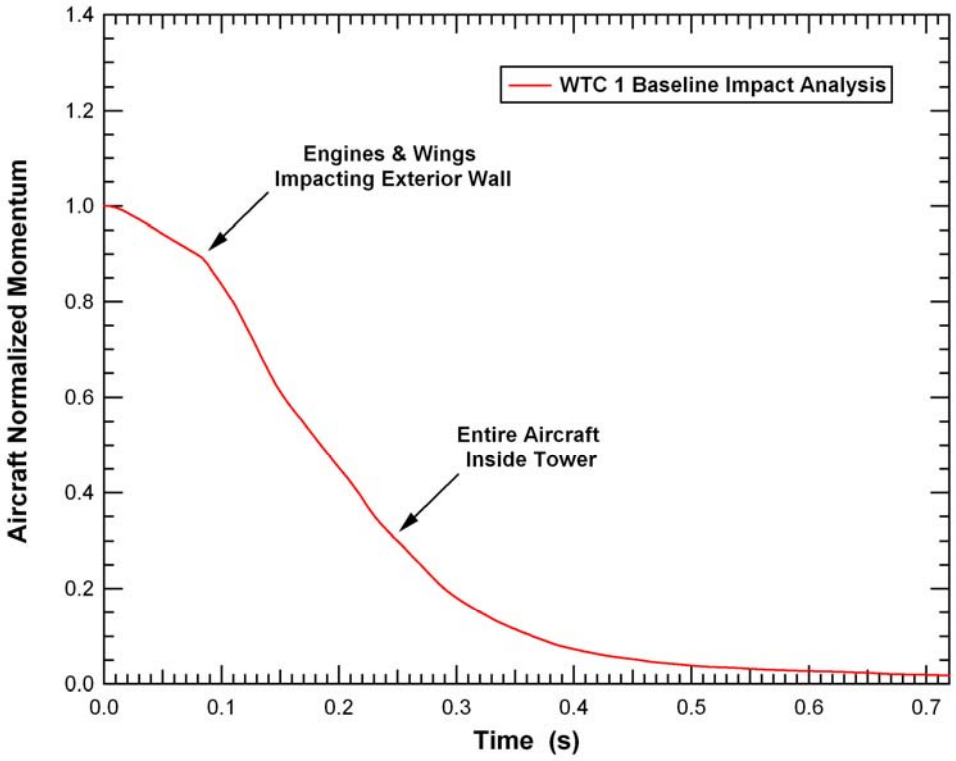

Figure E–27. Normalized aircraft momentum for the WTC 1 base case impact.

The aircraft was severely broken into debris as a result of the impact with the tower as shown in Figure E–28. At the end of the impact analysis, the aircraft was broken into thousands of debris fragments of various size and mass, as shown in Figure E–28(b). A closer inspection of the debris field shows that larger fragments still existed for specific components such as the engines, shown in Figure E–28(c). Both engines had significant impact damage with one of the engines broken into two large pieces. At the end of the simulation, the port engine was still inside the core, and the starboard engine was roughly one-third of the distance from the core to the south exterior wall. Each had a speed of less than 50 mph.

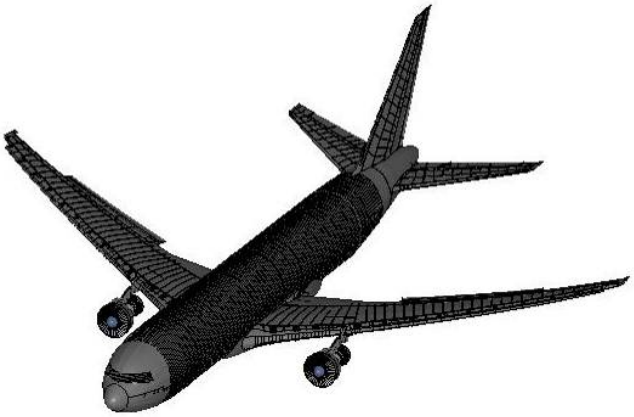

(a) Aircraft structure (time=0.00 s)

(b) Aircraft debris field (time=0.715 s)

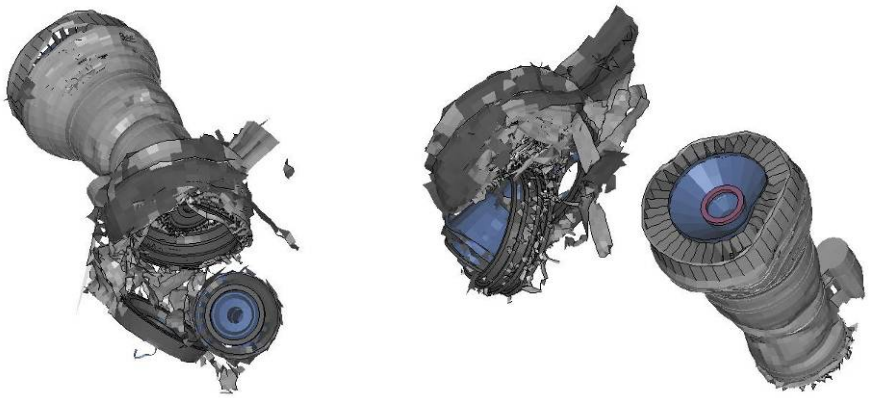

(c) Major engine debris (time=0.715 s)

Figure E–28. Aircraft break up and debris in the base case WTC 1 impact.

Exterior Wall Damage

The calculated damage to the exterior wall was significant for two reasons: (1) the exterior wall carried a significant portion of the load in the tower, and the degradation in exterior wall strength was important for the collapse analyses, and (2) the exterior wall was the one structural system for which direct visual evidence of the impact damage was available. Therefore, the comparison of the calculated and observed exterior wall damage could provide a partial validation of the analysis methodologies used in the global impact analyses.

Damage to the north exterior wall calculated in the base case WTC 1 global impact analysis is shown in Figure E–29. This damage was compared with a schematic of observed damage developed from inspections of the video and photographic data collected on the tower after impact. The calculated and observed damage in the impact damage zone were in good agreement. That both the position and shape of the impact damage agreed provided partial validation of the modeled geometry of the aircraft, including the aircraft orientation, trajectory, and flight distortions of the wings.

The calculated magnitude and mode of impact damage on the exterior wall also agreed well with the observed damage. The exterior wall completely failed in the regions of the fuselage, engine, and fuel-filled wing section impacts. Damage to the exterior wall was observed out to the wing tips, but the exterior columns were not completely failed in the outer wing and vertical stabilizer impact regions. Failure of the exterior columns occurred both at the bolted connections between column ends and at various locations in the column, depending on the local severity of the impact load and the proximity of the bolted connection to the impact. The agreement of both the mode and magnitude of the impact damage served to partially validate the constitutive and damage modeling of the aircraft and exterior wall of the tower.

Core Damage

The magnitude of damage to the core columns and core beams was important because this damage affected the residual strength of the tower. This strength was a critical input to subsequent structural stability and collapse analyses. The overall model for the core structure and calculated impact damage to the core is shown in Figure E–30. The figure shows that the core had significant damage in the region close to the impact point. The columns in line with the aircraft fuselage failed on the impact side, and several of the core beams were also severely damaged or failed in the impact zone.

A summary of the column damage is shown graphically in Figure E–31. The damage classification levels shown in the figure are light damage, moderate damage, heavy damage, and failed (severed). The light damage level was defined as showing evidence of impact (low level plastic strains), but without significant structural deformations. The moderate damage level had visible local distortions of the column cross section (e.g., bending in a flange), but no lateral displacements of the column centerline. The heavy damage classification was for impacts that produced global deformation of the column, resulting in a permanent deflection of the column centerline. The severed columns were completely failed and could carry no residual load. The calculated damage to the core of WTC 1 consisted of three severed columns and four heavily damaged columns.

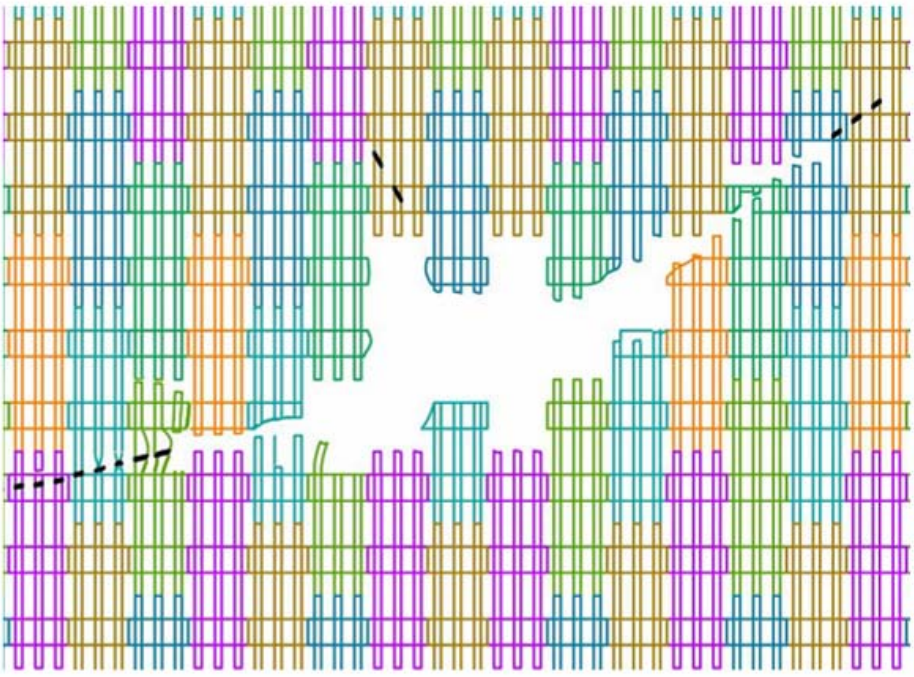

(a) Schematic of observed damage

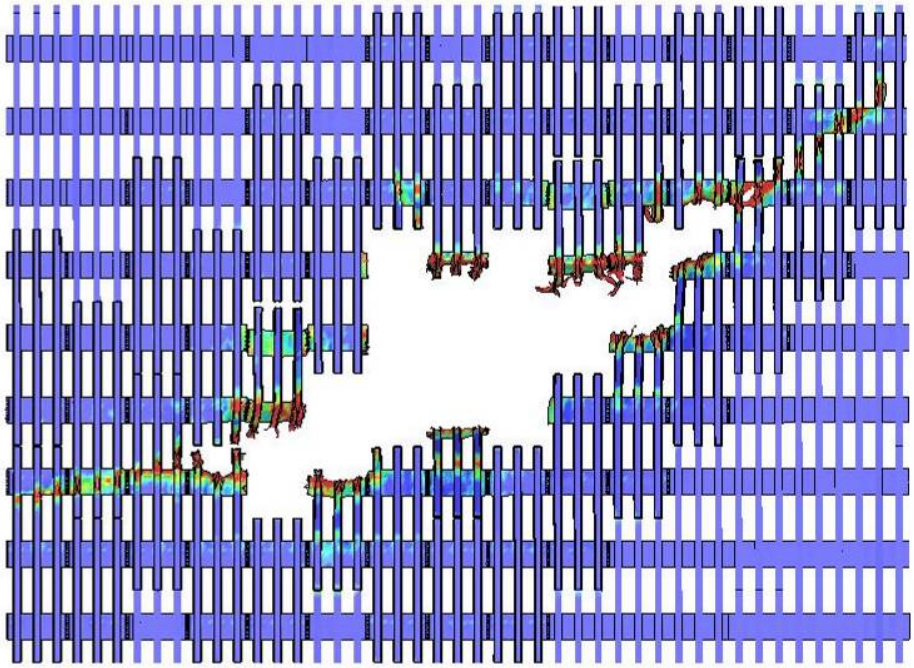

(b) Calculated damage (t=0.715 s)

Figure E–29. Base case impact damage to the WTC 1 exterior wall.

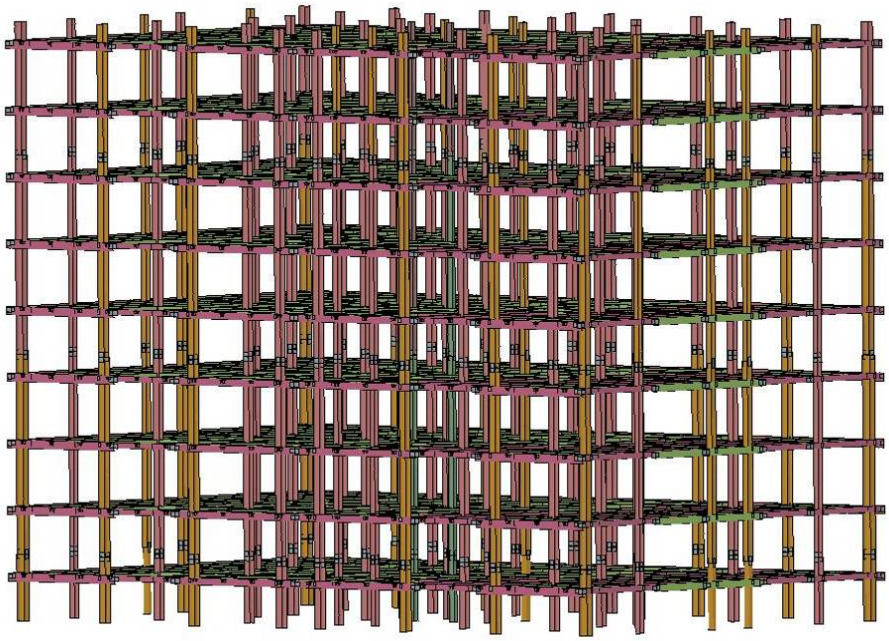

(a) Initial geometry

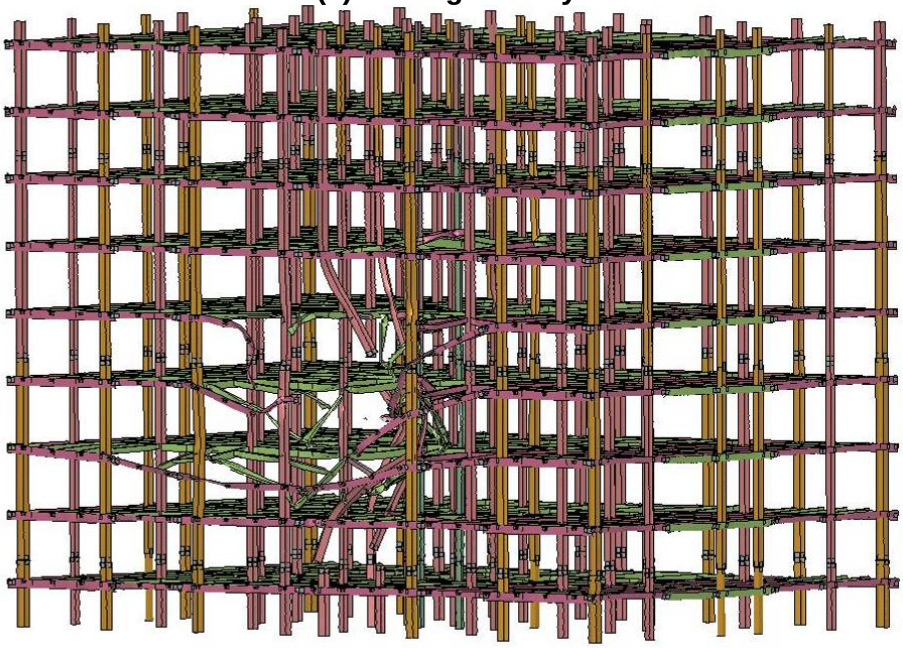

(a) Calculated impact damage

Figure E–30. Core column damage for the base case WTC 1 impact.

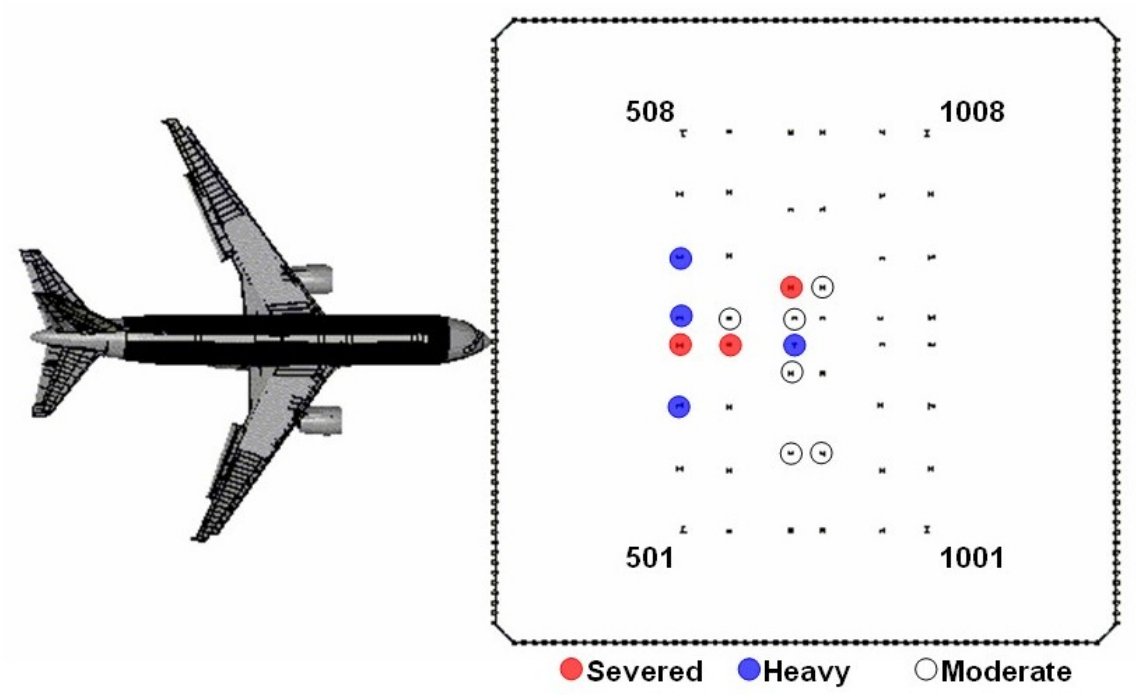

Figure E–31. Core column damage for the base case WTC 1 impact.

Truss Floor Damage

Impact damage to the floor trusses and floor slabs could have significantly contributed to the loss of structural strength and subsequent collapse. The truss floor sections provided lateral support to the exterior wall at each floor level. Any damage or holes in the concrete floor slab could provide a path for the fires to spread from floor-to-floor. Therefore, the calculation of the floor system damage was an important component of the global impact analyses.

An overall view of the floor truss structure in the impact zone, along with the calculated impact damage to the floor trusses, is shown in Figure E–32. The figure shows that the trusses experienced significant damage in the impact zone. The calculated impact response produced severe damage to the truss structures in the primary impact path of the fuselage. The truss structures were severely damaged from the exterior wall to the core. The truss floor system on floors 94 through 96 were damaged and sagging downward as a result of the impact loading.

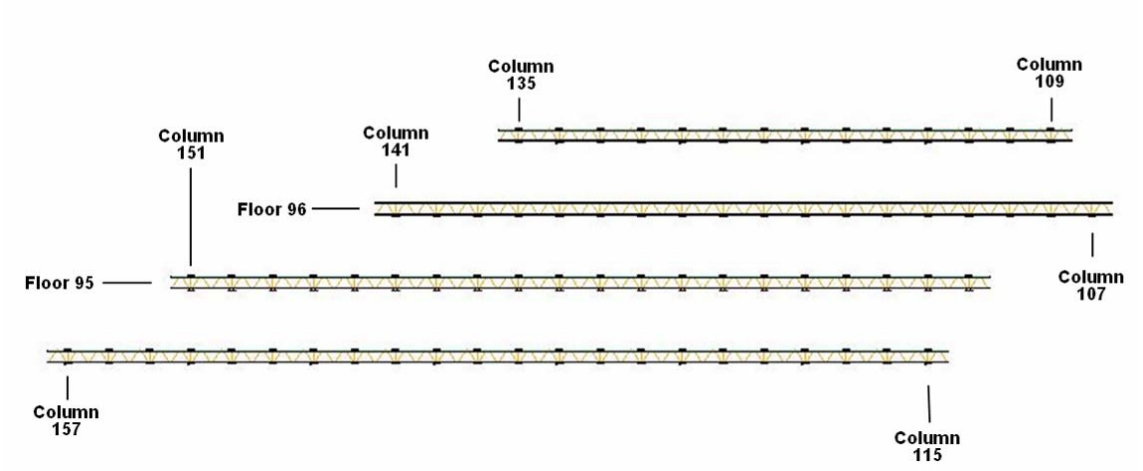

(a) Initial detailed truss structures

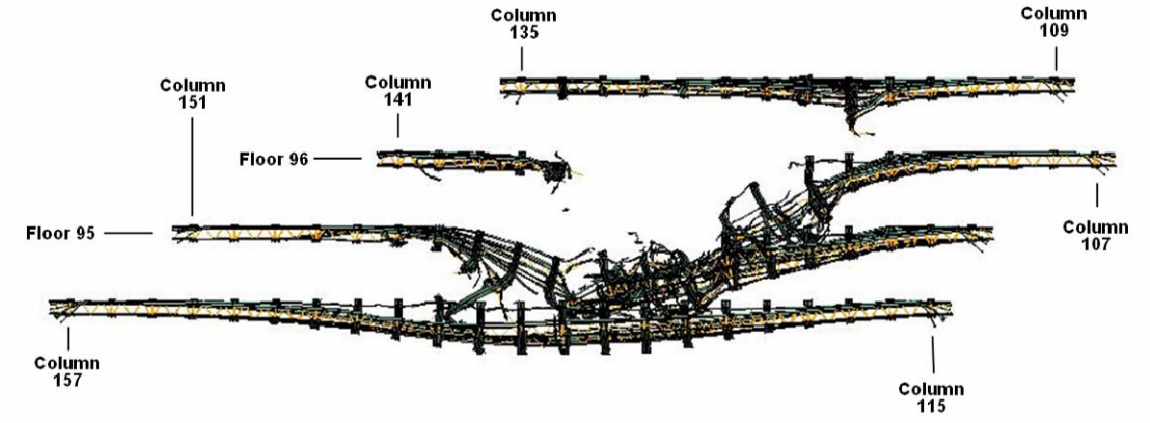

(b) Calculated damage (t=0.715 s)

Figure E–32. Base case impact damage to the WTC 1 floor truss (front view).

The calculated damage to the floor slabs on floors 94 through 97 of WTC 1 is shown in Figure E–33. Fringes of damage were set such that the concrete slab failed in the regions colored red (2 percent plastic strain was used corresponding to the zero strength strain limit for the concrete in unconfined compression). At these strain levels the concrete was severely damaged, indicating that it was probably removed, exposing the supporting metal decking.

After concrete failure, break up, and removal, the strength of the floor slab was severely reduced in the analyses to model the residual strength of the metal deck. At a plastic strain of 30 percent, corresponding to failure levels for the metal decking material, the elements were eroded (seen as holes ruptured in the floor slabs shown). Figure E–33 shows that the truss floor and associated slab were heavily damaged or completely destroyed in the impact zone. The zone of heavy damage to the floor slab extended beyond the truss floor and was approximately one-third of the distance through the core on floors 94 through 96.

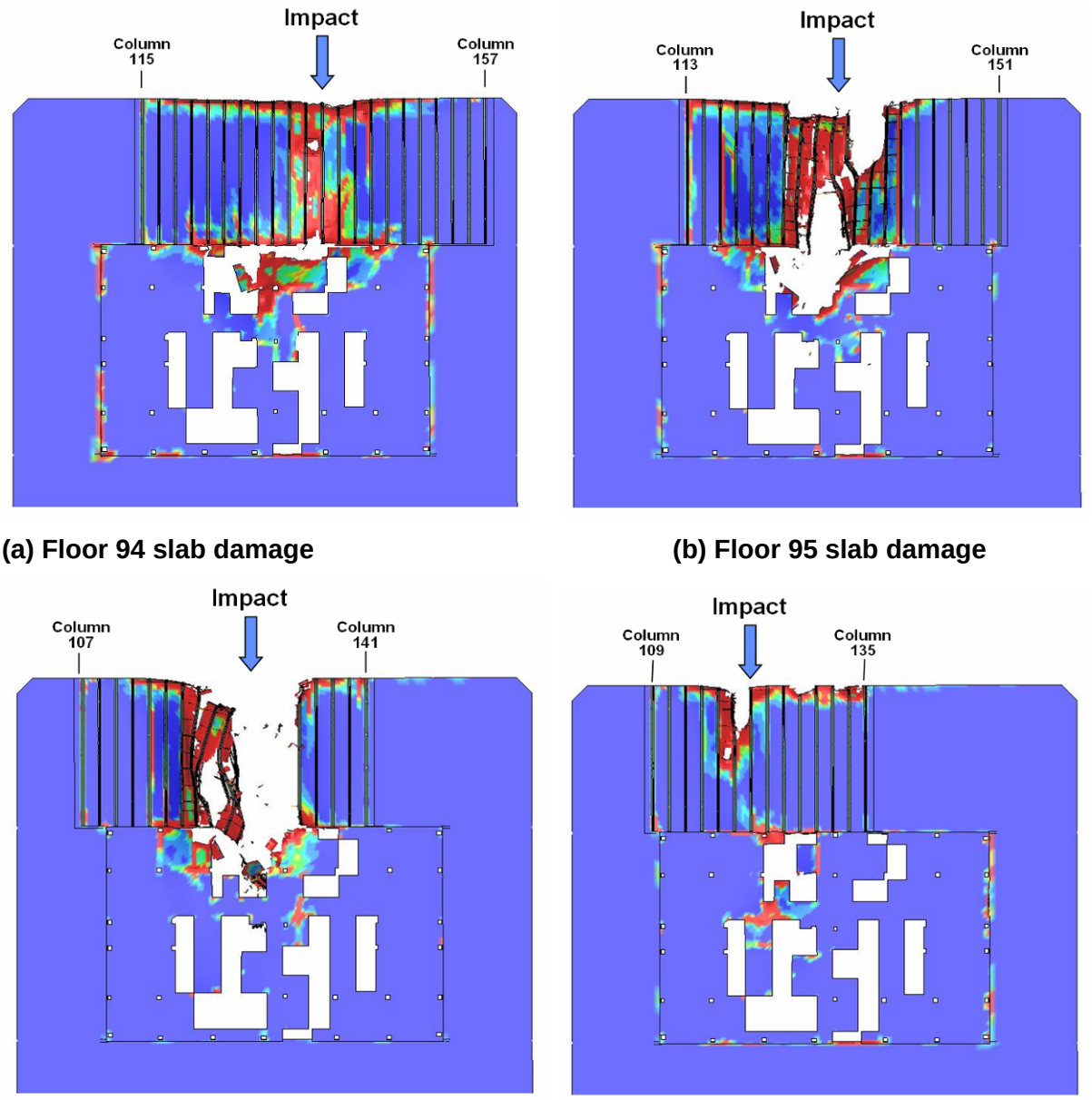

(a) Floor 94 slab damage **(b) Floor 95 slab damage**

(c) Floor 96 slab damage **(d) Floor 97 slab damage**

Figure E–33. Base case impact damage to the WTC 1 floor slab (plan view).

Fuel and Debris Distribution

Another primary objective of the global impact analyses was to determine the initial conditions that influenced the initiation and propagation of the fires in the towers. These initial conditions included the distribution of the jet fuel in the towers, the distribution of tower contents and aircraft debris that provided flammable materials for the fires, and the condition of the partitions and walls that provided barriers to air flow and spreading of the fires. The jet fuel was modeled using the smoothed particle hydrodynamics (SPH) algorithm in LS-DYNA. For the base case WTC 1 global impact analysis, the calculated distribution of the fuel in the tower and shape of the fuel cloud in a plan view and side view were shown

previously in Figure E–25 and Figure E–26, respectively. At the termination of the global impact analysis (0.715 s), the residual momentum of the jet fuel in the impact direction was less than 1 percent of the initial momentum, indicating that the fuel cloud was nearly at rest. The bulk of the aircraft debris and fuel was arrested prior to exiting the far side of the tower core. A small amount of aircraft debris was calculated to exit the far side of the tower (south wall of WTC 1).

A quantitative characterization of the fuel and aircraft debris distribution is given in Table E–4. The bulk of the fuel and aircraft debris was deposited on floors 93 through 97, with the greatest concentration on floor 94. The calculated debris cloud included 17,400 lb of debris and 6,700 lb of aircraft fuel outside of the tower at the end of the impact analysis, either rebounding from the impact face (north wall) or passing through the tower (south wall). This amount might have been larger in the calculation since the exterior walls were not modeled with windows that would contain the fuel cloud and other small debris inside the towers. In addition, the impact behavior of the aircraft fuel cloud did not include the ability to stick to, or wet, interior components. Rather, the aircraft fuel SPH particles tended to bounce off of internal structures.

Table E–4. Fuel and aircraft debris distribution for the base case WTC 1 impact.

Tower Location	Aircraft Fuel	Aircraft Debris
Total Outside Tower	6,700 lb	17,400 lb
WTC 1 Floor 92	810 lb	260 lb
WTC 1 Floor 93	6,100 lb	22,600 lb
WTC 1 Floor 94	16,100 lb	96,000 lb
WTC 1 Floor 95	12,200 lb	28,000 lb
WTC 1 Floor 96	11,700 lb	19,400 lb
WTC 1 Floor 97	9,500 lb	6,000 lb
WTC 1 Floor 98	2,200 lb	6,000 lb
WTC 1 Floor 99	770 lb	90 lb
Total Weight	66,100 lb	196,000 lb

E.9.2 WTC 2 Base Case Global Impact Analysis

The WTC 2 base case impact analysis was performed for a 0.62 s duration following initial impact of the aircraft nose with the south exterior wall. The side view and top view of the base case WTC 2 global impact response is shown in Figure E–34 and Figure E–35, respectively. Full penetration of the aircraft into the tower was completed at 0.2 s after impact. The aircraft impact response was very similar to that of the WTC 1 impact and was dominated by the penetration and fragmentation of the airframe structures. The fuselage structures were severely damaged both from the penetration through the exterior columns and the penetration of the 81st floor slab that sliced the fuselage structures in half. The downward trajectory of the aircraft structures caused the airframe to collapse against the floor, and the subsequent debris motion was redirected inward along a more horizontal trajectory parallel to the floor. The downward trajectory of the aircraft structures had transferred sufficient vertical load that the truss floor structures on the 80th and 81st floors began to collapse in the impact zone by the end of the simulation.

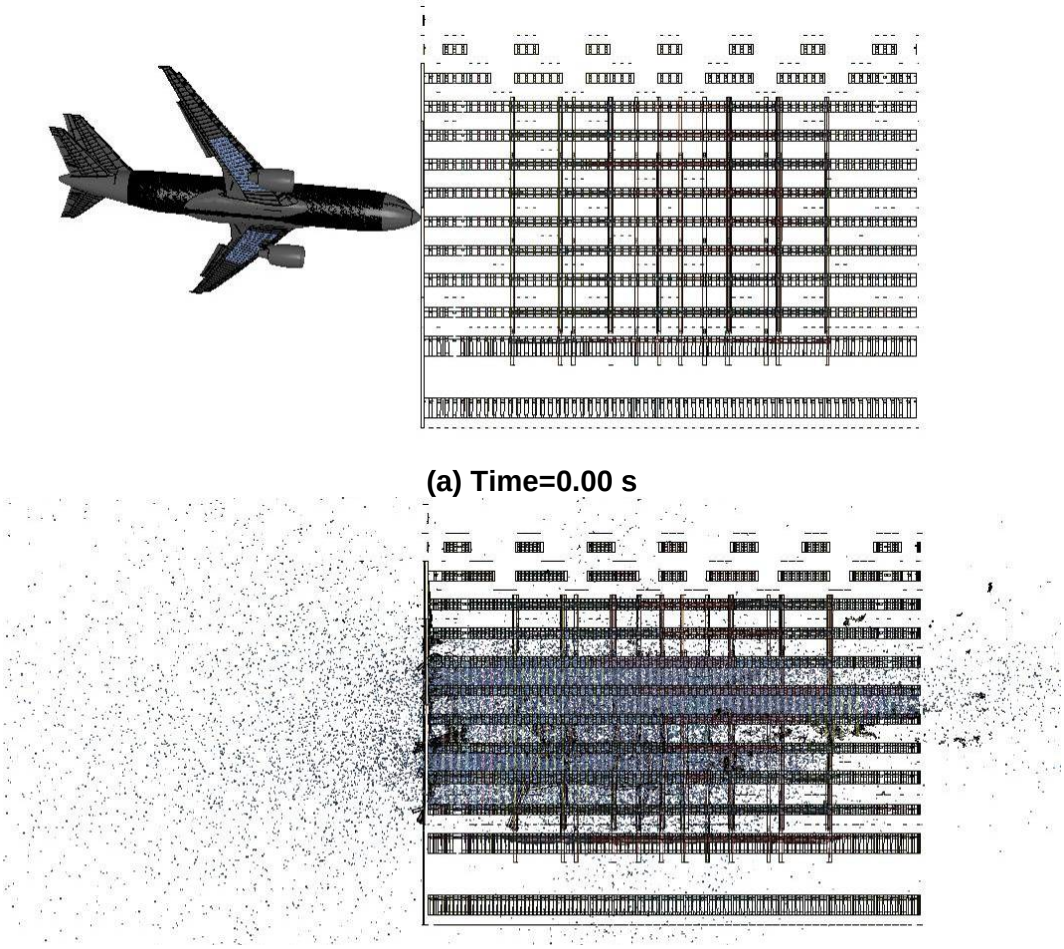

(a) Time=0.00 s

(b) Time=0.50 s

Figure E–34. WTC 2 base case global impact analysis – side view.

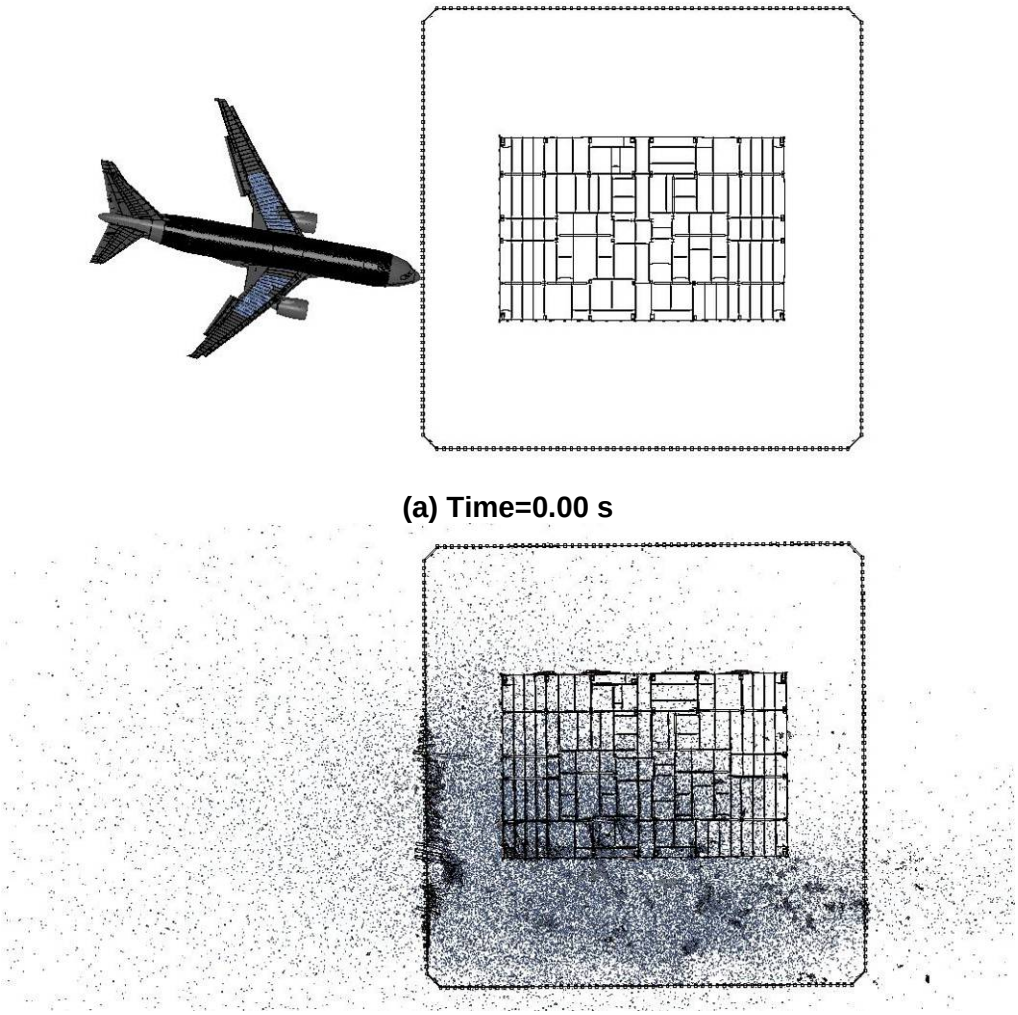

(a) Time=0.00 s

(b) Time=0.50 s

Figure E–35. WTC 2 base case global impact analysis – plan view.

The aircraft wing structures and fuel tank were fragmented by the impact with the tower exterior. The aircraft fuel cloud started to spread out immediately after impact, but the leading edge of the fuel remained relatively dense until passing approximately one-third of the lateral distance through the tower core (approximately 0.2 s after impact). At 0.3 s after impact, the aircraft fuel cloud had penetrated approximately two-thirds the distance through the core and was spreading out. Beyond this time, the subsequent motion of the aircraft fragments and fuel debris cloud was noticeably slowed. The spread of the fuel and debris cloud was more rapid and extensive in the open truss floor regions than through the core as a result of the open volume above the workstations in the truss floor zone.

Load transfer of the aircraft momentum into the tower structure is shown in Figure E–36. During the first 0.1 s of impact, the forward fuselage penetrated the exterior wall and impacted the interior structures. Between 0.1 s and 0.2 s a more rapid load transfer rate was observed as the area of the impact increased (extending outward in the wing impact regions) and a higher percentage of the aircraft mass impacted the interior structures. At 0.2 s, the aircraft completely penetrated the building and retained approximately 30 percent of its initial momentum. Beyond this time, the rate of load transfer steadily decreased with

very little load transfer after approximately 0.4 s. The behavior was very similar to that of the base case WTC 1 impact, shown in Figure E–27, but with a slightly compressed time scale due to the higher impact speed on WTC 2.

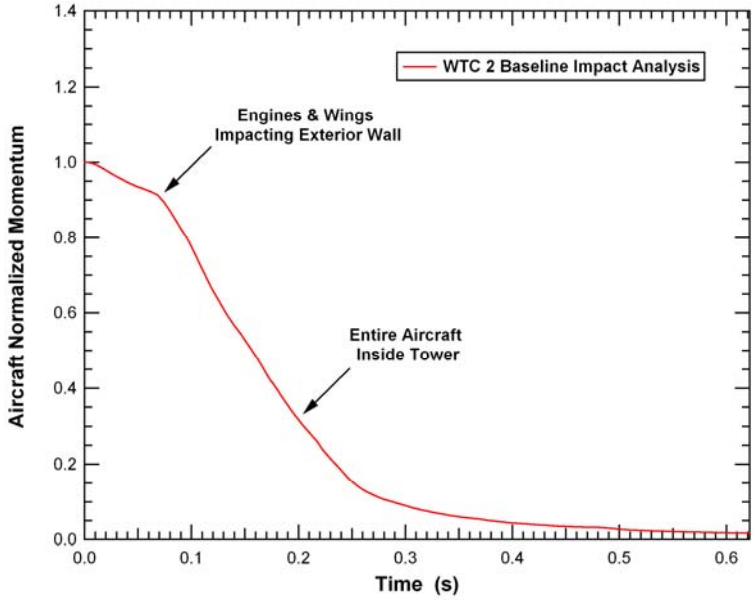

Figure E–36. Normalized aircraft momentum for the WTC 2 base case impact.

The aircraft was severely broken into debris as a result of the impact with WTC 2 as shown in Figure E–37. At the end of the impact analysis, the aircraft was broken into thousands of debris fragments of various size and mass, as shown in Figure E–37(b). A closer inspection of the debris field showed that larger fragments still occurred for specific components such as the engines and landing gear components. This behavior was very similar to the WTC 1 aircraft break up shown in Figure E–28.

Exterior Wall Damage

Damage to the north exterior wall calculated in the base case WTC 2 global impact analysis is shown in Figure E–38. The exterior wall completely failed in the regions where the fuselage, engine, and fuel-filled wing section impacted the structure. Damage to the exterior wall extended to the wing tips, but the exterior columns were not completely failed in the outer wing and vertical stabilizer impact regions. Failure of the exterior columns occurred both at the bolted connections between column ends and at various locations in the column, depending on the local severity of the impact load and the proximity of the bolted connection to the impact.

The calculated and observed geometry and magnitude of impact damage were in good agreement. That the position and shape of the impact damage agreed served to partially validate the geometry of the aircraft model, including the aircraft orientation, trajectory, and flight distortions of the wings. Agreement of both the mode and magnitude of the impact damage partially validated the constitutive and damage modeling of the aircraft and exterior wall of the tower.

(a) Aircraft structure (time=0.00 s)

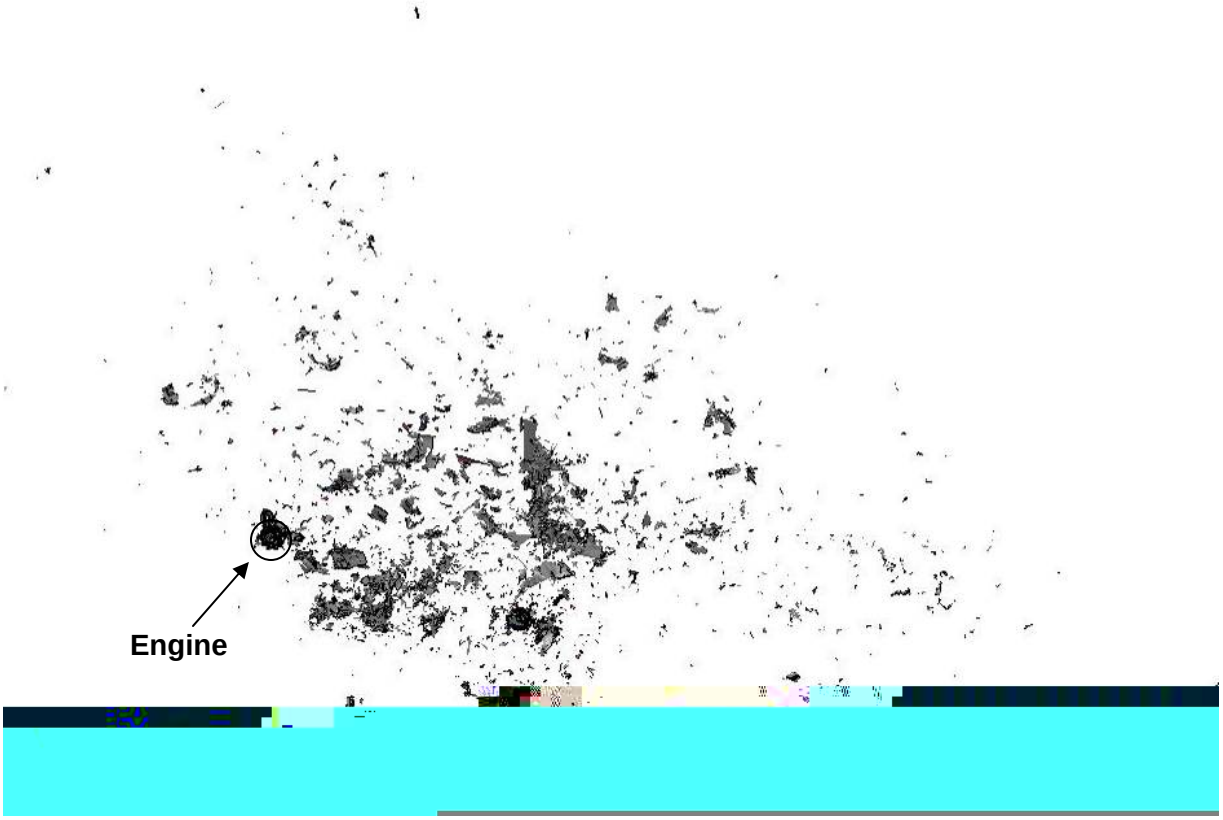

(b) Aircraft debris field (time=0.62 s)

Figure E–37. Aircraft break up and debris in the base case WTC 2 impact.

Core Damage

In the base case WTC 2 impact damage analysis, significant damage to the core was calculated in the region close to the impact point (the south east corner of the core). The columns in line with the aircraft fuselage failed on the impact side of the tower and several of the core beams were also severely damaged or failed in the impact zone. In some cases, failure of the column splices located on floors 77, 80, and 83 contributed significantly to the failure of the core columns. This was particularly true for the heavy column number 1001 at the southeast corner of the core that failed at three splice locations. A summary of the column damage is shown graphically in Figure E–39. A total of five columns were severed and four columns were heavily damaged.

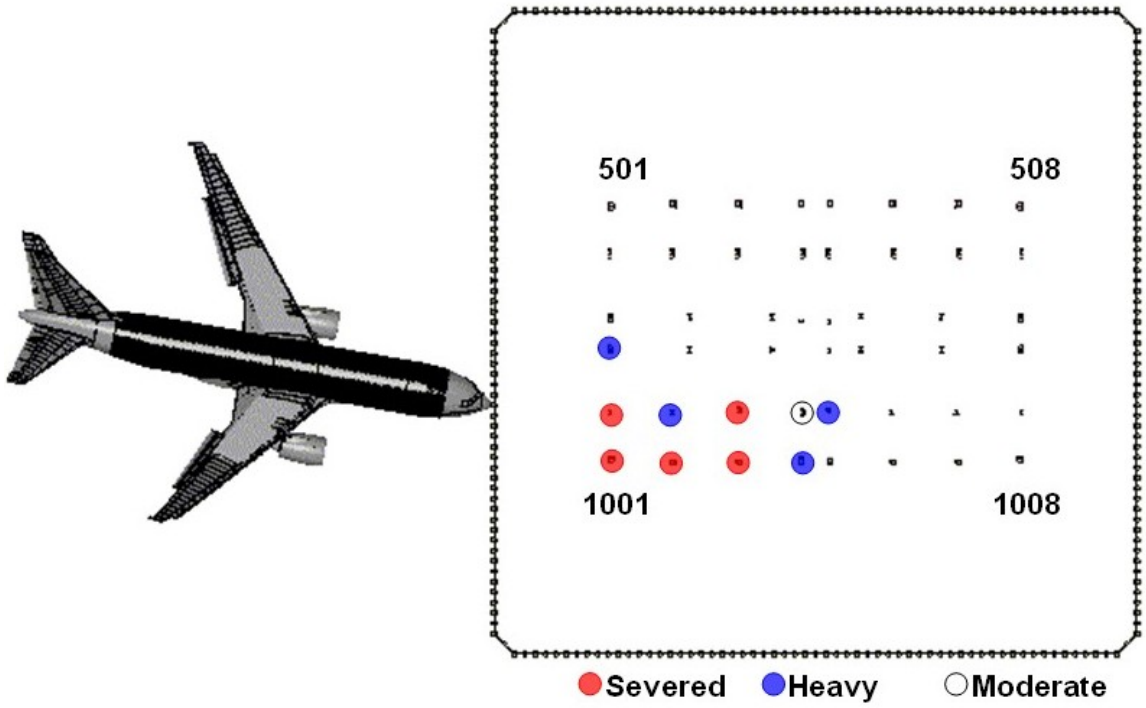

Figure E–39. Summary of core column damage for the base case WTC 2 impact.

Truss Floor Damage

An overall view for the floor truss structure in the WTC 2 impact zone, along with the calculated base case impact damage to the trusses, is shown in Figure E–40. The figure shows that the trusses experienced significant damage in the impact zone, with the greatest damage on floor 81. This severe damage to the floor 81 truss structure and floor slab was in the primary impact path of the fuselage and extended from the exterior wall to the core. The truss floor system on floors 79 and 81 had sufficient damage from the impact that truss floor sections were sagging downward as a result of the impact.

The calculated truss floor damage to WTC 2 was less than that of WTC 1, shown previously in Figure E–32, despite the higher aircraft impact energy for WTC 2. The higher truss floor damage and deflection in WTC 1 can be explained by two factors. The primary factor was that the WTC 1 downward impact trajectory was nearly twice as steep as that of the WTC 2 impact. As a result, the steeper impact

angle directed more impact energy normal to the floor slab. The vertical component of the impact load in WTC 1 was approximately 40 percent higher than in WTC 2. The secondary factor was that the damage to the long span truss floor in the WTC 1 impact zone produced larger displacements than the corresponding damage to the short span truss region in WTC 2.

(a) Initial detailed truss structures

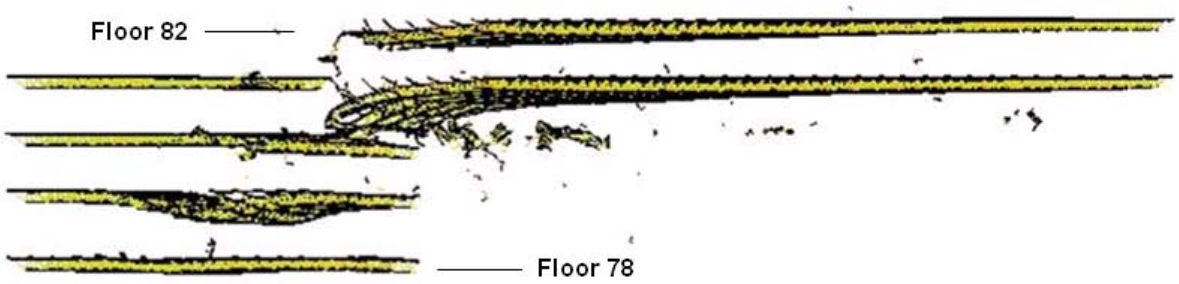

(b) Calculated damage

Figure E–40. Base case impact damage to the WTC 2 floor truss (front view).

Fuel and Debris Distribution

The calculated distribution of the aircraft debris and fuel cloud from the base case WTC 2 global impact analysis is shown in Figure E–34 and Figure E–35. At the end of the analysis, the residual momentum of the jet fuel in the impact direction was less than 1 percent of the initial momentum, indicating that the fuel cloud was nearly at rest at about 0.62 s. The bulk of the aircraft debris and fuel was arrested prior to exiting the tower structures. However, a significant amount of aircraft debris was calculated to exit the north and east sides of the tower (sides 300 and 200 of WTC 2). A portion of an engine exited the tower at the northeast corner of the building from the northeast corner of WTC 2. Based on the engine trajectory, it was estimated that the engine exited the building at approximately 120 mph. In the simulation, neither engine was calculated to exit WTC 2. At the end of the simulation, the speed of the aft portion of the starboard engine was below 80 mph and it was more than 60 ft away from the northeast corner of the building. For these calculations, it was estimated that the building contents would likely stop the engine fragment prior to impacting the northeast corner of the exterior wall. If the starboard engine impact location was lowered in the analysis by 1 to 2 ft, which is within the aircraft impact geometry uncertainty range, the engine would likely have not interacted with floor 82, and that would result in a larger residual speed inside the tower of over 100 mph. Also, if any portion of the east side of

WTC 2 was relatively free of office materials the engine fragment would have been free to move relatively unrestricted and would experience little loss of speed. As a result, in either case, the engine would likely have exited the tower in the simulation.

A quantitative characterization of the fuel and aircraft debris distribution is given in Table E–5. The bulk of the fuel and aircraft debris was deposited in floors 78 through 80, with the greatest concentration of aircraft debris on floor 80, and the largest concentration of aircraft fuel on floors 79, 81, and 82. The calculated debris distribution included 55,800 lb of debris and 10,600 lb of aircraft fuel outside of the tower at the end of the impact analysis, either rebounding from the impact face or passing through the tower. The calculated mass outside the tower is believed to be larger than is realistic since the exterior walls were not modeled with windows that could contain the fuel cloud and small debris inside the tower. In addition, treatment of the aircraft fuel cloud did not include the ability to stick to, or wet, interior components. Rather the aircraft fuel SPH particles would tend to bounce off of internal structures.

Table E–5. Fuel and aircraft debris distribution for the base case WTC 2 impact.

Tower Location	Aircraft Fuel	Aircraft Debris
Total Outside Tower	10,600 lb	55,800 lb
WTC 2 Floor 77	1,300 lb	400 lb
WTC 2 Floor 78	6,200 lb	4,800 lb
WTC 2 Floor 79	11,400 lb	16,200 lb
WTC 2 Floor 80	6,000 lb	83,800 lb
WTC 2 Floor 81	14,400 lb	27,300 lb
WTC 2 Floor 82	10,600 lb	3,600 lb
WTC 2 Floor 83	1,500 lb	4,300 lb
WTC 2 Floor 84	200 lb	500 lb
Total Weight	62,000 lb	197,600 lb

E.9.3 Different Severity Global Impact Analyses

Additional impact analyses were performed for each tower to provide a range of damage estimates due to the uncertainties in the calculated impact response. Two additional global impact analyses were performed for each tower in order to evaluate the impact response for a more severe and less severe impact scenario. The variations in impact conditions for the different severity global impact analyses were primarily obtained from the uncertainty analyses.

WTC 1 Global Impact Analyses

Impact conditions for the more and less severe WTC 1 impact scenarios are compared to the corresponding parameters in the base case analysis in Table E–6. The impact speeds were 414 mph and 472 mph in the less severe and more severe impact scenarios, respectively. These were the upper and lower bounds obtained from the analysis of aircraft impact conditions. The vertical trajectory of the aircraft was also varied from 13.6 degrees in the less severe case to 7.6 degrees for the more severe impact scenario. The reduced vertical trajectory angle resulted in a greater impact energy directed inward toward the core. The lateral trajectory was not varied since the impact was close to centered on the tower

and normal to the north face of WTC 1. A small variation in the lateral approach angle would have little effect on the energy of the aircraft debris entering the tower and core.

Table E–6. Input parameters for additional WTC 1 global impact analyses.

Analysis Parameters		Base case	More Severe	Less Severe
Flight Parameters	**Impact Velocity**	443 mph	472 mph	414 mph
	Trajectory - pitch	10.6°	7.6°	13.6°
	Trajectory - yaw	0.0°	0.0°	0.0°
	Orientation - pitch	8.6°	5.6°	11.6°
	Orientation - yaw	0.0°	0.0°	0.0°
Aircraft Parameters	**Weight**	100 percent	105 percent	95 percent
	Failure Strain	100 percent	125 percent	75 percent
Tower Parameters	**Failure Strain**	100 percent	80 percent	120 percent
	Live Load Weight[a]	25 percent	20 percent	25 percent

a. Live load weight expressed as a percentage if the design live load.

The calculated damage to the north exterior wall of WTC 1 from the three different severity impact analyses is shown in Figure E–41, along with a schematic of the observed damage. The overall agreement with the observed damage was good for all three analyses, with the base case global impact analysis providing the best match to the observed damage. The calculated damage magnitude was similar in each of the global analyses. The small differences in apparent damage were largely due to panels that may have severed columns in one case and were removed at the connections in another. In general, the trend was for a larger opening produced by the less severe impact and a smaller opening in the more severe impact. The increase in the opening with reduced severity impacts can be explained by the increased tower panel material toughness, resulting in a transition from severing of columns to the failure of connection bolts and panel removal.

Toward the wing tips, where the columns and spandrels were not completely severed, the more severe impact damage analysis calculated higher damage to the exterior wall panels. These columns had the largest amount of material with plastic strains above 5 percent (shown in red in the figure). As would be expected, the less severe impact damage analysis calculated lower damage to the exterior wall, and the base case analysis calculated an intermediate level of damage near the wing tips.

The calculated damage to the WTC 1 core columns for the three different severity impacts is shown in Figure E–42. The figure shows that the core damage was concentrated in the region of the core closest to the fuselage impact point, and there was a clear correlation in damage magnitude with the impact severity. A total of one column severed and two columns were heavily damaged in the less severe impact, compared to three columns severed and four columns heavily damaged in the base case impact analysis and six columns severed and three columns heavily damaged in the more severe WTC 1 impact analysis.

A strong correlation in core damage with impact severity was expected. All of the parameter variations in the three increasing severity analyses were selected to produce an increase in core damage. A higher impact speed and a shallower impact angle were selected to direct more energy toward the core. The aircraft mass was increased and given a higher material toughness. The mass of the tower contents was

reduced, and the tower materials were given a lower toughness. All of these variations contributed toward the increased core damage with impact severity.

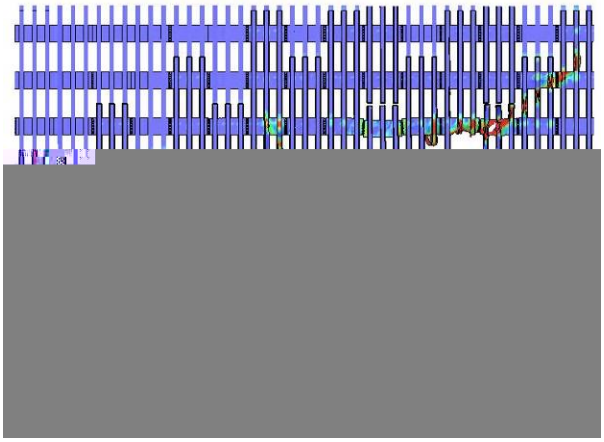

(a) Base case impact damage

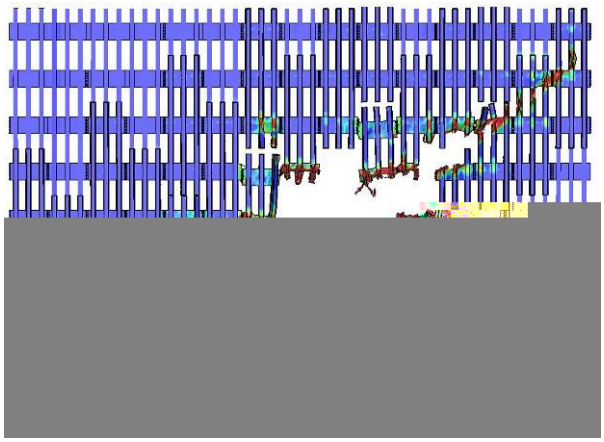

(b) More severe impact damage

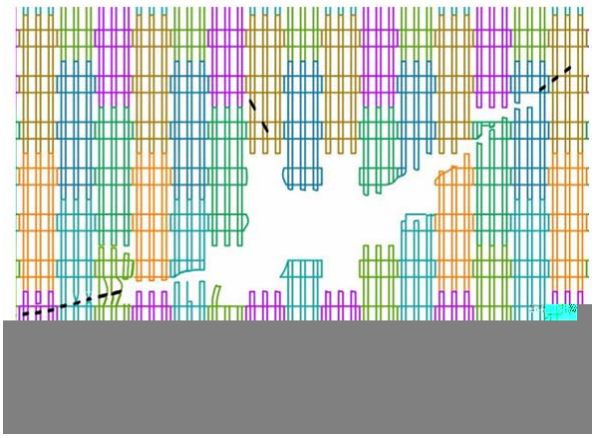

(c) Schematic of observed damage

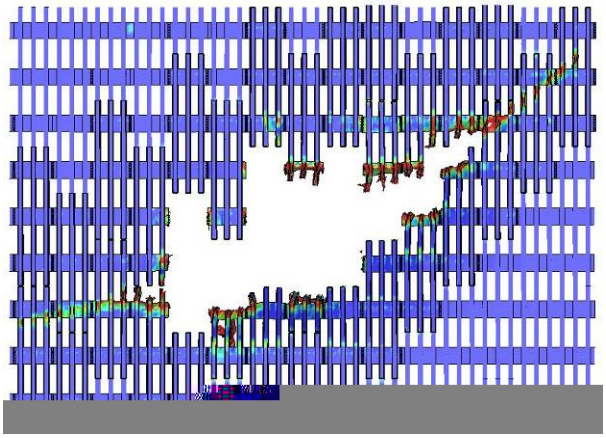

(d) Less severe impact damage

Figure E–41. Comparison of exterior wall damage for the WTC 1 impact analyses.

All of the WTC 1 global impact analyses resulted in a similar amount of damage to the truss floor and floor slab. Competing parameters cancel their respective effects on the floor damage. Variations in many of the parameters should cause greater damage to the floor system in the more severe impact analysis. However, the downward impact trajectory angle was also reduced to direct more energy into the core. Therefore, less of the impact energy was oriented into the floor system. The combined effects of varying these parameters led to very similar damage to the floor system in all of the analyses.

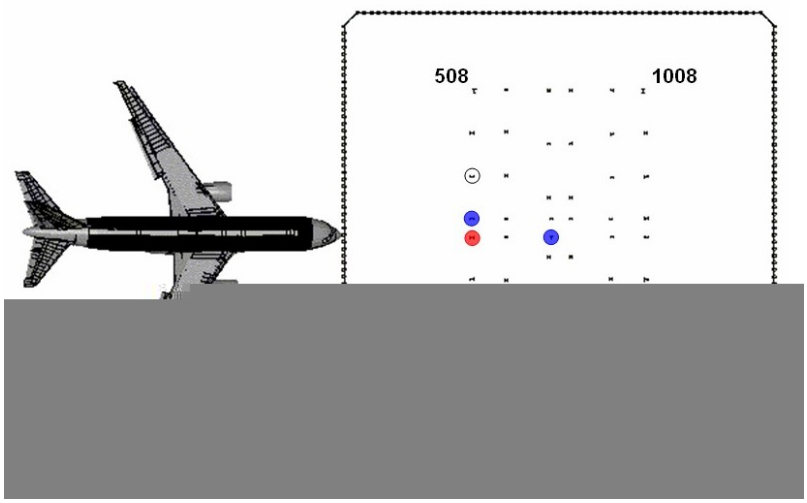

(a) Calculated less severe impact analysis

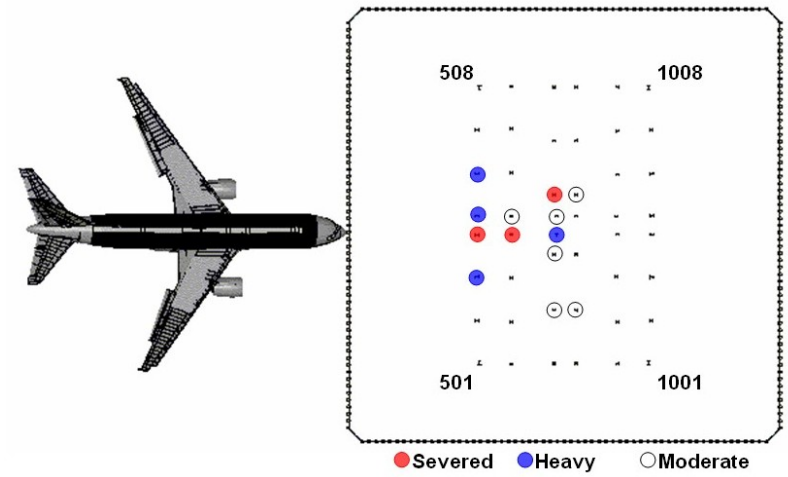

(b) Calculated base case impact damage

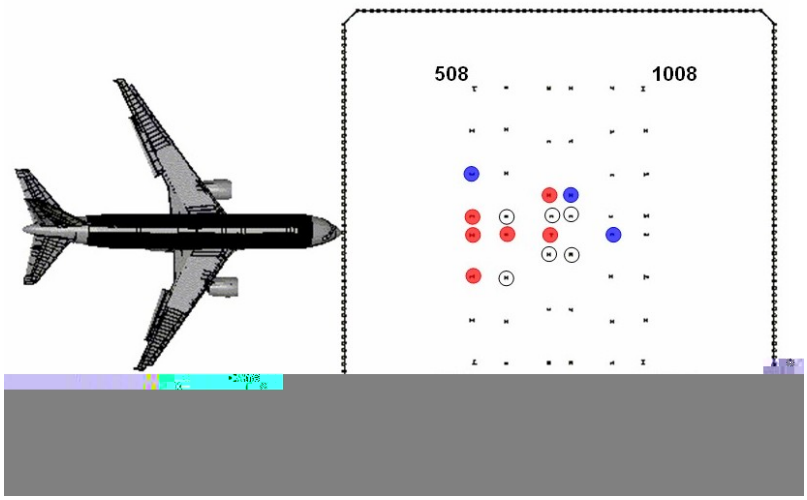

(c) Calculated more severe impact analysis

Figure E–42. Comparison of core column damage for the WTC 1 impact analyses.

WTC 2 Global Impact Analyses

Impact conditions for the more and less severe WTC 2 impact scenarios are compared to the corresponding parameters in the base case analysis in Table E–7. The impact speeds were 521 mph and 570 mph in the less severe and more severe impact scenarios, respectively. These speeds were the upper and lower bounds obtained from the analysis of aircraft impact conditions. The vertical trajectory of the aircraft was also varied from 5 (more severe case) to 8 degrees (less severe case) in order to direct less energy into the core for the less severe case.

Table E–7. Input parameters for additional WTC 2 global impact analyses.

Analysis Parameters		Base case	More Severe	Less Severe
Flight Parameters	**Impact Velocity**	546 mph	570 mph	521 mph
	Trajectory - pitch	6.0°	5.0°	8.0°
	Trajectory - yaw	13.0°	13.0°	13.0°
	Orientation - pitch	5.0°	4.0°	7.0°
	Orientation - yaw	10.0°	10.0°	10.0°
Aircraft Parameters	**Weight**	100 percent	105 percent	95 percent
	Failure Strain	100 percent	115 percent	75 percent
Tower Parameters	**Contents Strength**	100 percent	80 percent	100 percent
	Failure Strain	100 percent	90 percent	120 percent
	Live Load Weight[a]	25 percent	20 percent	25 percent

a. Live load weight expressed as a percentage if the design live load.

Calculated damage to the exterior wall and truss floor of WTC 2 showed similar trends to those seen in the WTC 1 analyses. Only slight changes in damage to these structures were calculated from the different severity impacts. Damage to the exterior was relatively insensitive to the parameter variations. Truss floor damage did not vary significantly due to the competing effect of the parameters varied.

Damage calculated for the WTC 2 core columns is shown in Figure E–43 for the three analyses performed. The figure shows that core damage was concentrated in the core region closest to the impact point. There is also a clear correlation in damage magnitude with the impact severity. A total of three columns were severed and two columns were heavily damaged in the less severe impact, compared to five columns severed and four columns heavily damaged in the base case analysis and ten columns severed and one columns heavily damaged in the more severe WTC 2 impact analysis.

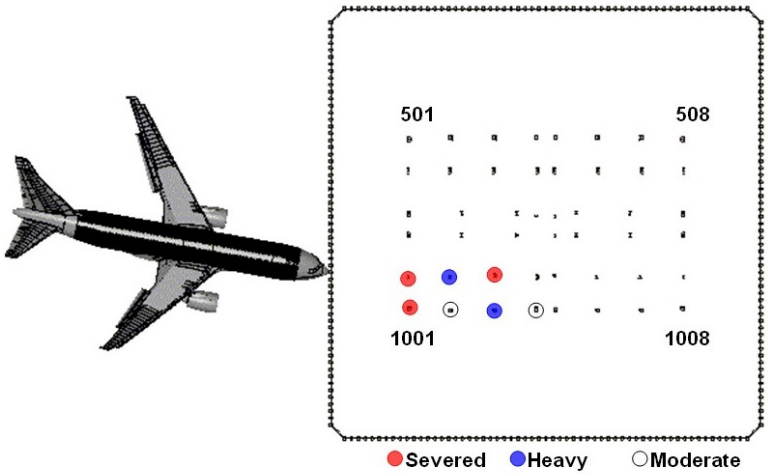

(a) Calculated less severe impact analysis

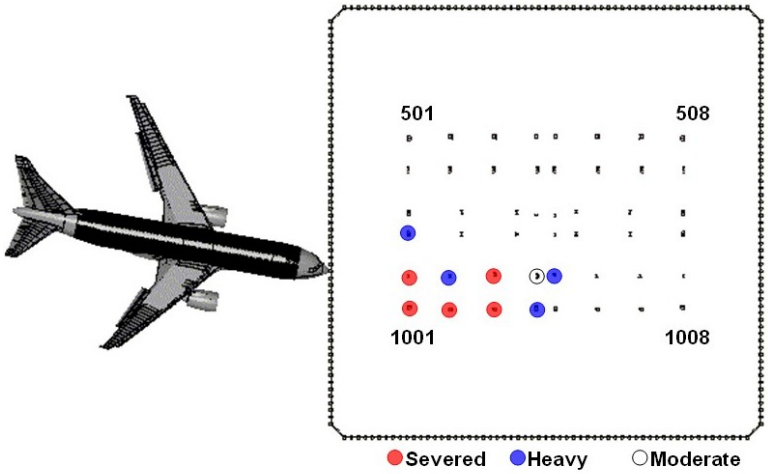

(b) Calculated base case impact damage

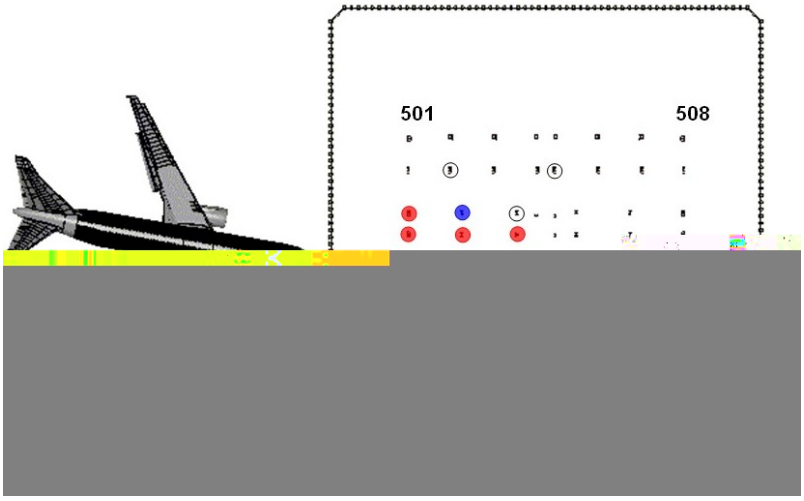

(c) Calculated more severe impact analysis

Figure E–43. Comparison of core column damage for the WTC 2 impact analyses.

E.9.4 Comparison with Observables

The observables available to help validate the global impact analyses included the following:

- Damage to the building exterior (exterior walls and floors in the immediate vicinity of the impact) documented by photographic evidence.
- Aircraft debris external to the towers (landing gear for WTC 1 and landing gear and engine for WTC 2) as documented by photographic evidence.
- Eyewitness accounts from survivors who were inside the towers (blocked or passable stairwells).

Not all of these observables were perfectly matched by the simulations due to the uncertainties in exact impact conditions, the imperfect knowledge of the interior tower contents, the chaotic behavior of the aircraft break up and subsequent debris motion, and the limitations of the models. In general, however, the results of the simulations matched the observables reasonably well.

E.9.5 Comparison with Previous Studies

Two studies to estimate the impact damage to the WTC towers were previously conducted. These studies were performed by staff at Massachusetts Institute of Technology (MIT) and Weidlinger Associates, Inc. (WAI). The MIT study used an energy balance approach to estimate damage to the core columns. The WAI study used the FLEX finite element code to calculate the aircraft impact damage to both towers. FLEX is an explicit, nonlinear, large deformation transient analysis finite element code with an overall code architecture similar to that of LS-DYNA. In the WAI calculations, the aircraft and WTC towers models were composed of beam and shell elements with 27,000 shell elements and 23,000 beam elements in the aircraft model. The aircraft fuel was included in the model by increasing the mass of the structures in the wing box.

Impact damage to the exterior north wall of WTC 1 calculated in this study is compared to the impact damage calculated by WAI in Figure E–44. The figure also shows a schematic of the damage observed in photographic evidence. The impact damage estimated in this study closely matched the observed damage for both towers. The damage profiles in the WAI impact simulations had some noticeable differences. Damage predictions from WAI included complete failure of the exterior columns over the entire length of the wings and top of the vertical stabilizer, and displayed local rupture of the columns adjacent to the impact point with less influence of the bolted connections on panel failure.

The differences in the damage profiles in the two calculations most likely resulted from a variety of differences in the models. One major difference between the two studies was in the fidelity of the aircraft models. The WAI aircraft model was based on their model of a Lockheed C-141B military transport rather than the Boeing 767. The NIST aircraft model contained an order of magnitude more elements and modeled the fuel explicitly. Secondary differences between the WAI and NIST impact analyses included, but were not limited to, variations in impact conditions (impact velocity, angle, location, etc.), aircraft model differences (airframe geometry, component thicknesses, mass distribution, material properties, etc.) and tower model differences (material properties, geometry, joint modeling, number of elements, etc.).

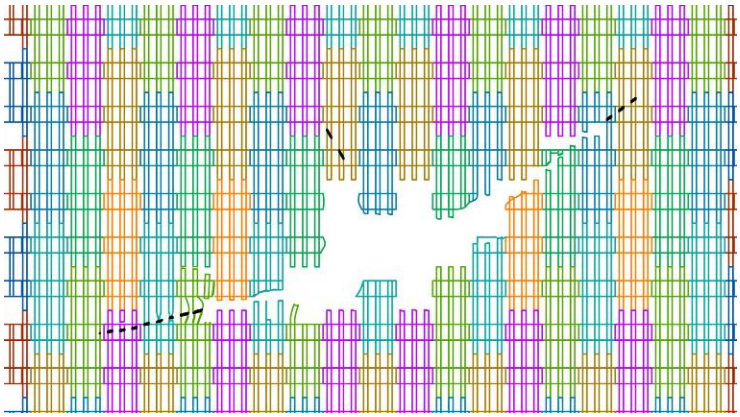

(a) Schematic of observed damage

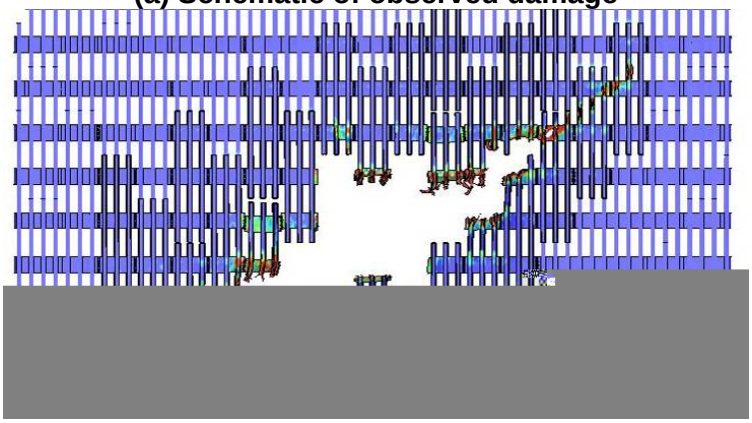

(b) NIST base case impact damage

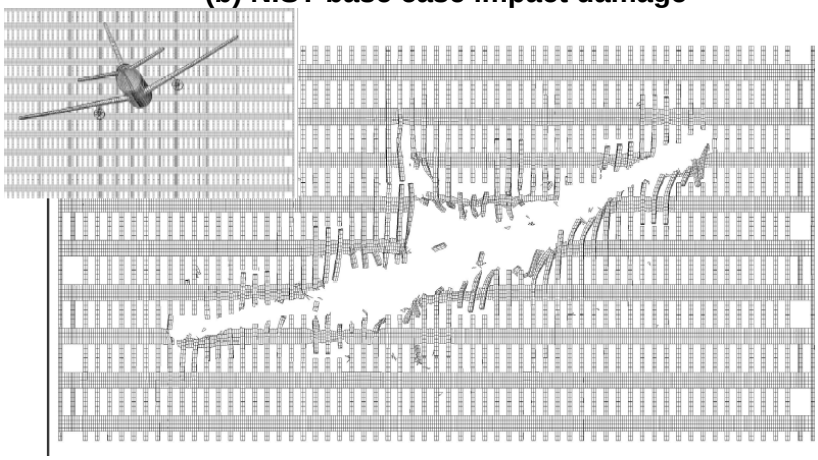

(c) WAI calculated damage

Figure E–44. Comparison of impact damage to the WTC 1 exterior wall.

Table E–8 compares the estimated core column damage from the various studies. For WTC 1, MIT estimated 4–12 core columns were failed (4 columns failed over a three-story length or 12 columns failed over a single floor length). The expected distribution of damage would fall between these bounds with some columns damaged on a single floor and others with damage distributed on multiple floors. WAI gave two estimates for core column failure. The first estimate of 23 core columns failed and 5 damaged was obtained from the FLEX impact analysis. The second estimate of 20 failed columns was the number

used in their collapse analysis. The NIST base case impact damage of 3 severed and 4 heavily damaged and less severe estimate of 1 severed and 2 heavily damaged falls below both the MIT and WAI estimates. The more severe estimate of 6 severed and 3 heavily damaged falls in the middle of the MIT range, but still well below the WAI estimates.

Table E–8. Comparison of damage to core columns from various studies.

WTC Impact Investigation	WTC 1 Core Column Damage	WTC 2 Core Column Damage
MIT Impact Analysis	4-12 Failed	7-20 Failed
WAI Impact Analysis	23 failed & significantly damaged Plus 5 Damaged	14 failed and significantly damaged Plus 10 damaged
WAI Collapse Analysis	20 Failed	5 Failed
NIST Base Case Impact Analysis	3 Severed Plus 4 Heavily Damaged	5 Severed Plus 4 Heavily Damaged
NIST More Severe Impact Analysis	6 Severed Plus 3 Heavily Damaged	10 Severed Plus 1 Heavily Damaged
NIST Less Severe Impact Analysis	1 Severed Plus 2 Heavily Damaged	3 Severed Plus 2 Heavily Damaged

A similar trend in the predicted damage to the core columns was found in the WTC 2 analysis. MIT estimated 7–20 columns failed (from 7 columns failed over a three-story length to 20 columns failed over a single floor length). WAI calculated 14 core columns failed and another 10 damaged in their FLEX analysis, but reduced the number of failed columns to 5 for their collapse analysis. The NIST base case impact damage of 5 severed and 4 heavily damaged, as well as the more severe estimate of 10 severed and 1 heavily damaged fell in the middle of the range predicted by MIT. The less severe impact scenario predicted fewer columns severed and heavily damaged than the MIT and WAI studies.

The MIT prediction for the number of failed core columns agrees remarkably well with the NIST estimates using their simplified analysis. The WAI impact analysis predicted higher core column failure and damage than the NIST estimates. One reason for the higher damage prediction may be attributed to the lack of internal tower contents in the WAI model, such as workstations and other building contents. Another reason for the higher damage prediction in the WAI study could result from the aircraft model.

In conducting a collapse analysis, WAI used engineering estimates to reduce the number of failed columns from that predicted by their FLEX model to stabilize the tower immediately after impact. For WTC 2 their adjusted estimate fell in line with the MIT and NIST studies.

E.10 SUPPORTING SIMPLIFIED ANALYSES

Approximate impact analyses were carried out to provide guidance to the global finite element impact analyses. The specific analyses included:

- The analysis of the overall aircraft impact forces: This analysis indicated that the momentum transfer was more important than the strength of the impacting aircraft in determining the overall impact loads on the building.

- The effects of the energy in the rotating engine components: This analysis indicated that the potential for the rotational kinetic energy of the engine to significantly change the magnitude of the tower impact damage is small.

- The influence of the static preloads on the calculated impact damage: This analysis showed that the initialization of a static preload in the columns of the towers would not have a significant effect on the tower impact response, damage, or residual strength.

- The analysis of the load characteristics required to damage core columns: This analysis determined the characteristics of a debris cloud (i.e., density and speed) necessary to fail a core column. Application of this analysis indicated that the dispersed fuel cloud alone would not be sufficient to fail core columns.

This page intentionally left blank.

Chapter 1
INTRODUCTION

The objective of this effort was to analyze the aircraft impacts into each of the World Trade Center (WTC) towers to provide the following: (1) estimates of probable damage to structural systems due to aircraft impact, including exterior walls, floor systems, and interior core columns; (2) estimates of the aircraft fuel dispersal during the impact; and (3) estimates of debris damage to the interior tower contents, including partitions and workstations. Thus, this analysis established the initial conditions for the fire dynamics modeling and for the thermal-structural response and collapse initiation analysis.

The WTC aircraft impact analysis is very complex, with large scale fracture and fragmentation of both tower and aircraft structures, nonlinear rate-dependent material behaviors, and the fluid-structure interaction of the aircraft fuel. The analyses of the aircraft impacts performed for this investigation are believed to be the highest-fidelity simulations ever performed for this type of impact behavior using state-of-the art analysis methodologies. Wherever possible, the models were validated against observables or supporting test data developed by the WTC Investigation.

The impact analyses were conducted at various levels of complexity including: (1) the component level, (2) the subassembly level, and (3) the global level to estimate the probable damage to the towers due to aircraft impact. Analyses of uncertainties using the component, subassembly, global, and simplified analyses were conducted to assess the effects of variability associated with various input parameters and identify the most influential parameters that affect the damage estimates using orthogonal factorial design. Based on the results of the sensitivity analyses, the most influential parameters that were identified were varied in the global models to provide a range of damage estimates for WTC 1 and WTC 2.

As part of the tower and aircraft models, constitutive relationships describing the actual behavior of the structures under the dynamic impact conditions of the aircraft were developed based on test results of the tower steels and from the open literature for other materials. Various grades of steels used in the exterior walls and core columns of the towers, weldment metal, bolts, reinforced concrete, and aircraft materials were considered. The constitutive relationships included high strain-rate effects and failure criteria for the various materials. Details on the development of the materials constitutive models are provided in Chapter 2.

The development of the tower and aircraft global models are explained in Chapters 3 and 4, respectively. The tower models were developed based on the original WTC drawings and the structural databases of the towers developed within the framework of the baseline structural performance. The tower models included the primary structural components of the towers in the impact zone, including exterior walls, floor systems, core columns, and connections. A refined finite element mesh was used for the areas in the path of the aircraft, and a coarser mesh was used elsewhere. The Boeing 767 aircraft model was developed based on information gathered from documentary aircraft structural information and data from measurements on a Boeing 767 aircraft. The model included the aircraft engines, wings, fuselage, empennage, and landing gear, as well as nonstructural components of the aircraft.

The WTC towers and Boeing 767 aircraft are complex structural systems. In the global model development process, the objective was to include all of the primary structural components and details of both the aircraft and towers. This approach, however, results in very large models. The component and subassembly analyses were used to determine model simplifications to reduce the overall model size while maintaining fidelity in the analysis. Therefore, a series of component impact and subassembly analyses were performed. The primary objectives of the component and subassembly modeling were to (1) develop an understanding of the interactive failure phenomenon of the aircraft and tower components and (2) develop the simulation techniques required for the global analysis of the aircraft impacts into the WTC towers, including variations in mesh density and numerical tools for modeling fluid-structure interaction for fuel impact and dispersion. The approach taken for component modeling was to start with finely meshed models of key components of the tower and aircraft structures and progress to relatively coarsely meshed beam and shell element representations that were used for the global models. An example of component level analysis is the analysis of exterior wall panels impacted by a segment of an aircraft wing with and without fuel. An example of the subassembly analysis is an aircraft engine impacting a strip from the exterior wall to the core of the tower. Component and subassembly analyses are described in Chapters 5 and 6, respectively.

Chapter 7 provides the initial conditions of the impact of the aircraft into the WTC towers. These include impact speed, aircraft orientation and trajectory, and impact location of the aircraft nose. This task utilized the two videos that captured the approach and impact of the American Airlines flight 11, which impacted WTC 1, and the several videos that captured United Airlines flight 175, that impacted WTC 2. In addition, a large body of photographic evidence was used to determine the impact location and orientation relative to the towers. These videos and photographs were analyzed to estimate, with the best accuracy possible, the speed, horizontal and vertical angles of incidence, and roll angle of each aircraft. Uncertainties in each of these parameters were also quantified.

The analysis of aircraft impact into the WTC towers is subject to large uncertainties in the input parameters, such as the initial conditions of the impact, material properties, mass properties of aircraft and building contents, connection behavior, modeling uncertainties, etc. Uncertainty analyses were performed at the component and subassembly levels, as reported in Chapter 8. The objectives of these analyses were to assess the effect of uncertainties on the level of damage to the towers after impact and to determine the most influential parameters that affect the damage estimates.

Chapter 9 presents the results of the global analyses of aircraft impact into WTC 1 and WTC 2 using the global tower and aircraft models. The analysis results included the estimation of the structural damage that degraded their strength and the condition and position of nonstructural contents such as partitions, workstations, aircraft fuel, and other debris that influenced the behavior of the subsequent fires in the towers. The global analyses included, for each tower, a “base case” based on a best estimate of all input parameters. They also provided more and less severe damage estimates based on variations of the most influential parameters. These more and less severe damage scenarios provided a range of damage estimates of the towers due to aircraft impact. Comparisons between the simulation results and observables obtained from video and photographic evidence, as well as eyewitness interviews, were also conducted. The chapter also provides a comparison with prior estimates of the damage obtained from other studies.

Approximate analyses were carried out to provide guidance to the global finite element impact analyses. As reported in Chapter 10, these analyses included: (1) the analysis of the overall aircraft impact forces and assessment of the relative importance of the airframe strength and weight distribution, (2) the evaluation of the potential effects of the energy in the rotating engine components on the calculated engine impact response, (3) the influence of the static preloads in the towers on the calculated impact damage and residual strength predictions, and (4) the analysis of the load characteristics required to damage core columns compared to the potential loading from impact of aircraft components.

This page intentionally left blank.

.

Chapter 2
MATERIAL CONSTITUTIVE MODELING

2.1 INTRODUCTION

An important requirement for high fidelity simulation of the aircraft impact damage is the development of constitutive models that represent the actual behavior of the World Trade Center (WTC) towers and aircraft structure under the dynamic impact conditions of the aircraft. The primary materials considered for the impact analyses included the several grades of steel used in the columns, spandrels, and floor trusses and beams of the WTC towers, the concrete floor slabs, and the aluminum airframe structure of the Boeing 767 aircraft. All of these materials played a significant role in the aircraft impact damage analyses. These materials exhibit significant nonlinear rate-dependent deformation and failure behavior over the range of strain rates expected in the impact scenario.

Secondary materials of interest included the nonstructural aircraft components and masses such as fuel, seats, interior trim, cargo, and luggage. Furthermore, a significant part of the mass of the WTC towers was material not included in the primary structural steel frame, such as nonstructural walls, partitions, furniture and other building contents, flooring, mechanical equipment, and insulation. The strength of these materials is relatively small compared to the structural materials, and a simple description of their constitutive behavior is adequate.

The analysis of the aircraft impact damage was performed with the LS-DYNA finite element code (LS-DYNA Version 971). LS-DYNA has an extensive library of more than 130 different constitutive models and was capable of accurately reproducing the important material behaviors required in this analysis. Material models currently available in LS-DYNA have been utilized for the analyses using material data from tests conducted by the National Institute of Standards and Technology (NIST) or available in the public domain.

2.2 WTC TOWER STEEL CONSTITUTIVE MODELS

Various constitutive models are available in LS-DYNA that can capture the nonlinear behavior of the steel under impact conditions, including strain rates effects and failure. The primary constitutive model applied was the Piecewise Linear Plasticity model. This model was sufficient to model the nonlinear dynamic deformation and failure of the steel structures. A tabular effective stress versus effective strain curve can be used in this model with various definitions of strain rate dependency.

The constitutive model parameters were developed for each grade of steel used in the construction of the WTC towers based on engineering stress-strain data provided by the NIST mechanical and metallurgical analysis of structural steel (see NIST NCSTAR 1-3).[1] The approach to developing the constitutive parameters for each grade of steel was:

[1] This reference is to one of the companion documents from this Investigation. A list of these documents appears in the Preface to this report.

- Convert the engineering stress-strain curve to a true stress versus true strain curve. The conversion process is described below and is valid up to the onset of necking in the specimen.
- Extrapolate the true stress-strain curve beyond the point of necking onset.
- Perform iterative finite element analyses of the tensile test and adjust the true stress-strain curve extrapolation and failure strain until the necking behavior and failure point were accurately captured. The primary criterion was the quantitative agreement of the measured and calculated engineering stress-strain behavior in the softening region beyond maximum stress. These analyses required a fine mesh resolution in the specimen to accurately model the large strain deformation response during necking.
- Perform a final finite element analysis of the material test using a coarser mesh resolution (medium mesh corresponding to the mesh resolution applied in the component analyses). Adjust the failure criteria (strain at failure) to obtain failure at the same engineering strain level.

The advantage of this approach was that the measured nonlinear material behavior up to failure was accurately captured in the constitutive model. In addition, the simulation of the material testing provided a validation that the constitutive model parameters were defined accurately and that the model could reproduce the measured response for the test conditions.

The tensile tests performed by NIST applied the ASTM 370 test standard (ASTM Designation A 370-03a 2003). Example finite element models of a rectangular test specimen with the fine and medium mesh resolutions are shown in Figure 2–1. This specimen type was used for all of the tests on WTC exterior column materials. A similar figure of the round bar specimen models used for testing of the WTC core column steels is shown in Figure 2–2. The typical element length used in the gage section for the fine meshes was approximately 0.015 in. and for the medium meshes was approximately 0.10 in. The use of the specimen models to develop the constitutive model parameters is described in the following sections.

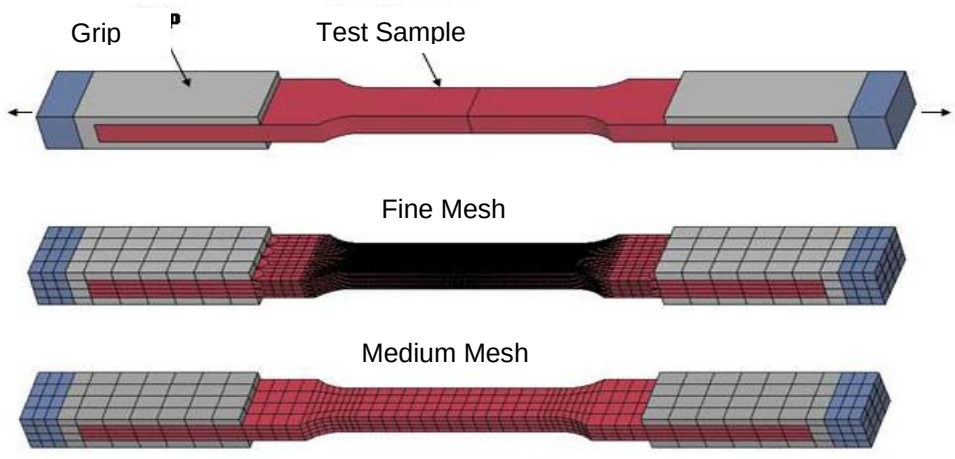

Figure 2–1. Example finite element models of the ASTM 370 rectangular tensile specimen.

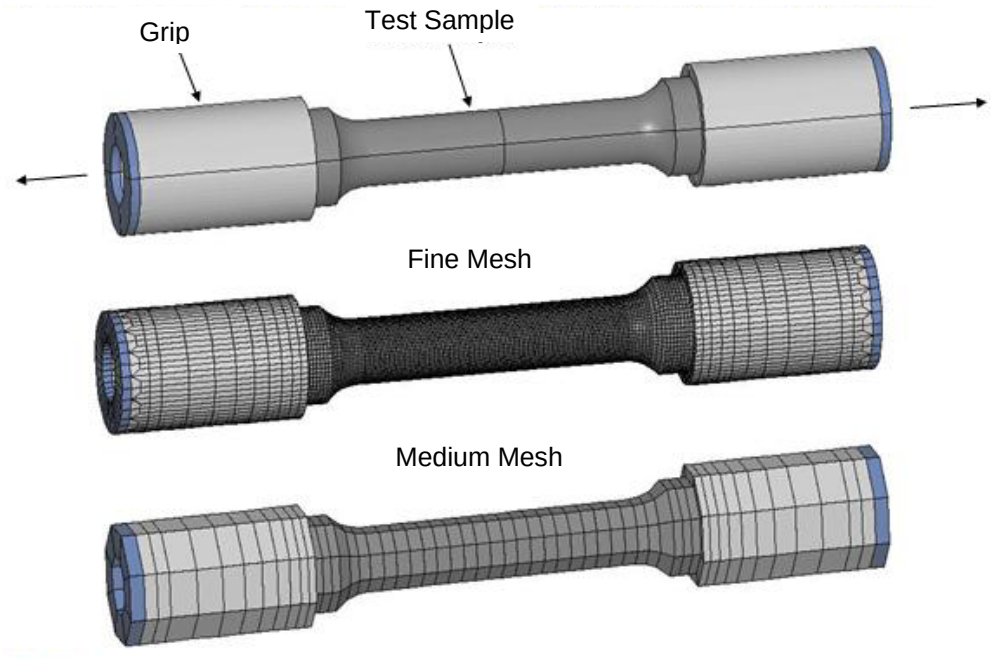

Figure 2–2. Example finite element models of the ASTM 370 round bar tensile specimen.

2.2.1 True Stress and True Strain Corrections

In most tensile tests, a plot is generated of the load measured at the cross head of the testing machine against the displacement of the specimen. A plot of engineering stress versus strain can be generated from this plot by dividing the load by the original cross sectional area of the specimen and the displacement by the original length of the specimen. If the changes in area and length are small during the test, these measures give a good indication of material behavior. However, in reality, the cross section changes (shrinks) significantly during the test, and the engineering stress does not yield the "true" stress in the cross section. Similarly, the engineering strain is not representative of the material behavior, especially when a general three-dimensional state of strain exists. As a result, the engineering stress decreases as some materials approach failure, implying a weakening of the material. In reality, the stress in the cross section is increasing due to the reduction in the cross sectional area (i.e., necking).

There are several different ways to measure stress and strain based on the coordinate system used. Some are based on material (Lagrangian) coordinates and some on spatial (Eulerian) coordinates. These give rise to terms such as "Green" and "Almansi" strain tensors. These are important in writing a computer code to solve large strain problems. An alternate approach is to define a "true" or "natural" stress and strain. The true stress is based on the load divided by the actual cross sectional area of the specimen and is equal to the engineering stress multiplied by a term to correct for the change in cross section.

$$\sigma_T = \sigma_{eng}(1+e) \tag{1}$$

where σ_T and σ_{eng} are the true and engineering stresses, respectively, and e is the engineering strain.

Prior to the onset of localization (necking), the natural or true strain, ε_T, is defined as

$$\varepsilon_T = \ln(\frac{l}{l_o}) = \ln(1+e) \tag{2}$$

This definition comes about from defining the incremental true or "natural" strain as the current "change in length" divided by the current length, or

$$d\varepsilon_T = \frac{dl}{l} \tag{3}$$

This is in contrast with the definition of engineering strain that references the change in length, Δl, divided by the original length, l_0, or

$$e = \frac{\Delta l}{l_0} \tag{4}$$

After the onset of localization, the determination of the true strain in the necked region becomes more complex and requires measurement of the local neck geometry.

2.2.2 Development of Steel Constitutive Properties

In this section, examples are provided to illustrate the methodology for constitutive model development of the WTC tower steels, as well as typical results. Figure 2–3 shows an example of the measured engineering stress-strain behavior for the 75 ksi perimeter column steel. Four tests were performed by the NIST Investigation (NIST NCSTAR 1-3) on each grade of steel, and the data clearly indicated anisotropy in the behavior introduced by the roll forming process (longitudinal tests L1 and L2 versus transverse tests T1 and T2 in the figure). This particular grade of steel had a larger anisotropy than seen in most of the other steel grades. Whenever anisotropy was observed, the material had greater ductility for specimens aligned with the rolling direction. The largest effects of the anisotropy were observed in the behavior after the onset of necking.

The first step in the constitutive model development process was to obtain a true stress-true strain curve. The typical approach was to select a representative test and perform the data conversion process described in Section 2.2.1. In this example, the data from test L1 was used to create the true stress-strain curve shown in Figure 2–3. This true stress-strain curve was then approximated by a piecewise linear curve in tabular form as shown in Figure 2–4. This tabular curve was the input used to specify the mechanical behavior in the constitutive model.

The final step was to apply the tabular true stress-strain behavior in the constitutive model to simulate the tensile test as shown in Figure 2–5. If necessary, the extrapolation of the true stress-strain behavior was adjusted until the simulation matched the measured engineering stress-strain response, including necking and failure (the portion of the stress-strain curve beyond the maximum engineering stress). A comparison of the calculated and measured tensile behavior for the 75 ksi perimeter steel is shown in Figure 2–6. In this example, the constitutive model was developed as an average between the longitudinal and transverse properties. Results of tests conducted by the NIST Investigation on the tower steels indicated that the stress-strain behavior was very similar in the longitudinal and transverse directions up to the onset of

necking. The difference between the longitudinal and transverse properties was in the ductility, where the average ratio of the longitudinal to transverse strain to failure in the exterior column steels is about 1.22:1. The approach used in the constitutive modeling was to use an average of the longitudinal and transverse properties and ignore the orthotropic characteristics of the material in the impact analyses. The effects produced by the variation of ductility between the longitudinal and transverse directions were assessed as part of the uncertainty analyses.

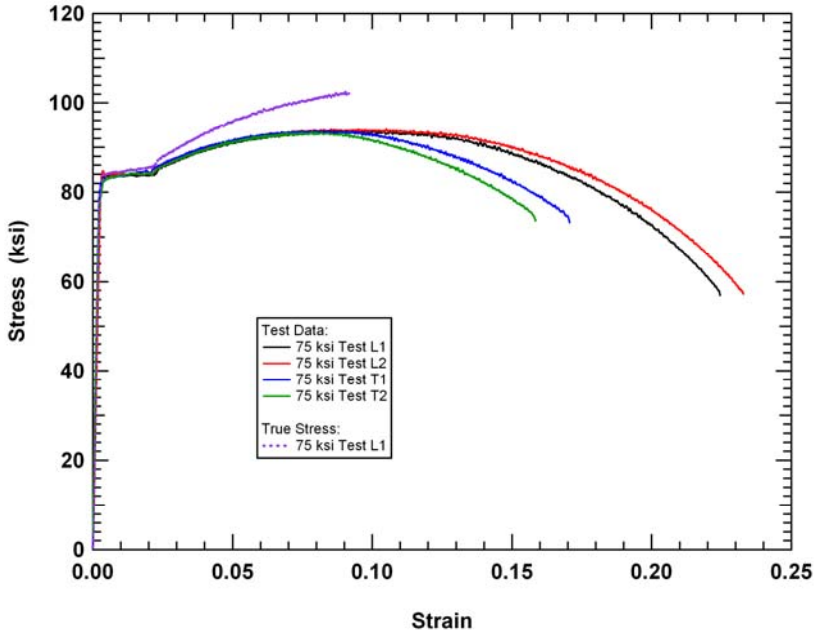

Figure 2–3. Test data and true stress-strain conversion for the 75 ksi steel.

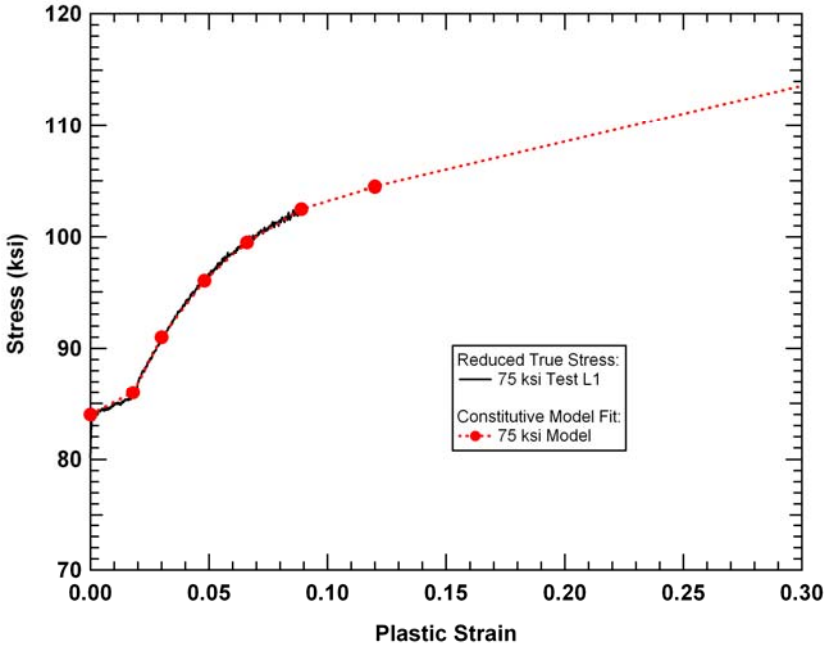

Figure 2–4. Tabular true stress-strain constitutive model curve for the 75 ksi steel.

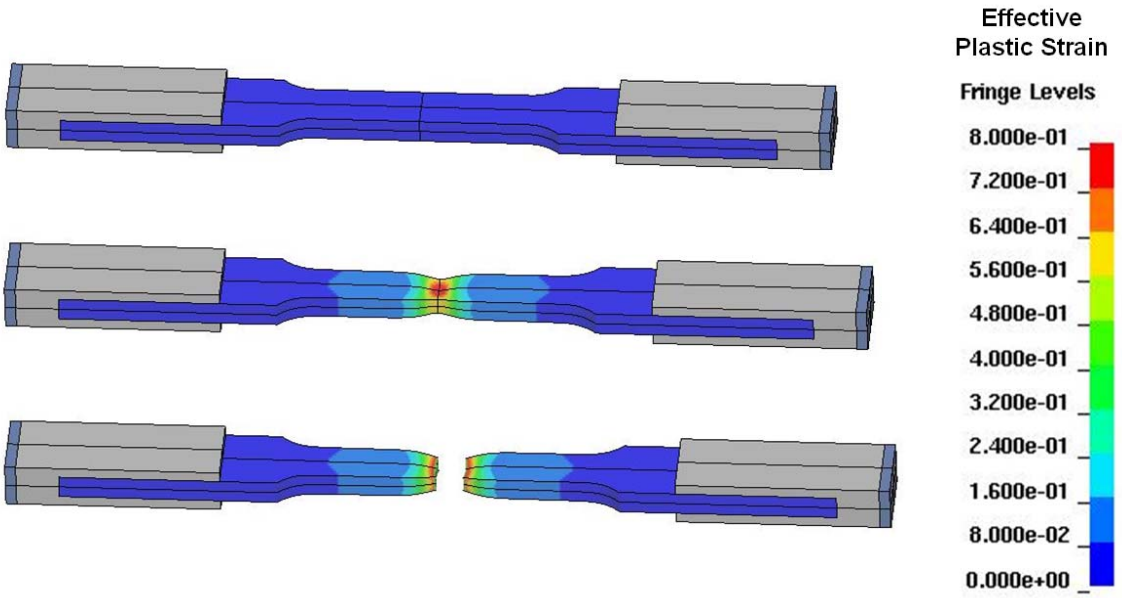

Figure 2–5. Calculated tensile test response with necking for the 75 ksi steel.

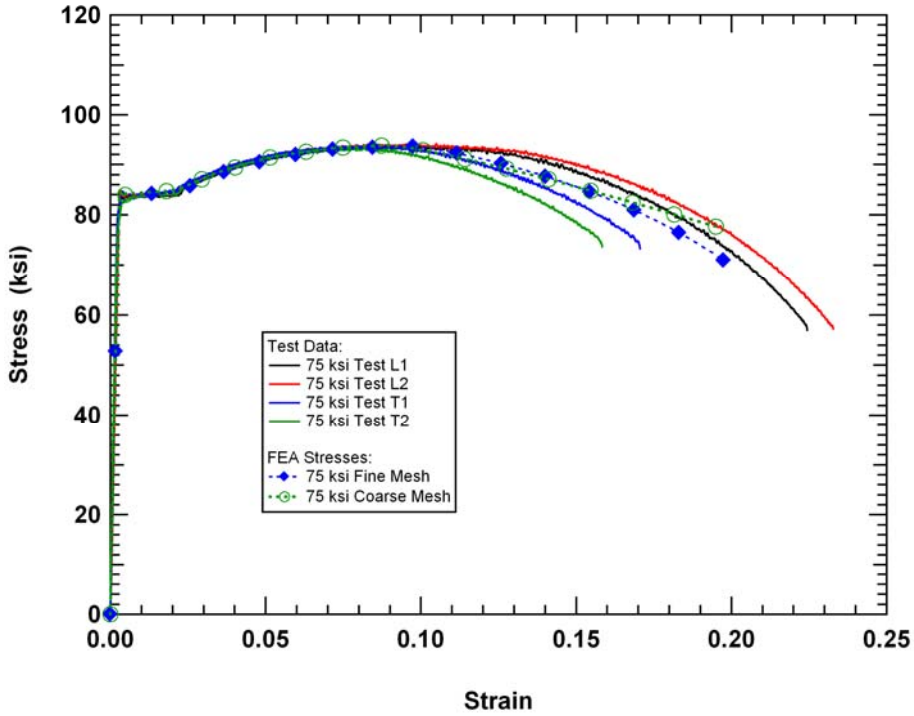

Figure 2–6. Comparison of measured and calculated engineering stress-strain curves for the 75 ksi steel.

The resulting true stress-true strain behavior incorporated into the constitutive model was representative of the steels tested in this Investigation. However, there were multiple sources (suppliers) of steel used in the construction of the WTC towers. The NIST Investigation (NIST NCSTAR 1-3) developed synthetic stress-strain curves for each grade of steel based on several data sources. As indicated in Section 2.2, the

test data were used as the input for the material modeling to provide validated stress-strain properties up to failure. A comparison of this synthetic curve with the constitutive model behavior for the 75 ksi steel is shown in Figure 2–7. There were observable differences in the curves, such as the representation of a yield point behavior in the constitutive model. However, the differences were not sufficiently large to produce a large variation in the calculated structural impact behavior. In addition, the effect of material strength variation on impact damage was assessed in the uncertainty analyses.

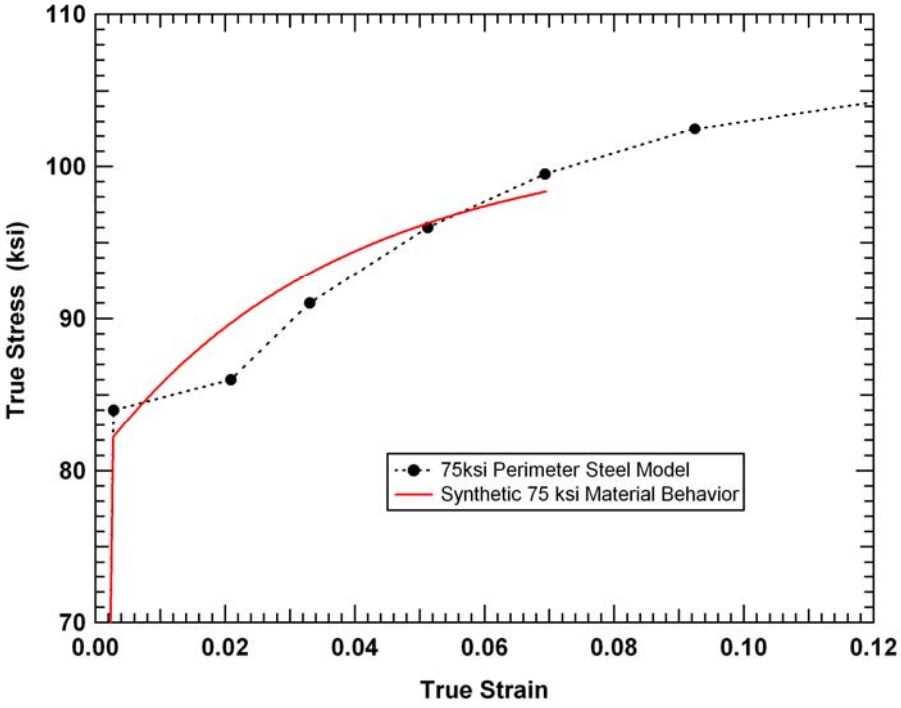

Figure 2–7. Comparison of the constitutive model and synthetic steel behaviors for the 75 ksi steel.

The procedure described above was applied to develop constitutive models for all of the WTC tower steels for which test data were provided by the NIST mechanical and metallurgical analysis.

2.2.3 Summary of Steel Constitutive Properties

A summary of the true stress-strain curves used in the constitutive models for the various WTC tower steels are summarized in Figure 2–8. Similarly, a comparison of the true stress-strain constitutive curves with the synthetic stress-strain curves, developed during the mechanical and metallurgical analysis of structural steel, for the various exterior column steels is shown in Figure 2–9 and Figure 2–10, and for core column steels in Figure 2–11. In general, the true stress-strain curves developed from the test data and the synthetic curves developed from multiple sources agreed to within approximately 10 percent. This variation in measured and expected material strengths was considered in the uncertainty analyses described in Chapter 8.

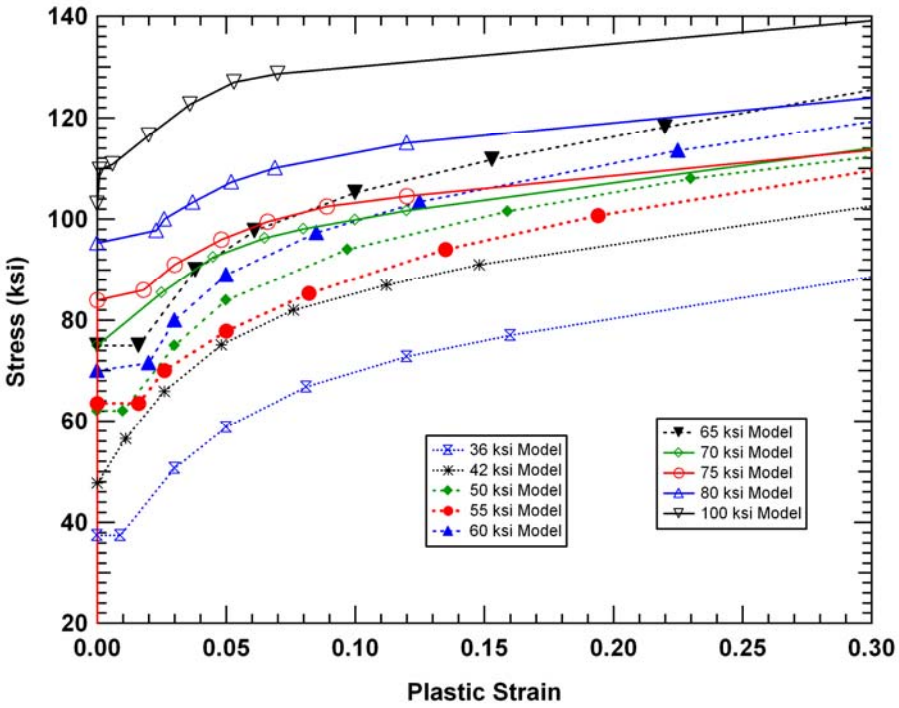

Figure 2–8. Tabular true stress-strain constitutive model curves.

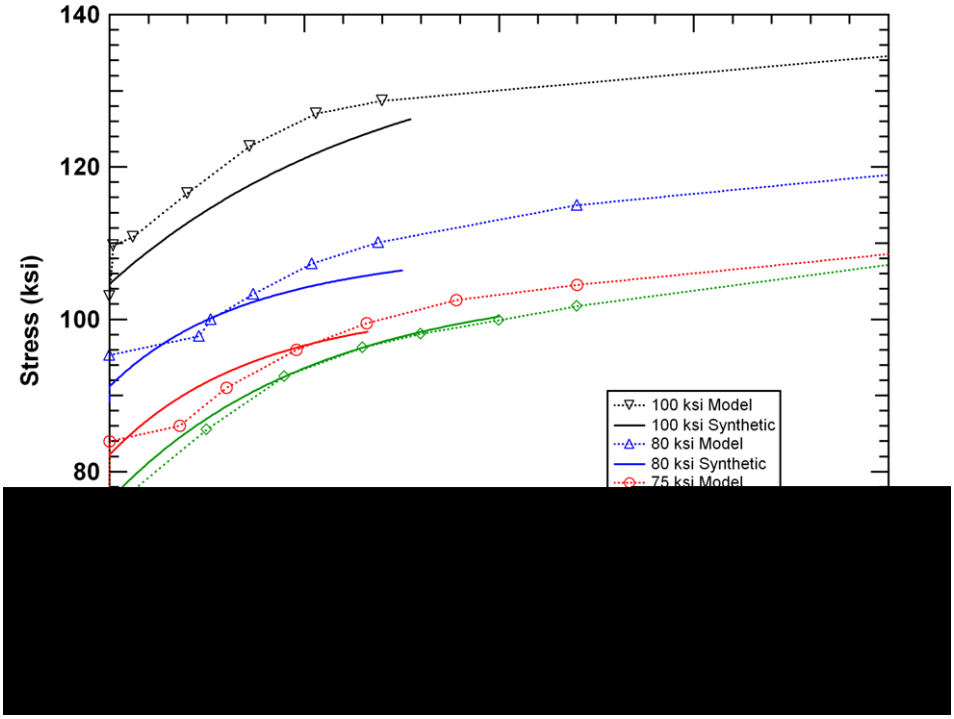

Figure 2–9. Comparison of the constitutive model and synthetic steel behaviors for the higher strength perimeter steels.

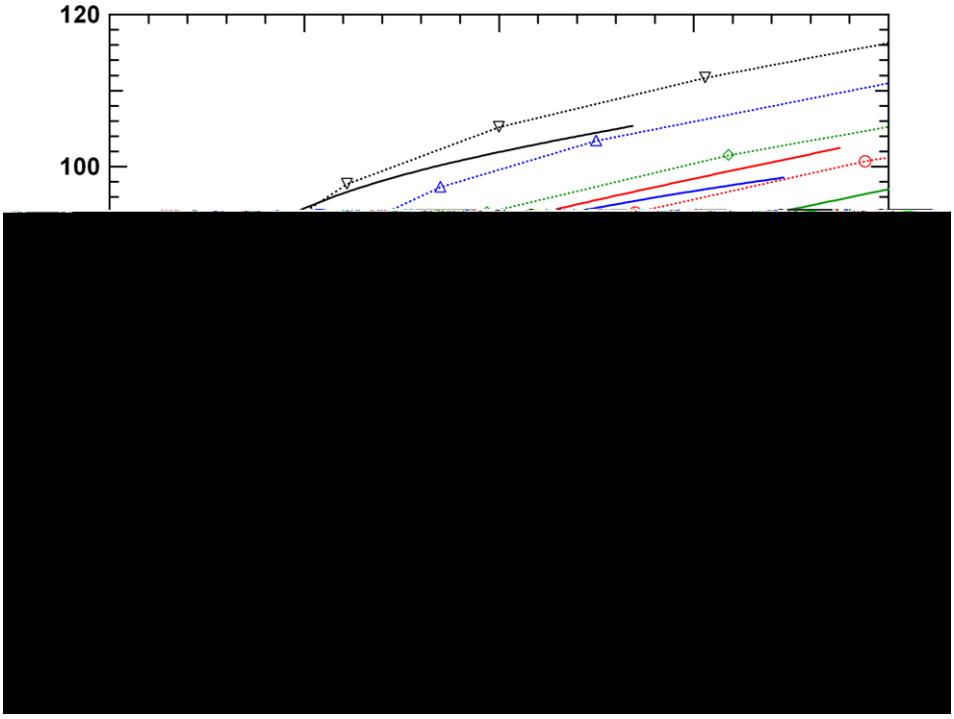

Figure 2–10. Comparison of the constitutive model and synthetic steel behaviors for the lower strength perimeter steels.

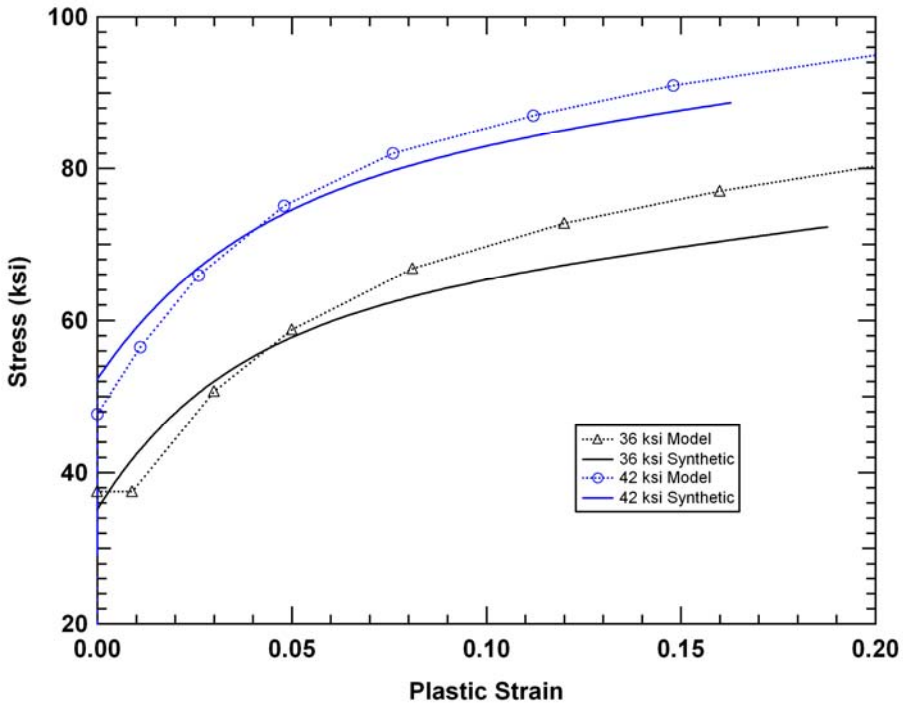

Figure 2–11. Comparison of the constitutive model and synthetic steel behaviors for the core steels.

2.2.4 Strain Rate Effects in Steel Constitutive Models

Elevated strain rates can influence the strength and ductility of structural materials. For the materials and strain rates of the WTC tower impact analyses, these strain rate effects are expected to be somewhat small compared to the effects of the baseline (static) strength and failure modeling. The strain-rate effects on the yield strength were included in the constitutive model for the tower steels with the Cowper and Symonds rate effect model. The functional form for the rate effects on strength is governed by the equation:

$$\sigma_y = \sigma_{y_0}[1 + (\frac{\dot{\varepsilon}}{C})^{1/p}] \quad (5)$$

where σ_y and σ_{y_0} are the yield strengths at strain rates of $\dot{\varepsilon}$ and zero, respectively. *C* and *p* are the Cowper and Symonds parameters.

A series of high-rate characterization tests was performed on tower steels as part of the NIST mechanical and metallurgical analysis of structural steel. In addition to quasi-static tests (performed at a rate below 0.001 s^{-1}), a series of high rate tests were performed, primarily at strain rates between 100 and 1000 s^{-1}. The Cowper and Symonds model parameters, C and p, were then fit to the test data and are provided in the following functional form for a strain rate in s^{-1} and a yield strength in ksi:

- $\text{Log}(C) = -7.55 + 0.324\sigma_{y0} - 0.00153(\sigma_{y0})^2$
- $p = 6.7824$

The specific values used for each of the different tower steels are summarized in Table 2–1. The 36 ksi and 42 ksi steels were materials used in the core columns, and the remaining steels were used in the exterior columns. The brick element failure strains in Table 2–1 are presented for the medium mesh resolution corresponding to the mesh density used in the component analyses. The resulting rate effects used in the constitutive modeling of tower steels, based on Equation (5), are compared to the measured high rate test data for the 50 ksi, 75 ksi, and 100 ksi tower steels in Figure 2–12. In the figure, the dashed lines with open symbols are the fits using the Cowper and Symonds model, while the corresponding solid symbols are the experimental data. The comparison shows that the Cowper and Symonds model is capable of reproducing the rate effects for the range of data available.

Test results indicated that the influence of strain rate on the ductility of the tower steels did not follow a consistent trend. Several grades of steel had an increased ductility at high rates (more common for low strength steels), some had a reduced ductility at high rates (more common for high strength steels), and some showed no significant effect of strain rate on ductility. The approach used in the constitutive modeling is to ignore the changes in ductility produced by elevated strain rates. The effects of the variation of ductility over the expected range of strain rates were assessed as part of the uncertainty analyses.

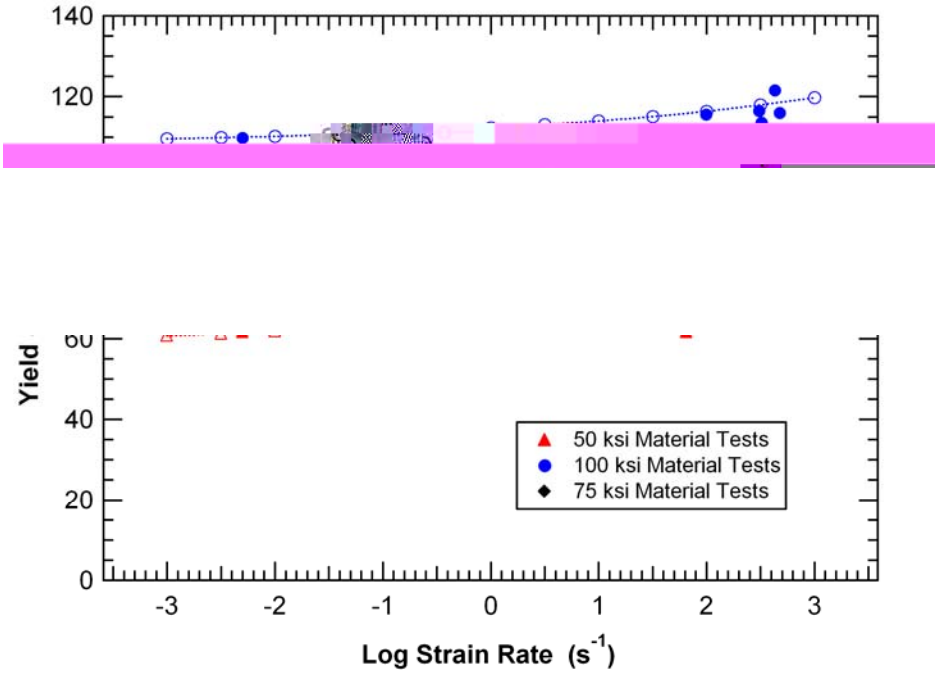

Figure 2–12. Comparison of rate effects model and test data.

Table 2–1. Material constitutive parameter table – WTC tower steels.

Material Yield Specification	Young's Modulus	Poisson's Ratio	Strain-Rate Coefficient (C)	Strain-Rate Exponent (p)	Brick Element Failure Strain
36 ksi	29.7 Msi	0.288	7.900e+01	6.782e+00	0.32
42 ksi	29.7 Msi	0.288	1.360e+05	6.782e+00	0.32
50 ksi	29.7 Msi	0.288	4.220e+06	6.782e+00	0.50
55 ksi	29.7 Msi	0.288	6.700e+06	6.782e+00	0.64
60 ksi	29.7 Msi	0.288	3.950e+07	6.782e+00	0.56
65 ksi	29.7 Msi	0.288	1.270e+08	6.782e+00	0.51
70 ksi	29.7 Msi	0.288	1.270e+08	6.782e+00	0.62
75 ksi	29.7 Msi	0.288	6.710e+08	6.782e+00	0.56
80 ksi	29.7 Msi	0.288	2.440e+09	6.782e+00	0.49
100 ksi	29.7 Msi	0.288	3.430e+09	6.782e+00	0.53

2.3 FAILURE MODELS

A challenge for calculating the aircraft impact response and damage to the WTC towers was the wide range of failure mechanisms that occurred in both the aircraft and tower structures. These failures resulted from severe loads and large scale deformations of the materials, as well as from exceeding the strength of bolted, welded, and riveted connections. At the connection locations, complex behaviors were influenced by variations in material cross sectional geometry and material properties that produced stress and strain concentrations.

The approach used to model the impact damage and failure of the structures was to apply engineering failure models within the framework of the LS-DYNA finite element analyses. Detailed fracture mechanics analysis of all of the failures that occurred was beyond the scope of this effort. Material failure in the impact analyses was calculated at the element where damage development was based on local (element) quantities including plastic strain and stress state. When the specified failure criterion in an element was exceeded, the element was eroded (deleted) from the calculation. The erosion of elements allowed for the propagation of failure through a structure.

Calculation of the failure of structural components was further complicated by the scale of the global impact analyses. Damage modeling is often applied to the analysis of smaller components and failure initiation. In these applications, a relatively fine mesh can be applied, and damage regions around a local fracture can be resolved on a fine scale. For the global impact of an aircraft into the WTC towers, element sizes had to be on average a few inches to maintain a model size at approximately 2 million elements. At this resolution, the gradients around a fracture cannot be accurately resolved, and the damage criteria required adjustment to obtain the appropriate strength and ductility of the structures. In the following sections, various failure modeling techniques applied to the aircraft and tower structures are described.

2.3.1 Mesh Refinement Effects

One of the significant modeling issues for the analysis of aircraft impact damage and failure is the effect of mesh refinement. The global impact analyses of the aircraft impacts into the WTC towers were very large analyses of complex structures and required the refinement of the model to be reduced significantly from the detailed component analyses. As the mesh refinement was reduced, it was important to ensure that the damage mechanisms and extent of impact damage were properly captured.

A preliminary example of the effects of mesh refinement on the response was introduced earlier in the analysis of the material tests on the WTC tower steels. Figure 2–1 showed both fine mesh and a coarser mesh (referred to as medium mesh) versions of the ASTM 370 rectangular tensile specimen for plate material. A comparison of the calculated necking behavior for the two 75 ksi specimen meshes immediately preceding failure is shown in Figure 2–13. The fine mesh was able to better resolve the strain gradients in the necking region and as a result had higher peak strain values at the same level of specimen displacement.

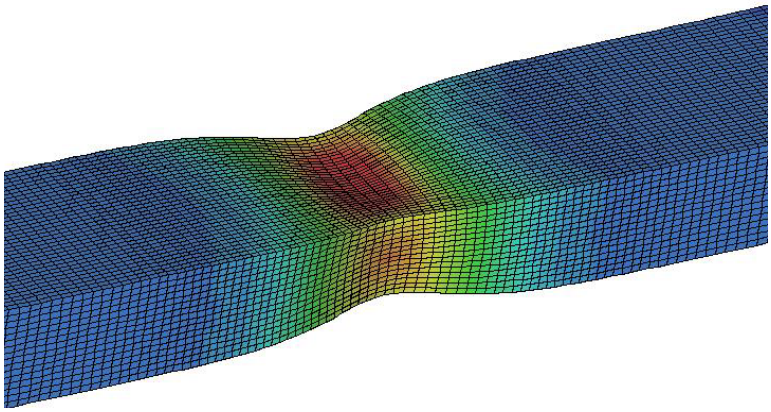

(a) Fine mesh necking behavior (red = 75 percent plastic strain)

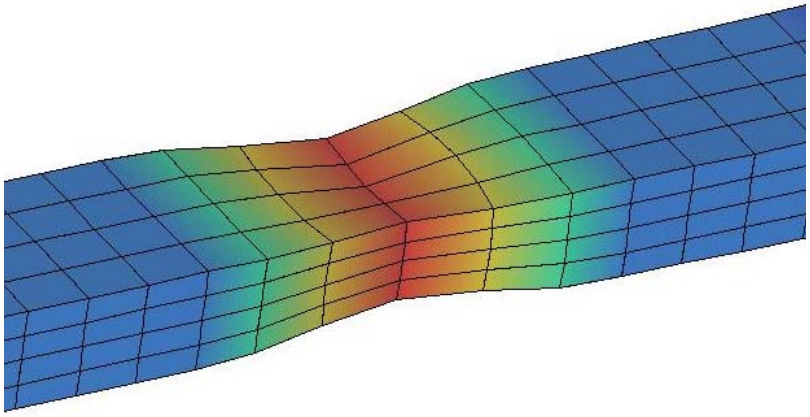

(b) Medium mesh necking behavior (red = 50 percent plastic strain)

Figure 2–13. Calculated necking response in the 75 ksi tensile specimen.

The effects of further reductions in mesh refinement required for global impact analyses can be demonstrated with the ASTM 370 tensile test example used in this section. To most closely resemble the mesh and element type used in the global analyses, three full width shell elements were used to model the entire specimen gage section, as shown in Figure 2–14. This coarse tensile specimen model had a single stress and a single strain value across the specimen gage section and did not have sufficient independent degrees of freedom to capture the localization that occurred during necking. To most closely match the behavior of the fine-mesh model, a failure strain of 0.18 was needed to model failure for this single shell element. Note that this closely matches the engineering failure strain of 0.20 for this material (see Figure 2–6).

The calculated engineering stress-strain behavior obtained with the three different mesh resolutions (fine, medium, and coarse) is shown in Figure 2–15. In these calculations, a maximum plastic strain criterion was used, and the critical failure strain was shifted until each calculation failed at a value matching the average measured engineering failure strain. The corresponding critical plastic strains were 1.00 for the fine mesh resolution, 0.56 for the medium mesh resolution, and 0.18 for the coarse mesh resolution (shell element model).

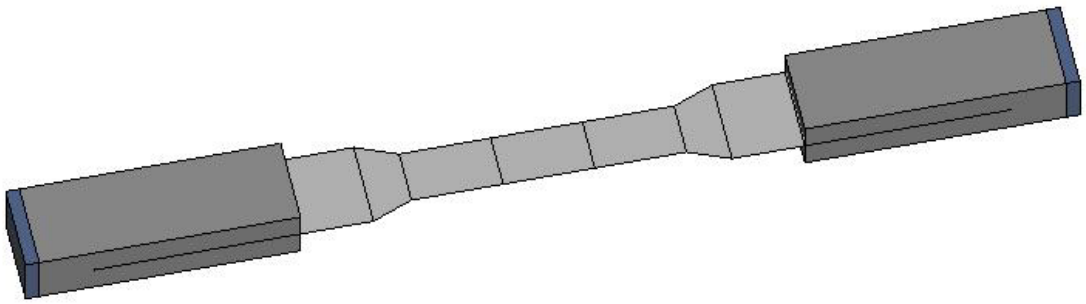

Figure 2–14. Coarse shell element mesh for the 75 ksi tensile specimen.

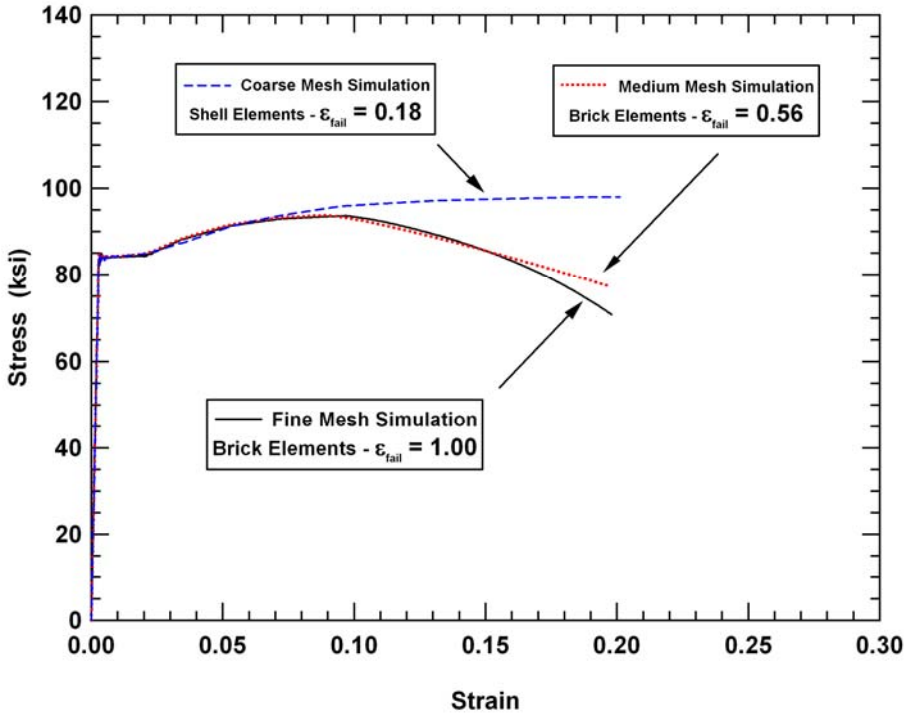

Figure 2–15. Mesh refinement effects in the calculated 75 ksi tensile test.

The medium mesh resolution used in the analysis of the tensile test described above corresponded to the mesh resolution applied in the exterior column component impact analyses described in Section 5.2.1. Therefore, the critical failure strain of 0.56 was carried forward to the detailed component analyses. The coarser shell element subassembly and global impact models were typically developed with shell elements and a resolution corresponding to the coarse model shown in Figure 2–14. Therefore, the measured engineering elongation of the specimens was used for the critical strain. Additional modification for the weld regions, with significant stress concentrations, is described below in Section 2.3.2.

2.3.2 Weld Zone Constitutive Modeling

Photographs of the WTC towers immediately after impact, and inspection of the recovered exterior wall panels in the impact zone, have shown that failure along the weld heat affected zone (HAZ) was a characteristic feature of the impact damage. An example exterior column from the impact zone that had significant fractures along the weld zone for the outer web is shown in Figure 2–16. Inspections of the weld zone failures indicated that these fractures were either brittle or very low energy ductile fractures (small plastic strains in the fracture zone). As a result, the amount of energy dissipated by these HAZ fractures was very small compared to the overall impact energy. The failure of the welds had little effect on the subsequent damage to the interior structures and contents of the towers. However, to capture the damage mechanisms of the impacted exterior columns and to develop models and failure criteria for the global impact analysis, a failure model for the weld zone was required.

Source: NIST.

Figure 2–16. Photograph of an exterior column with weld zone fractures.

Modeling of the constitutive behavior for the weld and HAZ material is a challenging task due to the lack of significant material testing in these regions. The data obtained on the weld and HAZ properties consisted of a micrographic characterization of an exterior column weld with microhardness indentation tests performed at various locations across the weld geometry. The specific weld geometry and microhardness characterization locations are shown in Figure 2–17. The corresponding hardness measurements across the base, HAZ, and weld materials are shown in Figure 2–18.

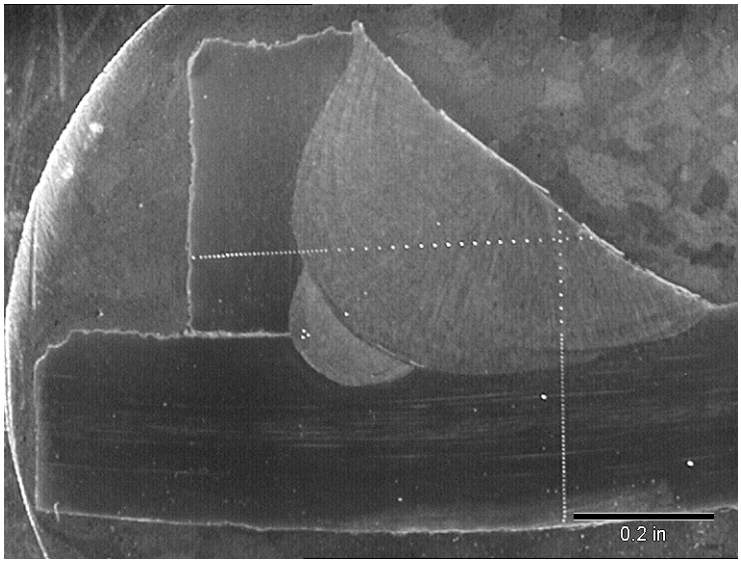

Source: NIST.

Figure 2–17. Micrograph of an exterior column weld geometry.

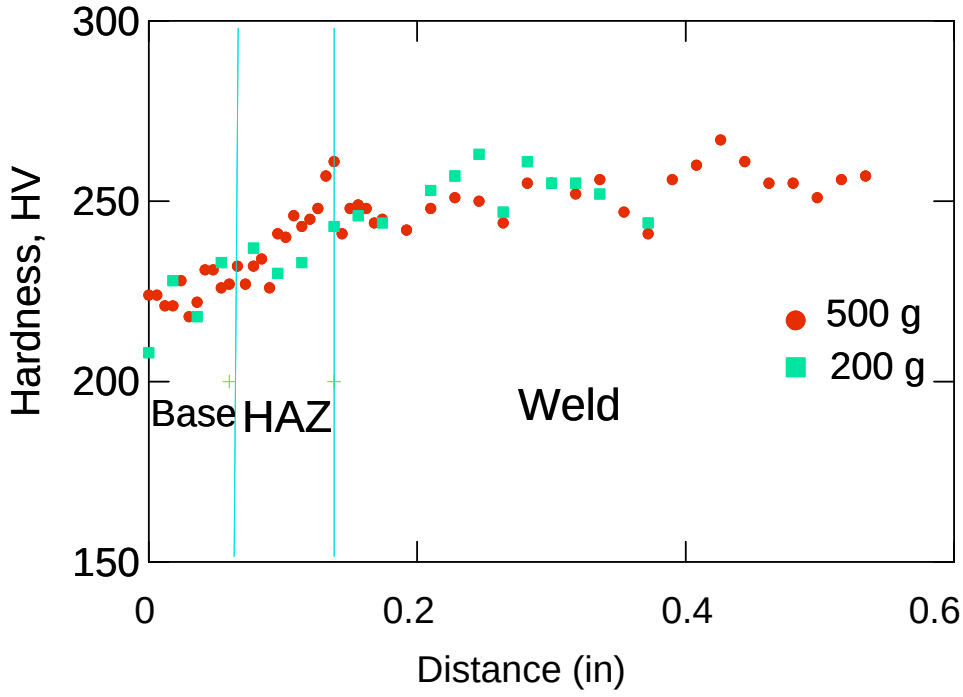

Figure 2–18. Microhardness characterization of the weld and HAZ materials.

Microhardness measurements shown in Figure 2–18 were used to develop approximate plasticity behaviors for the weld and HAZ material regions. The flow stresses of the HAZ and weld materials were increased from that of the base material by 12 percent and 18 percent, respectively. These shifts correspond to the relative magnitude of the average measured hardness in each material region.

The remaining stage in developing the weldment failure model was to perform three-dimensional component impact analyses of the external column and develop a coarser shell element description of the weld region that could be applied in the global aircraft impact analyses. The problem analyzed was the drop test configuration shown in Figure 2–19. The drop test configuration had a 550 lb steel impactor with an impact speed of 37.4 mph. The impactor was 12 in. wide and 5 in. across. The nose of the impactor had a reduced area, that is 12 in. wide and 2 in. across, with a 1/2 in. radius rounded edge around the impact face. The length of the column section represented a portion of an exterior column between spandrels.

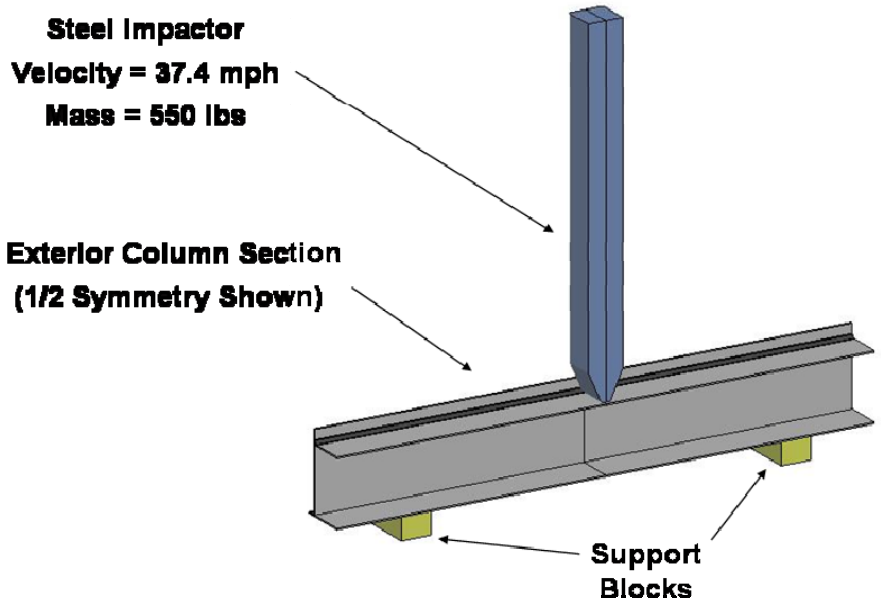

Figure 2–19. Drop test model for column weld fracture analysis.

The two different column models used for the weld zone failure analysis are shown in Figure 2–20. The brick element model had a mesh similar to the medium resolution tensile specimen model shown in Figure 2–13(b). This quarter-symmetry brick element column model contained 63,680 linear solid elements. The coarse shell element model had approximately 4 in. elements to define the column and 1 in. wide elements in the weld zone. The quarter-symmetry coarse shell element column model contained 144 linear shell elements. Obviously, the coarse shell-element model was not able to capture the stress and strain gradients in the weld zone to the same extent as the brick element model.

The drop test was simulated first using both the brick and shell element models. The results of the calculated impact response and failure were used to determine an upper bound for the failure strain of the weld zone. The strain profiles calculated in elements across the web in the weld region are plotted in Figure 2–21 (each black dot in the figure corresponds to a specific element plastic strain magnitude). The figure shows that the brick element model calculated a strong gradient in strain, with the peak strains near the toe of the weld, that were several times larger than the average strain in that region. The corresponding shell element model could calculate only a single strain value for the 1 in. wide weld zone as shown by the red line in Figure 2–21.

An average critical strain of approximately one-quarter of that in the corresponding base metal was selected for the 1 in. wide single shell element weld zone. This weld zone failure strain was 8 percent in the current example (55 ksi steel). The comparison of the resulting impact behavior for the brick and shell element models is shown in Figure 2–22. Both models had similar impact deformations, and the length of the weld failures were in good agreement. These analyses provided an upper bound value for the engineering fracture criteria in the weld region. Additional investigation of the weld failure and the effects of a more brittle fracture response were investigated in the subassembly analyses (Section 6.3.2). These subassembly impact analyses demonstrated that the weld zone fracture criterion had a negligible effect on the impact energy absorption and little significance on the impact damage.

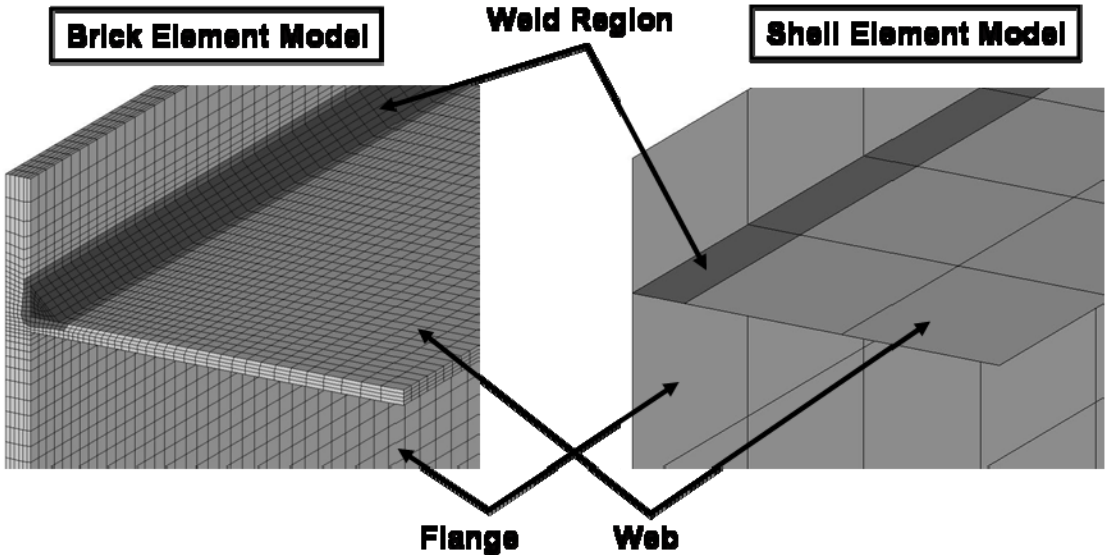

(a) Medium mesh resolution **(b) Coarse mesh resolution**

Figure 2–20. Models developed for column weld fracture analysis.

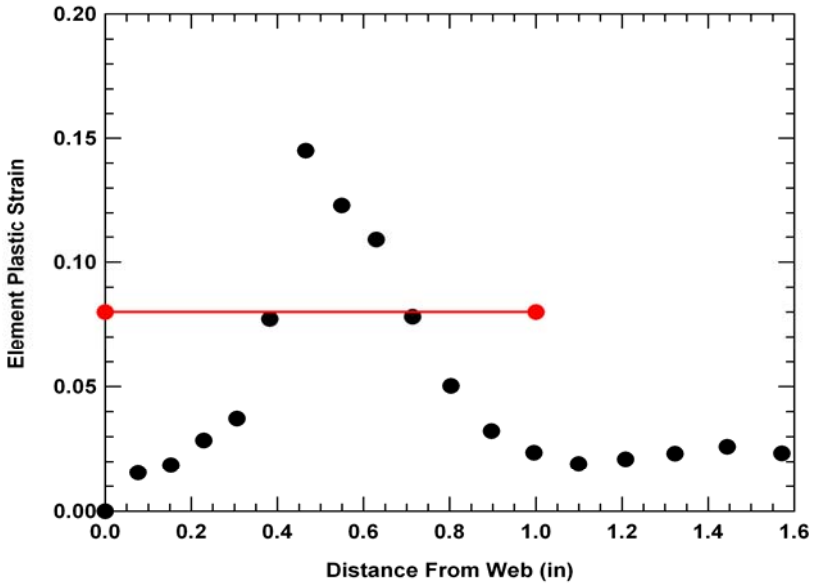

Figure 2–21. Calculated energy balance for the 2-D weldment models.

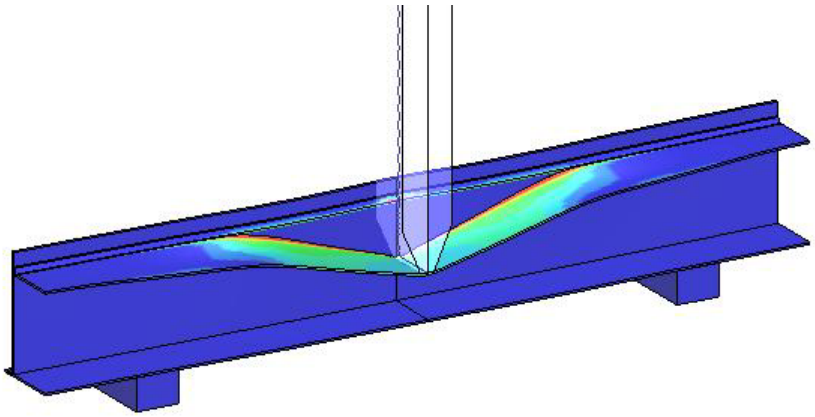

(a) Medium resolution brick element model

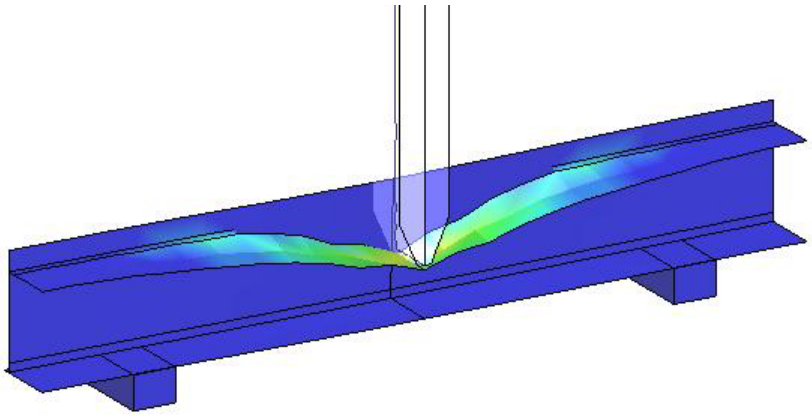

(b) Coarse resolution shell element model

Figure 2–22. Calculated drop test fracture behavior.

2.3.3 Bolt Material Constitutive Modeling

The primary bolts of interest for the impact analysis were those used at the connections between the exterior columns of the WTC towers. Within the impact zone, the connections were typically made using 0.875 in. diameter grade A325 steel bolts. Initially, there were no test data available that could be applied to develop a bolt model. The modeling approach was to develop a brick element model of the bolt and use it to develop a corresponding beam element bolt model for the majority of the impact analyses. A description of these bolt analyses are given in Section 5.2.3, along with the component analyses.

Subsequently, a series of tests was performed as part of the NIST mechanical and metallurgical analysis on bolts recovered from the WTC towers (NIST NCSTAR 1-3). A summary of the bolt testing is given in Figure 2–23. The bolts were found to yield at a load of approximately 50 kip and to have an ultimate failure load of approximately 68 kip. The measured elongation at failure was approximately 0.18 in. The bolts did not exhibit any significant strain rate dependency.

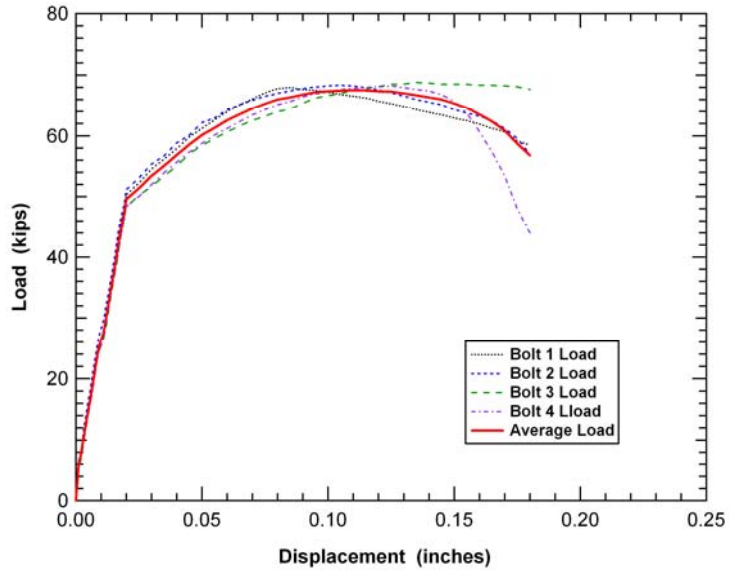

Figure 2–23. Measured bolt load-displacement behavior.

The beam element model for the bolt, described in Section 5.2.3, was compared to the bolt test data. The comparison showed good agreement in the strength of the bolt, but it also indicated that the beam model overestimated the ductility. This may be a result of not capturing the details of the stress concentrations in the region of the threaded connection and nut. The bolt test data were used to correct the ductility of the beam element bolt model, and the resulting comparison of the model and test data is shown in Figure 2–24. The bolt model shows a bilinear elastic-plastic behavior that is stiffer in the elastic region and yields at a higher stress level than the data. The inability of the simplified model to capture stress gradients in the regions of the bolt head, threads, and nut may cause this type of response. However, the overall strength and ductility of the model and data, as well as the strain energy capacity, agreed reasonably well so that further model development was not required.

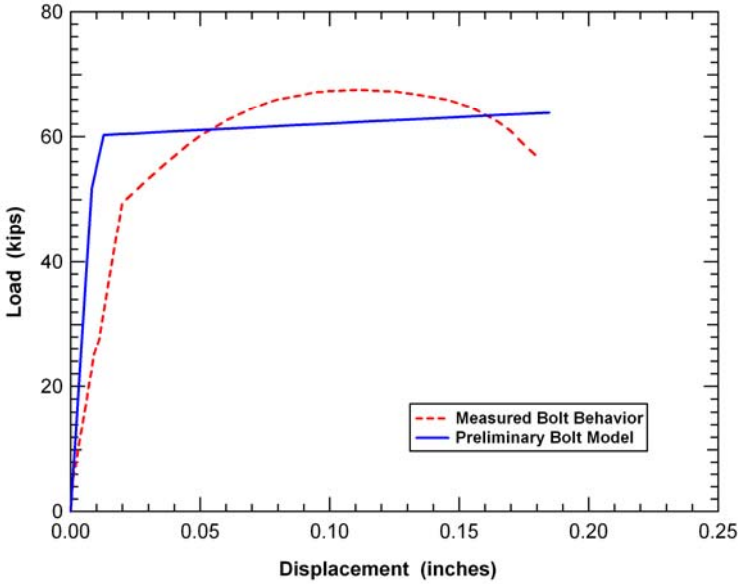

Figure 2–24. Comparison of the measured and calculated bolt behavior.

2.4 CONCRETE CONSTITUTIVE MODELS

There are several concrete models in LS-DYNA. Each has different capabilities for modeling rate effects and nonlinearity associated with damage and failure behavior. Potential concrete models in LS-DYNA include Types 5 (soil and crushable/non-crushable foam model), 16 (pseudo-tensor concrete model), 25 (kinematic hardening cap model), 78 (soil and concrete model), 84 (Winfrith concrete model) and 111 (Holmquist-Johnson-Cook concrete model). An important factor in determining the behavior of a concrete structure in compression or bending is its lateral confinement. The concrete floor slabs in the WTC towers were not highly confined, therefore, a material model suitable for this loading condition was needed.

In this study, the ability to accurately model the damage and softening behavior of concrete associated with low confinement conditions is important. Damage caused by cracking in the concrete degrades the strength in the low confinement regime. Inclusion of this damage growth provides a more accurate representation of the stress-strain response. Based on this capability, the LS-DYNA material Type 16 (pseudo-tensor concrete model) was selected for modeling the concrete floor slabs. This model also accounts for the sensitivity of concrete to high strain rates.

As implemented in LS-DYNA, the pseudo-tensor model can be operated in two major modes: (1) a simple tabular pressure-dependent yield surface, and (2) a complex model with two pressure-dependent yield functions and a damage-dependent function to migrate between curves. The first option is well suited for modeling standard geologic material behaviors such as a Mohr-Coulomb yield surface with a Tresca limit and has been used successfully for the analysis of ground shock and soil-structure interactions under high confinement. The second option, applied in this study, allows for implementation of tensile failure and damage scaling, which are more dominant material behaviors at low confinement.

The pseudo-tensor model, as applied to the analysis of the lightweight concrete in the WTC towers, has two pressure dependent yield functions in the form:

$$\sigma_y(p) = a_0 + \frac{p}{a_1 + a_2 p} \tag{6}$$

These yield functions are shown graphically in Figure 2–25, where the upper curve describes the maximum yield strength and the lower curve is the failed material curve. By defining suitable yield functions for the undamaged and fully damaged concrete and an appropriate tabular interpolation between the curves, the damage behavior under low confinement can be captured. For a detailed description of the model, the reader is referred to the LS-DYNA user's manual (2003).

Source: Reprinted from "LS-DYNA User's Manual," Livermore Software Technology Corporation, Version 970, April 2003, Figure 20.6, page 20.70, with permission from Livermore Software Technology Corporation.

Figure 2–25. Intact and completely damaged concrete strength as a function of pressure.

Material constitutive parameters for the pseudo-tensor model, Equation (6) and Figure 2–25, were developed for both 3 ksi and 4 ksi compressive strength lightweight concrete, as shown in Table 2–2. A tensile cutoff with a 500 psi tensile strength was used for this model. In the absence of experimental data on the concrete, a simulation was performed of a standard unconfined concrete compression test to check the constitutive model behavior. The simulated behavior of the concrete specimen is shown in Figure 2–26. The calculated compressive stress-strain response for the 3 ksi concrete is compared to measured compression data for 2.3 ksi and 3.8 ksi strength concretes in Figure 2–27 (Wischers 1978). The same material parameters were used for the concrete in both the core (normal weight concrete) and truss floor (lightweight concrete) areas.

Table 2–2. Strength parameters for the concrete material model.

Strength Parameter		f'_c =3 ksi	f'_c =4 ksi
a_o	(psi)	750	1000
a_1		0.333	0.333
a_2	$(psi)^{-1}$	1.11E-04	8.33 E-05
a_{0f}	(psi)	0.0	0.0
a_{1f}		0.385	0.385

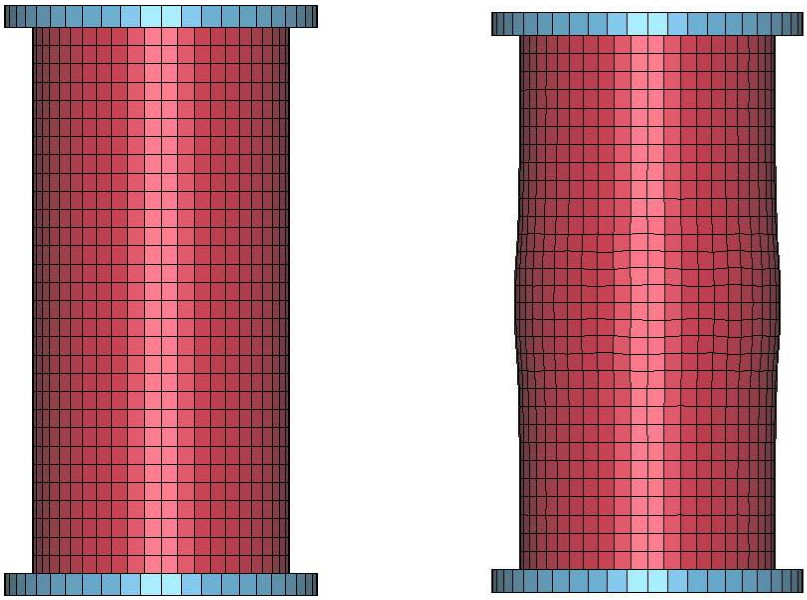

Initial configuration **2 percent compression**

Figure 2–26. Finite element analysis of the unconfined compression test.

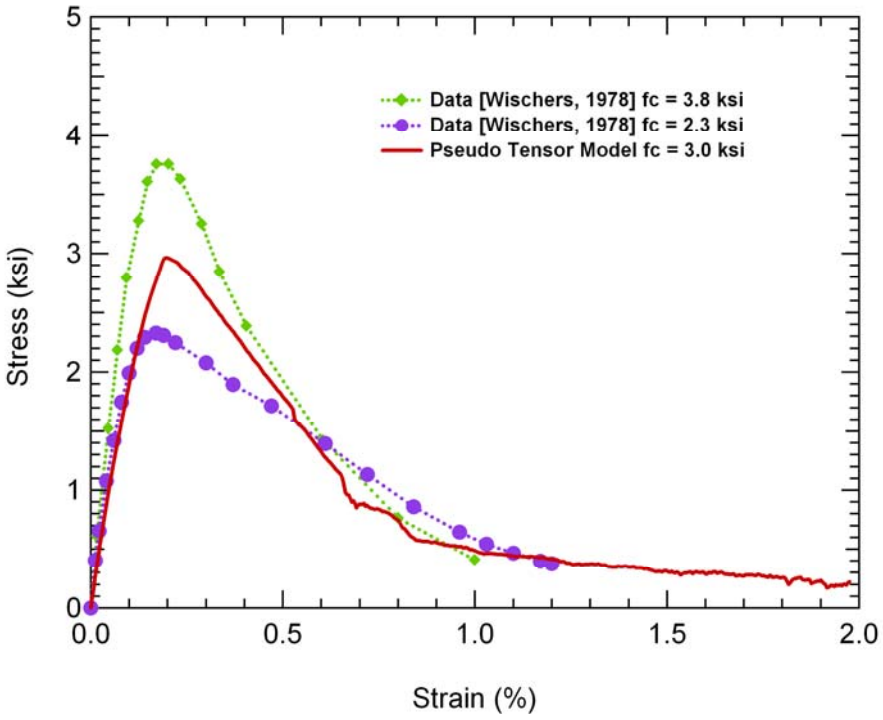

Figure 2–27. Comparison of the calculated unconfined compression behavior with concrete compression test data.

An additional comparison of the calculated compressive behavior to the stress-strain curve for the lightweight concrete response (Phan 1996) is shown in Figure 2–28. The agreement is good up to the

peak load point. The softening behavior was not specified beyond the requirement for the zero stress point corresponding to 2 percent strain. The calculated nonlinear softening behavior is typical of concrete materials. For subsequent global analyses, a 4 ksi concrete was used, instead of the 3 ksi concrete strength specified in the original design (NIST NCSTAR 1-6), to account for factors such as aging and difference between specified nominal and actual concrete strength. The pseudo-tensor model was then modified to have an unconfined compression strength of 4 ksi, as shown in Figure 2–29.

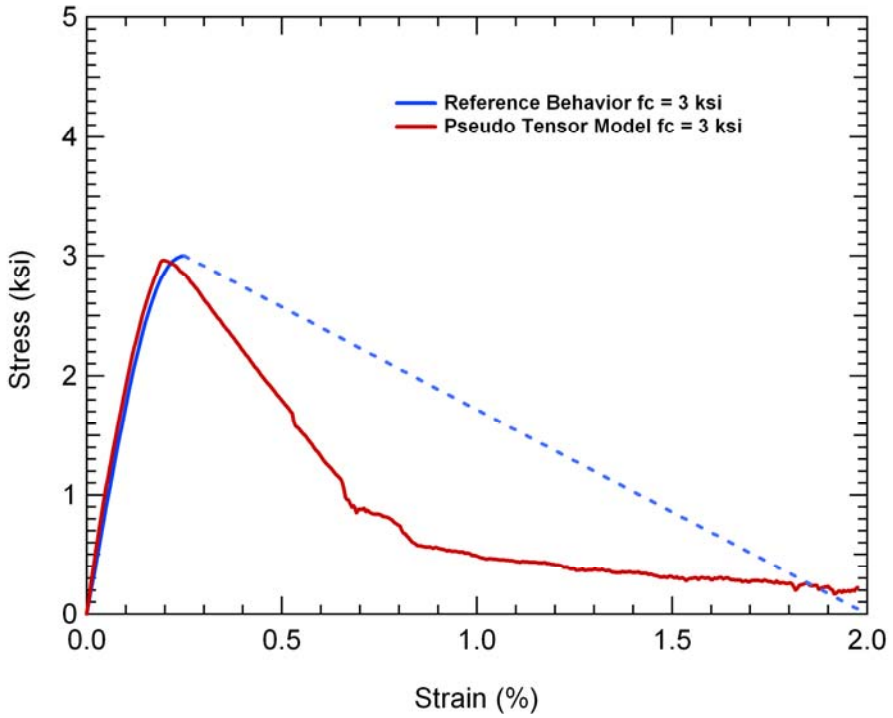

Source: Phan 1996.

Figure 2–28. Comparison of the calculated unconfined compression behavior with lightweight concrete behavior.

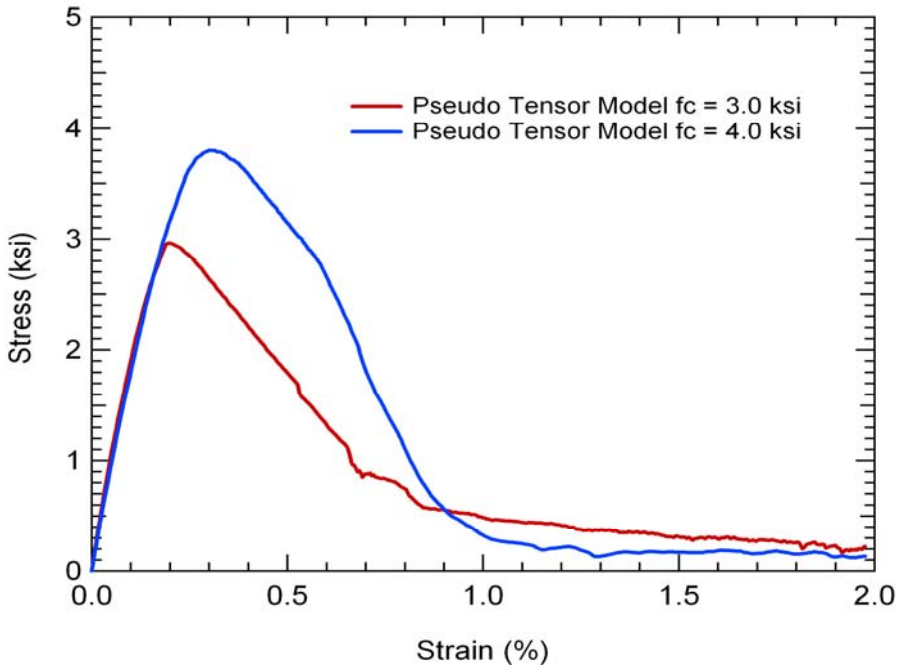

Figure 2–29. Comparison of the calculated unconfined compression behavior of 3 ksi and 4 ksi concrete.

Experimental characterization of the strain rate effects on concrete behavior is difficult, and there is a wide scatter in data that is influenced by concrete type, strength, and the testing methods applied. In general, elevated strain rate loading has a greater influence on the tensile strength than on the compressive strength. However, in the aircraft impact response of the WTC towers, the majority of the high-rate damage occurs with impact and penetration of the floor slab by hard components such as the engine. As a result, the strain rate effects for compressive loading were used for the constitutive model.

A collection of compressive strength data for elevated rates is shown in Figure 2–30 (Bischoff and Perry, 1991) and Figure 2–31 (see Ross et al., 1992). There is still a large scatter in the measured rate effects under compressive loading. In general, the effects of strain rate increase gradually up to a rate of approximately 30 s^{-1}. Beyond a rate of 30 s^{-1}, the compressive strength is more sensitive to strain rate. The majority of the aircraft impact damage to the concrete is expected to occur at loading rates below 30 s^{-1}.

The strain rate effects were added to the model in tabular form. The rate effects curve used in the model is shown in Figure 2–32. The curve was selected to provide a relatively smooth fit to the available compressive rate effects data on compressive strength.

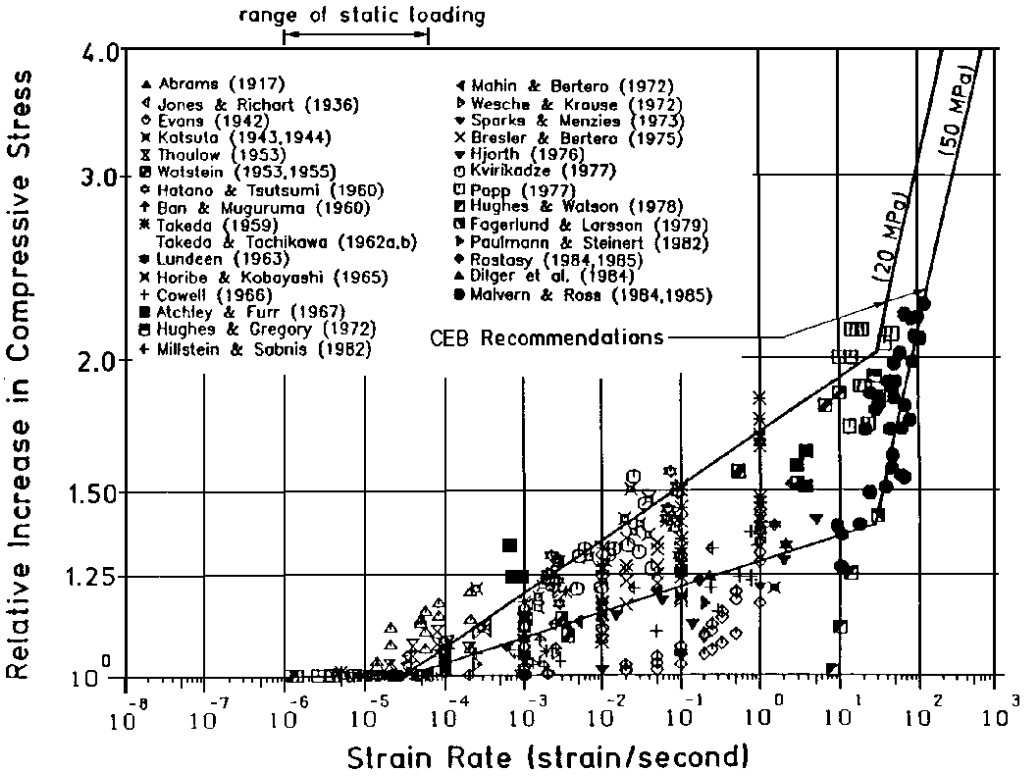

Source: From "*Compressive behavior of concrete at high strain rates*," published in *Mater. Struct.* **24** (1991) Courtesy RILEM.

Figure 2–30. Strain rate effects on concrete compressive strength.

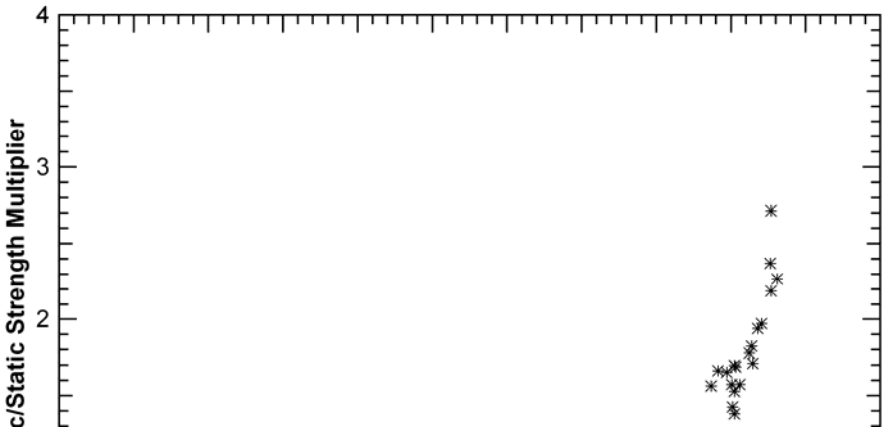

Figure 2–31. Strain rate effects on concrete compressive strength.

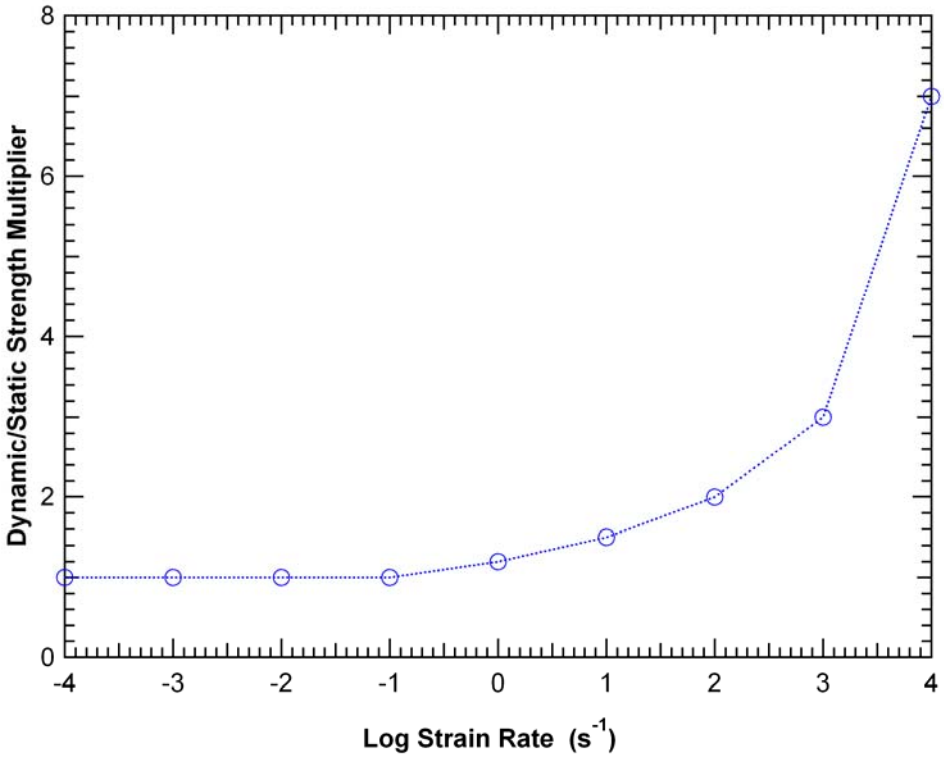

Figure 2–32. Tabular concrete strain rate effects curve.

2.5 AIRCRAFT MATERIALS CONSTITUTIVE MODELS

No material testing was performed to characterize the structural materials in the aircraft or develop the constitutive model parameters for these materials. Therefore, the constitutive and failure properties for the aircraft materials were developed from data available in the open literature. The principal sources of data for the airframe materials are the Military Handbook (MIL-HDBK-5F, 1987), and the Aerospace Structural Metals Handbook (Brown et al. 1991). Additional sources of data were used to verify and supplement the information obtained from these primary data sources.

Complete engineering stress-strain curves were provided in the MIL-HDBK-5F for various 2024 and 7075 aluminum alloys that are commonly used in the construction of the Boeing 767 airframe structures. These curves were digitized for the various 2024 and 7075 alloys as shown in Figure 2–33 and Figure 2–34, respectively. Representative stress-strain curves were then converted into true stress and true strain, as described in Section 2.2.1, and used to develop tabular curves for constitutive models. The calculated true stress-strain curves and tabular constitutive model fits are shown in Figure 2–35 and Figure 2–36, respectively. Appropriate failure criteria for the aircraft materials were developed using the fine and coarse wing component models discussed in Section 5.5.1.

Insufficient data were available on the effects of strain rates on the behavior of aircraft materials to determine appropriate values for the parameters for the Cowper and Symonds model. As a result, no rate sensitivity of the aircraft materials was explicitly included in the aircraft constitutive models. Alternatively, a larger variation in the strength and ductility of the aircraft materials was included in the uncertainty analyses in Chapter 8 to account for the potential effects of elevated strain rates.

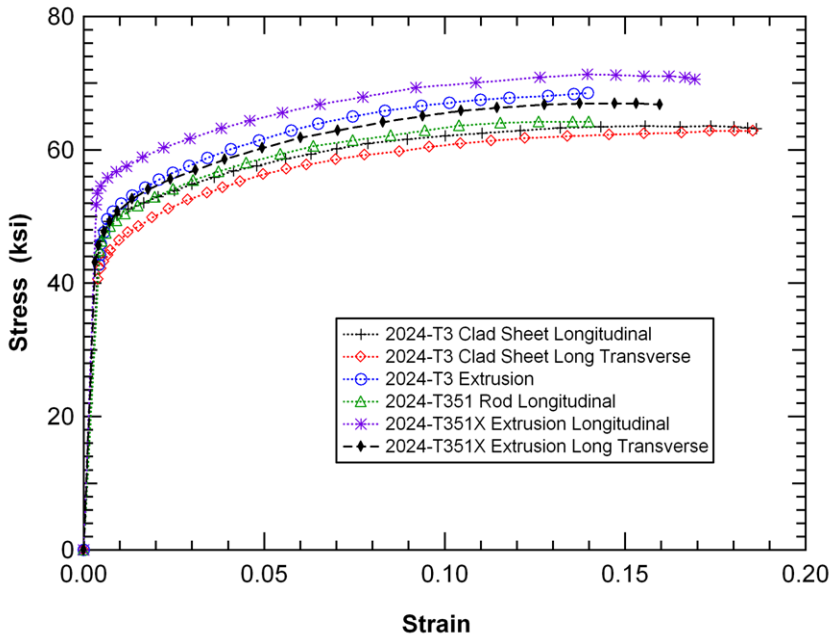

Figure 2–33. Digitized engineering stress-strain curves for various 2024 aluminum alloys.

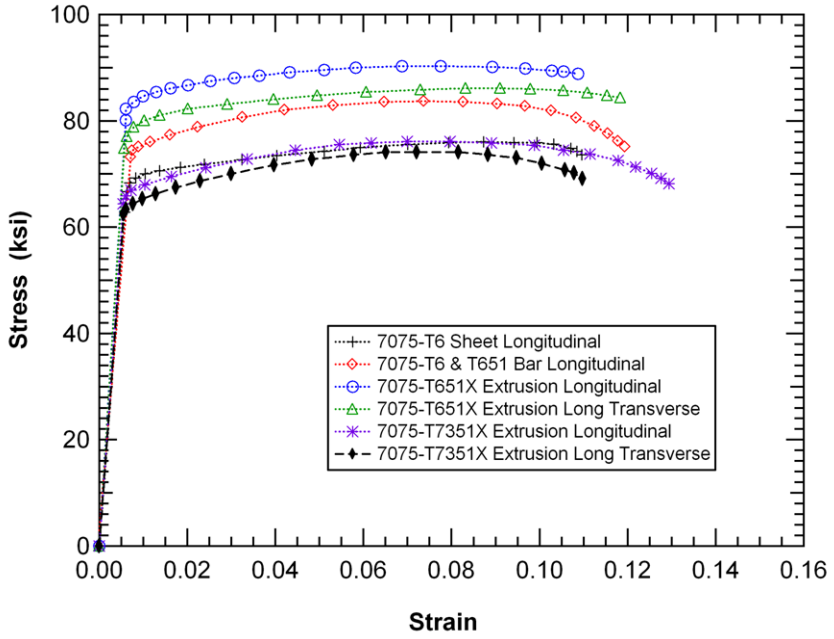

Figure 2–34. Digitized engineering stress-strain curves for various 7075 aluminum alloys.

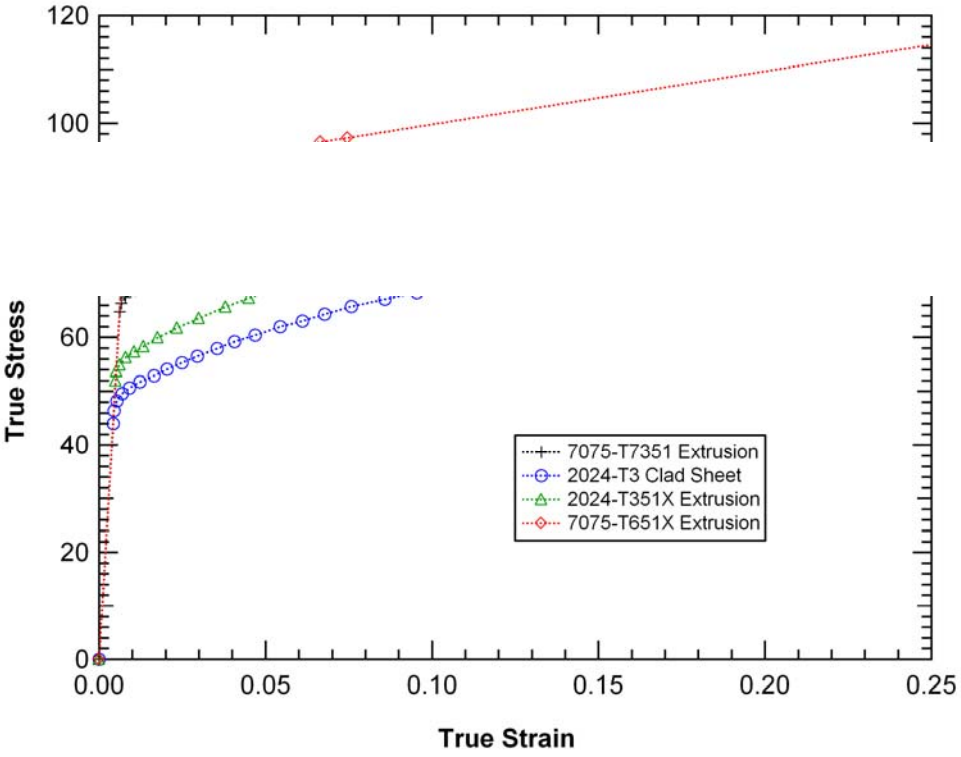

Figure 2–35. True stress-strain curves developed for various aircraft aluminum alloys.

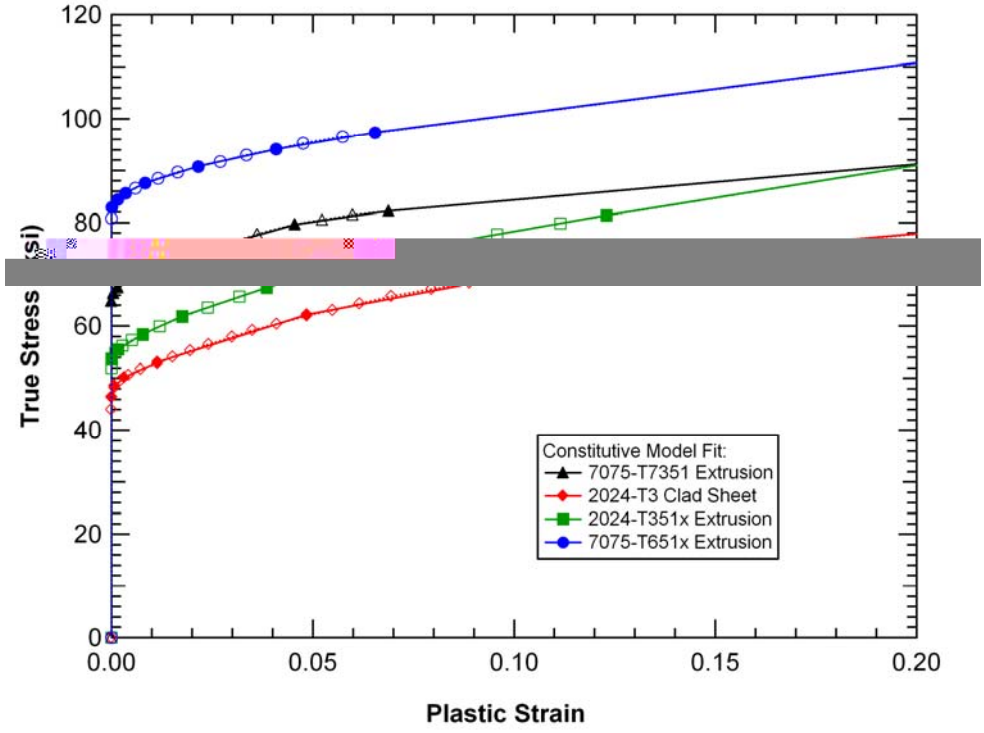

Figure 2–36. True stress-strain curves developed for various aircraft aluminum alloys.

2.6 NONSTRUCTURAL MATERIALS CONSTITUTIVE MODELS

No material testing was performed to characterize the nonstructural materials in the aircraft or tower. These include various components on the aircraft such as the landing gear tires and interior furnishings and the tower contents and nonstructural walls. In general, the primary influence of the nonstructural components on the impact behavior is their inertial contribution (mass). The effects of their strength are small. As a result, relatively simple approximations of their constitutive behavior can be used. Typically, a simple elastic-plastic model was applied for these materials to allow for efficient modeling of deformation and subsequent erosion from the calculations as their distortions become large. The ability to include material failure and erosion of these soft materials is important for the stability of the impact analyses.

The majority of the nonstructural components in the aircraft were not modeled explicitly but were included by distributing their mass into the airframe structures. These aircraft components included the interior wall paneling and fixtures, insulation, wiring, carpeting, etc. Similarly the luggage and cargo mass was distributed into the models for the Unit Load Devices (ULDs or cargo containers). The mass of the seats and passenger compartment cargo were lumped together in a simplified seat model. A bilinear elastic-plastic constitutive behavior was assumed for the effective seats with a yield strength of 1.45 ksi and a failure strain of 40 percent. The relatively large ductility was used to allow for the seats and cargo to be maintained in the simulation sufficiently long to transfer their inertial loading to the impacted tower components. Another nonstructural aircraft component modeled independently was the tires on the landing gear. Again, a bilinear elastic-plastic constitutive behavior was assumed for the tire material with a yield strength of 5.2 ksi and a failure strain of 50 percent.

The primary nonstructural components of the WTC towers included in the impact analyses were the tower contents. Models were developed for the workstations (cubicle partitions, desks, and cabinets) and for the nonstructural walls (partitions) made primarily of gypsum. A search of material properties of the nonstructural building materials (gypsum, wood, engineered materials, etc.) resulted in a wide range of specified properties. Wood strength properties vary greatly with the wood species, grain direction, and loading applied (tension, shear, or compression). For example, maximum shear strengths of various U.S. commercial wood species vary from approximately 800 psi to 2,500 psi (www.woodbin.com). The compression strengths, both parallel and perpendicular to the wood grain, have a significantly larger variation on reported values. Gypsum board properties also vary with thickness and direction with reported Modulus of Rupture values from 220 psi to 970 psi and compressive strength of approximately 400 psi. Engineered materials, such as medium density fiberboard (MDF), used in desk and cabinet construction has a reported Modulus of Rupture on the order of 5,000 psi. Workstation partitions are generally made of a very low density engineered materials and would be expected to have a significantly lower strength.

The constitutive model used for the building contents attempted to obtain an approximate strength for all of the various materials inside the towers. This is complicated by the details of connections in the assembly of workstations, etc. that were not included in the model. A bilinear elastic-plastic constitutive model was used with a yield strength of 500 psi and a failure strain of 60 percent. Again, the large failure strain for these materials was used to prevent large scale erosion of the contents before the momentum transfer from the aircraft debris had occurred.

2.7 REFERENCES

ASTM Designation A 370 - 03a, "Standard Test Methods and Definitions for Mechanical Testing of Steel Products," Approved June 10, 2003.

Bischoff, P.H., Perry, S.H., "Compressive Behavior of Concrete at High Strain Rates," Materials and Structures, vol. 24, 1991, pp. 425-450.

Brown, W. F. Jr., Mindlin, H., and Ho, C.Y., (Eds.). 1991. *Aerospace Structural Metals Handbook*, CINDAS/Purdue University Publishers, Volumes 3 & 4.

FEMA 304, May 2002, *World Trade Center Building Performance Study: Data Collection, Preliminary Observations, and Recommendations*, Federal Emergency Management Agency.

Kirkpatrick, S.W., Giovanola, J.H., and Simons, J.W., "DYNA3D Analysis of Dynamic Fracture of Weldments," IA'96, Proceedings of International Seminar on Quasi-Impulsive Analysis, Nov. 20-22, 1996, Osaka, Japan, pp. A6.1-15, K. Wakiyama, E. Tachibana, K. Imai and T. Kitano Eds.

"LS-DYNA Keyword User's Manual." 2003. Livermore Software Technology Corporation, Version 970, April.

Military Handbook, 1987, *Metallic Materials and Elements for Aerospace Vehicle Structures*, U.S. Dept. of Defense, MIL-HDBK-5F.

Phan, L.T. 1996. "Fire Performance of High-Strength Concrete: A Report of the State-of-the Art," NISTIR 5934, Gaithersburg, MD, December.

Ross, C.A., Kuennen, S.T., Tedesco, J.W. 1992. "Effects of Strain Rate on Concrete Strength," Session on Concrete Research in the Federal Government, ACI Spring Convention, Washington, D.C., March.

"TrueGrid Manual. 2001. Version 2.1.0," XYZ Scientific Applications, Inc., September.

"Welds and Heat Affected Zones (preliminary NIST results)."

Wischers, G. 1978. "Application of Effects of Compressive Loads on Concrete," Betontech, Berlin, Nos. 2 and 3.

This page intentionally left blank.

Chapter 3
TOWER MODEL DEVELOPMENT

3.1 INTRODUCTION

This chapter describes the methodology used in the development of the structural models of the two World Trade Center (WTC) towers for the global impact analyses. The initial efforts focused on the development of models for individual structural components used in the component and subassembly impact analyses (Chapters 5 and 6, respectively). These were developed in a parameterized form so that they could be used to generate the range of structural component models found throughout the towers. Additional information on the models used for the component impact analyses are provided in Chapter 5. The subsequent efforts were to use the parameterized part models to assemble the large models of complete sections of the towers for the global impact analyses (Chapter 9). All models were developed for the LS-DYNA finite element code (LS-DYNA Version 971) using the TrueGrid model generation program (TrueGrid Manual 2001). The input data for TrueGrid included a set of commands that define the geometries, materials, boundary conditions, and mesh properties. The output from TrueGrid is a complete LS-DYNA input file for the desired analysis.

One of the significant requirements in developing the tower models for the global impact analysis was to minimize the model size as much as possible while keeping sufficient fidelity in the impact zone to capture the deformations and damage distributions. The limitation was a model size that could be executed on a 32-bit computer. Based on this limitation, it was found that the combined aircraft and tower models should not exceed approximately 2.3 million nodes. Decomposition of a model with a larger number of nodes would require additional memory beyond the memory that can be addressed by a 32-bit system. The target for the global WTC tower model, thus, was a maximum of about 1.5 million nodes. The typical approach used to meet this objective was to develop models for the various tower components at different levels of refinement. Structures and components in the path of the impact and debris field were meshed with a higher resolution to capture the local impact damage and failure, while structures and components outside the impact zone were meshed more coarsely to primarily capture their structural stiffness and inertial properties.

3.2 METHODOLOGY FOR TOWER MODEL DEVELOPMENT

The global models for the WTC 1 and WTC 2 towers were assembled in subsections based on components developed in the component modeling phase (see Chapter 5). Given the complexity of the towers' structure, a key aspect of developing the global models was automating the mesh generation process. The component model generation files were all developed in a parameterized format to support automated mesh generation. For that purpose, the electronic structural databases developed by the firm of Leslie E. Robertson Associates, R.L.L.P. (LERA), under a contract to the National Institute of Standards and Technology (NIST) within the framework of Project 2 of the NIST Investigation; and reviewed and approved by NIST, were used (see NIST NCSTAR 1-2 and NIST NCSTAR 1-2A). Visual Basic (VB) programs were developed to interface with the structural databases and to automatically write master level TrueGrid input files for mesh generation.

A total of three VB programs were used for the tower mesh generation. Each program accessed different parts of the electronic structural database. The first program performed automatic core column generation, including column splice models connecting various sections of the columns. The user interface for this core column generation program is shown in Figure 3–1. The input to the column generation program included the tower being modeled (WTC 1 or WTC 2) and the upper and lower floor numbers for the desired model height. The program then read the appropriate databases and extracted the column details such as column type (box or wide-flange) and location, plate thicknesses, and material nominal yield strength. These column parameters were used to create a master TrueGrid input file that generated the desired core column models. The master TrueGrid input file contained a series of "include" statements for pre-existing parameterized generic column generation files. The core column models developed for the subassembly and global impact analyses consisted entirely of shell elements. Different mesh densities (e.g., inside and outside the impact zone in the global impact tower models) were generated by including different generic part generation files with various element size specifications.

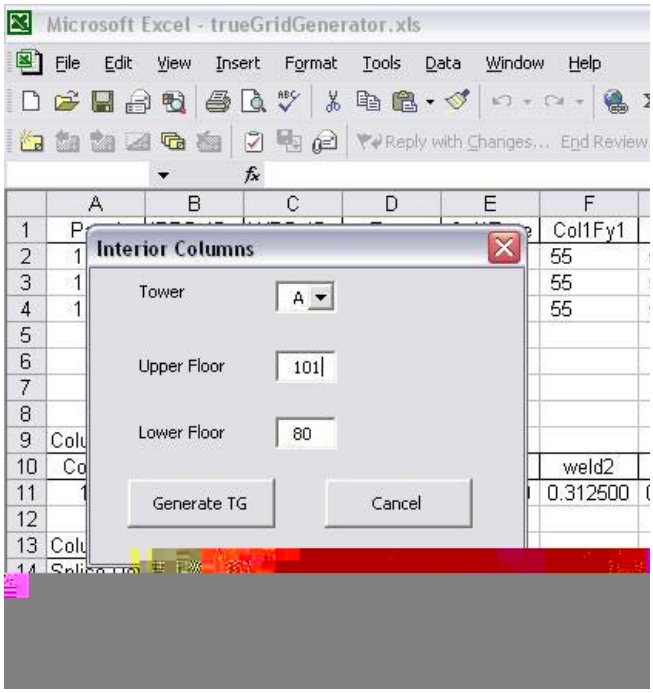

Figure 3–1. Model user interface for the core column generator.

The second program used the same input and a similar methodology as the first to generate a TrueGrid file for overall core assembly. The file included subassembly calls for core columns and core beam framing details. It also controlled mesh density and boundary condition assignment on a floor-by-floor basis. The user interfaces for programs 1 and 2 were very similar.

Figure 3–2 shows the user interface for the third program that generated a series of exterior wall panels. This program was the most complex of the three and required the user to identify the tower, upper and lower floor boundaries, and left and right (as viewed from outside the building) panel numbers. Additionally, the user could specify a fine mesh region, typically in the area of the aircraft impact. Similar to the other programs, this program extracted information from the database and generated a master TrueGrid file. Information not available in the database but included in the drawing books, such

as the weld specifications, were included in the VB program. The automatically generated TrueGrid files included the geometry and material specification for the columns, butt plates, spandrels, welds, bolts, and spandrel splice plates. Node tolerance specifications (nodal merging commands) were also automatically generated to define the connectivity of adjacent parts in the model. For example, the boundary nodes in the exterior spandrels and columns away from the impact zone were merged to create a perfect connection between adjacent panels. However, in the impact zone, the bolted connections were included in the model, and commands were generated to make sure that nodes in adjacent panels in the impact zone were not merged.

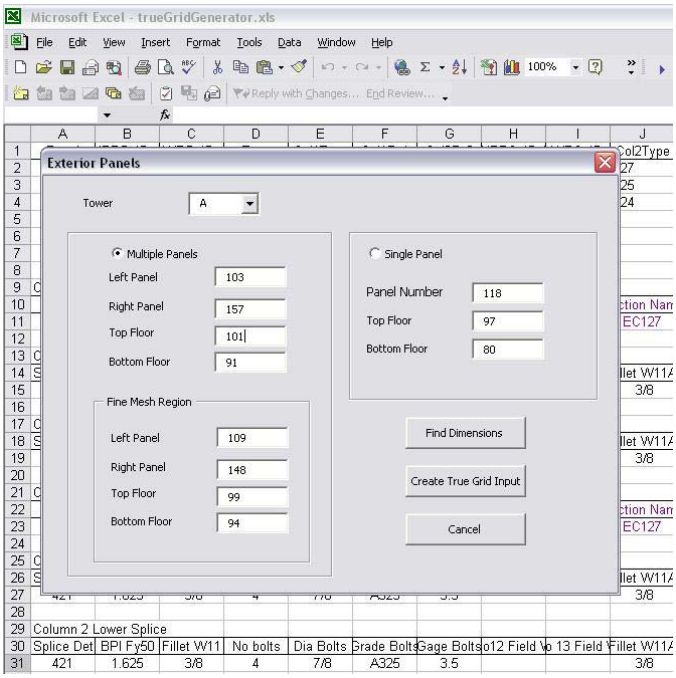

Figure 3–2. User interface for exterior panel generator.

Additional details of the model generation for various tower components are given in the following sections.

3.2.1 Core Model Development

Core column models were generated as a group in single floor sections. Dimensions and material specifications were assigned automatically, as specified in the WTC structural databases. The boundary conditions at the top and bottom of the core model and the column splices were automatically generated. An example model of the WTC 1 core columns for floors 95 to 97 is shown in Figure 3–3. Different colors correspond to different material assignments for the various column sections.

Both wide flange and box core columns were modeled with Belytschko-Tsay shell elements (LS-DYNA shell element type 2). These shell elements are four noded elements with single point integration, and are a computationally efficient alternative to the Hughes-Liu element in LS-DYNA. The Belytschko-Tsay shell elements are widely used for crash, impact, and metal forming applications. Results obtained with these elements typically agree with those obtained with the Hughes-Liu element. The reader is referred to the LS-DYNA Theoretical Manual for a complete discussion on this element type. Two mesh densities

were used in the global impact analysis, a refined density in the area of impact and a coarse far field density elsewhere (typical element dimensions of 2 in. in the impact zone and 8 in. in the far field, respectively). In the impact zone, the mesh topology and density for both column types were identical to those used in the component analysis. A single wide flange column in the impact zone had 552 shell elements and 600 nodes per floor. A box column in the impact zone had 864 shell elements and 900 nodes per floor.

Figure 3–3. Model of the WTC 1 95th–97th core columns and connections.

Details of column splices at floor 95 are shown in Figure 3–4 and Figure 3–5. The wide flange-to-wide flange core column connections were modeled by splice plates placed on the outside of each flange, as shown in Figure 3–4. The connection between the splice plate and column flange was modeled with a surface to surface tied interface without failure (LS-DYNA contact type 2). This effectively results in a perfect bond between the nodes of the splice plate and the flange of the adjacent column. If the columns

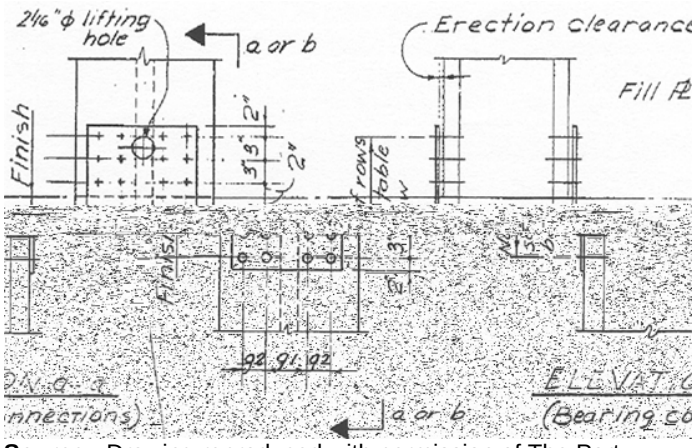

Source: Drawing reproduced with permission of The Port Authority of New York and New Jersey.

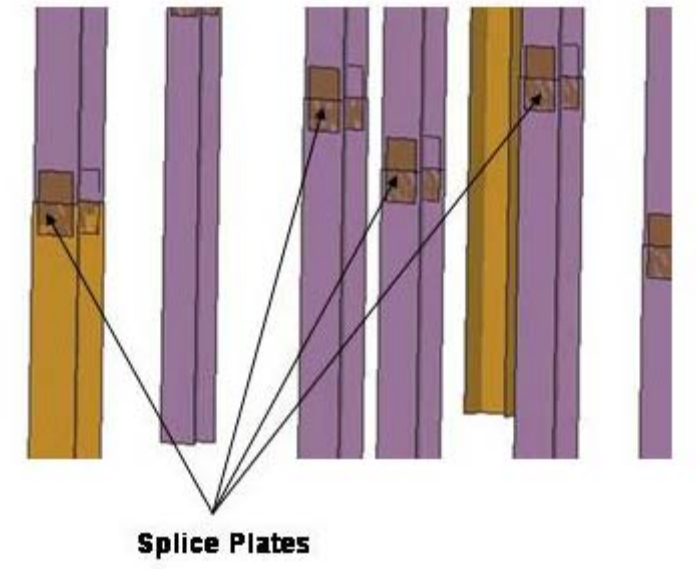

Figure 3–4. Detail of wide flange core columns splices.

A typical box column-to-wide flange column connection is shown in Figure 3–5. The thick box column cap was modeled with shell elements and was perfectly merged into the lower box column. The connection between the wide flange column and the box column cap was an edge-to-surface tied interface without failure (LS-DYNA contact type 7). This tied connection results in the nodes of the wide flange column being perfectly bonded to the element segments of the box column cap plate. Failure of this connection would occur only when deformations and strains of this connection are sufficiently high to fail the elements in the columns adjacent to the joint.

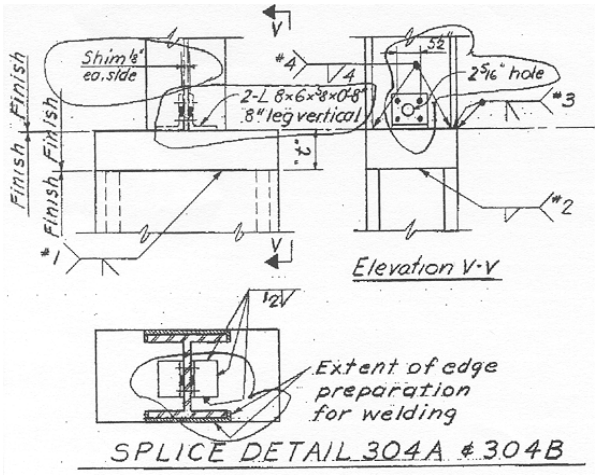

Source: Drawing reproduced with permission of The Port Authority of New York and New Jersey.

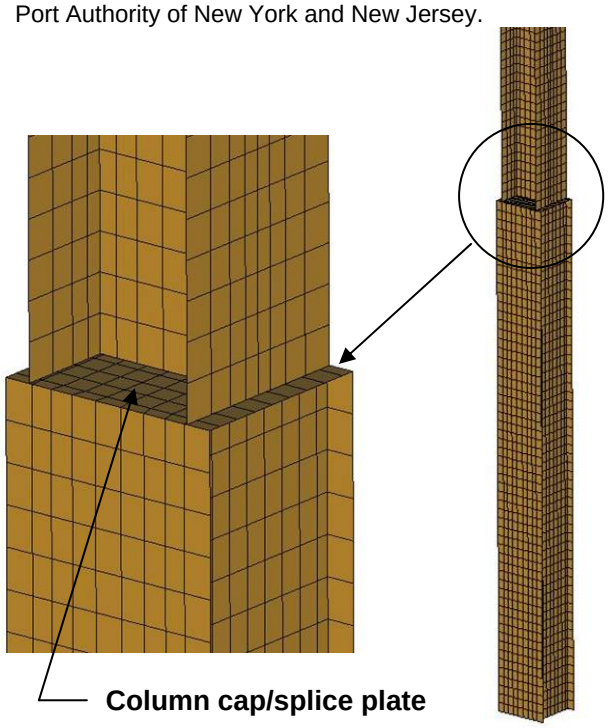

Figure 3–5. Detail of box columns-to-wide flange core columns splice.

The approach for assembling the core floors in the global model was to generate models of typical floors in the impact zone and repeat them in the surrounding floors. For WTC 1, a model of the 96th floor inside the core was developed and was used for modeling floors 92 through 100. This approach was also used for floors 77 through 85 as the impact zone in WTC 2. Special details for mechanical, lower and upper elevator, and sky lobby floors were sufficiently far away from the impact to warrant this simplification. Figure 3–6 shows the WTC 1 core prototype of the 96th floor with and without the concrete floor slab. The entire model was developed with Belytschko-Tsay shell elements. Mesh density can be set independently from floor to floor to obtain higher accuracy in the impact zone and computational economy in the surrounding floors. A typical core floor with the higher impact zone mesh

density (floor 96 of WTC 1 in this case) had approximately 66,000 shell elements and 76,000 nodes. This included core floor slab, floor beams, connections, and core columns over a height of one floor.

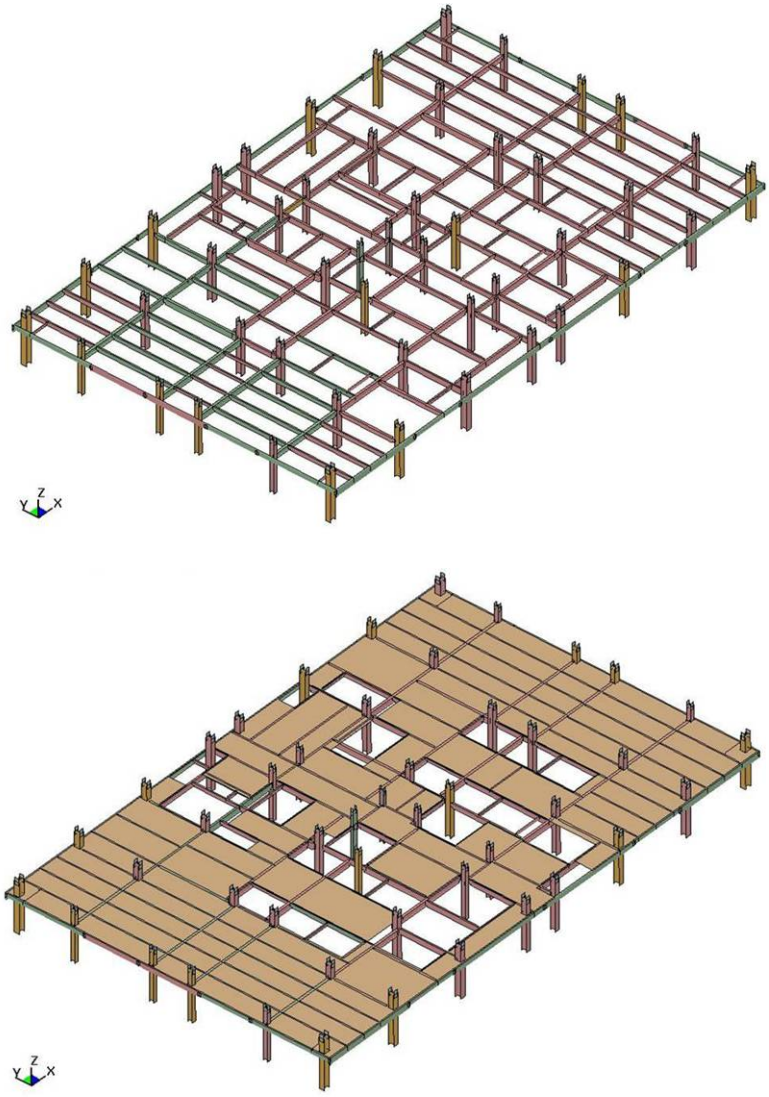

Figure 3–6. Model of the WTC 1 96th floor core columns and beams (with and without floor slab).

The various connection details between core beams are illustrated in Figure 3–7. Core perimeter beams were joined with splice plates in the same manner as wide flange column end connections described above. Interior beams were connected with node-to-surface tied connections (contact type 7). The node-to-surface contact algorithm constrains the nodes to move with the same relative motions as the adjacent surface elements and is appropriate for modeling a strong welded connection. An automatically generated model for the assembly of WTC 1 core floors 94 through 98 is shown in Figure 3–8. Floor beam and slab details in this model were replicates of the 96th floor prototype.

type 300 on the sides and panel type 210 in the corners. Examples of the models for these panel types are shown in Figure 3–9. The exterior wall in the WTC 2 impact zone included a mixture of 100, 200, 300, and 400 series panels due to the proximity of the mechanical floors.

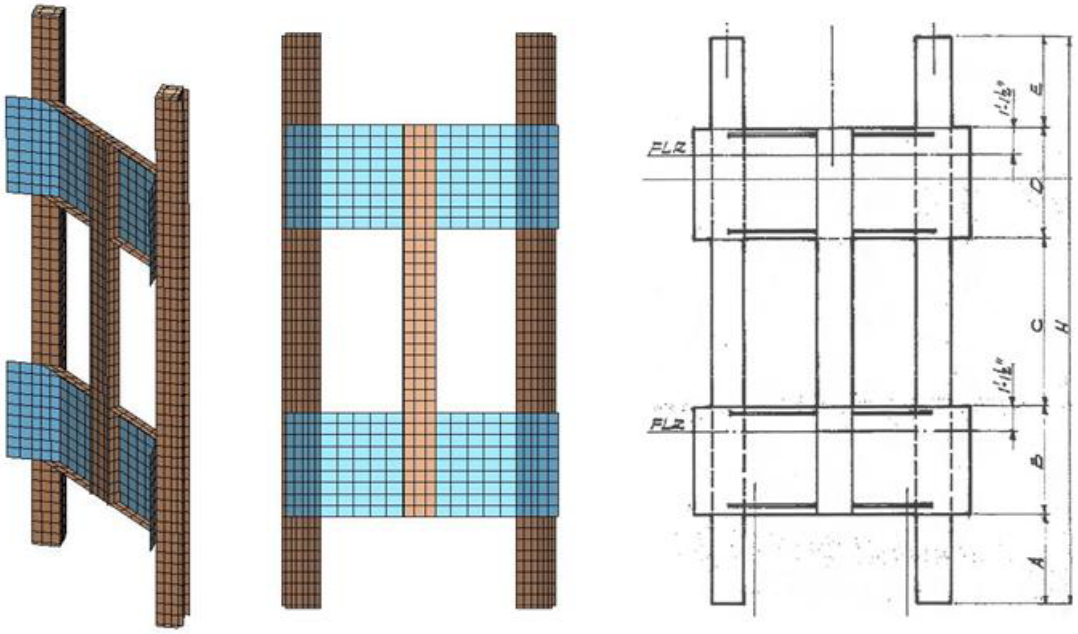

(a) Type 210 panel

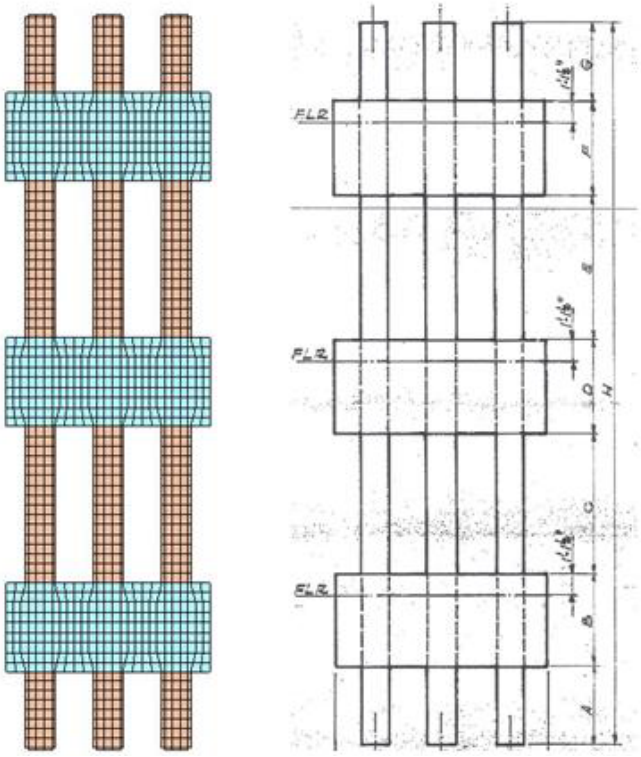

(b) Type 300 panel

Figure 3–9. Example models for exterior wall panel types.

The complete exterior wall model in the impact zone for each tower was generated by placing the various panels in the actual locations with their dimensions and material specifications. These material and geometric parameters were extracted automatically from the tower database using the third VB program to automatically generate the exterior wall models (see Section 3.2). The impact face for the global WTC 1 (north wall) and WTC 2 tower (south face) models are shown in Figure 3–10 and Figure 3–11, respectively. The figures show a mixture of coarse and fine meshed panels. A refined mesh was used in the immediate impact zone for improved accuracy of the impact response, and a coarse mesh was used outside the impact zone for improved computational efficiency. All panels were primarily constructed from Belytschko-Tsay shell elements. Constant stress brick elements (LS-DYNA solid element type 1) were used to model the butt plates in the refined panels. Hughes-Liu beam elements (LS-DYNA beam element type 1) were used to model bolts connecting the butt plates in the refined impact zone as described in Section 2.3.3. As an example, each type 300 panel in the impact zone contained 5,304 nodes, 5,202 shell elements, 78 brick elements, and 12 beam elements. The corresponding element sizes in the impact zone were a 1 in. element for the weld zone and 4 in. elements for the exterior column. A typical element dimension for the far field exterior panels was 14 in.

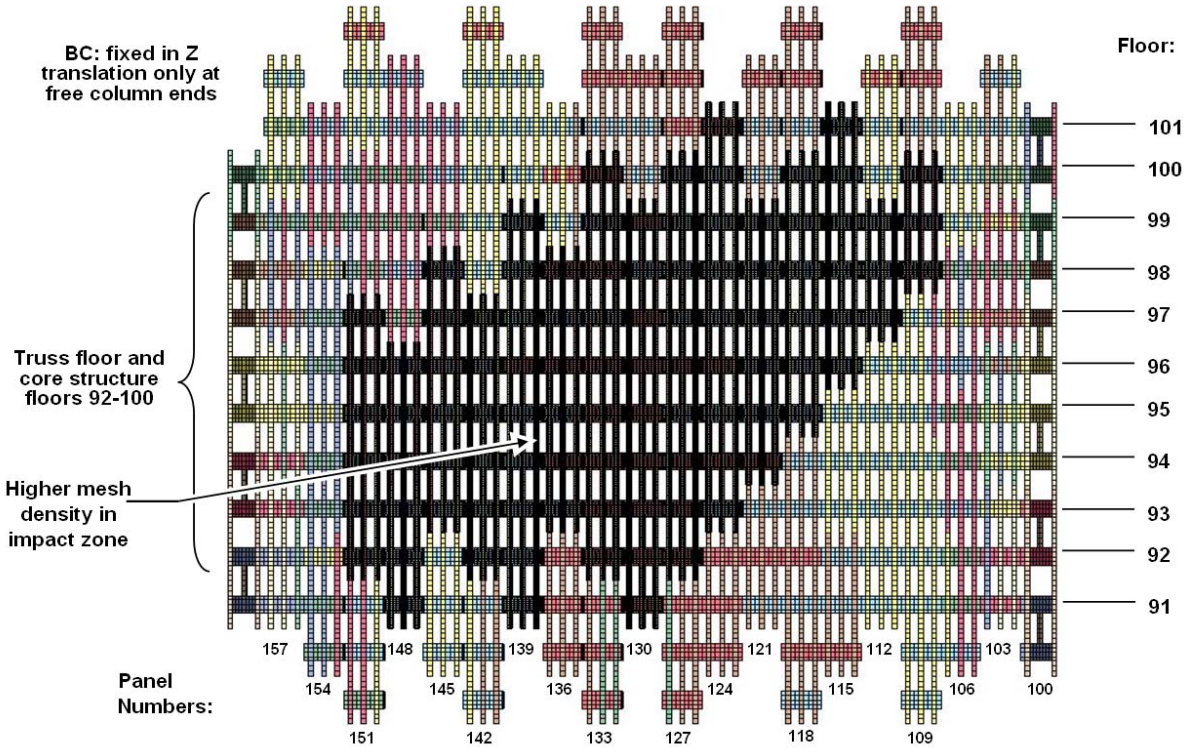

Figure 3–10. Impact face of the WTC 1 model - floors 91–101.

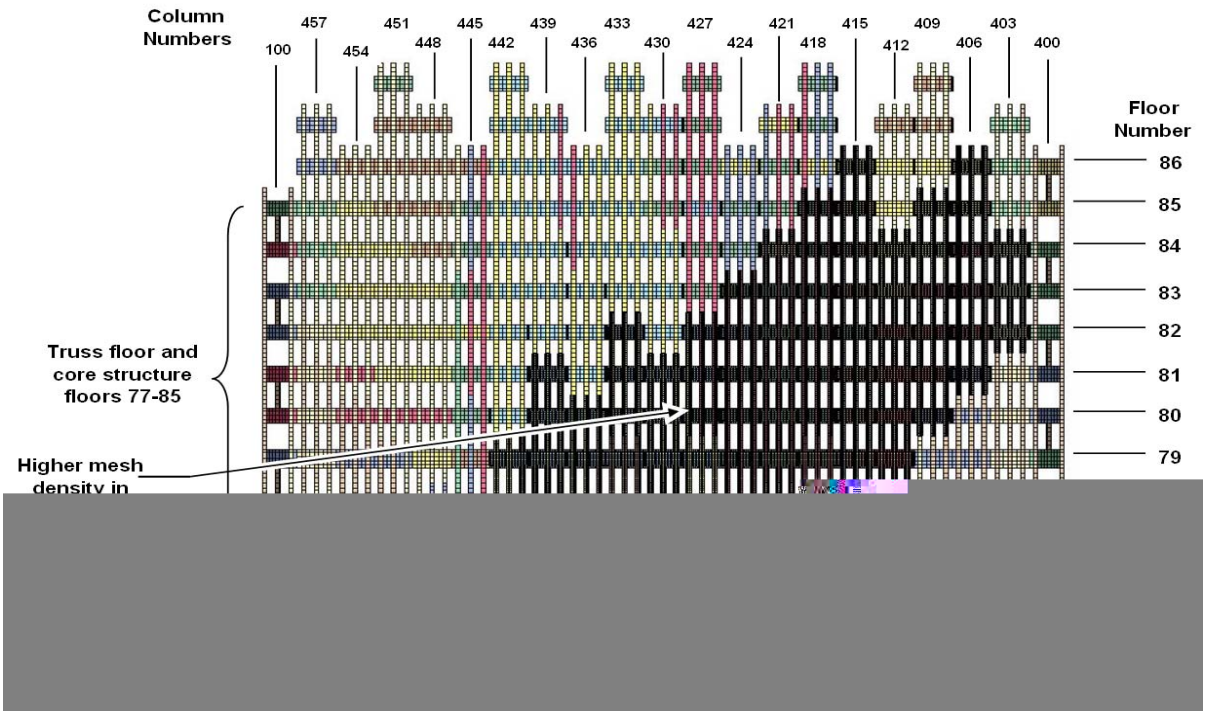

Figure 3–11. Impact face of the WTC 2 model - floors 75–86.

In addition to the generation of the exterior panels model, the VB program was also used to automatically specify the boundary conditions and various connection details between the panels. The boundary conditions at the top and bottom of the exterior wall were constrained vertical displacements. The lateral degrees of freedom and rotation about the vertical axis were not constrained. The free lateral displacements at the model boundary allowed for the tower model to have a rigid body velocity following the impact. Since the natural period of the tower was approximately 10 to 11 s, the tower would provide little structural resistance to the translation at the model boundary during the less than 1 s impact event. The connections between panels included the bolted connections across the column end butt plates and the bolted splice plate connections between spandrels of adjacent panels.

The bolted connection between exterior column ends was modeled using beam elements to represent the individual bolts. The behavior of these beam element bolts was compared to the measured tensile data for the bolts in Chapter 5. This representation of the bolted column butt plate connections was only provided in the higher mesh density impact zone panels. The column ends for the coarse far field exterior wall panels were merged together to create a perfect bond between column ends.

The model for the spandrel splice plate connection is shown in Figure 3–12. Twelve nodes on the splice plate were attached to the spandrels using the spot weld tied node algorithm (LS-DYNA Type 7 tied interface). The spot welds approximate the connection of the individual bolts connecting the spandrel splice plates. Failure of these connections occurred through deformation of the splice plates and/or spandrel and ductile failure of the materials.

The placement of the spandrel splice plates was again limited to the higher resolution impact zone for the exterior wall. The far-field coarse panel models were merged together as shown in Figure 3–13. The

influence of the spandrel splice connection on the impact response and exterior wall damage was investigated using engine component impact analyses as described in Chapter 5.

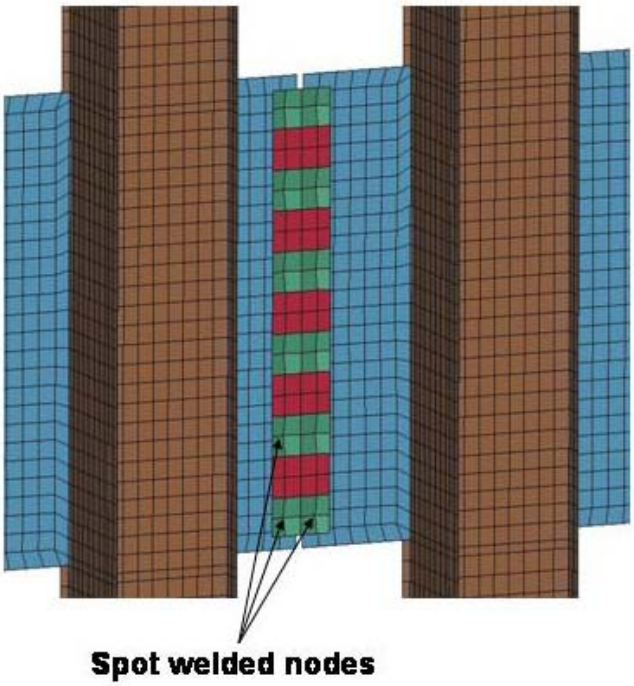

Figure 3–12. Model of spandrel splice plate connection.

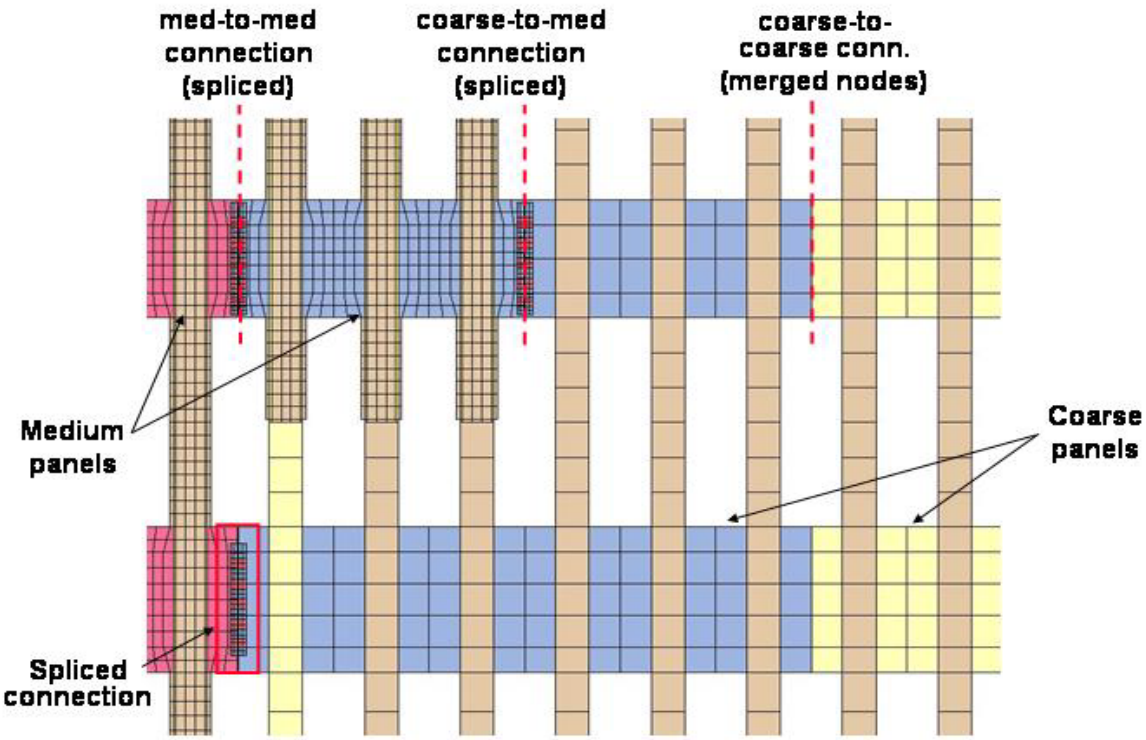

Figure 3–13. Placement of spandrel splice plates in the exterior wall model.

3.2.3 Truss Floor Model Development

The approach to the development of the truss floor model was very similar to other portions of the tower structure. Initially, parameterized component models were developed for segments of long-span trusses, short-span trusses, and corner two-way trusses. These parameterized models were then called repeatedly for generation and placement of the floor truss segments within the complete tower models. The individual truss floor segments spanned the distance from the exterior wall to the core. An example of a truss floor segment used in the global model is shown in Figure 3–14. In the double truss sections, the two trusses were modeled explicitly with the proper dimensions. The model of the floor trusses accounted for the potential for buckling of the bottom chord under impact loading.

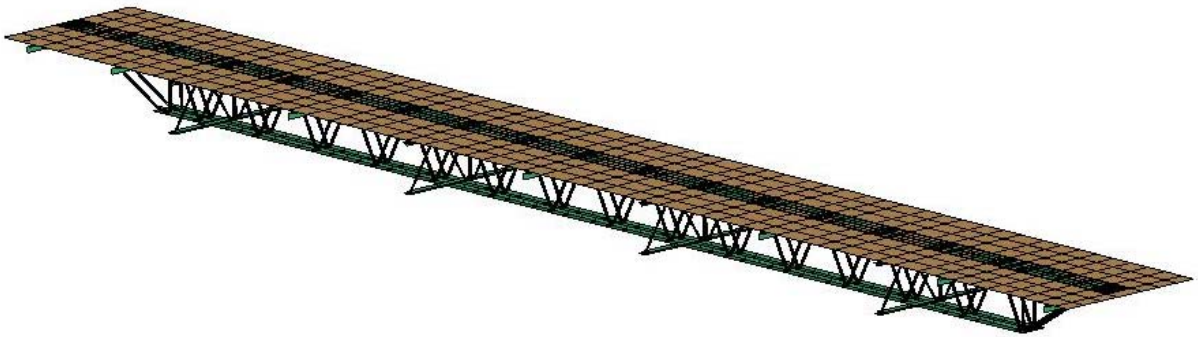

Figure 3–14. Model of a truss floor segment.

The model was developed using a uniform layer of Belytschko-Tsay shell elements for the combined floor slab and metal decking. Construction methodology was the same for both primary and bridging (secondary) trusses, using Belytschko-Tsay shell elements for the truss upper and lower chord components, Belytschko-Tsay shell elements for the cross supports, and Hughes-Liu beam elements for the round bar truss diagonals. The upper chords were attached to the floor slab using an offset tied interface for both the primary and bridging trusses. This approach, using shell elements as opposed to solid brick elements for the floor slab, was adapted to reduce the model size requirements. Development of a model with matching mesh density in the slab and truss structures (nodal alignment for a merged connection) resulted in a much larger model size.

The mesh refinement used in this model for the truss floor would result in a very large global tower model size if used throughout the structure. The model for the long-span truss floor segment, shown in Figure 3–14, contained 2,737 nodes, 362 beam elements, and 1,878 shell elements. Constructing a global impact tower model with these detailed floor segments was not practical due to model size limitations. A complete floor would result in approximately 200,000 nodes for a single truss floor structure. As a result, detailed floor segments were included only in the impact zone, and a simplified floor truss model was used elsewhere. Further discussion on the simplified model is included in Section 3.2.5.

Figure 3–15 and Figure 3–16 show truss floor connection details at the exterior wall and core, respectively. The models for the truss seat connections were developed using shell elements and attached using the tied interface algorithm. The failure of the seats only occurs as a result of exceeding the ductility of the seat or truss structures.

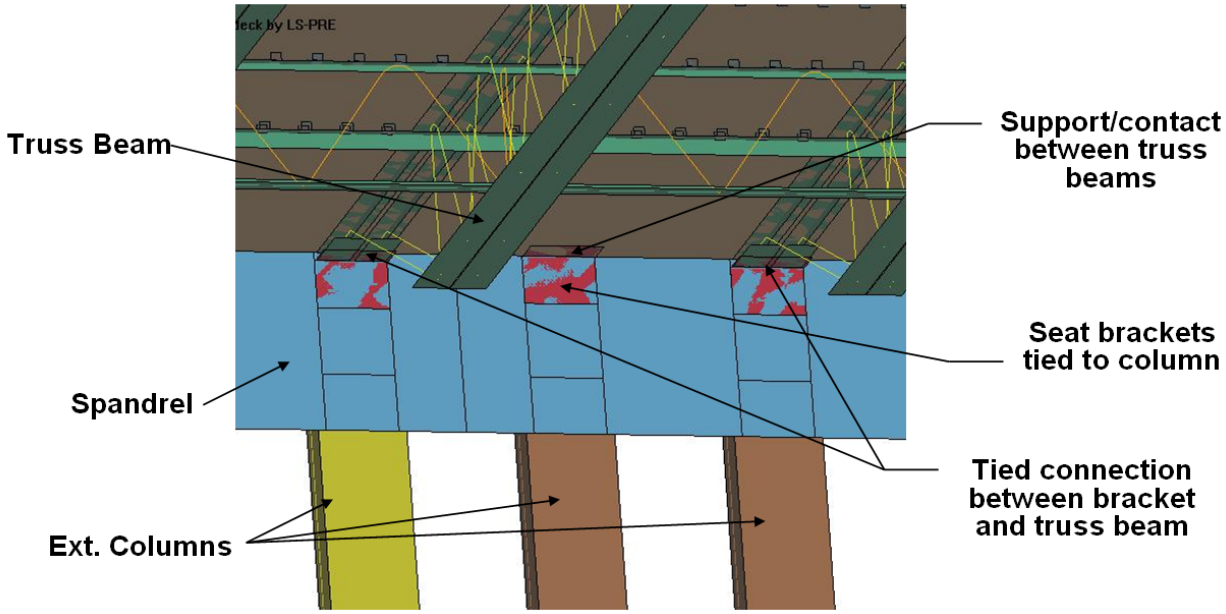

Figure 3–15. Truss floor connection detail at exterior wall.

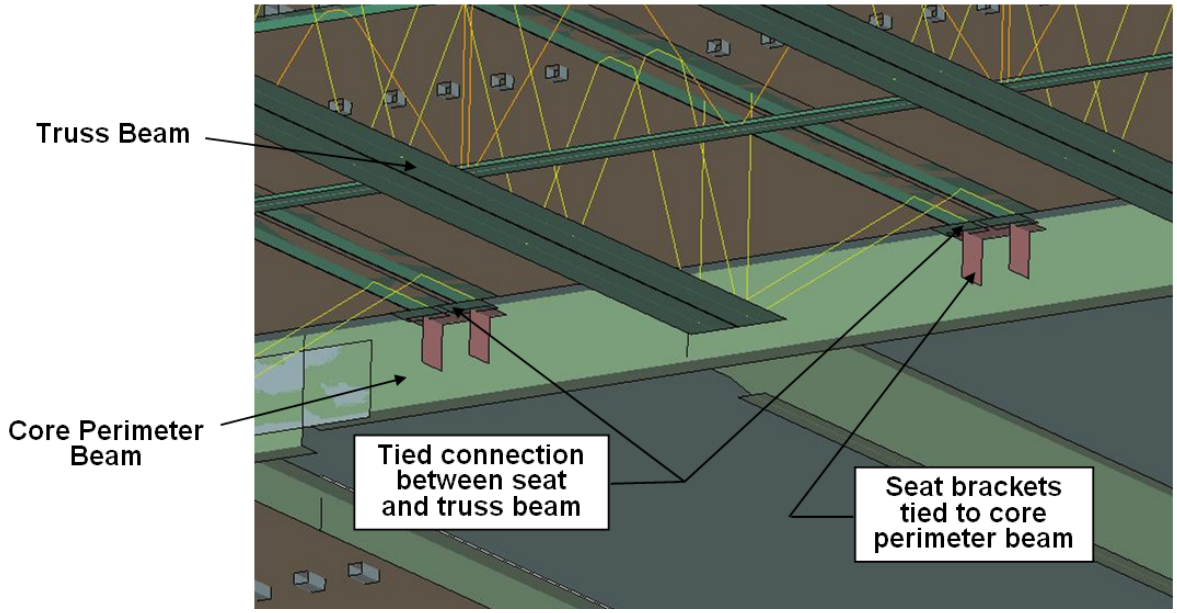

Figure 3–16. Truss floor connection detail at core perimeter.

A series of dampers were installed in the WTC towers between the floor truss lower chord and the spandrel on the exterior wall. The primary function of these dampers was to reduce the vibration of the building under wind loading. These dampers, however, were of low mass and the arrangement of the damper and saddle (member attaching the damper to the bottom chord of the truss), along with their connections, had virtually no strength in the transverse direction. Under impact conditions, the aircraft applied transverse forces to the damper assembly due to the downward motion of the aircraft (see Chapter 7). Also, due to the short duration of the impact event (less than 1 s), damping was not included

in the analyses. As a result, the dampers were considered to have sufficiently low mass and strength and were therefore not included in the impact analyses.

A model assembled for an entire floor (floor 96 of WTC 1), including the core and exterior wall structures, is shown in Figure 3–17. A comparison of the plan view and the associated framing plan drawing for this floor is shown in Figure 3–18.

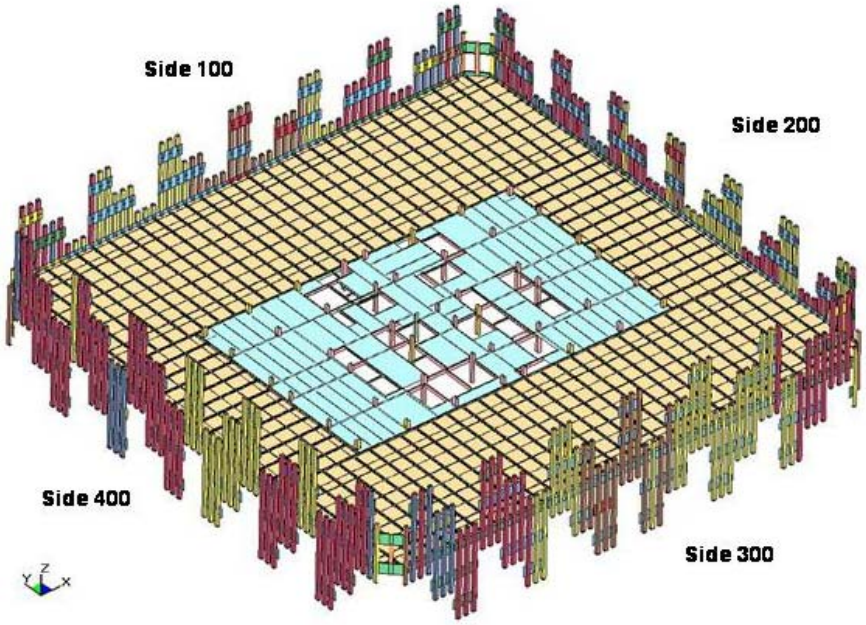

Figure 3–17. Model of the 96th floor of WTC 1.

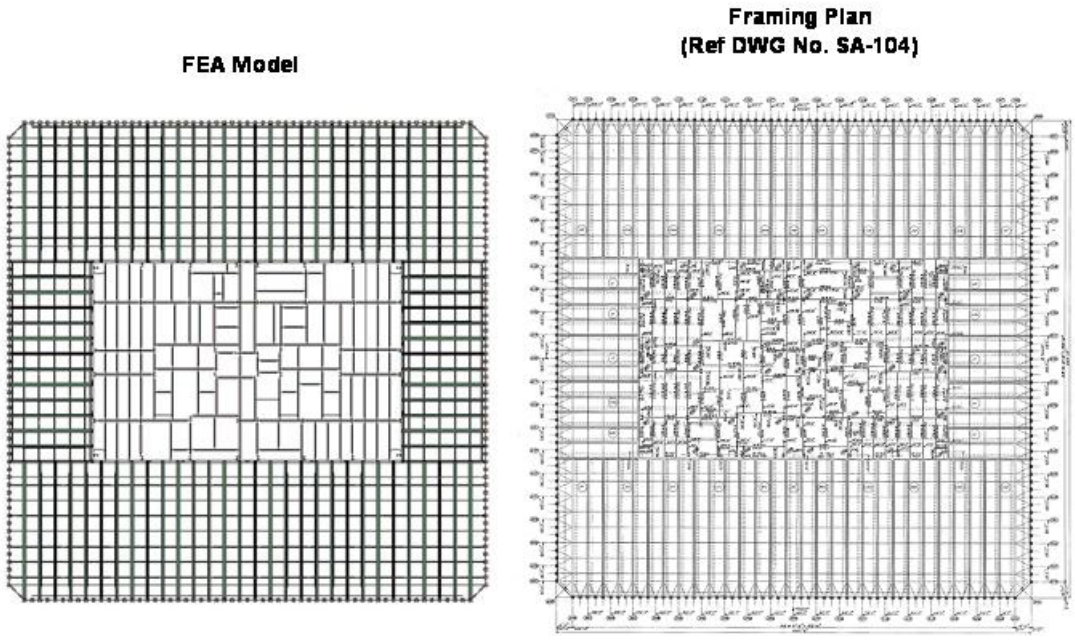

Source: Drawing reproduced with permission of The Port Authority of New York and New Jersey.

Figure 3–18. Model plan view and framing plan drawing of the 96th floor of WTC 1.

3.2.4 Interior Contents Model Development

The interior nonstructural contents of the towers were modeled explicitly in the tower models used for the global impact analyses. The live load mass was distributed between gypsum walls and cubicle workstations that covered the truss floor area. The distribution of the gypsum walls was obtained from architectural drawings and other information gathered as part of the NIST reconstruction of the thermal environment. Similarly, data gathered by NIST for the floor layout plans in the impact zone were used to develop the approximate placement of workstations over the truss floor area. The resulting model of a floor with interior contents is shown in Figure 3–19. Heavy elevator components such as elevator cars and counterweights inside the core's elevator shafts were not included in the models since there was no way of determining their locations at the time of impact.

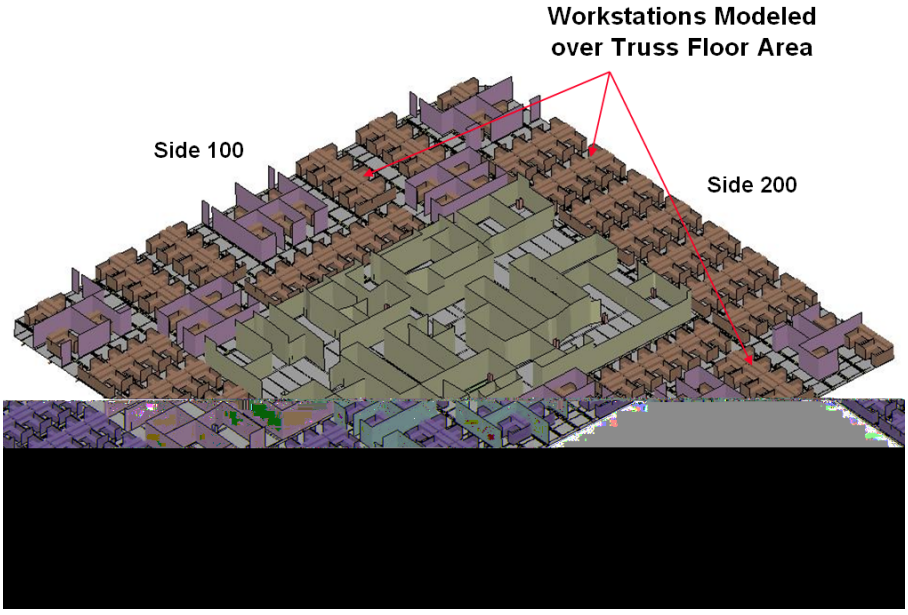

Figure 3–19. Model of the 96th floor of WTC 1, including interior contents.

The densities of specific materials were scaled to obtain the desired magnitudes for the live loads and superimposed dead loads. The densities of the tower contents (workstations and gypsum walls) were scaled by the appropriate ratios to get the desired distribution of live loads in the core and truss floor areas. The densities of all the remaining tower structural components were scaled proportionately to obtain the desired superimposed dead loads. These additional loads were important for obtaining an accurate mass distribution in the towers and inertial effects in the impact response. The live load used was based on a percentage of the design live load on the floors inside and outside the core. Using 25 percent of the design live loads resulted in 19.7 psf uniformly distributed over the core and 16.2 psf uniformly distributed over the outer truss floor area. Using the approximate floor areas of 8,700 ft^2 in the core and 31,250 ft^2 outside the core produced 170,000 lb and 500,000 lb of live load for the core and outer floor areas, respectively.

The superimposed dead loads added to the model were 36.2 psf for the core area and 11.5 psf outside the core producing 315,000 lb and 359,000 lb of superimposed dead load for the core and outer floor areas, respectively. These superimposed dead loads were included in the model by scaling the density of the structural components (slab, columns, beams, etc.) both inside the core and outside the core by uniform

scale factors to obtain the appropriate dead loads. Superimposed dead loads were applied to the columns to account for nonstructural components such as insulation, cladding, and windows.

A summary of the live loads and superimposed dead load magnitudes and density scale factors are provided in Table 3–1. The total amount of added weight from the superimposed dead load and live load for a single floor was 1.35 million lb resulting in a total weight for the floor of 4.41 million lb (after the addition of the self weight of the floor).

Table 3–1. Summary of superimposed dead loads and live loads (per floor).

	Area (ft^2)	Weighting (psf)	Added Weight (lb)	Density Multiplier
Core Dead Load	8,694	36.2	3.15E5	1.628
Outer Dead Load	31,257	11.5	3.59E5	1.218
Core Live Load	8,694	19.7	1.71E5	0.852
Outer Live Load	31,257	16.2	5.06E5	0.447/0.757[a]
Total	39,951	N/A	1.35E6	N/A

a. Value of multiplier dependent on model of workstation used.

The partitions and workstations were modeled using shell elements. The model of the building contents (partitions and workstations) over a single floor, as shown in Figure 3–19, had 101,733 nodes and 97,284 shell elements. To include the complete distribution of the building contents over five floors in the global impact model would require approximately 500,000 nodes. As a result, the global models included the partitions and workstations only in the region of each floor directly in the path of the aircraft impact and debris. Using this approach significantly reduced the computational requirements needed to include the building contents inertial contributions. For example, the WTC 1 global impact model included only 160,410 nodes and 148,858 shell elements for the partitions and workstations in the impact path over five floors (savings of about 300,000 elements). WTC 2 model simplification saved a similar amount of nodes and elements. These building content distributions for the two tower models are discussed in the following section.

All of the contents in the truss floor regions rested on the floor with a contact algorithm used to prevent penetration. Gravitational acceleration and friction included in the contact analyses resisted sliding motions of these contents. The bottoms of the gypsum walls in the core were rigidly connected to the floor slab using merged nodes. The core walls in the model did not extend the full height of the floor to avoid interference with the core beams of the floor above. As a result of this clearance, the tops of the core walls were not constrained. This approximation did not have a significant impact on the response in the core. An impact by a fragment with significant momentum resulted in a failure of the wall. The majority of the core wall damage in the simulations was failure and erosion rather than displacement or knocking over of the walls.

3.2.5 Global Model Assembly

The global model was assembled in the same coordinate system as defined in the structural databases. An assembly of exterior and core structure illustrating the global coordinate system is shown in Figure 3–20. The vertical (Z) coordinate was shifted to be centered on the floor closest to the impact point (e.g., Z=0 at floor 96 of the WTC 1 model). This reference was selected to eliminate numerical precision problems

associated with contact or small interference dimensions of components relative to large vertical coordinate values within the model.

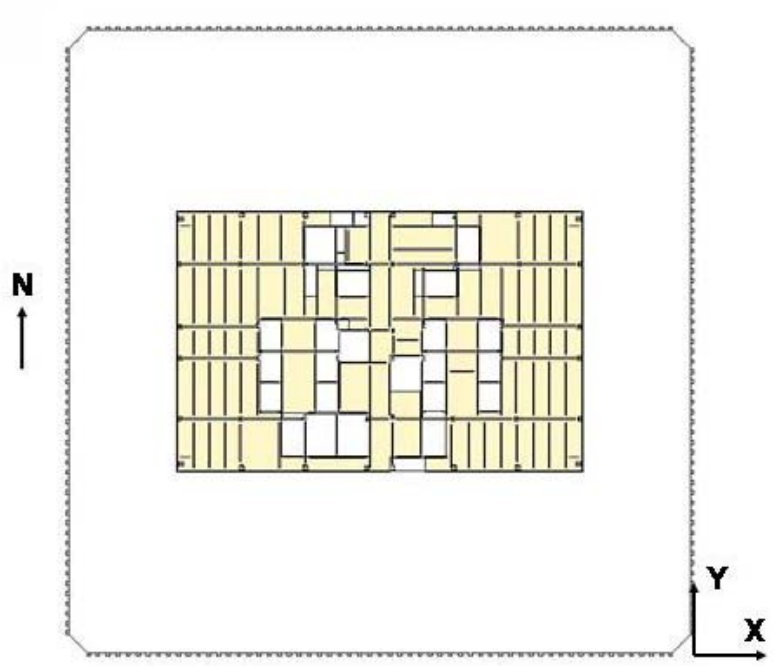

Figure 3–20. Coordinate system used for the WTC 1 model.

The multiple floor global model of the impact zone in WTC 1 is shown in Figure 3–21. The model included the complete floor inside and outside the core, the exterior walls, and core structures for floors 92 through 100. The boundary conditions for the ends of the exterior and core columns at the top and bottom of the model constrained vertical displacement. This allowed for free translations of the tower structure in the longitudinal and lateral directions and rotation about the vertical axis. The influence of these boundary conditions on the impact response was investigated separately, as described in Section 10.4, and found to have little influence on the impact damage. The higher resolution exterior wall panels in the impact zone, shown previously in Figure 3–10, can be seen on the impact face of the tower model (Side 100).

The WTC 1 global impact model with the exterior wall removed is shown in Figure 3–22. The figure shows how the model was optimized to reduce mesh size and eliminate computational requirements outside of the immediate impact and damage zone. The nonstructural building contents (partitions and workstations) were not modeled over the entire floors in the impact zone, but rather only in the path of the aircraft impact and debris cloud. These components are shown separately in Figure 3–23. As a result, the total live load mass modeled over the multiple floors within the impact zone was significantly less. The distribution and density of the building contents (partitions and workstations) in the path of the aircraft debris, however, were included in the model. The building contents outside this region were not expected to have a significant effect on the impact behavior since these components do not contribute significantly to the structural strength and they are not strongly coupled to the surrounding tower structures. The tower contents outside the impact zone were not sufficiently stiff or rigidly attached to the tower to have a

strong influence on the dynamic stress waves propagating through the structure as a result of the aircraft impact.

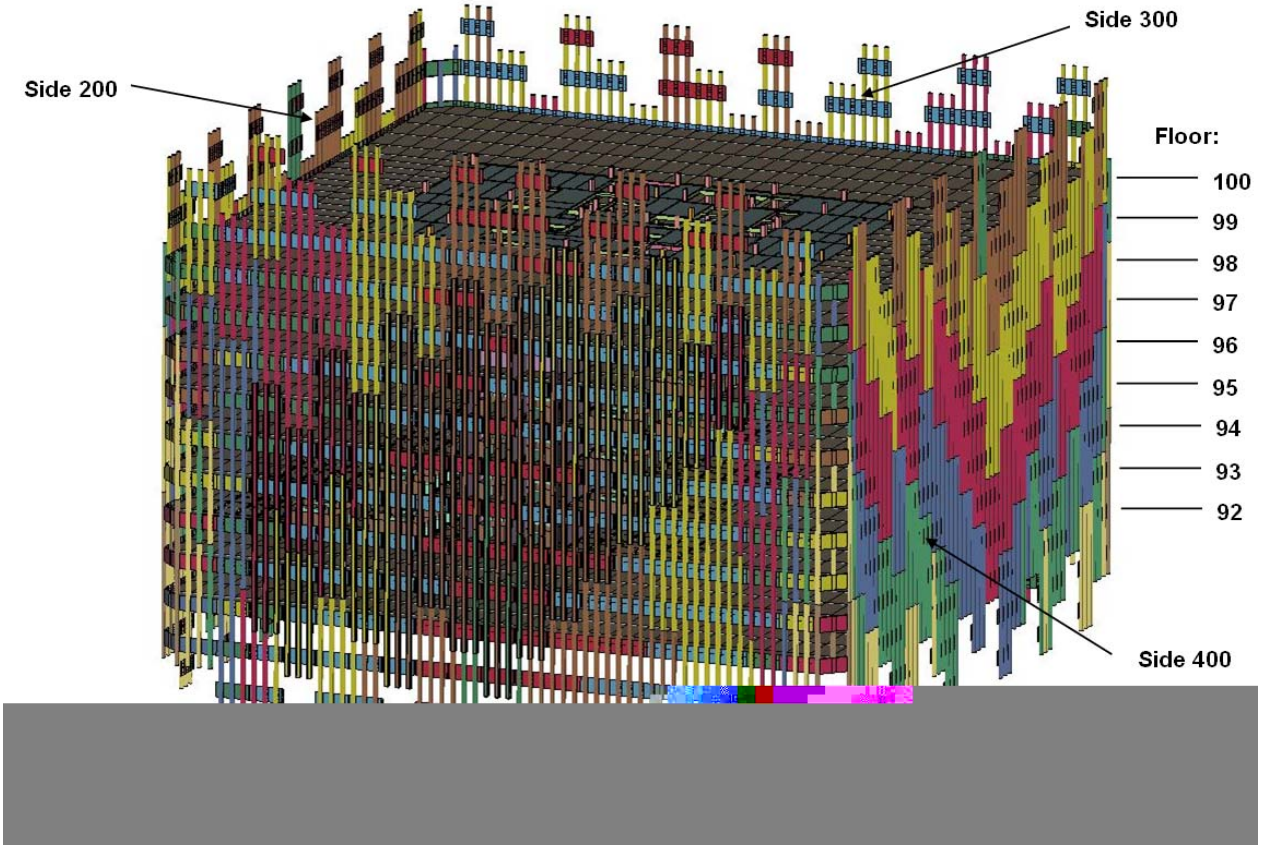

Figure 3–21. Multi-floor global impact model of the WTC 1 tower.

The truss floor structures near the impact zone were modeled in greater detail as seen in Figure 3–22(a). A separate view of the truss floor structures adjacent to Side 100 for floors 94 through 97 is shown in Figure 3–24. The sections of the truss floor in the path of the aircraft impact were modeled with the detailed truss floor model described in Section 3.2.3. The surrounding truss floor structures were modeled using a far-field truss model with a significantly reduced mesh resolution as shown in Figure 3–25. This far-field truss floor model was designed to have the appropriate inertial properties and structural stiffness. The truss was modeled with an effective shell element in place of the vertical truss structure and a beam element along the lower cord. These element dimensions were on the order of 30 in. and would not be able to accurately model a local collapse behavior of the truss. The floor slab was modeled with an identical approach as the floor slab in the impact zone, but with a typical element dimension of 30 in. compared to an element dimension of approximately 10 in. in the impact zone.

The side view of the internal structures, shown in Figure 3–22(b) looking from the west, illustrates that the core columns for floors 93 through 98 of WTC 1 were modeled with higher resolution than that in the floors above and below the direct impact zone. This higher mesh resolution was needed to capture the local damage that occurred from direct impact of aircraft structures and debris.

(a) Oblique view

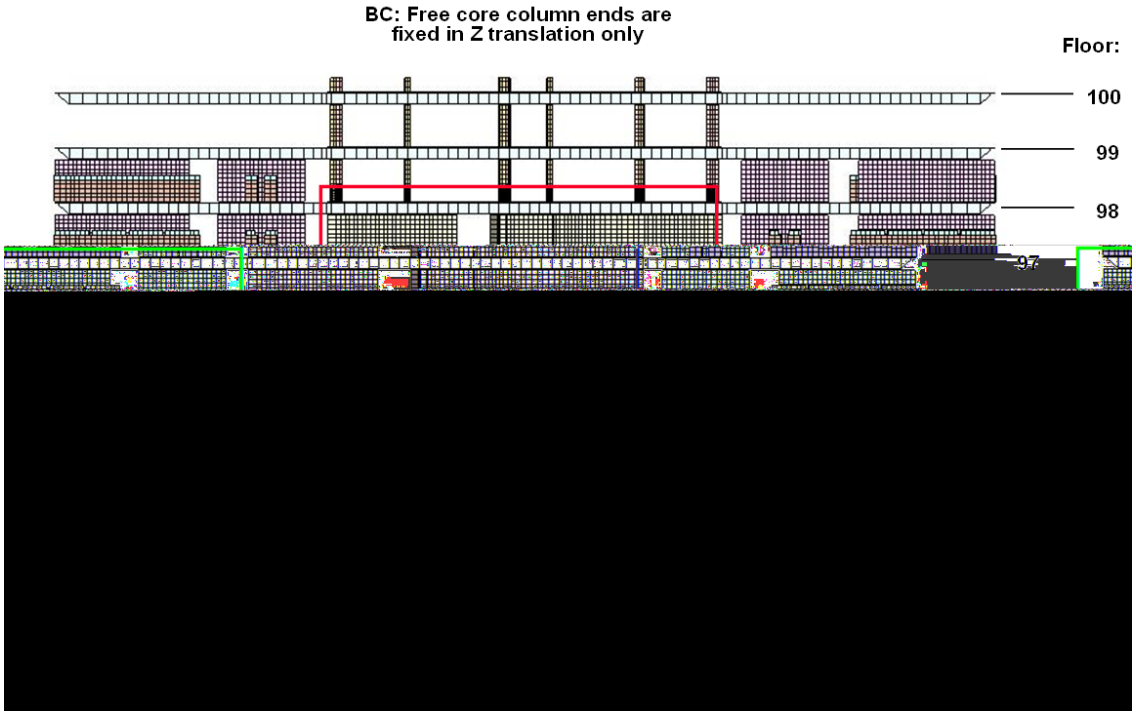

(b) West side view

Figure 3–22. Interior structures and contents of the WTC 1 global impact model.

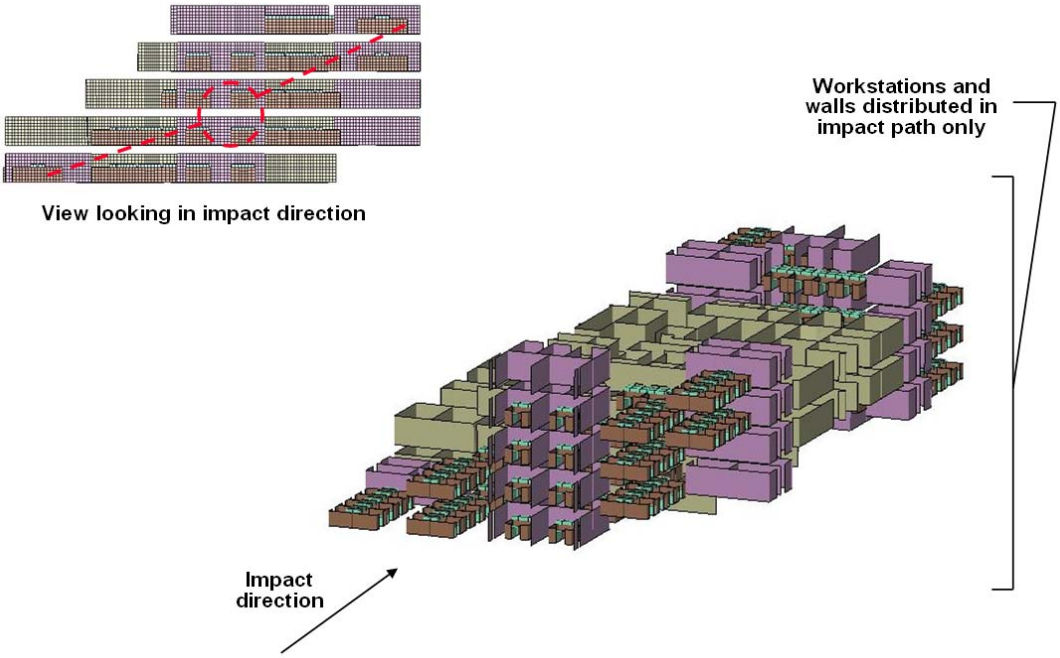

Figure 3–23. Building contents in the WTC 1 global impact model.

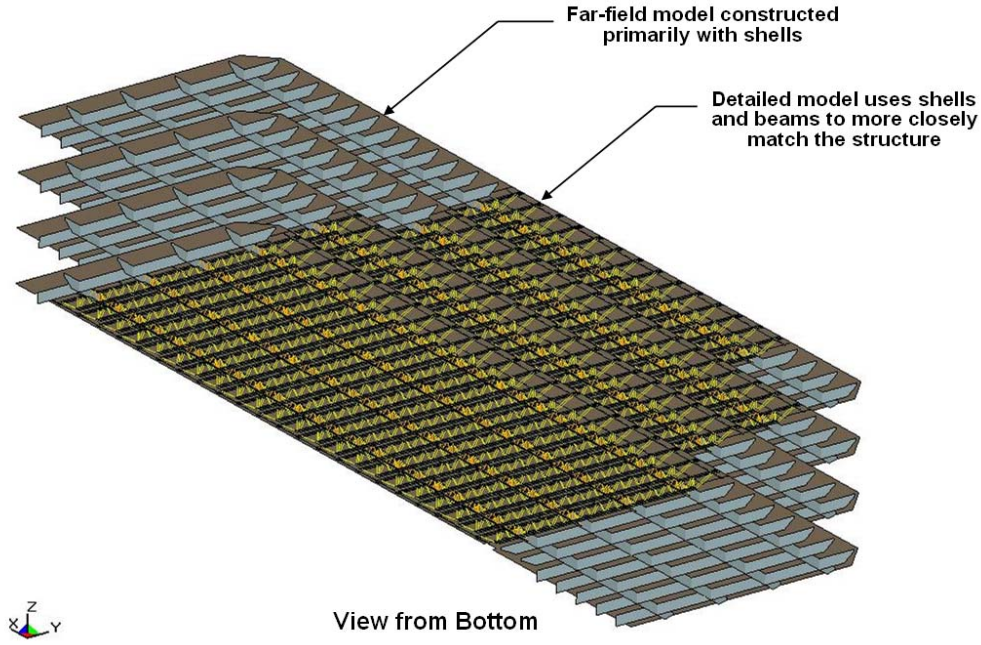

Figure 3–24. Truss floor components in the WTC 1 global impact model.

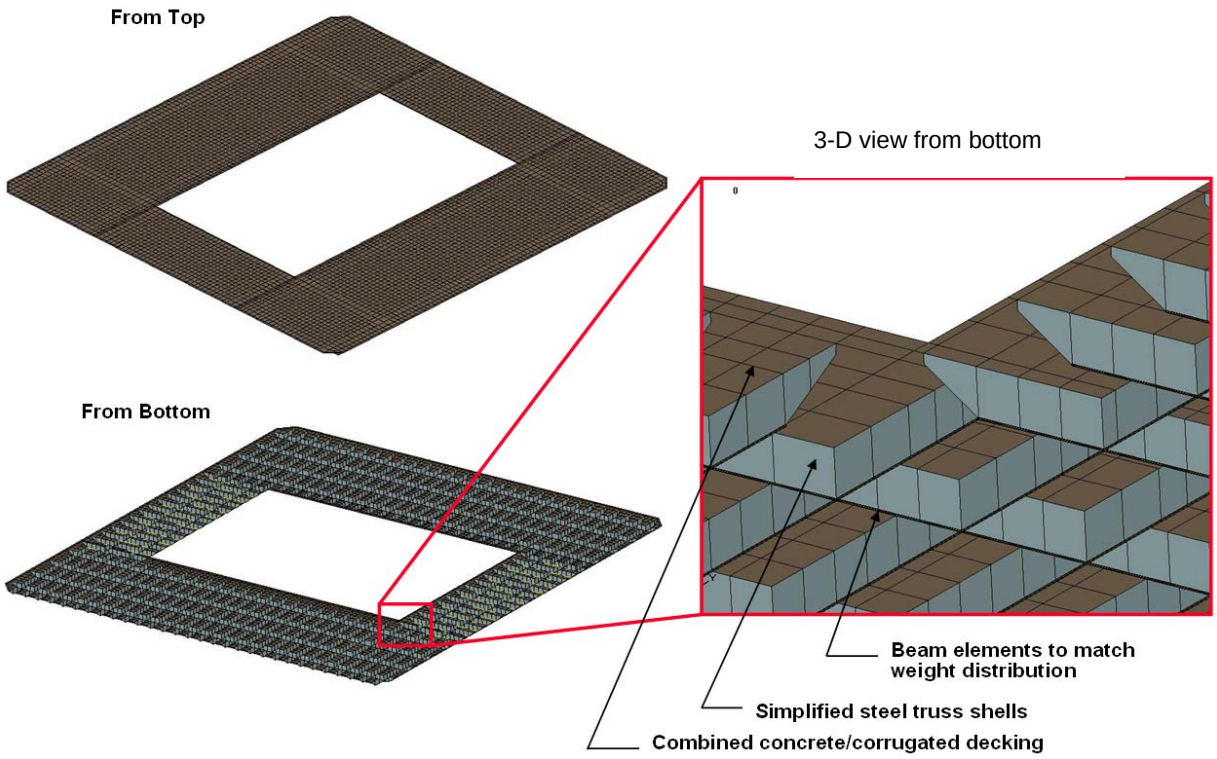

Figure 3–25. Far field truss floor model in the WTC towers.

The multiple floor global model for the impact zone of WTC 2 is shown in Figure 3–26. The model included the complete floor inside and outside the core for floors 77 through 85. The exterior wall panels at the bottom end of the model extended downward below floor 75. The boundary conditions for the ends of the exterior and core columns at the top and bottom of the model were the same as those for the WTC 1 model. The higher resolution exterior wall panels in the impact zone, shown previously in Figure 3–11, can be seen on the impact face of the WTC 2 tower model (Side 400).

The WTC 2 global impact model with the exterior wall removed is shown in Figure 3–27. This figure shows how the WTC 2 model was optimized to reduce the mesh size and eliminate computational requirements outside of the immediate impact and damage zone. The nonstructural building contents were again modeled only in the path of the aircraft impact and debris cloud. These components are shown separately in Figure 3–28. Similarly, the truss floor structures near the impact zone were modeled in greater detail as seen in Figure 3–27. These detailed sections of the truss floor were positioned adjacent to Side 400 (south face) for floors 78 through 81 and Side 300 (east face) for floors 81 and 82. The surrounding truss floor structures were again modeled with the far-field truss model shown previously in Figure 3–25.

To summarize, the approach adapted for the development of the global impact models for towers WTC 1 and WTC 2 was similar. The structures were modeled primarily with shell elements with some beam elements in the detailed truss floor sections and bolted connections between the column ends in the impact zone of the exterior wall. Some brick elements were used at the exterior column butt plates in the detailed impact zone. A summary of the model size and element types for the global tower models is presented in Table 3–2.

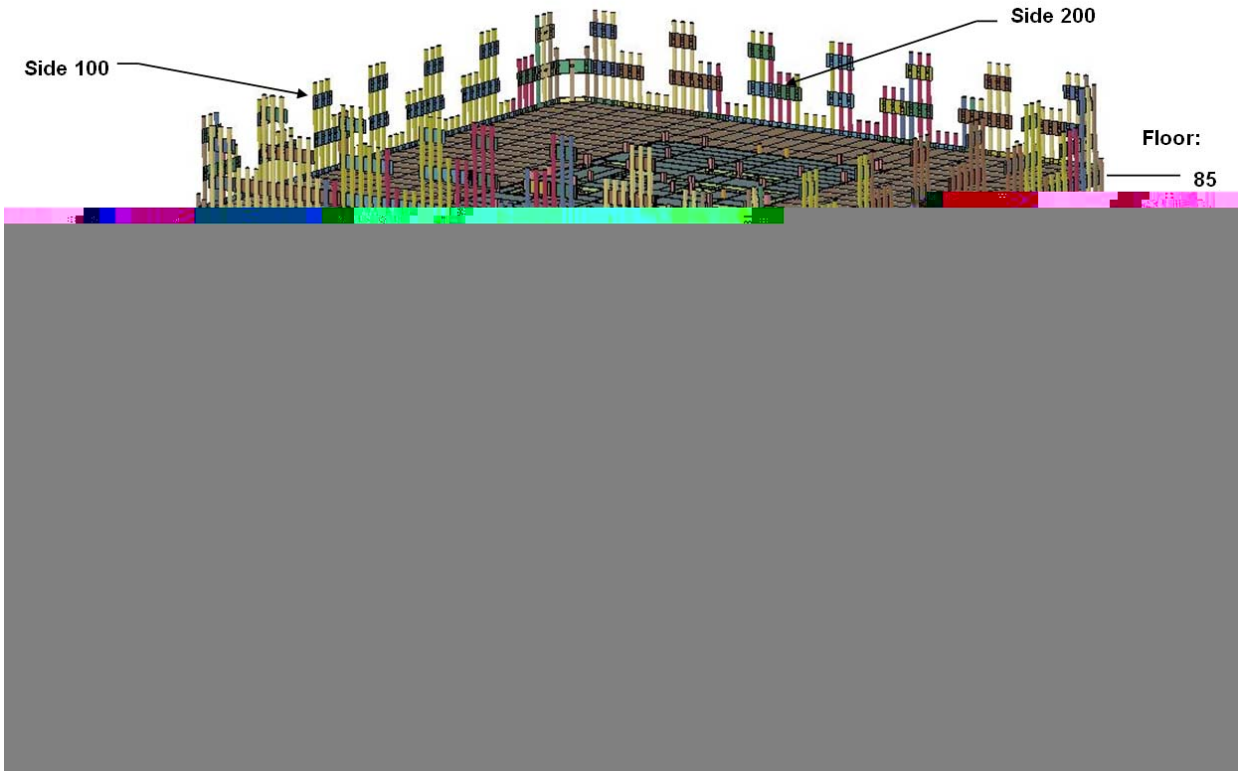

Figure 3–26. Multi-floor global impact model of the WTC 2 tower.

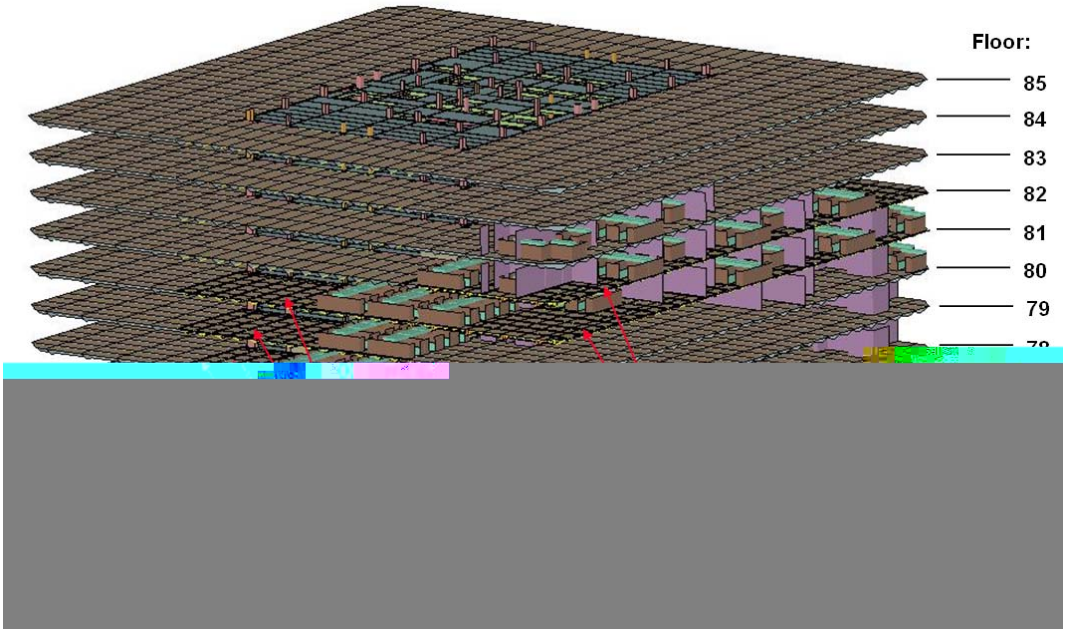

Figure 3–27. Interior structures and contents of the WTC 2 global impact model.

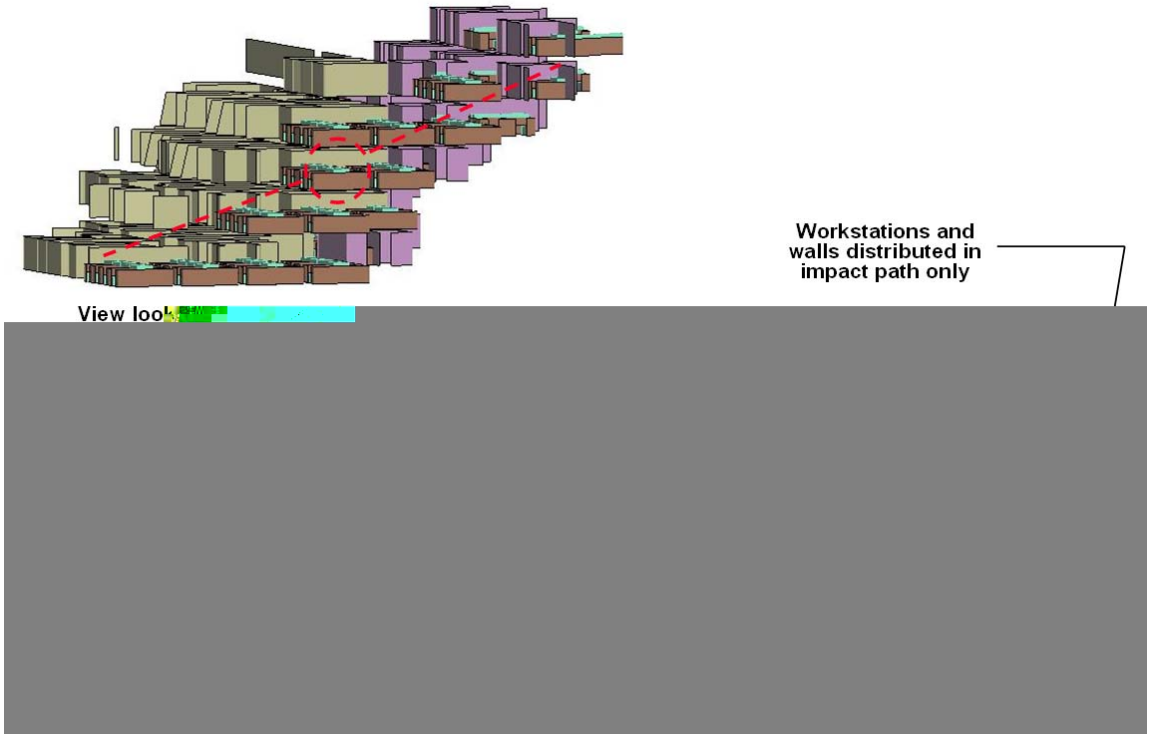

Figure 3–28. Building contents in the WTC 2 global impact model.

Table 3–2. Summary of the global impact models for the WTC towers.

	WTC 1 Tower Model	WTC 2 Tower Model
Number of Nodes	1,300,537	1,312,092
Hughes-Liu Beam Elements	47,952	53,488
Belytschko-Tsay Shell Elements	1,156,947	1,155,815
Constant Stress Solid Elements	2,805	2,498

3.3 REFERENCES

"LS-DYNA Keyword User's Manual," Livermore Software Technology Corporation, Version 970, April 2003.

"TrueGrid Manual, Version 2.1.0," XYZ Scientific Applications, Inc., September 2001.

"World Trade Center Building Performance Study: Data Collection, Preliminary Observations, and Recommendations," Federal Emergency Management Agency, FEMA 403, May 2002.

Chapter 4
AIRCRAFT MODEL DEVELOPMENT

4.1 INTRODUCTION

The finite element model for the Boeing 767-200ER aircraft was constructed through a three-step process: (1) data collection, (2) data interpretation and engineering analysis, and (3) meshing of the structure. The focus of this effort was on gathering sufficient structural data and including adequate detail in the aircraft model so that the mass and strength distribution of the aircraft and contents were properly captured for implementation in the impact analyses.

A fundamental limitation in the simulations described herein was the maximum finite element model size that could be executed on the available 32-bit computer clusters. Since LS-DYNA uses addressable memory for domain decomposition, the combined aircraft and tower model could not exceed approximately 2.3 million nodes. Due to this model size limitation, the Boeing 767-200ER model could not exceed 750,000 nodes.

The objective of the aircraft model development was to properly simulate the impact damage and aircraft break up and their effects on the World Trade Center (WTC) towers. Key requirements were to simulate the mass distribution, dynamic impact response, fragmentation, and progress of the aircraft components and debris into and through the towers. The modeling approach was to model the airframe completely using shell elements as opposed to a shell element skin and beam elements for the airframe. Shell elements in the airframe provided higher fidelity simulation of the impact response and fragmentation behavior. As a result of the model size constraints, some of the details and smaller structural elements were not modeled explicitly. Where modeling simplifications were required, component analyses were applied to ensure that the impact strength and break up behavior were maintained.

An example of this approach was the development of the wing model. A section of the aircraft wing structure was first modeled with a very fine mesh of the detailed wing structure to establish a baseline behavior for aircraft structural failure and fragmentation upon impacting the exterior wall of the WTC towers. A coarser and simplified version of the same wing section was subsequently developed and the failure criteria were modified to obtain similar impact and fragmentation behavior to the fine, detailed version. Section 4.3.2 describes how this model was constructed and the methodology used for developing the coarsely meshed wing section. A similar mesh resolution and failure criteria were used throughout the rest of the aircraft.

The following sections outline the overall aircraft model developed for the impact analysis. Details in modeling each major component including the wings, engines, fuselage, empennage, and landing gear are provided. The final section provides an analysis of the fuel distribution in the aircraft at the time of impact.

4.2 AIRCRAFT DATA COLLECTION

Structural data were collected for the Boeing 767-200ER aircraft from the open literature, electronic surface models and CAD drawings, an inspection of a 767-300ER, an Aircraft Structural Manual, Pratt and Whitney PW4000 Engine Reference Manuals, American and United Airlines, and the Boeing Company website. The following is a description of how these various sources were used for model development.

4.2.1 Electronic Surface Models

Two electronic surface models of a Boeing 767-200ER were obtained from Digimation. These surface models were part of a large database of models developed by several sources. As a result, Digimation was not able to provide reference information about the data used in the surface model development.

To evaluate the digital surface models, the model geometry was compared to electronic two-dimensional CAD descriptions obtained from the Boeing Company web site, as shown in Figure 4–1. The first model, VP3311 shown in Figure 4–1(a), did not match the CAD descriptions well. However, the second model, VP15710 shown in Figure 4–1(b), matched the CAD descriptions, showing only minor discrepancies in the position of the horizontal stabilizers. The VP15710 surface model geometry was subsequently modified to match the CAD description from Boeing and was used in the aircraft model generation to define the exterior surface geometry.

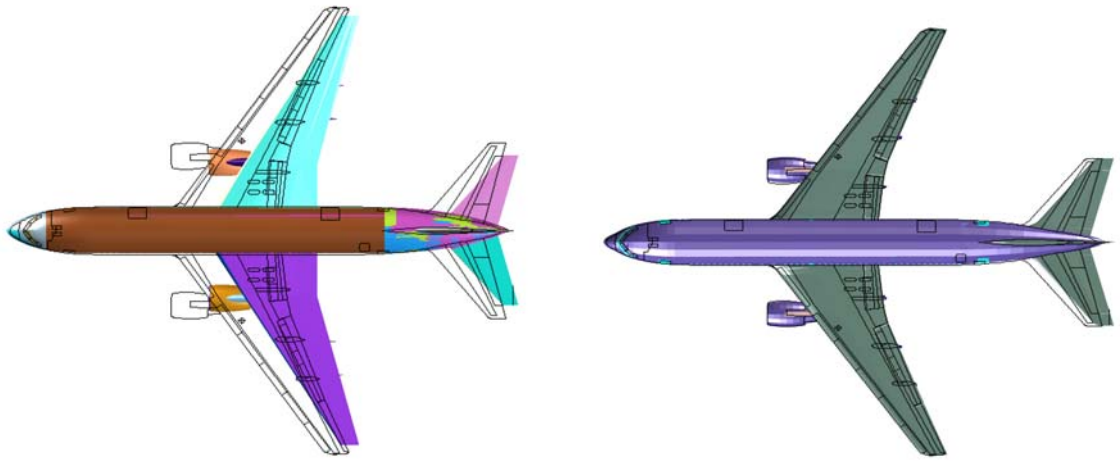

(a) Model VP3311 **(b) Model VP15710**

Figure 4–1. Surface models superimposed on Boeing CAD drawings of a 767-200ER.

4.2.2 Aircraft Inspection

No Boeing 767-200 aircraft was available for inspection. In order to obtain detailed structural information on the 767 aircraft, arrangements were made with an aviation company to inspect a 767-300ER. A comparison between the Boeing 767-200ER and the 767-300ER aircraft is shown in Figure 4–2. On the 767-300ER, the fuselage is extended, the horizontal stabilizers have a larger sweep angle, and parts of the structure are reinforced. Aside from these differences, the two aircraft are nearly identical.

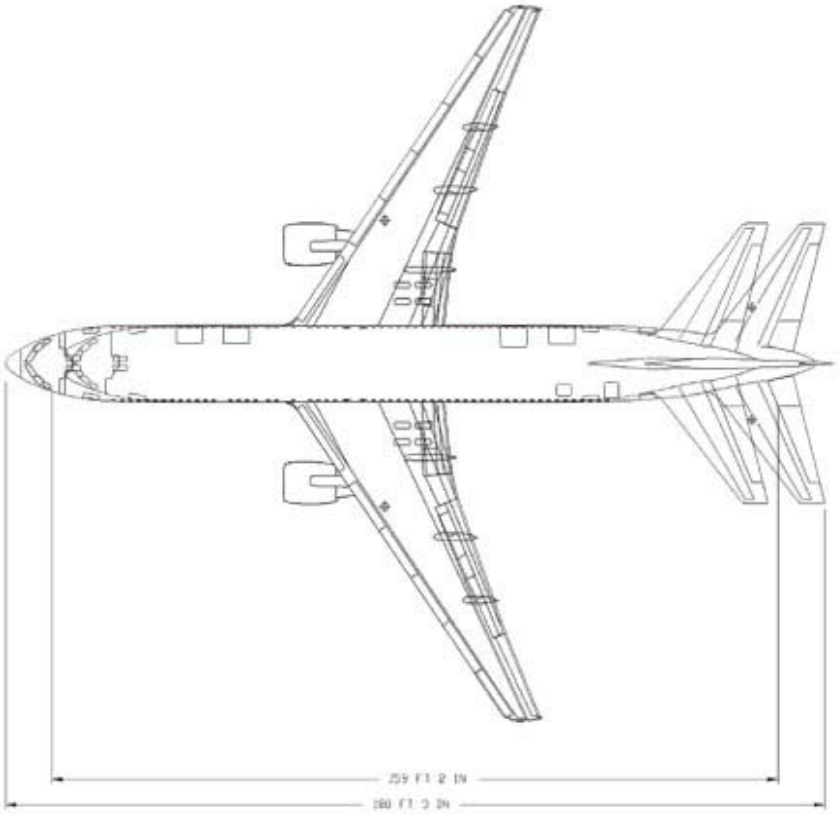

Used with permission. Enhanced by NIST.

Figure 4–2. Superimposed CAD drawings of the 767-200ER and 767-300ER.

Three ARA personnel visited the aircraft storage location where they were allowed access to the 767-300ER to take photographic and dimensional data of the aircraft. Photographic documentation of various aircraft components are shown in Figure 4–3. Photographs similar to these were critical in developing the model of the aircraft.

For the landing gear, global dimensions were taken along with ultrasonic thickness measurements of the major structural components, as shown in Figure 4–4. Ultrasonic measurement locations are marked in the photograph by the blue tape positions in Figure 4–4. Locations, dimensions, and approximate masses of various non-structural components such as the overhead luggage containers, overhead electronics, and under floor electronics were also documented, as shown in Figure 4–5.

(a) Control surfaces and linkage

(b) Main landing gear

(c) Non-structural contents

Source: NIST.

Figure 4–3. Photographic documentation of Boeing 767-300ER.

(a) Nose gear

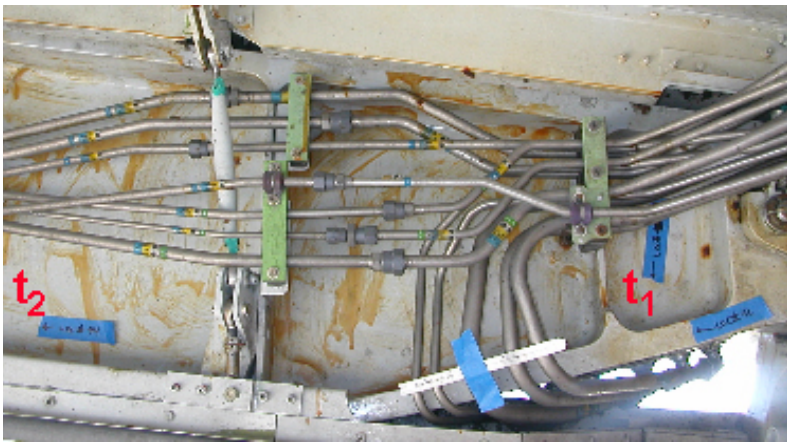

(b) Ultrasonic measurement locations

Source: NIST.

Figure 4–4. Ultrasonic thickness measurement of landing gear components.

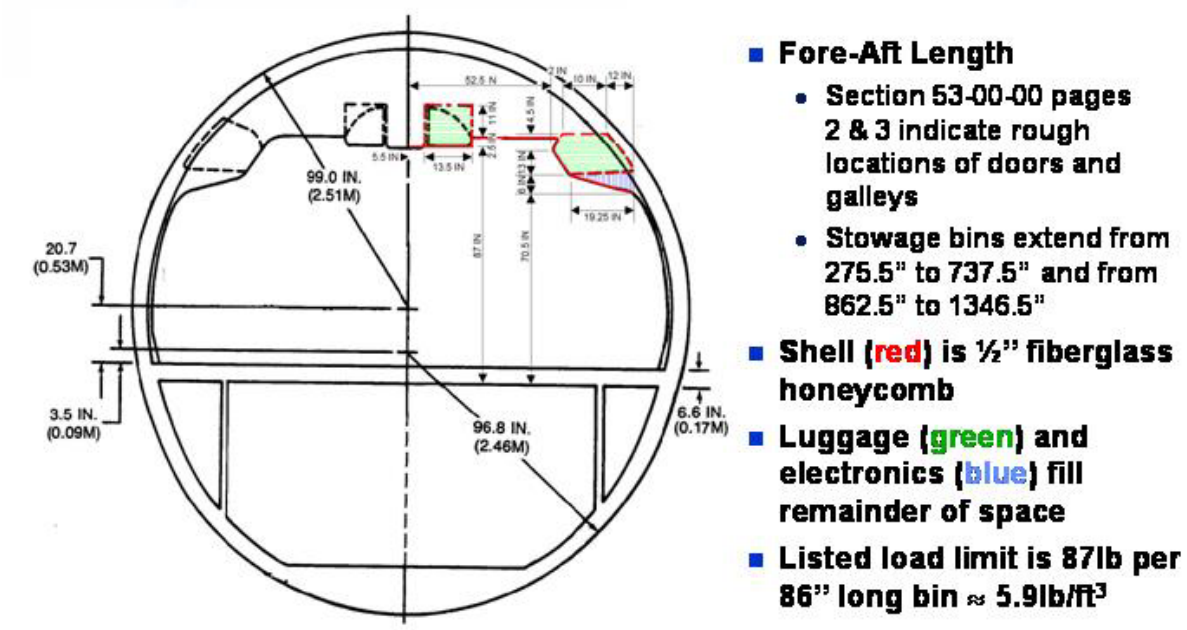

(a) Overhead luggage containers and contents

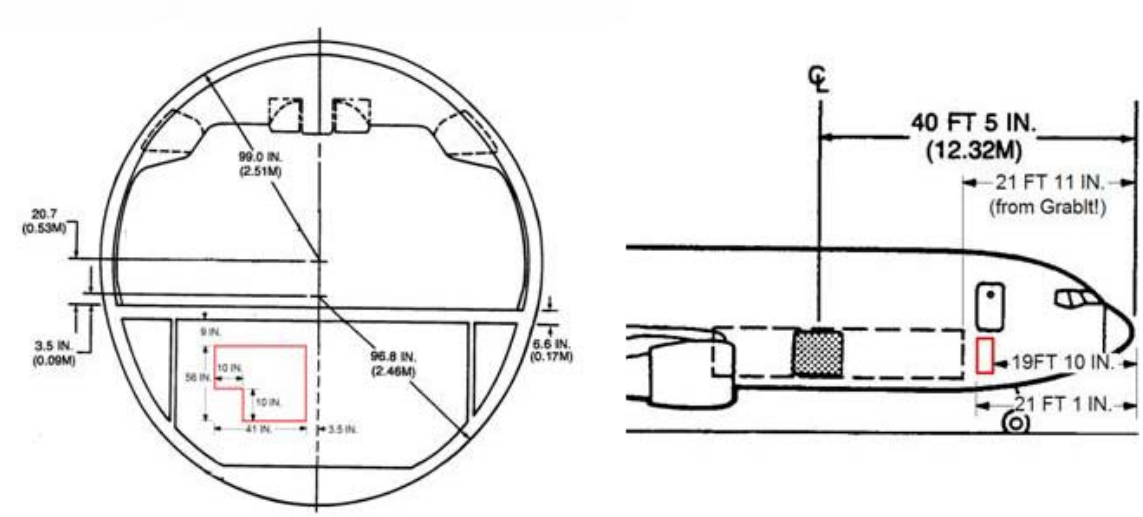

(b) Under floor electronics

Used with permission. Enhanced by NIST.

Figure 4–5. Non-structural mass locations in the fuselage.

4.2.3 Pratt & Whitney PW4000 Engine Reference Manuals

Initial sources indicated that the Pratt & Whitney PW4000 engine and the General Electric CF6-80 engine were on the aircraft that impacted the WTC towers (FEMA 2002). For this reason, the Engine Reference Manuals were obtained from Pratt & Whitney for the PW4000 turbofan engine. These manuals contained detailed information on the engine geometry and materials, as shown in Figure 4–6. A detailed finite element model of the PW4000 engine was developed from these manuals.

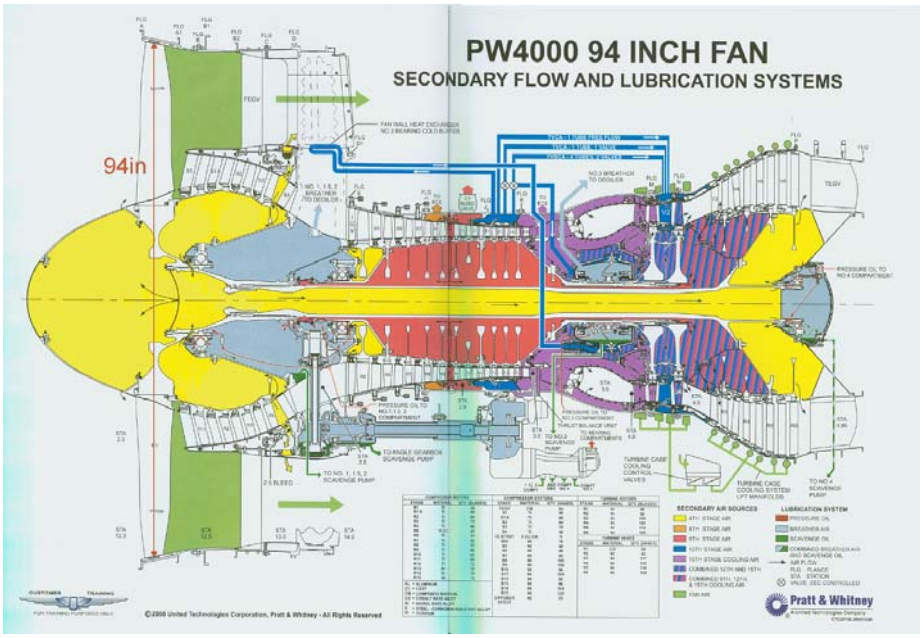

Used with permission.

Figure 4–6. Cutaway of a Pratt and Whitney PW4000 turbofan from the Engine Reference Manual.

After the engine model was developed, the engine types on each aircraft were clarified by the Aviation Safety Network (http://aviation-safety.net/). American Airlines flight 11 that impacted WTC 1 was powered by two General Electric CF6-80A2 engines. United Airlines flight 175 that impacted WTC 2 was powered by two Pratt & Whitney JT9D-7R4D engines. However, careful review of these engines indicated that the PW4000 turbofan engine is very similar to the General Electric CF6-80A2 and the PW JT9D-7R4D engines. Comparisons of specific physical characteristics of the engines are given in Table 4–1. In fact, the JT9D-7R4 and PW4000-94 are almost identical as they are in the same family of Pratt & Whitney aircraft engines. The PW4000 was labeled the "new technology JT9D" when it began replacing the latter engine on 767s built after 1987 where the PW4000-94 is 5.8 percent heavier than the JT9D-7R4 but produces up to 10 percent more thrust. Aside from an additional set of long stator blades and elongated exit nozzle, the CF6-80C2 is also of similar weight and dimensions to the PW4000. Due to these similarities, the PW4000 engine model was used for all impact simulations. Differences in the weights of aircraft components were included in the uncertainty analyses.

Table 4–1. Boeing 767 engine comparison.

Engine	Pratt & Whitney PW4000-94	Pratt & Whitney JT9D-7R4[a,b]	General Electric CF6-80C2[c,d]
Fan Blade Diameter	94 (in.)	94 (in.)	93 (in.)[e]
Length	153 (in.)	153 (in.)	161-168 (in.)[f]
Dry Weight	9,400 (lb)	8,885 (lb)	9,135-9,860 (lb)

a. The JT9D-7R4 and PW4000-94 are almost identical: (1) They are in the same family of Pratt & Whitney aircraft engines, and (2) the PW4000 was labeled the "new technology JT9D" when it began replacing the latter engine on 767s built after 1987.
b. The PW4000-94 is 5.8 percent heavier than the JT9D-7R4 but produces up to 10 percent more thrust.
c. The CF6-80C2 has an additional set of long stator blades for the excess fan air that is not present in the PW4000.
d. The second stage compressor blades in the CF6-80C2 are closer to the central shaft than the PW4000 and do not appear to have counter weights.
e. Reference value of 106 in. also found – may include cowling.
f. The "tail" of the CF6-80C2 is much longer than the PW4000. This potentially accounts for the additional 15 in. in length.

4.2.4 Airline Data and Data from the Boeing Company

The Boeing Company provides some general information on the layout of their aircraft at their website (www.Boeing.com). Useful data on the seating layout and dimensions and the Unit Load Devices (ULDs or cargo containers) were available, as shown in Figure 4–7 and Figure 4–8. The cargo, fuel, and passenger and crew masses were also provided by the airlines for American Airlines flight 11 (AA11) (Condon & Forsyth LLP, 2003) and United Airlines flight 175 (UAL175) [Midgett, 2003]. These data are outlined in Table 4–2. It was assumed in the global analyses that all 22 ULDs were onboard both flights for a total empty weight of 3,300 lb. Economy class seating was estimated at 25 lb per seat for a total of 6,625 lb when empty.

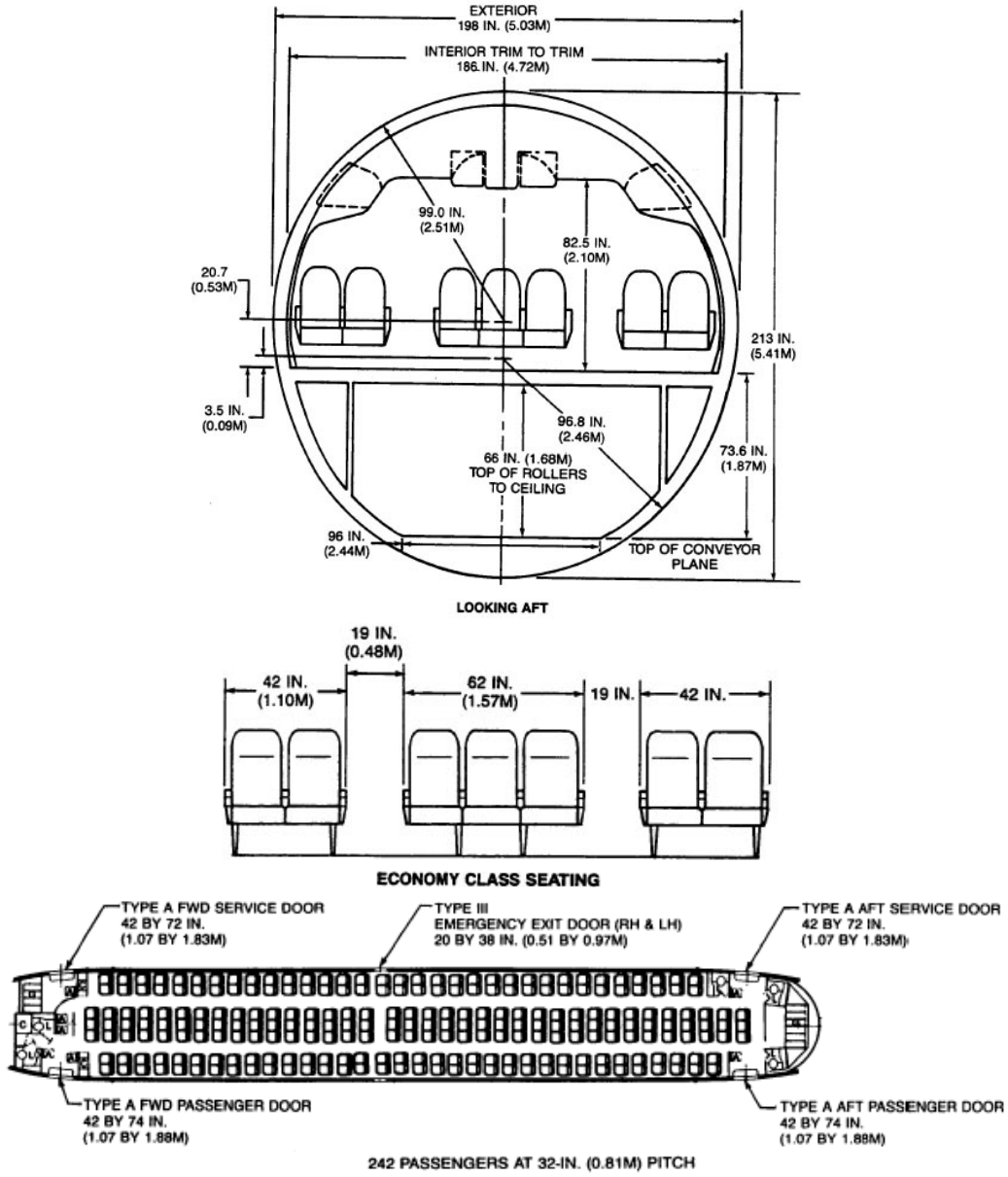

Used with permission.

Figure 4–7. Economy class seating location and dimensions (www.boeing.com).

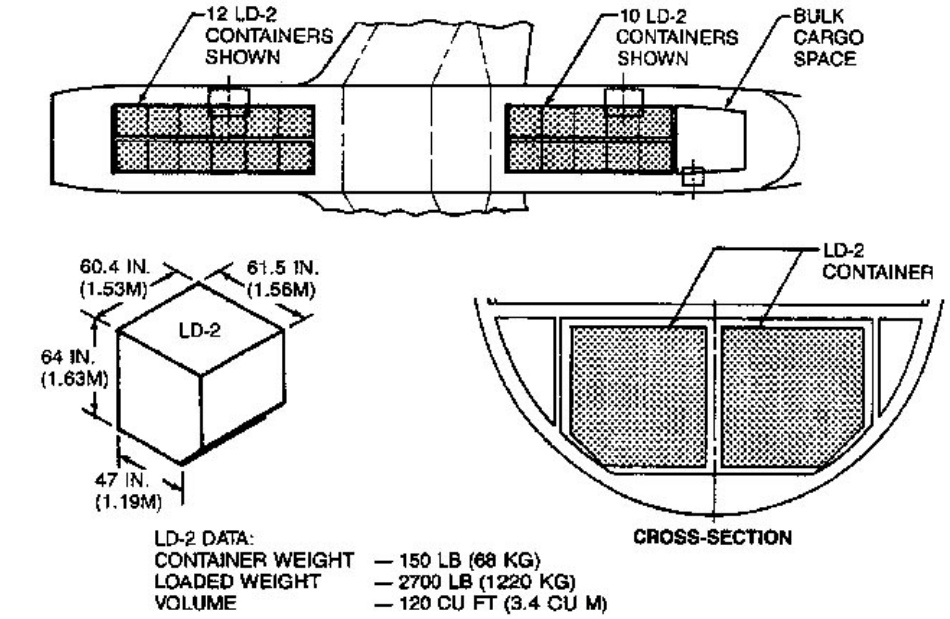

Used with permission.

Figure 4–8. Location and characteristics of the unit load devices (www.boeing.com).

Table 4–2. Cargo and passenger weights data.

	AA 11	UAL 175
Passengers and Crew	14,720 lb	9,410 lb
Freight	7,972 lb	16,970 lb
Luggage: Cargo hold	1,150 lb	1,390 lb
Luggage: Carry on	1,620 lb	1,010 lb
Catering	5,234 lb	-
Total	30,696 lb	28,780 lb

4.3 AIRCRAFT MODEL DEVELOPMENT

Similar to the global towers structural model, the LS-DYNA model of the aircraft was generated and meshed using the TrueGrid software (TrueGrid Manual 2001). The complete model for the Boeing 767-200ER is shown in Figure 4–9. A summary of the model parameters is presented in Table 4–3. The total empty mass represents an average cited by Jane's All the Worlds Aircraft (185,700 lb) (Jane's All the Worlds Aircraft 2001) and The Boeing Company (181,130 to 181,610 lb) (Boeing Company 1989) for an estimated empty weight of 183,500 lb. Notice that the weight cited for the ULD and seats includes the empty weights plus the passenger or cargo weight cited in Table 4–2. Carryon luggage and catering weight was distributed to the seats, and freight and cargo luggage weight was distributed to the ULDs.

Fuel was distributed in the wings as shown in Figure 4–10. Analysis of the fuel distribution is discussed later in Section 4.4. The wings of the aircraft were also deflected from the surface model geometry to represent their in-flight condition, as shown in Figure 4–11. A cubic function of the wing span was used with a tip deflection of approximately 52 in. Tip deflection was estimated from the impact pattern seen in photographs of the WTC towers and from the damage documented on the exterior panels by NIST.

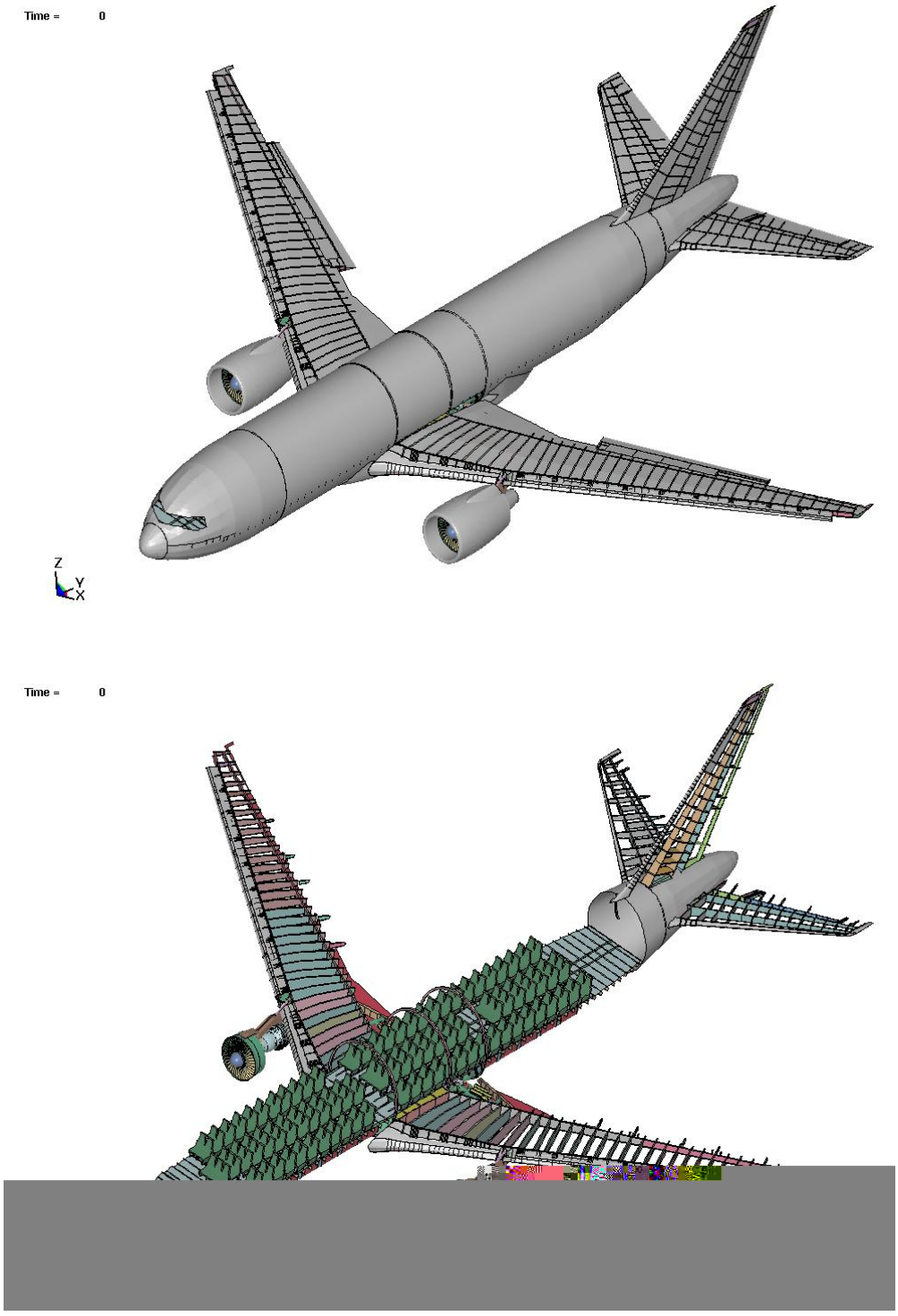

Figure 4–9. Finite element model of the Boeing 767-200ER.

Table 4–3. Boeing 767-200ER aircraft model parameters.

	AA 11	UAL 175
No. Brick Elements	70,000	70,000
No. Shell Elements	562,000	562,000
No. SPH Fuel Particles	60,672	60,672
Total Nodes	740,000	740,000
Total Weight (Empty)	183,500 lb	183,500 lb
ULD/Cargo Weight	12,420 lb	21,660 lb
Cabin Contents Weight	21,580 lb	10,420 lb
Fuel Weight	66,100 lb	62,000 lb
Total Weight (Loaded)	283,600 lb	277,580 lb

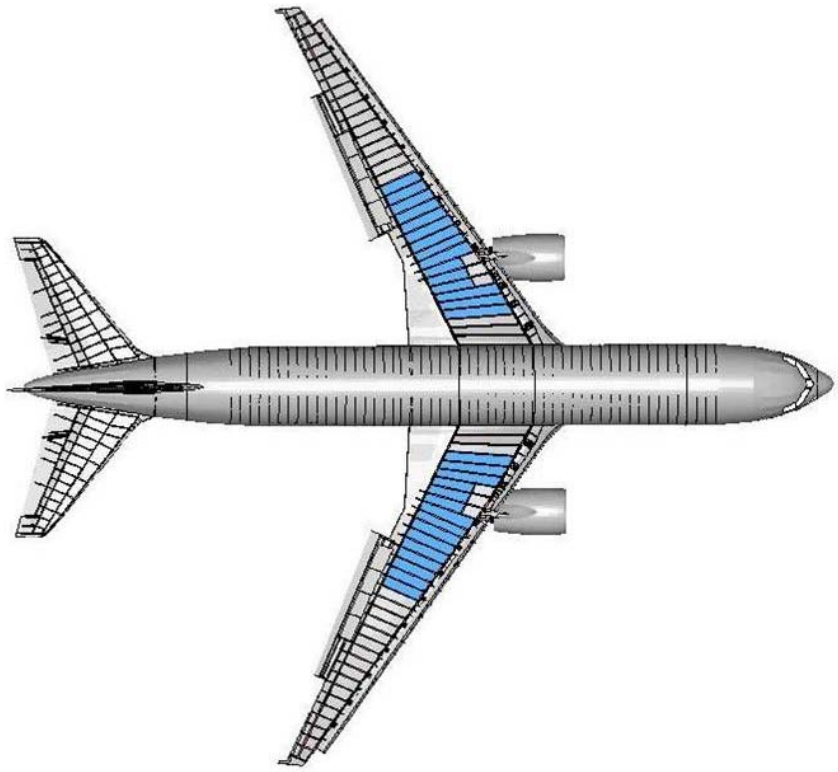

Figure 4–10. Boeing 767-200ER with fuel load at time of impact.

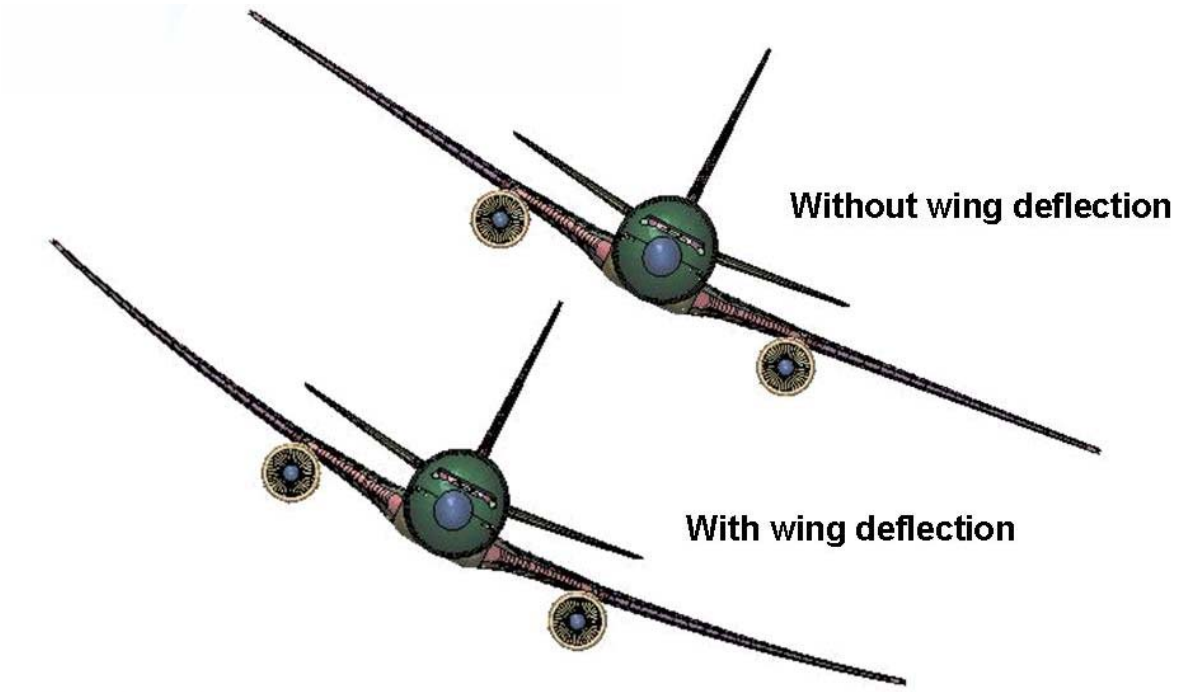

Figure 4–11. Boeing 767-200ER model wing deflections.

4.3.1 Airframe Model Development

The airframe model developed for the Boeing 767-200ER contained most of the significant structural components in the aircraft. The models of the fuselage, empennage, and wing structures were developed completely using Belytschko-Tsay shell elements. Models for the landing gear and engines were primarily developed using shell elements, but contained some brick elements as well. The model was developed in a parameterized form where the mesh resolution was determined by a single element characteristic size parameter. This approach was selected early in the development to allow flexibility in the model size and resolution as the model development and impact analyses progressed. The objective was to develop a mesh with typical element dimensions between 1 in. and 2 in. for small components, such as spar or rib flanges, and element dimensions of 3 in. to 4 in. for large parts such as the wing or fuselage skin.

Detailed models of the empennage and landing gear are shown in Figure 4–12 and Figure 4–13, respectively. Ribs, spars, rudder, and elevator were all modeled in detail in the empennage. Tires and hubs, the main strut and truck, and support bracing were all included in the landing gear model. The underside of the airframe in the model is shown in Figure 4–14, illustrating the position of the retracted main landing gear in the wheel well. Also shown in the figure are the Unit Load Devices (ULDs shown in red with blue edges). The density of these containers was scaled to include the weight of the cargo.

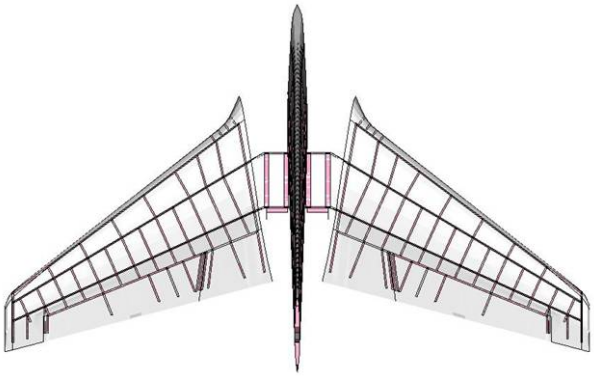

(a) Top view

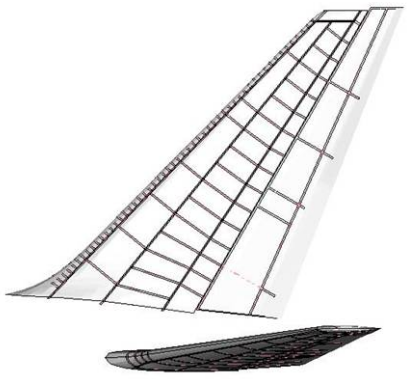

(b) Side view

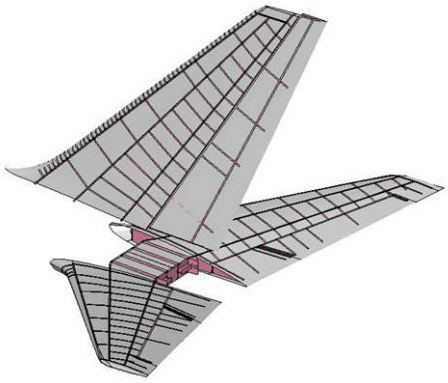

(c) Oblique view

Figure 4–12. Empennage model for the 767-200ER aircraft model.

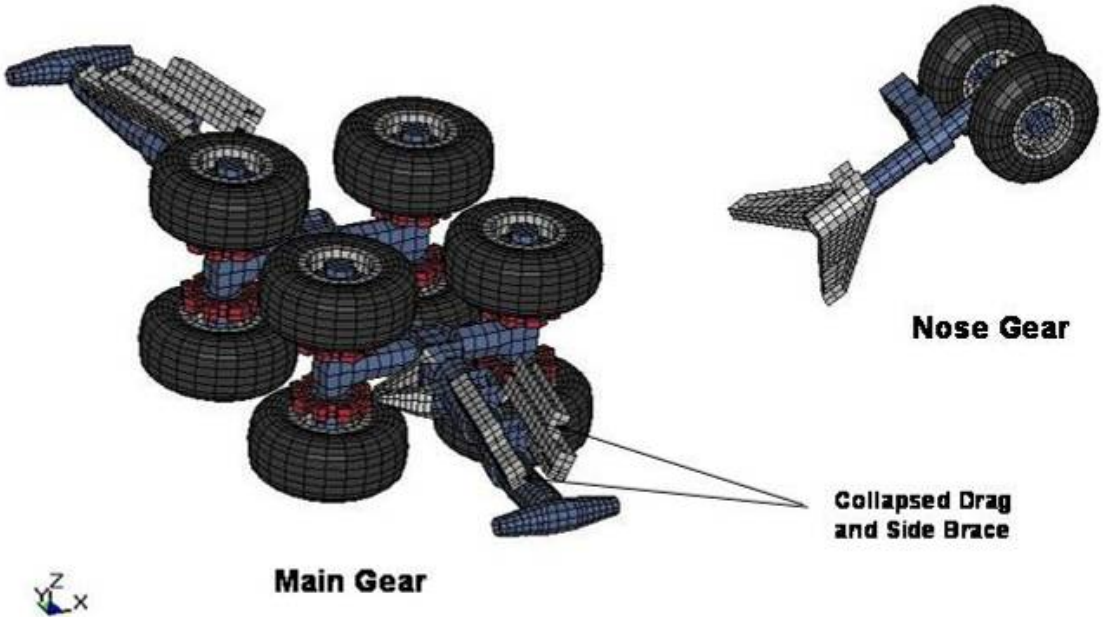

Figure 4–13. Retracted landing gear components for the 767-200ER aircraft model.

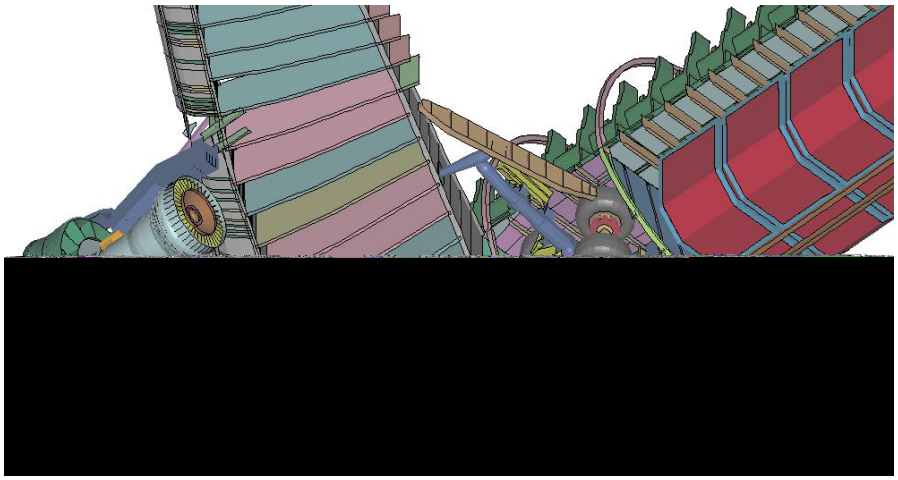

Figure 4–14. Underside of the 767 airframe model (skin removed) showing retracted landing gear.

Figure 4–15 shows the model of the wing structure, including the center wing, which attaches the port and starboard outboard wings. The wing stringers were not explicitly modeled to help reduce the size of the model. The stringers have a z-section geometry with typical dimensions of approximately 1 in. flanges and a two in. web with a thickness of approximately 1/8 in. These stringers run along the wing span over the top and bottom of the wing ribs as shown by part number 178 in Figure 4–16. To account for the weight and strength of the riveted skin/stringer construction, an 'effective' wing skin was used, as discussed in Section 4.3.2.

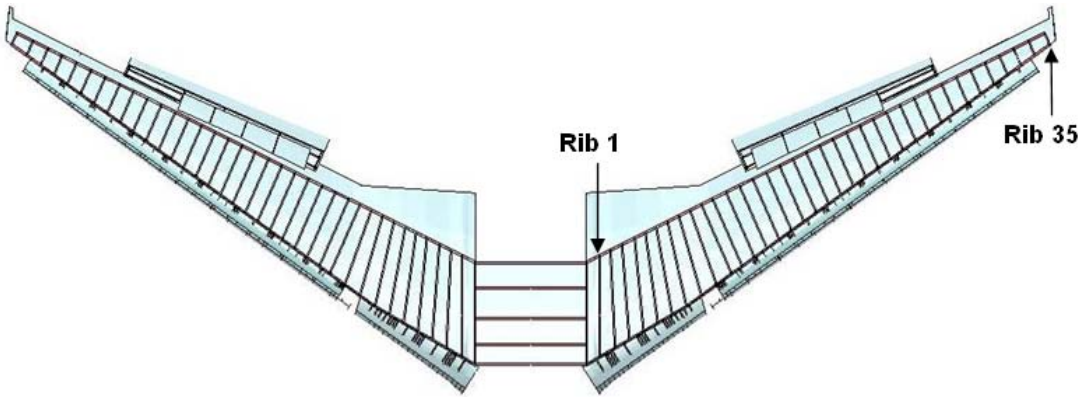

(a) Complete wing model

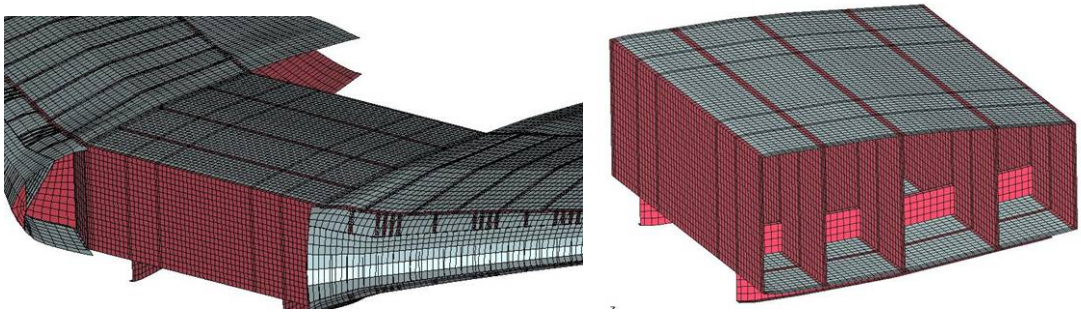

(b) Center wing structures

Figure 4–15. Complete wing structures for the Boeing 767 aircraft model.

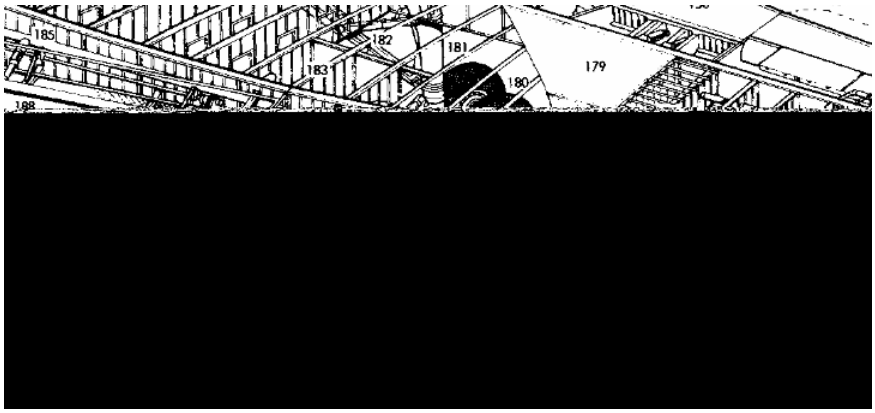

Source: Taken from Boeing Aircraft Cutaways. Cutaway © Mike Badrocke. Reproduced with permission of Osprey Publishing Ltd., www.ospreypublishing.com

Figure 4–16. Wing structural diagram of a Boeing 767-200.

A model of the fuselage was assembled with a stringer and frame construction supporting the external skin, as shown in Figure 4–17. A tied interface was used to connect the stringers to the frames and skin using the tied surface to surface contact algorithm in LS-DYNA. In this algorithm, nodes on a slave surface are constrained to nodes on a master surface provided they are within a certain distance of the master surface node. This distance is a function of the element thickness or diagonal length. The wing was integrated into the fuselage structure through attachment of the center wing to the keel and front and rear spar bulkheads, as shown in Figure 4–18. These components were also attached using a tied interface. Due to model size constraints, the forward and aft portions of the fuselage were modeled without the detailed stringer/frame construction. Instead, the weight of these components was smeared into the skin by increasing the skin thickness and scaling down the strength by a factor of 40 percent, as described in Section 4.3.2.

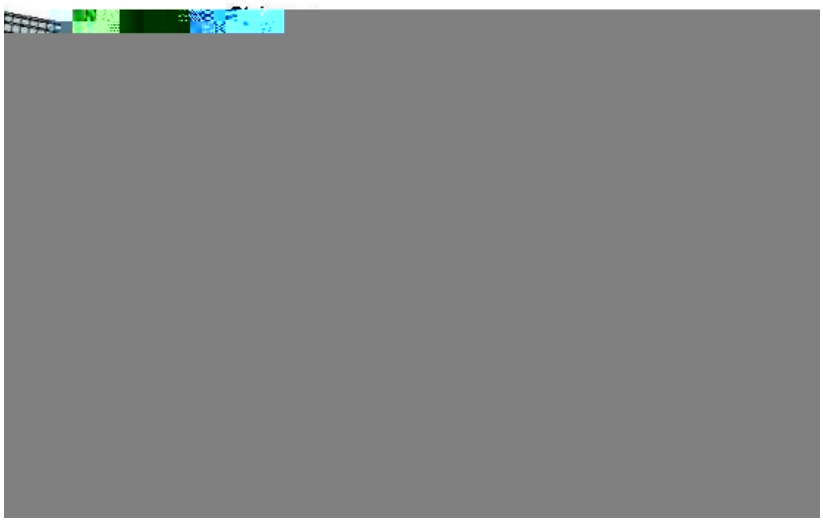

Figure 4–17. Model of fuselage interior frame and stringer construction.

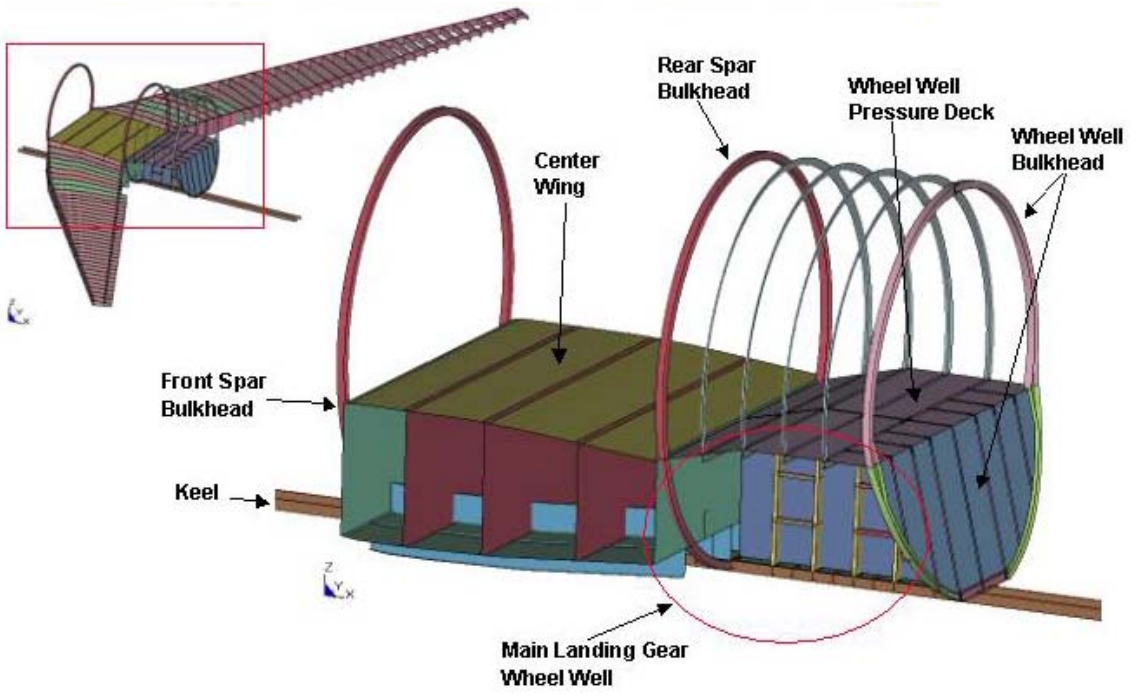

Figure 4–18. Integration of the fuselage and wing structures.

The density of various parts of the aircraft was increased to include the mass of parts of the structure not specifically modeled, as well as other non-structural components. Density scale factors and total weights for each major component are shown in Table 4–4. The difference in scale factors for flights AA 11 and UAL 175 were due to differences in passenger and cargo weight. In both cases the weight of the cargo, passengers, and crew were incorporated in the ULD (cargo weight) and the seats (passenger, crew, and carry on luggage weight). The weight of the modeled wings and empennage were doubled to account for the weight of small structural details, such as stiffeners, not specifically modeled, as well as hydraulic lines and fluid pumps, actuators, inboard flaps and outboard ailerons, flap and rudder connections, and other non-structural components. The weight of the landing gear was increased by a smaller amount (1.5) to account for hydraulic fluid and smaller structural components not included in the model. The weight of the fuselage was adjusted to match the published empty weight for the aircraft. That the scale factor for the fuselage was larger than for other components is reasonable as many heavy items in the fuselage were not specifically modeled (e.g., electronics, air conditioning, power units, ductwork, electronic wiring, cargo floor, actuator motors, insulation, hydraulics, galley, and lavatories). These structural and non-structural components could not be modeled in detail due to the constraints on model size.

4.3.2 Wing Section Component Model Development

A wing section model was developed to perform the component level and subassembly level analyses (Chapters 5 and 6, respectively). The full wing contains 35 ribs, with rib 1 closest to the fuselage and rib 35 near the wing tip, as seen in Figure 4–15(a). The wing section model developed in this section included the section of the wing from rib 14 to rib 18 as shown in Figure 4–19.

Table 4–4. Density scale factors and weights for aircraft components.

Major Aircraft Component	Density Scale Factor (AA11)	Total Weight (AA11)	Density Scale Factor (UAL175)	Total Weight (UAL175)
Wings	2.0	37,000 lb	2.0	37,000 lb
Empennage	2.0	8,350 lb	2.0	8,350 lb
Fuselage	6.68	103,050 lb	6.68	103,050 lb
Landing Gear	1.5	8,400 lb	1.5	8,400 lb
Engines (with cowlings)	1.2	20,100 lb	1.2	20,100 lb
ULD	1.43	12,400 lb	2.50	21,650 lb
Seats	1.29	28,200 lb	0.78	17,050 lb
Fuel	1.0	66,100 lb	1.0	62,000 lb
Total Weight		283,600 lb		277,600 lb

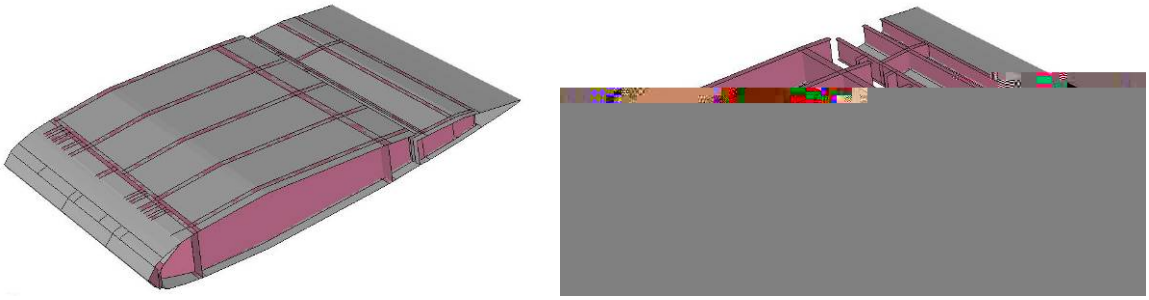

(a) Small wing section model **(b) Internal structure (skin removed)**

Figure 4–19. Wing section model for component level and subassembly analyses.

The main spars, wing ribs, leading edge ribs, nose beams, leading edge slats, and outboard flaps were all included in the wing section model. The internal structure of the wing (i.e., ribs, spars, nose beams, etc.), as shown in Figure 4–19(b), were attached to one another by merging nodes. To simulate the riveted connection between the external skin and the internal structure, the skin was attached to the leading edge ribs, the spars, and the ribs and spars of the trailing edge flap with a surface-to-surface tiebreak contact algorithm. This algorithm is discussed in more detail shortly. Nonstructural components, such as hydraulic lines, and mechanical components, such as slat actuators, were not included in the model geometry. The density of the spars, ribs, and other structural components were increased by a factor of two to account for this nonstructural mass.

The wing structure of the Boeing 767 contains a riveted stringer-skin construction between the front and rear spars as shown by part numbers 178 and 179 in Figure 4–16. The large number of relatively small stringers would require a large number of shell elements if modeled explicitly. The individual stringers were not expected to have a large effect on the impact response due to their relatively small cross section compared to tower structures. As a result, the stringers were not explicitly included in the wing model as they add significant complexity and size to the model. Instead, the stringers were included in an 'effective' wing skin in the model used for the component and subassembly analyses (Figure 4–19).

The effective wing skin was developed to account for the weight and strength of the riveted skin/stringer construction with a reduced overall model size. For this purpose, a simplified wing section model,

containing a uniform stringer-skin construction and a simple rectangular cross-section, was also developed (Figure 4–20) to evaluate different modeling options for the effective skin and determine the corresponding skin strength and weight. The wing section component models utilized Belytschko-Tsay shell elements.

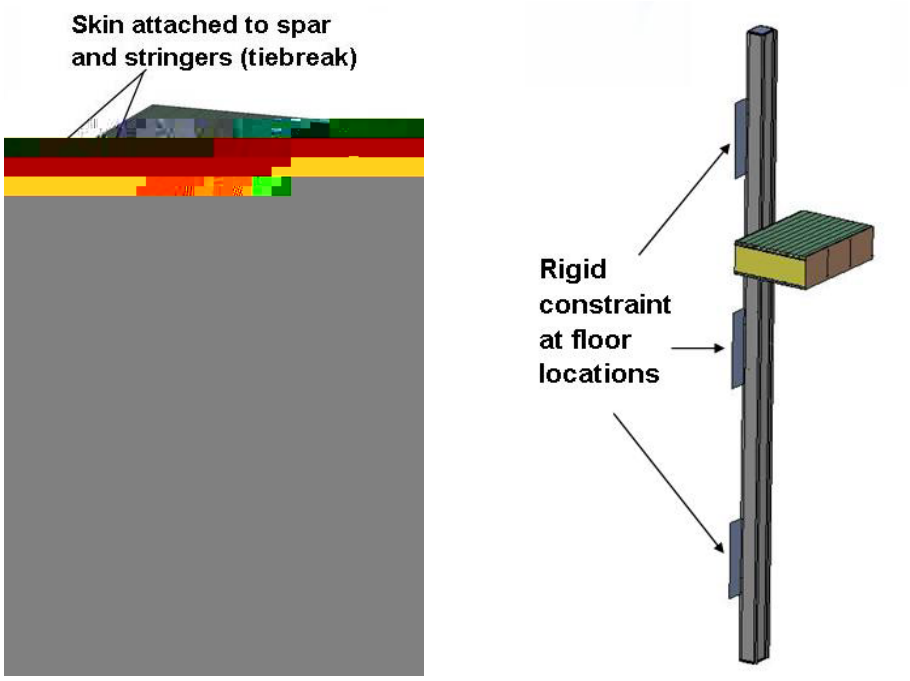

(a) Simplified wing construction **(b) Impact configuration**

Figure 4–20. Simplified wing section model and impact analysis used for the effective skin model development.

A suitable effective skin was developed by first modeling a wing segment containing the stringer and skin construction, as shown in Figure 4–20(a). The model consisted of four ribs of uniform height, a front and rear spar, ten z-stringers, and a top and bottom skin. In this model, both top and bottom skins and stringers were of the same materials as the top wing construction in the Boeing 767. The skin was attached to the stringers using the surface-to-surface tiebreak contact algorithm in LS-DYNA. A single rivet attachment was assumed for the skin-stringer and stringer-rib attachments in the simplified wing section model. The skin was also attached to the spars using a double-rivet tiebreak criterion. This model was impacted into an exterior column of the WTC tower, as shown in Figure 4–20(b). Ribs, stringers, spars, and skin were all meshed with 0.5 in. shell elements.

The surface-to-surface tiebreak contact algorithm uses a biaxial failure criterion governed by the equation:

$$\left(\frac{\sigma_n}{\sigma_n^f}\right)^2 + \left(\frac{\sigma_s}{\sigma_s^f}\right)^2 \geq 1 \qquad (7)$$

where σ_n and σ_s are the normal and shear stresses on an element, respectively. The σ^f are the corresponding magnitudes of the uniaxial normal and shear failure stresses. When this failure criterion is met, nodal displacements between tied nodes are no longer constrained, except to restrict penetrations of

one element segment through another. The reader is referred to the LS-DYNA Keyword User's Manual for a more complete discussion on this algorithm. Data from biaxial testing of riveted aluminum joints were used to estimate the values for ε_f, as shown in Figure 4–21. The data shown is for 5/32 in. rivets in 0.063 in. plates, where failure occurs at the interface of the countersunk head and the rivet shank. Assuming that the failure mode remained the same in the aircraft wing, failure data were scaled to those for 1/4 in. diameter rivets. Various rivet diameters were used, depending on plate thickness (5/32 in., 3/16 in., and 1/4 in.). The largest was used for the skin. The aircraft skin thickness in the simplified wing construction was assumed to be 0.1 in. The rivet spacing was four times the rivet diameter. Rivet spacing was needed to determine Y_f.

Source: Reprinted from Finite Elements in Analysis and Design, Vol. 30, Langrand, B., E. Deletombe, E. Markiewicz, and P. Drazetic, "Riveted join modeling for numerical analysis of airframe crashworthiness," Figure 1 on page 23 and Figure 12 on page 36, Copyright (2001), with permission from Elsevier.

Figure 4–21. Riveted joint configuration and failure data under mixed-mode loading.

Two alternatives were considered for an effective skin of the riveted stringer/skin construction. The first alternative was to increase the thickness of the skin to include the mass of the stringers. The second option was to increase the density of the skin to include the mass of the stringers. In both cases the skin yield strength was reduced by 40 percent to match the impact behavior of the effective skin wing segment with that of the riveted stringer/skin construction. In both options, the effective skin was only riveted to the front and rear spars and not the ribs. This behavior most closely resembled the skin behavior seen for the model with stringers and skin. Damage to each model immediately after impact with an exterior column is shown in Figure 4–22.

Internal energy of the exterior columns during impact by the various wing segment models is shown in Figure 4–24. Both effective skin options simulate reasonably well the damage to the exterior columns. This is also shown physically in Figure 4–25. However, the effective skin with increased density (i.e., 'Effective Skin 2') imparted less damage to the exterior column than did the stringer/skin construction or the first effective skin option. Therefore the first option with increased skin thickness was used in the subsequent wing and aircraft models.

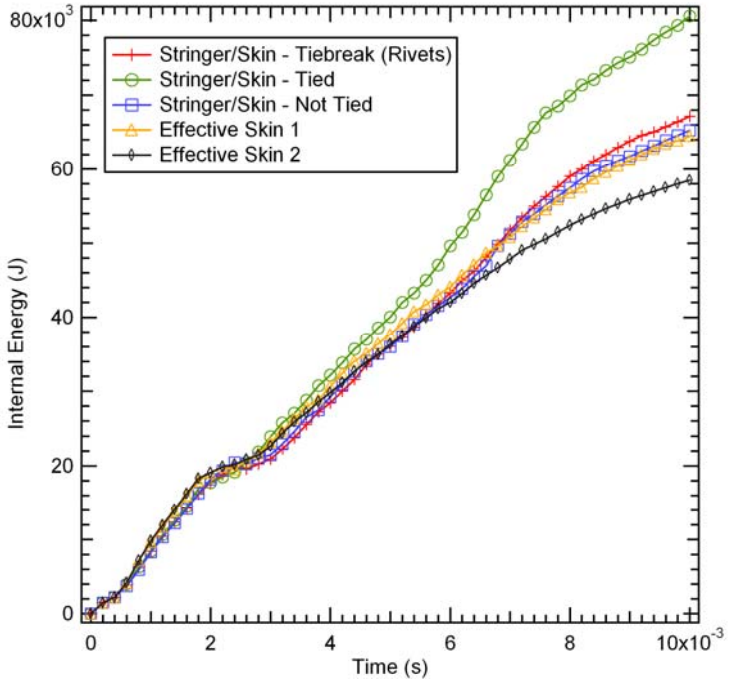

Figure 4–24. Internal energy of the exterior column.

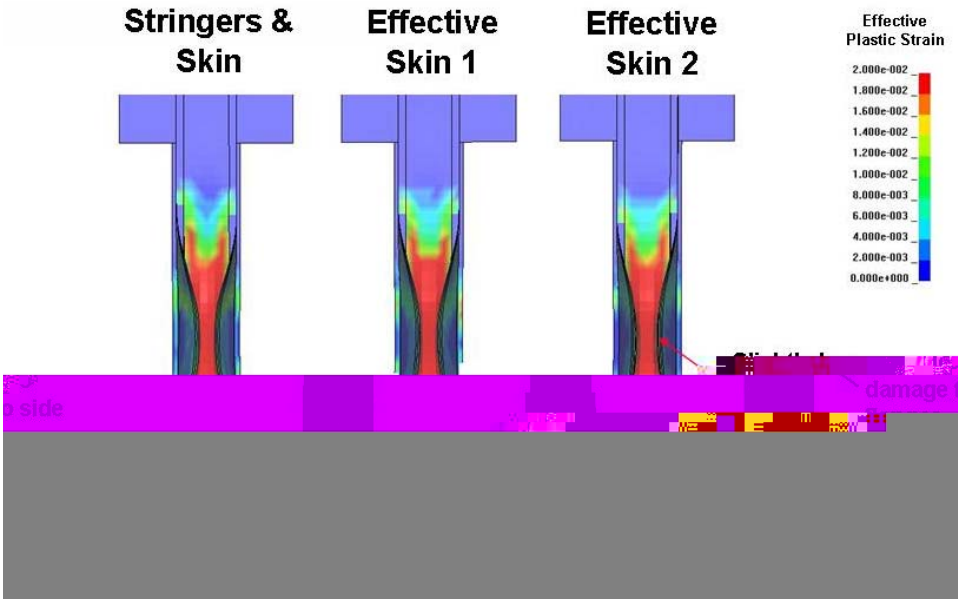

Figure 4–25. Damage to an exterior column from a wing section with each skin type.

4.3.3 Engine Model Development

The Pratt & Whitney PW4000 turbofan engine has a very complex structure as shown in Figure 4–26. The engine is an important component of the aircraft with the potential to produce significant impact damage to the WTC tower structures (e.g., fail core columns). As a result, special care was given to the development of the engine model to include all the details of the engine construction.

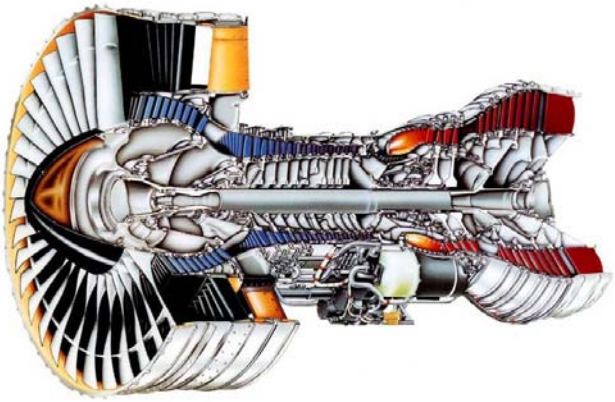

Used with permission.

Figure 4–26. Pratt & Whitney PW4000 turbofan engine.

The approach used to capture the geometry of the engine was to start with a cross-sectional drawing provided by Pratt & Whitney that clearly indicated many of the engine geometric details. In addition, the drawing had sufficient detail that the component thicknesses could be estimated. The primary structural components were identified and approximated with simplified geometry as illustrated in Figure 4–27. Known engine dimensions were used to determine the scale factor for the drawing. The simplified geometry of the engine structures could then be captured using a common digitization procedure. An example drawing with digitized coordinate locations included is shown in Figure 4–28.

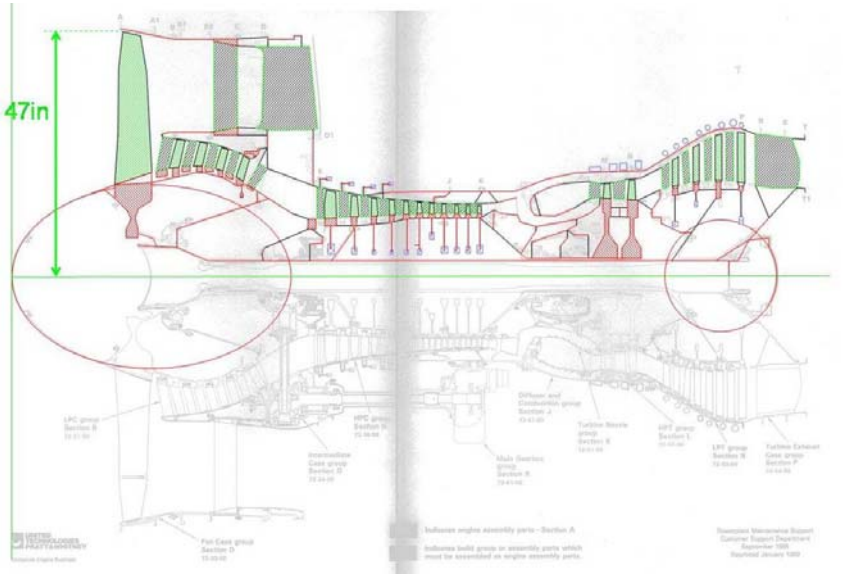

Used with permission. Enhanced by NIST.

Figure 4–27. PW4000 engine cross-sectional geometry and simplification.

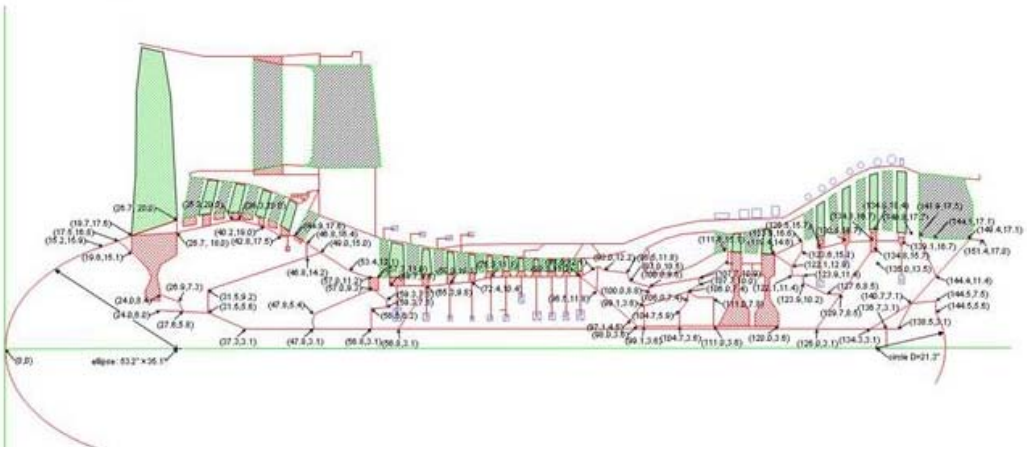

Used with permission. Enhanced by NIST.

Figure 4–28. PW4000 engine cross-sectional geometry digitization.

Once the engine internal geometry was captured, the digitized geometry was imported into TrueGrid and used to generate surface definitions and part geometries for the engine model. The engine model was developed with primarily shell elements. The objective was to develop a mesh with typical element dimensions between 1 in. and 2 in. However, smaller element dimensions were required at many locations to capture details of the engine geometry. Brick elements were used for some of the thicker hubs and the roots of the compressor blades. The various components of the resulting engine model are shown in Figure 4–29. A summary of the elements used in the engine model is given in Table 4–5.

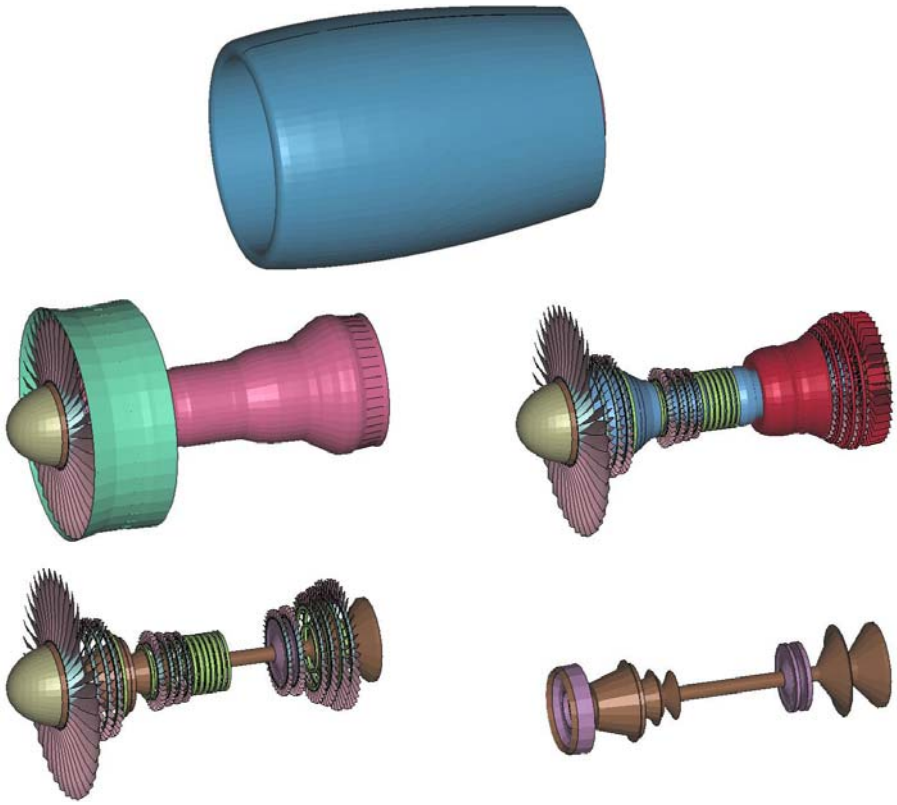

Figure 4–29. Pratt & Whitney PW4000 turbofan engine model.

Table 4–5. Engine model parameters.

	PW4000 Engine Model
No. Brick Elements	9,560
No. Shell Elements	54,788
Total Nodes	101,822
Preliminary Engine Model Mass	7,873 lb
Adjusted Engine Model Mass	9,447 lb

After the known primary structural components of the engine were included in the engine model, the mass of the model was calculated at 7,873 lb. The dry weight of the PW4000 engine was listed at 9,400 lb, and the JT9D-7R4 and CF6-80C2 engines weighed between 8,885 lb and 9,860 lb. These engine weights were approximately 20 percent larger than the initial model weight. The difference in weight potentially resulted from the nonstructural components (tubing, pumps, seals, bearings, etc.) that were not included in the model. To account for the difference, the density of all of the material models used for engine components was increased by 20 percent. This effectively smeared the missing mass in proportion to the original mass distribution in the model. The resulting adjusted engine model mass was 9,447 lb.

4.4 ANALYSIS OF FUEL DISTRIBUTION AT IMPACT

An important factor for determining impact damage and subsequent fire initiation was the distribution of the fuel in the aircraft. Both United Airlines and American Airlines provided estimates for the quantity and distribution of fuel for UAL flight 175 and AA flight 11 at the time of impact.[1,2] United Airlines estimated that flight 175 contained approximately 62,000 lb or 9,118 gal of fuel at impact with the "fuel evenly distributed between both main tanks."[1] American Airlines estimated that flight 11 contained 66,081 lb or 9,717 gal of fuel at impact and "the fuel was evenly distributed between left and right wing tanks of the aircraft."[2]

Fuel tank locations and capacities for the Boeing 767 are shown in Figure 4–30. The Boeing 767 uses an integral fuel tank where the wing skin, ribs, and spars serve as the fuel tank. There are three classes of fuel tanks onboard the 767-200ER, a main tank, a surge tank, and auxiliary tanks. The auxiliary tanks consist of port, starboard, and center fuel tanks. All tanks are shown for the port wing in Figure 4–31 along with the associated internal structures. The main tank is from rib 3 to rib 31, the port and starboard auxiliary tanks are from the inboard closure rib to rib 3. The center auxiliary tank is between the port and starboard closure ribs, and the surge tank is from rib 31 to rib 34. A dry bay is located above the engine at the forward part of the main tank between ribs 6 and 9. Baffle ribs are located at rib 5 and rib 18.

[1] Communication between United Airlines and NIST, September 5, 2003, "NIST WTC Flammable Contents Request."

[2] Communication between American Airlines and NIST, August 12, 2003, "In re September 11 Litigation C&F Ref.: DTB/MH28079."

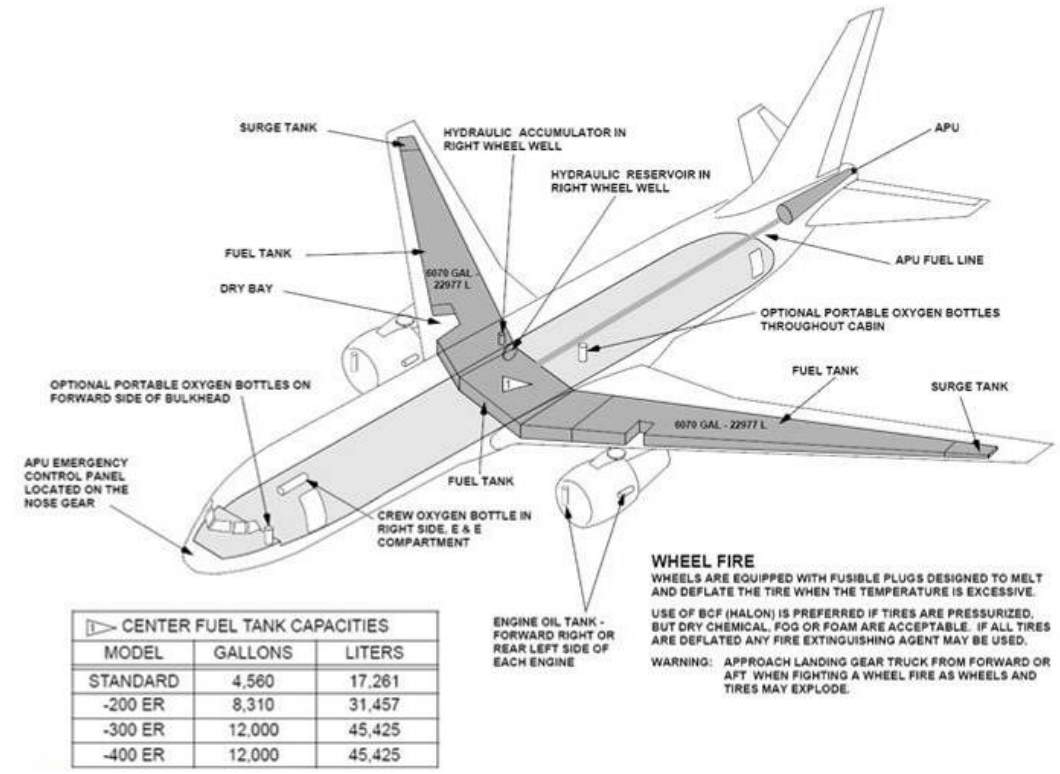

CENTER FUEL TANK CAPACITIES

MODEL	GALLONS	LITERS
STANDARD	4,560	17,261
-200 ER	8,310	31,457
-300 ER	12,000	45,425
-400 ER	12,000	45,425

Used with permission.

Figure 4–30. Flammable material locations in a Boeing 767 (www.boeing.com).

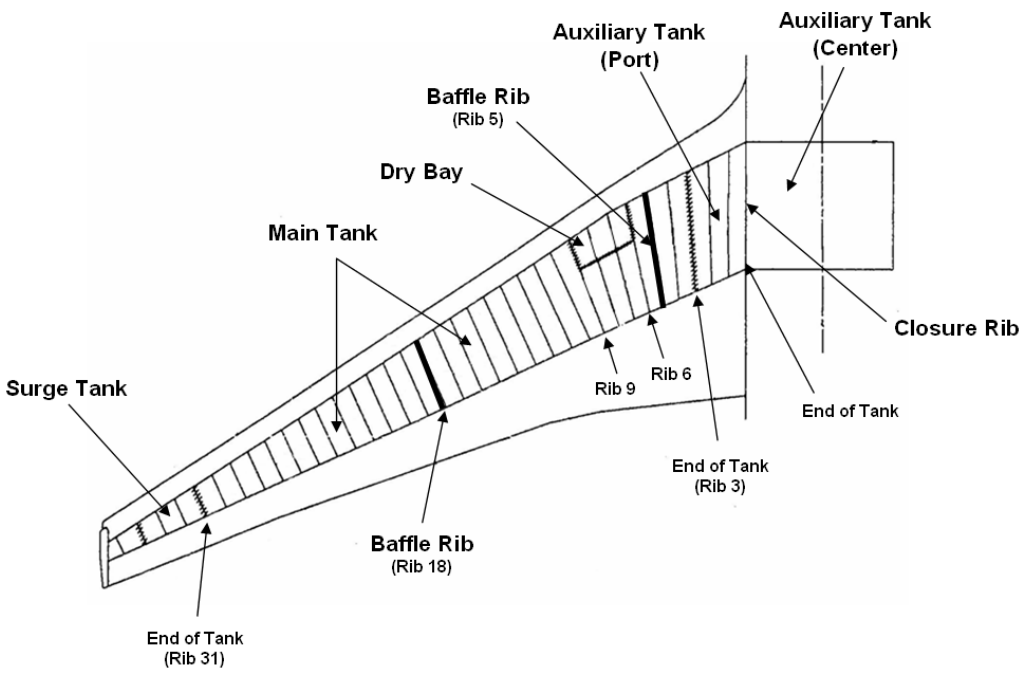

Figure 4–31. Layout of fuel tanks in the Boeing 767 wing.

Functionality of the wing fuel tanks is such that a typical wing rib allows some fuel to flow along the wing but acts as a two-way fuel baffle to minimize fuel slosh. However, there are special rib designs that alter the position and flow of fuel within the tank. The ribs in the dry bay region, between ribs 6 and 9, include a fuel barrier running parallel to the rear wing spar. In addition, baffle ribs (ribs 5 and 18) include a series of fuel dams that act as a one-way valve, allowing fuel flow inboard toward the sump areas (low point of tank). According to the statements from both airlines regarding fuel distribution, it is most likely that the surge tanks and all auxiliary tanks were dry at the time of impact.

Overall tank dimensions and geometry were estimated from aircraft structural references, the surface model from Digimation, and CAD drawings from Boeing. The dimensions and the approximated geometry used to calculate fuel tank capacity is shown in Figure 4–32. As shown in Figure 4–33, the front spar height is a good approximation for fuel depth in a full wing section. Using these approximate dimensions, the fuel tank capacity as a function of the distance along the wing buttock line (Figure 4–34) was calculated. The maximum capacity of each main tank was calculated to be approximately 6,500 gal. The actual main tank capacity is 6,070 gal (Figure 4–34), so the calculated fuel capacity distribution was modified to match this maximum value, as shown in Figure 4–34. Notice that the main tank capacity inboard of baffle rib 18 is approximately the same volume as the fuel onboard each aircraft at the time of impact.

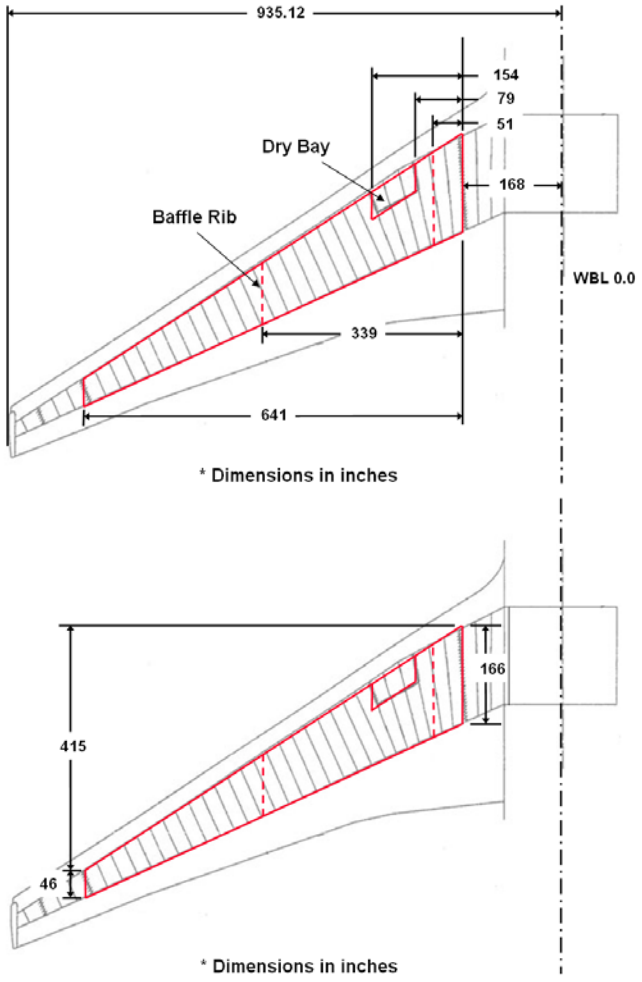

Figure 4–32. Approximate fuel tank dimensions (inches).

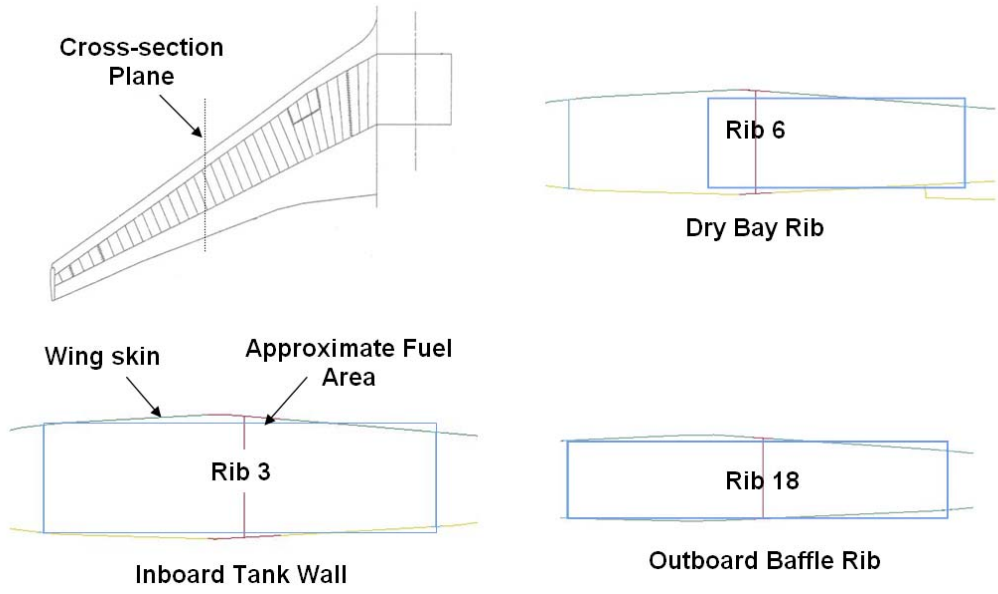

Figure 4–33. Wing cross-sections at various rib locations.

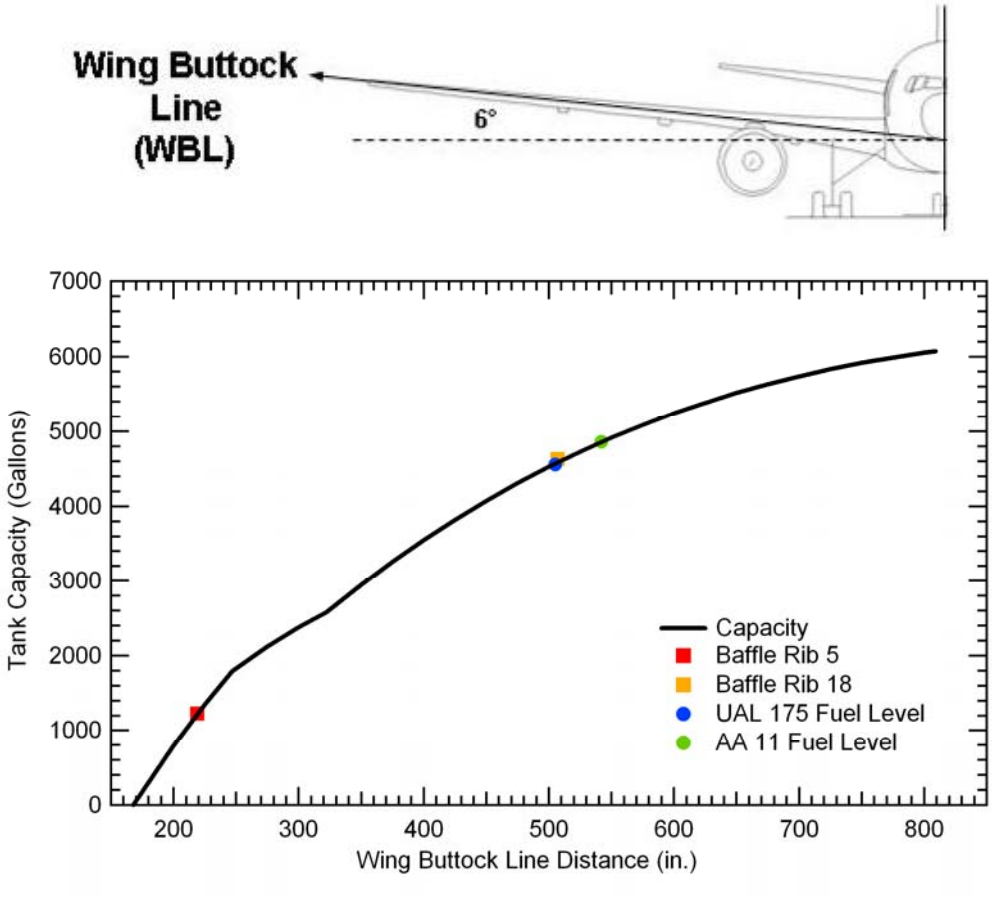

Figure 4–34. Fuel tank capacity.

The exact location and distribution of fuel at the time of impact was complicated by the flight conditions prior to and at the time of impact. The terrorist pilots likely performed extreme flight maneuvers prior to impact, causing most of the fuel to flow inboard. Extreme banking maneuvers with inappropriate trim could cause the fuel to flow inboard quickly. High loads on the wings due to the extreme flight regime at the time of impact would also cause fuel to flow inboard by increasing the dihedral angle of the wing. Since the baffle ribs restrict fuel from flowing outboard, it is reasonable that all fuel that could flow inboard was actually inboard at the time of impact.

For simplicity, it was assumed that all fuel had moved inboard at the time of impact. Since the fuel tank capacity at the outboard baffle rib and the fuel onboard are approximately the same, a good first estimate was that the main tanks were full inboard of baffle rib 18 at the time of impact. A small amount of fuel was outboard of this rib for AA flight 11. This is shown graphically in Figure 4–35 for smooth and level flight with an undeformed wing shape. A full wing out to baffle rib 18 and dry outboard of this rib was taken as the nominal case in subsequent analyses.

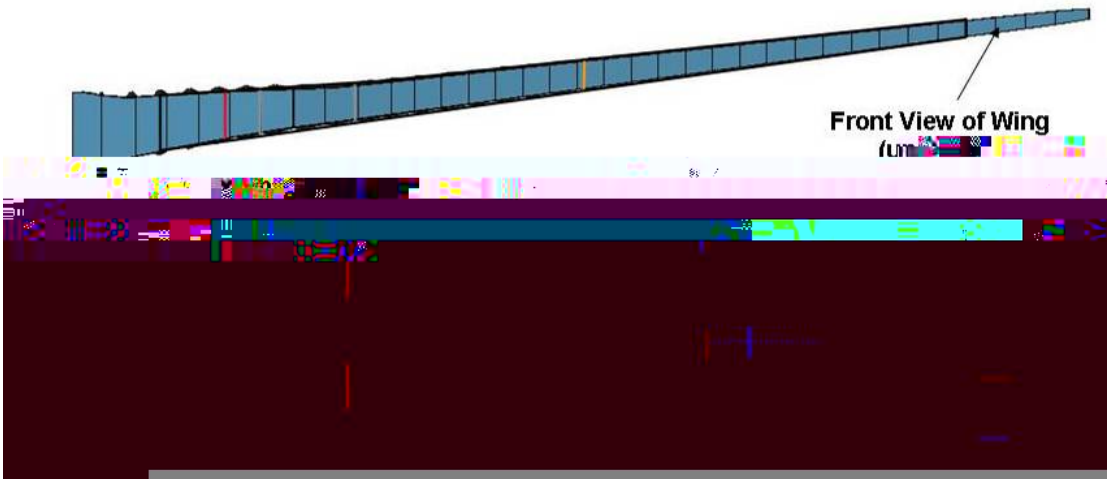

Figure 4–35. Approximate fuel locations for smooth and level flight.

4.5 REFERENCES

Badrocke, M. & Gunston, B. 1998. "Boeing Aircraft Cutaways – The History of the Boeing Aircraft Company." Osprey Publishing.

Boeing Company. 1989. Aircraft Description of Boeing 767, Section 2, Document number D6-58328, www.boeing.com.

Condon & Forsyth LLP. 2003. " In re September 11th Litigation C& F Ref: DTB/MH/28079," Correspondence between Condon & Forsyth LLP and NIST, NIST document number WTC1-155-1.

"Jane's All the Worlds Aircraft," McGraw-Hill, NY, 2001.

Langrand, B., E. Deletombe, E. Markiewicz, and P. Drazetic. 2001. "Riveted joint modeling for numerical analysis of airframe crashworthiness," Finite Elements in Analysis and Design, 38.

"LS-DYNA Keyword User's Manual," Livermore Software Technology Corporation, Version 970, April 2003.

Midgett, J. T. 2003. "NIST WTC Flammable Contents Request," Correspondence between United Airlines and NIST, NIST document number WTC1-156-1.

"TrueGrid Manual, Version 2.1.0," XYZ Scientific Applications, Inc., September 2001.

"World Trade Center Building Performance Study: Data Collection, Preliminary Observations, and Recommendations," Federal Emergency Management Agency, FEMA 403, May, 2002.

This page intentionally left blank.

Chapter 5
COMPONENT LEVEL ANALYSES

5.1 INTRODUCTION

The primary objectives of the component modeling were to (1) develop understanding of the interactive failure phenomenon of the aircraft and tower components, and (2) develop the simulation techniques required for the global analysis of the aircraft impacts into the World Trade Center (WTC) towers. The approach taken for component modeling was to start with finely meshed, brick and shell element models of key components of the tower structure and progress to relatively coarsely meshed beam and shell element representations to be used for the subassembly and global models. This was done to develop reduced finite element models appropriate for high fidelity global impact analyses, as modeling each component with fine details would be too demanding from a computational standpoint.

In addition to determining the optimal element size and type for global modeling, other key technical areas were addressed in the component modeling phase. These issues included material constitutive modeling, treatment of connections, and modeling of aircraft fuel. The following component modeling scenarios were outlined at the start of the project:

- An exterior column impacted by an aircraft engine
- An interior column impacted by an aircraft engine
- An exterior column impacted by an aircraft wing segment with and without fuel

In addition to the above component impact analysis scenarios, a range of additional component analyses were identified that were considered important and helpful in developing the global impact models and analysis methods. These additional component analysis scenarios included:

- Bolted column end-plate connections with approximated dynamic loading
- Bolted spandrel connections with approximated dynamic loading
- Floor system with concrete slab under impact loading

The approach used deviated somewhat from the tasks above to maximize efficiency and to produce the most meaningful structural loading scenarios. Once preliminary calculations were performed it was found, for example, that the load generated by an impacting engine would totally overwhelm an interior or exterior column. Reduced shell element models based on this severe loading would match the detailed brick model, but the subtle response from lesser loading might not be as accurate. To capture the more subtle response in the column components, wing section impactors were used as an alternate to the engine for the majority of component analyses. It was found that impact of an empty wing section produced damage to the exterior columns that was near the failure threshold. Similarly, a fuel-filled wing section impacting a core column produced damage near the failure threshold. As a result, the empty wing section

impacting an exterior column and a fuel-filled wing section impacting a core column were the primary component impact scenarios analyzed.

Development of the component models for the tower and aircraft structures were not completed at the same time. The component models for the aircraft wing were delayed by the data collection process for the aircraft structures. As a result, the wing section impact analyses on the exterior and interior core columns (Sections 5.2.1 and 5.2.2) used a preliminary wing section model that is of a lesser fidelity than the final wing model. However, the objective of these analyses was to develop the modeling methodologies for the tower components. The preliminary wing model was sufficient for obtaining a representative impact load.

5.1.1 Analysis Methodology

The impact analyses were performed using the LS-DYNA finite element code (LS-DYNA Version 971). LS-DYNA is a commercially available nonlinear explicit finite element code for the dynamic analysis of structures (LSTC 2003). The initial foundation of LS-DYNA was the public domain DYNA3D finite element code developed at the Lawrence Livermore National Laboratory (1986). Since 1987, the code has been extensively developed and supported by the Livermore Software Technology Corporation (LSTC) and is used for a wide variety of crash, blast, and impact applications.

LS-DYNA has several unique capabilities such as Arbitrary-Lagrangian-Eulerian (ALE) and Smooth Particle Hydrodynamics (SPH) algorithms that can be applied to the analyses of fluid-structure interaction and large-scale fracture and fragmentation of structures. These capabilities are critical for the analyses of the fuel tank break up and dispersion of fuel inside the towers upon impact. The fuel and debris dispersion is crucial for assessing the impact loads inside the tower structures and the corresponding damage to the mechanical systems.

The impact analyses described in this report used a variety of capabilities and algorithms in LS-DYNA. A brief description of these capabilities is described in this section. A significantly detailed description of the analysis methods is provided in the LS-DYNA Theoretical Manual (1998).

The fine mesh detailed component analyses typically used 8-node solid hexahedron (brick) elements with single point integration. This is the most commonly used solid element type in LS-DYNA due to its computational efficiency. The biggest disadvantage of the single point integration is the potential for hourglassing or zero energy modes. There are several methodologies for controlling hourglass modes in LS-DYNA. The typical approach used in these impact analyses was to apply a viscous hourglass control where a viscous damping was introduced that suppressed the formation of hourglass modes, but did not significantly influence the global modes.

The component impact analyses using solid elements typically had a fine mesh. As a result, damage and failure were included strictly through the constitutive algorithms. Damage criteria (such as maximum plastic strain) were tracked for each element within the constitutive model evaluation, and elements were eroded when the failure criteria were exceeded. This allowed for a direct evaluation of damage and failure within the impact simulations.

The eroded elements allowed for the initiation and extension of fracture in the model. Eroded elements no longer support any stress, and the strains in the eroded elements are no longer calculated. The

associated mass of the elements remains with the nodes in the calculation. If adjacent elements have not reached the failure surface, the nodes remain attached to the structure. If all of the elements connected to a specific node have failed, the node becomes a free particle. Free nodes can either be eliminated from the calculation or remain in the calculation with associated inertial properties and potential for impacts against other structural components (free nodes remain in contact algorithms).

As the mesh refinement and model size were reduced, the components were typically modeled using Belytschko-Lin-Tsay shell elements. These are four node shell elements with single point integration. The Belytschko-Lin-Tsay element is a computationally efficient alternative to the Hughes-Liu element in LS-DYNA and is a widely used shell element formulation within LS-DYNA for crash, impact, and metal forming applications. Results generated with the Belytschko-Lin-Tsay element typically agree with those generated using the Hughes-Liu element. As used in the solid elements, the most common approach to introducing damage and failure for the shell elements was through the constitutive models and element erosion.

In specific applications, unique algorithms were required to introduce failure modes in the analysis. An example is the interface between the skin and internal frame structures of the aircraft. Rivets were used for the primary connection between the airframe and skin (see Section 4.3.2). The approach used to model this connection and failure during the impact event was the tied interface with failure. In this approach, interface segments (shell elements) were constrained to move together until a failure criterion was exceeded. The failure criterion was a quadratic combination of the normal and shear failure stresses at the interface. After failure, the segments were allowed to move independently but not allowed to penetrate each other (typical contact algorithm behavior).

Overall contact in the impact analyses was modeled using the automatic single surface contact algorithms in LS-DYNA. Interacting components were defined by a material list, and contact segments were automatically generated by LS-DYNA. This greatly simplified the specification of contact between various components in the aircraft and tower structures. The type 1 soft constraint option was used in the contact algorithm that determined the contact stiffness based on stability considerations, time step size, and nodal mass. This soft constraint option was found to be more robust than the default penalty formulation for modeling the complex contact behaviors in large impact and crash simulations.

5.2 TOWER COMPONENT DEVELOPMENT AND ANALYSES

As described above, the development and analyses of the tower and aircraft components did not all proceed in parallel. Detailed models of the aircraft components, and in particular the wing components, were not initially available due to the time required to gather information about the details of the aircraft structures. Therefore, the initial component analyses focused on the behavior of the tower structures. In many of these analyses, preliminary models were used for the aircraft component impactors. The following sections describe the development and analysis of the tower components.

5.2.1 Exterior Column Impact Analyses

Various exterior column component impact analyses were performed with different objectives. The preliminary impact analyses were performed on a single column using a highly refined mesh of brick elements. These analyses were used to investigate details of the column response and to develop analysis

techniques that could be applied to the subassembly and global impact analyses. For these analyses, a simplified wing-section impactor was used since detailed structural information of the Boeing 767 wing design was not yet available. Subsequent exterior column impact analyses were performed using less refined models of the exterior columns in full panel configurations. More detailed wing section models were developed and used in these analyses with the primary objective of studying the impact response of the aircraft wing structures and investigating various modeling techniques for including aircraft fuel in the analyses. These analyses are discussed further in Section 5.5.

An example of a preliminary analysis was a fuel-laden wing section impacting an exterior column at 470 mph, as shown in Figure 5–1. The model of the exterior column consisted of three floors of a single exterior column with a relatively fine mesh of brick elements. The plates that make up the exterior column were modeled with four elements through the thickness resulting in a total of 467,232 brick elements for the exterior column model. Adjacent nodes in the web, flange, and spandrel plates were merged together (i.e., perfectly bonded), with no special treatment of the weld geometry or materials. The specific column modeled had a 60 ksi yield strength, while the spandrel plates had a yield strength of 42 ksi. A preliminary bilinear elastic-plastic constitutive model was used with a 30 percent plastic strain failure criterion. The fuel was added inside the wing, completely filling the wing section volume between the forward and rear spar. The fuel was modeled using brick elements and a simple constitutive model for the fluid that had a negligible strength and linear pressure-volume behavior. A large distortion of the fluid elements was allowed (250 percent strain) prior to removal from the calculation. This allowed the fuel to transfer its momentum to the impacted column without the subsequent distortion of the fluid elements terminating the calculation.

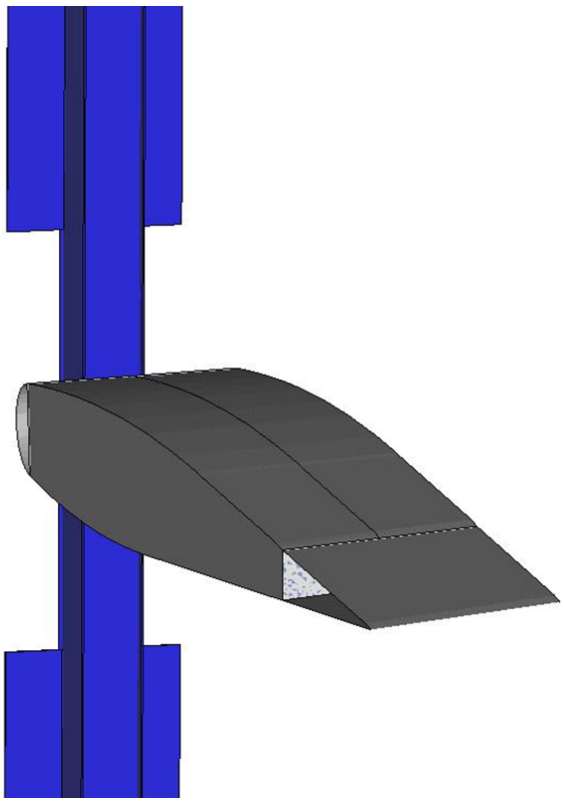

Figure 5–1. Preliminary model of a wing section with fuel impacting an exterior column.

The impact response of the wing section and column at 5 ms is shown in Figure 5–2(a), with the corresponding column damage shown in Figure 5–2(b). The subsequent impact loading of the wing section with fuel completely failed the exterior column. The early time impact response, shown in Figure 5–2, initiated various failure modes in the column. Connections at the front and back web plates were sheared away from the side flange plates, and the failure of the side plates had initiated. The momentum transfer and deformations of the front web were sufficient to result in a shear out failure at the position of the internal gusset plate at the location of the lower edge of the spandrel above the impact point. Although this analysis included preliminary models for the materials and structural details, many of these damage mechanisms were observed in the recovered exterior panels from the impact zone as shown in Figure 5–3. The photograph shows an exterior column with impact damage that sheared the front web free from the side flanges. The fracture progressed along the weld until it reached the internal stiffener plate at the location of the spandrel edge. The impact of the column front web with the internal stiffener sheared the forward web across the column width similar to the calculated response shown in Figure 5–2. Although the exact loading history that created the observed damage is not known, the qualitative agreement of the calculated and observed damage modes provided a level of confidence in the modeling methodologies used.

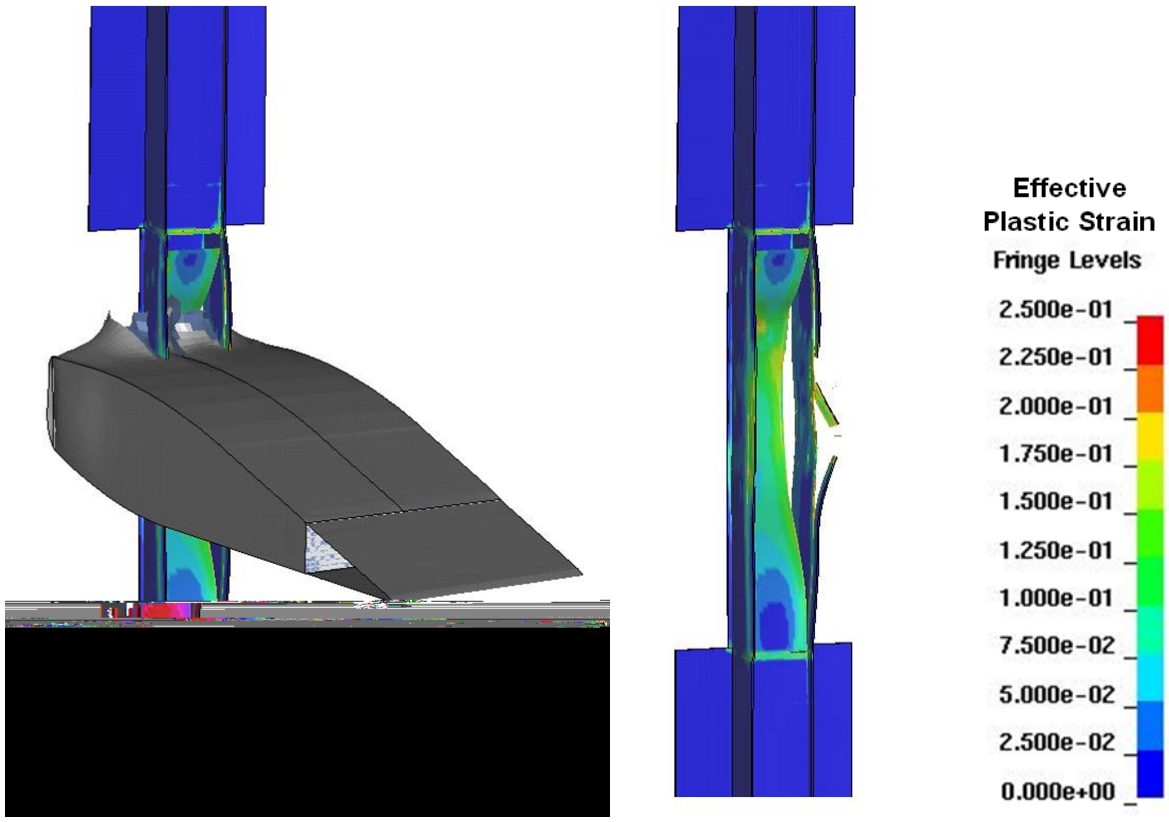

(a) Wing and column behavior **(b) Column damage**

Figure 5–2. Calculated wing with fuel impact response on the exterior column.

Source: NIST.

Figure 5–3. Observed impact damage in the recovered WTC exterior columns.

The objective of subsequent exterior column impact analyses was to develop a model with a coarser mesh that could be applied to the global impact analyses and still capture the impact damage properly. The analyses used the preliminary wing section impactor, shown in Figure 5–1, but with the fuel removed. This empty wing section model was selected to produce significant column damage at an impact speed of 470 mph without complete failure. This damage level was expected to be more sensitive to changes in the modeling methodologies than the complete failure produced by the impact of the wing section with fuel.

A series of these second generation exterior column impact analyses were performed to further refine modeling methods. These calculations used the updated constitutive models, described in Chapter 2, but with preliminary failure criteria. The exterior column modeled was constructed entirely with 55 ksi steel and the spandrel plates with 42 ksi steel. Both a model with a fine mesh of brick elements and a model with a coarser mesh of shell elements were develope

response, were failure strains of 12 percent and 2 percent for the base metal plates and weld zone, respectively. Contours of resultant displacements are shown on the column components. The overall response was similar in both magnitude and damage mode. The reduction in model refinement resulted in a significant reduction in run time from over 600 min to 9 min. This comparison demonstrated the significance of the mesh refinement on capturing local stress and strain concentrations and the resulting effect on the failure behavior.

Table 5–1. Exterior column component analyses comparison.

Column Model Type	Fine Brick Model	Coarse Shell Model 1	Coarse Shell Model 2
Number of Brick Elements	473,208	352	352
Number of Shell Elements	0	9,192	9,192
Number of Beam Elements	0	8	8
Minimum Element Dimension	0.0625 in.	1.0 in.	1.0 in.
Bulk Material Failure Strain	64 %	12 %	34 %
Weld Zone Failure Strain	64 %	2 %	8 %
Calculation Time (CPU)[a]	444 min	3 min	3 min
Elapsed Time	624 min	9 min	9 min

a. Simulation of 0.035 s duration impact response performed on 11 CPUs.

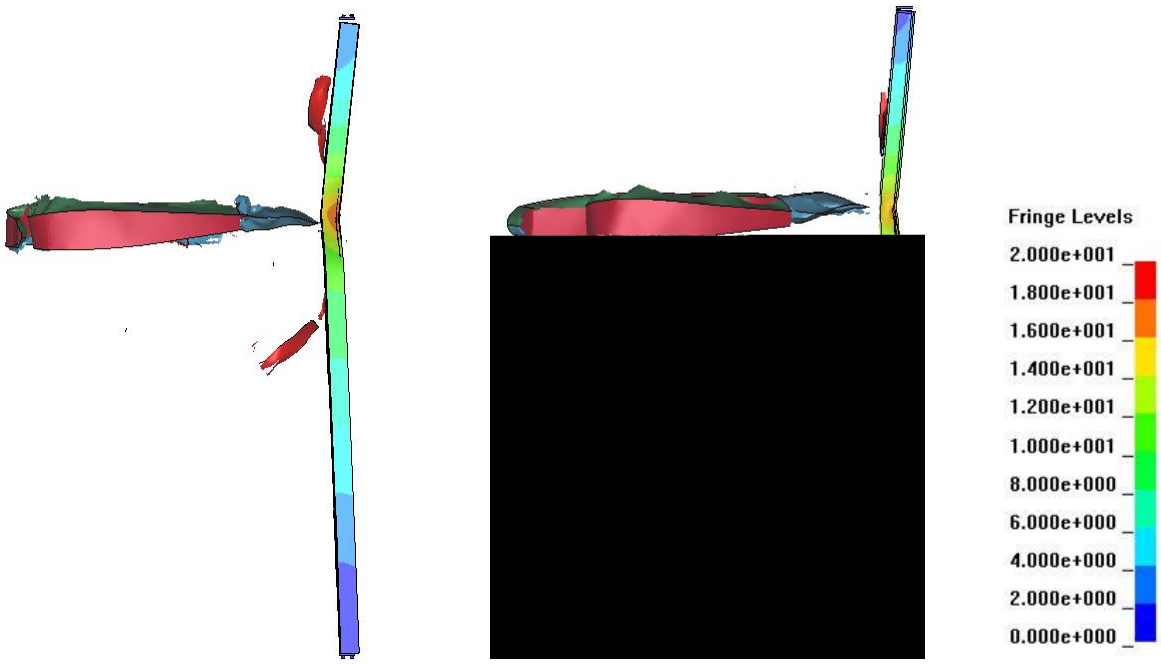

(a) Fine brick element column **(b) Coarse shell element column**

Figure 5–4. Exterior column response comparison, showing contours of the displacement magnitude (inches).

An additional exterior column impact analysis was performed using the coarse shell element model. This analysis was identical to the coarse shell element model shown above in Figure 5–4, but the failure

criteria were obtained from the mesh refinement study and weld zone failure analyses described in Section 2.3.1 and Section 2.3.3. These were the failure parameters used subsequently in the global impact analyses described in Chapter 9. The updated failure strains for the base metal plates and weld zone were set at 34 percent and 8 percent, respectively. A comparison of the impact response for the two different coarse shell element models is given in Figure 5–5. Although there were differences in the calculated column displacements and failure modes, many of the features, such as extent of weld failure and wing section damage, were similar. This comparison provided some guidance as to the bounds on uncertainties in failure criteria and range of expected damage in these analyses.

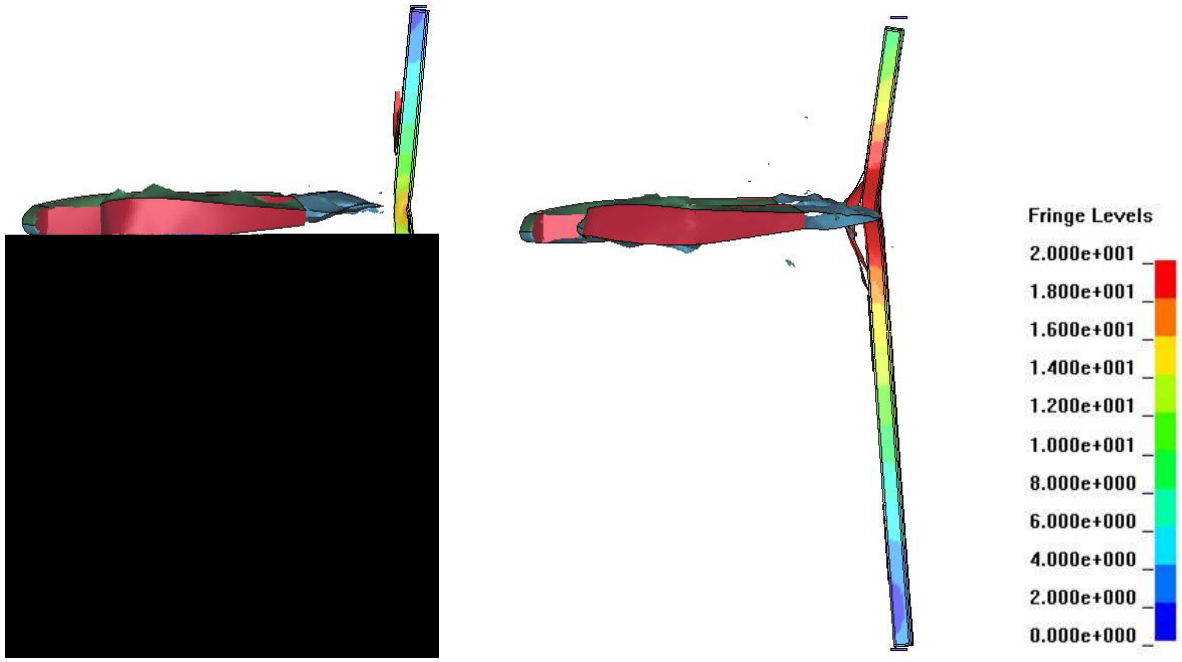

(a) Coarse shell element model 1 **(b) Coarse shell element model 2**

Figure 5–5. Exterior column response comparison, showing contours of the displacement magnitude (inches).

5.2.2 Core Column Impact Analyses

Engine Impact Analysis

Preliminary analyses of an engine impacting a single core column indicated that the impact load was sufficient to penetrate and overwhelm the column. To capture the more subtle response in the core column components, wing sections with and without fuel were studied as impactors. These studies are described in this section. Subsequent analyses of engine impacts focused on exterior panels and the combined impacts with exterior panels and core columns as described in Sections 5.2.4 and 5.3. Most useful were the engine-impact subassembly analyses described in Chapter 6, where there were sufficient tower structures to resist and potentially stop the engine.

Wing Section with Fuel Impact Analysis

Component analyses for core columns impacted by fuel-filled wing sections were conducted for both wide flange and box type columns. Similar to the exterior column analyses, the primary purpose was to progress from the initial finely meshed, brick element models to coarser shell element models. Figure 5–6 (wide flange core column) and Figure 5–8 (box section core column) compare the fine brick model and coarser shell model response under the same loading conditions. Figure 5–7 and Figure 5–9 show corresponding displacement and kinetic energy comparisons for, respectively, the wide flange and box section core column models. In these simulations, the constitutive and failure parameters used were identical between the fine brick model and coarser shell models. Material failure was not a significant factor for the impact behavior in this example, and the primary objective was to validate that the coarser shell element model could accurately reproduce the impact deformations. The figures indicate that the response of the coarser shell models was very similar to that of the fine brick models. Therefore, the shell element formulation and mesh refinement of the coarse model were sufficient to capture the impact damage mechanisms in this component impact scenario.

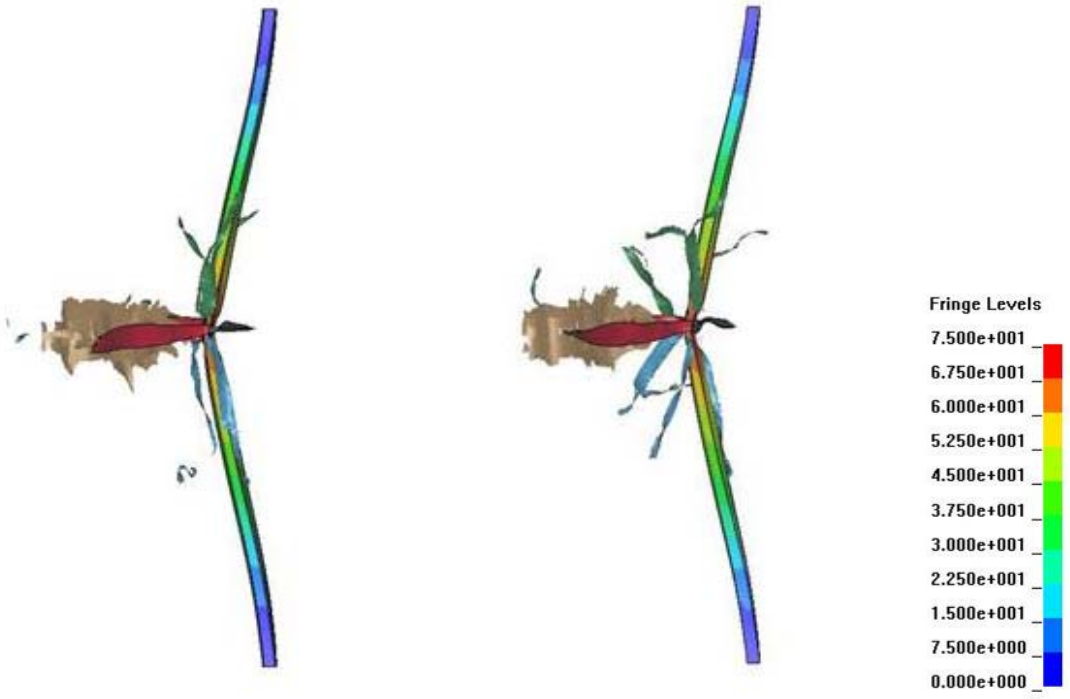

(a) Fine brick element column **(b) Coarse shell element column**

Figure 5–6. Wide flange core column response comparison, showing contours of the displacement magnitude (inches).

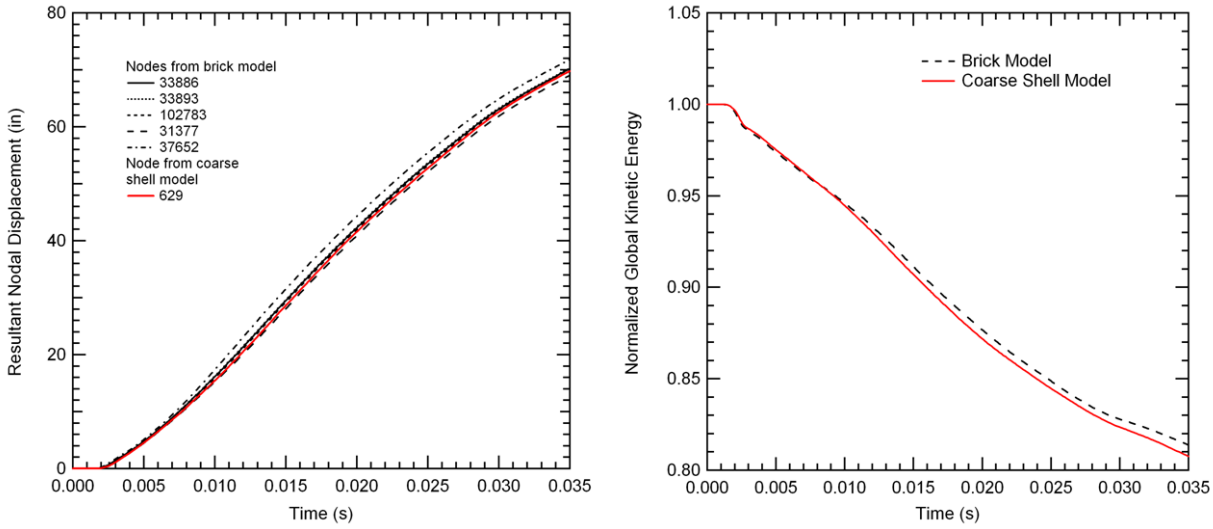

Figure 5–7. Displacement and kinetic energy comparison for wide flange core column wing impact analysis.

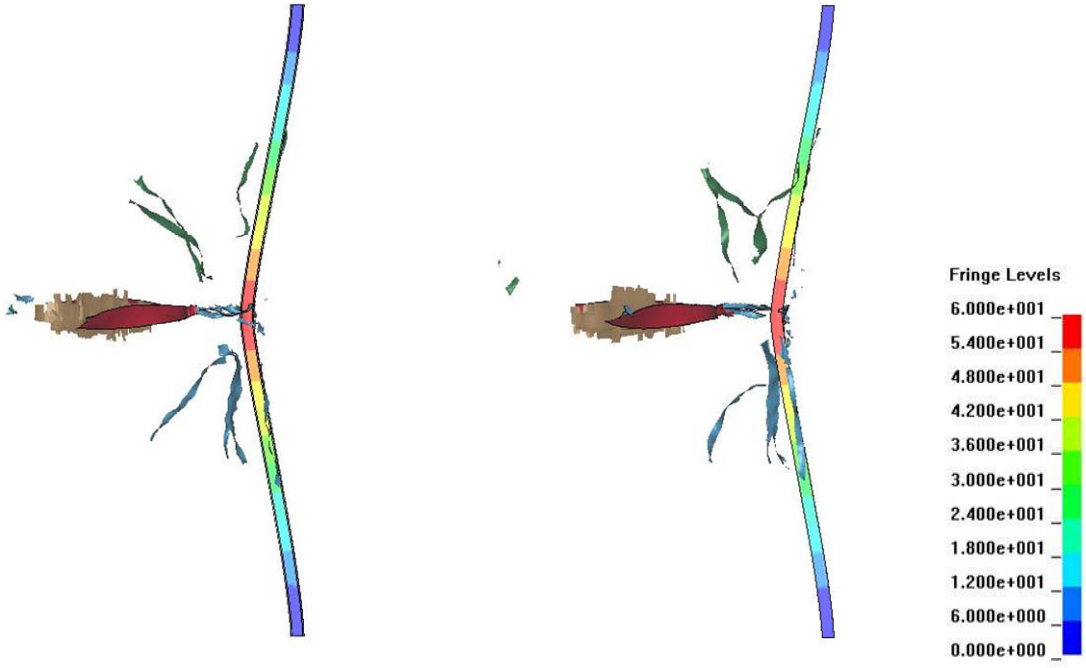

(a) Fine Brick element column **(b) Coarse shell element column**

Figure 5–8. Box core column response comparison, showing contours of the displacement magnitude (inches).

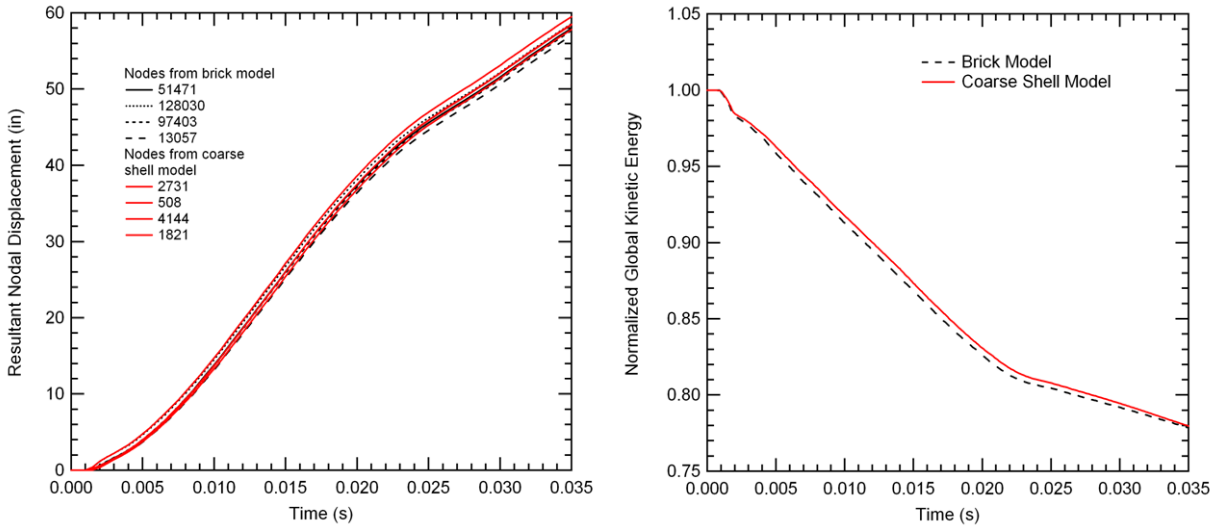

Figure 5–9. Displacement and kinetic energy comparison for box core column wing impact analysis.

5.2.3 Bolted Connection Modeling

There was a wide variety of different connections required for the assembly of the tower models. Wherever possible, evidence gathered from the WTC steel and photographs was applied to determine the importance of including connection details in the model and failure modes of those connections. Photographic and structural debris evidence clearly demonstrated that the external column connections played a significant role in the mode of column failure and extent of the external damage (FEMA 2002). For example, the bolted connections at exterior column butt plates, shown in Figure 5–10, failed primarily in the bolts. The bolted spandrel connections failed in several modes, including bearing strength failure where bolts pulled through the spandrel material, as shown in Figure 5–11.

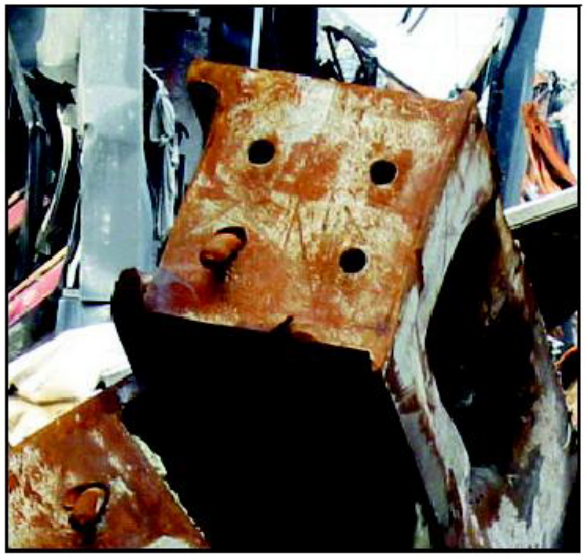

Source: FEMA 2002.

Figure 5–10. Failure behavior observed in the external column bolted joints.

Source: NIST.

Figure 5–11. Typical bolt bearing shear failures of spandrel connections.

The objective of the connection component analyses was to develop connection models for the global impact analyses that accurately captured the capacity and failure modes of the connection. Various connection component models developed included both fine models of these complex connection components (e.g., 3-D brick element models of bolts), and simple models such as simple beam element bolt models and tied constraints with failure. A tied constraint with failure requires that two nodes or a node and a surface segment (shell element or solid element face) have tied degrees of freedom until a failure criterion is exceeded.

The coarse component models utilized many of the simplified connection and element types available in LS-DYNA to approximate the behavior observed in the fine models. For example, in the exterior column bolted connections, the bolts were modeled with elastic-plastic beam elements calibrated to match the fine model. The constitutive behavior of the beam element bolt was described previously in Section 2.3.4. Bolted joints, such as in the spandrel connections, were approximated with a tied node algorithm that constrained degrees of freedom of adjacent nodes and element faces. Various options were investigated in these component analyses, and final selections of the modeling methodology were based on both the fidelity and efficiency of the modeling approaches.

Component models of the exterior column butt plate connections are shown in Figure 5–12. The detailed model included individual bolts modeled with solid brick elements. The simplified model used coarse brick butt plates joined by beam elements representing the bolts. A dynamic analysis was carried out to calibrate the beam element bolt model. The loading condition was a dynamic separation of the two butt plates. The velocity profile used to separate the butt plates was obtained from a preliminary engine impact analysis against the exterior wall, similar to those described in Section 5.2.4. The profile was a

linearly increasing separation velocity between the butt plates with an initial velocity of zero and a velocity of 43 fps at a time of 5.0 ms.

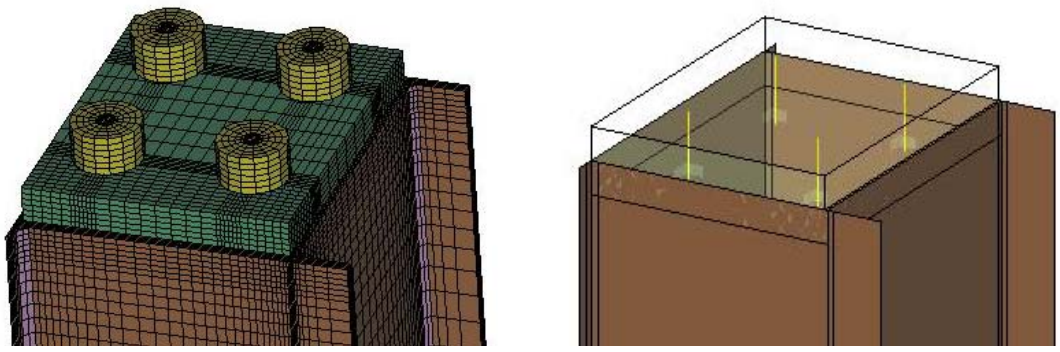

(a) Brick element bolts **(b) Beam element bolts (butt plates shown as transparent)**

Figure 5–12. Exterior column end connection treatments.

Failure strain in the beam models was calibrated such that the beam bolts failed at the same time as the brick element bolts. Failure of the bolts occurred at a time of approximately 3.0 ms. These connection models were used in the corresponding brick and shell models of the exterior column component impact analyses shown previously in Figure 5–4. Connection failure at the column ends was quite similar in both cases, as shown in Figure 5–13. Failure of the connection is illustrated for both connection models at the same time, 35 ms, after impact with the empty wing segment. The primary failure mode for both models was a tensile failure of the bolts and subsequent separation of the column end butt plates.

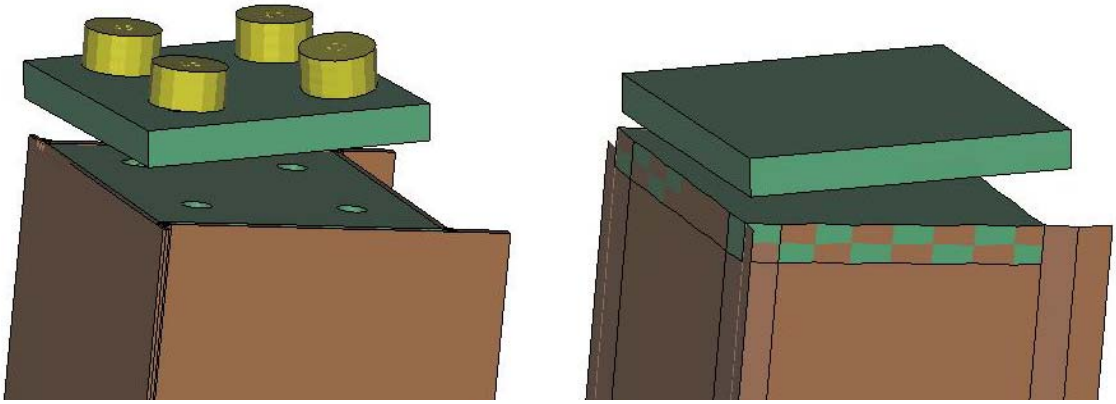

(a) Brick element bolts **(b) Beam element bolts**

Figure 5–13. Failure comparison of exterior column end connection treatments.

The spandrel connections consisted of an overlapping splice plate across a spandrel joint with rows of bolts on both sides of the joint. Typical failure of these spandrel joints in the impact zone resulted from bolt bearing shear failures, typically in the spandrel plate, as shown in the photographs in Figure 5–11. A common configuration in the impact zone would be six bolts on either side of the joint. Modeling the spandrel connection bolts using beam elements was not appropriate at this location, where the dominant response mechanism was a bolt bearing shear failure. In the exterior columns, the bolts failed primarily

in tension, and details of the contact between bolts and butt plates were not as important for capturing the failure behavior. As a result, an alternate modeling approach was required for the spandrel splice failures.

Spandrel connections were modeled using a splice plate made up of shell elements, as shown in Figure 5–14. Connections corresponding to individual bolts were treated by tying single nodes on the splice plates (center of green squares in Figure 5–14) to the spandrels. Two material definitions were used to make up the splice plate to allow for contact between the splice plates and the spandrels, as well as having tied contact. Use of a single material definition can sometimes result in numerical instability due to conflicting constraint and interface algorithms on those segments.

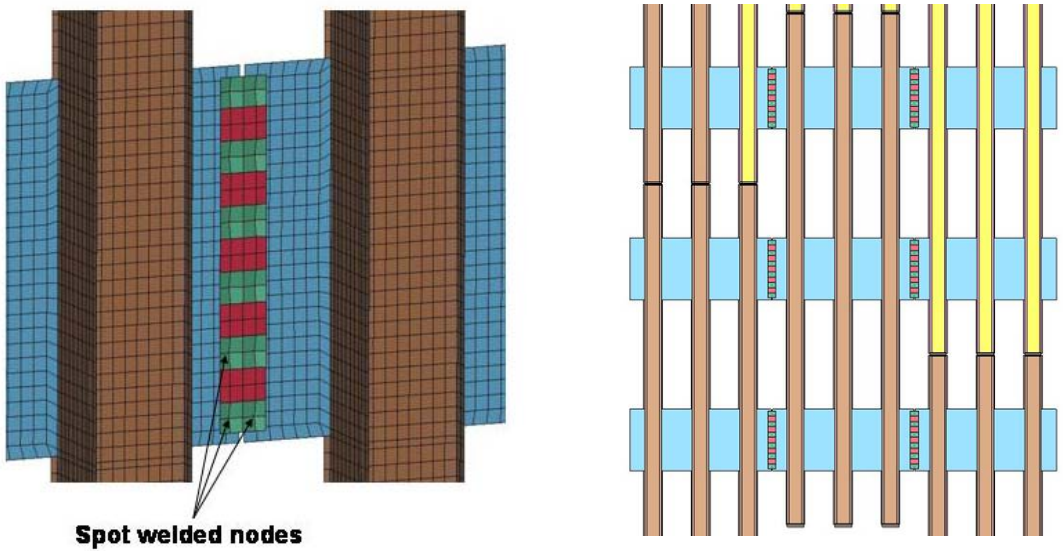

(a) Detail of connection **(b) Multiple panel connections**

Figure 5–14. Bolted spandrel connection treatments.

The first splice plated material definition (shown in green in Figure 5–14) was used to allow the center node tied constraint (representing the bolt connection) to be aligned with the center of the spandrel plate. Since this material included the tied constraint, it was not included in the automatic contact definition. The second material definition in the splice plate (shown in red in Figure 5–14) had a standoff distance equal to one half of the combined thickness of the spandrel and splice plate and was included in the automatic contact definition. Both material definitions had the same constitutive properties. The application of the spandrel splice plate connection model was demonstrated in the following engine impact component analyses (see Figure 5–17).

5.2.4 Engine Impact Analysis

An example of an engine impacting an assembly of exterior panels is shown in Figure 5–15. The analysis included an engine impacting an exterior panel of WTC 1 and was centered on panel 124 at floor 96 (the impact was centered on the middle spandrel). The initial engine impact speed was 500 mph. In this example, a shell element panel with medium mesh density was used (typical exterior panel element size on the order of 2 in.). Columns were connected with beam element representations of individual bolts. Spandrels were merged together in this model (i.e., splice plates were not used). Fixed butt plates were bolted at the free column end, and no boundary conditions were applied to represent the floors. Velocity

time-histories for representative engine core materials are shown in Figure 5–16. The plot shows an overall reduction in speed of about 67 mph after impact with the exterior wall.

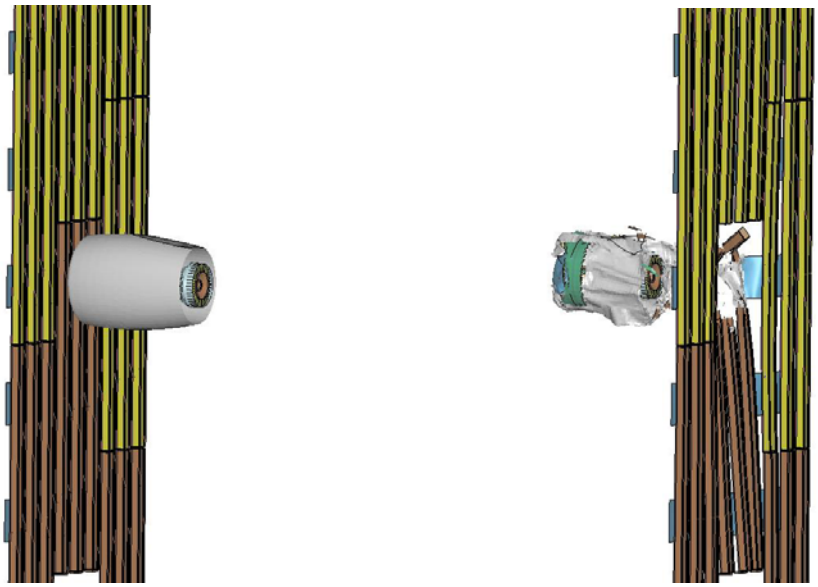

(a) Initial configuration **(b) Impact response at 40 ms**

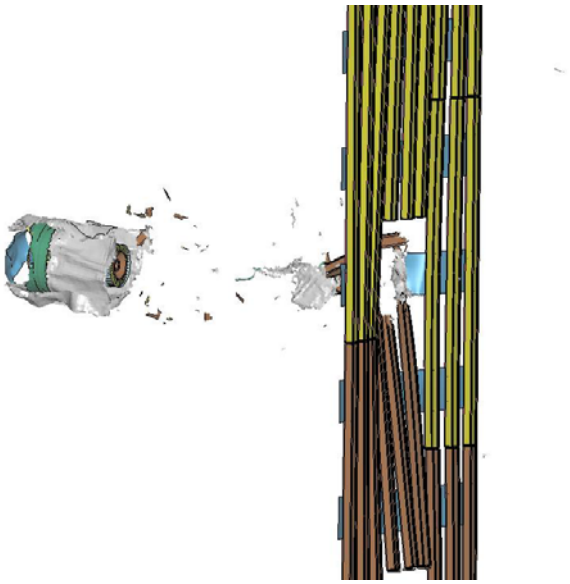

(b) Impact response at 80 ms

Figure 5–15. Example engine impact analysis with exterior columns.

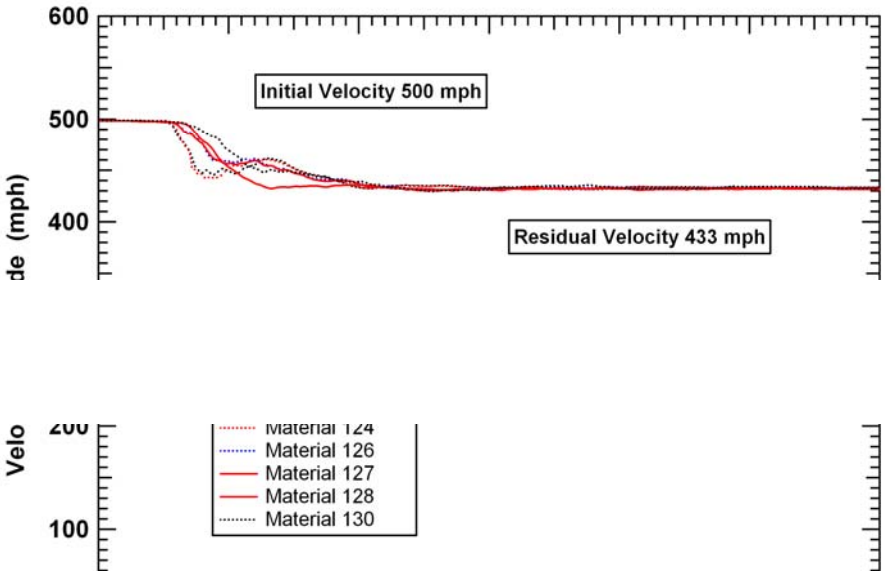

Figure 5–16. Engine velocity history for the exterior wall impact.

A second engine impact analysis was performed with similar conditions except that the impact location was moved downward by one half of a floor height to create an impact centered between spandrels. A comparison of the two calculated impact behaviors is shown in Figure 5–17. In both analyses the engine broke through the exterior wall with relatively little break up of the engine core. The impact centered between spandrels resulted in a reduction of the engine core speed by about 56 mph.

A final revision of the analysis described above included adding splice plates at the spandrel connections as explained in Section 5.2.3. Figure 5–18 shows a comparison of both models. The figure shows exterior wall damage as seen from the outside without engine components. Contours of plastic strain are shown in the plot with blue being zero strain and red being at the failure strain threshold (20 percent in this case). Material exceeding the maximum failure strain was eroded and no longer shown in Figure 5–17. The analyses differed most in spandrel failure modes. Spandrels failed at the column connection in the merged spandrel case, while the splice plate connection failed when the splice plate was included in the model. In the latter case, a realistic bearing stress type tear-out mode was observed in the splice plate. Engine core velocities for the three engine impact analyses are compared in Figure 5–19 for a single representative engine component. The splice plate model resulted in a 74 mph speed reduction of the engine core. The splice model resulted in the largest reduction in the speed of the engine. In this case, the entire spandrel was carried away by the engine, resulting in a larger transfer of momentum.

The comparison described above suggests that the splice plate had a relatively small influence on the exterior wall strength. The addition of the splice plate had approximately a 10 percent effect on the change in engine velocity during impact and penetration of the exterior wall. However, the spandrel connection model did not introduce a large computational cost and resulted in a more appropriate failure

mode for the spandrels in the impact zone. Therefore, the spandrel splice connections were maintained in subsequent impact analyses.

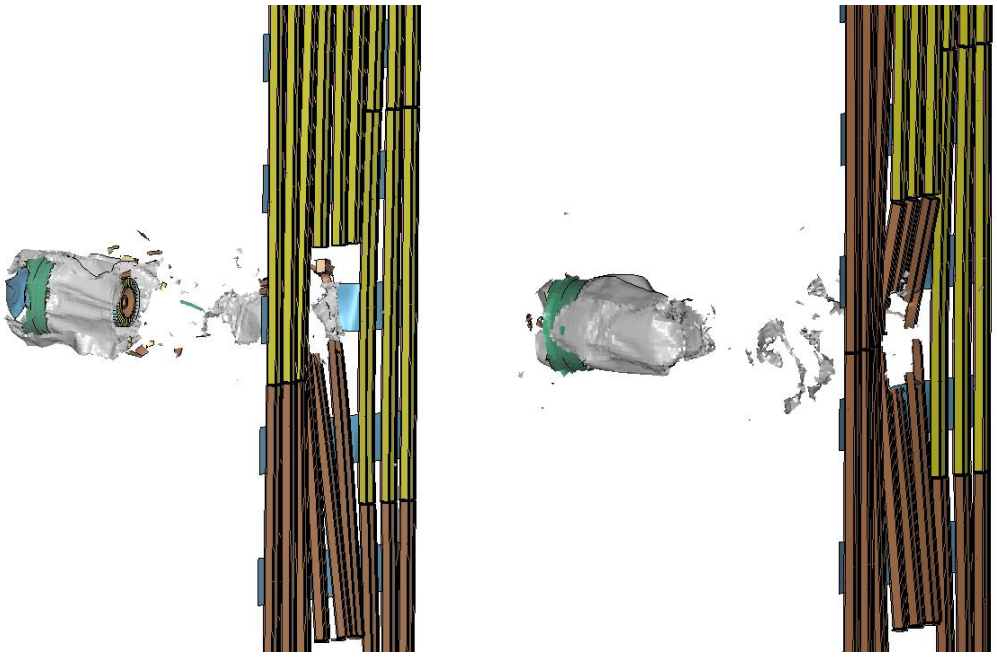

(a) Spandrel centered impact **(b) Between spandrel impact**

Figure 5–17. Example engine impact analysis with different impact locations.

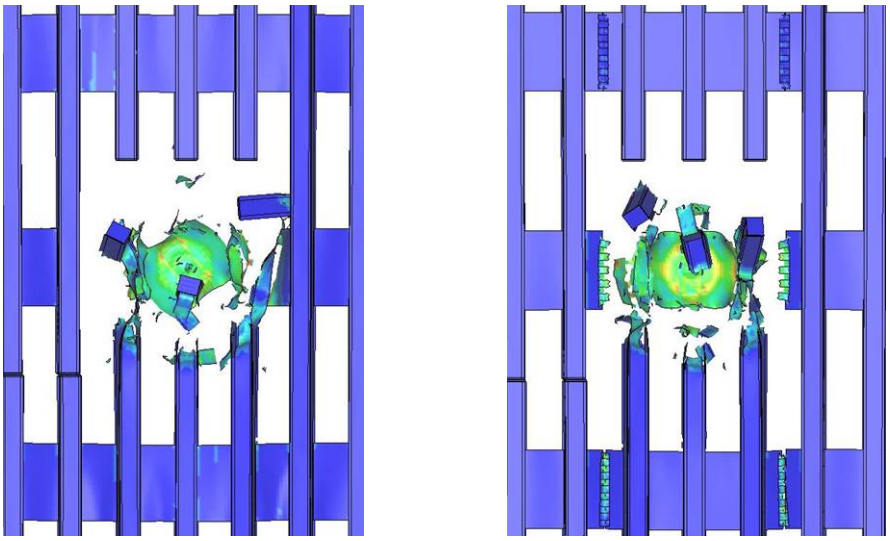

(a) Merged spandrel analysis **(b) Spliced spandrel analysis**

Figure 5–18. Example engine impact analysis with different spandrel connection treatments.

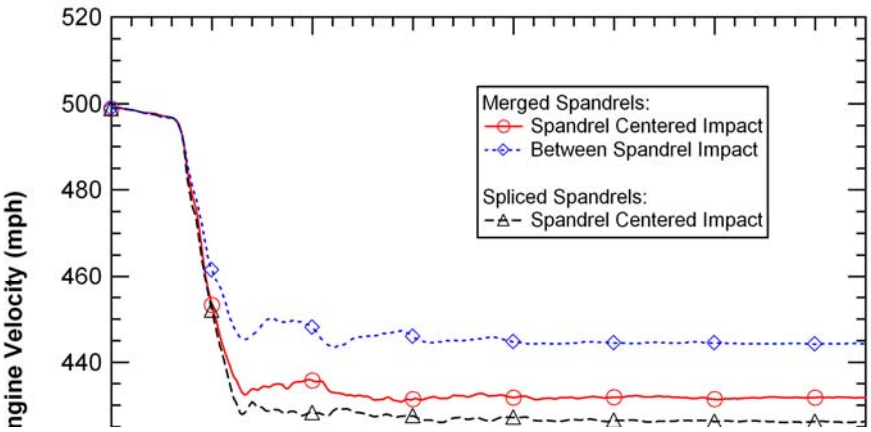

Figure 5–19. Engine velocity history for the exterior wall impact.

5.3 COMBINED ENGINE IMPACT ANALYSES

A combined engine impact analysis was performed to demonstrate the damage response to both exterior and interior columns. The impact configuration was an engine impacting at 560 mph against a set of exterior columns in a single exterior panel, an interior box column, and an interior wide flange column. The columns were modeled using shell elements. The spacing between exterior and core columns was reduced to shorten the run time necessary for the complete impact scenario. The simulation included three external panels stacked vertically such that the impacted column was bolted to additional panels both above and below. The core column models were several floors tall to reduce the influence of the clamped boundary conditions at the ends.

The impact scenario is illustrated in Figure 5–20(a). The calculated impact damage is shown at a time of 90 ms in Figure 5–20(b). The calculated engine impact response completely failed all of the columns with a residual velocity of the engine of approximately 224 mph. The deformations of the column included large lateral displacements, which would be significantly reduced if the constraint effects of the concrete floor slab were included in the model. The deceleration profile of the major engine debris fragment is shown in Figure 5–21. The majority of the engine structure had been broken into fragments by the combination of the three impacts. The resulting size, strength, and velocity of the engine debris were not likely to produce severe impact damage or failure to a subsequent core column.

This example illustrates the large level of damage produced by a massive aircraft component, such as an engine, at high impact velocity. The impact energy was sufficient to overwhelm a single core column and, therefore, made it difficult to determine the effects of column component modeling parameters on the impact response.

(a) Initial configuration

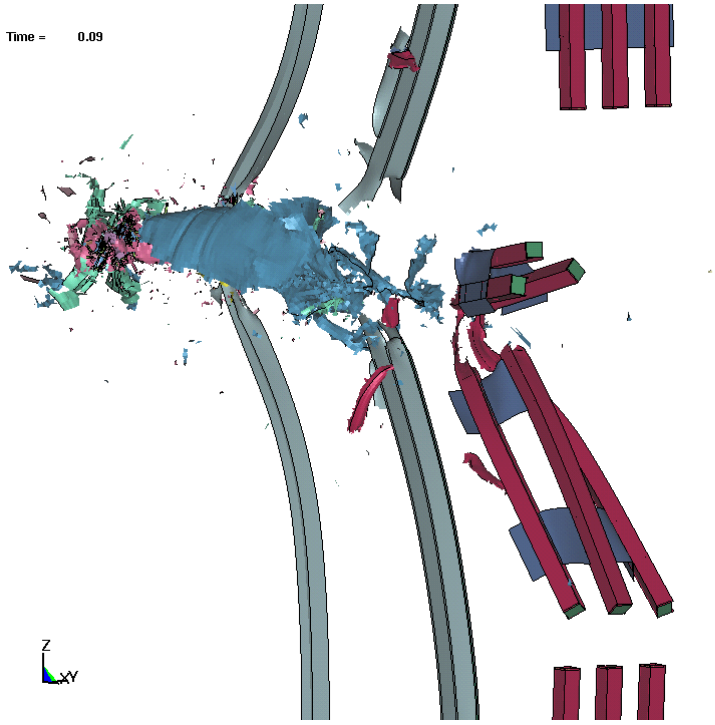

(b) Impact response at 90 ms

Figure 5–20. Example engine impact analysis with interior and exterior columns.

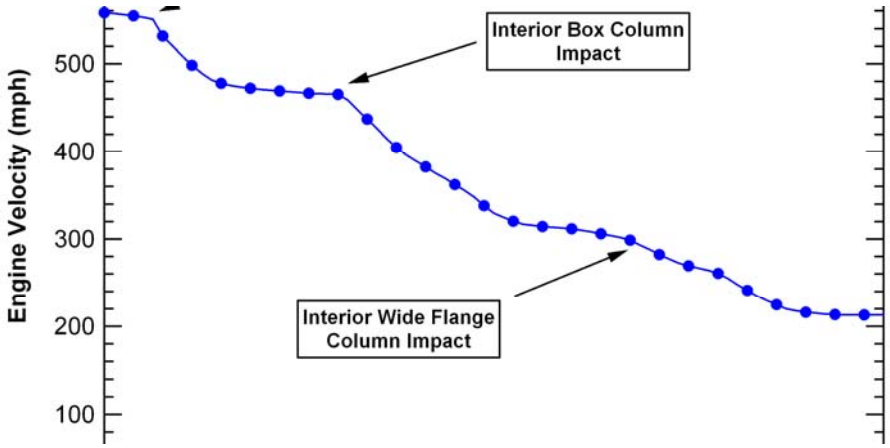

Figure 5–21. Example engine impact analysis with exterior and interior columns.

5.4 FLOOR ASSEMBLY COMPONENT ANALYSES

The truss floor structures outside the core played a significant role in the aircraft impact and penetration resistance of the towers. The failure and penetration of the floor structures were important for assessing the extent of damage and the spread of fuel and debris through the structure. The integrity of the floor structures could also be significant in the analysis of the subsequent fire behavior in the towers. As a result, floor truss component impact analyses were performed to ensure that the impact and penetration resistance of the simplified truss floor models used in the global impact analyses were properly modeled. Dynamic loading of the truss floor structure was achieved by direct impact by a simplified impactor.

Component models of a section of the composite floor assembly outside the core were generated and used in the impact analyses. The models included the concrete slab, the metal decking, and the primary and bridging trusses. The dampers were not included in the models for the reasons explained in Section 3.2.3. Detailed floor component models used a combination of brick elements for the concrete slab, beam elements for the truss round bar diagonals, and shell elements for the remainder of the structures, including the truss upper and lower chords and metal decking. This model is shown in Figure 5–22. A simplified model was then developed with coarser shell and beam elements as shown in Figure 5–23. The less-refined floor assembly models reduced the size of the model by an order of magnitude and the run times by more than 80 percent as can be seen from Table 5–2.

Table 5–2. Truss floor assembly component analyses comparison.

Model Type	Fine Brick Model	Coarse Shell Model
No. Beam Elements	6,928	3,440
No. Brick Elements	230,778	0
No. Shell Elements	148,256	39,000
Total Nodes	372,084	48,971
CPU Time	16,796 s (4.7 h)	2,482 s (0.7 h)
Elapsed Time	26,553 s (7.3 h)	4,454 s (1.2 h)

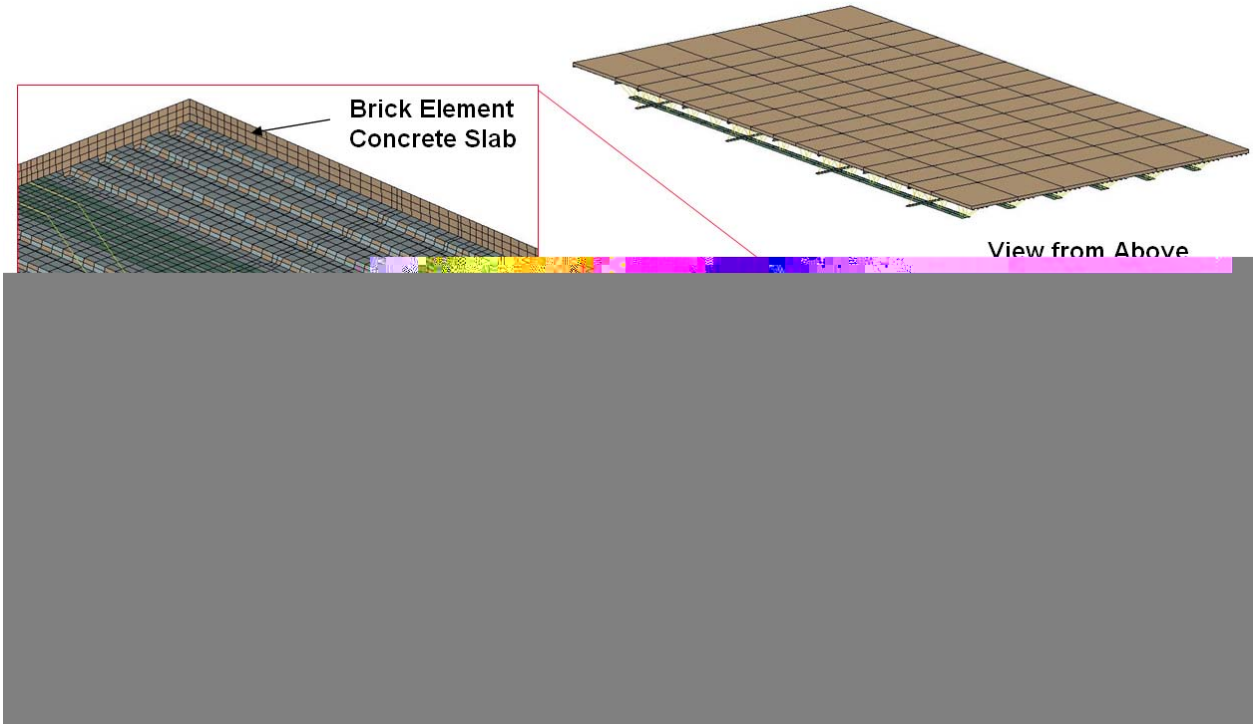

Figure 5–22. Detailed model of the truss floor.

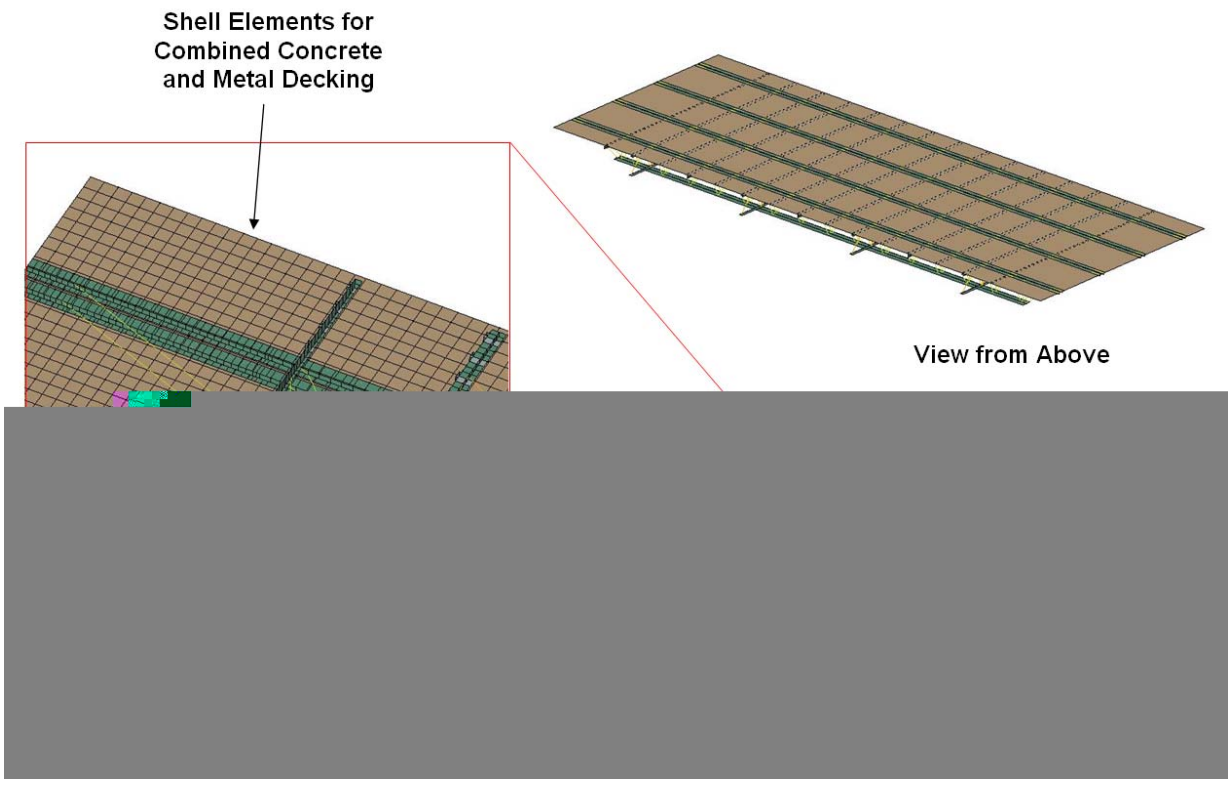

Figure 5–23. Simplified model of the truss floor.

The concrete constitutive model used in the brick elements of the detailed floor model was described previously in Section 2.4. The design for the floor truss structures specified that material yield strength was to be taken equal to 50 ksi for all steel members unless otherwise specified. Therefore, the constitutive model developed for the 50 ksi tower steel, described in Section 2.2, was used for all of the truss structure components and metal decking. The exact strength of the metal decking could not be confirmed; however, the relative contribution of the metal deck was small compared to the much thicker concrete slab (see Figure 5–24). Therefore, the uncertainty on metal deck strength was not expected to have a significant effect on the truss floor strength.

The coarse floor model used an effective material model for the combined concrete slab and metal decking so that these parts would not need to be meshed separately. As the concrete constitutive model described in Section 2.4 (pseudo-tensor model) was developed for brick elements, and does not work for shell elements, a piecewise plasticity model was used for the effective slab-decking behavior. A tabular yield strength was developed based on the rule of mixtures of the elastic-plastic metal decking with the unconfined compressive behavior for the concrete. The combined slab and decking stress-strain curve was compared to the concrete unconfined compressive behavior in Figure 5–24. The strength of the combined floor slab was dominated by the concrete strength at low strain levels (below 1 percent strain). However, as the concrete was fragmented and removed as debris, the residual strength was equivalent to that of the metal deck alone and remained ductile until a strain of 30 percent was reached, corresponding to the failure strain of the 50 ksi material. This combined slab material model had the same rate effect multiplier as the concrete constitutive model described previously in Section 2.4 and shown in Figure 2–32.

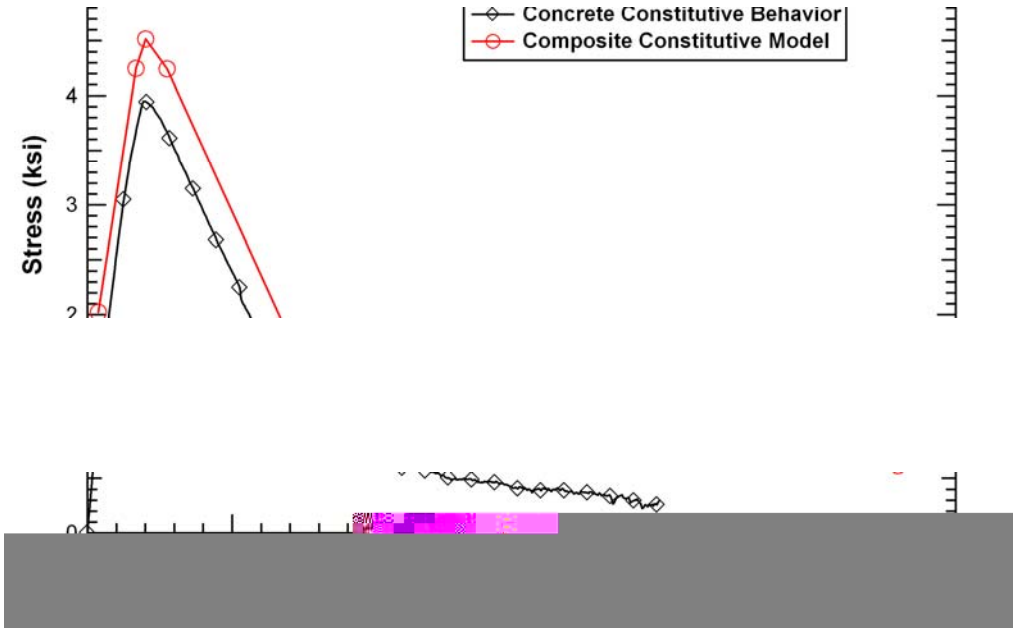

Figure 5–24. Constitutive behavior for the combined concrete and metal decking.

The impactor used in the component modeling was a simplified plow type impactor which promoted repeatable damage, not complicated by all the debris and randomness associated with an engine-floor impact. The weight of the plow impactor was comparable to an engine, and the impact velocity was 500 mph, applied horizontally. The response of the floor to the plow type impactor was similar to the response to an aircraft engine, but without the complications of the detailed engine impact behavior, based on preliminary engine-floor impact simulations. An example analysis with a plow impactor and the fine mesh floor model is shown in Figure 5–25. The calculated impact damage with the coarser shell element floor system model is shown in Figure 5–26. This component impact configuration was useful for comparing the differences in response with changes in the modeling methods or refinement. The calculated plow impactor deceleration profile for the brick and shell element models are compared in Figure 5–27. The comparison shows that the simplifications did not significantly change the impact loads in the floor assembly.

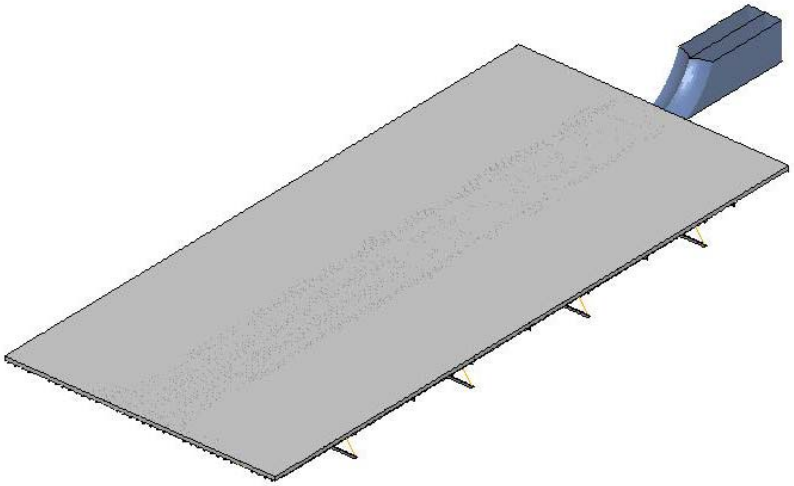

(a) Initial configuration

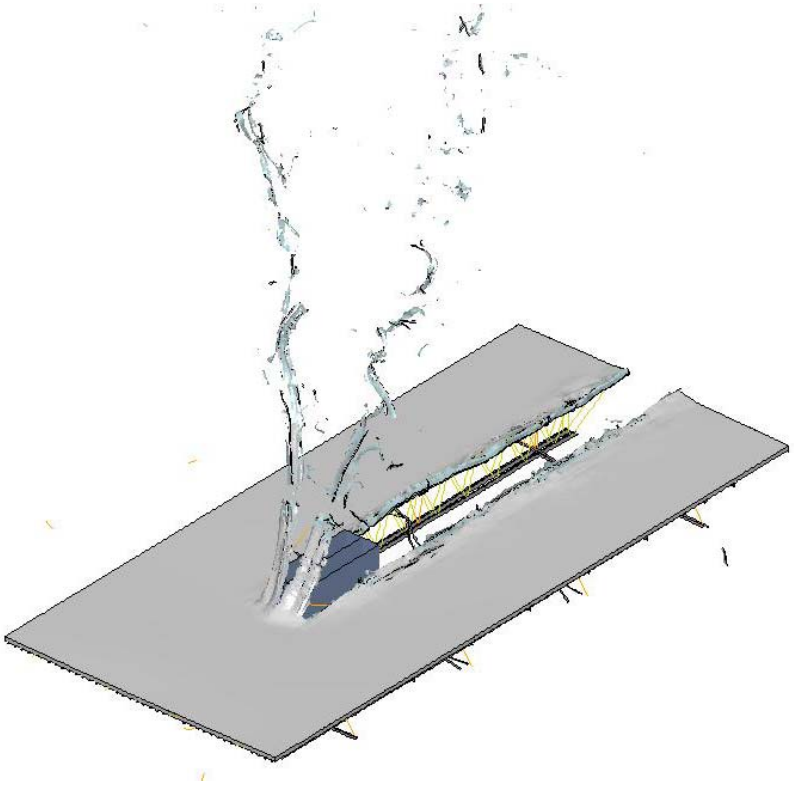

(b) Impact response at 0.10 s

Figure 5–25. Floor assembly impact analysis with brick element concrete slab.

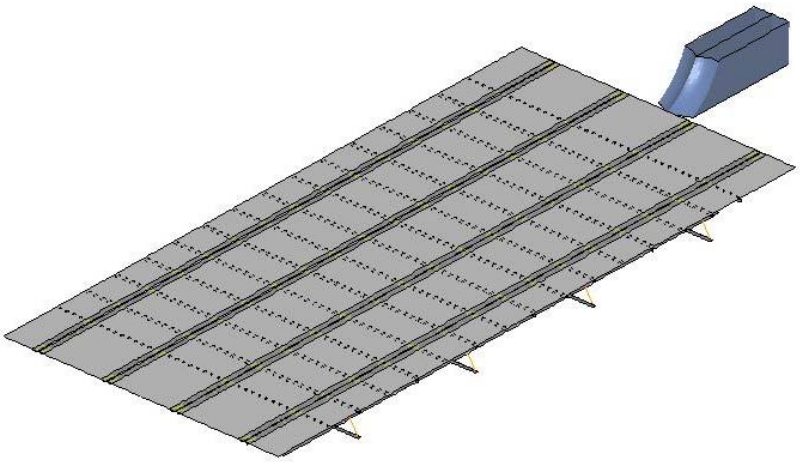

(a) Initial configuration

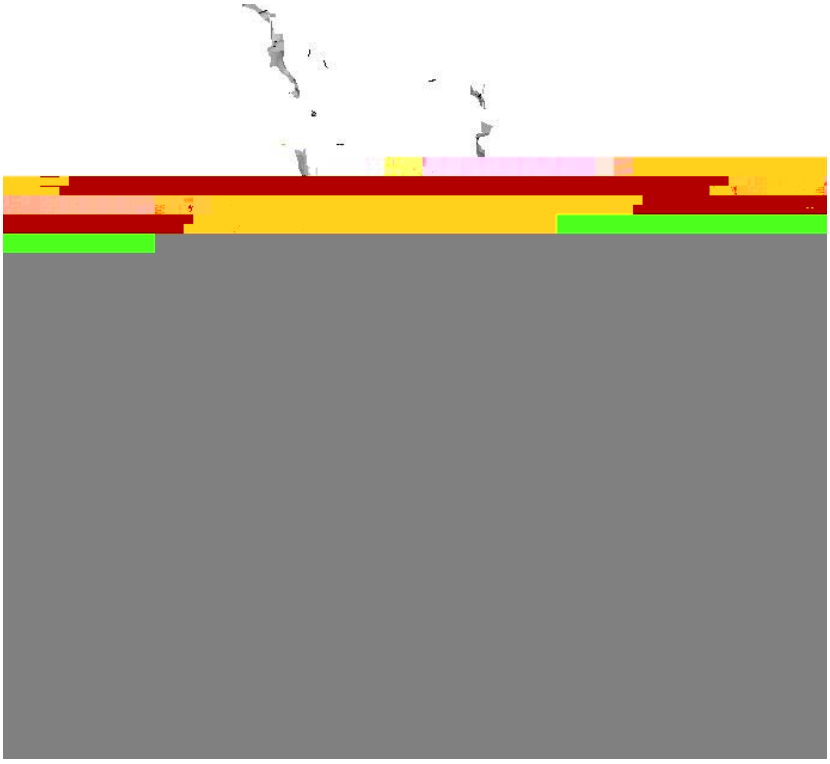

(b) Impact response at 0.10 s

Figure 5–26. Floor assembly impact analysis with shell element concrete slab.

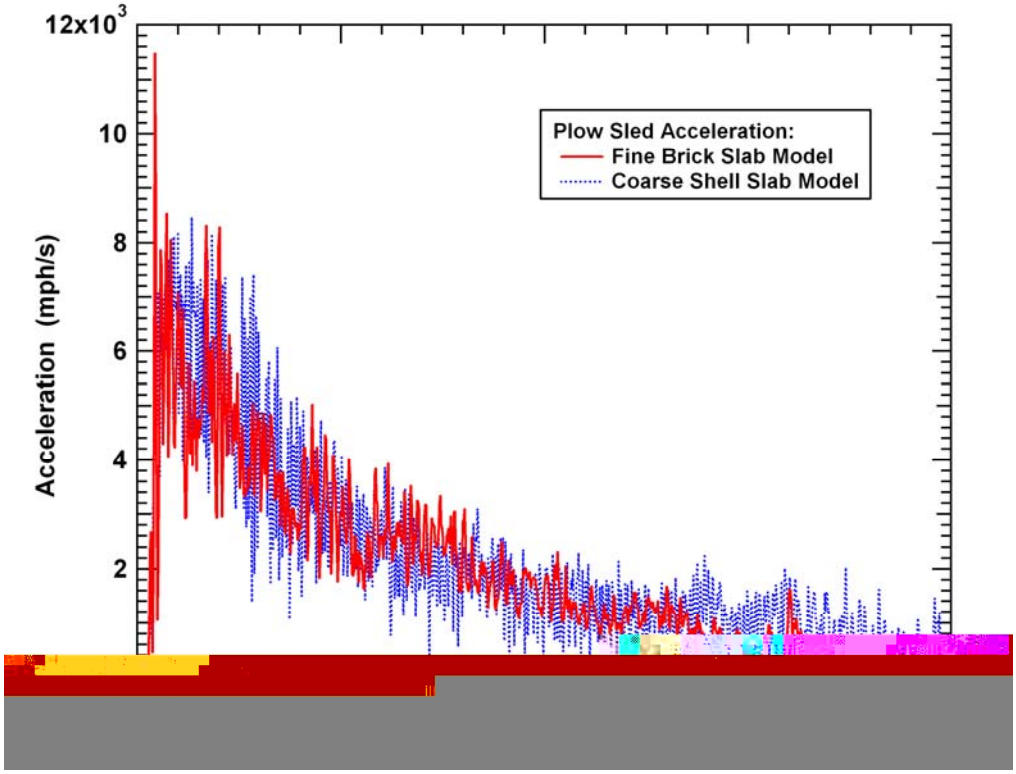

Figure 5–27. Comparison of brick and shell element floor assembly impact analyses.

5.5 AIRCRAFT WING SECTION COMPONENT ANALYSES

The aircraft wing section component models were the last of the component models to be developed. Having established acceptable tower component models, the exterior panel model type 300 was then used to evaluate an aircraft wing section component model. Construction of the wing section model was previously discussed in Section 4.3.2. The focus in this section is on developing a coarse wing model for the global impact analysis and evaluating methods for modeling fuel in the wing. This coarse model of the aircraft wing and associated failure modeling criteria are important not only for modeling the wing accurately, but also to establish the modeling methodology for the entire airframe. Element size, tied interfaces, and failure criteria developed in this section were implemented in the model for the entire airframe.

5.5.1 Empty Wing Section Component Model Development and Analysis

A significant challenge in developing an aircraft model suitable for performing the global analyses was to reduce the number of nodes and elements in the model to a manageable size. This was a challenging task because the detailed geometry of the fracture and tearing of aluminum that occurred during impact could not be modeled well with the coarse mesh needed in the global model. Instead, elements were given a reduced failure strain in the coarse mesh model so that the energy absorbed approximated that of the tearing aluminum structure. An appropriate reduction in failure strain was found by conducting component analyses of coarse and fine mesh wing section models. In both cases, the wing section was impacted into a pair of exterior panels of a WTC tower.

Development of the wing section component model was previously described in Section 4.3.2. The finely meshed wing component model had a mesh fine enough to capture the tearing of the wing. In this analysis, the fine and coarse wing models impacted the same target panel in order to maintain accurate failure modeling of the panels and a reasonable runtime appropriate for the uncertainty analyses. The resulting model for the exterior panel had 10,400 shell elements (columns and spandrels), 264 solid brick elements for the butt plates, and 48 beam elements for the bolts. This model is shown with the wing in its initial position in Figure 5–28.

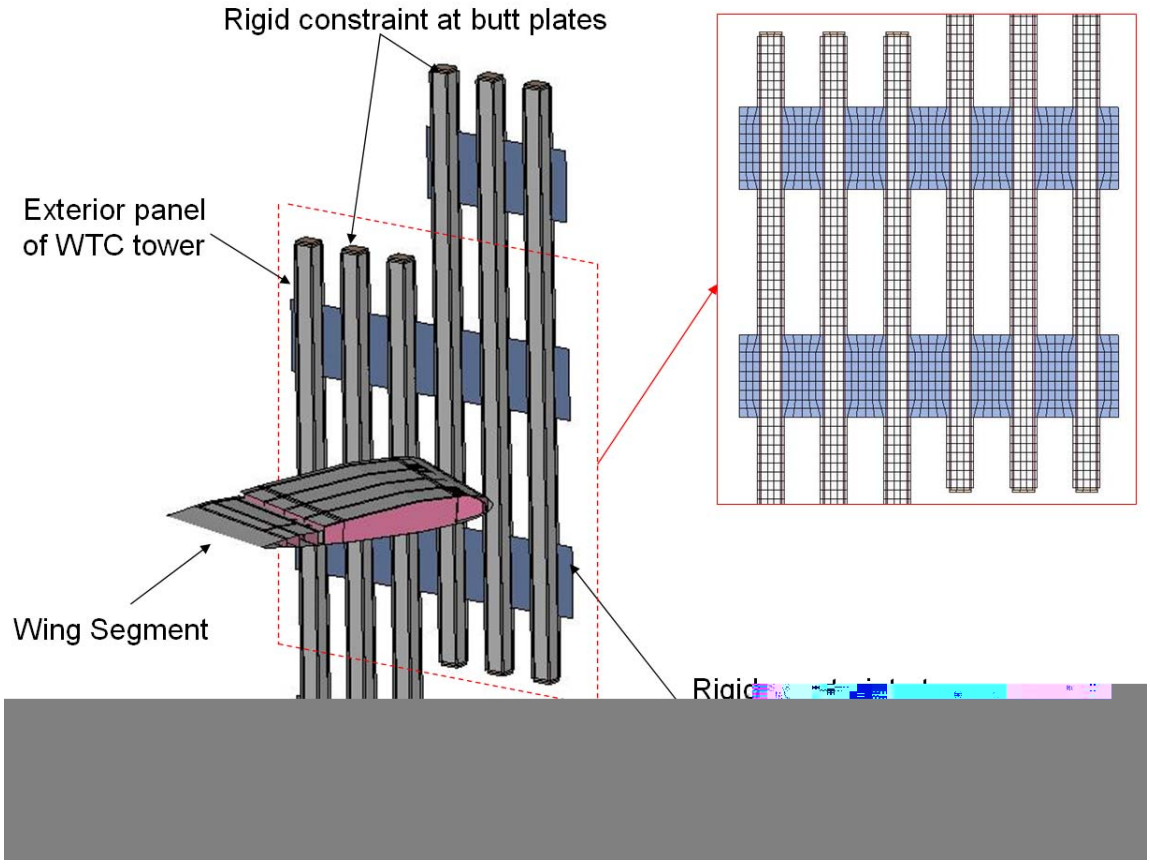

Figure 5–28. Empty wing section impact model with two exterior panels.

The wing section impacted the panels half way between spandrels at 442 mph. The wing section impacted with a lateral trajectory offset 3 degrees relative to the panel normal, as shown in Figure 5–29. This was done to impart a less symmetric loading on the exterior columns, which was more realistic for the global impact. The wing was oriented with no pitch or roll, so the angle of the leading edge was that of the sweep angle of the wing relative to the fuselage.

The fine component model of the aircraft wing, as shown in Figure 5–30, was modeled with a typical element size of approximately 0.5 in. for a total model size of approximately 245,000 shell elements. Material properties and constitutive models discussed in Section 2.5 were used in the component model. Data from the Military Handbook (MIL-HDBK-5F 1987) for elongation at failure were used as the failure criteria of the 0.5 in. elements. Elements were eroded when the effective plastic strain in the element met

this failure criterion. Total run time for this fine component model was approximately 7 hours on 12 processors.

Figure 5–29. Wing segment showing the initial impact conditions on the exterior panels.

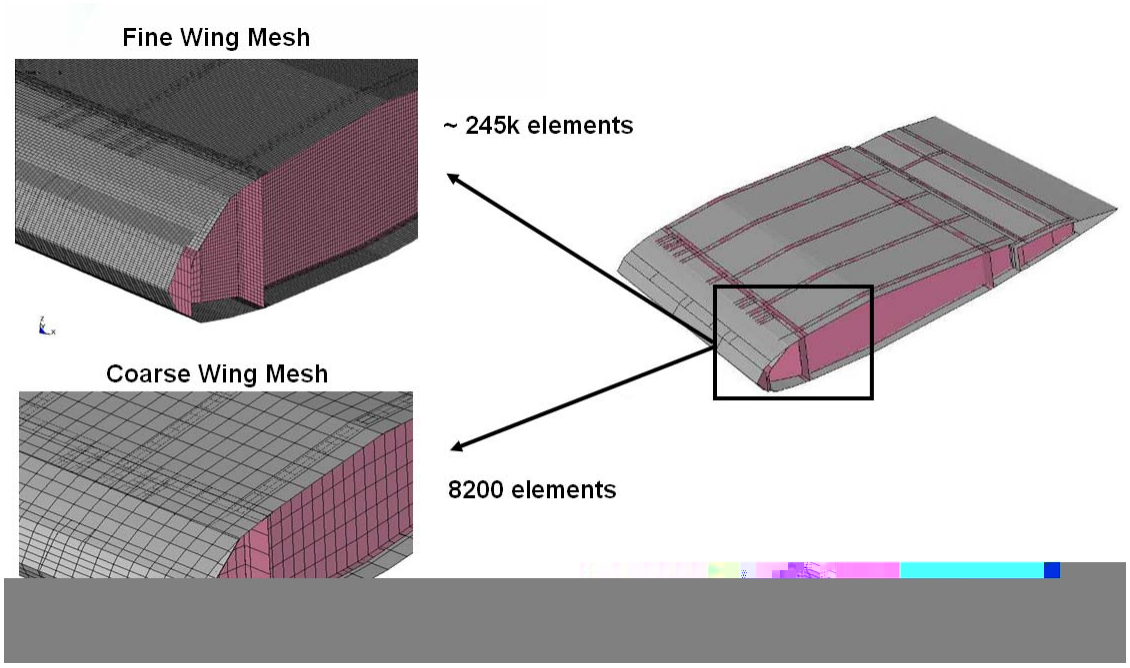

Figure 5–30. Coarse and fine mesh used in the small wing component model.

The fine-mesh empty wing section impacting two exterior panels of the WTC tower is shown in Figure 5–31. The spars, ribs, and skin were torn by the impact against each column. As a result, significant material was free to pass between the columns. The residual kinetic energy of the aircraft debris was 43 percent of the initial kinetic energy. Damage to the exterior panel is shown in Figure 5–32.

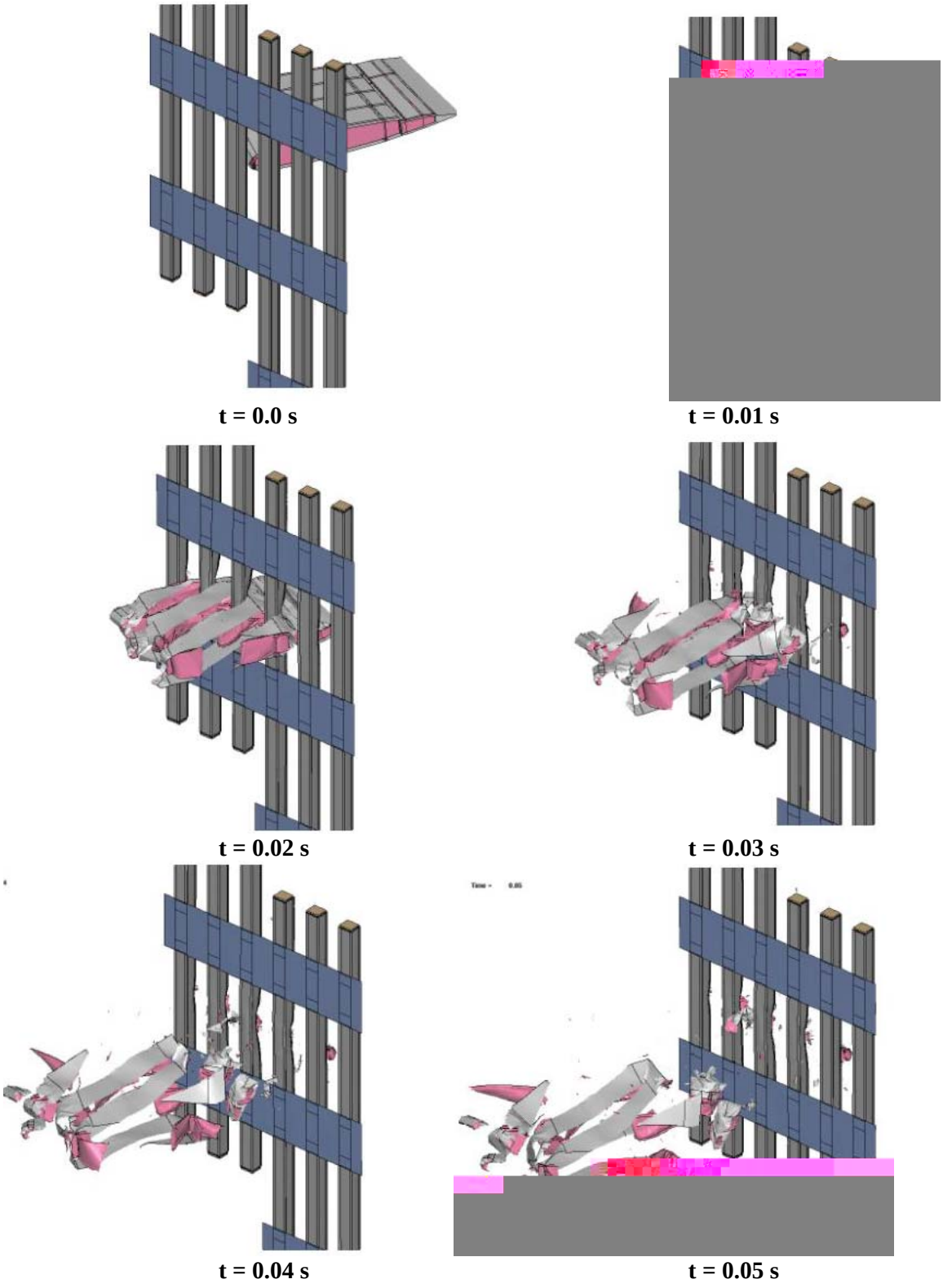

Figure 5–31. Calculated impact of a fine-mesh empty wing section with two exterior panels at 442 mph.

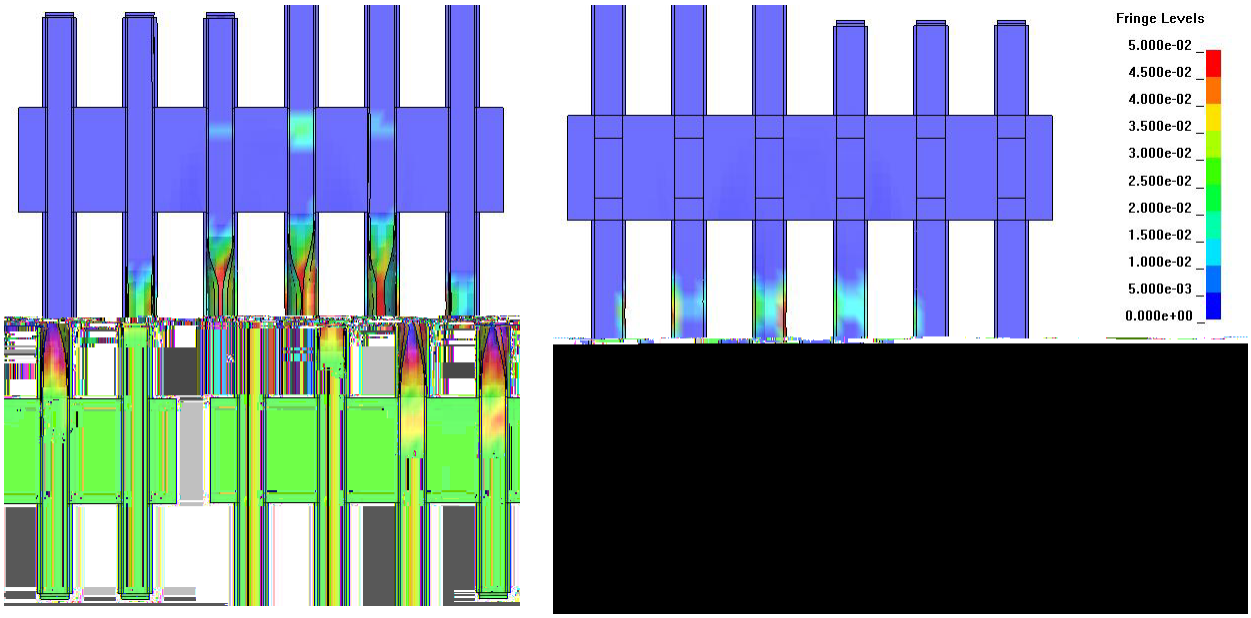

(a) Front (building exterior) **(b) Back (building interior)**

Figure 5–32. Fine-mesh empty wing section impact damage to the exterior panel.

The calculated impact response produced large-scale damage and fragmentation of the empty wing section and moderate damage to the exterior columns. The internal energy absorbed by the panels was 4 percent of the initial kinetic energy. The damage included distortion of the columns, plastic strains, and fracture of the welded front web connections within the columns. However, the columns were not completely severed and still maintained some load carrying capacity.

In order to meet the size constraints imposed by the global analyses, the coarse mesh size required for the wing structure needed to be an order of magnitude larger than that for the finely-meshed wing section. The coarse-mesh wing component is shown in Figure 5–30. This model had a typical element size of approximately 4 in. to 5 in. for the primary components. The total model size of the coarse wing section component model was approximately 8,200 elements.

When the coarse wing section model was used in the impact analysis without any adjustment in the failure strain, the impact response was significantly different. More of the wing material was eroded, and the wing structures had a much tougher behavior resulting in lower residual velocities of the wing debris. The residual kinetic energy of the wing section debris was reduced from 43 percent to 18 percent of the initial kinetic energy. Much of the additional kinetic energy loss for the coarse wing section model was absorbed in the panels. The damage to the columns was significantly larger with the internal energy increasing from 4 percent to 18 percent of the initial kinetic energy.

Additional wing section-panel impact analyses were used to determine failure models for the coarse mesh model in order to most closely match the impact response of the fine mesh model. Obtaining an exact match was not possible due to competing mechanisms in the calculation. Reducing the failure strains for the wing materials would reduce the damage to the exterior panel (improved agreement with the fine mesh analysis). However, the greater amount of erosion in the wing section structures resulted in reduced residual kinetic energy for the wing debris (poorer agreement with the fine mesh analysis). The final

model parameters were determined by balancing the observed impact response, the damage to the panels, and the residual kinetic energy of the wing debris. The difficulty in developing the coarse wing model was that the plastic strain at failure needed to be reduced significantly for the large elements used. It was found that reductions in the plastic failure strain of over 70 percent were necessary. The initial approach, shown in Figure 5–33(a), was to simply reduce the element erosion strain to the appropriate value depending on the element size (see Section 2.3.1).

(a) Initial failure model.

(b) Modified failure model.

Figure 5–33. Failure modeling approaches for the coarse wing section model.

The problem with using very low erosion strains to represent material failure was that elements eroded quickly, and their inertia was not completely transferred to the columns prior to being eroded. An alternative approach was applied that avoided the potential shortcomings of the first method for treating material failure. The modified approach was to reduce the load carrying capacity of an element at a given value of plastic strain, representing 'failure', but to only erode the element at larger strains. An example of this treatment of material failure is shown in Figure 5–33(b). In this example, the true stress in an element was decreased at 20 percent of the original fine mesh failure strain. Beyond this strain, a degraded true stress of 7 ksi was used. This level was selected to balance the need for a reduced strength in the material with stability of the degraded element behavior. Note that the strain energy of the modified failure model, Figure 5–33(b), was very similar to that of the initial failure model, Figure 5–33(a).

Wing sections modeled with both the initial and modified failure modeling methodologies are shown in Figure 5–34 for a time when the wing section partially penetrated the exterior columns. For the initial failure approach, shown in Figure 5–34(a), the elements in the path of the column showed little strains as they impacted and eroded against the column. There may not have been sufficient time to transfer the momentum of these elements to the columns prior to element erosion. Element strains near the impact zone for the modified failure approach, shown in Figure 5–34(b), were much larger. This indicates that elements stayed in the calculation longer, allowing more time for load to be transferred between the wing structures and exterior columns. Therefore, this modified modeling approach was adopted for subsequent wing impact analyses.

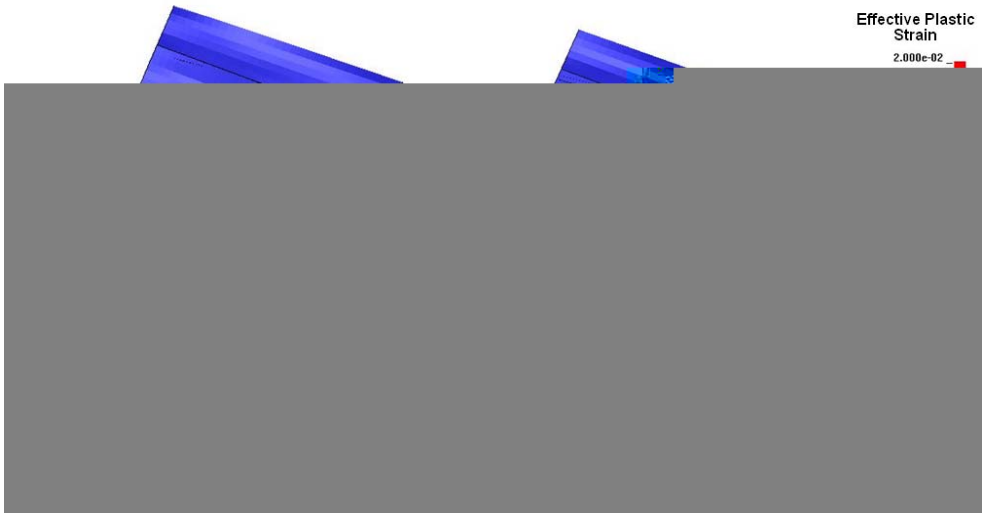

(a) Baseline failure model **(b) Modified failure model**

Figure 5–34. Wing section response for two material failure criteria.

A final parameter investigated in the coarse wing section component analyses was the modeling of wing structure connectivity on impact response. Analyses were performed with both a tied interface (i.e., without failure, between the internal structure and skin) and with a tiebreak interface. The surface-to-surface tiebreak and surface-to-surface tied contact algorithms were discussed in Section 3.3.2. It was found that the connection between the internal structure and the skin did influence the failure of wing elements. When a tied contact was used, the model response improved. The fragmented debris of the

fine and coarse mesh models with tied and tiebreak contact are shown in Figure 5–35. Note that debris with the tied coarse mesh most closely resembles that of the finely meshed wing..

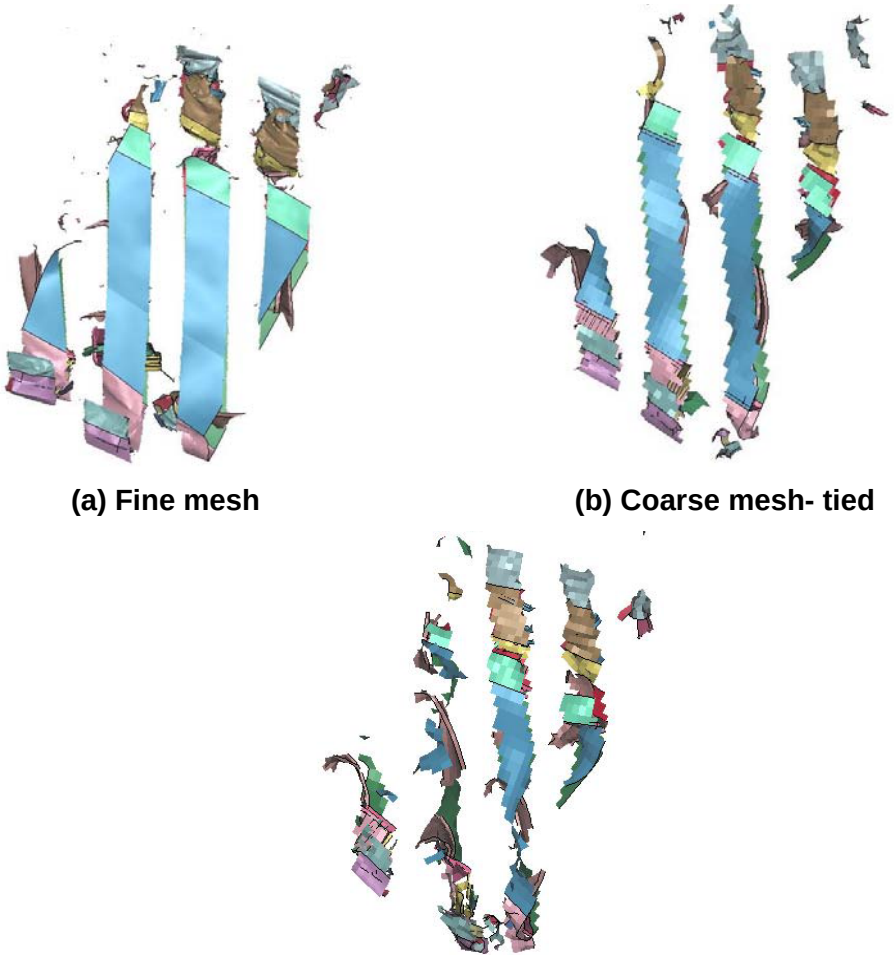

(a) Fine mesh **(b) Coarse mesh- tied**

(b) Coarse mesh- tiebreak

Figure 5–35. Fine and coarse mesh fragmentation.

The calculated impact response for the final coarse wing section model is shown in Figure 5–37. The corresponding damage to the exterior panels is shown in Figure 5–38. The calculated impact behavior was reasonably close to that of the detailed wing section response shown previously in Figure 5–31 and Figure 5–32. The tabulated true stress-plastic strain data used in the final model for the various aircraft aluminum alloys are shown in Figure 5–36.

Overall, the coarse-mesh model did a reasonable job of approximating the fine-mesh behavior despite the challenge of simulating the tearing and fragmentation of aluminum with such large elements. In both cases the damage extended over approximately one floor, and the columns were still intact. The front plate was pushed inward, but did not fail. The side flanges were also bent inward, but did not fail. The back plate sustained minor damage. Most of the difference in damage appeared to be in the side flanges, resulting in larger internal energy absorption in the panel. The larger elements of the wing section and their limited ability to conform well with the column geometry resulted in more damage to these flanges. Despite the coarse wing section having a lower residual kinetic energy, the wing broke up in a similar

fashion to the finely meshed model, as shown by the debris in Figure 5–35(a) and (b). This debris had more eroded material and, therefore, less mass and kinetic energy, because of the inability of large elements to smoothly conform to the line of material tearing.

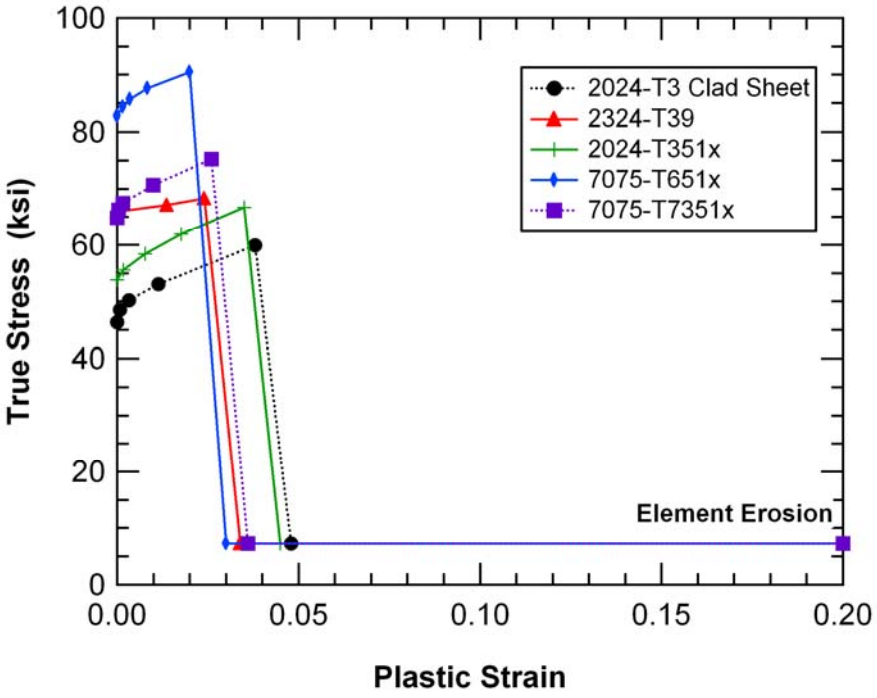

Figure 5–36. Aluminum model for coarse-mesh aircraft components.

A final check of the methodology developed here for failure of the coarsely meshed aircraft components is the visible impact results from the global analysis. As will be further discussed in Chapter 9, the damage pattern predicted in the global analyses agreed reasonably well with that observed in photographs. This is even true in the outboard parts of the wings where there was no fuel and the exterior columns did not completely fail.

5.5.2 Modeling of Aircraft Wing Section Impact with Fuel

A significant portion of the weight of a Boeing 767 wing is from the fuel in its integral fuel tanks. At the time of impact, it is estimated that each aircraft had approximately 10,000 gal of fuel onboard. Upon impact, this fuel was responsible for large distributed loads on the exterior columns of the WTC towers and subsequently on interior structures, as it flowed into the building. Therefore, it could have a significant effect on the damage inflicted on the building structure. Modeling of the fluid-structure interaction is necessary to predict the extent of this damage and the fuel dispersion within the building to help establish the initial conditions for the fire dynamics modeling.

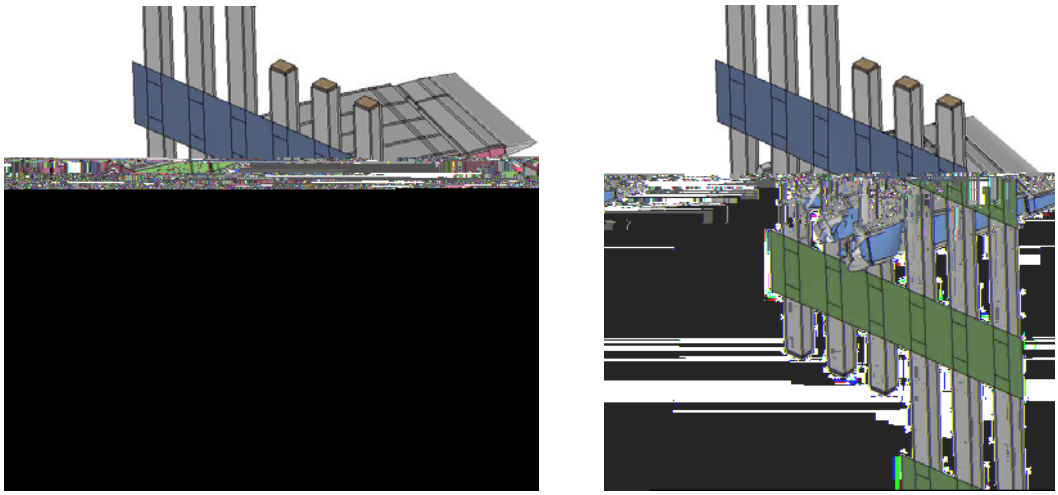

t = 0.0 s

t = 0.01 s

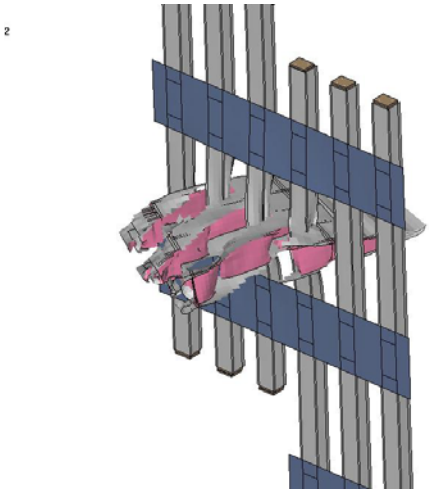

t = 0.02 s

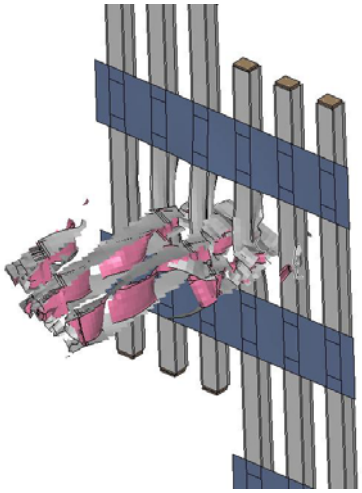

t = 0.03 s

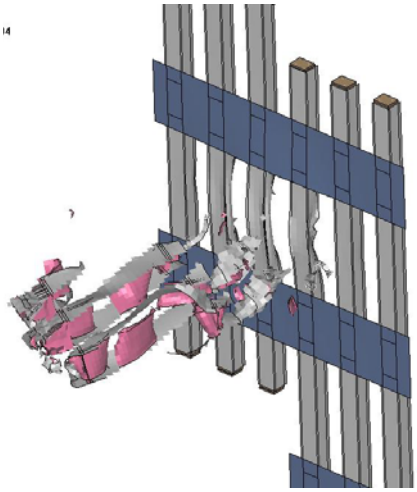

t = 0.04 s

Figure 5–37. Calculated impact of a coarse-mesh empty wing section with two exterior panels at 442 mph.

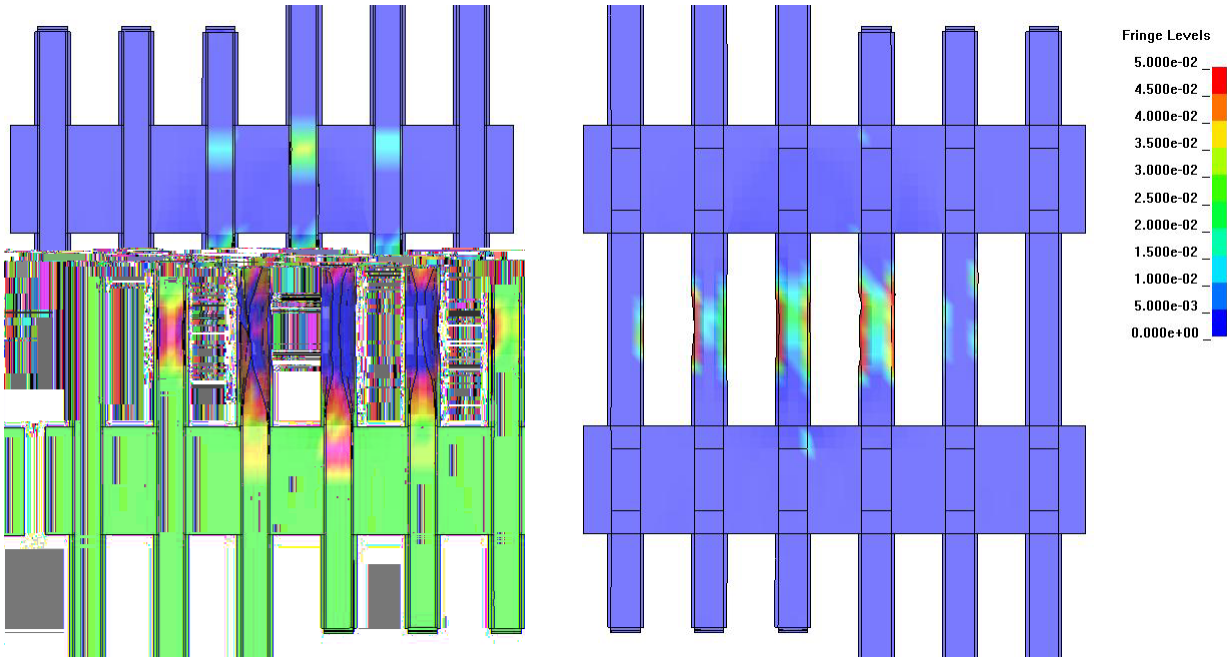

(a) Front (building exterior) **(b) Back (building interior)**

Figure 5–38. Impact damage to the exterior panel from a coarse-mesh empty wing section at 442 mph contours of effective plastic strain are shown.

A number of approaches to solving Fluid-Structure Interaction (FSI) problems are available in LS-DYNA. One approach is the standard Lagrangian finite element analysis with erosion, where the fuel is modeled using a deformable mesh. This approach accounts for the inertial effects of the fuel, but does not simulate the fuel flow during impact well due to limitations on mesh distortion. The Arbitrary-Lagrangian-Eulerian (ALE) method has been developed as one good approach to solve fluid and solid material interaction. With this methodology, fluids are modeled with an Eulerian mesh, which allows for materials to flow between mesh elements. Solid materials are modeled with a moving Lagrangian mesh. With ALE, both mesh types can interact.

An alternative approach is to use mesh-free methods such as Smoothed Particle Hydrodynamics (SPH). SPH modeling for fuel effects has the advantage of a smaller mesh size and, potentially, much faster run times than ALE analyses. Both ALE and SPH methods were applied to the analysis of fuel impact and dispersion and are compared here.

5.5.3 Impact Analysis of a Wing Section with Fuel

The small wing segment was used for performing component level analyses of the wing with fuel. The small wing segment was from rib 14 to rib 18, the outboard baffle rib. For this location, the segment was considered to be completely filled with fuel (approximately 850 gal). Figure 5–39 shows the fuel-filled wing section model with an SPH and ALE mesh for the fuel, shown in blue. The fuel was modeled with 6,720 SPH fuel particles and 110,825 ALE elements for the fuel and surrounding air region, shown in Figure 5–40. The wing section model was finer than that for the empty wing component analysis (24,000 shell elements for this model versus 8,200 in the previous analysis).

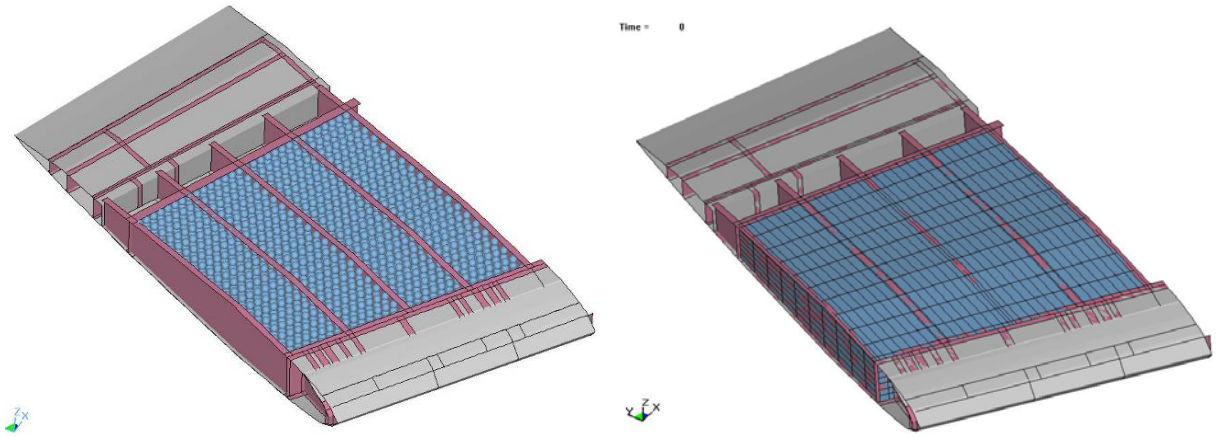

(a) SPH mesh **(b) ALE mesh**

Figure 5–39. SPH and ALE fuel in the small wing segment.

For these component analyses, the impacted structures were the same two exterior panels used in the empty wing section analysis described in Section 5.5.1. Model size and parameters are shown in Table 5–3. The exterior panel also contained 48 beam elements for the bolts connecting the butt plates. In these initial wing section impact analyses, water was used to model the fuel, although it was later changed to JP-4 jet fuel for the global analyses. The only significance of using water in the analyses here was that the density of water is 62.3 lb/ft^3 where that for JP-4 is approximately 48.3 lb/ft^3.

Table 5–3. Wing with fuel component modeling parameters.

	Exterior Panel	Wing Component
Shell Elements	54,096	23,733
Solid/ALE Elements	2,112	110,825
Mass	16,854 lb	1,014 lb

The model configuration for the component analysis with an ALE treatment of the fuel is shown in Figure 5–40. An ALE mesh surrounding the wing segment and the panels was needed for the fuel to flow into. In ALE analyses, material is advected from one element to the next so that a mesh is needed for initially "empty" regions. In this case, this mesh was filled with stationary air to interact with the fuel. The wing segment trajectory was that of a normal impact at 500 mph at mid-height between spandrels. The wing was oriented with no pitch, yaw, or roll. Therefore, the leading edge impacted the panels with the sweep angle of the wing relative to the fuselage, as shown in Figure 5–41. The two exterior panels were constrained rigidly at the butt plates and at the floor slab locations. For comparison, it is important to note that subsequent runs of the empty wing section at a speed of 500 mph, not specifically discussed in the previous section, resulted in more damage than shown in Figure 5–38, but still did not completely fail the columns.

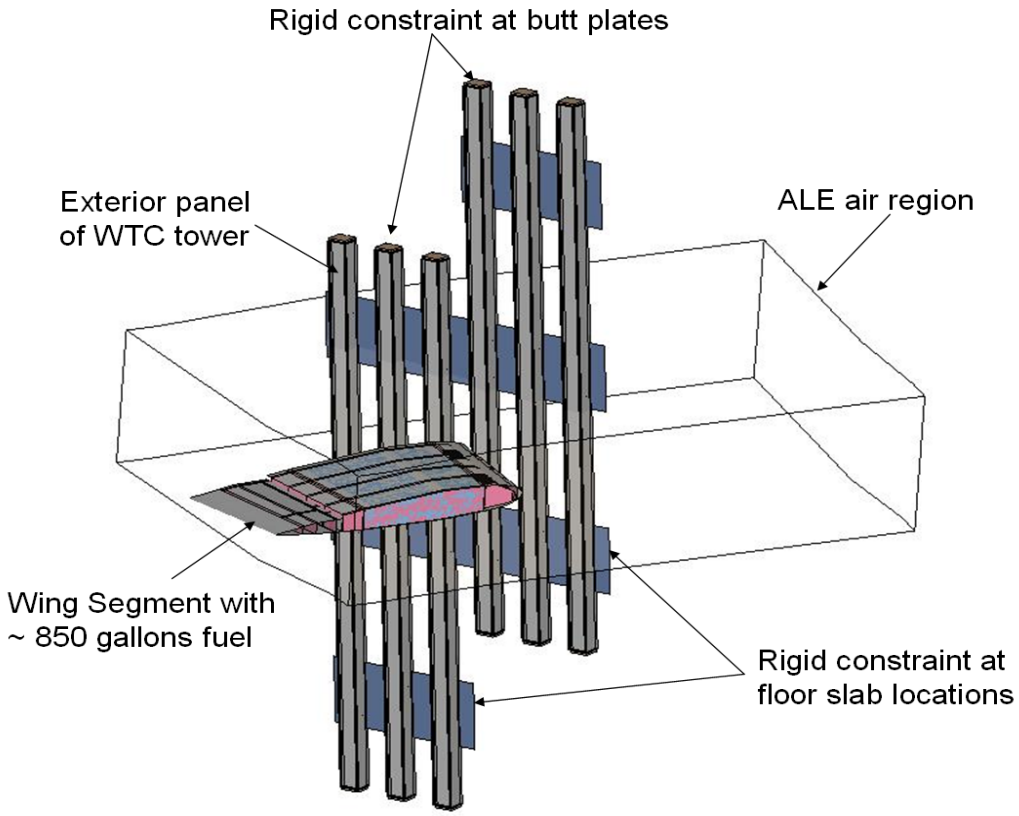

Figure 5–40. Wing segment, fuel, and exterior panel configuration.

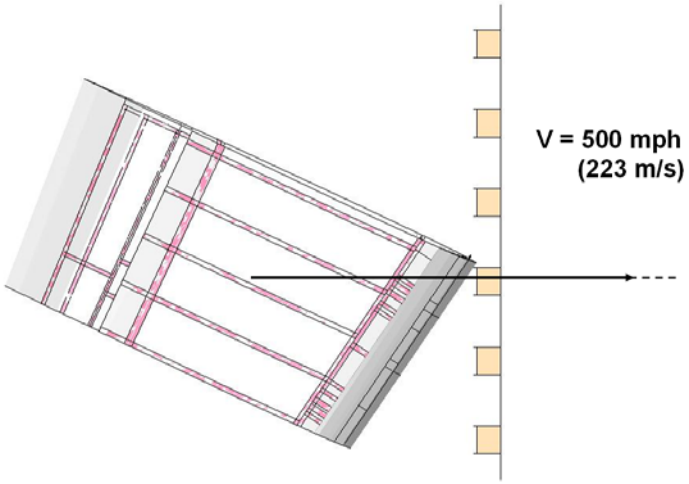

Figure 5–41. Wing segment orientation prior to impact.

Fuel was modeled with both the ALE and SPH models using the MAT_NULL material model and Gruneisen equation of state model. The pressure in the Gruneisen equation of state is estimated as

$$p = \frac{\rho_o C^2 \mu[1 + (1 - \frac{\gamma_0}{2})\mu - \frac{a}{2}\mu^2]}{[1 - (S_1 - 1)\mu - \frac{\mu^2}{\mu + 1}S_2 - \frac{\mu^3}{(\mu + 1)^2}S_3]^2} + (\gamma_o + a\mu)E \quad (1)$$

for compressed materials and

$$p = \rho_o C^2 \mu + (\gamma_o + a\mu)E \quad (2)$$

for expanded materials. The E is the internal energy, $\mu = \rho/\rho_o - 1$, and ρ is density. Air in the ALE mesh was modeled as an ideal gas using the Ideal Gas equation of state model. Parameters for these models are shown in Table 5–4. The reader is referred to the LS-DYNA user's manual (2003) for a more complete description of these models. These material models were used in order to appropriately treat the constitutive behavior of the fuel, which had no deviatoric strength, only a viscosity. However, the constitutive behavior is of secondary importance as the predominant effect of the fuel is an exchange of momentum with the impacted structure.

Table 5–4. Fuel and air model parameters.

	Fuel (Water)	Air
MAT_NULL		
Density - ρ_o (lb/ft^3)	62.3	0.0737
Dynamic Viscosity Coefficient (lb·s/ft^2)	1.82E-05	3.66E-07
EOS_GRUNEISEN		
C (in/s)	6.48E+04	-
S_1	1.921	-
S_2	-0.096	-
S_3	0.0	-
γ_o	0.35	-
Eo (ft-lb)	2.14e+05	-
EOS_ IDEAL_GAS		
C_p (Btu/lb·F)	-	0.172
C_v (Btu/lb·F)	-	0.240
T_o (R)	-	1,028
V_o	-	1.0

Fluid-structure interaction was modeled using two separate algorithms, one for ALE and the other for SPH. The first, when using an ALE mesh for fuel, is the CONSTRAINED_LAGRANGE_IN_SOLID algorithm. The second, for an SPH fuel mesh, is the automatic nodes to surface contact algorithm. The

reader is referred to the LS-DYNA user's manual for a more complete description of both the ALE and SPH approaches for solving fuel-structure interaction problems.

Impact of the wing section using the ALE and SPH methods are shown in Figure 5–42 and Figure 5–43, respectively. In both cases the columns of the exterior panels were completely destroyed due to impact. Recall that this was not the case for the empty wing section with an equivalent initial impact speed. Close-ups of the damage to the exterior panels are shown in Figure 5–44. Figure 5–45 through Figure 5–48 show close-up plan and side view comparisons of the fuel dispersion and wing break up predicted by the two fuel modeling methods. While both modeling approaches gave comparable results for the damage to the exterior wall panels, the SPH modeling method predicted greater fuel dispersion and wing break up than when using ALE, as can be shown clearly in the side view. Without experimental data, it is difficult to evaluate which method provides a more accurate solution.

Run-times from these component analyses clearly indicate that the SPH method is more practical for the global impact analyses. The current SPH model runs significantly faster than the ALE method as it requires a smaller mesh and does not need to rezone after each time step, as is done in the ALE method. In addition, the ALE method requires a mesh for both the fuel region and the air zone into which the fuel can flow. In the example shown, this required the addition of approximately 100,000 solid elements for the ALE analysis. These calculations indicate that the ALE analysis run-times are as much as 10 times longer than those for the SPH analyses. Therefore, the SPH method was selected as the modeling technique for the global analyses.

5.6 SUMMARY

The set of engine impact analyses described in this chapter demonstrates how an engine traveling at speeds of approximately 500 mph completely overwhelms a single column. Therefore, such component analyses are not as useful as desired in determining the sensitivity of modeling parameters in the impact response. A final configuration consisting of twenty interior core columns was developed for performing the uncertainty analyses during engine impact. This analysis is described further in Chapter 8.

The WTC towers and Boeing 767 aircraft are extremely complex structural systems, and including all of the structural details of both the aircraft and towers in the global impact analyses would result in very large models. The component analyses were used to determine model simplifications that could reduce the overall model size while maintaining fidelity in determination of the impact damage.

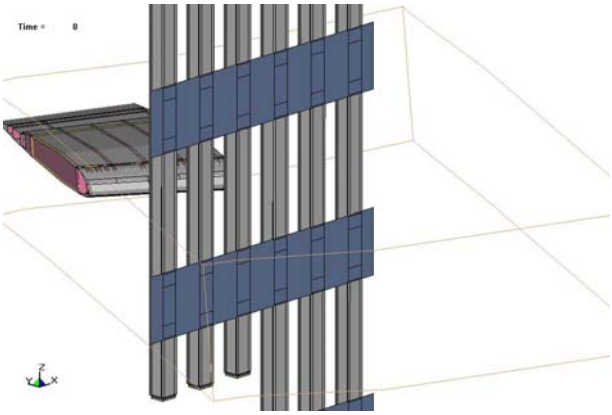

t = 0.0 s

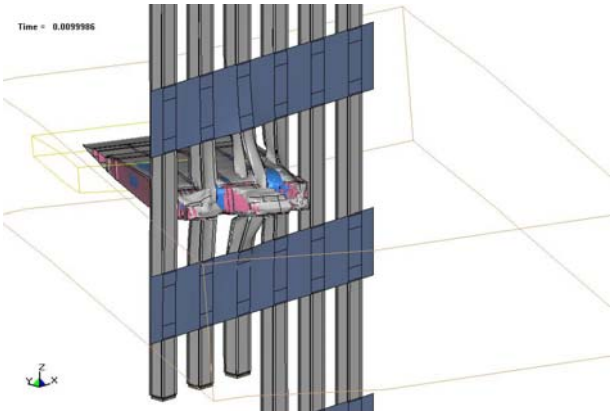

t = 0.01 s

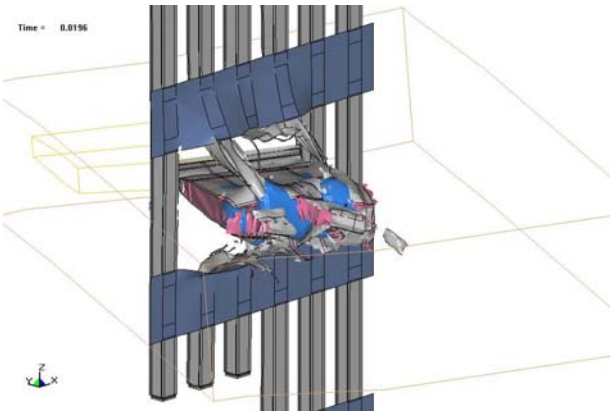

t = 0.02 s

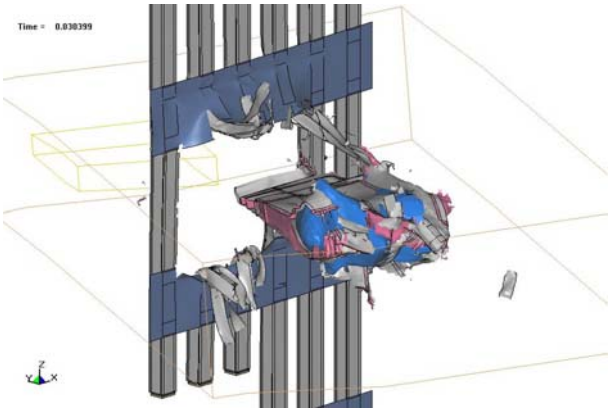

t = 0.03 s

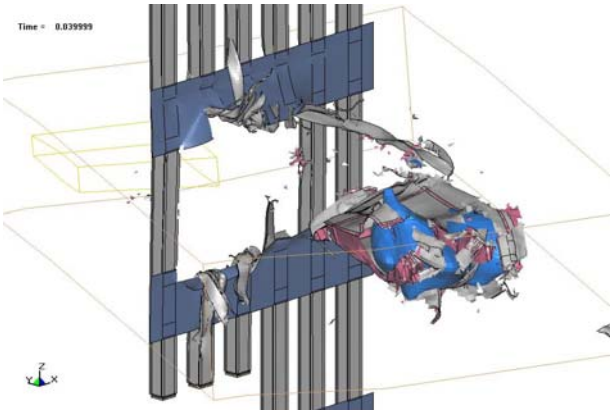

t = 0.04 s

Figure 5–42. Calculated impact of a coarse mesh wing section laden with fuel modeled using ALE elements.

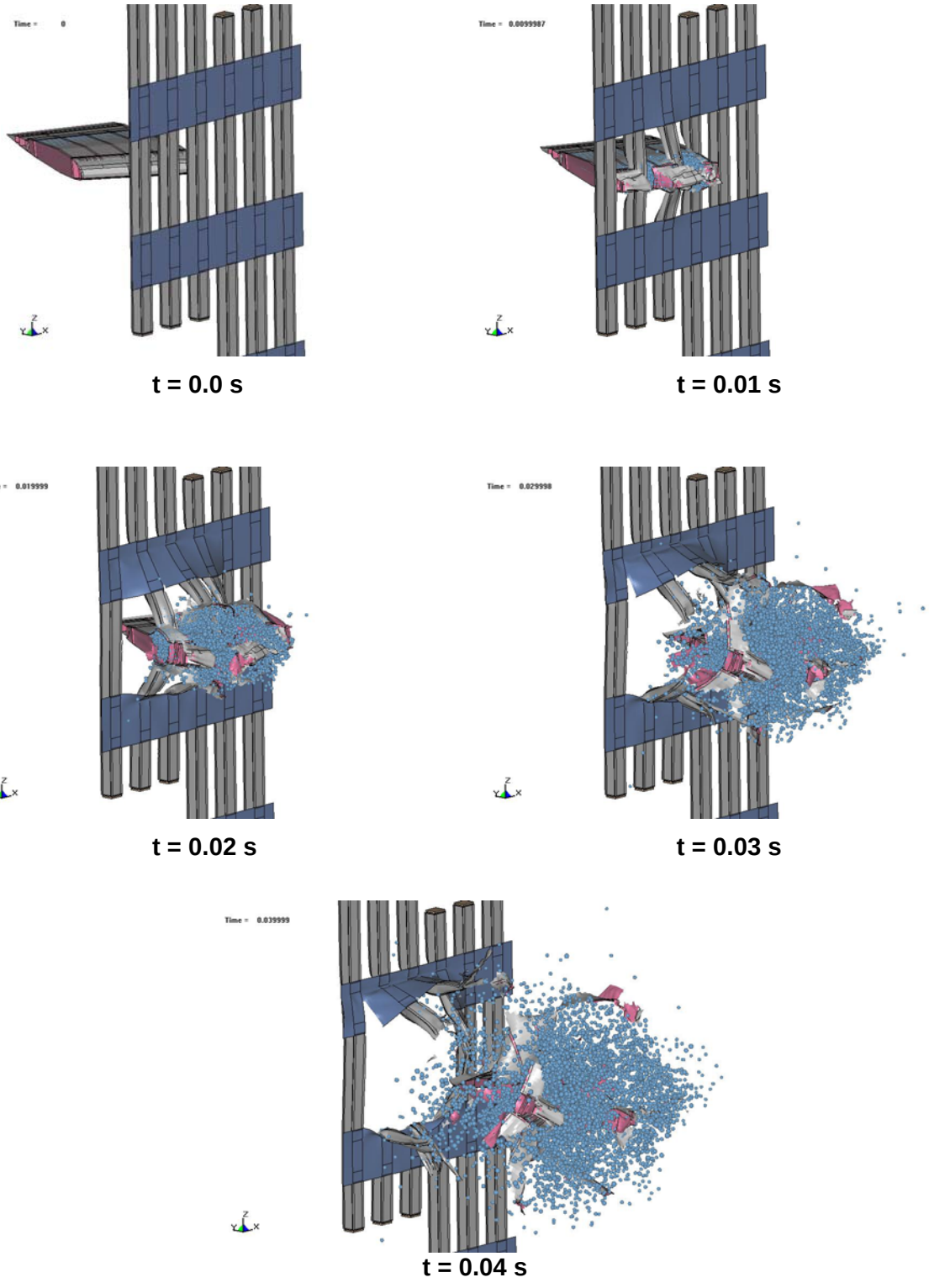

Figure 5–43. Calculated impact of a coarse mesh wing section laden with fuel modeled using SPH particles.

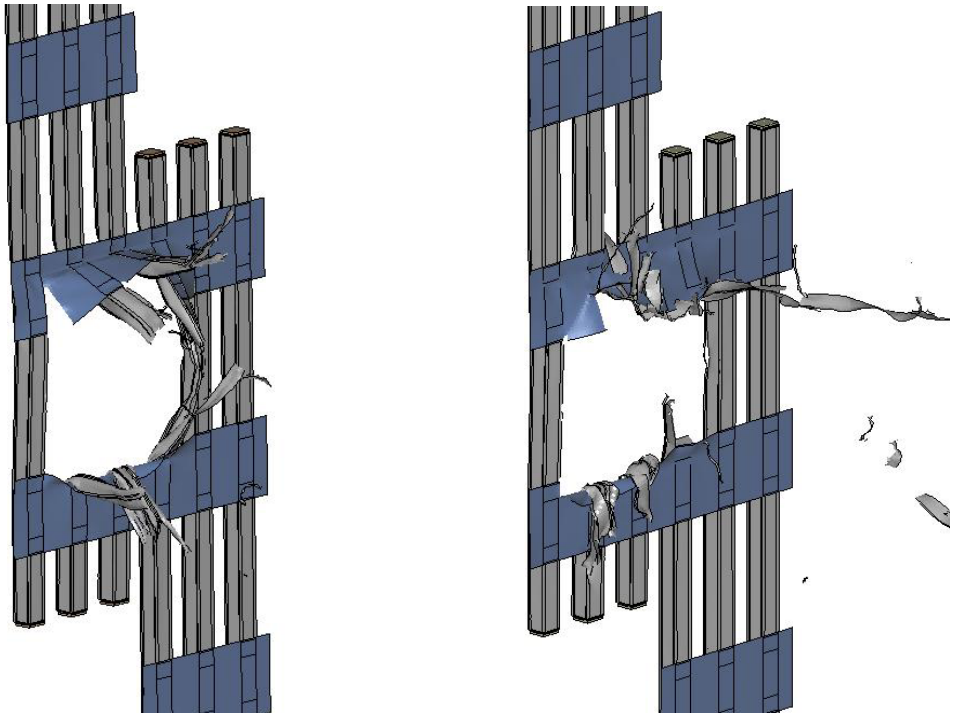

(a) With SPH fuel **(b) With ALE fuel**

Figure 5–44. Exterior panels after impact with a wing segment with fuel.

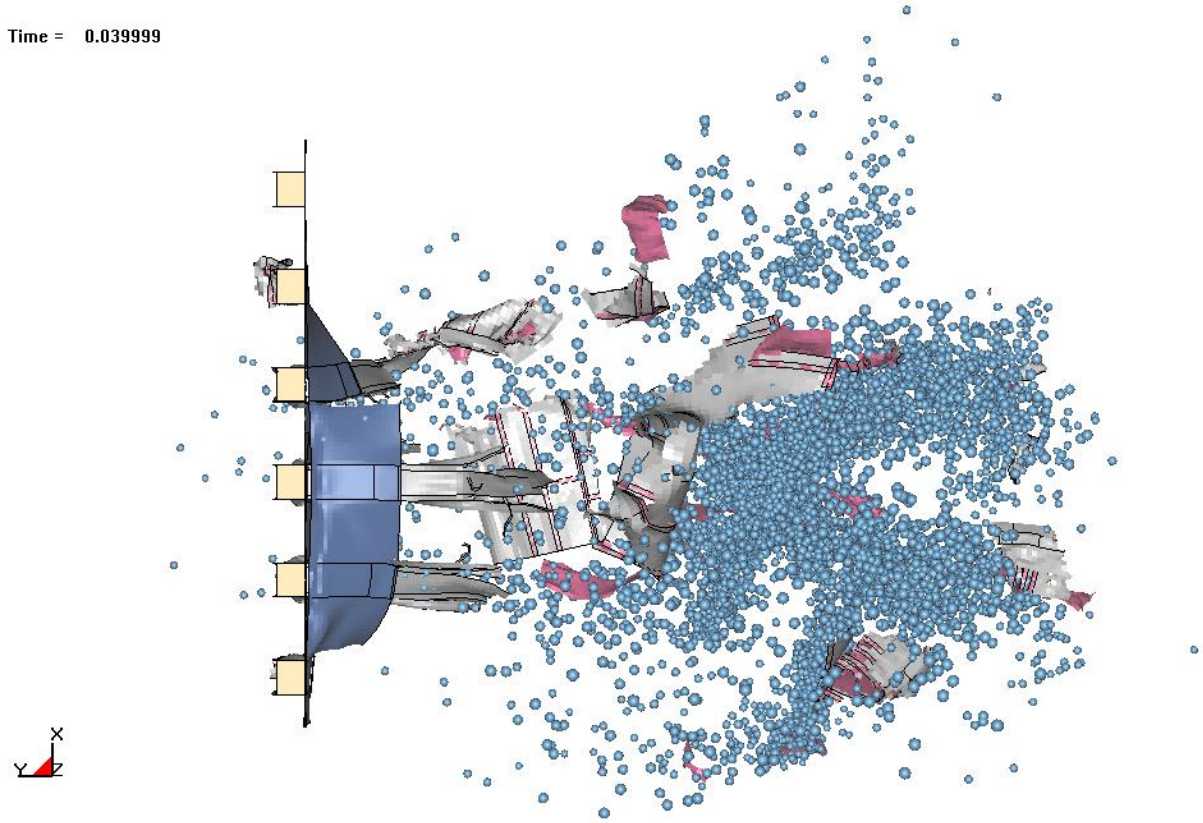

Figure 5–45. SPH analysis of structural damage and fuel dispersion at 0.04s (top view).

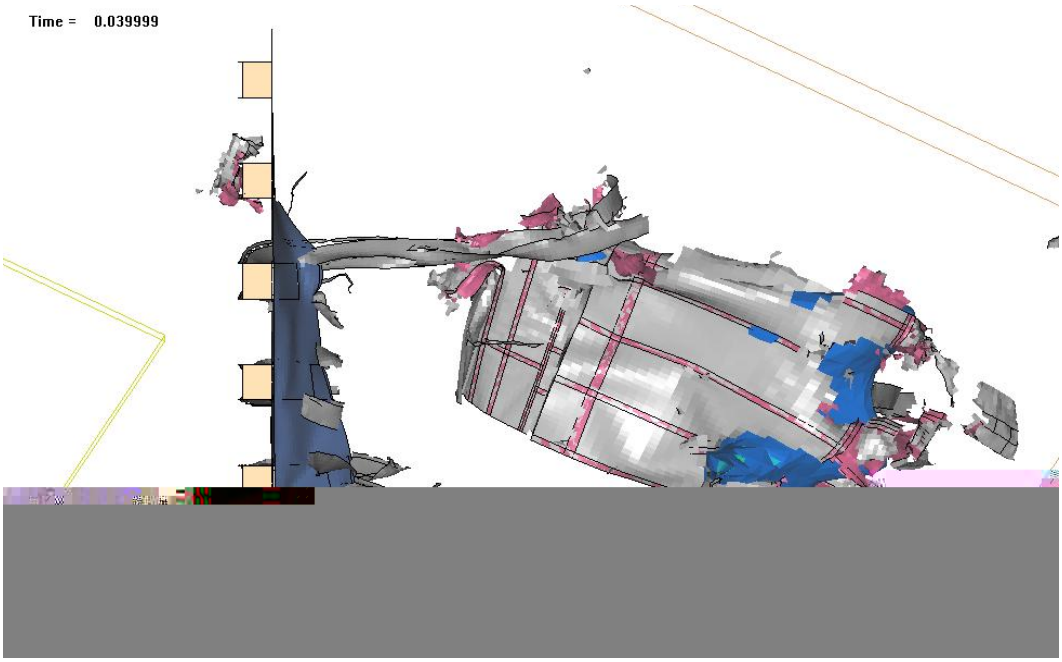

Figure 5–46. ALE analysis of structural damage and fuel dispersion at 0.04s (top view).

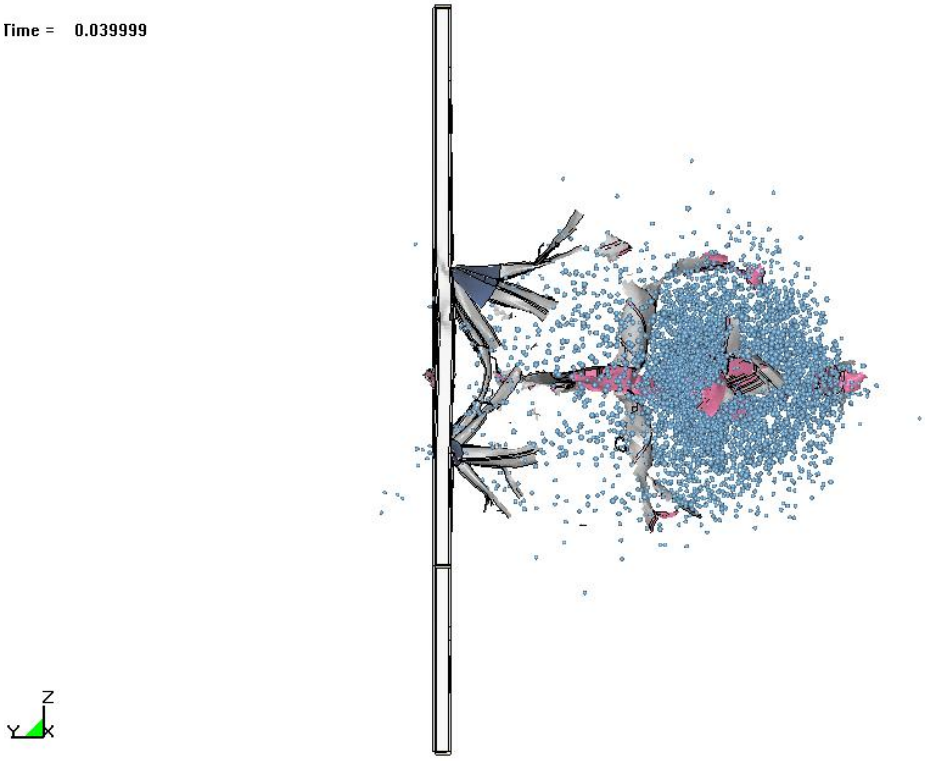

Figure 5–47. SPH analysis of structural damage and fuel dispersion (side view).

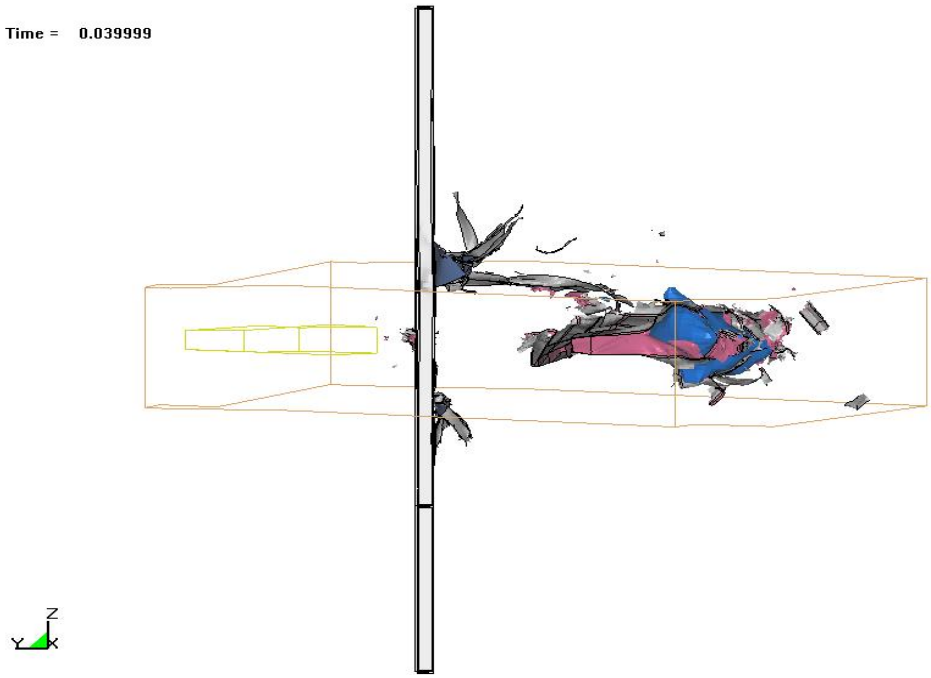

Figure 5–48. ALE analysis of structural damage and fuel dispersion (side view).

A series of component impact analyses were performed using models of tower exterior columns, core columns, and floor assemblies with wing section and engine models as impactors. These models were used to develop the simulation techniques required for the global analysis of the aircraft impacts into the WTC towers. The following results were obtained from the component impact analyses:

- A 500 mph engine impact against an exterior wall panel resulted in a penetration of the exterior wall and failure of impacted exterior columns. If the engine did not impact a floor slab, the majority of the engine core remained intact through the exterior wall penetration with a reduction in velocity between 10 percent and 20 percent. The residual velocity and mass of the engine after penetration of the exterior wall was sufficient to fail a core column in a direct impact condition.

- A normal impact of the exterior wall by an empty wing segment outboard of rib 14 of the Boeing 767 wing produced significant damage to the exterior columns, but not necessarily complete failure. This is consistent with photographs showing the exterior damage to the towers due to impact.

- A fuel-filled wing section impact resulted in complete failure of the exterior columns. This is also consistent with photographs of the exterior damage. The resulting debris propagating into the building maintained the majority of the initial momentum prior to impact.

- Three different numerical techniques were investigated for modeling impact effects and dispersion of fuel: (1) standard Lagrangian finite element analysis with erosion, (2) Smoothed Particle Hydrodynamics (SPH) analysis, and (3) Arbitrary-Lagrangian-Eulerian (ALE) analysis. Of these approaches, SPH analyses were adopted for modeling fuel in the global impact analysis due to computational efficiency.

5.7 REFERENCES

FEMA 304, May 2002, *World Trade Center Building Performance Study: Data Collection, Preliminary Observations, and Recommendations*, Federal Emergency Management Agency.

Hallquist, J.O., "DYNA3D User's Manual (Nonlinear, Dynamic Analysis of Solids in Three Dimensions)," University of California, Lawrence Livermore National Laboratory, Report UCID-19156, Revision 2, 1986.

"LS-DYNA Keyword User's Manual," Livermore Software Technology Corporation, Version 970, April 2003.

"LS-DYNA Theoretical Manual," Livermore Software Technology Corporation, May 1998.

"TrueGrid Manual, Version 2.1.0," XYZ Scientific Applications, Inc., September 2001.

Chapter 6
SUBASSEMBLY IMPACT ANALYSES

6.1 INTRODUCTION

The subassembly analyses are a transition between the component analyses described in Chapter 5 and the global impact analyses described in Chapter 9. The analyses were separated into two primary sets: preliminary and final subassembly analyses. The preliminary subassembly analyses were used mainly to investigate different modeling techniques and associated model size, run times, numerical stability, and impact response. These preliminary subassembly analyses were performed concurrently with the component analyses described in Chapter 5. Therefore, many components in the preliminary subassembly model were not those ultimately used in the global impact models. As a result, some of the constitutive properties, failure criteria, and mesh resolutions were modified later. An example of these preliminary subassembly analyses is presented in this Chapter.

The final subassembly analyses were performed using the same modeling methodologies as the global impact analyses, described in Chapter 9. The constitutive models and mesh refinement were identical to those used subsequently in the impact zone of the global impact analyses. The final subassembly model was used to investigate the sensitivity of the impact response to modeling parameters, as well as for the uncertainty analyses described in Chapter 8.

6.2 PRELIMINARY SUBASSEMBLY ANALYSES

A preliminary analysis of the tower subassembly impacted by an aircraft engine was performed using the tower structures in the impact area of World Trade Center (WTC) 1. The subassembly model for this analysis consisted of a single width exterior panel (panel number 121A), three floor assemblies (floor 95 to floor 97) of the same width extending from the exterior panel to the core, and two core columns, as shown in Figure 6–1. The core framing and slab were not included in the model with the exception of the core perimeter beams. The core columns used in the model were numbers 503 and 603 between floor 94 and floor 98. A detailed model of the truss floor structure was used. The floor model contained many more elements than the subsequent truss floor model used in the global impact analyses. The concrete slab was modeled with brick elements, and the diagonal round bar members in the floor trusses were modeled with beam elements. The remainder of the structures, including the columns, metal decking, and truss upper and lower chord components, were modeled with shell elements. The final model contained approximately 793,000 nodes, 404,000 brick elements, 385,000 shell elements, and 11,000 beam elements.

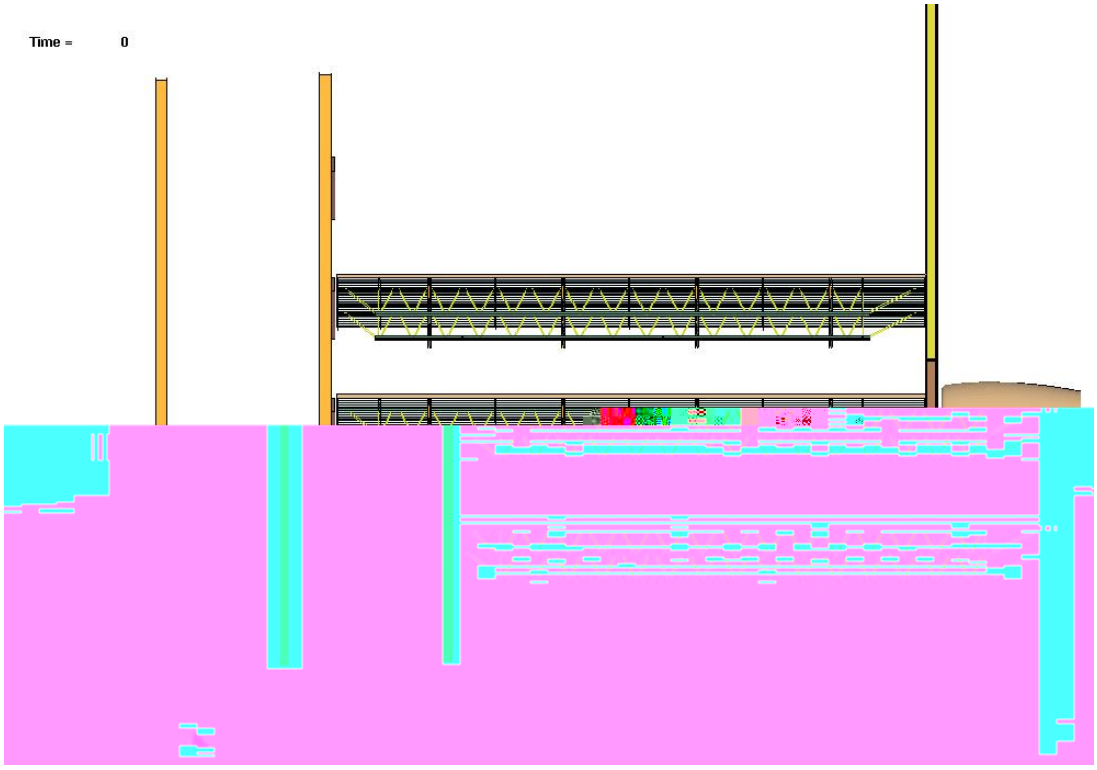

(a) Initial configuration

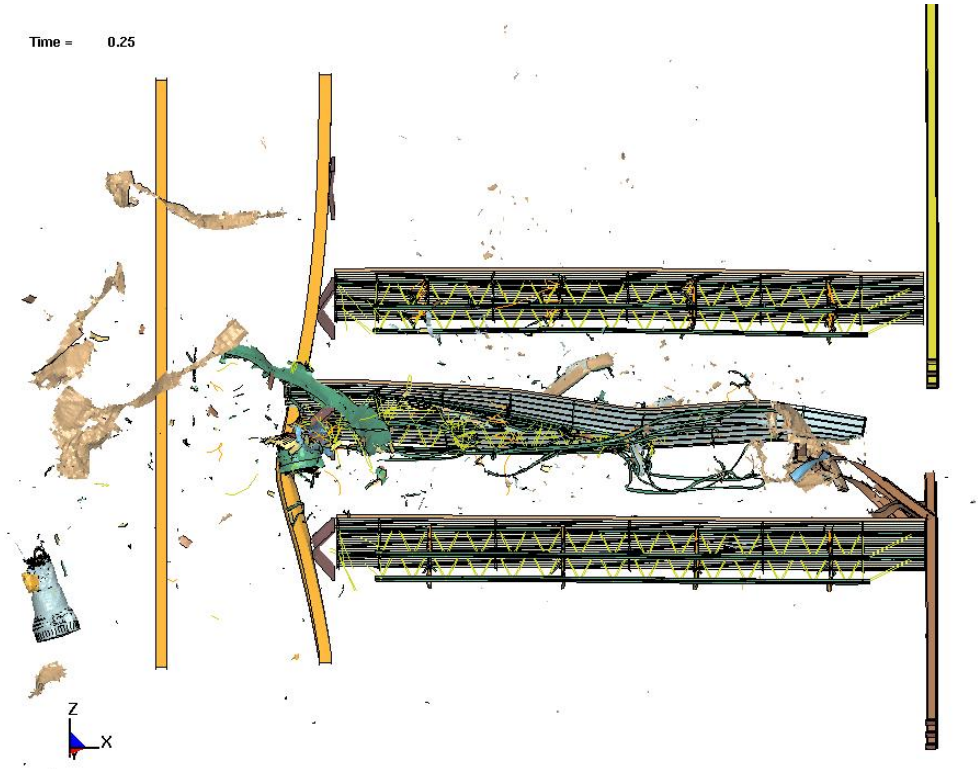

(b) Impact response at 0.25 s

Figure 6–1. Example engine impact subassembly analysis.

The impact response of the tower subassembly when impacted by an engine at 500 mph is shown in Figure 6–1(b) and Figure 6–2. Engine impact was centered on the spandrel at floor 96. The trajectory of the engine was normal to the exterior panel. The engine significantly penetrated the floor structure and caused significant damage to the core column (503) upon impact.

Figure 6–2. Oblique view of the subassembly engine impact damage.

The impact response of this preliminary subassembly model was influenced by many of the preliminary modeling assumptions applied. Unconstrained boundary conditions on the side of the floor slab influenced the deformation of the truss floor structures. In addition, the concrete in this analysis was assumed to have an unconfined compressive strength of 3 ksi and strain rate hardening was not yet included in the concrete constitutive model. The result was an over estimation of the impact damage to the floor structures in the model. However, the preliminary subassembly analyses still were useful in developing simplified models for the bolted column connections, as described in Section 5.2.3, and to refine the modeling approach for various impact conditions. Additional applications of the final subassembly models are described in the following sections.

6.3 FINAL SUBASSEMBLY ANALYSES

The final subassembly model was developed using structural components from the impact zone on the north face of WTC 1 (Side 100). The model, shown in Figure 6–3, was used to further evaluate the response of structural connections, material and failure models, and other issues affecting global impact analyses. The model was three floors tall, spanning floors 95–97, three exterior panels wide, and extended from the exterior wall through to the first two rows of core columns. The core columns included in the subassembly model were column numbers 502–504 and 602–604. The exterior wall in the subassembly model included the exterior panels that extended into floors 95–97, as well as two panels above and below the panel spanning all three floors. Exterior column numbers in the model ranged from

column 117 through 125. The structural components in the final subassembly model included the exterior panels, core framing, truss floor structures, and interior contents (workstations). These structural components are shown separately in Figure 6–4. The concrete slab in the core was not included in this model.

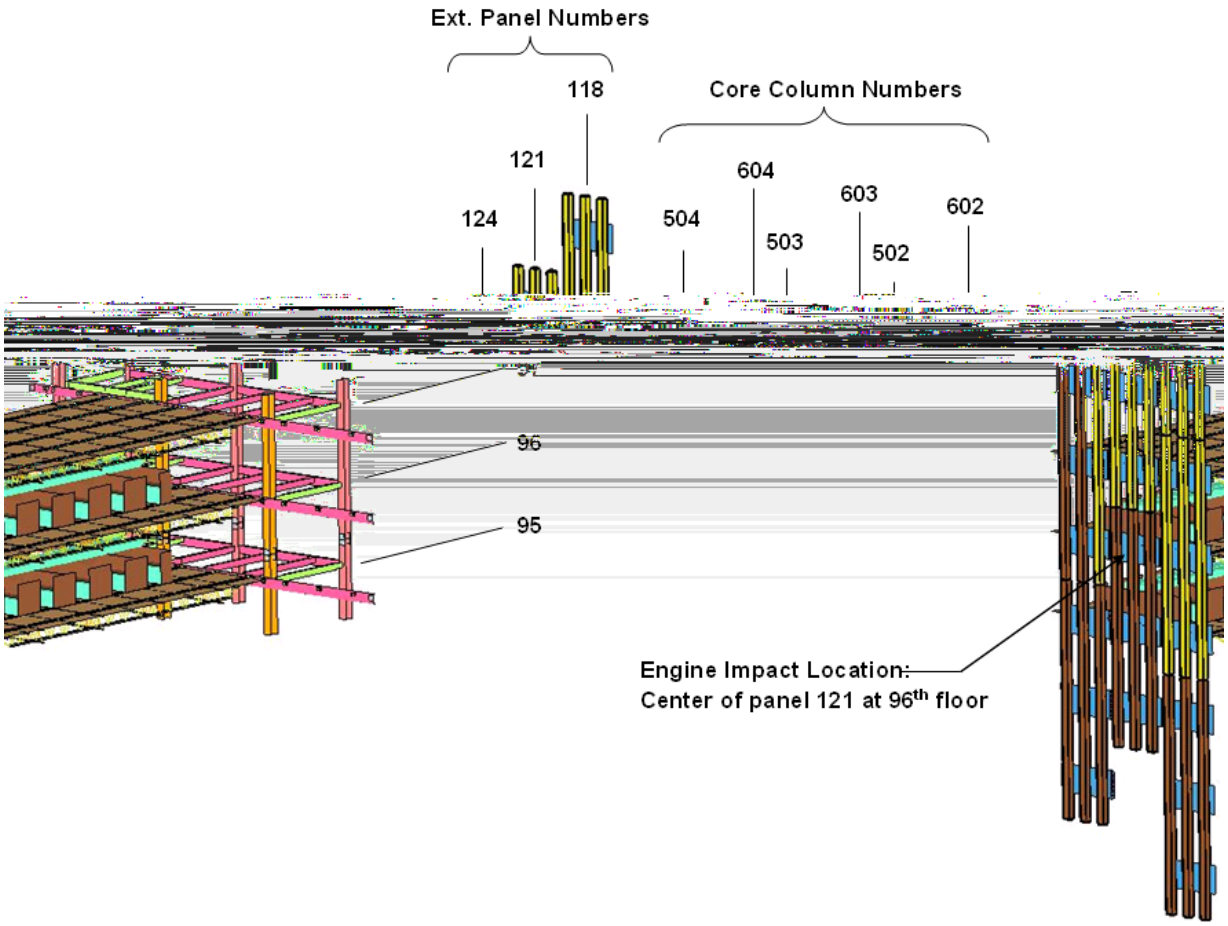

Figure 6–3. Final WTC tower subassembly model.

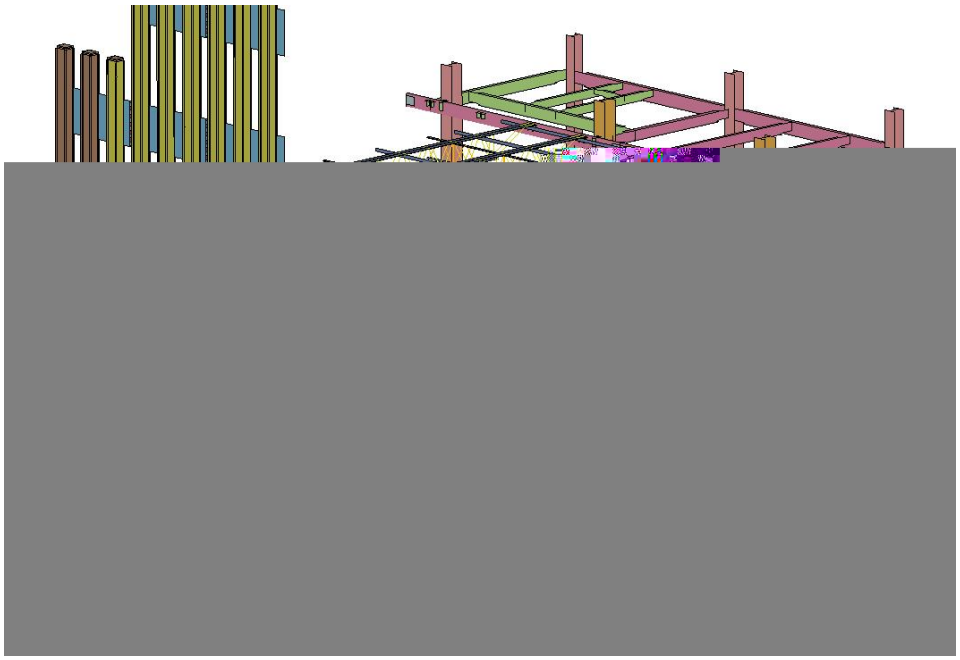

(a) Framing for the subassembly model

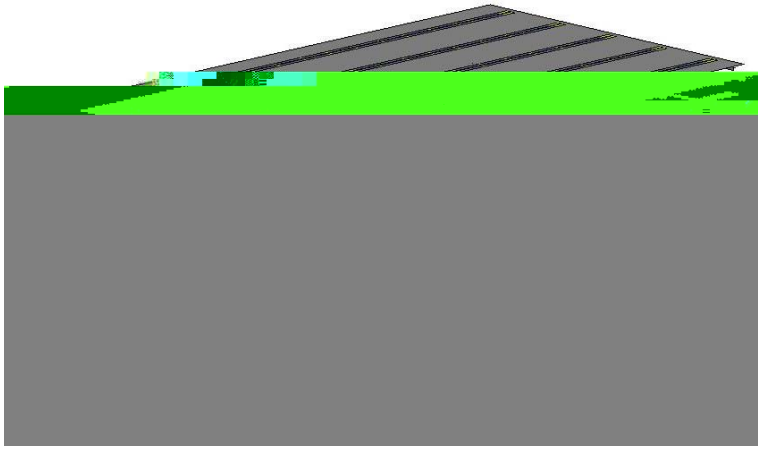

(b) Truss floor components in the subassembly model

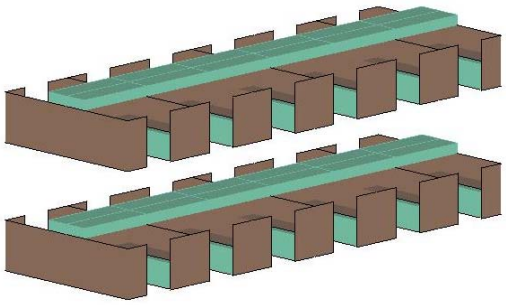

(c) Workstations in the subassembly model

Figure 6–4. Details of the final WTC tower subassembly model.

The vertical displacements were constrained at the top and bottom of the free ends of the core columns. For the exterior columns, a bolted connection was added to an adjacent butt plate for which the vertical motions were constrained. The lateral displacements were constrained at the free spandrel edges and at the sides of the truss floor structures. This model offered much more realistic boundary conditions on the impacted portion of the structure than the preliminary model discussed in Section 6.2. In addition, the greater width of the exterior wall and truss floor structures in this model reduced the influence of the boundary conditions on the impact response.

6.3.1 Engine Impact Subassembly Analyses

The engine model used in the subassembly analyses was based on the structural design information from the Pratt & Whitney PW4000 turbofan engine. The development of the engine model was described previously in Section 4.3.3. The objective of these analyses was to investigate the impact response to a variety of impact conditions while using different modeling methodologies. Most of these engine impact analyses are described in Chapter 8 as part of the uncertainty analyses. A few specific engine impact analyses are described here to illustrate the characteristic engine impact behavior and the effects of specific model parameters on the impact response.

The initial position and orientation of the aircraft engine in one sample calculation is shown in Figure 6–5. The engine had an initial velocity of 413 mph and a trajectory with a lateral approach angle of 4 degrees from the exterior panel normal and a vertical approach angle of 7.6 degrees below the horizontal. The impact point was centered approximately 6 ft below the 97th floor so that the initial impact did not engage a significant portion of the truss floor structures. The calculated impact response of the subassembly is shown in Figure 6–6. The engine penetrated the exterior wall and continued into the interior of the building along the initial downward trajectory. As the engine continued into the subassembly model, it plowed through the interior building contents (workstations) and eventually skipped off of the truss floor slab at the 96th floor.

A side view of the impact behavior at different times is shown in Figure 6–7. The engine penetrated the exterior wall following the initial downward trajectory. As the engine continued downward it impacted the workstations and the truss floor structures of floor 96. The engine motion was redirected by the impact with the truss floor and continued its motion toward the core, penetrating additional workstations. At a time of 0.25 s the engine entered the core as shown in Figure 6–7(c). The impact conditions of this analysis resulted in a collision of the engine with core column 503. The speed-time history of the engine core in this impact analysis is shown in Figure 6–8. The deceleration that occurred in the first 5 ms was primarily from the penetration of the exterior wall and the floor slab and truss of floor 97. This deceleration was larger than that observed in Section 5.2.4 by approximately 25 percent. The analysis in Section 5.2.4 was that of only exterior panels without any floors attached or boundary conditions to approximate their effect. This difference in deceleration was due to the reinforcing effect of the floor structure on the exterior panel, as well as impact with the floor structure.

Figure 6–5. Final subassembly model for engine impact analysis.

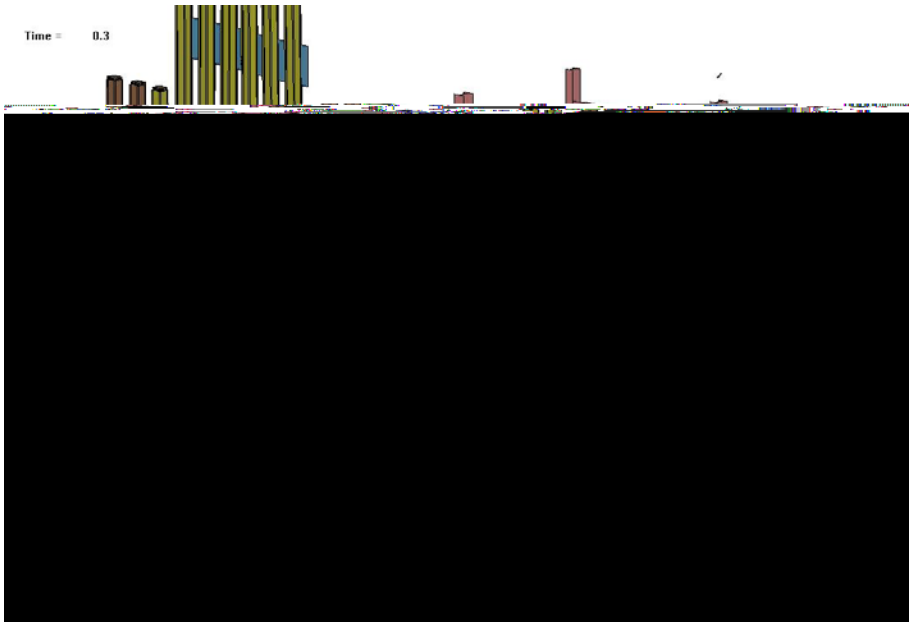

Figure 6–6. Calculated response for the baseline engine impact analysis.

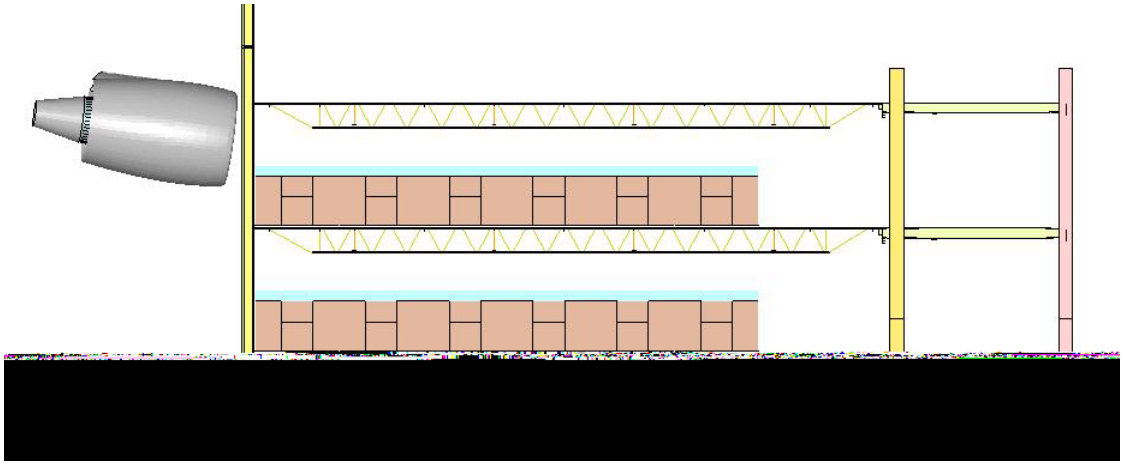

(a) Time = 0.00 s

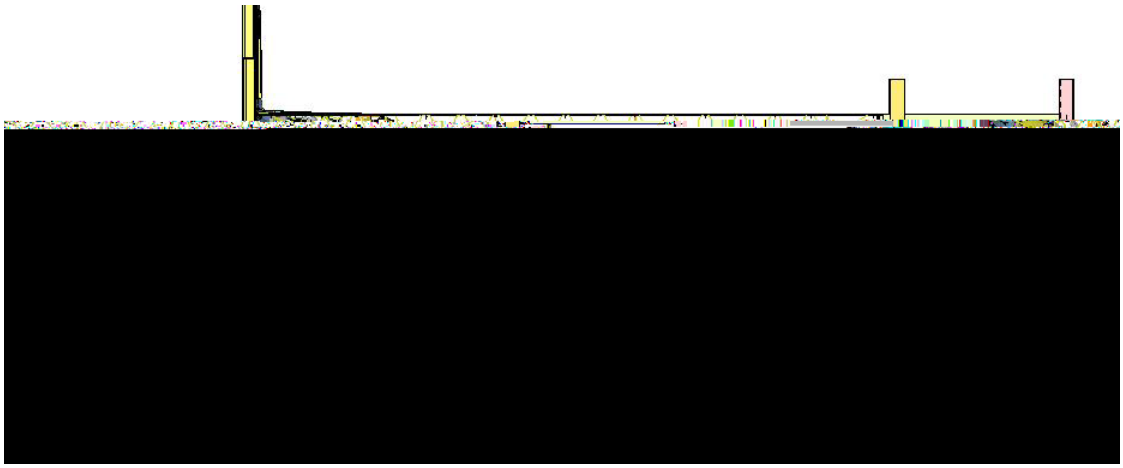

(b) Time = 0.05 s

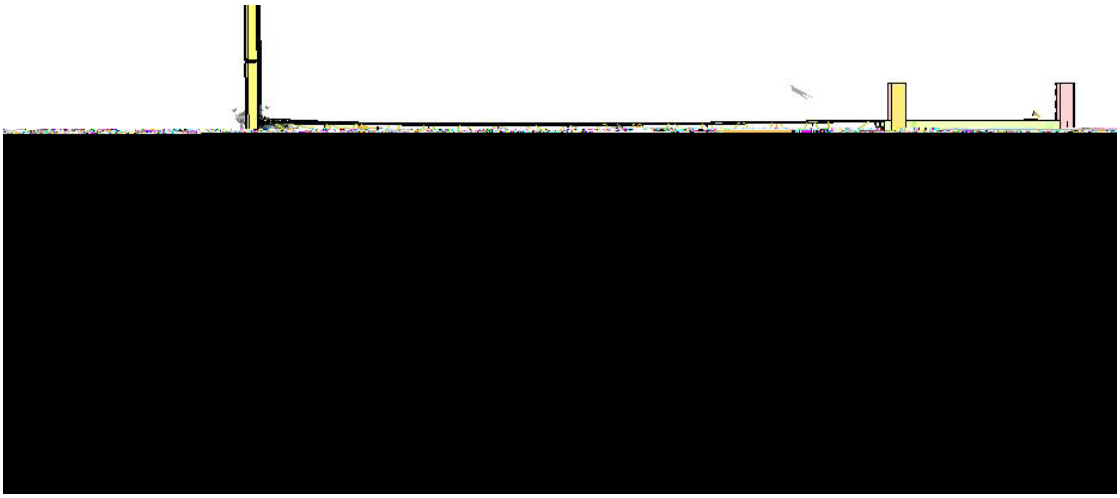

(c) Time = 0.25 s

Figure 6–7. Baseline engine impact and break up behavior (side view).

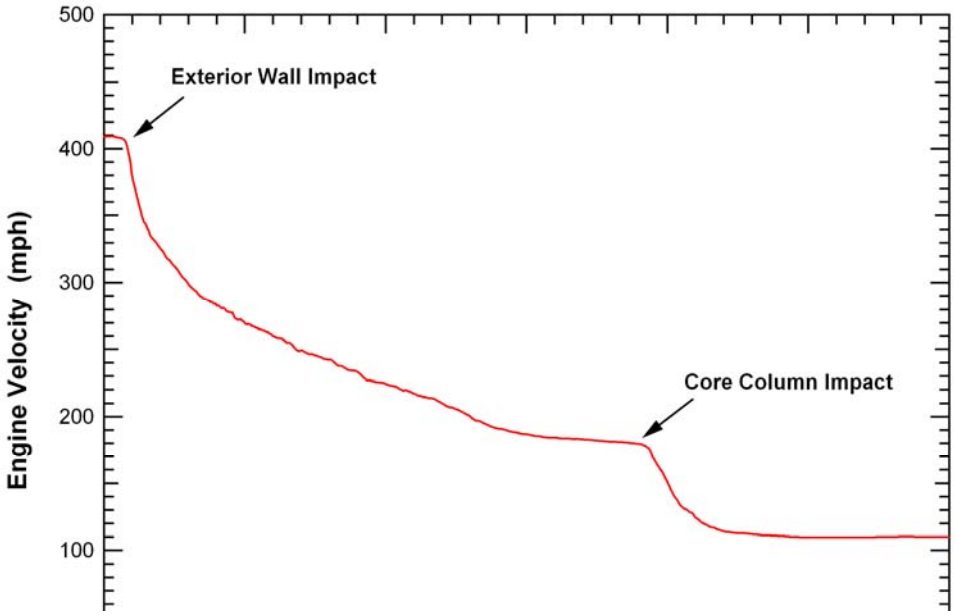

Figure 6–8. Speed history for the baseline engine subassembly impact analysis.

Building Contents Strength Effects

Two subassembly engine impact analyses were performed to investigate the influence of the strength of the building contents (in this case, workstations) on the impact response. The baseline strength of the building contents (partitions and workstations) was estimated to be 500 psi. As a comparison, the second calculation used identical impact conditions, but the building contents had virtually no strength (0.5 psi).

The deceleration histories for the engine core in the two subassembly analyses are compared in Figure 6–9. The deceleration that occurred in the first 3 to 5 ms was primarily from the penetration of the exterior wall. In this phase of the impact response, the engine speed was reduced from the impact speed of 413 mph to approximately 375 mph. The majority of the subsequent deceleration to a time of 0.25 s was the result of the engine impacting the workstations. For the 500 psi workstations, the engine was decelerated to a speed of 100 mph as the engine entered the core. The engine impacting the low strength workstations had a residual speed of 130 mph entering the core. Although there was a 30 mph difference in the impact response as a result of the workstation strength, the total loss of speed produced by the impact with the building contents was about 150 mph. Therefore, the deceleration was dominated by the mass of the workstations.

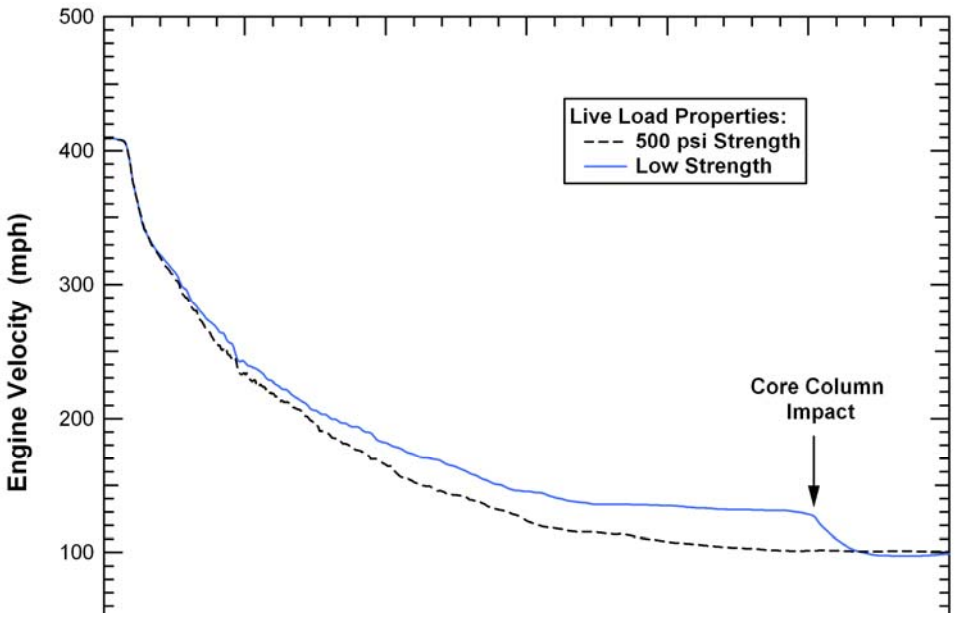

Figure 6–9. Effect of the building content strength on engine impact behavior.

Truss Floor Concrete Strength Effects

A pair of subassembly engine impact analyses was performed to investigate the influence of the floor concrete strength on the impact response. For this evaluation, initial conditions of the engine were selected so that there was significant interaction of the impacting engine with the truss floor structures, as shown in Figure 6–10. The building contents (workstations) are not visualized in Figure 6–10(b) and (c) so the engine impact response can be more clearly seen. The engine impact was close to being centered on the truss floor slab with a downward trajectory of 13.6 degrees and an impact speed of 473 mph. The impact response resulted in a significant penetration of the truss floor slab. As a result of the downward trajectory, the engine ended up on the lower of the two floors and at a time of 0.25 s was approaching the core structures.

The concrete used in the truss floor section was a lightweight concrete with a design compressive strength of 3 ksi. However, due to aging and material variation above the specified minimum strength, the expected strength of the truss floor concrete at the time of the impact was above the 3 ksi specification. The engineering estimate of the actual strength was approximately 4 ksi (NIST NCSTAR 1-6). This strength was used in the majority of the analyses in this study. To demonstrate the effect of the concrete strength on the impact behavior, an additional engine subassembly impact analysis was performed with the specified 3 ksi strength to demonstrate the influence of the concrete strength on the impact behavior.

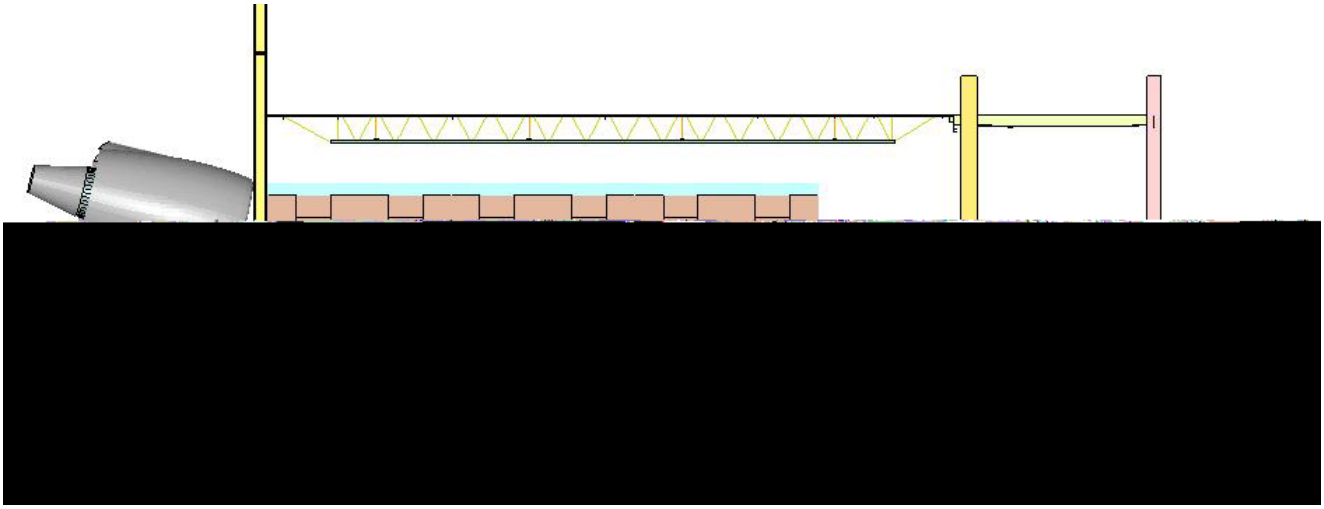

(a) Time = 0.00 s

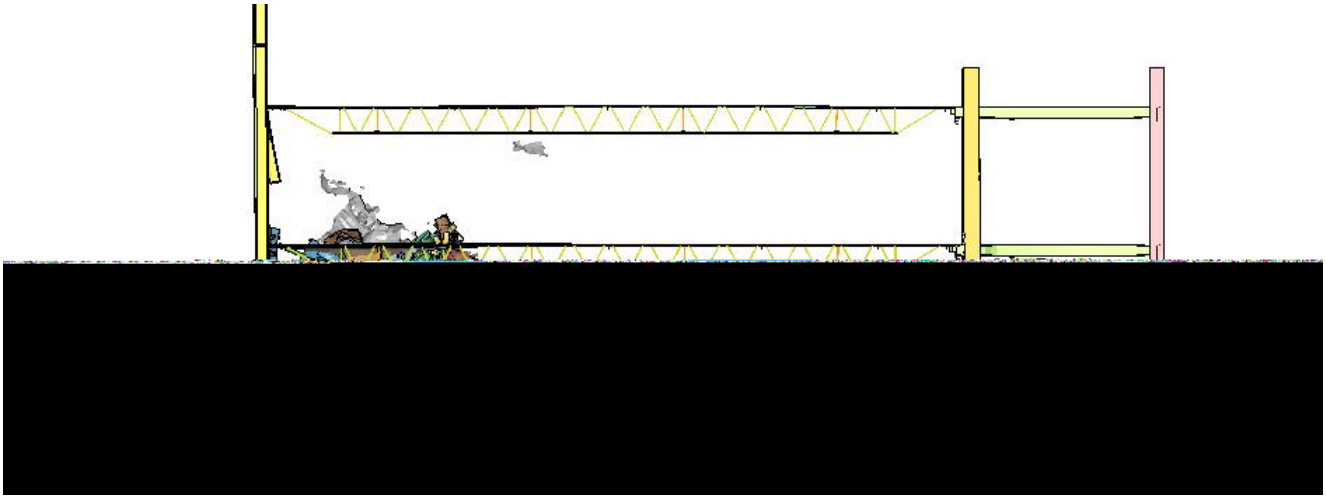

(b) Time = 0.05 s

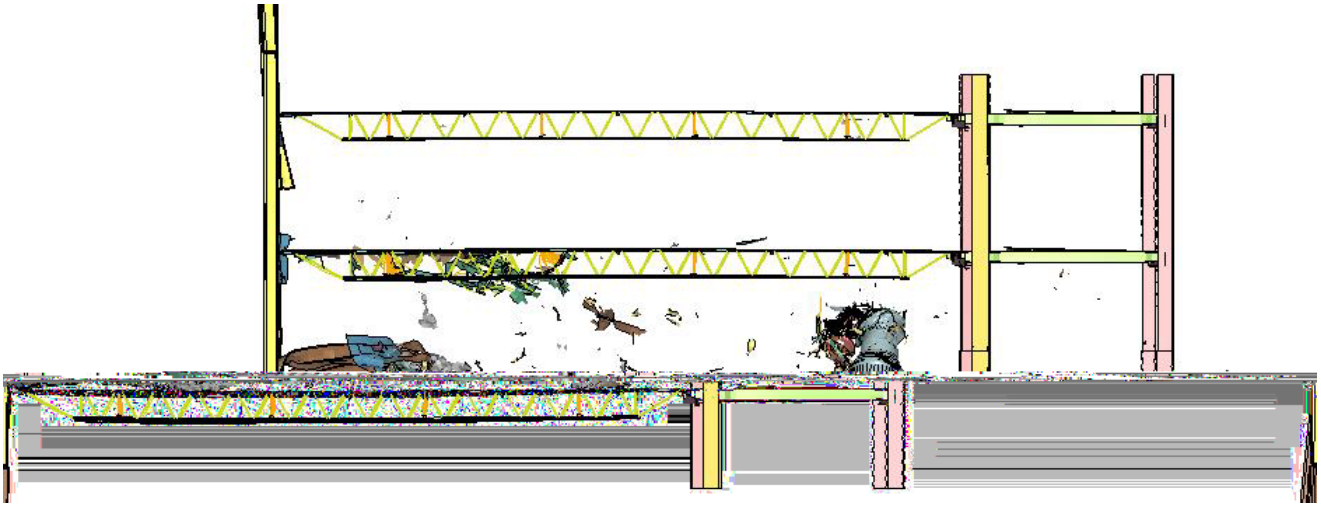

(c) Time = 0.25 s

Figure 6–10. Engine impact for concrete strength evaluation (side view).

The engine speed-time histories for the analyses with 3 ksi and 4 ksi concrete are compared in Figure 6–11. The engines had nearly identical speeds at 50 ms when the interaction with the truss floor was complete and approximately a 5 mph difference in speed at the end of the simulation. The speed difference was introduced by a slightly different rolling behavior of the two engines as they moved through the building contents. When the rotational axis of the engine was not coincident with the engine trajectory, a larger amount of mass was engaged and the engine was decelerated more rapidly.

Figure 6–11. Effect of the concrete strength on engine impact behavior.

A comparison of the engine impact damage to the truss floor structures with the 3 ksi and 4 ksi strength concrete is shown in Figure 6–12. The comparison shows that the two truss floors had very similar impact damage. A hole was created in both floors that extended from the outer wall back to approximately the second bridging truss. The mass of the concrete slab appears to have a greater effect on the engine deceleration and damaged floor than does the concrete strength.

6.3.2 Wing Section Impact Subassembly Analyses

Fuel-filled wing section impact subassembly analyses were performed using the final subassembly model discussed in Section 6.3.1. The development of the wing section impactor was described previously in Chapter 4. The combined wing section and tower subassembly model for the baseline impact conditions is shown in Figure 6–13. The fuel-structure interaction in this analysis was modeled using SPH particles, as discussed in Section 5.5.3.

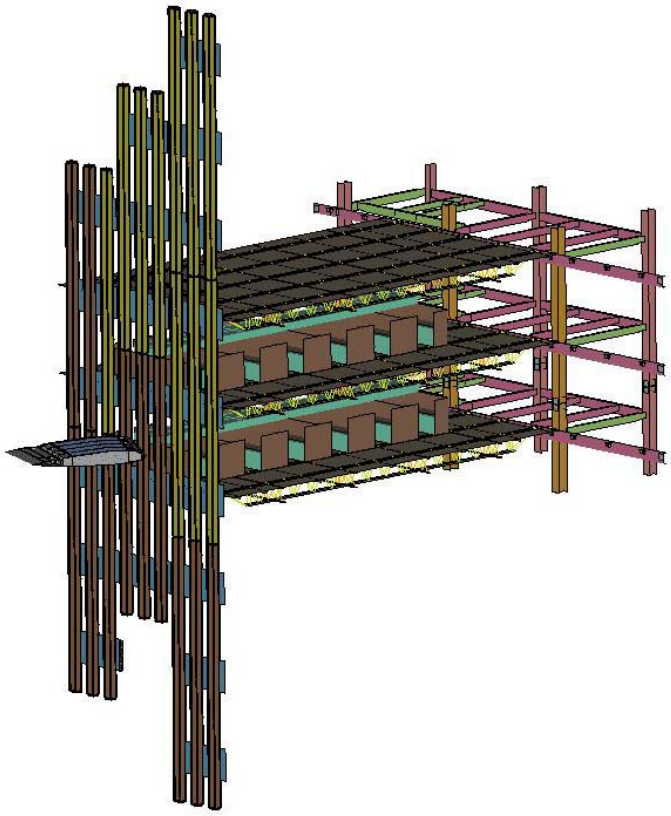

Figure 6–13. Final subassembly model for wing section impact analysis.

The impact response for the baseline subassembly wing section impact analysis is shown in Figure 6–14. In the first 50 ms, the wing section penetrated the exterior wall and was torn apart by the interaction with the exterior columns. The aircraft fuel formed a relatively dense cloud that covered the full height of the floor and extended 20 ft to 30 ft into the building. At a time of 0.25 s, as shown in Figure 6–14(c), the wing section impact caused significant damage to the workstations on the impact floor, and the fuel cloud expanded through to the core of the subassembly.

(a) Time = 0.00 s

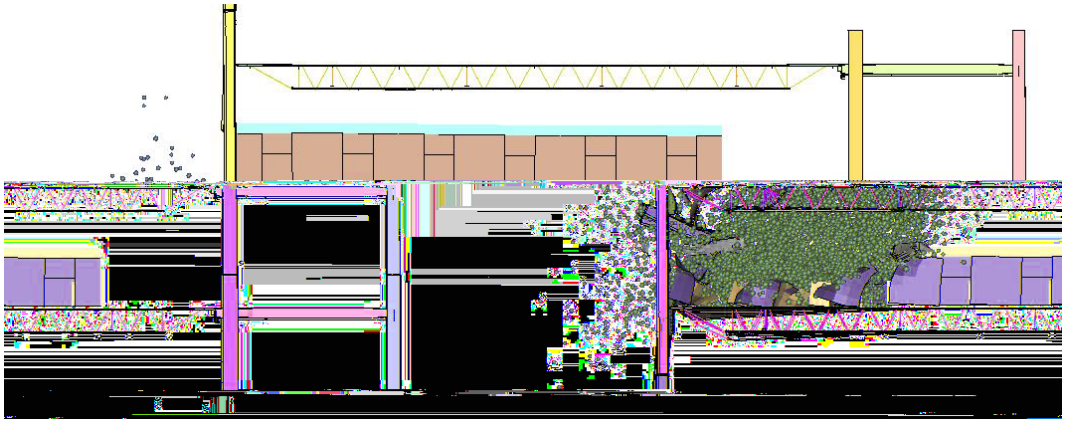

(b) Time = 0.05 s

(c) Time = 0.25 s

Figure 6–14. Baseline wing section impact and break up behavior (side view).

The damage produced by the wing section impact, shown in Figure 6–14, is different in many ways from the engine impact analyses shown in Figure 6–7. Both impactors started with similar kinetic energies; the wing-section impactor had an initial kinetic energy of 5.0×10^7 lb·ft and the engine impactor had 5.8×10^7 lb·ft. The wing impactor completely destroyed the workstations, where the engine only cut a path through the center of the subassembly. The wing caused extensive floor buckling despite having no initial vertical component to its velocity, unlike the engine. With the wing section, damage

predominantly occurred from the exterior panel to the core with little to no damage to the core. The difference in response is due to the break up and expansion of the wing components and fuel cloud. This debris and fuel expands more than the damaged engine components and can, therefore, engage more tower materials before reaching the core.

The difference in the impact behavior for the engine and wing section can be shown by the comparison of the impactor resultant momentum histories, shown in Figure 6–15. Although the wing section initially had approximately 20 percent lower momentum than the engine, the wing section impact transferred a larger percentage of the momentum to the tower in a much shorter duration. Therefore, the wing section resulted in greater damage near the impact point at the tower exterior. However, for comparable impact mass, the engine had a significantly larger energy entering the core and corresponding potential for damaging the core columns.

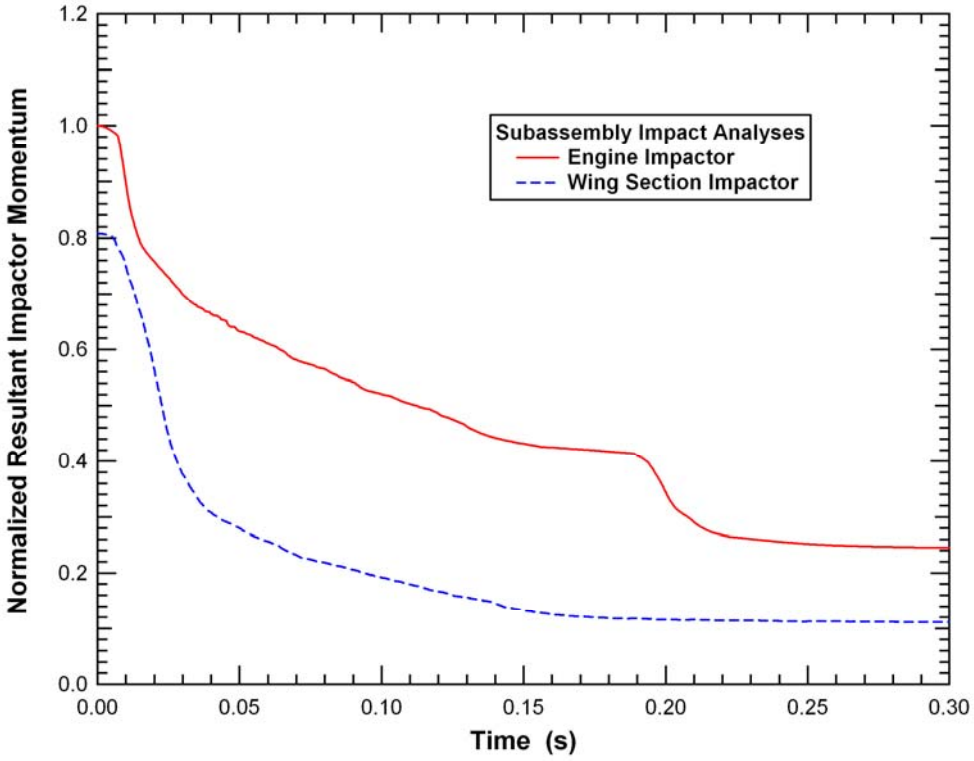

Figure 6–15. Impactor momentum histories for the engine and wing section analyses.

Weld Zone Ductility Effects

The wing section impact analyses were used to investigate the effect of the exterior column weld toughness on the impact response. This weld existed between the four plates comprising the column cross sections. As described in Chapter 2, the ductility of the weld zones was developed based on experimental characterization of the steel behavior, as well as simulation of the weld fractures in column segments subjected to impact loads. In the analyses, the maximum average weld zone ductility for the various grades of steel in the exterior columns was set at 8 percent. The extension of the weld fractures at elevated strain rates and under the very high stress concentrations at the crack tip can result in a

significantly reduced ductility from that required for crack initiation. Therefore, it was of interest to investigate the influence of a significantly reduced ductility of the weld zone on the impact response.

Two wing section impact analyses were performed to investigate the influence of the weld ductility on the impact response. In the first analysis, the baseline value of 8 percent for the weld ductility was used for the 55 ksi steel columns. In the second analysis, a failure strain of 1 percent was used to investigate the effects of a more brittle crack extension. This low ductility would more accurately simulate the conditions of a brittle crack extension along the exterior column welds.

Damage to the exterior panels due to both the baseline and brittle weld behavior is shown in Figure 6–16. The damage was very similar with only subtle differences in the fragmentation of the failed columns. The calculated global energy balance and the absorption of energy by the exterior panels are shown in Figure 6–17. Of the approximately 8.9×10^6 lb·ft of energy absorbed by the exterior wall, approximately 1 percent to 2 percent of that energy was absorbed in the weld zone. The impact response in the two analyses was nearly identical, indicating that weld ductility had a negligible effect on the impact behavior and damage to the tower.

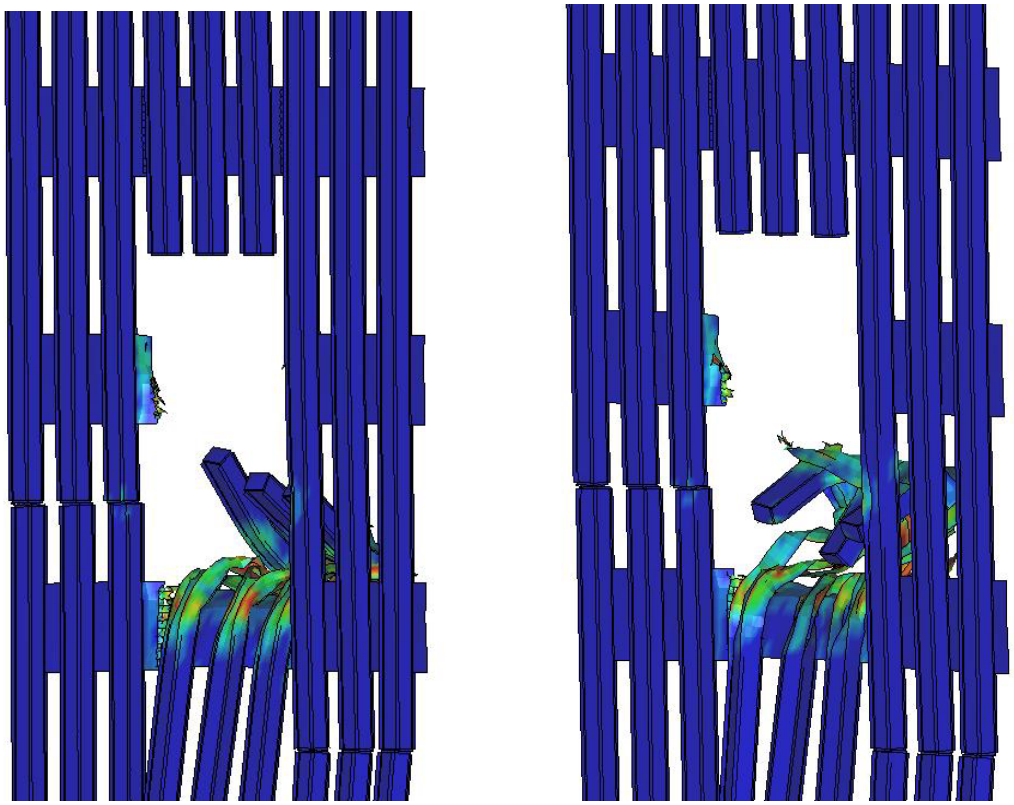

(a) Baseline response **(b) Brittle weld response**

Figure 6–16. Exterior wall damage for the wing section impact analyses.

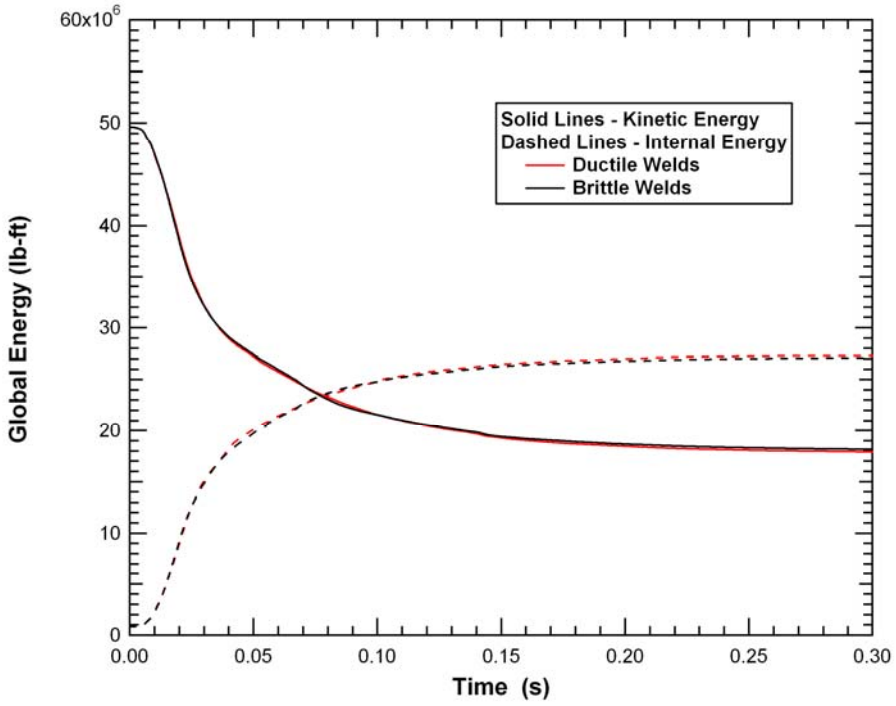

(a) Global energy balance

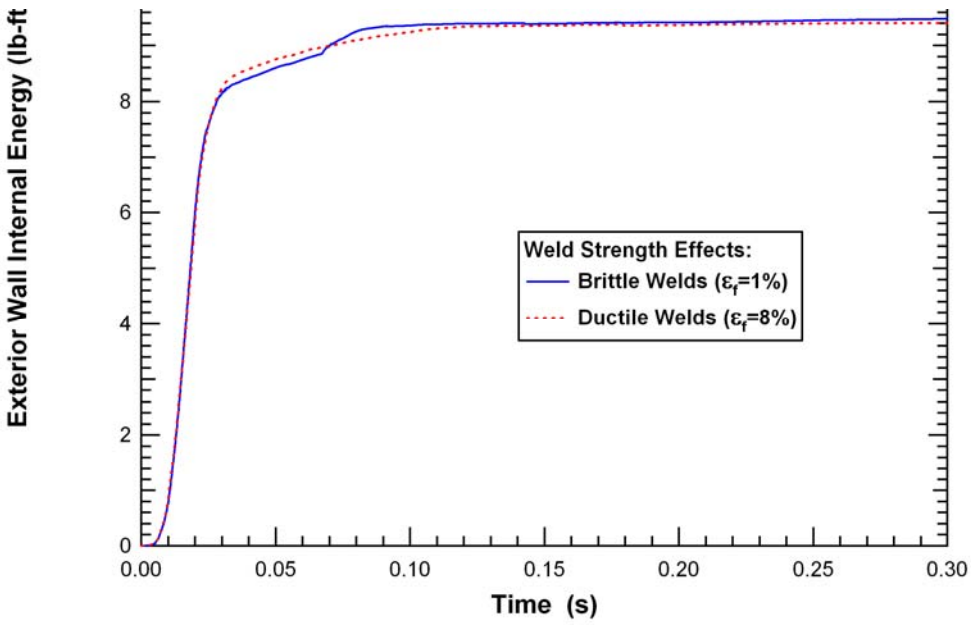

(b) External wall energy absorption

Figure 6–17. Effect of the weld strength on wing section impact response.

6.4 SUMMARY

The subassembly analyses were used as a transition between the component level analyses and the global impact analyses. With the subassembly analyses, more complex structural behavior not captured in the component analyses could be investigated with significantly shorter run times than required for the global analyses. The subassembly analyses were primarily used to investigate different modeling techniques and associated model size, run times, numerical stability, and impact response. The final subassembly model used structural components from the impact zone on the north face of WTC 1. The structural components in the final subassembly model included the exterior panels, core framing, truss floor structures, and interior contents (workstations).

The subassembly model was impacted by an aircraft engine and by a segment of a fuel-filled wing. The subassembly model was used to investigate the effect of a number of modeling parameters on the response and damage estimates. For the engine impact simulations, these parameters included the strength of both the building nonstructural contents and the concrete slab. For the wing impact simulations, the effect of the ductility of the exterior column weldment on the impact response was investigated. The results of these parametric studies indicated the following:

- The deceleration profile of the impacting engine indicated that the response of the nonstructural building contents was dominated by the mass of the workstations, rather than by their strength.

- Varying the strength of the floor concrete slab from 4 ksi to 3 ksi did not result in significant change in the impact response. It appears that the mass of the concrete slab had a greater effect on the engine deceleration and damage to the floor than did the concrete strength.

- Varying the ductility of the weld zone in the exterior columns from 8 percent to 1 percent did not result in any noticeable difference in the damage pattern or the energy absorbed by the exterior panels, indicating that the weld ductility had a negligible effect on the impact response.

6.5 REFERENCES

"LS-DYNA User's Manual: Nonlinear Dynamic Analysis of Structures in Three Dimensions," Livermore Software Technology Corporation, Version 940, June 1, 1997.

This page intentionally left blank.

Chapter 7
ANALYSES OF AIRCRAFT IMPACT CONDITIONS

7.1 INTRODUCTION

This chapter describes the estimation of the initial impact conditions of the aircraft which hit the World Trade Center (WTC) towers from available evidence. Important initial conditions for the impact analysis included impact speed, aircraft orientation and trajectory, and location of aircraft nose at impact. Two videos captured the approach and impact of the American Airlines flight 11 (AA 11) aircraft that impacted the WTC 1 tower, and several videos captured the United Airlines flight 175 (UAL 175) aircraft that impacted the WTC 2 tower. In addition, there is a large body of photographic evidence that was used to determine the impact location and orientation relative to the towers. These videos and photographs were analyzed to estimate, with the best accuracy possible, the velocity magnitude (speed), horizontal and vertical angles of incidence, and roll angle of each aircraft during impact with each tower.

The analysis of the initial aircraft impact conditions was performed in two steps. The first step was to perform an analysis of the video footage of the two impact events. This analysis compared the various videos and used visual references and known dimensions and positions of towers to determine the flight conditions prior to impact (Section 7.2). The second step was to use the photographic evidence of the impact damage to refine the details of the impact position, orientation, and trajectory (Section 7.3). The impact orientation and trajectory parameters are defined in Figure 7–1.

Two vectors are defined in Figure 7–1, one for the velocity vector of the aircraft (the trajectory) and one for the orientation of the aircraft. There is no reason to assume that these two vectors were coincident, although they could have been at the time of impact. Both vectors are described in terms of a vertical angle around structure east as shown in the figure, and a lateral angle, which is measured clockwise around the tower axis from structure north. The orientation is also described in terms of a wing-tip roll angle, as shown in the figure.

The resolution of the video footage was not sufficient to measure wing deflections or impact points more accurately than within ± 6 ft. In the two videos that captured the WTC 1 impact, there also was not enough resolution to obtain an accurate orientation of the aircraft. Consequently, the impact point and roll angle of AA 11 were determined using only the still frame photographs of the impact damage to the north side of WTC 1. Since UAL 175 impact was captured by several videos, the trajectory and orientation measurements could be made from the available video footage. The still frame photography of the damaged WTC 2 structure again was used as the primary source to determine the impact location. The following sections describe the analysis methodologies used to determine the motion parameters and impact conditions.

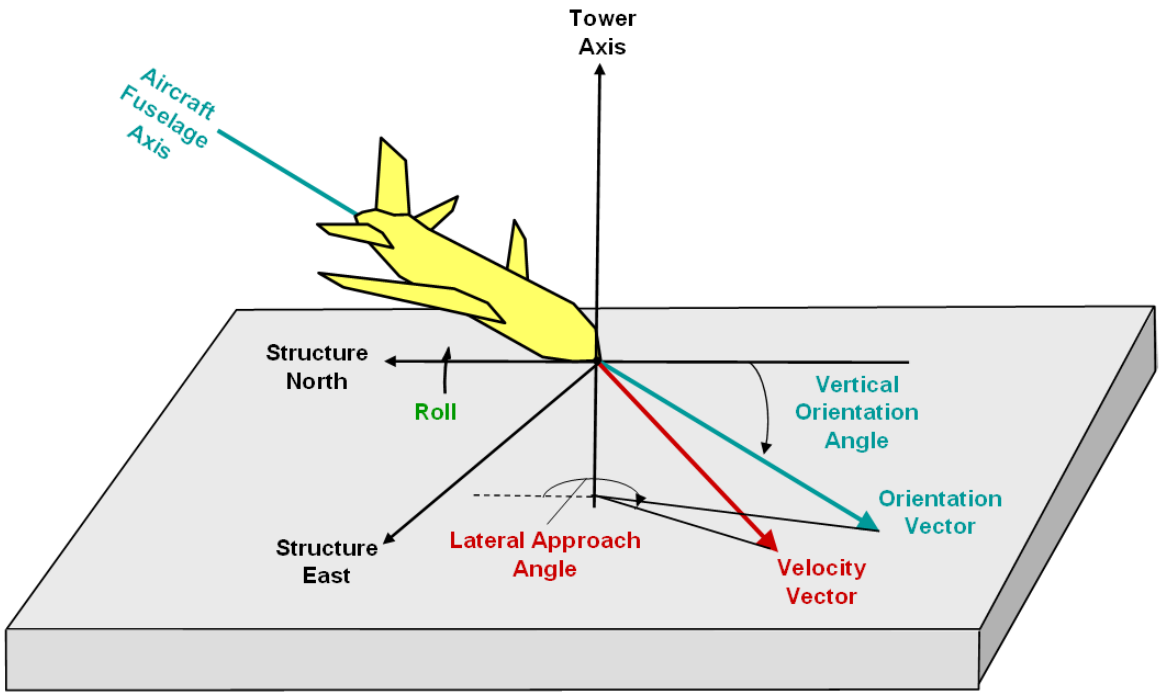

Figure 7–1. Definitions of the aircraft impact parameters.

7.2 MOTION ANALYSIS METHODOLOGY

7.2.1 Videos Used in the Analysis

The first task in the analysis of the aircraft impact conditions was the review and selection of appropriate video and photographic data. An extensive library of video and photographic evidence of the WTC tower impacts has been collected by the National Institute of Standards and Technology (NIST). The available videos in the NIST WTC collection were reviewed to select the best video footage of the aircraft's approach and impact with each tower. NIST had already digitized the footage, which was stored in files with AVI formats. The WTC 1 aircraft impact was captured in two videos, and both were used in the analysis. Several videos captured the aircraft impact into WTC 2 tower, and seven of them were used in the analysis. The image coordinates of the aircraft nose, tail, wing tips, aileron, and several locations on the towers were measured in each frame of the videos. Adobe Photoshop was used to determine the X and Y image coordinates. Table 7–1 provides a summary of the videos used to analyze impact conditions. Still images from each of these video records are provided in Appendix A.

Table 7–1. Videos used for the analysis of aircraft impact conditions.

Digitized Video	Original Video Format	Tower Impact	Description
V1	NTSC	WTC 1	Footage taken at ground level at the corner of Church and Lispenard streets. Taken north and east of the towers.
V2	PAL	WTC 1	Footage taken from the entrance of the Brooklyn Battery Tunnel, heading west. Taken south and east of the towers.
V3	NTSC	WTC 2	Footage taken from a helicopter north and west of the towers.
V4	NTSC	WTC 2	Footage taken at ground level near the Castle Clinton National Monument. Footage taken south and east of the towers.
V5	NTSC	WTC 2	Footage taken from Brooklyn, south and east of the towers.
V6	NTSC	WTC 2	Footage taken from the 13th floor of John Street, east of the towers.
V7	NTSC	WTC 2	Footage taken at ground level from the corner of Church and Liberty. Taken south and east of the towers.
V8	NTSC	WTC 2	Footage taken from a helicopter north of the towers.
V9	NTSC	WTC 2	Footage taken from a moving vehicle on FDR drive, heading west just before the Brooklyn Bridge. Footage taken north and east of the towers.

The second column in Table 7–1 lists the original format of the various videos that were analyzed. The National Television System Committee (NTSC) video format is the standard television format in the United States. The Phase Alternating Line (PAL) video format is common in Europe and parts of Asia. Any image data from the interlaced field of the videos were neglected. It was also assumed that the digitized NTSC videos had a rate of 29.97 images per second, while the PAL videos had a rate of 25 images per second. The digitized images had sizes of 720×480 pixels (NTSC) and 720×576 pixels (PAL). The original video footage was assumed to have an aspect ratio of 1.33/1, so the X-values of the measured image coordinates were adjusted to account for the actual aspect ratio. The image coordinates were also shifted relative to the locations of fixed points in the field of view (corners of a tower) to eliminate the effects of movement and shaking of the camera.

7.2.2 Complex Motion Analysis Procedures

A complex motion analysis was the method originally used in this study to calculate the speed, orientation, and trajectory vectors of the aircraft. However, subsequent analysis methodologies, as discussed in the following sections, provided more accurate estimates of speed and orientation. The quality and limited video footage available produced greater uncertainty using the complex motion analysis methodology. Therefore, this analysis was only used to define the aircraft trajectory. The following is a discussion of the complex motion analysis and an assessment of its accuracy.

The methodology used in this analysis to determine the aircraft impact conditions was previously developed for other applications (Cilke 1995). Figure 7–2 depicts the analysis procedure. The image coordinates of the moving object (the aircraft) and two stationary positions on the structures within the field of view were triangulated with the known real-world positions of the structures and camera. The camera was assumed to be a pin hole type camera, i.e., all the light rays pass through a single focal point and project onto a flat surface that records the image. The result was the definition of the vector

extending from the camera to the measured object. Note that the position of the object along the vector was unknown. The vector was then intersected with a surface defined by a set of vectors extending from a second camera to the measured object in multiple frames. The result was the real world position of the object at one instant in time. The global positions of other points on the object and positions of the object in multiple frames were then used to define the orientation and trajectory of the object. Note that in ideal test conditions, where the video cameras and reference positions are precisely surveyed and the camera field of view is designed, the uncertainties in the measured object velocities range from 1 percent to 1.5 percent.

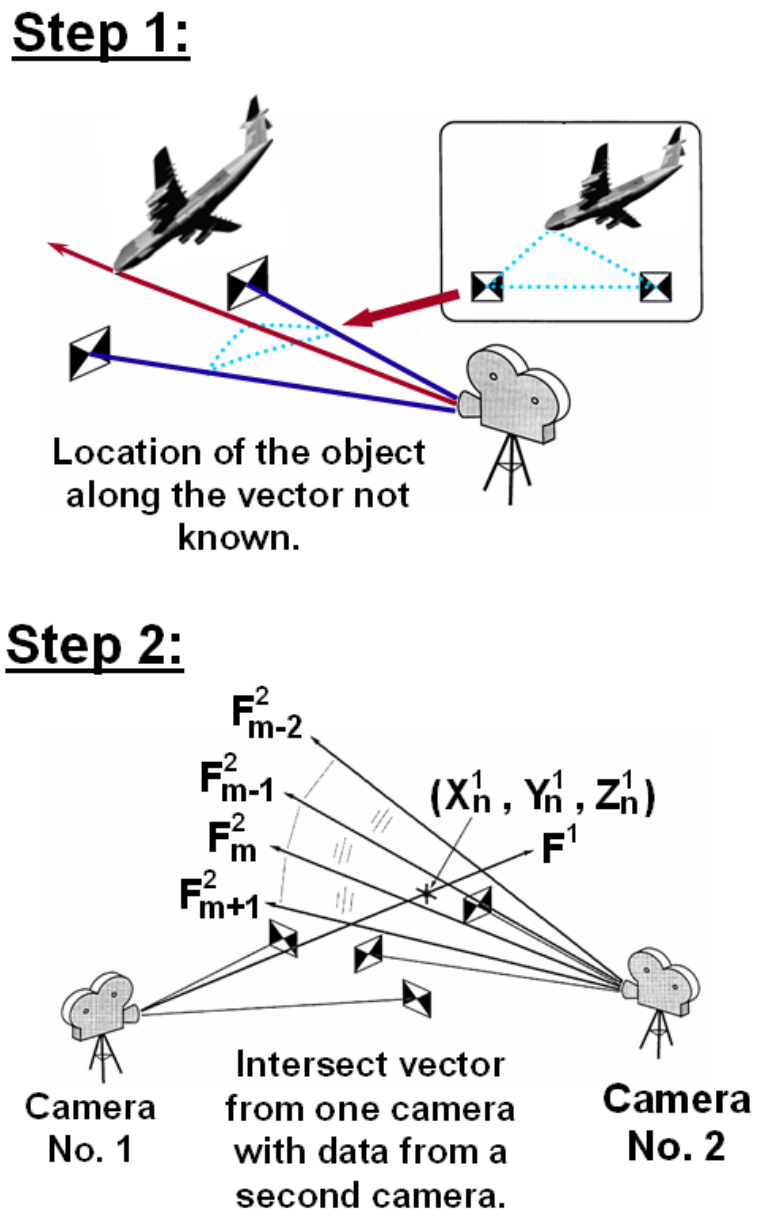

Figure 7–2. Procedures to measure object motions using multiple cameras.

For the WTC aircraft motion analysis, various locations on the two towers were used as fixed reference locations. The four corners of the towers at three floor levels were used, as they could be easily identified in the video footage. Additional points on the WTC 1 antenna were also used as reference locations. Figure 7–3 shows the reference locations used on the towers. The tower reference positions were at the center of each beveled corner. Similarly, Figure 7–4 shows a plan view of the reference locations of the corners. Note that a local coordinate system is defined in the figure that is orthogonal to the sides of the structures. Structure north is approximately 29° clockwise from True North. The coordinates of the reference locations were determined by using the original construction drawings of the towers. While the locations on the structure could be determined with high fidelity, the coordinates (X, Y, and Z) of the cameras had to be estimated through an iterative process.

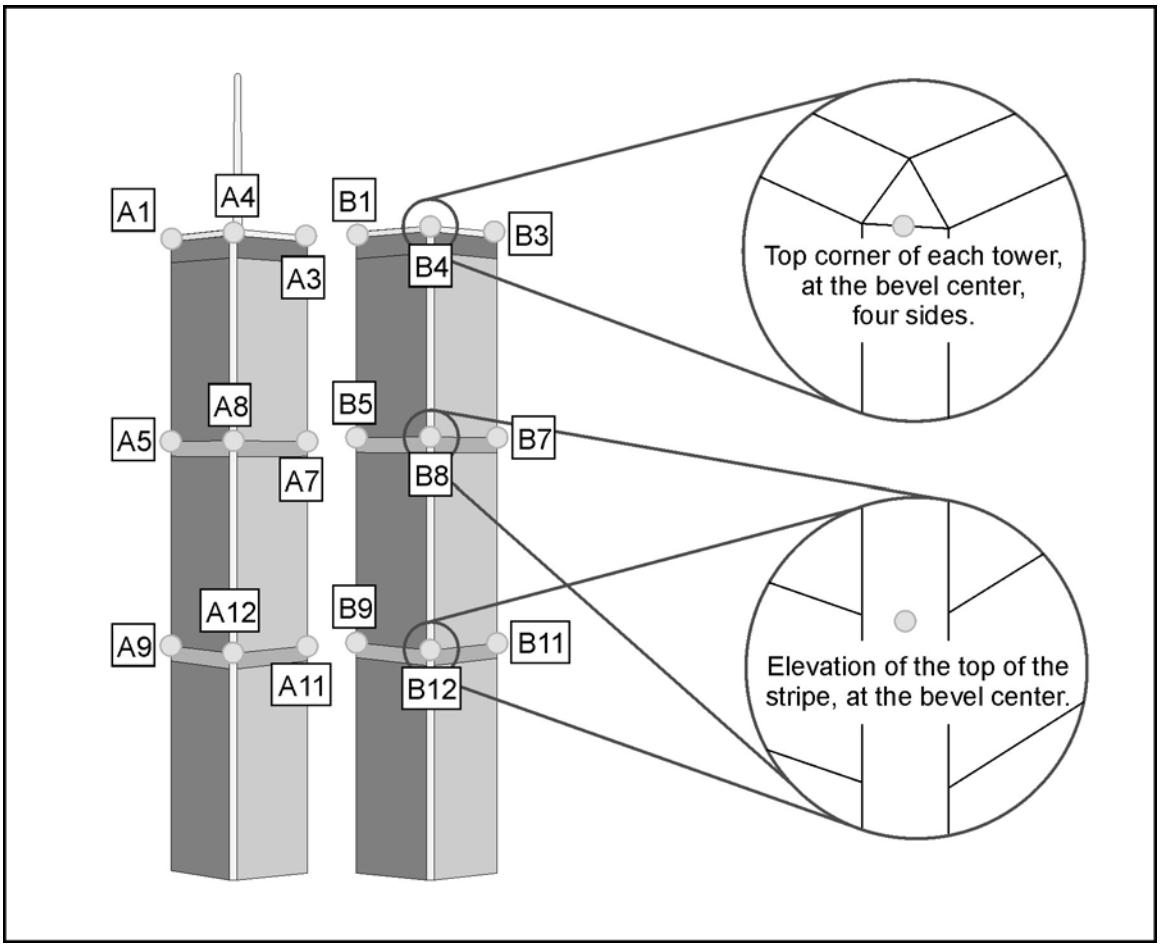

Figure 7–3. Reference locations on the WTC towers for video footage motion analysis.

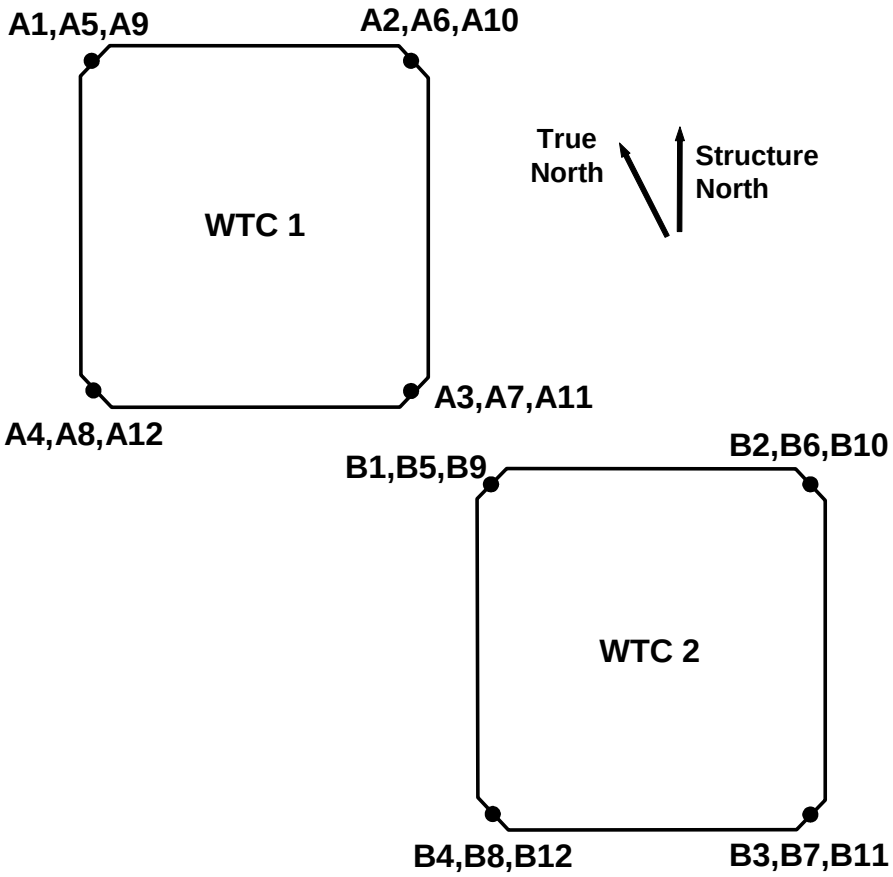

Figure 7–4. Plan view of the reference locations on the WTC towers.

With the camera locations estimated, motion analyses were performed using the complex motion analysis technique. For the WTC 1 aircraft impact, image data from the V1 video were correlated with the data from the V2 video. The analysis produced a speed of 435 ± 30 mph for the WTC 1 aircraft at time of impact.

For the WTC 2 aircraft impact, data from each of the V1, V5, and V9 videos were correlated with the other two cameras to determine the motion of the aircraft prior to impact. The other cameras were less effective with this analysis technique. Videos V6 and V7 viewed the aircraft for only a few frames, which could not be intersected with many frames from the other cameras. Videos V3 and V8 were both taken from the north. The last second before the aircraft struck the WTC 2 tower was obscured by the towers. As a result, the cameras' data did not intersect with the other cameras' fields of view. Data from the two helicopters, V3 and V8, could not be effectively correlated with each other, as their viewpoints were too similar.

Image data from videos V4, V5, and V9 converged to a tight set of trajectory angles and aircraft orientations. These angles are provided later in Table 7–3. The uncertainties in the measured angles were derived from three components. First, there was a significant amount of scatter in the measured image coordinates. The perceived motion and orientation of the aircraft varied between frames, due to the relatively low resolution of the images and the motion of the camera fields of view. The scatter in the image data contributed to approximately ±2° to ±4° of the image uncertainty. The tips of the aircraft

wings were more difficult to define accurately; the scatter in the wing measurements led to an estimated uncertainty of ±4° in the roll angle. Second, the uncertainties in the camera locations contributed to the uncertainties in measured angles. Since there was more uncertainty in the cameras' horizontal positions than the vertical positions, the measured horizontal azimuths had larger uncertainties (±2°). Third, the potential distortion in the field of view distorted the measured angles. The uncertainty of the measured angles due to image distortion was estimated to be ±1°.

The initial analyses using the complex motion methodology indicated the UAL 175 aircraft impact speed to be about 497 mph, which was heavily based on the V4 footage. However, subsequent analyses showed that the cameras did not provide an accurate aircraft impact speed. The cause of this inaccuracy was traced to three possible causes. First, the range of the camera could only be estimated. If the camera was close to the object motion, the range of the camera would have a significant effect on the perceived scale of the object in motion. Second, the scale of the image was determined from the dimensions of the towers in the field of view, which took up a relatively small portion of the field of view. As a result, the uncertainties in the measured image distances increased. Third, and most important, there were measurable distortions in the camera fields of view. For example, in the V5 footage, the camera pans from left to right, tracking UAL 175 as it approaches the south tower. The tower initially appears from the right edge of the image and moves to the center. The length of the aircraft (which remained in the center of the field-of view) appeared to decrease by 1.5 percent. However, the width of the south tower's east edge appeared to decrease by 7 percent, indicating a significant distortion in the field of view. As a result, a simplified motion analysis procedure was used to determine the speed of the WTC 2 aircraft (Section 7.2.3). The complex motion analysis was used only to define the aircraft orientation and trajectory vectors.

7.2.3 Simplified Motion Analysis Procedures

The simplified motion analysis procedure determined the impact speed by scaling the displacement of the aircraft within the field of view with the aircraft's apparent fuselage length. Figure 7–5 depicts the simplified procedure to determine the aircraft speed. For several videos of the WTC tower impacts, linear regressions were performed for the image X and Y coordinates as functions of time. The displacements of the nose, tail, and wing tips were measured. The apparent length of the fuselage within each image was determined from the nose and tail regression lines, and the apparent displacement of the aircraft between images was normalized to the apparent length of the fuselage. Multiplying the result by the length of the aircraft determined the aircraft speed (there are constant time steps between frames). Finally, a geometric correction was made if the fuselage orientation and trajectory were not aligned.

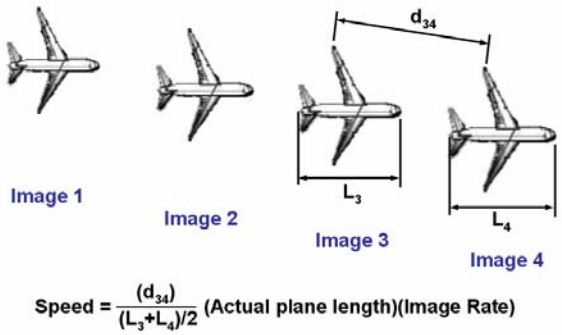

Figure 7–5. Simplified motion analysis procedure to determine aircraft speed.

The fuselage length of the Boeing 767-200ER aircraft is 155 ft as shown in Figure 7–6. However, for the simplified motion analysis the fuselage was assumed to have an apparent length of 153 ± 2 ft. The adjustment in apparent fuselage length was a result of the relatively low resolution of the video footage. As a sharp object enters a region captured by a single pixel, the background dominates the pixel color value until the object has entered by a significant fraction. The low resolution could not accurately capture the shape of the aircraft nose and tail, and the aircraft nose in the videos appeared to be blunter than the actual Boeing 767-200ER nose. The average length of the fuselage in the videos analyzed was approximately 75 pixels (but varied depending on the footage). It was assumed that the resolution effect resulted in an apparent loss of approximately a half pixel at each end of the fuselage (1 ft at each end of the fuselage). As a result, the apparent length of the fuselage in the video footage was approximately 2 ft less than the specified length.

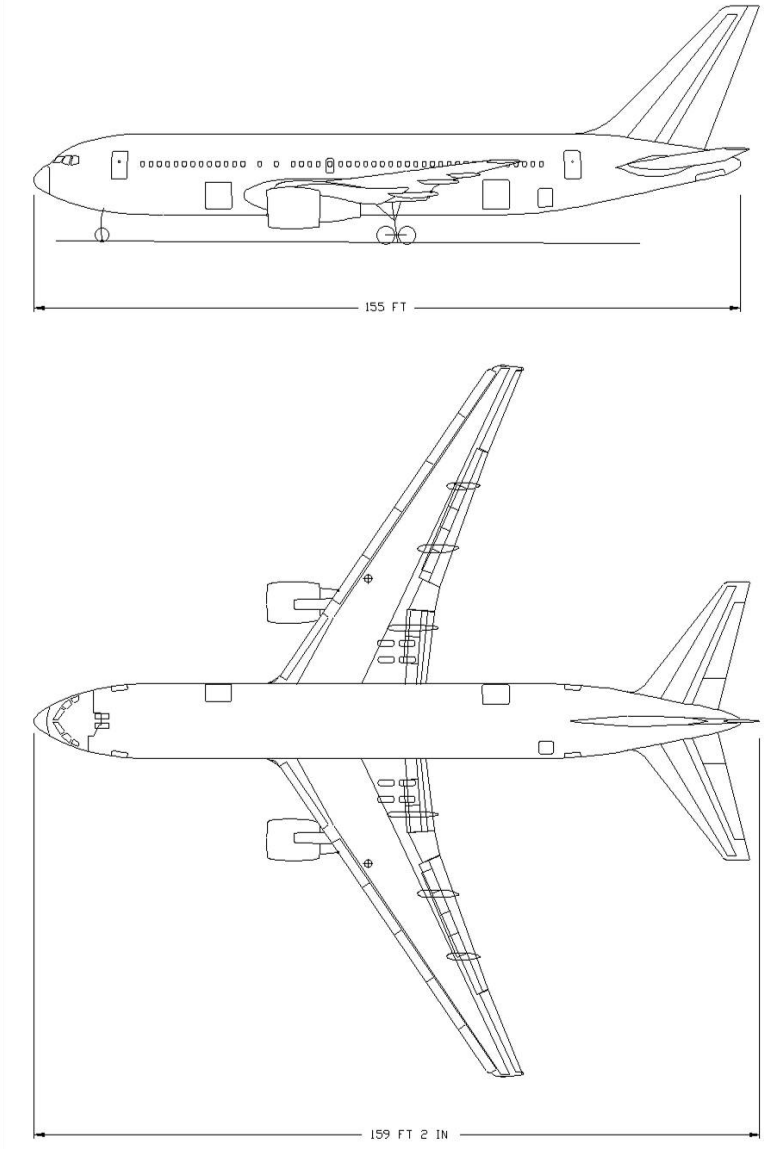

Used with permission.

Figure 7–6. Dimensions of the Boeing 767-200 aircraft and fuselage.

The simplified motion analysis technique was used for the analysis of aircraft speed for both tower impacts. For the WTC 1 impact, only the V1 video could be used to determine the aircraft speed with this technique. The second video, V2, could not be used to obtain an accurate measure of speed as the aircraft was traveling away from the camera. The simplified analysis produced a speed of 451 mph ± 30 mph, which is 16 mph higher than the value obtained from the complex motion analysis technique. Both of these values for the WTC 1 impact speed fall within the uncertainties in the corresponding analyses. As a result, the WTC 1 aircraft impact speed provided in Table 7–3 is the average of the two speeds obtained using the complex and simplified motion analysis techniques.

The videos with a viewing angle approximately perpendicular to the UAL 175 flight direction were used to estimate impact speed. The results of the simplified motion analyses from each camera for UAL 175 are provided in Table 7–2. The uncertainties in Table 7–2 were based on the scatter in the measured displacements, the aircraft length within the image, and uncertainty in the actual aircraft length as seen in the images due to unknown orientation. A systematic error in calculating the aircraft speed was introduced due to the lateral fuselage orientation relative to trajectory. The uncertainty in this value was due to the aircraft maneuvers during approach. In calculating the uncertainty in speed, an uncertainty of ±3 degrees in orientation was assumed.

Table 7–2. Measured UAL 175 impact speed using the simplified analysis technique.

Video Reference	Calculated Aircraft Speed
V4	573 mph ± 55 mph
V5	556 mph ± 27 mph
V6	535 mph ± 23 mph
V7	523 mph ± 31 mph
V9	557 mph ± 53 mph
Best Estimate Speed	542 mph ± 24 mph

A speed estimate was then calculated from the individual videos. A mean value was calculated using the weighted average of the mean values. The measurement precision (the reciprocal of the variance) was used as a weight factor on the mean values. If measurements were independent, the uncertainty in the mean could be calculated by summing the individual measurement precisions, giving 443 mph ± 21 mph for AA11 and 542 mph ± 14 mph for UAL 175. However, some uncertainties were systematic, and the actual bound on the uncertainty was larger as a result. Therefore, this uncertainty range was increased to ± 30 mph and ± 24 mph for AA 11 and UAL 175, respectively. A summary of the impact conditions derived from video analysis is shown in Table 7–3.

The simplified motion analysis technique was used for the analysis of aircraft speed for both tower impacts. For the WTC 1 impact, only the V1 video could be used to determine the aircraft speed with this technique. The second video, V2, could not be used to obtain an accurate measure of speed as the aircraft was traveling away from the camera. The simplified analysis produced a speed of 451 mph ± 30 mph, which is 16 mph higher than the value obtained from the complex motion analysis technique. Both of these values for the WTC 1 impact speed fall within the uncertainties in the corresponding analyses. As a result, the WTC 1 aircraft impact speed provided in Table 7–3 is the average of the two speeds obtained using the complex and simplified motion analysis techniques.

Table 7–3. Summary of measured aircraft impact conditions from video analysis.

	AA 11 (WTC 1)	UAL 175 (WTC 2)
Impact Speed (mph)	443 ± 30	542 ± 24
Vertical Approach Angle (Velocity vector)	10.6° ± 3° below horizontal (heading downward)	8° ± 4° below horizontal (heading downward)
Lateral Approach Angle (Velocity vector)	180.3° ± 4° clockwise from Structure North[a]	19° ± 6° clockwise from Structure North[a]
Vertical Fuselage Orientation from horizontal	—	3° ± 4° below horizontal (heading downward)
Lateral Fuselage Orientation from Structure North	—	8° ± 6° clockwise from Structure North[a]
Roll Angle (left wing downward)	25° ± 4°	38° ± 4°

a. Structure North is approximately 29 degrees clockwise from True North.

The videos with a viewing angle approximately perpendicular to the UAL 175 flight direction were used to estimate impact speed. The results of the simplified motion analyses from each camera for UAL 175 are provided in Table 7–2. The uncertainties in Table 7–2 were based on the scatter in the measured displacements, the aircraft length within the image, and uncertainty in the actual aircraft length as seen in the images due to unknown orientation. A systematic error in calculating the aircraft speed was introduced due to the lateral fuselage orientation relative to trajectory. The uncertainty in this value was due to the aircraft maneuvers during approach. In calculating the uncertainty in speed, an uncertainty of ±3 degrees in orientation was assumed.

A speed estimate was then calculated from the individual videos. A mean value was calculated using the weighted average of the mean values. The measurement precision (the reciprocal of the variance) was used as a weight factor on the mean values. If measurements were independent, the uncertainty in the mean could be calculated by summing the individual measurement precisions, giving 443 mph ± 21 mph for AA11 and 542 mph ± 14 mph for UAL 175. However, some uncertainties were systematic, and the actual bound on the uncertainty was larger as a result. Therefore, this uncertainty range was increased to ± 30 mph and ± 24 mph for AA 11 and UAL 175, respectively. A summary of the impact conditions derived from video analysis is shown in Table 7–3.

Original results from the simplified motion analysis produced a mean speed for UAL 175 of 546 mph. Therefore, this speed was used in running the global impact analysis, discussed in Chapter 9. Subsequent refinement of the analysis and associated uncertainties produced the slightly lower mean value of 542 mph as discussed above. Because this difference in speed is less than 1 percent and well within the uncertainty range, the speed used for the baseline impact analysis was not modified.

7.3 REFINEMENT OF AIRCRAFT IMPACT CONDITIONS

Estimates for the aircraft impact locations, orientations, and trajectories were further refined based on the damage patterns documented on the exterior of the WTC towers. The general approach was to visualize the aircraft within the range of flight conditions estimated from the video analysis (Section 7.2) and project the impact points of the wings, fuselage, engines, and vertical stabilizer onto the exterior wall of

each tower. A damage pattern was then estimated and compared to that obtained previously from analysis of the video and photographic evidence.

The estimated damage to the north face of WTC 1 is shown in Figure 7–7 along with approximate impact locations for various aircraft components of AA 11. Estimated impact locations for various aircraft components (wind tips, vertical stabilizer tip, and engines) were added to the figure to fit the damage profile. For AA 11, it was found that the fuselage orientation needed to be 2 degrees above the vertical approach angle (2 degrees nose-up). The difference in the lateral approach angle and the fuselage orientation from structure north is 0 degrees.

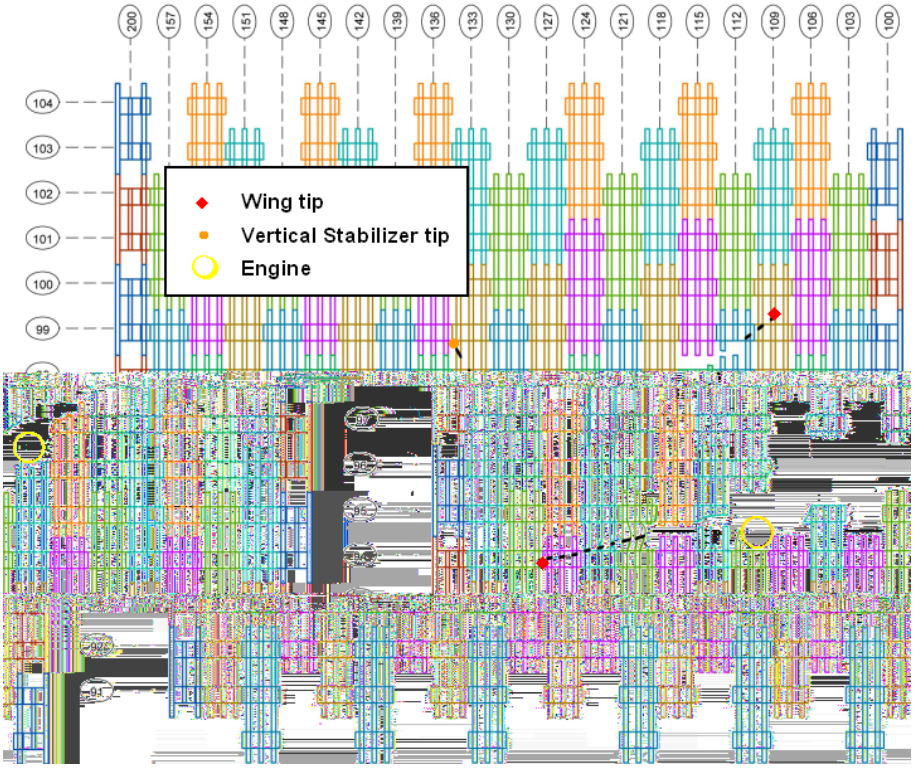

Figure 7–7. Estimated impact locations of aircraft components superimposed on the damaged face of WTC 1.

An example impact condition is shown in Figure 7–8 where the vertical approach angle was 10.6 degrees (fuselage orientation from horizontal = 8.6 degrees) and the lateral approach angle was 180 degrees (fuselage orientation from structure north = 180 degrees). The position of the vertical stabilizer tip was the most critical factor in determining this relationship. The impact points of the wing tips were known to within approximately ± 2 ft. This corresponded to an uncertainty in the roll angle of approximately ±2 degrees. Since no accurate orientation information could be derived from the video analysis, analysis of the damage pattern was critical in determining the aircraft orientation at the time of impact.

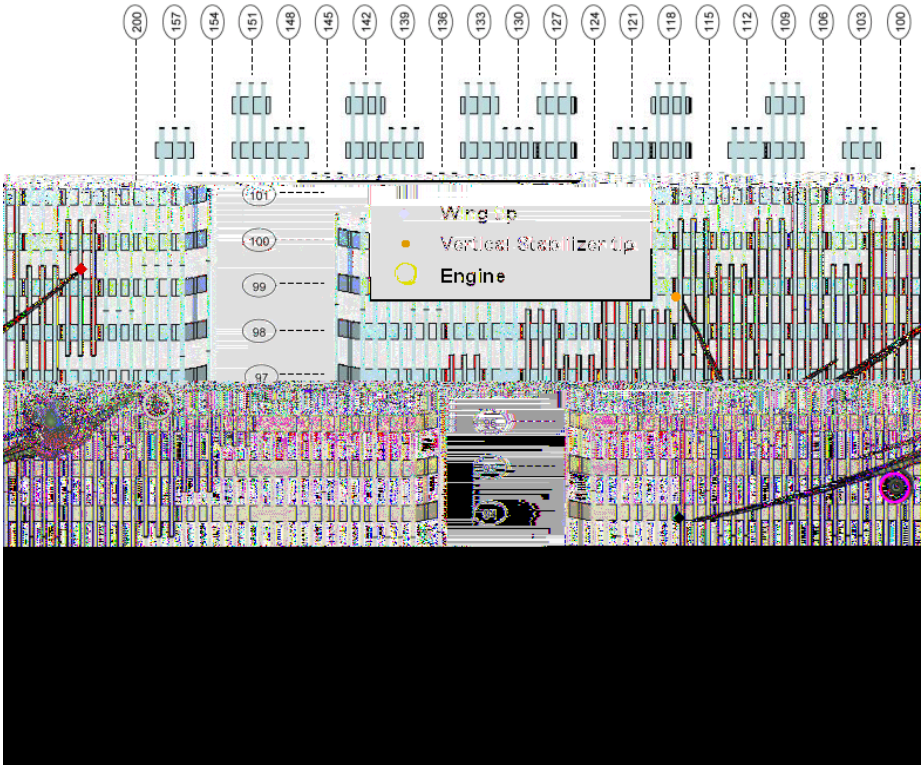

Figure 7–8. An orientation and trajectory of AA 11 that matches the impact pattern (vertical approach angle = 10.6°, lateral approach angle = 0°).

The estimated damage to the face of WTC 2 is shown in Figure 7–9, along with approximate impact locations for various aircraft components of UAL 175. From these impact locations, the combinations of flight conditions that were consistent with the observed impact damage could be determined.

Figure 7–10 shows the south face of WTC 2 with the aircraft model positioned in the impact orientation and location estimated from the video analysis, as summarized in Table 7–3. The viewpoint of the figure is along the trajectory axis so that the projection of each aircraft component onto the tower face represents its approximate impact location, assuming no significant structural deformation prior to impact of an aircraft component with the building exterior. During the impact simulation, little structural deformation was observed in parts of the aircraft that had not yet impacted the towers. The vertical stabilizer, the last part of the aircraft to enter the building and which has the longest time to experience structural deformation, impacted close to this projected impact location.

The impact conditions shown in Figure 7–10, which were based on video analysis alone, would cause the starboard wing tip to miss the building and are, therefore, not physically reasonable. Also shown in the figure are the estimated impact locations for the wing tips, vertical stabilizer, and engines. These also did not align well with the observed impact damage. Translation of the aircraft alone does not account for the discrepancy in the impact point shown in the figure. Both a translation of 3.3 ft higher and 9.8 ft further west was needed, along with a specific relationship between the trajectory and orientation, in order for the impact pattern to match. The final impact points, defined as the location where the nose of each aircraft initially contacted the towers, are provided in Table 7–5.

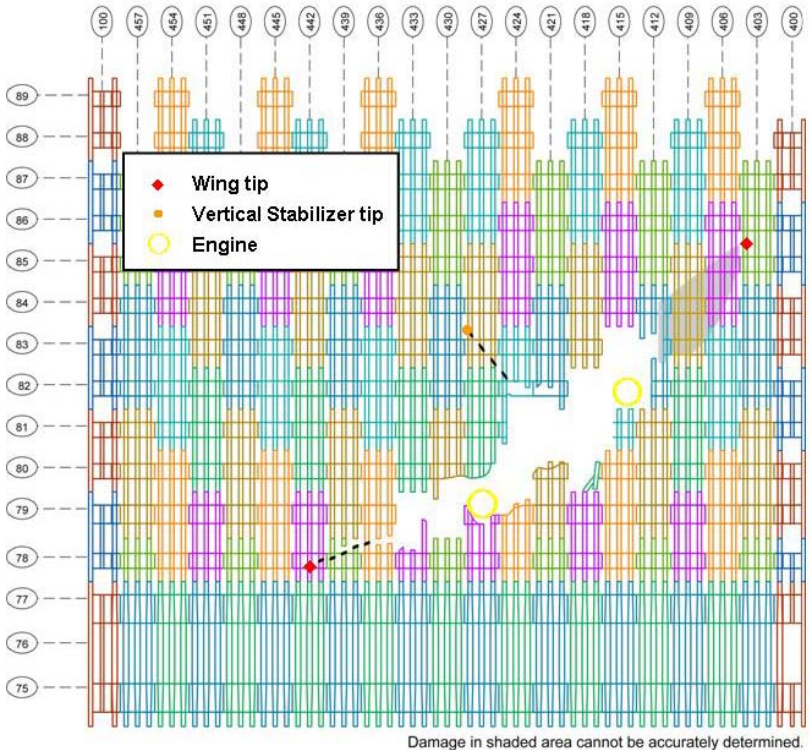

Figure 7–9. Estimated impact locations of aircraft components superimposed on the damaged face of WTC 2.

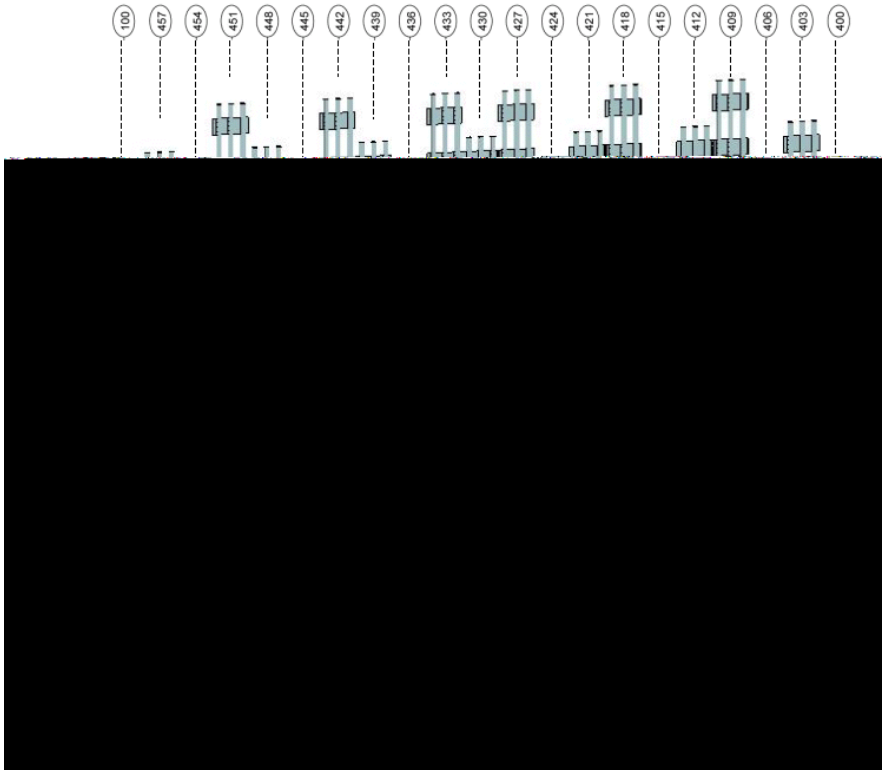

Figure 7–10. Baseline orientation and trajectory of UAL 175 from video analysis.

It was found that a strict relationship between the aircraft trajectory and orientation needed to be maintained in order to achieve an impact pattern consistent with the damage observed on the south wall of WTC 2. The fuselage orientation needed to be 1° above the vertical approach angle (i.e., 1 degree nose-up). The difference in the lateral approach angle and the fuselage orientation from structure north was 3 degrees as listed in Table 7–4. An example impact condition for UAL 175 is shown in Figure 7–11, where the vertical approach angle was 6 degrees (fuselage orientation from horizontal = 5 degrees) and the lateral approach angle was 13 degrees (fuselage orientation from structure north = 10 degrees). Larger or smaller angles resulted in projected impact points with the engines spaced too far horizontally or vertically or with the tip of the vertical stabilizer in the wrong location. Also, note that the impact point of the nose had been moved from original estimates, as previously discussed, and that the roll angle was maintained. A second example of an acceptable impact condition, this time with a lateral approach angle of 17 degrees, is shown in Figure 7–12.

Table 7–4. Summary of refined aircraft impact conditions.

	AA 11 (WTC 1)	UAL 175 (WTC 2)
Impact Speed (mph)	443 ± 30	542 ± 24
Vertical Approach Angle (Velocity vector)	10.6° ± 3° below horizontal (heading downward)	6° ± 2° below horizontal (heading downward)
Lateral Approach Angle (Velocity vector)	180.3° ± 4° clockwise from Structure North[a]	15° ± 2° clockwise from Structure North[a]
Vertical Fuselage Orientation Relative to Trajectory	2° nose-up from the vertical approach angle	1° nose-up from the vertical approach angle
Lateral Fuselage Orientation Relative to Trajectory	0° clockwise from lateral approach angle	-3° clockwise from lateral approach angle
Roll Angle (left wing downward)	25° ± 2°	38° ± 2°

a. Structure North is approximately 29 degrees clockwise from True North.

Table 7–5. Aircraft impact locations on the WTC towers.

	Horizontal Location	Vertical Location
AA 11 (WTC 1)	2.0 ± 3 ft west of centerline	1.6. ± 4 ft above 96th floor
UAL 175 (WTC 2)	23.1 ± 3 ft east of centerline	0.6. ± 4 ft above 81st floor

The relationship between aircraft trajectory and orientation was then used to reduce the uncertainty of these parameters. The uncertainty in the vertical approach angle from the video analysis varied from 4 degrees to 12 degrees, as shown in Table 7–3, and the fuselage orientation from horizontal from –1 degree to 7 degrees. As a 1 degree difference needed to be maintained in order for the impact pattern to match the observed damage, uncertainty in the vertical approach angle was reduced to 6 degrees ± 2 degrees and the fuselage orientation from horizontal to 4 degrees ± 1 degree. Uncertainty in the lateral approach angle and the fuselage orientation from structure north was similarly reduced, as shown in Table 7–4. The impact points of the wing tips were known to within approximately ± 2 ft. This corresponded to an uncertainty in the roll angle of approximately ± 2 degrees.

Figure 7–11. An orientation and trajectory of UAL 175 that matches the impact pattern (vertical approach angle = 6°, lateral approach angle = 13°).

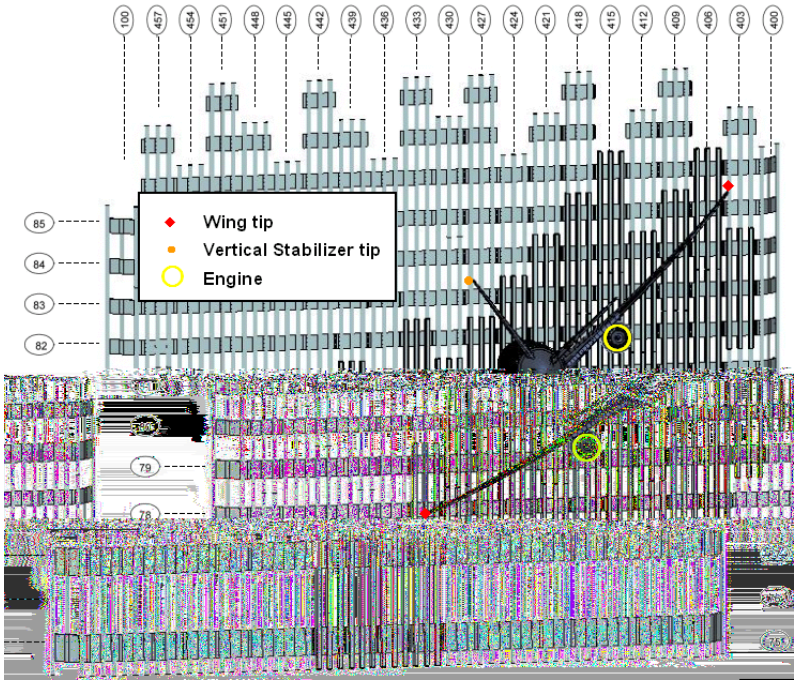

Figure 7–12. An orientation and trajectory of UAL 175 that matches the impact pattern (vertical approach angle = 6°, lateral approach angle = 17°).

Although the lateral approach angle of UAL 175 had a nominal value of 15 degrees, additional observable information was used to define a most probable flight condition. Figure 7–13 shows the top view of WTC 2 with the engines and landing gear in their pre-impact location. Also shown is the projected trajectory of the starboard engine of UAL 175 with an initial lateral approach trajectory of 13° instead of 15°, assuming the engine was not significantly deflected as it passed through the building. With this lateral trajectory, the starboard engine would exit the tower at the northeast corner, consistent with the observables from video and photographic evidence.

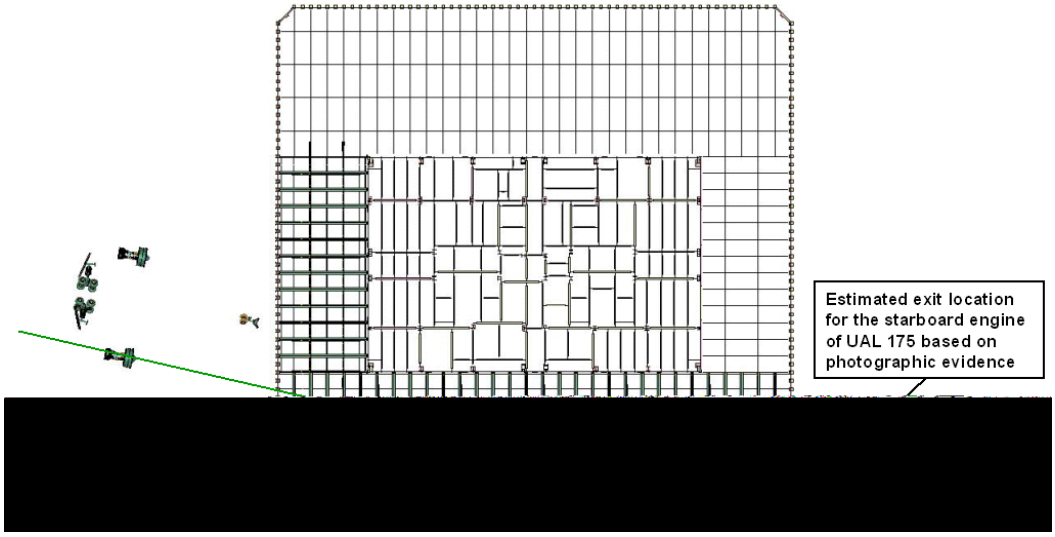

Figure 7–13. Projected trajectory of the starboard engine of UAL 175 with an initial lateral approach angle of 13°.

It is possible that the tower structure and/or contents deflected the engine from its initial lateral trajectory. The global simulations described in Chapter 9 used a standard configuration for building contents similar to WTC 1. This configuration did not cause substantial deviation in the trajectory of the starboard engine. This lateral trajectory was, therefore, the most likely and was adopted for the global analyses.

7.4 COMPARISON WITH ALTERNATE AIRCRAFT IMPACT CONDITIONS

Alternate analyses and values of the aircraft impact initial conditions have been performed and reported by other studies. The objective of this analysis was to provide an independent assessment using the full database of video and photographic evidence collected and maintained by NIST. Many of these data sources may not have been available in the previous analyses. In this section, a comparison is presented between the aircraft impact conditions estimated in this study and those reported earlier. This comparison provides an opportunity to review the methodologies applied, as well as assists in the determination of the uncertainties in the impact conditions. The comparison includes estimates or analyses performed by the Federal Emergency management Agency (FEMA), Hart-Weidlinger, and Massachusetts Institute of Technology (MIT) and the analyses presented in this chapter (NIST). The analysis methodologies or data sources used for the FEMA estimate of the impact conditions were not available. As a result, an evaluation of those estimates of impact conditions and determination of their uncertainties could not be made.

Table 7–6 compares the results of the motion analyses for the AA 11 impact. Both the Hart-Weidlinger and MIT analyses utilized the Doppler shift of the engine noise to determine the aircraft speed. The Hart-

Weidlinger velocity analysis was based on AA 11 approaching the north tower at an angle 4º shallower than the analyses presented here (NIST analysis in Table 7–6). If the Hart-Weidlinger analysis had the aircraft approaching at a steeper angle, it would have reported a speed much closer to the MIT and NIST analyses. One significant difference in the analyses of the AA 11 impact conditions was that none of the previous analyses had the opportunity to utilize the V2 video. This second video from a different location was very helpful in determining the motion parameters of the AA 11.

Table 7–6. AA 11 (WTC 1) aircraft impact analysis comparison.

	FEMA[a]	Hart-Weidlinger[b]	MIT[c]	NIST
Best Estimate Speed (mph)	470	500	429	443
Speed Error Estimate (mph)		+ 30 / - 50	± 51	± 30
Lateral Approach Angle (clockwise)		4.3º		0.3º ± 4º
Vertical Approach Angle (downward)		6.2º		10.6° ± 3°
Aircraft Roll (left wing down)		20.7º		25º± 2°

a. FEMA World Trade Center Building Performance Study, May 2002. Analysis methodology or data source not available.
b. Levy, M., and Abboud, N., 2002, "World Trade Center – Structural Engineering Investigation," Hart-Weidlinger.
c. The Towers Lost and Beyond, Massachusetts Institute of Technology, Eduardo Kausel.

Table 7–7 compares the results of the various motion analyses for the UAL 175 impact. The Hart-Weidlinger and the analyses presented here were consistent with the exception of the lateral approach angle. The MIT estimates of impact speed are low compared to the other analyses. However, assuming a lateral approach angle of 20º would have increased the MIT estimate of the UAL 175 impact speed to 524 mph.

Table 7–7. UAL 175 (WTC 2) aircraft impact analysis comparison.

	FEMA[a]	Hart-Weidlinger[b]	MIT[c]	NIST
Best Estimate Speed (mph)	590	550	503	542
Speed Error Estimate (mph)			± 38	± 24
Lateral Approach Angle (clockwise)		11.7º	15º	15° ± 2°
Vertical Approach Angle (downward)		2.7º	0º	6° ± 2°
Aircraft Roll (left wing down)		30.1º		38°± 2°

a. FEMA World Trade Center Building Performance Study, May 2002. Analysis methodology or data source not available.
b. Levy, M., and Abboud, N., 2002, "World Trade Center – Structural Engineering Investigation," Hart-Weidlinger.
c. The Towers Lost and Beyond, Massachusetts Institute of Technology, Eduardo Kausel.

7.5 SUMMARY

Three different methods were used to determine the impact conditions for the two aircraft that impacted the WTC towers. The initial impact conditions included aircraft speed, horizontal and vertical angles of incidence, roll angle of each aircraft, and the location of nose impact with each tower. The first method used a comparison of videos from different positions to calculate the three-dimensional trajectory of the aircraft. The second method used the relative frame-by-frame motion in a single video, scaled to the length of the aircraft in the video to calculate the impact speed. Finally, analysis of the impact damage on the face of each tower was used to refine the relative impact orientation and trajectory. This was done by

matching the projected impact points of the wings, fuselage, engines, and vertical stabilizer onto the exterior wall of each tower to the observed damage pattern.

7.6 REFERENCES

Cilke, R.W., 1995, "Motion Picture Analysis Procedures for Impact Parameters of Air-Delivered Weapons," FCT-LR-95-6, prepared by Applied Research Associates, Inc., Letter Report to the Defense Nuclear Agency, June.

FEMA, 2002, "World Trade Center Building Performance Study: Data Collection, Preliminary Observations and Recommendations," FEMA 403, May.

Foecke, T., and Pitts, W., NIST Predecisional Documents, Presentations, and Personal Communications.

Kausel, E., "The Towers Lost and Beyond," Massachusetts Institute of Technology, May 2002, http://web.mit.edu/civenv/wtc/index.html.

Levy, M., and Abboud N., 2002, "World Trade Center – Structural Engineering Investigation," Hart-Weidlinger Technical Report, Prepared for Wachtel, Lipton, Rosen, and Katz, August 1.

Lipton, E., and J. Glanz, 2002, "First Tower to Fall Was Hit at Higher Speed, Study Finds," The New York Times, February 23.

The Boeing Company Website, www.boeing.com.

Chapter 8
UNCERTAINTY ANALYSES

8.1 INTRODUCTION

The objectives of the uncertainty analyses were to assess the effect of uncertainties associated with the aircraft and World Trade Center (WTC) towers on the level of impact-induced damage to the towers and to determine the most influential modeling parameters that affect the damage estimates. Uncertainty arises in these analyses from the following key parameters:

1. Aircraft impact parameters: aircraft speed, horizontal and vertical angles of incidence, orientation, and location of impact.
2. Material properties: high strain rate material constitutive behavior and failure criteria for the towers and the aircraft.
3. Aircraft mass and stiffness properties and the jet fuel distribution in the aircraft.
4. Tower parameters: Structural strength and mass distribution, connection and joint positions relative to impact and joint failure behavior.
5. Nonstructural building contents that may absorb energy imparted by the aircraft impact.

An important class of uncertainty that is not listed in these key parameters is the inaccuracy associated with mathematical or numerical models. These uncertainties, also known as modeling errors, are deterministic in nature, but are often treated as random variables to characterize the effects of the analysis methodologies on the calculated response. All of these variables do not necessarily have a significant effect on the estimated impact damage to the WTC towers. An example of such modeling parameters is the resolution of the finite element model and the associated element sizes. Other examples include modeling of erosion and contact in the finite element calculations (see Section 8.2.1 for description of some of these parameters).

Because of the complexity of the problem, down-selection of all possible uncertainty parameters to a refined list applicable to a limited number of global impact analyses needs to be justified. Engineering experience and intuition alone are not sufficient. Therefore, parameter screening was conducted using design of experiments methodology. Screening was first conducted at the component and subassembly levels using orthogonal factorial design techniques in order to identify the most influential parameters and reduce the number of parameters to a more manageable number for the global impact analyses. These component and subassembly uncertainty analyses are the subject of this chapter.

A Plackett-Burman experimental design (Plackett, R.L., and Burman, J.P. 1947) was used for the screening of parameters in the analyses discussed in this chapter. Plackett-Burman (P-B) designs are two-level designs, run at high and low values for each parameter. For k parameters, Plackett-Burman designs require $4\times[\text{int}(k/4)+1]$ runs, i.e., the least multiple of 4, greater than k. One additional run, with all parameters held at their nominal or central values, is also performed. There are several advantages to using a Plackett-Burman design for the screening of parameters. First, P-B designs require fewer runs

than the usual k+1 runs needed for a “one at a time plus center point” design. Parameters are also allowed to vary throughout the entire set of runs, each parameter simultaneously in the presence of each other's variation.

8.2 COMPONENT AND SUBASSEMBLY LEVEL UNCERTAINTY ANALYSES

Two sets of component-level uncertainty analyses were performed. The first set of uncertainty analyses was that of an aircraft engine impacting a collection of core columns. As discussed in Chapter 5, a single core column impacted solidly by an engine was completely overwhelmed and destroyed. This response made it difficult to determine differences in impact behavior caused by uncertainties in the impact parameters. A collection of columns was, therefore, selected to obtain a more sensitive measure of column damage to engine impact. The second set of component level uncertainty analyses was for an empty aircraft wing section impacting two exterior panels, the same configuration discussed in Section 5.5.1. Finally, the subassembly uncertainty analysis was that of the configuration discussed in Chapter 6 impacted by an aircraft engine.

8.2.1 Engine - Core Column Component Uncertainty Analyses

The impact configuration for the engine and core column impact uncertainty analysis is shown in Figure 8–1. The assembly of core columns was selected from the core column arrangement on floor 96 of WTC 1. The first column impacted by the engine was column 503 in the assembly (Figure 8–1). The other columns in the assembly had the same positions relative to each other as existed in the core structure, but were moved closer together. The reduced column spacing was used so that the subsequent motion of the engine and debris following the initial impact would interact with additional columns. This is shown for a sample configuration in Figure 8–1(b). In this arrangement, a range of impact orientations and severity were obtained in each simulation as appropriate for the engine interacting with the tower core structures.

The core columns’ top and bottom were attached to a steel plate of the same material as the column. These plates were rigidly constrained around their edges. These boundary conditions were selected to approximate the compliance of the continuous columns in the tower core frame structure. A more rigid constraint at the column ends was found to initiate failures at column ends with small column impact deformations and energy absorption. Columns were one story in height.

Thirteen uncertainty parameters were used in the engine-core column impact analyses, as shown in Table 8–1. The flight parameters, including speed and vertical and horizontal impact locations, were varied in this analysis. Impact speed in this analysis was based on previous estimates for the impact speed of flight UAL 175 that impacted the WTC 2 tower. A wide range of uncertainty in impact speed was used in these analyses for two reasons. First, these uncertainty analyses were performed before the analysis of the impact conditions was performed and the impact speed was more accurately determined. The second reason was that the aircraft engine lost an unknown amount of speed when penetrating the exterior of the building. Therefore, the velocity at which the engine reached the core was not accurately known. The variations in the horizontal and vertical impact locations were selected to be appropriate for the problem geometry used, and thus, the impact point was moved from being centered on the first column to half the width between columns horizontally and to the top of the engine at the ceiling height

vertically. The minimum values for horizontal and vertical impact locations were the same as the baseline values for symmetry considerations.

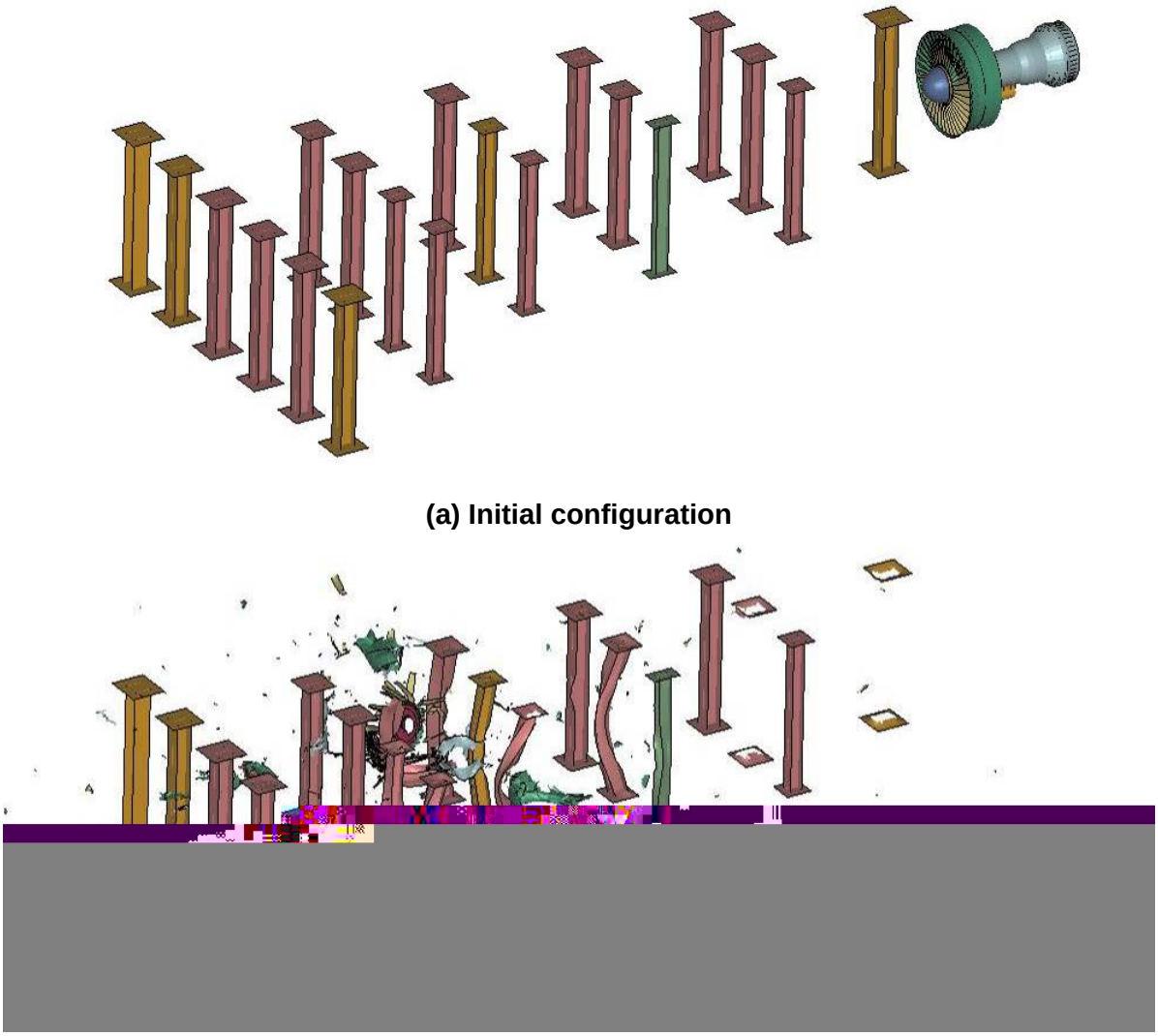

(a) Initial configuration

(b) Impact response at 0.20 s

Figure 8–1. Example engine impact into an assembly of core columns.

Strength and failure strain were varied in both the engine and tower columns. The tower material strengths were varied by 15 percent, and the engine material strengths were varied by 35 percent. For the tower steels, the baseline strength values were those obtained from the test data. A large variation in failure strain was considered for both structures. Strain rate effects on both the column and engine materials strength were also considered. A magnitude of 1 in the table was the baseline strain rate enhancement of strength discussed in Chapter 2 (obtained by modification of the parameter C in the Cowper and Symonds model). A magnitude of 10 was ten times this enhancement. At the time of this study, final data were not yet available for strain rate effects in the tower materials, so this large variation was selected. Subsequent data, as discussed in Chapter 2, was used to reduce this uncertainty to a scale factor of 0.1 to 2.0 in the rest of the uncertainty analyses. In addition to these material parameter

uncertainties, different data sources cited different materials for many of the engine components, so the two different material sets were considered here.

Table 8–1. Engine-core column impact uncertainty parameters.

Uncertainty Parameters		Parameter ID	Minimum Value	Baseline Value	Maximum Value
Flight Parameters	**Speed**	1	392 mph	485 mph	579 mph
	Vertical Impact Location	2	0.00 ft	0.00 ft	2.03 ft
	Horizontal Impact Location	3	0.00 ft	0.00 ft	3.00 ft
Engine Parameters	**Material Assignment Set**[a]	4	1	1	2
	Material Strength	5	65 %	100 %	135 %
	Failure Strain	6	50 %	100 %	150 %
	Strain Rate Effects	7	10 %	100 %	1000 %
Tower Parameters	**Material Strength**	8	85 %	100 %	115 %
	Failure Strain	9	50 %	100 %	150 %
	Strain Rate Effects	10	10 %	100 %	1000 %
Model Parameters	**Erosion Parameter**[a]	11	1	1	2
	Contact Parameter[a]	12	1	1	2
	Friction Coefficient	13	0.0	0.3	0.6

a. Discrete parameter.

Several deterministic parameters, or modeling parameters, were also considered. The first was the erosion parameter in the contact algorithm of LS-DYNA. When an element exceeds the failure criterion, the element is eroded or removed from the calculation. When all of the elements attached to a specific node have eroded, that node becomes free or unattached from any of the other structures in the calculation. However, the free nodes still have mass and momentum. Depending on the selection of the erosion parameter, the free nodes can be maintained or eliminated in the contact algorithms. Deleting nodes may reduce the impact loads on the structure by eliminating their momentum from subsequent impacts. However, maintaining the deleted nodes in the contact algorithms can sometimes lead to computational instability. Provided the failed part of the structure had lost the majority of its initial momentum, the removal of free nodes from contact calculations should have had little effect on the results. Varying the erosion parameter in the uncertainty analyses helped to evaluate the significance of this effect.

Finally, two additional contact parameters were considered. These are the contact type and the friction coefficient between contacting parts. The contact parameter alternates the numerical algorithm used to model contact. A parameter set to 0 uses a penalty treatment and 1 uses the soft constraint algorithm. The penalty formulation is the default option in LS-DYNA and is the most efficient contact algorithm. The soft constraint option uses the nodal mass and global time step to calculate the local interface stiffness. This algorithm typically is more robust and often necessary for calculations with large variations in material elastic bulk moduli (e.g., steel and tower internal contents). A more complete explanation of the differences in these contact types can be found in the LS-DYNA user's manual. For the coefficient of friction between contacting parts, a large variation was considered. This large uncertainty stems from various sources. Reference values for the coefficient of friction for aluminum on steel is approximately 0.45 (Oberg et. al. 1990). However, in this impact situation there were many

possible complexities that served to modify the effective friction coefficient. These factors included, among others, painted and unpainted surfaces, erosion of metal and painted surfaces, and changes in properties of paint and metal from heating. In addition, the ability of the contact algorithms to smoothly calculate the interface normal and frictional forces is reduced with a coarser mesh resolution. The friction coefficient was therefore varied from 0.0 to 0.6.

A fractional factorial 2^{13-9} experimental design was selected for this study, as shown in Table 8–2, with the intent of identifying the significant parameters affecting the impact response. The uncertainty factor IDs are listed across the top of the table, with the run number on the left hand side. Minimum and maximum cases from Table 8–1 are shown by –1 and +1, respectively. Baseline cases are shown by 0.

Table 8–2. Fractional factorial 2^{13-9} experimental design (with centerpoint) for the engine-core column impact analyses.

The reduction in load carrying capacity of the damaged assembly of columns as a fraction of the original capacity was selected as the response parameter for this study. The complex variation in the damage modes and nonlinear damage behavior made it difficult to estimate the reduction in load carrying capacity. Therefore a set of simplified engineering analyses were used to calculate the change in load carrying capacity for each column. The baseline strength was assumed to be the full plastic load level or yield strength multiplied by the cross sectional area. The main factors that were considered for the reduction in load carrying capacity were the reduction in cross sectional area from failed material, deflections of the column centerline that influence the global collapse behavior, and cross-section damage or distortions that modify the local stress distribution.

The first factor that reduced the load carrying capacity was the fraction of the cross-section that had failed under the impact load. The load carrying capacity was reduced by the ratio of the remaining to initial cross-sectional areas. The second factor used to calculate the residual column strength was the maximum centerline displacement of the column produced by the impact damage. The effect of the centerline displacement was determined using classical solid mechanics analysis of an axial compressive load, centered on the column ends and aligned with the original longitudinal axis of the column. At the point of maximum centerline displacement, the axial compressive load resulted in both a uniform compressive force and a moment equal to the force multiplied by the centerline displacement. The column was assumed to fail when the maximum compressive stress in the column reached the yield stress. For simplicity, the bending was assumed to be aligned with the direction of the maximum principal moment of inertia for the column.

The last factor that reduced the load carrying capacity of a column was the local distortion in the cross-sectional shape. The magnitude and type of distortion of the cross-section was difficult to quantify due to the large variation in impact conditions and damage. To simplify this characterization, a cross-section damage scale was developed, where the damage was classified in integer magnitudes varying from 0 to 5, where 0 indicates no damage to the cross-section and 5 represents the greatest damage (large distortions and close to failure). The cross-section distortion of each column was evaluated in the final state of the simulation, and engineering judgment was used to categorize the damage magnitude for each column. Example cross-section damage levels for various core columns are shown in Figure 8–2. For each level of increasing damage, the load carrying capacity was reduced by 10 percent.

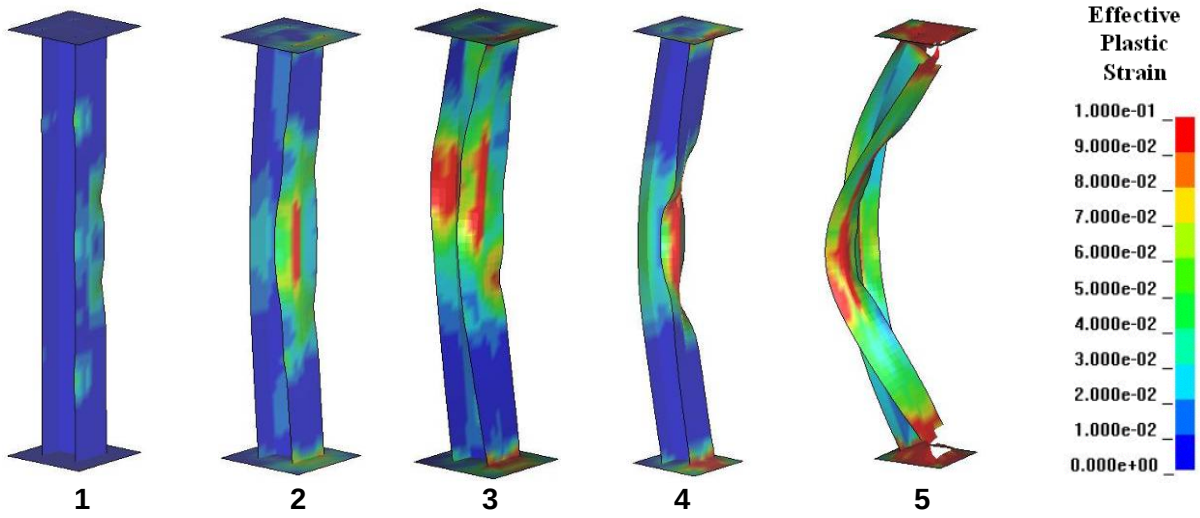

Figure 8–2. Measures of cross-section damage to a core column.

The total reduction in load carrying capacity of a single column was calculated by multiplying the reductions from each factor: the global centerline displacement, cross-section area reductions, and cross-section distortion. The total reduction in capacity of the collection of columns was calculated by summing over all the columns in the model.

A main effects plot for the engine-core column impact analyses is shown in Figure 8–3. The strain rate effect (parameter 10) on column steel strength, horizontal impact location (parameter 3), column materials failure strain (parameter 9), and engine materials strength (parameter 5) had the largest impact on the residual load carrying capacity of the assembly of core columns. The uncertainty in the strain rate effects had the largest effect on the response for these analyses. However, the effect of strain rate was exaggerated by the large variation considered in these analyses. Data made available after the conclusion of this set of engine impact calculations reduced the uncertainty in this parameter to a factor of 2, not 10, for the maximum variation. If the magnitude of uncertainty in the strain rate parameter was reduced by a factor of 5, it is expected that the importance of this uncertainty parameter would be significantly less.

Horizontal impact location (parameter 3) was the second most significant parameter affecting the residual load capacity of the columns. The importance of the horizontal impact position was probably magnified by the problem geometry used. For the baseline and minimum value analyses, the impact was aligned horizontally with a row of columns, and the impact would typically result in complete failure of several columns aligned with the engine trajectory. For the maximum value analyses, the horizontal impact

location was centered between rows of columns, and the impact typically had several glancing impacts as the engine passed between columns. For this impact scenario, significantly fewer columns were completely failed by a solid engine impact.

Figure 8–3. Main effects plot for the engine - core column impact analyses.

Interpretation of this strong significance of the horizontal impact location for the subassembly or global impact analyses was difficult since variations in the flight conditions and initial impact location on the tower exterior were not easily related to the resulting trajectory of the engine through the core. This argument also applies to the vertical impact location.

Although the variation in engine speed resulted in nearly a 50 percent increase in the engine impact momentum, the engine speed did not have a dominant effect on the residual load capacity of the core columns. The relative importance of some parameters can be easily seen. The impact location was more dominant than impact speed since a solid impact at lower speed caused more damage than a glancing impact at higher speed. The impact response mechanisms controlling the relative importance of other parameters were less clear. A contributing mechanism seen was the introduction of tumbling motions of the engine. A side-on impact by the engine produced significantly less damage than a head-on impact (impact trajectory and orientation both aligned with the engine axis of rotation). Similarly, the impact of engine debris caused significantly less damage than a relatively intact engine. As a result, the changes in material ductility and strength could introduce engine impact responses that resulted in significant changes in the cumulative column damage.

The uncertainty parameters with the smallest effect on the load carrying capacity were the core column strength, erosion parameter, and friction coefficient (parameters 8, 11, and 13, respectively). Note that

the friction and erosion parameters were found to have an insignificant effect in this problem geometry compared to a more observable effect in the wing section impact (Section 8.2.2). This is potentially a result of the much larger surface area of failed material and element erosion in the relatively low strength empty wing section as it was torn apart in passing through the exterior columns. Remaining portions of the light empty wing sections were not likely to have sufficient momentum to impart significant structural damage to the core columns.

Based on these results, the following parameters were considered to be potentially significant in the subassembly and global impact analyses:

- Aircraft materials strength.
- Tower materials failure strain.
- Tower material strain rate dependence.
- Engine materials set (possibly secondary significance).

8.2.2 Empty Wing Segment - Exterior Panel Uncertainty Analysis

The empty wing segment and exterior panel models discussed in Section 5.5.1 were selected as an impact configuration to perform the second component-level uncertainty analysis in this study. The wing segment and panel model are shown in Figure 8–4. The impact of a fuel-laden wing segment was found to overwhelm the exterior panel and was, therefore, not used here. The impact of an empty wing section was expected to produce significant damage to the exterior columns, but not catastrophic failure. This level of damage was observed in the photographs of the damage to the exterior columns of the WTC towers where the wing was not laden with fuel.

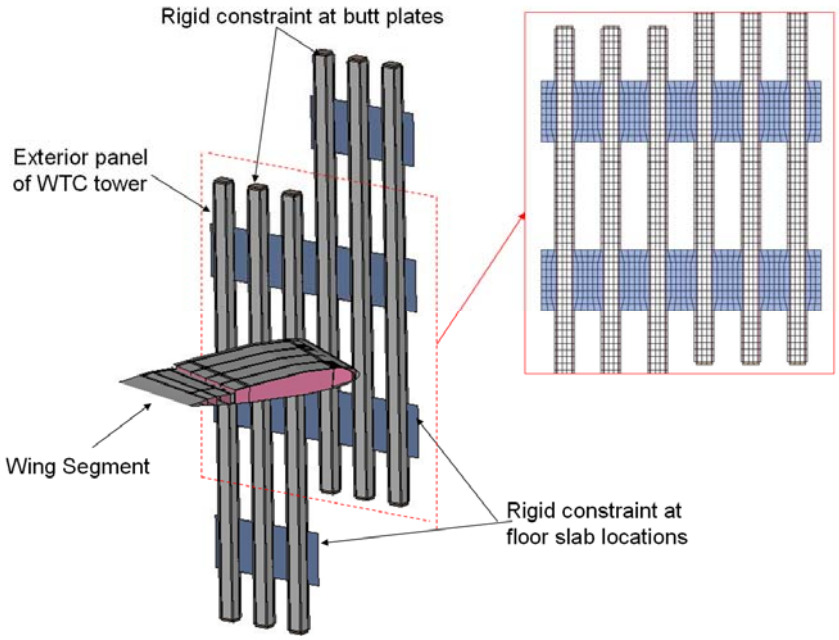

Figure 8–4. Impact configuration for the wing-panel analyses.

Thirteen uncertainty parameters were selected for the wing-panel impact analyses, as listed in Table 8–3. The flight or trajectory parameter uncertainties were obtained from the video and photographic analysis of impact conditions of the impact of AA 11 into the WTC 1 tower, as discussed in Chapter 7. The trajectory angle of the wing segment was varied between –4° and +4°, as shown in Figure 8–5. Strength and failure strain were varied in both the wing and tower structures. Strength of the tower materials were probably known with greater certainty than the aircraft materials due to the detailed testing performed by National Institute of Standards and Technology (NIST). The tower material strengths were, therefore, varied by 15 percent, while the wing material strengths were varied by 35 percent. The element erosion strain, at which elements of the wing structure were deleted from the calculation, was also varied. This parameter was not a reflection of material failure, as discussed in Section 5.5.1, but rather a reflection of how long the nodes and mass of an element remained in the calculation after material failure. Therefore, the erosion strain was included in this example as a modeling parameter. The reader is referred to Chapter 5 for more discussion on this parameter. In addition to these material uncertainties, strain rate effects on the tower materials strength were also considered.

Table 8–3. Wing-panel impact uncertainty parameters.

Uncertainty Parameters		Parameter ID	Minimum Value	Baseline Value	Maximum Value
Flight Parameters	**Speed**	1	413 mph	443 mph	521 mph
	Lateral Approach Angle	2	-4.0°	0.0°	4.0°
Wing Parameters	**Material Strength**	3	65 %	100 %	135 %
	Failure Strain	4	50 %	100 %	150 %
	Rivet Strength	5	50 %	100 %	150 %
	Weight Factor	6	1.5	2.0	3.0
Tower Parameters	**Material Strength**	7	85 %	100 %	115 %
	Failure Strain	8	50 %	100 %	150 %
	Strain Rate Effects	9	10 %	100 %	200 %
Model Parameters	**Erosion Parameter**[a]	10	1	1	2
	Erosion Strain	11	0.2	0.3	0.4
	Contact Parameter[a]	12	1	1	0
	Friction Coefficient	13	0.0	0.3	0.6

a. Discrete parameter.

The weight of the tower exterior panels is known from the detailed structural design information. However, there is significant uncertainty in the weight of the wing, since not all of the minor structural details and non-structural masses were modeled explicitly in the wing. The weight scale factor of the wing was, therefore, varied. This scale factor was based on engineering estimates, as described in Chapter 4. Therefore, a significant variation in the wing section weight scale factor was considered here. The rivet connection strength between the interior structure and skin was also varied. Rivet sizes used between each component in the wing were not known. A large variation in strength was, therefore, considered.

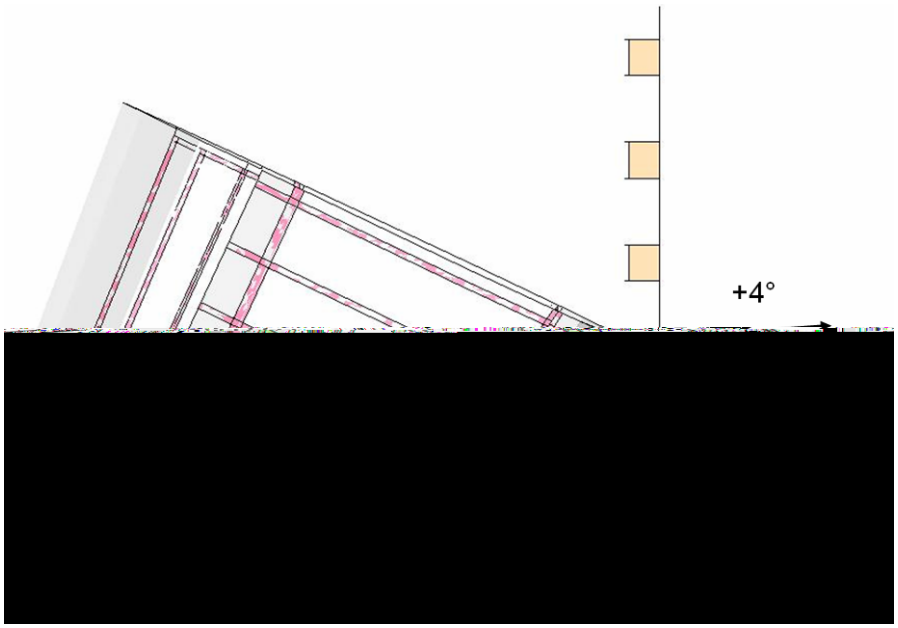

Figure 8–5. Wing segment showing the variation in impact conditions on the exterior panels.

Three deterministic parameters, or modeling parameters, were considered. These parameters were the erosion parameter and two contact parameters, contact type and friction coefficient. These parameters were the same as those used in the wing section exterior panel uncertainty analysis and were discussed in Section 8.2.1.

The matrix of uncertainty parameters used for the engine-core column and the wing-panel impact uncertainty analyses were very similar, as listed in Table 8–1 and Table 8–3, respectively. The primary differences were the uncertainty parameters used for the impact conditions. The uncertainty range used for the engine-core column impact speed was much larger to allow for variations in the impact speed at the core. The engine-core column impact parameters included variations in the horizontal and lateral impact location, while the wing impact analyses varied the lateral approach angle as an impact parameter. The uncertainties in the material properties for the aircraft and tower components were quite similar, with the exception of the uncertainty bounds on the strain rate effects for the tower materials that were reduced significantly for the wing section impact as a result of additional data obtained on the tower steels.

A 2^{13-9} fractional factorial experimental design was used for the wing-panel impact analyses as shown in Table 8–4. The uncertainty factor IDs are listed across the top of the table, with the run number on the left hand side. Minimum and maximum cases from Table 8–3 are shown by –1 and +1, respectively. Baseline cases are shown by 0. The residual linear momentum of the wing and panel debris was used as the response parameter for this analysis. It represents a measure of the potential of the debris to inflict damage to interior structures and to move non-structural masses. This residual momentum was measured by placing a rigid wall in the path of the debris field and recording the change in momentum of the wall. The wall was placed at a sufficient distance from the panel such that contact with the wall had no influence on components impacting the panel.

Table 8–4. Fractional factorial 2^{13-9} experimental design (with centerpoint) for the wing-panel impact analyses.

A main effects plot for the wing-panel impact analyses is shown in Figure 8–6. To generate a main effects plot, all responses at the minimum and maximum cases for a parameter were averaged and denoted as the '-' and '+' values for a parameter, as shown in the figure. The figure indicates that uncertainty in the wing weight had the largest effect on the response of the wing-panel study. However, the relative uncertainty in the total aircraft mass was much smaller than that of the wing itself. The aircraft mass was known to within 5 percent, as discussed in Chapter 4. Redistributing the wing mass with the baseline scale factor of 2 to 3 (a 50 percent change in wing mass), for example, resulted in only an 18 percent change in fuselage weight. The wing weight was also dominated by the mass of the fuel, which weighs approximately twice as much as the empty wing itself. Therefore, in the context of the global analyses, this result was interpreted as the variation in the total aircraft weight was more important than any uncertainty in the wing weight distribution.

Figure 8–6. Main effects plot for the wing-panel impact analyses.

Secondary uncertainty factors included the erosion parameter, impact speed, wing material yield strength and ductility, tower materials ductility, and the friction coefficient. The erosion parameter had a larger effect than the other factors. Although the erosion parameter was significant in these analyses, it caused computational stability problems in some analyses. The negative effect of maintaining the free nodes in contact outweighed the benefit of keeping this momentum in the global impact calculation.

Based on these results and the above discussion, variation in the following parameters were considered to be potentially significant in the subassembly and global impact analyses (not listed in order of importance):

- Impact speed.
- Aircraft materials strength.
- Aircraft materials ductility.
- Total aircraft weight.
- Tower materials ductility.
- Friction coefficient.
- Erosion parameter

8.2.3 Engine-Subassembly Uncertainty Analysis

Figure 8–7 shows the configuration selected to perform the engine-subassembly uncertainty analysis. The subassembly model is the same as that described in Chapter 6. The analysis included an engine impacting a strip of the tower with a width of three exterior wall panels and extending through the truss floor system to the core for a height of three floors. Eleven parameters were selected as the critical uncertainty factors in this analysis, as shown in Table 8–5. Four flight parameters, including speed, vertical impact location, horizontal approach angle, and lateral approach angle were varied in this analysis. Uncertainties from the video and photographic analysis of impact conditions of flight AA 11 impacting the WTC 1 tower were used. Analyses of these impact conditions and associated uncertainties were described in Chapter 7. The baseline vertical impact location was approximately centered between spandrels on the 96th floor. Variation in the vertical impact locations moved the impact point by 3.28 ft as shown in Figure 8–8. The initial vertical approach angle was considered important because this parameter contributed significantly to the vertical load magnitude on the truss floor structures. The lateral approach angle in this analysis determined the path of the engine through the building contents and influenced the potential for an impact on a core column. Horizontal impact location was not varied because variations in the lateral approach angle yielded a similar result on the impact behavior.

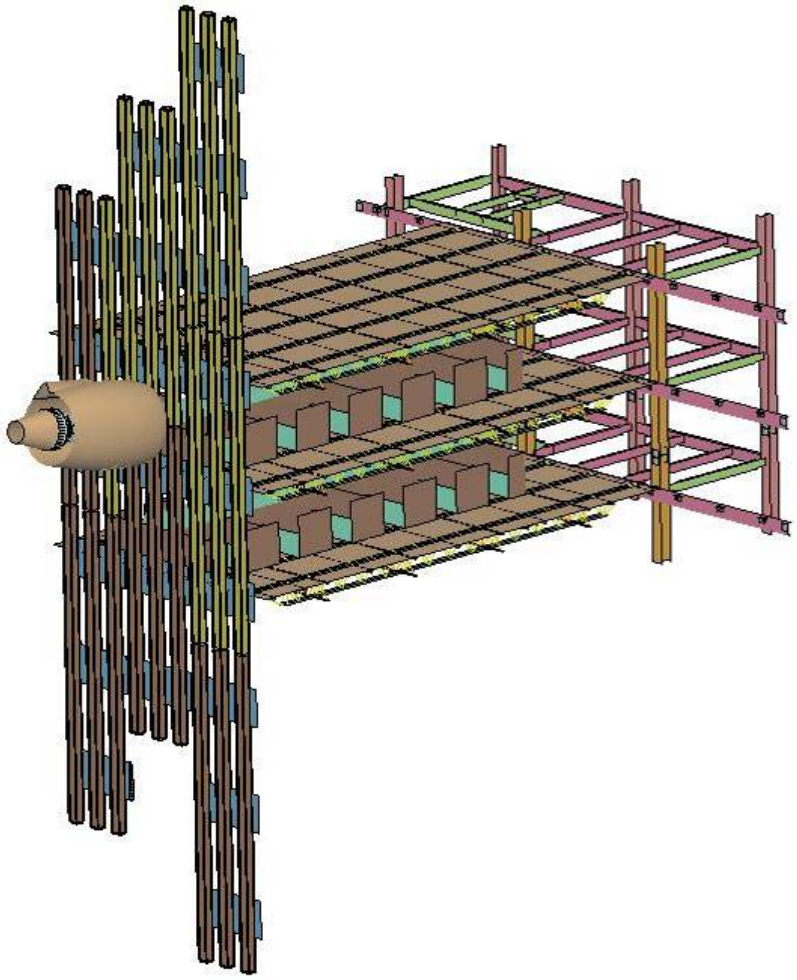

Figure 8–7. Impact configuration for the engine-subassembly impact analyses.

Table 8–5. Engine-subassembly impact uncertainty parameters.

Uncertainty Parameters		Parameter ID	Minimum Value	Baseline Value	Maximum Value
Flight Parameters	**Speed**	1	414 mph	443 mph	472 mph
	Vertical Impact Location	2	-3.28 ft	0.00 ft	3.28 ft
	Vertical Approach Angle	3	7.6°	10.6°	13.6°
	Lateral Approach Angle	4	0.0°	2.0°	4.0°
Engine Parameters	**Material Assignment Set**[a]	5	1	1	2
	Material Strength	6	65 %	100 %	135 %
Tower Parameters	**Material Strength**	7	85 %	100 %	115 %
	Failure Strain	8	50 %	100 %	150 %
	Strain Rate Effects	9	10 %	100 %	200 %
	Tower Contents Weight	10	60 %	100 %	160 %
Model Parameters	**Erosion Parameter**[a]	11	1	1	2

a. Discrete parameter.

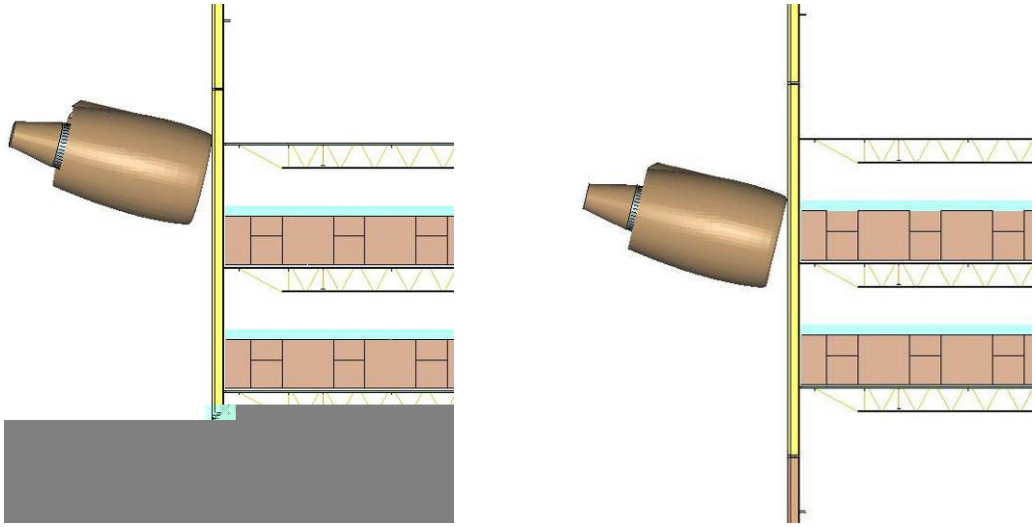

(a) Maximum **(b) Mininimum**

Figure 8–8. Variation in vertical impact location for the engine-subassembly impact analyses.

Tower materials failure strain and strain rate effects were considered in this analysis because of their importance as indicated in the engine-core column component analysis. However, the magnitude of the uncertainty in the strain rate effects was reduced to a more appropriate level as high rate material test data were obtained and evaluated. Engine material strength and the engine material set were included in this study for the same reason. Strength uncertainties were varied in the same way as in the component-level uncertainty analyses. Tower material strength was also considered, as the strength of the exterior columns, floor trusses, and concrete slab had not been investigated in the previous uncertainty analyses.

An additional source of uncertainty that is appropriate for the subassembly analysis was the weight of the interior building contents (modeled here with partitions and workstations) of the towers. A description of the building contents and assumed weight distribution in the global tower models were described in Chapter 3. The variations used for the weight (densities) of the building contents were 60 percent and 160 percent of the baseline weight. Finally, the only modeling uncertainty parameter included was the erosion parameter. Neither variation in the contact parameter or the coefficient of friction parameter had a significant effect in the component-level uncertainty analyses, and thus, their variations were not considered in the global analyses.

A Placket-Burman experimental design of 11 factors was selected for this study, as shown in Table 8–6. The residual kinetic energy of the engine materials as it entered the core of the building was selected as the response parameter for this study. This energy reflected the potential of the engine to inflict damage to the core columns after penetrating through the tower exterior and truss floor region of the building.

Table 8–6. Placket-Burman experimental design of 11 factors for the engine-subassembly impact analyses.

A main effects plot for the engine-subassembly impact analyses is shown in Figure 8–9. Vertical impact location, tower materials strength, and the engine vertical approach angle had the largest effect on the residual kinetic energy of the engine materials. Parameters with the smallest effect on the residual kinetic energy of the engine were the engine materials' set and strength.

Figure 8–9. Main effects plot for the engine subassembly impact analyses.

The vertical impact location had the largest effect on the impact response. For the uppermost engine impact location, the engine tended to glance off the floor slab and continued into the core on the same floor, as shown in Figure 8–10. In four of the six runs where the impact point was in the lower position (runs 3, 4, 6, and 7) the engine was stopped before reaching the core. In these runs, there was significant penetration and interaction with the floor slab, which resulted in a large deceleration and deflection of the engine trajectory.

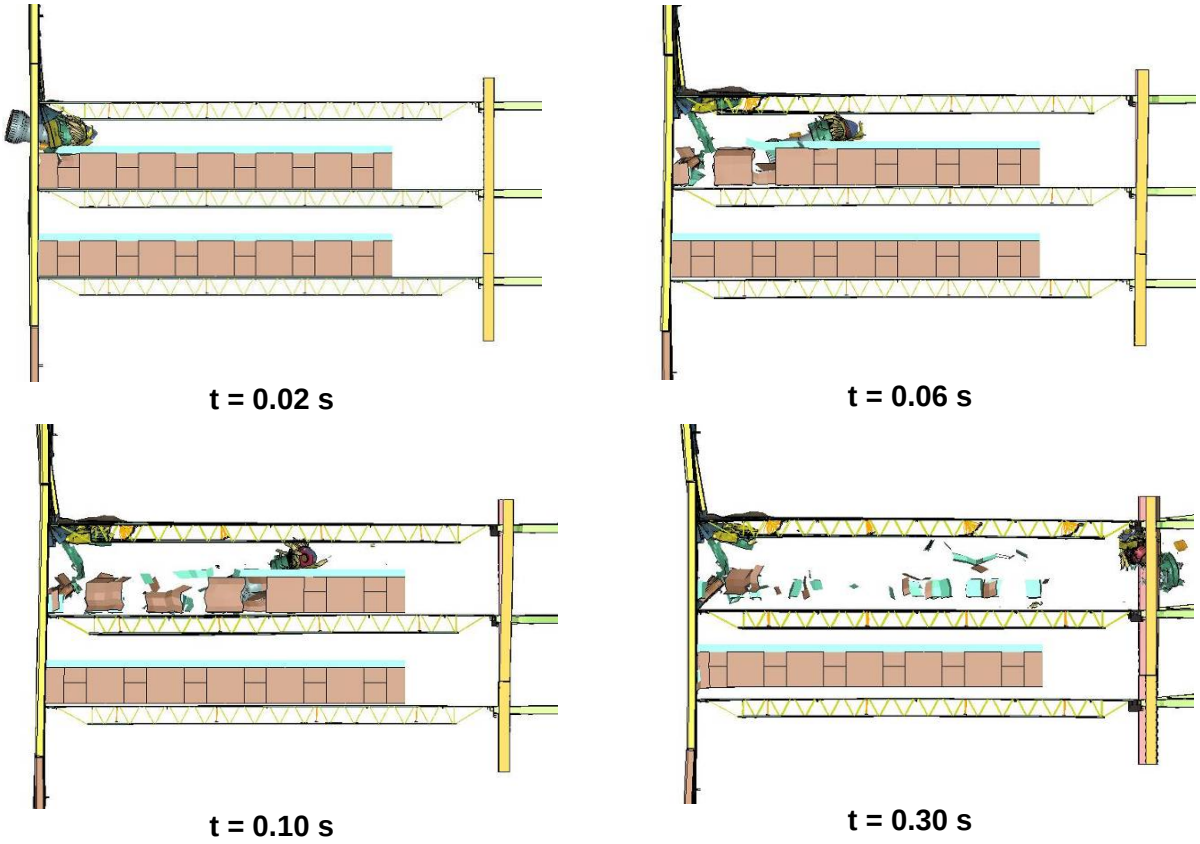

Figure 8–10. Engine impact response and trajectory for run 1.

Based on these results, the following parameters were of primary importance in the subassembly uncertainty analyses:

- Vertical impact location.
- Tower materials strength.
- Engine vertical approach angle.

Of secondary importance, but still yielding appreciable change in the impact response were

- Impact speed.
- Engine lateral approach angle.
- Building contents weight.
- Strain rate effects.
- Tower materials ductility.

Of the primary factors, the vertical impact location uncertainty was difficult to interpret for the global impact analyses. The vertical impact location of an engine relative to the floor slab was obviously

important for the subsequent response of that engine. However, the global impact analyses included the impact response of the entire aircraft. This spanned several floors and included two engines, landing gear, the fuselage, luggage and cargo, and many other components. Altering the vertical impact point for the aircraft, as well as the trajectory (roll, vertical approach, and lateral approach angles), and the aircraft orientation influences where various aircraft components impact the tower relative to floor levels. Therefore, modification of the vertical impact location for a specific engine in these subassembly analyses has a much different effect (and stronger influence on impact damage) than changing the vertical impact location of the entire aircraft. In addition, changing impact parameters, such as the aircraft pitch, changes the vertical impact point of the engines.

8.3 GLOBAL IMPACT ANALYSES PARAMETER SELECTION

Based on the three uncertainty analyses described above, the modeling parameters found to be significant in each analysis are summarized in Table 8–7. Secondary parameters are identified with a '-'. Based on these results and on engineering judgment as explained below, the following parameters were selected for variation in the global impact analyses:

- Impact velocity.
- Vertical approach angle.
- Lateral approach angle.
- Total aircraft weight.
- Aircraft materials failure strain.
- Tower materials failure strain.
- Building contents weight.

The impact speed and vertical approach angle were selected as significant parameters in the global analysis due to their importance in the component and subassembly impact response. The vertical approach angle played a primary role in the magnitude of the vertical impact loads on the truss floor structures. Lateral approach angle was also selected, despite its secondary importance in the component and subassembly analyses, as this parameter dictated to a large extent where aircraft debris traveled and what part of the core was affected by this debris, an effect not captured in the component or subassembly analyses. The vertical impact location was not considered in the global impact analysis, despite being significant in the subassembly analysis. However, the aircraft contained a large collection of components. A change in the vertical location may increase the damage imparted from a particular component, but will simultaneously decrease the damage due to another component, resulting in less pronounced overall effect.

Table 8–7. Summary of significant modeling parameters.

		Engine – Core Column Component	Wing Section – Exterior Panel Component	Engine – Subassembly Impact
Flight Parameters	Impact velocity		9	9-
	Vertical impact location			9
	Vertical Approach Angle			9
	Lateral Approach Angle			9-
Aircraft Parameters	Aircraft materials strength	9	9	
	Aircraft materials failure strain		9-	
	Wing section weight		9	
	Engine materials set	9-		
Tower Parameters	Tower materials strength			9
	Tower materials failure strain	9	9-	9-
	Tower materials strain rate effects	9		9-
	Live load weight			9-
Model	Friction coefficient		9-	
	Erosion Parameter		9	

Variations in the strength and ductility (failure strain) of materials had a similar effect on the amount of energy absorbed. An increase in yield strength or an increase in failure strain resulted in an increase in the energy absorbing capacity of the structure. The yield strength of materials was typically known more accurately than the failure strains. This is particularly true within the finite element analyses, where the value of the failure strain needed to be assigned based on the model resolution and failure criteria used. This effect was described in detail in Section 2.3.1. As a result, only the uncertainties in the material failure strain were used as a material uncertainty parameter for both the aircraft and tower in the subsequent global impact analyses.

The uncertainty in the weights associated with building contents (corresponding to service live loads) was found to be of secondary importance in the engine-subassembly impact analysis. In the global impact analyses, the live load contents were expected to play a more significant role in confining the fuel and debris dispersion. In addition, the partition walls were significant for controlling the subsequent spread of fire through the towers. As a result, the uncertainty in building contents weight was included as an uncertainty parameter in the global analysis.

The wing section weight was found to be an important parameter for the wing section - exterior panel impact analyses. For the global analyses, the total aircraft weight was carried forward as an uncertainty parameter. The uncertainty in the total aircraft weight was, however, significantly smaller than the uncertainty in the weight of the empty wing section impactor. An uncertainty of ±5 percent was used for total aircraft weight.

The engine materials set and the friction coefficient were not found to be sufficiently significant in any of the uncertainty analyses and were, therefore, not included in the global analysis. Similarly, the erosion parameter was found to be significant only for the wing-section impact analyses. The importance of this

parameter was amplified in this example as a result of the relatively low weight and strength of the empty wing-section impactor and the large amount of material failure and erosion as the wing was segmented by the exterior columns. The fact that the erosion parameter uncertainty had a negligible effect on the other analyses and potentially had negative consequences for the stability of the global impact analyses led to the elimination of this parameter from the global impact analyses.

8.4 REFERENCES

"LS-DYNA Keyword User's Manual," 2003. Livermore Software Technology Corporation, Version 970, April.

Oberg, E., F. D. Jones, and H. L. Horton. 1990. *Machinery's Handbook, 23rd Edition*, Industrial Press Inc., NY, p. 2202-2203.

Plackett, R. L., and Burman, J. P., 1947. "The Design of Optimum Multifactorial Experiments," Biometrika, 33.

This page intentionally left blank.

TABLE OF CONTENTS

LIST OF FIGURES

Add a paragraph return between each major section after updating the list.

This page intentionally left blank.

LIST OF TABLES

Add a paragraph return between each major section after updating the list.

This page intentionally left blank.

Chapter 9
GLOBAL IMPACT ANALYSES

9.1 INTRODUCTION

The primary objective of this project was to determine the condition of the two World Trade Center (WTC) towers immediately following the aircraft impacts. This assessment includes both the determination of the structural damage that adversely affected their strength and the condition and position of nonstructural contents such as partitions, workstations, aircraft fuel, and other debris that influenced the behavior of the subsequent fires in the towers. The global impact analyses were the primary method by which most of the information on the tower damage was obtained. The analyses described in the other chapters of this report, such as the component and subassembly impact analyses, were performed to support the development and validation of these global impact models.

9.2 ASSUMPTIONS AND LIMITATIONS

A fundamental limitation of the global impact simulations was the maximum finite element model size that can be executed on the available 32-bit computer clusters. Since LS-DYNA uses addressable memory for domain decomposition, the combined aircraft and tower model could not exceed approximately 2.3 million nodes. The primary assumptions and limitations of the global impact analyses were the result of reducing the model size to meet these decomposition limitations as well as to achieve a run time that allowed the necessary global impact analyses to be completed within the duration of the investigation.

Although the analyses were performed on a 32 bit computer cluster, the precision used in the analyses can be controlled by the analysis software. Both single precision and double precision versions of LS-DYNA were available for the impact analyses. In general, single precision analyses are more efficient and the precision is sufficient for the type of impact simulation being performed. However, when the dimensions of the structure being analyzed are sufficiently large, the single precision analyses can introduce rounding errors in the analyses. The rounding errors occur since the analysis is resolving deformations or analyzing element penetrations on a local scale that is several orders of magnitude smaller than the controlling dimension.

In preliminary simulations, the coordinate system for the models of the tower structures was located near the base of the tower. As a result, the largest dimensions were the vertical position of the structures in the impact zone. This large vertical dimension controlled the size scale in the impact analyses and introduced rounding errors that were manifested as unstable element behaviors. To eliminate this precision problem, the tower model coordinate system was moved to be centered on the impact zone of the tower. The largest controlling dimension was therefore the distance across tower (significantly smaller than the height of the tower). After adjusting the coordinate location, the unstable element behaviors were no longer observed.

To confirm the adequacy of the single precision analyses, subassembly impact analyses (Chapter 6) were performed on the same model in both single and double precision. The comparison of the two analyses showed no substantial difference in the impact response and damage.

Specific assumptions and limitations introduced in the analyses to meet the computational constraint included:

- Tower structures away from the impact zone had a coarse mesh resolution. Therefore, damage in those regions may not be as accurately captured as that in the impact zone. An example is the potential damage to the exterior panels on the far side of the tower (opposite to impact). As debris passed through the building and struck a panel on the far side of the building, the coarse mesh refinement and merged boundary conditions at column ends (as opposed to bolted connections in the impact zone) underestimated the secondary impact damage.

- Tower contents (workstations and nonstructural walls) were only included in the expected path of the aircraft impact and subsequent debris cloud. Therefore, debris and fuel that passed beyond this region could move more freely through the structure, only interacting with primary structural components.

- The analysis of the impact response of the aircraft-fuel cloud had several limitations. Smooth Particle Hydrodynamics (SPH) was used to model the fuel in the impacting aircraft, and approximately 60,000 SPH particles were used for the approximately 60,000 lb of fuel in each aircraft. Therefore, the particle size in the fuel cloud was approximately one pound. The air in and around the towers was not modeled, so the deceleration of the fuel particles in the cloud by aerodynamic resistance was not included. The contact algorithm for the fuel particles and tower did not include a sticking or "wetting" behavior so the fuel particles bounce off of components in the tower. The lack of these limitations would spread the fuel cloud over a larger region in the simulation. Finally, the deflagration of the fuel was not modeled, and the resulting dynamic over-pressure in the tower from the combustion process were not included in the analysis.

- Windows were not modeled on the exterior of the tower. The open space between the exterior columns allowed fuel particles and small debris fragments from the aircraft and tower to escape that may have been contained if the windows were included. Note that the weight of the windows was added to the columns as part of the superimposed dead loads (see Section 3.2.4).

- The rotational velocity of the spinning aircraft engine components was not modeled. The effects of the rotational kinetic energy, stabilization of the engine trajectory, and potential for engine thrust during impact were, therefore, not included in the analysis. An analysis was performed to estimate the magnitude of this assumption, as described in Section 10.3. The analyses indicated that the rotational kinetic energy of each engine was approximately one percent of the aircraft initial kinetic energy. In addition, much of this rotational energy was probably dissipated by internal deformations of the engine components following impact with the tower exterior. Therefore, this approximation should have a small influence on the global impact damage.

- Aeroelastic forces were not applied to the aircraft wings since the generated stresses were not expected to affect the impact response of the tower. The energy associated with the aeroelastic stresses are much less than the energy absorbed during impact. Note that a wing tip deflection was applied as explained in Section 4.3.

- Initial service loads (stresses) in the tower and aircraft were not included. The material internal energy associated with the elastic service loads were small compared to the material internal energy capacity. Therefore, it was not expected to have a significant influence on the dynamic impact response and deformation. Simplified analyses were performed to evaluate the magnitude of this assumption for the impact response of a core column, as described in Section 10.4. These analyses indicated that ignoring the static preload in the column had little influence on either the dynamic column deformations or the resulting collapse strength of the column. Gravitational acceleration was modeled during the impact analyses to include the gravitational acceleration on debris movement and potential contributions to the collapse of the damaged truss floor regions.

- The impact analyses are subject to uncertainties in the input parameters, such as initial impact conditions, material properties and failure criteria, aircraft mass and stiffness properties, mass distribution inside the towers, the jet fuel distribution and dispersion, connections behavior, the presence of nonstructural building contents, etc. (see Chapter 8 for further details). The global analyses presented in this chapter not only provide a "base case" based on a best estimate of all input parameters (based on photographic and video evidence, material testing, and data in the open literature), but also provide more and less severe damage estimates based on variations of the most influential parameters, identified in the sensitivity analyses (Chapter 8). These more and less severe damage scenarios provide a range of damage estimates of the towers due to aircraft impact.

9.3 MODELS FOR THE BASE CASE IMPACT ANALYSES

The development of the tower models and the development of the Boeing 767 aircraft model were described in detail in Chapters 2 and 3, respectively. Similarly, the analysis of the aircraft impact conditions was described in Chapter 7. In this section, a brief description of the combined global model of the tower and aircraft used for the impact simulations is provided. Similar to the component and subassembly analyses, the global impact analyses were performed using the LS-DYNA general purpose finite element software package.

The combined aircraft and tower models developed for the base case global impact conditions of WTC 1 and WTC 2 are shown in Figure 9–1 and Figure 9–2, respectively. The global impact models were each in excess of two million nodes. A detailed summary of the number and types of elements in each model is provided in Table 9–1. The bulk of the aircraft and tower structures were modeled using shell elements. Solid elements were used for specific components, such as the exterior wall butt plates and for some of the thick hubs and flywheels in the aircraft engines. Beam elements were used primarily in the WTC tower floor truss structures and for the bolted connections in the impact zone of the exterior wall.

Table 9–1. Summary of the WTC global impact models.

	WTC 1 Tower Model	WTC 2 Tower Model
Number of Nodes	2,068,736	2,110,970
Belytschko-Tsay Shell Elements	1,682,615	1,716,249
Constant Stress Solid Elements	73,189	72,906
Hughes-Liu Beam Elements	47,952	53,488
SPH Fuel Particles	60,672	60,672

The objective of the base case impact analyses was to provide an estimate of the impact scenario based on an analysis with a best estimate of all the data obtained from photographic and video evidence, material testing, and data in the open literature. A summary of the aircraft impact conditions used for the base case global impacts of the towers is provided in Table 9–2.

Table 9–2. Summary of base case impact conditions.

	WTC 1	WTC 2
Impact Speed (mph)	443	546
Vertical Approach Angle (Velocity vector)	10.6° below horizontal (heading downward)	6° below horizontal (heading downward)
Lateral Approach Angle (Velocity vector)	180.3° clockwise from Structure North	13° clockwise from Structure North
Vertical Fuselage Orientation Relative to Trajectory	2° nose-up from vertical approach angle	1° nose-up from vertical approach angle
Lateral Fuselage Orientation Relative to Trajectory	0° clockwise from lateral approach angle	-3° clockwise from lateral approach angle
Roll Angle (left wing downward)	25°	38°
Total Aircraft Weight	283,600 lb	277,600 lb
Aircraft Fuel Weight	66,100 lb	62,000 lb
Aircraft Cargo Weight	40,600 lb	38,700 lb

(a) Plan view

(b) Side view

Figure 9–1. WTC 1 global impact model.

(a) Plan view

(b) Side view

Figure 9–2. WTC 2 global impact model.

9.4 WTC 1 BASE CASE IMPACT ANALYSIS

This case is referred to as Case A for the remainder of the WTC Investigation reports. The WTC 1 base case analysis was performed for a 0.715 s duration following initial impact of the aircraft nose with the north exterior wall. The analysis was performed on a computer cluster using twelve 2.8 GHz Intel Xeon processors, each on a separate node of the cluster. The run time for this analysis was approximately two weeks. The progress of the global impact simulations was monitored on average every two days. The calculations were terminated when the damaged towers reached a steady state and the motion of the debris was reduced to a level that was not expected to produce significant impact damage. A typical value for the residual kinetic energy in the airframe components at the termination of a global impact simulation was less than one percent of the initial kinetic energy at impact.

A side view of the base case WTC 1 global impact model is shown in Figure 9–3. The tower interior contents were removed, and the tower structures shown as transparent, so that the impact response in the tower interior could be seen. The floor numbers and core columns for the tower model are labeled in the figure. The corresponding side view was used to illustrate the base case global aircraft impact response in Figure 9–4. The response is shown at intervals of 0.1 s from impact through the initial 0.5 s of the response. Corresponding plan view images of the progression of aircraft impact response are shown in Figure 9–5.

Figure 9–3. WTC 1 base case global impact model.

The initial 0.1 s of the base case global aircraft impact response, shown in Figure 9–4(b) and Figure 9–5(b), was dominated by the impact, penetration, and fragmentation of the forward fuselage structures. The engines and wing sections were just starting to impact the exterior wall. The forward fuselage structures were severely damaged both from penetration through the exterior columns and the penetration of the 96th floor slab that sliced these fuselage structures in half. The downward trajectory of

the aircraft structures caused the airframe to collapse against the floor, and the subsequent debris motion was redirected inward along a more horizontal trajectory parallel to the floor.

(a) Time=0.00 s

(b) Time=0.10 s

(c) Time=0.20 s

Figure 9–4. WTC 1 base case global impact analysis (side view).

(d) Time=0.30 s

(e) Time=0.40 s

(f) Time=0.50 s

Figure 9–4. WTC 1 base case global impact analysis (side view) (continued).

(a) Time=0.00 s

(b) Time=0.10 s

(c) Time=0.20 s

Figure 9–5. WTC 1 base case global impact analysis (plan view).

(d) Time=0.30 s

(e) Time=0.40 s

(f) Time=0.50 s

Figure 9–5. WTC 1 base case global impact analysis (plan view) (continued).

At 0.2 s after impact, the wings had completely penetrated the exterior wall, and only the tail structures were still outside of the tower, as shown in Figure 9–4(c) and Figure 9–5(c). The wing structures were completely fragmented by the penetration through the exterior wall. The aircraft fuel cloud was starting to spread out, but was still relatively dense, and the leading edge of the fuel was just reaching the tower core. By 0.2 s, the downward trajectory of the aft structures had transferred sufficient vertical load that the truss floor structures on the 95th and 96th floors were starting to collapse in the impact zone.

At 0.3 s after impact, the aircraft was completely inside of the tower (full penetration completed at approximately 0.25 s), as shown in Figure 9–4(d) and Figure 9–5(d). The airframe was mostly broken up, but some large sections of the aft fuselage and tail were still intact, having penetrated through the opening in the tower wall produced by the forward fuselage structures. The aircraft fuel cloud penetrated approximately half the distance through the core and was spreading out. However, the subsequent motion of the aircraft fragments and fuel debris cloud began to be noticeably slowed beyond this time. The fuel and debris did continue to spread through the tower, but at a much slower rate, as seen in the remaining images in Figure 9–4 and Figure 9–5.

The load transfer of the aircraft impact can be seen by the history of the resultant momentum of the aircraft as shown in Figure 9–6. The momentum plotted for all of the aircraft structures and contents (including fuel) and is normalized by the initial momentum magnitude. The curve illustrates an initial rate of load transfer during the first 0.1 s of impact as the forward fuselage penetrated the exterior wall and impacted the interior structures. Between 0.1 s and 0.25 s, a more rapid load transfer rate was observed, as the area of the impact was greater (extending outward in the wing impact regions), and a higher percentage of the aircraft mass was impacting the interior structures. At 0.25 s, as indicated in Figure 9–6, the aircraft completely penetrated the building and retained approximately 30 percent of its initial momentum. Beyond this time, the rate of load transfer was steadily decreasing, with very little load transfer after approximately 0.5 s.

Figure 9–6. Normalized aircraft momentum for the WTC 1 base case impact.

The aircraft was severely broken into debris as a result of the impact with the tower, as shown in Figure 9–7. At the end of the impact analysis, the aircraft was broken into thousands of debris fragments of various size and mass, as shown in Figure 9–7(b). A closer inspection of the debris field shows that larger fragments still occurred for specific components such as the engines, shown in Figure 9–7(c). At the end of the simulation, the port engine was still inside the core, and the starboard engine was roughly one third of the distance from the core to the southern exterior wall. Both had a speed of less than 50 mph.

(a) Aircraft structure (time=0.00 s)

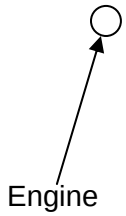

(b) Aircraft debris field (time=0.715 s)

(c) Major engine debris (time=0.715 s)

Figure 9–7. Aircraft breakup and debris in the base case WTC 1 impact.

9.4.1 WTC 1 Base Case Impact Analysis - Structural Damage

The structural damage to the WTC 1 tower by the base case impact conditions is described in this section. The primary structural components of interest were the exterior wall, core columns and core framing components, and the floor structures and concrete slab. The response of the internal contents, walls, and partitions were also of interest to provide the initial conditions for the fire dynamics simulations.

Exterior Wall Damage

The calculated damage to the exterior wall is significant for two reasons: (1) the exterior wall contributed significantly to the strength of the tower, and the degradation in exterior wall strength was important for the collapse analyses, and (2) the exterior wall was the only structural system for which direct visual evidence of the impact damage was available. Therefore, the comparison of the calculated and observed exterior wall damage can provide a partial validation of the analysis methodologies used in the global impact analyses.

A comparison of the north exterior wall observed and calculated damage from the base case WTC 1 global impact analysis is shown in Figure 9–8. The calculated impact damage to the exterior wall is shown with color fringes representing plastic strain magnitude, with undamaged sections in blue and strains at or above 5 percent shown in red. The schematic of observed damage was developed from inspections of the video and photographic data collected on the tower after impact. Both the observed and calculated damage wall regions shown in Figure 9–8 illustrate a region of the exterior wall from column 108 to column 152, extending from floor 91 to floor 100 (spandrels at floors 92 through 100).

The first observation from the comparison of the calculated and observed damage was that the geometry and location of the impact damage zone were in good agreement. This agreement in the position and shape of the impact damage served to validate the geometry of the aircraft model, including the aircraft orientation, trajectory, and flight distortions of the wings.

The second observation was the agreement in the magnitude and mode of impact damage on the exterior wall. The exterior wall completely failed in the regions of the fuselage, engine, and fuel-filled wing section impacts. Damage to the exterior wall was observed all the way out to the wing tips, but the exterior columns were not completely failed in the outer wing and vertical stabilizer impact regions. Failure of the exterior columns occurred both at the bolted connections between column ends and at various locations in the column, depending on the local severity of the impact load and the proximity of the bolted connection to the impact. The agreement in both the mode and magnitude of the impact damage served to partially validate the constitutive damage modeling of the aircraft and exterior wall of the tower.

Core Structural Damage

The determination of the damage to the core columns and core beams was important in determining the residual strength for the subsequent analyses of structural stability and collapse. The overall model for the core structure and calculated impact damage to the core is shown in Figure 9–9. The figure shows that the core had significant damage in the regions close to the impact point. The columns in line with the

aircraft fuselage failed on the impact side, and several of the core beams were also severely damaged or failed in the impact zone.

(a) Schematic of observed damage

(b) Calculated damage (t=0.715 s)

Figure 9–8. Base case impact damage to the WTC 1 exterior wall.

(a) Initial geometry

(a) Calculated impact damage

Figure 9–9. Base case impact damage to the WTC 1 core frame structures.

The calculated damage to the core columns by is shown in Figure 9–10. The columns are shown with color fringes representing plastic strain magnitude, with undamaged sections in blue and strains at or above 5 percent shown in red. A summary of column damage is listed in Table 9–3 and shown graphically in Figure 9–11. The qualitative classification of the column damage levels is shown in Figure 9–12. The classification levels were light damage, moderate damage, heavy damage, and failed (severed). The light damage level was defined as having evidence of impact (low level plastic strains), but without significant structural deformations. The moderate damage level had visible local distortions of the column cross section (e.g. bending in angle) but no lateral displacements of the column centerline. The heavy damage classification was for impacts that produced global deformation of the column, resulting in a permanent deflection of the column centerline. The severed columns were completely failed and could carry no residual loads. A summary of the floor-by-floor damage to the core framing is shown in Figure 9–13.

P–' effects generated due to the sway of the towers after impact, as observed in video evidence (see NIST NCSTAR 1-5A), were not expected to affect or impose additional damage to the core columns. The core columns were designed as axially loaded members without continuity of framing, and thus would not develop significant P–moments (see Chapter 5 of NIST NCSTAR 1-2A).

Floor Truss and Slab Damage

The impact damage to the floor trusses and floor slabs could contribute significantly to the loss of structural strength and subsequent collapse. The trusses and floor sections provided lateral support to the exterior wall at each floor level. Any damage or holes in the concrete floor slab could provide a path for the fires to spread from floor-to-floor. Therefore, the calculation of the floor system damage was an important component of the global impact analyses.

An overall front view of the floor truss structure in the impact zone, along with the calculated impact damage to the floor trusses, is shown in Figure 9–14. The truss structures shown are for the detailed truss floor section models described in Section 3.2.3 and Section 3.2.5. The figure is from a view point exterior to the tower, looking toward the impact point, and shows that the trusses experienced significant damage in the impact zone. A plan view of the calculated damage to the truss on each floor is shown in Figure 9–15. The calculated impact response produced severe damage to the truss structures in the primary impact path of the fuselage. The truss structures were severely damaged from the exterior wall to the core. The truss floor system on floors 94 through 96 were damaged and sagging downward as a result of the impact loading.

(a) Columns 501-1001 (b) Columns 502-1002 (c) Columns 503-1003

(d) Columns 504-1004 (e) Columns 505-1005 (f) Columns 506-1006

(g) Columns 507-1007 (h) Columns 508-1008 (i) Reference scale

Figure 9–10. Base case impact damage to the WTC 1 core columns.

Table 9–3. Summary of core column damage for the base case WTC 1 impact.

Column	Location	Damage Level	Lateral Deflection of Column Centerline (in.)
Column 503	Floor 96	Heavy	18
Column 504	Floors 92–96	Severed	
Column 505	Floors 93–96	Heavy	20
Column 506	Floors 93–94	Heavy	10
Column 604	Floors 92–96	Severed	
Column 605	Floors 94–95	Moderate	
Column 702	Floor 96	Moderate	
Column 703	Floor 96	Moderate	
Column 704	Floor 94	Heavy	18
Column 705	Floor 95	Moderate	
Column 706	Floors 93–95	Severed	
Column 802	Floor 96	Moderate	
Column 805	Floor 94	Moderate	

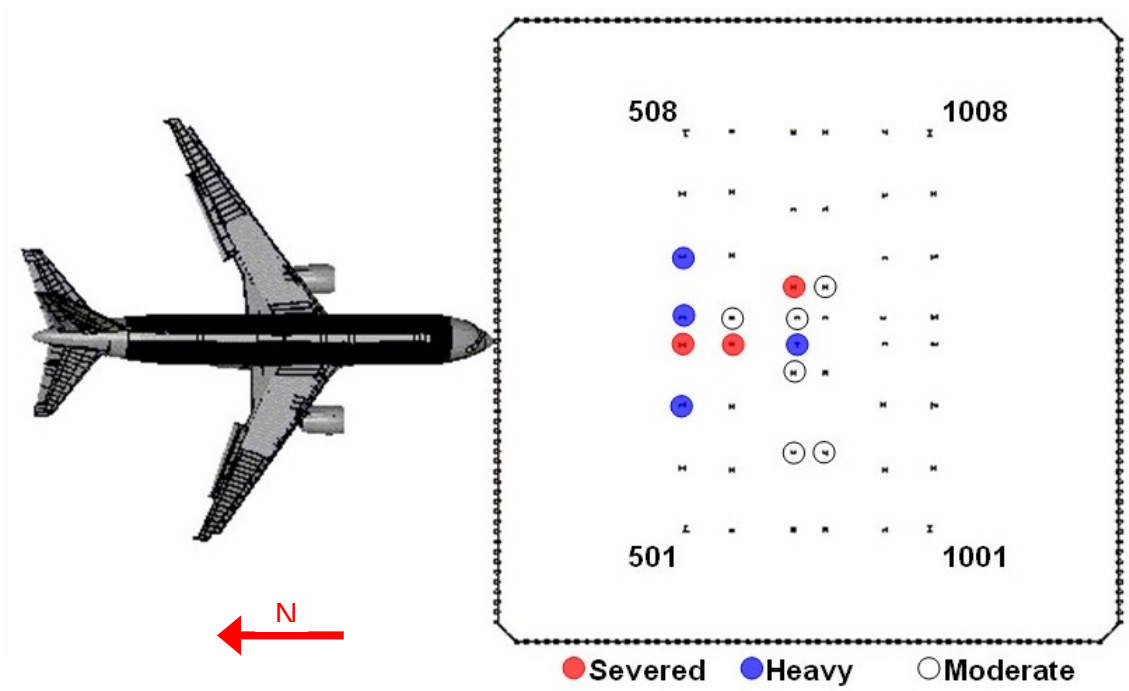

Figure 9–11. Summary of core column damage for the base case WTC 1 impact.

(a) Light (b) Moderate (c) Heavy (d) Severed

Figure 9–12. Classification of damage levels in core columns.

(a) Floor 93 core framing damage

(b) Floor 94 core framing damage

(c) Floor 95 core framing damage

(d) Floor 96 core framing damage

(e) Floor 97 core framing damage

(f) Floor 98 core framing damage

Figure 9–13. Base case impact damage to the WTC 1 core floor framing (plan view).

(a) Initial detailed truss structures

(b) Calculated damage (t=0.715 s)

Figure 9–14. Base case impact damage to the WTC 1 floor trusses (front view).

The calculated damage to the WTC 1 floor slab for floors 94 through 97 is shown in Figure 9–16. The fringes of damage were set such that the concrete slab failed in the regions colored red (2 percent plastic strain was used corresponding to the zero stress strain limit for the concrete in unconfined compression). At these strain levels, the concrete was severely damaged and probably removed, exposing the supporting metal decking. Beyond 2 percent plastic strain, the strength of the floor slab was severely reduced in the analyses to model the residual strength of the metal deck after the concrete failure, breakup, and removal. At a plastic strain of 30 percent, corresponding to failure levels for the metal decking material, the elements were eroded (seen as ruptured in the floor slabs shown). The line of damage, visible around the edge of the core in Figure 9–16, is believed to be the result of numerical precision errors and interference in the modeling methodology at the connection of the floor slab rather than impact damage.

(a) Floor 94 truss damage

(b) Floor 95 truss damage

(c) Floor 96 truss damage (d) Floor 97 truss damage

Figure 9–15. Base case impact damage to the WTC 1 floor trusses (plan view).

(a) Floor 94 slab damage

(b) Floor 95 slab damage

(c) Floor 96 slab damage

(d) Floor 97 slab damage

Figure 9–16. Base case impact damage to the WTC 1 floor slab (plan view).

9.4.2 WTC 1 Base Case Impact Analysis – Fuel and Debris Distributions

The objectives of the global impact analyses included the determination of both the structural damage and the initial conditions that influenced the initiation and propagation of the fires in the towers, including the distribution of the jet fuel in the towers, the distribution of tower contents and aircraft debris that provided flammable materials for the fires, and the condition of the partitions and walls that provided barriers to air flow and spreading of the fires.

The global impact results presented in this section include the distribution of the jet fuel inside the tower, the damage to the building contents (partition walls and workstations), and the aircraft debris distribution in the towers. The jet fuel was modeled using a smoothed particle hydrodynamics (SPH) algorithm in

LS-DYNA, as described in Section 5.5.3. For the baseline case WTC 1 global impact analysis, the calculated distribution of the fuel in the tower and shape of the fuel cloud in a plan view and side view are shown in Figure 9–17 and Figure 9–18, respectively. At the termination of the global impact analysis, the residual momentum of the jet fuel in the impact direction was less than one percent of the initial momentum, indicating that the fuel cloud was nearly at rest at about 0.715 s.

To more clearly present the calculated response of the structures that influenced the fire propagation, the structural components were removed from the visualization, with the exception that the core columns were maintained in the visualizations for reference positions. A plan view of the response of the remaining building contents and aircraft debris is shown in Figure 9–19. Similar plan views of floor-by-floor slices through the building contents and debris field are provided in Figure 9–20 through Figure 9–24 for floors 94 through 98, respectively. The bulk of the aircraft debris and fuel were arrested prior to exiting the far side of the tower core. A small amount of aircraft debris was calculated to exit the far side of the tower (south wall of WTC 1).

A quantitative characterization of the fuel and aircraft debris distribution was obtained by slicing the model at vertical floor locations and calculating the mass at each floor level. A summary of the floor-by-floor fuel and debris distributions is given in Table 9–4. The bulk of the fuel and aircraft debris was deposited in floors 93 through 97, with the greatest concentration on floor 94. Approximately 18,000 lb, or 7 percent, of aircraft mass was eliminated from the debris cloud at the final state as a result of the erosion in the aircraft structures due to impact and breakup. This mass was not accounted for in the fuel and debris distributions provided in Table 9–4. A first approximation would be to increase the airframe debris distribution proportionately to account for the eroded mass. This eroded mass was maintained in the calculation but was no longer included in the contact algorithm. As a result, any residual momentum at the time of erosion could not be subsequently transferred to the tower.

The calculated debris distribution included 17,400 lb of debris and 6,700 lb of aircraft fuel outside of the tower at the end of the impact analysis, either bounding from the impact face (north wall) or passing through the tower (south wall). These estimates of mass outside the tower were expected to be overestimated in the calculation since the external walls were not modeled with windows that could contain the fuel cloud and small debris inside the tower. In addition, the impact behavior of the aircraft fuel cloud did not include the ability to stick to, or wet, interior components. Rather, the aircraft fuel SPH particles tended to bounce off of internal structures.

The physics of fuel impact and dispersion in this type of impact event is complex and no appropriate validation data could be found. The fuel starts as a continuous fluid within the tanks and ends up distributed both on the tower structures and as droplets that interact with the atmosphere surrounding the impact zone. No single analysis technique is currently available that can analyze this full range of fuel dispersion without significant uncertainties.

Both the SPH and ALE analysis techniques (see Section 5.5.3) available for the analysis of the fuel impact and dispersion had limitations. Details of the fuel behavior such as the wetting of the fuel against tower structures and interior contents or the physics of the fuel breakup into droplets are not accurately reproduced in either analysis technique. However, the momentum transfer from the fuel to the tower structures and subsequent impact damage produced by the fuel can be modeled by both analysis techniques.

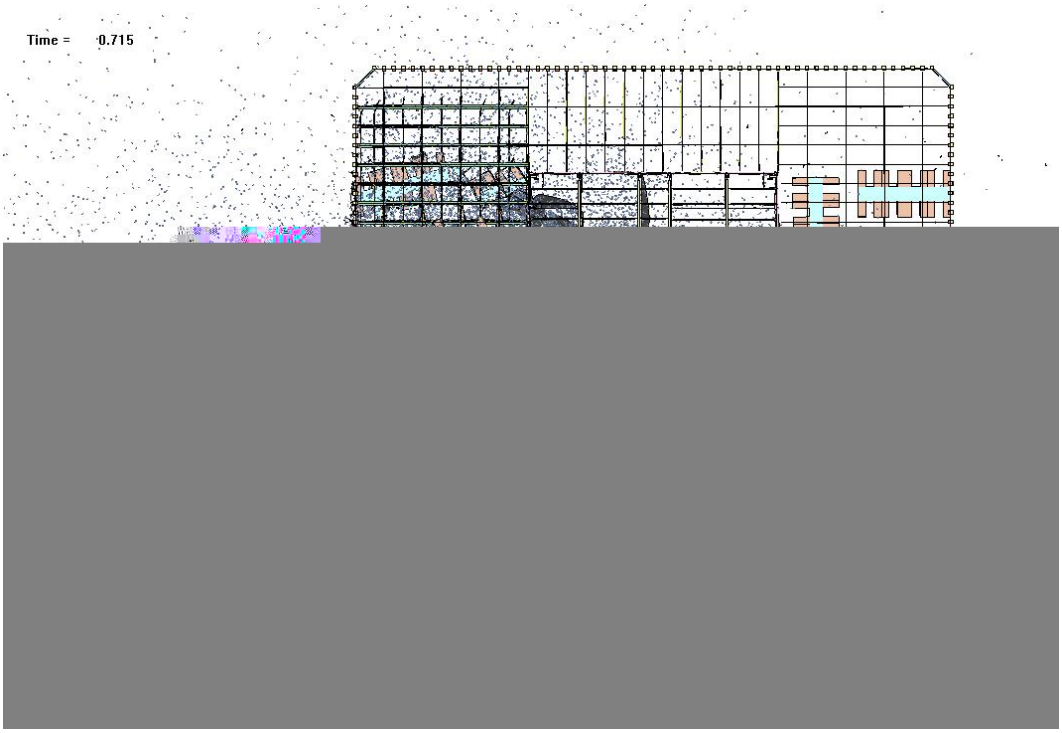

(a) Calculated impact response (floor slab removed)

(b) SPH fuel distribution

Figure 9–17. Calculated fuel distribution in the base case WTC 1 analysis (plan view).

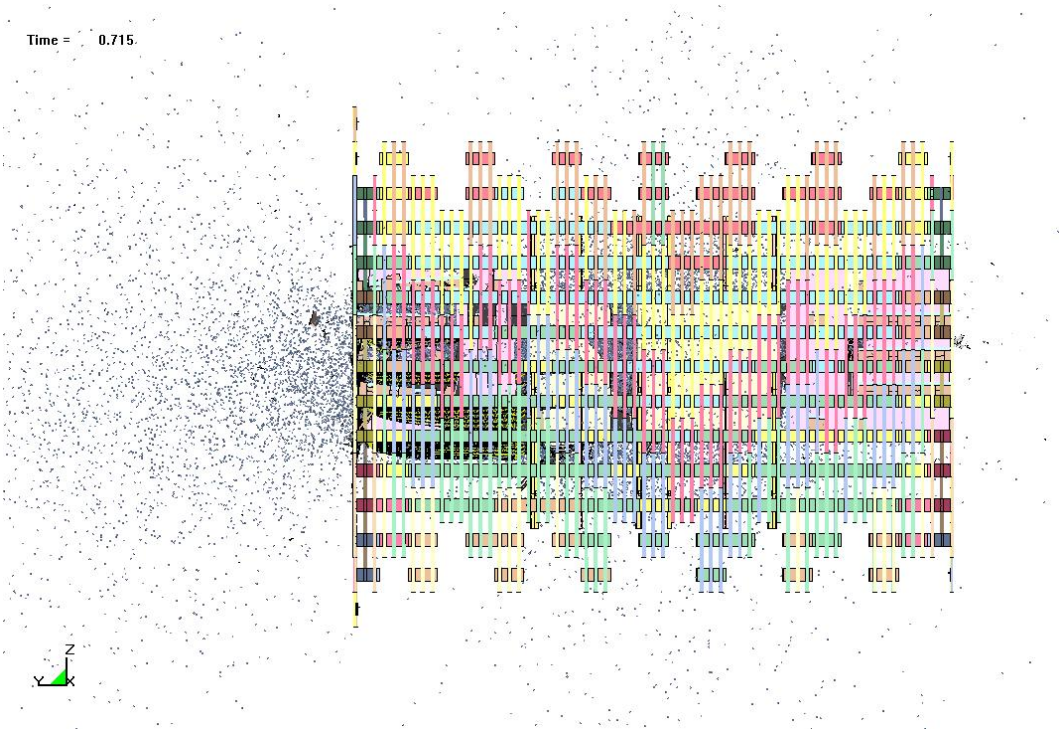

(a) Calculated impact response

(b) SPH fuel distribution

Figure 9–18. Calculated fuel distribution in the base case WTC 1 analysis (side view).

(a) Impact configuration (plan view)

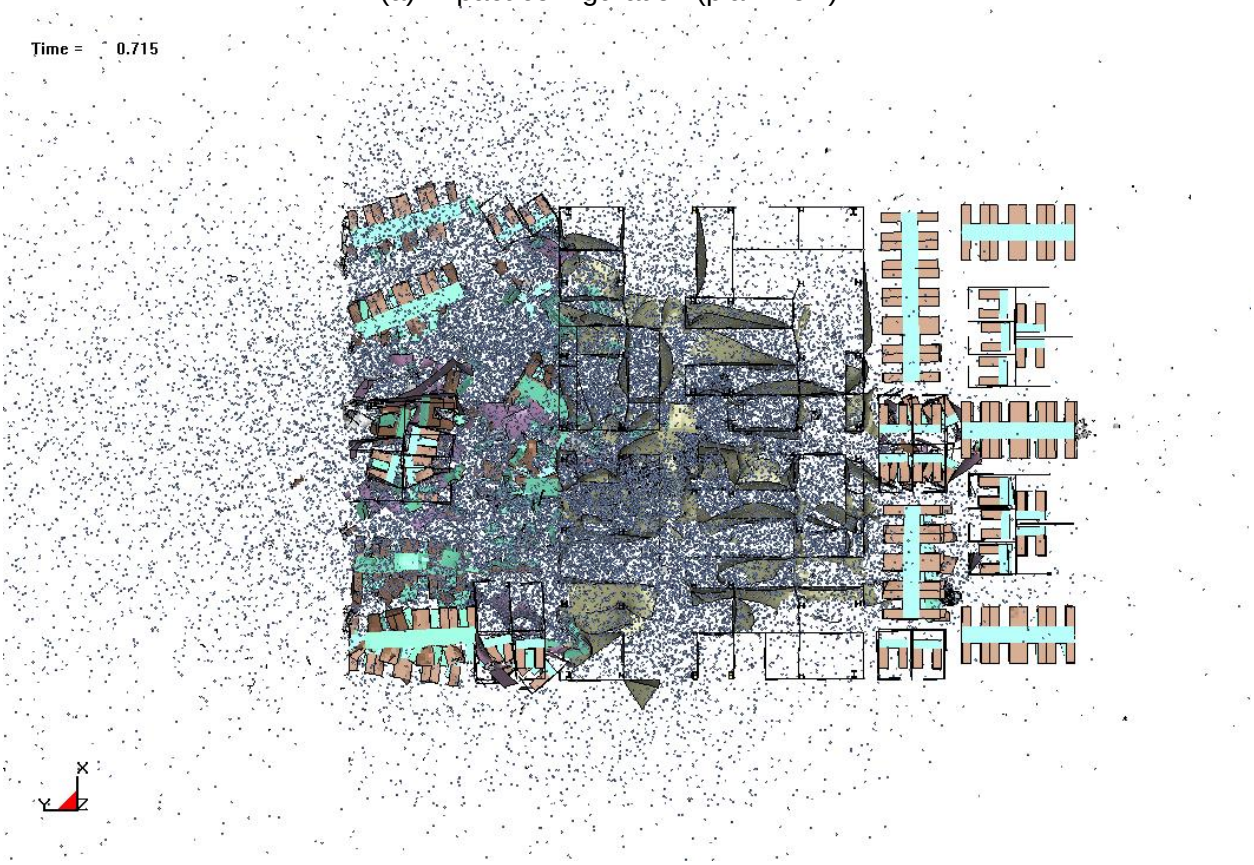

(b) Calculated impact response (t=0.715)

Figure 9–19. Calculated WTC 1 building contents, fuel, and aircraft debris distribution.

(a) Initial impact configuration

(b) Calculated impact response

(c) Calculated impact response (fuel removed)

(d) Calculated aircraft debris

Figure 9–20. Calculated floor 94 contents, fuel, and aircraft debris distribution.

(a) Initial impact configuration

(b) Calculated impact response

(c) Calculated impact response (fuel removed)

(d) Calculated aircraft debris

Figure 9–21. Calculated floor 95 contents, fuel, and aircraft debris distribution.

(a) Initial impact configuration

(b) Calculated impact response

(c) Calculated impact response (fuel removed)

(d) Calculated aircraft debris

Figure 9–22. Calculated floor 96 contents, fuel, and aircraft debris distribution.

(a) Initial impact configuration

(b) Calculated impact response

(c) Calculated impact response (fuel removed)

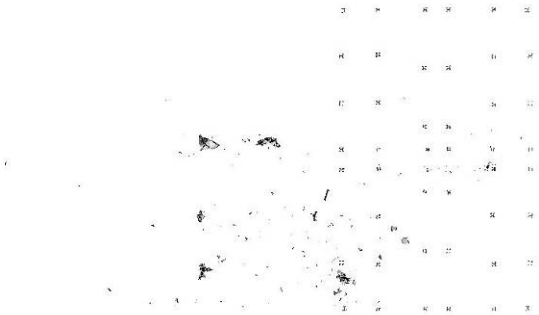

(d) Calculated aircraft debris

Figure 9–23. Calculated floor 97 contents, fuel, and aircraft debris distribution.

(a) Initial impact configuration

(b) Calculated impact response

(c) Calculated impact response (fuel removed)

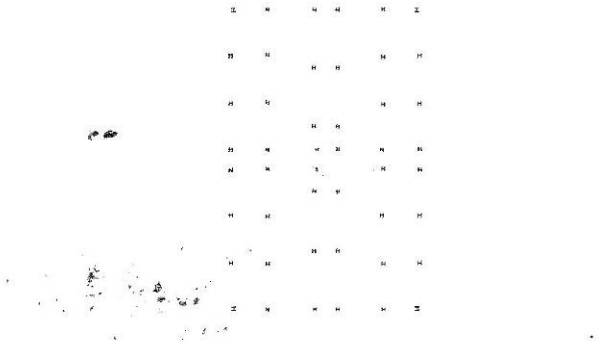

(d) Calculated aircraft debris

Figure 9–24. Calculated floor 98 contents, fuel, and aircraft debris distribution.

The detailed predictions of the fuel dispersion and distribution using SPH in the global impact analyses had significant uncertainties in the absence of improved validation testing. However, some aspects of the distribution had a higher confidence. The floors confined the vertical motion of the fuel, and the floor-by-floor distribution of fuel was controlled more by the geometry of the tower and impact conditions. As a result, this distribution by floor has a higher level of confidence. Similarly, the interior contents and partition walls, and the damage to these structures, controlled the spread of fuel.

Table 9–4. Fuel and aircraft debris distribution for the base case WTC 1 impact.

Tower Location	Aircraft Fuel	Aircraft Debris
Total Outside Tower	6,700 lb	17,400 lb
WTC 1 Floor 92	810 lb	260 lb
WTC 1 Floor 93	6,100 lb	22,600 lb
WTC 1 Floor 94	16,100 lb	96,000 lb
WTC 1 Floor 95	12,200 lb	28,000 lb
WTC 1 Floor 96	11,700 lb	19,400 lb
WTC 1 Floor 97	9,500 lb	6,000 lb
WTC 1 Floor 98	2,200 lb	6,000 lb
WTC 1 Floor 99	770 lb	90 lb
Total Weight	66,100 lb	196,000 lb

9.5 WTC 2 BASE CASE IMPACT ANALYSIS

This case is referred to as Case B for the remainder of the WTC Investigation reports. The WTC 2 base case impact analysis was performed for a 0.62 s duration following initial impact of the aircraft nose with the south exterior wall. A side view of the base case WTC 2 global impact model is shown in Figure 9–25. The tower interior contents were removed, and the tower structures were shown as transparent in the figure so that the impact response of the tower interior was visible. The floor numbers and core columns for the tower model are labeled in the figure. The corresponding side view is used to illustrate the base case global aircraft impact response in Figure 9–26. The response is shown at intervals of 0.1 s from impact through the initial 0.5 s of the response. Corresponding plan view images of the progression of aircraft impact response are shown in Figure 9–27.

Figure 9–25. WTC 2 base case global impact model.

(a) Time=0.00 s

(b) Time=0.10 s

(c) Time=0.20 s

Figure 9–26. WTC 2 base case global impact analysis (side view).

(d) Time=0.30 s

(e) Time=0.40 s

(f) Time=0.50 s

Figure 9–26. WTC 2 base case global impact analysis (side view) (continued).

(a) Time=0.00 s

(b) Time=0.10 s

(c) Time=0.20 s

Figure 9–27. WTC 2 base case global impact analysis (plan view).

(d) Time=0.30 s

(e) Time=0.40 s

(f) Time=0.50 s

Figure 9–27. WTC 2 base case global impact analysis (plan view) (continued).

The initial 0.1 s of the base case global aircraft impact response, shown in Figure 9–26(b) and Figure 9–27(b), was dominated by the impact, penetration, and fragmentation of the forward fuselage structures. The engines and leading portions of the wings penetrated the exterior wall. The forward fuselage structures were severely damaged both from penetration through the exterior columns and the penetration of the 81st floor slab that sliced the fuselage structures in half. The downward trajectory of the aircraft structures caused the airframe to collapse against the floor, and the subsequent debris motion was redirected inward along a more horizontal trajectory parallel to the floor. The higher impact speed and short truss floor span in this impact orientation had the forward fuselage structures well into the tower core by this time.

At 0.2 s after impact, the full penetration of the aircraft into the tower was just completed, as shown in Figure 9–26(c) and Figure 9–27(c). The airframe was mostly broken up, but some large sections of the aft fuselage and tail were still intact, having penetrated through the opening in the tower wall produced by the forward fuselage structures. The aircraft fuel cloud was starting to spread out but was still relatively dense, and the leading edge of the fuel was approximately one-third through the tower core. By 0.2 s, the downward trajectory of the aircraft structures had transferred sufficient vertical load that the truss floor structures on the 80th and 81st floors were starting to collapse in the impact zone.

At 0.3 s after impact, the aircraft fuel cloud had penetrated approximately two-thirds the distance through the core and was spreading out, as shown in Figure 9–26(d) and Figure 9–27(d). However, the subsequent motion of the aircraft fragments and debris cloud began to be noticeably slowed beyond this time. The fuel and debris did continue to spread through the tower, but at a much slower rate, as seen in the remaining images in Figure 9–26 and Figure 9–27. The spread of the fuel and debris cloud was more rapid and extensive in the open truss floor zones than through the core as a result of the open volume above the workstations in the truss floor zone.

The load transfer of the base case WTC 2 aircraft impact can be shown by the history of the resultant momentum as shown in Figure 9–28. The curve illustrates an initial rate of load transfer during the first 0.1 s of impact as the forward fuselage penetrated the exterior wall and impacted the interior structures. Between 0.1 s and 0.2 s, a more rapid load transfer rate was observed, as the area of the impact was larger (extending outward in the wing impact regions), and a higher percentage of the aircraft mass was impacting the interior structures. At 0.2 s, as indicated in Figure 9–28, the aircraft completely penetrated the building and retained approximately 30 percent of its initial momentum. Beyond this time, the rate of load transfer was steadily decreasing with very little load transfer after approximately 0.4 s. The behavior was very similar to that of the base case WTC 1 impact, shown in Figure 9–6, but with a slightly compressed time scale resulting from the higher impact speed on WTC 2.

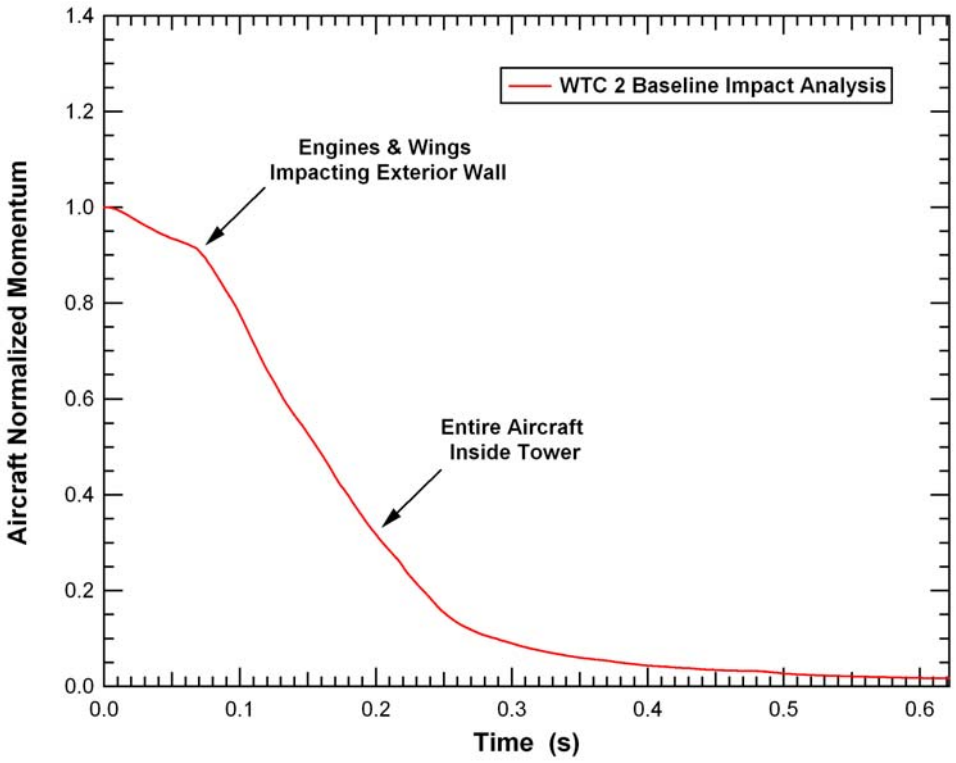

Figure 9–28. Normalized aircraft momentum for the WTC 2 base case impact.

The aircraft was severely broken into debris as a result of the impact with WTC 2 as shown in Figure 9–29. At the end of the impact analysis, the aircraft was broken into thousands of debris fragments of various size and mass, as shown in Figure 9–29(b). A closer inspection of the debris field showed that larger fragments still occurred for specific components such as the engines and landing gear components. This behavior was very similar to the WTC 1 aircraft breakup shown in Figure 9–7.

9.5.1 WTC 2 Base Case Impact Analysis - Structural Damage

The structural damage to the WTC 2 tower by the base case impact conditions is described in this section. The details of the base case WTC 2 aircraft impact conditions were summarized previously in Section 9.3 (shown in Figure 9–2 and summarized in Table 9–2). The primary structural components of interest were the exterior wall, core columns and core framing components, and the floor structures and concrete floor slab. The response of the internal contents, walls, and partitions as well as fuel dispersion was also of interest as initial conditions for the fire analysis.

(a) Aircraft structure (time=0.00 s)

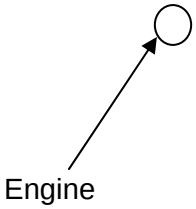

(b) Aircraft debris field (time=0.62 s)

Figure 9–29. Aircraft breakup and debris in the base case WTC 2 impact.

Exterior Wall Damage

A comparison of the south exterior wall observed and calculated damage from the base case WTC 2 global impact analysis is shown in Figure 9–30. The calculated impact damage to the exterior wall is shown with color fringes representing plastic strain magnitude with undamaged sections in blue and strains at or above 5 percent shown in red. The schematic of observed damage was developed from inspections of the video and photographic data collected on the tower after impact. Both the observed and calculated damage regions shown in Figure 9–30 illustrate a region of the exterior wall from column 402 to column 446, extending from floor 76 to floor 86 (spandrels at floors 77 through 86).

The exterior wall completely failed in the region of the fuselage, engine, and fuel-filled wing section impacts. Damage to the exterior wall extended to the wing tips, but the exterior columns were not completely failed in the outer wing and vertical stabilizer impact regions. Failure of the exterior columns occurred both at the bolted connections between column sections and at various locations in the column, depending on the local severity of the impact load and the proximity of the bolted connection to the impact.

The initial observation from the comparison of the calculated and observed damage was that the geometry and location of the impact damage zone were in good agreement. This agreement in the position and shape of the impact damage served to validate the geometry of the aircraft model, including the aircraft orientation, trajectory, and flight distortions of the wings. The agreement of both the mode and magnitude of the impact damage served to partially validate the constitutive and damage modeling of the aircraft and exterior wall of the tower.

Core Structural Damage

The estimation of the damage to the core columns and core beams was important for the subsequent analysis of structural stability and collapse. The overall model for the WTC 2 core structure and calculated impact damage to the core is shown in Figure 9–31. The figure shows that the core had significant damage in the region close to the impact point, in particular the southeast corner of the core. The columns in line with the aircraft fuselage failed on the impact side, and several of the core beams were also severely damaged or failed in the impact zone. In some cases, failure of the column splices located on floors 77, 80, and 83 contributed significantly to the failure of the core columns. This was particularly true for the heavy column number 1001 at the corner of the core that failed at the three splice locations.

The calculated damage to the core columns by floor is shown in Figure 9–32. The columns are shown with color fringes representing plastic strain magnitude with undamaged sections in blue and strains at or above 5 percent shown in red. A summary of the column damage is listed in Table 9–5 and shown graphically in Figure 9–33. The qualitative classification of the column damage levels were provided previously in Figure 9–12. A summary of the floor-by-floor damage to the core framing is shown in Figure 9–34.

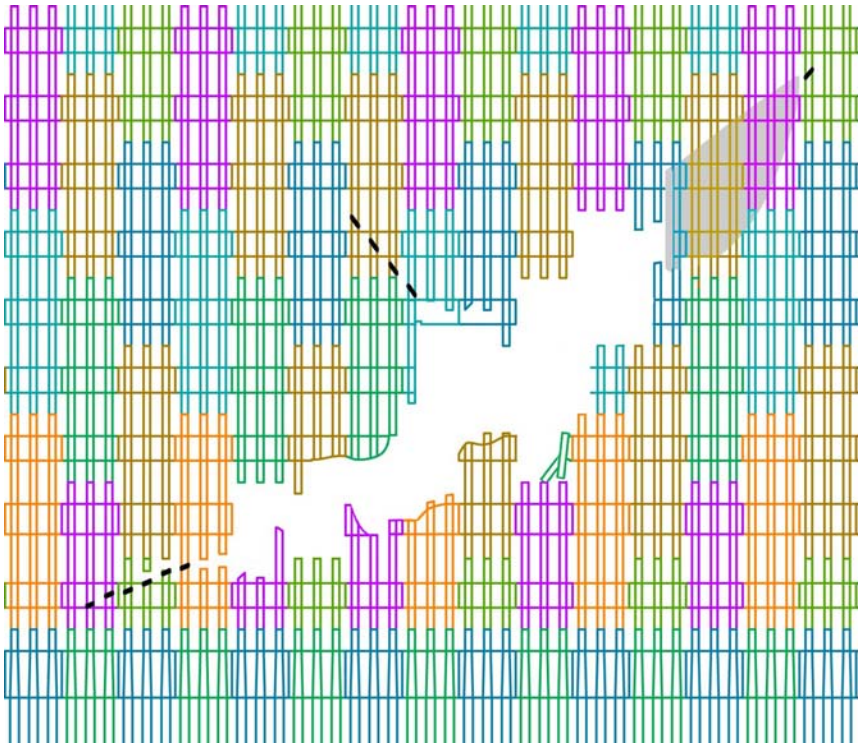

(a) Schematic of observed damage

(b) Calculated damage (t=0.62 s)

Figure 9–30. Base case impact damage to the WTC 2 exterior wall.

(a) Initial geometry

(a) Calculated impact damage

Figure 9–31. Base case impact damage to the WTC 2 core.

(a) Columns 1001-1008 (b) Columns 901-908

(c) Columns 801-807 (d) Columns 701-708

Figure 9–32. Base case impact damage to the WTC 2 core columns.

Table 9–5. Summary of core column damage for the base case WTC 2 impact.

Column	Location	Damage Level	Lateral Deflection of Column Centerline (in.)
Column 801	Floor 79	Heavy	10
Column 901	Floors 79-82	Severed	
Column 902	Floor 79	Heavy	32
Column 903	Floors 77-83	Severed	
Column 904	Floor 79	Moderate	
Column 905	Floor 79	Heavy	18
Column 1001	Floors 77-83	Severed	
Column 1002	Floors 79-81	Severed	
Column 1003	Floor 80	Severed	
Column 1004	Floor 80	Heavy	18

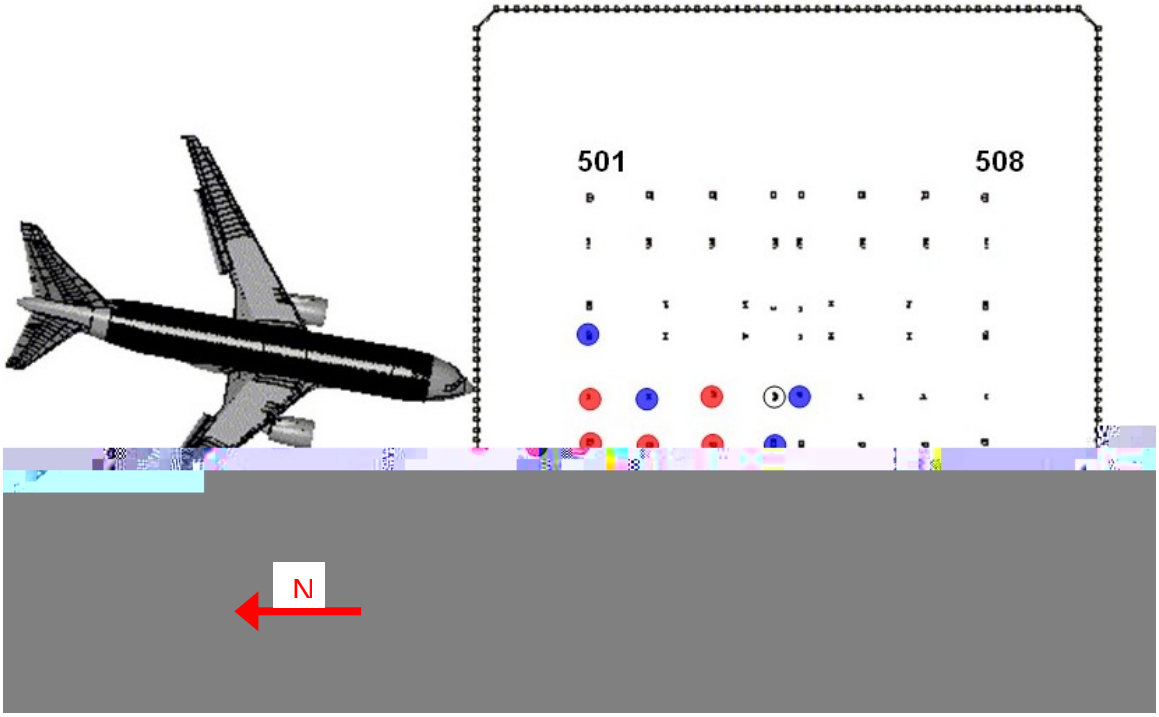

Figure 9–33. Summary of core column damage for the base case WTC 2 impact.

(a) Floor 77 core framing damage

(b) Floor 78 core framing damage

(c) Floor 79 core framing damage

(d) Floor 80 core framing damage

(e) Floor 81 core framing damage

(f) Floor 82 core framing damage

Figure 9–34. Base case impact damage to the WTC 2 core floor framing (plan view).

Floor Truss and Slab Damage

An overall view for the floor truss structure in the WTC 2 impact zone, along with the calculated base case impact damage to the trusses, is shown in Figure 9–35. The figure shows a front view of the trusses that were modeled in detail before and after impact by the aircraft. Note that the coarsely meshed trusses on these floors are not shown in the figure. These trusses experienced significant damage in the impact zone, with the largest damage on floor 81. A plan view of the calculated damage to the trusses on each floor is shown in Figure 9–36. The calculated impact response produced severe damage to the truss structures in the primary impact path of the fuselage. The truss structures were severely damaged from the exterior wall to the core. The truss floor system on floors 79 and 81 had sufficient damage from the impact that truss floor sections were sagging downward as a result of the impact.

(a) Initial detailed truss structures

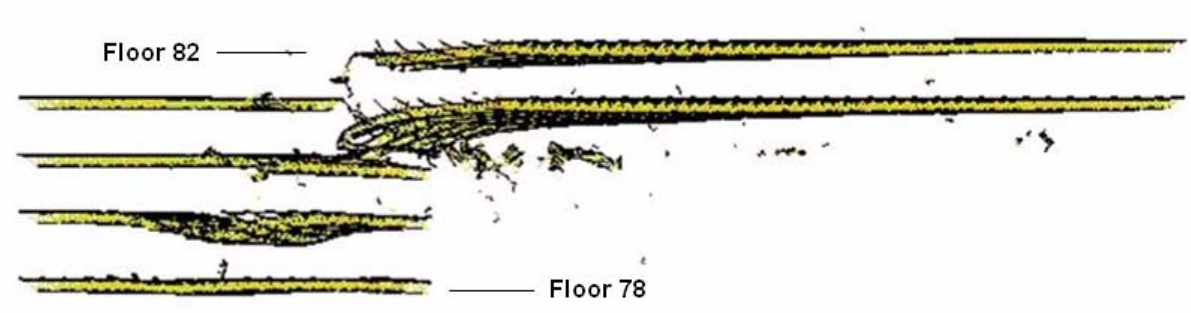

(b) Calculated damage

Figure 9–35. Base case impact damage to the WTC 2 floor truss (front view).

The calculated damage to the WTC 2 floor slab for floors 78 through 83 are shown in Figure 9–37. The fringes of damage were set such that the concrete in the regions colored red (2 percent plastic strain). In these regions, it is expected that the concrete had been severely damaged and potentially removed, exposing the supporting metal decking. The strength of the floor slab was severely reduced in the analysis beyond this strain to model the residual strength of the metal deck after the concrete failure, breakup, and removal. At a plastic strain of 30 percent, corresponding to failure levels for the metal decking material, the elements were eroded (seen as ruptured in the floor slab shown). The line of damage, visible around the edge of the core in Figure 9–37, was believed to be the result of numerical precision errors and interference in the modeling methodology at the connection of the floor slab rather than impact damage.

(a) Floor 79 truss damage

(b) Floor 80 truss damage

(c) Floor 81 truss damage

(d) Floor 82 truss damage

Figure 9–36. Base case impact damage to the WTC 2 floor trusses (plan view).

(a) Floor 78 slab damage

(b) Floor 79 slab damage

(c) Floor 80 slab damage

(d) Floor 81 slab damage

(e) Floor 82 slab damage

(f) Floor 83 slab damage

Figure 9–37. Base case impact damage to the WTC 2 floor slab (plan view).

9.5.2 WTC 2 Base Case Impact Analysis – Fuel and Debris Distributions

The global impact results presented in this section include the distribution of the jet fuel and aircraft debris in the WTC 2 tower, and the damage to the building contents (partition walls and workstations). For the base case WTC 2 global impact analysis, the calculated distribution of the fuel in the tower and shape of the fuel cloud in a plan view and side view are shown in Figure 9–38 and Figure 9–39, respectively. At the end of the analysis, the residual momentum of the jet fuel in the impact direction was less than one percent of the initial momentum, indicating that the fuel cloud was nearly at rest at about 0.62 s.

To more clearly present the calculated response of the structures that influenced the fire propagation, the structural components were removed from the visualization, with the exception that the core columns were maintained in the visualizations for reference positions. A plan view of the response of the remaining building contents and aircraft debris is shown in a plan view in Figure 9–40. Similar plan views of floor-by-floor slices through the building contents and debris field are provided in Figure 9–41 through Figure 9–46 for floors 78 through 83, respectively. The bulk of the aircraft debris and fuel was arrested prior to exiting the tower structures. However, a significant amount of aircraft debris was calculated to exit the north and east sides of the tower (Sides 300 and 200 of WTC 2).

A quantitative characterization of the fuel and aircraft debris distribution was obtained by slicing the model at vertical floor locations and calculating the mass at each floor level. A summary of the floor-by-floor fuel and debris distributions is given in Table 9–6. The bulk of the fuel and aircraft debris was deposited in floors 78 through 80, with the greatest concentration of aircraft debris on floor 80, and the largest concentration of aircraft fuel on floors 79, 81, and 82. Approximately 14,000 lb, or 5 percent, of the total aircraft mass was eliminated from the debris cloud in the final state as a result of the erosion in the aircraft structures due to impact and breakup. The eroded mass was maintained in the calculation but eliminated from consideration in the contact algorithm. As a result, any residual momentum at the time of erosion could not be subsequently transferred to the tower.

The calculated debris distribution included 55,800 lb of debris and 10,600 lb of aircraft fuel outside of the tower at the end of the impact analysis, either from bounding from the impact face or passing through the tower. These estimates of mass outside the tower are expected to be overestimated in the calculation since the exterior walls were not modeled with windows that could contain the fuel cloud and small debris inside the towers. In addition, the impact behavior of the aircraft fuel cloud did not include the ability to stick to, or wet, interior components. Rather, aircraft fuel SPH particles tended to bounce off of internal structures (see Section 9.4.2).

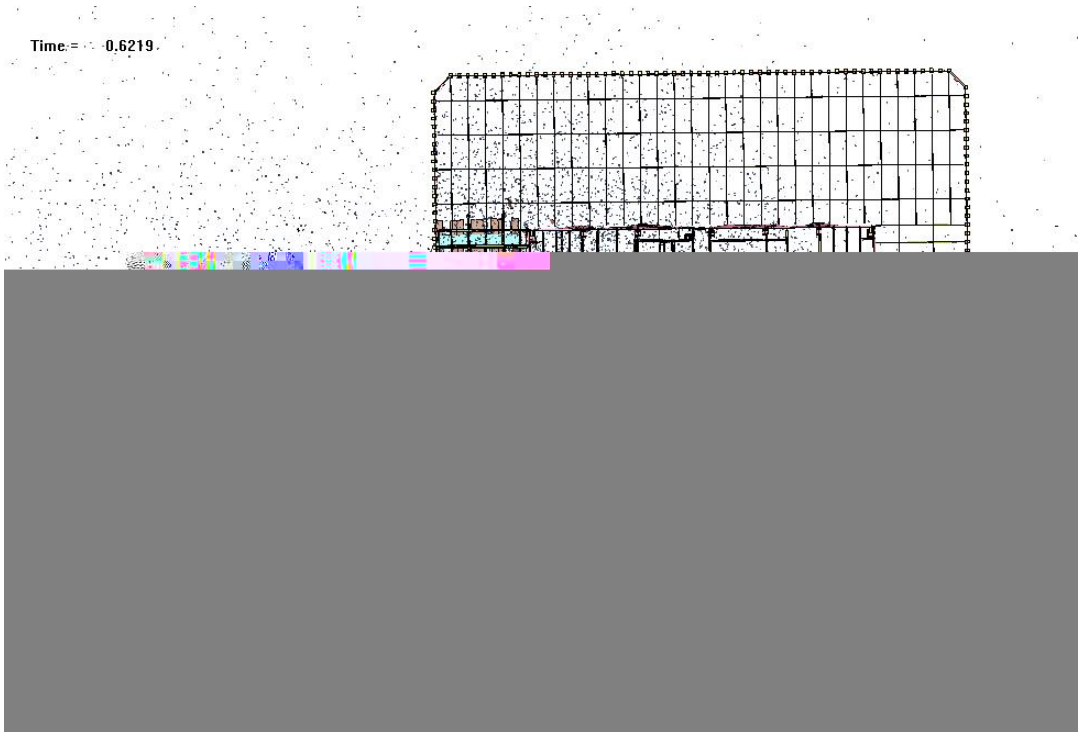

(a) Calculated impact response (floor slab removed)

(b) SPH fuel distribution

Figure 9–38. Calculated fuel distribution in the base case WTC 2 analysis (plan view).

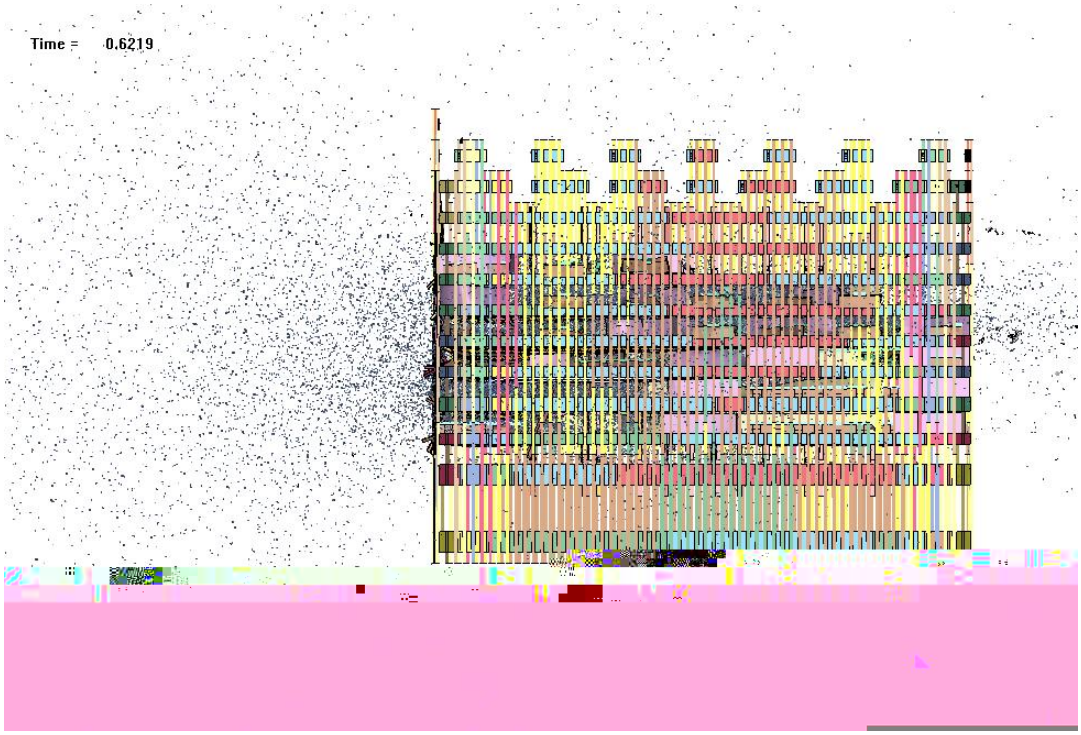

(a) Calculated impact response

(b) SPH fuel distribution

Figure 9–39. Calculated fuel distribution in the base case WTC 2 analysis (side view).

(a) Impact configuration (plan view)

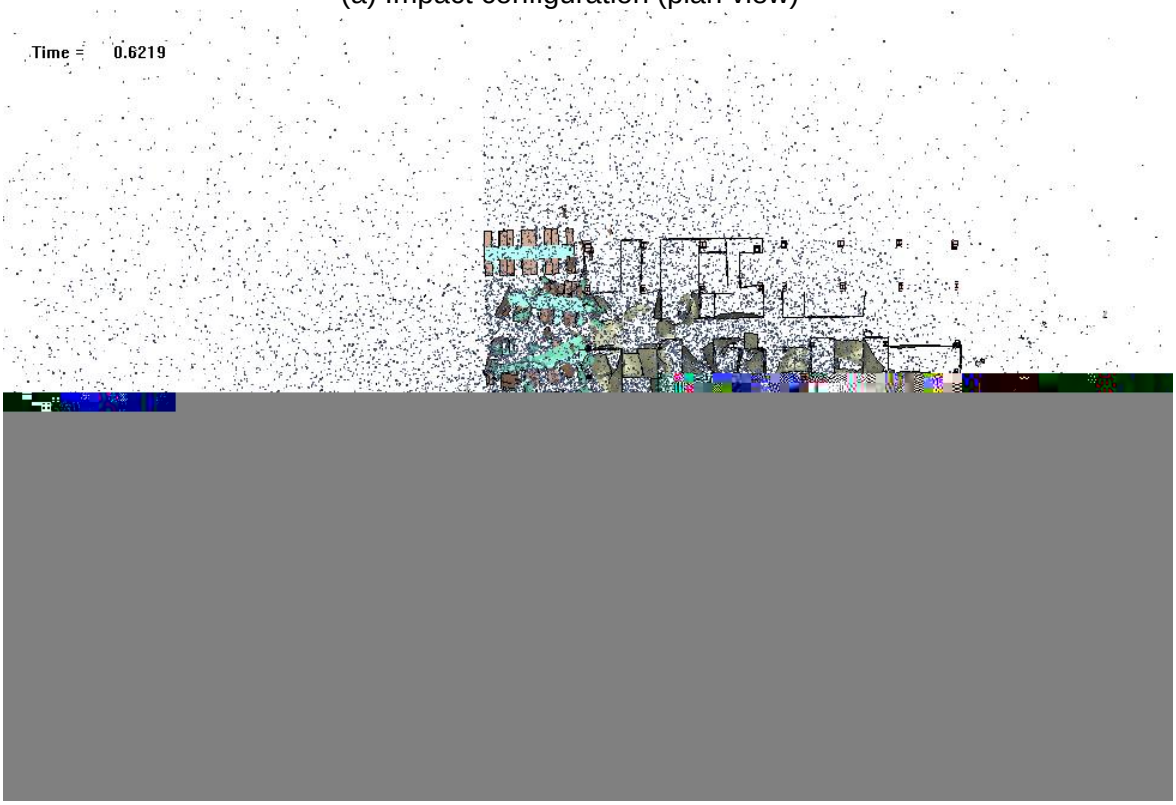

(b) Calculated impact response (t=0.622)

Figure 9–40. Calculated WTC 2 building contents, fuel, and aircraft debris distribution.

(a) Initial impact configuration

(b) Calculated impact response

(c) Calculated impact response (fuel removed)

(d) Calculated aircraft debris

Figure 9–41. Calculated floor 78 contents, fuel, and aircraft debris distribution.

(a) Initial impact configuration

(b) Calculated impact response

(c) Calculated impact response (fuel removed)

(d) Calculated aircraft debris

Figure 9–42. Calculated floor 79 contents, fuel, and aircraft debris distribution.

(a) Initial impact configuration

(b) Calculated impact response

(c) Calculated impact response (fuel removed)

(d) Calculated aircraft debris

Figure 9–43. Calculated floor 80 contents, fuel, and aircraft debris distribution.

(a) Initial impact configuration

(b) Calculated impact response

(c) Calculated impact response (fuel removed)

(d) Calculated aircraft debris

Figure 9–44. Calculated floor 81 contents, fuel, and aircraft debris distribution.

(a) Initial impact configuration

(b) Calculated impact response

(c) Calculated impact response (fuel removed)

(d) Calculated aircraft debris

Figure 9–45. Calculated floor 82 contents, fuel, and aircraft debris distribution.

(a) Initial impact configuration

(b) Calculated impact response

(c) Calculated impact response (fuel removed)

(d) Calculated aircraft debris

Figure 9–46. Calculated floor 83 contents, fuel, and aircraft debris distribution.

Table 9–6. Fuel and aircraft debris distribution for the base case WTC 2 impact.

Tower Location	Aircraft Fuel	Aircraft Debris
Total Outside Tower	10,600 lb	55,800 lb
WTC 2 Floor 77	1,300 lb	400 lb
WTC 2 Floor 78	6,200 lb	4,800 lb
WTC 2 Floor 79	11,400 lb	16,200 lb
WTC 2 Floor 80	6,000 lb	83,800 lb
WTC 2 Floor 81	14,400 lb	27,300 lb
WTC 2 Floor 82	10,600 lb	3,600 lb
WTC 2 Floor 83	1,500 lb	4,300 lb
WTC 2 Floor 84	200 lb	500 lb
Total Weight	62,000 lb	197,600 lb

9.6 ADDITIONAL WTC 1 GLOBAL IMPACT ANALYSES

In addition to the base case impact analyses, additional impact analyses were performed for each tower to provide a range of calculated impact-induced damage. Variations in impact analysis parameters were developed based on the result of the uncertainty analyses described in Chapter 8 and additional evaluations of the parameter uncertainties. Additional guidance on the combination of parameters was obtained by engineering analysis of expected responses.

Two additional global impact analyses were performed for each WTC tower impact to evaluate a more severe and less severe impact scenario. The combinations of impact conditions for the more and less severe WTC 1 impact scenarios are compared to the corresponding parameters in the base case analysis in Table 9–7. The impact speeds were 414 mph and 472 mph in the less severe and more severe impact scenarios, respectively. These were the upper and lower bounds obtained from the analysis of aircraft impact conditions described in Chapter 7. The aircraft vertical trajectory angle was also varied from 13.6 degrees to 7.6 degrees for the less severe and more severe impact scenarios, respectively. This resulted in more impact energy directed inward toward the core in the more severe impact scenario and less impact energy imparted to the core for the less severe impact. The lateral trajectory was not varied since the impact was close to centered on the tower and normal to the north face of WTC 1. A small variation in the lateral approach angle would have little effect on the energy of the aircraft debris entering the tower and core.

The parameters varied for the aircraft model were the weight of the aircraft and the ductility of the aircraft materials. A 5 percent variation on the total aircraft weight was considered, with the additional weight applied for the more severe impact. The failure strain was varied from 75 to 125 percent of the baseline value for the less severe and more severe impact scenarios, respectively. This relatively large variation in aircraft material ductility was applied for multiple reasons. First, no material characterization testing of specimens cut from a Boeing 767 were performed as a part of this investigation. All of the material properties used for the aircraft were obtained from sources available in the open literature, as described in Section 2.5. Second, the variation in ductility was used as the single parameter in these additional analyses to evaluate the uncertainties in aircraft material energy absorption capacity. An increase in aircraft material strength would have a similar effect to an increase in material ductility for producing

increased impact damage to the towers. Finally, the material failure parameters were influenced by the resolution of the models in the impact analysis. This effect was described previously in Section 2.3.1, and the material models were developed for the resolution in the global impact analysis. However, the mesh refinement effects introduced an increased uncertainty on the failure strains in these analyses.

Table 9–7. Input parameters for additional WTC 1 global impact analyses.

Analysis Parameters		Base Case	More Severe	Less Severe
Flight Parameters	Impact speed	443 mph	472 mph	414 mph
	Trajectory - pitch	10.6°	7.6°	13.6°
	Trajectory - yaw	0.0°	0.0°	0.0°
	Orientation - pitch	8.6°	5.6°	11.6°
	Orientation - yaw	0.0°	0.0°	0.0°
Aircraft Parameters	Weight	100 percent	105 percent	95 percent
	Failure Strain	100 percent	125 percent	75 percent
Tower Parameters	Failure Strain	100 percent	80 percent	120 percent
	Live Load Weight[a]	25 percent	20 percent	25 percent

a. Live load weight expressed as a percentage of the design live load.

Finally, the parameters varied for the tower model were the ductility of the steel used in the tower construction and the weight of the contents inside the tower. A variation of 20 percent was used to account for the uncertainty in failure strain for the two materials. However, for the tower the material, failure strain was increased for the less severe impact analysis. The combination of reducing all of the aircraft material ductilities by 25 percent and increasing the tower material ductilites by 20 percent for the less severe impact scenario covered a wide range of relative aircraft and tower strength assumptions.

The variations in internal tower contents (live load weight in Table 9–7) are specified as a percentage of the design live load as described in Section 3.2.4.

9.6.1 More Severe WTC 1 Global Impact Analysis

This case is referred to as Case C for the remainder of the WTC investigation reports. A side view of the more severe WTC 1 global impact response is shown in Figure 9–47. The tower interior contents were removed and the tower structures were shown as transparent so that the impact response in the tower interior can be seen. Similar plan view images of the progression of aircraft impact response are shown in Figure 9–48. The corresponding views were used previously to illustrate the base case global aircraft impact response in Figure 9–4 and Figure 9–5, respectively.

The more severe impact response is qualitatively very similar to that of the base case impact analysis. The initial 0.1 s of the base case global aircraft impact response, shown in Figure 9–47(b) and Figure 9–48(b), was dominated by the impact, penetration, and fragmentation of the forward fuselage structures. The engines and forward wing sections impacted the exterior wall. At 0.2 s after impact, the wings had completely penetrated the exterior wall and only the tail structures were still outside of the tower, as shown in Figure 9–47(c) and Figure 9–48(c). The wing structures were completely fragmented by the penetration through the exterior wall. The aircraft fuel cloud was starting to spread out, but was still relatively dense and the leading edge of the fuel was entering the tower core. At 0.3 s after impact,

the aircraft was completely inside of the tower (penetration completed at approximately 0.24 s), as shown in Figure 9–47(d) and Figure 9–48(d). The aircraft fuel cloud penetrated approximately three-quarters of the distance through the core and was slowing out. However, the subsequent motion of the aircraft fragments and fuel debris cloud began to be noticeably slowed beyond this time. The fuel and debris did continue to spread through the tower but at a much slower rate as seen in the remaining images in Figure 9–47 and Figure 9–48.

Exterior Wall Damage for the More Severe WTC 1 Impact

A comparison of the north exterior wall observed and calculated damage from the more severe WTC 1 global impact analysis is shown in Figure 9–49. The calculated impact damage to the exterior wall is shown with color fringes representing plastic strain magnitude, with undamaged sections in blue and strains at or above 5 percent shown in red. The regions shown in Figure 9–49 illustrate a region of the exterior wall from column 108 to column 152, extending from floor 91 to floor 100 (spandrels at floors 92 through 100). The calculated and observed magnitude and mode of impact damage on the exterior wall was still in good agreement for this more severe impact analysis.

Core Structural Damage for the More Severe WTC 1 Impact

The overall model for the WTC 1 core structure and calculated response for the more severe global impact analysis is shown in Figure 9–50. The figure shows that the core had extensive damage in the region close to the impact point. The columns in line with the aircraft fuselage failed on the impact side, and several of the core beams were also severely damaged or failed in the impact zone. In some cases, failure of the column splices located on floors 92, 95, and 98 contributed significantly to the failure of the core columns.

The calculated damage to the core columns by floor is shown in Figure 9–51, and the floor-by-floor damage to the core framing is shown in Figure 9–52. The core structures are shown with color fringes representing plastic strain magnitude, with undamaged sections in blue and strains at or above 5 percent shown in red. A summary of the core column damage is provided in Table 9–3 and shown graphically in Figure 9–53, with the qualitative classification of the column damage levels provided previously in Figure 9–12. A total of six columns were severed and three columns were heavily damaged, compared to three columns severed and four columns heavily damaged in the base case WTC 1 impact analysis.

(a) Time=0.00 s

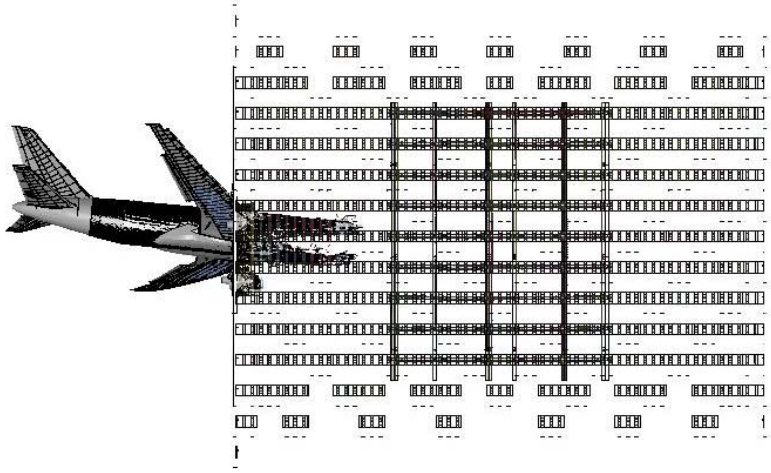

(b) Time=0.10 s

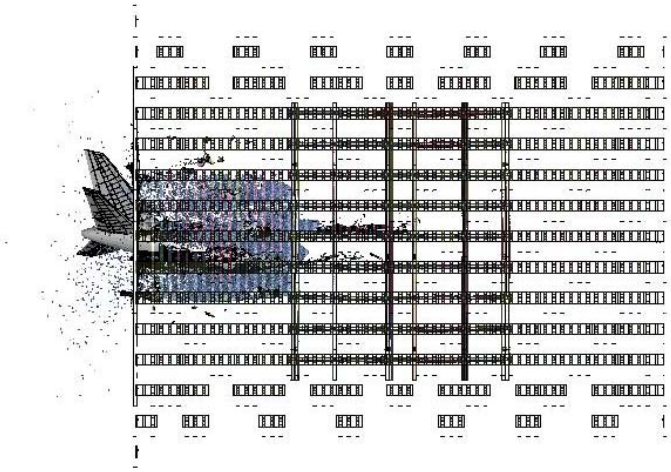

(c) Time=0.20 s

Figure 9–47. More severe WTC 1 global impact analysis (side view).

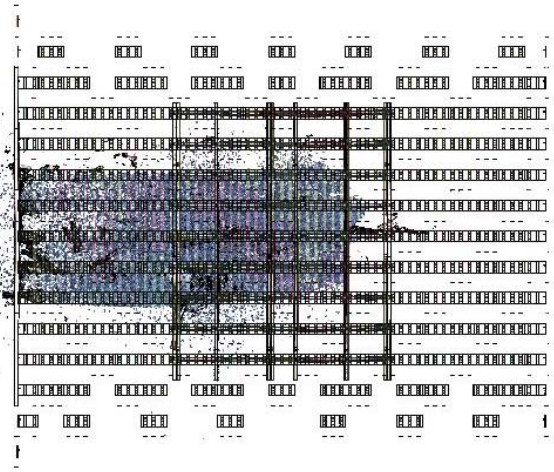

(d) Time=0.30 s

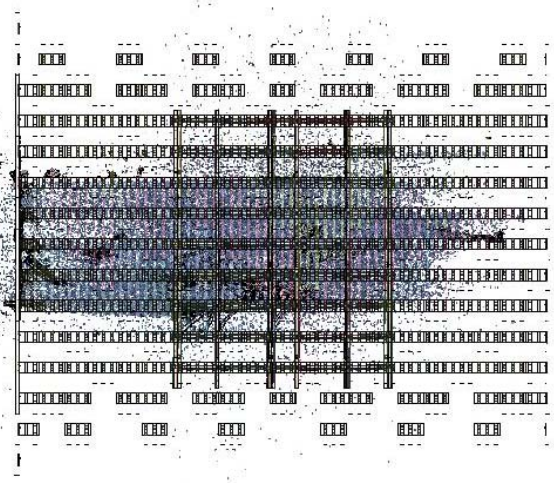

(e) Time=0.40 s

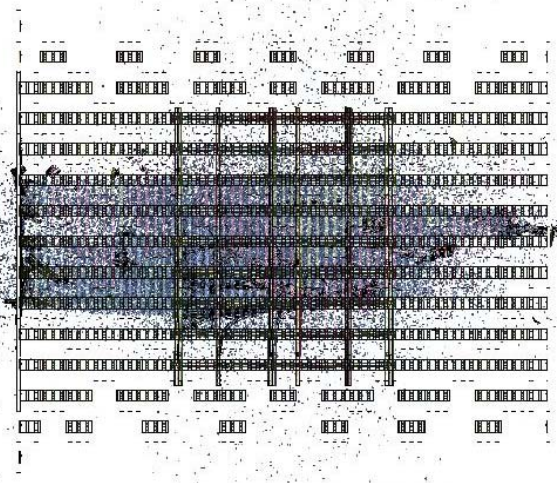

(f) Time=0.50 s

Figure 9–47. More severe WTC 1 global impact analysis (side view) (continued).

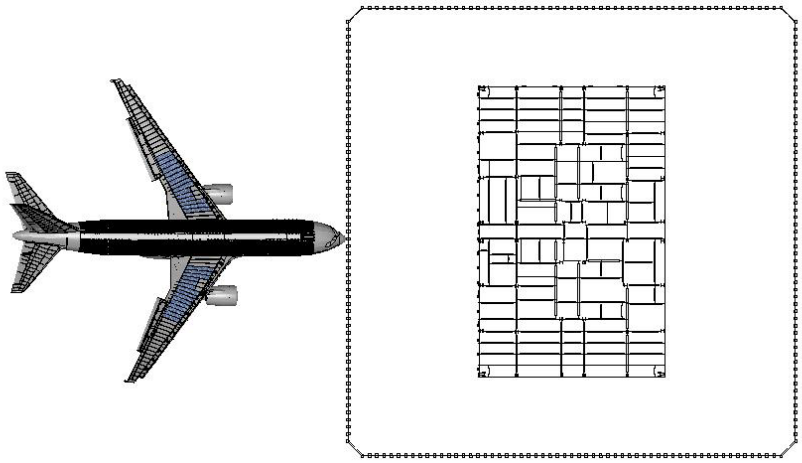

(a) Time=0.00 s

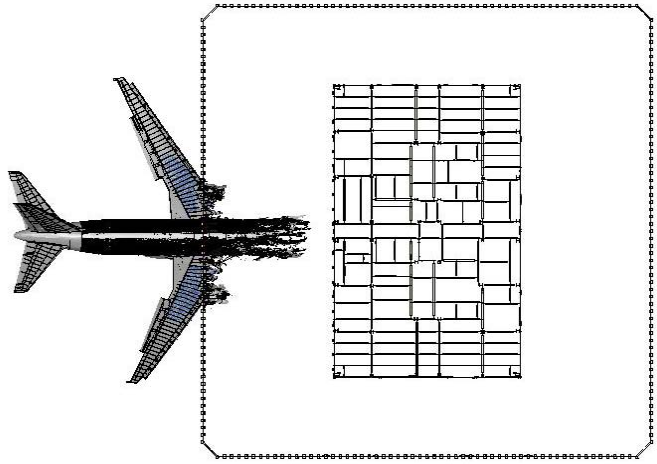

(b) Time=0.10 s

(c) Time=0.20 s

Figure 9–48. More severe WTC 1 global impact analysis (plan view).

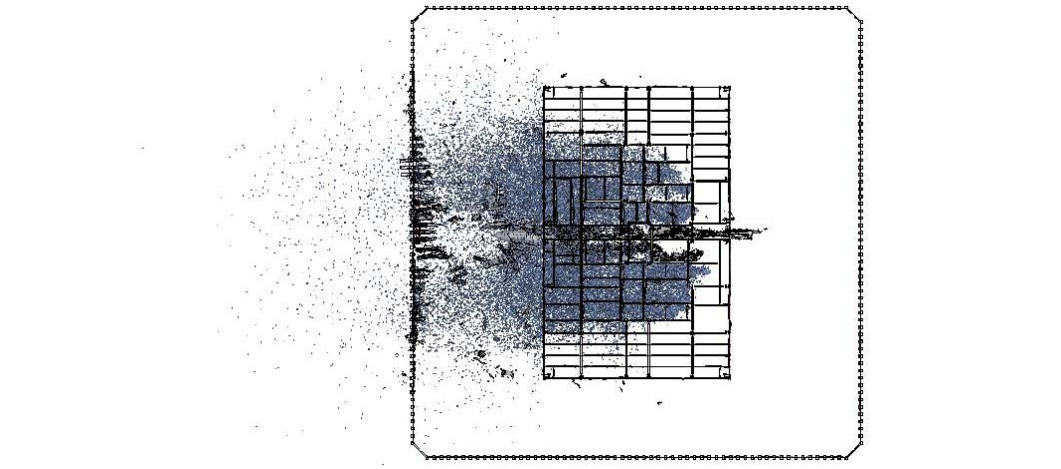

(d) Time=0.30 s

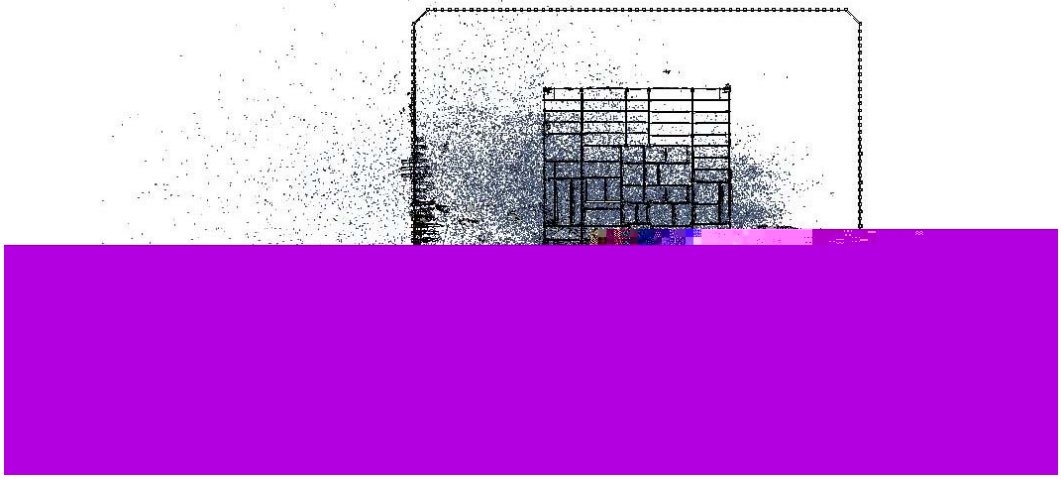

(e) Time=0.40 s

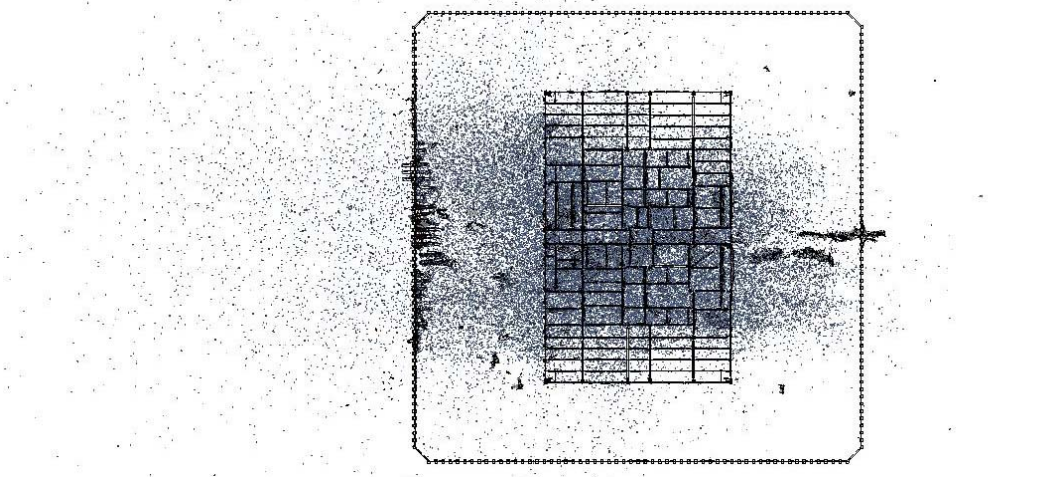

(f) Time=0.50 s

Figure 9–48. More severe WTC 1 global impact analysis (plan view) (continued).

(a) Schematic of observed damage

(b) Calculated damage (t=0.685 s)

Figure 9–49. More severe impact damage to the WTC 1 exterior wall.

(a) Initial geometry

(a) Calculated impact damage

Figure 9–50. More severe impact response of the WTC 1 core.

(a) Columns 501-1001 (b) Columns 502-1002 (c) Columns 503-1003

(d) Columns 504-1004 (e) Columns 505-1005 (f) Columns 506-1006

(a) Floor 93 core framing damage

(b) Floor 94 core framing damage

(c) Floor 95 core framing damage

(d) Floor 96 core framing damage

(e) Floor 97 core framing damage

(f) Floor 98 core framing damage

Figure 9–52. More severe impact damage to the WTC 1 core floor framing (plan view).

Table 9–8. Core column response for the more severe WTC 1 impact.

Column	Location	Damage Level	Lateral Deflection of Column Centerline (in.)
Column 503	Floor 95-96	Severed	
Column 504	Floors 92-96	Severed	
Column 505	Floors 93-96	Severed	
Column 506	Floors 93-95	Heavy	24
Column 603	Floors 96-97	Moderate	
Column 604	Floors 92-96	Severed	
Column 605	Floors 94-95	Moderate	
Column 606	Floors 94	Light	
Column 702	Floor 97	Light	
Column 703	Floor 96	Moderate	
Column 704	Floors 92-96	Severed	
Column 705	Floor 95	Moderate	
Column 706	Floors 93-95	Severed	
Column 802	Floor 96	Light	
Column 803	Floors 96-97	Moderate	
Column 804	Floor 94-96	Moderate	
Column 805	Floors 93-95	Heavy	20
Column 903	Floor 96	Light	
Column 904	Floors 95-96	Heavy	19
Column 905	Floor 95	Light	

Figure 9–53. Summary of core column damage for the more severe WTC 1 impact.

Floor Truss and Slab Damage for the More Severe WTC 1 Impact

An overall view of the floor truss structure in the impact zone, along with the calculated more severe impact damage to the floor trusses, is shown in Figure 9–54. The figure shows that the trusses experienced significant damage in the impact zone. A plan view of the calculated damage to the truss on each floor is shown in Figure 9–55. The calculated impact response produced severe damage to the truss structures in the primary impact path of the fuselage. The truss structures were severely damaged from the exterior wall to the core. The truss floor system on floors 94 through 96 were damaged and sagging downward as a result of the impact loading.

The magnitude of truss floor damage was very similar for the base case and more severe global impact analyses. When the floor-by-floor damage was compared for the base case and more severe impact analyses, Figure 9–15 and Figure 9–55 respectively, the damage appears to be slightly less for the more severe impact analysis. The parameters used in the more severe global impact analysis would primarily contribute to an increased damage magnitude for the tower structures. However, the downward impact trajectory angle was reduced from the 10.6 degree angle in the base case analysis to a 7.6 degree angle in the more severe impact analysis. This would have the effect of directing more of the impact energy inward toward the tower core but reducing the total downward force on the floor structures in the impact zone. As a result, the combined effects of the analysis parameter variations produced slightly less damage to the truss structure in the more severe impact analysis scenario.

(a) Initial detailed truss structures

(b) Calculated damage (t=0.685 s)

Figure 9–54. More severe impact damage to the WTC 1 floor truss (front view).

(a) Floor 94 truss damage

(b) Floor 95 truss damage

(c) Floor 96 truss damage

(d) Floor 97 truss damage

Figure 9–55. More severe impact damage to the WTC 1 floor truss (plan view).

The calculated more severe impact damage to the WTC 1 floor slab for floors 94 through 97 are shown in Figure 9–56. The fringes of damage were set such that concrete is failed in the regions colored red (2 percent plastic strain was used corresponding to zero strength strain limit for the concrete in unconfined compression). At these strain levels, concrete was severely damaged and probably removed, exposing the supporting metal decking. At 2 percent plastic strain, the strength of the floor slab was severely reduced in the analyses to model the residual strength of the metal deck after the concrete failure, breakup, and removal. At a plastic strain of 30 percent, corresponding to failure levels for the metal decking material, the elements were eroded (seen as holes ruptured in the floor slab shown). The line of damage, visible around the edge of the core, was believed to be the result of numerical precision errors and interference in the modeling methodology at the connection of the floor slab rather than impact damage.

(a) Floor 94 slab damage

(b) Floor 95 slab damage

(c) Floor 96 slab damage

(d) Floor 97 slab damage

Figure 9–56. More severe impact damage to the WTC 1 floor slabs (plan view).

The magnitude of floor slab damage was, in general, very similar for the base case and more severe global impact analyses. When the floor-by-floor damage was compared for the base case and more severe impact analyses, Figure 9–16 and Figure 9–56 respectively, the damage appears to be slightly less for the more severe impact analysis. Similar to the truss damage, the reduced damage in the floor slab was believed to be the result of the reduction in the downward impact trajectory angle from 10.6 to 7.6 degrees in the more severe impact analysis, reducing the normal downward force on the floor structures.

Damage to WTC 1 Contents for the More Severe Impact

The calculated damage to the WTC 1 contents for the more severe impact is shown in plan views in Figure 9–57 through Figure 9–61 for floors 94 through 98, respectively. A comparison to the calculated damage for the base case WTC 1 impact analysis, shown previously in Figure 9–20 through Figure 9–24, indicated that the content damage zone is very similar in width but extended further south through the tower in the more severe impact. The more severe impact produced significantly greater content damage on the far side of the core and extended more fully through the tower.

(a) Initial impact configuration

(b) Calculated response of contents

Figure 9–57. Calculated more severe WTC 1 impact response of floor 94 contents.

(a) Initial impact configuration

(b) Calculated response of contents

Figure 9–58. Calculated more severe WTC 1 impact response of floor 95 contents.

(a) Initial impact configuration

(b) Calculated response of contents

Figure 9–59. Calculated more severe WTC 1 impact response of floor 96 contents.

(a) Initial impact configuration

(b) Calculated response of contents

Figure 9–60. Calculated more severe WTC 1 impact response of floor 97 contents.

(a) Initial impact configuration

(b) Calculated response of contents

Figure 9–61. Calculated more severe WTC 1 impact response of floor 98 contents.

9.6.2 Less Severe WTC 1 Global Impact Analysis

Exterior Wall Damage for the Less Severe WTC 1 Impact

A comparison of the north exterior wall observed and calculated damage from the less severe WTC 1 global impact analysis is shown in Figure 9–62. The calculated impact damage to the exterior wall is shown with color fringes representing plastic strain magnitude, with undamaged sections in blue and strains at or above 5 percent shown in red. The wall regions shown in Figure 9–62 are from column 108 to column 152, extending from floor 91 to floor 100 (spandrels at floors 92 through 100). The magnitude and mode of impact damage on the exterior wall is still in good agreement with the observed damage for this less severe impact scenario.

(a) Schematic of observed damage

(b) Calculated damage (t=0.735 s)

Figure 9–62. Less severe impact damage to the WTC 1 exterior wall.

Core Structural Damage for the Less Severe WTC 1 Impact

The overall model for the WTC 1 core structure and calculated response for the less severe global impact analysis is shown in Figure 9–63. The figure shows that the core had a limited damage confined to the region nearest to the impact point. The calculated damage to the core columns by row is shown in Figure 9–64, and the floor-by-floor damage to the core framing is shown in Figure 9–65. The core structures are shown with color fringes representing plastic strain magnitude, with undamaged sections in blue and strains at or above 5 percent shown in red. A summary of the column damage is provided in Table 9–9 and shown graphically in Figure 9–66, with the qualitative classification of the column damage levels provided previously in Figure 9–12. Only one column was severed, and two columns were heavily damaged, compared to three severed columns and four heavily damaged columns in the base case WTC 1 impact analysis. The failure of the column splices located on floors 92 and 95 contributed to the failure of the core column.

Table 9–9. Core column response for the less severe WTC 1 impact.

Column	Location	Damage Level	Lateral Deflection of Column Centerline (in.)
Column 504	Floors 92-96	Severed	
Column 505	Floors 93-96	Heavy	14
Column 506	Floors 93-94	Moderate	
Column 604	Floor 96	Light	
Column 606	Floors 94	Light	
Column 702	Floor 96	Moderate	
Column 703	Floor 96	Light	
Column 704	Floor 96	Heavy	12
Column 705	Floor 96	Light	
Column 802	Floor 96	Moderate	
Column 805	Floor 96	Light	

(a) Initial geometry

(a) Calculated impact damage

Figure 9–63. Less severe impact response of the WTC 1 core.

(a) Columns 501-1001 (b) Columns 502-1002 (c) Columns 503-1003

(d) Columns 504-1004 (e) Columns 505-1005 (f) Columns 506-1006

(g) Columns 507-1007 (h) Columns 508-1008 (i) Reference scale

Figure 9–64. Less severe impact response of the WTC 1 core columns.

(a) Floor 93 core framing damage

(b) Floor 94 core framing damage

(c) Floor 95 core framing damage

(d) Floor 96 core framing damage

(e) Floor 97 core framing damage

(f) Floor 98 core framing damage

Figure 9–65. Less severe impact damage to the WTC 1 core floor framing (plan view).

Figure 9–66. Summary of core column damage for the less severe WTC 1 impact.

Floor Truss and Slab Damage for the Less Severe WTC 1 Impact

An overall view of the floor truss structure in the impact zone, along with the calculated less severe impact damage to the floor trusses, is shown in Figure 9–67. The figure shows that the trusses experienced significant damage in the impact zone. A plan view of the calculated damage to the truss on each floor is shown in Figure 9–68. The calculated impact response produced severe damage to the truss structures in the primary impact path of the fuselage. The truss structures were severely damaged from the exterior wall to the core. The truss floor system on floors 94 through 96 were damaged and sagged downward as a result of the impact loading.

(a) Initial detailed truss structures

(b) Calculated damage (t=0.735 s)

Figure 9–67. Less severe impact damage to the WTC 1 floor truss (front view).

The magnitude of truss floor damage was very similar for the base case and more severe global impact analyses. When the floor-by-floor damage was compared for the base case and less severe impact analyses, Figure 9–15 and Figure 9–68, respectively, the damage was slightly increased for the less severe impact analysis. The parameters used in the less severe global impact analysis would primarily contribute to a reduced damage magnitude for the tower structure. However, the downward impact trajectory angle was increased from the 10.6 degree angle in the base case analysis to a 13.6 degree angle in the more severe impact analysis. This would have the effect of directing more of the impact energy downward, increasing the normal force on the floor structures in the impact zone. As a result, the combined effects of the analysis parameter variations produced a small increase in the damage to the truss structure in the less severe impact analysis scenario.

(a) Floor 94 truss damage

(b) Floor 95 truss damage

(c) Floor 96 truss damage

(d) Floor 97 truss damage

Figure 9–68. Less severe impact damage to the WTC 1 floor truss (plan view).

The calculated less severe impact damage to the WTC 1 slab for floors 94 through 97 are shown in Figure 9–69. The magnitude of floor slab damage was very similar for the base case and less severe global impact analyses. When the floor-by-floor damage was compared for the base case and less severe impact analyses, Figure 9–16 and Figure 9–69, respectively, the damage appeared to be slightly increased in the truss floor impact zone for the less severe impact. Similar to the truss damage, the increased

damage in the floor slab was believed to be the result of the increase in the downward impact trajectory angle from 10.6 to 13.6 degrees in the more severe impact analysis, increasing the normal downward force on the floor structures. In contrast to the floor slab, the core floor slab damage was reduced in the less severe impact analysis. This was a result of less impact energy imparted to the core frame. In the base case analysis, the core frame was more severely damaged, resulting in coupled damage to the core slab.

(a) Floor 94 slab damage

(b) Floor 95 slab damage

(c) Floor 96 slab damage

(d) Floor 97 slab damage

Figure 9–69. Less severe impact damage to the WTC 1 floor slab (plan view).

Damage to WTC 1 Contents for the Less Severe Impact

The calculated damage to the WTC 1 contents for the less severe impact is shown in plan views in Figure 9–70 through Figure 9–74 for floors 94 through 98, respectively. A comparison to the calculated damage for the base case WTC 1 impact analysis is shown previously in Figure 9–20 through Figure 9–24,

indicated that the building contents damage zone was very similar in width but did not extend as far through the tower in the less severe impact. The less severe impact produced little content damage on the far side of the core and did not extend fully through the tower. Little or no debris penetration of the south wall of the tower was expected for the less severe impact condition.

(a) Initial impact configuration

(b) Calculated response of contents

Figure 9–70. Calculated less severe WTC 1 impact response of floor 94 contents.

(a) Initial impact configuration

(b) Calculated response of contents

Figure 9–71. Calculated less severe WTC 1 impact response of floor 95 contents.

(a) Initial impact configuration

(b) Calculated response of contents

Figure 9–72. Calculated less severe WTC 1 impact response of floor 96 contents.

(a) Initial impact configuration

(b) Calculated response of contents

Figure 9–73. Calculated less severe WTC 1 impact response of floor 97 contents.

(a) Initial impact configuration

(b) Calculated response of contents

Figure 9–74. Calculated less severe WTC 1 impact response of floor 98 contents.

9.7 ADDITIONAL WTC 2 GLOBAL IMPACT ANALYSES

Two additional global impact analyses were performed for the WTC 2 impact to evaluate a more severe and less severe impact scenario. The combination of impact conditions for the more and less severe impact scenarios are compared to the corresponding parameters in the base case analysis in Table 9–10. The impact speeds were 521 mph and 570 mph in the less severe and more severe impact scenarios, respectively. These were the upper and lower bounds obtained from the analysis of aircraft impact conditions described in Chapter 7. The aircraft vertical trajectory angle was also varied from 8 to 5 degrees for the less severe and more severe impact scenarios, respectively. This resulted in more impact energy directed inward toward the core in the more severe impact scenario and less impact energy in the core for the less severe impact. The lateral trajectory was not varied in these analyses so that the starboard engine trajectory was aligned with exiting the northeast corner of the tower, as was observed from photographic evidence (see Section 9.11).

Table 9–10. Input parameters for additional WTC 2 global impact analyses.

Analysis Parameters		Base Case	More Severe	Less Severe
Flight Parameters	Impact Velocity	546 mph	570 mph	521 mph
	Trajectory - pitch	6.0°	5.0°	8.0°
	Trajectory - yaw	13.0°	13.0°	13.0°
	Orientation - pitch	5.0°	4.0°	7.0°
	Orientation - yaw	10.0°	10.0°	10.0°
Aircraft Parameters	Weight	100 percent	105 percent	95 percent
	Failure Strain	100 percent	115 percent	75 percent
Tower Parameters	Contents Strength	100 percent	80 percent	100 percent
	Failure Strain	100 percent	90 percent	120 percent
	Live Load Weight[a]	25 percent	20 percent	25 percent

a. Live load weight expressed as a percentage of the design live load.

The parameters varied for the aircraft model were the weight of the aircraft and the ductility of the aircraft materials. A 5 percent variation of the total aircraft weight was considered, with the additional weight applied for the more severe impact. The failure strain was varied from 75 to 115 percent of the baseline value for the less severe and more severe impact analyses, respectively. This variation in aircraft material ductility was used as the single parameter in these additional analyses to evaluate the uncertainties in aircraft material energy absorption capacity.

The parameters varied for the tower model were the ductility of the steel used in the tower construction and the weight and strength of the contents in the tower. The less severe impact analysis used a 20 percent increase in failure strain for the tower material and the baseline values for the contents weight and strength. The more severe impact analysis used a 10 percent reduction in tower material ductility with a corresponding 20 percent reduction in strength of the internal contents and a reduction of the weight of the content from 25 percent to 20 percent of the design live load capacity for the truss and core floor areas. The design live load is described in Section 3.2.4.

For WTC 2, the variations in the parameters from the base case were similar to those for WTC 1 (see Table 9–7), with two exceptions. The first exception was introduction of the strength of the building contents as a parameter. There was less information available about the layout of building contents in the WTC 2 impact zone and therefore a larger uncertainty associated with the contents was assumed. Recall that the workstation layout from WTC 1 was used for WTC 2. Thus, in the more severe case, the contents strength was reduced to 80 percent of the baseline value.

The second exception was the failure strains for the aircraft and tower materials. For the more severe WTC 1 analysis, 125 percent and 80 percent of the baseline values were used for the aircraft and tower failure strains, respectively. For the more severe WTC 2 analysis, 115 percent and 90 percent of the baseline values were used. The more severe WTC 2 analysis was the final global impact analysis performed. Based on the previous analyses, the variation in damage levels indicated that the WTC 2 more severe impact analysis would produce impact damage state that was not viable (e.g., the amount of debris exiting the north wall). To ensure that a viable damage state was obtained, the aircraft and tower materials were adjusted to the values presented in Table 9–10.

9.7.1 More Severe WTC 2 Global Impact Analyses

This case is referred to as Case D for the remainder of the WTC investigation reports. A side view of the more severe WTC 2 global impact model is shown in Figure 9–75. The tower interior contents were removed and the tower structures were shown as transparent in the figure so that the impact response in the tower interior was visible. Similar plan views of the progression of aircraft impact response are shown in Figure 9–76. The responses are shown at intervals of 0.1 s from impact through the initial 0.5 s of the response. Corresponding images of the base case WTC 2 impact response were shown previously in Figure 9–26 and Figure 9–27, respectively.

The initial 0.1 s of the more severe global aircraft impact response, shown in Figure 9–75(b) and Figure 9–76(b), was dominated by the impact, penetration, and fragmentation of the forward fuselage structures. The engines and forward wing structures also penetrated the exterior wall. At 0.2 s after impact, the full penetration of the aircraft into the tower was completed, as shown in Figure 9–75(c) and Figure 9–76(c). The airframe was mostly broken up, but some large sections of the aft fuselage and tail were still intact, having penetrated through the opening in the tower wall produced by the forward fuselage structures. The aircraft fuel cloud was starting to spread out, but was still relatively dense and the leading edge of the fuel was approximately one-half through the tower core. At 0.3 s after impact, the aircraft fuel cloud had penetrated the distance through the core and was spreading out, as shown in Figure 9–75(d) and Figure 9–76(d). The subsequent motion of the aircraft fragments and fuel debris cloud began to be noticeably slowed beyond this time. The slower spread of fuel and debris through the tower is seen in the remaining images in Figure 9–75 and Figure 9–76. The spread of the fuel and debris cloud was more rapid and extensive in the open truss regions than through the core as a result of the open volume above the workstations in the truss floor zone.

Exterior Wall Damage for the More Severe WTC 2 Impact

A comparison of the south exterior wall observed and calculated damage from the more severe WTC 2 global impact analysis is shown in Figure 9–77. The calculated impact damage to the exterior wall is shown with color fringes representing plastic strain magnitude, with undamaged sections in blue and strains at or above 5 percent shown in red. The region shown in Figure 9–77 includes column 402 to column 446, extending from floor 76 to floor 86 (spandrels at floors 77 through 86). The mode and magnitude of the calculated and observed impact damage on the exterior wall were still in good agreement in this more severe impact analysis.

(a) Time=0.00 s

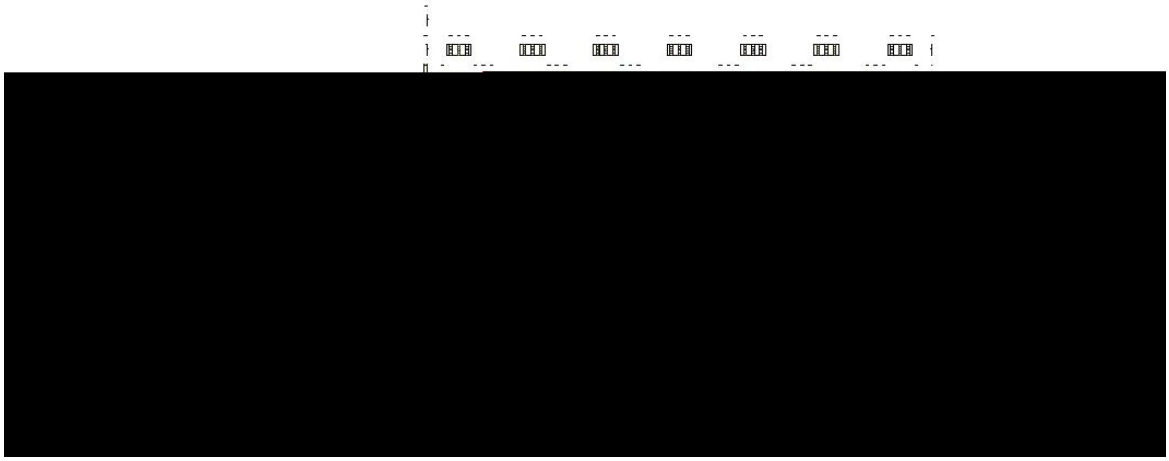

(b) Time=0.10 s

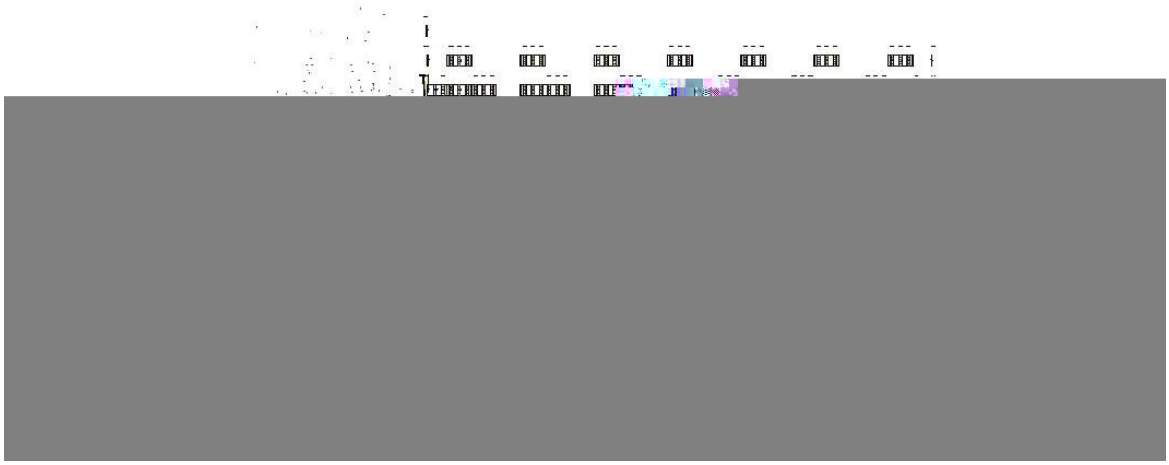

(c) Time=0.20 s

Figure 9–75. More severe WTC 2 global impact analysis (side view).

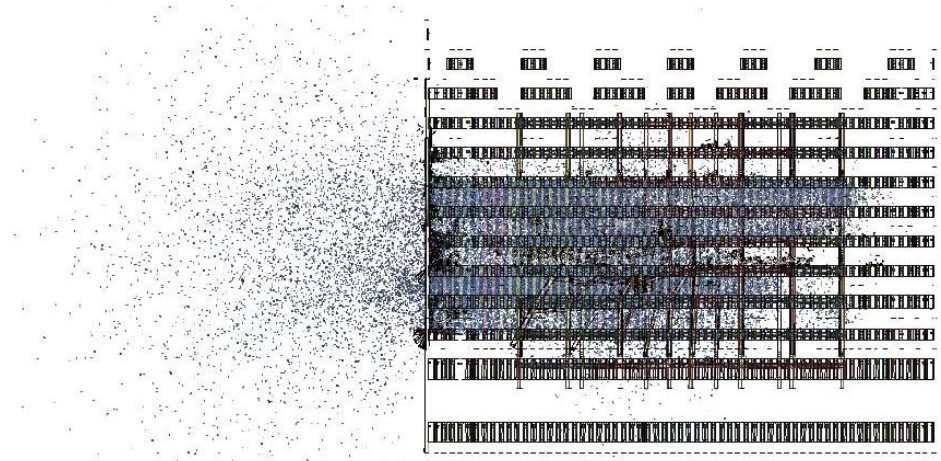

(d) Time=0.30 s

(e) Time=0.40 s

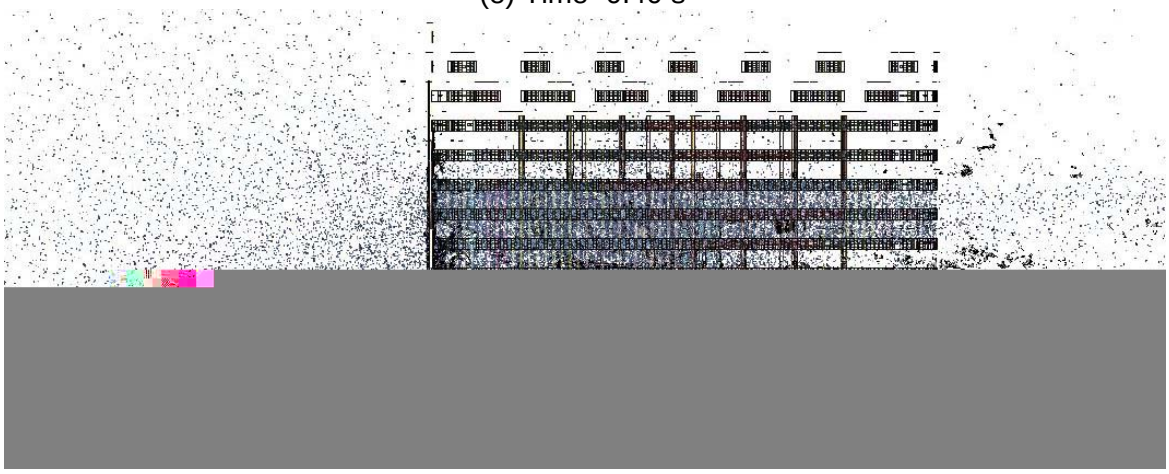

(f) Time=0.50 s

Figure 9–75. More severe WTC 2 global impact analysis (side view) (continued).

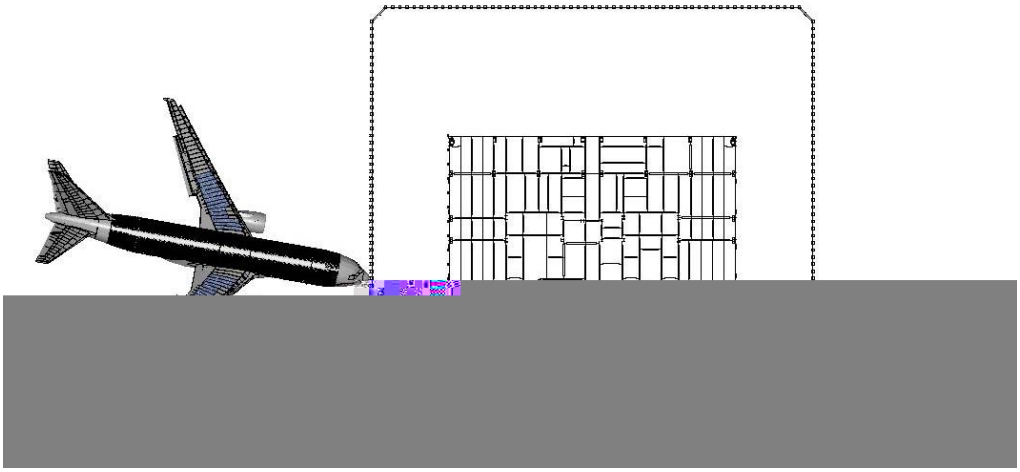

(a) Time=0.00 s

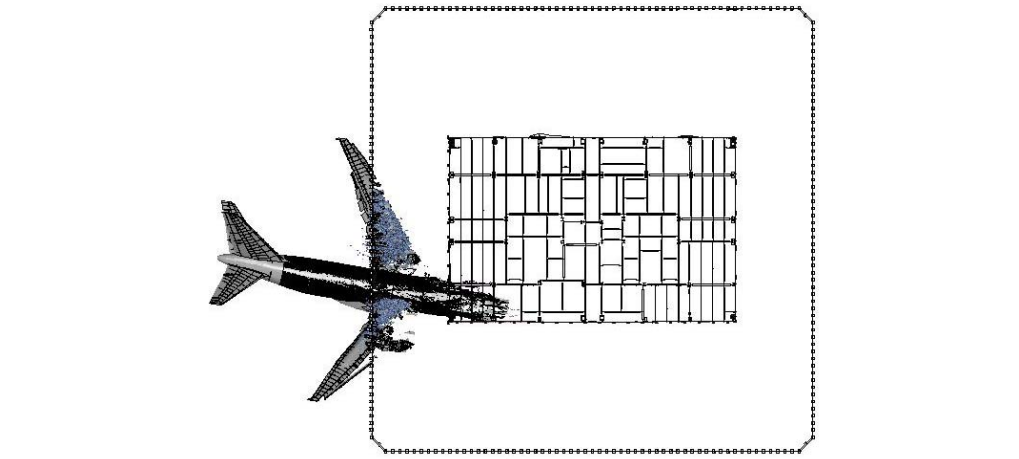

(b) Time=0.10 s

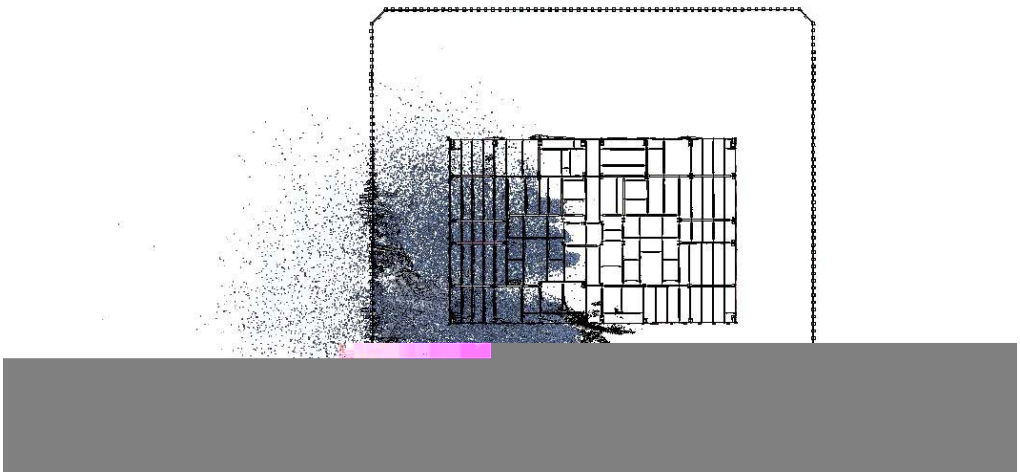

(c) Time=0.20 s

Figure 9–76. More severe WTC 2 global impact analysis (plan view).

(d) Time=0.30 s

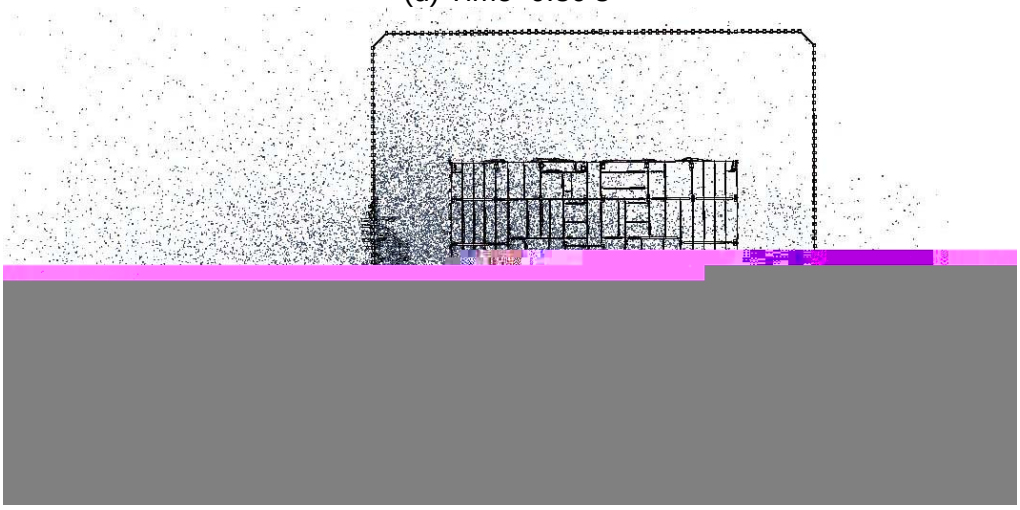

(e) Time=0.40 s

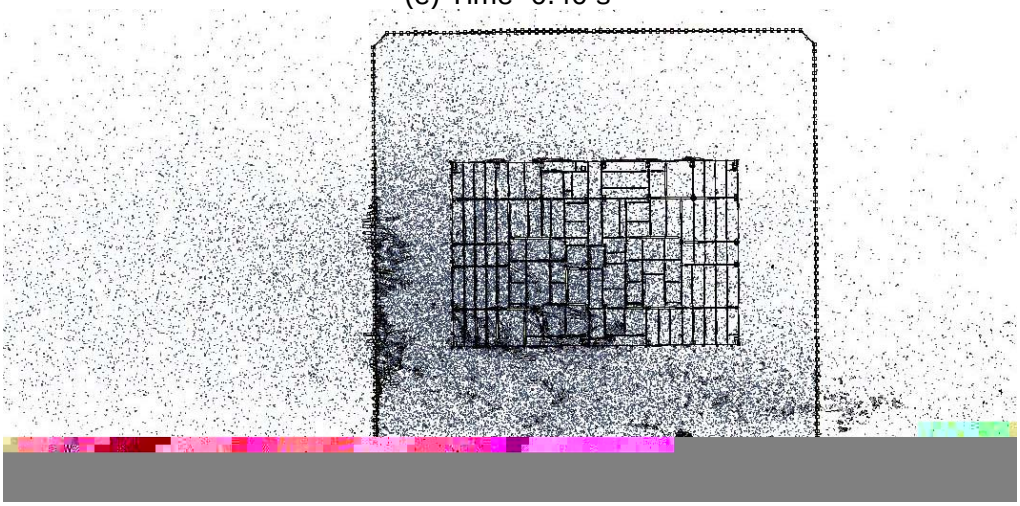

(f) Time=0.50 s

Figure 9–76. More severe WTC 2 global impact analysis (plan view) (continued).

(a) Schematic of observed damage

(b) Calculated damage (t=0.62 s)

Figure 9–77. More severe impact damage to the WTC 2 exterior wall.

Core Structural Damage for the More Severe WTC 2 Impact

The overall model for the WTC 2 core structure and calculated response for the more severe damage analysis is shown in Figure 9–78. The figure shows that the core had extensive damage in the region close to the impact point. The columns in line with the aircraft fuselage failed on the impact side, and several of the core beams were also severely damaged or failed in the impact zone. In some cases, failure of the column splices located on floors 77, 80, and 83 contributed significantly to the failure of the core columns.

The calculated damage to the core columns by is shown in Figure 9–79, and the floor-by-floor damage to the core framing is shown in Figure 9–80. The core structures are shown with color fringes representing plastic strain magnitude, with undamaged sections in blue and strains at or above 5 percent shown in red. A summary of the column damage is provided in Table 9–11 and shown graphically in Figure 9–81, with the qualitative classification of the column damage levels provided previously in Figure 9–12. A total of 10 columns were severed, and one column was heavily damaged, compared to five columns severed and four columns heavily damaged in the base case WTC 2 impact analysis.

(a) Initial geometry

(a) Calculated impact damage

Figure 9–78. More severe impact response of the WTC 2 core.

(a) Columns 1001-1008 (b) Columns 901-908

(c) Columns 801-807 (d) Columns 701-708

Figure 9–79. More severe impact response of the WTC 2 core columns.

(a) Floor 78 core framing damage

(b) Floor 79 core framing damage

(c) Floor 80 core framing damage

(d) Floor 81 core framing damage

(e) Floor 82 core framing damage

(f) Floor 83 core framing damage

Figure 9–80. More severe impact damage to the WTC 2 core floor framing (plan view).

Table 9–11. Core column response for the more severe WTC 2 impact.

Column	Location	Damage Level	Lateral Deflection of Column Centerline (in.)
Column 602	Floor 79	Moderate	
Column 605	Floor 79	Moderate	
Column 701	Floors 79-80	Severed	
Column 702	Floor 79	Heavy	16
Column 703	Floor 79	Moderate	
Column 704	Floor 79	Light	
Column 705	Floors 78-79	Light	
Column 705	Floor 78	Light	
Column 801	Floors 79-80	Severed	
Column 802	Floors 77-80	Severed	
Column 803	Floors 77-80	Severed	
Column 804	Floor 79	Light	
Column 901	Floors 80-81	Severed	
Column 902	Floor 79	Moderate	
Column 903	Floors 77-83	Severed	
Column 904	Floors 79-81	Moderate	
Column 905	Floors 79 & 81	Light	
Column 907	Floor 81	Light	
Column 1001	Floors 77-83	Severed	
Column 1002	Floors 79-83	Severed	
Column 1003	Floors 79-83	Severed	
Column 1004	Floors 79-83	Severed	
Column 1005	Floors 79-81	Moderate	

Figure 9–81. Summary of core column damage for the more severe WTC 2 impact.

Strain Rate Observations for the More Severe WTC 2 Impact

The more severe WTC 2 impact analysis had the highest impact speed of any of the global impact analyses. As a result, the more severe WTC 2 impact is an appropriate case for bounding the expected strain rates for the deformation of the WTC tower structural materials. Fringes of Von Mises effective strain rate for the south exterior wall and core framing are shown in Figure 9–82 and Figure 9–83, respectively. The corresponding times shown are at 90 ms and 200 ms for the exterior wall and core framing, respectively. These times were selected as representative of instants when rapid impact deformations over a significant portion of the structure were observed in the calculation.

The strain rates in the exterior wall were significantly higher than those in the core. Peak strain rates were calculated at specific locations for short durations. These strain rates were on the order of a few thousand per second. However, these high strain rates were localized to small regions of the structure and for very short durations. Figure 9–82 shows that the majority of the deformations occurred with strain rates at or below approximately 100 per second. Similarly, the localized peak strain rates in the core were a few hundred per second, and Figure 9–83 shows that the majority of the deformation in the core occurred with strain rates at or below approximately 20 per second.

The expected influence of these elevated strain rates on strength is small. The dominant strain rates seen in the figures are between 1 and 100 per second. The rate material testing, described previously in Section 2.2.4, shows that the yield stress for the WTC tower materials typically increased by less than 10 percent at these calculated rates.

Figure 9–82. Representative exterior wall strain rates for the more severe WTC 2 impact (view from tower exterior).

Figure 9–83. Representative core frame strain rates for the more severe WTC 2 impact (impact from the left of the figure).

Floor Truss and Slab Damage for the More Severe WTC 2 Impact

An overall view of the floor truss structure in the WTC 2 impact zone, along with the calculated more severe impact damage to the trusses, is shown in Figure 9–84. The figure shows that the trusses experienced significant damage in the impact zone, with the heaviest damage on floor 81. A plan view of the calculated damage to the trusses on each floor is shown in Figure 9–85. The calculated impact response produced severe damage to the truss structures in the primary impact path of the fuselage. The truss structures were severely damaged from the exterior wall to the core. The truss floor system on floors 79 through 82 had sufficient damage from the impact that portions of the truss floor sections sagged downward as a result of the impact.

(a) Initial detailed truss structures

(b) Calculated damage (t=0.58 s)

Figure 9–84. More severe impact damage to the WTC 2 floor truss (front view).

The magnitude of truss floor damage was very similar for the base case and more severe global impact analyses. The parameters used in the more severe global impact analysis would primarily contribute to increased damage for the tower structures. However, the downward impact trajectory angle was reduced from the 6 degree angle in the base case analysis to a 5 degree angle in the more severe impact analysis. This would have the effect of directing more of the impact energy inward toward the tower core, but reducing the normal downward force on the floor structures in the impact zone. As a result, the combined effects of the analysis parameter variations produced very similar damage to the truss structure.

The calculated damage to the WTC 2 floor slab for floors 78 through 83 for the more severe impact is shown in Figure 9–86. The fringes of damage were set so that the concrete failed in the regions colored red (2 percent plastic strain). In these regions, it is expected that the concrete slab was severely damaged and potentially removed, exposing the supporting metal decking. At a plastic strain of 30 percent, corresponding to failure levels for the metal decking material, the elements were eroded (seen as holes ruptured in the floor slab shown). The line of damage, visible around the edge of the core, was believed to be the result of numerical precision errors and interference in the modeling methodology at the connection of the floor slab rather than impact damage.

(a) Floor 79 truss damage

(b) Floor 80 truss damage

(c) Floor 81 truss damage

(d) Floor 82 truss damage

Figure 9–85. More severe impact damage to the WTC 2 floor truss (plan view).

Similar to the damage levels in the floor truss structures, the magnitude of floor slab damage was very similar for the base case and more severe global impact analyses. The parameters used in the more severe global impact analysis would primarily contribute to an increased damage magnitude for the tower structures. However, the downward impact trajectory angle was reduced from the 6 degree angle in the base case analysis to a 5 degree angle in the more severe impact analysis. This would have the effect of directing more impact energy inward toward the tower core, but reducing the normal downward force on the floor structures in the impact zone. As a result, the combined effects of the analysis parameter variations produced very similar damage magnitudes to the floor slab.

Damage to WTC 2 Contents for the More Severe Impact

The calculated damage to the WTC 2 contents for the more severe impact is shown in plan views in Figure 9–87 through Figure 9–92 for floors 78 through 83, respectively. A comparison to the calculated damage for the base case WTC 2 impact analysis, shown previously in Figure 9–41 through Figure 9–46, indicated that the tower contents damage zone was similar, with a slight increase in damage for the more severe impact.

(a) Initial impact configuration

(b) Calculated response of contents

Figure 9–87. Calculated more severe WTC 2 impact response of floor 78 contents.

(a) Initial impact configuration

(b) Calculated response of contents

Figure 9–88. Calculated more severe WTC 2 impact response of floor 79 contents.

(a) Initial impact configuration

(b) Calculated response of contents

Figure 9–89. Calculated more severe WTC 2 impact response of floor 80 contents.

(a) Initial impact configuration

(b) Calculated response of contents

Figure 9–90. Calculated more severe WTC 2 impact response of floor 81 contents.

(a) Initial impact configuration

(b) Calculated response of contents

Figure 9–91. Calculated more severe WTC 2 impact response of floor 82 contents.

(a) Initial impact configuration

(b) Calculated response of contents

Figure 9–92. Calculated more severe WTC 2 impact response of floor 83 contents.

9.7.2 Less Severe WTC 2 Global Impact Analyses

Exterior Wall Damage for the Less Severe WTC 2 Impact

A comparison of the south exterior wall observed and calculated damage from the less severe WTC 2 global impact analysis is shown in Figure 9–93. The calculated impact damage to the exterior wall is shown with color fringes representing plastic strain magnitude, with undamaged sections in blue and strains at or above 5 percent shown in red. The region shown in Figure 9–93 includes column 402 to column 446, extending from floor 76 to floor 86 (spandrels at floors 77 through 86). The mode and magnitude of the calculated and observed impact damage on the exterior wall are still in good agreement in this less severe impact analysis.

(a) Schematic of observed damage

(b) Calculated damage (t=0.66 s)

Figure 9–93. Less severe impact damage to the WTC 2 exterior wall.

Core Structural Damage for the Less Severe WTC 2 Impact

The overall model of the WTC 2 core structure and calculated response for the less severe global impact analysis is shown in Figure 9–94. The figure shows that the core had significant damage in the region close to the impact point. The columns in line with the aircraft fuselage failed on the impact side, and several of the core beams were also severely damaged or failed in the impact zone. In some cases, failure of the column splices located on floors 77, 80, and 83 contributed significantly to the failure of the core columns.

The calculated damage to the core columns by axis is shown in Figure 9–95, and the floor-by-floor damage to the core framing is shown in Figure 9–96. The core structures are shown with color fringes representing plastic strain magnitude, with undamaged sections in blue and strains at or above 5 percent shown in red. A summary of the column damage is provided in Table 9–12 and shown graphically in Figure 9–97, with the qualitative classification of the column damage levels provided previously in Figure 9–12. A total of three columns were severed, and two columns heavily damaged, compared to five severed columns and four heavily damaged columns in the base case WTC 2 impact analysis.

Floor Truss and Slab Damage for the Less Severe WTC 2 Impact

An overall front view of the floor truss structure in the WTC 2 impact zone, along with the calculated less severe impact damage to the trusses, is shown in Figure 9–98. The truss floor system on floors 79 through 82 had sufficient damage from the impact that portions of the truss floor sections sagged downward as a result of the impact. A plan view of the calculated damage to the trusses on each floor is shown in Figure 9–99. The figure shows that the trusses experienced significant damage in the impact zone, with the heaviest damage on floor 81. The calculated impact response produced severe damage to the truss structures in the primary path of the fuselage. The truss structures were completely destroyed along the impact path on floor 81 from the exterior wall to the core.

(a) Initial geometry

(a) Calculated impact damage

Figure 9–94. Less severe impact response of the WTC 2 core.

(a) Columns 1001-1008 (b) Columns 901-908

(c) Columns 801-807 (d) Columns 701-708

Figure 9–95. Less severe impact response of the WTC 2 core columns.

(a) Floor 78 core framing damage

(b) Floor 79 core framing damage

(c) Floor 80 core framing damage

(d) Floor 81 core framing damage

(e) Floor 82 core framing damage

(f) Floor 83 core framing damage

Figure 9–96. Less severe impact damage to the WTC 2 core floor framing (plan view).

Table 9–12. Core column response for the less severe WTC 2 impact.

Column	Location	Damage Level	Lateral Deflection of Column Centerline (in.)
Column 801	Floor 79	Light	
Column 901	Floors 79-80	Severed	
Column 902	Floors 78-79	Heavy	24
Column 903	Floors 77-81	Severed	
Column 1001	Floors 77-83	Severed	
Column 1002	Floors 80-81	Moderate	
Column 1003	Floors 79-80	Heavy	16
Column 1004	Floor 80	Moderate	

Figure 9–97. Summary of core column damage for the less severe WTC 2 impact.

(a) Initial detailed truss structures

(b) Calculated damage (t=0.661 s)

Figure 9–98. Less severe impact damage to the WTC 2 floor truss (front view).

The magnitude of truss floor damage was very similar for the base case and less severe global impact analyses. The parameters used in the less severe global impact analysis would primarily contribute to a reduced damage magnitude for the tower structures. However, the downward impact trajectory angle was increased from the 6 degree angle in the base case analysis to a 8 degree angle in the less severe impact analysis. This would have the effect of directing more of the impact energy downward, increasing the normal force on the floor structures in the impact zone. As a result, the combined effects of the analysis parameter variations produced very similar damage to the truss structure.

The calculated damage to the WTC 2 floor slab for floors 78 through 83 for the less severe impact is shown in Figure 9–100. Similar to the damage levels in the floor truss structures, the magnitude of floor slab damage was very similar for the base case and less severe global impact analyses. The increase in the impact trajectory angle from 6 to 8 degrees offset the effects of the other analysis parameters for producing damage to the floor slab.

(a) Floor 79 truss damage

(b) Floor 80 truss damage

(c) Floor 81 truss damage

(d) Floor 82 truss damage

Figure 9–99. Less severe impact damage to the WTC 2 floor truss (plan view).

(a) Floor 78 slab damage

(b) Floor 79 slab damage

(c) Floor 80 slab damage

(d) Floor 81 slab damage

(e) Floor 82 slab damage

(f) Floor 83 slab damage

Figure 9–100. Less severe impact damage to the WTC 2 floor slab (plan view).

Damage to WTC 2 Contents for the Less Severe Impact

The calculated damage to the WTC 2 contents for the less severe impact is shown in plan views in Figure 9–101 through Figure 9–106 for floors 78 through 83, respectively. A comparison to the calculated damage for the base case WTC 2 impact analysis, shown previously in Figure 9–41 through Figure 9–46, indicated that the content damage zones were very similar, with a slight reduction in damage for the less severe impact.

(a) Initial impact configuration

(b) Calculated response of contents

Figure 9–101. Calculated less severe WTC 2 impact response of floor 78 contents.

(a) Initial impact configuration

(b) Calculated response of contents

Figure 9–102. Calculated less severe WTC 2 impact response of floor 79 contents.

(a) Initial impact configuration

(b) Calculated response of contents

Figure 9–103. Calculated less severe WTC 2 impact response of floor 80 contents.

(a) Initial impact configuration

(b) Calculated response of contents

Figure 9–104. Calculated less severe WTC 2 impact response of floor 81 contents.

(a) Initial impact configuration

(b) Calculated response of contents

Figure 9–105. Calculated less severe WTC 2 impact response of floor 82 contents.

(a) Initial impact configuration

(b) Calculated response of contents

Figure 9–106. Calculated less severe WTC 2 impact response of floor 83 contents.

9.8 COMPARISON OF DIFFERENT SEVERITY WTC 1 IMPACT ANALYSES

9.8.1 Exterior Wall Damage for WTC 1

The calculated damage to the north exterior wall of WTC 1 for the three different severity impacts is shown in Figure 9–107, along with a schematic of the observed damage. The overall agreement with the observed damage was good for all three analyses, with the base case global impact analysis providing the best match to the observed damage. The calculated damage magnitude was similar in each of the global analyses with small differences, as shown in the figure.

The differences in apparent damage were largely due to panels that may have severed columns in one case and were removed at the connection in another. Visually this looks substantial as portions of panels that were damaged but still attached to the wall in the more severe impact, shown in the Figure 9–107(b), were completely removed in the less severe impact, as shown in Figure 9–107(c). In general, the trend was for a larger opening produced by the less severe impact to a smaller opening in the more severe impact. The increase in the opening with reduced severity impact can be explained by the increased tower panel

material toughness, resulting in a transition from column severing to connection bolt failure and panel removal.

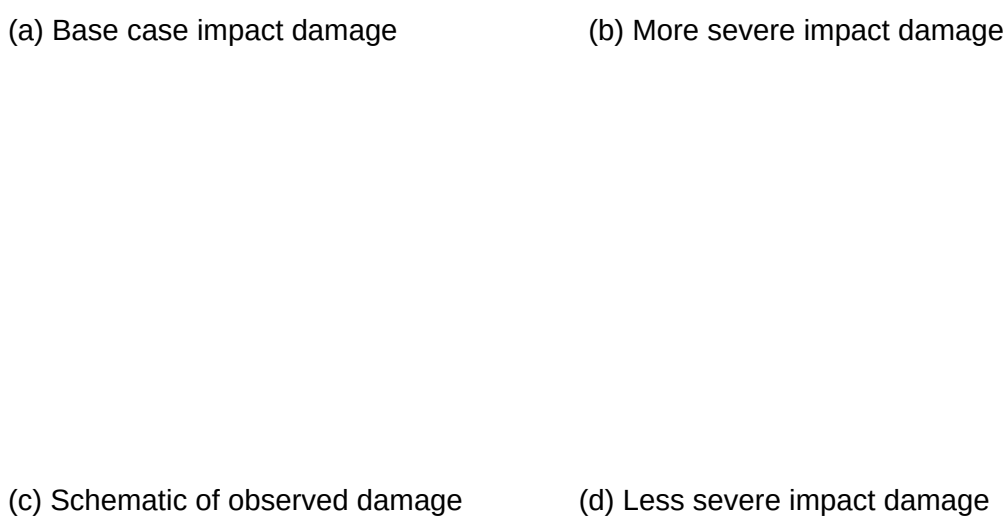

(a) Base case impact damage (b) More severe impact damage

(c) Schematic of observed damage (d) Less severe impact damage

Figure 9–107. Impact damage to the north exterior wall of WTC 1.

Toward the wing tips, where the columns and spandrels were not completely severed, the more severe impact damage analysis calculated higher damage to the exterior wall panels. These columns had the largest amount of material with plastic strains above 5 percent (shown in red in the figure). As would be expected, the less severe impact damage analysis calculated lower damage to the exterior wall, and the base case analysis calculated an intermediate level of damage near the wing tips.

9.8.2 Core Column Damage for WTC 1

The calculated damage to the WTC 1 core columns for the three different severity impacts is shown in Figure 9–108. The figure shows that the core damage was concentrated in the region of the core closest to the impact point, and there was a clear correlation in damage magnitude with the impact severity. A total of one column was severed, and two columns were heavily damaged in the less severe impact, compared to three columns severed and four columns heavily damaged in the base case impact analysis and six columns severed and three columns heavily damaged in the more severe WTC 1 impact analysis.

(a) Calculated less severe impact analysis

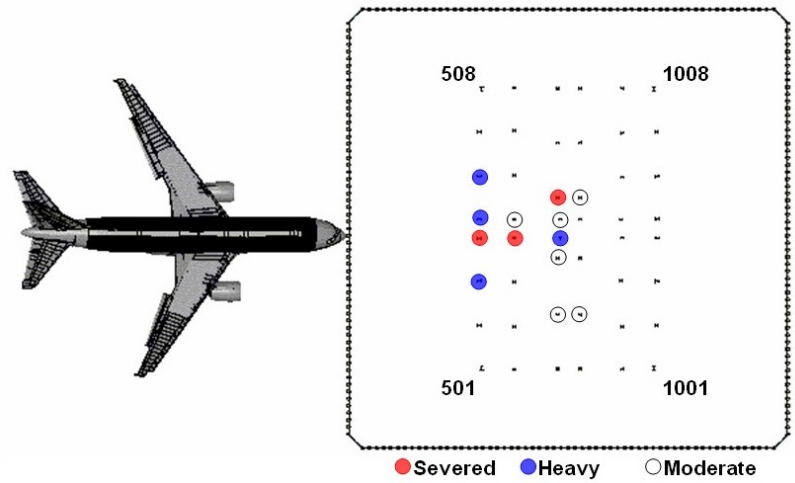

(b) Calculated base case impact damage

(c) Calculated more severe impact analysis

Figure 9–108. Comparison of core column damage for the WTC 1 impact analyses.

The strong correlation in the core damage with increasing severity was expected. All of the parameter variations in the three increasing severity analyses would be expected to produce an increase in core damage. The flight parameters had an increasing impact speed and a shallower impact angle, directing more energy toward the core. The aircraft had increasing weight and higher material toughness. The tower had reduced mass in the contents and added material toughness. All of these variations contributed toward the increased core damage with increased impact severity.

9.8.3 Floor Truss Damage for WTC 1

The calculated damage to the WTC 1 floor trusses for the three different severity impacts is shown in Figure 9–109. The magnitude of truss floor damage was very similar for the different severity WTC 1 global impact analyses. The parameters used in the increasing severity global impact analyses would primarily contribute to an increased damage magnitude for the tower structures. However, the downward impact trajectory angle was correspondingly reduced from 13.6 degrees in the less severe impact to 10.6 and 7.6 degrees in the base case and severe impact scenarios, respectively. This would have the effect of directing less of the impact energy downward, reducing the normal force on the floor structures in the impact zone. As a result, the combined effects of the analysis parameter variations produced very similar damage to the truss structure for the three different severity impact scenarios.

(a) Calculated less severe impact analysis

(b) Calculated base case impact damage

(c) Calculated more severe impact analysis

Figure 9–109. Comparison of floor truss damage for the WTC 1 impact analyses.

9.9 COMPARISON OF DIFFERENT SEVERITY WTC 2 IMPACT ANALYSES

9.9.1 Exterior Wall Damage for WTC 2

The predicted impact damage to the south exterior wall of WTC 2 for the three different severity impacts is shown in Figure 9–110, with a schematic of the observed damage for comparison. As was the case for WTC 1, there were small differences in the predictions from each of the global analyses shown in the figure. Overall, the agreement with the observed damage from photographs was very good. The most

obvious differences were largely due to portions of beams that may have severed columns in one case or have been removed at the connections in another.

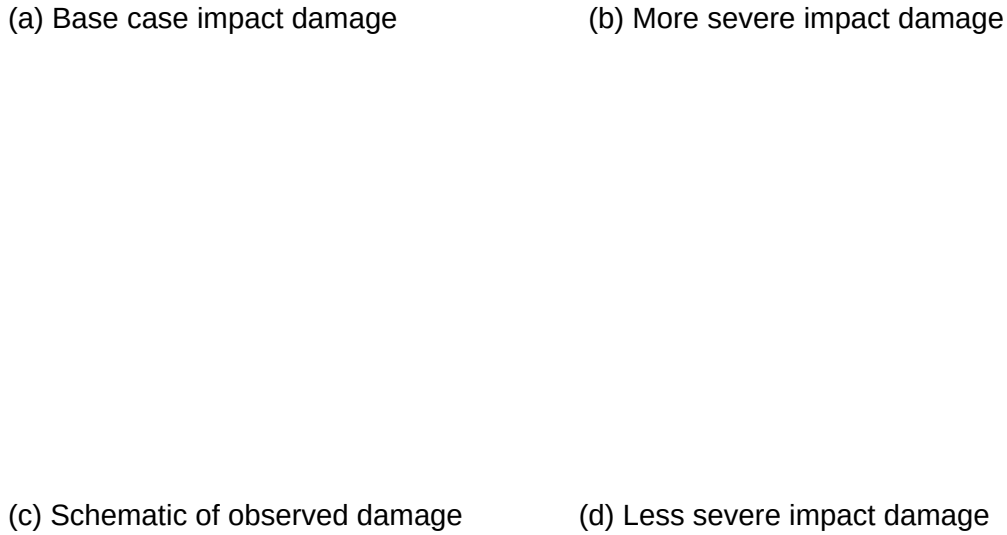

(a) Base case impact damage (b) More severe impact damage

(c) Schematic of observed damage (d) Less severe impact damage

Figure 9–110. Impact damage to the south exterior wall of WTC 2.

9.9.2 Core Column Damage for WTC 2

The calculated damage to the WTC 2 core columns for the three different severity impacts is shown in Figure 9–111. The figure shows that the core damage was concentrated in the region of the core closest to the impact point, and there was a clear correlation in damage magnitude with the impact severity. A total of three columns were severed and two columns were heavily damaged in the less severe impact, compared to five columns severed and four columns heavily damaged in the base case analysis and ten columns severed and one column heavily damaged in the more severe WTC 2 impact analysis.

The strong correlation in the core damage with impact severity was expected. All of the parameter variations in the three increasing severity analyses would be expected to produce an increase in core damage. The flight parameters had an increasing impact speed and a shallower impact angle, directing more energy toward the core. The aircraft had increasing weight and higher material toughness. The

tower had reduced mass in the contents and added material toughness. All of these variations contributed toward the increased core damage with increased impact severity.

(a) Calculated less severe impact analysis

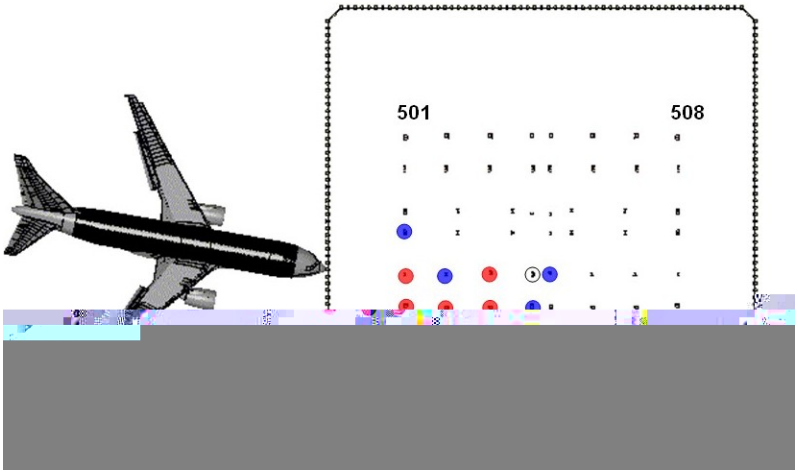

(b) Calculated base case impact damage

(c) Calculated more severe impact analysis

Figure 9–111. Comparison of core column damage for the WTC 2 impact analyses.

9.9.3 Floor Truss Damage for WTC 2

The calculated damage to the WTC 2 floor truss structures for the three different severity impacts is shown in Figure 9–112. The magnitude of truss floor damage was very similar for the different severity WTC 2 global impact analyses. The parameters used in the increasing severity global impact analyses would primarily contribute to an increased damage magnitude for the tower structures. However, the downward impact trajectory angle was correspondingly reduced from 8 degrees in the less severe impact to 6 and 5 degrees in the base case and more severe impact scenarios, respectively. This would have the effect of directing less of the impact energy downward, reducing the normal force on the floor structures in the impact zone. As a result, the combined effects of the analysis parameter variations produced very similar damage to the truss structure for the three different severity impact scenarios.

(a) Calculated less severe impact analysis

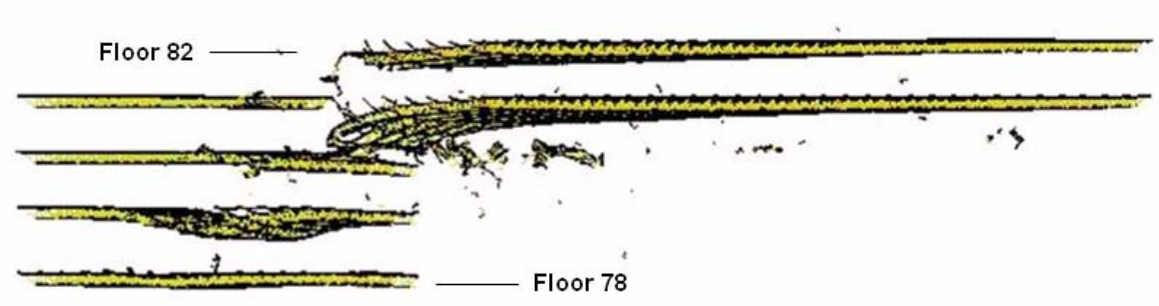

(b) Calculated base case impact damage

(c) Calculated more severe impact analysis

Figure 9–112. Comparison of floor truss damage for the WTC 2 impact analyses.

9.10 COMPARISON BETWEEN WTC 1 AND WTC 2

The comparison of the aircraft impact response and resulting tower damage for WTC 1 and WTC 2 was complicated by the differences in the two impact scenarios. The base case WTC 1 impact was close to centered and perpendicular on the face of the tower, with the long span trusses between the impact point and the core. The base case WTC 1 impact scenario led to a debris trajectory where almost all of the aircraft debris passed through the core. The baseline impact conditions for WTC 1 were a 443 mph collision with a downward impact trajectory angle of 10 degrees. In contrast, the baseline WTC 2 impact was off center and angled away from the core, resulting in a significant fraction of the aircraft debris cloud outside (east) of the core. The WTC 2 impact had short span trusses between the impact point and the core. Finally, the baseline impact conditions for WTC 2 were a 546 mph collision with a downward impact trajectory angle of 6 degrees.

Exterior Wall Damage

The calculated exterior wall damage for the base case WTC 1 and WTC 2 impacts are compared in Figure 9–113. Despite the differences in impact conditions, the mode and magnitude of damage to the exterior walls were quite similar in both towers. This was because the impact loads distributed over the majority of the aircraft structures were much larger than the exterior column rupture strength. The details of the failure mode (column deformation and rupture or failure and separation of bolted column end connections) were determined by the proximity of the floor slab and column joints to the impact point. For both impacts, the wing tip structures impacted and damage, but did not completely fail the columns.

Core Column Damage

The calculated core column damage for the base case WTC 1 and WTC 2 impacts are compared in Figure 9–114. In the WTC 1 impact, there were three columns severed and four columns heavily damaged. The calculated region of significant core column damage appears to extend three column rows deep into the core. In contrast, the calculated damage for the WTC 2 impact included five columns severed and four columns heavily damaged, and the region of significant core column damage appears to extend four column rows deep. This increase in core damage was even more significant since the impact zone was 15 floors lower in WTC 2 (and therefore designed to carry more gravity loads), and as a result the core columns were heavier and more resistant to impact damage in the WTC 2 impact zone.

The differences in the core column damage between WTC 1 and WTC 2 can be explained by two primary factors. The first was that the WTC 2 impact speed was 23 percent higher (approximately 50 percent higher impact energy), and the shallower impact angle directed more impact energy inward toward the core. The second factor was that the orientation of the core relative to the impact was different in the two towers, as the core was closer to the impact point in WTC 2. As a result, WTC 2 had reduced energy absorbing capacity due to the shorter floor structures and less building contents between the impact point and the core.

(a) WTC 1 calculated damage (t=0.715 s)

(b) WTC 2 calculated damage (t=0.62 s)

Figure 9–113. Comparison of base case impact damage to the exterior wall.

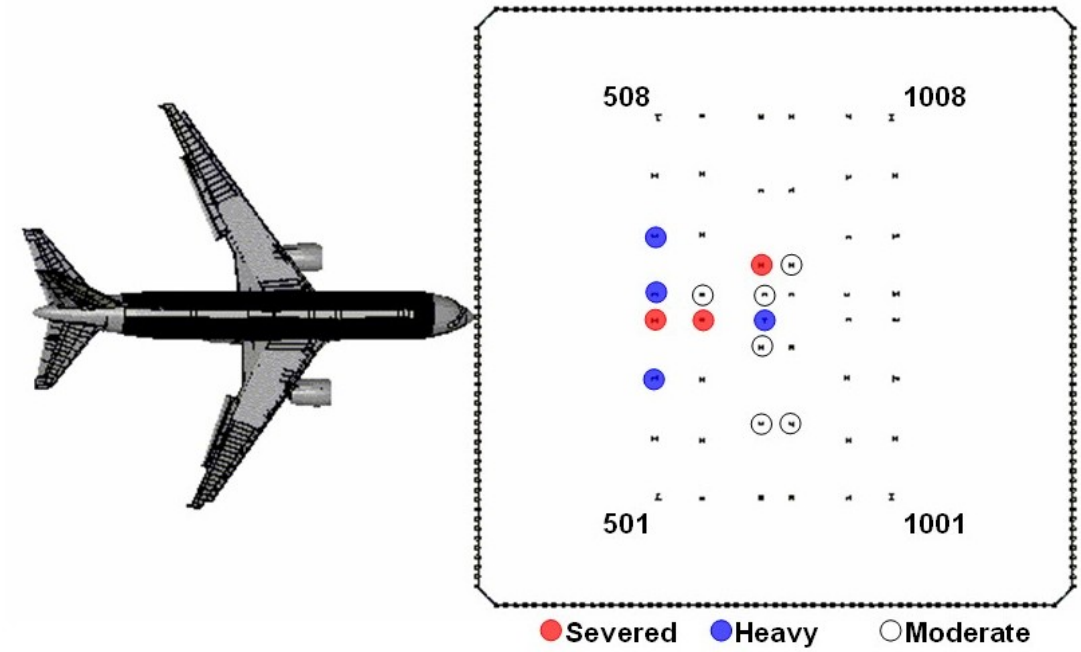

(a) WTC 1 calculated damage (t=0.715 s)

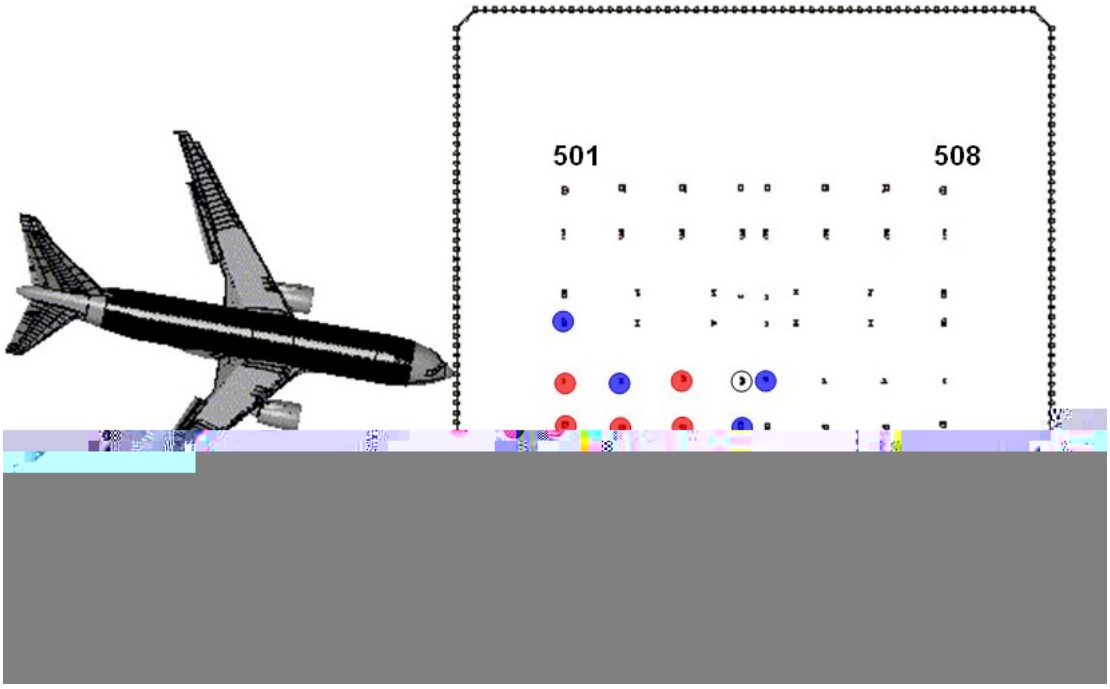

(b) WTC 2 calculated damage (t=0.62 s)

Figure 9–114. Comparison of base case impact damage to the core columns.

Floor Truss Damage

The calculated floor truss damage for the base case WTC 1 and WTC 2 impacts are compared in Figure 9–115. The comparison shows that the WTC 1 floor truss had greater damage and collapse of the truss floor despite the lower aircraft impact energy. The higher amount of truss floor damage and

deflection in WTC 1 can be explained by two factors. The primary factor was that the WTC 1 downward impact trajectory was nearly twice as steep as that of WTC 2 impact. As a result, the steeper impact angle directed more impact energy normal to the floor. The vertical component of the impact load in WTC 1 was approximately 40 percent higher than in WTC 2 (the vertical momentum of the aircraft that impacted WTC 1 was about 40 percent higher than that of the aircraft that impacted WTC 2). The secondary factor was that the damage to the long span floors in the WTC 1 impact zone produced larger displacements than a corresponding damage level to a short span truss region.

(a) WTC 1 calculated damage (t=0.715 s)

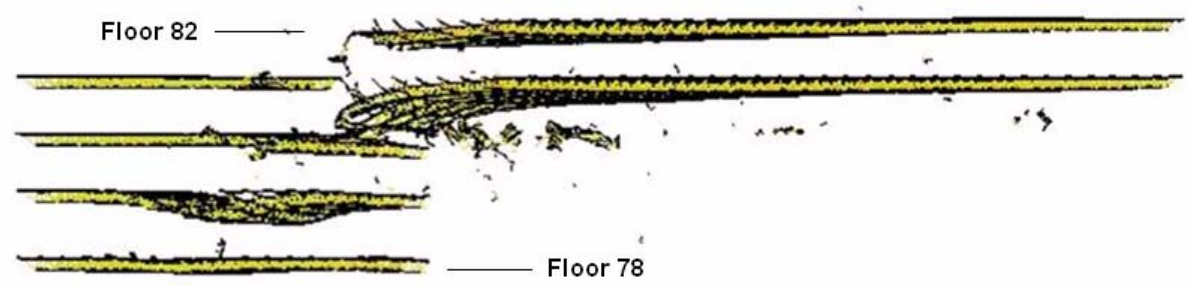

(b) WTC 2 calculated damage (t=0.715 s)

Figure 9–115. Comparison of base case impact damage to floor truss (front view).

9.11 COMPARISON WITH OBSERVABLES

The observable evidence available to help validate the global impact analyses included the following:

- Damage to the buildings' exteriors documented by photographic evidence.
- Floor damage visible from the buildings' exteriors documented by photographic evidence.
- Aircraft debris external to the towers as documented by photographic evidence.
- Eyewitness accounts from survivors who were inside portions of the buildings.

The most valuable observable from a modeling standpoint was the damage to the impacted exterior wall of each tower. The impact damage to the exterior tower walls was well documented, and the response did not depend much on unknown parameters, such as the detailed office layout on each floor. Good agreement of the calculated and observed damage indicated that the geometric modeling of the aircraft and the initial trajectory and orientation of the aircraft were accurate. The agreement of both the mode and magnitude of the structural damage in the impact wall served to partially validate the constitutive and damage modeling of the aircraft and exterior wall structures of the tower. The agreement in exterior wall damage, based on the modeling methods described in this report, contributed to the confidence that the damage predictions for the interior of the towers were reasonably estimated.

The calculated and observed impact damage to the exterior walls were described previously in this chapter and are summarized in Figure 9–116 for the base cases. There were small differences in the damage details, but the overall agreement with the observed damage is very good.

(a) Base case WTC 1 impact analysis

(b) Schematic of observed WTC 1 damage

(c) Base case WTC 2 impact analysis

(d) Schematic of observed WTC 2 damage

Figure 9–116. Impact damage to the exterior walls of the WTC towers.

9.11.1 Comparison with Observables on WTC 1

Damage on the South Exterior Wall of WTC 1

The exterior panel from column 329 to column 331 between floors 94 through 96 on the south face of WTC 1 was knocked free by landing gear and possibly other debris. These columns were located in the center of the south wall of WTC 1, as shown in Figure 9–117. In both the base case and more severe damage global analyses, aircraft debris impacted the south face of the tower, as shown in Figure 9–118 and Figure 9–119, and exited the building. In the more severe damage analysis, as shown in Figure 9–120, none of the aircraft debris that passed through the west wall was calculated to exit the building. The figures also show the calculated landing gear debris for similar impacts. None of the debris impacting the south wall happened to contain landing gear fragments. In the base case analysis, the debris impacted columns 328 to 330 at floor 96. In the more severe impact analysis, debris impacted columns 328 to 333 on both floors 95 and 96. In the base case analysis, very little damage was done to the exterior panels on the south wall. However, damage was heavy in the more severe damage analysis, as shown in Figure 9–121.

Figure 9–117. Representative floor plan (based on floors 94 to 95 of WTC 1).

(a) Calculated aircraft debris (t = 0.71 s)

(b) Calculated landing gear debris (t = 0.71s)

Figure 9–118. Base case aircraft debris distribution in WTC 1.

(a) Calculated aircraft debris (t = 0.685 s)

(b) Calculated landing gear debris (t = 0.685 s)

Figure 9–119. More severe damage aircraft debris distribution in WTC 1.

(a) Calculated aircraft debris (t = 0.735 s)

(b) Calculated landing gear debris (t = 0.735 s)

Figure 9–120. Less severe damage aircraft debris distribution in WTC 1.

Figure 9–121. Damage to the south face of WTC 1 from the more severe damage global analysis.

Because of model size constraints, the panels on the south face of WTC 1 were modeled with a very coarse resolution. Neither the spandrel splice joints nor exterior column butt joints were modeled. Column ends and spandrel edges were merged together. The model, therefore, underestimates the damage to the tower on this face. The calculated damage produced by the more severe impact is shown in Figure 9–121. Columns 329–331 on floors 94 through 96 sustained substantial damage. Had a fine mesh been used on these columns, it is likely that they would have failed on floor 95, and possibly on 94 and 96. Based on the failure modes observed on the face and on the speed and mass of the debris, the panel would potentially be knocked free by failing at the connections.

Landing Gear Trajectory

It is believed that a portion of the main landing gear of AA 11 exited WTC 1 at the 94th or 95th floor and landed at the corner of Rector and West Streets. This debris is believed to be a tire, wheel, brake assembly, and hub of a main landing gear, as shown in Figure 9–122. Based on the final position of the landing gear and assuming the landing gear to be a projectile with a horizontal initial velocity, the exit speed of the landing gear from the south wall of WTC 1 can be estimated to be about 105 mph. Note that there is a significant uncertainty in this estimate associated with the exit trajectory, aerodynamic effects, landing position rather than final resting position of debris, etc. Another piece of landing gear debris, shown in Figure 9–123, was found embedded in what is postulated to be the panel containing columns 329, 330, 331, running from the 93rd to the 96th floors. This panel was dislodged from the building and found at Cedar Street near its intersection with West Street. As little other damage had been

documented on the south face of WTC 1, it is postulated that the landing gear debris that landed at the corner of Rector St. and West St. also exited through this panel location.

The amount of aircraft debris found to exit WTC 1 in the global impact analyses varied, as shown in Figure 9–118 to Figure 9–120. However, no portion of the landing gear was observed to exit the tower in the simulations, but rather was stopped inside, or just outside, of the core. In order to simulate the trajectory of specific pieces of aircraft debris, a very precise knowledge of the internal configuration of the building would be needed. This is especially true with components passing through the core of the building, where some of the most massive building contents and partition walls were present. Uncertainties regarding the internal layout of each floor, such as the location of hallways or walls, can make the difference between debris from a specific component passing through or being stopped inside the structure. Modeling uncertainties may also have contributed to the inability to predict the trajectory of specific aircraft components.

Figure 9–122. Landing gear found at the corner of West and Rector streets.

Figure 9–123. Landing gear found embedded in exterior panel knocked free from WTC 1.

Stairwell Disruption

According to eyewitness interviews, stairwells 1 (referred to also as stairwell A), 2 (stairwell C), and 3 (stairwell B) inside the core were impassable on floor 92 and possibly above after the impact of AA 11. The calculated base case stairwell disruption is shown in Figure 9–124 for floors 93 through 97. Stairwell positions are outlined with red boxes in the figure. Debris or disruption was observed to the core on floor 92 in the calculation; therefore, it is not shown in the figure. Recall that the global model for WTC 1 only contained partition walls in the core for floors 94 through 97. Therefore, the ability to ascertain damage and/or debris in the stairwells on floors 92 and 93 was limited. The floor slab was removed from view on floors 94 through 97 so that debris is more visible.

Based on the calculated damage to, or debris in, the stairwells on floors 94 to 96, all three stairwells appear impassable. Given that falling debris in these areas would cause further subsequent damage to the floors below, as well as block passage on these floors, this result was reasonably consistent with the eyewitness accounts.

Floor Damage Visible on the North Face of WTC 1

One location where the damage to the WTC 1 truss floors could be observed was through the opening in the tower exterior produced by the aircraft impact. A photograph of the impact damage on the north face of WTC 1 is shown in Figure 9–125(a). The magnitude of damage is difficult to quantify as a result of the strong contrast in lighting between the tower interior and exterior and the smoke inside the building. However, the photograph shows that the truss floors were heavily damaged and/or removed in the primary impact zone. The depth of the floor damage extending into the tower could not be determined.

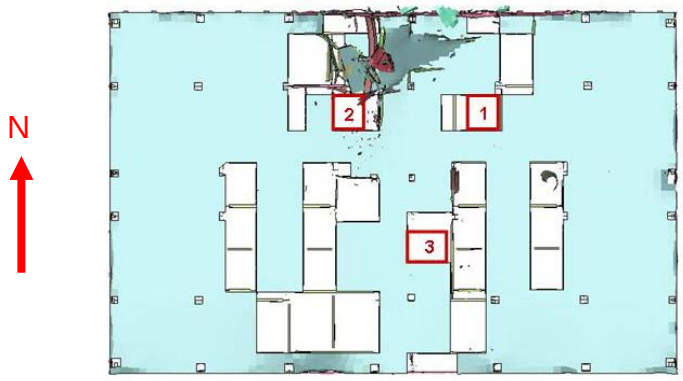

(a) Floor 93

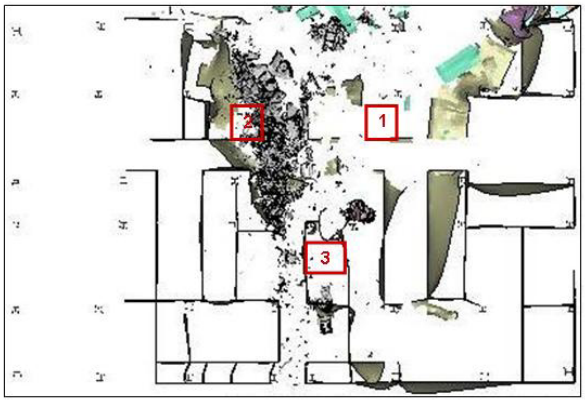

(b) Floor 94

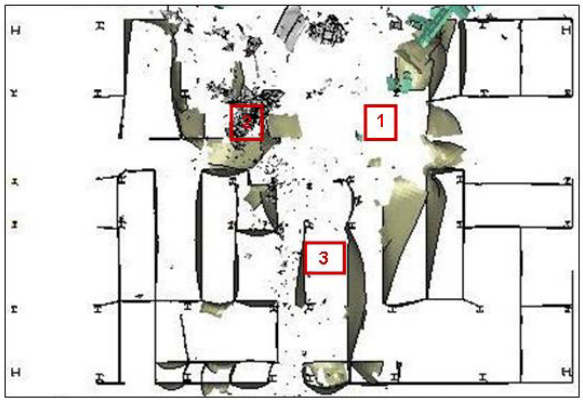

(c) Floor 95

(d) Floor 96

(e) Floor 97

Figure 9–124. Base case stairwell disruption in WTC 1.

(a) Damage photograph

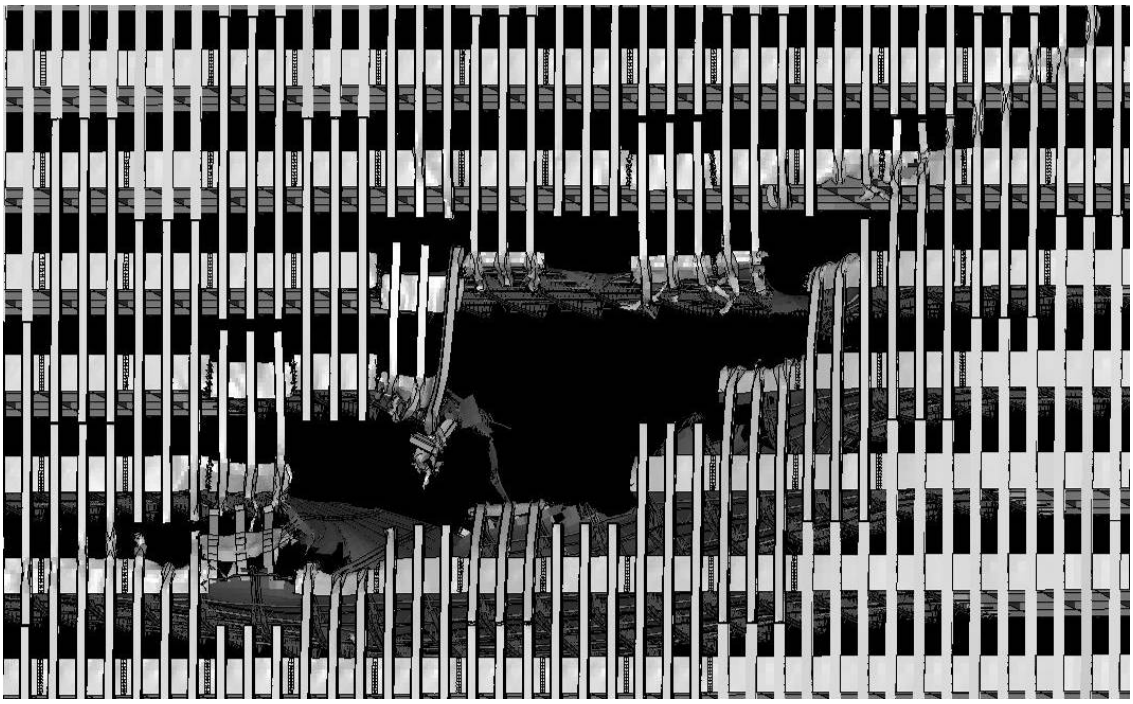

(b) Calculated damage

Figure 9–125. Calculated and observed WTC 1 damage (front view).

A corresponding image of the calculated damage to the other structures is shown in Figure 9–125(b). The structures beyond the start of the core were removed and replaced with a black background for comparison with the photograph. Although a quantitative comparison of the calculated and observed damage could not be made from the available damage photographs, the truss floor damage appeared to be consistent.

9.11.2 Comparison with Observables on WTC 2

Damage on the North Exterior Wall

From photographic evidence, such as that shown in Figure 9–126, damage on the north wall at the northeast corner of WTC 2 was documented and is shown in Figure 9–127. As mentioned earlier, there was significant uncertainty as to the actual layout of the workstations and other building contents on the impacted floors of the towers. Recall that generic workstation configurations were used to model these building contents, as shown in the northeast corner of WTC 2 in Figure 9–128(a). Uncertainties regarding this layout, such as missing partition walls and workstations, can make the difference between debris from a specific component passing through or being stopped inside the structure. The base case impact response of the northeast corner of WTC 2 on the 81st floor is shown in Figure 9–128(b).

Figure 9–126. Impact Damage to the Northeast Corner of the Exterior Wall of WTC 2.

Figure 9–127. Documented damage to the 81st floor of the northeast corner of WTC 2.

(a) Initial workstation configuration

(b) Debris field at t = 0.62 s

(c) Residual speed of aircraft debris (contours in mph)

Figure 9–128. Base case analysis on the 81st floor of the northeast corner of WTC 2.

Aircraft debris on the 81st floor is shown in Figure 9–128(c), with the coloring depicting the residual speed of the debris field. Notice that some of the debris in this figure, weighing approximately 3,800 lb, was traveling at 110-150 mph and was projected to impact between columns 252 and 256. The leading debris was in fact portions of the starboard main landing gear main strut and main landing gear beam. That significant debris was projected to impact in the region of significant damage shows positive agreement with damage evidence available for the north wall of WTC 2.

Stairwell Disruption

According to eyewitness interviews, stairwells 2 and 3 on floor 78 of WTC 2 were impassable. Stairwell 1 (referred to also as stairwell A), which was located in the northwest corner of the core, was passable. The calculated base case stairwell disruption is shown in Figure 9–129. Stairwells 1 and 2 (stairwell C) on floor 78 of WTC 2 were outside of the core column region. These stairwells were not included in the WTC 2 model. Therefore, a good assessment could not be made for stairwell 2. However, disruption to stairwell 3 (stairwell B) is shown in Figure 9–129. From the damage shown in the figure, the stairwell appears to be impassable. As damage or debris was seen in the northwest corner of the core, the top right in the figure, stairwell 1 in this area of the core was likely unaffected. Both of these assessments were consistent with the eyewitness accounts.

Figure 9–129. Base case stairwell disruption on floor 78 in WTC 2.

Landing Gear Trajectory

A portion of the landing gear of UAL 175 exited WTC 2 and landed on the roof of 45 Park Place. No photographic evidence was available to document the size of the fragment and whether this was a nose or main landing gear. From the damage to the building, it was believed that the landing gear fragment might have exited somewhere along the north wall between column 251 and the northeast corner on floor 81. Based on the final position of the landing gear and assuming the landing gear to be a projectile with a horizontal initial velocity, the exit speed of the landing gear from the north wall of WTC 2 can be estimated to be about 102 mph. Note that there is significant uncertainty in this estimate associated with the exit trajectory, aerodynamic effects, landing position other than final resting position of debris, etc.

The calculated aircraft debris distribution and landing gear and engine debris distributions for UAL 175 are shown in Figure 9–130 to Figure 9–132 for the less severe scenarios. A portion of the port main landing gear was seen to exit the building at approximately 230 mph in the more severe impact analysis, as shown in Figure 9–131(b). No landing gear debris exited the building in either the base case or less severe simulations. At the conclusion of the simulation, the base case analysis had a substantial piece of the starboard main landing gear still at approximately 180 mph that was expected to impact the northeast corner.

Engine Trajectory

A portion of an engine also exited the tower at the northeast corner of the building and was found at the intersection of Murray and Church Streets. From damage to the building, it was believed that the engine exited the building in this corner of WTC 2. Based on this trajectory, it was estimated that the engine exited the building at approximately 120 mph. The engine trajectories predicted from the base case global analysis are shown in Figure 9–133, which indicates that the engine that exited from the northeast corner is likely the starboard engine. The red line indicates the extrapolated engine flight path based on the initial trajectory of the starboard engine. Notice that this trajectory would result in engine fragments exiting at the northeast corner. In the simulations, the engines were projected to stop short of this position, although they followed the extrapolated trajectory reasonably well.

Speed histories for the aft portion of the starboard engine are shown in Figure 9–134. The engine would typically break up into smaller fragments from the forward section of the engine and a larger section from the aft end, as shown in Figure 9–135. In the simulations, the speed was seen to drop by approximately 200 mph due to impact with the exterior panel, floor slab, and floor truss. Interaction with these portions of the structure ends by approximately 0.12 s. This initial impact is shown in Figure 9–136. The engine debris then continued through the tenant space of the 81st floor, plowing through the workstations and contents. Whether or not the fragment passes over these contents, or if other debris and fuel remove the contents from the engine's path, affects the deceleration of the fragment. At the end of the simulation, the speed of the aft portion of the engine was below 80 mph, and it was more than 60 ft from the northeast corner of the building. For these calculations, it was estimated that the building contents would likely stop the engine fragment prior to impacting the northeast corner of the exterior wall.

None of the three WTC 2 global impact simulations resulted in a large engine fragment exiting the tower. However, the impact behavior suggests that only minor modifications would be required to achieve this response. For example, if the starboard engine impact location was lowered by 1 to 2 ft, which is within the aircraft impact geometry uncertainty range, the engine would likely have a greater residual speed inside the tower (over 100 mph). In the global analyses performed, the engine impacted the underside of the 82nd floor, as shown in Figure 9–136. This resulted in a large reduction in speed of approximately 200 mph. In the component analyses discussed in Chapter 5, the engine speed decreased by roughly 60 mph when impacting an exterior panel alone. Additional speed would likely result in a large engine fragment exiting the northeast corner of the tower.

(a) Calculated aircraft debris (t = 0.62 s)

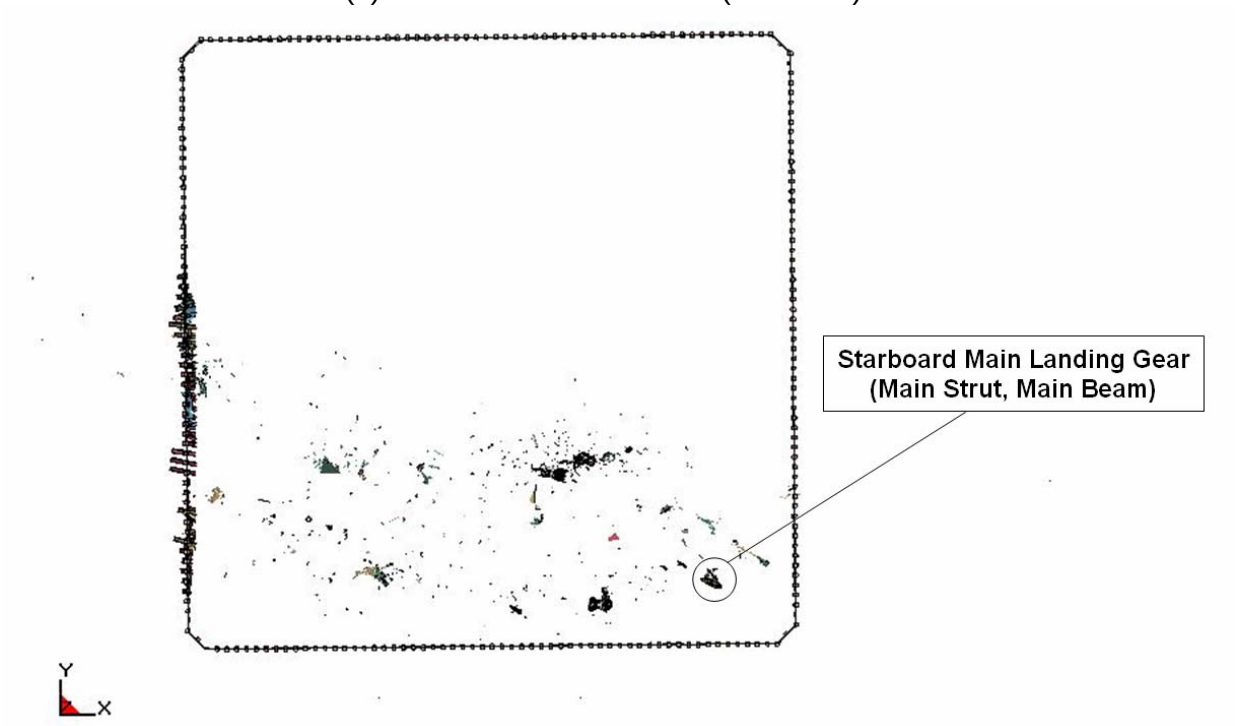

(b) Calculated engine and landing gear debris (t = 0.62 s)

Figure 9–130. Base case damage aircraft debris distribution in WTC 2.

(a) Calculated aircraft debris (t = 0.58 s)

(b) Calculated engine and landing gear debris (t = 0.58 s)

Figure 9–131. Aircraft debris distribution in the more severe WTC 2 impact.

(a) Calculated aircraft debris (t = 0.66 s)

(b) Calculated engine and landing gear debris (t = 0.66 s)

Figure 9–132. Aircraft debris distribution in the less severe WTC 2 impact.

t = 0 t = 0.10 s

t = 0.20 s t = 0.30 s

t = 0.40 s t = 0.62 s

Figure 9–133. Starboard engine fragment trajectory in the base case global analysis of WTC 2.

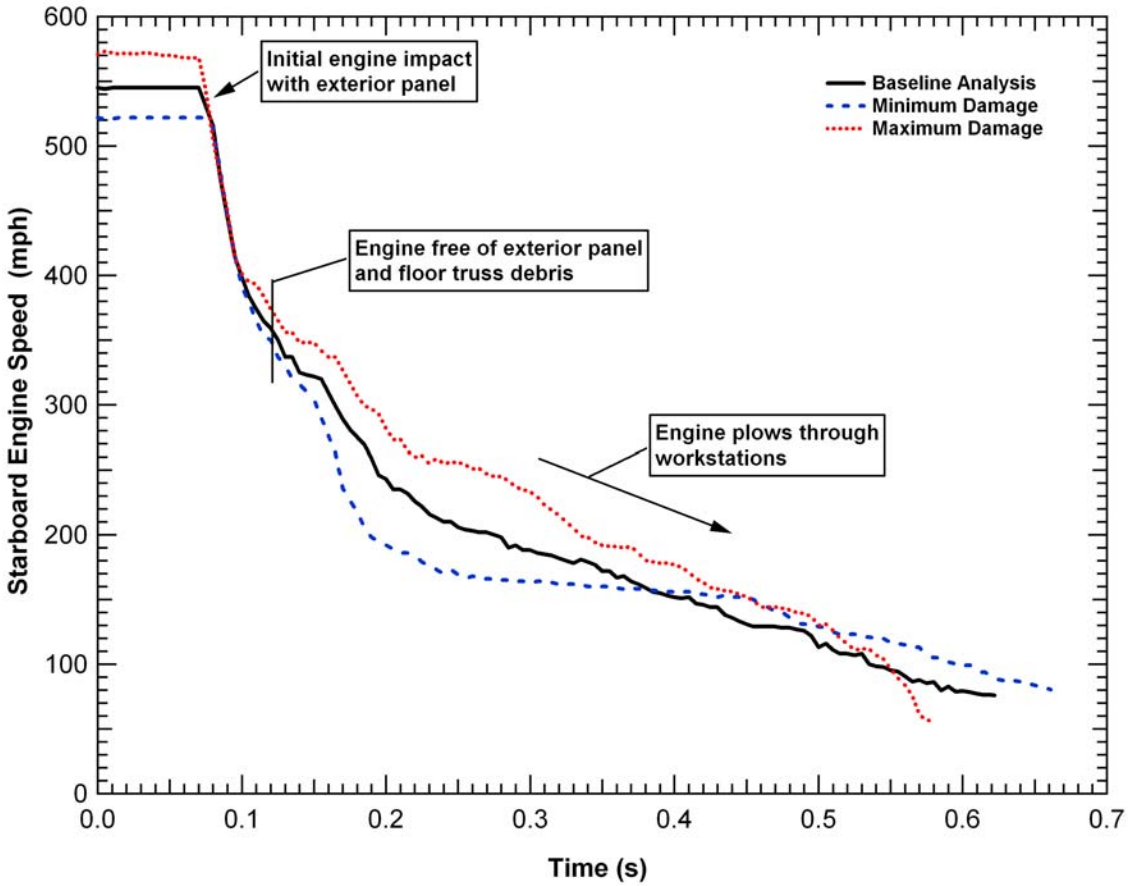

Figure 9–134. Speed of the aft portion of the starboard engine.

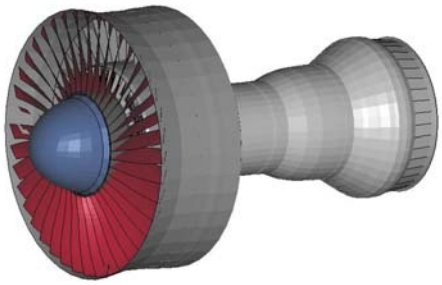

(a) Undamaged engine

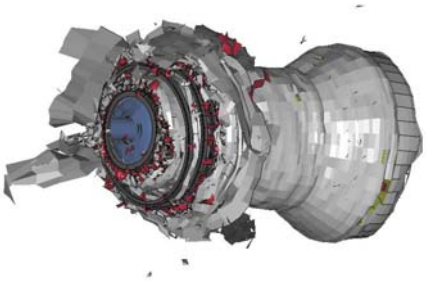

(b) Large engine fragment

(c) Engine fragment found at Murray and Church St.

Figure 9–135. Calculated and observed engine damage.

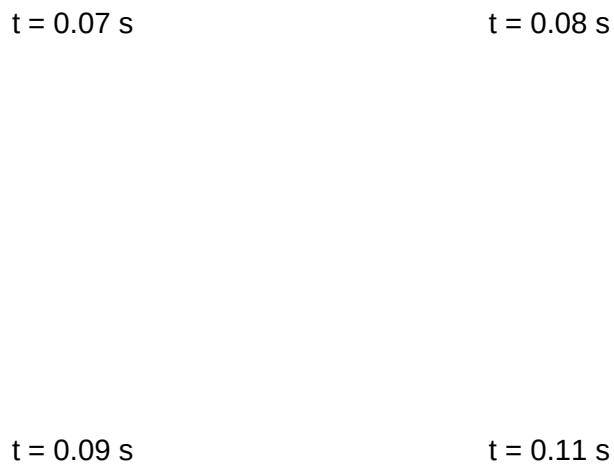

Figure 9–136. Starboard engine impact with the south face of WTC 2 in the base case global analysis.

Other minor modifications to the model could also result in a large engine fragment exiting the building. As mentioned previously, there was significant uncertainty in the distribution of building contents on the floors of the impact area. If any portion of the east side of WTC 2 was relatively free of office materials, the engine fragment would have been free to move relatively unrestricted and would have experienced little loss of speed. After the engine entered the structure, and without office materials, the engine fragment would only slow due to friction with the floor slab and occasional interaction with floor trusses above. After initially entering the building, the engine did not further penetrate the floor slab. Removing much of these building contents from the east side would result in the starboard engine fragment impacting the northeast corner of the tower with sufficient speed to exit the building. Little or no difference in core damage would result, as debris in this area had no chance of impacting the core.

Floor Damage Visible on the South Face of WTC 2

One location where the damage to the WTC 2 truss floor could be observed was through the opening in the tower exterior produced by the aircraft impact. A similar comparison for the WTC 1 truss floor damage was shown in Figure 9–125. The magnitude of damage was difficult to quantify as a result of the strong contrast in lighting between the tower interior and exterior and the smoke inside the building. This was worse for WTC 2, where the prevailing wind and fire conditions resulted in larger quantities of smoke exiting through the opening on the impact face. The partial photographic evidence did suggest that

a similar level of truss floor damage in the impact zone occurred for WTC 2. The severity and the depth of the floor damage extending into the tower could not be determined. Although a quantitative comparison of the calculated and observed damage could not be made from the available damage photographs, the truss floor damage appears to be consistent.

The ‘Cold Spot’ on the North Face of WTC 2

A ‘cold spot’ was observed on the north face of the tower between columns 238 and 250 on floors 80, 81, and 82. The cold spot was a region of the tower where no debris could be seen from the exterior of the tower, and no significant fires were observed prior to tower collapse.

Much of the explanation for the cold spot was obtained from an analysis of the debris trajectory aligned with the cold spot. The debris path, obtained by projecting the width of the cold spot along the initial lateral impact trajectory of the aircraft, is shown in Figure 9–137 (13 degrees relative to the tower face normal). This region was aligned laterally with the left side of the fuselage and the port wing structures. Considering the baseline impact orientation and trajectory, shown in Figure 9–138, it can be seen that much of the wing debris impacted on floors lower than the observed cold spot. Only debris from very close to the fuselage would be expected on floor 80 or above. The debris from the port wing, including the majority of the aircraft fuel in the left side tanks, entered at floors 78 and 79.

The base case WTC 2 global analysis calculated an amount of aircraft debris passing through the cold zone on floors 80 and 81. However, the building contents were not completely modeled over the entire path in this section. After clearing the core region, the debris in the calculation had primarily an open path to the cold spot on the North wall of WTC 2. If all of the internal contents had been included, it is likely that all of this debris would have been stopped before reaching the cold spot.

The comparison of the calculated and observed impact response cold spot is inconclusive. Much of the absence of damage and aircraft debris in this region is explained by the impact orientation and trajectory. Much of this region is not directly in the path of significant aircraft fuel and debris. In addition, the debris aligned with the cold spot would be required to pass through a significant portion of the core. A more accurate analysis of the impact mechanics leading to the formation of a cold spot would require a specific survey of the tenant layout, including both contents that acted as a barrier to the debris and walls that provided a barrier to subsequent fire propagation.

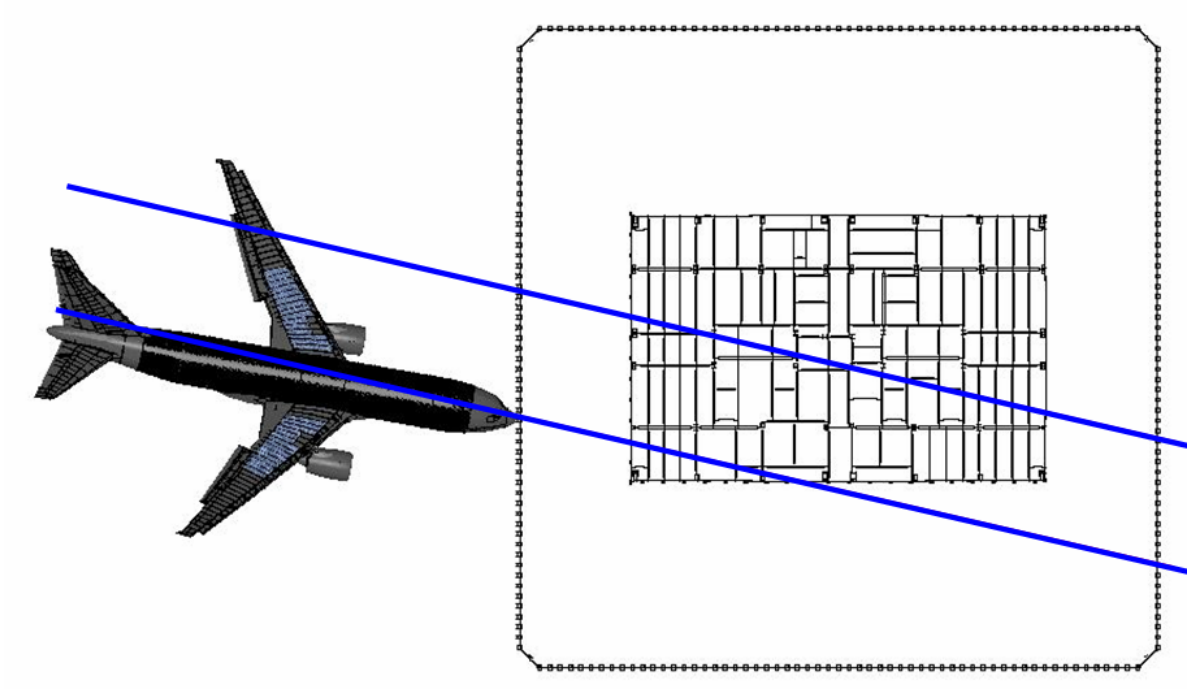

Figure 9–137. Projected debris path for the WTC 2 north face cold spot.

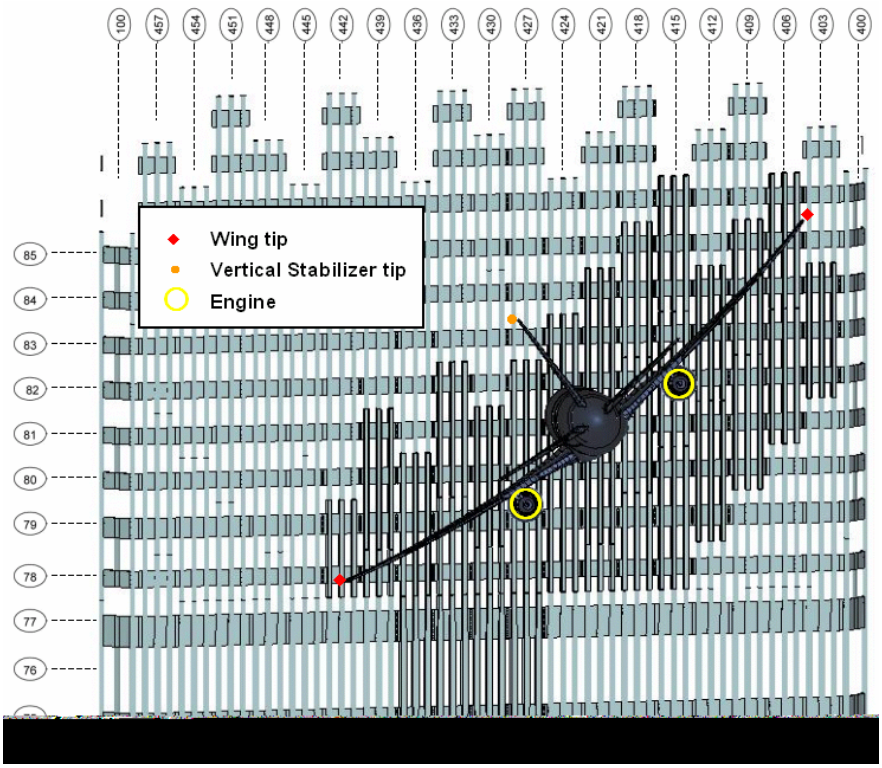

Figure 9–138. Base case WTC 2 impact orientation and trajectory (vertical approach angle = 6 q lateral approach angle = 13 q).

9.11.3 Comparison with Observables - Summary

A summary of the observables, their relative significance, and the level of agreement with these observables seen in the simulations is shown in Table 9–13 and Table 9–14 for WTC 1 and WTC 2, respectively. The most valuable observable was the damage to the impacted exterior wall of each tower. The impact damage to the exterior walls was well documented and the response did not depend as much on unknown parameters, such as the detailed office configuration on each floor. Eyewitness accounts of damage to stairwells and visible floor damage were also significant as they were the only available data on the damage to the tower interiors. That these observables were in good agreement adds greater credibility to the predicted damage to the tower interiors.

Observed trajectories of specific aircraft components, such as the landing gear and engines, were considered to be of lower importance in validating the simulated damage to the tower. A fairly precise knowledge of the internal configuration of the building would be needed in order to simulate the trajectory of specific aircraft debris. Damage to the opposite side of each tower from the point of impact was also of lower importance. These parts of the tower were modeled with lower resolution and as a result, the models were not sufficient to capture the detailed damage. The actual damage was also predominantly caused by the landing gear and engine components already discussed. Overall, agreement between the observables and simulations is good.

Table 9–13. Comparison with observables from WTC 1.

Observable	Importance	Agreement
Damage to the north exterior wall	Very significant	Very good
Damage to the south exterior wall	Slightly significant	Fair
Landing gear trajectory	Slightly significant	Poor
Stairwell disruption	Significant	Good
Floor damage visible on the north face	Significant	Good (unclear)

Table 9–14. Comparison with observables from WTC 2.

Observable	Importance	Agreement
Damage to the south exterior wall	Very significant	Very good
Damage to the north exterior wall	Slightly significant	Good
Stairwell disruption	Significant	Good
Landing gear trajectory	Not significant	Fair
Engine trajectory	Slightly significant	Good
Floor damage visible on the south face	Significant	Good (unclear)
The ‘cold spot’ on the north face	Slightly significant	Unclear

9.12 COMPARISON WITH PREVIOUS STUDIES

Two previous studies were conducted to estimate the impact damage to the WTC towers. These studies were performed by staff from Massachusetts Institute of Technology (MIT) (Wierzbicki, Xue, and

Hendry-Brogan 2002) and Weidlinger Associates, Inc. (WAI) (Levy and Abboud 2002). The MIT study used an energy balance approach to estimate damage to the core columns. Estimates were made for the initial kinetic energy of the impacting aircraft and the internal energy absorbed in fragmentation of the aircraft and damage to the tower exterior columns, floor slab, and core columns. The energy absorbed by the core was used to estimate the number of failed core columns.

The WAI study used the FLEX finite element code to calculate the aircraft impact damage to both towers. The FLEX family of finite element modeling software (Vaughan 1997) was developed and maintained by WAI. FLEX is an explicit, nonlinear, large deformation transient analysis finite element code for the analysis of structures subjected to blast, impact, and shock loadings. The overall code architecture is very similar to that of LS-DYNA, used to calculate the aircraft impact damage in this investigation.

In the WAI calculations, the aircraft and WTC towers models were composed of beam and shell elements. The aircraft model consisted of 27,000 shell elements and 23,000 beam elements. The aircraft fuel was included in the model by increasing the mass of the structures in the wing box. The tower models included the exterior wall on the impact face, the floor structures, and the core frame for floors 91-101 and floors 76 through 86 for WTC 1 and WTC 2, respectively. The tower models had fixed boundary conditions at the top and bottom floors.

Comparison of Exterior Wall Damage

The calculated base case impact damage to the exterior wall of WTC 1 from this study is compared to the impact damage calculated by WAI in Figure 9-139. The figure also shows a schematic of the damage observed in photographic evidence. Figure 9-140 shows a similar comparison for the south wall of WTC 2. In both towers, the base case impact damage estimated in this study closely matched the observed damage. The damage profiles in the WAI simulations had some noticeable differences. The first is that the damage profile included complete failure of the exterior columns over the entire length of the wings and to the top of the vertical slab. The second difference is that the failure mode of the exterior walls was dominated by local rupture of the columns adjacent to the impact point, with less influence of the bolted connections on panel failure and removal.

The differences in the damage profiles in the calculations most likely resulted from a variety of differences in the models. One major difference between the two studies was in the fidelity of the aircraft models. The WAI Boeing 767 model was based on their model of a Lockheed C-141B military transport. In the WAI model, the external geometry of the C-141B was modified to fit the dimensions of the Boeing 767, but the internal components, such as stiffener configuration and material thicknesses and properties, remained the same. The differences in the internal structure and materials could affect the way the aircraft responded to the impact. The aircraft model used in this study also contained an order of magnitude more elements (70,000 bricks, 562,000 shells, and 61,000 SPH particles) than the WAI model (27,000 shell elements and 23,000 beam elements). The higher resolution of the NIST model could also account for significant differences in the determination of the impact load distribution and resulting exterior damage. Additionally, the NIST model explicitly modeled the fuel. If the fuel mass in the WAI model was spread out further toward the wing tips as part of the wing structure, it would be expected that the calculated column damage would extend over a wider portion of the wings.

(a) Schematic of observed damage

(b) NIST base case impact damage

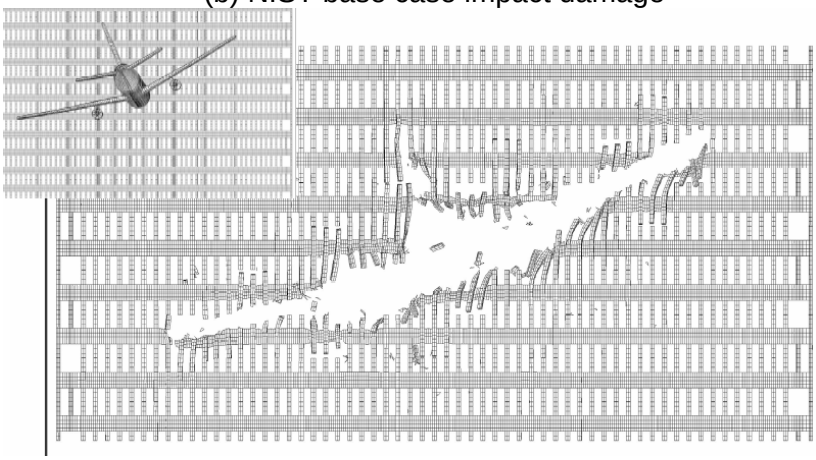

(c) WAI calculated damage (Levy and Abboud, 2002)

Figure 9–139. Comparison of impact damage to the WTC 1 exterior wall.

(a) Schematic of observed damage

(b) NIST base case impact damage

(c) WAI calculated damage (Levy and Abboud, 2002)

Figure 9–140. Comparison of impact damage to the WTC 2 exterior wall.

Secondary differences in the WAI and NIST impact analyses included, but were not limited to, variations in impact conditions (impact velocity, angle, location, etc.), aircraft model differences (airframe geometry, component thicknesses, mass distribution, material properties, etc.) and tower model differences (material properties, geometry, joint modeling, number of elements, etc.).

Comparison of Core Column Damage

Table 9–15 compares the estimated core column damage from the various studies. For WTC 1, MIT (Wierzbicki, Xue, and Hendry-Brogan 2002) estimated that four to 12 core columns failed. This MIT estimate of core columns was based on energy balance calculations and corresponded to a damage distribution ranging from four columns failed over a three-story length to 12 columns failed over a single floor length. The expected distribution of damage would fall between these bounds, with some columns damaged on a single floor and others with damage distributed on multiple floors. WAI gave two estimates for core column failure. The first estimate of 23 core columns failed and five damaged was obtained from the FLEX impact analysis. The second estimate of 20 failed columns was the number used in their collapse analysis. The NIST base case impact damage of three severed and four heavily damaged and less severe estimate of one severed and two heavily damaged falls below both the MIT and WAI estimates. The more severe estimate of six severed and three heavily damaged falls in the middle of the MIT range, but still well below the WAI estimates.

Table 9–15. Comparison of damage to core columns from various studies.

WTC Impact Investigation	WTC 1 Core Column Damage	WTC 2 Core Column Damage
MIT Impact Analysis	4-12 Failed	7-20 Failed
WAI Impact Analysis	23 failed and significantly damaged Plus 5 damaged	14 failed and significantly damaged Plus 10 damaged
WAI Collapse Analysis	20 Failed	5 Failed
NIST Base Case Impact Analysis	3 Severed Plus 4 Heavily Damaged	5 Severed Plus 4 Heavily Damaged
NIST More Severe Impact Analysis	6 Severed Plus 3 Heavily Damaged	10 Severed Plus 1 Heavily Damaged
NIST Less Severe Impact Analysis	1 Severed Plus 2 Heavily Damaged	3 Severed Plus 2 Heavily Damaged

A similar trend in the predicted damage to the core columns was found in the WTC 2 analysis. MIT estimated seven to 20 columns failed (from seven columns failed over a three-story length to 20 columns failed over a single floor length). WAI calculated 14 core columns failed and another 10 damaged in their FLEX analysis, but reduced the number of failed columns to only five for their collapse analysis. The NIST base case impact damage of five severed and four heavily damaged, as well as the more severe estimate of 10 severed and one heavily damaged fall in the middle of the range predicted by MIT. The less severe impact scenario predicted fewer columns severed and heavily damaged than the MIT and WAI studies.

The MIT prediction for the number of failed core columns agrees remarkably well with the NIST estimates using their simplified analysis. Differences may be a result of the estimates of material properties and structural geometry used (MIT did not have access to the detailed structural drawing of the WTC towers for their study), approximations in the estimates of damage mode and resulting energy absorption, as well as the fact that the MIT study did not include the energy absorbed by internal tower contents.

The WAI impact analysis predicted much higher core column failure and damage than the NIST estimates. One reason for the higher damage prediction may be attributed to the lack of internal tower contents, such as workstations and other live loads, in the WAI model. This study found that the internal tower material absorbed a significant amount of the impact energy and, therefore, reduced the loads applied to the core columns. Another reason for the higher damage prediction in the WAI study could result from the aircraft model. As noted above, the WAI aircraft impact simulation overpredicted the extent of column damage and failure on the exterior wall. It is possible to assume that the aircraft model would also overpredict the damage to the core columns, especially that this damage configuration resulted in an unstable tower (Levy and Abboud, 2002).

In conducting a collapse analysis, WAI used engineering estimates to reduce the number of failed columns from that predicted by their FLEX m

to be warranted for evaluation of the impact damage. As a result, the rotational kinetic energy of the spinning aircraft engine components was not included in the impact analyses.

An analysis was performed to quantify the potential effect of the rotational kinetic energy of the engine turbine and compressor components on the aircraft impact response. This was investigated using simple energy and momentum principals. The inertial properties of the engine components were calculated from the finite element engine model using LS-DYNA. The inertial properties were automatically generated for each part (material assignment) by LS-DYNA as part of the model initialization.

The internal engine components for which some portion would be rotating are shown in Figure 10–1. The engine components in the model were separated to estimate the rotating engine mass and obtain an estimated percentage of the engine that is rotating. The approximation used was that 3,500 lb, or 37 percent of the total engine mass, was rotating.

Figure 10–1. Internal components of the aircraft engine model.

Both the kinetic energy from translation and rotation were calculated based on an assumed impact speed of 500 mph and an engine rotational speed of 5,000 RPM. The results are shown in Table 10–1. The initial rotational kinetic energy of the engine components was approximately 2.2×10^7 lb·ft, which was approximately one-quarter of the translational kinetic energy for the engine or less than one percent of the initial kinetic energy for the aircraft impact.

Table 10–1. Kinetic energy partitioning in aircraft.

Component	Weight	Moment of Inertia about Engine Axis	Translational Kinetic Energy	Rotational Kinetic Energy
Total Engine	9400 lb	3.3×10^4 lb·ft^2	8.1×10^7 lb·ft	3.5×10^6 lb·ft
Rotor Components	3500 lb	5.2×10^3 lb·ft^2	3.0×10^7 lb·ft	2.2×10^7 lb·ft
Entire Aircraft	290,000 lb		2.4×10^9 lb·ft	

Since the rotational kinetic energy is a nontrivial percentage of the total engine kinetic energy, additional consideration was given to the rotational effects on the engine impact response. The concern is the coupling of the rotational energy into the tower and the potential of the rotating engine parts to stabilize the engine trajectory during the impact. However, as the engine impacted and penetrated the exterior wall of the tower, a significant amount of debris from the tower steel, glass, aluminum trim, and concrete floor slab was forced into the engine. It is expected that this would produce significant internal damage and lock up the rotating engine components in a relatively short duration. The forces produced by the internal angular deceleration of the rotating engine components would either be reacted by the engine support

structures or cause the entire engine to roll about its major rotational axis. Using conservation of angular momentum for the engine, it was estimated that the rotational energy after the engine locked up was about 3.5×10^6 lb-ft, or 16 percent of the initial rotational kinetic energy. Therefore, the bulk of the initial engine rotational energy would most likely be dissipated by deformation of the internal engine components rather than damage to the tower. As a result, the potential for the rotational kinetic energy to significantly change the magnitude of the tower impact damage is small.

10.4 EFFECTS OF STATIC STRUCTURAL PRELOAD

The global impact analyses required the use of very large and complex tower models of approximately 1.5 million nodes. The global WTC tower impact analysis run times were on the order of two weeks on twelve processors for a 0.65 second impact event. Initialization of a static preload in these tower models was difficult and computationally intensive. As a result, an analysis was performed to determine the importance of the preload effect on the tower impact response and damage. The internal energy associated with the elastic service loads was small compared to the material internal energy capacity that was utilized under impact response and damage. Therefore, the static preload was not expected to have a significant influence on the dynamic impact response and deformation.

A wide flange core column was used for this analysis with the applied loading and boundary conditions as shown in Figure 10–2. The column dimensions were 16-in. flange width and 16-in. length between outer flange faces, with a flange thickness of 1.72 in. and a web thickness of 1.07 in. These dimensions were typical for the range of wide flange core columns in the impact zones of the WTC towers. A static compressive axial load, P_{static}, was applied to the upper end of the column, as shown in Figure 10–2(a). An impulsive load per unit area, $P_{dynamic}$, was centered between floors at the middle of the column over a distance of 60 in. The pressure was applied perpendicular to the flange. The lateral constraints allowed the ends of the horizontal beam sections connected to the column to translate only in the direction of the static load, as shown in Figure 10–2(b).

(a) Loading detail (b) Lateral constraint detail

Figure 10–2. Problem geometry for analysis of axial preload effects.

Three cases were analyzed to study the effects of the axial preload:

Case 1: A static axial load was applied with no impulsive pressure ($P_{dynamic}$ = 0.0). The column collapsed when the axial force reached 3,360,000 lbf.

Case 2: An impulsive load was applied with $P_{dynamic}$ = 2,538 psi and without a static preload. The pressure pulse had a characteristic time of 4 ms, resulting in a total impulse of I = 10.2 psi-s. A static axial load was subsequently applied and increased until collapse. The column collapsed when axial load reached 2,300,000 lbf.

Case 3: An axial preload was applied until stresses in the column equaled 40 percent of the column's yield strength. Then, the lateral impulsive load used in Case 2 was applied. Finally, the axial load was increased until collapse. Collapse occurred when axial load reached 2,240,000 lbf.

Comparing Case 1 with Case 2, it was found that the damage produced by the dynamic load reduced the amount of axial force the column was able to support by about 32 percent. In Case 3, with an axial preload, the column required 2.6 percent less axial force for collapse than in Case 2 with no axial preload. This result suggests that the time at which the axial load was applied relative to the application of the dynamic load had little effect on the amount of axial force required to collapse the column. Figure 10–3 shows a comparison of the damage and plastic strains for Case 2 and Case 3, immediately after the application of the dynamic load. The plastic strains for these two cases were very similar. Therefore, the static preload has little effect on the damage developed by a lateral impulsive load.

These comparisons show that the initialization of axial preload in the columns of the towers would not have a significant effect on the tower impact response, damage, or residual strength.

(a) Case 4, no static load (b) Case 3, static load

Figure 10–3. Dynamic column response with and without axial preload.

10.5 SIMPLIFIED ANALYSIS OF CORE COLUMN DAMAGE

In order to better understand the importance of the initial impact and breakup of the aircraft on damage to the WTC tower core structures, a model of resultant impact damage from an aircraft debris cloud on core columns was developed. This model was based on simple momentum and energy conservation concepts, similar to the simplified global analysis discussed in Section 10.2. The fundamental premise of the analysis is that the aircraft debris has negligible strength on impact, and the load on the building columns is due to momentum transfer. As a consequence, the load on the columns is determined by the debris density and impact kinematics. The impact pressure delivered to the column is determined by momentum change. The pulse duration is determined by the debris speed and size. This analysis was used to study the effects of the dispersed fuel cloud on core column response.

The critical loads required to fail a core column were determined based on a combination of the peak impact pressure and impulse intensity. A good description of this characterization of critical loads as Pressure-Impulse or "P-I" damage curves is given by Abrahamson and Lindberg [1972]. The concept that broad definitions of critical loads can be made based on peak pressure or load and impulse intensity or total impulse is well established. The P-I damage analysis method has been commonly used for evaluation of blast damage to structures and is appropriate for structures where the impacting body has a low strength. This P-I damage curve approach provides a useful way to make a quick evaluation of the damage potential of aircraft debris cloud on core columns.

10.5.1 Development of P-I Curves

An example of the process used to develop the P-I curves for a structure is demonstrated in Figure 10–4. A series of simple finite element calculations with various pressure and impulse combinations are performed to bracket the conditions required to initiate damage or failure of the structure. Each calculation is represented by a circle in the figure. The load conditions that resulted in no damage or incipient damage are represented by a solid blue circle. Load combinations resulting in failure of the structure are represented with a solid red circle. Intermediate levels of damage are displayed with open black circles. The results from the simulations are fit with two P-I curves, one representing the onset of significant damage and the other representing complete failure. The P-I curves have a form that is similar in shape to a hyperbolic curve. The load combinations which fall above and to the right of the red P-I curve in Figure 10–4 produce structural failure. Similarly, load combinations which fall below and to the left of the blue P-I curve in Figure 10–4 produce little or no damage.

Individual P-I curves correspond to a specific magnitude of damage. In this example, separate P-I curves are generated for the onset of damage and for failure. A comparison of the two P-I curves in Figure 10–4 shows that at the limit of a long duration loading, the P-I curves are representing damage and failure are equal for this structure (lower right portion of the P-I curves with a low pressure magnitude and large impulse intensities). This results from unstable buckling of this structure under quasi-static pressure loads. As a result, the quasi-static pressure magnitude that is sufficient to produce yielding will also result in a complete rupture. The knee of the P-I curves in this example corresponds to an effective load duration between one and ten milliseconds, which corresponds to the characteristic response times of the structure (natural frequencies of the important damage modes such as column buckling modes, etc.).

Figure 10–4. Development of damage and failure P-I curves for a structure.

10.5.2 Core Column Damage Analyses

Using the procedure outlined in the previous section, P-I curves were developed for core column failure. The column dimensions and boundary conditions were identical to those used in Section 10.4 and shown in Figure 10–2, but without an axial preload. Three different P-I curves were developed for three heights of dynamic pressure loading, as shown in Figure 10–5. Pressure and impulse combinations were applied over 30 in., 60 in., and 120 in. spans on the column. The P-I curves were then used to determine the characteristics of a fuel cloud impact that would be sufficient to fail a core column.

The core column response was analyzed for the aircraft fuel impact loads at four positions along the wing. The impact loading of the fuel was considered separately in this example since it represents a significant fraction of the total mass in the wings. Initially, the effect of a direct impact by a section of the fuel on the core column (no dispersion of the fuel cloud) was considered. To calculate the impact pressure and impulse, the fuel tank dimensions at each location were approximated by a rectangle. Near the root of the wing the approximate tank dimensions were 43 in. tall by 161 in. across. The position nearest the wing tip had approximate tank dimensions of 14 in. tall by 50 in. across. The other two positions had relatively uniform spacing and had dimensions of 18 in. tall by 91 in. across and 22 in. tall by 132 in. across, respectively. The peak pressure for the fuel impact was found from the momentum change, which is governed by the fuel density and impact velocity. The duration of the load was calculated using the dimension across the fuel tank divided by the impact velocity. The pressure multiplied by the duration gives the impulse intensity for this impact scenario.

The impact loads for the four different positions of the fuel tank were calculated for three impact speeds, 537, 430, and 268 mph. The corresponding positions of the impact loads in pressure and impulse are shown in Figure 10–5. The comparison of the impact loads to the P-I curve for the 30 in. load span (green curve) is most appropriate since the loaded area in this example varies from 43 in. at the wing root to 14 in. at the wing tip. These data show that a section of fuel directly impacting the core columns at 430 mph or above would cause failure. However, the loads produced by a lower impact speed of 268 mph would not be sufficient to fail this core column.

Figure 10–5. Core column P-I failure curves and concentrated fuel impact loading.

The fuel impact loads used in the above example were an upper bound on the damage that could be produced by the fuel at the core since the fuel was still assumed to be in a solid rectangular section at full density. In reality, the impact with the exterior wall broke up the wing structures, and the fuel cloud spreads out to some extent prior to reaching the core columns. The impact with the internal building contents also reduced the severity of the fuel impact at the core.

A first approximation of the effects of the fuel cloud dispersion on the core column loading was performed by assuming that the fuel cloud spread vertically to fill the full floor height prior to reaching the core. A uniform fuel cloud density was used that was scaled by the ratio of the initial fuel section height to the full floor height. No spreading in the longitudinal or lateral direction was assumed. The spreading of the debris cloud, thus, reduced the pressure without changing the load duration. These positions of the impact loads in pressure and impulse are shown in Figure 10–6. The comparison of the impact loads to the P-I curve for the 120 in. load span (black curve) was most appropriate since the loaded area in this example was uniform over the full length of the column. The comparison shows that an expanded fuel cloud did not produce sufficient loading to fail a core column with the exception of points close to the wing root at the highest impact speeds considered. A more realistic fuel cloud dispersion would have included lateral and longitudinal spreading, as well as removal of some fuel from the cloud as

a result of impact with the outer wall and building contents. Under these conditions, it is expected that the fuel cloud alone would not be sufficient to fail core columns.

Figure 10–6. P-I curves and expanded fuel cloud impact loading.

10.6 REFERENCES

Abrahamson, G.R., and Lindberg, H.E., 1972. "Peak-Impulse Characterization of Critical Pulse Loads in Structural Dynamics," in Dynamic Response of Structures, G. Herrmann & N. Perrone, Eds., Pergamon Press, Inc., New York, pp. 31-52.

Gardner, J.W., 1984. "Calculation of the Forces Acting Upon a Rigid Structure from an Aircraft Impact," Int. J. Impact Engineering, Vol. 2, No. 4, pp. 345-356.

Riera, J.D., 1980. "A Critical Reappraisal of Nuclear Power Plant Safety Against Accidental Aircraft Impact," Nuclear Engineering and Design, Vol. 57.

Zimmerman, Th., Rodriguez, C., and Rebora, B., 1981. "Nonlinear Analysis of a Reactor Building for Aircraft Impact loadings," Trans. 6th International Conference on Structural Mechanics in Reactor Technology, Vol. J, August.

This page intentionally left blank.

Chapter 11
SUMMARY

11.1 INTRODUCTION

The objective of this project was to analyze the aircraft impacts into the World Trade Center (WTC) towers to provide the following: (1) estimates of the probable damage to structural systems, including the exterior walls, floor systems, and interior core columns, (2) estimates of the aircraft fuel dispersal during the impact; and (3) estimates of debris damage to the interior tower contents, including partitions and workstations to be used for estimating damage to the fireproofing and to the mechanical and architectural systems inside the towers. This project, thus, established the initial conditions for the fire dynamics modeling in Project 5 and the thermal-structural response and collapse initiation analysis in Project 6 of the National Institute of Standards and Technology (NIST) Investigation.

The WTC aircraft impact analysis is very complex with large scale fracture and fragmentation of both tower and aircraft structures, nonlinear rate-dependent material behaviors, and the fluid-structure interaction of the aircraft fuel. The analyses of the aircraft impacts performed for this investigation are believed to be the highest-fidelity simulations ever performed for this impact behavior using state-of-the art analysis methodologies. Wherever possible, the models were validated against observables or supporting test data developed by the WTC Investigation.

The impact analyses were conducted at various levels of complexity including: (1) the component level, (2) the subassembly level, and (3) the global level to estimate the probable damage to the towers due to aircraft impact. Analysis of uncertainties using the component, subassembly, and global analyses were also conducted to assess the effect of uncertainties associated with various parameters on the damage estimates and to identify the most influential parameters that affect the impact response.

11.2 MATERIAL CONSTITUTIVE MODELING

An important requirement for high fidelity simulation of the aircraft impact damage was the development of constitutive models that represented the actual behavior of the WTC towers and aircraft under the dynamic impact conditions. The materials that were considered included: (1) the several grades of steel used in the columns, spandrels, and floor trusses and beams of the WTC towers, (2) the concrete floor slabs, (3) the various aluminum and titanium alloys used in the aircraft, and (4) the nonstructural contents of the towers. These materials exhibit significant nonlinear, rate-dependent deformation and failure behavior that need to be represented in the constitutive relationship.

The primary constitutive model that was used for the tower steels was the Piecewise Linear Plasticity model in LS-DYNA. This model is sufficient to model the nonlinear rate-dependent deformation and failure of the steel structures. The constitutive model parameters for each grade of steel were based on engineering stress-strain data obtained by Project 3 of the NIST Investigation. Finite element analyses of the test specimens were conducted with a fine and medium mesh to capture the nonlinear material behavior up to failure. The finite element analysis provided a validation that the constitutive model

parameters were defined accurately and that the model reproduce the measured response for the test conditions. Strain-rate effects on the steel yield strength were included in the constitutive model for tower steels with the Cowper and Symonds rate effect model.

The LS-DYNA material Type 16 (pseudo-tensor concrete model) was selected for modeling the concrete floor slabs due to its ability to accurately model the confinement damage and softening behavior of concrete. The model uses two pressure-dependent yield functions and a damage-dependent function to migrate between curves. This allows for implementation of tensile failure and damage scaling, which are more dominant material behaviors at low confinement. The pseudo-tensor model also accounts for the high strain-rate sensitivity of concrete.

The constitutive and failure properties for the aircraft materials were developed from data available in the open literature. Complete engineering stress-strain curves were obtained for various 2024 and 7075 aluminum alloys that are commonly used in the construction of the Boeing 767 airframe structures. These curves were digitized for the various aluminum alloys. Representative stress-strain curves were then converted into true stress and true strain and used to develop tabular curves for the constitutive models. No rate sensitivity of the aircraft materials was considered.

The primary influence of the nonstructural components on the impact behavior was their inertial contribution. The effects of their strength were small. As a result, relatively simple approximations of their constitutive behavior were used. Typically, a linear elastic-plastic constitutive model was applied for these materials to allow for efficient modeling of deformation and subsequent erosion from the calculations as their distortions became large.

11.3 TOWER MODEL DEVELOPMENT

One of the significant challenges in developing the tower and aircraft models for the global impact analyses was to minimize the model size while keeping sufficient fidelity in the impact zone to capture the deformations and damage distributions. The limitation was that the combined aircraft and tower models should not exceed approximately 2.3 million nodes. These were distributed between the global WTC tower model and the aircraft so that the tower model would be about 1.5 million nodes and the aircraft about 0.8 million nodes. The approach used to meet this objective was to develop models for the various tower components at different levels of refinement. Components in the path of the impact and debris field were meshed with a higher resolution to capture the local impact damage and failure, while components outside the impact zone were meshed coarsely to primarily capture their structural stiffness and inertial properties.

The towers were modeled primarily with shell elements, with the exception of the exterior wall bolted connections (beam and brick elements) and the floor truss diagonals (beam elements). The WTC 1 model extended between floors 92 and 100, while the WTC 2 model extended between floors 85 and 77. The global impact models of the WTC towers included the following components:

- Core columns and floors: Core columns were modeled using shell elements with two mesh densities, a refined density in the direct impact area and a coarser far field density elsewhere. The spliced column connections were included in the model with proper failure criteria. The floors within the core were modeled using shell elements representing the floor slabs and beams.

- Exterior walls: The exterior columns and spandrels were modeled using shell elements with two mesh densities, a refined density in the immediate impact zone and a coarser far field density elsewhere. For the bolted connections between exterior panels in the refined mesh areas, brick elements were used to model the bolt plates, and beams elements were used for the bolts.

- Truss floor: In the direct impact area, the floor model included shell elements for the combined floor slab and metal decking and the upper and lower chords of the trusses. Beam elements were used for the truss diagonals. In the far field floor segments, simplified shell element representations were used for the floor slab and trusses. The dampers were not included in the models due to their low mass and strength, particularly in the transverse direction.

- Interior building contents: The interior nonstructural contents of the towers were modeled explicitly. These included the partitions and workstations, which were modeled with shell elements in the path of the aircraft debris. The live load mass was distributed between the partitions and cubicle workstations.

11.4 AIRCRAFT MODEL DEVELOPMENT

The finite element model for the Boeing 767-200ER aircraft was constructed through a three-step process: (1) data collection, (2) data interpretation and engineering analysis, and (3) meshing of the structure. The focus of this effort was on gathering sufficient structural data and including adequate detail in the aircraft model so that the mass and strength distributions of the aircraft and contents were properly captured for implementation in the impact analyses. Structural data were collected for the Boeing 767-200ER aircraft from (1) documentary aircraft structural information and (2) data from measurements on Boeing 767 aircraft.

The airframe model contained most of the significant structural components in the aircraft. The models of the fuselage, empennage, and wing structures were developed completely using shell elements. Models for the landing gear and engines were primarily developed using shell elements, but contained some brick elements as well. The typical element dimensions were between one and two in. for small components, such as spar or rib flanges, and three to four in. for large parts, such as the wing or fuselage skin.

Special emphasis was placed on modeling the aircraft engines due to their potential to produce significant damage to the tower components. The engine models were developed primarily with shell elements. The objective was to develop a mesh with typical element dimensions between one and two inches. However, smaller element dimensions were required at many locations to capture details of the engine geometry. Brick elements were used for some of the fan hubs and the roots of the compressor blades.

A detailed analysis was carried out to estimate the fuel distribution in the aircraft wings at the time of impact.

11.5 COMPONENT LEVEL ANALYSES

The primary objectives of the component modeling were (1) to develop understanding of the interactive failure phenomenon of the aircraft and tower components and (2) develop the simulation techniques required for the global analysis of the aircraft impacts into the WTC towers. The approach taken for component modeling was to start with finely meshed brick and shell element models of key components of the tower and aircraft structures and progressively coarsen the relatively coarsely meshed beam and shell element representations used in the global models. In addition to determining the optimal element size and type for global modeling, other key technical areas were addressed in the component modeling, including material constitutive modeling, treatment of connections, and modeling of aircraft fuel. Examples of the component impact analyses included:

- Impact of a segment of an aircraft wing with an exterior column.
- Impact of a segment of an aircraft wing with a core column.
- Detailed and simplified modeling of exterior panel bolted connection under impact loading and modeling of the bolted spandrel connection.
- Impact of an aircraft engine with exterior wall panels.
- Impact of a simplified plow type impactor with truss floor assembly.
- Impact of an empty wing segment with exterior wall panels.
- Impact of fuel-filled wing segment with exterior wall panels.

The following results were obtained from the component impact analyses:

- A 500 mph engine impact against an exterior wall panel resulted in a penetration of the exterior wall and failure of impacted exterior columns. If the engine did not impact a floor slab, the majority of the engine core would remain intact through the exterior wall penetration with a reduction in speed between 10 percent and 20 percent. The residual velocity and mass of the engine after penetration of the exterior wall was sufficient to fail a core column in a direct impact condition. Interaction with additional interior building contents prior to impact or a misaligned impact against the core column could change this result.
- A normal impact of the exterior wall by an empty wing segment from approximately mid-span of the wing produced significant damage to the exterior columns but not complete failure. Impact of the same wing section, but filled with fuel, resulted in extensive damage to the external panels of the tower, including complete failure of the exterior columns. The resulting debris propagating into the building retained the majority of its initial momentum prior to impact.
- Three different numerical techniques were investigated for modeling impact effects and dispersion of fuel: (1) standard Lagrangian finite element analysis with erosion, (2) Smoothed Particle Hydrodynamics (SPH) analysis, and (3) Arbitrary-Lagrangian-Eulerian (ALE)

analysis. Of these approaches, use of the SPH offered the best viable option due to its computational efficiency.

11.6 SUBASSEMBLY IMPACT ANALYSES

The subassembly analyses were considered as a transition between the component level analyses and the global impact analyses. With the subassembly analyses, more complex structural behavior not captured in the component analyses could be investigated with significantly shorter run times than required for the global analyses. The subassembly analyses were primarily used to investigate different modeling techniques and associated model size, run times, impact stability, and impact response. The final subassembly model used structural components from the impact zone on the north face of WTC 1, and included exterior panels, core framing, truss floor structures, and interior contents (workstations). The subassembly model was impacted by an aircraft engine and by a segment of a fuel-filled wing.

The subassembly model was used to investigate the effect of a number of modeling parameters on the impact response and damage estimates. For the engine impact simulations, these parameters included the strength of the building nonstructural contents and the concrete slab strength. For the wing impact simulations, the effect of the ductility of the exterior column weldment on the impact response was investigated. The results of these parametric studies indicated the following:

- The deceleration profile of the impacting engine indicated that the response of the nonstructural building contents was dominated by the mass of the workstations, rather than by their strength.

- Varying the strength of the floor concrete slab from 4 ksi to 3 ksi did not result in significant change in the impact response. It appears that the mass of the concrete slab had a greater effect on the engine deceleration and damage to the floor than did the concrete strength.

- Varying the ductility of the weld zone in the exterior columns from 8 percent to 1 percent did not result in any noticeable difference in the damage pattern or the energy absorbed by the exterior panels, indicating that the weld ductility had a negligible effect on the impact response.

11.7 ANALYSIS OF AIRCRAFT IMPACT CONDITIONS

The initial aircraft impact conditions included aircraft speed, horizontal and vertical angles of incidence, roll angle of each aircraft, and the location of nose impact with each tower. Three different methods were applied to determine the impact conditions for the aircraft that impacted the towers. The first method used a comparison of videos from different positions to calculate the three-dimensional trajectory of the aircraft. The second method used the relative frame-to-frame motion in a single video scaled to the length of the aircraft in the video to calculate the impact speed. Finally, analysis of the impact damage on the face of each tower was used to define the relative impact orientation and trajectory. This was done by matching the projected impact points of the wings, fuselage, engines, and vertical stabilizer onto the exterior wall of each tower to the observed damage pattern.

The analysis indicated that the impact speed on WTC 2 (542 mph) was about 23 percent larger than the impact speed on WTC 1 (443 mph). The aircraft that impacted the north tower was steeper than the aircraft that impacted the south tower (vertical approach angle of 13 deg for WTC 1 versus 6 deg for WTC 2). The roll angle for WTC 1 was 25 deg while that for WTC 2 was 38 deg.

11.8 UNCERTAINTY ANALYSES

The objectives of the uncertainty analyses were to assess the effect of uncertainties associated with the aircraft and WTC towers parameters on the level of damage to the towers after impact and to determine the most influential modeling parameters that affect damage estimates. Uncertainty arises in these analyses from the following key parameters: (1) aircraft impact parameters (speed, horizontal and vertical angles of incidence, orientation, and location of impact), (2) material properties and failure criteria for the towers and the aircraft, (3) aircraft parameters (mass and stiffness properties, and jet fuel distribution), (4) tower parameters (structural strength and mass distribution, connections behavior), and (5) nonstructural building contents that may share in absorbing energy imparted by the aircraft impact.

Another important source of uncertainty is the inaccuracy associated with mathematical or numerical models. These uncertainties, also known as modeling errors, are deterministic in nature, but are often treated as random variables to characterize the effects of the analysis methodologies on the calculated response. All of these variables did not necessarily have a significant effect on the estimated impact damage to the WTC towers.

Because of the complexity of the problem and the total number of parameters that could be varied in the global analyses, it was necessary to down-select a manageable list of uncertainty parameters from all of the possible parameters. Therefore, parameter screening was conducted using design of experiments methodology. Screening was first conducted at component and subassembly levels using orthogonal factorial design techniques in order to identify the most influential parameters and reduce the number of parameters to a more manageable number for the global impact analyses. The sensitivity analyses included engine impacts against core columns, wing section impacts against exterior panels, and engine-impact subassembly analyses.

Based on the three sensitivity analyses, the set of influential modeling parameters was reduced. The following parameters were selected for variation in the global impact analyses:

- Impact speed.
- Vertical approach angle of the aircraft.
- Lateral approach angle of the aircraft.
- Total aircraft weight.
- Aircraft materials failure strain.
- Tower materials failure strain.
- Building contents weight.

The impact speed and vertical approach angle were selected as significant parameters in the global analyses due to their importance in the component and subassembly impact response. The vertical approach angle played a primary role in the magnitude of the vertical impact loads on the truss floor structures. Lateral approach angle was also selected, as this parameter dictated to a large extent where aircraft debris traveled and what part of the core was affected by this debris.

Uncertainties in the strength and ductility (failure strain) of materials had a coupled effect. An increase in yield strength or an increase in failure strain resulted in an increase in the energy-absorbing capacity of the structure. The yield strength of materials was typically known more accurately than the failure strains. This was particularly true within the finite element analyses, where the value of the failure strain needed to be assigned based on the model resolution and failure criteria used. As a result, only the uncertainties in the material failure strain were used as a material uncertainty parameter for both the aircraft and the towers in the subsequent global impact analyses.

The uncertainty in the weights associated with building contents (corresponding to service live loads) was found to be of secondary importance in the engine subassembly impact analysis. In the global impact analyses, the live load contents were expected to play a more significant role in confining the fuel and debris dispersion. In addition, the partition walls were significant for controlling the subsequent spread of fire through the towers. As a result, the uncertainty in building contents weight was included as an uncertainty parameter in the global analyses.

11.9 GLOBAL IMPACT ANALYSES

The primary objective of this project was to determine the condition of the WTC towers immediately following the aircraft impacts. This assessment included the estimation of the structural damage that degraded their strength and the condition and loss of nonstructural contents such as partitions, workstations, aircraft fuel, and other debris that influenced the behavior of the subsequent fires in the towers. The global impact analyses were the primary method by which the damage to the towers was estimated. The global analyses included, for each tower, a "base case" based on a best estimate of all input parameters. They also provided more and less severe damage estimates based on variations of the most influential parameters. These more and less severe damage scenarios provided a range of damage estimates for the towers due to aircraft impact.

11.9.1 WTC 1 Base Case Global Impact Analysis

The base case impact analysis was performed for 15.0 s duration following initial impact of the aircraft nose with the north exterior wall. The analysis was performed on a computer cluster using twelve 2.8 GHz Intel Xeon processors, each on a separate node of the cluster. The run time for this analysis was approximately two weeks. The residual kinetic energy of the airframe components at the termination of a global impact simulation was typically less than one percent of the initial kinetic energy at impact.

The aircraft impact response was dominated by the impact, penetration, and fragmentation of the airframe structures. The entire aircraft fully penetrated the tower at approximately 0.25 s. The fuselage structures were severely damaged both from the penetration through the exterior columns and the penetration of the 96th floor slab that sliced the fuselage structures in half. The downward trajectory of the aircraft structures caused the airframe to collapse against the floor, and the subsequent debris motion was

redirected inward along a more horizontal trajectory parallel to the floor. The downward trajectory of the aircraft structures transferred sufficient vertical load that the truss floor structures on the 95th and 96th floors collapsed in the impact zone.

The wing structures were completely fragmented by the exterior wall. The aircraft fuel cloud began to spread out after impact but remained relatively dense until the leading edge of the fuel reached the tower core. The aircraft fuel and debris cloud eventually penetrated most of the distance through the core before their motion was halted.

Exterior Wall Damage

The calculated and observed damage in the impact zone were in good agreement. The agreement in the position and shape of the impact damage provided partial validation of the modeled geometry of the aircraft, including the aircraft orientation, trajectory, and flight distortions of the wings.

The calculated magnitude and mode of impact damage on the exterior wall also agreed well with the observed damage. The exterior wall completely failed in the regions of the fuselage, engine, and fuel-filled wing section impacts. Damage to the exterior wall was observed out to the wing tips, but the exterior columns were not completely failed in the outer wing and vertical stabilizer impact regions. Failure of the exterior columns occurred both at the bolted connections between column ends and at various locations in the column, depending on the severity of the impact load and the proximity of the bolted connection to the impact. The agreement of both the mode and magnitude of the impact damage served to partially validate the constitutive damage modeling of the aircraft and exterior wall of the tower.

Core Damage

The core had significant damage in the region close to the impact point. The columns in line with the aircraft fuselage failed on the impact side, and several of the core beams were also severely damaged or failed in the impact zone. The calculated damage to the core of WTC 1 consisted of three severed columns and four heavily damaged columns.

Truss Floor Damage

The trusses experienced significant damage in the impact zone. The calculated impact response produced severe damage to the truss structures in the primary impact path of the fuselage. The truss structures were severely damaged from the exterior wall to the core. The truss floor system on floors 94 through 96 were damaged and sagged downward as a result of the impact loading.

The truss floor and associated slab was heavily damaged or completely destroyed in the impact zone ahead of the fuselage. The zone of heavy damage to the floor slab extended beyond the truss floor and was approximately one-third of the distance through the core on floors 94 through 96.

Fuel and Debris Distribution

The bulk of the fuel and aircraft debris was deposited on floors 93 through 97, with the greatest concentration on floor 94. The calculated debris cloud included 17,400 lb of debris and 6,700 lb of aircraft fuel outside of the tower at the end of the impact analysis, either rebounding from the impact face (north wall) or passing through the tower (south wall). This amount might have been over-estimated in the calculation since the exterior walls were not modeled with windows that would contain the fuel cloud and other small debris inside the tower. In addition, the impact behavior of the aircraft fuel cloud did not include the ability to stick to, or wet, interior components. Rather, the aircraft fuel SPH particles tended to bounce off of internal structures.

11.9.2 WTC 2 Base Case Global Impact Analysis

The WTC 2 base case impact analysis was performed for a 0.62 s duration following initial impact of the aircraft nose with the south exterior wall. Full penetration of the aircraft into the tower was completed at 0.2 s after impact. The aircraft impact response was very similar to that of the WTC 1 impact and was dominated by the penetration and fragmentation of the airframe structures. The fuselage structures were severely damaged both from the penetration through the exterior columns and the penetration of the 81st floor slab that sliced the fuselage structures in half. The downward trajectory of the aircraft structures caused the airframe to collapse against the floor, and the subsequent debris motion was redirected inward along a more horizontal trajectory parallel to the floor. The downward trajectory of the aircraft structures transferred sufficient vertical load that the truss floor structures on the 80th and 81st floors began to collapse in the impact zone by the end of the simulation.

The aircraft wing structures and fuel tank were fragmented by the impact with the tower exterior. The aircraft fuel cloud started to spread out immediately after impact, but the leading edge of the fuel remained relatively dense until passing approximately one-third of the lateral distance through the tower core (approximately 0.2 s after impact). At 0.4 s after impact, the aircraft fuel cloud had penetrated approximately two-thirds the distance through the core and was spreading out. Beyond this time, the subsequent motion of the aircraft fragments and debris cloud was noticeably slowed. The spread of the fuel and debris cloud was more rapid and extensive in the open truss floor regions than through the core as a result of the open volume above the workstations in the truss floor zone.

Exterior Wall Damage

The exterior wall completely failed in the regions where the fuselage, engine, and fuel-filled wing section impacted the structure. Damage to the exterior wall extended to the wing tips, but the exterior columns were not completely failed in the outer wing and vertical stabilizer impact regions. Failure of the exterior columns occurred both at the bolted connections between column ends and at various locations in the column, depending on the local severity of the impact load and the proximity of the bolted connection to the impact.

The calculated and observed geometry and magnitude of impact damage were in good agreement. That served to partially validate the geometry of the aircraft model, including the aircraft orientation, trajectory, and flight distortions of the wings. Agreement of both the mode and magnitude of the impact damage partially validated the constitutive and damage modeling of the aircraft and exterior wall of the tower.

Core Damage

In the base case WTC 2 impact damage analysis, significant damage to the core was calculated in the region close to the impact point (the southeast corner of the core). The columns in line with the aircraft fuselage failed on the impact side of the tower, and several of the core beams were also severely damaged or failed in the impact zone. In some cases, failure of the column splices located on floors 77, 80, and 83 contributed significantly to the failure of the core columns. This was particularly true for the heavy column number 1001 at the southeast corner of the core that failed at three splice locations. A total of five columns were severed and four columns were heavily damaged.

Truss Floor Damage

The trusses experienced significant damage in the impact zone, with the greatest damage on floor 81. This severe damage to the floor 81 truss structure and floor slab was in the primary impact path of the fuselage and extended from the exterior wall to the core. The truss floor system on floors 79 and 81 had sufficient damage from the impact that truss floor sections sagged downward as a result of the impact. Trusses on floor 80 also sustained significant damage as a result of impact.

The calculated truss floor damage to WTC 2 was less than that of WTC 1, despite the higher aircraft impact energy for WTC 2. The larger truss floor damage and deflection in WTC 1 can be explained by two factors. The primary factor was that the WTC 1 downward impact trajectory was nearly twice as steep as that of the WTC 2 impact. As a result, the steeper impact angle directed more impact energy normal to the floor slab. The secondary factor was that the damage to the long span truss floor in the WTC 1 impact zone produced larger displacements than the corresponding damage level to the short span truss region in WTC 2.

Fuel and Debris Distribution

The bulk of the fuel and aircraft debris was deposited in floors 78 through 80, with the largest concentration of aircraft debris on floor 80, and the largest concentration of aircraft fuel on floors 79, 81, and 82. The calculated debris distribution included 8,655 lb of debris and 10,600 lb of aircraft fuel outside of the tower at the end of the impact analysis, either rebounding from the impact face or passing through the tower. Similar to WTC 1, the calculated debris outside the tower is believed to be larger than is realistic.

11.9.3 Different Severity Global Impact Analyses

Additional impact analyses were performed for each tower to provide a range of damage estimates due to the uncertainties in the calculated impact response. Two additional global impact analyses were performed for each tower in order to evaluate the impact response for a more severe and less severe impact scenario. The variations in impact conditions for the different severity global impact analyses were primarily obtained from the uncertainty analyses.

WTC 1 Global Impact Analyses

The impact speeds were 414 mph and 472 mph in the less severe and more severe impact scenarios, respectively. These were the upper and lower bounds obtained from the analysis of aircraft impact conditions. The vertical trajectory of the aircraft was also varied from 13.6 degrees in the less severe case

to 7.6 degrees for the more severe impact scenario. The reduced vertical trajectory angle resulted in a greater impact energy directed inward toward the core. The lateral trajectory was not varied since the impact was close to centered on the tower and normal to the north face of WTC 1. A small variation in the lateral approach angle would have little effect on the energy of the aircraft debris entering the tower and core.

A comparison of the calculated damage to the north exterior wall of WTC 1 from the three different severity impact analyses with the observed damage indicated that the overall agreement with the observed damage was good for all three analyses, with the base case global impact analysis providing the best match to the observed damage. The calculated damage magnitude was similar in each of the global analyses. The small differences in apparent damage were largely due to panels that may have severed columns in one case and were removed at the connections in another. In general, the trend was for a larger opening produced by the less severe impact and a smaller opening in the more severe impact. The increase in the opening with reduced severity impact can be explained by the increased tower panel material toughness in the less severe scenarios, resulting in a transition from severing of columns to the failure of connection bolts and panel removal.

Toward the wing tips, where the columns and spandrels were not completely severed, the more severe impact damage analysis calculated larger damage to the exterior wall panels. These columns had the largest amount of material with plastic strains above 5 percent. As would be expected, the less severe impact damage analysis calculated lower damage to the exterior wall, and the base case analysis calculated an intermediate level of damage near the wing tips.

The core damage was concentrated in the region of the core closest to the fuselage impact point, and there was a clear correlation in damage magnitude with impact severity. A total of one column was severed, and two columns were heavily damaged in the less severe impact, compared to three columns severed and four columns heavily damaged in the base case impact analysis and six columns severed and three columns heavily damaged in the more severe WTC 1 impact analysis. A strong correlation in core damage with impact severity was expected. All of the parameter variations in the three increasing severity analyses were selected to produce an increase in core damage. A higher impact speed and a shallower impact angle were selected to direct more energy toward the core. The aircraft mass was increased and given a higher material toughness. The mass of the tower contents was reduced, and the tower materials were given a lower toughness. All of these variations contributed toward the increased core damage with impact severity.

All of the WTC 1 global impact analyses resulted in a similar amount of damage to the truss floor and floor slab. Competing parameters canceled their respective effects on the floor damage. Variations in many of the parameters should have caused greater damage to the floor system in the more severe impact analysis. However, the downward impact trajectory angle was also reduced to direct more energy into the core. Therefore, less of the impact energy was directed into the floor system. The combined effects of varying these parameters led to very similar damage to the floor system in all of the analyses.

WTC 2 Global Impact Analyses

The impact speeds were 521 mph and 570 mph in the less severe and more severe impact scenarios, respectively. These speeds were the upper and lower bounds obtained from the analysis of aircraft impact

conditions. The vertical trajectory of the aircraft was also varied from 5 (more severe case) to 8 degrees (less severe case) in order to direct less mass into the core for the less severe case.

Calculated damage to the exterior wall and truss for WTC 2 showed similar trends to those seen in the WTC 1 analyses. Only slight changes in damage to these structures were calculated from the different severity impacts. Damage to the exterior wall was relatively insensitive to the parameter variations. Truss floor damage did not vary significantly due to the competing effect of the parameters varied.

The core damage was concentrated in the core region closest to the impact point. There is also a clear correlation in damage magnitude with the impact severity. A total of three columns were severed, and two columns were heavily damaged in the less severe impact, compared to five columns severed and four columns heavily damaged in the base case analysis. Seven columns severed and one columns heavily damaged in the more severe WTC 2 impact analysis.

11.9.4 Comparison with Observables

The observables available to help validate the global impact analyses included the following:

- Damage to the building exterior (exterior walls and floors in the immediate vicinity of the impact) documented by photographic evidence.
- Aircraft debris external to the towers (landing gear for WTC 1 and a landing gear and an engine for WTC 2) as documented by photographic evidence.
- Eyewitness accounts from survivors who were inside the towers (blocked or passable stairwells).

Not all of these observables were perfectly matched by the simulations due to the uncertainties in exact impact conditions, the imperfect knowledge of the interior tower contents, the chaotic behavior of the aircraft break up and subsequent debris motion, and limitations of the models. In general, however, the results of the simulations matched these observables reasonably well.

11.9.5 Comparison with Previous Studies

Two studies were previously conducted to estimate the impact damage to the WTC towers. These studies were performed by staff at Massachusetts Institute of Technology (MIT) and Weidlinger Associates, Inc. (WAI). The MIT study used an energy balance approach to estimate damage to the core columns. The WAI study used the FLEX finite element code to calculate the aircraft impact damage to both towers.

In both towers, the impact damage to the external wall calculated in this study closely matched the observed damage. The damage profiles in the WAI simulations had some noticeable differences. The first was that damage predictions from WAI included complete failure of the exterior columns over the entire length of the wings and top of the vertical stabilizer. The second was that the WAI predictions displayed local rupture of the columns adjacent to the impact point with less influence of the bolted connections on panel failure. Neither is consistent with the observed damage.

The differences in the damage profiles between the WAI and NIST calculations most likely resulted from a variety of differences in the aircraft and tower models. The WAI aircraft model was based on their model of a Lockheed C-141B military transport rather than the Boeing 767. The NIST aircraft model also contained an order of magnitude more elements and explicit modeling of the fuel. There were also differences in the aircraft impact conditions.

In general, the MIT and WAI studies appeared to predict more damage to the core columns compared to the NIST estimates. For WTC 1, MIT estimated that between four to 12 core columns failed. WAI gave two estimates for core column failure. The first estimate of 23 core columns failed and five damaged was obtained from the FLEX impact analysis. The second estimate of 20 failed columns was the number used in their collapse analysis. The NIST base case impact damage of three severed and four heavily damaged core columns and less severe estimate of one severed and two heavily damaged core columns fell below both the MIT and WAI estimates. The more severe estimate of six severed and three heavily damaged columns fell in the middle of the MIT range, but still well below the WAI estimates.

A similar trend in the predicted damage to the core columns was found in the WTC 2 analysis. MIT estimated between seven to 20 columns failed. WAI calculated 14 core columns failed and another 10 damaged in their FLEX analysis, but reduced the number of failed columns to five for their collapse analysis. The NIST base case impact damage of five severed and four heavily damaged columns, as well as the more severe estimate of 10 severed and heavily damaged columns fell in the middle of the range predicted by MIT. The less severe impact scenario predicted fewer severed and heavily damaged columns when compared with the MIT and WAI studies.

One reason for the higher damage predictions from WAI may be attributed to the lack of internal tower contents in the WAI model, such as workstations and other building contents. Another reason for the higher damage prediction in the WAI study could result from the aircraft model. In conducting a collapse analysis, WAI used engineering estimates to reduce the number of failed columns from that predicted by their FLEX model to stabilize the tower immediately after impact. Despite this adjustment, the WAI study still estimated significantly higher damage for WTC 1 than the MIT and NIST studies. For WTC 2 their adjusted estimate fell in line with the MIT and NIST studies.

11.10 SUPPORTING SIMPLIFIED ANALYSES

Approximate analyses were carried out to provide guidance to the global finite element impact analyses. The specific analyses included:

- The analysis of the overall aircraft impact forces: This analysis indicated that that the momentum transfer was more important than the strength of the impacting aircraft in determining the overall impact loads on the building.

- The effects of the energy in the rotating engine components: This analysis indicated that the potential for the rotational kinetic energy of the engine to significantly change the magnitude of the tower impact damage is small.

- The influence of the static preloads on the calculated impact damage: This analysis showed that the initialization of a static preload in the columns of the towers would not have a significant effect on the tower impact response, damage, or residual strength.

- The analysis of the load characteristics required to fail undamaged core columns: This analysis determined the characteristics of a debris cloud (i.e. density and speed) necessary to fail a core column. Application of this analysis indicated that the dispersed fuel cloud alone would not be sufficient to fail core columns.

APPENDIX A
STILL IMAGES OF THE VIDEO RECORDS USED IN CHAPTER 7

This appendix provides still images of the video records used to estimate the initial impact conditions of the aircraft that impacted World Trade Center (WTC) 1 and WTC 2 (see Chapter 7). A short description of each of these videos is provided in Table 7–1.

Figure A–1. Still image from Video V1 (WTC 1 impact).

Figure A–2. Still image from Video V2 (WTC 1 impact).

Figure A–3. Still image from Video V3 (WTC 2 impact).

Figure A–4. Still image from Video V4 (WTC 2 impact).

Figure A–5. Still image from Video V5 (WTC 2 impact).

Figure A–6. Still image from Video V6 (WTC 2 impact).

Figure A–7. Still image from Video V7 (WTC 2 impact).

Figure A–8. Still image from Video V8 (WTC 2 impact).

Figure A–9. Still image from Video V9 (WTC 2 impact).

This page left intentionally blank